

Walter Kaminsky
Editor

Metalorganic Catalysts for Synthesis and Polymerization

Recent Results
by Ziegler-Natta
and Metallocene
Investigations



Springer

Metalorganic Catalysts for Synthesis and Polymerization

Springer

Berlin

Heidelberg

New York

Barcelona

HongKong

London

Milan

Paris

Singapore

Tokyo

Walter Kaminsky (Ed.)

Metalorganic Catalysts for Synthesis and Polymerisation

Recent Results by Ziegler–Natta
and Metallocene Investigations

With 302 Figures and 177 Tables



Springer

Prof. Dr. Walter Kaminsky

University of Hamburg

Institute for Technical and Macromolecular Chemistry

Bundesstraße 45

D-20146 Hamburg

Germany

Library of Congress Cataloging-in-Publication Data

Metalorganic catalysts for synthesis and polymerization: recent results
by Ziegler-Natta and metallocene investigations / W. Kaminsky (ed.).

p. cm.

Includes bibliographical references.

ISBN-13: 978-3-642-64292-0

e-ISBN-13: 978-3-642-60178-1

DOI: 10.1007/978-3-642-60178-1

1. Organometallic catalysts. I. Kaminsky, W. (Walter), 1941-.

QD411.M494 1999

547' .0504595--dc21

99-25652 CIP

This work is subject to copyright. All rights are reserved, whether the whole or part of the material is concerned, specifically the rights of translation, reprinting, re-use of illustrations, recitation, broadcasting, reproduction on microfilm or in other ways, and storage in data banks. Duplication of this publication or parts thereof is permitted only under the provisions of the German Copyright Law of September 9, 1965, in its current version, and permission for use must always be obtained from Springer-Verlag. Violations are liable for prosecution act under German Copyright Law.

© Springer-Verlag Berlin Heidelberg 1999

Softcover reprint of the hardcover 1st edition 1999

The use of general descriptive names, registered names, trademarks, etc. in this publication does not imply, even in the absence of a specific statement, that such names are exempt from the relevant protective laws and regulations and therefore free for general use.

Production: ProduServ GmbH Verlagsservice, Berlin

Typesetting: Camera-ready by author

Cover design: Erich Kirchner, Springer Heidelberg

SPIN:10692582

2/3020-5 4 3 2 1 0 - Printed on acid-free paper

Preface

45 years after the discovery of transition metals and organometallics as catalysts for the polymerization of olefins and for organic synthesis, these compounds have not lost their fascination. The 100th birthday of Karl Ziegler, the great pioneer in this metallorganic catalysis, was in this year.

Since 1953 when Karl Ziegler has discovered the catalytic polymerization of ethylene leading to plastically formable polymers, synthetic polymers and rubbers becoming one of the most growing commercial markets. The stereoselective polymerization of propylene and other long-chain α -olefins, first detected by Giulio Natta, leads to an even broadened field of applications.

Today the importance of plastics is appreciated by many politicians. During the reception of the participants of this symposium in the Rathaus of Hamburg (townhall), the Mayor of the City of Hamburg emphasized: „Chemistry has changed the world. Even those only dealing a little bit with this topic see that particularly polymer chemistry has given important impulses for the growth of our economy and prosperity.“

Polyolefins and polybutadienes produced by metallorganic catalysts are not only the most important plastics but they show an unbroken production increase. Containing only carbon and hydrogen atoms, polyolefins will substitute other plastics which cannot be produced or recycled under the same environmental conditions.

A great development in this field was given by the discovery of metallocene/methylaluminoxane catalysts in our Hamburg laboratory. Since the last ten years over 300 patents are announced every year from industrial and academic research groups all over the world dealing with metallocene and „single site“ catalysts. Why is there so much interest in this field of research? Metallocene catalysts are soluble in hydrocarbons, show only one type of active site and their chemical structure can be easily changed. These properties allow one to predict accurately the properties of the resulting polyolefins by knowing the structure of the catalyst used during their manufacture and to control the resulting molecular weight and distribution, comonomer content and tacticity by careful selection of the appropriate reactor conditions. In addition, their catalytic activity is 10–100 times higher than that of the classic Ziegler–Natta systems.

This „International Symposium on Metalorganic Catalysts for Synthesis and Polymerization“, held in Hamburg from September 13–17, 1998 gave an overview of today's point of research for olefine polymerizations with metalorganic compounds. The goals of the symposium were to show the ways for further development of catalysts, to find proper methods in molecular modeling, to investigate the kinetics and the overall mechanisms of the catalysis with heterogeneous and homogeneous catalysts, to provide with synthetic pathways for new polyolefins and copolymers with different properties and finally to develop tools and techniques for a comprehensive characterization of the polymers and processes.

In many aspects there remain a lot of yet (unsolved) problems and possibilities for the future.

On this symposium, 49 lectures and over 90 posters were presented. We are pleased to announce that 59 manuscripts of lectures and posters could be included in this proceedings book.

The organizers like to express their special thanks to the University of Hamburg, to the Gesellschaft Deutscher Chemiker, and to companies which have sponsored the symposium and this monograph, to all authors who prepared manuscripts, and to all participants for discussions.

Hamburg, May 1999

Walter Kaminsky

Table of Contents

1. Heterogeneous Ziegler-Natta Catalysis

| | |
|--|----|
| Polyethylene: Polymer with Future (<i>L.L. Böhm, J. Berthold, H.-F. Enderle, M. Fleissner</i>) | 3 |
| Polypropylene: 44 Years Young! The Challenge for the 21 st Century (<i>P. Galli, G. Cecchin, J.C. Chadwick, D. Del Duca, G. Vecellio</i>) | 14 |
| Characterization of PP Prepared with the Latest Metallocene and MgCl ₂ -supported TiCl ₄ Catalyst Systems (<i>N. Kashiwa, S.-I. Kojoh, J.-I. Imuta, T. Tsutsui</i>) | 30 |
| An Absolute Test of Rival Theories for MWDs in Heterogeneous Polymerization-MWDs during Quasi-Living Polymerization (<i>T. Keii, T. Matsuzawa</i>) | 38 |
| Olefin Polymerization with Novel Type of Ziegler Catalysts (<i>K. Soga, E. Kaji, T. Uozumi</i>) | 50 |
| Kinetics and Mechanism of Ethylene Polymerization and Copolymerization Reactions with Heterogeneous Titanium-Based Ziegler-Natta Catalysts (<i>Y.V. Kissin, R.I. Mink, T.E. Nowlin, A.J. Brandolini</i>) | 60 |
| New Insight into Propene Polymerization Promoted by Heterogeneous Ziegler-Natta Catalysts (<i>V. Busico, R. Cipullo, G. Monaco, G. Talarico, M. Vacatello, J.C. Chadwick, A.L. Segre, O. Sudmeijer</i>) | 76 |
| Energy Distribution of Active Sites in Heterogeneous Ziegler-Natta Catalysts. Method of Study of Active Site Non-uniformity (<i>L.A. Novokshonova, N.Y. Kovaleva, Y.A. Gavrilov, V.G. Krashenninikov, T.A. Ladygina, I.O. Leipunskii, A.M. Zhigach, M.L. Kuskov</i>) | 89 |
| Ziegler-Natta and Metallocene Polymerisation of Olefins with Heterogeneous Catalysts (<i>K. Weiss, S. Botzenhardt, M. Hofmann</i>) | 97 |

2. Homogeneous Catalysis, Synthesis and Polymerization

| | |
|--|-----|
| Formation, Structure and Mechanism of Oligomeric Methylaluminoxanes (MAO) (<i>H. Sinn, I. Schimmel, M. Ott, N. von Thienen, A. Harder, W. Hagendorf, B. Heitmann, E. Haupt</i>) | 105 |
| The Activation of Metal-Fluorine Bonds in Compounds of Group 4 by Aluminum Alkyls (<i>H. Wessel, A. Herzog, P. Yu, H.W. Roesky</i>) | 123 |
| A DFT Quantum-chemical Study of the Structures and Reactive Sites of Polymethylalumoxane (<i>I.I. Zakharov, V.A. Zakharov, G.M. Zhidomirov</i>) | 128 |
| In situ FTIR Spectroscopy Shows no Evidence of Reaction between MAO and TMA (<i>J.L. Eilertsen, E. Rytter, M. Ystenes</i>) | 136 |
| Alumoxanes alternative to MAO: Synthesis and characterization (<i>T. Dall'Occo, M. Galimberti, I. Camurati, M. Destro, O. Fusco, D. Brita</i>) . | 142 |
| Expanding the Scope of Metallocene Catalysis: Beyond Indenyl and Fluorenyl Derivatives (<i>J.A. Ewen, R.L. Jones, M.J. Elder</i>) | 150 |
| New C ₁ -Symmetric Metallocenes for the Polymerization of Olefins (<i>W. Kaminsky, R. Werner</i>) | 170 |
| New Catalyst Concepts for the Polymerization of Ethylene with Metallocenes (<i>A. Akimoto, A. Yano</i>) | 180 |
| Synthesis of Novel Complex with Bridged Bis(indenyl)Ligand and its Polymerization Behavior of Propylene (<i>T. Kato, H. Uchino, N. Iwama, K. Imaeda, M. Kashimoto, Y. Osano, T. Sugano</i>) | 192 |
| Linked Amido-Cyclopentadienyl Complexes of Group 3 and 4 Metals: The First „Post-Metallocenes“ (<i>J. Okuda</i>) | 200 |
| Late Transition Metal Catalysts for Olefin Polymerization (<i>O. Pyrlík, M. Gosmann, M. Arndt-Rosenau</i>) | 212 |

3. Homogeneous Catalysis, Mechanism of Polymerization

- Chain Growth in Zirconocene-catalyzed Olefin Polymerization -DFT Studies on Possible Reaction Paths and the Influence of a Second Olefin Ligand
(*M.-H. Proscenc, F. Schaper, H.-H. Brintzinger*) 223
- Syndiotactic and Isotactic Specific Metallocene Catalysts with Hapto-flexible Cyclopentadienyl-Fluorenyl Ligand
(*A. Razavi, V. Bellia, Y. De Brauwer, K. Hortmann, M. Lambrecht, O. Miserque, L. Peters, S. Van Belle*) 236
- Current Vitality of Ziegler's Monumental Discovery of Zirconium Catalysis in Olefin Polymerization: Metallocene and Nonmetallocene Catalysts via Reductive Dimerization
(*J.J. Eisch, X. Shi, F.A. Owuor*) 248
- Kinetic Features of Living Polymerization of Propene with the [t-BuNSiMe₂Flu]TiMe₂/B(C₆F₅)₃ Catalyst
(*T. Shiono, H. Hagihara, S. Yoshida, T. Ikeda*) 264
- Quantitative Structure-Activity Relationships for Unbridged Zirconocene Catalysts During Ethene Polymerization
(*J.A. Støvneng, A. Stokvold, K. Thorshaug, E. Rytter*) 274
- Coexistence of two Active Species in the Polymerization of 1-Hexene Catalyzed with Zirconocene/MAO Catalysts
(*H. Frauenrath, H. Keul, H. Höcker*) 283
- In-depth Investigation of Unsaturated Chain-end Groups: A Tool for Understanding Hydrogen Activation Mechanism in Zirconocene Catalysed Propene Polymerization
(*M.C. Sacchi, F. Forlini, I. Tritto, P. Locatelli, A. Carvill*) 294

4. Supported Metallocene Catalysts

- Supported Metallocene Catalysts for Propene Polymerization
(*P.J.T. Tait, R. Ediat*) 307
- Influence of the Particle Size of Silica Support on the Kinetics and the Resulting Polymer Properties at the Polypropylene Polymerization with Heterogeneous Metallocene Catalysts; Part I: Experimental Studies and Kinetic Analysis
(*C. Przybyla, J. Zechlin, B. Steinmetz, B. Tesche, G. Fink*) 321

| | |
|---|-----|
| Influence of the Particle Size of Silica Support on the Kinetics and the Resulting Polymer Properties at the Polypropylene Polymerization with Heterogeneous Metallocene Catalysts; Part II: Development of a Model as well as a Mathematical Simulation (<i>C. Przybyla, B. Weimann, G. Fink</i>) | 333 |
| Supported Metallocene Catalysts in Olefin Polymerization: Toward High Performances (<i>R. Spitz, N. Verdel, V. Pasquet, J. Dupuy, J.P. Broyer, T. Saudemont</i>) | 347 |
| Zeolite Supported Metallocene Catalysts: Effect of Support Structure and Surface Groups on the Polymerization Process (<i>F. Ciardelli, A. Altomare, M. Michelotti, G. Arribas, S. Bronco</i>) | 358 |
| Preparation of Novel Supported Metallocene and their Olefin Polymerization Capabilities (<i>Y.S. Ko, T.S. Seo, D.S. Hong, S.I. Woo</i>) | 368 |
| Development of Supported Single-site Catalysts and Produced Polyethylene (<i>A. Muñoz-Escalona, L. Méndez, J. Sancho, P. Lafuente, B. Peña, W. Michiels, G. Hidalgo, M.F. Martínez-Nuñez</i>) | 381 |
| Ethylene Polymerization with the Heterogeneous Single Site CpIndZrCl ₂ Catalyst (<i>D.-H. Lee, S.K. Noh</i>) | 397 |
| The Impact of the Cocatalyst on the Polymerisation Behaviour of Supported Metallocenes (<i>E. Ernst, J. Reußner, P. Denifl</i>) | 406 |
| Heterogenised MAO-free Metallocene Catalysts (<i>S.J. Lancaster, S.M. O'Hara, M. Bochmann</i>) | 413 |
| A New Supported Zirconocene Catalyst for Ethylene Polymerization (<i>W. Ochedzan-Siodlak, M. Nowakowska, M. Wasielewski</i>) | 426 |

5. Polystyrene and Copolymers

| | |
|---|-----|
| Syndiospecific Polymerization of Styrene (<i>K. Yokota, T. Inoue, S. Naganuma, H. Shozaki, N. Tomotsu, M. Kuramoto, N. Ishihara</i>) | 435 |
|---|-----|

| | |
|---|-----|
| Monocyclopentadienyl Titanium Catalyst (<i>J.C.W. Chien, M.D. Rausch</i>) | 446 |
| The Effects of the Bridge Structure and the Ligand System of Zirconocene Catalysts on the Copolymerization of Styrene and Ethylene (<i>T. Arai, T. Ohtsu, S. Suzuki</i>) | 465 |
| Branched Polyethenes Prepared via Olefin Copolymerization and Migratory Insertion (<i>J. Heinemann, P. Walter, D. Mäder, R. Schnell, J. Suhm, R. Mülhaupt</i>) | 473 |
| Metallocene Catalyzed Alternating Copolymerization of Olefins (<i>I. Beulich, F. Freidanck, A.-M. Schauwienold, U. Weingarten, M. Arndt-Rosenau, W. Kaminsky</i>) | 485 |
| Copolymer Microstructures of Ethylene Norbornene Copolymers Prepared with Homogeneous Metallocene Based Catalysts (<i>I. Tritto, L. Boggioni, M.C. Sacchi, P. Locatelli, D.R. Ferro, A. Provasoli</i>) | 493 |
| Studies on Properties of Metallocene Catalysed Copolymers of Ethylene and Linear, Non-conjugated Dienes (<i>P. Pietikäinen, A. Malmberg, B. Löfgren, J. Seppälä</i>) | 502 |
| Ethylene/ α -Olefin Copolymerization with Dimethylsilyl-bis-(2-methyl-4-phenyl-indenyl)zirconium dichloride and Methylaluminumoxane: Influences on Polymerization Activity and Molecular Weight (<i>M. Miri, D. Hetzer, A. Miles, M. Pecak, B. Riscili</i>) | 509 |

6. Functional Polyolefins and Polydienes

| | |
|--|-----|
| The Role of the Cyclopentadienyl Ligand in Catalysts for 1,3-Diene Polymerization (<i>L. Porri, G. Ricci, A. Giarrusso</i>) | 519 |
| Catalytic Reaction Mechanisms and Structure-Reactivity Relationships in the Stereospecific Butadiene Polymerization (<i>R. Taube</i>) | 531 |
| Styrene and Conjugated Dienes Polymerization with Half Sandwich Titanocene Catalysts (<i>A. Zambelli, A. Grassi, P. Longo</i>) | 548 |

| | |
|--|-----|
| Half-Vanadocene Catalyst for Butadiene Polymerization (<i>S. Ikai, M. Suzuki, N. Tsujimoto, Y. Iwamoto, S. Yuasa, J. Yamashita, M. Murakami, Y. Kai, T. Yano</i>) | 558 |
| Chemical Functionalization of Polypropylene with a V-based Living Polymerization Catalyst (<i>M. Murata, Y. Fukui, K. Soga</i>) | 566 |
| Copolymerization of Ethylene/ ω -Hydroxy α -Olefins (<i>M.M. Marques, S.G. Correia, J. Ascenso, A.R. Dias, M. Blais, M.D. Rausch, J.C.W. Chien</i>) | 576 |
| Stereospecific Polymerization of Methacrylates with Dimethylsilylene-bridged Zirconocene Catalysts (<i>N. Saegusa, T. Saito, T. Shiono, T. Ikeda, H. Deng, K. Soga</i>) | 583 |
| Development of Catalytic Systems based on Lanthanoid Complexes for Olefin Polymerization (<i>K. Bujadoux, T. Chenal, C. Fouga, X. Olonde, J.-F. Pelletier, A. Mortreux</i>) | 590 |

7. Polymer Characterization and Processes

| | |
|--|-----|
| Initial 2,1-Insertions in Metallocene Polymerizations of Polypropylene (<i>J.C. Randall, C.J. Ruff, J.C. Vizzini, A.N. Speca, T.J. Burkhardt</i>) | 601 |
| Olefin Polymerization with DuPont's Versipol™ Catalyst System (<i>S.D. Ittel</i>) | 616 |
| Features of Cyclopentadienyl Metal Catalysts for Ethylene Copolymerization in Gas and Liquid Phase (<i>F.J. Karol, S.-C. Kao, E.P. Wasserman, Z. Yu</i>) | 629 |
| How to Avoid Gas-Liquid Mass Transfer Limitations During Polymerization of Olefins (<i>P. Kittilsen, R. Tøgersen, E. Rytter, H. Svendsen</i>) | 643 |
| Ternary Metallocene Based Catalysts in High Temperature, High Pressure Polymerization (<i>G. Luft, A. Rau, A. Dyroff, C. Götz, S. Schmitz, T. Wiczorek, R. Klimesch, A. Gonioukh</i>) | 651 |

| | |
|---|-----|
| Advances in the Use of Stopped-flow Techniques for Olefin Polymerization (<i>M. Terano, M. Yamahiro, H. Mori</i>) | 658 |
| Contributors | 671 |

1. Heterogeneous Ziegler–Natta Catalysis

Polyethylene: Polymer with Future

L. L. Böhm, J. Berthold, H.-F. Enderle, M. Fleissner

Hostalen Polyethylen GmbH,
D-65926 Frankfurt (M), Germany

Abstract

Polyethylenes play a very important role today, because these polymers have a lot of advantages in comparison to other materials. They are produced using easily accessible, reasonable raw materials, they are environmentally harmless, and they can be recycled or energetically exploited after loss of performance. However, the most important aspect is, that they can be tailored in an excellent way using well established modern, energy saving, and non-polluting technologies of large scale.

To make these products and to run these processes appropriate catalysts mostly together with cocatalysts are required. The catalyst or the catalyst/cocatalyst system plays the key role for catalytic polymerization of olefins. Now, a broad spectrum of high mileage catalyst systems is available and some new ones are under development. New catalyst systems open prospectives for future progress. The catalyst system and the polymerization process are forming the polymerization technology and both parts must be well-balanced to reach a high level of effectiveness.

Besides the polymerization technology, the correlations between polymer structure and polymer properties must be known to tailor products. Based on these three legs: catalyst or catalyst system, process, polymer properties/polymer structure relations, polyethylenes with new and so far unknown properties can be designed and brought to the market. With these polymers consumers needs can be better met saving material and energy for processing, transportation and finally, waste management.

Introduction

Polymers are today materials used in all fields of life. These materials have been discovered within this century and are now produced overall in the world [1]. Nowadays (1995) around 160 Mt of polymer-based materials (plastics, fibers, elastomers, duromers, dispersions) are consumed per annum. The largest part are plastics with around 100 Mt/a and among these the polyolefins have a share of about 60 Mt/a [2,3].

Within the next 10 years production and consumption of polyolefins will considerably increase to reach between 100 and 110 Mt/a. The key success factors for polyolefins are the following ones: the raw materials (monomers) are easily accessible and reasonable based on oil or natural gas. The production costs are low due to modern, energy saving and non-polluting large volume processes. The products are saving resources and they are environmentally harmless thus contributing to the principle of sustainable development [4,5]. After loss of

performance these polymers can be burned having combustion energies like oil. Therefore, they are also called solid white oil [6,7]. Finally a broad product portfolio of polyolefins is accessible by catalytic polymerization processes ranging from very low up to ultrahigh molecular mass compounds and covering a broad range of densities. All these products can be tailored to reach excellent product quality in respect to processing and final product performance. Some of these products can be identified as polymer alloys [8-11]. Starting from easily accessible, reasonable raw materials like ethene, propene or other 1-olefins and using catalytic polymerization processes a broad spectrum of valuable polymer products can be synthesized as demonstrated on fig. 1.

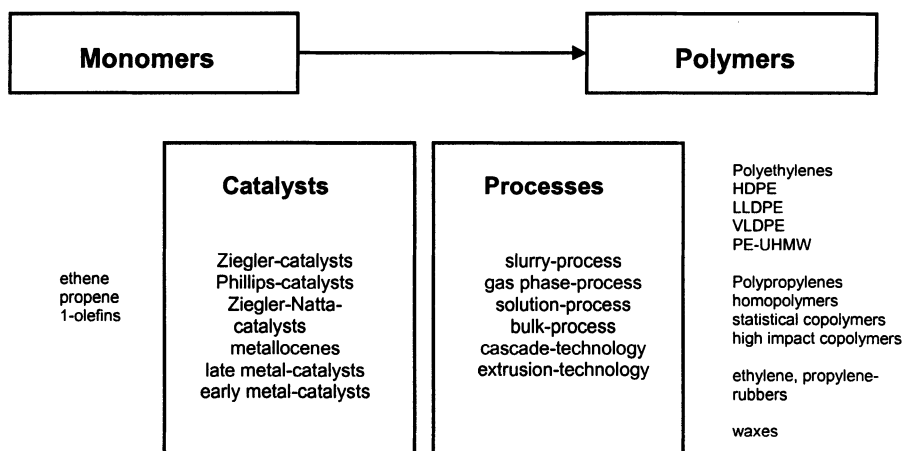


Fig. 1. Catalysts, Processes for Polyolefins Production

Polymerization Technology

To make tailored polyethylenes meeting customer needs in a well-performing way, there must be a proper technology together with a detailed know-how of polymer structure and polymer properties relations. For catalytic polymerization processes the catalyst, mostly in combination with a cocatalyst, and the polymerization process are regarded as the polymerization technology. This means that both are forming an integrated whole and both must be well-balanced in respect to each other [12,13]. However, it must be pointed out that the catalyst or catalyst system plays the key role as shown on fig. 2. It determines the polymerization behavior, the polymer structure and for heterogeneous processes the polymer powder morphology. The catalyst system must perfectly fit to the polymerization process.

In heterogeneous processes (slurry or gas phase technology) the polymerization reaction only takes place inside the polymer particles. Each of these polymer particles is a small reactor (micro reactor) with its own energy and mass balance [13-15]. They grow from the catalyst particles by polymer formation around the catalyst fragments (primary particles) [16]. This process is called particle forming process and it is a must that it runs in a certain way which means: only negligible temperature and monomer concentration gradients exist within the polymerizing

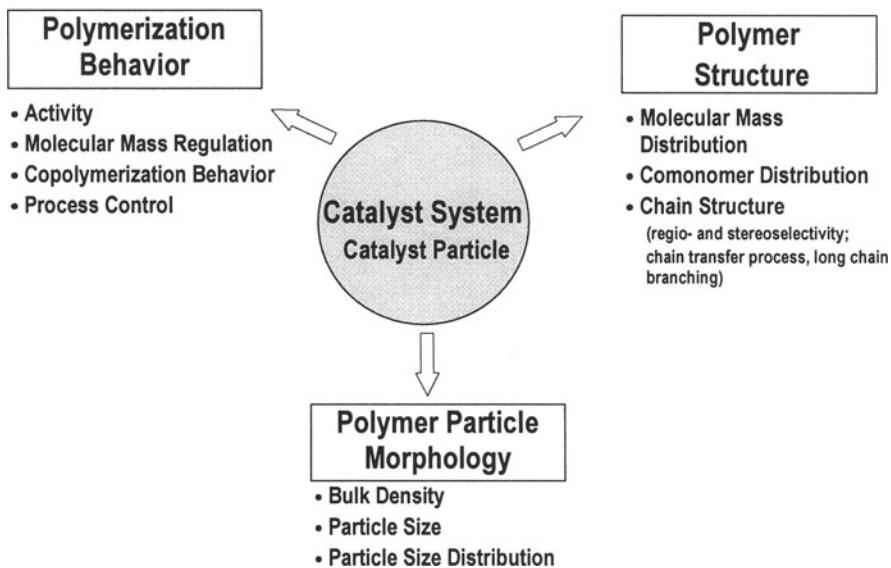


Fig. 2. The Key Role of the Catalyst System

particle and at the surface (see curves 1 in fig. 3). Especially in the start-up phase of polymerization at the fresh catalyst particle after its entrance in the polymerization reactor, this may not be the case. To avoid almost certainly overheating of the particle (hot spot formation) and monomer concentration gradients inside the particle (although this is not critical for technically used catalyst systems [17,18]) the rate of polymerization must be small in this stage as shown in fig. 3.

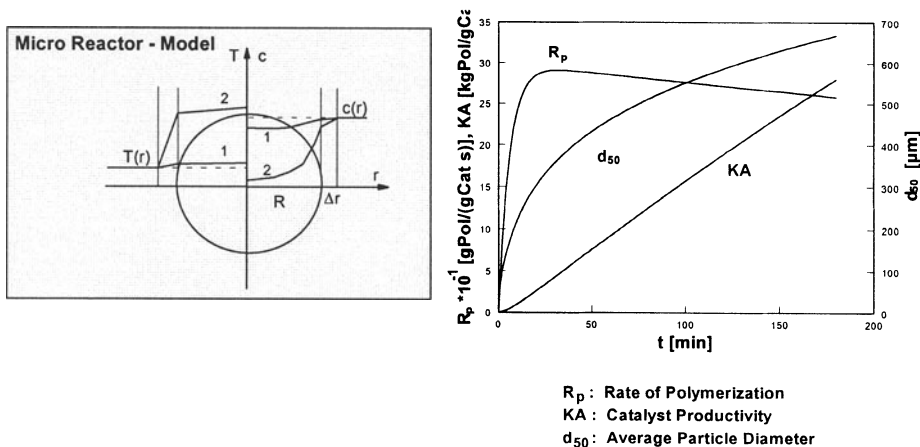


Fig. 3. Optimized Polymerization Behavior of the Catalyst System

When the polymerizing particle expands and the micro reactor becomes larger then the rate of polymerization can also increase because heat transfer and monomer flow increase simultaneously. To reach a high catalyst productivity (mass of polymer/mass of catalyst used) the polymerization rate must then stay at a high level as long as the polymerizing particle remains in the reactor (average residence time).

Under such conditions the particle forming process runs as shown on fig. 4, which means that every primary particle is covered by a polymer layer and all catalyst fragments are evenly distributed over the whole polymer particle.

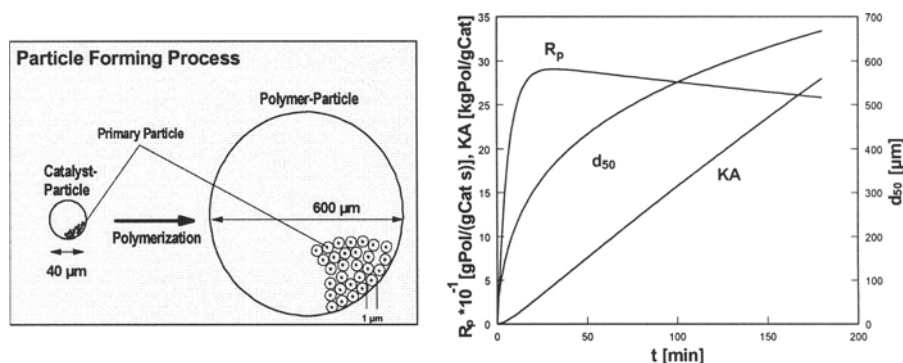


Fig. 4. Particle Forming Process

Such optimized catalyst systems are today state of the art and only those catalyst systems can be used in technical processes.

For the technical process stability and flexibility are the main recommendations: a polymerization reactor is an open system in which a sensitive metallorganic system is used to catalyze polymerization. To stabilize this process against uncontrolled entrance of impurities a sufficient high level of an aluminumorganic compound is established as a scavenger. This compound further acts as cocatalyst. The catalyst system must be sensitive to a limited number of process parameters to control polymer data over a wide range. By variation of this limited set of process parameters strong changes of the product data average molecular mass and density can be achieved (good process flexibility) [19]. Fig. 5 shows the data set (extensive and intensive parameters) which controls polymer data. The underlined parameters should be kept constant under technical process conditions.

Product Portfolio

Using modern advanced technologies a broad range of products with different average molecular mass or melt flow rate (MFR) [20], density, molecular mass distribution and comonomer distribution can be produced as shown on fig. 6.

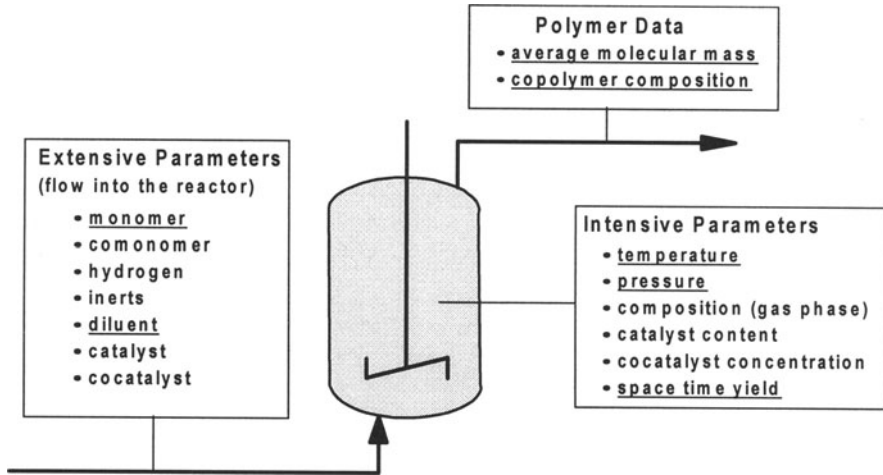


Fig. 5. Process Parameters for Product Data Control

Applying the detailed knowledge about the relation between polymer structure and polymer properties [21-26] tailored products in respect to processibility and final product performance can be produced for a wide field of applications. There are 2 general trends: with decreasing density the comonomer distribution in the polymer should become homogeneous, and with increasing average molecular mass or

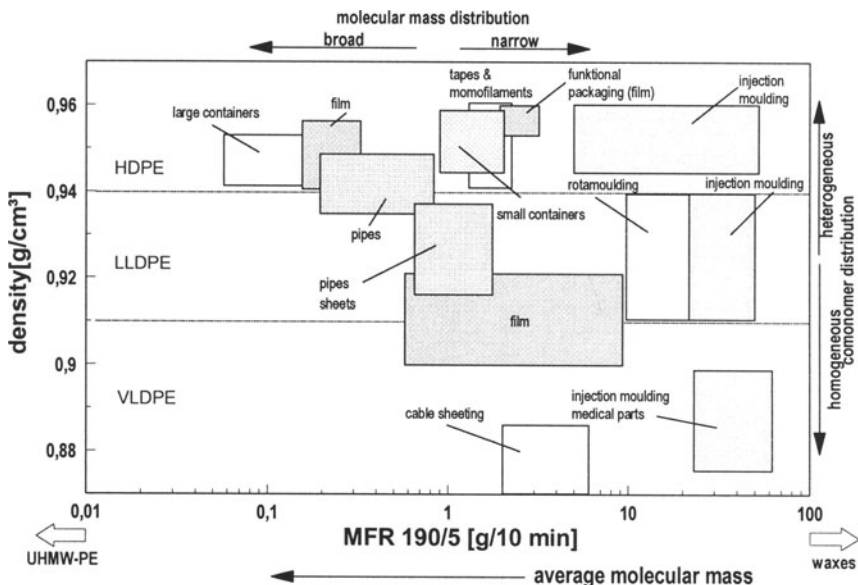


Fig. 6. Polyethylene Product Map

decreasing melt flow rate (MFR) the molecular mass distribution moves from narrow to broad, going from unimodal to bimodal. In the LLDPE and VLDPE product field, it is advantageous to produce polymers with narrow molecular mass distribution and homogeneous comonomer distribution as shown on fig. 7 [27].

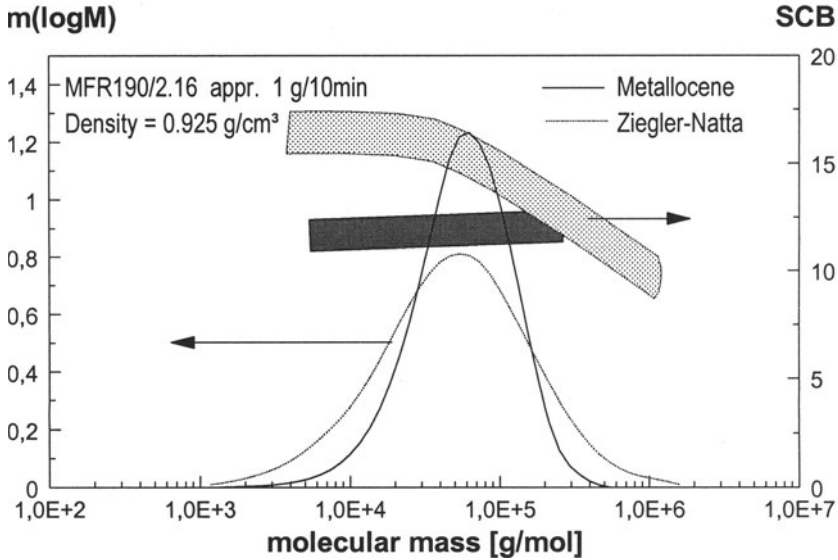


Fig. 7. Molecular Mass and Comonomer Distribution (SCB: short chain branches)

These copolymers can be produced with single site catalysts now available by combining metallocenes and methylalumoxane [28-30]. Products with nearly the same processing behavior due to the same shear viscosity in the processing window differ considerably in weight (M_w) and number average molecular mass (M_n) depending on the polydispersity M_w/M_n (see fig. 8).

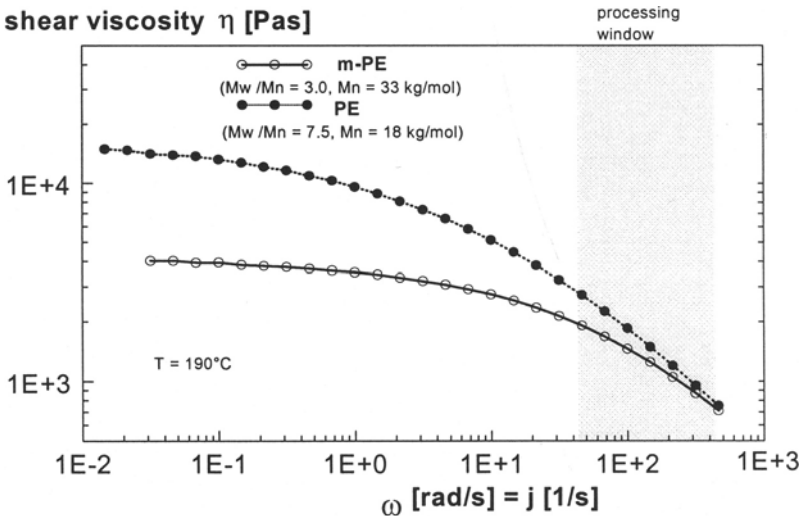


Fig. 8. Viscosity Functions: metallocene vs. conventional PE

For polymers with unimodal molecular mass distributions there is a master curve correlating toughness and number average molecular mass M_n [21]. This opens the possibility to design products with improved mechanical properties in the same processing window compared to state of the art products with broader molecular mass distributions. Fig. 9 shows some results for PP-fibres [31]

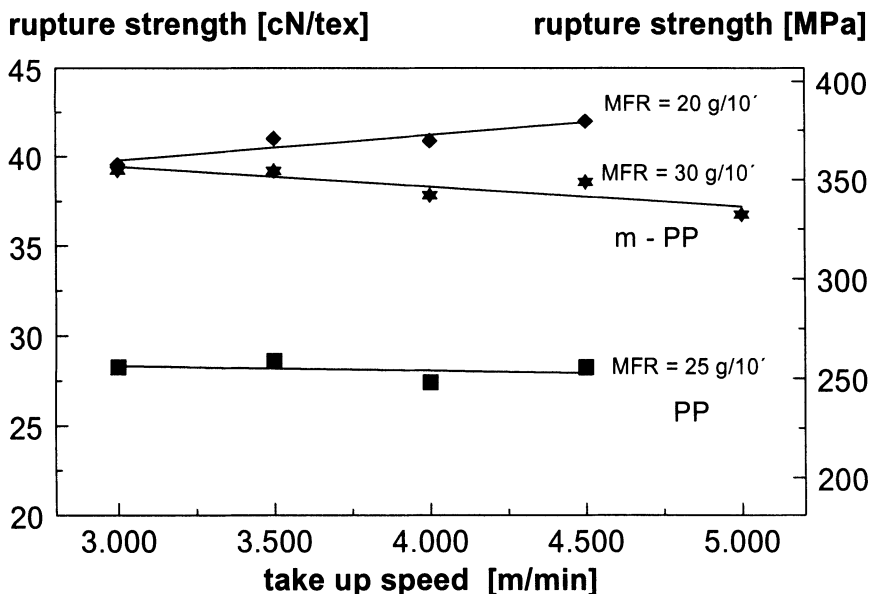


Fig. 9. Tensile Strength of PP-fibres (m-PP: metallocene-made polymer, PP: standard polymer)

In summary these products with narrower molecular mass distributions, and homogeneous comonomer distributions have higher toughness, higher tensile strength, lower extractables, narrower melting ranges, higher stress crack resistance and higher melt strength than known products. Improved products for injection moulding, rotamoulding, films and fibres in the whole density range with a clear focus on low to very low densities can be produced.

Looking on high density, high average molecular mass products, advantageous products have a very broad, bimodal molecular mass distribution and an inhomogeneous comonomer distribution with the comonomer built into the long chains [10].

These products are made using the cascade technology with 2 polymerization reactors in series [32]. The catalyst is only introduced in the 1st reactor to form the very low molecular mass homopolymer, then the polymer particles with the still active catalyst move into the 2nd reactor to form the very high molecular mass copolymer. Again the catalyst system plays the key role. Molecular mass regulation with hydrogen must be possible over a broad range as shown in fig. 10 without losing the activity by inhibition with hydrogen.

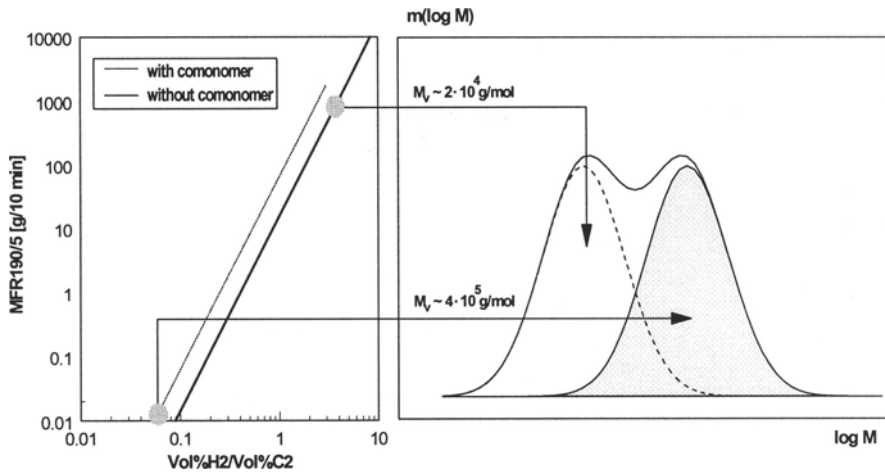


Fig. 10. Molecular Mass Regulation to Produce a Bimodal PE-HD

The particle forming process must run in such a way that each catalyst fragment is covered by layers of the low molecular mass homopolymer and the high molecular mass copolymer, and all catalyst fragments must be evenly distributed over the polymer particle. Fig. 11 shows this in a schematic representation.

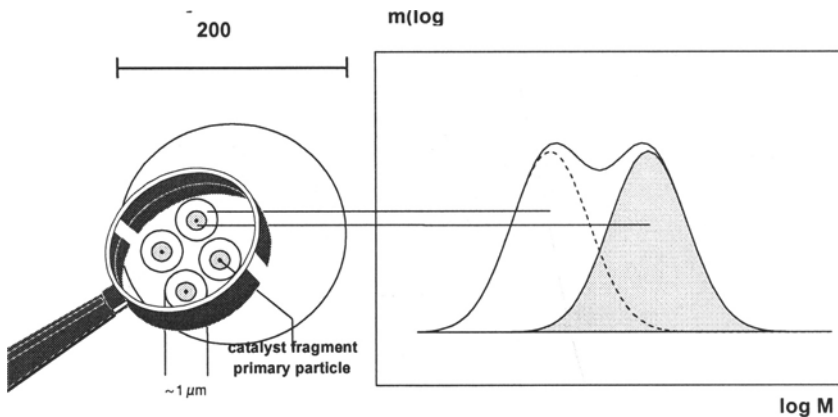


Fig. 11. Polymer Particle Structure for Cascade-Made Bimodal PE-HD

Finally to reach the full performance of these materials the polymer powder must be transferred in a homogeneous polymer melt by extrusion. This can be achieved because already in each polymer particle the high and the low molecular mass fractions are finely divided in each other (in situ-blend). These polymers have an outstanding combination of desired properties for pipe applications (water and gas pipes) and films. Therefore they can be addressed as a polymer alloy or an engineering resin. Fig. 12 summarizes the properties.

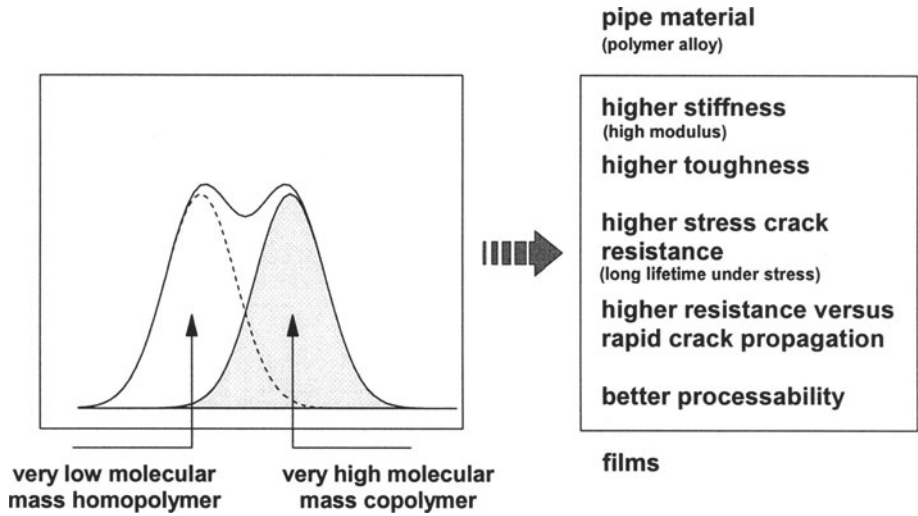


Fig. 12. Advantageous Properties of Bimodal Pipe Materials

The properties of the products and their applications were described in detail for pipes [10,33-36] and films [32] elsewhere.

Conclusions

Polyolefins in general and polyethylenes as part of this product family are polymers of the future. This is demonstrated by the great increase in production and consumption forecasted between 1995 and 2005 [3].

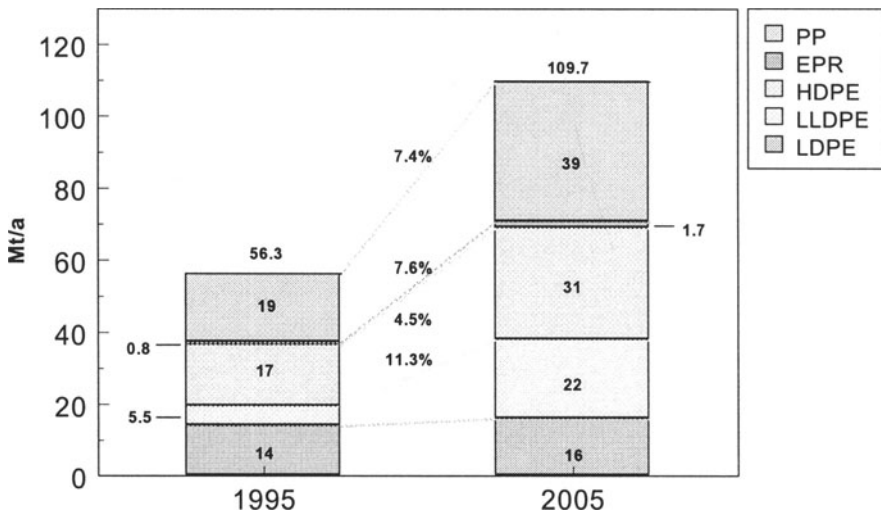


Fig. 13. Production and Consumption of Polyolefins

These growth rates must be driven by strong economic and technical factors. The most important driving force is that polyolefines are often the better problem solvers in various fields of application as shown e. g. for packaging materials [4]. After loss of performance these products can be recycled or energetically exploited [6,7,37]. So these materials contribute strongly to the concept of sustainable development [5].

The most relevant technical aspects are the availability of a broad range of catalyst systems and advanced polymerization processes. Using these technologies together with the profound knowledge in polymer structure/polymer properties relations tailored products with excellent performance can be designed to meet customer needs. New materials have been developed in the last few years which can be addressed as engineering resins like the PE 100 pipe material. There are still potentials for new, surprising developments which will be realized in near future. In addition, the discovery of new catalyst or catalyst systems is driving this innovation process [38].

Literature

1. L. A. Utracki, *Polym. Eng. & Sci.* **35**, 2 (1995)
2. D. Freitag, *Chem. Ind. Nordrhein-Westfalen* **1997**, 33
3. Data: Marktforschung Hostalen Polyethylen GmbH
4. Survey Report of Life Cycle Assessment (LCA) for Plastics and other Packaging Materials, Plastic Waste Management Institute Japan (1995)
5. B. Weßling, *Kunststoffe* **84**, 524 (1994)
6. H. Kindler, N. Nikles, *Kunststoffe* **70**, 802 (1982)
7. J. Brandrup, in *Blasformen '97. Innovationen und Perspektiven*, VDI-Verlag GmbH, Düsseldorf, 1997, p. 131
8. T. Sasaki, T. Ebara, H. Johoji *Polym. Adv. Techn.* **4**, 406 (1993)
9. *Catalyst Design for Tailor-Made Polyolefins*, K. Soga, M. Terano, Eds., Kodansha, Tokyo, 1994
10. J. Scheirs, L. Böhm, J. C. Boot, P. S. Leever, *TRIP* **4**, 408 (1996)
11. L. L. Böhm, H.-F. Enderle, M. Fleissner, F. Kloos, *Angew. Makromol. Chem.* **244**, 93 (1997)
12. L. L. Böhm, in *5th International Workshop on Polymer Reaction Engineering*, Dechema Monograph. **131**, 191 (1995)
13. T. Xie, K. B. McAuley, J.C.C. Hsu, D.W. Bacon, *Ind. Eng. Chem. Res.* **33**, 449, (1994)
14. L. L. Böhm, R. Franke, G. Thum, in *Transition Metals and Organometallics as Catalysts for Olefin Polymerization*, W. Kaminsky, H. Sinn, Eds., Springer-Verlag, Berlin 1988, p. 391
15. L. L. Böhm, D. Bilda, W. Breuers, H.-F. Enderle, R. Lecht, in *Ziegler, Catalysts*, G. Fink, R. Mülhaupt, H.-H. Brintzinger, Eds., Springer-Verlag, Berlin 1995, p. 387
16. M. Kakugo, H. Sodatoshi, M. Yokoyama, K. Kojima, in ref. (14), p. 433
17. L. L. Böhm, *Chem. Ing. Techn.* **56**, 674 (1984)
18. T. F. McKenna, F. Barbotin, R. Spitz, *J. Appl. Polym. Sci.* **62**, 1835 (1996)
19. L. L. Böhm, P. Goebel, P.-R. Schöneborn, *Angew. Makromol. Chem.* **174**, 189 (1990)

20. ISO (International Standard) 1133-1981
21. M. Fleißner, *Angew. Makromol. Chem.* 105, 167 (1982)
22. L. L. Böhm, H.-F. Enderle, M. Fleißner, *Adv. Mater.* 4, 234 (1992)
23. M. Takahashi, N. Kashiwa, A. Todo, M. Ohigizawa, *Structure and Properties of Metallocene LLDPE in the Gas Phase Process, Metallocenes '95, Brussels 1995*
24. J. Everaert, *Kunststoffe* 87, 73 (1997)
25. L. L. Böhm, M. Fleißner, *Kunststoffe* 88 (1998) in press
26. H. Domininghaus, *Die Kunststoffe und ihre Eigenschaften*, VDI-Verlag GmbH, Düsseldorf 1992
27. N. Kashiwa, in ref. (9), p. 381
28. W. Kaminsky, *Chemistry in Britain*, February 1998, p. 43
29. H. Sinn, W. Kaminsky, H.-J. Vollmer, R. Woldt, *Angew. Chem.* 92, 39 (1980)
30. H. Sinn, W. Kaminsky, *Adv. Organomet. Chem.* 18, 99 (1980)
31. L. L. Böhm, V. Dolle, H.-F. Enderle, M. Fleißner, A. Winter, in ref. (7), p. 113
32. L. L. Böhm, H.-F. Enderle, M. Fleißner, *Plastics, Rubber and Composites Proc. & Appl.* 27, (1998) in press
33. J. Berthold, L. L. Böhm, H.-F. Enderle, P. Göbel, H. Lüker, R. Lecht, U. Schulte, *Plastics, Rubber and Composites Proc. & Appl.* 25, 368 (1996)
34. L. L. Böhm, H.-F. Enderle, M. Fleißner, in ref. (9), p. 351
35. U. Schulte, R. Lecht, *Swiss Plastics* 20, 15 (1998)
36. U. Schulte, *Kunststoffe* 87, 203 (1997)
37. *Energetische Verwertung von Kunststoffen, Expertenworkshop am 03.06.1998, VKE Verband Kunststoffherzeugende Industrie e. V., VGB Technische Vereinigung Großkraftwerksbetreiber e. V.*
38. P. M. Morse, *New Catalysts renew Polyolefins*, C & EN, July 6, 1998, p. 11

POLYPROPYLENE: 44 YEARS YOUNG! THE CHALLENGE FOR THE 21ST CENTURY

P. Galli, G. Cecchin, J.C. Chadwick, D. Del Duca, G. Vecellio
Montell Polyolefins

Abstract. Polypropylene is one of the most versatile and successful materials in the market because of the ever-increasing spectrum of polymer composition and properties which have originated from continuing breakthroughs in catalyst and process technology. Industrial polypropylene production is based on Ziegler-Natta supported catalysts. The success of $MgCl_2$ -supported catalysts is also due to the development of spherical catalysts with controlled particle size and porosity, used in bulk liquid monomer and gas-phase processes for production of a broad range of homo- and copolymers and multiphase polymer alloys via "Reactor Granule" technology. The most recent development is the discovery of $MgCl_2/TiCl_4$ /diether catalysts which can give PP yields twice as high as those obtained with previous catalysts. The achievement of a better control of the polymer structure has resulted in an increased capability to tailor the products according to the performance requirements, both in the conversion technologies and in the application life cycle, as well as to extend their application to new market areas.

Introduction

It was in March 1954 that Natta and his coworkers at the Politecnico di Milano first synthesized crystalline isotactic polypropylene using the catalyst system $TiCl_4 - AlEt_3$, following Ziegler's discovery of similar systems for ethene polymerization in 1953 [1-3]. Commercial production of polypropylene started in Ferrara in 1957 (one reactor can be seen in its original position at the site) and over the past forty years has undergone continuous growth, such that current worldwide manufacturing capacity exceeds 20 million tonnes per annum, forecasted to be increased in the future.

The catalytic system played a key role for the development and the innovation of industrial technologies, leading to the achievement of sophisticated polymerization processes and materials.

1. Early catalyst and process development

The first and second generation catalysts were based on $\text{TiCl}_3/\text{AlEt}_2\text{Cl}$ systems and allowed the development of polymerization processes in solvent suspension (slurry). These processes exhibited low productivity and stereospecificity and deashing, for catalyst residues removal, and separation of the atactic polymer fraction were necessary [4].

Early processes in liquid monomer were also developed, with the advantage of higher polymerization rates due to higher monomer concentration. This process simplification also led to cost reduction by eliminating the requirement for solvent purification and recycling [5].

The products achievable through these complex, expensive and polluting manufacturing processes were limited to homopolymers with different molecular weights and copolymers with low comonomer (ethene) content.

The progress accomplished since the first generation of catalysts has been outstanding.

Fig. 1 shows the increases in yield which have been achieved with successive generations of catalysts:

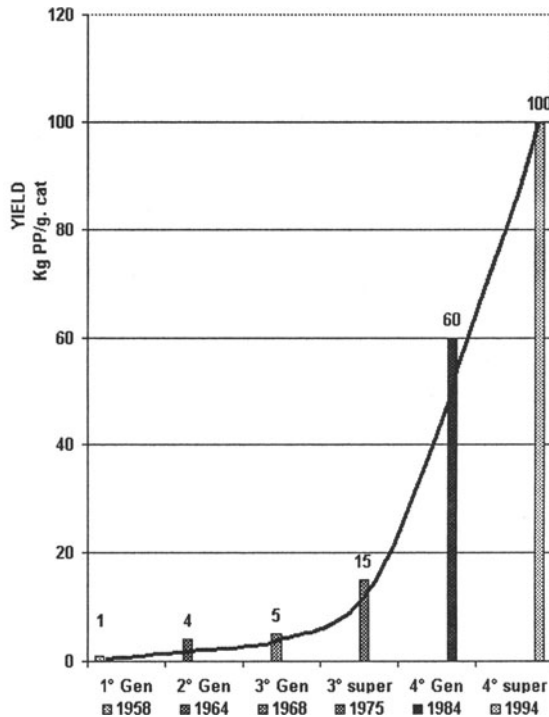


Fig. 1. Yield increase for different catalyst generations How has it been made possible?

The process has involved a deep meticulous understanding and control of the different chemical steps involved in the catalysis.

2. The “high yield” catalysts

The basis for the development of the high-activity supported catalysts lay in the discovery, in the late 1960's, of “activated” $MgCl_2$ able to support $TiCl_4$ [6] and give high catalyst activity, and the subsequent discovery, in the mid-1970's, of electron donors (Lewis bases) capable of increasing the stereospecificity of the catalyst so that (highly) isotactic polypropylene could be obtained [7-9].

High-activity Ziegler-Natta catalysts comprise $MgCl_2$, $TiCl_4$ and an “internal” electron donor and are typically used in combination with an aluminium alkyl cocatalyst such as $AlEt_3$ and an “external” electron donor added in polymerization.

The first catalyst systems contained ethyl benzoate as internal donor and a second aromatic ester as external donor, but nowadays the catalysts most widely used in polypropylene manufacture contain a diester (e.g. diisobutyl phthalate) as internal donor and are used in combination with an alkoxysilane external donor of type $RR'Si(OMe)_2$ or $RSi(OMe)_3$.

The function of the internal donor in $MgCl_2$ -supported catalysts is twofold. One function is to stabilize small primary crystallites of magnesium chloride; the other is to control the amount and distribution of $TiCl_4$ in the final catalyst. Activated magnesium chloride has a disordered structure comprising very small lamellae.

Giannini [7] has indicated that, on preferential lateral cleavage surfaces, the magnesium atoms are coordinated with 4 or 5 chlorine atoms, as opposed to 6 chlorine atoms in the bulk of the crystal. These lateral cuts correspond to (110) and (100) faces of $MgCl_2$, as shown in Fig. 2.

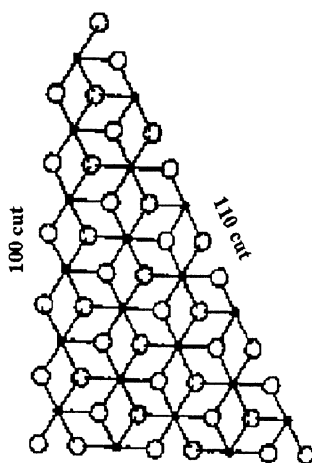


Fig. 2 Model of $MgCl_2$ layer showing the (100) and (110) cuts.

Bridged dinuclear Ti_2Cl_8 species can coordinate to the (100) face of $MgCl_2$ and on contact with an alkylaluminium cocatalyst these species will be reduced to Ti_2Cl_6 units in which the environment of the Ti atoms is chiral [10-11] as illustrated in Fig. 3.

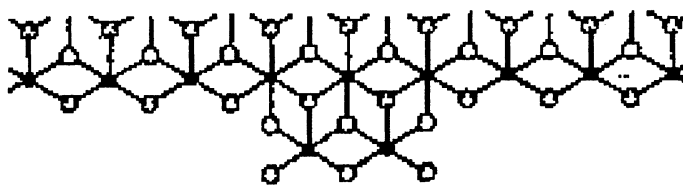


Fig. 3. Ti_2Cl_6 epitaxially placed on a (100) cut of MgCl_2

These sites have the stereoregulating ability required for isospecific polymerization. Coordination of TiCl_4 to the (110) face of MgCl_2 , on the other hand, will lead to monomeric Ti species which may lack the necessary stereoregulating ability for isospecific propagation.

In the absence of a Lewis base, TiCl_4 will coordinate to both the (100) and the (110) faces of MgCl_2 . In the presence of a base, however, there will be a competition between the base and TiCl_4 for the available coordination sites. Due to the higher acidity of the coordination sites on the (110) face [11], preferential coordination of the base rather than TiCl_4 on these sites will avoid the formation of Ti species having poor specificity.

Analytical studies [12] have indicated that a monoester internal donor such as ethyl benzoate is coordinated to MgCl_2 and not to TiCl_4 . In the search for donors giving catalysts having improved performance, it was considered [13] that bidentate donors should be able to form strong chelating complexes with tetracoordinate Mg atoms on the (110) face of MgCl_2 , or binuclear complexes with two pentacoordinate Mg atoms on the (100) face. This led to the development of the $\text{MgCl}_2/\text{TiCl}_4/\text{phthalate ester}$ catalysts, used in combination with an alkoxysilane as external donor.

The requirement for an external donor when using catalysts containing an ester as internal donor is due to the fact that, when the catalyst is brought into contact with the cocatalyst, a large proportion of the internal donor is lost as a result of alkylation and/or complexation reactions. In the absence of an external donor, this leads to poor stereospecificity due to increased mobility of the titanium species on the catalyst surface. When the external donor is present, contact of the catalyst components leads to replacement of the internal donor by the external donor. An alkoxysilane cannot be used effectively as internal donor, as under the conditions of catalyst preparation (at ≥ 100 °C, in the presence of excess TiCl_4) reaction between the alkoxysilane and titanium tetrachloride would take place, generating chlorosilanes and alkoxytitanium species.

Most recently, research on $MgCl_2$ -supported catalysts has led to systems not requiring the use of an external donor. This required the identification of bidentate internal donors which not only had the right oxygen-oxygen distance for effective coordination with $MgCl_2$ but which, unlike esters, were not removed from the support on contact with $AlEt_3$ and which, in contrast to alkoxysilanes, were unreactive with $TiCl_4$ during catalyst preparation. It was found [13,14] that certain 2,2-disubstituted-1,3-dimethoxypropanes met all these criteria. The best performance was obtained when bulky substituents in the 2-position resulted in the diether having a most probable conformation with an oxygen-oxygen distance in the range 2.8 - 3.2 Å.

The successive “generations” of high-activity $MgCl_2$ -supported catalyst systems for polypropylene are summarised below.

| <i>Catalyst type</i> | <i>Cocatalyst</i> | <i>External donor</i> |
|------------------------------------|-------------------|-----------------------|
| $MgCl_2/TiCl_4$ /ethyl benzoate | AlR_3 | aromatic ester |
| $MgCl_2/TiCl_4$ /dialkyl phthalate | AlR_3 | alkoxysilane |
| $MgCl_2/TiCl_4$ /diether | AlR_3 | - |

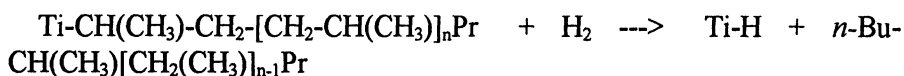
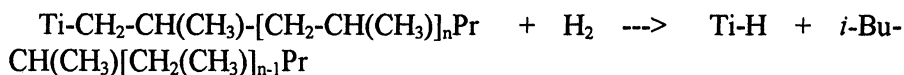
Catalyst performance has improved considerably with each generation. The polypropylene yield obtained under typical polymerization conditions (liquid monomer, in the presence of hydrogen, 70 °C, 1-2 hours) has increased from 15-30 kg/g cat. for the third generation to 30 - 80 kg/g cat. for the fourth generation. With the recently developed fifth generation catalysts containing a diether as internal donor, yields of 80-160 kg/g cat. can be achieved.

The significant improvements which have been made, and which indeed are still continuing, in the performance of $MgCl_2$ -supported catalysts for polypropylene have been accompanied and assisted by an increase in our fundamental understanding of heterogeneous Ziegler-Natta catalysis.

One example has been the use of molecular modelling in defining the required characteristics of a diether donor. It was found [15] that the most effective stereoregulating donors exhibited preferential coordination on the (110) rather than the (100) face of $MgCl_2$, and that the presence of the donor in the vicinity of titanium species was able to transform non-stereospecific isolated $TiCl_4$ and/or Ti_2Cl_8 units into isospecific species.

In addition to very high activity, an added advantage of catalysts containing a diether donor is high sensitivity to hydrogen, so that relatively little hydrogen is required for molecular weight control. Recently, we have established¹⁶ that this effect can be ascribed to a high probability of chain transfer after the occasional secondary (2,1-) rather than the usual primary (1,2-) insertion.

The activating effect of hydrogen in propene polymerization with heterogeneous catalysts, which for a long time was regarded as one of the unsolved problems in Ziegler-Natta catalysis, can be largely attributed to reactivation of "dormant" (2,1-inserted) species via chain transfer with hydrogen. These conclusions have been based on the ¹³C NMR determination of the relative proportions of *i*-Bu and *n*-Bu terminated chains, resulting from chain transfer with hydrogen after primary and secondary insertion respectively.



Other studies have demonstrated that chain transfer is dependent not only on *regio*- but also on *stereoselectivity* [17]. This explains the fact that, with catalyst systems of type MgCl₂/TiCl₄/phthalate ester - AlR₃ - alkoxy silane, the silanes which give the most stereoregular isotactic polymer also tend to give a relatively low hydrogen response. By varying the catalyst composition, and in particular the nature of the electron donors (esters, silanes, diethers) present in the catalyst system, we are now able to control the polypropylene tacticity, molecular weight and molecular weight distribution to produce a range of polymers having the processing and end-use properties required for very different applications.

The progress achieved in catalyst performance has been accompanied by a parallel expansion of the polypropylene property envelope. The main properties reported in Fig. 4 (Flex modulus, izod impact, transparency = 100-haze) give an indicative idea of the impressive progresses made!

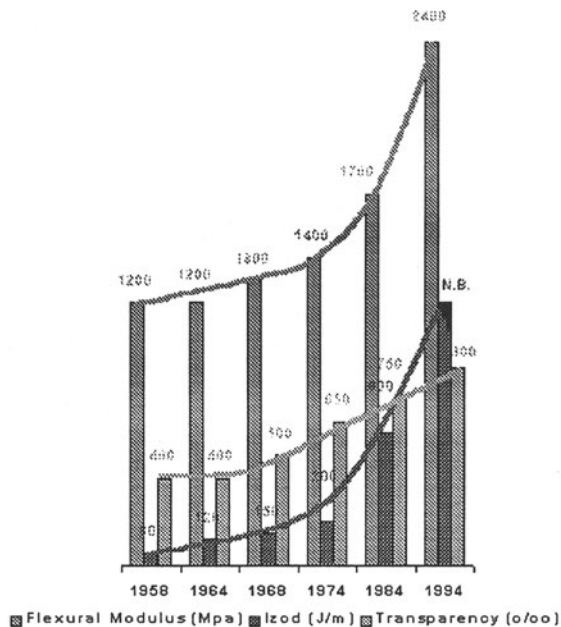


Fig 4 Variation of properties for polymers by different catalyst generations

3. The related process technology development

With the introduction of these high-yield, high-stereospecificity catalyst systems, production processes could be simplified because deashing and atactic removal became unnecessary [18]. The elimination of hydrocarbon diluents was also possible, using either liquid or gaseous monomer as the polymerization medium. These new processes allowed reduction of capital and operating costs, so an expansion of polypropylene production was induced.

A key factor in this achievement has been the development of products with controlled spherical morphology based on the catalyst “replication” phenomenon, allowing an effective control of the particle size and porosity [19]. The understanding and the full control achieved on the catalyst “replication” phenomenon has given a real “new dimension” [20] in heterogeneous catalysis.

The morphology of the catalyst particle is replicated in the final polymer as particle growth takes place during polymerization [19] (Fig. 5).

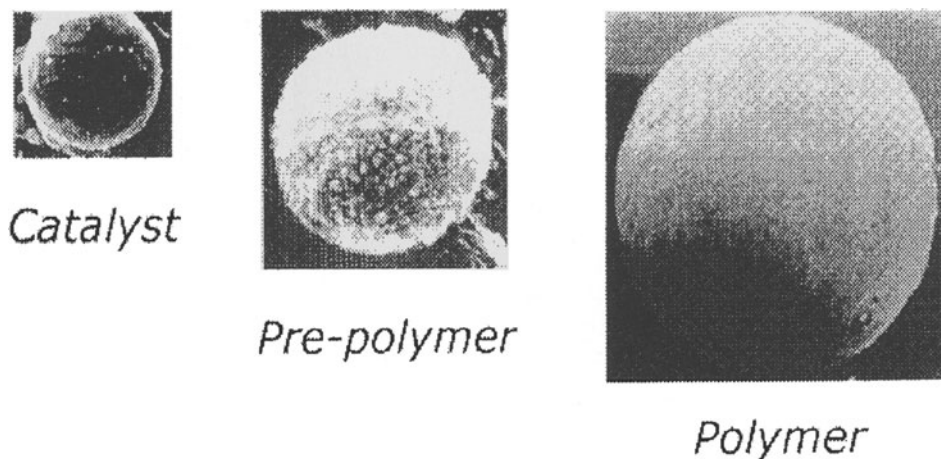


Fig. 5 “Replication” phenomenon during the polymerization

A new degree of freedom in tailoring the polymeric structures opens the way to the generation of new polymer properties. A broad range of homo- and copolymers and multiphase polymer alloys has become accessible by what we have termed “Reactor Granule Technology” [21]. The concept includes the possibility of planning the structure and the distribution of the phases inside the granule itself.

It is important that the mechanical strength of the catalyst be high enough to prevent fragmentation, but low enough to allow progressive expansion of the particle as polymerization proceeds [22]. It is the result of a sophisticated catalyst construction, or better “ARCHITECTURE” [23,24].

Under appropriate polymerization conditions, polymer particles can be obtained that have an internal morphology which can range from compact to “onion” structure to porous structure [25] (Fig. 6).

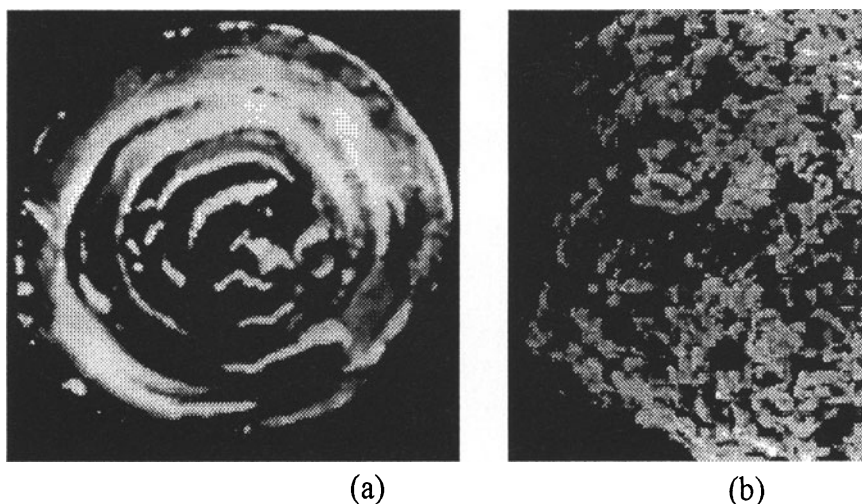


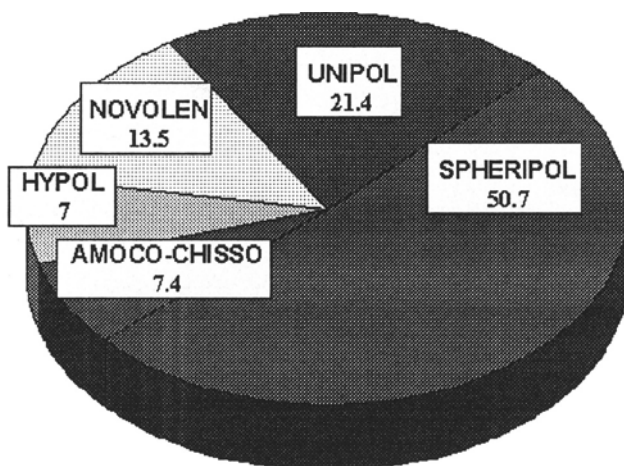
Fig. 6. (a) “onion” and (b) porous morphological structures

Porous polymer particles produced through R.G.T can act as a microreactor for the polymerization of other monomers within the solid granule, the second polymer being intimately dispersed throughout the host polymer matrix, and this has led to the development of processes for gas-phase production of rubber-rich polyolefin alloys without the inconvenience of reactor fouling that previously affected these processes.

4. The Spheripol process technology

Such a basic approach has been adopted for the Spheripol process, a hybrid liquid monomer/gas-phase process where homopolymerization and “random” copolymerization are carried out in liquid monomer while the ethene/propene elastomer is produced in gas-phase.

Montell’s Spheripol process is the technology most widely adopted today in the world for the production of polypropylene. The amount of PP produced with this technology is about 50% of total PP obtained through high-yield processes (Fig. 7), the others being Mitsui’s Hypol, involving polymerization in liquid monomer using a continuous stirred reactor, and the gas-phase processes with fluidized bed (Unipol–Union Carbide) or mechanically agitated reactors (Novolen–Targor, Amoco-Chisso).



| | Plants | MI mt/Y | Market Share (%) |
|---------------------|-----------|-------------|------------------|
| SPHERIPOL | 81 | 11.6 | 50.7 |
| UNIPOL | 28 | 4.9 | 21.4 |
| NOVOLEN | 34 | 3.1 | 13.5 |
| AMOCO-CHISSO | 9 | 1.7 | 7.4 |
| HYPOL | 18 | 1.6 | 7 |

Fig. 7 PP Licensing competitive position for HY-HS processes

The multistep polymerization approach, based on the use of long lasting, controlled morphology catalyst systems, allowed the development of an articulated product-mix:

- Homopolymers with a wider range of molecular weight, from low fractional MFR up to 1000 MFR, with a broader crystallinity control through

stereoregularity and/or Molecular Weight Distribution. As a consequence PP grades with improved processability for films and fibers were made available as well as higher stiffness products allowing downgauging in the rigid packaging segment.

- Random copolymers with improved optical properties and lower seal initiation temperature were developed for the flexible packaging area.

- Heterophasic copolymers with a higher amount of better-distributed rubbery phase, expanding the application in the more demanding impact performance automotive and technical market segments. Heterophasic copolymers with high crystallinity matrix and appropriate rubbery phase composition, characterized by a relevant improvement of the impact/stiffness balance were developed.

5. The Catalloy process technology

The concept of step polymerization addressed to the achievement of a prefixed polymer structure was further implemented with the development of the Catalloy process.

The process is based on a multistage, highly flexible, sequential, gas-phase polymerization technology with a fully independent control of gas composition in each reactor.

The use of the 4th generation of Ziegler-Natta catalyst, allowing, already in the polymerization step, a homogeneous distribution of the various phases in each polymer particle, coupled with the full freedom to control the amount and the composition of each phase, has dramatically expanded the property spectrum of the resulting materials, opening new application areas to the propylene based “alloys” produced by this process.

New families of materials have been generated, exploiting better performance in the consolidated application segments and increasing the inter-materials competitiveness in application areas where other thermoplastics were dominant.

A typical example is given by products characterized by high flexibility and softness and retaining high mechanical strength, toughness and environmental friendly characteristics and which have entered application areas typically covered by plastified PVC, PE and rubbers. Examples are geo-membranes, roof-protection foils, synthetic leather for automotive applications, toughness modifiers, etc.

6. The Hivalloy process technology

The “Reactor Granule” technology has been extended to allow the incorporation of non-olefinic monomers into the polyolefinic matrix. The porous polyolefinic granule is a suitable substrate for easy reaction with non-olefinic monomers, by radical grafting and polymerization.

The combination between olefinic component and the non-olefinic one, achieved through an in-reactor compatibilization, yields structures with a continuous polyolefin matrix and a dispersed amorphous phase, giving polymers with excellent uniformity and properties. The chemical resistance, processability and ductility peculiar to the polyolefins are coupled with the dimensional stability, thermal and surface properties characteristic of the non-olefinic materials.

Through the selection of the non-olefinic monomer, it is possible to enhance specific set properties. The resulting product families, characterized by a significantly lower density than various engineering materials, can easily be modified with fillers and reinforcing agents, allowing a further expansion of properties.

Products from Hivalloy technology offer a competitive advantage in various applicational areas vs. engineering materials, like Nylon, PC/PBT, PC/ABS.

7. The “integrated system” approach

The availability of materials characterized by widely different properties but having a similar polymeric matrix allowed the development of integrated systems.

The performances required to satisfy the processing and applicative needs is achieved with materials that complement each other.

The „Montell Integrated System Technology“ allows, in addition, the solution of a growing problem in the wider consumer acceptance of plastics: the environmental need to recycle plastic parts. The advantage is that separation of different plastics in recycling is no longer required.

8. The new frontiers

The metallocene homogeneous catalysts, more recently developed at industrial level, can produce polyolefins characterized by a homogeneous and effective

comonomer distribution, a relevant issue in the polymer structural design. On the other hand, they typically give a very narrow molecular weight distribution, which results in a poor processability in several conversion technologies. In addition, they lack morphology control.

Based on the “Reactor Granule” technology a new path has been undertaken combining the heterogeneous Ziegler-Natta catalysis with the homogeneous catalysis, including both metallocene and other single-centre organometallic polymerization catalysts.

This new approach, termed Multicatalyst Reactor Granule Technology (M.R.G.T.) [26], is based on a first step of polymerization with a spherical $MgCl_2$ -supported catalyst, generating a spherical polymer having controlled porosity which is then impregnated with an activated metallocene or other single-site catalyst prior to a second polymerization step (Fig. 8).

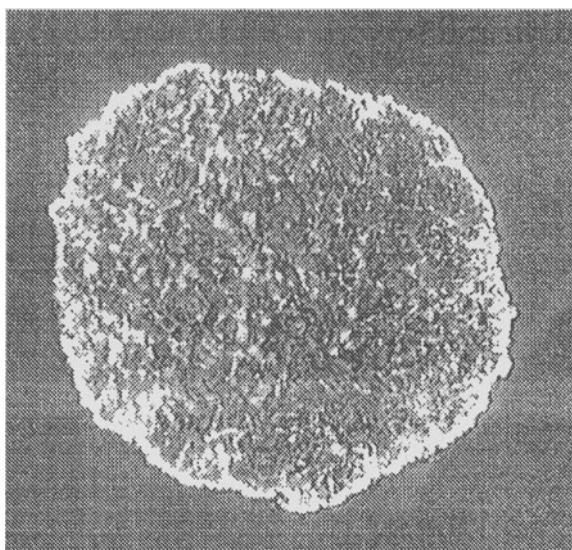


Fig. 8 Micrographical section of a polymer granule by mixed catalysis.

It is now generally recognised that the use of a supported catalyst is an essential prerequisite for wide industrial application of homogeneous catalysis. The M.R.T.G. approach offers an effective solution to this problem, opening the way to a range of new polymeric materials where the respective performance advantages of Ziegler-Natta and single-centre polymers are combined.

As already happened in the PP past industrial history, an advancement in the catalyst system area is often followed by an advancement in the Process technology. This is happening again. A new Process technology has been conceived to polymerize alpha-olefins in gas-phase: the Multi Zone Circulating Reactor [27] is addressing a wide exploitation of the M.R.G.T potentiality.

9. Conclusions

What could be the polypropylene future?

A further diversification potential can be perceived through the exploitation of the technology innovation options we have previously described:

-the **Reactor Granule Technology** will expand the capability to directly polymerize polymer alloys;

-the **Single-Centre** catalysts offer the opportunity to develop and specialize new polymeric structures;

-the **Mixed Catalysis** approach offers the opportunity to get synergies between the two above-mentioned areas;

-finally the **Multi Zone Circulating Reactor** will offer the opportunity to get a level of homogeneity in the phase combination and distribution not available today.

10. References

1. Ziegler, K., Breil, H., Martin, H., Holzkamp, R. Ger. Pat. 973,626 (filed Nov. 17, 1953)
2. Natta, G., Pino, P., Mazzanti, G. U.S. Pat. 3,715,344 (Ital. priority June 8, 1954).
3. Natta, G. (1955) *J. Polym. Sci.* 16: 143.
4. Galli, P. (1981) International Union of Pure and Applied Chemistry, Structural Order on Polymers, Ciardelli F., Giusti P., Eds., Pergamon Press, p. 63.
5. Kirschner, H.G., Gumbolt, A.G.M., Bier, B., (1961) U.S. Patent 3 002 961 Farbenwerke Hoechst Aktiengesellschaft.
6. Mayr, A., Galli, P., Susa, E., Di Drusco, G., Giachetti, E., (1970) Ger. Pat. 1.958,488; C.A., 73, 35929u (1970).
7. Giannini, U. (1981) *Makromol. Chem. Suppl.* 5: 216.
8. Galli, P., Luciani, L., Cecchin, G. (1981) *Angew. Makromol. Chem.* 94: 63.
9. Barbè, P.C., Cecchin, G., Noristi, L. (1987) *Adv. Polym. Sci.*, 81: 1.

10. Corradini, P., Busico, V., Guerra, G. (1988) In: Kaminsky, W. and Sinn, H. (eds.) *Transition Metals and Organometallics as Catalysts for Olefin Polymerization*, p. 337, Springer-Verlag, Berlin.
11. Busico, V., Corradini, P., De Martino, L., Proto, A., Savino, V., Albizzati, E. (1985) *Makromol. Chem.* 186: 1279.
12. Terano, M., Kataoka, T., Keii, T. (1987) *Makromol. Chem.* 188: 1477.
13. Albizzati, E., Giannini, U., Morini, G., Smith, C.A., Zeigler, R.C. (1995) In Fink, G., Mülhaupt, R., Brintzinger, H.H. (eds.) *Ziegler Catalysts. Recent Scientific Innovations and Technological Improvements*, p. 413, Springer-Verlag, Berlin.
14. Albizzati, E., Giannini, U., Morini, G., Galimberti, M., Barino, L., Scordamaglia, R. (1995) *Macromol. Symp.* 89: 73.
15. Barino, L., Scordamaglia, R. (1995) *Macromol. Symp.* 89: 101.
16. Chadwick, J.C., Morini, G., Albizzati, E., Balbontin, G., Mingozzi, I., Cristofori, A., Sudmeijer, O., van Kessel, G.M.M. (1996) *Macromol. Chem. Phys.* 197: 2501.
17. Chadwick, J.C., van Kessel, G.M.M., Sudmeijer, O. (1995) *Macromol. Chem. Phys.* 196: 1431.
18. Di Drusco, G., Rinaldi, R., (1981) *Hydrocarbon Processing* 60(5):153
19. Galli, P., Barbè, P.C., Noristi, L. (1984) *Angew. Makromol. Chem.* 120: 73.
20. Galli, P., (1992) *Proceedings of the II International Conference "The future of science has begun - chemical, biochemical and cellular topology"*, Milan, p. 43.
21. Galli, P. (1994, 1996) *Macromol. Symp.* 78: 269 and 112:1.
22. Simonazzi, T., Giannini, U. (1994) *Gazz. Chim. Ital.* 124: 533.
23. Galli, P., Cecchin, G., Simonazzi, T. (1988) 32nd IUPAC Int. Symp. "Frontiers of macromolecular science", Kyoto, p. 91
24. Galli, P. (1996) *J. Macromol. Sci.-Phys.* 35:427
25. Galli, P., (1994) *Progr. Poly. Sci.* 19: 959.
26. Collina, G., Pelliconi, A., Sgarzi, P., Sartori, F., Baruzzi, G. (1997) *Polym. Bull.* 39: 241.
27. Govoni, G., Rinaldi, R., Covezzi, M., Galli, P., (1997) U.S. Pat. 5,698,642.

Characterization of PP prepared with the latest metallocene and MgCl₂-supported TiCl₄ catalyst systems

Norio Kashiwa, Shin-ichi Kojoh*, Jun-ichi Imuta and Toshiyuki Tsutsui

Petrochemicals R&D Center, Mitsui Chemicals, Inc., 1-2, Waki 6-chome, Waki-cho, Kuga-gun, Yamaguchi 740-0061, Japan

Norio.Kashiwa@mitsui-chem.co.jp, Shinichi.Kojoh@mitsui-chem.co.jp, Junichi.Imuta@mitsui-chem.co.jp, Toshiyuki.Tsutsui@mitsui-chem.co.jp

Abstract. A novel metallocene, *rac*-Me₂Si[2-*n*-Pr-4-(9-Phenanthryl)-Ind]₂ZrCl₂, was synthesized and employed for propylene polymerization in conjunction with Ph₃CB(C₆F₅)₄ as a cocatalyst. The resulting polypropylene (*m*-PP) shows 99.6 % of *m*mmm by ¹³C NMR and 162.8 °C of melting temperature (*T*_m) by DSC. In addition, *m*-PP was compared with the polypropylene (Ti-PP) produced by our latest MgCl₂-supported TiCl₄ catalyst system, which shows 99.0 % of *m*mmm and 165.7 °C of *T*_m, by TREF analysis. TREF indicated that *m*-PP has narrower stereo-regularity distribution than Ti-PP and *T*_m of the fraction eluted from *m*-PP at the highest temperature is 163.6 °C, while that from Ti-PP reaches to 167.3 °C. The individualities of both catalyst systems are discussed.

1. Introduction

Since the discovery of isotactic polymerization of propylene with the C₂-symmetrical metallocene catalyst system[1], much effort has been invested in the molecular design of its ligands[2,3] and the optimization of the polymerization conditions[3,4] in order to enhance the stereo-specificity. Consequently, the stereo-specificities of the developed metallocenes[2,3] have reached to the comparative level to the commercial MgCl₂-supported TiCl₄ catalyst systems. These metallocenes contribute to the enhancement of the regio-specificity as well as the stereo-specificity, but it is still lower than that with the commercial MgCl₂-supported TiCl₄ catalyst systems which forbid chain propagation after the regio-irregular insertion of propylene monomer by the formation of dormant sites[5]. Therefore, the further investigation has been continuing without a break. In this paper, a newly designed metallocene, which has extremely high stereo-specificity and regio-specificity, is synthesized and the obtained polypropylene (PP) with it was characterized by ¹³C NMR, DSC, GPC and Temperature-rising elution fractionation (TREF) analyses.

On the other hand, the further improvement of the stereo-specificity of the commercial MgCl₂-supported TiCl₄ catalyst system is desired for the application of car use and much effort is being devoted to it. Recently, we have developed the MgCl₂-supported TiCl₄ catalyst system that has higher stereo-specificity than any commercial MgCl₂-supported TiCl₄ catalyst systems. The comparison of it with the above-mentioned metallocene would be significant for a step toward the development of PP having no defect. TREF is an effective method for such comparison[6]. In fact, there have been a number of reports where TREF gives the clear interpretation for the relation between the features of the obtained PP and the natures of the active sites of the MgCl₂-supported TiCl₄ catalyst system[7-10]. In this paper, TREF is carried out for the comparison between the PP produced by our latest MgCl₂-supported TiCl₄ catalyst system and the PP obtained by our new metallocene catalyst system.

2. Experimental

2.1. Catalysts

2.1.1. *rac*-Me₂Si[2-Me-4-(1-Naphtyl)Ind]₂ZrCl₂ (metallocene-A)

Metallocene-A was synthesized according to the literature[2].

2.1.2. *rac*-Me₂Si[2-*n*-Pr-4-(9-Phenanthryl)Ind]₂ZrCl₂ (metallocene-B)

Metallocene-B was synthesized as follows. To a 1 L glass flask, 37 g of potassium *t*-butoxide, 400 ml of toluene and 32 ml of 1-methyl-2-pyrrolidone were added. Then, the solution prepared by dissolving 60.7 g of *n*-propylmalonic diethyl ester in 50 ml of toluene was dropped at 10 °C into the flask and reacted at 65 °C for 1 hour (h). Next, the solution prepared by dissolving 75 g of 2-bromobenzyl bromide in 50 ml of toluene was dropped into the flask at 10 °C and heated to reflux for 1 h. The resulting mixture was poured into 500 ml of water, acidified with H₂SO₄ to pH=1 and extracted with toluene. The combined organic layers were washed with brine, dried with MgSO₄ and the solvent was removed. The concentrated liquid (114g) was added into a 2 L glass flask with 237 g of potassium hydroxide, 520 ml of methanol and 180 ml of water and it was heated to reflux for 5 h. After the removal of methanol, the resulting mixture was poured into 500ml of water, acidified with H₂SO₄ to pH=1 and extracted with diethyl ether. The combined organic layers were dried with MgSO₄ and the solvent was removed. The concentrated semisolid (94g) was added into a 1 L glass flask and heated to 180°C for 10 minutes(min), followed by cooling. Thus, 78 g of liquid, which is 2-(2-bromophenyl)-1-*n*-propylpropionic acid (compound-A), was obtained. Then, 67 g of 4-bromo-2-*n*-propyl-1-indanone

(compound-B) was prepared with the same operations as the synthesis of 2-methyl-4-phenyl-1-indanone in the literature[2] except for the use of compound-A in stead of 2-(2-phenylbenzyl)propionic acid. Next, 66 g of compound-B was dissolved in 200 ml of ethanol and dropped into the 1 L glass flask containing 4.96 g of sodium borohydride and 300 ml of ethanol at 0 °C. The reaction mixture was stirred at room temperature for 3 h and 200 ml of water was added. After the removal of ethanol, it was extracted with diethyl ether. The combined organic layers were dried with MgSO_4 and the resulting powder (66.5g) was obtained by the removal of solvent. The powder was added in a 1 L glass flask with 68 ml of triethylamine and 200 ml of diethyl ether, followed by the dropping of the mixture of 55 ml of trimethylsilyl chloride and 100 ml of diethyl ether at 0 °C. Then, it was stirred for 7 h and poured into 400 ml of aqueous solution of sodium hydrogencarbonate. It was extracted with diethyl ether and the combined organic layers were washed with brine. It was dried with MgSO_4 , followed by the removal of solvent and vacuum distillation. Thus, 76 g of 4-bromo-2-n-propyl-1-trimethylsilyloxyindane (compound-C) was obtained. To a 300 ml glass flask, 10 g of compound-C, 50 ml of diethyl ether and 112 mg of PdCl_2 were added. Then, 42 ml of 1.45 M diethyl ether solution of 9-phenanthrylmagnesium bromide was dropped in it and they were refluxed for 10 h. The reaction mixture was poured into 300 ml of aqueous solution of ammonium chloride and extracted with diethyl ether. The combined organic layers were washed with brine and dried with MgSO_4 . After the removal of solvent, 20.3 g of semisolid was obtained. It was added into a 300 ml glass flask with 50 ml of diethyl ether and 60 ml of 5 N HCl was dropped in it. After the stirring for 6.5 h, it was extracted with diethyl ether. The combined organic layers were washed with aqueous solution of sodium hydrogencarbonate and dried with MgSO_4 . The obtained semisolid by the removal of solvent was refined with a column chromatography. The refined powder was added in a 200 ml glass flask with 80 ml of methylene chloride, 12.8 ml of triethylamine and 187 mg of 4-dimethylaminopyridine and the mixture of 4.72 ml of methylsulfonyl chloride and 20 ml of methylene chloride was dropped at 5 °C. After the stirring for 4 h at room temperature, it was poured into 100 ml of water and extracted with methylene chloride. The combined organic layers were washed with aqueous solution of sodium hydrogencarbonate and dried with MgSO_4 . The obtained semisolid by the removal of solvent was refined with a column chromatography. Thus, 7.2 g of 2-n-propyl-7-(9-phenanthryl)-indene (compound-D) was obtained. Then, metallocene-B was prepared from compound-D, which procedures were same as the preparation of metallocene-A from 2-mehtyl-7-(1-naphthyl)-indene in the literature[2].

2.1.3. The latest MgCl_2 -supported TiCl_4 catalyst system (Mg/Ti-A)

The latest MgCl_2 -supported TiCl_4 catalyst system in our laboratry was used as Mg/Ti-A.

2.2. Polymerizations

2.2.1. Method-A

In a 500 ml glass autoclave equipped with a stirrer, 400 ml of toluene was added and the system was charged with propylene. Then, the temperature of it was heated to 50 °C and 0.144 mmol of *i*-Bu₃Al was added. In the minimum amount of toluene, 8.0×10^{-4} mmol of metallocene-A or metallocene-B and 0.28 mmol of methylaluminoxane (MAO) were dissolved. This toluene solution was added in the reactor and the polymerization was carried out under atmospheric pressure for 15 min. During the polymerization, 100 L/h of propylene was supplied continuously. At the end of the polymerization, the feed of propylene was stopped and a small amount of methanol was added. Then, the whole product was poured into 4 L of methanol containing a small amount of HCl. The obtained polymer was filtered, washed with a plenty of methanol and dried at 80 °C for 12 h.

2.2.2. Method-B

In a 2 L glass autoclave equipped with a stirrer, 1 L of toluene was added and the system was charged with propylene. Then, the temperature of it was cooled to 0 °C and the toluene solution dissolving 1.0×10^{-3} mmol of metallocene-B and 0.9 mmol of *i*-Bu₃Al was added in it. Next, 2.0×10^{-3} mmol of Ph₃CB(C₆F₅)₄ was added in it and the polymerization was carried out under atmospheric pressure for 30 min. During the polymerization, 150 L/h of propylene and 3 L/h of hydrogen were supplied continuously. After the polymerization, the polymer was obtained by the same operations as method-A.

2.2.3. Method-C

In a 1 L stainless-steel autoclave equipped with a stirrer, 400 ml of *n*-heptane was added and the system was charged with propylene. Then, 0.4 mmol of Et₃Al, 0.4 mmol of an external donor and 8.0×10^{-3} mmol of Mg/Ti-A in terms of Ti were added in this order at 60 °C. Next, 100 ml of hydrogen was added and the system was pressurized to 0.49 MPa by propylene and heated to 70 °C. The polymerization was carried out at 70 °C for 1 h and propylene was fed continuously to keep 0.49 MPa. After the polymerization, the resulting slurry was filtered to separate into a powder and a liquid phase portion. The powder was washed with *n*-hexane and vacuum dried at 80 °C. The liquid phase portion was concentrated to obtain the solvent-soluble polymer.

2.3. Polymer analyses

TREF was carried out as follows. The stainless-steel column (21.5 mm in diameter and 150mm in length) was packed with glass beads which diameters were 100 μm and maintained at 145 °C. Then, 7.5 ml of *o*-dichlorobenzene (ODCB) solution

dissolving 37.5 mg of the polymer sample at 145 °C was injected into the column. The cooling step was performed at 10 °C/h from 145 °C to 25 °C and subsequent elution step was carried out by pumping ODCB at 1.0 ml/min and rising the temperature at 15 °C/h from 25 °C to 145 °C. The amount of the eluted polymer was monitored for every 2.5 min by a Mercury Cadmium Telluride detector of Nicolet FT-IR Magna-550. The whole solution was fractionated into 4 fractions and they were poured into five times volume of methanol. The precipitated polymer was collected by filtration and washed with methanol, followed by vacuum-dry.

The analyses of the microstructures with ^{13}C NMR, the number-average (M_n) and the weight-average molecular weights (M_w) with GPC and the melting temperatures (T_m) with DSC were performed in the same manners as our previous paper[5].

3. Results and Discussion

Figure 1 shows the structures of two types of the bridged metallocenes exhibiting C_2 symmetry. Metallocene-A is already well-known for its high stereo-specificity[2] owing to the steric effects of methyl substituent in the 2-position and naphthyl substituent in the 4-position of the indenyl group. On the other hand, metallocene-B is newly synthesized in order to enhance the stereo- and the regio-specificities, which has the bulkier substituents in 2- and 4-positions of the indenyl group.

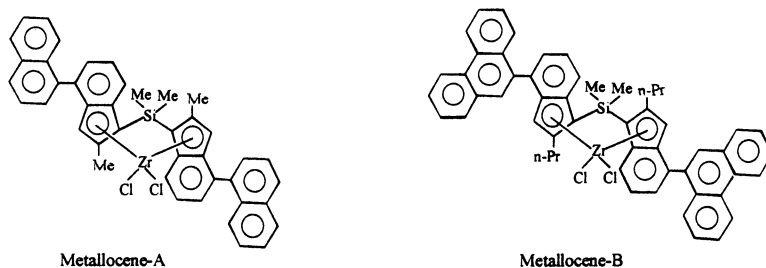


Fig. 1. Structures of metallocene-A and metallocene-B. Metallocene-A; $\text{rac-Me}_2\text{Si}[2\text{-Me-4-(1-Naphtyl)Ind}]_2\text{ZrCl}_2$, Metallocene-B; $\text{rac-Me}_2\text{Si}[2\text{-n-Pr-4-(9-Phenanthryl)Ind}]_2\text{ZrCl}_2$.

The catalyst performance of metallocene-B was compared with that of metallocene-A for propylene polymerization at 50 °C with MAO as a cocatalyst (Table 1). The activity of metallocene-B is twice as high as that of metallocene-A. According to expectation, both the stereo- and the regio-specificities of metallocene-A are improved into those of metallocene-B by the changes of substituents in 2- and 4-positions of the indenyl group, resulting in the enhancement of T_m . While, these substituent changes seem not to influence the chain-propagation and the chain-transfer reactions, because M_w of the PP produced with metallocene-B is almost

same as that with metallocene-A. Although it would be worthy of notice that mmmm of the PP prepared with metallocene-B reaches to 99.2 %, 159.8 °C of its T_m is lower than that with the latest MgCl₂-supported TiCl₄ catalyst system (Mg/Ti-A) which shows the equivalent mmmm. T_m and mmmm of the PP obtained by Mg/Ti-A are 165.7 °C and 99.0 %, respectively, as shown in Table 2 as Ti-PP.

Table 1. Results of propylene polymerizations with metallocene-A and metallocene-B. Polymerization conditions: method-A; 50 °C, 15 min, propylene 100 L/h, atmospheric pressure, toluene 400 ml, [Zr] = 2.0 × 10⁻³ mM, [MAO] = 0.70 mM, [i-Bu₃Al] = 0.36 mM.

| Catalyst | Activity(kg -PP/mmol- Zr*h) | mmmm (%) | 2,1-in- version (mol%) | 1,3-in- version (mol%) | T _m (°C) | M _w (× 10 ⁵) |
|-------------------|-----------------------------------|-------------|------------------------------|------------------------------|------------------------|--|
| Metallocene- A | 22.5 | 98.6 | 0.29 | 0.05 | 156.2 | 3.8 |
| Metallocene- B | 46.8 | 99.2 | 0.15 | 0.07 | 159.8 | 4.0 |

Next, propylene polymerization at low temperature such as 0 °C was performed, using metallocene-B in conjunction with Ph₃CB(C₆F₅)₄ in stead of MAO. T_m and mmmm of the resulting PP (m-PP in Table 2) reaches to 99.6 % and 162.8 °C, respectively, and 2,1-inversion of it decreases to 0.10 mol%. However, T_m is still lower than the expectation from mmmm. It would show that the existence of a small amount of inversion causes the significant drop of T_m.

Table 2. PP samples for TREF analysis. m-PP: PP obtained by method-B with metallocene-B, Ti-PP: PP produced by method-C with Mg/Ti-A, n.d. means "not detected".

| Sample | Catalyst | mmmm (%) | 2,1- inversion (mol%) | 1,3- inversion (mol%) | T _m (°C) | M _w (× 10 ⁵) |
|--------|-------------------|-------------|-----------------------------|-----------------------------|------------------------|--|
| m-PP | Metallocene -B | 99.6 | 0.10 | < 0.05 | 162.8 | 1.4 |
| Ti-PP | Mg/Ti-A | 99.0 | n.d. | n.d. | 165.7 | 4.9 |

The TREF analysis of m-PP was carried out in comparison with Ti-PP. The relation between elution temperature and the amount of the PP eluted from each sample is shown in Figure 2. Ti-PP was eluted in the temperature range of 110 - 140 °C and m-PP was done in that of 105 - 135 °C. In both cases, the amount of the eluted PP was negligible below each eluted temperature range, indicating that the amount of atactic PP is too small to detect. Figure 2 shows that the elution curve of Ti-PP has two peaks and that of m-PP has single peak. It would reflect the plural active species of Mg/Ti-A and the homogeneity of the active species of metallocene-B.

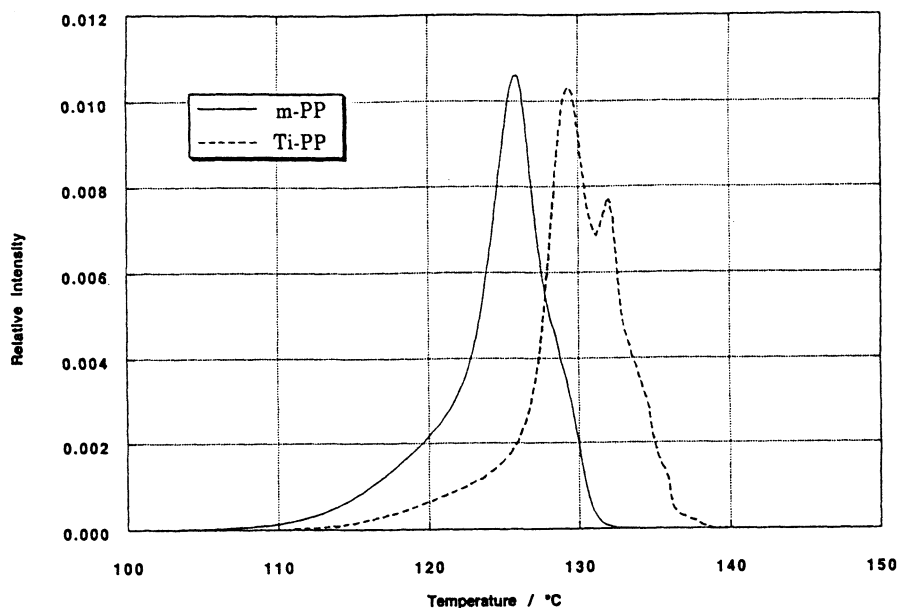


Fig. 2. TREF profiles of m-PP and Ti-PP.

Table 3. The results of TREF, DSC and GPC analyses. m-PP: PP sample obtained by method-B with metallocene-B, Ti-PP; PP sample obtained by method-C with Mg/Ti-A.

| Sample | Elution temp.(°C) | Proportion (wt%) | Tm (°C) | Mw ($\times 10^5$) | Mw/Mn |
|--------|-------------------|------------------|---------|----------------------|-------|
| m-PP | whole | - | 162.8 | 1.4 | 2.1 |
| | Fr.1 | 105 - 115 | - | - | - |
| | Fr.2 | 115 - 123 | 162.0 | 0.7 | 1.7 |
| | Fr.3 | 123 - 127 | 163.3 | 1.4 | 1.7 |
| | Fr.4 | 127 - 135 | 22.8 | 163.6 | 1.8 |
| Ti-PP | whole | - | 165.7 | 4.9 | 4.0 |
| | Fr.1 | 110 - 123 | 160.4 | - | - |
| | Fr.2 | 123 - 128 | 164.1 | 1.7 | 2.1 |
| | Fr.3 | 128 - 131 | 166.4 | 4.4 | 2.5 |
| | Fr.4 | 131 - 140 | 34.7 | 167.3 | 7.0 |

In addition, both m-PP and Ti-PP were fractionated into 4 fractions in order to analyze themselves with DSC and GPC and the results are shown in Table 3. Tm and Mw of the fractions increased with rising the elution temperature and the increase in the case of Ti-PP is far more than m-PP. It would indicate that the higher stereospecific active sites produce the higher molecular weight PP especially in the use of Mg/Ti-A.

Regarding Fr.3 and Fr.4, T_m varies from 166.4 °C to 167.3 °C and M_w ranges from 440 000 to 700 000 in the case of Ti-PP, while T_m varies from 163.3 °C to 163.6 °C and M_w ranges from 140 000 to 180 000 in the case of m-PP. Namely, the microstructure of Fr. 3 from Ti-PP differs from that of Fr. 4 from it, while Fr.3 from m-PP would have fundamentally same microstructure as Fr. 4 from it. It would be noticeable that T_m of Fr. 4 from Ti-PP is obviously higher than that of the whole sample which shows 99.0 % of mmmm and no regio-irregularity. It is distinctly expectable that mmmm of Fr. 4 from Ti-PP exceeds 99.0 % and no regio-irregularity is detected in it.

In conclusion, we believe that there are two ways toward the development of a perfect PP in stereo-regularity and regio-regularity. One is the enhancement of the regio-specificity of metallocene-B and the other is to unify the plural active sites of Mg/Ti-A into the active sites which can produce the PP eluted as Fr. 4 from Ti-PP.

4. References

- [1] W. Kaminsky, K. Kulper, H.H. Brintzinger, F.R.W.P. Wild, *Angew. Chem., Int. Ed. Engl.* 24, 507 (1985).
- [2] W. Spalek, F. Kuber, A. Winter, J. Rohrmann, B. Bachmann, M. Antberg, V. Dolle, E.F. Paulus, *Organometallics* 13, 954 (1994).
- [3] H. Deng, H. Winkelbach, K. Taeji, W. Kaminsky, K. Soga, *Macromolecules* 29, 6371 (1996).
- [4] A. Toyota, T. Tsutsui, N. Kashiwa, *J. Mol. Catal.* 56, 237 (1989).
- [5] S. Kojoh, M. Kioka, N. Kashiwa, M. Itoh, A. Mizuno, *Polymer* 36, 5015 (1995).
- [6] A. Mizuno, T. Abiru, M. Motowoka, M. Kioka, M. Onda, *J. Appl. Polym. Sci: Appl. Polym. Symp.* 52, 159, (1993).
- [7] M. Kakugo, T. Miyatake, Y. Naito, K. Mizunuma, *Macromolecules* 21, 314 (1989).
- [8] M. Kioka, H. Makio, A. Mizuno, N. Kashiwa, *Polymer* 35, 580 (1994).
- [9] J. XU, F. Feng, S. Yang, Y. Yang, X. Kong, *Polym. J.* 29, 713 (1997).
- [10] I. Mingozzi, G. Cecchin, G. Morini, *Int. J. Polym. Anal. & Charact.* 3, 293 (1997).

An Absolute Test of Rival Theories for MWDs in Heterogeneous Polymerization-MWDs during Quasi-Living Polymerization

Tominaga Keii and Teruo Matsuzawa

Japan Advanced Institute of Science and Technology, 1-1 Asahidai, Tatsunokuchi, Ishikawa 923-1292 Japan

Abstract. Many rival theories proposed for the origin of the broad MWDs of polymers produced with heterogeneous catalysts still persist. As an absolute test for them, the importance of the transitional behavior of MWDs during the quasi-living stage of polymerization is emphasized. Based upon the different mechanisms, all the rival theories have been constructed so as to explain the broad MWDs at the stationary state. Therefore, all competing rate processes are balanced in the stationary state, and any specification of the kinetic mechanism can not be tested by the stationary MWDs. However, for the transitional MWD from the living stage to the stationary state, all the rival theories predict respective behavior in response to their different mechanisms. The observed transitional MWDs show that MWDs in the living stages are always broad and then mostly narrow or remain unchanged for which all the rival theories are invalid. To understand this situation, a new theory of non-uniform sites not only with propagation but also slightly with transfer rate is proposed. The non-uniformity that conforms to a popular kinetic model gives a unified explanation about the abnormal decay kinetics recognized in many systems as well as that of the supported Ziegler catalyst.

1. Phenomenological Review of Rival Theories

It is generally accepted that the molecular weight distribution (MWD) of polyolefins produced with heterogeneous Ziegler-Natta or Phillips catalysts is broad. The reasons for this wide distribution have not yet been clearly established, though many rival theories have been proposed. Although the absence of any decisive test method is responsible for the situation, there is some confusion in the assessment of the rival theories. First all the rival theories are discussed in a phenomenological manner.

The MWD is characterized by the size distribution function $F(n)$ and its corollary. The number of growing (living) n -mer chains is denoted by N_n^* and that of the dead n -mer by N_n . The size distribution function is defined by $F(n)=(N_n^*+N_n)/\Sigma(N_n^*+N_n)$ and its corollary: Weight distribution function,

$W(n)=nF(n)/\Sigma nF(n)$, Number average degree of polymerization, $\bar{n}=\Sigma nF(n)$ and Polydispersity, $Q=\Sigma n^2F(n)/(\Sigma nF(n))^2$. The summation with n from unity to infinity is abbreviated as Σ .

All the rival theories have been constructed so as to explain the broad MWDs at the stationary state which are most adequately described by Wesslau's log-normal distribution¹,

$$F(n) = (\sqrt{2\pi}\sigma n)^{-1} \exp[-\ln^2(n/n_0)/2\sigma^2] \quad (1)$$

and by Tung's exponential distribution²

$$W(n) = abn^{b-1} \exp(-an^b) \quad (2)$$

in some cases. All the theoretical approaches have been made so as to obtain (1), (2) and related ones by modifying Flory's most probable distribution³ that was established for a stationary MWD during homogeneous polymerization,

$$F(n) = (k_t/k_p) \exp(-nk_t/k_p) \quad (3)$$

where k_t and k_p denote the rates of transfer and propagation per a growing chain, respectively. It is well-known that (3) is derived for polymerizations of constant rates. The possibilities of modification of (3) are limited within the three factors; k_t , k_p and their ratio β . Also, the modifications made are referred to the popular kinetic mechanisms of heterogeneous catalyses; the non-uniform surface sites with respect to rate constant, the chain-length dependent rate constant and the slowest diffusion in a porous catalyst.

1.1 Chain-length Dependent Rates

Referring to the surface-chemical mechanism of polymer desorption, Gordon and Roe⁴ derived the chain-length dependent transfer rate,

$$k_{t,n}/k_p = G/2\sqrt{n}(\sqrt{n} + A) \quad (4)$$

where G and A are experimentally determinable parameters. On the other hand, Mussa⁵ suggested that k_p might be increased with n , referring to the possibility of overheating with polymer accumulation. These suppositions can not be tested by experimental MWD at a stationary state, as shown below.

The MWD in these cases can be obtained from the following set of difference-differential equations.

$$\begin{aligned}
 dN_n^* / dt &= k_{\rho,n-1} N_{n-1}^* - (k_{\rho,n} + k_{t,n}) N_n^* \\
 dN_1^* / dt &= \sum k_{t,n} N_n^* - (k_{\rho,1} + k_{t,1}) N_1^* \\
 dN_n / dt &= k_{t,n} N^*
 \end{aligned} \tag{5}$$

with the boundary condition at $t=0$

$$\begin{aligned}
 N_n^* &= 0 & n > 1 \\
 &= \sum N_n^* = C_0^* & n = 1
 \end{aligned}$$

where C_0^* is a constant. The solution of (5) is easily obtained for the stationary state. Denoting $k_{t,n}/k_{\rho,n}$ by β_n , the size distribution is expressed by

$$F(n)_\infty = N_n / \sum N_n = \beta_n \exp(-\sum_{n=1}^n \beta_n) \tag{6}$$

The inverse relation⁶ of the above equation is

$$\beta_n = F(n)_\infty / \sum_{n=n}^{\infty} F(n)_\infty \tag{7}$$

which guarantees that from any experimental MWD, its corresponding β_n can always be estimated. Therefore, it is clear that β_n , the ratio $k_{t,n}/k_{\rho,n}$, is only the factor to determine the stationary MWD, and then many combinations of $k_{t,n}$ and $k_{\rho,n}$ can also be assumed, as long as the functional form of β_n is fixed. The combinations with various values of ρ , for example,

$$k_{t,n} = k_{t,1} n^{\rho-\alpha} \quad \text{and} \quad k_{\rho,n} = k_{\rho,1} n^\rho \tag{8}$$

correspond to the same stationary MWD with $\beta_n n^{-\alpha}$, the polydispersity of which is $2 \leq Q \leq \infty$ in accordance to $0 \leq \alpha \leq 1$. It is noted that the combination of (4) can not explain the MWDs of $Q \leq 6$.

1.2 Non-uniform Surface Sites

Since the suggestions of Wesslau¹ and Natta⁷, the non-uniformity of polymerization centers with respect to activity, as the origin of broad MWDs in the heterogeneous polymerization, has been discussed by many chemists⁸.

The first quantitative theory was proposed by Clark and Bailey⁹, who assumed that the surface sites are exponentially distributed with adsorption energy of growing chains and desorption (transfer) is the slowest step. Denoting the values averaged with the site-distribution function by $\langle \rangle$, the observable values at the stationary state in this case may be represented by

$$\langle Q_\infty \rangle = 2 \langle k_t \rangle \langle 1/k_t \rangle \quad \text{and} \quad \langle \bar{n}_\infty \rangle = k_p \langle 1/k_t \rangle \quad (9)$$

In the case of the non-uniformity with k_p ¹⁰, they are represented by

$$\langle Q_\infty \rangle = 2 \langle k_p^2 \rangle / \langle k_p \rangle^2 \quad \text{and} \quad \langle \bar{n}_\infty \rangle = \langle k_p \rangle / k_t \quad (10)$$

The importance of the non-uniformity with respect to $\beta (=k_t/k_p)$ ¹¹ for characterizing the polymerization catalyst has been emphasized by Kissin¹² who recommends the step-wise distribution of sites, f_i , obtained numerically from GPC-curve, using

$$\langle W(\ln n) \rangle = n^2 \sum_i f_i \beta_i^2 \exp(-n\beta_i) \quad (11)$$

It can be shown that these three non-uniformities, however, are equivalent for MWDs at the stationary state. The form of the size distribution function of dead polymers depends on the non-uniformity,

$$\langle F(n)_\infty \rangle = N_n / \sum N_n = \langle \beta^2 \exp(-n\beta) \rangle / \langle \beta \rangle \quad (12)$$

for the case with k_t , while

$$\langle F(n)_\infty \rangle = \langle \beta \exp(-n\beta) \rangle = \int_0^\infty \beta e^{-n\beta} T(\beta) d\beta \quad (13)$$

for the case with k_p . Denoting the site distribution functions by $T(\beta)$, $T(k_t)$ and $T(k_p)$ respectively, we have the relation between them, apart from normalization constants,

$$T(\beta) = T(k_t) = \beta^3 T(k_p) \quad (14)$$

which can easily be proved, remembering that the averaging procedure (13) is a Laplace-transform, the inverse form of which is $\beta T(\beta)$.

$$\beta T(\beta) = L^{-1} \left\{ \int_0^\infty \beta e^{-n\beta} T(\beta) d\beta \right\} \quad (15)$$

It is then clear that the supposition of non-uniformity with β , that with k_t , and that with k_p are equally corresponding to the same stationary MWD, as shown in Fig. 1.

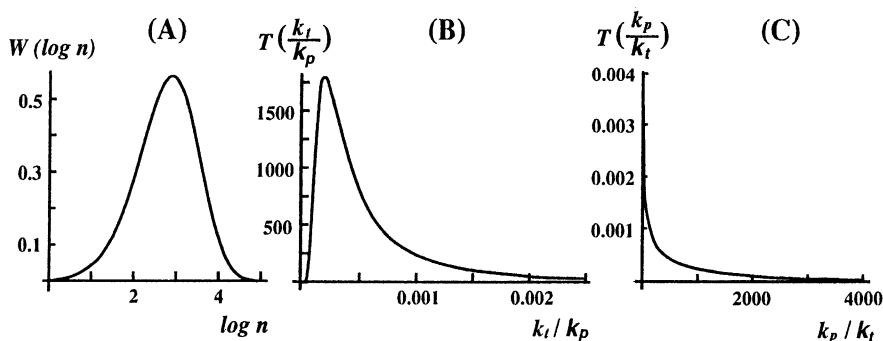


Fig. 1. Site-distributions obtained from a given $F(n)_\infty$; A: $W(\log n)$ for $\log n$, B: $T(k_t/k_p)$ for k_t/k_p , or $T(\beta)$ for β , C: $T(k_p/k_t)$ for k_p/k_t , or $T(1/\beta)$ for $1/\beta$.

1.3 Relation between Theories of Non-uniform Sites and Chain-length Dependent Rates

Gordon and Roe commented on the theory of non-uniform sites as "Almost any MWD (broader than an exponential distribution) can be fitted *a posteriori* by assuming a suitable distribution of site activities¹³." This comment is correct but it is also correct for their own theory too, because their specific function is also obtained from experimental MWD using (7).

To examine the effect of hydrogen addition on the stationary MWD proposed by Roe¹⁴ for testing the rival theories is useful to distinguish the theory of non-uniform sites from other theories including that of monomer diffusion control. His assumption made about the kinetic mechanism of transfer by hydrogen appears to be plausible but it is not so absolute as to refute any other assumption. In fact, Vizen and Yakobson¹⁵ derived a different conclusion on the effect of hydrogen based on a different assumption. Therefore, for testing the rival theories some absolute method should be needed.

2 MWDs during Quasi-living Polymerization

The importance of MWD during the transitional state from living polymerization to stationary polymerization is emphasized. It is well-known that the MWD at the living stage of homogeneous polymerization can be described by a Poisson distribution³. All the rival theories, which issue their modifications of Flory's distribution for explaining MWD at the stationary state, should then issue the same modifications of the Poisson distribution for MWD at the living stage. For MWD at the living polymerization, the theory of non-uniform sites with k_p , for example, should give

$$\langle F(n)_1 \rangle = \langle [(k_p t)^{n-1} / P(n)] e^{-k_p t} \rangle \quad (16)$$

$$\text{and} \quad \langle Q_1 \rangle = \langle k_p^2 \rangle / \langle k_p \rangle^2$$

The Poisson distribution is the function of k_p and independent of k_t , therefore, the theories based upon modifications of k_t give always the narrowest MWD of $Q_t = 1$. The theory of monomer diffusion control should give also the same result. However, to identify MWD at the living polymerization is experimentally difficult, because of observing the living stages under the condition that $k_p t \gg 1$ and $k_t t \ll 1$. Then, MWDs at the transition stages from the living to the stationary state ($k_t t \gg 1$), especially those at the quasi-living stage, the duration from the living to the time when $k_t t \sim 1$ is practically more useful. For the transitional behavior of the MWDs, all the rival theories should predict using their modifications applied to the transitional MWD during homogeneous polymerization. The latter MWD is represented by (17) obtained by solving the set of difference-differential equations (5) with constant rates.

$$\begin{aligned}
 F^*(n) &= N_n^* / \sum N_n^* = N_n^* / C_0^* \\
 &= [(k_p t)^{n-1} e^{-k_p t} / \Gamma(n)] e^{-k_t t} + [(k_t / k_p) e^{-n k_t / k_p}] \gamma(n, (k_p + k_t) t) / \Gamma(n) \quad (17) \\
 \text{and} \quad F(n) &= (1 + k_t t)^{-1} \{ F^*(n) + k_t \int_0^t F^*(n) dt \}
 \end{aligned}$$

where $\gamma(n, (k_p + k_t) t)$ is the incomplete Gamma function. The corresponding forms of Q and \bar{n} of polymerization have been obtained by Cabrerizo and Guzman¹⁶ as

$$\begin{aligned}
 Q &= 2(k_p / k_t)^2 (k_t t - 1 + e^{-k_t t})(1 + k_t t) / (k_p t)^2 \\
 \bar{n} &= k_p t / (1 + k_t t) = \bar{n}_\infty (k_t t / 1 + k_t t) \quad (18)
 \end{aligned}$$

These are the objects with respect to the modification of the rival theories.

2.1 Chain-length Dependent Rates.

From the set of difference-differential equations (5) we have

$$\begin{aligned}
 \sum (N_n^* + N_n) &= C_0^* + \int_0^t \sum k_{t,n} N_n^* dt \\
 \sum n(N_n^* + N_n) &= \int_0^t \sum k_{t,n} N_n^* dt \quad (19) \\
 \text{and} \quad \sum n^2 (N_n^* + N_n) &= 2 \int_0^t \sum n k_{t,n} N_n^* dt
 \end{aligned}$$

Then, the observables are represented by

$$\begin{aligned}
 \bar{n} &= \int_0^t \sum k_{p,n} N_n^* dt / (C_0^* + \int_0^t \sum k_{t,n} N_n^* dt) \\
 Q &= \{ 2 \int_0^t \sum n k_{p,n} N_n^* dt \} \{ (C_0^* + \int_0^t \sum k_{t,n} N_n^* dt) \} / \\
 &\{ \int_0^t \sum k_{p,n} N_n^* dt \}^2 \quad (20)
 \end{aligned}$$

Further results must be obtained by rather cumbersome numerical calculations. Some results obtained for the cases, $k_{t,n}/k_p$ and $k_t/k_{p,n}$ together with the general case (8) are illustrated in Fig. 2.

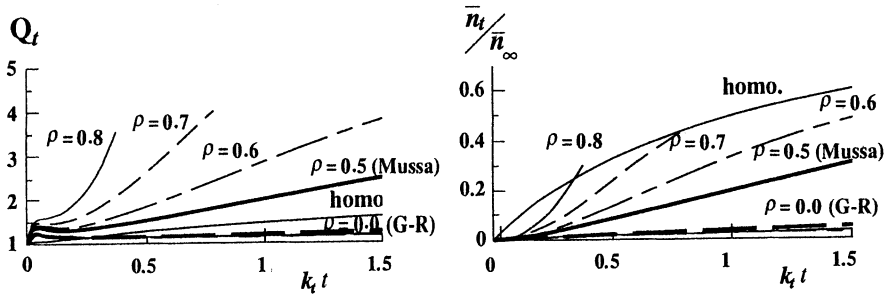


Fig. 2. Transitional changes of MWD predicted from (4) by Gordon-Roe⁴ and Mussa⁵ together with those from (8) or $Q_\infty \equiv 6$ ($\alpha=0.5$).

2.2 Non-Uniform Sites

The observables in the theories of non-uniform sites are given by

$$\begin{aligned} \langle Q \rangle &= 2\{ \langle k_p^2/k_t \rangle t - \langle k_p^2/k_t^2 \rangle + \langle (k_p^2/k_t^2) \exp(-k_t t) \rangle \\ &\{ 1 + \langle k_t \rangle t \} / \{ \langle k_p \rangle t \}^2 \} \quad (21) \\ \langle \bar{n} \rangle &= \langle k_p \rangle t / 1 + \langle k_t \rangle t = \bar{n}_\infty \{ \langle k_t \rangle t / 1 + \langle k_t \rangle t \} \end{aligned}$$

As can be seen from these results, the change of $\langle \bar{n} \rangle$ with time is always the same form as that of the homogeneous polymerization (18). The polydispersity in the non-uniformity with $\langle k_p \rangle$ increases from $\langle k_p^2 \rangle / \langle k_p \rangle^2$ to its double, $2 \langle k_p^2 \rangle / \langle k_p \rangle^2$, as that from 1 to 2 in the homogeneous case. On the contrary, in the case with $\langle k_t \rangle$, the polydispersity slowly increases from 1, as illustrated in Fig. 3.

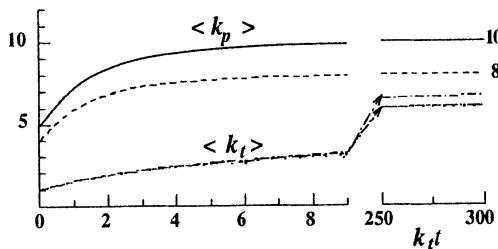


Fig. 3. Comparison of results derived from the two non-uniformities, for the cases $\langle Q_\infty \rangle = 10$ and 8.

2.3 Comparison with Experiments

The observed MWDs, which are identified as those during the quasi-living stages where \bar{n} is increasing, are not very many. Similar to Chein¹⁶, such observations of MWDs have been made mainly for the ethene and propene polymerizations with $\text{TiCl}_3/\text{Al}(\text{C}_2\text{H}_5)_2\text{Cl}$ or MgCl_2 -supported $\text{TiCl}_4/\text{Al}(\text{C}_2\text{H}_5)_3$.⁸ Summarizing the time-dependencies of the observed MWDs of polypropene, which appear to be mostly in good agreement each others, we may conclude follows.

Number average molecular weight always increases similar to that during homogeneous polymerization.

Polydispersity

- (I) decreased monotonously^{15,17,18} or remain unchanged¹¹ from broad MWDs ($Q=8\sim 12$) to stationary ones in the case of $\text{TiCl}_3/\text{Al}(\text{C}_2\text{H}_5)_2\text{Cl}$, or
- (II) remained unchanged from broad MWDs ($Q\sim 4$) in the case of highly active supported- $\text{TiCl}_4/\text{Al}(\text{C}_2\text{H}_5)_3$.^{19,20} In addition, we may note some quantitative observations.
- (III) polydispersity increased from broad MWD ($Q=7\sim 9$) at 2min to its double, $Q\sim 20$, at 30min in the case of the traditional Ziegler catalyst, $\text{TiCl}_4/\text{Al}(\text{C}_2\text{H}_5)_3$.²¹ Tailings of a very broad MWDs ($Q>>20$) at 15s and broad stationary ones ($Q=7$) of polyethene produced with supported catalyst agreed with each other²².

These results show that (A) ***MWDs at the beginning stages (almost living stage) are broad.*** The beginning stage is very limited by the minimum amount of produced polymers which is sufficient for measuring the MWD in each experiment. In the propene polymerization of MgCl_2 -supported $\text{TiCl}_4/\text{Al}(\text{C}_2\text{H}_5)_3$ at 20°C¹⁹, it was 0.1s when the number average degree was 100 and volume of polypropene was 0.2 of that of the catalyst. As the number average degree was expressed by $k_p t$ up to 0.2s, the beginning stage up to 0.2s can be considered the living stage. Conclusion (A) refutes all the rival theories, except the theory of non-uniformity with k_p . Of course, the theory of slowest monomer-diffusion, in any style, is refuted.

The experimental results also show that (B) ***MWDs during the quasi-living stages are monotonously narrow or remain unchanged (polydispersities decrease or keep constant) with time.*** This conclusion (B) refutes all the rival theories, including that of non-uniform sites with k_p . A few results, where the Q -value doubled²¹, may support the non-uniformity with k_p . A slight increase in the Q (from 10 ± 2 at 5min to 14 ± 2 at 50min) of MWD was observed with $\text{TiCl}_3/\text{Al}(\text{C}_2\text{H}_5)_3$ at 41°C, but the MWD could not be identified as that during the quasi-living stage¹¹. The increase in MWD should then be confirmed.

3 A New Non-Uniformity of Surface Sites

For the narrowing of the MWD during the quasi-living stage, a theory of non-uniformity with both k_p and k_t has been proposed by Vizen and Yakobson¹⁵. It

could explain their own experimental result, i.e., polydispersity decreased from ~ 9 to ~ 2 . In addition, they assumed that the rate of transfer by hydrogen is constant and independent of site-distribution for explaining their result that hydrogen addition broadens the stationary MWD. Although their experimental results and assumption on the stationary MWD can not be generally accepted, the non-uniformity proposed should be noted. For it is plausible that the rates of propagation and transfer of a growing polymer on a surface site would be similarly affected by a change from site by site.

3.1 A New Non-Uniformity of Sites with Both Rates

Suppose a non-uniformity with respect to k_p together with the relation

$$k_i / \bar{k}_i = (k_p / \bar{k}_p)^\alpha \quad (22)$$

where \bar{k}_i and \bar{k}_p are their averages. Using this, (21) is represented by

$$\begin{aligned} \langle Q \rangle &= 2\{(\bar{k}_i t) \langle x^{2-\alpha} \rangle - \langle x^{2(1-\alpha)} \rangle + \\ &\langle x^{2(1-\alpha)} \exp(-(\bar{k}_i t)x) \rangle\} \{1 + (\bar{k}_i t) \langle x \rangle\} / \{(\bar{k}_i t) \langle x \rangle\}^2 \end{aligned} \quad (23)$$

where x denotes k_p / \bar{k}_p . From this we have

$$\begin{aligned} \langle Q_1 \rangle &= \langle k_p^2 \rangle / \langle k_p \rangle^2 \\ \text{and} \quad \langle Q_\infty \rangle &= 2 \langle k_p^{2-\alpha} \rangle \langle k_p^\alpha \rangle / \langle k_p \rangle^2 \end{aligned} \quad (24)$$

Further details are determined by the nature of the non-uniformity $T(k_p)$. If we take a log-normal distribution as $T(x)$

$$T(x) = (\sqrt{2\pi\sigma^2})^{-1} \exp\{-(\ln x)^2 / 2\sigma^2\} \quad (25)$$

we have $\langle Q_1 \rangle = \exp(-\sigma^2)$

$$\text{and} \quad \ln(\langle Q_\infty \rangle / 2 \langle Q_1 \rangle) = (1-\alpha)^2 \quad (26)$$

If we take a Gamma-distribution,

$$T(x) = \{v^v / \Gamma(v)\} x^{v-1} \exp(-vx) \quad (27)$$

we have $\langle Q_1 \rangle = 1 + (1/v)$

$$\text{and} \quad \langle Q_\infty \rangle / 2 \langle Q_1 \rangle = \Gamma(v-\alpha)\Gamma(v+\alpha) / \Gamma(v) \quad (28)$$

In Figs. 4 and 5, some results of the calculations are illustrated.

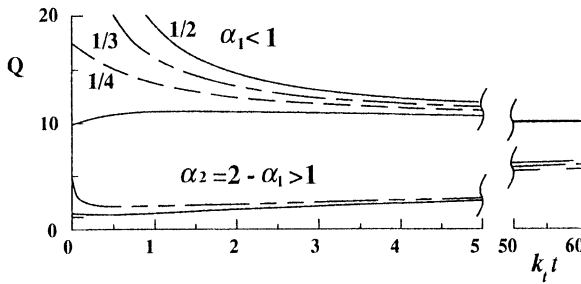


Fig. 4. Polydispersity during quasi-living stage in the case of log-normal site distribution. $\langle Q_\infty \rangle$ is fixed to 10.

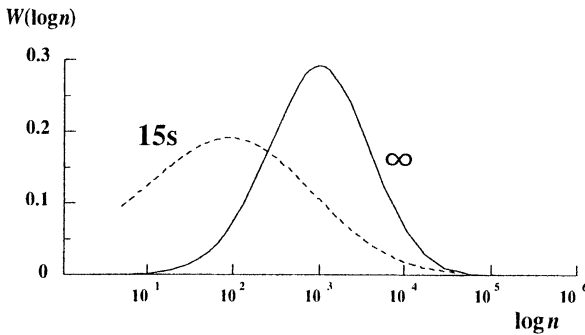


Fig. 5. MWDs at the living stage and the stationary ($\langle Q_\infty \rangle \equiv 7$) state, in the case $\alpha = 0.5$ with Log-normal distribution.

3.2 Kinetic Mechanism and Application of New Non-uniformity

The plausibility of the new non-uniformity is now discussed. The changes in potential energy along the reaction path in terms of bond distance between the end-carbon of the growing chain and Ti of the catalyst may be postulated as those in Fig. 6.

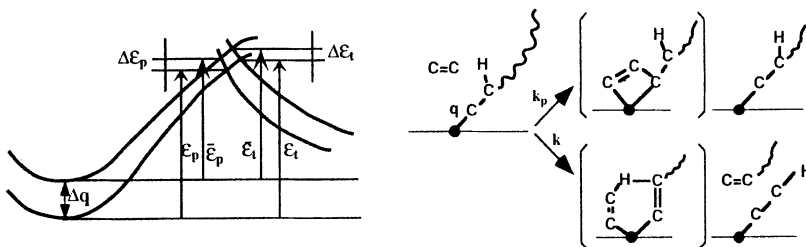


Fig. 6. Potential energy change along with reaction path.

Some correlation exist between the changes in activation energies $\Delta \varepsilon$ and adsorption energy Δq . The rule of Horiuti and Polanyi²³ may be proposed.

$$\begin{aligned} & |\Delta \varepsilon_p| = \gamma |\Delta q| \quad \text{and} \quad |\Delta \varepsilon_t| = \gamma' |\Delta q| \quad 0 < \gamma, \gamma' < 1 \\ \text{and then} \quad & |\Delta \varepsilon_t| = (\gamma' / \gamma) |\Delta \varepsilon_p| \end{aligned} \quad (29)$$

which corresponds to the relation (22), providing $\alpha = \gamma' / \gamma$. It is noted that the site distribution which is expressed by the Gaussian distribution of Δq with variance $(\sigma')^2$ corresponds to the log-normal distribution $T(k_p)$, (25), provided that $\sigma = \sigma' \gamma RT$, which has been reported by the author²⁴.

These discussions suggest that all the reactions of the growing chains have some correlation among them. In this connection, the abnormal decay kinetics during propene polymerization with a supported catalyst, reported by Giannini²⁵, Hsu et al.²⁶ and us¹¹ are important. It is the abnormal decay (first order at the initial, after the stationary state was performed, while a higher order during decay) rate of polymerization centers

$$R_d = -dC^* / dt = k_d C_0^* (C^* / C_0^*)^\delta \quad \delta > 1 \quad (31)$$

and the rate of polymerization (with C^* first order initially while higher order during decay)

$$R_p = k_d C_0^* (C^* / C_0^*)^\delta \quad (32)$$

For this abnormality the above non-uniformity with k_p together with (33) can give a plausible explanation.

$$k_d / k_a = (k_p / k_p)^\xi \quad (33)$$

For the sake of simplicity, using a Gamma-distribution (27) for the case with $\xi = 1$, we have $\delta = 1 + (1/\nu)$. Other than the above, abnormal decay kinetics have been recognized in many systems and summarized as "stretched time" or the law of Kholrausch who found first it in 1854 with discharge in a Leyden jar.²⁷ For those abnormal kinetics, the non-uniformity proposed here gives also a unified explanation, which will be published elsewhere.

Acknowledgement: The authors thank Prof. M. Terano and Dr. H. Mori for kind discussion.

References

- 1) H. Wesslau, *Makromol. Chem.* **20**, 111 (1956)
- 2) L. H. Tung, *J. Polym. Sci.* **24**, 333 (1957)
- 3) L. H. Peebles, "Molecular Weight Distribution in Polymers", New York, J. Wiley-Interscience, 1971
- 4) M. Gordon and R-J. Roe, *Polymer* **2**, 41 (1961)
- 5) C. Mussa I. V., *J. Appl. Polym. Sci.* **1**, 300 (1959)
- 6) E. F. G. Herrington and A. Robertson, *Trans. Faraday Soc.* **40**, 236 (1944)
- 7) G. Natta, *J. Polym. Sci.* **34**, 21 (1959)
- 8) U. Zucchini and G. Cecchin, *Adv. Polym. Sci.* **51**, 101 (1983)
- 9) A. Clark and G. C. Bailey, *J. Catal.* **2**, 2301 (1963)
- 10) T. Keii, *Preprint in IUPAC 28th Macromol. Symp.* (1982) p.237.
- 11) T. Keii et al., *Makromol. Chem.* **185**, 1537 (1984)
- 12) Y. V. Kissin, *Makromol. Chem., Macromol. Symp.* **66**, 83 (1993)
- 13) Ref.4, p.57.
- 14) R-J. Roe, *Polymer* **2**, 60 (1961)
- 15) Y. I. Vizen and F. I. Yakobson, *Polym. Sci., USSR* **20**, 1046 (1978)
- 16) J. Largo-Cabrerizo and J. Guzman, *Macromolecules* **12**, 526 (1979)
- 17) J. C. W. Chien, *J. Polym. Sci.* **A1**, 411 (1963)
- 18) H. Schnecko, K. A. Jung, W. Kern, "Coordination Polymerization", J. C. W. Chien ed., (1975) p.73.
- 19) T. Keii, M. Terano, K. Kimura, K. Ishii, "Transition Metals and Organometallics as Catalysts for Olefin Polymerization", W. Kaminsky, H. Sinn, eds., Springer-Verlag (1988) p.3.
- 20) M. Murata et al., "Catalytic Olefin Polymerization", T. Keii, K. Soga, eds. Kodansha-Elsevier (1990) p.165.
- 21) M. C. Taylor and L. H. Tung, *J. Polym. Sci., Polym. Lett.* **1**, 157 (1963)
- 22) L. L. Bohm, *Polymer* **19**, 562 (1978)
- 23) J. Horiuti and M. Polanyi, *Nature(London)*, **132**, 819, 931 (1933)
- 24) T. Keii, *Macromol. Theory Simul.* **4**, 947 (1995)
- 25) U. Giannini, *Makromol. Chem., Suppl.* **5**, 216 (1981)
- 26) C. C. Hsu et al., "Transition Metal Catalyzed Polymerizations", R.P. Quirk, ed., Camb. Univ. Press (1988) p.136.
- 27) J. T. Bendler and M. F. Shlesinger, "New Trends in Kramers' Reaction Rate Theory", P. Talkner and P. Hanggi, eds., Kluwer Acadm Pub. (1995) p.189.

Olefin Polymerization with Novel Type of Ziegler Catalysts

Kazuo Soga, Eiichi Kaji and Toshiya Uozumi

School of Materials Science,

Japan Advanced Institute of Science and Technology,

1-1 Asahidai, Tatsunokuchi, Nomi-gun,

Ishikawa Prefecture 923-1612, Japan

Abstract : A series of dichlorobis(β -diketonato)titanium complexes were synthesized and the corresponding $MgCl_2$ -supported catalysts were prepared by impregnation method. Those complexes combined with MAO or alkylaluminums hardly showed the activity for propene polymerization. Whereas, the $MgCl_2$ -supported catalysts displayed high activity even using alkylaluminums as cocatalyst. The catalyst isospecificity was drastically increased by adding a suitable Lewis base as an external donor. Isotactic polypropene (PP) with T_m over 169 °C could be thus obtained under appropriate polymerization conditions.

On the other hand, copolymerization of ethene and propene over them gave poly(ethene-*co*-propene) with a fairly high molecular weight and a narrow chemical composition in high yield.

This paper summarizes the characteristics of the $MgCl_2$ -supported catalysts for propene polymerization and ethene-propene copolymerization.

INTRODUCTION

Synthesis of heterogeneous Ziegler-Natta catalysts with a single-site character is not easy due to the formation of $TiCl_3$ clusters in the alkylation process ¹⁾. Whereas, homogeneous metallocene catalysts can afford to give polyolefins with narrow MMD's as well as olefin copolymers with narrow chemical compositions ²⁾.

More recently, some non-metallocene complexes have also been claimed as catalysts for olefin polymerizations ³⁾. Among them, the homogeneous catalyst system composed of a zirconium β -diketonato complex and methylaluminoxane (MAO) or

$\text{AlR}_n\text{Cl}_{3-n}$ (R = Me, Et and *i*-Bu, $n = 2, 3$), which gives polyethene or ethene oligomer depending upon the cocatalyst, seems to be peculiarly interesting because of an easy synthesis of the complex. However, the catalyst system is inactive for propene polymerization.

We have synthesized a series of titanium analogues and supported them on MgCl_2 . The resulting catalysts showed very high activity for propene polymerization even using ordinary alkylaluminums as cocatalyst. The catalyst isospecificity was drastically improved by the addition of a suitable Lewis base. From the elemental analysis of the supported catalysts before and after subjecting to cocatalyst, it was demonstrated that one of the β -diketone ligands is attached to the active Ti⁴⁺. As a result, the catalyst performance was markedly dependent upon the β -diketone ligand. In addition, the formation of titanium clustrates, which is frequently observed during the alkylation process of conventional MgCl_2 -supported TiCl_4 catalysts¹⁾, might be suppressed due to the steric hindrance caused by a bulky β -diketone ligand. Therefore, the active species formed in the supported catalysts could be assumed to be more uniform as compared to those in the ordinary MgCl_2 -supported TiCl_4 catalysts. The test of those catalysts to ethene-propene copolymerization actually yielded give poly(ethene-*co*-propene) with a narrow chemical composition. The copolymerization results also gave us an invaluable information on the oxidation states of active Ti species.

This paper summarizes the characteristics of the novel Ziegler-type catalysts.

EXPERIMENTAL PART

Materials : MgCl_2 (surface area measured by BET method = 80 m²/g) and triethylaluminum (TEA) donated by Toho Titanium Co. Japan and Tosoh Akzo Co. Japan were used without further purification. $\text{Ti}(\text{acetylacetonato})_2\text{Cl}_2$ [$\text{Ti}(\text{AA})_2\text{Cl}_2$], $\text{Ti}(1\text{-benzoylacetonato})_2\text{Cl}_2$ [$\text{Ti}(\text{BA})_2\text{Cl}_2$], $\text{Ti}(2,2,6,6\text{-tetramethyl-3,5-heptanedionato})_2\text{Cl}_2$ [$\text{Ti}(\text{DPM})_2\text{Cl}_2$] and $\text{Ti}(4,4,4\text{-trifluoro-1-phenyl-1,3-butanedionato})_2\text{Cl}_2$ [$\text{Ti}(\text{BFA})_2\text{Cl}_2$] were prepared according to the literature⁵⁾. Ethene and propene of research grade purchased from Takachiho Chem. Co. Japan were further purified by passing through NaOH and P₂O₅ columns. The other chemicals commercially obtained from Kanto Chemical Co. Japan were purified according to the usual procedures.

Preparation of the MgCl₂-supported catalysts : All the reactions were performed under nitrogen atmosphere using a standard Schlenk technique. The supported catalysts were prepared by allowing the titanium compounds to react with MgCl₂ in toluene at room temperature overnight. The solid products were washed with a plenty of toluene, followed by drying i. vac. at 40 °C. The contents of Ti in the catalysts were analyzed by ICP-AES spectrometer (Inductively Coupled Plasma Atomic Emission Spectrometer, Seiko Instruments SPS7700).

Propene polymerization : Polymerization of propene was conducted under atmospheric pressure in a 300 cm³ glass reactor equipped with a magnetic stirrer. *n*-Heptane (100 cm³) was used as the solvent. Polymerization was quenched with acidic methanol and the polymer produced was washed with a plenty of methanol. The polymer was subsequently extracted with boiling heptane. Isotactic index (I.I.) of PP was measured as the weight fraction of polymer insoluble in boiling heptane.

Copolymerization of ethene with propene : The copolymerization was carried out in a 1 dm³ glass autoclave reactor equipped with a mechanical stirrer under a total pressure of 1 atm. *n*-Heptane (300 cm³) was used as the solvent. Ethene and propene were continuously supplied by using two sets of gas flow controllers (MC-1AS, KOFLOC Inc.). The concentrations of ethene and propene in *n*-heptane (C_M) were estimated by using the following Kissin's equation ⁶⁾,

$$C_M = K_M \cdot \exp(Q/RT) \cdot P_M$$

where the Henry constants (K_M) for ethene and propene are 1.15 × 10⁻³ mol/dm³ · atm and 2.72 × 10⁻³ mol/dm³ · atm, and the heats of solution (Q) for ethene and propene are 11.3 kJ/mol and 13.4 kJ/mol, respectively. Copolymerization was started by adding 1.0 mmol of TEA and 1 μ mol of the Ti(BFA)₂Cl₂/MgCl₂ catalyst, and terminated with acidic methanol. The precipitated polymer was separated by filtration and adequately washed with methanol, followed by drying i. vac. at 40 °C.

Characterization of the (co)polymers : The ¹³C-NMR spectra of (co)polymers were recorded at 140 °C using a Varian GEM-300 spectrometer operating at 75 MHz. The sample solution of (co)polymer was prepared in 1,2,4-trichlorobenzene/benzene-*d*₆ (vol. ratio 9/1). Differential scanning calorimetry (DSC) measurement was made using a Seiko DSC (SSC-5200) at a heating rate of 10 °C/min. The TREF (on-line temperature-rising

elution fractionation)-SEC (size exclusion chromatography) analysis of copolymer was made using a Mitsubishi Yuka CFC (cross fractionation chromatography, T-105A) system.

RESULTS AND DISCUSSION

Propene polymerization : Four kinds of MgCl_2 -supported $\text{Ti}(\beta\text{-diketonato})_2\text{Cl}_2$ complexes [$\text{Ti}(\text{AA})_2\text{Cl}_2/\text{MgCl}_2$; Ti content = 0.062 (mmol-Ti/g-cat.), $\text{Ti}(\text{BA})_2\text{Cl}_2/\text{MgCl}_2$; 0.038, $\text{Ti}(\text{DPM})_2\text{Cl}_2/\text{MgCl}_2$; 0.037, $\text{Ti}(\text{BFA})_2\text{Cl}_2/\text{MgCl}_2$; 0.017] were tested to propene polymerization at 40 °C using TEA as cocatalyst. From a detailed analysis of the $\text{Ti}(\text{AA})_2\text{Cl}_2/\text{MgCl}_2$ - TEA catalyst system, it was confirmed that one of the ligands is left unremoved even after contacting the catalyst with TEA. The polymerization activity decreased as follows: $\text{Ti}(\text{BFA})_2\text{Cl}_2/\text{MgCl}_2 > \text{Ti}(\text{BFA})_2\text{Cl}_2/\text{MgCl}_2 \cong \text{Ti}(\text{BFA})_2\text{Cl}_2/\text{MgCl}_2 > \text{Ti}(\text{BFA})_2\text{Cl}_2/\text{MgCl}_2$. The highest activity [$\text{Ti}(\text{BFA})_2\text{Cl}_2/\text{MgCl}_2$] was ca. 900 kg-PP/mol-Ti · atm · h, which is comparable to those obtained with the conventional MgCl_2 -supported TiCl_4 catalysts. It may be considered that the activity is enhanced by an electron-withdrawing substituent on the β -diketonato ligand. Whereas, the catalyst isospecificity measured as the weight fraction of boiling heptane insoluble polymer (I.I.) was approximately 25 % independently of the substituent.

Addition of a Lewis base like ethyl benzoate (EB), di-*n*-butyl phthalate (DNBP)

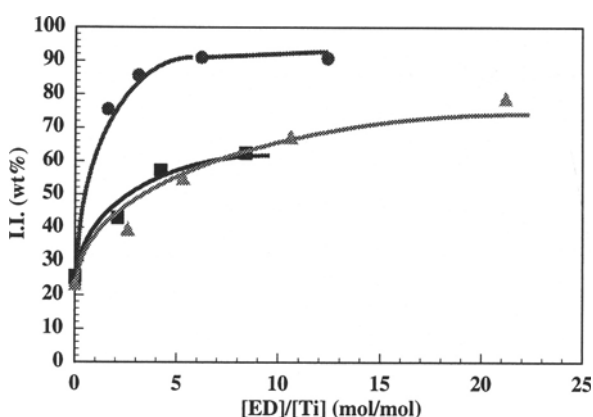


Fig. 1 Plots of I.I. against the $[\text{ED}]/[\text{Ti}]$ ratio

Cat. = $\text{Ti}(\text{BFA})_2\text{Cl}_2/\text{MgCl}_2$ (0.017 mmol/g), Ti = 0.001 mmol, $[\text{Al}]/[\text{Ti}] = 70$, $P = 1$ atm, *n*-heptane = 100 cm^3 at 40 °C for 1 h.

▲ : EB ■ : DNBP ● : DIPDMS

or di-*i*-propyl-dimethoxysilane (DIPDMS) as an external donor (ED) caused to increase the I.I. to a great extent as frequently observed with the conventional Ziegler-Natta catalysts⁷⁾. For reference, the results obtained with the $\text{Ti}(\text{BFA})_2\text{Cl}_2/\text{MgCl}_2$ catalyst are illustrated in Fig. 1. DIPDMS was found to be

most effective among the three donors.

To check the formation of clustrate active species, a set of $\text{Ti}(\text{BFA})_2\text{Cl}_2/\text{MgCl}_2$ catalysts with different Ti contents [0.017, 0.011, 0.007, 0.002 (mmol-Ti/g)] were prepared

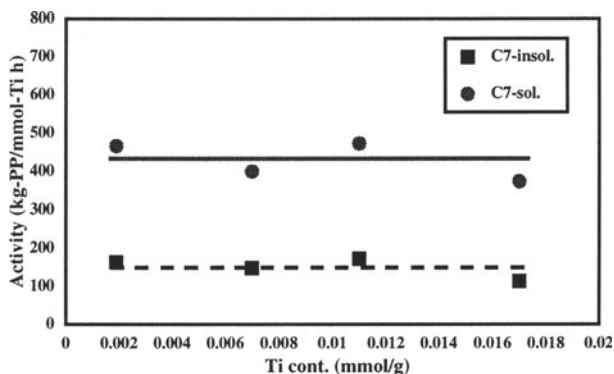


Fig. 2 Effect of the Ti content on the activity

Cat. = $\text{Ti}(\text{BFA})_2\text{Cl}_2/\text{MgCl}_2$, Ti = 0.01 mmol, $[\text{Al}]/[\text{Ti}] = 70$,

$P = 1$ atm, n -heptane = 100 cm^3 at 40°C for 1 h.

isolated with one another.

Polymerization of propene was then conducted over those catalysts using DIPDMS as the external donor, the typical results of which are given in Tab. 1. The rise in the I.I.

and tested to propene polymerization in the absence of an external donor. The specific activities for both isotactic and atactic polymerizations did not change so much as shown in Fig. 2, suggesting that the active species formed in the present catalysts are

Tab. 1 Effect of the $[\text{Si}]/[\text{Ti}]$ ratio on propene polymerization^{a)}

| Ti cont. (mmol/g) | $[\text{Si}]/[\text{Ti}]$ (mol/mol) | Activity (kg-PP/mol-Ti h) ^{b)} | | \bar{M}_n (* 10^4) | I.I. ^{c)} (%) | T_m ^{d)} ($^\circ \text{C}$) | $[mmmm]$ ^{e)} (%) |
|----------------------|--|---|---------------|-------------------------|---------------------------|--|-------------------------------|
| | | C7-insol.(Iso.) | C7-sol.(Ata.) | | | | |
| 0.017 | 0 | 114 | 378 | 3.2 | 23.4 | 158.1 | 88.9 |
| | 1.6 | 208 | 67 | 6 | 75.5 | 163.7 | 91.2 |
| | 3.1 | 113 | 18 | 8.4 | 85.7 | 164.9 | 93.2 |
| | 6.2 | 98 | 9 | 10.5 | 91.0 | 164.3 | 94.3 |
| | 12.4 | 62 | 7 | 15.1 | 90.8 | 165.7 | 94.9 |
| 0.007 | 0 | 149 | 400 | 3.9 | 27.1 | 161.8 | 86.4 |
| | 3.3 | 401 | 172 | 6.2 | 70.0 | 163.9 | -- |
| | 6.5 | 429 | 33 | 11.1 | 92.9 | 166.2 | 94.8 |
| | 13.0 | 271 | 10 | 10.6 | 96.4 | 166.8 | 97.0 |
| 0.002 | 0 | 164 | 466 | 3.8 | 26.0 | 161.2 | -- |
| | 31.1 | 817 | 29 | 7.1 | 96.6 | 167.5 | 95.2 |
| | 62.5 | 416 | 10 | 10.4 | 97.7 | 168.0 | 98.3 |

^{a)} Polymerization conditions : Cat. = $\text{Ti}(\text{BFA})_2\text{Cl}_2/\text{MgCl}_2$, $[\text{Ti}] = 0.01$ mmol, $[\text{Al}(\text{TEA})]/[\text{Ti}] = 70$,

n -heptane = 100 cm^3 , $P = 1$ atm at 40°C for 1 h. Si = di-*i*-propyldimethoxysilane. ^{b)} Iso.; isotactic part,

Ata.; atactic part. ^{c)} Isotactic index(I.I.); weight % of boiling heptane insoluble fraction. ^{d)} T_m :^{e)}

$[mmmm]$ for boiling heptane insoluble part.

and $[mmmm]$ pentad fraction by the addition of DIPDMS become more prominent with a decrease in the Ti content. Thus, isotactic PP with $T_m = 168.0\text{ }^\circ\text{C}$ was obtained with the catalyst containing as low as 0.002 mmol-Ti/g.

Whereas, the effect of EB on propene polymerization was found to be different, i. e., with an increase in the $[\text{EB}]/[\text{Ti}]$ ratio, the I.I. was markedly increased from 20 to 90 %,

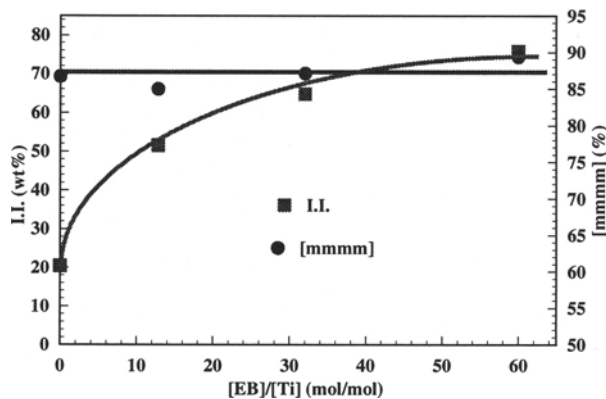


Fig. 3 Plots of I.I. and $[mmmm]$ against the $[\text{EB}]/[\text{Ti}]$ ratio

Cat. = $\text{Ti}(\text{BFA})_2\text{Cl}_2/\text{MgCl}_2$ (0.002 mmol/g), Ti = 0.01 mmol,

$[\text{Al}]/[\text{Ti}] = 70$, $P = 1\text{ atm}$, n -heptane = 100 cm^3 at 40 $^\circ\text{C}$ for 1 h.

but the $[mmmm]$ pentad fraction was kept almost unchanged as shown in Fig. 3.

Copolymerization of ethene with propene: The copolymerization of ethene with propene was first carried out at 40 $^\circ\text{C}$ with the $\text{Ti}(\text{BFA})_2\text{Cl}_2/\text{MgCl}_2$ [0.002 mmol-Ti/g]-TEA catalyst system in the presence of DIPDMS

($[\text{DIPDMS}]/[\text{Ti}] = 50$). In the ^{13}C -NMR spectra of resulting copolymers, any peaks attributed to the chemical inversion were not observed.

Tab. 2 summarizes the results of ethene-propene copolymerization together with the triad sequence distributions in the copolymers determined by ^{13}C -NMR. Even the copolymer with a high content of propene displayed a melting temperature (T_m). To get a better information on this point, a typical copolymer (obtained in run 3) was analyzed by TREF-SEC (Fig. 4). The majority of the copolymer (ca. 96 wt%) was extracted below 80 $^\circ\text{C}$ and the rest at around 100 $^\circ\text{C}$. It is known that the $\text{Ti}(\text{II})$ species, which is inactive for propene homopolymerization, also catalyzes the copolymerization with ethene to yield poly(ethene-co-propene) with less content of propene⁸⁾. The fraction extracted at around 100 $^\circ\text{C}$ might thus result from the $\text{Ti}(\text{II})$ species. It may be considered, therefore, that the catalyst contains a small portion of the over-reduced $\text{Ti}(\text{II})$ species, which could not be confirmed by propene polymerization.

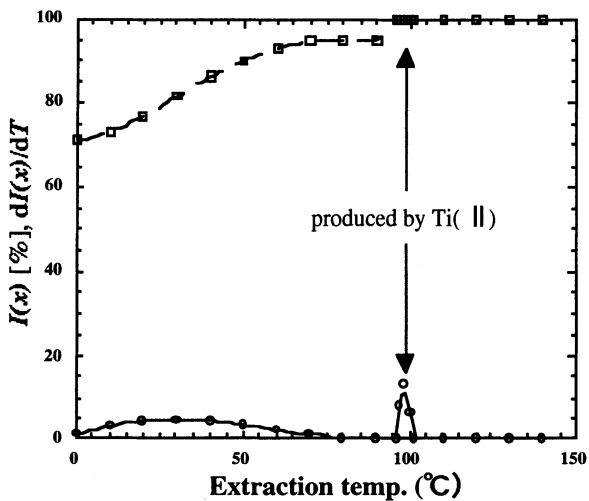


Fig. 4 TREF diagrams of poly(ethene-co-propene)

Sample ; run 3 (propene cont. = 43.3 mol%)

Solid and broken lines indicate the differential data, $dI(x)/dT$, and the summation of fractions, $I(x)$, respectively.

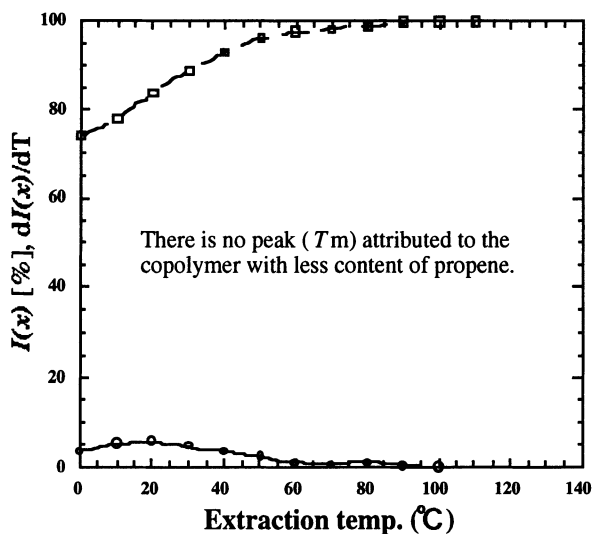


Fig. 5 TREF diagrams of poly(ethene-co-propene)

Sample ; run 8 (propene cont. = 36.9 mol%)

Solid and broken lines indicate the differential data, $dI(x)/dT$, and the summation of fractions, $I(x)$, respectively.

Tab. 2 Results of ethene-propene copolymerization with DIPDMS^{a)}

| Run No. | Conc. of monomers in heptane | | Yield g | P mol% | T _m °C | [PPP] | [PPE] | [PEP] | [EPE] | [PEE] | [EEE] |
|---------|------------------------------------|------------------------------------|---------|--------|-------------------|---------|---------|-------|-------|-------|-------|
| | C _E mol/dm ³ | C _P mol/dm ³ | | | | + [EPP] | + [EEP] | | | | |
| 1 | 0.051 | 0.137 | 0.57 | 16.4 | 122.2 | 3.4 | 7.8 | 3.9 | 10.3 | 19.6 | 55.0 |
| 2 | 0.039 | 0.205 | 1.116 | 25.8 | 122.6 | 7.3 | 16.4 | 5.0 | 9.7 | 20.5 | 41.1 |
| 3 | 0.026 | 0.273 | 0.845 | 43.3 | 124.2 | 18.2 | 20.8 | 7.7 | 8.5 | 17.7 | 27.0 |
| 4 | 0.008 | 0.369 | 0.334 | 77.8 | 108.6 | 56.7 | 18.6 | 7.6 | 3.9 | 7.1 | 6.1 |

^{a)} Ti(BFA)₂Cl₂/MgCl₂ (Ti cont. = 0.002 mmol/g) = 1 μ mol, [Al(TEA)/[Ti] = 1000,

[di-*i*-propyldimethoxysilane]/[Ti] = 50, *n*-heptane = 300 cm³ at 40 °C. ^{b)} not determined

Copolymerization of ethene with propene was then conducted at 40 °C under similar conditions without adding an external donor. The results of copolymerization together with the triad sequence distributions are shown in Tab. 3. Contrary to the results obtained above in the presence of DIPDMS, the melting points of the copolymers decreased monotonously to disappear completely with an increase in the propene content. The TREF diagram of a typical copolymer (obtained in run 8) is illustrated in Fig. 5, which clearly shows that all the copolymers are extracted below 90 °C. The absence of other fractions extractable at

Tab. 3 Results of ethene-propene copolymerization without DIPDMS^{a)}

| Run No. | Conc. of monomers in heptane | | Yield g | P mol% | T _m °C | [PPP] | [PPE] | [PEP] | [EPE] | [PEE] | [EEE] |
|---------|------------------------------------|------------------------------------|---------|--------|---------------------|---------|---------|-------|-------|-------|-------|
| | C _E mol/dm ³ | C _P mol/dm ³ | | | | + [EPP] | + [EEP] | | | | |
| 5 | 0.047 | 0.159 | 0.815 | 5.6 | 120.1 ^{b)} | 0 | 3.0 | 0 | 2.6 | 10.0 | 84.4 |
| 6 | 0.038 | 0.205 | 0.861 | 13.4 | 119.0 ^{b)} | 0 | 5.8 | 0.9 | 7.6 | 14.3 | 71.4 |
| 7 | 0.023 | 0.289 | 0.881 | 27.4 | 114.5 ^{b)} | 6.1 | 10.8 | 4.6 | 10.5 | 21.0 | 47.1 |
| 8 | 0.013 | 0.339 | 0.437 | 36.9 | n. d. ^{c)} | 11.5 | 16.8 | 8.0 | 8.6 | 23.1 | 32.0 |
| 9 | 0.007 | 0.371 | 0.422 | 39.9 | n. d. ^{c)} | 10.2 | 18.8 | 7.0 | 10.9 | 23.2 | 29.9 |

^{a)} Ti(BFA)₂Cl₂/MgCl₂ (Ti cont. = 0.002 mmol/g) = 0.15 μ mol, [Al(TEA)/[Ti] = 1000,

n-heptane = 300 cm³ at 40 °C, ^{b)} very weak, ^{c)} not detected.

higher temperatures might deny the formation of Ti(II) species in the donor-free catalyst. Accordingly, it may be said that the catalyst possesses a single-site character.

Conclusion : From the results described above, we have come to the following conclusions. 1) the MgCl_2 -supported $\text{Ti}(\beta\text{-diketonato})_2\text{Cl}_2$ catalysts effectively catalyze propene polymerization. 2) the active species formed in those catalysts are isolated with one another. 3) the catalyst isospecificity is drastically improved by adding a suitable electron donor, especially organic silane compound like DIPDMS. 4) the $\text{Ti}(\text{BFA})_2\text{Cl}_2/\text{MgCl}_2$ catalyst modified by DIPDMS contains an appreciable amount of the Ti (II) species, and consequently gives the copolymer with less content of comonomer as a by-product. 5) such an over-reduction of the titanium species is not observed in the donor-free catalyst, i. e., the donor-free catalyst possesses a single-site character (all the active species are Ti(III) and isolated with one another). 6) the activity for ethene-propene copolymerization is quite high, and thus, 7) the present novel Ziegler-type catalysts may be of use for the production of LLDPE with a narrow chemical composition.

A further study is now in progress to make the structure of active species clear.

REFERENCES

- 1) (a) K. Soga, Y. Doi, and T. Shiono, *Makromol. Chem.*, **189**, 1531 (1988); (b) J. Kratochvila, T. Shiono, and K. Soga, *Makromol. Chem. Rapid Commun.*, **14**, 85 (1993).
- 2) (a) H. Sinn, W. Kaminsky, H. J. Vollmer, and R. Woldt, *Angew. Chem. Int. Ed. Engl.*, **19**, 390 (1980); (b) F. R. W. P. Wild, L. Zsolnai, G. Huttner, and H. H. Brintzinger, *J. Organomet. Chem.*, **232**, 233 (1982); (c) F. R. W. P. Wild, M. Wasiucionek, G. Huttner, and H. H. Brintzinger, *J. Organomet. Chem.*, **288**, 63 (1985); (d) J. A. Ewen, *J. Am. Chem. Soc.*, **106**, 6355 (1984); (e) W. Kaminsky, K. Kulper, H. H. Brintzinger, and F. R. W. P. Wild, *Angew. Chem. Int. Ed. Engl.*, **24**, 507 (1985); (f) T. Mise, S. Miya, and H. Yamazaki, *Chem. Lett.*, 1853 (1989); (g) J. A. Ewen, M. J. Elder, L. R. Jones, S. Curtis, and N. H. Cheng, *Stud. Surf. Catal.*, **56**, 4392 (1990); (h) N. Ishihara, M. Kuramoto, and M. Uoi, *Macromolecules*, **21**, 3356 (1988); (i) W. Kaminsky and K. Heiland, *Makromol. Chem.*, **193**, 601 (1992); (j) E. Shamshoum, *Metallocene Conference '93*, 173 (1983); (k) D. Rauscher, *Metallocene Conference '93*, 189 (1983).
- 3) (a) L. Matilainen, M. Klinga, and M. Leskela, *J. Chem. Soc. Dalton Trans.*, 219 (1996); (b) K. Koyama, E. Ihara, and H. Yasuda, *Polymer prep. Jpn.*, **45**(2), 171(1996); (c) C. Janiak, T. G. Scharmann, and K. C. H. Lange, *Macromol. Rapid Commun.* **15**, 655 (1994);

- (d) K. Oouchi, M. Mitani, M. Hayakawa, T. Yamada, and T. Mukaiyama, *Macromol. Chem. Phys.*, **197**, 1545 (1996); (e) T. Miyatake, K. Mizunuma, Y. Seki, and M. Kakugo, *Makromol. Chem. Rapid Commun.*, **10**, 349 (1989).
- 4) K. Soga, E. Kaji, T. Uozumi, *J. Polym. Sci.: part A, Polym. Chem.*, in printing.
- 5) (a) T. J. Pinnavaia and R. C. Fay, *Inorg. Synth.*, **12**, 88 (1970); (b) R. C. Fay and R. N. Lowry, *Inorg. Chem.*, **6**, 1512 (1967).
- 6) Y. V. Kissin, *"Isospecific Polymerization of Olefins with Heterogeneous Ziegler-Natta Catalysts"*, Springer Verlag, New York 3 (1985).
- 7) (a) N. Kashiwa, *Polym. Bull.*, **12**, 99 (1984); (b) N. Kashiwa, J. Yoshitake, A. Toyota, *Polym. Bull.*, **19**, 333 (1988).
- 8) (a) K. Soga, T. Sano, R. Ohnishi, *Polym. Bull. (Berlin)* **4**, 157 (1981); (b) K. Soga, S. Chen, R. Ohnishi, *Polym. Bull. (Berlin)* **8**, 473 (1982); (c) K. Soga, M. Ohtake, R. Ohnishi, Y. Doi, *Polym. Commun.* **25**, 171 (1984); (d) K. Soga, M. Ohtake, R. Ohnishi, Y. Doi, *Makromol. Chem.* **186**, 1129 (1985).

Kinetics and Mechanism of Ethylene Polymerization and Copolymerization Reactions with Heterogeneous Titanium-Based Ziegler-Natta Catalysts

Yury V. Kissin, Robert I. Mink, Thomas E. Nowlin, Anita J. Brandolini

Edison Research Lab., Mobil Chemical Co., P.O.Box 3029, Edison, NJ 08818-3029, USA

A detailed kinetic analysis of ethylene homopolymerization reactions and its copolymerization reactions with 1-hexene with a supported Ti-based Ziegler-Natta catalyst shows a number of kinetic features which are interpreted as a manifestation of multi-site catalysis. The catalyst contains several types of active centers which differ in stability and formation rates, the molecular weights of polymer molecules they produce and in their response to the presence of an α -olefin. Several kinetic effects in ethylene polymerization reactions require an introduction of a special kinetic mechanism which postulates an unusually low reactivity of the growing polymer chain containing one ethylene unit, the Ti-C₂H₅ group. This peculiarity of the Ti-C₂H₅ group, which is probably caused by its β -agostic stabilization, predicts two features of ethylene polymerization reactions which have not been described in the literature yet: (a) formation of deuterated ethylenes in ethylene homopolymerization reactions in the presence of deuterium, and (b) an apparently increased reactivity of α -olefins in chain initiation reactions involving the Ti-H bond. Both effects were confirmed experimentally.

1 Introduction

Ethylene polymerization reactions with Ti-based heterogeneous and supported Ziegler-Natta catalysts exhibit several features which distinguish them from polymerization reactions of other α -olefins with the same catalysts:

1. Based on the values of its reactivity ratios in copolymerization reactions with various α -olefins, ethylene is the most reactive among all olefins in polymerization reactions with all Ziegler-Natta catalysts [1-3]. However, ethylene never exhibits the high reactivity in homopolymerization reactions expected based on its relative reactivity in copolymerization reactions.
2. Introduction of α -olefins to the ethylene polymerization reactions always results in significantly higher polymerization rates [4-11]. Literature data on ethylene copolymerization reactions in solutions at high temperatures suggest a kinetic rather than a physical (diffusion) mechanism of the effect [11].

3. The overall rate of ethylene homopolymerization has a reaction order with respect to the ethylene concentration significantly exceeding one, usually in the 1.7-1.9 range [6,12,13].
4. Introduction of hydrogen causes a significant immediate decrease of the ethylene polymerization rate. This rate depression effect is completely reversible suggesting a chemical nature [6].

We have attempted to provide the experimental basis for a single explanation of all these specific features of ethylene polymerization reactions. We have carried out a detailed kinetic investigation of ethylene polymerization and ethylene/1-hexene copolymerization reactions with a supported Ti-based Ziegler-Natta catalyst using the concept of multi-center catalysis with different centers responding differently to changes in reaction parameters. As a result of these studies, we have proposed a kinetic mechanism which explains most of the above-listed features of ethylene polymerization kinetics. The proposed mechanism predicts several new features of ethylene polymerization reactions which have not yet been described in the literature. We have examined these new effects and have provided experimental proofs of their existence.

2 Experimental Part

Ethylene homopolymerization and copolymerization reactions were carried out in a stainless-steel 500-cm³ reactor equipped with a heating jacket, a magnet-drive stirrer and several ports for adding solvents, liquid monomers and catalyst components. Most reactions were carried out at 80-85°C using *n*-heptane as the solvent and AlEt₃ (1.5-1.6 mmol) as the cocatalyst. The ethylene partial pressure, P_E, varied from 0.4 to 1.3 MPa (this corresponds to an ethylene concentration in solution, C_E, from 0.30 to 1.0 M), the hydrogen partial pressure, P_H, ranged from 0 to 0.3 MPa (hydrogen concentration, C_H, varied from 0 to 0.03 M), and the 1-hexene concentration in solution, C_{Hex}, varied from 0 to 2.2 M. A single Ti-based, silica-supported catalyst with a Ti content of ca. 3 wt. % was used in all experiments [14].

Polymers and copolymers were characterized by several techniques. GPC analysis was performed at 145°C with a Waters 150C Liquid Chromatograph (two columns 10⁶, 10⁴ and 10³ Å). Resolution of GPC curves into Flory components was carried out with Scientist program (MicroMath Scientific Software) as described earlier [15]. Copolymer compositions were measured by the IR method using a Perkin-Elmer Paragon 1000 FTIR spectrophotometer. ¹³C NMR and ²H NMR analyses of polymers were performed with a JEOL Eclipse 400 NMR spectrometer at 130°C using polymer solutions in 1,3,5-trichlorobenzene. Analyses of light products, gases and liquids, generated in the polymerization reactions were carried out using the GC method [with a Hewlett-Packard 5890 Gas Chromatograph, a 60-meter MTX-1 column, (Restek Co.)] and the GC/MS method [with a Varian 3400 Gas Chromatograph, a 50-meter Chromopack Al₂O₃-plot column and a Finnigan MAT 8230 mass-spectrometer (mass range from 10 to 1000)].

3 Kinetic Studies of Ethylene Polymerization Reactions

3.1 Principal Procedure of Kinetic Studies

The cornerstone of our kinetic study is the analysis of the molecular weight distribution data. It is performed under the assumption that all heterogeneous Ziegler-Natta catalysts contain several types of active centers. Our earlier experience suggests that Ti-based catalysts used for ethylene polymerization usually contain four or five types of centers [16,17]. These centers differ one from another in the following kinetic properties:

1. The centers have different stabilities. Some centers deactivate more rapidly whereas other remain active for many hours.
2. Each type of center produces polymer molecules with a narrow molecular weight distribution described by the Flory theory ($M_w/M_n = 2.0$). Figure 1 gives one example of a GPC curve analysis for an ethylene/1-hexene copolymer prepared in the absence of hydrogen.
3. The centers produce polymer chains of different average molecular weights. For example, Table 1 shows that when an ethylene homopolymerization reaction is performed 85°C, the centers produce Flory components with widely different weight-average molecular weights M_w .
4. The centers have different copolymerization abilities.

Table 1. Molecular weights of Flory components in ethylene homopolymer

| Component: | II | III | IV | V |
|------------|---------------|-----------------|-----------------|---------------------|
| M_w : | 51,000-55,000 | 143,000-165,000 | 450,000-490,000 | 1,480,000-1,610,000 |

We adopted the following procedure for determining kinetic parameters of the active centers [16,17]. A series of polymerization experiments (from 3 to 6) was carried out under the same conditions (temperature, monomer concentrations) for different periods of time. Every polymer was analyzed by GPC, contents of each Flory component (produced by a single type of active center) were determined, and the copolymer composition was measured. Polymerization kinetics on a single type of active center is described by the following equations for the reaction rate, $R(t)$, and the yield, $Q(t_r)$, at time t_r . These equations assume the first-order reaction kinetics with respect to C_E for a given center:

$$R(t) = k_{\text{eff}} k_f C_E \cdot [\exp(-k_f t) - \exp(-k_d t)] / (k_d - k_f) \quad (1)$$

$$Q(t_r) = k_{\text{eff}} C_E \cdot [k_f / (k_d - k_f)] \cdot \{ [1 - \exp(-k_f t_r)] / k_f + [1 - \exp(-k_d t_r)] / k_d \} \quad (2)$$

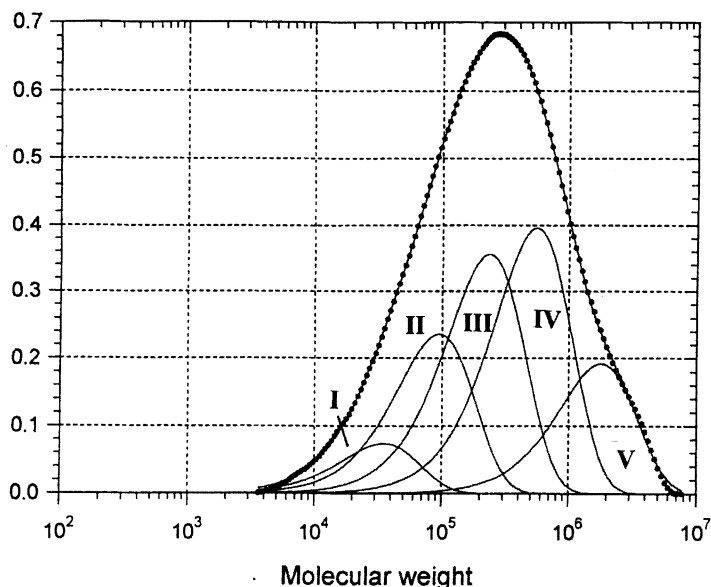


Fig. 1. GPC curve of ethylene/1-hexene copolymer. Flory components are numbered in the order of increasing molecular weight

Each type of active center has different values of all three kinetic parameters in Eqs. 1 and 2, the effective rate constant, k_{eff} (the product of the propagation rate constant, k_p , and the concentration of a particular active center, C^* , which itself is a function of C_E), the rate constant of center formation, k_f , and the rate constant of center deactivation, k_d . Every experimental kinetic curve is regarded as the sum of kinetic curves for each type of active center. Combination of reaction rates, $\Sigma R(t)$, for several types of active centers is calculated to comply with two criteria: (a) the calculated total reaction rate should fit the experimental kinetic curve, and (b) the yield of each Flory component at different reaction times should match the contribution of the respective component to the total polymer mixture (from GPC data, see Fig. 1). Figure 2 gives one example of such a kinetic analysis for the case of an ethylene/1-hexene copolymerization reaction at 85°C in the absence of H_2 .

3.2 Ethylene Concentration Effect on Polymerization Kinetics

Kinetics of homopolymerization reactions at temperatures $< 90^\circ\text{C}$ at P_E 0.3 to 1.2 MPa is relatively stable; reaction rates rapidly reach a plateau and then slowly decrease by ca. 30% over a period of 4 hours. The analysis of the polymerization reaction kinetics provides several means of evaluating overall reaction orders, n , with respect to the ethylene concentration:

1. Plotting total polymer yields after 4 hours as a function of C_E gave the n value range of 1.7-2.0.
2. Comparison of reaction rates (at 60 or 120 minutes) at different C_E gave $n =$

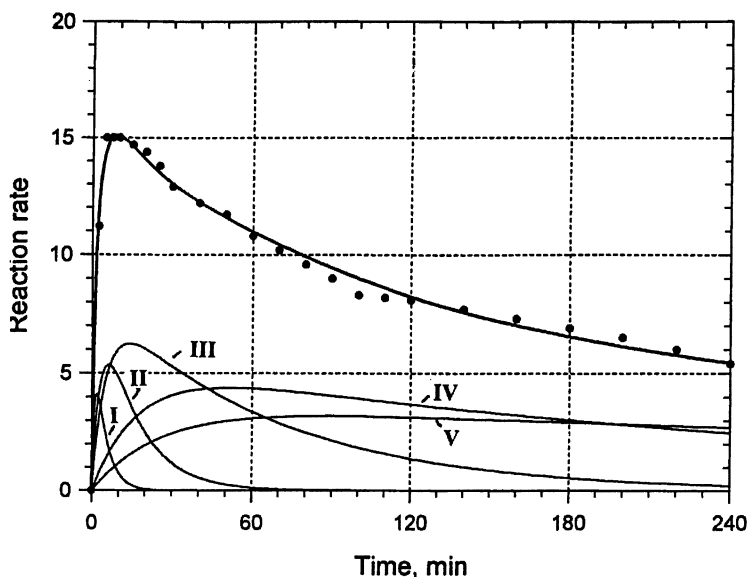


Fig. 2. Kinetics of ethylene/1-hexene copolymerization reaction at 85°C in the absence of H_2 at $C_E = 0.556$ M, $C_{Hex} = 1.12$ M. Points - experimental data, lines - calculated reaction rates for each type of active center

1.6-1.7.

3. Experiments in the slurry in which P_E was increased step-wise from 0.2 to 1.1 MPa in the course of a single run gave $n = 1.8-1.9$.
4. Several multi-stage gas-phase polymerization experiments during which the reaction pressure was repeatedly changed gave $n \sim 1.8$.

We also evaluated the reaction order with respect to C_E within the framework of the multi-center catalyst model. Two methods were used, (a) measuring the product of the total polymer yield, $Q(t_r)$, and the content of a given Flory component (this product corresponds to the output of a given active center as a function of C_E), and (b) from k_{eff} values. The data in Table 2 show that the reaction order for the centers with the highest reactivity, centers III, IV and V, with respect to C_E is significantly higher than one and can approach the second order.

Table 2. Reaction orders with respect to C_E for different centers

| Reaction order n | Center III | Center IV | Center V |
|-----------------------|------------|-----------|----------|
| From component yields | 1.7 | 1.8 | 2.2 |
| From k_{eff} values | 1.5 | 1.6 | 2.1 |

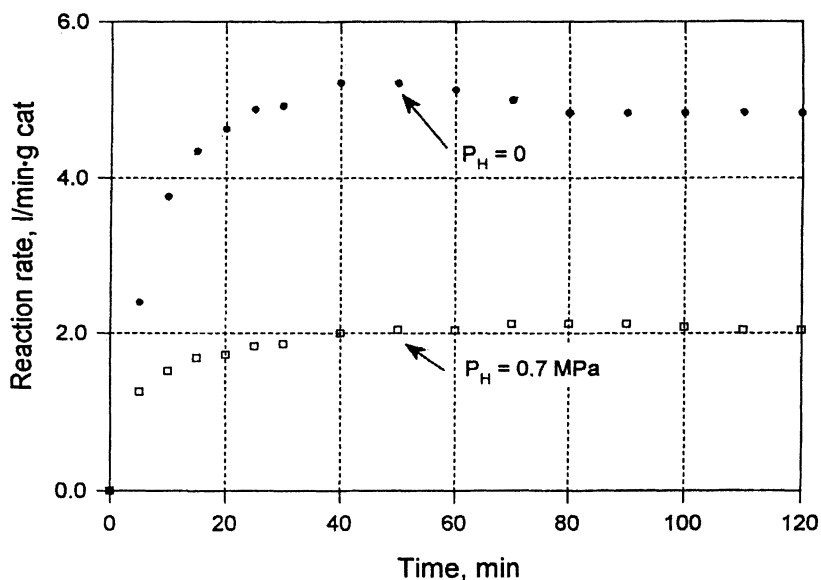


Fig. 3. Hydrogen effect on ethylene homopolymerization kinetics at 80°C, $P_E = 0.38$ MPa

3.3 Hydrogen Effects on Ethylene Homopolymerization

Hydrogen significantly (and reversibly) reduces ethylene polymerization rates (Fig. 3) and, of course, reduces molecular weights of the polymers [3]. Table 3 gives the magnitude of the last effect for each type of active center in 1-hour reactions at 80°C. The data in the last column of Table 3 show that hydrogen depresses activities of all active centers nearly equally and, as a result, their contributions to the overall catalyst productivity remain mostly unaffected.

Table 3. Hydrogen effect on molecular weights of Flory components

| P_H | P_E | Center | M_w | Fraction |
|----------|----------|--------|-----------|----------|
| 0 MPa | 0.38 MPa | I | 10,700 | 3.2% |
| | | II | 47,500 | 10.6% |
| | | III | 146,600 | 27.0% |
| | | IV | 462,800 | 38.0% |
| | | V | 1,577,000 | 21.1% |
| 0.69 MPa | 0.38 MPa | I | 1,550 | 2.6% |
| | | II | 6,200 | 9.2% |
| | | III | 18,500 | 24.9% |
| | | IV | 50,300 | 45.2% |
| | | V | 145,800 | 18.0% |

3.4 Ethylene/1-Hexene Copolymerization Kinetics

Copolymerization reactions of ethylene and α -olefins activate much faster and initially proceed at much higher rates; however, at longer reaction times, effective rates in both types of reactions become similar (Fig. 4). As the reaction progresses, the content of an α -olefin in copolymers declines. GPC measurements showed that molecular weights of Flory components in both types of reactions, homo- and copolymerization, are approximately the same, especially for the material produced by centers III, IV and V. The main difference between homopolymerization and copolymerization reactions lies in relative contributions from each center: when an α -olefin is present, relative contributions of centers IV and V decrease whereas relative contributions of centers I, II and III increase.

These changes afford a simple qualitative explanation: α -olefins activate centers I, II, and III but do not significantly affect centers IV and V. Because centers I, II and III decay relatively rapidly (Fig. 2), mostly centers IV and V remain active after ca. 2-3 hours both in homopolymerization and in copolymerization reactions, and the latter centers have similar activities independent of the presence of an α -olefin. For this reason, relative contents of Flory components produced by centers IV and V gradually increase with time at the expense of material produced by centers I, II and III. Table 4 gives kinetic parameters of different centers in ethylene/1-hexene copolymerization reactions at 85°C in the absence of hydrogen. 1-Hexene does not affect reactivities of centers IV and V (they poorly copolymerize olefins with ethylene) but greatly increases k_{eff} values of centers I, II and III. 1-Hexene also increases formation rate constants of most centers (unfortunately, these values cannot be estimated with a good precision).

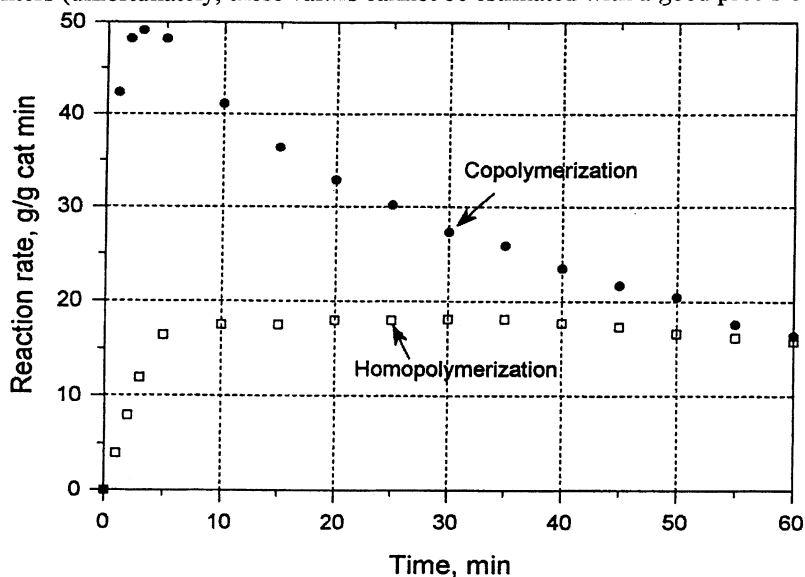


Fig. 4. Comparison of ethylene homopolymerization and copolymerization kinetics at 85°C

Table 4. Kinetic parameters of active centers in ethylene/1-hexene copolymerization reactions at 85°C in the absence of hydrogen

| | | | |
|----------------------------|--------------------------------|--------|--------|
| Ethylene concentration, M: | | 0.482 | 0.529 |
| 1-Hexene concentration, M: | | 0 | 2.24 |
| Center I | k_{eff} , l/g cat·min | 0.034 | 0.205 |
| | k_f , min ⁻¹ | 0.540 | ~10 |
| | k_d , min ⁻¹ | 0.070 | 0.070 |
| Center II | k_{eff} , l/g cat·min | 0.082 | 0.237 |
| | k_f , min ⁻¹ | 0.15 | 2.41 |
| | k_d , min ⁻¹ | 0.018 | 0.018 |
| Center III | k_{eff} , l/g cat·min | 0.128 | 0.443 |
| | k_f , min ⁻¹ | 0.04 | 0.95 |
| | k_d , min ⁻¹ | 0.007 | 0.013 |
| Center IV | k_{eff} , l/g cat·min | 0.211 | 0.247 |
| | k_f , min ⁻¹ | 0.060 | 0.20 |
| | k_d , min ⁻¹ | 0.0009 | ~0.004 |
| Center V | k_{eff} , l/g cat·min | 0.156 | 0.128 |
| | k_f , min ⁻¹ | 0.04 | 0.19 |
| | k_d , min ⁻¹ | 0.0009 | 0.0009 |

3.5 Hydrogen Effects on Copolymerization Kinetics

Hydrogen effects in ethylene/1-hexene copolymerization reactions are, in general terms, similar to those in ethylene homopolymerization reactions (see above).

- Centers I, II, and III remain quite unstable whereas centers IV and V are much more stable. The decay rates of the centers are unaffected by hydrogen. Because of the differences in the decay rates, the average 1-hexene content in the copolymers produced in the presence of hydrogen, $[1\text{-Hexene}]_{\text{copol}}$, decreases as copolymerization reactions progress (Table 5).
- Copolymerization abilities of different centers vary in a wide range independent upon the presence of hydrogen in the reaction, as shown in Table 6.

Table 5. Copolymer composition vs. reaction time. Copolymerization reaction at 85°C in the presence of hydrogen

| | | | | | |
|--|-----|------|------|------|-----|
| Time, min: | 5 | 15 | 60 | 120 | 240 |
| Normalized yield, %: | 6.0 | 17.2 | 47.8 | 69.2 | 100 |
| $[1\text{-Hexene}]_{\text{copol}}$, mol. %: | 3.4 | 2.6 | 2.2 | 2.1 | 2.0 |

Table 6. Copolymer compositions of Flory components (reaction at 85°C, $C_E/C_{Hex} = 0.237$ in the presence of hydrogen) and reactivity ratios r_1 of different centers

| Flory component: | I | II | III | IV | V |
|---------------------------------------|-------|---------|---------|------|-------|
| [1-Hexene] _{copol} , mol. %: | 7-8 | 3.5-3.9 | 2.9-3.4 | ~0.5 | ~0.3 |
| r_1 : | 45-55 | 100-115 | 120-140 | ~800 | ~1400 |

Centers IV and V copolymerize ethylene with α -olefins extremely poorly and produce virtually linear polyethylene even in the presence of high α -olefin concentrations.

These differences in the properties of various active centers are similar to those found earlier for other supported Ti-based catalysts [16] in ethylene copolymerization reactions and they are probably universal for all such catalysts. Kinetic analysis of ethylene/1-hexene copolymerization reactions in the presence of hydrogen reveals an additional subtle kinetic effect: whereas hydrogen decreases activities of all types of active centers in ethylene homopolymerization reactions to approximately the same extent (see Table 3), it does not affect reactivities of centers I, II and III anymore if an α -olefin is present, as shown in Table 7.

Table 7. Reactivities of active centers. Ethylene/1-hexene copolymerization reactions at 85°C, $C_E = 0.51-0.55$ M and $C_{Hex} = 1.12$ M for 1 hour

| Hydrogen conc., M | 0 | 0.0204 | 0.0400 |
|--------------------------------------|--------|-----------------------|--------|
| [1-Hexene] _{copol} , mol. % | 0.6 | 1.2 | 1.3 |
| | | Yields, g/g cat-hour: | |
| Center I | 58.1 | 79.5 | 40.6 |
| Center II | 249.7 | 264.6 | 249.9 |
| Center III | 714.4 | 868.3 | 767.7 |
| Center IV | 1213.9 | 639.8 | 459.3 |
| Center V | 667.9 | 133.1 | 105.5 |

4 Kinetic Interpretation of Ethylene Polymerization Reactions

The following peculiarities of ethylene polymerization reactions should be accounted for in a comprehensive kinetic mechanism:

1. In ethylene homopolymerization reactions, most active centers have the effective reaction order with respect to C_E greatly exceeding one and often close to two.

2. In ethylene/ α -olefin copolymerization reactions, the centers which have a poor copolymerization ability (centers IV and V) retain the same high reaction order whereas the centers that have a good copolymerization ability decrease the reaction order to one.
3. In homopolymerization reactions, introduction of hydrogen depresses reactivities of all centers in a reversible manner and to approximately the same degree. However, reactivities of centers that copolymerize ethylene and α -olefins well (centers I, II and III) are not depressed when an α -olefin is present.
4. Introduction of an α -olefin significantly increases activity of centers which are capable of copolymerization (centers I, II and III) but does not affect centers that copolymerize α -olefins poorly (centers IV and V).

All these features of ethylene polymerization reactions can be reconciled if one introduces a single assumption about the reaction mechanism, that the Ti-C₂H₅ bond (a growing polymer chain with one ethylene unit attached to the Ti atom) is unusually stable. As a hypothesis, we propose that the stability of the Ti-C₂H₅ bond is the result of a relatively strong β -agostic interaction between one of the hydrogen atoms of its methyl group and the Ti atom.

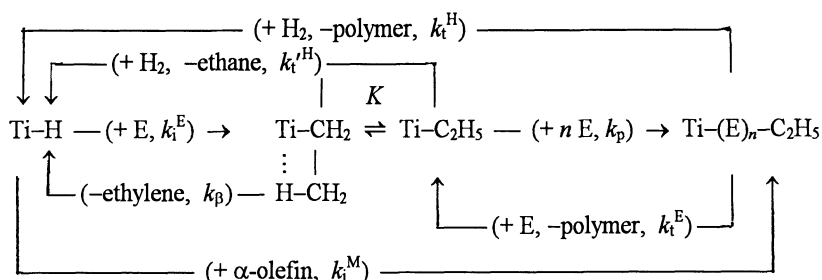
Literature data on model olefin insertion reactions into metal-carbon bonds indeed show the existence of some β -agostically stabilized complexes containing ethyl groups:

1. A strongly β -agostic Co complex [(C₅H₅)Co[P(OMe)₃(CH₂-CH₂)H]⁺ coordinates an ethylene molecule by breaking the Co...H bond and then inserts the coordinated molecule into the Co-C bond [18].
2. The ethylene insertion rate into the Sc-C bond in the (C₅Me₅)₂Sc-C₂H₅ complex at -80°C is 14 times lower than that for the (C₅Me₅)₂Sc-C₃H₇ complex due to β -agostic stabilization of the former complex [19].
3. Theoretical calculations [20,21] confirm the existence of β -agostic interactions in various [(C₅H₅)₂Zr-R]⁺ complexes, although reasons for a stronger agostic interaction of a β -CH₃ group vs. a β -CH₂ group we observe are not clear.

Scheme 1 shows the proposed kinetic scheme of ethylene polymerization reactions. It differs from the standard kinetic schemes in the following respects:

1. Based on preliminary kinetic analysis, we assume that the equilibrium in the reaction between the non-coordinated Ti-C₂H₅ group and the β -agostically stabilized Ti-C₂H₅ group strongly favors the stabilized species.
2. Only the non-coordinated Ti-C₂H₅ species can insert ethylene whereas the β -agostically stabilized Ti-C₂H₅ group is inert.
3. A reaction between the Ti-H bond and ethylene immediately produces the stabilized Ti-C₂H₅ group.
4. The stabilized Ti-C₂H₅ group may undergo β -hydride elimination producing an ethylene molecule and forming the Ti-H bond even in the absence of hydrogen.

This kinetic scheme affords a uniform explanation of most observed kinetic effects. For example, the rate-depressing effect of hydrogen is explained as due to the formation of the stabilized Ti-C₂H₅ group from the Ti-H group. Stabilized



Scheme 1. Kinetic model of ethylene polymerization reactions

Ti-C₂H₅ groups can react with hydrogen with the formation of ethane, a kinetic feature which explains the disproportionately high yields of ethane in ethylene polymerization reactions. Finally, when α -olefin is present in a reaction system, it inserts into the Ti-H bond with the immediate formation of the Ti-Polymer bond and thus bypasses the β -agostically stabilized Ti-C₂H₅ bond.

The proposed kinetic mechanism predicts two chemical/kinetic features of ethylene homopolymerization and copolymerization reactions which were not described earlier:

1. If one uses D₂ instead of H₂ in ethylene homopolymerization reactions, then, in addition to polymer molecules with two deuterium atoms on the ends of each polymer chain (due to chain transfer with deuterium and chain re-initiation with Ti-D species), Ziegler-Natta catalysts should generate deuterium-substituted ethylene molecules because, after the Ti-CH₂-CH₂D species is formed, an exchange between β -agostically coordinated C-H and C-D bonds followed by β -hydride elimination should produce free CH₂=CHD molecules. Deuterated ethylene has approximately the same reactivity as CH₂=CH₂ and a large part of it should be incorporated into polyethylene chains.
2. Scheme 1 predicts that chain initiation via the insertion of any α -olefin into the Ti-H bond should proceed with a relatively increased probability vs. the ethylene insertion into the same bond.

5 Structure of Ethylene Polymers Produced with Deuterium

To verify the first of the predictions, several ethylene homopolymerization reactions were carried with the same catalyst in the presence of large quantities of deuterium. Analysis of the reaction products, both gases and the homopolymers, showed that the products formed in the presence of deuterium differ from the products formed in the presence of hydrogen under the same conditions:

1. GC/MS analysis of the gas phase showed that both its major components, ethane and ethylene, have deuterium atoms:

Ethylene: ca. 2.2 % has formula C₂H₃D and ca. 1.1% C₂H₂D₂.

Ethane (20% of gas phase): most molecules contain one to three D atoms. (One should keep in mind that, according to the standard polymerization scheme, only formation of 1,2-dideuterated ethane is expected.)

The large yield of deuterated ethanes and the presence of several deuterium-substituted isomers can be readily explained in Scheme 1 by the existence of a large concentration of stabilized $\text{Ti-C}_2\text{H}_{5-x}\text{D}_x$ groups.

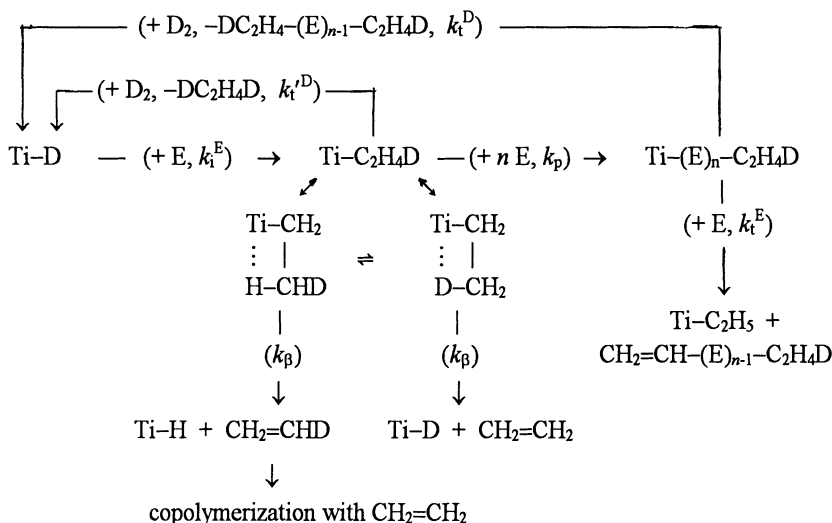
- IR analysis of the gas products confirmed the results of the GC/MS analysis: the spectra contain bands due to ν_7 (b_{1u}) modes [22,23] of three deuterated ethylenes, $\text{CH}_2=\text{CHD}$ (main component), $\text{CH}_2=\text{CD}_2$, and *cis*- and *trans*- $\text{CHD}=\text{CHD}$.
- IR spectra of polyethylenes prepared in the presence of D_2 have several rocking mode bands of deuterated units [24-26]:
 - isolated $-\text{CHD}-$ groups (major component), at 660 cm^{-1} ,
 - $-\text{CH}_2-\text{CHD}-\text{CHD}-\text{CH}_2-$ sequences, at 621 and 615 cm^{-1} ,
 - $-\text{CD}_2-\text{CHD}-$ and $-\text{CH}_2-\text{CD}_2-\text{CD}_2-\text{CH}_2-$ (minor comp.), 588 and 560 cm^{-1} .
- The ^{13}C NMR spectrum of one of the polymers prepared in the presence of D_2 showed the presence of $-\text{CH}_2\text{D}$ and $-\text{CH}_3$ chain ends in a ratio of ca. 1:2. The CH_3 end-groups are due to $\text{Ti}\cdots\text{H} \leftrightarrow \text{Ti}\cdots\text{D}$ isomerization in the β -agostically stabilized ethyl group followed by formation of the $\text{Ti}-\text{H}$ bond. Accordingly, the α - CH_2 region in the spectrum exhibited two peaks assigned to $-\text{CH}_2(\text{CH}_2\text{D})$ and $-\text{CH}_2(\text{CH}_3)$ groups, also in the 1:2 ratio.
- The ^2H NMR spectrum showed two broad signals, one arising from $-\text{CH}_2\text{D}$ groups, at 0.9 ppm, and another due to $-\text{CHD}-$ groups, at 1.4 ppm.

All these effects are explained in Scheme 2 which represents the extension of Scheme 1 in the case of deuterium-affected reactions. Formation of dideuterated ethylenes can be similarly explained by H-D exchange reactions in β -agostically stabilized $\text{Ti}-\text{CH}_2-\text{CH}_2\text{D}$ species.

6 Chain Ends in Ethylene/ α -Olefin Copolymers

Scheme 1 predicts that the chain initiation via insertion of any α -olefin molecule into the $\text{Ti}-\text{H}$ bond should proceed with an increased effective probability vs. ethylene insertion into the $\text{Ti}-\text{H}$ bond, when these reactions are compared to respective chain growth reactions. As a result, an unproportionally high fraction of polymer chains in ethylene/ α -olefin copolymerization reactions should contain α -olefin units as "starting" units in polymer chains. These effects can be directly examined if the polymer molecules are very short and are easily distinguished one from another [27]. Some copolymer molecules formed by Ti-based Ziegler-Natta catalysts (mostly those produced by center I) have very low molecular weights and are, in effect, oligomers. Analysis of the oligomers is a key to determining structures of "starting" chain-ends. To produce oligomers in significant quantities (0.2-

0.4% of a polymer yield), copolymerization reactions were carried out at a high P_H , ca. 0.7 MPa. In such reactions, most chains are terminated in chain transfer with hydrogen and the Ti-H species is the principal chain initiation center.



Scheme 2. Ethylene homopolymerization reactions in the presence of deuterium

In order to determine unambiguously the precise structures of the shortest polymer molecules (oligomers) formed in ethylene copolymerization reactions with α -olefins, we chose olefins (OL) which produce chain ends different from those in ethylene homo-oligomers: 1-pentene (Fig. 5) and 4-methyl-1-pentene. This choice can be demonstrated by comparing the most important oligomer structures:

Ethylene homo-oligomers H-E_x-H:

H-(CH₂-CH₂)_{x-1}-CH₂-CH₃, n -alkanes with even C_n (n -C₁₂ and n -C₁₄ in Fig. 5).

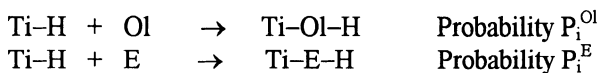
Ethylene/ α -olefin co-oligomers with the "starting" α -olefin unit, H-E_x-OL-H: in ethylene/1-pentene copolymerization reaction,

H-(CH₂-CH₂)_x-CH₂-CH₂-C₃H₇, n -alkanes with odd C_n (n -C₁₃ in Fig. 5).

in ethylene/4-methyl-1-pentene copolymerization reaction,

H-(CH₂-CH₂)_x-CH₂-CH₂-CH₂-CH(CH₃)₂, 2-methyl-branched alkanes.

Calculations of relative probabilities of the "starting" reactions with ethylene and with an α -olefin (their insertion reactions into the Ti-H bond) were carried out as described elsewhere [28]:



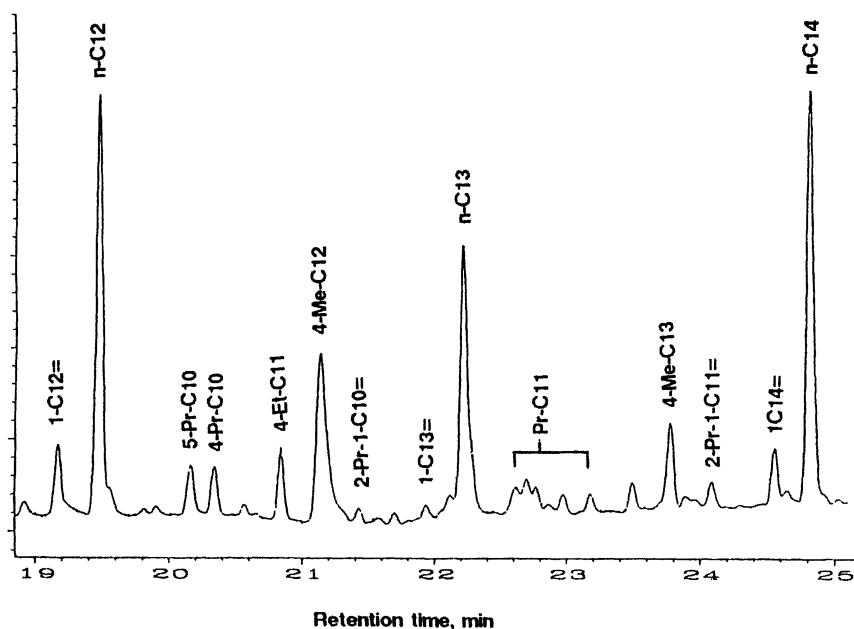
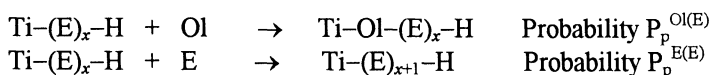


Fig. 5. GC (C_{12} - C_{14} range) of ethylene/1-pentene co-oligomers. n - C_{12} and n - C_{14} - ethylene homo-oligomers, n - C_{13} - co-oligomer with the "starting" 1-pentene unit, 4-Me- C_{12} - co-oligomer with the "end"-1-pentene unit

Probabilities of chain propagation reactions (insertion of ethylene and an α -olefin into the Ti-C bond) were calculated in a similar manner from the relative contents of all oligomer molecules produced in a series of steps after the following reactions:



The results of these estimations confirmed the second conclusion from the reaction mechanism in Scheme 1: the probabilities of chain initiation reactions with both α -olefins are significantly higher than the relative probabilities of chain growth reactions with the same olefins: in ethylene/1-pentene co-oligomerization, the $P_i^{\text{Ol}}/P_i^{\text{E}}$ ratio is 5-6 times higher than the average $P_p^{\text{Ol(E)}}/P_p^{\text{E(E)}}$ value, and, in ethylene/4-methyl-1-pentene co-oligomerization, the $P_i^{\text{Ol}}/P_i^{\text{E}}$ value is 7-8 times higher than the average $P_p^{\text{Ol(E)}}/P_p^{\text{E(E)}}$ value. These conclusions are supported by the ^{13}C NMR study of the ethylene/4-methyl-1-pentene copolymer. The spectrum shows a prominent fraction of chain ends starting with 4-methyl-1-pentene units inserted into the Ti-H bond (structure C in Fig. 6).

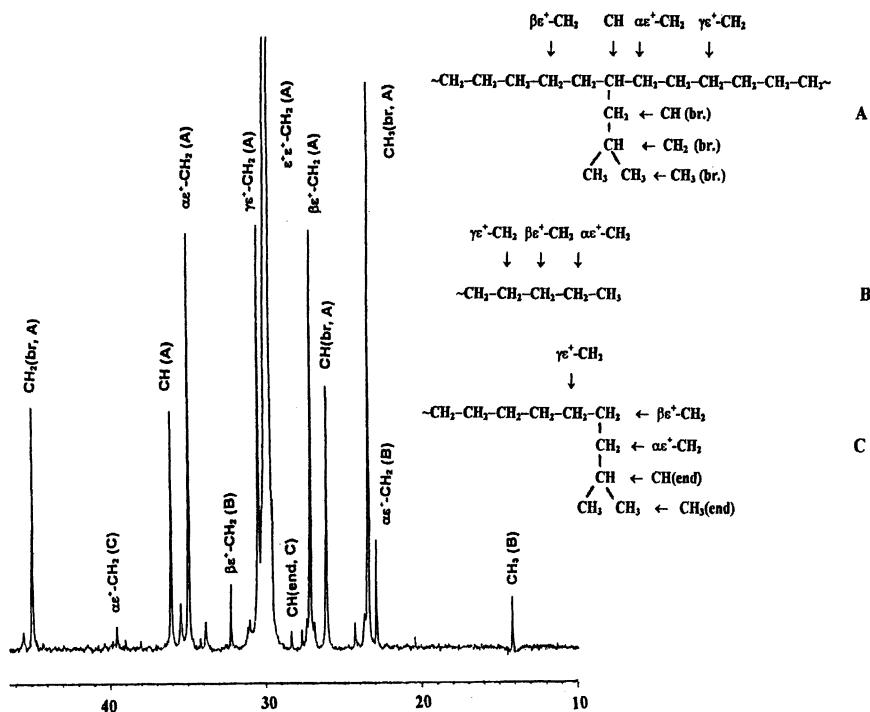


Fig. 6. ^{13}C NMR spectrum of ethylene/4-methyl-1-pentene copolymer. Peak assignment is based on calculations according to refs. 29 and 30. A - main-chain 4-methyl-1-pentene unit, B - ethylene "starting" unit, C - 4-methyl-1-pentene "starting" unit

7 Acknowledgments

The experimental work of J. Garlick and J. Fisher (polymer synthesis), B. Harrison and J. Orvos (GPC measurements), and M. Brezina (NMR spectroscopy) is greatly appreciated. GC/MS analysis was carried out by Dr. T. G. Hartman (Rutgers University). The authors thank Professors J. C. W. Chien (University of Massachusetts) and W. Piers (University of Calgary, Canada) for their helpful discussions.

8 References

1. Kissin YV (1985) *Isospecific Olefin Polymerization with Heterogeneous Ziegler-Natta Catalysts*, Springer Verlag, New York, 1985.
2. Kissin YV (1983) In Quirk RP (ed) *Transition Metal Catalyzed Polymerizations: Alkenes and Dienes*, Harwood Academic Publishers, New York, Part B, p. 597.
3. Krentsel BA, Kissin YV, Kleiner VI, Stotskaya LL (1997) *Polymers and Copolymers of Higher Alpha-Olefins*, Hanser Publishers, Munich.
4. Munoz-Escalona A, Garcia H, Albornoz A (1987) *J Appl Polym Sci* 34: 977.

5. Calabro DC, Lo FY (1988), In Quirk RP (ed) Transition Metal Catalyzed Polymerizations. Ziegler-Natta and Metathesis Polymerizations, Cambridge University Press, New York, p. 729.
6. Kissin YV (1989) *J Molec Catal* 46: 220.
7. Wang JG, Zhang WB, Huang BT (1992) *Makromol Chem, Macromol Symp* 63: 245.
8. Tait PJT, Downs GW, Akinbami AA (1988), In Quirk RP (ed) Transition Metal Catalyzed Polymerizations. Ziegler-Natta and Metathesis Polymerizations, Cambridge University Press, New York, p. 834.
9. Bobrov BN, Echevskaya LG, Kleiner VI, Zakharov VA, Krentsel BA (1990) *Vysokomol Soed B32*: 457.
10. Koivumaki J, Seppala JV (1993) *Macromolecules* 215: 535.
11. Stanovaya SS, Kreitser TV, Sigalova GS, Ivanchev SS (1986) *Vysokomol Soed B28*: 174.
12. Han-Adebkun GC, Ray WH (1997) *J Appl Polym Sci* 65: 1037.
13. Kryzhanovskii AF, Gapon II, Ivanchev SS (1990) *Kinetics & Catalysis* 31: 90.
14. Mink RI, Nowlin TE (1995) US Patent 5,470,812.
15. Kissin YV (1995) *J Polym Sci, Part A: Polym Chem* 33: 227.
16. Kissin YV (1993) *Makromol Chem, Macromol Symp* 66: 83.
17. Kissin YV (1995) *Macromol Chem, Macromol Symp* 89: 113.
18. Brookhart M, Schmidt GF, Lincoln MD, Rivers D (1988) In Quirk RP (ed) Transition Metal Catalyzed Polymerizations. Ziegler-Natta and Metathesis Polymerizations, Cambridge University Press, New York, p. 497.
19. Burger BJ, Thompson ME, Cotter WD, Bercaw JE (1990) *J Amer Chem Soc* 112: 1566.
20. Lohrenz JCW, Woo TK, Ziegler T (1995) *J Amer Chem Soc* 117: 12793.
21. Margl P, Lohrenz JCW, Ziegler T, Blöschl PE (1996) *J Amer Chem Soc* 118: 4434.
22. Crawford BL, Lancasrer JE, Inskiep RG (1953) *J Chem Phys* 21: 678.
23. Whitfield RG, Leroi GE (1978) *J Chem Phys* 68: 4384.
24. Ikeda S, Yamamoto A, Tanaka H (1963) *J Polym Sci, Part A-1*: 2925.
25. Tasumi M, Shimanouchi T, Kenjo H, Ikeda S (1966) *J Polym Sci, Part A-1* 4: 1011.
26. Tasumi M, Shimanouchi T, Ikeda S (1966) *J Polym Sci, Part A-1* 4: 1023.
27. Kissin YV, Nowlin TE, Mink RI (1993) *Macromolecules* 26: 2151.
28. Kissin YV, Mink RI, Nowlin TE, Brandolini AJ *J Polym Sci*, in press.
29. Grant DM, Paul EG (1964) *J Amer Chem Soc* 86: 2984.
30. Carman CJ, Tarpley AR, Goldstein JH (1973) *Macromolecules* 6: 719.

New insight into propene polymerization promoted by heterogeneous Ziegler-Natta catalysts

Vincenzo Busico^{*a)}, Roberta Cipullo^{a)}, Guglielmo Monaco^{a)}, Giovanni Talarico^{a)}, Michele Vacatello^{a)}, John C. Chadwick^{b)}, Anna Laura Segre^{c)}, Olof Sudmeijer^{d)}

^{a)}Dipartimento di Chimica - Università di Napoli «Federico II»

Via Mezzocannone, 4 - 80134 Napoli (Italy)

^{b)}Montell Polyolefins – Centro Ricerche «Giulio Natta»

Piazzale Donegani, 12 - 44100 Ferrara (Italy)

^{c)}Istituto di Strutturistica Chimica e Servizio NMR del CNR - Area della Ricerca di Roma
C.P. 10 - 00165 Monterotondo Stazione (Italy)

^{d)}Shell Research and Technology Centre, Amsterdam (Shell International Chemicals, B.V.)
P.O. Box 38000 – 1030 BN Amsterdam (The Netherlands)

SUMMARY:

The configurational analysis of polypropylenes made with coordination catalysts has received a tremendous impulse by the recent application of high-field ¹³C NMR techniques. In particular, unprecedented determinations of stereosequence distribution at heptad/nonad level have made more realistic and sophisticated models of chain propagation applicable for the first time in a statistically significant manner. In this presentation, the most recent applications to «high-yield» MgCl₂-supported Ziegler-Natta catalysts are illustrated.

Introduction

In the stereochemical study of 1-alkene polymerizations promoted by heterogeneous Ziegler-Natta catalysts, NMR spectroscopy represents an indirect but most powerful tool for the mechanistic investigation of active species which remain inaccessible to a direct observation [1].

The concept of polymer chain microstructure as a catalyst «fingerprint» dates back to the early 60's, when pioneering studies of ¹H NMR provided the first information on the configuration of stereoregular vinyl polymers at *triad* level, and it was recognized that different mechanisms of chain propagation may result in distinctive triad distributions [2,3]. For isotactic propagation, in particular, it was shown that the two simple limiting cases in which the stereocontrol is exerted by the configuration of the last-inserted monomeric unit of the growing chain («chain-end» control [2]) or by the chirality of the transition metal active species («enantiomorphic-sites» control [3]) correspond to the formation of stereoerrors of the type ...*mmmmrrmmmm*... and ...*mmmmrrrrmmmm*..., respectively.

In the case of poly(1-alkene)s, whose ^1H NMR spectra in the latter respect are relatively uninformative [4], this approach had to wait ten years more, till the development of FT ^{13}C NMR.

However, from the very first experiments on polypropylene with rather primitive low-field spectrometers [5], it became clear that the new technique was able to provide stereochemical information at an unprecedented *pentad* level.

This easily allowed the origin of highly isotactic control in Ziegler-Natta polymerization to be traced to the intrinsic chirality of the active species [1], in agreement with the hypothesis of Cossee and Arlman [6], and also opened the way to more complex studies, such as the stereochemical analysis of the «atactic» by-products in terms of multi-site statistical models [1,7].

Elegant studies on polymers at natural isotope abundance or selectively enriched in ^{13}C rapidly led to a thorough understanding of the mechanisms of asymmetric induction in Ziegler-Natta catalysis, and provided the experimental basis for the development of the first realistic models of active sites, made possible by innovative applications of molecular mechanics [1].

Twenty years after these brilliant achievements, the microstructural approach has still a long way to go. Indeed, with the advent of high-field spectrometers, the resolution in polypropylene analysis has now reached the *heptad/nonad* level [8,9].

In our laboratories, high-field ^{13}C NMR has been applied for the first time to the stereochemical investigation of MgCl_2 -supported «high-yield» catalysts for propene polymerization [8]. In this presentation, we report the results of a comparative high-resolution ^{13}C NMR microstructural analysis of an «atactic» and an «isotactic» polypropylene fraction prepared with a MgCl_2 -supported catalyst, from which we derive new insight in the structure of the polymer and – correspondingly – in the behaviour of the catalytic species.

Results and Discussion

Choice of the polypropylene fractions

Heterogeneous Ziegler-Natta catalysts contain different classes of active species, some of which undergo reversible interconversions. As a result, they afford polypropylenes which are complicated mixtures of highly isotactic, poorly isotactic («isotactoid») and syndiotactic sequences, at least in part chemically linked to form stereoblock chains [1,8,10].

A rough but practical method for evaluating the stereoregularity of a given polymer sample is to measure the weight fraction that is insoluble in a certain solvent under certain conditions and as such is conventionally referred to as «isotactic» [1]. Two popular (and substantially equivalent) procedures are extraction with boiling heptane and crystallization from xylene solution. Although it is well known that polymer solubility depends on the molecular mass as well, it is commonly assumed that in the range of average molecular masses of commercial grade polypropylenes this dependence is only marginal, and that the fractionation is mainly governed by tacticity [1]; as a matter of fact, typical «isotactic» fractions (*i.e.*, heptane- or xylene-insoluble) have a content of *mmmm* pentads (measured by ^{13}C NMR) in excess of 90% [10j,o].

The soluble polymer fraction, in turn, is often referred to as «atactic», although it has long been recognized that this notation is not appropriate. Indeed, no truly atactic chains are found in such fraction, which contains instead isotactic and syndiotactic sequences [1,7,8,10].

Quite surprisingly, however, recent ^{13}C NMR investigations proved that most «isotactic» fractions are also stereoblock materials, in which very long blocks of almost ideal isotacticity are spanned by short syndiotactic blocks [8b,10 l-p].

Thus, it is now being realized that the difference between «isotactic» and «atactic» polypropylene is less clearcut than has been assumed, and that the mechanisms of stereocontrol leading to their formation are intimately related.

For our investigation, we selected a diethylether-insoluble/pentane-soluble fraction (A) and a xylene-insoluble fraction (B) of a polypropylene sample prepared in the presence of the catalyst system $\text{MgCl}_2/\text{TiCl}_4 - 2,6\text{-dimethylpyridine}/\text{Al}(\text{C}_2\text{H}_5)_3$ [8d]. This system is peculiar in that it affords polypropylenes with relatively high contents of crystallizable syndiotactic sequences both in soluble and insoluble fractions; therefore, in the statistical analysis of polymer configuration, it can be assumed that the average length of such sequences is high enough to neglect the possible presence of block junctions, that would represent a major source of complication.

We also checked that in both fractions the concentration of chain end-groups is below the limit for ^{13}C NMR detectability ($M_v = 1.5 \times 10^5$ dalton for fraction A, 5.7×10^5 dalton for fraction B).

Configurational analysis of the «atactic» fraction A

In Fig. 1, we compare the methyl resonance of fraction A, as it appears in

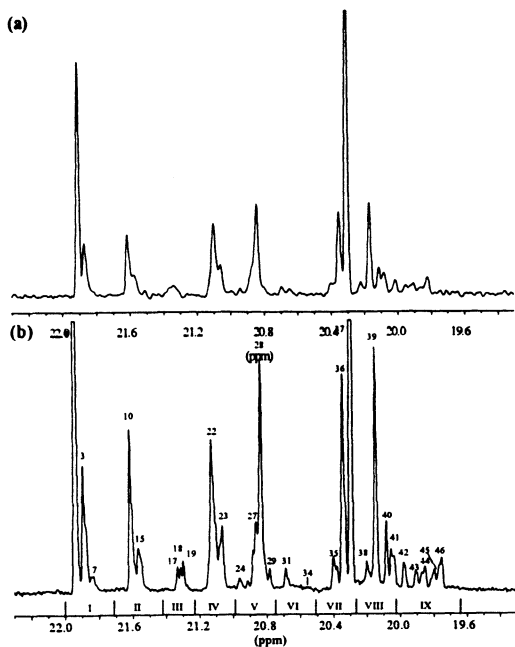


Figure 1 ^{13}C NMR spectra (methyl region) of polypropylene fraction A (see text), at 100 MHz (a) and 150 MHz (b). The chemical shift scale is in ppm downfield of TMS. Peak numbering in the latter spectrum refers to the assignment given in ref. 9a.

a «routine» ^{13}C NMR spectrum recorded at 100 MHz (a) and in a high-resolution spectrum run at 150 MHz (b). In both cases, the acquisition temperature was 70°C .

In the former spectrum, the nine multiplets corresponding to the ten non equivalent steric pentads are significantly overlapped. Any attempt of deconvolution is precluded by the fact that the fine structure is largely hidden; as a result, the evaluation of the pentad distribution is affected by a relatively large uncertainty (Tab. 1).

Table 1 – 100 MHz ^{13}C NMR pentad distribution of polypropylene fraction A, and best-fit distribution in terms of the ES/CE model (see text).

| <i>Pentad</i> | <i>Normalized fraction</i> | |
|--------------------|----------------------------|-------------------|
| | <i>Experimental</i> | <i>Calculated</i> |
| <i>mmmm</i> | .183 (10) | .1863 |
| <i>mmmr</i> | .075 (10) | .0824 |
| <i>rmmr</i> | .022 (10) | .0148 |
| <i>mmrr</i> | .103 (10) | .0898 |
| <i>mmrm + rrmr</i> | .106 (10) | .1178 |
| <i>rmrmm</i> | .018 (10) | .0296 |
| <i>rrrr</i> | .338 (10) | .3387 |
| <i>rrrm</i> | .104 (10) | .0956 |
| <i>mrrm</i> | .050 (10) | .0449 |

$$\Sigma(y_i - y_i^0)^2 \times 10^4 = 6.6$$

$$\chi_r^2 = 1.1$$

$$\sigma = 0.82$$

$$P_r = 0.90$$

$$w = 0.50$$

It is common practice to reproduce such data in terms of a simple two-site model, which assumes the sample to be a physical mixture of two basic types of stereosequences: predominantly isotactic (or «*m*-rich» or isotactoid) and predominantly syndiotactic (or «*r*-rich» or syndiotactoid) [7,10]. The configuration of the former is described in terms of the enantiomorphic-sites (ES) statistics [3]; that of the latter, in terms of the chain-end (CE) statistics [2]. The underlying mechanistic implication is that the stereocontrol of isotactic propagation is exerted by intrinsically chiral transition metal active species, whereas syndiotactic propagation would be due to a 1,2-*unlike* (*ul*) asymmetric induction involving the last-inserted monomeric unit of the growing chain.

The model has only three adjustable parameters: σ , conditional probability of monomer insertion with the preferred enantioface during site-controlled isotactoid propagation; P_r , conditional probability of generating a *r* diad during chain-end controlled syndiotactic propagation; w , weight fraction of isotactoid sequences.

When the analysis is limited to the steric pentads, it is easy to solve in the

least-squares sense the overdetermined set of equations that give the probability of occurrence for each single pentad [7]. For the data in Tab. 1, as shown in the same table, this results in a value of the χ_r^2 function close to 1, which means that the model is adequate and that more complex ones, necessarily requiring a higher number of adjustable parameters, lead to overfitting.

The situation changes completely when high resolution ^{13}C NMR data like those of Fig. 1-b are available. Although the complete fine structure at nonad/undecad level is not accessible even at 150 MHz, all nine multiplets corresponding to the steric pentads are well separated, and a number of peaks associated with longer sequences (heptads and, to some extent, nonads) can be deconvoluted and integrated with good accuracy; moreover, additional information can be obtained from the methylene and methine resonance [8,9].

In the examined case, we were able to extract 27 independent normalized integrals corresponding to a collection of steric nads from pentads to nonads (Tab. 2, columns 1-3). The evaluation of the experimental uncertainty was made with integration codes specifically developed for spectral patterns of intrinsically low resolution [11].

When the data in Tab. 2 are subjected to statistical analysis in terms of the «ES/CE» two-site model (in this case, matrix multiplication methods are more convenient, as is described in ref. 8c), the fit is far from being satisfactory, as the unacceptably high value of χ_r^2 (= 18.5) indicates.

Table 2 – 150 MHz ^{13}C NMR stereosequence distribution of polypropylene fraction A, and best-fit ones in terms of various statistical models (see text and ref. 9 for range and peak numbering)

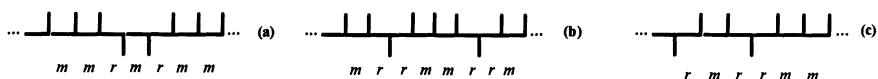
| Range/ Peak No. | Assignment | Normalized fraction | | | |
|-----------------------|------------|---------------------|----------------------|-----------------------------------|--------------------------------------|
| | | Experimental | Calculated, ES/CE | Calculated, C ₁ /CE | Calculated, ES/C ₁ /CE |
| I | mmmm | .1937(50) | .2094 | .2024 | .1978 |
| XXII | mmmmmm | .1514(38) | .1509 | .1433 | .1527 |
| XXIII | mmmmmr | .0389(35) | .0537 | .0539 | .0384 |
| II | mmmr | .0708(29) | .0758 | .0770 | .0708 |
| II/10 | mmmmrr | .0426(33) | .0538 | .0634 | .0509 |
| III | rmmr | .0141(31) | .0122 | .0127 | .0161 |
| III/17 | mrrmmrrm | .0042(15) | .0035 | .0047 | .0058 |
| III/18 | mrrmmrrr | .0044(22) | .0019 | .0033 | .0057 |
| IV | mmrr | .0999(32) | .0837 | .0998 | .1004 |
| IV/22 | mmrrm + | .0709(22) | .0642 | .0758 | .0694 |
| V | mmrrrr | .1048(79) | .0538 | .0589 | .0479 |
| | mmrrm + | | .0104 | .0169 | .0215 |
| | rmrr | | .0166 | .0026 | .0026 |
| | | | .0934 | .0945 | .0991 |
| VI | rmrm | .0110(16) | .0245 | .0112 | .0101 |
| VI/31 | rrmrmr | .0090(10) | .0092 | .0080 | .0066 |

Table 2 (ctd.)

| | | | | | |
|------------|----------------------------------|-----------|--|--|---|
| VI/34 | <i>mrmrmm</i> | .0010(10) | .0097 | .0010 | .0013 |
| VII | <i>rrrr</i> | .3423(47) | .3490 | .3509 | .3504 |
| VII/37 | <i>rrrrrr</i> | .2736(36) | .2759 | .2695 | .2683 |
| VIII/38 | <i>mrrrmr</i> | .0086(13) | .0092 | .0080 | .0067 |
| VIII/39 | <i>rrrrmr</i> | .0665(15) | .0647 | .0671 | .0643 |
| VIII/40+41 | <i>rrrrmm</i> + <i>mrrrmm</i> | .0364(30) | .0196 { .0168 .0028 | .0280 { .0268 .0012 | .0348 { .0336 .0012 |
| IX/42 | <i>rmrrmr</i> | .0090(15) | .0046 | .0046 | .0056 |
| IX/43+44 | <i>mmrrmr</i> | .0189(36) | .0104 | .0102 | .0168 |
| IX/45+46 | <i>mmrrmm</i> | .0248(36) | .0269 | .0308 | .0244 |
| XI | <i>mrmrr</i> | .0043(10) | .0120 | .0091 | .0077 |
| XII | <i>rmrrr</i> + <i>mrrrm</i> | .0486(7) | .0467 { .0407 .0060 | .0473 { .0427 .0046 | .0496 { .0457 .0039 |
| XIII+ | <i>mrrrr</i> + | .4946(52) | .490 { .0813 | .5004 { .0940 | .5025 { .0979 |
| XIV+ | <i>rmrrm</i> + | | .0049 | .0014 | .0012 |
| XV | <i>rrrrr</i> + | | .3083 | .3040 | .3015 |
| | <i>rmrrr</i> + | | .0196 | .0240 | .0311 |
| | <i>mmrrm</i> + | | .0117 | .0012 | .0014 |
| | <i>mmrrr</i> | | .0642 | .0758 | .0694 |
| XIII/10 | <i>mmrrrrm</i> | .0200(12) | .0088 | .0158 | .0198 |
| XIII/11 | <i>rmrrrrr</i> | .0525(11) | .0568 | .0579 | .0525 |
| | | | $\sum(y_i - y_i^0)^2 \times 10^3 =$ 1.88 $\chi_r^2 = 18.5$ $\sigma = .85$ $P_r = .90$ $w = .47$ | $\sum(y_i - y_i^0)^2 \times 10^3 =$ 1.32 $\chi_r^2 = 8.2$ $\sigma_1 = .99$ $\sigma_2 = .60$ $P_{12} = .53$ $P_{21} = 1.00$ $P_r = .89$ $w = .47$ | $\sum(y_i - y_i^0)^2 \times 10^3 =$.311 $\chi_r^2 = 2.5$ $\sigma = .99_5$ $\sigma_1 = 1.00$ $\sigma_2 = .31$ $P_{12} = .45$ $P_{21} = .97$ $P_r = .90$ $w_1 = .10$ $w_2 = .42$ |

By comparison of the experimental and calculated distributions in columns 3 and 4 of Tab. 2, it can be noted that the largest disagreement (in relative sense) affects the *mrmr*-centred sequences: the fractional abundance of the *mrmr* pentad according to the ES/CE model is more than twice the experimental one, and the reason for that is a 10-fold overestimate of the *mrmrmm* heptad (whereas the *rrmrrmr* heptad is correctly reproduced).

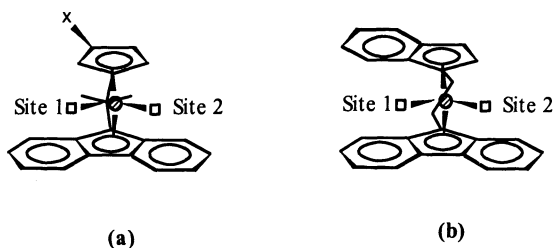
$m_x m_r m_r m_y$ *n*Ads should derive from isotactoid sequences containing two consecutive stereoerrors (Scheme 1-a).



Scheme 1

According to the enantiomorphic-sites statistics [3], all *nads* of equal length and equal number of stereoirregular units are equiprobable. This is clearly not the case for the investigated sample, in which only *nads* with non consecutive stereoerrors (such as, e.g., *mrrmmrrm* and *rmrrmm*, Scheme 1-b and 1-c) were detected.

In ref. 8d, we noted that this feature is typical of predominantly isotactic polypropylenes prepared with homogeneous catalysts based on C_1 -symmetric *ansa*-metallocenes of the 4th column of the type sketched in Scheme 2-a (with X a bulky group such as, e.g., *t*-butyl or trimethylsilyl) [12] or Scheme 2-b [13], with two diastereotopic [14] active sites (denoted in the schemes as 1 and 2).



Scheme 2

For such catalysts, it is generally accepted that the polymerization proceeds with a «defective chain migratory» mechanism [12,13,15]. Indeed, molecular mechanics calculations [15] pointed out a preference of the growing chain for the sterically more open coordination site 2; as a result, monomer insertion occurs preferentially at site 1. The fact that only site 1 is highly enantioselective has the following consequences:

- i) Chain propagation is predominantly isotactic.
- ii) The stereoselectivity increases with decreasing monomer concentration, because this favours chain «back-skip» relative to monomer insertion at the weakly enantioselective site 2.
- iii) The probability of two consecutive insertions at site 2 (and hence that of two consecutive stereoerrors) is very low, which means that sequences of the type $m_x r m r m_y$ are virtually «prohibited».

Importantly, we proved [8d] the existence of an inverse correlation between stereoselectivity and monomer concentration also for the active species of the heterogeneous Ziegler-Natta systems responsible for the formation of the isotactoid sequences. This finding, along with the discussed selection rule of stereosequence generation, suggests a close similarity with the case of the quoted C_1 -symmetric metallocenes.

Therefore, we replaced the ES model with a more general one, apt to describe site-controlled chain propagation at a C_1 -symmetric active species with two diastereotopic sites. Four adjustable parameters are needed: σ_1 and σ_2 , conditional probabilities that the prochiral monomer inserts with a given enantioface (either *re* or *si*) at each of the two sites (1 and 2, respectively), as a result of their chirotopicity [14]; P_{12} and P_{21} , conditional probabilities of monomer insertion at site 2 after a previous insertion at site 1 and *vice versa*. A linear combination with the CE model results in a « C_1 /CE» two-site model with 6 adjustable parameters ($\sigma_1, \sigma_2, P_{12}, P_{21}, P_r, w$).

In the 5th column of Tab. 2, we report the corresponding best-fit stereosequence distribution for fraction A. The value of $\chi_r^2 = 8.2$ is indicative of a substantial improvement of the fit compared with the ES/CE model; in particular, the experimental distribution of the $m_x r m r m_y$ sequences is now nicely matched.

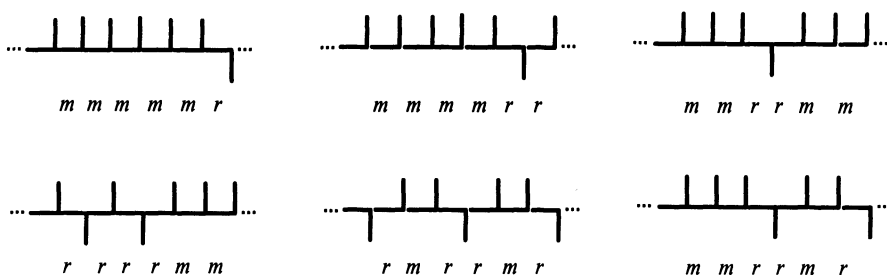
The best-fit values of P_r (= 0.89) and of the mixing coefficient w (= 0.47) are identical to those found for the ES/CE model, and the differences concern entirely isotactoid propagation. According to the C_1 /CE model, this would take place at active species inserting the monomer preferentially at one of the two active sites (site 1; $P_{12} < P_{21}$), and the probability ($1 - P_{21}$) of two consecutive insertions at the other site (site 2) is practically 0.

The minimum of the χ_r^2 function, however, is very shallow, and acceptable values of χ_r^2 are obtained for all solutions in which $P_{12}(1 - \sigma_2) = 0.21$ and $0 < \sigma_2 < 0.5$; this leaves some margins of ambiguity on the enantioselectivity of site 2. Indeed, similar distributions of configurations can be achieved in all cases comprised between the following two limiting hypotheses:

- Site 1 is highly enantioselective ($\sigma_1 \approx 1$), whereas site 2 is non-enantioselective ($\sigma_2 \approx 0.5$);
- Site 1 and 2 are enantiotopic and both highly enantioselective ($\sigma_1 \approx 1, \sigma_2 \approx 0$ or $\sigma_1 \approx 0, \sigma_2 \approx 1$),

provided that the probability of monomer insertion at site 2 (P_{12}) is adjusted so as to result in the same value of $P_{12}(1 - \sigma_2)$, *i.e.* in the same fraction of stereoerrors.

Let us now examine the residual mismatches between experimental and best-fit calculated stereosequence distribution. By comparing columns 3 and 5 of Tab. 2, it can be seen that the calculations tend to overestimate the *mmmmmmr*, *mmmmrr* and *mmrrmr* heptads, and to underestimate the *rrrrmm*, *rmrrmr* and *mmrrmr* ones (Scheme 3). This is a strong indication that the stereoerrors in the isotactoid part tend to concentrate in blocks.



Scheme 3

The co-presence of «less defective» and «more defective» isotactic sequences, along with syndiotactic sequences, clearly calls for the adoption of a three-site model.

A « $C_1/C_1/CE$ » model, with as many as 11 adjustable parameters (4 for each C_1 -symmetric site, 1 for the site with chain-end control and two mixing coefficients) would be unreasonably complicated even for the high-resolution data in Tab. 2. However, due to the fact that the ES and C_1 statistics tend to degenerate with increasing stereoselectivity of chain propagation [8d], we can tentatively adopt the former for describing the configuration of the «less defective» isotactic sequences. This results in a more simple «ES/ C_1/CE » model with 8 adjustable parameters (σ for ES propagation; σ_1 , σ_2 , P_{12} , P_{21} for C_1 propagation; P_r for CE propagation; two mixing coefficients w_1 and w_2).

The best-fit stereosequence distribution for fraction A in terms of such a model is given in the last column of Tab. 2. At the absolute minimum, χ_r^2 is now as low as 2.5 (hence not too far from the «ideal» value of $\chi_r^2 = 1$), and most $|(y_i - y_i^\circ)|$ values are actually lower than the experimental uncertainties. Also in this case, however, as already discussed for the C_1/CE model, the χ_r^2 function is almost invariant for all solutions in which $P_{12}(1 - \sigma_2)$ (that is, the fraction of stereoregular units in the isotactoid sequences) is ≈ 0.30 and $0 < \sigma_2 < 0.5$ (the other parameters remaining constant within the experimental uncertainty).

According to the model, the investigated polypropylene fraction consists of *three* different types of stereosequences: highly isotactic, isotactoid and syndiotactic. The former, in low amount ($\approx 10\%$ by weight), would be close to ideal isotacticity, with ≈ 1 mol% of isolated stereoirregular units. The isotactoid sequences would amount to $\approx 40\%$ by weight, and contain ≈ 30 mol% of stereoirregular units, distributed in accordance with the C_1 statistics. The remaining $\approx 50\%$ by weight of the material would be formed by syndiotactic sequences, with ≈ 10 mol% of stereoirregular units whose structure is consistent with chain-end control.

Configurational analysis of the «isotactic» fraction B

Due to the comparatively high stereoregularity of fraction B, its ^{13}C NMR characterization had to be carried out at 130°C instead of 70°C . This resulted in appreciable variations of the ^{13}C NMR chemical shift values and in a significant decrease of their spreading, compared with the spectrum of fraction A.

However, due to the lower fraction of «defective» stereosequences, a less crowded spectrum was obtained, with an adequate resolution already at 125 MHz. By integration of the methyl and methylene regions, a set of 20 independent data ranging from pentads to nonads was achieved (Tab. 3).

In the same table, we report the best-fit distributions calculated according to the ES/CE two-site model, and to the ES/C₁/CE three-site model.

Also in this second case and for the same reasons, the ES/CE model was found not to be adequate ($\chi_r^2 = 7.8$).

Conversely, the application of the ES/C₁/CE model resulted in a very good match between experimental and calculated data, with a value of $\chi_r^2 = 2.0$. Interestingly, the configuration of the three types of constituting stereosequences turned out to be similar to fraction A (cfr. Tab. 2), in spite of strong differences in their relative amounts. Fraction B, indeed, was found to be made predominantly of highly isotactic sequences ($\approx 60\%$ by weight), with only minor amounts of isotactoid ($\approx 30\%$) and syndiotactic ($\approx 10\%$) sequences.

Table 3 – 150 MHz ^{13}C NMR stereosequence distribution of polypropylene fraction B, and best-fit ones in terms of various statistical models (see text and ref. 9 for range and peak numbering)

| Range/ Peak No. | Assignment | Normalized fraction | | |
|-----------------------|----------------|---------------------|----------------------|--------------------------------------|
| | | Experimental | Calculated, ES/CE | Calculated, ES/C ₁ /CE |
| I | mmmm | .6515(18) | .6528 | .6523 |
| II | mmmr | .0621(12) | .0635 | .0593 |
| III | rmmr | .0065(5) | .0036 | .0067 |
| III/17 | mrrmmrrm | .0025 (7) | .0013 | .0035 |
| III/18 | mrrmmrrr | .0019(9) | .0005 | .0015 |
| IV | mmrr | .0670(8) | .0670 | .0682 |
| V | mmrm + rmrr | .0378(13) | .0358 { .0320 | .0363 { .0317 |
| VI | rmrm | .0060(5) | .0072 | .0066 |
| VI/31 | rrmrmr | .0020(10) | .0033 | .0022 |
| VI/34 | mrmrmm | .0010(10) | .0097 | .0013 |
| VII | rrrr | .1045(7) | .1046 | .1046 |

Table 3 (ctd.)

| | | | | | | |
|------------|------------------------|------------|-------------------------------------|--|---|--|
| VIII/38+39 | <i>mrrrmr+</i> | .0180(14) | .0256 | $\left\{ \begin{array}{l} .0223 \\ .0033 \end{array} \right.$ | .0196 | $\left\{ \begin{array}{l} .0174 \\ .0022 \end{array} \right.$ |
| VIII/40+41 | <i>rrrrmm + mrrrrm</i> | .0130(20) | .0064 | | $\left\{ \begin{array}{l} .0058 \\ .0006 \end{array} \right.$ | |
| IX | <i>mrrm</i> | .0341(8) | .0335 | | | .0340 |
| IX/43+44 | <i>mmrrmr</i> | .0129(33) | .0032 | | .0089 | |
| IX/45+46 | <i>mmrrmm</i> | .0192(17) | .0287 | | .0235 | |
| XI | <i>mrmmr</i> | .0040(12) | .0038 | | .0030 | |
| XII | <i>rrmrr + mrrrr</i> | .0151(17) | .0160 | $\left\{ \begin{array}{l} .0141 \\ .0019 \end{array} \right.$ | .0159 | $\left\{ \begin{array}{l} .0144 \\ .0015 \end{array} \right.$ |
| XIII | <i>mrrrr</i> | .0277(41) | .0282 | | | |
| XIV+ | <i>rmmrm +</i> | .1584(118) | .1612 | $\left\{ \begin{array}{l} .0008 \\ .0905 \\ .0064 \\ .0030 \\ .0605 \end{array} \right.$ | .1629 | $\left\{ \begin{array}{l} .0012 \\ .0902 \\ .0122 \\ .0033 \\ .0560 \end{array} \right.$ |
| XV | <i>rrrrr +</i> | | | | | |
| | <i>rrmrr +</i> | | | | | |
| | <i>mmrmr +</i> | | | | | |
| | <i>mmrrr</i> | | | | | |
| | | | $\Sigma(y_i - y_i^0)^2 \times 10^4$ | | $\Sigma(y_i - y_i^0)^2 \times 10^4$ | |
| | | | = 3.17 | | = .75 | |
| | | | $\chi^2 = 7.8$ | | $\chi^2 = 2.0$ | |
| | | | $\sigma = .95$ | | $\sigma = 1.00$ | |
| | | | $P_r = .88$ | | $\sigma_1 = .97$ | |
| | | | $w = .83$ | | $\sigma_2 = .10$ | |
| | | | | | $P_{12} = .15$ | |
| | | | | | $P_{21} = 1.00$ | |
| | | | | | $P_r = .91$ | |
| | | | | | $w_1 = .50$ | |
| | | | | | $w_2 = .36$ | |

Conclusions

The stereosequence distribution of the «atactic» and «isotactic» fractions of a polypropylene sample made with a $MgCl_2$ -supported catalyst, determined by means of high-resolution ^{13}C NMR, was analyzed in terms of statistical models of increasing sophistication.

Two-site models, including the ES/CE one normally used for the interpretation of «routine» ^{13}C NMR data at pentad level [7,10], were shown to be inconsistent with the much finer high-resolution data. A good agreement between experimental and calculated stereosequence distributions could be obtained only in terms of an ES/C₁/CE three-site model, describing each fraction as a mixture of highly isotactic, weakly isotactic (isotactoid) and syndiotactic sequences.

According to such model, the two fractions would comprise the same three building blocks (the configuration of the three different types of stereosequences being almost invariant), and differ merely in their relative amounts; this conclusion necessarily implies a stereoblock nature.

We note that the model fits nicely with the observed physical properties of the materials. In particular, on the one hand, it provides a simple explanation for the fact that fraction B, with an *average* content of stereoirregularities in the isotactic part of almost 5 mol%, has a DSC melting peak with the maximum at 157°C, whereas polypropylene samples with the same amount of *uniformly distributed* defects, made with «single-site» metallocene catalysts, melt around 130°C [16].

On the other hand, it easily accounts for the observation of weak isotactic crystallinity in the X-ray diffraction spectrum of fraction A as well. In fact, this can be traced to the low amounts of highly isotactic blocks, the isotactoid blocks being substantially uncrystallizable.

The experimental basis discussed so far is also an important starting point for the development of better defined models of the active species in MgCl₂-supported Ziegler-Natta catalysts. This aspect will be addressed in forthcoming dedicated papers.

Experimental Part

The synthesis of the polypropylene sample was described in ref. 8d. The ¹³C{¹H} NMR spectrum of fraction A was recorded with a Bruker AMX 600 spectrometer operating at 150.9 MHz, on a 5 mg/mL polymer solution in tetrachloroethane-1,2-*d*₂ at 70°C. Experimental setup: acquisition time, 2.3 s; relaxation delay, 2.0 s; pulse angle, 45°; 64K data points; 25K transients. Proton broad-band decoupling was achieved with the GARP sequence. The ¹³C{¹H} NMR spectrum of fraction B was recorded with a Bruker DRX 500 spectrometer operating at 125.76 MHz, on a 150 mg/mL polymer solution in tetrachloroethane-1,2-*d*₂ at 130°C. Experimental setup: acquisition time, 3.25 s; relaxation delay, 1.0 s; pulse angle, 90°; 64K data points; 16.7K transients. Proton broad-band decoupling was achieved with the WALTZ 16 sequence.

References

- [1] For a review on the stereoselectivity of 1-alkene polymerization promoted by Ziegler-Natta catalysts, see: Corradini, P.; Busico, V.; Guerra, G. In *Comprehensive Polymer Science*; Pergamon Press: Oxford, 1988; Vol. 4, pp. 29-50.
- [2] Bovey, F.A.; Tiers, G.V.D. *J. Polym. Sci.* **1960**, *44*, 173.
- [3] Shelden, R.A.; Fueno, T.; Tsunetsugu, T.; Furukawa, J. *J. Polym. Sci., Polym. Lett.* **1965**, *3*, 23.
- [4] Bovey, F.A. *Chain Structure and Conformation of Macromolecules*; Academic Press: New York, 1982; Chapter 3, pp. 75-78 and refs. therein.
- [5] (a) Johnson, L.F.; Heatley, F.; Bovey, F.A. *Macromolecules* **1970**, *3*, 175; (b) Inoue, Y.; Nishioka, A.; Chûjô, R. *Makromol. Chem.* **1972**, *152*, 15; (c) Zambelli, A.; Dorman, D.E.; Brewster, A.I.R.; Bovey, F.A. *Macromolecules* **1973**, *6*, 925; (d) Zambelli, A.; Locatelli, P.; Bajo, G.; Bovey, F.A. *Macromolecules* **1975**, *8*, 687.

- [6] (a) Cossee, P. *J. Catal.* **1964**, *3*, 80; (b) Arlman, E.J. *J. Catal.* **1964**, *3*, 89; Arlman, E.J.; Cossee, P. *J. Catal.* **1964**, *3*, 99; (d) Cossee, P. In *The Stereochemistry of Macromolecules*; Ketley, A.D., Ed; Marcel Dekker: New York, 1967; Vol. 1, Chapter 3.
- [7] Doi, Y. *Makromol. Chem., Rapid Commun.* **1982**, *3*, 635.
- [8] (a) Busico, V.; Corradini, P.; De Biasio, R.; Landriani, L.; Segre, A.L. *Macromolecules* **1994**, *27*, 4521; (b) Corradini, P.; Busico, V.; Cipullo, R. *Catalyst Design for Tailor-Made Polyolefins*; Soga, K., Terano, M., Eds.; Kodansha: Tokyo, 1994; pp. 21-34; (c) Busico, V.; Cipullo, R.; Corradini, P.; Landriani, L.; Vacatello, M.; Segre, A.L. *Macromolecules* **1995**, *28*, 1887; (d) Busico, V.; Cipullo, R.; Talarico, G.; Segre, A.L.; Chadwick, J.C. *Macromolecules* **1997**, *30*, 4787.
- [9] (a) Busico, V.; Cipullo, R.; Monaco, G.; Vacatello, M.; Segre, A.L. *Macromolecules* **1997**, *30*, 6251; (b) Busico, V.; Cipullo, R.; Monaco, G.; Vacatello, M.; Bella, J.; Segre, A.L. *Macromolecules*, in press.
- [10] ¹³C NMR microstructural characterizations of polypropylene fractions at pentad level: (a) Wolfsgruber, C.; Zannoni, G.; Rigamonti, E.; Zambelli, A. *Makromol. Chem.* **1975**, *176*, 2765; (b) Pavan, A.; Provasoli, A.; Moraglio, G.; Zambelli, A. *Makromol. Chem.* **1977**, *178*, 1099; (c) Zhu, S.-N.; Yang, X.-Z.; Chûjô, R. *Polymer J.* **1983**, *12*, 859; (d) Inoue, Y.; Itabashi, Y.; Chûjô, R.; Doi, Y. *Polymer* **1984**, *25*, 1640; (e) Martuscelli, E.; Avella, M.; Segre, A.L.; Rossi, E.; Di Drusco, G.; Galli, P.; Simonazzi, T. *Polymer* **1985**, *26*, 259; (f) Cheng, H.N. *J. Appl. Polym. Sci.* **1988**, *35*, 1639; (g) Kakugo, M.; Miyatake, T.; Naito, Y.; Mizunuma, K. *Macromolecules* **1988**, *21*, 314; (h) Hayashi, T.; Inoue, Y.; Chûjô, R.; Doi, Y. *Polymer* **1989**, *30*, 1714; (i) Busico, V.; Corradini, P.; De Martino, L.; Graziano, F.; Iadicicco, A. *Makromol. Chem.* **1991**, *192*, 49; (j) Chadwick, J.C.; Miedema, A.; Ruisch, B.J.; Sudmeijer, O. *Makromol. Chem.* **1992**, *193*, 1463; (k) van der Burg, M.; Chadwick, J.C.; Sudmeijer, O.; Tulleken, H.J.A.F. *Makromol. Chem., Theory Simul.* **1993**, *2*, 385; (l) Paukkeri, R.; Väänänen, T.; Lehtinen, A. *Polymer* **1993**, *34*, 2488; (m) Paukkeri, R.; Iiskola, E.; Lehtinen, A.; Salminen, H. *Polymer* **1994**, *35*, 2636; (n) Härkönen, M.; Seppälä, J.V.; Salminen, H. *Polym. J.* **1995**, *27*, 256; (o) Busico, V.; Cipullo, R.; Corradini, P.; De Biasio, R. *Macromol. Chem. Phys.* **1995**, *196*, 491; (p) Randall, J.C. *Macromolecules* **1997**, *30*, 803.
- [11] "SHAPE" Program, by Monaco, G., University of Naples "Federico II"; Monaco, G., manuscript in preparation.
- [12] (a) Ewen, J.A.; Elder, M.J. *Eur. Pat. Appl.* 537130 (1993); (b) Ewen, J.A. *Macromol. Symp.* **1995**, *89*, 181 and refs. therein; (c) Razavi, A.; Peters, L.; Nafpliotis, L.; Verecke, D.; Den Dauw, K.; Atwood, J.L.; Tewald, U. *Macromol. Symp.* **1995**, *89*, 345 and refs. therein.
- [13] Rieger, B.; Jany, G.; Fawzi, R.; Steinmann, M. *Organometallics* **1994**, *13*, 647.
- [14] Farina, M. *Macromol. Symp.* **1995**, *89*, 489.
- [15] Guerra, G.; Cavallo, L.; Moscardi, G.; Vacatello, M.; Corradini, P. *Macromolecules* **1996**, *29*, 4834.
- [16] Unpublished results from our laboratory. See also: Mülhaupt, R. *Macromol. Chem. Phys.* **1994**, *195*, 1433.

ENERGY DISTRIBUTION OF ACTIVE SITES IN HETEROGENEOUS ZIEGLER-NATTA CATALYSTS. METHOD OF STUDY OF ACTIVE SITE NON-UNIFORMITY

L.A.Novokshonova*, N.Yu.Kovaleva*, Yu.A.Gavrilov*, V.G.Krasheninnikov*, T.A.Ladygina*, I.O. Leipunskii**, A.M. Zhigach**, M.L. Kuskov**

*Institute of Chemical Physics, RAS, 117977 Moscow, Russia

**Institute of Energy Problems of Chemical Physics, RAS, 117977 Moscow, Russia
lnov@center.chph.ras.ru

Abstract.

The new method of investigation of active site non-uniformity was developed. The method is based on mass-spectrometric study of temperature programmed desorption (TPD) products from the catalyst surface at initial stages of olefin polymerization (up to 10 – 15 monomer units in chain). The method allows to obtain the information concerning the energy non-uniformity of active sites in terms of a distribution of active sites over activation energy of active Mt-C bond thermal destruction. By the method, the initial stages of ethylene and deuterioethylene polymerization with Ti-supported catalysts of different structure were studied. It is shown that the view of energy distribution of active sites depends on catalyst structure. The values of activation energy of thermal destruction of Ti-C bonds in differing active sites were estimated and energy spectra of active sites for catalysts were obtained.

Introduction

The distinctive property of heterogeneous Ziegler-Natta catalysts is a non-uniformity of active sites. It influences on kinetic regularities of olefin polymerization and characteristics of polymers obtained. Multicenter character of heterogeneous catalysts manifests itself in broadening of molecular mass distribution, chemical non-uniformity of copolymers, complicated order of catalyst deactivation reactions over the active site number observed often on an analysis of olefin polymerization kinetics.

In this paper, new method for an analysis of non-uniformity of heterogeneous catalyst active sites is presented. The method is based on mass-spectrometric study of temperature programmed desorption (TPD) products from a surface of catalyst on initial stages of olefin polymerization. By developed technique [1-3],

the initial stages of ethylene and deuterioethylene polymerization with different titanium supported catalysts were studied.

Experimental

Essence of method

By the method, the hydrocarbon (polyolefin) molecules evolved in thermal degradation of active (living) Ti-polymer bonds, when polymer chains are very short (up to 10-15 monomer units in chain), are recorded depending on temperature of heating. Linear heating of samples gets the information of energy distribution of active sites. The experimental data allow to calculate the activation energies of thermal degradation of active "Ti-C" bonds located in differing active sites and to get an energy spectrum of catalyst active sites.

The sample of pre-formed catalyst was placed in special cell connected directly with mass-spectrometer. The gas-phase polymerization was carried out also in this cell. The sample investigated was heated with constant rate from room temperature to 500° C. A continuous cyclic scanning of mass-spectra in range of m/z up to 400 was used. The ratio m/z is the mass to ion charge ratio, as z in our experiments was equal to one, and hence this ratio characterises ion mass. TPD products from surface of pre-formed catalysts were investigated prior to and after monomer polymerization. The polymerization was carried out at low pressure (0.13 - 2.15 kPa) and room temperature for a short time (1-10 min) to produce small amount of polymer and the short macromolecules on catalyst surface which can be desorbed and analyzed from gas phase. The additional amount of Al-alkyl was not injected into cell.

Objects of investigation

Supported catalyst based on titanium chloride covalent-bonded to aerosil through OH groups ($\text{SiO}_2/\text{TiCl}_4/\text{AlEt}_2\text{Cl}$) and supported catalyst containing clusters of TiCl_3 on aerosil surface ($\text{SiO}_2/\text{AlEt}_3/\text{TiCl}_3$) were used for investigations. The catalysts were obtained by sequential adsorption of catalyst components on aerosil in Mac-Ben balance device [4].

Results and discussion

TPD spectra from catalyst surface prior to and after polymerization.

TPD products contain hydrocarbons. The most intense lines in mass-spectra for $\text{SiO}_2/\text{TiCl}_4/\text{AlEt}_2\text{Cl}$ catalyst after polymerization are attributed to a family of unsaturated hydrocarbons C_nH_{2n} with $n > 3$, the amount of saturated hydrocarbons $\text{C}_n\text{H}_{2n+2}$ is much lower. For $\text{SiO}_2/\text{AlEt}_3/\text{TiCl}_4$ catalyst, the amounts of saturated and unsaturated hydrocarbons are correlated. The maximum value of n is not less than 28 corresponding to 10–15 monomer units in chain.

For tested catalysts after polymerization, the presence of maxima of complicated shape on TPD curves in temperature range of 180–350°C is observed (Fig. 1, curve 1). These maxima are absent on TPD curves prior to polymerization (Fig. 1, curve 2). Desorption of physically adsorbed hydrocarbons (“dead” macromolecules) takes place at temperature of about 100°C. Intense evolution of hydrocarbons as a result of thermal destruction of PE begins at temperature higher than 350°C (Fig. 1, curve 3).

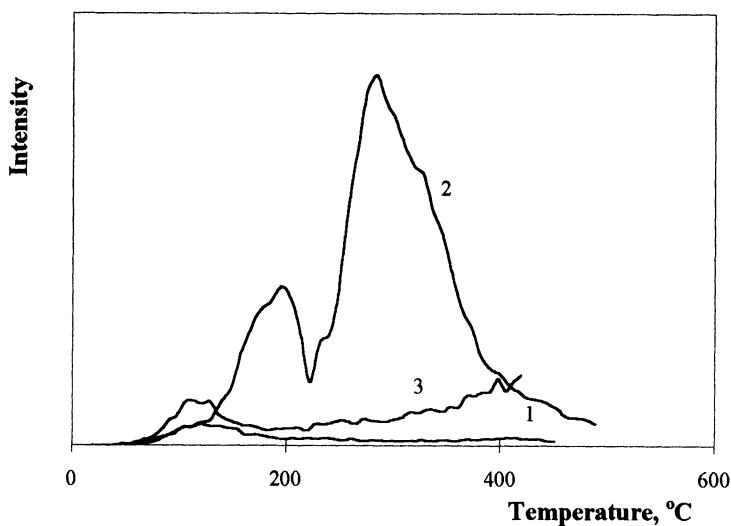


Fig. 1. TPD curves from surface of pre-formed $\text{SiO}_2/\text{TiCl}_4/\text{AlEt}_2\text{Cl}$ catalyst prior to (1) and after (2) ethylene polymerization (5 min. under 2,15 kPa) for $m/z=140$; (3) - the catalyst after ethylene polymerization when polyethylene has $M_n=20000$.

If the catalyst was inhibited by CO prior to contact with monomer, TPD curves

do not have maxima in temperature interval of 180-350°C. If the living catalyst was treated with hydrogen after polymerization and all living polymer chains were terminated, TPD curves do not have the maxima in this temperature range also.

Similar results are obtained in deuterioethylene polymerization.

Above results show that the presence of TPD maxima in temperature range of 180 – 350°C from catalyst surface is due to the evolution of hydrocarbon molecules with different length in thermal destruction of living Ti-C bonds in active sites.

TPD results for $\text{SiO}_2/\text{TiCl}_4/\text{AlEt}_2\text{Cl}$ catalyst

The spectra of TPD products from this catalyst surface after ethylene polymerization contain two intense maxima at temperature of 180-210°C and 280-320°C (Fig.1, Fig. 2). The curves presented are typical for all mass lines observed. The intensity of the lines decreases quickly with increase of mass. The plot of three-dimensional TPD surface is shown in Fig. 3. These two maxima seem to be a weakly resolved superposition of several maxima, the relative intensities of which change with an increase of m/z . At higher m/z the resolution of the peaks is improved (Fig.1, Fig. 2).

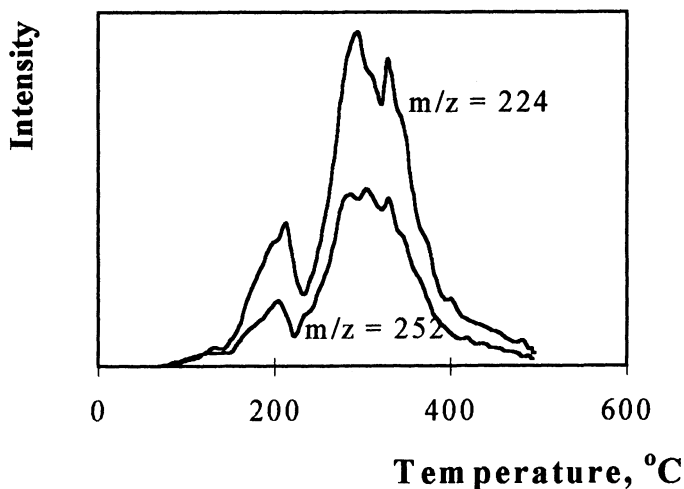


Fig. 2. TPD curves from the surface of $\text{SiO}_2/\text{TiCl}_4/\text{AlEt}_2\text{Cl}$ catalyst after ethylene polymerization (5 min. under 2,15 kPa) for m/z equal to 224 and 252.

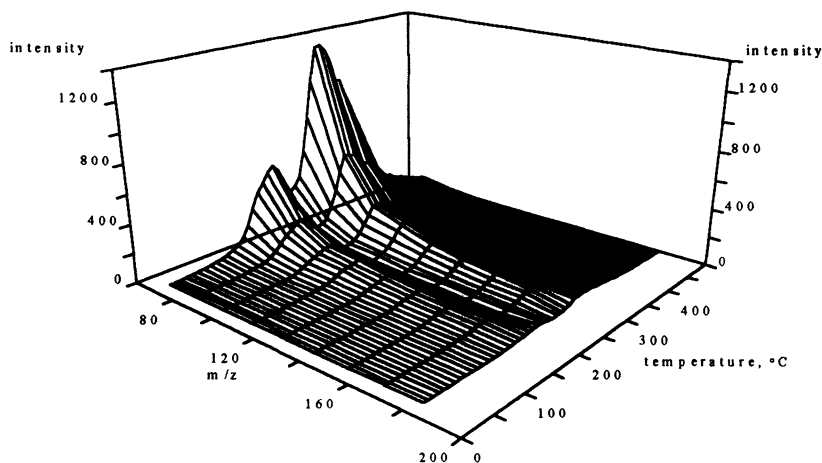


Fig. 3. Three-dimensional plot, showing TPD curves for $\text{SiO}_2/\text{TiCl}_4/\text{AlEt}_2\text{Cl}$ catalyst after ethylene polymerization (5 min under 2,15 kPa) for different $m/z=28n$.

The results allow to conclude that in $\text{SiO}_2/\text{TiCl}_4/\text{AlEt}_2\text{Cl}$ catalyst containing titanium chloride chemically bonded to aerosil surface there are at least two types of active sites varying in the activation energy of thermal destruction of Ti-C bonds. Complex shape of both maxima indicates that there is a distribution over activation energy for both site types.

TPD results for $\text{SiO}_2/\text{AlEt}_3/\text{TiCl}_4$ catalyst

The spectrum of TPD products from surface of catalyst containing clusters of TiCl_3 on aerosil after ethylene polymerization are significantly different from those of the above catalyst (Fig. 4). The maximum in the range of 250 - 350°C involving, in essence, at least two peaks at 250°C and 350°C is observed. The maximum at lower temperature (about 200°C) is absent.

It is interesting that intensities of both peaks at 250°C and 350°C change with time of polymerization (Fig. 4). At the beginning they increase in time and thereafter fall off, the maximal intensity of lower temperature peak being achieved more quickly. As a result the relation between peaks changes in time. Similar picture is observed for all masses. For living polymerization, from these data it follows that the peak at lower temperature is attributed to more active sites, which produce the macromolecules more quickly.

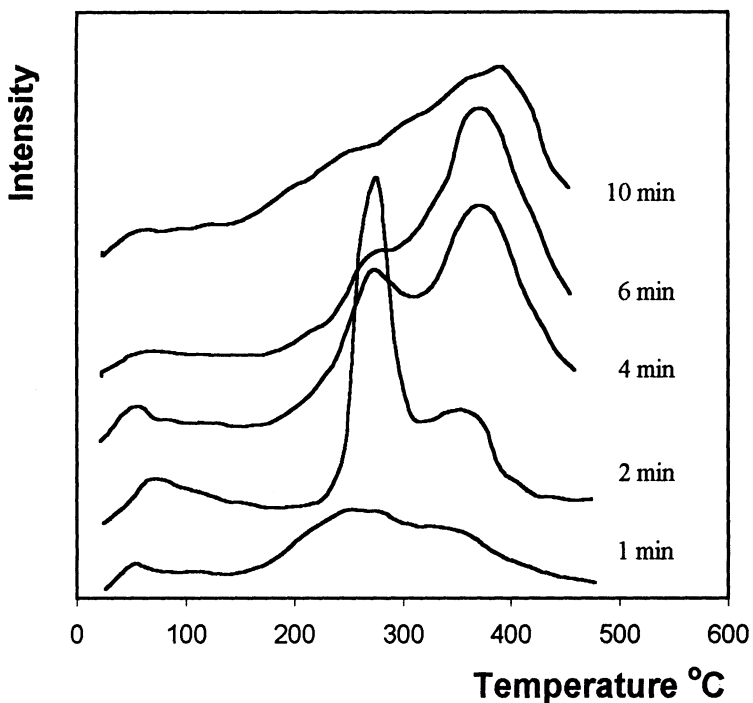


Fig. 4. TPD curves from $\text{SiO}_2/\text{AlEt}_3/\text{TiCl}_4$ catalysts after ethylene polymerization for $m/z = 140$ depending on polymerization time (ethylene pressure of 0.13 kPa).

Energy spectra of active sites for some catalysts

Based on the experimental dependence of evolution rate of desorption products on temperature, the activation energies of thermal destruction of “Ti-polymer chain” bonds in active sites were calculated using equation like to Wigner-Polanyi equation:

$$F(T) = \int_{E_1}^{E_2} k(E, T) \cdot C(E, T) dE,$$

where $k(E, T) = A \cdot \exp(-E/RT)$ is the rate constant of Ti-C bond destruction, $C(E, T)$ is the current concentration of active sites, E is an activation energy of Ti-C bond destruction. The calculation was made in the assumption that the active site distribution over activation energy is continuous and $A = 10^8$. The calculated energy spectra are given in Fig. 5.

The energy spectrum calculated for $\text{SiO}_2/\text{TiCl}_4/\text{AlEt}_2\text{Cl}$ catalyst (Fig.5, curve 1) consists of two groups of energy peaks in range of 20-23 kcal/mol and 25-30 kcal/mol. The average values of thermal destruction of "Ti-polymer chain" bonds in these two groups of active sites differ about 1.5 times.

The energy spectrum for $\text{SiO}_2/\text{AlEt}_3/\text{TiCl}_4$ catalyst containing clusters of TiCl_3 (Fig. 5, curve 2) does not contain the peaks in the range of about 20-23 kcal/mol and has several peaks in the range of 25-30 kcal.

The obtained results lead to conclusion that active sites of catalyst based on titanium chloride covalent-bonded to aerosil surface are more non-uniform in comparison with catalyst containing clusters of TiCl_3 on aerosil.

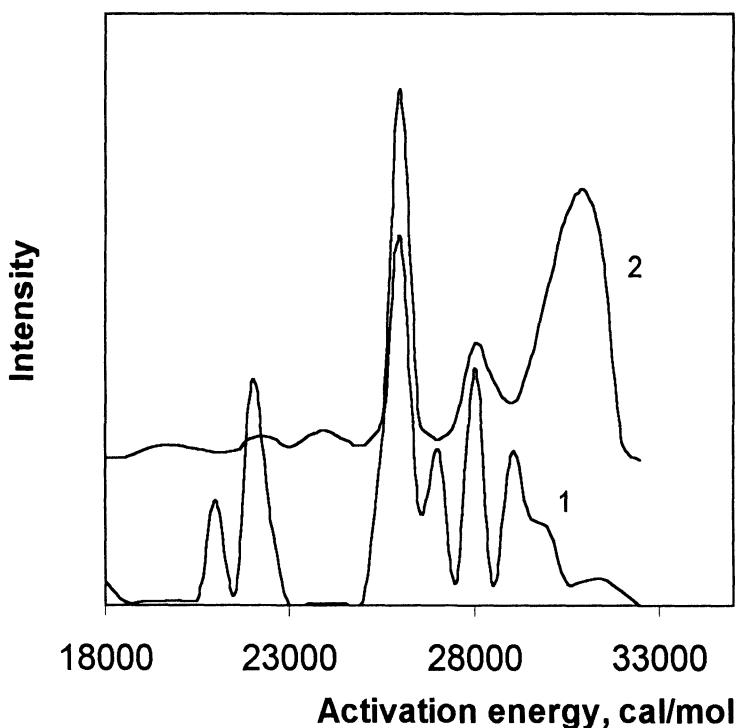


Fig. 5. Energy spectra of active sites for $\text{SiO}_2/\text{TiCl}_4/\text{AlEt}_2\text{Cl}$ (1) and $\text{SiO}_2/\text{AlEt}_3/\text{TiCl}_4$ (2) catalysts calculated on the base of TPD experiments in the terms of active site distribution over activation energy of thermal destruction of Ti-C bonds.

Actually, the study of molecular mass characteristics of polyethylene showed that both catalysts give the polymer with rather wide MWD. However, polyethylene produced by $\text{SiO}_2/\text{TiCl}_4/\text{AlEt}_2\text{Cl}$ catalyst based on titanium chloride covalent-bonded to supporter surface has more wide MWD (M_w/M_n is equal to

10-11) than polymer obtained by $\text{SiO}_2/\text{AlEt}_3/\text{TiCl}_4$ catalyst containing clusters of TiCl_3 , for which M_w/M_n is equal to 7-8. The distinction of catalysts on non-uniformity of active sites reflects itself also in the kinetics of polymerization. The ethylene polymerization with $\text{SiO}_2/\text{AlEt}_3/\text{TiCl}_4$ catalyst occurs with more stable in time rate. Evidently this fact is connected with an absence of the active sites responsible for TPD peaks in the lower temperature range (about 200°C) and characterizing by less activation energy of thermal destruction of active Ti-C bonds hence less stability in polymerization.

Conclusion

The obtained results show that the developed method allows to extract an information about the character of active site non-uniformity of olefin polymerization heterogeneous catalysts and to obtain a distribution of active sites over activation energy of Mt-C bond thermal destruction. As evident from data obtained, the view of energy distribution of active sites depends on catalyst structure. It is possible to trace the effect of method of catalyst heterogenization on energy distribution of active sites formed on supporter surface, in particular, to trace the extent of uniformity of active sites of supported Zr-cene catalysts depending on heterogenization method.

References:

1. L.A.Novokshonova, N.Yu.Kovaleva, Yu.A.Gavrilov, V.G.Krashenninnikov, I.O.Leipunskii, A.N.Zhigach. 6-th Seminar on Organometallic complexes as catalyst of vinyl compound polymerization, Kamien Sl., Poland, Sept. 1996, p. 27.
2. L.A.Novokshonova, N.Yu.Kovaleva, Yu.A.Gavrilov. V.G.Krashenninnikov, I.O.Leipunskii, A.N.Zhigach, M.N.Larichev, M.V.Chebunin, Pol.Bull., 1997, v.39, p.59-65.
3. L.A.Novokshonova, N.Yu.Kovaleva, Yu.A.Gavrilov. V.G.Krashenninnikov, I.O.Leipunskii, A.N.Zhigach, M.N.Larichev, M.V.Chebunin, Polimery 1998, 43, N4, pp 239-242.
4. N.Yu.Kovaleva, Yu.A.Gavrilov, L.A.Novokshonova. Polimery, 1997, vol. 42, N 10, p.616.

Ziegler-Natta and Metallocene Polymerisation of Olefins with Heterogeneous Catalysts

Karin Weiss, Sandra Botzenhardt and Monika Hofmann

University Bayreuth, Department of Inorganic Chemistry, D-95440 Bayreuth, Germany

karin.weiss@uni-bayreuth.de

Abstract. The reactions of AlMe_3 or $\text{Al}(\text{iBu})_3$ (TIBA) with the clay mineral montmorillonite form surface fixed aluminoxanes. By further addition of metallocenes – Cp_2ZrCl_2 or $\text{Et}(\text{Ind})_2\text{ZrCl}_2$ – heterogeneous metallocene complexes are produced. The activities of these catalysts in ethylene or propylene polymerisation are as high as the activities known of similar homogeneous catalyst systems with MAO as cocatalyst. The reaction of AlMe_3 with montmorillonite and the further addition of TiCl_4 or VCl_4 yields very active heterogeneous Ziegler-Natta catalysts. Both types produce high molecular weighted polyethylenes.

Some years ago we started to study the polymerisation of ethylene and propylene with Ti-, Zr- and Hf-metallocenes as homogeneous catalysts and with MAO as cocatalyst [1, 2].

For technical applications heterogeneous metallocene catalysts are favoured, because they give less reactor fouling in olefin polymerisation. Following our experience in syntheses of heterogeneous metathesis catalysts [3], we started in 1997 to heterogenize metallocene catalysts together with cocatalysts. Many publications existed already in this field. Most of them are focused on inorganic carriers: silica and alumina [4, 5]. As cocatalyst MAO in combination with AlMe_3 was often used. Because MAO is not a well defined compound and therefore has some disadvantages, we tried to produce heterogeneous metallocene catalysts without using MAO.

As inorganic carrier we tested clay minerals which are alumina silicates and found that montmorillonite was the best carrier for AlR_3 /metallocene catalysts. The heterogeneous catalysts were formed by reaction of a toluene solution of trialkyl aluminum with the carrier for 2 hours. After removing the solvent the residue was washed twice with toluene. A heterogeneous aluminoxane can be formed by reaction of surface - OH - groups of the carrier with the aluminum alkyls (AlMe_3 or $\text{Al}(\text{iBu})_3$) (figure 1).

In the next reaction step a toluene solution of the metallocene (Cp_2ZrCl_2 or $\text{Et}(\text{Ind})_2\text{ZrCl}_2$) forms with montmorillonite/ AlR_3 the active olefin polymerisation catalyst. The solvent was removed and the residue again was washed twice with toluene. The catalyst was either used immediately for ethylene or propylene polymerisation, or stored.

No further addition of aluminum alkyls or MAO was necessary for the olefin polymerisations. In ethylene and propylene polymerisation the metallocene catalysts formed by reactions with montmorillonite / $\text{Al}(\text{iBu})_3$ are as active as those formed with montmorillonite / AlMe_3 (tables 1 to 4).

As postulated for homogeneous metallocene / MAO catalysts the heterogeneous catalysts on montmorillonite can also form weakly coordinating aluminate anions and Ti, Zr or V cations.

Fig. 1. Formation of active heterogeneous Ziegler-Natta and Metallocene Catalysts by Surface Reactions with Montmorillonite

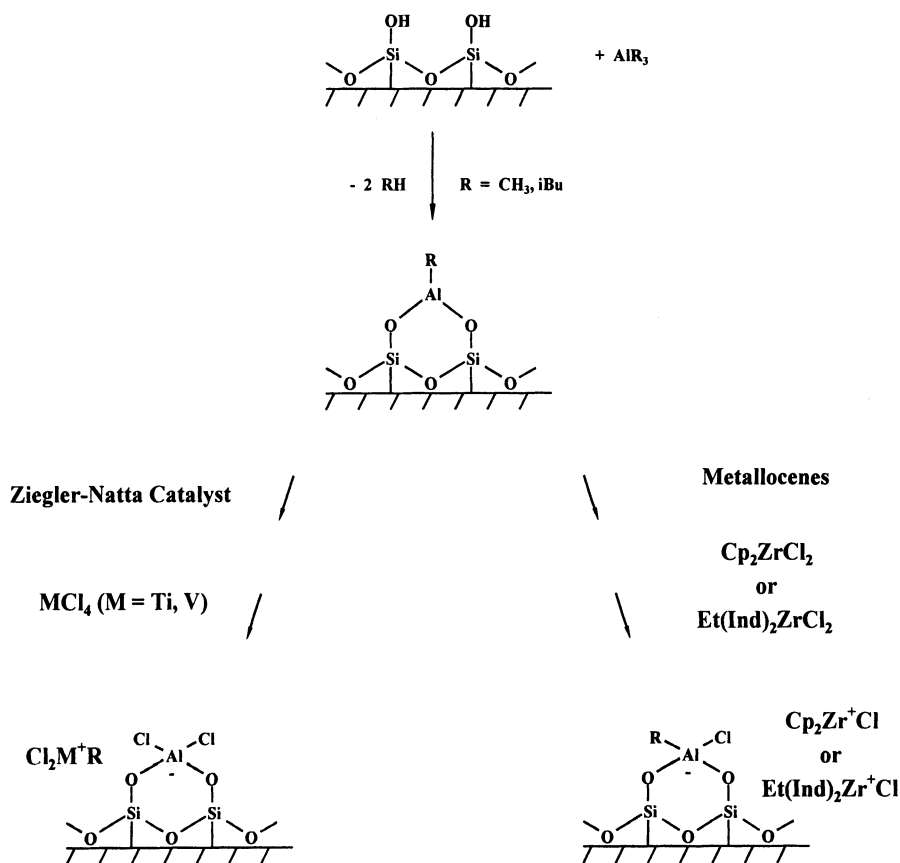


Table 1. Ethylene - Polymerisation with Montmorillonite / AlMe₃ / Cp₂ZrCl₂

5 g Montmorillonite; solvent: heptane; pressure [C₂H₄]: 10 bar; T_{pol.} = 50°C; reaction time: 60 min; no fouling;

¹ 2.5 g Montmorillonite; ² stored for 1 week at - 30°C

| mmol | | Molar ratio | Yield PE | Activitiy A | M _n • 10 ⁻⁶ | T _M |
|------------------|-------|-------------|----------|------------------|-----------------------------------|----------------|
| Al | Zr | Al / Zr | [g] | [kg PE/mol Zr h] | [g / mol] | [°C] |
| 6 | 0.024 | 250 / 1 | 100 | 4 200 | 0.37 | 135.3 |
| 12 | 0.006 | 2 000 / 1 | 81.1 | 13 500 | 0.34 | 136.5 |
| 6 ¹ | 0.012 | 500 / 1 | 75.1 | 6 300 | 0.38 | 136.1 |
| 6 ^{1,2} | 0.012 | 500 / 1 | 64.1 | 5 300 | 0.34 | 136.1 |

Table 2. Ethylene - Polymerisation with Montmorillonite / Al(iBu)₃ / Cp₂ZrCl₂

reaction conditions see table 1

| mmol | | Molar ratio | Yield PE | Activitiy A | M _n • 10 ⁻⁶ | T _M |
|------|-------|-------------|----------|------------------|-----------------------------------|----------------|
| Al | Zr | Al / Zr | [g] | [kg PE/mol Zr h] | [g / mol] | [°C] |
| 12 | 0.024 | 500 / 1 | 43.5 | 21 800 | 0.20 | 137.0 |
| 12 | 0.006 | 2 000 / 1 | 84.5 | 14 100 | 0.40 | 136.1 |
| 6 | 0.012 | 500 / 1 | 81.0 | 6 800 | 0.35 | 136.3 |

Table 3. Propylene - Polymerisation with Montmorillonite / AlMe₃ / rac-EtInd₂ZrCl₂

5 g montmorillonite; 250 ml propylene; T_{pol.} = 40°C; reaction time: 60 min; purification of propylene: 12 mmol Al(iBu)₃;

¹ reactive, stopped after 20 minutes; ² 2.5 g Montmorillonite

| mmol | | Molar ratio | Yield PP | Activitiy A | M _n | T _M | mmmm |
|-----------------|--------|-------------|----------|------------------|----------------|----------------|------|
| Al | Zr | Al / Zr | [g] | [kg PP/mol Zr h] | [g / mol] | [°C] | [%] |
| 12 ¹ | 0.03 | 400 / 1 | 110.2 | 11 000 | 8 500 | 113.8 | 59.5 |
| 6 ² | 0.0075 | 800 / 1 | 115.0 | 15 300 | 14 000 | 123.6 | - |
| 3 | 0.0038 | 800 / 1 | 25.3 | 6 800 | 15 000 | 128.6 | - |

Table 4. Propylene - Polymerisation with Montmorillonite / Al(iBu)₃ / rac-EtInd₂ZrCl₂

reaction conditions see table 3; ¹ 1 g Montmorillonite

| mmol | | Molar ratio | Yield PP | Activitiy A | M _n | T _M | mmmm |
|----------------|--------|-------------|----------|------------------|----------------|----------------|------|
| Al | Zr | Al / Zr | [g] | [kg PP/mol Zr h] | [g / mol] | [°C] | [%] |
| 12 | 0.03 | 400 / 1 | 117.4 | 3 900 | 15 000 | 128.3 | - |
| 6 | 0.0075 | 800 / 1 | 109.9 | 14 600 | 14 000 | 127.7 | - |
| 6 ¹ | 0.0075 | 800 / 1 | 96.9 | 12 900 | 14 000 | 126.8 | - |
| 6 | 0.0019 | 3 200 / 1 | 113.1 | 60 300 | 11 000 | 122.8 | 72.1 |

The heterogeneous metallocene catalysts on the montmorillonite carrier have activities in ethylene and propylene polymerisation like those known of homogeneous metallocene catalysts (table 5).

Table 5. Ethylene and Propylene Polymerisation Activities of homogeneous and heterogeneous Zirconocene Catalysts on Silica (already published by W. Kaminsky and K. Soga) and our results with heterogeneous Zirconocene Catalysts on Montmorillonite

¹ Activities: kg PP (PE) / mol Zr h; ² very reactive, stopped after 1 minute

| Metallo- cene | published results ¹ | | our results ¹ |
|---|--------------------------------|---------------------------|------------------------------------|
| | homogeneous (MAO) | heterogeneous (Silica) | heterogeneous (Montmorillonite) |
| PP Cp ₂ ZrCl ₂ | 140 | 99 | 4 600 |
| PP rac-Et(Ind) ₂ ZrCl ₂ | 1700 | 26 | 14 800 |
| PE Cp ₂ ZrCl ₂ | 60 900 | - | 13 300 |
| PE rac-Et(Ind) ₂ ZrCl ₂ | 12 000 | 121 | ca. 40 000 ² |

The heterogeneous aluminoxane does not only form metallocene catalysts, but also heterogeneous Ziegler-Natta catalysts by reactions with TiCl₄ or VCl₄ (figure 1). Both types of Ziegler-Natta catalysts produce high molecular weighted polyethylenes (table 6).

Table 6. Ethylene Polymerisation with Montmorillonite / AlMe₃ / TiCl₄ and Montmorillonite / AlMe₃ / VCl₄

5 g Montmorillonite; solvent: heptane; pressure [C₂H₄]: 10 bar; T_{pol.} = 50°C; reaction time: 60 min; no fouling; ¹ 1 g Montmorillonite

| Catalyst | mmol | | Molar ratio Al / M | Yield PE [g] | Activity [kg PE / mol M h] | M _η · 10 ⁻⁶ [g / mol] | T _M [°C] |
|-------------------------------|------|-------|-----------------------|-----------------|-------------------------------|--|---------------------|
| | Al | M | | | | | |
| TiCl ₄ | 6 | 0.08 | 75 / 1 | 58.3 | 729 | 4.8 | 134.1 |
| TiCl ₄ | 6 | 0.06 | 100 / 1 | 85.2 | 1 420 | 3.2 | 133.7 |
| VCl ₄ | 3 | 0.012 | 250 / 1 | 33.5 | 2 792 | 1.4 | - |
| VCl ₄ ¹ | 1.2 | 0.012 | 100 / 1 | 89.1 | 7 428 | 3.6 | 134.1 |

References

- [1]H. Lang, S. Blau, A. Muth, K. Weiss and U. Neugebauer *J. Organomet. Chem.* (1995), 490 ,C 32 - 36.
- [2]K. Weiss, U. Neugebauer, S. Blau and H. Lang *J. Organomet. Chem.* (1996), 520, 171 – 179.
- [3]K. Weiss and G. Lössel *Angew. Chem. Int. Ed. Engl.* (1989), 28, 62 – 64.
- [4]W. Kaminsky and F. Renner *Makromol. Chem. Rapid Commun.* (1993), 14, 239 – 243.
- [5]K. Soga and T. Shiono *Prog. Polym. Sci.* (1997), 22, 1503 – 1546.

2. Homogeneous Catalysis, Synthesis and Polymerization

Formation, structure and mechanism of oligomeric methylaluminoxanes (MAO)

Hansjörg Sinn*, Ingrid Schimmel*, Mathias Ott*, Norbert von Thienen*, Annette Harder*, Wiebke Hagendorf*, Bernd Heitmann*, Erhard Haupt**

*Institut für Technische und Makromolekulare Chemie
Universität Hamburg
Bundesstraße 45
D 20146 Hamburg, Deutschland

**Institut für Anorganische und Angewandte Chemie
Universität Hamburg
Martin-Luther-King-Platz 6
D 20146 Hamburg, Deutschland

Abstract. Evidence for hexa-methyl-tetra-aluminoxane as a main product of MAO is demonstrated. Stability and measured molecular weights in benzene, trimethylaluminum, dioxane and tetrahydrofurane are explained by self-association. A new band reactor is described to produce MAO in a small temperature range. NMR-spectra during preparation and after the completion of the reaction allow to understand the mechanism of formation. A compound $[Al_2(CH_2)_3]_n$ insoluble in hydrocarbons is prepared.

Introduction

Aluminumalkyls activate metallocenes like Cp_2TiCl_2 , $Cp_2Ti(CH_3)Cl$, Cp_2ZrCl_2 and $Cp_2Zr(CH_3)Cl$ to polymerize ethene^{1,2,3}, but MAO activates the above mentioned metallocenes **and in addition** $Cp_2Ti(CH_3)_2$ and $Cp_2Zr(CH_3)_2$ to polymerize ethene **and** alpha-olefines⁴.

MAO is produced from aluminumtrimethyl and water. Unfortunately the activating power is different when aluminumtrimethyl and water or MAO - prepared separately - is added to metallocenes in solution.

It was summarized⁵: „recent works demonstrates that the transition metal is

1 G.Natta, P.Pino, G.Mazzanti, J.Giannini, JACS 79 (1957) 2975

2 D.S.Breslow, N.R.Newburg, JACS 79 (1957) 5073

3 F.Patat, H.Sinn, Angew.Chemie 70 (1958) 496

4 H.Sinn, W.Kaminsky, H.-J.Vollmer, R.Woldt, DE 3007725, US 4404344

associated with the aluminoxane in activated metallocene-aluminoxane complexes.“ Therefore we try to get more insight in the formation and structure of MAO and whether the structure of MAO allows to understand his specific cocatalytic power.

Section I. Evidence for hexa-methyl-tetra-aluminoxane

There is evidence that a compound with a ratio $\text{CH}_3/\text{Al} = 1,5$ plays an important role forming the MAO.

1°: If we add diethyl-ether to a solution of methylaluminoxane MAO and trimethylaluminum TMA in toluene, a phase separation takes place ⁶. After phase separation all TMA will be found in the upper phase.

The lower phase - after washing with toluene - has a composition: one diethyl-ether molecule for 8 aluminum atoms, 12 methyl groups and 6 oxygen atoms.

The lower phase - after washing with diethylether - has a composition: one toluene molecule and 3-4 diethylether molecules for 16 aluminum atoms, 24 methyl groups and 12 oxygen atoms .

From the upper phase trimethylaluminum-etherate can be condensed off; the composition of the residue is 1-2 diethylether molecules for 8 aluminum atoms, 10-12 methylgroups and 6 oxygen atoms.

2°: Of interest is the reaction of MAO mixed with TMA with an excess of tertiary butyl alcohol: All the methyl groups bound to aluminum react rapidly under methane evolution.

The formed alcoholate of aluminum is totally insoluble in dimethoxyethane. Thus it is possible to find out the amount of TMA originally present, after digesting and washing with dimethoxyethane and quantitative estimation of the precipitation⁷. The purity was shown by X-ray diffraction.

In the solution remains the alcoholate of the „true“ MAO. By mass-balance it was shown, that the true MAO in solution has had the composition: methylgroups to aluminum atoms equal to 1.44 to 1.5. Looking at the numerical value 1.44 we will remember, that the alcoholate of MAO splits off further alcoholate of aluminum in a slow reaction.

-
- 5 W.R.Beard,D.R.Blevins,D.W.Imhoff,B.Kneale,L.S.Simeral, Conf.Proceed.,The Material Institute London, The International Polyethylene Conference 1997
 - 6 J.Bliemeister, W.Hagendorf, A.Harder, B.Heitmann, I.Schimmel, E.Schmedt, W.Schnuchel, H.Sinn (correspondence), L.Tikwe, N.von Thienen, K.Urlass, H.Winter, O.Zarncke in *Ziegler Catalysts*, G.Fink,R.Mülhaupt, H.H.Brintzinger(Eds.), Springer 1995, p.57
 - 7 W.Hagendorf, A.Harder, H.Sinn, *Macromol.Symp.*97 (1995) 127.

3°: In a very nice investigation of Thorn-Csányi and Dehmel in our institute it was shown⁸, that TMA reacts with tungsten-oxychloride in a very fast reaction, whereas MAO reacts only slow. So it is possible to distinguish between TMA and the „true“ MAO. They estimated with this method the ratio of $\text{CH}_3\text{-/Al}$ in true MAO to be 1.48 to 1.52.

4°: Recently a group from Albemarle Corporation was able to determine the ratio of TMA to MAO using proton nuclear magnetic resonance. They determined the $\text{CH}_3\text{-/Al}$ ratio in „true“ MAO to be 1.5 - 1.4⁹ and 1.5 - 1.3¹⁰. In combination with molecular weight determinations in dioxane they calculated the molecular weight of the „true“ MAO to be 850 with standard deviation of 100.

5°: During this conference Eilertsen, Rytter and Ystenes reported: „The MAO sample has a $\text{CH}_3\text{-/Al}$ ratio close to 1.5 and should contain no or little free TMA“. The result is based on IR-investigations¹¹.

6°: Deconvolution of a NMR-signal of a MAO free of TMA shows two different methyl groups in the ratio 4/2¹².

Concluding we identify hexa-methyl-tetra-aluminoxane as a brick of MAO; this brick as well as the formed MAO shows a ratio of methyl-groups to aluminum atoms of 1.5 and the hexa-methyl-tetra-aluminoxane shows two different methyl-groups in the ratio 4/2, which is in agreement with the NMR-observations.

Thus, two questions arise:

- How is hexa-methyl-tetra-aluminoxane build up and why is the reaction stopped after the formation of hexamethyltetraaluminoxane?
- Why do we find in apolar and polar solvents different molecular weights which correspond to a multiple of hexamethyltetraaluminoxane ?

To the first question there is one very simple answer. A further build up is stopped by the self-coordination of the hexa-methyl-tetra-aluminoxane.

8 E.Thorn-Csányi, J.Dehmel, O.Halle, W.Sciborski, Makromol.Chem.Phys. **195** (1994) 3017

9 D.W.Imhoff, L.S.Simeral, S.A.Sangokoya, J.H.Peel, Organometallics **17** (1998) 1941.

10 Cf. 5

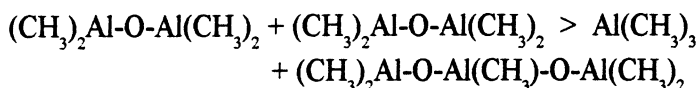
11 J.L.Eilertsen, E.Rytter, M.Ystenes, Proc.of the Int.Symp.on Metalorganic Catalysts for Synthesis and Polymerisation, W.Kaminsky(Ed.) Springer 1999.

12 H.Sinn, Macromol.Symp.,**97** (1995) 27.

Perhaps not the first, but the second or third step in the formation of MAO, using TMA and frozen water, is undoubtedly the formation of tetra-methyl-di-aluminoxane.

A sequence of reactions characterised by intermolecular splitting off TMA from two molecules of tetramethyldialuminoxane forming pentamethyltrialuminoxane and TMA or intermolecular splitting off TMA from one molecule of tetramethyldialuminoxane and one molecule of pentamethyltrialuminoxane forming hexamethyltetraaluminoxane and TMA is shown in the sketch Figure 1.

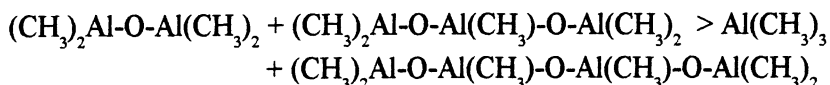
The sequence starts with two molecules of tetramethyldialuminoxane which are shown in orthogonal position. The reaction



proceeds nearly without changing a position of any atom. The bonds can be arranged forming TMA and pentamethyltrialuminoxane. The formation of TMA is proven experimentally. The next line of the sketch shows the pentamethyltrialuminoxane molecule in his „in situ“ position and the third line the same molecule in a stretched position.

The next line of the sketch shows pentamethyltrialuminoxane in a stretched position with one molecule of tetramethyldialuminoxane added in orthogonal position comparable to the position in the first line.

Renewed splitting off of TMA is possible in the same manner as before and in this reaction the hexamethyltetraaluminoxane is formed.



The last line in the sketch of Figure 1 shows the hexamethyltetraaluminoxane in its „in situ“ position. It is shown how the molecule coordinates itself. This selfcoordination of hexamethyltetraaluminoxane prevents a new and further addition of a tetramethyldialuminoxane or a pentamethyltrialuminoxane in a position from which splitting off of TMA is possible and this leads to hexamethyltetraaluminoxane as the main product. Nevertheless, side reactions may produce heptamethylpentaaluminoxane from two molecules of pentamethyltrialuminoxane. But this reaction is suppressed due to kinetic reasons.

However, in the hexamethyltetraaluminoxane molecule three of the four aluminumatoms and two of the three oxygen atoms are coordinatively unsaturated; this causes further selfassociation.

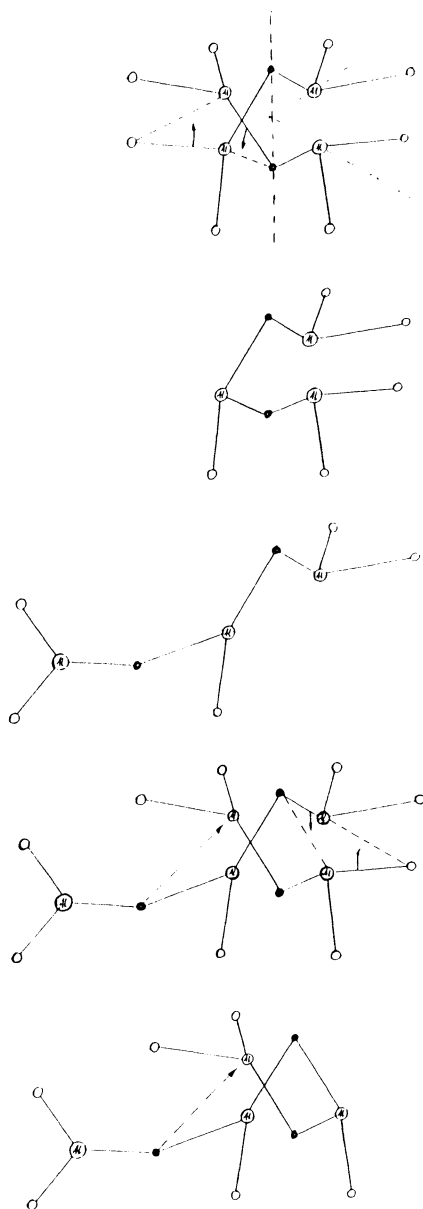


Fig. 1. Sketch to explain the reaction sequence forming hexamethyltetraaluminoxane and to show the selfcoordination which stops the reaction; cf. text.
 O = methyl group; o = oxygen atom; (Al) = aluminum atom.

Section II. Selfassociation of hexamethyltetraaluminumoxane and interpretation of the molecular weights cryoscopically found in benzene, TMA and dioxane and ebullioscopically found in tetrahydrofurane.

As mentioned before the Albemarle group reported molecular weights of „true“ MAO in the range of 850 with a standard deviation of 100.

Claiming the catalyst system methylaluminumoxane/MAO and organozirconium compounds, especially dimethylzirconocen, in 1980¹³ it was said, that best results were obtained if the degree of oligomerisation of the MAO is greater five, especially greater ten.

We measured with cryoscopy for mixtures of MAO and TMA in benzene molecular weights of 1,200. Later we found that the same products showed in tetrahydrofurane by ebullioscopic measurements molecular weights of 350 to 400¹⁴. In the meantime we measured the molecular weights of a lot of MAO samples in benzene, in trimethylaluminum and in dioxane. The results are reported in some PhD thesis^{15,16,17} and summarized in¹⁸. Normally we found 1,100-1,200 in benzene and TMA and 400 - 500 in dioxane.

The results correspond with the formula $\{[Al_4O_3(CH_3)_6]_4\} * nAl(CH_3)_3$. In benzene or TMA this complex is found as *one* particle. In polar solvents like dioxane or tetrahydrofurane it is found as *two particles* if $n = 1$ and as *three particles* if $n = 2$. This means that molecular weight of „true“ MAO is 984. If for one molecule of „true“ MAO two molecules of TMA in benzene are present, it will be found a molecular weight of 1128 due to the strong association of TMA with MAO which forms $\{[Al_4O_3(CH_3)_6]_4\} * 2Al(CH_3)_3$.

If the same composition of one „true“ MAO and two molecules of TMA is dissolved in dioxane or tetrahydrofurane a molecular weight of 376 is expected.

The ratio of CH_3-/Al for the whole complex is 27/17 if $n = 1$ and 30/18 if $n = 2$. So it is possible to estimate the value of n with this ratio. This is the weak point. It is very difficult to differentiate between a ratio CH_3-/Al of 1.51 and 1.49 or 1.67 and 1.65. It is an additional problem, that the molecular weight determinations are only accurate within 5-10%.

13 Cf. 4

14 J.Bliemeister, Dissertation Universität Hamburg 1990

15 H.Winter, Dissertation Universität Hamburg 1990

16 W.Schnuchel, Dissertation Universität Hamburg 1993

17 B.Heitmann, Dissertation Universität Hamburg, will be published in 1999

18 K.v.Lacroix, B.Heitmann, H.Sinn, Macromol.Symp.,97 (1995) 137

Within these limits the Albemarle-measurements cited above¹⁹, where the content of TMA is determined by NMR spectroscopy, are in agreement with our results.

However, if hexamethyltetraaluminoxane is four-fold associated it satisfies the most measured molecular weights and furthermore all oxygen atoms and every three of four aluminum atoms are saturated coordinatively. The possible molecular models are shown in Figures 2 and 3. The shown neighbourhood of the dimethylaluminum groups prepare for split off of TMA. In addition it is shown that all methyl-groups are located on an „outer“ shell, surrounding an „inner“ shell of Al-O-network.

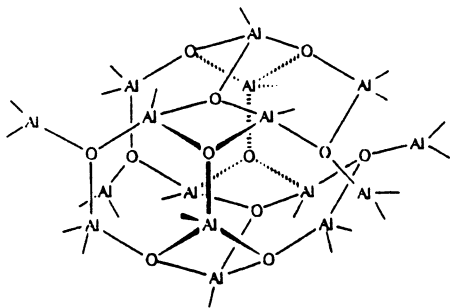


Fig.2. Model type A of $[Al_4O_3(CH_3)_6]_4$
Type A has four- and six-membered rings and has a certain flexibility. Every bond-dash bears a methyl-group.

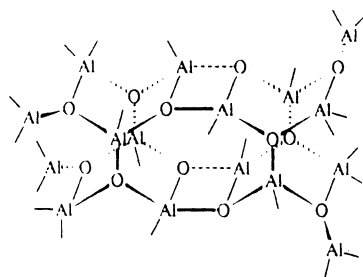


Fig.3. Model type B of $[Al_4O_3(CH_3)_6]_4$
Type B has four-, six- and eight-membered rings and has a rigid structure. Every bond-dash bears a methyl-group.

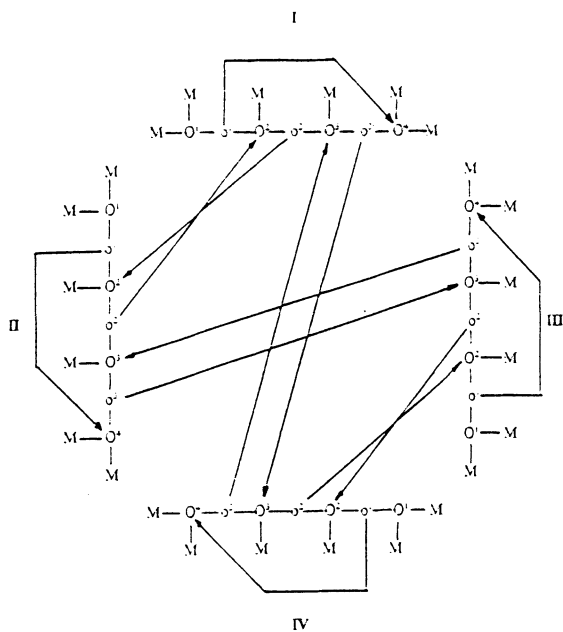
The model shown in Figure 2 was published²⁰ accompanied by a proposal how the catalytically active complex together with metallocene may be formed. Looking at the structure of MAO it seems to be possible that MAO works as a „wrapper“ or „envelope“ for one tetramethyl-aluminum ion, which may be centered within the MAO, inside the positively charged inner shell of the MAO micella, which is there coordinatively saturated and binds the more cationic part of the metallocene.

The formation of the coordination bonds is shown in Figures 4 and 5.

19 Cf. 5 and cf. 9

20 Cf. 6 p.75 Fig. 13 and cf. 12

Model A



Model B

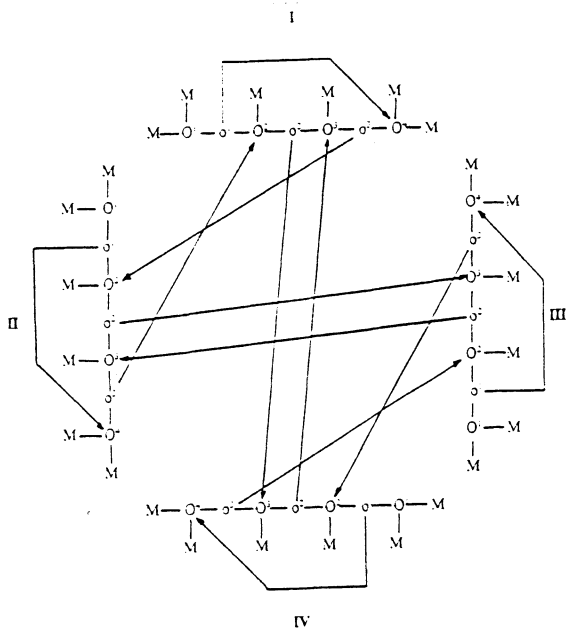


Fig.4 (A) and 5 (B) Me = methyl; o = oxygen atom; O = aluminatom.
 In every molecule I,II,III and IV a free pair of electrons of o^1 coordinates to the
 electroneficiency of O^4 . The rings I,II,III and IV are formed. The two possibilities
 of the association $4 [Al_4O_3(CH_3)_6] \longleftrightarrow [Al_4O_3(CH_3)_6]_4$ are demonstrated.

It is believed that the catalytic activity of the metallocene center is stimulated by its surroundings in a similar sense as Calvin demonstrated comparing different surroundings of an iron-ion (cf. Figure 6)²¹.

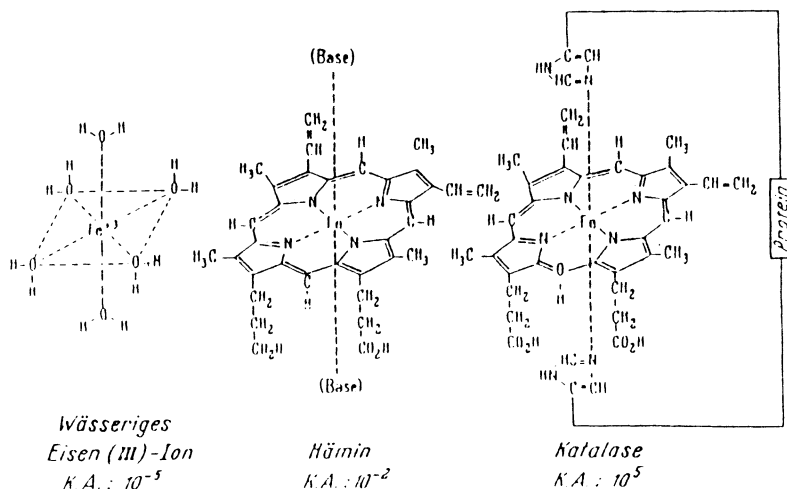


Fig.6. A comparison given by Calvin on the catalytic activity K.A. of an iron(III)-ion as a function of its surroundings. If the hydrate is replaced by the haemine and this is replaced by the haemine-enzyme the activity is increased 10 powers of 10.

There is no doubt that beside of such structures other species of MAO are present. Perhaps it was only a lucky chance when in an experiment where we added diethylether to a solution of MAO in toluene, the content of $[(\text{CH}_3)_6\text{Al}_4\text{O}_3]_4$ was high, so that we got a strong phase separation. However, if we got strong phase separations, the samples showed also good cocatalytic activities. Therefore we are engaged to find the conditions where a high amount of $[(\text{CH}_3)_6\text{Al}_4\text{O}_3]_4$ is produced (Section III).

One side reaction is the reaction between two neighbouring $-\text{Al}(\text{CH}_3)_2$ -groups with splitting off of one TMA. Because we have eight $-\text{Al}(\text{CH}_3)_2$ -groups it is theoretically possible to split off four TMA molecules.

If all the eight $-\text{Al}(\text{CH}_3)_2$ groups react the formula $[(\text{CH}_3)_6\text{Al}_4\text{O}_3]_4$ changes to $[(\text{CH}_3)_3\text{Al}_3\text{O}_3]_4$ which would be the ideal formula of a methylaluminoxane. Such products with tertiary butyl groups instead of methyl groups were iso-

21 The comparison was made by Melvin Calvin, nobelprize winner in 1961. As a vision this picture accompanies us since more than 40 years. Unfortunately we are missing the original source.

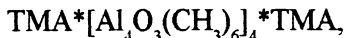
lated and characterized by Barron²². With methyl groups it was not possible to reach such a composition. Trying to do so products get insoluble and cocatalytic activity is decreased.

If only one TMA is split off the formula $[(CH_3)_6Al_4O_3]_4 = (CH_3)_{24}Al_{16}O_{12}$ is changed to $(CH_3)_{21}Al_{15}O_{12}$ with a ratio of $CH_3-/Al = 1.40$ and a molecular weight of 912.

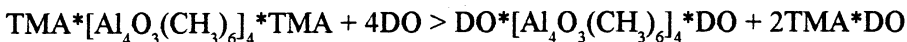
If two molecules of TMA are split off, the formula $(CH_3)_{24}Al_{16}O_{12}$ changes to $(CH_3)_{18}Al_{14}O_{12}$ with a ratio of $CH_3-/Al = 1.29$ and a molecular weight of 840 (cf. the results of the Albemarle group).

With a view on the models Figure 2 and 3 it is obvious, that not only the described intramolecular cleavage reactions are possible but also intermolecular reactions. If two $-Al(CH_3)_2$ groups of two different molecules $(CH_3)_{24}Al_{16}O_{12}$ react with each other, splitting off one molecule of TMA, a big molecule $(CH_3)_{45}Al_{31}O_{24}$ is produced with a ratio $CH_3-/Al = 1.45$ and a molecular weight 1,896. Values up to 3,600 were found.

In the MAO molecule $\{[Al_4O_3(CH_3)_{6,4}]\} * 2Al(CH_3)_3$, where the „true“ MAO molecule is complexed with two molecules of TMA:



the TMA will be replaced with polar compounds (donors DO) like diethylether, tetrahydrofurane or dioxane:



Inspecting the model of MAO it is seen that four $-Al(CH_3)_2$ -groups are coordinatively unsaturated. This means that it is allowed to formulate



to explain the determined ratio of (diethylether molecules)/Al-atoms of $4/16 = 1/4$.

We have to distinguish between the following reactions which evolve methane:

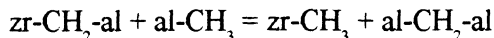
1°) A methylgroup of a metallocene (me- CH_3 , preferred ti- CH_3) reacts with a methylgroup of TMA or a methylgroup of $-Al(CH_3)_2$ in MAO forming ti- CH_2 -al²³. The $-CH_2$ -al group reacts as a normal ligand and is especially

22 M.R.Mason, J.M.Smith, S.G.Bott, R.Barron, JACS 115 (1993) 4971-4984

23 ti = one valency of titanium, al = one valency of aluminum.

exchanged against other alkylgroups. Thus, in a stepwise catalytic process, a polymer $-Al(CH_3)CH_2[Al(CH_3)CH_2]_n Al(CH_3)CH_2-$ is formed²⁴(which is iso-electronic with $-Al(CH_3)-O-[Al(CH_3)-O-]_n Al(CH_3)-O-$).

Especially in the zirconocenesystem the equilibrium

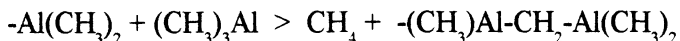


will explain some of the so-called „dormant“ species.

2°) As mentioned before, in an intermolecular reaction two methylgroups of two $-Al(CH_3)_2$ groups react under methane evolution:



As far as we can see also the reaction between a aluminumdimethylgroup of MAO and a molecule of TMA takes place



We have found, that only the methyl groups of the aluminum atoms of MAO, which are not saturated coordinatively, and all the methyl groups of TMA are able to react.

3°) K.Ziegler reported the thermal decomposition of TMA and postulated a compound $[Al_2(CH_2)_3]_n$ as an intermediate²⁵. We showed that a solution of TMA in a high boiling hydrocarbon decomposes slowly at 175-185°C under methane evolution and the reaction is stopped accurately when 3 moles of CH_4 per 2 moles of TMA are evolved. The product is insoluble in hydrocarbons and we have therefore no molecular weight, but elementary analysis and analysis by decomposition with water agree with $[Al_2(CH_2)_3]_n$. We have prepared some kilograms of this interesting compound which will be used as scavenger and also to heterogenize MAO. This will be published separately.

As mentioned earlier²⁶, after phase separation the lower phase shows an unexpected high density of 0.95 g/ml. This proofs a very dense package of the dissolved MAO. Unfortunately we were never able to get crystals. However, we have done diffraction experiments with synchrotron radiation. The results are given in the Figure 7.

24 H.Sinn, H.Hinck, F.Bandermann, H.F.Grützmacher, Angew.Chemie Int.Ed.,7 (1968) 217

25 K.Ziegler, K.Nagel, M.Patheiger, Z.anorg.allg.Chem., 282 (1955) 345

26 Cf. 12, p. 30, table II

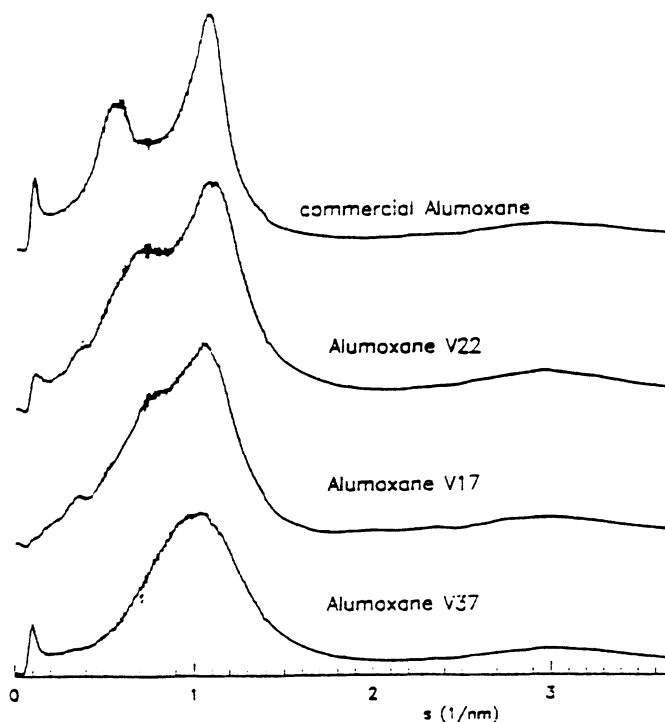


Fig.7. Scattering curves of various MAO samples done by N.von Thienen and R. Gehrke, both DESY, Deutsches Elektronensynchrotron Hamburg. The s value corresponds with distances 1.0, 1.4 and 1.7 nm, equal to the distances of model A.

It is too early to try an interpretation, but the fact that different MAO samples showed different diffraction curves stimulates once more to prepare MAO under very precise conditions and to correlate conditions of production with the activity.

Section III. A new thinfilm reactor to prepare MAO, the „Eisbandreaktor“

We know by numerous experiments²⁷, that at -40°C from a surface of ice of about 300 cm^2 with a 1 molar solution of TMA about 3 moles of methane are evolved per hour, corresponding of 27 grams of ice used for the reaction with the methyl groups of TMA. This means $27,000\text{ mm}^3 / (3,600\text{ sec } 30,000\text{ mm}^2) = 0.25\text{ }\mu\text{m/sec}$ of the ice are reacted.

If it would be possible to deposit such a thin film of ice on a carrier and to bring this carrier into a solution of TMA, a reaction would proceed within one or some seconds and no more reaction would be possible because all the ice is

²⁷ Cf.15 and cf. 16

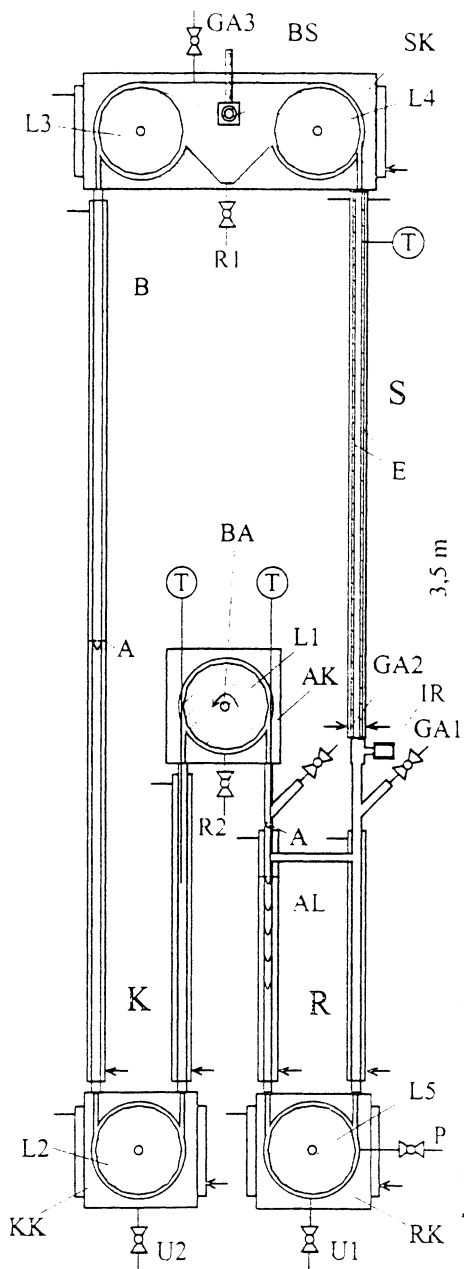


Fig.8. Cross section of the „Eisbandreaktor“. The cooled steelband driven with BA picks up ice E by sublimation in the sublimation chamber S and introduces the ice into the reaction chamber R where the ice reacts with a solution of TMA producing MAO and methane. The band passes some skimmers AL which strip adsorbed MAO and runs to the cooling chamber K .

used and the carrier could be able to catch the reaction heat and to transport it away. To get more reaction, more carrier is needed. To realize this an endless-carrier may be the best. This requires the following steps a) - c):

- a) To deposit ice of defined thickness on a carrier;
- b) To bring this carrier into the solution of TMA
- c) To clean the carrier and to bring it back to the point where a) starts.

This is the simple idea of what we call the „Eisbandreaktor“²⁸. It was realized with an endless band of stainless steel, 10mm broad and 0.2mm thick. It was also realized with a wire with 0.4mm diameter. MAO was produced at -40°C and at -5°C in toluene but also in n-heptane. The samples showed a good phase separation and a good cocatalytic activity. The deposition of the ice on the carrier was done by sublimation.

The realized „Eisbandreaktor“ is somewhat simpler than that described in the patent. We worked without the proposed „washing chamber“. The essential dates of the reactor shown in Figure 8 are:

- a) Endless steelband, $0.2 \cdot 10^{-3}\text{m}$ thick, $1.0 \cdot 10^{-2}\text{m}$ broad;
- b) heat capacity of 10^{-4}m^2 steelband is $63.2 \cdot 10^{-3}$ Joule/grd;
- c) ice-film by sublimation at both sides $0.1 \cdot 10^{-4}\text{m}$ thick;
- d) heat capacity of 10^{-4}m^2 ice-film is $20.9 \cdot 10^{-6}$ Joule/grd;
- e) reaction enthalpy in 10^{-4}m^2 ice-film is 0.22 Joule (calculated with the estimated value of 200 KJoule/mole methane evolution);
- f) adiabatic temperature increase of the steelband is < 7 grd;
- g) the reaction proceeds within some seconds after insertion of the steelband into the reaction chamber with a TMA solution
- h) TMA solutions with concentrations up to 2 moles/l were used
- i) proposed band velocities are between 0.1 and 0.7 m/s. For a short time we used 1.5 m/s.

As it is seen in Figure 8 we have the possibility to take off small samples at the valve U1 during the reaction from the reaction chamber. This was done.

The reaction was either stopped by introducing immediately the sample into cold diethylether or the sample was worked up in the usual manner. The results are given in Section IV.

Section IV. Remarks on NMR investigations ²⁹

With numerous samples of MAO which were prepared in toluene we got the same or very similar results in NMR spectroscopy as recently reported^{30, 31}.

²⁸ German Patent 19626245

²⁹ Cf. M.Boleslawski, J.Serwatowski, J.Organometal.Chem, **255** (1983) 269-278

Perhaps it is interesting to note that the sharp signal, usually attributed to TMA, disappears if the MAO is made solvent free in a vacuum, dissolved in TMA, the resulting solution is frozen and subsequently freeze-dried³². This signal disappears also if a MAO sample is dissolved in dioxane and precipitated with n-pentane. If solving and precipitating is repeated eight times, nothing of the sharp signal is to be seen.

Examples are given in Figure 10 and Figure 11. Unfortunately these examples were measured 1992 and 1995 only with 100 Mhz ¹H-frequency.

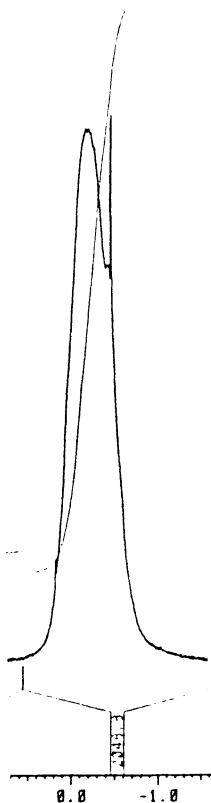


Fig.10. NMR-Signal of MAO, prepared in toluene, dried, dissolved in dioxane, precipitated with n-pentane and dried. The process of dissolution and precipitation was repeated three times.

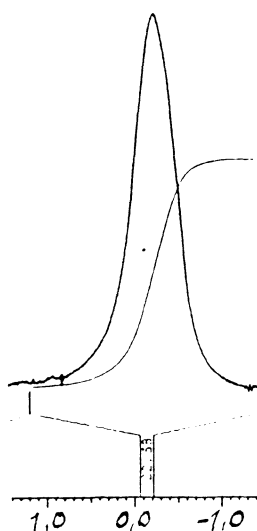


Fig.11. NMR-Signal of MAO, prepared in toluene, dried, dissolved in dioxane, precipitated with n-pentane and dried. The process of dissolution and precipitation was repeated eight times.

30 Cf. 5

31 Cf. 9

32 Cf. 12, p. 39

In contrast to this, if we reacted TMA with water in dioxane or in tetrahydrofuran we got significant structured NMR-signals in the range of the methylprotons bound to aluminum. Such spectra are shown in Figures 12 and 13.

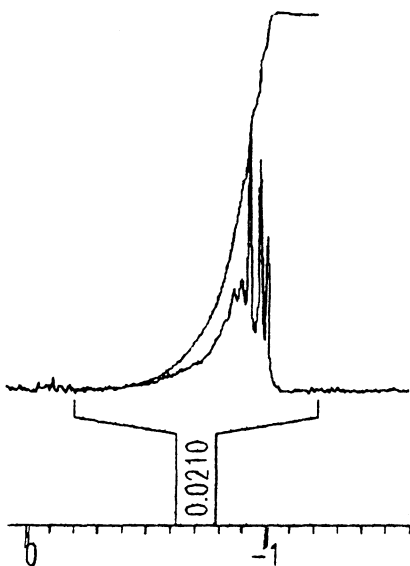


Fig.12. NMR-spectrum of MAO prepared in tetrahydrofuran. To the solution of TMA in tetrahydrofuran was added water (Ott, v. Thienen 305, 30.06.1995)

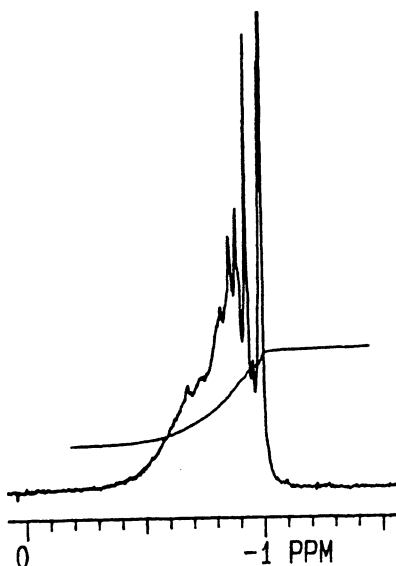


Fig.13. NMR-spectrum of MAO prepared in dioxane. To the solution of TMA in dioxane was added water till 50% of the methyl-groups were evolved as methane.

Now, after we had the band reactor, it was very surprising to see that samples prepared in toluene by reaction of a solution of TMA with the ice-film on the stainless steel band showed initially the same significant structured NMR-signals. After a conversion of 19% of the methyl groups at -27°C a sample was let out and flown immediately in a vessel with diethylether. This sample was dried in vacuum for 12 hours, then dissolved in dioxane- d_8 (Figure 14).

The reaction was stopped when 24,5% of the methyl groups were evolved as methane. About one hour later a part of the reaction mixture was given into diethylether, warmed up, dried in a vacuum for 12 hours and dissolved in dioxane- d_8 (Figure 15).

With additional two samples of the same reaction mixture, the usual procedure of working up was done. From the reaction mixture the volatile compounds, solvent and a part of the TMA was condensed off and the residue dried in a vacuum of 10^{-3} Pa for 12 hours.

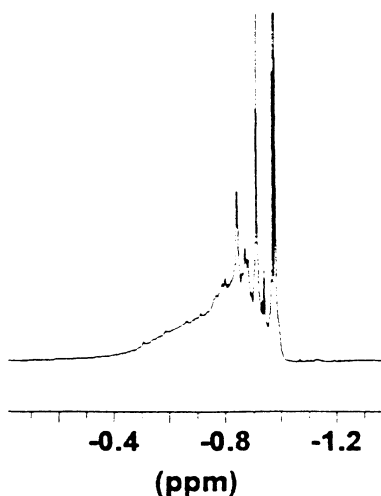


Fig.14. Sample of a reaction mixture in toluene; the icefilm is reacted with TMA; 19%³³ conversion of the methyl groups; sample immediately given into diethylether, dried in vacuum for 12 hours, dissolved in dioxane-d₈ and measured.

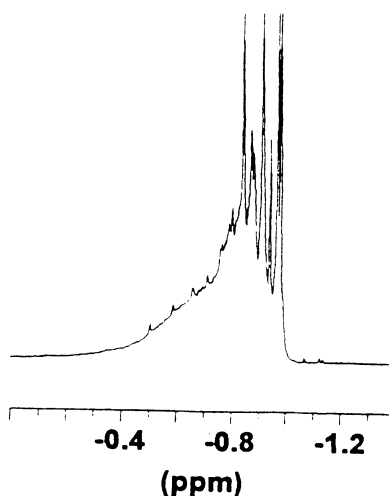


Fig.15. Sample of a reaction mixture in toluene; the icefilm is reacted with TMA; 24,5%³⁴ conversion of the methyl groups; sample one hour later given into diethylether, dried in vacuum for 12 hours, dissolved in dioxane-d₈ and measured.

One sample was than dissolved in toluene and diethylether was added to test the phase-separation. Without separation the phases, the mixture was dried as before and the residue dissolved in dioxane-d₈. The NMR-spectrum is shown in Figure 16. Another sample was dissolved in toluene only; the solution was dried in a vacuum of 10^{-3} Pa for 12 hours - that is identical how we normally isolate the MAO - and the residue dissolved in dioxane-d₈. The NMR-spectrum is shown in Figure 17.

When after the described interruptions of the reactions the products were worked up in the usual manner, what means that solvent and most of the excess of TMA were condensed off, the significant structured signals as seen in Figures 14 and 15 are disappeared.

33 Conversion was measured by methane evolution; because of the methane solubility at deep temperatures the value will be corrected to 23%.

34 Conversion was measured by methane evolution; because of the methane solubility at deep temperatures the value will be corrected to 29%.

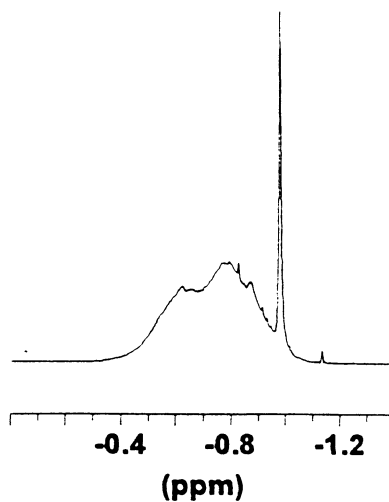
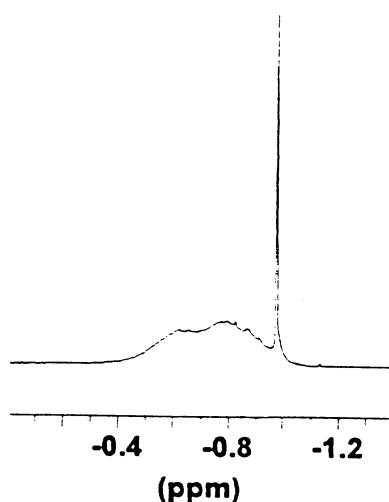


Fig.16. Sample of the same reaction mixture as in Figure 15 used but without any addition of a polar substance dried; after drying dissolved in toluene, diethyl-ether added, dried again and dissolved in dioxane-d8 and measured.

Fig.17. Sample of the same reaction mixture as in Figure 15 used but without any addition of a polar substance dried; after drying without any addition dissolved in dioxane-d8 and measured.

These results will be reported in more detail in the near future. In the moment we conclude, that there are the same steps in the reaction system consisting of TMA and ice, in an apolar solvent like toluene or benzene as well as in a polar solvent like diethylether^{35,36}, tetrahydrofuran or dioxane which serves as donators. In a solvent which serves as donator the intermediates $(\text{CH}_3)_2\text{AlOH}$, $(\text{CH}_3)_2\text{Al-O-Al}(\text{CH}_3)_2$, $(\text{CH}_3)_2\text{Al-O-Al}(\text{CH}_3)_2\text{-O-Al}(\text{CH}_3)_2$, etc. will be stabilized as donator complexes thus preventing some fast consecutive reactions. To form the final products which we call MAO (combined one „true“ MAO with 2-4 donator molecules) it needs some days, even at room temperature.

If the system is free of donators a complexation of the intermediates is done with the acceptor molecule TMA. The intermediates have now high reactivity and can be caught at decreased temperatures only. And to form the final product MAO, that is $\{[\text{Al}_4\text{O}_3(\text{CH}_3)_{6,4}]\} * n\text{Al}(\text{CH}_3)_3$ only minutes or hours are needed.

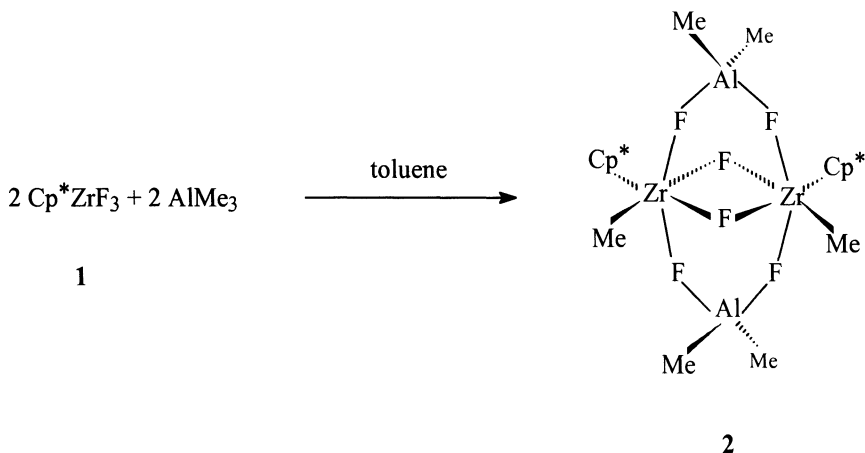
The Activation of Metal-Fluorine Bonds in Compounds of Group 4 by Aluminum Alkyls

Helge Wessel, Axel Herzog, Peihua Yu, Herbert W. Roesky*

Institut für Anorganische Chemie, Tammannstr. 4, 37077 Göttingen
hroesky@gwdg.de

Abstract. In recent years we have developed the facile preparation of group 4-6 and main-group fluorides from the corresponding chlorides using Me_3SnF as a fluorinating reagent. Reactions of group 4 organometallic fluorides with alkyls of group 13 elements, especially those of aluminum, are of particular interest with regard to the mechanism of homogeneous catalysis for the polymerization of olefins. The formation of adducts of group 4 metallocene halides with AlMe_3 is assumed to be the first step of activation of a polymerization catalyst when AlMe_3 containing methylaluminoxane (MAO) is used. The following methylation of the metallocene centers is markedly facilitated by this electrophilic support. In order to understand the catalytic activity of those compounds, it is necessary to examine whether a selective coordination of the fluorine atoms and an exchange for alkyl and amino groups, respectively, is possible using aluminum compounds.

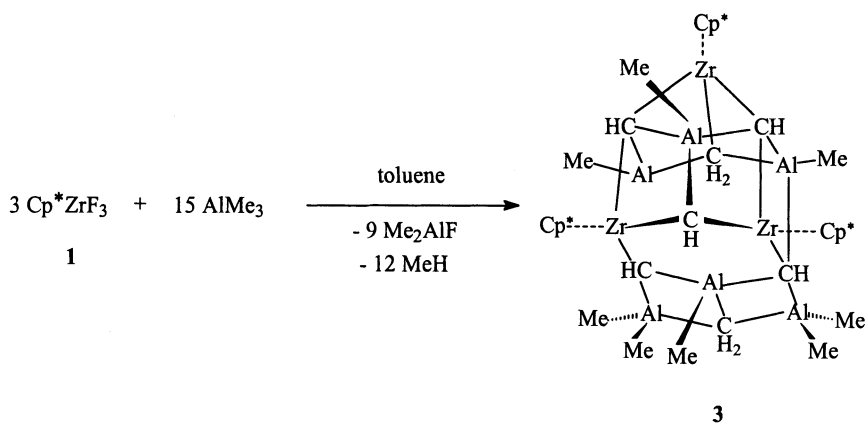
The reaction of Cp^*ZrF_3 (**1**) ($\text{Cp}^* = \eta^5\text{-C}_5\text{Me}_5$) and AlMe_3 in an equimolar ratio in toluene as well as in *n*-hexane leads to a Me-F exchange, and the fluorine-bridged dimer *cis*- $\{[\text{Cp}^*\text{ZrMe}(\mu_2\text{-F})][(\mu_2\text{-F})_2\text{AlMe}_2]\}_2$ (**2**) is formed stereoselectively (Scheme 1). The X-ray crystal structure of this complex has been



Scheme 1.

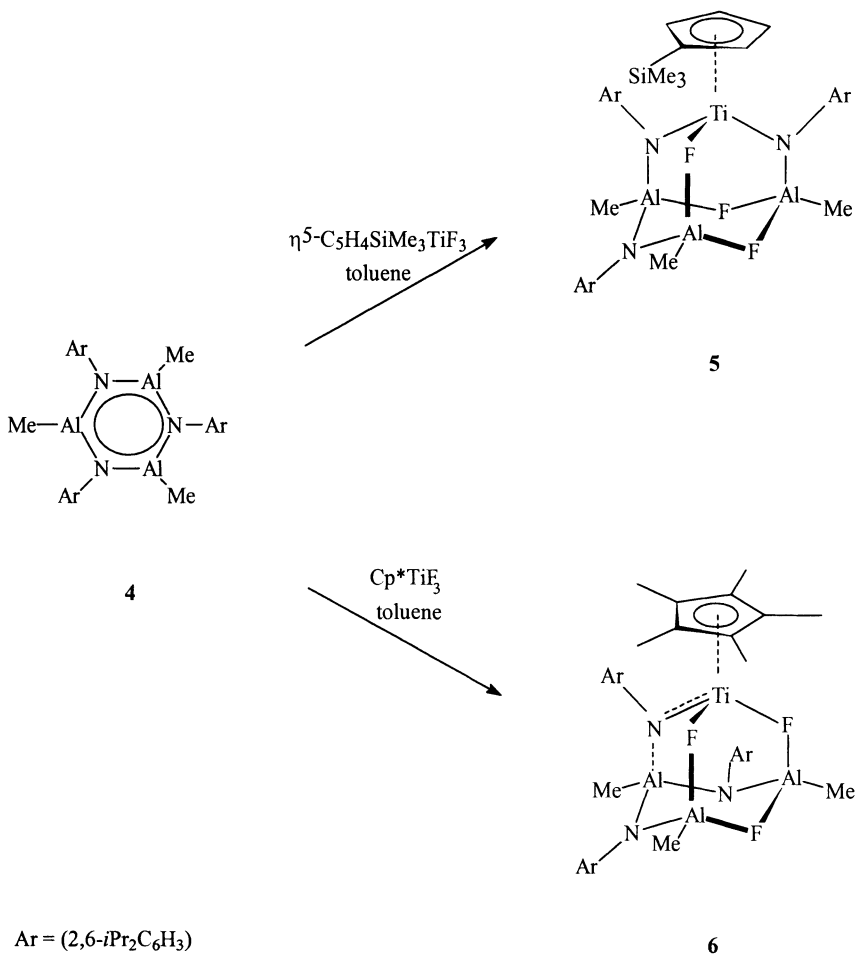
determined and shows Me_2AlF for the first time as a complex ligand; the fluorine atoms are in a bridging position.[1, 2]

When an excess of AlMe_3 is reacted with **1** in *n*-hexane, all the fluorine atoms are replaced from the zirconium and methane evolution can be observed. The maximum amount of methane (3.5 equiv) can be achieved when 5 equiv of AlMe_3 is reacted with **1**. Finally, the $\text{Zr}_3\text{Al}_6\text{C}_7$ cluster $(\text{Cp}^*\text{Zr}_3)\text{Al}_6\text{Me}_8(\text{CH}_2)_2(\text{CH})_5$ (**3**) can be isolated in yields of 30 (pure) and 70 % (crude) as a yellow crystalline solid. From the relation of the evolved amount of methane and the theoretical required one (Scheme 2) a maximum yield of 88 % for **3** can be calculated. Single crystals of **3** could be obtained only from freshly prepared material by slowly evaporating the solvent. The X-ray crystal structure of **3** has been determined. [1, 2]

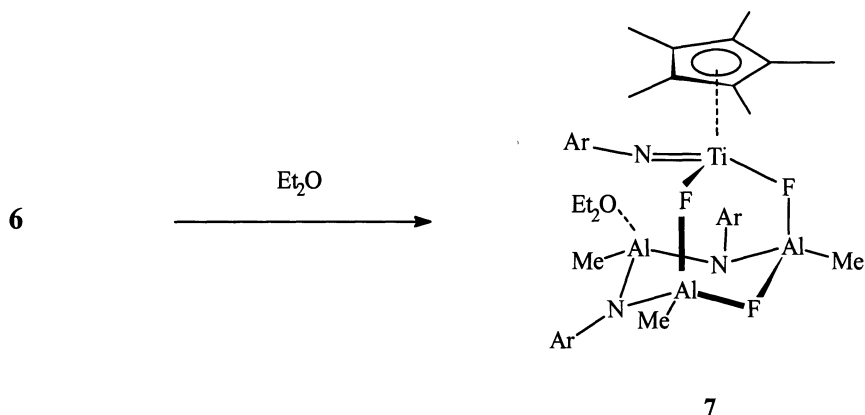


Scheme 2.

Furthermore, we report on the reaction of cyclopentadienyl titanium trifluorides with the trimeric iminoalane (**4**), which exhibits quasaromatic properties and contains Lewis-acidic, three-coordinate aluminum centers.[3] The reaction of **4** with $\eta^5\text{-C}_5\text{H}_4\text{SiMe}_3\text{TiF}_3$ and Cp^*TiF_3 in toluene leads under fluorine-nitrogen metathesis to the adamantane-like cage compounds **5** and **6**, respectively (Scheme 3). These novel titanocene compounds were characterized by IR and NMR spectroscopy, mass spectrometric, and elemental analysis. The structure of **5** has been determined by X-ray crystal structural analysis.[4, 5]

**Scheme 3.**

Treatment of **6** with the donor solvent diethyl ether leads to **7** through cleavage of an aluminum-nitrogen bond (Scheme 4). **7** is the first compound containing a titanium-nitrogen double bond obtained by a metathesis reaction; hereby an intramolecular stabilization of a titanium-nitrogen double bond by fluorine was established for the first time.



Scheme 4.

The ^{19}F NMR spectra of **5-7** contain signals for the Al-Ti-bridging fluorine atoms (**5**: $\delta = -151.9$; **6**: $\delta = -168.2, -158.4$; **7**: $\delta = -168.1, -158.4$), which are strongly shifted to higher field with respect to those of the starting materials ($\delta = 164.5$ and 124.0). This was also observed for other compounds with Al-F bonds.[6] The signals at $\delta = -135$ are assigned to the Al-bridging fluorine atoms. These findings indicate that the structures of the compounds are similar in the solid state and in solution.

Conclusions. As expected, in contrast to organo transition metal chlorides, reversible reactions of the corresponding fluorides with an excess of AlMe_3 are not observed due to the generation of Me_2AlF . This is one reason as well as the elimination of methane from the involved CH activation process, which finally results in the facile formation of the Zr-C-Al cluster. These results show the ability of the fluorine complexes to function as Ziegler-Natta catalysts. Moreover, it was demonstrated that hypervalent CH units are involved in catalytic cycles. Such species are thought to persist in MAO-activated zirconocene catalyst solutions from which methane evolution can be observed, and it is assumed that this process inhibits the polymerization catalysts. This suggestion corresponds with the result of the catalytical inactivity of the described Zr clusters, when no cocatalyst is added.

Furthermore, we have shown that reactions of group 4 cyclopentadienyl metal trifluorides with a trimeric iminoalane lead to intramolecular fluorine-nitrogen exchange, activation of metal-fluorine bonds, and the formation of adamantane-like cages. Moreover, the reported synthesis is a new route to aluminum-containing mixed amidofluorides of group 4 elements.

Acknowledgement. We are grateful for financial support of the Deutsche Forschungsgemeinschaft, the Witco GmbH, Bergkamen, the Bundesministerium für Bildung und Forschung, and the Göttinger Akademie der Wissenschaften. H. W. is grateful to the Fonds der Chemischen Industrie for a fellowship.

References.

- [1] A. Herzog, H. W. Roesky, Z. Zak, M. Noltemeyer, *Angew. Chem.* **1994**, *106*, 1035; *Angew. Chem. Int. Ed. Engl.* **1994**, *33*, 967.
- [2] A. Herzog, H. W. Roesky, F. Jäger, A. Steiner, M. Noltemeyer, *Organometallics* **1996**, *15*, 909.
- [3] P. P. Power, K. M. Waggoner, H. Hope, *Angew. Chem.* **1988**, *100*, 1765; *Angew. Chem. Int. Ed. Engl.* **1988**, *27*, 1699.
- [4] H. Wessel, M. L. Montero, C. Rennekamp, H. W. Roesky, P. Yu, I. Usón, *Angew. Chem.* **1998**, *110*, 862; *Angew. Chem. Int. Ed. Engl.* **1998**, *37*, 843.
- [5] H. Wessel, C. Rennekamp, H. W. Roesky, M. L. Montero, P. Müller, I. Usón, *Organometallics* **1998**, *26*, 1919.
- [6] P. Yu, H. W. Roesky, A. Densar, T. Albers, H.-G. Schmidt, M. Noltemeyer *Angew. Chem.* **1997**, *109*, 1846; *Angew. Chem. Int. Ed. Engl.* **1997**, *36*, 1766.

A DFT quantum-chemical study of the structures and reactive sites of polymethylalumoxane

Ivan I. Zakharov, Vladimir A. Zakharov, Georgii M. Zhidomirov

Boreskov Institute of Catalysis, Pr.Akad. Lavrentieva 5, Novosibirsk 630090, Russia

Abstract.

DFT quantum-chemical calculations have been performed to elucidate the geometrical and electronic structure of methylalumoxanes $(-\text{Al}(\text{Me})\text{O}-)_n$ with different size ($n=6,8,12$). The three-dimensional oxo-bridged (cage) structures of methylalumoxane (MAO) have been analyzed.

It has been found that the cage structure consisting of three layers of $[-\text{Al}(\text{CH}_3)_2\text{O}-]_4$ units is the most stable for MAO with $n=12$. Trimethylaluminum reacts with MAO by cleavage of a Al-O dative bond and the formation of acidic tricoordinated Al-atoms and basic dicoordinated O-atoms in the MAO molecule. Two molecules of AlMe_3 are associated with these sites. The total heat of the TMA interaction with MAO depends on the n value and the MAO structure. The reactive sites of MAO are proposed based on the obtained data.

Introduction

The polymethylalumoxane is recognized as an efficient co-catalyst for highly active homogeneous metallocene catalysts in the ethylene polymerization [1, 2]. Polymethylalumoxane (or methylalumoxane, MAO) is the key element determine not only extremely high activity but also kinetic peculiarities of these catalytic systems. The unique feature of MAO and some other activators (perfluoroborates in particular) consists in their ability - while reacting with metallocenes - to form cation-like alkyl complexes $\text{M}(\text{IV})$ ($\text{M}=\text{Ti}, \text{Zr}, \text{Hf}$) which act as the catalyst's active centers [3-9].

MAO is an oligomeric product of incomplete hydrolysis of trimethylaluminum (TMA) and consists of monomer $[-\text{Al}(\text{CH}_3)_2\text{O}-]$ units. It has the following compositional and structural peculiarities:

- 1) The MAO molecular mass (oligomerization degree n in structure $[-\text{Al}(\text{CH}_3)_2\text{O}-]_n$) varies over a wide range ($n=6-30$) and depends on the preparation procedure [10-12]. The activity of zirconocene catalysts in the ethylene polymerization depends on the MAO oligomerization degree and increases with increasing value of n . [10, 11].
- 2) The MAO samples always contain a significant amount of TMA (2-30% with respect to Al) [12,13], which is either strongly associated with MAO or in a free

state. The MAO molecular mass depends on the TMA content and increases with decreasing TMA content [12]. The TMA content in MAO affects the metallocene catalysts activity which declines if TMA is removed from MAO [12-15].

These peculiarities impede the studies of the MAO structure and identification of reactive centers which interact with metallocenes forming the catalysts active centers. Barron et al. [16] obtained reliable structural data for tert-butylalumoxane of the composition $[(t\text{-Bu)Al}(\mu_3\text{-O})]_6$. This alumoxane has been shown to form a three-dimensional oxo-bridged structure (cage structure) comprised by coordinatively saturated aluminium and oxygen atoms (tetra- and triple-coordinated, respectively).

Regarding the results of work [16], the authors of [12] suggested that MAO, formed from TMA on the surface of ice, consists of sphere molecules $[\text{Al}_4\text{O}_3(\text{CH}_3)_6]_4$, each associated to four molecules $\text{Al}(\text{CH}_3)_3$. Similar to the Barron cage structure all the aluminium and oxygen atoms in this compound are coordinatively saturated.

^{27}Al -, ^{17}O -, ^1H - and ^{13}C -NMR spectroscopy has been used to study the structure of MAO in work [17]. The obtained data are consistent with the cage alumoxane clusters $[(t\text{-Bu)Al}(\mu_3\text{-O})]_6$ and $[(t\text{-Bu)Al}(\mu_3\text{-O})]_9$ [16], suggesting that the studied MAO oligomers have the cage structure as well.

Recent EPR spectroscopic studies [18] of the MAO reaction with the stable nitroxyl radical TEMPO provided experimental data for the presence of the Lewis acidic centers in MAO. It has been found that MAO contains one acidic center per 50 ± 15 aluminium atoms. Most likely, the TMA contained in MAO is adsorbed at these centers and equilibrium of type (1) exists in the system MAO/TMA:



Recently we have presented the first data on the structures and reactive sites of MAO obtained via DFT quantum-chemical study [19]. It has been found:

- 1) Starting from $n=6$, the three-dimensional oxo-bridged (cage) structure of MAO is more stable than the cycle structure.
- 2) The Lewis acidity of Al atoms in MAO depends on the size of MAO and increases with increasing MAO size.
- 3) Trimethylaluminium reacts with the cage structure of MAO by cleavage of the Al-O dative bond; two molecules of AlMe_3 are associated with acidic Al^ν and basic O^ν sites formed by interaction of MAO with TMA.

In the present work we have carried out the more detail DFT analysis of the cage structures of MAO with different sizes ($n=6, 12$). Three-dimensional oxo-bridged structures consisting of three layers of $[-\text{Al}(\text{CH}_3)\text{O}-]_m$ units ($m=2,4$; triple-cage) have been calculated. The obtained data is compared to those for cage structures of MAO consisting of two layers of $[-\text{Al}(\text{CH}_3)\text{O}-]_m$ units ($m=3,4,6$; double-cage).

Method and calculation details.

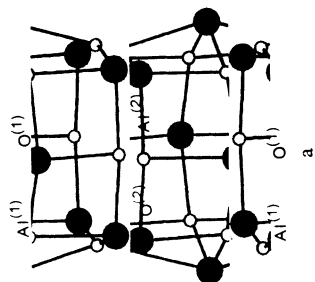
All the calculations were carried out using of the Gaussian92/DFT package [20]. The geometries of various forms of the oligomers $[-\text{Al}(\text{CH}_3)\text{O}]_n$, ($n=4-12$) have been calculated using density functional theory (DFT), the LANL1 effective core potential for inner shells of Al [21] and basis set single- ξ (Minimal Basis) for valence shells of Al and for the carbon, the oxygen and hydrogen atoms. The Vosko-Vilk-Nusair [22] (VWN) local correlation parameters (LDA) were applied to evaluate the density functions. The total charge densities of the $[-\text{Al}(\text{CH}_3)\text{O}]_n$ oligomers were calculated using the Mulliken population analysis. The accuracy of the calculated by geometries was tested for dimeric TMA. The length of Al-C bonds calculated using DFT/LANL1MB level agree well with those values obtained in crystallographic studies [23]: 2.26 \AA (calc.) vs. 2.24 \AA (exper.) for bridging bonds Al-Me-Al, and 2.02 \AA (calc.) vs. 2.00 \AA (exper.) for terminal bonds Al-Me. Experimental data for the dissociation enthalpy of dimeric TMA (19.0 kcal/mol) [24] are comparable to those calculated at the DFT/LANL1MB level (9.0 kcal/mol). Comparison between calculated and experimental dissociation enthalpy for Al_2Me_6 shows the underestimation of the calculated reaction energy: 9.0 kcal/mol (calc.) vs. 19.0 kcal/mol (exper.), which unusual for the LDA level. This is connected with the minimal basis sets (single- ξ) employed. But the calculations at the LDA level with double- ξ basis sets considerably overestimates reaction energy and we have preferred to use the minimal basis sets.

Results and Discussion

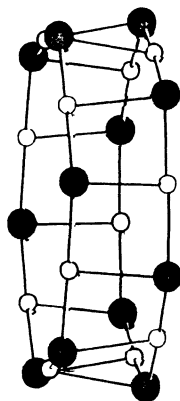
The data of the calculation of the geometric and electronic characteristics of the various cage structures of MAO are presented in Tab.1. Two types of the structures have been considered. One of them (double-cage) is consisted of two layers of $[-\text{Al}(\text{CH}_3)\text{O}]_m$ units ($m=3, 4$ and 6) and another one (triple-cage) is consisted of three layers of $[-\text{Al}(\text{CH}_3)\text{O}]_m$ units ($m=2$ and 4). The examples of the structures calculated for the double-cage ($n=12, m=6$) and the triple-cage ($n=12, m=4$) are presented in Figs.1a and 2a. The results of the net energy calculation (Tab.1) clearly show that the double-cage structure is more stable in comparison to the triple-cage structure for $n=6$, but that the formation of the triple-cage structure is more preferable for MAO with $n=12$. The results calculated for MAO with $n=6$ and 12 (Tab.1) match well with the experimental X-ray data [16] of tert-butylaluminum with $n=6$ and 9 . According to reference [16] the double-cage structure is formed for tert-butylaluminum with $n=6$ and the triple-cage is formed for tert-butylaluminum with $n=9$. Basing on these data and results of our calculations we propose the triple-cage structure to be the most probable for MAO with $n \geq 9$.

The essential characteristic of the triple-cage structure is the inhomogeneity of the aluminium and the oxygen atoms (Tab.1). Particularly atoms of Al in the outer layers are four-fold coordinated and the oxygen atoms are three-fold coordinated, while atoms of Al in the inner layer are five-fold coordinated and oxygen atoms are four-fold coordinated (Fig.2a). Accordingly atoms of aluminium

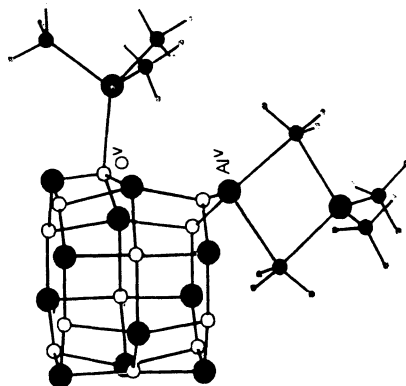
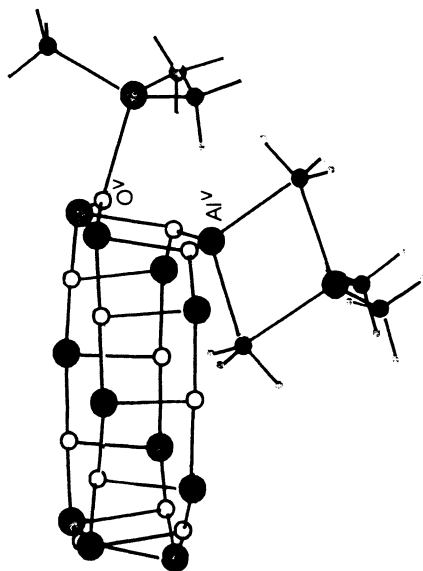
$Al^{(1)} - O^{(1)} = 1.770$
 $Al^{(2)} - O^{(2)} = 1.921$
 $Al^{(1)} - O^{(2)} = 1.920$
 $Al^{(2)} - O^{(1)} = 1.978$
 $Al^{(1)} - C = 1.986$
 $Al^{(2)} - C = 1.976$
 $C - H = 1.090$



○ - oxygen
 ● - aluminium
 ○ - carbon



a



b

Fig. 1 Calculated at the DFT/LANL1MB level the cage-double structure of $(MeAlO)_2$ before (a) and after (b) interaction with Al_2Me_6 (methyl groups of MAO are omitted for clarity)

Fig. 2 Calculated at the DFT/LANL1MB level the cage-triple structure of $(MeAlO)_2$ before (a) and after (b) interaction with Al_2Me_6 (methyl groups of MAO are omitted for clarity)

Table 1. Calculated geometric and electronic characteristics of the various cage-structures of $(\text{MeAlO})_n$ ($D_{n/2}$ d -symmetry for double-cage, $C_{n/3}$ v -symmetry for triple-cage).

| [Al(CH ₃)O] _n | Calculated geometry (Å) | | Net charges of Al | DFT/LANL1MB energy (a.u.) |
|--------------------------------------|--|--|--|---------------------------|
| | Al-O | Al [*] -O [*] | | |
| n=6 (double) m=3 | 1.813 | 1.924 | +0.493 | -695.10815 |
| n=6 (triple) m=2 | 1.856(Al ¹ -O ¹) ^{a)} 2.154(Al ² -O ²) ^{a)} | 1.836(Al ¹ -O ²) 1.902(Al ² -O ¹) | +0.494 (Al ¹) +0.410 (Al ²) | -695.04832 |
| n=8 (double) m=4 | 1.780 | 1.972 | +0.511 | -926.84935 |
| n=12 (double) m=6 | 1.775 | 1.990 | +0.520 | -1390.20901 |
| n=12 (triple) m=4 | 1.770(Al ¹ -O ¹) 1.921(Al ² -O ²) | 1.920(Al ¹ -O ²) 1.978(Al ² -O ¹) | +0.535 (Al ¹) +0.492 (Al ²) | -1390.44271 |

^{a)} The Al¹ and O¹ atoms are in the outer layers of triple-cage structure of MAO, the Al² and O² atoms are in the inner layer. All the Al and O atoms in the double-cage structure of MAO are equivalent.

in the outer layers (Al^1) are more acidic; they possess the higher net charges in comparison to atoms aluminium in the inner layer (Al^2) (Tab.1). The distance of covalent bond Al-O and dative bond Al^*-O^* differs notably, too, for the outer and the inner layers (Tab.1.).

As we mentioned above, MAO always contains relatively large amounts of TMA, as well associated with MAO as in a free form [12, 13]. Several authors note that the presence of TMA in MAO is essential for the high activity of metallocene catalysts [13-15]. Regarding this fact we carried out the quantum-chemical calculations of the reaction between dimeric TMA and the MAO with different size and structures. The results of the calculation of the geometric and the electronic structure of MAO after interaction with TMA are presented in Tab. 2 and in Figs. 1b and 2b. As we mentioned above there are two types of aluminium atoms (Al^1 - Al^2) in the triple-cage structure of MAO. So there are two possibilities for the interaction of Al_2Me_6 with dative Al^*-O^* bonds of MAO (Fig.2a):

i) interaction with an Al^1-O^2 bond; ii) interaction with an Al^2-O^1 bond. Our previous results obtained for the triple-cage structure with $n=6$ show that the interaction of Al_2Me_6 with a dative bond Al^1-O^2 is more preferable. Therefore we have carried out the calculation of Al_2Me_6 interaction with an Al^1-O^2 dative bond for the triple-cage structure with $n=12$. The results obtained are presented in Tab.2 and Fig.2b in comparison to the data obtained for the double-cage structure with $n=8$ and 12 (Tab.2, Fig. 1b).

So, as MAO reacts with Al_2Me_6 , the opening of one of the four-membered faces of MAO occurs by adding molecules of $AlMe_3$ to Al^* and O^* atoms (Figs. 1b and 2□). After interaction with Al_2Me_6 , the distances $Al^v - O^v$ in the MAO molecules increase by ca. 0.4 \AA for the double cage and by ca. 1.1 \AA for the triple-cage structure (compare the data of Tab. 1 and Tab.2). As the cage-structure increases in size, the acidity of Al^v -centers amplifies (the charge on Al^v atom increases and distance $Al^v-(AlMe_3)$ shortens (Tab. 2). On the contrary, interaction of TMA with the O^* -centers weakens with increasing n , the value and the distance $O^v-(AlMe_3)$ increases.

The heat of the addition reaction between Al_2Me_6 and MAO (Q value) remarkably changes with the size of the MAO and with the type of the cage-structure (Tab.2). The Q value decreases for MAO with a double-cage structure from -26.8 kcal/mol for $n=8$ to -20.2 kcal/mol for $n=12$ and on the contrary the Q value increases for MAO with a triple cage structure from $+13.7 \text{ kcal/mol}$ for $n=6$ to -0.9 kcal/mol for $n=12$.

Basing on the performed calculations, we represent the process of the TMA interaction with MAO as a combination of two reactions:

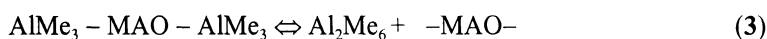


Table 2. Calculated geometric and electronic characteristics of the various cage-structures of MAO ($n=6, 8, 12$) after interaction with Al_2Me_6 .

| [$-Al(CH_3)O-$] $_n$ | Calculated geometry, (Å) | | Net charges of Al^y , (LUMO, eV) | DFT/LANL1MB total energy (a. u.) | Reaction heat ^{a)} (Q) (kcal/mol) |
|--------------------------|--------------------------|-----------------|------------------------------------|----------------------------------|--|
| | $Al^y - O^{yb)}$ | $Al^y - AlMe_3$ | | | |
| $n=6$ (triple) $m=2$ | 3.068 | 2.891 | 1.972 | -936.03356 | + 13.7 |
| $n=8$ (double) $m=4$ | 2.391 | 2.788 | 2.080 | -1167.89916 | - 26.8 |
| $n=12$ (double) $m=6$ | 2.368 | 2.759 | 2.184 | -1631.24836 | - 20.2 |
| $n=12$ (triple) $m=4$ | 3.085 | 2.813 | 2.378 | -1631.45136 | - 0.9 |

^{a)}The reaction heat is computed with respect to the free Al_2Me_6 and MAO molecules; the total DFT energies for MAO are given in Tab.1 the total DFT energy for Al_2Me_6 is -241.00712 a.u

^{b)} Al^y and O^y are the atoms of aluminum and oxygen in the MAO molecule interacted with Trimethylaluminium.

Reaction (2) proposes that the initial cage-structure of MAO (I) (Figs. 1a and 2a) transforms to the structure (II) (Figs. 1b and 2b) in which two molecules AlMe_3 are associated with an acidic center of Al^{ν} and a basic center of O^{ν} . According to equilibrium reaction (3) structure (II) transforms to the reactive form of MAO (III) containing two active centers (acidic Al^{ν} and basic O^{ν}). The probability of the formation of the MAO(III) structure (reaction 3) is the highest if the binding energy of two AlMe_3 molecules in MAO(II) is equal to the dimerization energy of the reaction: $2\text{AlMe}_3 \rightleftharpoons \text{Al}_2\text{Me}_6$. It is just this correspondence is observed for the triple-cage structure with $n=12$ (Tab.2).

Acknowledgement: this research was supported by the Russian Fund of Basic Research, grant No. 98-03-33132

References:

- 1) H. Sinn, W. Kaminsky, *Adv. Organomet. Chem.* **18**, 99 (1980)
- 2) W. Kaminsky, M. Miri, H. Sinn, R. Woldt, *Macromol. Chem. Rapid Commun.* **4**, 417 (1983)
- 3) R.F. Jordan, *Adv. Organomet. Chem.* **32**, 325 (1991)
- 4) C. Sishta, R.H. Hathorn, T.J. Marks, *J. Am. Chem. Soc.* **114**, 1112 (1992)
- 5) X. Yang, C.L. Stern, T.J. Marks, *J. Am. Chem. Soc.* **116**, 10015 (1994)
- 6) M. Bochmann, S.J. Lancaster, *Angew. Chem., Int. Ed. Engl.*, **33**, 1634 (1994)
- 7) I. Tritto, M.C. Sacchi, G. Zannoni, *Macromolecules* **26**, 7112 (1993)
- 8) I. Tritto, M.C. Sacchi, S. Li, *Macromol. Rapid Commun.* **15**, 217 (1994)
- 9) I. Tritto, R. Donetti, M.C. Sacchi, P. Locatelli, G. Zannoni, *Macromolecules* **30**, 1247 (1997)
- 10) K.Q. Peng, S.J. Xiao, *J. Mol. Catal.*, **90**, 201 (1994)
- 11) E. Giannetti, G.M. Nicoletti, R. Mazzochi, *J. Polym. Sci., Polym. Chem. Ed.*, **23**, 2117 (1985)
- 12) H. Sinn, *Macromol. Symp.* **97**, 27 (1995)
- 13) I. Tritto, C. Mealares, M.C. Sacchi, P. Locatelli, *Macromol. Chem. Phys.* **198**, 3963 (1997)
- 14) S. Reddy, G. Shaashider, S. Sivaram, *Macromolecules* **26**, 1180 (1993)
- 15) B. Reiger, C. Janiak, *Angew. Makromol. Chem.*, **215**, 35 (1994)
- 16) M.R. Mason, J.M. Smith, S.G. Bott, A.R. Barron, *J. Am. Chem. Soc.* **115**, 4971 (1993)
- 17) D.E. Babushkin, N.V. Semikolenova, V.N. Panchenko, A.P. Sobolev, V.A. Zakharov, E.P. Talsi, *Macromol. Chem. Phys.* **198**, 3845 (1997)
- 18) E.P. Talsi, N.V. Semikolenova, V.N. Panchenko, A.P. Sobolev, D.E. Babushkin, A.A. Shubin, V.A. Zakharov, *J. Mol. Catal.*, in press
- 19) I.I. Zakharov, V.A. Zakharov, G.M. Zhidomiriv, *Macromol. Theory Simul.* (1999) in press
- 20) M.J. Frisch, G.W. Trucks, H.B. Schlegel, P.M.W. Gill, B.G. Johnson, M.W. Wong, J.B. Foresman, M.A. Robb, M. Head-Gordon, E.S. Replogle, R. Gomperts, J.L. Andres, K. Raghavachari, J.S. Binkley, C. Gonzalez, L. Martin, D.J. Fox, D.J. Defrees, J. Baker, J.J.P. Stewart, J.A. Pople, *Gaussian 92/DFT, Revision G.2, Gaussian, Inc.*, Pittsburgh PA, 1993.
- 21) P.J. Hay, W.R. Wadt, *J. Chem. Phys.* **82**, 270 (1985)
- 22) S.J. Vosco, L. Wilk, M. Nusair, *Can. J. Phys.* **58**, 1200 (1980)
- 23) P.H. Lewis, R.E. Rundle, *J. Chem. Phys.* **21**, 986 (1953)
- 24) M.B. Smith, *J. Organomet. Chem.* **70**, 13 (1974)

***In situ* FTIR spectroscopy shows no evidence of reaction between MAO and TMA.**

Jan L. Eilertsen¹, Erling Rytter², Martin Ystenes¹.

¹Dept. of Inorganic Chemistry, Norwegian University of Science and Technology, N-7034 Trondheim, Norway.

²Statoil Research Centre, Postuttak, N-7005 Trondheim, Norway

/ Dept. of Industrial Chemistry, Norwegian University of Science and Technology.

jan.lasse.eilertsen@chembio.ntnu.no, err@statoil.com, martin.ystenes@chembio.ntnu.no

Abstract.

In situ infrared spectra of TMA depleted commercial MAO with increasing additions of TMA have been recorded at 25 °C in toluene solution. The spectra of the mixtures are the sums of the spectra of TMA depleted MAO (CH₃/Al ratio 1.5) and of TMA. There is no evidence of any reaction between these compounds; the basic MAO entity seems to be completely uninfluenced by additions of TMA at this temperature.

Introduction

Methyl aluminoxane (MAO) is the most studied cocatalyst for metallocene based catalysts for olefin polymerization. Although several papers are dedicated to the study of MAO, its structure is still obscure. Also very little is known about possible reactions between MAO and trimethyl aluminium (TMA), which is crucial as commercial "MAO" in fact is a mixture of MAO and TMA. It is recognized that the content of TMA influences the activity of the MAO as cocatalyst, but the role of TMA is not fully established [1-4]. Multiple equilibria are proposed to be present in MAO/TMA mixtures, and are assumed to influence the structure and properties of MAO [2-8]. This assumption has been based on several observations, e.g. that "TMA free" MAO releases TMA when heated for some time [4,9], and that NMR peaks assigned to TMA are broader for MAO/TMA mixtures than for pure TMA [6]. Eisch et al. have studied the addition of Al₂(CD₃)₆ to "TMA free" MAO by ¹H NMR [11]. A rapidly rising signal from free TMA showed methyl group exchange between MAO and TMA.

It is difficult to reduce the CH₃/Al ratio to less than 1.5 by evaporation of volatile components. In consistence with this, Sinn proposed the basic formula of MAO to be [Al₄O₃(CH₃)₆]₄ [7]. The proposed formula is in agreement with ¹H NMR results, which indicate the general formula to be [AlO_{0.8-0.75}(CH₃)_{1.4-1.5}]_n [8].

As one has not yet succeeded in crystallizing MAO, one has to rely on indirect studies to reveal its structure. A suitable tool is vibrational spectroscopy, which can

reveal important information about structure and reactions. Hitherto not many IR studies have been performed on MAO or MAO/TMA mixtures [12]. As MAO is reactive towards moisture and air, the recording of such spectra is an experimental challenge. The few IR studies published, including studies of other aluminoxanes, are almost exclusively done with salt windows. However, we have found that these materials are not inert to MAO.

In the present work we use an *in situ* FTIR-cell, which has proven useful in the study of Ziegler-Natta catalysts [13]. The cell has also been used in the study of very delicate triethylaluminium-ester complexes, and the IR study turned out to reveal crucial and clear information about the structure and reactions of these complexes [14].

The present results have been obtained at 25 °C; studies at higher temperatures are under preparation.

Experimental

All operations were carried out with Schlenk techniques under dry nitrogen (99.99%) atmosphere. The toluene was dried over sodium. Commercial MAO (Albemarle, 10 wt% in toluene) was dried under reduced pressure (0.08 mbar, 25 °C, held for 2 h at the minimum pressure). The dry residue was dissolved in toluene (10 wt% MAO). TMA (Aldrich) was diluted in toluene (10 vol% TMA). The solutions were transferred and dosed by lubricant free PE/PP syringes (Fortuna, W. Graf). The methyl content was determined by volumetric measurement of the evolved methane during hydrolysis, and the aluminium content was determined by EDTA back titration. The CH₃/Al ratio of the dried MAO was determined to be 1.48±0.05.

The IR spectra were recorded with a liquid flow cell equipped with silicon and germanium windows. The cell was placed in a loop consisting of a magnet drive gear liquid pump and a mixing tank (for details see ref. [13]). The loop was connected to a Schlenk line. The equipment was thoroughly dried, evacuated overnight and flushed with dry toluene before use. The spectra of the MAO/TMA mixture were recorded 5-10 minutes after each TMA addition.

Results and Discussion

Fig. 1 shows the spectrum of MAO, where excess TMA has been removed by evaporation, and the spectra obtained after consecutive additions of TMA. The TMA/MAO ratio ranges from 0 to 0.5 (by Al content), corresponding to a total CH₃/Al ratio from 1.5 to 2. The solvent spectrum has been subtracted from the sample spectra. Absolute concentrations of the solutes could not be determined, as the amount of toluene left in the loop after the initial flushing was not known, but concentrations were estimated from the intensity of the Al-O band at 809 cm⁻¹.

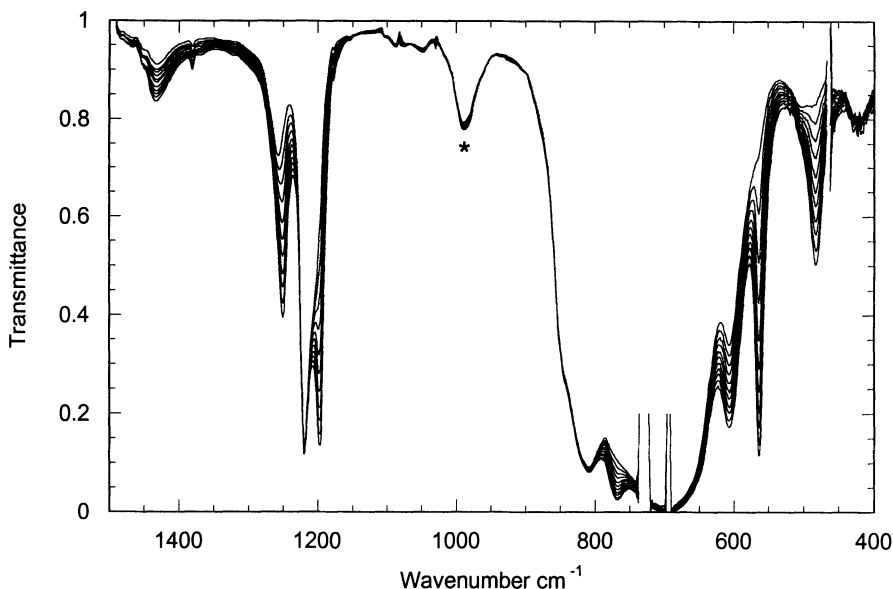


Fig. 1. The IR spectrum of TMA depleted MAO in toluene and the spectra obtained after consecutive additions of TMA. The solvent spectrum has been subtracted. The band at 990 cm^{-1} , marked with an asterisk, is attributed to methoxy groups.

Fig. 1 shows that all bands due to TMA increase linearly with increasing TMA additions. The eleven most prominent TMA bands all have absorbance intensities that increase linearly to the added amount of TMA with R-values of at least 0,999. The results therefore strongly indicate that TMA does not react with the TMA depleted MAO, and that the spectrum of the mixture is just a superposition of the spectra of the two components.

Fig. 2 verifies the interpretation. The spectra marked B and C are obtained by subtracting the spectrum of the starting TMA depleted MAO from the spectrum obtained after the first (B) and the last (C) TMA addition. Both difference spectra (B,C) correspond perfectly to the spectrum of TMA within the experimental accuracy. Scaled spectra of TMA are plotted together with each of the difference spectra, to demonstrate the close fit.

Fig. 2 (A) shows the residual spectrum obtained by subtracting the spectrum of TMA depleted MAO from the spectrum of the MAO before drying. The most prominent feature of the spectrum is the distinct signature of TMA. The methoxy band at 990 cm^{-1} is negative in the difference spectrum because the amount of methoxy groups has increased during the drying. Methoxy groups are known to appear on oxygen contamination [12], and are often present in MAO solutions after the storage cylinder has been opened several times. The actual amount of methoxy groups in the MAO used in this work is currently not known. It appears unlikely that a limited amount of methoxy groups should influence the reactivity of the MAO to the extent that the main conclusion of this work is offset. Precautions will be taken to avoid this ambiguity in future work. The changes above 800 cm^{-1} are

not easily interpreted, but they could be connected to the increase of methoxy groups. Regarding the IR spectrum, the MAO is basically unchanged by the drying process, except for removal of free TMA, and the formation of methoxy groups.

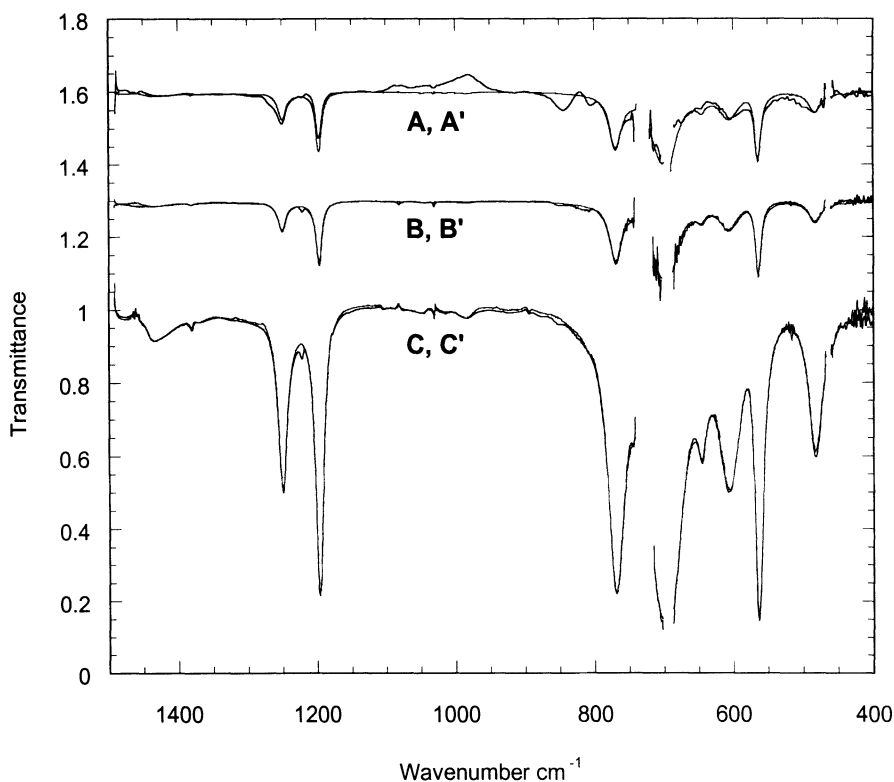


Fig. 2. Difference spectra obtained by subtracting the spectrum of the TMA depleted MAO from the original MAO (A) and from the spectrum obtained after the first (B) and the last (C) TMA addition. Scaled spectra of TMA (A', B' and C'; thin line) are plotted for comparison. The gaps are regions blocked by toluene bands. Spectrum couples A/A' and B/B' are offset on the transmittance scale.

The spectra were recorded 5-10 minutes after the additions. To check for any slow reaction, the time was increased to 30 minutes, but there was no observable change in the spectrum during this period. Reactions on a wider time span cannot be ruled out. Nevertheless, the present result is clearly in contradiction to the conclusions drawn by Tritto et al. [3,6], who proposed a rapid equilibrium between TMA and TMA depleted MAO, with a significant lowering of the molecular weight as the result. The broadening of ^1H NMR peaks as observed by Tritto et al. [6] and the methyl exchange as observed by Eisch et al. [11] indicate an interaction, however, observable changes in the IR spectra should be expected, if the intermediate complex was present in significant quantity. No such changes are seen in our spectra.

However, our results are in agreement with findings of von Lacroix et al. [10], who determined the molecular weight of dried MAO by the freezing point method with TMA as the solvent. The molecular weights determined in TMA were comparable with those obtained in benzene. This indicates the absence of a disproportionation reaction, but precaution should be taken, as the temperature during preparation of these samples is not reported.

To make sure that the spectra show the dissolved species, we recorded spectra during flushing with toluene after the last addition of TMA. The spectra showed that the sample was quickly diluted. Only a trace of MAO was seen in the spectrum obtained after the final flushing.

The amount of TMA evaporated during drying was collected in a liquid nitrogen trap and determined by titration to contain 7 % of the total aluminium. This is in reasonable agreement with a 5% loss estimated from the IR spectra.

TMA was added to the TMA depleted MAO, and it was tested for activity as cocatalyst in ethylene polymerization. The activity was comparable to that of the original MAO.

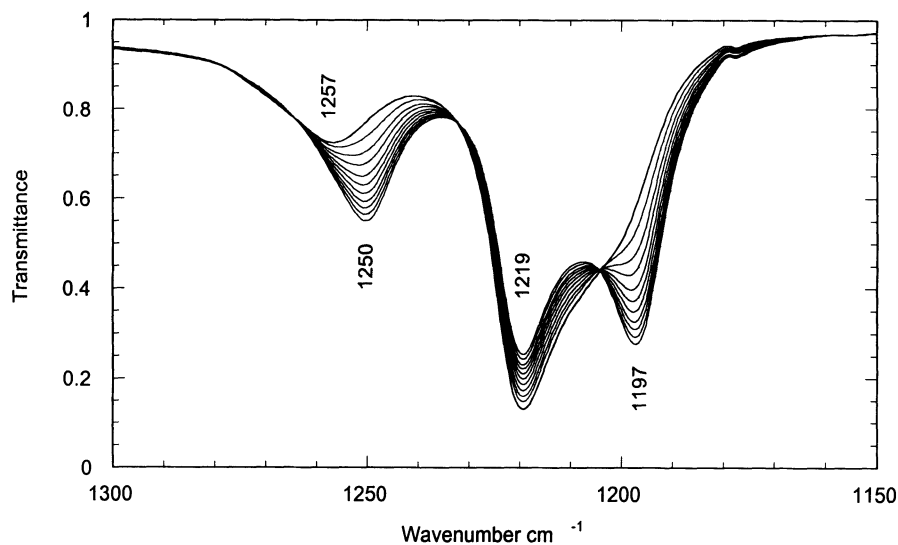


Fig. 3. Detailed view of the IR spectrum of MAO in toluene, showing the symmetric methyl deformation bands (umbrella). The solvent spectrum has been subtracted. The spectra have not been corrected for decreasing concentration.

Fig. 3 shows the bands attributed to symmetric methyl deformation. The spectra in this figure are not corrected for decreasing concentration of the sample. The two isosbestic points, at 1232 and 1204 cm^{-1} , verify that the spectra contain only two independent components. As it is established that both TMA and MAO are present, there can be no reaction between them, as this would introduce a third component and the isosbestic points should not be expected. The isosbestic points also verify that there are no significant surface compounds on the windows.

The bands at 1250 and 1197 cm^{-1} , which increase with TMA additions, are assigned to umbrella deformation of bridging and terminal methyl groups, respectively. The TMA depleted MAO has a band at 1257 cm^{-1} and a shoulder at 1200 cm^{-1} which cannot be attributed to free TMA, because of the absence of the strong TMA band at 564 cm^{-1} . The band at 1257 cm^{-1} indicates that methyl bridges are present in TMA depleted MAO. The band at 1219 cm^{-1} and the broad shoulder at 1200 cm^{-1} indicate the presence of at least two different types of terminal methyl groups. The band at 1257 cm^{-1} decreases sharply on addition of donors, which supports the assumption that it is attributed to methyl bridges.

Conclusions

FTIR spectroscopy shows no evidence of any reactions between TMA and TMA depleted MAO, and the basic MAO entity seems to be completely uninfluenced by additions of TMA. It should nevertheless be pointed out that these results are obtained at 25 °C, and may not apply for higher temperatures.

References

- 1 a) J.C.W. Chien, B.-P. Wang, *J. Polym. Sci. A.*, 26, 3089-3102 (1988); b) S. Srinivasa Reddy, G. Shashidhar, S. Sivaram, *Macromolecules*, 26, 1180-1182 (1993); c) P.A. Charpentier, S. Zhu, A.E. Hamielec, M.A. Brook, *Polymer*, 39, 6501-6511 (1998); d) I. Tritto, R. Donnetti, M.C. Sacchi, P. Locatelli, G. Zannoni, *Macromolecules*, 30, 1247-1252 (1997)
- 2 a) E. Giannetti, G. Martino, M. Nicoletti, R. Mazzocchi, *J. Polym. Sci., Polym. Chem.*, 23, 2117-2133 (1985); c) W. Michiels, A. Muñoz-Escalona, *Macromol. Symp.* 97, 171-183 (1995); e) I. Tritto, C. Méalares, M.C. Sacchi, P. Locatelli, S.X. Li, *Macromol. Symp.* 97, 101-108 (1995)
- 3 I. Tritto, C. Méalares, M.C. Sacchi, P. Locatelli, *Macromol. Chem. Phys.* 198, 3963-3977 (1997)
- 4 L. Resconi, S. Bossi, *Macromolecules*, 23(20), 4489-4491 (1990)
- 5 a) S. Pasynkiewicz, *Polyhedron*, 9, 429-453 (1990); d) D.W. Imhoff, L.S. Simeral, S.A. Sangokoya, J.H. Peel, *Organometallics*, 17, 1941-1945 (1998);
- 6 I. Tritto, M.C. Sacchi, P. Locatelli, S.X. Li, *Macromol Chem. Phys.* 197, 1537-1544 (1996)
- 7 H. Sinn, *Macromol. Symp.* 97, 27-52 (1995)
- 8 D.W. Imhoff, L.S. Simeral, S.A. Sangokoya, J.H. Peel, *Organometallics*, 17, 1941-1945 (1998)
- 9 A.R. Barron, *Organometallics*, 14, 3581-3583 (1995)
- 10 K. Von Lacroix, B. Heitmann, H. Sinn, *Macromol. Symp.* 97, (1995);
- 11 J.J. Eisch, S.I. Pombrik, S. Gürtzgen, R. Rieger, W. Uzick, in "Catalyst Design for Olefin Polymerization", K. Soga, M. Terano, Eds, Elsevier, Amsterdam 1994, 221-235;
- 12 S. Lasserre, J. Derouault, *Nouveau Journal de Chimie*, 7, 659-665 (1983);
- 13 Ø. Bache, M. Ystenes, *Appl. Spectrosc.*, 48, 8, 985-993 (1993)
- 14 Ø. Bache, M. Ystenes, *J. Mol. Str.*, 408/409, 291-299 (1997)

Alumoxanes alternative to MAO: Synthesis and characterization

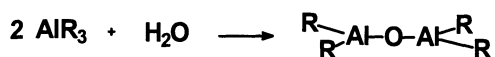
T. Dall'Occo, M. Galimberti, I. Camurati, M. Destro, O. Fusco, D. Brita.

Montell Italia S.p.A., G. Natta Research Centre, P.le G. Donegani 12, 44100 Ferrara, Italy

Abstract. A new alumoxane alternative to MAO was synthesised, characterized and used as cocatalyst for metallocene based polymerizations. It is based on Al(2,4,4-trimethylpentyl)₃ (TIOA). Alumoxanes were prepared by reacting TIOA and H₂O with different molar ratios. ¹H NMR spectra of these products are characterized by the presence of broad bands and of resolved multiplets. Their relative amount in the region between 1.9 and 2.5 ppm was identified as the “*finger-print*” of the polymerization activity.

Introduction

Since the late 80's, Montell scientists have developed new alumoxanes as cocatalysts for metallocene based polymerizations[1]. These alumoxanes are based on reaction products between AlR₃, where R is an alkyl or aryl radical, and H₂O (see Scheme 1.), and are alternative to polymethylalumoxane (MAO), traditionally employed in this field.



Scheme 1.

These products are obtained by different methods of synthesis, for example by:

- using a water saturated nitrogen flow
- direct reaction of AlR₃ and water in organic solvents
- using hydrate metal salts as water source.

In particular, tetra-iso-butyl alumoxane (TIBAO) and reaction products of Al(*i*-Bu)₃ (TIBA) and H₂O in the molar ratio Al/H₂O=2, have been studied[2,3].

A number of these cocatalysts were tested in ethene polymerization with some metallocenes and showed catalytic activities dependent on the type of zirconocene[3]. For example (Table 1) the simple Cp₂ZrCl₂, in the adopted polymerization conditions, is active only with MAO or AlMe₃/H₂O. Traces of polymer, if any, were obtained with the other aluminum-alkyls. On the other hand the stereorigid *racemic*-ethylenebisindenylzirconium dichloride (*rac*-EBIZrCl₂) was active with Al(*i*-Bu)₃/H₂O and TIBAO, but not with the polyisobutylaluminoxane (IBAO). Only low activities were achieved with AlR₃/H₂O as cocatalyst when R was an unbranched alkyl radical.

This work is focussed on a new cocatalytic system based on **Al(2,4,4-trimethylpentyl)₃** (TIOA = Al(*i*-Octyl)₃) and is aimed at correlating the catalytic performances with the structure of the alumoxane.

Table 1. Ethylene polymerization with different cocatalytic systems based on AlR₃/H₂O reaction products

| <u>Metalloocene</u> | | <u>Cocatalyst</u> | | Al/H ₂ O | Yield | <u>Activity</u> | | [η] |
|---------------------------------------|-----------|---|------|---------------------|-------|---------------------|-------------------------|------------|
| mg | μ mol | | mmol | molar | g | kg/g _{cat} | kg/(g _{Zr} ·h) | dL/g |
| Cp₂ZrCl₂ | | | | | | | | |
| 0.29 | 0.99 | AlMe ₃ /H ₂ O | 5 | 2 | 19.1 | 65.9 | 211.1 | 2.6 |
| 0.29 | 0.99 | MAO | 5 | - | 26.2 | 90.34 | 289.6 | 1.9 |
| 1 | 3.42 | AlEt ₃ /H ₂ O | 17.1 | 2 | 0 | | | |
| 1 | 3.42 | Al(<i>n</i> -Bu) ₃ /H ₂ O | 17.1 | 2 | 0 | | | |
| 0.29 | 0.99 | Al(<i>i</i> -Bu) ₃ /H ₂ O | 5 | 2 | 0 | | | |
| 0.29 | 0.99 | TIBAO | 5 | | 0 | | | |
| 1 | 3.42 | Al(<i>n</i> -Oct) ₃ /H ₂ O | 17.1 | 2 | 0.05 | 0.05 | 0.2 | n.d. |
| <i>rac</i>-EBIZrCl₂ | | | | | | | | |
| 0.17 | 0.41 | AlMe ₃ /H ₂ O | 2 | 2 | 19 | 111.8 | 512.9 | 1.4 |
| 0.17 | 0.41 | MAO | 2 | - | 33 | 194.1 | 890.8 | 1.6 |
| 0.42 | 1.00 | Al(<i>i</i> -Bu) ₃ /H ₂ O | 5 | 2 | 19 | 45.2 | 207.6 | 1.5 |
| 0.42 | 1.00 | TIBAO | 5 | - | 15 | 35.7 | 163.9 | 1.7 |
| 0.42 | 1.00 | IBAO | 5 | - | 0 | | | |
| 1 | 2.39 | Al(<i>n</i> -Oct) ₃ /H ₂ O | 12.0 | 2 | 10 | 10.0 | 45.9 | 1.0 |

Experimental conditions: 2.3 L stainless steel reactor; Hexane, 1 L; pP_E = 9.6 bar; T: 80°C; [Zr] = 0.5÷3.4 · 10⁻⁶ M; Al/Zr = 5000 mol/mol, time: 60 min.

Experimental part

All manipulations were performed under dry nitrogen atmosphere.

Materials: AlMe₃, MAO, Al(Et)₃, Al(*n*-Bu)₃, Al(*i*-Bu)₃, TIBAO, IBAO Al(*n*-Oct)₃, DIBAH were all purchased from WITCO GmbH. Cp₂ZrCl₂ and (Me₅Cp)₂ZrCl₂ were purchased from STREM Chemical Inc. *rac*-EBIZrCl₂ and *rac*-EBTHIZrCl₂ were purchased from WITCO GmbH. Bis-(4,7-dimethyl-indenyl)ZrCl₂ (BDMIZrCl₂) and *rac*-Ethylenebis-(4,7-dimethyl-indenyl)ZrCl₂ (*rac*-EBDMIZrCl₂) were synthesized following the method reported in the literature[6].

Synthesis of *tris-i-Octyl Aluminum (TIOA)*. 128 ml of 2,4,4-trimethyl-1-pentene (0.82 mol) were introduced in a round bottomed flask, working under anidrous nitrogen atmosphere. 15 ml (0.0082 mol) of di-isobutylaluminum-hydride (DIBAH) were slowly added under stirring in 30 minutes, at a temperature of 30°C. The temperature was then slowly warmed up to 108°C (refluxing conditions), collecting in a trap (cooled at -80°C) the formed isobutene. The

reaction mixture was maintained under stirring at 108°C for 20 hours. At the end, the residual olefin was removed by distillation at 80°C (0.1 mmHg). TIOA was left as residue (24 g). From elemental analysis: Al = 7.9 wt.% (Al_{calcd} = 7.4 wt.%).

¹H NMR (C₆D₆), (Figure 1): 2.15-1.92 ppm (m, 1H, **H2**), 1.31 ppm (d, J=5.40 Hz, 2H, **H3**), 1.10 ppm (d, J= 6.64 Hz, 3H, **H5**), 0.98 ppm (s, 9H, **H4**), 0.65-0.17 (bs, 2H, **H1**)

Reference compounds:

2,4,4-trimethyl-1-pentene (starting olefin); ¹H NMR (C₆D₆): 4.82 ppm (s, 1H), 4.61 ppm (s, 1H), 1.86 ppm (s, 2H), 1.69 ppm (s, 3H), 0.87 ppm (s, 9H).

2,4,4-trimethyl-2-pentene (side product of the starting olefin); ¹H NMR (C₆D₆): 5.17 ppm (s, 1H), 1.62 ppm (s, 3H), 1.59 ppm (s, 3H), 1.07 ppm (s, 9H).

2,2,4-trimethyl-pentane (product of TIOA hydrolysis); ¹H NMR (C₆D₆): 1.73-1.48 ppm (m, 1H), 1.10 ppm (d, J=5.40 Hz, 2H), 0.91 ppm (d, J=6.64, 6H), 0.88 ppm (s, 9H).

Synthesis of TIOAO. 5.0 g (0.0137 mol) of TIOA and 8 ml of n-hexane were introduced in a 50 ml Schlenk tube. The solution was cooled to a -5±0°C and 115 μl (0.0064 mol) of distilled water were added under vigorous stirring, maintaining the temperature below 0°C. The solution was allowed to achieve room temperature, under stirring. 1 ml was taken, the solvent removed under reduced pressure, and the viscous oil left as a residue was dissolved in 0.5 ml of C₆D₆ for ¹H NMR analysis.

¹H NMR (C₆D₆) (Figure 2): 2.50-1.90 ppm (bs+m, 1H), 1.70-1.15 ppm (bs+d, 2H), 1.15-1.05 ppm (bs+d, 3H), 0.97 ppm (bs, 9H), 0.80-0.20 (m+bs, 2H)

Synthesis of Polyisooctylalumoxane (TAO). The same aforementioned procedure was applied to the synthesis of TAO by using 5.0 g of TIOA and 243 μl (0.0135 mol) of distilled water.

¹H NMR (C₆D₆) (Figure 3): 2.50-1.90 ppm (bs, 1H), 1.70-1.15 ppm (bs, 2H), 1.15-0.95 ppm (bs, 3H+9H), 0.80-0.20 (bs, 2H)

¹H NMR Analysis. Spectra were acquired at room temperature on a Bruker DPX 200 working at 200.13 MHz using C₆D₆ as solvent. Chemical shifts were referred to the signal of the residual C₆H₆ (7.15 ppm). 128 transients were acquired for each spectrum with a 15° pulse and 1 s of delay between pulses.

To optimise peak area measurements a selected region of the NMR spectra was fitted as a sum of Gaussian functions with the Bruker WINNMR™ program according to the following procedure:

- I. selection of the region (1.9 ÷ 2.5 ppm)
- II. base line correction (to eliminate the interference due to the base of the large peaks at higher fields)
- III. choice of the number and positions of the Gaussian functions for the fitting (1 for the broad signal (**A**) and 8 for the multiplet (**B**), see figure 4)
- IV: starting of the fitting till a maximum number of iterations is reached or a minimum difference between the experimental and the calculated spectra is obtained
- V. the area of each peak is obtained and combined in a suitable way to obtain the contribution of the two components.

Polymerization procedures

Ethene polymerization was performed in a 2.3 L thermostatted stainless-steel autoclave purified by purged with ethene at 80 °C. 1.0 L of *n*-hexane and 9.6 bar of ethene were introduced, and the temperature was risen to 80 °C. The cocatalyst and the metallocene in toluene solution (0.1-0.5 mg in 5 ml), were introduced in a 10 ml Schlenk tube; stirred for 5 minutes and injected into the autoclave through a stainless steel vial with ethene overpressure. The total pressure was maintained constant by continuously feeding ethene. After one-hour polymerization at 80°C, the reactor was degassed, the polymer was recovered by filtration and dried in vacuum at 70°C.

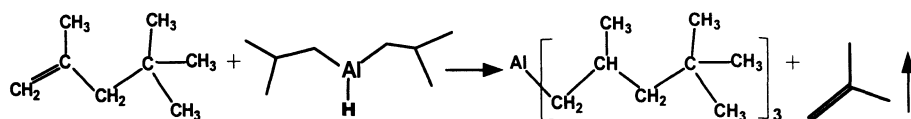
Ethene/propene copolymerization was performed at 50°C, in a 250 ml glass reactor, equipped with a mechanical stirrer, a thermometer and a pipe for monomers feeding. 100 ml of toluene and the cocatalyst (1.725 mmol of Aluminum) were introduced in the nitrogen-purged reactor, kept in a thermostatic bath. At the polymerization temperature, a monomers mixture was fed and continuously discharged with a flow of 1.5 L/min. When the equilibrium pressure (80 mmHg of overpressure) was reached, 0.74 mg (1.725 μmol) of catalyst, dissolved in 5 ml of toluene, were added to start the polymerization. During the polymerization, the temperature was kept within ± 0.2°C. The polymerization was stopped after 15 min by adding 1 ml of methanol and the copolymer recovered by precipitation in methanol/HCl and filtration, was finally dried at 50°C under reduced pressure.

Intrinsic viscosity was measured in tetrahydronaphthalene at 135 °C.

Results and discussion

TIOA synthesis

TIOA was easily obtained by the common insertion reaction of 2,4,4-trimethyl-1-pentene in the Al-H bond of di-*i*-butylaluminum hydride[5] (DIBA-H) followed by the elimination of 2-methyl-propene (see Scheme 2). An excess of 1-olefin and the separation of the formed 2-methyl-propene allowed the complete conversion of DIBA-H in TIOA.



Scheme 2.

Essentially pure tris(2,4,4-trimethylpentyl)aluminum was obtained after distillation of the excess of 2,4,4-trimethyl-1-pentene. The starting olefins were present in a low amount, less than 5 wt.%, as revealed by ¹H NMR spectrum (see Figure 1).

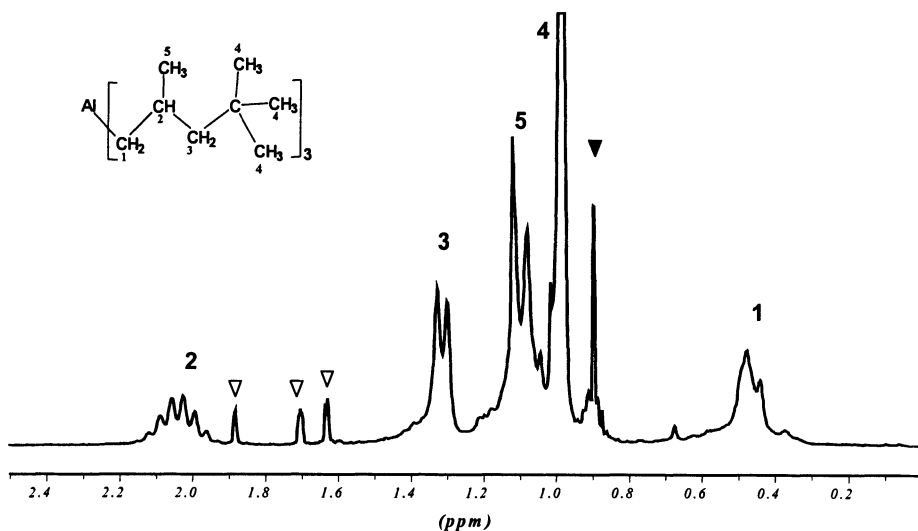
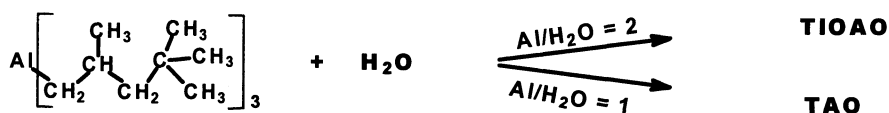


Fig. 1. ^1H NMR spectrum of TIOA. The peaks marked with Δ are due to the starting olefins; the peak marked with (∇) is due to the 2,4,4-trimethylpentane (see experimental part)

Alumoxane synthesis

TIOAO, formally tetra-*i*-octyl alumoxane, was prepared by reacting TIOA with H_2O (see Scheme 1), under controlled conditions, in a stoichiometric ratio of 2 : 1⁴. Poly-*i*-octyl alumoxane (TAO), from the reaction of TIOA and H_2O in a 1=1 ratio was also prepared (Scheme 3).



Scheme 3.

Figure 2a-2b show the ^1H NMR spectra of TIOAO and of TAO respectively.

The spectrum of TIOAO consists of two overlapping set of signals. One set is made of broad peaks typical of a poly-alkyl-aluminum-oxane, the other of sharper peaks and resolved multiplets as in TIOA. In the TAO spectrum only broad peaks are present. In both cases, 2,2,4-trimethyl-pentane is present as the product of the hydrolysis reaction between AlR_3 and H_2O .

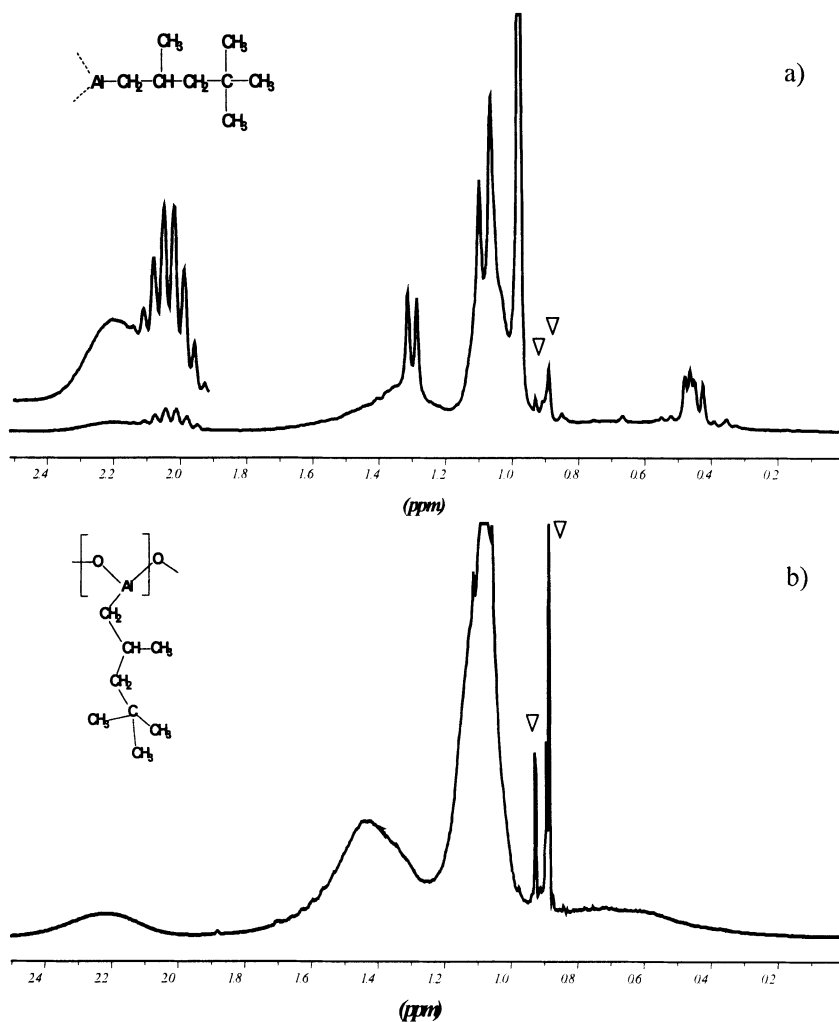


Fig. 2. ¹H NMR of TIOAO (2a) and of TAO (2b). The marked peaks (▽) are due to the alkane

Catalytic performances of TIOA, TIOAO and TAO in ethene-based polymerization

TIOA, TIOAO and TAO were tested as cocatalysts in ethene polymerization in the conditions of Table 1 by using *rac*-EBIZrCl₂ as the metallocene. The catalytic system was completely inactive with TIOA, while only traces of polymer were obtained with TAO. Only TIOAO allowed the synthesis of polyethene in high yield (600 KgPE/g_{Zr}/h). The same catalytic behaviour was obtained with *rac*-EBTHIZrCl₂ in the low-pressure ethene/propene copolymerization carried out in toluene solution at 50°C (see experimental part). Alumoxanes alternatives to MAO seem to give polymers with very similar molecular masses as shown by data of Table 1 and confirmed by results reported elsewhere[7].

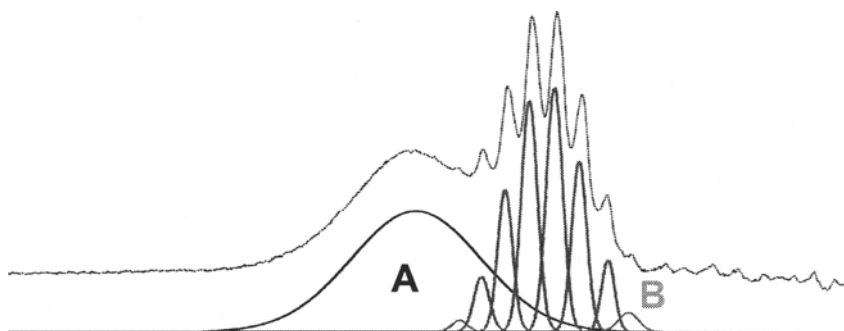


Fig. 3. Fitting of ^1H NMR “finger-print” region of TIOAO

Ethene polymerization from metallocenes

The catalytic ability of TIOAO and of other alumoxanes was compared in ethene polymerization promoted by a number of metallocenes. Figure 4 and 5 show that the catalytic activity is strongly dependent on the metallocene. However TIOAO based systems are definitely more active than the other investigated cocatalysts alternative to MAO.

Furthermore the catalytic performances are due not only to the structure of the metallocene, but should be rather attributed to the whole catalytic system. This emphasises the role played by the cocatalytic system.

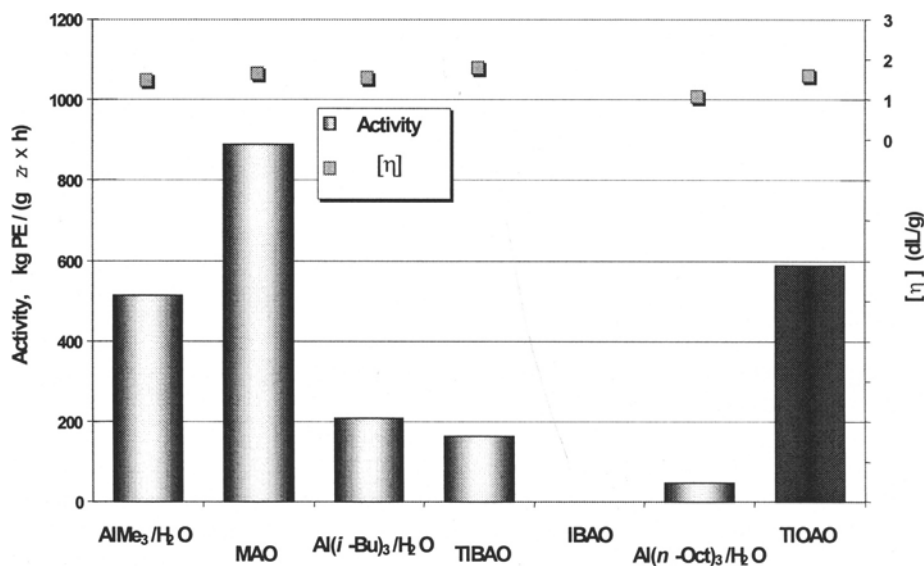


Fig. 4. Ethene polymerization with $r\text{-EBIZrCl}_2$ and various cocatalyst vs TIOA/H₂O. Experimental conditions: 2.3 L stainless steel reactor; Hexane, 1 L; $p_{\text{PE}} = 9.6$ bar; T 80°C; $[\text{Zr}] = 0.5 \div 2.4 \cdot 10^{-6}$ M; Al/Zr = 5000 mol/mol, time 60 min.

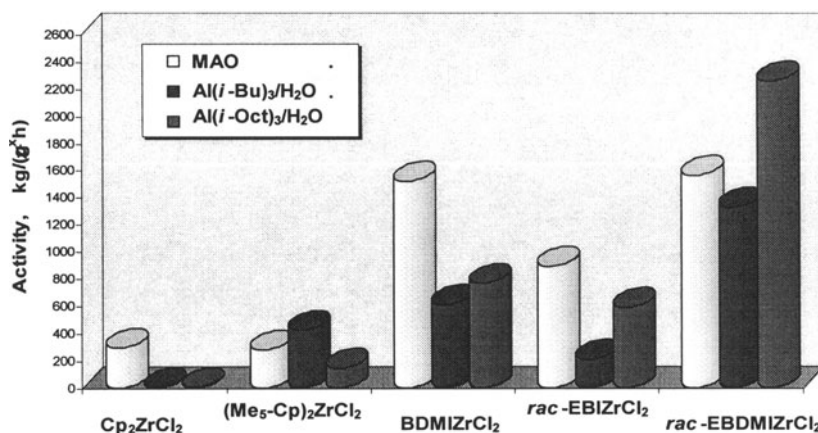


Fig. 5. Comparison in Ethene polymerization, between the three main cocatalysts and different metallocenes. Experimental conditions: 2.3 L stainless steel reactor; Hexane, 1 L; $P_E = 9.6$ bar; $T = 80^\circ\text{C}$; $[\text{Zr}] = 0.5 \pm 2.4 \cdot 10^{-6}$ M; Al/Zr = 5000 mol/mol, time 60 min.

Conclusions

- A new alumoxane, TIOAO, alternative to MAO and based on Al(*i*-Octyl)₃, was discovered and developed.
- A number of different procedures for the synthesis of TIOAO, providing stable compounds, were optimised.
- An analytical “*finger-print*” of the cocatalyst was chosen and a correlation with the catalytic performances was established.
- In ethene (co) polymerization, remarkable catalytic activities, comparable or even better than those obtained with MAO were observed.

References

1. Resconi, L.; Giannini, U.; Albizzati, E.; EP 0384171 to Montell Technology B.V., **1990**.
2. Resconi, L.; Galimberti, M.; Piemontesi, F.; Guglielmi, F.; Albizzati, E.; EP 0575875 to Montell Technology B.V., **1993**.
3. Resconi, L.; Dall’Occo, T.; Giannini, U.; to be published
4. (a) Dall’Occo, T.; Galimberti, M.; Resconi, L.; Albizzati, E.; Pennini, G.; WO 96/02580 to Montell Technology B.V., **1996**. (b) Galimberti, M. WO 97/00897 to Montell Technology B.V., **1997**
5. K. Ziegler in *Organometallic Chemistry* (ACS monograph. n 147, H. Zeiss, ed.), Reinhold, New York, **1960**, pp. 194-269.
6. N. Piccolrovazzi, P. Pino, G. Consiglio, A. Sironi, M. Moret, *Organometallics*, **9**, **1990**, 3098.
7. I. M. Lee, J. A. M. Ball, B. Iyengor, S. Collins, *Organometallics*, **11**, **1992**, 2115.
8. M. Galimberti, M. Destro, O. Fusco, F. Piemontesi, I. Camurati, accepted by *Macromolecules* for publication

Expanding the Scope of Metallocene Catalysis: Beyond Indenyl and Fluorenyl Derivatives.

John A. Ewen^a, Robert L. Jones^b, Michael J. Elder^b

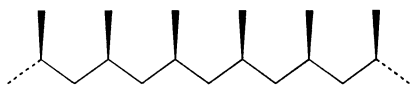
^a Catalyst Research Corporation, 14311 Golf View Trail, Houston, Texas 77059 (USA)

^b Montell USA Inc., Elkton Research and Development Center, 912 Appleton Road, Elkton, Maryland 21921 (USA)

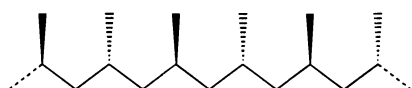
1. Introduction.

Group 4 metallocenes with bridged and substituted Ind and Cp/Flu ligands have produced high-molecular-weight isotactic (I-PP), syndiotactic (S-PP), atactic (A-PP) and hemi-isotactic (HIT-PP) (Scheme 1) polypropylenes.ⁱ

Scheme 1.



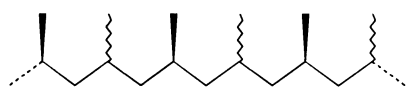
I-PP from C_{2v}, C₂ and C₁ Symmetry



S-PP from C_s Symmetry

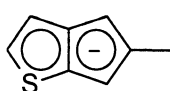


A-PP from C₂ and C_s Symmetry

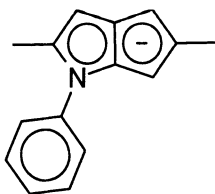


HIT-PP from C₁ Symmetry

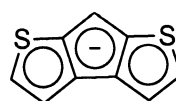
In this contribution we report on catalysts bearing instead thiophene and pyrrole heterocycles ring-fused to Cp (Figs. 1 and 2). Preliminary investigations of the effects of 5/5 rings and heteroatoms on the control of the polymerization stereochemistries, stereospecificities, polypropylene molecular weights, and catalyst activities are reported on.ⁱⁱ



L₁



L₂



L₃

Fig. 1. Ligand structures of heterocycles ring fused to Cp.

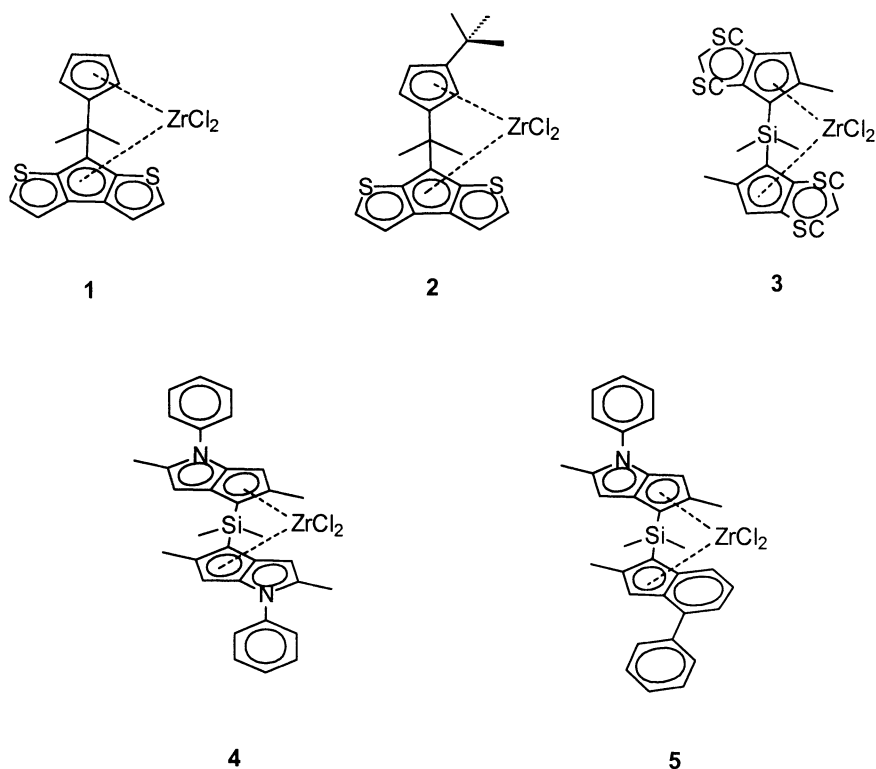


Fig. 2. Heterocenes with C_s (1), C_1 (2), C_2 (3, 4) and pseudo- C_2 (5) crystallographic symmetries. The monoalkyl cation derived from “meso”-5 is chiral.

The heterocenes depicted in Fig. 2 with C_s (1), C_1 (2) and C_2 (3, 4) and pseudo- C_2 (5) crystallographic symmetries were prepared to determine if they obey the same polypropylene-tacticity *versus* catalyst-structure rules first observed with the indenyl and fluorenyl ligands.ⁱⁱⁱ The C_2 symmetric structures also include a Me_2Si bridge for rigidity,^{iv} methyl groups α to the bridgehead carbon with L_1 and L_2 for MW control^v and an N-phenyl ring with L_2 for high activity and stereospecificity.^{vi} The mixed heterocene/indenocene 5 was investigated to determine if the observed ligand effects were cumulative.

The heterocene catalysts are compared throughout with the analogously structured $\text{Me}_2\text{C}(1\text{-Cp-9-Flu})\text{ZrCl}_2$,^{vii} $\text{Me}_2\text{C}(3\text{-}t\text{-Bu-1-Cp-9-Flu})\text{ZrCl}_2$,^{viii} $\text{Me}_2\text{Si}(2\text{-Me-1-Ind})_2\text{ZrCl}_2$ ^{ix} and $\text{Me}_2\text{Si}(2\text{-Me-4-Ph-1-Ind})_2\text{ZrCl}_2$.^{vi} The heterocenes obey the same metallocene symmetry rules, produce polypropylenes with high molecular weights, and do indeed rival their forerunners in both activities and stereospecificities. Interesting differences are noted between PP MWs with the heterocenes and the traditional prototypes. The identical trends in activities and stereospecificities *versus* ligand structures confirms that steric effects largely determine catalyst performance.

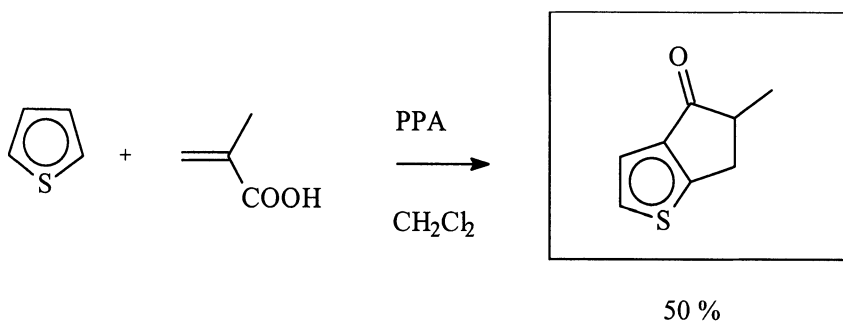
2. Experimental

The syntheses of $L_1 - L_3$ and 1 - 5 are partially illustrated in Schemes 2 - 4. The depicted carbonyl precursors to L_1 and L_2 were converted to olefins by tosylhydrazone elimination with *n*-BuLi; following Volz's use of the Shapiro reaction. L_3 was prepared in moderate yield according to Kraak. The metallocenes were prepared with our standard procedures for the corresponding indenyl and fluorenyl derivatives.^x

2.1 Syntheses of L_1 and 3.

2.1.1 5-Methyl-5,6-dihydrocyclopenta[1,2-b]thiophen-4-one and 5-methyl-4,5-dihydrocyclopenta[2,1-b]thiophen-6-one.^x A solution containing thiophene (65.7 g, 781 mmol), methacrylic acid (66.56 g, 773 mmol), and methylene chloride (50 mL) were added dropwise to 87% polyphosphoric acid (PPA) over a 1 h. period, while maintaining the temperature at 50 °C (Scheme 1). The reaction mixture was stirred an additional 2h and then poured onto 1 L of ice. The organic layer was collected with a methylene chloride/hexane solution (30 vol.%, 100 mL), washed with water (250 mL), sodium bicarbonate (saturated solution, 2 x 250 mL), then water (2 x 250 mL). The organic layer was dried over magnesium sulfate, filtered, and dried in vacuo yielding 93.5 g of a dark brown, slightly viscous oil. Distillation of this material produced 52.2 g (1 mbar, 92 °C – 98 °C) of the target materials (a mixture of the two positional isomers.) Yield: 44%. ¹H-NMR, CD₂Cl₂ ppm δ; 7.85 (d, 1H), 6.95 (d, 1H), 2.4 - 3.3 (m, 2H), 1.25 (d, 3H).

Scheme 2



2.1.2 5-Methyl-5,6-dihydrocyclopenta[1,2-b]thiophen-4-sulfonylhydrazide.^{xii} Absolute ethanol (300 g) was treated with a vigorous stream of gaseous hydrochloric acid until saturated. Toluene-4-sulfonyl hydrazine (64 g, 343 mmol) was added as a dry powder, forming a white slurry. 4,5-Dihydro-5-methyl-6H-cyclopenta(b)thiophene-6-one (52.2 g, 343 mmol) was added dropwise over a 30

minute period. The solution turned to a clear, straw colored liquid, then formed a white precipitate which was collected by filtration. The precipitate was washed with THF (800 mL) then dried *in vacuo*. Yield: 100 g (91.5%). ¹H-NMR, DMSO-*d*₆ ppm δ; 9.1 (s, 1H), 6.4-6.6 (m, 3H), 6.15 (d, 2H), 5.7 (d, 1H), 2.1 (s, 1H), 1.9 (m, 2H), 1.2 (m, 3H), 0.2 (d, 3H).

2.1.3 5-methyl-4-hydrocyclopenta[2,1-b]-thiophene (L₁). 5-Methyl-5,6-dihydrocyclopenta[1,2-b]thiophen-4-sulfonohydrazide (165.5g, 517 mmol) was slurried in anhydrous THF (300 mL) and the temperature lowered to -10 °C. *n*-Butyllithium (1,525 mmol, 2.5 M solution in hexane, 610 mL) was added dropwise. The temperature was allowed to rise to ambient and stirring was continued for 16 h with the color turning deep purple. The reaction was quenched with the dropwise addition of water (50 mL), the color of the solution turned yellow. The organic layer was collected with diethyl ether (500 mL) and washed repeatedly with water (3 x 300 mL). The organic fraction was then dried over magnesium sulfate, filtered, and the solvents were removed *in vacuo* to yield a dark orange oil (47.3g). Distillation of the oil (short path, 18 mtorr, 37 °C), produced 24.5g (35 %) of the purified product. Mass spectrum (typical, first isomer; *m/e* (RA): 136 (11.4), 134 (100), 121 (25), 77 (12). ¹H-NMR (both isomers), CD₂Cl₂ ppm δ; 6.8-7.2 (4d, 2H), 6.4 (2s, 1H), 3.1, 3.3 (2s, 2H), 2.25 (2s, 3H).

2.1.4 Dimethylsilylbis(2-methyl-2-hydrocyclopenta[2,1-b]-thiophene). 5-Methyl-4-hydrocyclopenta[2,1-b]-thiophene (13.6 g, 100 mmol) was dissolved in 20 mL of THF and the temperature lowered to -10 °C. *n*-Butyllithium (100 mmol, 2.5 M of a hexane solution, 40 mL), was added dropwise. The flask and contents were allowed to warm to room temperature and stirring was continued for 2 h. In a separate flask, dimethyldichlorosilane (6.5 g, 50 mmol, 6.5 mL) was dissolved in 20 mL of THF and the temperature was lowered to -10°C. The solution containing the 5-methylcyclopenta[2,1-b]-thiophene anion was added dropwise to the stirred solution. The flask and contents were then allowed to warm to room temperature and stirring continued overnight. The contents of the flask were cooled to -10 °C, then a solution containing 2.5 mL water in 20 mL THF was added dropwise. After addition was complete, stirring continued for 1h, then the organic layer was collected with diethyl ether (100 mL) and washed with water (100 mL), saturated sodium bicarbonate solution (100 mL), then water (100 mL). The organic fraction was dried over magnesium sulfate, filtered, and the solvents were removed *in vacuo* to yield a dark orange oil (15.6g). Kugelrohr distillation (30 mtorr, 200 °C) of the product yielded 7.3g (22 mmol, 45 %) desired product. Mass spectrum, *m/e* (RA), 328 (43), 193 (100), 177 (42), 159 (56); CD₂Cl₂ ppm δ (both isomers); 6.9-7.4 (m, 4H), 6.5-6.8 (m, 2H), 3.1- 3.8 (m, 4H), 2.0-2.4 (m, 6H), 0.1-0.3 and -0.3 (m, 6H).

2.1.5 Dimethylsilylbis(2-methylthiapentenyl)zirconium dichloride (3). A solution containing 7.33 g (22.3 mmol) of dimethylsilylbis(2-methyl-2-hydrocyclopenta[2,1-b]-thiophene) in diethylether prepared at -10 °C was treated with methylithium (44.6 mmol, 1.4 M solution in diethylether, 35 mL). The

contents were allowed to warm to room temperature and stirring was continued for 16 h. Solvents were decanted and the solids were washed with fresh diethylether (2 x 30 mL). Zirconium tetrachloride was added as a dry powder, and pentane (100 mL) was added. Stirring was continued overnight, then the pentane was removed in vacuo and the solids recovered (10.2 g). Portions of the solids were filtered from toluene and the filtrate dried in vacuo. Slow evaporation of a concentrated dichloromethane solution of the product produced crystals suitable for x-ray diffraction studies. Yield: 2 g of a mixture of stereoisomers (3 *rac*- and 3 *meso*- ; Figure 3). $^1\text{H-NMR}$ δ (CD_2Cl_2): 6.7-7.7(m, 4H), 6.4-6.7 (m, 2H), 2.0-2.5 (m, 6H), 0.9-1.2 (m, 6H).

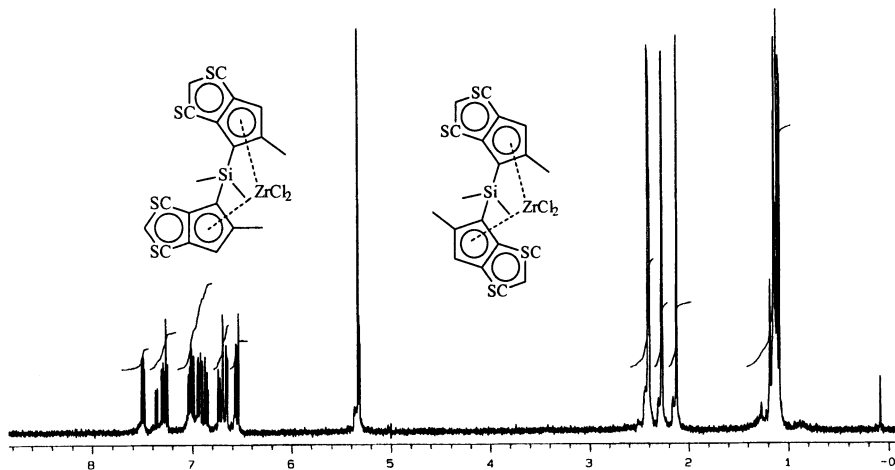
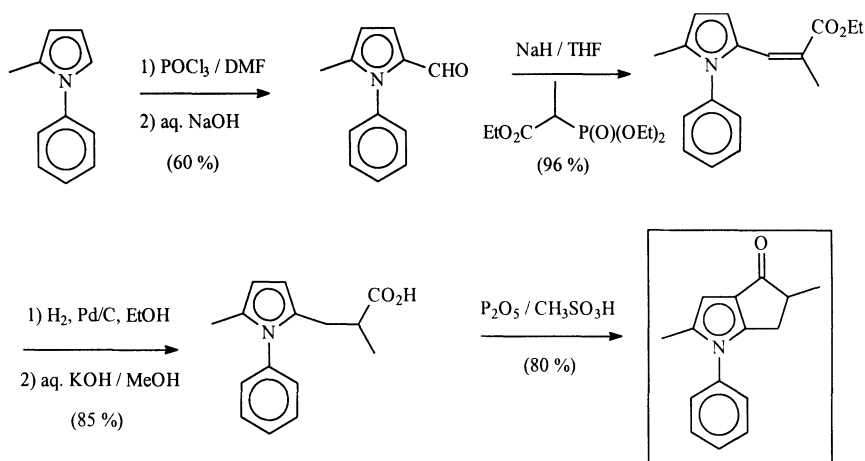


Fig. 3. ^1H NMR of the six S/C positional isomers of *meso*- and *rac*- $\text{Me}_2\text{Si}(\text{L}_1)_2\text{ZrCl}_2$.

2.2 Syntheses of L_2 , 4 and 5.

2.2.1 1-Phenyl-2-methylpyrrole. Butyllithium (0.700 mol, 280 mL of 2.5 M solution in hexanes) was added slowly at room temperature to a mixture of 1-phenylpyrrole (0.695 mol, 100g) and TMEDA (0.700 mol, 106 mL) in hexane (80 mL) and stirred for 3 h. The slurry was diluted with 300 mL of THF and iodomethane (0.771 mol, 48 mL) was added slowly while maintaining the temperature between 35-40 °C. After stirring overnight at room temperature, 250 mL of water were added and the organic layer was separated. The aqueous layer was extracted with ether (2 x 100 mL) and the combined organic fractions were dried over MgSO_4 . Evaporation of solvents and TMEDA yielded 107 g of light brown oil (98% yield, +95% purity by GC). $^1\text{H-NMR}$ δ (CDCl_3): 7.3-7.4 (m, 5H), 6.8 (m, 1H), 6.2 (m, 1H), 6.1 (m, 1H), 2.2 (s, 3H).

Scheme 3^{xiii}

2.2.3 5-Methyl-1-phenylpyrrole-2-carbaldehyde. POCl_3 (0.375 mol, 35 mL) was added dropwise to 37 mL of DMF and stirred for 10 min. The temperature was lowered to 0 °C and a mixture of 1-phenyl-2-methylpyrrole (55 g, 0.340 mol) and DMF (7 mL) were added dropwise. The viscous solution was slowly warmed to 50 °C and stirred for 1 h. After cooling to room temperature, the flask was opened to the air and charged with 350 g of crushed ice. A 20 wt% aqueous solution of NaOH (430 mL) was added cautiously and the mixture was immediately heated to 90–95 °C and stirred for 10 min. The flask was placed in an ice bath and the product solidified upon cooling. The solids were collected on a filter funnel, washed with water, redissolved in dichloromethane, and dried over MgSO_4 . Evaporation of the solvent yielded 38 g of light brown solids (60 % yield). $^1\text{H-NMR}$ showed the crude product to be a mixture of 5-methyl-1-phenylpyrrole-2-carbaldehyde and 5-methyl-1-phenylpyrrole-3-carbaldehyde in *ca.* 4:1 ratio. Spectroscopically pure 1-phenyl-5-methyl-2-pyrrolicarboxaldehyde was obtained by recrystallization from ether. Analysis of 1-phenyl-5-methyl-2-pyrrolicarboxaldehyde: $^1\text{H-NMR}$ δ (CDCl_3): 9.3 (s, 1H, Py-COH), 7.4 (m, 3H, ArH), 7.2 (m, 2H, ArH), 7.0 (d, 1H, PyH), 6.1 (d, 1H, PyH), 2.0 (s, 3H, PyCH₃). $^{13}\text{C-NMR}$ δ (CDCl_3): 178.3 (-CHO), 140.1, 137.6, 133.8 (Ar and py quat. C) 129.4, 129.0, 128.0 (Ar-CH), 110.5 (py-CH), 12.9 (py-CH₃). mp 85 °C. Analysis of 1-phenyl-2-methyl-3-pyrrolicarboxaldehyde: $^1\text{H-NMR}$ δ (CDCl_3): 9.9 (s, 1H, PyCOH), 7.4 (m, 3H, ArH), 7.2 (m, 2H, ArH), 6.7 (d, 1H, PyH), 6.6 (d, 1H, PyH), 2.4 (s, 3H, PyCH₃).

2.2.4 Ethyl[2Z]-2-methyl-3-[5-methyl-1-phenylpyrrol-2-yl]prop-2-enoate. Triethyl 2-phosphonopropionate (93.3 mmol, 20 mL) was diluted with THF (15 mL) and added slowly to NaH (130 mmol, 3.16 g) in THF (40 mL) at 0 °C. The mixture was slowly warmed to room temperature and stirring was continued for 0.5 h after gas evolution had ceased. The temperature was lowered to -10 °C and a solution of 5-methyl-1-phenylpyrrole-2-carbaldehyde (86.5 mmol, 16.0 g) in 50

mL THF was added dropwise. The flask and contents were warm to room temperature over a 30 min. period resulting in a thick precipitate. A saturated aqueous solution of NH_4Cl (50 mL) was added cautiously dissolving the precipitate to give a two phase solution. After evaporating the THF, the crude product was extracted with ether (2 x 100 mL), washed with brine solution, dried over MgSO_4 , and evaporated to a brown oil. Yield: 22.5 g (96.5 %) of spectroscopically pure product. $^1\text{H-NMR}$ δ (CDCl_3): 7.4 (m, 3H, ArH), 7.2 (m, 3H, ArH (2 H's) + $\text{PyCHC}(\text{CH}_3)(\text{CO}_2\text{Et})$), 6.6 (d, 1H, PyH), 6.1 (d, 1H, PyH), 4.0 (q, 2H, OCH_2CH_3), 2.1 (s, 3H, $\text{PyCHC}(\text{CH}_3)(\text{CO}_2\text{Et})$), 2.0 (s, 3H, PyCH_3), 1.1 (t, 3H, OCH_2CH_3).

2.2.5 Ethyl-2-methyl-3-[5-methyl-1-phenylpyrrol-2-yl]propanoate. A solution of ethyl[2Z]-2-methyl-3-[5-methyl-1-phenylpyrrol-2-yl]prop-2-enoate (10g, 37 mmol) in ethanol (50 mL) was stirred under 3.5 bar of hydrogen pressure at room temperature with 300 mg of 10% Pd on carbon for 1 h. Evaporation of the filtered golden solution gave ethyl-2-methyl-3-[5-methyl-1-phenylpyrrol-2-yl]propanoate as a yellow syrup (9.4 g, 95% pure by GC). $^1\text{H-NMR}$ δ (CDCl_3): 7.4 (m, 3H, ArH), 7.2 (m, 2H, ArH), 5.9 (m, 2H, PyH), 4.0 (q, 2H, OCH_2CH_3), 2.7 (m, 1H, $\text{PyCH}_2\text{CH}(\text{CH}_3)(\text{CO}_2\text{Et})$), 2.5 (m, 2H, PyCH_2CH), 2.0 (s, 3H, PyCH_3), 1.2 (t, 3H, OCH_2CH_3), 1.1 (d, 3H, $\text{CH}(\text{CH}_3)(\text{CO}_2\text{Et})$). $^{13}\text{C-NMR}$ δ (CDCl_3): 176.4 (CO), 129.4, 128.7, 128.0, (Ar), 106.2, 106.0 (Py), 60.4 (O- CH_2), 39.7 (PyCH_2CH), 31.2 (PyCH_2CH), 25.5 (PyCH_3), 17.3 ($\text{PyCH}_2\text{CH}(\text{CH}_3)$). ms (m/e) (rel intensity): 271 ($[\text{M}^+]$, 23), 170 (100), 154 (12), 128 (6), 77 (10).

2.2.6 2-Methyl-3-[5-methyl-1-phenylpyrrol-2-yl]propanoic acid. A mixture of ethyl-2-methyl-3-[5-methyl-1-phenylpyrrol-2-yl]propanoate (9.4 g of crude oil, ca. 33 mmol) and Claisen's reagent (18 mL) were heated at 90-95 °C for 1 h. After cooling to room temperature, the solution was diluted with 15 g of crushed ice and acidified to pH 1-2 with 6 N HCl. The brown oily precipitate was dissolved in ether, washed with brine solution, dried over MgSO_4 , and evaporated to give a waxy solid. Triteration of the solids with pentane afforded 6.6 g of 2-methyl-3-[5-methyl-1-phenylpyrrol-2-yl]propanoic acid as a tan powder (84.7 % yield). $^1\text{H-NMR}$ δ (CDCl_3): 7.4 (m, 3H, ArH), 7.2 (m, 2H, ArH), 5.9 (m, 2H, PyH), 2.7 (dd, 1H, $\text{PyCH}_2\text{CH}(\text{CH}_3)(\text{CO}_2\text{Et})$), 2.5 (m, 2H, PyCH_2CH), 2.0 (s, 3H, PyCH_3), 1.1 (d, 3H, $\text{PyCH}_2\text{CH}(\text{CH}_3)$). $^{13}\text{C-NMR}$ δ (CDCl_3): 183.2 (-COOH), 139.0, 130.6; 129.7, 129.1, 128.4 (Ar-CH), 106.7, 106.4 (py-CH), 39.8 (- $\text{CH}(\text{CH}_3)(\text{COOH})$), 31.0 (py- CH_2CH -), 17.4 (CH_3), 13.3 (CH_3). mp 85 °C.

2.2.7 2,5-Dimethyl-1-phenyl-4,5-dihydrocyclopenta[2,1-b]pyrrole-6-one. Phosphorus pentoxide (57.9g, 204 mmol) was dissolved in methanesulfonic acid (288g, 3.0 mol) by heating at 100°C with stirring for 1 h. The solution was cooled to 70°C and 48.6g (200 mmol) of 2-methyl-3-[5-methyl-1-phenylpyrrol-2-yl]propanoic acid were added slowly and stirred for 30 minutes. The mixture was then heated to 100° for an additional 1 h. After cooling to room temperature, the reaction mixture was poured onto crushed ice and the organic fraction was

collected with dichloromethane, dried over magnesium sulfate, filtered, and rotovaped to an oil. Yield: 50.6 g of crude oil. The oil solidified upon standing and the solids were triterated with hexane/ether and dried under vacuum. $^1\text{H-NMR}$ δ (CDCl_3): 7.4 (m, 3H, ArH), 7.2 (m, 2H, ArH), 6.1 (s, 1H, PyH), 2.9 (m, 2H, PyCH₂), 2.3 (d, 1H, PyCH₂CH(CH₃)CO-), 2.1 (s, 3H, PyCH₃), 1.2 (d, 3H, PyCH₂CH(CH₃)CO-). ms (EI) (rel intensity): 223 ($[\text{M}^+ - 2]$, 4), 205 (4), 149 (100), 121 (3), 104 (5), 93 (3), 76 (5). mp 106 °C.

2.2.8 Hydrazone of 2,5-Dimethyl-1-phenyl-4,5-dihydrocyclopenta[2,1-b]pyrrole-6-one. The ketone 2,5-dimethyl-1-phenyl-4,5-dihydrocyclopenta[2,1-b]pyrrole-6-one (31 mmol, 7.0 g), *p*-toluenesulfonylhydrazide (36 mmol, 6.7 g), and *p*-toluenesulfonic acid monohydrate (6.3 mmol, 1.2 g) were dissolved in 50 mL of ethanol and stirred at 65 °C for 24 h. After cooling to room temperature and standing for several hours, the precipitated product was collected on a filter funnel, washed with ether and dried under vacuum (yield 5.0 g). The solvent was removed from the filtrate and an additional 1.2 g of product was crystallized from an ether/toluene solution of the oily residue. Total yield: 6.2 g (51 %) of light gray powder. $^1\text{H-NMR}$ δ (CDCl_3): 7.8 (d, 2H, ArH), 7.4 (m, 3H, ArH), 7.2 (m, 4H, ArH), 6.2 (s, 1H, PyH), 3.3 (tt, 1H, PyCH₂CH(CH₃)CN-), 2.9 (dd, 1H, PyCH₂), 2.4 (s, 3H, PyCH₃), 2.2 (dd, 1H, PyCH₂), 2.1 (s, 3H, Me), 1.2 (d, 3H, PyCH₂CH(CH₃)CN-). mp 156 °C

2.2.9 2,5-Dimethyl-1-phenyl-4-hydrocyclopenta[2,1-b]pyrrole (L₂-H). 11.9g (30 mmol) of the hydrazone of 2,5-dimethyl-1-phenyl-4,5-dihydrocyclopenta[2,1-b]pyrrole-6-one were dissolved in 50 mL THF. The solution was cooled to -78 °C and 69 mmol of *n*-butyllithium was added dropwise (69 mmol, 27.6 mL of a 2.5 M sol. in hexanes). After addition was complete the flask was heated to reflux an additional 2 h., then cooled to -10 °C, and a solution containing 0.7 mL water in 10 mL THF was added slowly and stirred an additional 30 minutes. The reaction mixture was washed with water and the organic layer collected with ether. The organic fraction was dried over magnesium sulfate, filtered, and rotovaped to a dark brown oil. Yield: 5.36g. The crude oil was further extracted with hexane, filtered and evaporated to a light oil. Yield = 3.2 g (L₂-H, + 85% purity by GC). $^1\text{H-NMR}$ δ (CDCl_3): *Isomer 1* - 7.3 (m, 5H, ArH), 6.0 (s, 1H), 5.9 (s, 1H), 3.2 (s, 2H, CH₂ of C₅ ring), 2.2 (s, 3H, PyCH₃), 2.0 (s, 3H, CH₃ at C-5). *Isomer 2* - 7.3 (m, 5H, ArH), 6.1 (s, 1H), 5.85 (s, 1H), 3.2 (s, 2H, CH₂ of C₅ ring), 2.2 (s, 3H, PyCH₃), 2.0 (s, 3H, CH₃ at C-5). ms (EI) (rel intensity): 209 (100), 194 (27), 167 (5), 117 (4), 91 (5), 77 (13).

2.2.10 Chlorodimethyl(L₂-H)silane. L₂-H (10.9 mmol, 2.28 g) was dissolved in ether (60 mL), treated with butyllithium (13 mmol, 5.2 mL of a 2.5 M sol. in hexanes) at -78 °C, and warmed to room temperature. After stirring for 4 h and refluxing for 1 h, pentane (30 mL) was added to precipitate the lithium salt. Liquids were decanted with a cannula and the solids were slurried in fresh ether (60 mL), cooled to -78 °C, and dichlorodimethylsilane (16.5 mmol, 2.13 g) was added by syringe. The mixture was brought to room temperature, stirred for 16 h,

filtered, and evaporated to an oil. The oil was further dried *in vacuo* (50 °C) to remove all traces of dichlorodimethylsilane. Yield - 3.0 g (9.9 mmol). $^1\text{H-NMR}$ δ (CD_2Cl_2): 7.5 (m, 2H), 7.4 (m, 3H), 6.3 (s, 1H), 6.0 (s, 1H), 3.3 (s, 1H), 2.4 (s, 3H), 2.3 (s, 3H), 0.5 (s, 3H), 0.1 (s, 3H). $^{13}\text{C-NMR}$ δ (CD_2Cl_2): 129.4, 126.5, 125.7, (Ar), 117.3, 104.3 (2 olefinic CH groups), 44.7 (Si-CH group), 17.5, 13.6 (2 CH_3 groups), 0.7, -1.6 (2 Si- CH_3 groups).

2.2.11 Dimethyl(L_2 -H) $_2$ silane. L_2 -H (9.9 mmol, 2.06 g) was dissolved in THF (40 mL), cooled to -78 °C, and treated with butyllithium (11 mmol, 4.4 mL of a 2.5 M solution in hexanes). The dark blue solution was brought to room temperature and stirred 4 h (The anion partially precipitated from solution. The mixture was added slowly to a solution of chlorodimethyl(L_2 -H)silane (9.9 mmol) in THF (20 mL) at -78 °C and warmed to room temperature. The reaction mixture was then stirred for 16 h at 55 °C. After removing solvents *in vacuo*, the residue was extracted with pentane (75 mL), filtered, and evaporated to give a tan solid (4.53 g, 9.5 mmol). $^1\text{H-NMR}$ δ (CD_2Cl_2): (*rac* isomer) 7.5 (m, 10H), 6.35 (ss,4H), 3.75 (s, 2H), 2.39 (s, 6H), 2.35 (s, 6H), -0.20 (s, 6H); (*meso* isomer) 7.5 (m, 10H), 6.30 (s, 2H), 6.10 (s, 2H), 3.75 (s, 2H), 2.33 (s, 6H), 2.24 (s, 6H), -0.19 (s, 3H), -0.24 (s, 3H). $^{13}\text{C-NMR}$ δ (CD_2Cl_2): (*rac* / *meso* mixture) 145.5, 145.4, 144.1, 144.0, 142.0, 131.3, 129.4, 129.3, 128.4, 127.7, 118.3, 107.0, 106.6, 44.7, 44.4, 20.0, 15.8, -5.2, -5.4, -5.6. ms (EI) (rel. intensity): 474 (18, PM), 266 (100), 208 (21), 165 (4), 77 (8).

2.2.12 $\text{Me}_2\text{Si}(L_2)_2\text{ZrCl}_2$ (4). Butyllithium (19 mmol, 7.6 mL of a 2.5 M sol. in hexanes) was added slowly to a solution of dimethyl(L_2 -H) $_2$ silane (8.8 mmol) in 60 mL of ether at -78 °C. The solution was stirred for 16 h at room temperature and solvents were evaporated *in vacuo*. The orange dilitho salt was slurried in pentane (60 mL) and treated with zirconium chloride (8.6 mmol, 2.0 g). Ether (1.0 mL) was added by syringe and the mixture was stirred vigorously for 24 h. The resulting yellow solids were collected on a closed frit, washed with pentane, and dried under vacuum. Yield - 5.6 g of 4 as a 1:1 *rac:meso* mixture and 2 equivalents of $\text{LiCl}\cdot\text{Et}_2\text{O}$. $^1\text{H-NMR}$ δ (CD_2Cl_2): (1:1 *rac:meso* mixture) 7.4 (m, 10H *meso*, 10H *rac*), 6.14 (s, 2H), 6.08 (s, 2H), 6.06 (s, 2H), 5.97 (s, 2H), 2.35 (s, 3H), 2.33 (s, 3H), 2.22 (s, 3H), 2.19 (s, 3H), 1.14 (s, 3H), 1.11 (s, 3H), 1.09 (s, 6H). LiCl was removed by redissolving the complex in dry dichloromethane, filtering, and removing the solvent *in vacuo*. The *rac* isomer (Figure 4) was recrystallized from a concentrated toluene solution. $^1\text{H-NMR}$ δ (CD_2Cl_2): 7.5 (m, 10H), 6.09 (s, 2H), 6.04 (s, 2H), 2.29 (s, 3H), 2.15 (s, 3H), 1.06 (s, 6H). $^{13}\text{C-NMR}$ δ (CD_2Cl_2): 143.0, 139.1, 129.6, 129.6, 127.0, 126.0, 121.7, 104.2, 102.6, 18.6, 14.3, 0.08. ms (EI, confirmed with Chem. I.) m/z 634 ($\text{C}_{32}\text{H}_{32}\text{N}_2\text{Cl}_2\text{SiZr}$).

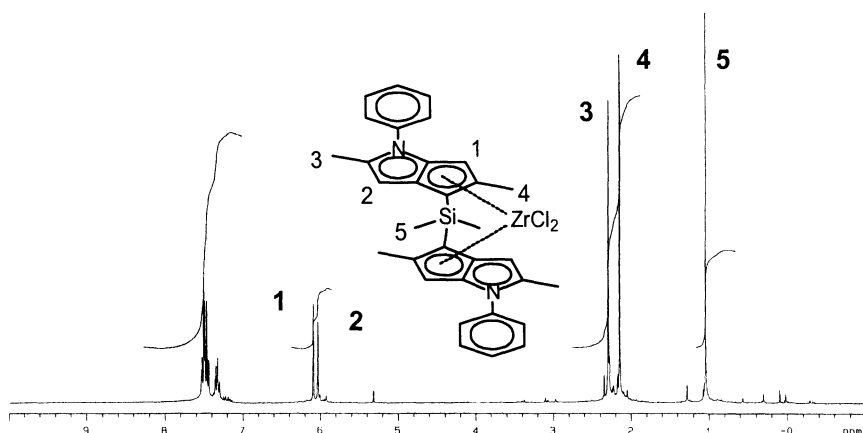


Fig. 4. ^1H NMR of *rac*- $\text{Me}_2\text{Si}(\text{L}_2)_2\text{ZrCl}_2$.

2.2.13 Dimethyl(*L*₂-*H*)(2-*Me*-4-*Ph*-*Ind*)silane. 2-Methyl-4-phenylindene (6.8 mmol, 1.4 g) was dissolved in ether (60 mL), cooled to $-78\text{ }^\circ\text{C}$, and treated with butyllithium (7.0 mmol, 2.8 mL of a 2.5 M solution in hexanes). The solution was brought to room temperature, stirred 4 h, and added dropwise to a solution of chlorodimethyl(*L*₂-*H*)silane (6.8 mmol, 2.0 g) in THF (40 mL) stirring at $-78\text{ }^\circ\text{C}$. The reaction mixture was warmed to $55\text{ }^\circ\text{C}$ and stirred for 16 h. Solvents were evaporated under reduced pressure and the residue was extracted with pentane (120 mL). The extract was filtered and evaporated to a sticky foam. Yield = 3.1 g (97%) of dimethyl(*L*₂-*H*)(2-*Me*-4-*Ph*Ind)silane. ^1H -NMR δ (CD_2Cl_2): 7.2-7.6 (m, 13H, Ar), 6.9, 6.4, 6.3, 6.1 (4 s, 3H, olefinic CH, major isomers), 2.2-2.4 (m, 9H, 3 methyls), -0.20 - -0.15 (m, 6H, $(\text{CH}_3)_2\text{Si}$). *ms* (EI) (rel. intensity): 472 (39, PM), 341 (6), 267 (100), 247 (18), 209 (48), 165 (23).

2.2.14 *Me*₂*Si*(*L*₂)(2-*Me*-4-*Ph*Ind)*ZrCl*₂ (5). The ligand dimethyl(*L*₂-*H*)(2-*Me*-4-*Ph*Ind)silane (6.6 mmol, 3.1 g) was dissolved in ether (60 mL), cooled to $-78\text{ }^\circ\text{C}$, and treated with butyllithium (14.5 mmol, 5.8 mL of a 2.5 M sol. in hexanes). The solution was warmed to room temperature, stirred for 3 h, and then refluxed for 1 h. Heating was stopped and the solvents were removed under reduced pressure. The residue was washed with pentane and dried to a yellow powder *in vacuo*. ZrCl_4 (6.6 mmol, 1.53 g) and pentane (40 mL) were added to the dianion powder and stirring was started. 1 mL of ether was added by syringe to the slurry and stirring continued for 16 h. The bright yellow solids were collected on a closed frit, washed with pentane, and dried under vacuum. 3.8 g of the crude **5** were obtained as a 1:1 mixture of the *rac* and *meso* forms (78% based on $\text{Me}_2\text{Si}(\text{DPA})(2\text{-Me-4-Ph-Ind})\text{ZrCl}_2 \cdot 2\text{LiCl} \cdot 0.25(\text{Et}_2\text{O})$). The LiCl ether complex was removed by redissolving the complex in dichloromethane, filtering, and evaporating the solvent. A *rac* isomer enriched sample was precipitated from toluene/pentane solutions. ^1H -NMR δ (CD_2Cl_2) *rac* form: 7.1-7.7 (m, 13H), 6.9 (s, 1H), 6.0 (s, 1H), 5.9 (s, 1H), 2.45 (s, 3H), 2.3 (s, 3H), 2.2 (s, 3H), 1.3 (s, 3H),

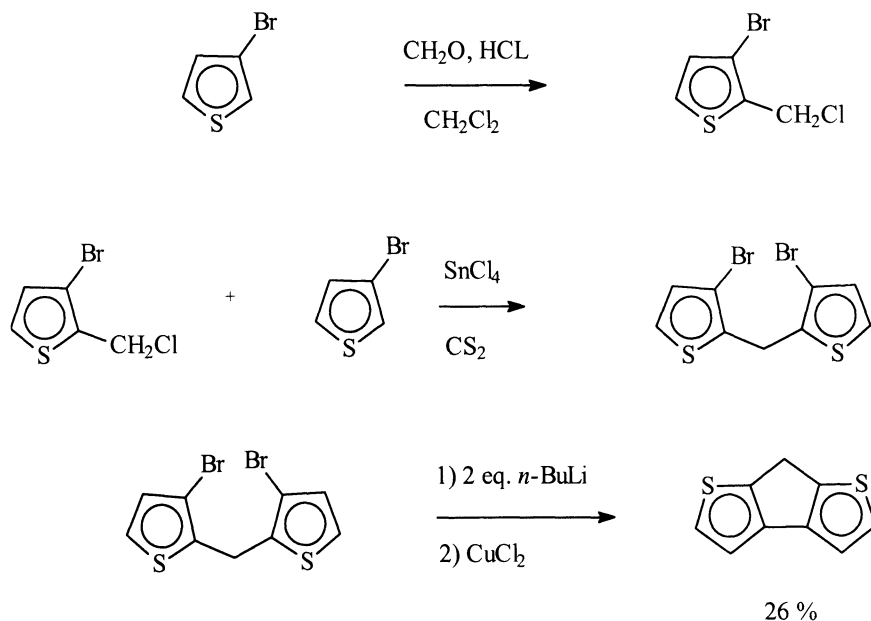
1.2 (s, 3H). $^1\text{H-NMR } \delta$ (CD_2Cl_2) *meso* form: 7.1 7.7 (m, 13H), 6.8 (s, 1H), 6.2 (s, 1H), 6.1 (s, 1H), 2.4 (s, 3H), 2.3 (s, 3H), 2.2 (s, 3H), 1.3 (s, 3H), 1.2 (s, 3H). ms (EI, confirmed with chemical ionization MS), m/z 631 ($\text{C}_{33}\text{H}_{31}\text{NCl}_2\text{SiZr}$).

2.3 Syntheses of L_3 , **1** and **2**.

2.3.1 7*H*-Cyclopenta[1.2-*b*:4.3-*b'*]dithiophene ($\text{L}_3\text{-H}$). 3,3'-Dibromo-2,2'-dithienylmethane^{xiv} (13 mmol, 4.5 g) in THF (30 mL) was added to a solution of *n*-butyllithium (28 mmol, 11.2 mL of a 2.5 M solution in hexanes) cooled to -78°C . The yellow solution was stirred at -50°C for 0.5 h, followed by addition of solid anhydrous CuCl_2 (56 mmol, 7.5 g) over a 5-10 min. period. The reaction mixture was stirred for 2 h, maintaining the temperature between -50 and -30°C , and then slowly warmed to room temperature and stirred for an additional 12 h. The product mixture was poured into 60 mL of aqueous NH_4Cl , shaken, and the two layers were separated. The aqueous layer was extracted with ether and the combined organic fractions were washed with water, dried over MgSO_4 , filtered, and evaporated to a dark oil. The oil was chromatographed on aluminum oxide (neutral, Brockmann I) using 10 vol.% dichloromethane in hexane. $\text{L}_3\text{-H}$ was obtained as white solids by evaporation of the 2nd eluting fraction and washing the residue with methanol (0.6 g, 26% yield). $^1\text{H-NMR } \delta$ (CDCl_3) ppm; 7.31 (d, 2H), 7.13 (d, 2H), 3.80 (s, 2H).

2.3.2 2-cyclopentadienyl-2-(7- $\text{L}_3\text{-H}$)propane. A solution of $\text{L}_3\text{-H}$ (5.62 mmol, 1.0 g) in ether (15 mL) was cooled to -78°C and treated with *n*-butyllithium (5.8 mmol, 2.3 mL of a 2.5 M sol. in hexanes). After stirring at 0°C for 2 h, a solution of 6,6-dimethylfulvene (5.62 mmol, 0.60 g) in ether (5 mL) was added over a 30 minute period and stirred for 1 h. The flask and contents were warmed to room temperature, and stirring continued for 16 h. A saturated aqueous solution of NH_4Cl (15 mL) was added and the organic layer was separated, washed with water (2 x 15 mL), and dried over MgSO_4 . After filtration, the solvents were evaporated from the filtrate and the product was crystallized from a mixture of methanol / acetone to give 0.7 g (44%) of **1** as a white solid. Proton NMR δ (CDCl_3) ppm; (2 isomers) 7.23 (d, 2H), 7.10 (d, 2H) 6.1-6.8 (m, 3H), 3.1 (m, 2H), 1.18, 1.29 (2s, 6H). Mass spectrum: ($\text{C}_{17}\text{H}_{16}\text{S}_2$, 284 MW), $\text{PM} = 284$.

Scheme 4



2.3.3 $\text{Me}_2\text{C}(1\text{-Cp})(7\text{-L}_3)\text{ZrCl}_2$ (1). A solution of 2-cyclopentadienyl-2-(7- L_3 -H)propane (1.9 mmol, 540 mg) in THF (20 mL) was cooled to -78°C and treated with *n*-butyllithium (4.0 mmol, 1.6 mL of a 2.5 M sol. in hexanes). The solution was slowly warmed to 0°C , stirred for 4 h, and solvents were removed *in vacuo*. The reddish-purple residue was cooled to -78°C , partially dissolved in ether (15 mL), and treated with a slurry of ZrCl_4 (1.9 mmol, 0.443 g) in pentane (10 mL). The reaction mixture was slowly warmed to room temperature and stirred overnight. The precipitated crude product was collected on a closed frit, washed with small amounts of ether, and dried *in vacuo* to give 1.0 g of an orange powder. An analytical pure sample of **2** was obtained by extraction with CH_2Cl_2 . $^1\text{H-NMR}$ δ (CD_2Cl_2): 7.42 (d, $J=5.5$, 2H), 7.21 (d, $J=5.5$, 2H), 6.44 (t, $J=5.4$, 2H), 5.84 (t, $J=5.4$, 2H), 2.05 (s, 6H).

2.3.4 2-(3-*t*-Bu-1-cyclopentadiene)-2-(7- L_3 -H)propane. The ligand $\text{L}_3\text{-H}$ (4.9 mmol, 0.87 g) was dissolved in dry ether (20 mL), cooled to -78°C , and treated with 1 eq. of butyllithium (1.9 mL of a 2.5 M sol. in hexanes). The reaction mixture was warmed to 0°C and stirred for 4 h. A solution of 3-*t*-butyl-6,6-dimethylfulvene (4.9 mmol, 0.79 g) in 10 mL of ether was added dropwise, stirred for 2 h at 0°C , and then at room temperature for 16 h. The reaction was quenched by slowly adding a saturated aqueous solution of NH_4Cl (10 mL). The aqueous layer was separated, washed with ether, and discarded. The organic fractions were combined, dried over MgSO_4 , and evaporated to an oil. The oil was redissolved in a mixture of methanol / acetone and the product was crystallized by cooling on dry ice (yield - 800 mg, 48 %).

2.3.5 $\text{Me}_2\text{C}(3\text{-}t\text{-Bu-1-Cp})(7\text{-}L_3)\text{ZrCl}_2$ (2). 2-(3-*t*-Bu-1-cyclopentadiene)-2-(7- L_3 -H)propane (800 mg) were dissolved in 20 mL of THF, cooled to -78°C , and treated with butyllithium (4.8 mmol, 1.92 mL of a 2.5M sol. in hexanes). The solution turned dark brown and was stirred an additional 10 minutes at -78°C before warming to room temperature. After stirring for 3 h, the THF was removed *in vacuo*. The remaining solids were washed with pentane and dried under vacuum. Zirconium tetrachloride (2.5 mmol, 0.56 g) was added to the flask and the mixture of solids were suspended in 50 mL pentane and stirred overnight. Stirring was stopped, pentane was decanted with a cannula, and the solids dried *in vacuo* yielding 1.21 g. of a light brown powder. The product (1.2 g) was purified by stirring the material in 30 mL of dichloromethane, filtering off the insolubles, and evaporating the filtrate to a dry powder. In this fashion, 150 mg of complex **1** were isolated. $^1\text{H-NMR}$ δ (CD_2Cl_2): 7.4 (d, 2H), 7.22 (m, 2H), 6.3 (t, 1H), 5.85 (t, 1H), 5.65 (t, 1H), 2.0 (s, 6H), 1.2 (s, 9H).

2.4 Propylene Polymerizations.

Toluene solutions of methylalumoxane (10 wt% MAO) purchased from Witco Corp. were used in all polymerizations. An MAO/metallocene mixture (Al/Zr molar ratio of 14300) was added to a 4 or 5 liter reactor containing liquid propylene, MAO (approx. 11 mmol in terms of Al), and hydrogen (optionally); the reactor being at 30°C . After 2-3 minutes the temperature was raised to the run temperature (50 or 70°C) and maintained for one hour. Polymerization was stopped by means of methanol (or CO) injection. Polymerization in a 1 L Autoclave followed a similar method using 400 g of propylene with MAO approx. 8 mmol Al).

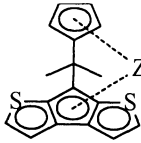
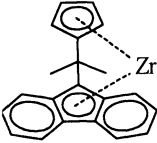
3. Polymerization Results

3.1 **1** and $\text{Me}_2\text{C}[1\text{-Cp-9-Flu}]\text{ZrCl}_2$.

The results of 50°C bulk polymerization tests of the C_s symmetric metallocenes **1** and $\text{Me}_2\text{C}[1\text{-Cp-9-Flu}]\text{ZrCl}_2$ are compiled in Table 1. Both catalysts produced S-PP with $M_v \approx 100,000$ and were intrinsically equally as site-stereospecific with the same level of site-control or mm triad stereochemical imperfections in the polymers.

On the other hand the lower m.pt. of the S-PP from **1** resulted from a higher level of skipped-out insertions or meso dyads; consistent with a higher $R_{\text{back-skip}} / R_{\text{insertion}}$ ratio for the 5/5/5 ring system. The tabulated difference in catalyst activities is attributed in part to an inadvertent impurity in the polymerization test with **1** because 5/5 and 5/6 analogs are typically equally active (*vide infra*).

Table 1. Bulk polymerization with **1** and Me₂C[1-Cp-9-Flu]ZrCl₂ at 50 °C. ^{a)}

| Metallocene, (mg) | Activity (kg/mmol.h) | 10 ⁻³ .M _v (g/mol) | m.pt., (°C) | rrrr, % | rmmr, % | rrmr, % |
|---|-------------------------|---|----------------|---------|---------|---------|
|  ZrCl ₂ (1) | 14 | 98 | 110 | 74 | 1.8 | 8.1 |
|  ZrCl ₂ (0.3) | 90 | 133 | 140 | 82 | 1.7 | 2.8 |

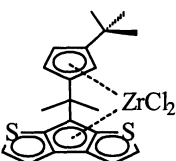
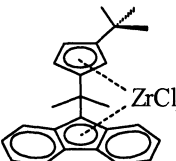
^{a)} Conditions: 1 L autoclave, 1 h, 8 mmol Al, 400 g propylene.

3.2 2 and Me₂C[3-*t*-Bu-1-Cp-9-Flu]ZrCl₂.

Bulk polymerization test results with C₁ symmetric **2** and the fluorenyl analog Me₂C[3-*t*-Bu-1-Cp-9-Flu]ZrCl₂ at 50 °C are listed in Table 2. Both metallocenes are isospecific with a site-control mechanism, make I-PP with the same catalyst activity, and once more produce polymers with M_v ≈ 100,000. The higher site-isospecificity for the more open structure **2** as evidenced by the higher I-PP m.pt., the higher mmmm pentad, and the lower mrrm pentad was somewhat surprising in view of past observations of isospecific catalyst structures *versus* their relative stereospecificities.

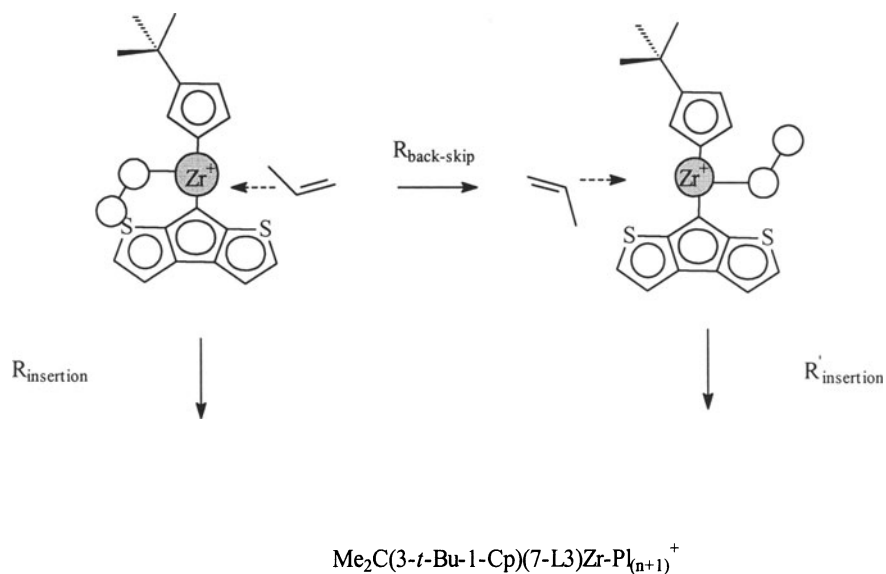
A kinetic ambiguity in evaluating C₁ symmetric catalyst stereospecificities was recognized years ago (Scheme 5).^{viii} The catalysts are isospecific with the preferred conformation of the chain-end acting as a molecular lever by directing the same monomer π-face coordination irregardless as to which side of the catalyst it is attached to.

Table 2. Bulk polymerization with **2** and $\text{Me}_2\text{C}[1\text{-Cp-9-Flu}]\text{ZrCl}_2$ at 50 °C. ^{a)}

| Metallocene | Activity (kg/mmol.h) | $10^{-3} \cdot \text{Mv}$ (g/mol) | m.pt., (°C) | mmmm, mrrm, % | |
|---|-------------------------|--------------------------------------|----------------|------------------|-----|
|  | 13 | 91 | 130 | 84 | 3.1 |
|  | 13 | 91 | 125 | 80 | 3.7 |

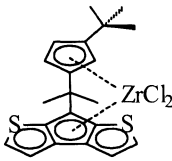
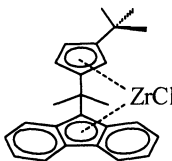
^{a)}Conditions: 1 mg metallocene, 1 L autoclave, 1 h, 8 mmol Al, 400 g propylene

Scheme 5



Molecular mechanics calculations teach us that propylene insertions are more stereospecific with the monomer coordinated at the more crowded sides of the catalysts than with it at the more open sides of the catalysts due to a steric contact between the propylene methyl group and the catalyst *t*-Bu group when the “wrong” π -face is coordinated in S_{re} and R_{si} molecular assemblies.^{xv} Furthermore, the crowded chain-end / *t*-Bu arrangement with the chain-end at the crowded side provides a driving force for the chain to back-skip to the more open side.^{xv(e)} Lower propylene concentrations slow insertion rates and thus the chain back-skips more frequently to the more stereospecific, less congested construction between insertions.

Table 3. Toluene slurry polymerization results with **2** and $\text{Me}_2\text{C}[3\text{-}t\text{-Bu-1-Cp-9-Flu]ZrCl_2$ at 50 °C.^{a)}

| Metallocene (mg) | $[\text{C}_3\text{H}_6]$, M | Activity, (kg/mmol.h) | m.pt., (°C) | mmmm, mrrm, % | mmmm, mrrm, % | |
|--|---------------------------------|--------------------------|----------------|------------------|------------------|-----|
|  | (3.6) | 0.9 | 9 | 130 | 84 | 2.9 |
| | (2.0) | 1.7 | 14 | 129 | 84 | 2.9 |
| | (1.0) | Bulk | 25 | 130 | 83 | 3.2 |
|  | (3.5) | 0.9 | 1 | 134 | 87 | 2.5 |
| | (3.5) | 1.7 | 2.2 | 129 | 85 | 2.8 |
| | (1.0) | Bulk | 25 | 125 | 80 | 3.7 |

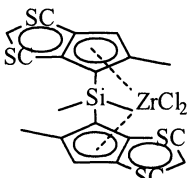
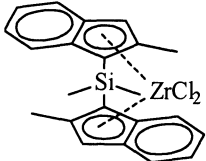
^{a)}Conditions: 250 mL glass reactor, 3 mL MAO, 100 mL toluene, 1 h.

2 and $\text{Me}_2\text{C}[3\text{-}t\text{-Bu-1-Cp-9-Flu]ZrCl_2$ were polymerization tested in toluene slurries as a function of propylene concentration to address the ambiguity (Table 3). **2** was about 8 times more active than $\text{Me}_2\text{C}[3\text{-}t\text{-Bu-1-Cp-9-Flu]ZrCl_2$ in these tests. **2** remained unchanged in stereospecificity as a function of propylene whereas the stereospecificity of $\text{Me}_2\text{C}[3\text{-}t\text{-Bu-1-Cp-9-Flu]ZrPI}^+$ increased at lower propylene; to the point where the latter was the most stereospecific at 1 M C_3H_6 . The data is in accord with all the insertions with **2**, even in bulk, occurring with the chain at the more open side of the catalyst due to a high $R_{\text{back-skip}} / R_{\text{insertion}}$ ratio with the heterocene and with $\text{Me}_2\text{C}[3\text{-}t\text{-Bu-1-Cp-9-Flu]ZrPI}^+$ being 0.4 % more stereospecific than $\text{Me}_2\text{C}[3\text{-}t\text{-Bu-1-Cp-6-L}_3]ZrPI}^+$ with the monomer located at the more crowded sides of the catalysts.

3.3 **3** and $\text{Me}_2\text{Si}[2\text{-Me-1-Ind}]_2\text{ZrCl}_2$.

Bulk polymerization test results with **3** and *rac*- $\text{Me}_2\text{Si}[2\text{-Me-1-Ind}]_2\text{ZrCl}_2$ are summarized in Table 4.

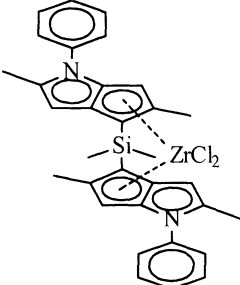
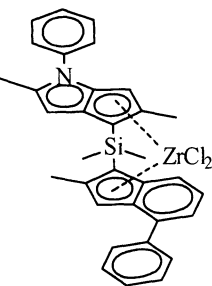
Table 4. Bulk polymerization with **3** and *rac*- $\text{Me}_2\text{Si}[2\text{-Me-1-Ind}]_2\text{ZrCl}_2$.^{a)}

| Metallocene | Pol. Temp., (°C) | Activity, (kg/mmol.h) | $10^{-3} \cdot M_w$, (g/mol) | m.pt., (°C) | mmmm, % |
|---|---------------------|--------------------------|----------------------------------|----------------|------------|
|  | 50 | 55 | 161 | 127 | 78 |
| | 70 | 97 | 113 | 125 | 79 |
|  | 50 | 40 | 340 | 148 | 97 |
| | 70 | 99 | 195 | 145 | - |

a) Conditions: 4 L autoclave, 1 mg cat., 10 mL 10 % MAO in toluene, 1 hour.

The *meso*- and *rac*-**3** stereoisomers were equally active and produced a 50/50 mixture of I-PP and A-PP with the same M_w . Thus all 6 isomers of **3** produced a mixture of two polymers with a $MWD \approx 2$; close to the most probable value for a single-site catalyst. The mmmm pentad for *rac*-**3** was calculated from the ^{13}C NMR spectrum of as-polymerized samples using the 2-site enantiomorph-atactic model free of regio-irregularities.^{vii(b)} **3** and *rac*- $\text{Me}_2\text{C}[2\text{-Me-1-Ind}]_2\text{ZrCl}_2$ were equally as active as each other at 50 and 70 °C and twice active as the C_1 symmetric catalysts in Table 3. The more open heterocene structure made I-PP with $\frac{1}{2}$ of the M_w and with a melting point 20 °C lower than *rac*- $\text{Me}_2\text{C}[2\text{-Me-1-Ind}]_2\text{ZrCl}_2$. The 125 °C m.pt. with the heterocene **3** is interesting because high MW I-PP with a m.pt. less than 145 °C cannot be obtained with indenyl analogs.^{xvi}

3.4 4, 5 and *rac*-Me₂Si[2-Me-4-Ph-1-Ind]₂ZrCl₂Table 5. Bulk polymerization with 4, 5 and *rac*-Me₂Si[2-Me-4-Ph-1-Ind]₂ZrCl₂.^{a)}

| Metallocene | Pol. Temp., (°C) | Activity, (kg/mmol.h) | 10 ⁻³ ·M _w , (g/mol) | m.pt., (°C) | mmmm, % |
|--|---------------------|--------------------------|---|----------------|------------|
|  | 70 | 560 | 198 | 155 | 96 |
|  | 50 | 550 | 997 | 161 | 95 |
| | 50 ^{b)} | 1,420 | 170 | 161 | 97 |
| | 70 | 865 | 709 | 156 | 95 |
| <i>rac</i> -Me ₂ Si(2-Me-4-Ph-1-Ind) ₂ ZrCl ₂ | 70 | 755 | 1,287 | 156 | 95 |

(a) 4 L autoclave, 0.16 mg cat., 4.5 mmol MAO, 2.5 mmol TIBAL, 1 hour.

(b) H₂ added.

The *meso*-4 isomer is polymerization silent whereas the chiral *meso*-5 appears to be activated at 70 °C. The activity of *rac*-4 is five times higher than for *rac*-3 which is comparable to the activity change on going from *rac*-Me₂Si(2-Me-1-Ind)₂ZrCl₂ to *rac*-Me₂Si(2-Me-4-Ph-1-Ind)₂ZrCl₂. The I-PP M_w with 4 is only twice that of 3; as compared to the six fold increase on going from *rac*-Me₂Si(2-Me-1-Ind)₂ZrCl₂ to *rac*-Me₂Si(2-Me-4-Ph-1-Ind)₂ZrCl₂.

The ligand effects on M_w are additive; as seen by the threefold increase on comparing 4 to the mixed ligand 5. A noteworthy similarity between the C₂ symmetric heterocenes and indenyl systems is evident from M_w = 997,000 obtained at 50 °C with 5 being reduced fivefold with H₂ while tripling the already

ultra-high catalytic activity, halving $P_{2,1}$ from 0.2 to 0.1 mole-%, and giving $mmmm = 97\%$.

The stereospecificities of **4** and **5** are comparable with *rac*-Me₂Si(2-Me-4-Ph-1-Ind)₂ZrCl₂. This observation is not inconsistent with the earlier noted difference between **3** and *rac*-Me₂Si(2-Me-1-Ind)₂ZrCl₂ since the methyls α to the pendant N-phenyls make **4** and **5** inexact structural analogs of *rac*-Me₂Si(2-Me-4-Ph-1-Ind)₂ZrCl₂.

4. Conclusions

The heterocene catalysts' performances in general surely rival those of earlier fluorenyl and indenyl based systems and the observed trends are readily understandable with models based on chain migratory insertion and back-skip reactions. It is clear from the forgoing results and discussion that there is no polymer accessible with conventional metallocenes that cannot be made equally as well with heterocenes.

Heterocenes were selected in this study for polypropylene catalysis on the premise that the novel 5/5 ring-fused structures and the range of group 15 and 16 elements would provide interesting new tools for controlling polymer stereochemistry and molecular weights. Our preliminary investigations indicate that indeed they do and the heterocene catalyst symmetries have also been found to control the polymer tacticities. The entire field of single site catalysis has clearly been expanded enormously.

5. Acknowledgements

We thank the following for assistance in this work: F. Testoni, I. Camurati, F. Piemontesi, and L. Resconi at Montell Polyolefins in Ferrara, Italy; J. van Baar and P. Schut at Shell International Chemicals B. V. Amsterdam, and M. Beverin at Montell Polyolefins USA.

6. References

- ⁱ Review: Brintzinger, H. H., Fischer, D.; Mulhaupt, R., Rieger, B., Waymouth, R. M. (1995) *Angew. Chem. Int. Ed. Engl.* 34: 1143.
- ⁱⁱ Ewen, J. A., Jones, R. L., Elder, M. J., Rheingold, A. L., and Liable-Sands, L.M. (1998) *J. Amer. Chem. Soc.* 120: 10786.
- ⁱⁱⁱ Ewen, J. A. (1997) *Scientific American*, 276, (5): 6355.
- ^{iv} Ewen, J. A., Haspeslagh, L., Elder, M. J., Atwood, J. L., Zhang, H., and Cheng, H. N. (1988) in *Transition Metals and Organometallics as Catalysts for Olefin Polymerization*, W. Kaminsky and H. Sinn, Eds.; Springer-Verlag: New York, pp. 281-289.
- ^v (a) Miya, S., Yoshimura, T., Mise, T., Yamazaki, H. (1988). *Polym. Prepr. Jpn.* 37: 285
(b) Miya, S., Mise, T., Yamazaki, H. (1989) *Chem. Lett.*, 1953 (c) Miya, S., Mise, T., Yamazaki, H., (1990) *Stud. Surf. Sci. Catal.* 56: 531.
- ^{vi} Spaleck, W., Küber, F., Winter, A., Rohrmann, J., Bachmann, B., Antberg, M., Dolle, V., Paulus, E. F. (1994) *Organometallics*, 13: 954.
- ^{vii} (a) Ewen, J. A., Jones, R. L., Razavi, A., Ferrara, J. D. (1988) *J. Amer. Chem. Soc.* 110: 6255 (b) Ewen, J. A., Elder, M. J., Jones, R. L., Curtis, S., and Cheng, H. P. (1990) *Stud. Surf. Sci.* 56: 271.
- ^{viii} Ewen, J. A., Elder, M. J., (1995) in *Ziegler Catalysts*, (G. Fink, R. Mulhaupt, H. H. Brintzinger, Eds.) Springer-Verlag, Berlin, Heidelberg, New York, London, Paris, Tokyo, Hong Kong, Barcelona, Budapest, p. 99.
- ^{ix} Spaleck, W., Antberg, M., Rohrman, J., Winter, A., Bachmann, B., Kiprof, P., Behm, J., Herrmann, W. A. (1992) *Angew. Chem. Int. Ed. Engl.* 31: 1347
- ^x Ewen, J. A., Elder, M. J., Jones, R. L., Haspeslagh, L. Atwood, J. L., Bott, S. G., Robinson, K. (1991) *Makromol. Chem., Macromol. Symp.* 48/49: 253.
- ^{xi} O. Meth-Cohn, S. Gronowitz, (1966) *Acta Chemica Scandinavica*, 20: 1577.
- ^{xii} Volz, H. and Kowarsch, H. (1976) *Tet. Lett.* 48: 4375.
- ^{xiii} (a) Volz, H., Zirngib, U., Meßner, B. (1970) *Tetrahedron Lett.* 4: 3593. (b) Voltz, H., Meßner, B. (1969) *Tetrahedron Lett.* 47: 4111. (c) Hidetsra, C., Shinsuke, M. (1996) *Heterocycles*, 43:127. (d) Shapiro, R. H.; Heath, M. J. (1967) *J. Am. Chem. Soc.* 89: 5374.
- ^{xiv} Kraak, A., Wiersema, A. K., Jordans, P., Wynberg, H. (1968) *Tetrahedron*, 24: 3381.
- ^{xv} (a) van der Leek, Y., Angermund, K., Reffke, M., Kleinschmidt, R., Goretzki, R., Fink, G. (1997) *Chem. Eur. J.* 3: 585. (b) Cavallo, L., Guerra, G., Vacatello, M., Corradini, P. (1991) *Macromolecules*, 24: 1784. (c) Corradini, P., Busico, V., Cipullo, R. (1992) *Makromol. Chem. Rapid Commun.* 13: 21. (d) Guerra, G., Corradini, P., Cavallo, L., Vacatello, M. (1995) *Makromol. Symp.*, 307. (e) Cavallo, L., Guerra, G. (1996) *Macromolecules*, 29: 2729.
- ^{xvi} Spaleck, W., Antberg, M., Rohrmann, J., Winter, A., Bachmann, B., Kiprof, P., Behm, J., Herrmann, A. (1995) in: Fink, G.; Mulhaupt, R., Brintzinger, H. H. *Ziegler Catalysts*; Springer-Verlag, Berlin: p. 84.

New C₁-Symmetric Metallocenes for the Polymerization of Olefins

Walter Kaminsky, Ralf Werner

Institut für Technische und Makromolekulare Chemie
Universität Hamburg, Bundesstr. 45, D-20146 Hamburg, Germany
kaminsky@chemie.uni-hamburg.de

Abstract. For the polymerization of propene in solution three new C₁-symmetric metallocenes, (I) (Me₂C(PhCp)(Flu)]ZrCl₂, (II) [Me₂C(cHCp)(Flu)]ZrCl₂, and (III) [PhMe₃PenFlu)]ZrCl₂, were compared. The zirconocene (III) is more stereorigid than (I) and (II) and, therefore, has special properties. At a polymerization temperature of 30 °C, (I) in combination with MAO exhibits the highest activity of 7500 kg PP/(mol Zr h*c_p), which is about 5 times higher than the unsubstituted [Me₂C(Cp)(Flu)]ZrCl₂ catalyst. At 60 °C however, compound (III) is much more active than the others due to the higher thermal stability. A strong dependence of the activity on the propene concentration is observed with all catalysts. The high molecular weight of the polypropene produced by (III) is of particular interest; it is two to four times higher than that of polymers synthesized with the other C₁-symmetric zirconocenes. All three catalysts produce polymers with a hemiisotactic microstructure. (III) affords a polymer with more isotactic blocks while polymer produced by (I) has more syndiotactic blocks.

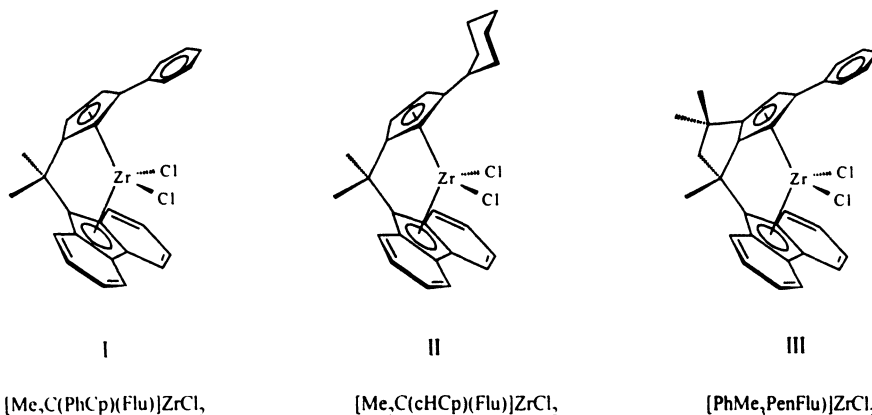
1. Introduction

C_s or C₁ symmetric zirconocenes with an isopropylidene bridge and substituted cyclopentadienyl and fluorenyl ligands are of great interest as catalysts for the polymerization of propene, which leads to syndiotactic and hemiisotactic polymers [1-4]. They are stable and can be synthesized without achiral side products. For an industrial use some disadvantages have to be solved. The polymers often show a low molecular mass, and the catalysts are not very stable at higher temperatures and deactivate fast. In many cases these catalysts are not active enough and give only low stereoselectivities.

Therefore there is an interest to increase the activity and to make the metallocenes more stable for higher temperatures [5]. It is known from the bisindenylzirconocenes that substitution by phenyl groups increases the activity [6]. A stronger bridge should increase the thermal stability.

2. Results and Discussion, Synthesis

Three C_1 -symmetric metallocenes were synthesized with a phenyl or cyclohexyl substitution at the cyclopentadienyl ligand.



For the synthesis of the phenyl substitution, phenyl cyclopentadiene [7] was produced first. In a reaction vessel 3 cyclopentene-1-on [8] in diethylether was reacted with phenyllithium. The mixture was quenched after 2 hours by a cold solution of NH_3 and NH_4Cl . The product was extracted and dried which yielded 86 % of a yellow solid compound.

The next step was the synthesis of 2-phenyl-6,6-dimethyl fulvene, similar to the reactions published by Ewen and Razavi [1].

Butyllithium in hexane was added to a mixture of phenylcyclopentadiene in toluene at $-50\text{ }^\circ\text{C}$. After reaching room temperature, a white product separated which was treated with acetone and washed. The yield after crystallization was 43 %. A similar reaction was used to synthesize 2-cyclohexyl-6,6-dimethyl fulvene from cyclohexylcyclopentadiene.

To obtain 1,3,3-trimethyl-5-phenyl-2,3-dihydropentalen, a mixture of acetone and pyrrolidine in methanol was stirred at room temperature for one hour at least; then phenylcyclopentadiene was added and allowed to react for 40 hours, and the product was dried in vacuum (see also Erker, Ref. 9).

The combination of the fulvene together with the fluorene was carried out as described in the literature. For example, the 1-fluorenyl-1,3,3-trimethyl-5-phenyl-1,2,3,4-tetrahydropentalen was produced by reaction of the fluorene with

butyllithium in THF and at $-50\text{ }^{\circ}\text{C}$. Then the 1,3,3-trimethyl-5-phenyl-2,3-dihydropentalene in THF was added and reacted over night. After extraction with ether and recrystallization, the solid product was received in 20 % yield. In the last step the obtained ligand was treated with butyllithium and reacted with zirconium tetrachloride in hexane after which a crystalline red compound precipitated in a yield of 31 %.

Fig. 1 shows the x-ray structure of the [1-fluorenyl-1,3,3-trimethyl-5-phenyl-tetrahydropenta-lenyl]zirconium dichloride. It can be seen that the centroids form

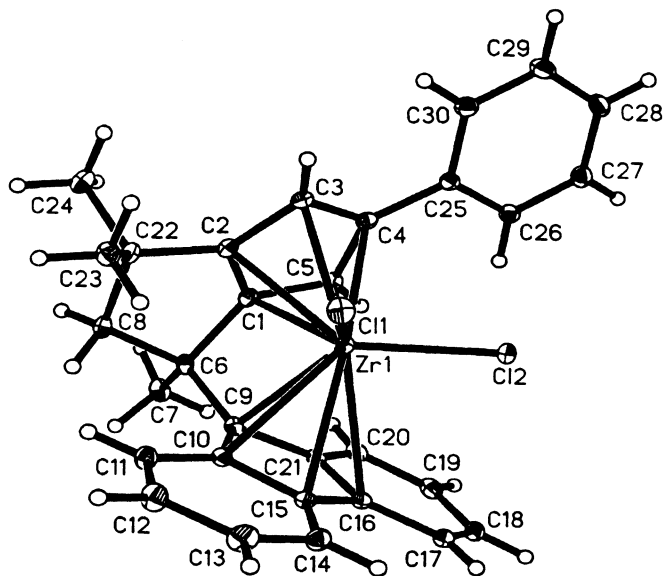


Fig. 1. X-ray structure of $[\text{PhMe}_3\text{PenFlu}]\text{ZrCl}_2$

a similar open angle (118 °) to the other C_1 - and C_s -symmetric zirconocenes.

3. Polymerization of Propene

For comparison of activity and stereoselectivity, the polymerization with these catalysts has to be carried out under the same conditions [10]. Table 1 shows the conditions; the runs have been carried out. In every case, methylaluminoxane (MAO) was used as cocatalyst. The experiments were carried out in a 1-liter-autoclave. The catalyst concentration was between $2 \cdot 10^{-5}$ to $2 \cdot 10^{-6}$ mol/l.

Table 1. Polymerization under Standard Conditions

| Experimental Parameters | |
|-------------------------|-------------|
| Volume | 200 ml |
| Solvent | toluene |
| Monomer | propene |
| Monomer concentration | 1.29 mol/l |
| Temperature | 30 °C |
| Cocatalyst | MAO |
| Al:Zr-ratio | 4000 - 5500 |

Table 2 summarizes the activities of the three zirconocenes in dependence on the temperature. The phenyl substituted zirconocene I gives the highest activities at low temperatures. This activity is up to nine times higher than that of the unsubstituted compound. Whereas metallocenes I and II show a fast thermal deactivation at higher polymerization temperatures, an increase in activity was found for complex III by raising the temperature; this may be an effect of the very rigid structure of this compound. The cyclohexyl substitution gives a lower activity than the phenyl substitution at all temperatures.

Table 2. Polymerization Activity as a Function of the Temperature

| T [°C] | [Me ₂ C(PhCp)(Fl)]ZrCl ₂ [kg PP/(molZr h)] | [Me ₂ C(cHCp)(Flu)]ZrCl ₂ [kg PP/(molZr h)] | [PhMe ₃ PenFlu]ZrCl ₂ [kg PP/(molZr h)] |
|--------|---|--|--|
| 15 | 6 630 | 1 880 | 100 |
| 30 | 8 400 | 3 600 | 890 |
| 30 | 11 400 | 4 060 | 1 200 |
| 45 | 4 950 | 4 460 | 1 700 |
| 60 | 1 300 | 1 100 | 7 600 |

The Arrhenius plot (Fig. 2) confirms the thermal instability of the complexes I and II. Only for zirconocene III can an activation energy of 70 kJ/mol be calculated.

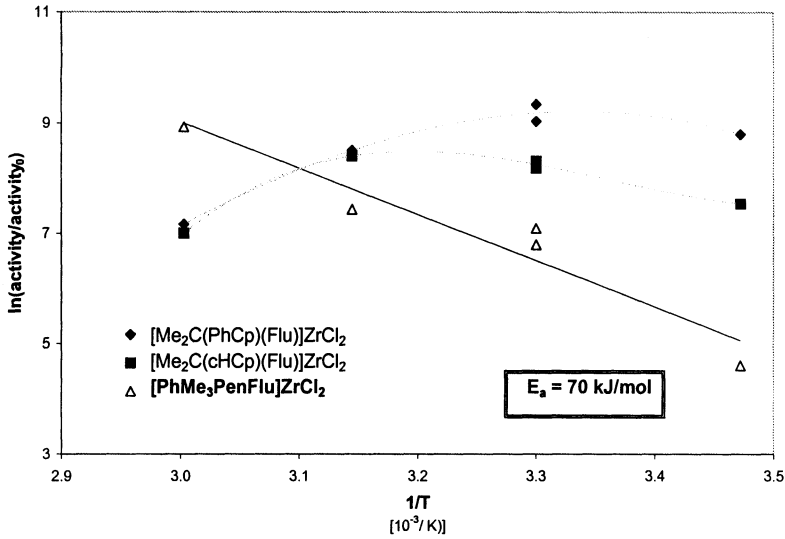


Fig. 2. Arrhenius plot of 3 different catalysts

There is a great difference in the dependence of the activities on the proper concentration. Fig. 3 compares the polymerization activities of the metallocenes as a function of the monomer concentration.

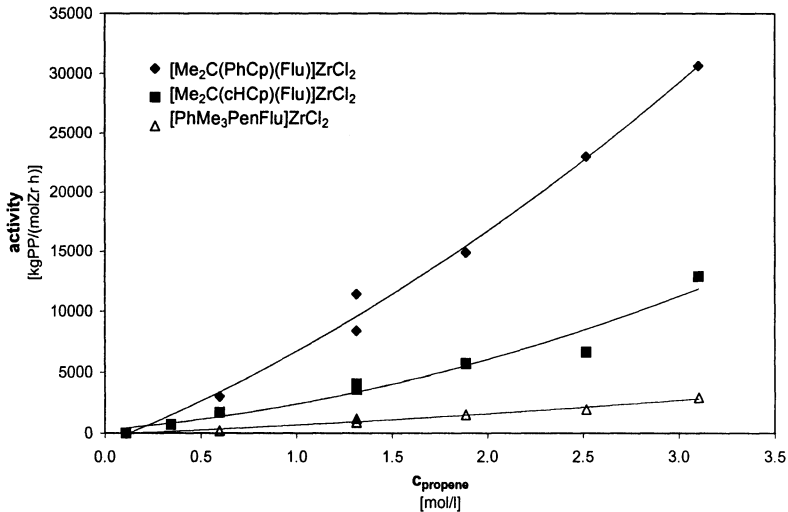


Fig. 3. Activity as a function of the monomer concentration

For all metallocenes an increase of the activity at higher monomer concentrations is observed. Catalyst I shows the strongest increase, compound III the lowest. The reaction order for propene is in all cases 1.4 to 1.5.

While the polymerization activity is very important for the technical process, the molecular mass and the microstructures are relevant for the properties of the polymer.

Fig. 4 shows the molecular masses of the polypropylenes obtained. Catalyst III gives a polymer with a very high molecular mass of up to 480 000. This is

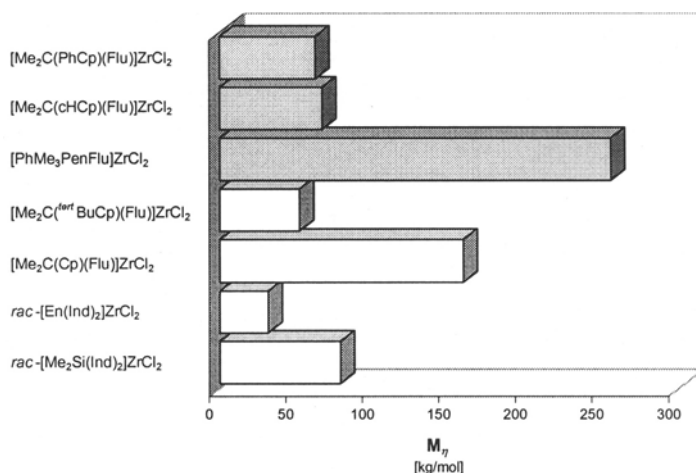


Fig. 4. Comparison of viscosimetric average molecular weight of polypropene polymerized under standardized conditions

16 times higher than that of the isotactically working system $\text{rac-}[\text{En}(\text{Ind})_2]\text{ZrCl}_2$ [10]. Compared to the other complexes, a factor of three is given. There could be a dependence of the high molecular mass of the polypropylene produced and the unusual geometry of the pentalene structure of zirconocene III. The stereorigid structure poses the polymer chain in such a position that β -agostic interaction with the metal center is hindered. This decreases chain termination and leads to a higher molecular mass.

The molecular masses show a strong dependence on the polymerization temperature (Fig. 5). Between 15 and 60 °C the molecular mass decreases by

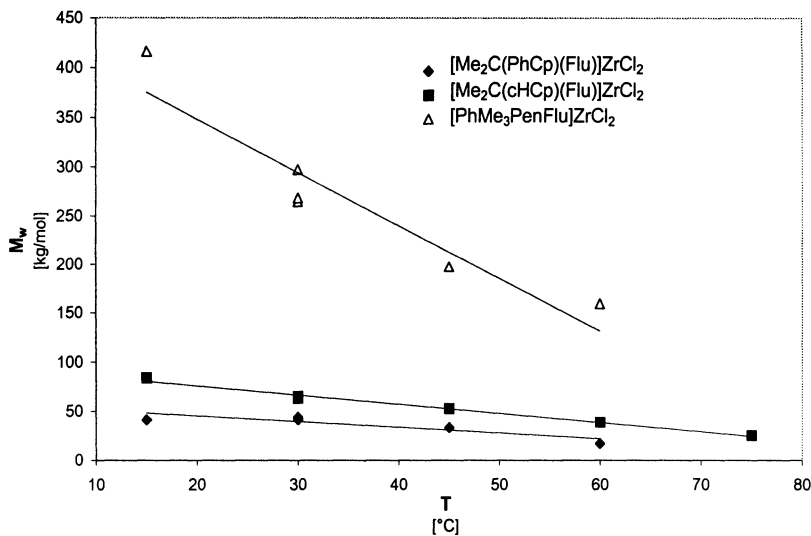


Fig. 5. Molecular weight as a function of the polymerization temperature

a factor of 3. On the other hand, the molecular mass can be decreased with the propene concentration (Fig. 6). Especially the more stereorigid complex III gives

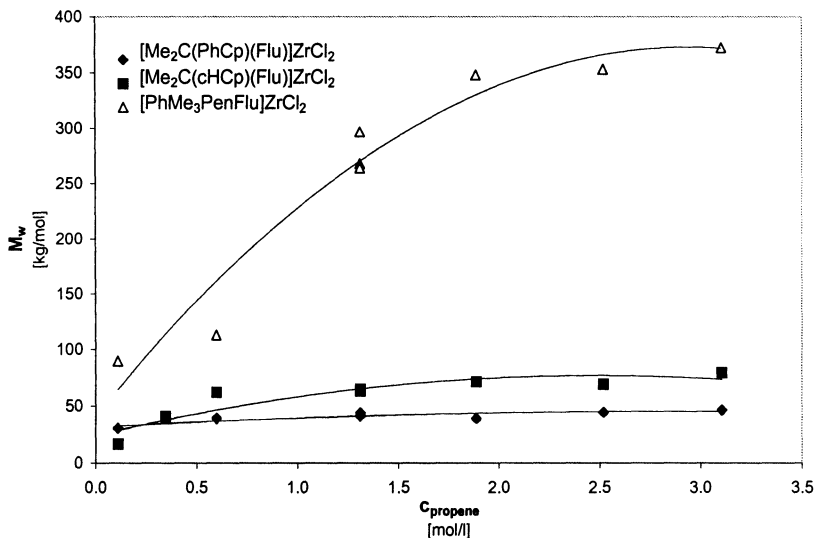


Fig. 6. Molecular weight as a function of the monomer concentration

much higher molecular masses with increasing propene concentration while those of the other catalysts are more independent. After a propene concentration of 3

mol/l, in all cases, the molecular mass becomes independent. While the propagation step is always bimolecular and depends strongly on the monomer concentration, the chain transfer reaction is monomolecular. At a limit propene concentration, there is no increase in the molecular mass.

4. Microstructure of the Polypropylene.

The microstructure of the polypropylene has a significant influence on the polymer properties. There are some mechanistic and calculatory models to interpret the microstructure of the polymer in dependence on the structure of the catalyst [11,12]. Fig. 7 gives an overview on the microstructure of the

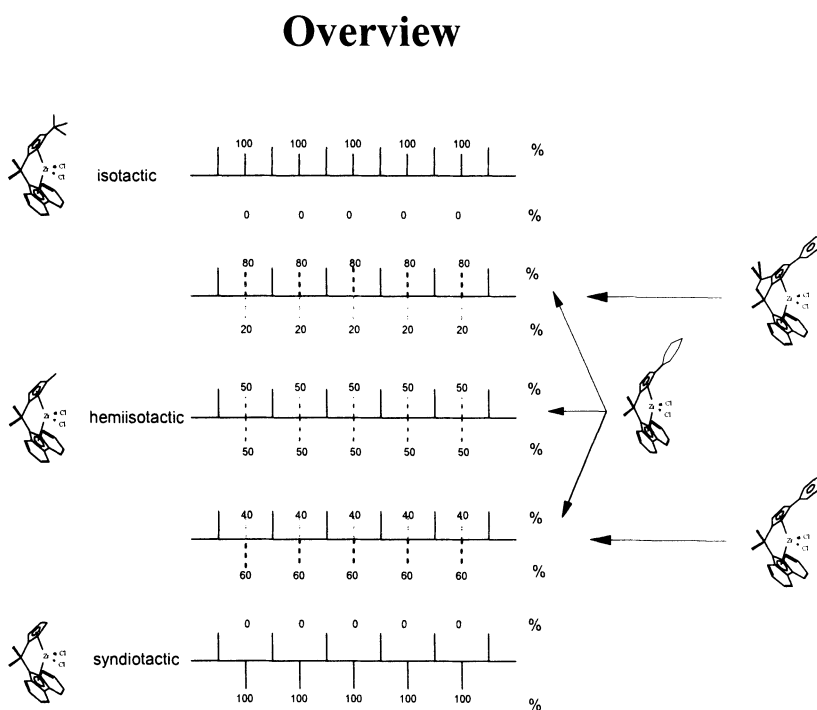


Fig. 7. Microstructure of polypropylene produced with different catalysts

polypropylenes prepared with the three catalysts compared with some other systems. Catalysts I and II produce polypropylenes with high amounts of syndiotactic pentads - I more than II (Table 3). Both metallocenes have two

different half sides which are the background for the rrrr-pentads. On the other side the concentration of mrrr-pentads is low.

A partially isotactic polymer is yielded by zirconocene III (Table 3). The mmmm-pentads reaches values of 58 %, which means that the isotactic sequence length is about 10.

Table 3. Parts of ^{13}C -NMR measured pentades (in %) of polypropylenes synthesized with the catalysts I, II, III at 30 °C

| Catalyst | I | II | III |
|-----------|------|------|------|
| mmmm | 9,6 | 11,8 | 57,5 |
| mmmr | 8,8 | 9,7 | 11,4 |
| rmmr | 8,1 | 5,7 | 1,9 |
| mmrr | 22,7 | 21,2 | 15,7 |
| mrrm+rmrr | 2,3 | 3,8 | 0,4 |
| mrrr | 0 | 0 | 0,3 |
| rrrr | 32,7 | 33,5 | 2,8 |
| rrrm | 11,8 | 11,5 | 3,4 |
| mrrm | 4,2 | 2,9 | 6,6 |

An explanation can be given if the polymer chain is located on the pentalenyl side while the coordination of the propene takes place at the phenyl substituted side of the metallocene. The phenyl group interacts with the monomer and leads to a preferred orientation of the propene. By this an isotactic polymer is formed. No regio errors such as 2.1 or 3.1 insertion can be found.

There is nearly no influence of the temperature or monomer concentration on the microstructure of the polypropylene prepared with catalyst III. In contrast to this the cyclohexyl substituted catalyst II shows a strong dependence of the microstructure with increasing polymerization temperature (Fig. 8).

At low polymerization temperatures, zirconocene II produces a polymer with more syndiotactic structures while at temperatures over 50 °C more isotactic structures are formed. There are different steric arrangements of the hexyl group in

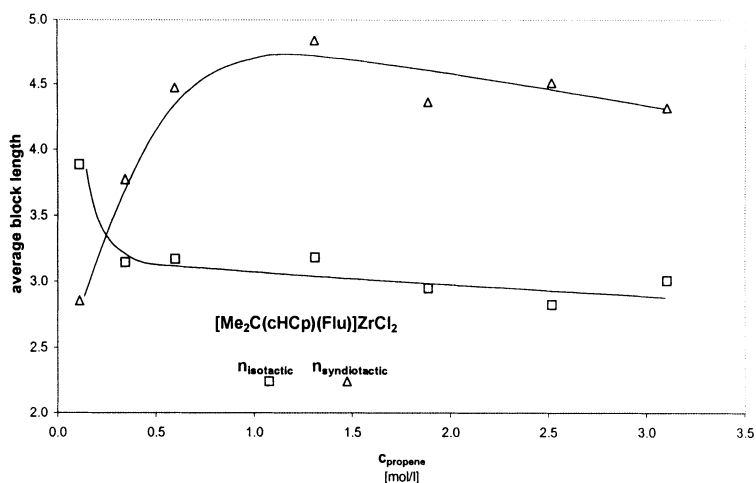


Fig. 8. Monomer concentration dependency of the average block length of the iso- and syndiotactic polypropylene sequences polymerized with $[\text{Me}_2\text{C}(\text{cHCp})(\text{Flu})]\text{ZrCl}_2$

dependence on the temperature so that there is a higher sterical hindrance of the cyclohexyl group that brings the incoming propene into an isotactic position.

5. References

- [1] J.A. Ewen, R.L. Jones, A. Razavi, *J. Am. Chem. Soc.* 110, 6255 (1988)
- [2] J.A. Ewen, M.J. Elder, R.L. Jones, L. Haspeslagh, J.L. Atwood, S.G. Bott, K. Robinson, *Makromol. Chem. Macromol. Symp.* 48/49, 253 (1991)
- [3] W. Spaleck, M. Antberg, V. Dolle, R. Klein, J. Rohrmann, A. Winter, *New J. Chem.* 14, 499 (1990)
- [4] J.A. Ewen, M.J. Elder inventors (Fina Technology) EP 0537130A1, CA 119, 2507262 (1993)
- [5] W. Kaminsky, *Macromol. Chem. Phys.* 197, 3907 (1996)
- [6] W. Spaleck, W.A. Hermann, J. Rohrmann, E. Hertweck, *Angew. Chem. Int. Ed. Engl.* 29, 1511 (1989)
- [7] R. Riemschneider, R. Nehring, *Mh. Chem.* 91, 829 (1960)
- [8] K. Alder, F.H. Flock, *Chem. Ber.* 89, 1732 (1956)
- [9] G. Erker, C. Psiorz, C. Krüger, M. Nolte, *Chem. Ber.* 127, 1551 (1994)
- [10] W. Kaminsky, R. Engehausen, K. Zoumis, W. Spaleck, J. Rohrmann, *Makromol. Chem.* 193, 1643 (1992)
- [11] P. Pino, U.W. Suter, *Polymer* 18, 412 (1977)
- [12] M. Farina, G. di Silvestro, P. Sozzani, *Macromolecules* 15, 1451 (1982)

New Catalyst Concepts for the Polymerization of Ethylene with Metallocenes

A. Akimoto, A. Yano

TOSOH Corporation Yokkaichi Research Laboratory
1-8 Kasumi Yokkaichi Mie 510-8490 Japan
akimoto@tosoh.co.jp

Abstract. Diphenylmethylidene(cyclopentadienyl)(2-dimethylamino-fluorenyl)zirconium dichloride ($\text{Ph}_2\text{C}(\text{Cp})(2\text{-Me}_2\text{NFlu})\text{ZrCl}_2$) catalyst activated with dimethylanilinium tetrakis(pentafluorophenyl)borate ($\text{Me}_2\text{PhNH}\cdot\text{B}(\text{C}_6\text{F}_5)_4$)/triisobutylaluminum ($i\text{-Bu}_3\text{Al}$) or methylaluminoxane (MAO) produced a high molecular weight polyethylene with a high activity at high temperatures. The molecular weight of the polyethylene was significantly decreased with an increase in the concentration of the aluminum compounds, followed by the formation of vinyl end groups. This phenomenon was not observed for the $\text{Ph}_2\text{C}(\text{Cp})(\text{Flu})\text{ZrCl}_2$ based catalysts.

Introduction

Since Ewen et al.[1] first reported the syndiospecific polymerization of propylene with $\text{Me}_2\text{C}(\text{Cp})(\text{Flu})\text{ZrCl}_2/\text{MAO}$, there has been a lot of interest in the syndiospecific polymerization of propylene. The effect of substituent groups of the fluorenyl ligand on the catalyst performance for the propylene polymerization was also studied and it was reported that the kind of the substituent groups and the substituted position significantly influence the stereospecificity and the molecular weight of the polypropylene. However, the introduction of substituent groups containing oxygen or nitrogen atom such as $\text{Me}_2\text{N-}$ or MeO- result in a drastic decrease in the molecular weight of the polypropylene[2].

On the other hand, we have already reported that $\text{Ph}_2\text{C}(\text{Cp})(\text{Flu})\text{ZrCl}_2/\text{Me}_2\text{PhNH}\cdot\text{B}(\text{C}_6\text{F}_5)_4/i\text{-Bu}_3\text{Al}$ produce high molecular weight ethylene/ α -olefin copolymers with a high activity at high temperatures[3]. We have also studied the relationship between ligand structure and catalyst performance for the ethylene polymerization at high temperatures using modified catalyst based on $\text{Ph}_2\text{C}(\text{Cp})(\text{Flu})\text{ZrCl}_2$ and showed that the introduction of methyl or t-butyl substituent groups at 2,7-positions of the fluorenyl ligand gave rise to an increase in the molecular weight of the polyethylene without a loss a activity[3]. This motivated us to study the effects of the introduction of $\text{Me}_2\text{N-}$ or MeO- substituent groups on the catalyst performance for the ethylene polymerization at high temperatures although a decrease in the molecular weights of polypropylene with these catalysts was observed. We report the results of ethylene homo- and

copolymerization of 1-hexene with $\text{Ph}_2\text{C}(\text{Cp})(\text{Flu})\text{ZrCl}_2$ derivatives containing a heteroatom on the fluorenyl ligand under different ethylene pressures at high temperatures. The effect of the Al/Zr ratio on the activity, the molecular weight of the polyethylene and chain transfer reactions is discussed.

Experimental

Materials

$\text{Me}_2\text{PhNH}\cdot\text{B}(\text{C}_6\text{F}_5)_4$, MAO and $i\text{-Bu}_3\text{Al}$ from Tosoh Akzo Co. were used without purification. Toluene, C9-C13 hydrocarbon solvent, ethylene, 1-butene and 1-hexene were commercially obtained and purified according to the usual procedures. $\text{Ph}_2\text{C}(\text{Cp})(\text{Flu})\text{ZrCl}_2$ was prepared according to the literature[4]. $\text{Ph}_2\text{C}(\text{Cp})(2\text{-Me}_2\text{NFlu})\text{ZrCl}_2$ and $\text{Ph}_2\text{C}(\text{Cp})(2\text{-MeOFlu})\text{ZrCl}_2$ were prepared by the modified literature method. Other alkyl amino or methoxy derivatives were prepared with the same method as the preparation of $\text{Ph}_2\text{C}(\text{Cp})(2\text{-Me}_2\text{NFlu})\text{ZrCl}_2$.

Solution polymerization

Polymerizations were carried out in a 1L autoclave equipped with a magnetic stirrer, a thermometer tube and various inlets. The autoclave was flushed several times with nitrogen and filled with 600ml of C9-C13 mixed hydrocarbon solvent and 1-hexene was added. After that, the autoclave was heated to the polymerization temperature. Polymerization was started by adding the catalyst components. Ethylene was continuously supplied to keep a constant pressure during the polymerization. The polymerization was terminated by adding ethanol and the ethylene was released. The obtained polymer was washed with plenty of ethanol and dried at 60°C under reduced pressure to constant weight.

Ethylene/ α -olefin copolymerization procedure in a high pressure process

Copolymerization reactions were carried out in our pilot plant where the operating conditions are very close to those in industry. The polymerization temperature can be changed from 120°C to 280°C. The ethylene pressure range is up to 2000 bar. The polymerization temperature is controlled by the catalyst feed rate. The average residence time is 60 seconds. Polymerization reactions are continuously carried out and unreacted ethylene and α -olefin are recycled. The molten polymer flows out of the separator and can be pelletized.

Characterization of polymers

Differential scanning calorimetry (DSC) measurements were made using a SEIKO DSC-200 at a heating rate of 10°C/min. Molecular weight and molecular weight distribution of the polymers were determined by gel-permeation chromatography (GPC) using *o*-dichlorobenzene as solvent. Numbers of short chain branching was analyzed by IR spectrometry measured with a Perkin Elmer FT-IR 1760X or by $^1\text{H-NMR}$ spectra measured with a JEOL GSX-400 operating at 400MHz. Cross fractionation chromatography (CFC) was carried out using a Mitsubishi petrochemical CFC T-101.

Results and discussion

Ethylene homopolymerization

The results of the ethylene polymerization with $\text{Ph}_2\text{C}(\text{Cp})(2\text{-Me}_2\text{NFlu})\text{ZrCl}_2$ and $\text{Ph}_2\text{C}(\text{Cp})(2\text{-MeOFlu})\text{ZrCl}_2$ catalysts activated with $\text{Me}_2\text{PhNH}\cdot\text{B}(\text{C}_6\text{F}_5)_4/i\text{-Bu}_3\text{Al}$ at 170°C are shown in Tab. 1. Both catalysts produce higher molecular weight polyethylene than the $\text{Ph}_2\text{C}(\text{Cp})(\text{Flu})\text{ZrCl}_2$ based catalyst though a slight loss of activity is observed.

Table 1. The results of ethylene polymerization with $\text{Ph}_2\text{C}(\text{Cp})(2\text{-Me}_2\text{NFlu})\text{ZrCl}_2/\text{Me}_2\text{PhNH}\cdot\text{B}(\text{C}_6\text{F}_5)_4/i\text{-Bu}_3\text{Al}$ catalyst

| Run No | Metalloocene | (μmol) | Activity ($\text{kg}/\text{mmol}\cdot\text{Zr}$) | Mw ($\times 10^{-4}$) | Mw/Mn |
|--------|---|---------------------|---|----------------------------|-------|
| 525 | $\text{Ph}_2\text{C}(\text{Cp})(\text{Flu})\text{ZrCl}_2$ | 0.25 | 134 | 8.3 | 1.9 |
| AF-7 | $\text{Ph}_2\text{C}(\text{Cp})(2\text{-Me}_2\text{NFlu})\text{ZrCl}_2$ | 1.0 | 32 | 12.9 | 2.0 |
| 1340 | $\text{Ph}_2\text{C}(\text{Cp})(2\text{-MeOFlu})\text{ZrCl}_2$ | 0.5 | 40 | 12.0 | 2.0 |

Polymerization conditions: Ethylene pressure: 20bar, Solvent: C9-C13 hydrocarbon, 600ml, Polymerization time: 20minutes, Polymerization temperature: 170°C

Catalyst: Metalloocene/ $\text{Me}_2\text{PhNH}\cdot\text{B}(\text{C}_6\text{F}_5)_4/i\text{-Bu}_3\text{Al}$ =1/1.2/250

We have already reported that the introduction of alkyl substituent groups such as methyl and t-butyl results in a slight increase in the molecular weight of the polyethylene. Compared with these results, the molecular weight enhancement effect of substituent groups having an oxygen or a nitrogen atom was significantly high. It was already reported that the introduction of MeO-substituents at 4,7-positions of the indenyl ligands of $\text{Ind}_2\text{ZrCl}_2$ [5] or $\text{Et}(\text{Ind})_2\text{ZrCl}_2$ [6] results in a significant loss of activity and molecular weight for the ethylene polymerization. Ewen et al. investigated isopropylidene-(Cp)(2-Me₂NFlu)ZrCl₂ and (Cp)(2-MeOFlu)ZrCl₂ as propylene polymerization catalysts, and reported that the molecular weight of the polypropylene prepared with the $\text{Me}_2\text{C}(\text{Cp})(2\text{-Me}_2\text{NFlu})\text{ZrCl}_2/\text{MAO}$ catalyst drastically decreases[2]. Similar results were observed with the $\text{Ph}_2\text{C}(\text{Cp})(2,7\text{-(MeO)}_2\text{Flu})\text{ZrCl}_2/\text{MAO}$ catalyst[7]. Therefore, the enhancement of the molecular weight by the introduction of substituent groups having a hetero atom is unique.

The effect of the Al/Zr ratio on the $\text{Ph}_2\text{C}(\text{Cp})(2\text{-Me}_2\text{NFlu})\text{ZrCl}_2/\text{Me}_2\text{PhNH}\cdot\text{B}(\text{C}_6\text{F}_5)_4/i\text{-Bu}_3\text{Al}$ catalyst on the activity and the molecular weight of the polyethylene obtained is summarised in Tab. 2. The activity slightly decreases and surprisingly the molecular weight of the polyethylene significantly decreases with increasing Al/Zr ratio.

Unsaturated bond structures of the polyethylene obtained with this catalyst and the $\text{Ph}_2\text{C}(\text{Cp})(\text{Flu})\text{ZrCl}_2$ based catalyst for comparison are given in Tab. 3. For the $\text{Ph}_2\text{C}(\text{Cp})(\text{Flu})\text{ZrCl}_2$ based catalyst the molecular weight of the polyethylene was not influenced by the Al/Zr ratio and also the unsaturated end group structures were not changed.

Table 2. The effect of the Al/Zr ratio on the catalyst performance for ethylene polymerization with $\text{Ph}_2\text{C}(\text{Cp})(2\text{-Me}_2\text{NFlu})\text{ZrCl}_2/\text{Me}_2\text{PhNH}\cdot\text{B}(\text{C}_6\text{F}_5)_4/\text{i-Bu}_3\text{Al}$ catalyst

| Run No | Zr | B (μmol) | Al/Zr | Activity ($\text{kg}/\text{mmol}\cdot\text{Zr}$) | Mw ($\times 10^{-4}$) | Mw/Mn |
|--------|-----|--------------------------|-------|---|----------------------------|-------|
| AF-13 | 1.0 | 1.2 | 100 | 31 | 15.4 | 2.1 |
| AF-07 | 1.0 | 1.2 | 250 | 32 | 12.9 | 2.0 |
| AF-12 | 1.0 | 1.2 | 1000 | 20 | 9.0 | 2.6 |
| AF-11 | 1.0 | 1.2 | 4000 | 22 | 3.9 | 3.1 |

Polymerization conditions: Ethylene pressure: 20bar, Solvent: C9-C13 hydrocarbon, 600ml, Polymerization time: 20 minutes, Polymerization temperature: 170°C

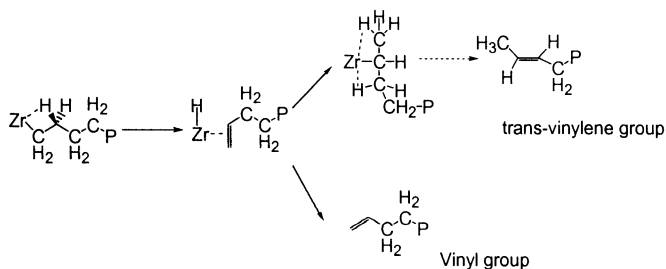
Table 3. The effect of Al/Zr ratio on terminal bond structures of polyethylene obtained with $\text{Ph}_2\text{C}(\text{Cp})(2\text{-Me}_2\text{NFlu})\text{ZrCl}_2$ and $\text{Ph}_2\text{C}(\text{Cp})(\text{Flu})\text{ZrCl}_2$ catalysts

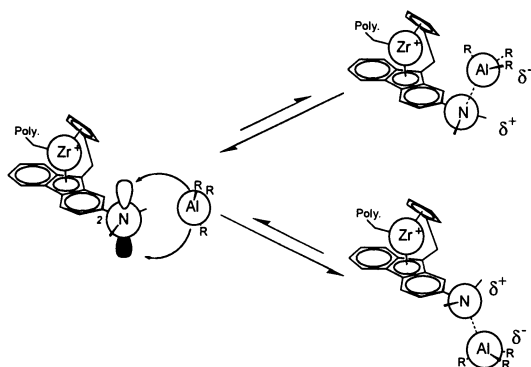
| Run No | Metallocene | Al/Zr | Mn ($\times 10^{-4}$) | Trans-vinylene (No/1000C) | Vinyl (No/1000C) | Vinylidene (No/1000C) |
|--------|-------------|-------|----------------------------|------------------------------|---------------------|--------------------------|
| AF-13 | (a) | 100 | 7.4 | 0.11 | 0.11 | trace |
| AF-07 | (a) | 250 | 6.4 | 0.16 | 0.13 | trace |
| AF-12 | (a) | 1000 | 3.5 | 0.06 | 0.19 | trace |
| AF-11 | (a) | 4000 | 1.3 | 0.07 | 0.58 | trace |
| A-1 | (b) | 250 | 4.2 | 0.11 | 0.21 | trace |
| A-2 | (b) | 1000 | 3.6 | 0.26 | 0.26 | trace |
| A-3 | (b) | 4000 | 3.8 | 0.14 | 0.24 | trace |

(a) $\text{Ph}_2\text{C}(\text{Cp})(2\text{-Me}_2\text{NFlu})\text{ZrCl}_2$, (b) $\text{Ph}_2\text{C}(\text{Cp})(\text{Flu})\text{ZrCl}_2$, Polymerization conditions: see Tab. 2

We have already reported that trans-vinylene end groups[8] are formed by β -H transfer after isomerization and vinyl end groups are formed by β -H transfer from the last inserted ethylene unit as shown in Scheme 1. Furthermore, the formation of trans-vinylene end groups enhanced under high temperature and low ethylene pressure. [9]

Chain transfer after ethylene insertion

**Scheme 1.** The formation mechanism of vinyl and trans-vinylene end groups



Scheme 2. Postulated mechanism for the interaction of the substituent groups with the organoaluminium compound

On the other hand, for the $\text{Ph}_2\text{C}(\text{Cp})(2\text{-Me}_2\text{NFlu})\text{ZrCl}_2$ based catalyst, an increase in the content of vinyl end groups and no change of trans-vinylene content as well as a decrease in the molecular weight of the polyethylene were observed. In this catalyst system, $i\text{-Bu}_3\text{Al}$, which is easily decomposed to isobutene and diisobutylaluminum hydride at high temperatures, was used as alkylation agent. Therefore, chain transfer reactions of this catalyst at high temperatures may be very complicated. Nevertheless, we speculated that chain transfer to Al was the major chain transfer reaction and responsible for the decrease in the molecular weight with increasing Al/Zr ratio. Actually, it is well known that aluminum-alkyl bonds are unstable at high temperatures and alkenes are formed by elimination reactions from aluminium-alkyl bonds.

In these catalysts, bimolecular complexation by coordination of the dimethylamino or methoxy groups on one molecule with the metal center of another may occur. Actually, $\text{Cp}_2\text{ZrMe}(\text{THF})[\text{BPh}_4]$ was prepared by reaction of Cp_2ZrMe_2 with 1 equiv. of $\text{Ag}[\text{BPh}_4]$ in CH_3CN followed by recrystallization from THF[10]. Nevertheless, Alt et al. indicated that $\text{Ph}_2\text{C}(\text{Cp})(2,7\text{-(MeO)}_2\text{Flu})\text{ZrCl}_2$ does not react with 2,7-dimethoxy fluorene, indicating that no dimerization of this complex does occur and is therefore not the reason for the decrease in activity and molecular weight. Therefore, the interaction of the nitrogen atom of substituent groups with organoaluminium compounds like $i\text{-Bu}_3\text{Al}$ may be related to the decrease in molecular weight of the polyethylene.

Increase in the local Lewis acidity at the zirconium atom should increase the tendency to undergo β -elimination and decrease the molecular weight of the produced polymer[11]. This suggests that the interaction of substituent groups with $i\text{-Bu}_3\text{Al}$ is related to the decrease in the molecular weight of the polyethylene obtained with this catalyst.

Scheme 2 shows the interaction of the substituent groups with $i\text{-Bu}_3\text{Al}$. When the lone pair of electrons on the nitrogen atom is used in the complexation to an acidic center, a positive charge is created on the hetero atom. As a consequence, the positive center withdraws electrons from the fluorene thus drastically

decreasing its basicity. This results in low polymerization efficiencies and low polymer molecular weights.

The cocatalyst is the other important factor for the catalyst performance. Tab. 4 shows the results of ethylene polymerizations with $\text{Ph}_2\text{C}(\text{Cp})(2\text{-Me}_2\text{NFlu})\text{ZrCl}_2/\text{MAO}$ catalyst at 170°C . As with the $\text{Me}_2\text{PhNH}\cdot\text{B}(\text{C}_6\text{F}_5)_4/i\text{-Bu}_3\text{Al}$ activated catalyst, the molecular weight of the polyethylene synthesized by the $\text{Ph}_2\text{C}(\text{Cp})(2\text{-Me}_2\text{NFlu})\text{ZrCl}_2/\text{MAO}$ catalyst decreases with increasing Al/Zr ratio. On the other hand, the activity increases with increasing Al/Zr ratio, which was vice versa for the $\text{Me}_2\text{PhNH}\cdot\text{B}(\text{C}_6\text{F}_5)_4/i\text{-Bu}_3\text{Al}$ activated catalyst.

Table 4. The results of ethylene polymerizations with $\text{Ph}_2\text{C}(\text{Cp})(2\text{-Me}_2\text{NFlu})\text{ZrCl}_2/\text{MAO}$

| Run No | Zr | Al/Zr | Activity (kg/mmol·Zr) | Mw ($\times 10^{-4}$) | Mw/Mn |
|--------|-----|-------|--------------------------|----------------------------|-------|
| AF-5 | 1.0 | 1000 | 31 | 12.0 | 2.2 |
| AF-3 | 1.0 | 4000 | 54 | 3.5 | 2.0 |
| AF-6 | 1.0 | 10000 | 73 | 1.7 | 2.0 |

Polymerization conditions: Ethylene pressure: 20bar, Solvent: C9-C13 hydrocarbon, 600ml, Polymerization time: 20minutes, Polymerization temperature: 170°C

Tab. 5 shows the end group structures of polyethylene obtained with $\text{Ph}_2\text{C}(\text{Cp})(2\text{-Me}_2\text{NFlu})\text{ZrCl}_2$ and $\text{Ph}_2\text{C}(\text{Cp})(\text{Flu})\text{ZrCl}_2$ catalysts activated with MAO at different Al/Zr ratio.

Table 5. End group structures of polyethylene obtained with $\text{Ph}_2\text{C}(\text{Cp})(2\text{-Me}_2\text{NFlu})\text{ZrCl}_2/\text{MAO}$ and $\text{Ph}_2\text{C}(\text{Cp})(\text{Flu})\text{ZrCl}_2/\text{MAO}$ catalysts

| Run No | Metallocene | Al/Zr | Mn ($\times 10^{-4}$) | Vinylene (No/1000C) | Vinyl (No/1000C) | Vinylidene (No/1000C) |
|--------|-------------|-------|----------------------------|------------------------|---------------------|--------------------------|
| AF-5 | (a) | 1000 | 5.5 | 0.07 | 0.13 | trace |
| AF-3 | (a) | 4000 | 1.7 | 0.07 | 0.48 | 0.04 |
| AF-6 | (a) | 10000 | 0.86 | 0.07 | 0.93 | 0.01 |
| A-4 | (b) | 1000 | 3.9 | 0.29 | 0.25 | trace |
| A-5 | (b) | 4000 | 4.6 | 0.17 | 0.21 | trace |
| A-6 | (b) | 10000 | 4.4 | 0.12 | 0.22 | trace |

(a) $\text{Ph}_2\text{C}(\text{Cp})(2\text{-Me}_2\text{NFlu})\text{ZrCl}_2$, (b) $\text{Ph}_2\text{C}(\text{Cp})(\text{Flu})\text{ZrCl}_2$, Polymerization conditions: see Tab. 4

A significant increase in the number of vinyl end groups, no change of trans-vinylene end groups and a decrease in the molecular weight of the polyethylene were observed for $\text{Ph}_2\text{C}(\text{Cp})(2\text{-Me}_2\text{NFlu})\text{ZrCl}_2/\text{MAO}$, whereas the molecular weight and the chain end structures of the polyethylene obtained with $\text{Ph}_2\text{C}(\text{Cp})(\text{Flu})\text{ZrCl}_2/\text{MAO}$ were not changed by the Al/Zr ratio. Nevertheless, the molecular weight of the ethylene synthesized with $\text{Ph}_2\text{C}(\text{Cp})(2\text{-Me}_2\text{NFlu})\text{ZrCl}_2/\text{MAO}$ at a low Al/Zr ratio was higher than that of the polyethylene obtained with $\text{Ph}_2\text{C}(\text{Cp})(\text{Flu})\text{ZrCl}_2/\text{MAO}$.

In general, it is assumed that chain transfer to Al is the minor chain transfer reaction for conventional MAO activated metallocene catalysts[12]. Nevertheless,

Brintzinger et al. already reported that polypropylene obtained with *rac*-dimethylsilylbis(2-*N,N*-dimethylaminoindenyl)zirconium dichloride/MAO was comparable in the molecular mass with polypropylene obtained with *rac*-dimethylsilylbis(indenyl)zirconium dichloride/MAO. It was also indicated that the dominant chain transfer reaction is chain transfer to aluminum[13]. Furthermore, Leino et al. studied the dependency of the molecular weight of the polypropylene on the Al/Zr ratio using *rac*-[ethylenebis(2-(*tert*-butyldimethylsiloxy)indenyl)]zirconium dichloride or *rac*-[ethylenebis(2-(*tert*-butyldimethylsiloxy)-4,5,6,7-tetrahydroindenyl)]zirconium dichloride catalysts in combination with MAO, and reported that the molecular weight of the polypropylene decreases with increasing Al/Zr ratio due to chain transfer to aluminium. [14] Similar Zr to Al chain transfer reactions have been observed with sterically congested zirconocene catalysts[15].

These results indicate that the major chain transfer reaction for the ethylene polymerization with the $\text{Ph}_2\text{C}(\text{Cp})(2\text{-Me}_2\text{NFlu})\text{ZrCl}_2/\text{MAO}$ catalyst is the chain transfer to aluminium and the significant decrease of the molecular weight under high Al/Zr ratios arises from this chain transfer reaction. These phenomena were also observed for the $\text{Me}_2\text{PhNH}\cdot\text{B}(\text{C}_6\text{F}_5)_4/i\text{-Bu}_3\text{Al}$ activated catalysts, which means that the complexation of the amino substituent group with aluminum compounds such as MAO or *i*-Bu₃Al results in a decrease of the molecular weight of the polyethylene obtained with the $\text{Ph}_2\text{C}(\text{Cp})(2\text{-Me}_2\text{NFlu})\text{ZrCl}_2$ based catalyst.

The $\text{Ph}_2\text{C}(\text{Cp})(2\text{-MeOFlu})\text{ZrCl}_2$ based catalyst also showed the same Al/Zr dependency on the molecular weight, but the degree of the decrease in molecular weight was smaller than that of the $\text{Ph}_2\text{C}(\text{Cp})(2\text{-Me}_2\text{NFlu})\text{ZrCl}_2/\text{MAO}$ catalyst.

Tab. 6 shows the influence of the alkyl substituent groups on the nitrogen atom. *Me*₂*N*- substituted metallocene based catalyst shows the highest activity. The activity decreases in the following order: *Me*₂*N*>*Et*₂*N*>(PhCH₂)₂*N*; whereas the (PhCH₂)₂*N*-substituted metallocene based catalyst produces the highest molecular weight polyethylene and the order of the molecular weight was opposite to the order of the activity.

Table 6. The effect of the substituent of the amino group on catalyst performance for ethylene polymerization

| Run No | Metallocene | Activity (kg/mmol·Zr) | Mw (×10 ⁻⁴) | Mw/Mn |
|--------|--|--------------------------|----------------------------|-------|
| AF-29 | $\text{Ph}_2\text{C}(\text{Cp})(2\text{-Me}_2\text{NFlu})\text{ZrCl}_2$ | 45.6 | 7.6 | 1.9 |
| EAF-2 | $\text{Ph}_2\text{C}(\text{Cp})(2\text{-Et}_2\text{NFlu})\text{ZrCl}_2$ | 24.9 | 13.0 | 2.1 |
| BAF-1 | $\text{Ph}_2\text{C}(\text{Cp})(2\text{-(PhCH}_2)_2\text{NFlu})\text{ZrCl}_2$ | 8.6 | 20.0 | 1.9 |
| BF-2 | $\text{Ph}_2\text{C}(\text{Cp})(2,7\text{-(Et}_2\text{N)}_2\text{Flu})\text{ZrCl}_2$ | 9.8 | 18.7 | 1.9 |
| DBAF-2 | $\text{Ph}_2\text{C}(\text{Cp})(2,7\text{-(PhCH}_2)_2\text{Flu})\text{ZrCl}_2$ | 2.3 | 17.4 | 1.8 |

Polymerization conditions: Ethylene pressure:20bar, Solvent:C9-C13hydrocarbon, 600ml, Polymerization time:20minutes, Polymerization temperature: 200°C

Catalyst:Metallocene/*Me*₂PhNH·B(C₆F₅)₄/*i*-Bu₃Al=1/1.2/100

The introduction of *Et*₂*N*- or (PhCH₂)₂*N*- substituent groups in 2,7- positions of the fluorenyl ligand resulted in a significant decrease of the activity and the molecular weight of the polyethylene.

The effect of the Al/Zr ratio on the activity and the molecular weight of the polyethylene with these catalysts is shown in Fig. 1. Surprisingly, the molecular weight of the polyethylene obtained with the $(\text{PhCH}_2)_2\text{N}$ -substituted metallocene based catalyst does not change with the Al/Zr ratio, which is totally different for Me_2N - and Et_2N - substituted metallocene based catalysts. As already reported, we speculate that the decrease in the molecular weight arises from the complexation of the amino group with $i\text{-Bu}_3\text{Al}$. Therefore, the interaction of the $(\text{PhCH}_2)_2\text{N}$ -substituent group with $i\text{-Bu}_3\text{Al}$ may be weak especially compared to Me_2N - and Et_2N - substituent groups presumably due to the steric bulk of benzyl substituents.

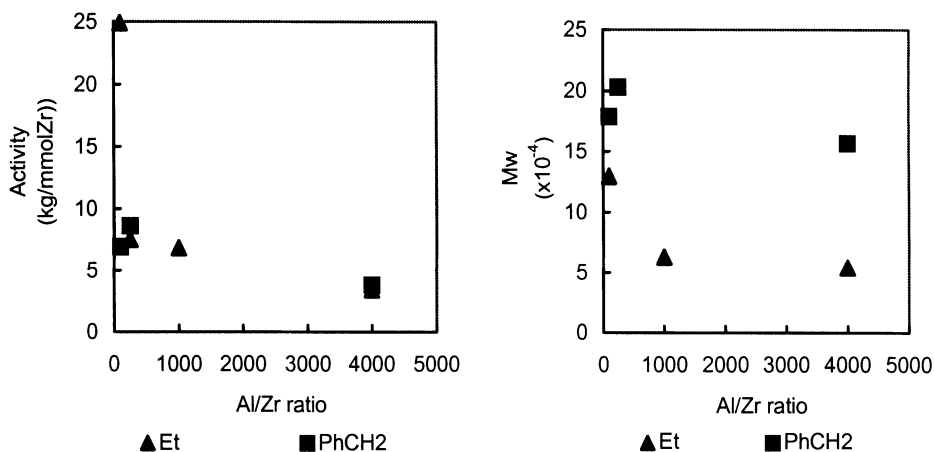


Fig. 1. Effect of Al/Zr ratio on activity and the molecular weight of polyethylene obtained with $\text{Ph}_2\text{C}(\text{Cp})(2\text{-Et}_2\text{NFlu})\text{ZrCl}_2$ and $\text{Ph}_2\text{C}(\text{Cp})(2\text{-(PhCH}_2)_2\text{NFlu})\text{ZrCl}_2$ based catalysts

Ethylene/1-hexene copolymerization

The results of ethylene/1-hexene copolymerization with $\text{Ph}_2\text{C}(\text{Cp})(2\text{-Me}_2\text{NFlu})\text{ZrCl}_2/\text{Me}_2\text{PhNH}\cdot\text{B}(\text{C}_6\text{F}_5)_4/i\text{-Bu}_3\text{Al}$ catalyst are shown in Tab. 7.

Table 7. The results of ethylene/1-hexene copolymerization with $\text{Ph}_2\text{C}(\text{Cp})(2\text{-Me}_2\text{NFlu})\text{ZrCl}_2/\text{Me}_2\text{PhNH}\cdot\text{B}(\text{C}_6\text{F}_5)_4/i\text{-Bu}_3\text{Al}$ catalyst at 170°C

| Run No | Zr (μmol) | Al/Zr | 1-hexene (ml) | Activity (kg/mmol \cdot Zr) | Mw ($\times 10^4$) | Mw/Mn |
|--------|---------------------------|-------|------------------|----------------------------------|-------------------------|-------|
| AF-13 | 1.0 | 100 | 0 | 31 | 15.4 | 2.1 |
| AF-23 | 1.0 | 100 | 20 | 35 | 16.0 | 1.8 |
| AF-24 | 1.0 | 100 | 40 | 21 | 16.3 | 1.8 |
| AF-41 | 1.0 | 100 | 80 | 30 | 10.5 | 2.2 |
| AF-43 | 1.0 | 250 | 80 | 44 | 9.1 | 2.1 |
| AF-44 | 1.0 | 1000 | 80 | 29 | 7.0 | 2.0 |
| AF-45 | 1.0 | 4000 | 80 | 23 | 4.9 | 2.1 |

Polymerization conditions: Ethylene pressure: 20bar, Solvent: C9-C13 hydrocarbon, 600ml, Polymerization time: 20minutes, Polymerization temperature: 170°C
 $\text{Ph}_2\text{C}(\text{Cp})(2\text{-Me}_2\text{NFlu})\text{ZrCl}_2/\text{Me}_2\text{PhNH}\cdot\text{B}(\text{C}_6\text{F}_5)_4=1/1.2$

This catalyst produces high molecular weight ethylene/1-hexene copolymers with high activity under low Al/Zr ratio but the molecular weight drastically decreases with increasing Al/Zr ratio.

Tab. 8 shows the unsaturated bond groups of the copolymers obtained. A significant increase in the vinyl content and no change of vinylidene, trans-vinylene and trisubstituted contents were observed as well as a decrease in the molecular weight of the copolymers. These results also indicate that chain transfer to aluminum is the major chain transfer reaction of this catalyst.

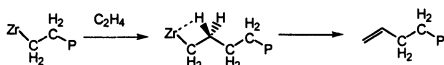
Table 8. Unsaturated bond structures of ethylene/1-hexene copolymers obtained with $\text{Ph}_2\text{C}(\text{Cp})(2\text{-Me}_2\text{NFlu})\text{ZrCl}_2$ catalyst activated with $\text{Me}_2\text{PhNH}\cdot\text{B}(\text{C}_6\text{F}_5)_4/\text{i-Bu}_3\text{Al}$

| Run No | Al/Zr | Trans-vinylene (No/1000C) | Vinyl (No/1000C) | Vinylidene (No/1000C) | Trisubstituted (No/1000C) |
|--------|-------|------------------------------|---------------------|--------------------------|------------------------------|
| AF-41 | 100 | 0.21 | 0.06 | 0.04 | 0.28 |
| AF-43 | 250 | 0.26 | 0.07 | 0.06 | 0.34 |
| AF-44 | 1000 | 0.16 | 0.13 | 0.04 | 0.22 |
| AF-45 | 4000 | 0.21 | 0.33 | 0.06 | 0.38 |

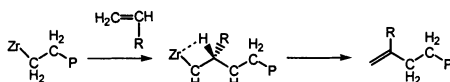
Polymerization condition: see Tab. 7

Possible chain transfer reactions of ethylene/ α -olefin polymerization with usual catalysts are shown in Scheme 3.

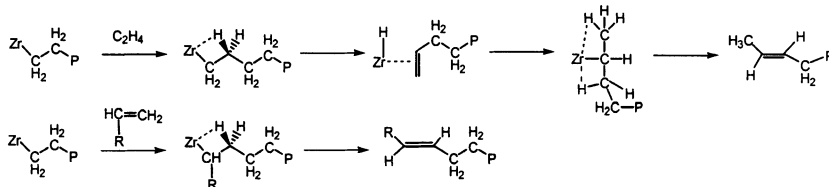
1) Vinyl end group



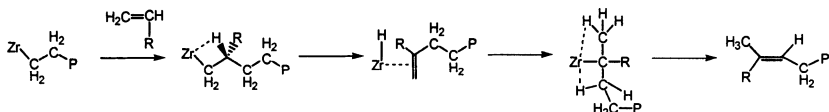
2) Vinylidene end group



3) Trans vinylene end group



4) Trisubstituted end group



Scheme 3. Possible chain transfer reactions in the ethylene/ α -olefin copolymerization

Vinyl and vinylidene end groups are formed by β -H transfer from propagating chains containing ethylene and primary inserted α -olefin as terminal units respectively. Trans-vinylene end groups are formed by two mechanism, one of which is the β -H transfer from propagating chains containing secondary inserted α -olefin as terminal units, the other one is the β -H transfer after isomerization. Trisubstituted end groups [16] are formed by β -H transfer from species that are formed by rearrangement after primary insertion of α -olefin.

Employing the usual metallocene catalysts for ethylene/ α -olefin copolymerization at high temperatures produced low molecular weight copolymers with mainly vinylidene end groups, indicating that β -H transfer from propagating chains containing primary inserted α -olefin as terminal units is the major chain transfer reaction. [9] We have already reported that this chain transfer reaction can be controlled by using the $\text{Ph}_2\text{C}(\text{Cp})(\text{Flu})\text{ZrCl}_2$ catalyst activated with $\text{Me}_2\text{PhNH}\cdot\text{B}(\text{C}_6\text{F}_5)_4/i\text{-Bu}_3\text{Al}$ even at high temperatures and that this catalyst is able to produce high molecular weight ethylene/ α -olefin copolymers with a high activity[17]. Therefore, it was clear that the chain transfer reactions of the $\text{Ph}_2\text{C}(\text{Cp})(2\text{-Me}_2\text{NFlu})\text{ZrCl}_2$ based catalyst are different from those of conventional metallocene catalysts or the $\text{Ph}_2\text{C}(\text{Cp})(\text{Flu})\text{ZrCl}_2$ based catalyst.

Tab. 9 shows the comparison of the $\text{Ph}_2\text{C}(\text{Cp})(2\text{-MeOFlu})\text{ZrCl}_2$ with the $\text{Ph}_2\text{C}(\text{Cp})(2\text{-Me}_2\text{NFlu})\text{ZrCl}_2$ catalyst activated with $\text{Me}_2\text{PhNH}\cdot\text{B}(\text{C}_6\text{F}_5)_4/i\text{-Bu}_3\text{Al}$. Both catalysts produce higher molecular weight copolymers than the $\text{Ph}_2\text{C}(\text{Cp})(\text{Flu})\text{ZrCl}_2$ based catalyst though they show a slightly lower 1-hexene incorporation ability. The $\text{Ph}_2\text{C}(\text{Cp})(2\text{-MeOFlu})\text{ZrCl}_2$ based catalyst exhibits a bigger 1-hexene incorporation ability than the $\text{Ph}_2\text{C}(\text{Cp})(2\text{-Me}_2\text{NFlu})\text{ZrCl}_2$ based catalyst, but the molecular weight is lower than that of the copolymers obtained with the $\text{Ph}_2\text{C}(\text{Cp})(2\text{-Me}_2\text{NFlu})\text{ZrCl}_2$ based catalyst.

Table 9. Comparison of $\text{Ph}_2\text{C}(\text{Cp})(2\text{-Me}_2\text{NFlu})\text{ZrCl}_2$ with $\text{Ph}_2\text{C}(\text{Cp})(2\text{-MeOFlu})\text{ZrCl}_2$ catalyst activated with $\text{Me}_2\text{PhNH}\cdot\text{B}(\text{C}_6\text{F}_5)_4/i\text{-Bu}_3\text{Al}$

| Run No | Metallocene | Mw ($\times 10^{-4}$) | Mw/Mn | Methyl (No/1000C) | Tm ($^{\circ}\text{C}$) |
|--------|---|----------------------------|-------|----------------------|------------------------------|
| AF-43 | $\text{Ph}_2\text{C}(\text{Cp})(2\text{-Me}_2\text{NFlu})\text{ZrCl}_2$ | 9.1 | 2.1 | 10.4 | 111 |
| 1348 | $\text{Ph}_2\text{C}(\text{Cp})(2\text{-MeOFlu})\text{ZrCl}_2$ | 8.4 | 1.9 | 12.5 | 103 |
| 1347 | $\text{Ph}_2\text{C}(\text{Cp})(\text{Flu})\text{ZrCl}_2$ | 6.8 | 1.8 | 12.7 | 99 |

Polymerization conditions: Ethylene pressure:20bar, Solvent:C9-C13hydrocarbon, 600ml, Polymerization time: 20minutes, Polymerization temperature: 170 $^{\circ}\text{C}$, 1-hexene: 80ml
Catalyst: Metallocene/ $\text{Me}_2\text{PhNH}\cdot\text{B}(\text{C}_6\text{F}_5)_4/i\text{-Bu}_3\text{Al}$ =1/1.2/250

Ethylene/1-butene copolymerization in a high pressure process

The results of ethylene/1-butene copolymerization with the $\text{Ph}_2\text{C}(\text{Cp})(2\text{-Me}_2\text{NFlu})\text{ZrCl}_2$ catalyst activated with $\text{Me}_2\text{PhNH}\cdot\text{B}(\text{C}_6\text{F}_5)_4/i\text{-Bu}_3\text{Al}$ are shown in Tab. 10. This catalyst produced higher molecular weight copolymers than the $\text{Ph}_2\text{C}(\text{Cp})(\text{Flu})\text{ZrCl}_2$ based catalyst though slightly lower comonomer incorporation and lower activity. Nevertheless, it is very important that this catalyst can produce polyethylene with a very low density and high molecular weight.

Fig. 2 shows a CFC diagram of this copolymer and it was clear that this catalyst produces copolymers with narrow chemical composition distribution, which indicates that this catalyst is a so called single site catalyst in a high pressure process.

Table 10. The results of ethylene/1-butene copolymerization with $\text{Ph}_2\text{C}(\text{Cp})(2\text{-Me}_2\text{NFlu})\text{ZrCl}_2/\text{Me}_2\text{PhNH}\cdot\text{B}(\text{C}_6\text{F}_5)_4/i\text{-Bu}_3\text{Al}$ catalyst

| Run No | Metalocene | $\text{C}_4^=$ (mol%) | $\text{T}_p^{(1)}$ ($^\circ\text{C}$) | Activity ($\text{Kg}/\text{mmol}\cdot\text{Zr}$) | Mw ($\times 10^{-4}$) | Mw/Mn | Methyl (No/1000C) |
|--------|------------|--------------------------|--|---|----------------------------|-------|----------------------|
| 4ZX010 | 1) | 70 | 160 | 620 | 5.4 | 1.9 | 43.9 |
| 5YX009 | 2) | 72 | 168 | - | 8.3 | 1.8 | 36.9 |
| 52X001 | 2) | 78 | 145 | 160 | 9.8 | 1.9 | 43.0 |

Polymerization conditions: Ethylene pressure: 800bar, 1-butene: 70mol%

1): $\text{Ph}_2\text{C}(\text{Cp})(\text{Flu})\text{ZrCl}_2$, 2): $\text{Ph}_2\text{C}(\text{Cp})(2\text{-Me}_2\text{NFlu})\text{ZrCl}_2$

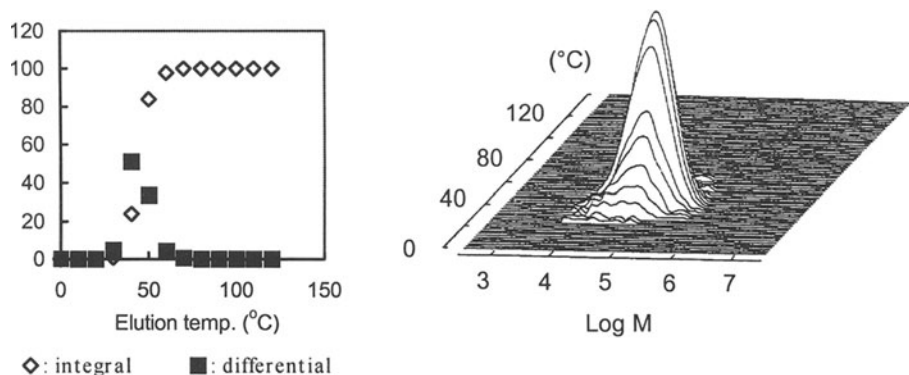


Fig. 2. CFC diagram of ethylene/1-butene copolymers obtained with $\text{Ph}_2\text{C}(\text{Cp})(2\text{-Me}_2\text{NFlu})\text{ZrCl}_2$ based catalyst (5YX009)

Reference

- [1] J. A. Ewen, R. L. Jones, A. Razavi, J. D. Ferrara, *J. Am. Chem. Soc.* 110, 6255 (1988)
- [2] J. A. Ewen, *Macromol. Chem., Symp.* 89, 181 (1995)
- [3] A. Akimoto, *Metalocene'95*, 439 (1995)
- [4] A. Razavi, J. L. Atwood, *J. Organomet. Chem.* 459, 117 (1993)
- [5] N. Piccolrovazzi, P. Pino, G. Consiglio, A. Sironi, M. Moret, *Organometallics* 9, 3098 (1990)
- [6] I. M. Lee, W. J. Gauthier, J. M. Ball, B. Iyengar, S. Collins, *Organometallics* 11, 2115 (1992)
- [7] H. G. Alt, R. Zenk, *J. Organomet. Chem.* 522, 39 (1996)
- [8] K. Thorshaug, E. Rytter, M. Ystenes, *Macromol. Chem., Rapid Commun.* 18, 715 (1997)

- [9] A. Yano, M. Sone, S. Yamada, S. Hasegawa, A. Akimoto, *Macromol. Chem., Phys.* Accepted
- [10] R. F. Jordan, W. E. Dasher, S. Eshols, *J. Am. Chem. Soc.* 108, 1718 (1986)
- [11] W. Spaleck, M. Antberg, J. Rohrmann, A. Winter, B. Bachmann, P. Kiprof, J. Behm, W.A. Harrmann, *Angew. Chem. Int. Ed. Engl.* 31, 1347 (1992)
- [12] J. C. W. Chien, B. P. Wang, *J. Polym. Sci., Part A, Polym. Chem.* 28, 15 (1990)
- [13] E. Barsties, S. Schaible, M-H. Prosenc, U. Rief, W. Röhl, O. Weyand, B. Dorer, H-H. Brintzinger, *J. Organomet. Chem.* 520, 63 (1996)
- [14] R. Leino, H. J. G. Luttikhedde, P. Lehmus, C-E. Wilen, R. Sjöholm, A. Lehtonen, J. V. Seppälä, J. H. Näsman, *Macromolecules* 30, 3477 (1997)
- [15] B. Rieger, A. Reinmuth, W. Röhl, H. H. Brintzinger, *J. Mol. Catal.* 82, 67 (1993)
- [16] A. Rossi, J. Zhang, G. Odian, *Macromolecules* 29, 2331 (1996)
- [17] A. Yano, M. Sone, S. Hasegawa, M. Sato, A. Akimoto, *Macromol. Chem., Phys.* accepted

Synthesis of Novel Complex with Bridged Bis(indenyl) Ligand and its Polymerization Behavior of Propylene

Taku KATO, Hideshi UCHINO, Naoshi IWAMA, Kaori IMAEDA, Masami KASHIMOTO, Yasuko OSANO and Toshihiko SUGANO

Yokohama Research Center, Mitsubishi Chemical Corporation
1000 Kamoshida-cho, Aoba-ku, Yokohama 227-8502 (Japan)
taku@rc.m-kagaku.co.jp

Abstract. Novel *ansa*-zirconocenes characterized by a bis(indenyl) *ansa* ligand bridged between 4 and 4' positions were synthesized. The behavior of these complexes as polymerization catalysts in the presence of methylalumoxane and properties of the polymers thus obtained were studied. Isotactic polypropylene was obtained by using C_2 -symmetrical zirconocene. Especially, *rac*-Me₂Si[4,4'-(3-methyl-1-phenylindenyl)₂]ZrCl₂ produced polypropylene with high tacticity, and a small amount of 3,1-type regiodeflect. By the polymerization test with above complex at various propylene pressures, the depression of melting point of polymer was observed with decrease of monomer pressure, which seemed to be due to the lowering of isotacticity mainly. And by the plot of $1/P_N$ versus $1/[\text{propylene}]$, we got a relatively large value of k_{T0}/k_p , and it is suggested that β -H transfer to propylene was not suppressed by substituent at 3 position effectively. Changing substituent at 3 position from methyl group to ethyl group resulted in increasing of molecular weight of polymer.

1 INTRODUCTION

Chiral *ansa*-zirconocenes having two indenyl groups linked by bridge between 1 and 1' positions have proved to be useful for catalyst for producing isotactic polypropylene in combination with cocatalyst[1]. The bridge was important for conferring the rigidity and symmetry on the complex, but the bridging position was almost restricted to 1 position of indenyl moiety.

Among the reasons that led us to change the bridging position 1 to 4 in the first place, there was a hope that the complex would maintain C_2 -symmetry. And another hope was that two remote parts linking two indenyl groups, one is bridging group "Q" and the other is zirconium, would confer the increased rigidity on the complex, compared with 1,1'-bridged type complex in which the bridge is adjacent to zirconium. And it would be possible to place substituents which would play the role for improvement of stereoregularity and molecular weight of isotactic polypropylene, corresponding to the substituents at 2 position and 4 position of

1,1'-bridged type zirconocenes. In addition, it would be possible to control the spatial position of the substituents by changing the length of bridging group "Q" (Figure 1).

In this paper, we describe a brief outline of syntheses of complexes and their propylene polymerization behaviors.

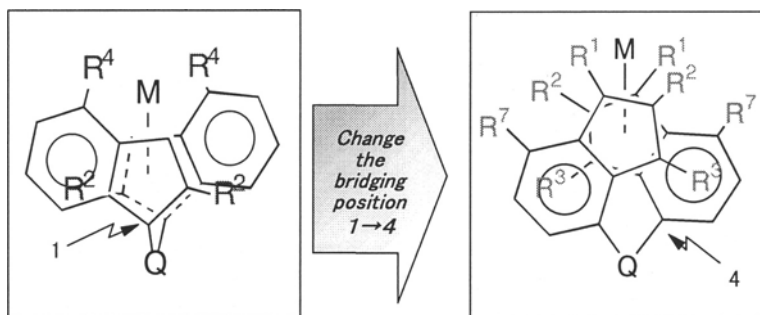


Fig. 1. Changing the Bridging Position 1 to 4

2 EXPERIMENTAL

Polymerization of propylene with novel complexes was carried out in 1 L autoclave with methylalumoxane ("MMAO" produced by TOSOH AKZO CORP.) as cocatalyst (Al/Zr = 10,000), in toluene, under the conditions of 8 bar propylene pressure at 40°C.

In the case of *rac*-Me₂Si[4,4'-(3-methyl-1-phenylindenyl)₂]ZrCl₂ (2), polymerization experiment was conducted in 1 L autoclave with MMAO (Al/Zr = 5,000) in toluene at 50 °C under a constant propylene pressure for the evaluation of the effect of monomer concentration on the polypropylene microstructure. Liquid propylene monomer polymerization was carried out in 1 L autoclave with MMAO or triisobutylaluminium ("TiBA", Al/Zr = 250) /N,N-dimethylanilinium tetrakis(pentafluorophenyl)borate ("PNBF₄", B/Zr = 2) at 50 or 70°C.

The polymer obtained was analyzed by GPC, DSC and ¹³C-NMR.

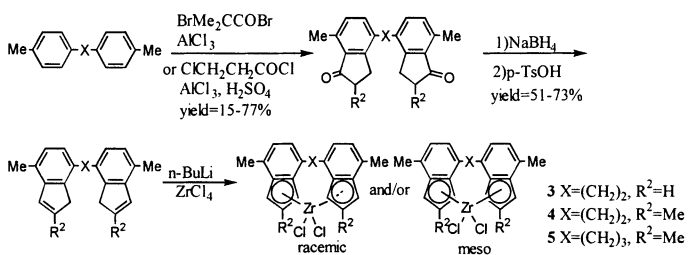
3 RESULTS AND DISCUSSION

3.1. Syntheses of Bis(indenyl) Zirconocenes

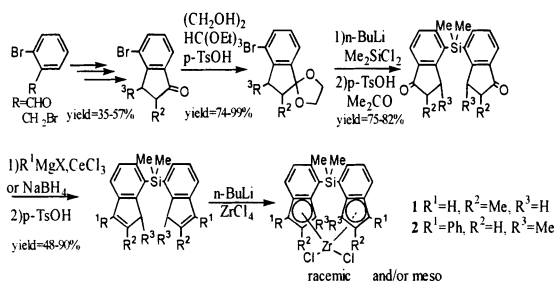
The outline of synthesis of ethylene or trimethylene bridged bis(indenyl) zirconocene was described in Scheme 1. In the case of C₂H₄[4,4'-(2,7-

dimethylindenyl)₂]ZrCl₂ (**4**), meso form was generated in preference to racemic one.

Dimethylsilylene bridged type zirconocene was synthesized by using the protected 4-bromo-1-indanone as key intermediate. The dimethylsilylene bridge was introduced by lithiation of the protected 4-bromo-1-indanone and reaction of the resulting aryllithium compound with 0.5 equiv. of dichlorodimethylsilane. Synthetic route of this type was depicted in Scheme 2.



Scheme 1. Synthetic Pathway to Ethylene or Trimethylene Bridged Type Zirconocene



Scheme 2. Synthetic Pathway to Dimethylsilylene Bridged Type Zirconocene

3.2. Crystal and Molecular Structure

Molecular structure of meso **4** and racemic **2** were confirmed by X-ray analysis.

In the case of *meso-4*, no crystallographic symmetry was observed within the molecule. This means that the indenyl moieties are slightly shifted from complete stack (Figure 2). Selected bond lengths and angles for **4** are listed in Table 1.

Zirconocene **2** has a crystallographic C_2 axis. The carbons, which form 5-membered ring, are on the plane with deviation within $\pm 0.028(2)$ Å, but C5 and C6 are 0.444(6) Å and 0.514(6) Å distant from the plane containing the 5-membered ring, respectively. This deviation may be caused by the result of repulsive effect between C5 and 3'-Me C atoms (interatomic bond distance = 3.38 Å Figure 3). Two conformers of methyl groups at 3 and 3' position were found in

the crystalline state, causing a disorder with site occupancy factor of 0.5 and 0.5. Selected bond lengths and angles for **2** are listed in Table 2.

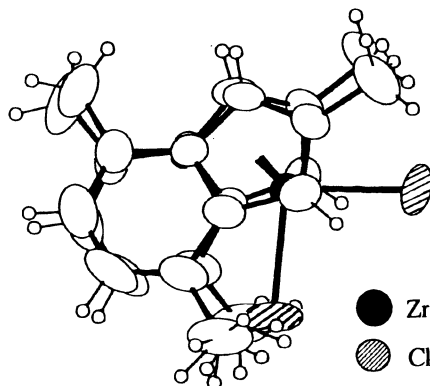


Fig. 2. Molecular Structure of *meso*-C₂H₄[4,4'-(2,7-dimethylindenyl)₂]ZrCl₂ **4**

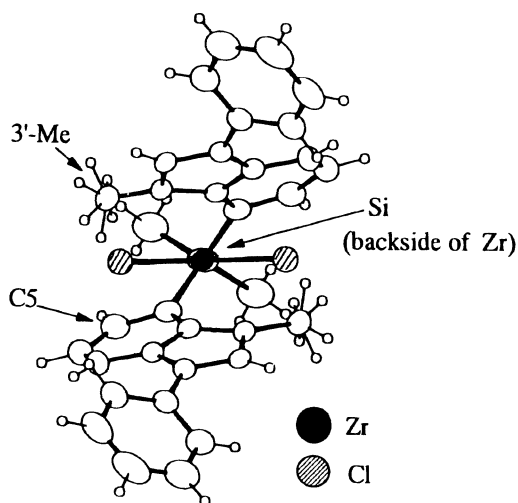


Fig. 3. Molecular Structure of *rac*-Me₂Si[4,4'-(3-methyl-1-phenylindenyl)₂]ZrCl₂ **2**

Table 1. Selected Distances(Å) and Angles(deg) for *meso*-**4**

| | | | |
|-------|----------|-----------|----------|
| Zr-Cl | 2.435(2) | Cl-Zr-Cl' | 94.69(7) |
| Zr-CR | 2.226 | CR-Zr-CR' | 131.8 |
| | | PL-PL' | 52.9 |

CR and CR': centroids of C₅ rings.

PL and PL': planes of C₅ rings.

Table 2. Selected Distances(Å) and Angles(deg) for *rac*-**2**

| | | | |
|---------|----------|---------------|----------|
| Zr-Cl | 2.470(2) | Cl-Zr-Cl' | 97.74(7) |
| Zr-CR | 2.281 | CR-Zr-CR' | 132.8 |
| Si-C | 1.865(3) | C-Si-C | 106.9(3) |
| Si-C(4) | 1.886(3) | C(4)-Si-C(4)' | 102.5(2) |
| | | PL-PL' | 50.2(1) |

CR and CR': centroids of C₅ rings. PL and PL': planes of C₅ rings. C: methyl carbon of Me₂Si<.

3.3. Polymerization of Propylene

The properties of novel complexes **1**, **2**, **4** and **5** as catalysts for the polymerization of propylene were studied in reaction systems containing the respective complex, together with MMAO in toluene at 40°C under a constant propylene pressure of 8 bar. Polymerization activities of these catalysts and properties of their polymer products are summarized in Table 3.

Table 3. Propylene Polymerization with Zirconocene/MAO Catalysts

| Complex | Polymn. Activity ^a | T _m (°C) | mm (%) | 2,1-unit(%) 3,1-unit(%) | M _n (x10 ⁴) |
|---------------------------------|-------------------------------|------------------------|-----------|--------------------------------------|---------------------------------------|
| 1 racemic | 2,600 | 103.6 | 77.8 | n.d. 0.0 ₄ | 6.2 |
| 2 racemic | 61,900 ^b | 158.8 | 99.0 | n.d. 0.1 ₁ | 12.0 |
| 4 meso | 18,600 | n.d. | 24.4 | n.d. n.d. | 18.4 |
| 5 mix. of r. and m. | 0 | --- | --- | --- | --- |
| cf. EIZ ^c racemic | 50,200 | 135.2 | 92.5 | 1.0 ₃ 0.0 ₆ | 2.1 |

^a Polymn. Activity: g-polymer/mmolZr/hr, Polymerization time = 2 h.

^b Polymerization time = 1 h. ^c Ethylene bis(1-indenyl)zirconium dichloride

The catalyst systems examined were found to have moderate polymerization activities. As expected, *meso*-**4** produced atactic polypropylene. On the other hand, racemic complexes **1** and **2** gave isotactic polypropylene with *mm* of ca. 78 and 99%, respectively. The feature of the polymer from dimethylsilylene bridged type is the low amounts of 3,1-type regiodefects and lack of 2,1-type ones.

The influence of polymerization temperature and cocatalyst on the catalyst system containing *rac*-**2** was investigated under the condition of liquid propylene or toluene slurry at 50 or 70°C (Table 4).

Table 4. Propylene Polymerization with *rac*-**2**

| Polymn. Condition ^a | Cocatalyst | Polymn. Activity ^b | T _m (°C) | mmmm ^c (%) | 2,1-unit(%) 3,1-unit(%) | M _n (x10 ⁴) |
|------------------------------------|--|-------------------------------|------------------------|--------------------------|---------------------------------------|---------------------------------------|
| 40°C Toluene Slurry PPY = 8 bar | MMAO | 61,900 | 158.8 | 98.4 | n.d. ^e 0.1 ₁ | 12.0 |
| 50°C Liquid Monomer | MMAO | 105,600 | 158.5 | 98.3 | n.d. 0.1 ₀ | 12.2 |
| 50°C Liquid Monomer | PNBF ₄ ^f TiBA | 72,800 | 158.1 | 98.6 | n.d. 0.0 ₆ | 2.6 |
| 70°C Toluene Slurry PPY = 8 bar | MMAO ^d | 36,700 | 150.6 | 95.6 | n.d. 0.2 ₁ | 5.3 |
| 70°C Liquid Monomer | MMAO | 224,700 | 155.0 | 98.2 | n.d. 0.1 ₂ | 6.2 |

^a Polymerization time = 1 h. ^b Polymn. Activity: g-polymer/mmolZr/hr. ^c [mmmm] = 1 - 5[mrrm]

^d Al/Zr = 5,000. ^e not detected. ^f N,N-Dimethylanilinium tetrakis(pentafluorophenyl)borate.

In liquid monomer condition, the depression of T_m was relatively small with increasing of polymerization temperature from 50 to 70°C, while the depression of M_n was large. When TiBA/PNBF₄ were used as cocatalyst, the T_m was not changed so much comparing with MMAO, but molecular mass fell to less than a quarter.

The molecular mass from *rac-2* was not so high as to be expected, nevertheless of the lack of 2,1-type regiodefects[2]. So the effect of monomer concentration on the polymer structure was examined to get a clue for increasing the polymer mass [3]. The results of monomer pressure dependence test are listed in Table 5 and the plot of $1/P_N$ versus $1/[\text{propylene}]$ is illustrated in Figure 4.

Table 5. Propylene Polymerization with *rac-2*/MAO at 50°C

| PPY (bar) | [PPY] ^{1,a} | Polymn. Activity ^b | T_m (°C) | <i>mmmm</i> ^c (%) | 2,1-unit(%) 3,1-unit(%) | M_n (x10 ⁴) | P_N ³ (x10 ⁻⁴) |
|-----------|----------------------|-------------------------------|------------|------------------------------|---------------------------------------|---------------------------|---|
| 1.9 | 1.625 | 22,800 | 150.1 | 93.3 | n.d. ^d 0.1 _s | 3.8 | 11.1 |
| 3.1 | 0.970 | 39,100 | 153.4 | --- | --- | 5.0 | 8.4 |
| 3.8 | 0.785 | 51,900 | 154.9 | --- | --- | 5.8 | 7.3 |
| 6.0 | 0.491 | 106,000 | 156.7 | 97.7 | n.d. 0.1 ₂ | 7.0 | 6.0 |

^a Calculated as ref 3. ^b Polymn. Activity: g-polymer/mmolZr/hr, Polymerization times have been chosen so as to yield ca. 20 to 35 g of polymer, Cocatalyst: MMAO (Al/Zr = 5,000). ^c [*mmmm*] = 1 - 5[*mrrm*]. ^d not detected

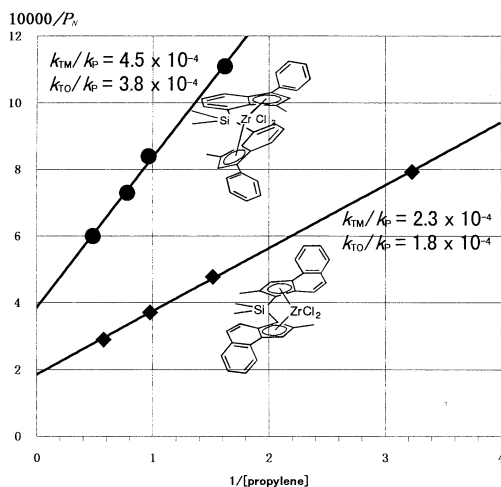


Fig. 4. Reciprocal Degree of polymerization, $1/P_N$, with Dependence on Reciprocal Propylene Concentration, $1/[\text{propylene}]$, for *rac-2*/MAO, and $\text{Me}_2\text{Si}(2\text{-methylbenz[e]indenyl})_2\text{ZrCl}_2$ as comparison. The comparison data is cited in ref. [3].

We got a relatively large value of k_{TO}/k_p (3.8×10^{-4}), comparing with $\text{Me}_2\text{Si}(2\text{-methyl}[e]\text{benzindenyl})_2\text{ZrCl}_2$ ($k_{TO}/k_p = 1.8 \times 10^{-4}$) [3], and it is suggested that β -H transfer to monomer was not suppressed effectively by methyl groups at 3 and 3' position. Actually, molecular mass of polypropylene by using $\text{Me}_2\text{Si}[4,4'-(3\text{-ethyl-1-phenylindenyl})_2]\text{Zr}(\text{NMe}_2)_2$ (**6**) turned out to be higher than the polymer from $\text{Me}_2\text{Si}[4,4'-(3\text{-methyl-1-phenylindenyl})_2]\text{Zr}(\text{NMe}_2)_2$ (**2-amide**) (Table 6).

Table 6. Propylene Polymerization with **6** and **2-amide**/MAO

| Complex | Polymn. Condition ^a | T_m (°C) | M_w ($\times 10^4$) |
|----------------|-------------------------------------|---------------|----------------------------|
| 6 | 50°C n-Hexane Slurry PPY = 5 bar | 158.3 | 19.0 |
| 2-amide | 50°C n-Hexane Slurry PPY = 5 bar | 159.0 | 16.5 |

^a Polymerization time = 1 h, Cocatalyst: MMAO (Al/Zr = 5,000).

The T_m of isotactic polypropylenes from *rac*-**2** were highly dependent on monomer concentration. The depression of T_m was observed with decrease of monomer pressure, which seemed to be due to the lowering of the isotacticity mainly in the pressure range of our examination (See Table 5). This effect of propylene pressures on stereoselectivities may be ascribed to the epimerization of the polymer chain at its active site.[4]

4 Conclusions

Novel *ansa*-metallocene complexes having bis(indenyl) ligands bridged at 4 position were synthesized. Ethylene or trimethylene bridged type zirconocene was prepared from bis(*p*-tolyl)ethane or bis(*p*-tolyl)propane as starting material, respectively. Dimethylsilylene bridged type zirconocene was synthesized from the protected 4-bromo-1-indanone derivative.

The structures of *meso*- $\text{C}_2\text{H}_4[4,4'-(2,7\text{-dimethylindenyl})_2]\text{ZrCl}_2$ (**4**) and *rac*- $\text{Me}_2\text{Si}[4,4'-(3\text{-methyl-1-phenylindenyl})_2]\text{ZrCl}_2$ (**2**) were confirmed by X-ray analysis.

As expected, atactic polypropylene was obtained in the case of *meso*-**4**. Trimethylene bridged complex had no polymerization activities, and it could be presumed that trimethylene bridge was too long, and indenyl ligand would cover the vacant site of zirconium. Dimethylsilylene bridged racemic complex gave isotactic polypropylene. Especially, *rac*-**2** could produce polypropylene with high isotacticity and a small amount of 3,1-type regiodeflect under certain conditions.

The influence of polymerization temperature, cocatalyst and propylene pressure on catalyst performances with regard to *rac*-**2** is reported. In liquid monomer polymerization condition, the depression of T_m was relatively small (3.5°C) with increasing of polymerization temperature from 50 to 70°C, while M_n fell to a half (from 12.2×10^4 to 6.2×10^4). The *rac*-**2**/PNBF₄/TiBA catalyst system produced

polypropylene with low molecular weight. By plotting of $1/P_N$ versus $1/[\text{propylene}]$, we got a relatively large value of k_{TO}/k_p (3.8×10^{-4}) and it is suggested that β -H transfer to monomer was not suppressed effectively by methyl groups at 3 and 3' position. As a result of change of the substituent at 3 position from methyl to ethyl, the molecular mass of polypropylene went up a little. The drop of T_m was observed with decreasing of monomer concentration, and it seemed to be due to the lowering of the isotacticity derived from the epimerization of the polymer chain at its active site.

References

- [1] (a) Ewen, J. *J. Am. Chem. Soc.* **1984**, *106*, 6355. (b) Kaminsky, W.; Kulper, K.; Brintzinger, H. H.; Wild, F. R. W. P. *Angew. Chem. Int. Ed. Engl.* **1985**, *24*, 507. (c) For recent review, see Brintzinger, H. H.; Fisher, D.; Mulhaupt, R.; Rieger, B.; Waymouth, R. M. *Angew. Chem. Int. Ed. Engl.* **1995**, *34*, 1143.
- [2] Resconi, L.; Piemontesi, F.; Camurati, I.; Balboni, D.; Sironi, A.; Moret, M.; Rychlicki, H.; Zeigler, R. *Organometallics* **1996**, *15*, 5046.
- [3] Stehling, U.; Diebold, J.; Kirsten, R.; Roll, W.; Brintzinger, H. H.; Jungling, S.; Mulhaupt, R.; Langhauser, F. *Organometallics* **1994**, *13*, 964.
- [4] (a) Busico, V.; Cipullo, R. *J. Am. Chem. Soc.* **1994**, *116*, 9329. (b) Busico, V.; Caporaso, R.; Landriani, L. *J. Am. Chem. Soc.* **1996**, *118*, 2105. (c) Leclerc, M. K.; Brintzinger, H. H. *J. Am. Chem. Soc.* **1996**, *118*, 9024. (d) Busico, V.; Brita, D.; Caporaso, L.; Cipullo, R.; Vacatello, V. *Macromolecules* **1997**, *30*, 3971.

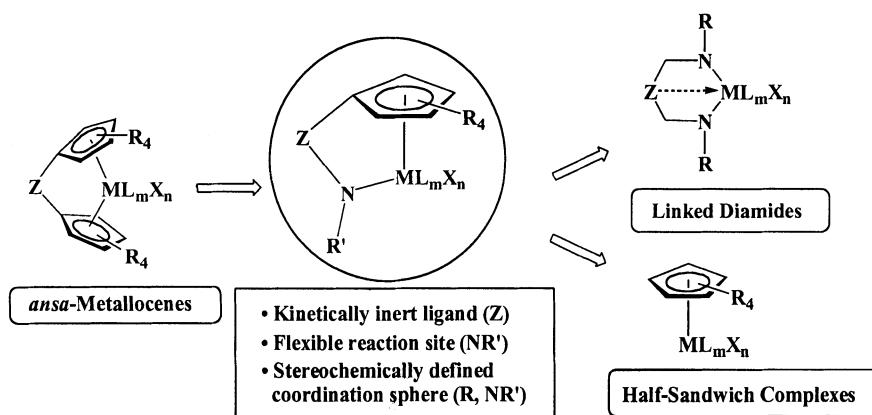
Linked Amido–Cyclopentadienyl Complexes of Group 3 and 4 Metals: The First “Post-Metalloenes”

Jun Okuda

Institut für Anorganische Chemie und Analytische Chemie,
Johannes Gutenberg-Universität Mainz,
Johann-Joachim-Becher-Weg 24, D-55099 Mainz, Germany

Introduction

Linked amido–cyclopentadienyl ligands were introduced by Bercaw and Shapiro in the late eighties with the catalysts of the type $\text{Sc}(\eta^5\text{:}\eta^1\text{-C}_5\text{Me}_4\text{SiMe}_2\text{N}^t\text{Bu})\text{X}$ ($\text{X} = \text{H}$, alkyl) [1]. These electronically more unsaturated and sterically more accessible analogs of *ansa*-scandocene complexes were found to be capable of catalyzing the living oligomerization of the α -olefins propylene, 1-butene, and 1-pentene. In these complexes the steric constraint [2] of Brintzinger-type *ansa*-metalloenes is alleviated by the replacement of one cyclopentadienyl ligand by an amido ligand NR' (Scheme 1). In order to explore sterically demanding derivatives of this dianionic ligand $(\text{C}_5\text{R}_4\text{ZNR}')^{2-}$, iron and titanium complexes were synthesized shortly thereafter [3].



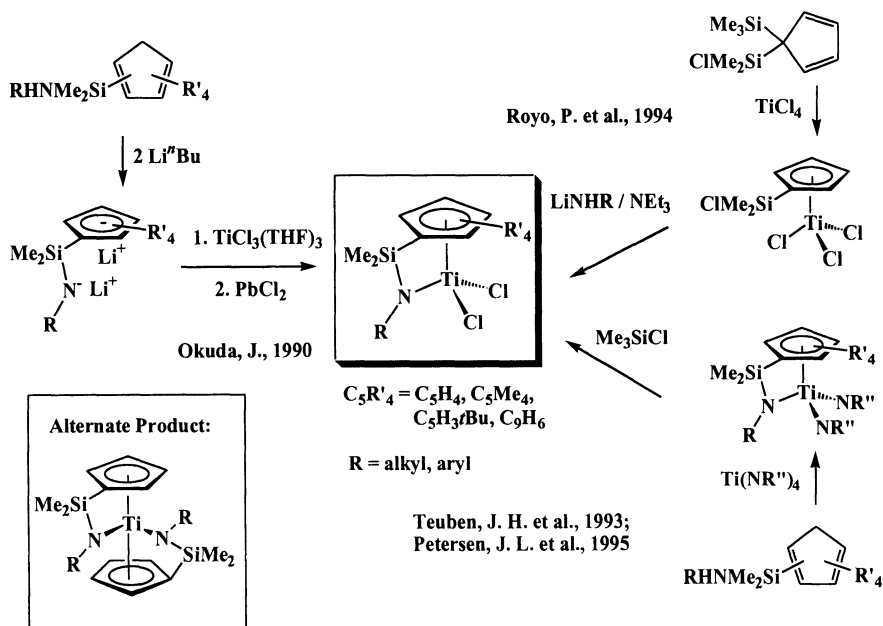
Scheme 1.

Based on these bridged amido–cyclopentadienyl ligands, a flurry of development occurred independently in the research laboratories of Dow Chemical and Exxon Chemical and culminated in their patent applications filed within two weeks of each other in 1990 [4]. A deluge of patents has appeared in the meantime and

most of the data on this subject resides in the patent literature. The great interest in the group 4 metal complexes containing the linked amido–cyclopentadienyl ligand stems from their unprecedented potential as a new generation of homogeneous olefin polymerization catalysts [5]. In particular, the possibility of producing copolymers of ethylene with new rheological properties and good processability at high temperatures, has stimulated a frantic activity in synthesizing and testing such complexes [6]. We summarize here some coordination chemical aspects relevant to polymerization catalysis [3c].

Synthesis and Structure of Group 4 Metal Complexes

Following the traditional route to metallocene complexes, bridged amido–cyclopentadienyl complexes of group 4 metals are most commonly bridged synthesized by first assembling the ligand $(C_5R_4H)Z(NHR')$ and then coordinating it at the metal center according to a suitable protocol. For the complexation several different synthetic procedures have been developed (Scheme 2). The metathetical reaction of the doubly metalated ligand precursor $(C_5R_4ZNR')^{2-}$ with appropriate metal halides appears to be the most common [7].



In order to avoid the problems associated with the metathesis method, such as the the formation of solvent adducts and dimerization of some zirconium complexes, reaction of homoleptic metal amides $M(NR'')_n$ with the functionalized

cyclopentadienes, with amine elimination has been applied [8]. Another approach consists of introducing the amido linkage within the preformed half-sandwich complex [9]. This method can only be applied to the unsubstituted cyclopentadienyl system C_5H_4 [10] and could not be extended to metal centers other than titanium.

The synthesis of alkyl complexes, important as precursors for α -olefin polymerization catalysts, from the chloro or amido derivatives can be achieved using suitable alkylating reagents, organolithium or Grignard reagents with methyl, benzyl, trimethylsilylmethyl, neophyl, and neopentyl residues [7,8,10]. Generally, the bulkier alkyl groups provide more thermally and photochemically stable complexes.

In the context of explaining the specific polymerization properties of group 4 metal complexes containing the linked amido-cyclopentadienyl ligand, single-crystal structure analyses of numerous dichloro complexes of the type $M(\eta^5:\eta^1-C_5R_4ZNR')Cl_2$ have been performed. Some representative examples are compiled in Table 1.

Table 1. Selected structural characteristics of complexes containing linked amido-cyclopentadienyl ligands (Cp denotes the centroid of the cyclopentadienyl, N denotes the appended amido-nitrogen)

| Compound | Cp-M-N, ° | M-Cp, Å | M-N, Å | Ref. |
|--|-----------|---------|----------|------|
| Ti($\eta^5:\eta^1-C_5H_4SiMe_2N^tBu$)Cl ₂ | 107.0 | 2.019 | 1.901(3) | [7] |
| Ti($\eta^5:\eta^1-C_5Me_4SiMe_2N^tBu$)Cl ₂ | 107.6 | 2.030 | 1.908(6) | [5] |
| Ti($\eta^5:\eta^1-C_5Me_4(CH_2)_2N^tBu$)Cl ₂ | 107.9 | - | 1.909(5) | [5] |
| Ti($\eta^5:\eta^1-C_5H_4SiMe_2N^iPr$)Cl ₂ | 105.5 | 2.017 | 1.878(2) | [11] |
| Ti($\eta^5:\eta^1-C_5H_4(CH_2)_2N^iPr$)Cl ₂ | 104.4 | 2.008 | 1.864(2) | [8] |
| Ti($\eta^5:\eta^1-C_5H_4(CH_2)_3N^iPr$)Cl ₂ | 112.6 | 2.027 | 1.867(2) | [8] |
| Ti($\eta^5:\eta^1-C_5H_4SiMe_2N^tBu$)(NMe ₂) ₂ | 105.5 | 2.083 | 1.972(4) | [7] |
| Zr($\eta^5:\eta^1-C_5Me_4SiMe_2N^tBu$)Cl ₂ | 102.0 | 2.163 | 2.056(6) | [11] |
| Zr($\eta^5:\eta^1-C_5Me_4SiMe_2N^tBu$)(NMe ₂) ₂ | 100.2 | 2.233 | 2.108(4) | [7] |

Single X-ray structural analysis of $(-)-(S_C, S_{Ti})-Ti(\eta^5:\eta^1-C_5R_4SiMe_2NCHMePh)-Cl(CH_2SiMe_3)$ (Fig. 1), an optically active titanium complex containing an amido-cyclopentadienyl ligand [10], reveals a structure in which the phenyl group is arranged coplanarly to the C_5H_4 ring, turned away from the metal center. NOE measurements suggest restricted rotation about the nitrogen-methine carbon bond based on a larger NOE between the methyl group of the stereogenic center and one of the two diastereotopic methyl groups of the silanediyl link.

A similar characteristic feature for complexes containing a secondary amido substituent R', is the tendency of the methine proton to orientate itself towards the metal center. This phenomenon is consistently found in *iso*-propyl-amido com-

plexes such as $\text{Ti}(\eta^5:\eta^1\text{-C}_5\text{H}_4\text{SiMe}_2\text{N}^i\text{Pr})\text{Cl}_2$ [11], $\text{Ti}\{\eta^5:\eta^1\text{-C}_5\text{H}_4(\text{CH}_2)_2\text{N}^i\text{Pr}\}\text{Cl}_2$ and $\text{Ti}\{\eta^5:\eta^1\text{-C}_5\text{H}_4(\text{CH}_2)_3\text{N}^i\text{Pr}\}\text{Cl}_2$ [8].

Values for the $\text{Ti-N-C}_{\text{Methine}}$ angle and the $\text{Ti-H}_{\text{Methine}}$ distances are given in Table 2. A β -agostic interaction is not observed by ^1H NMR spectroscopy in complexes with $Z = \text{SiMe}_2$. However, it is detected in complexes containing less constrained, longer links ($Z = (\text{CH}_2)_3$). Here the $\text{Ti-N-C}_{\text{Methine}}$ angle and the $\text{Ti-H}_{\text{Methine}}$ distance for the β -agostic interaction are similar to those found in the non-bridged cyclopentadienyl amido complex $\text{Ti}(\eta^5\text{-C}_5\text{H}_5)(\text{N}^i\text{Pr}_2)\text{Cl}_2$ [12], where one of the isopropyl groups is directed towards the metal center due to a β -agostic interaction of the methine proton, resulting in a $\text{Ti-H}_{\text{Methine}}$ distance of 2.25 Å and a $\text{Ti-N-C}_{\text{Methine}}$ angle of $101.4(2)^\circ$.

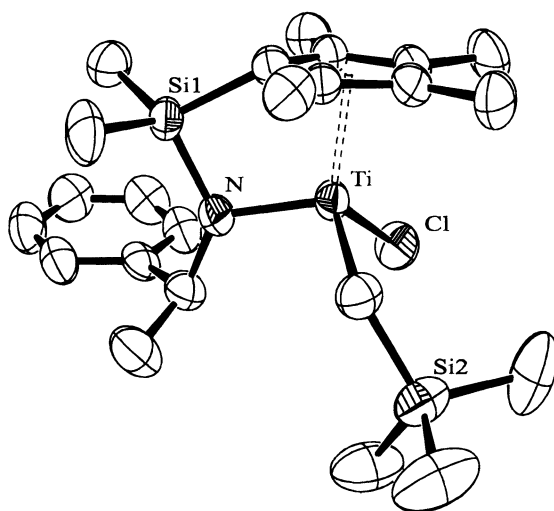


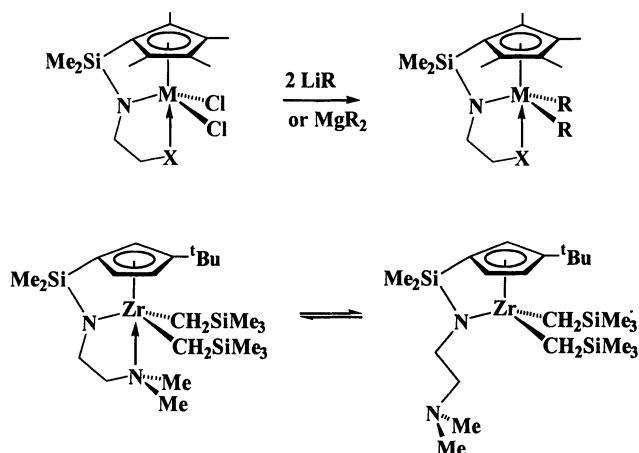
Figure 1. Molecular structure of $(-)(S_C, S_{Ti})\text{-Ti}(\eta^5:\eta^1\text{-C}_5\text{H}_4\text{SiMe}_2\text{NCHMePh})\text{Cl}(\text{CH}_2\text{SiMe}_3)$.

Table 2. Characteristics of complexes with secondary amido substituents

| Compound | $\text{Ti-H}_{\text{Methine}}$, Å | $\text{Ti-N-C}_{\text{Methine}}$, ° | $\delta(\text{H}_{\text{Methine}})$, ppm | Ref. |
|--|---------------------------------------|---|--|------|
| $(-)(S)\text{-Ti}(\eta^5:\eta^1\text{-C}_5\text{H}_4\text{SiMe}_2\text{NCHMePh})\text{Cl}_2$ | 2.84 | 120.5(3) | 6.54 | [10] |
| $\text{Ti}(\eta^5:\eta^1\text{-C}_5\text{H}_4\text{SiMe}_2\text{N}^i\text{Pr})\text{Cl}_2$ | 2.79 | 117.4(1) | 5.69 | [11] |
| $\text{Ti}\{\eta^5:\eta^1\text{-C}_5\text{H}_4(\text{CH}_2)_2\text{N}^i\text{Pr}\}\text{Cl}_2$ | 2.67 | 114.2(2) | 5.92 | [8] |
| $\text{Ti}\{\eta^5:\eta^1\text{-C}_5\text{H}_4(\text{CH}_2)_3\text{N}^i\text{Pr}\}\text{Cl}_2$ | 2.38 | 104.5(1) | 6.57 | [8] |

Complexes with a Tridentate Amido–Cyclopentadienyl Ligand

In order to attenuate the Lewis acidity of early transition metal centers, a new ligand system with a side chain incorporating an additional weak neutral donor site within the chelating amido–cyclopentadienyl ligand framework has been introduced [13]. Donor groups such as OMe or NMe₂ attached to the amido functionality offer new possibilities in tailoring the coordination sphere around a reactive transition metal center. Using the metathetical pathway, a series of group 4 metal complexes $M(\eta^5:\eta^1\text{-C}_5\text{Me}_4\text{SiMe}_2\text{NCH}_2\text{X})\text{Cl}_2$ ($M = \text{Ti, Zr, Hf; X} = \text{CH}=\text{CH}_2, \text{CH}_2\text{OMe, CH}_2\text{NMe}_2$) [13] have been prepared (Scheme 3). The bridged unsubstituted cyclopentadienyl titanium derivatives $\text{Ti}(\eta^5:\eta^1\text{-C}_5\text{H}_4\text{SiMe}_2\text{NCH}_2\text{X})\text{Cl}_2$ ($X = \text{CH}_2\text{OMe, CH}_2\text{NMe}_2$) are accessible from $\text{Ti}(\eta^5:\eta^1\text{-C}_5\text{H}_4\text{SiMe}_2\text{Cl})\text{Cl}_3$ [14].



Scheme 3.

Since the molecules contain a mirror plane irrespective of the coordination of the appended donor group in solution, the question whether the additional donor is bonded rigidly or in a fluxional manner cannot be decided by ¹H or ¹³C NMR spectroscopy, including variable-temperature NMR spectra. The corresponding dimethyl complexes offer the possibility to record NOE measurements and to study the coordination mode. Whereas in titanium compounds $\text{Ti}(\eta^5:\eta^1\text{-C}_5\text{Me}_4\text{-SiMe}_2\text{NCH}_2\text{X})\text{Me}_2$ a spatial relationship between the TiMe_2 signal and OMe and NMe₂ groups could not be established, homologous zirconium complexes $\text{Zr}(\eta^5:\eta^1\text{-C}_5\text{Me}_4\text{SiMe}_2\text{NCH}_2\text{X})\text{Me}_2$ exhibit an NOE between the proton signals of the ZrMe_2 groups and the additional donor function OMe or NMe₂. Thus, the zirconium (and hafnium) complexes retain the intramolecular coordination in solution. This can be ascribed to the higher Lewis acidity of zirconium and hafnium compared to titanium. For example, the crystal structure of the complex

$\text{Hf}(\eta^5:\eta^1\text{-C}_5\text{Me}_4\text{SiMe}_2\text{NCH}_2\text{CH}_2\text{OMe})\text{Cl}_2$ shows a rather unusual trigonal bipyramidal configuration at the hafnium center with the OMe group occupying a site trans to the ring ligand (Fig. 2).

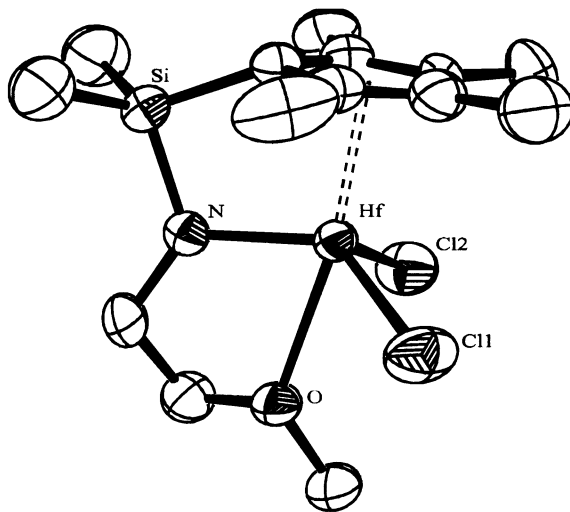


Fig. 2. Molecular structure of $\text{Hf}(\eta^5:\eta^1\text{-C}_5\text{Me}_4\text{SiMe}_2\text{NCH}_2\text{CH}_2\text{OMe})\text{Cl}_2$ [13b].

Dialkyl complexes $\text{M}(\eta^5:\eta^1\text{-C}_5\text{Me}_4\text{SiMe}_2\text{NCH}_2\text{CH}_2\text{OMe})\text{R}''_2$ ($\text{M} = \text{Zr}, \text{Hf}$) can be synthesized with the alkyl ligands R'' including Me, Ph, CH_2SiMe_3 , and CH_2Ph , but most remarkably, dialkyls with β -hydrogen atoms ($\text{R}'' = \text{Et}, {}^n\text{Pr}, {}^n\text{Bu}$) can be isolated in this series. The crystal structure of the thermally most stable (dec. > 90 °C) complex $\text{Hf}(\eta^5:\eta^1\text{-C}_5\text{Me}_4\text{SiMe}_2\text{NCH}_2\text{CH}_2\text{OMe})({}^n\text{Bu})_2$ shows two undistorted *n*-butyl groups [13,15].

NMR spectra of the planar chiral derivatives $\text{M}\{(\eta^5:\eta^1\text{-C}_5\text{H}_3{}^t\text{Bu})\text{SiMe}_2\text{NCH}_2\text{CH}_2\text{NMe}_2\}\text{Cl}_2$ ($\text{M} = \text{Ti}, \text{Zr}$) directly reveal the presence or absence of rigid intramolecular coordination of the NMe_2 function. A rigid coordination of the NMe_2 group prevents nitrogen inversion, giving rise to two inequivalent methyl signals as in fact observed in the case of the zirconium complex $\text{Zr}\{(\eta^5:\eta^1\text{-C}_5\text{H}_3{}^t\text{Bu})\text{SiMe}_2\text{NCH}_2\text{CH}_2\text{NMe}_2\}\text{Cl}_2$. In the case of the titanium derivative, $\text{Ti}\{(\eta^5:\eta^1\text{-C}_5\text{H}_3{}^t\text{Bu})\text{SiMe}_2\text{NCH}_2\text{CH}_2\text{NMe}_2\}\text{Cl}_2$, only one signal for the NMe_2 group is observed in the temperature range of $+80$ to -80 °C, suggesting that the coordination is not occurring or is fluxional on the NMR time scale [13]. A fluxional bonding mode is detected for the bulky dialkyl $\text{Zr}\{(\eta^5:\eta^1\text{-C}_5\text{H}_3{}^t\text{Bu})\text{SiMe}_2\text{NCH}_2\text{CH}_2\text{NMe}_2\}(\text{CH}_2\text{SiMe}_3)_2$ with an activation energy of $\Delta G^\ddagger(7 \text{ °C}) = 13.1 \text{ kJ}\cdot\text{mol}^{-1}$.

Alkyl Cation Formation and Ethylene Polymerization

In contrast to the 14-electron group 4 metallocenium polymerization catalysts $[M(\eta^5-C_5R_5)_2R]^{+}$, but in analogy to the scandium catalysts $Sc(\eta^5:\eta^1-C_5Me_4SiMe_2-N^tBu)X$, the 12-electron alkyl cation of the type $[M(\eta^5:\eta^1-C_5R_4ZNR')R]^{+}$ is thought to be the active species for the linked amido-cyclopentadienyl catalysts [16]. It can be generated either by the reaction with methylaluminumoxane, or by reacting a dialkyl complex with a Lewis acid such as $B(C_6F_5)_3$. Activity-structure relationships [5] show that these catalysts form, depending on the nature of the ligand framework, high molecular weight polyethylene with long-chain branching, resulting from the incorporation of oligoethylene chains formed by β -hydride elimination. Also, superior properties as copolymerization catalysts were recognized, allowing efficient and uniform incorporation of higher α -olefins such as 1-octene, styrene, norbornene, and even isobutylene [6].

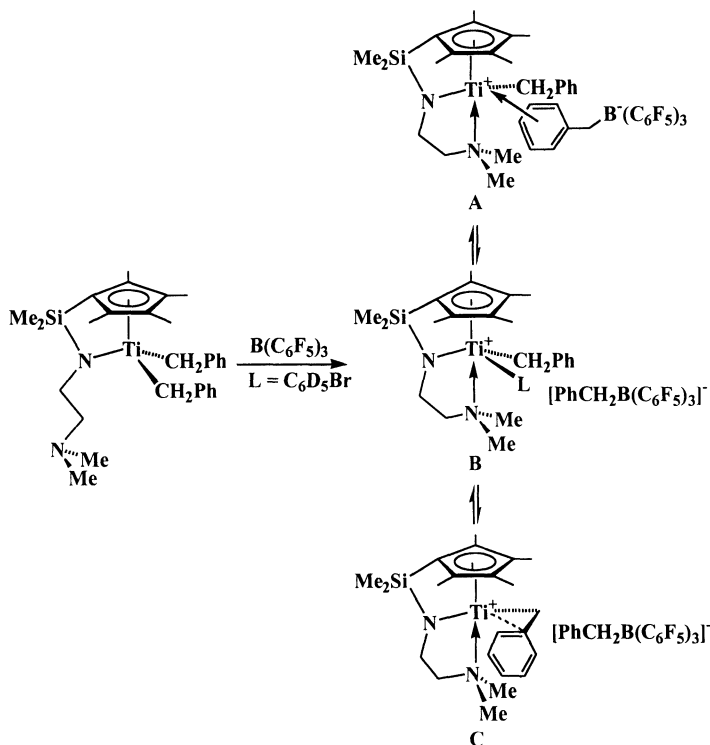
This pronounced ability of these catalysts to incorporate bulky monomers can be ascribed to the more open coordination sphere, compared to conventional metallocene systems. The nature of the ligand substituents R in the C_5R_4 ring, R' of the amido substituent NR', and the length of the bridge Z was found to influence the catalytic activity. Since catalyst precursors with the short bridge $Z = SiMe_2$ were found to give the best polymerization characteristics, the bite angle of the chelating ligand (angle Cp-Ti-N) was proposed to be a crucial geometrical criteria for a catalyst to perform well [17]. However, there is still no clearly obvious universal structure-activity relationship and we have noticed that the activity values for ethylene polymerization are also remarkably sensitive to the nature of the amido substituent R' [18].

Table 3.

| Compound | Activity, kg PE / mol Ti•h•mol/l |
|--|----------------------------------|
| Ti($\eta^5:\eta^1-C_5Me_4SiMe_2N^iPr$)Cl ₂ | 100 |
| Ti($\eta^5:\eta^1-C_5Me_4SiMe_2CH_2N^iPr$)Cl ₂ | 330 |
| Ti($\eta^5:\eta^1-C_5Me_4SiMe_2N^tBu$)Cl ₂ | 950 |
| Ti($\eta^5:\eta^1-C_5Me_4SiMe_2CH_2N^tBu$)Cl ₂ | 1320 |
| Ti($\eta^5:\eta^1-C_5Me_4SiMe_2NAd$)Cl ₂ | 460 |
| Ti($\eta^5:\eta^1-C_5Me_4SiMe_2NCH_2Ph$)Cl ₂ | 3090 |
| Ti($\eta^5:\eta^1-C_5Me_4SiMe_2CH_2NCH_2Ph$)Cl ₂ | 120 |
| Ti($\eta^5:\eta^1-C_5Me_4SiMe_2NCMe_2CH_2^tBu$)Cl ₂ | 72 |
| Ti($\eta^5:\eta^1-C_5Me_4SiMe_2NCMe_2Ph$)Cl ₂ | 54 |
| Ti($\eta^5:\eta^1-C_5Me_4SiMe_2NCH_2CH_2Ph$)Cl ₂ | 15 |

Polymerization conditions: Ethylene 3 bar, cat. 25 μ mol/l in toluene, Ti: Al(MAO) ratio 1:500, reaction time 2 h, temperature 23 °C.

When the titanium dibenzyl complexes $\text{Ti}(\eta^5\text{-}\eta^1\text{-C}_5\text{Me}_4\text{SiMe}_2\text{NCH}_2\text{CH}_2\text{X})\text{-(CH}_2\text{Ph)}_2$ ($\text{X} = \text{OMe}, \text{NMe}_2$) were reacted with equimolar amounts of $\text{B}(\text{C}_6\text{F}_5)_3$ in bromobenzene at room temperature, the clean formation of $[\text{Ti}(\eta^5\text{-}\eta^1\text{-C}_5\text{Me}_4\text{SiMe}_2\text{NCH}_2\text{CH}_2\text{NMe}_2)(\text{CH}_2\text{Ph})]^+ [\text{PhCH}_2\text{B}(\text{C}_6\text{F}_5)_3]^-$, stable for several hours, resulted. Based on NMR spectroscopic evidence, we believe it to be a solvent-separated ion pair rather than a contact ion pair (**B** favored over **A** in Scheme 4). The anion shows ^{19}F NMR spectroscopic features that are indicative of a free $[\text{PhCH}_2\text{B}(\text{C}_6\text{F}_5)_3]^-$ ion [19]. The methylene protons of the benzyl group bonded to the boron appears at δ 3.27 as a broad singlet and all aromatic protons are recorded well below δ 6.5, excluding the possibility of any strong interaction of the aromatic ring with the cationic metal center. There is no evidence for agostic or dihapto bonding of the benzyl group attached to the cationic titanium center [20]. From NMR evidence, including variable temperature NMR studies, we assume that at room temperature the side chain is engaged in a fluxional (“weak”) bonding without halting the nitrogen inversion. Apparently the strongly electrophilic, formally 12-electron cation is sufficiently stabilized by this mode of fluxional coordination.



Scheme 4.

Polymerization of ethylene and 1-hexene was observed with these cations, but with erratic results. Therefore study of ethylene polymerization was conducted with $\text{Ti}(\eta^5\text{:}\eta^1\text{-C}_5\text{Me}_4\text{SiMe}_2\text{NCH}_2\text{CH}_2\text{OMe})\text{Cl}_2$ and $\text{M}(\eta^5\text{:}\eta^1\text{-C}_5\text{Me}_4\text{SiMe}_2\text{N-CH}_2\text{CH}_2\text{OMe})\text{R}$ ($\text{M} = \text{Zr, Hf}$; $\text{R} = \text{Me, }^n\text{Bu}$). Compared to similar complexes containing the bidentate ligand such as $\text{Ti}(\eta^5\text{:}\eta^1\text{-C}_5\text{Me}_4\text{SiMe}_2\text{N}^t\text{Bu})\text{Cl}_2$ under identical conditions, it is evident that side chain modification results in significantly lower activities (12 vs. 950 kg polyethylene/mol $\text{Ti}\cdot\text{h}$) [21]. We tentatively ascribe this to the occupation of one additional site at the metal that blocks the π -complex formation of ethylene.

Yttrium Complexes

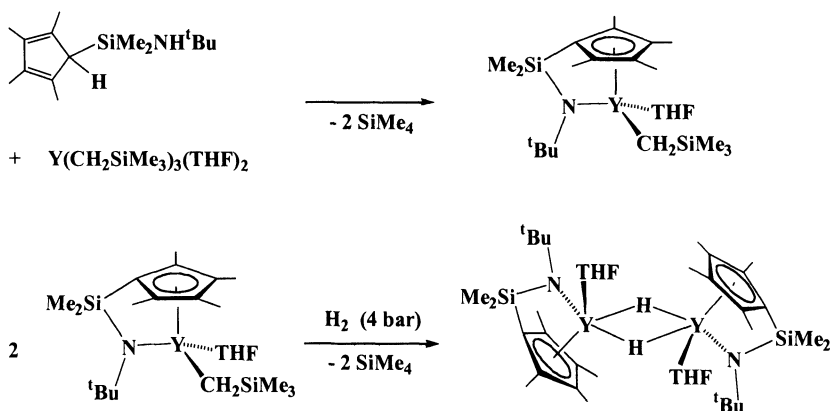
The double coordination of the linked amido-cyclopentadienyl ligands sometimes hampers the synthesis of the desired mono(ligand) complexes. Group 4 metals give neutral C_2 -symmetric metallocene complexes $[\text{M}(\eta^5\text{:}\eta^1\text{-C}_5\text{R}_4\text{ZNR}')_2]$ [22] whereas the heavier group 3 metals give rise to anionic complexes of the type $[\text{M}(\eta^5\text{:}\eta^1\text{-C}_5\text{R}_4\text{ZNR}')_2]^-$. Such complexes form exclusively when tridentate ligands of the type $\text{C}_5\text{R}_4\text{SiMe}_2\text{NCH}_2\text{CH}_2\text{X}$ ($\text{X} = \text{OMe, NMe}_2$) are used [23]. The reaction of anhydrous yttrium or lutetium trichloride with $\text{Li}_2(\text{C}_5\text{R}_4\text{SiMe}_2\text{NCH}_2\text{CH}_2\text{X})$ produces, in high yields, hydrocarbon-soluble heterobimetallic complexes of the composition $\text{Li}[\text{M}(\eta^5\text{:}\eta^1\text{-C}_5\text{R}_4\text{SiMe}_2\text{NCH}_2\text{CH}_2\text{X})_2]$ ($\text{M} = \text{Y, Lu}$) in which the metallocene unit tightly coordinates the lithium ion together with the ligand side chains.

The half-sandwich yttrium complex $(\eta^5\text{:}\eta^1\text{-C}_5\text{Me}_4\text{SiMe}_2\text{N}^t\text{Bu})\text{Y}(\text{CH}_2\text{SiMe}_3)\text{-}(\text{THF})$ along with tetramethylsilane can be obtained from the σ -bond metathesis between $\text{Y}(\text{CH}_2\text{SiMe}_3)_3(\text{THF})_2$ with $(\text{C}_5\text{Me}_4\text{H})\text{SiMe}_2\text{NH}^t\text{Bu}$. Hydrogenolysis of $(\eta^5\text{:}\eta^1\text{-C}_5\text{Me}_4\text{SiMe}_2\text{N}^t\text{Bu})\text{Y}(\text{CH}_2\text{SiMe}_3)(\text{THF})$ in pentane at room temperature afforded the dimeric hydrido complex $[(\eta^5\text{:}\eta^1\text{-C}_5\text{Me}_4\text{SiMe}_2\text{N}^t\text{Bu})\text{YH}(\text{THF})_2]_2$ (Scheme 5) [24]. $[(\eta^5\text{:}\eta^1\text{-C}_5\text{Me}_4\text{SiMe}_2\text{N}^t\text{Bu})\text{YH}(\text{THF})_2]_2$ exists as a 4:1 mixture of two asymmetric diastereomers in toluene- d_8 solution. The crystal contains racemic pairs of C_2 -symmetric homochiral dimers. Thus the two linked amido-cyclopentadienyl yttrium units are connected by two hydrogen atoms in a *transoid* fashion.

Table 4.

| Monomer | [Mon]/[Y] | % Yield | $10^{-3} M_n$ | M_w/M_n | % mm | % mr | % rr |
|-----------------------------|-----------|---------|---------------|-----------|------|------|------|
| <i>tert</i> -butyl acrylate | 95 | 85 | 25 | 1.56 | 21 | 50 | 29 |
| <i>tert</i> -butyl acrylate | 201 | 90 | 38 | 1.61 | 25 | 49 | 26 |
| acrylonitrile | 328 | 24 | 3.3 | - | 27 | 41 | 32 |
| acrylonitrile | 198 | 48 | 5.0 | - | 30 | 44 | 26 |

a) Reaction conditions: temperature 25 °C, reaction time 16 h in toluene. b) Reaction conditions: temperature -30 °C, reaction time 48 h in toluene.



Scheme 5.

Ethene as well as α -olefins such as 1-hexene or styrene react sluggishly with alkyl complexes $(\eta^5\text{-}\eta^1\text{-}C_5Me_4SiMe_2N^tBu)Y(CH_2SiMe_3)(THF)$ (25 °C, C_6D_6 , several days), but are not unexpectedly polymerized by the hydride complex $[(\eta^5\text{-}\eta^1\text{-}C_5Me_4SiMe_2N^tBu)YH(THF)]_2$. However, in contrast to the lanthano-cene hydride and alkyl complexes, $(\eta^5\text{-}\eta^1\text{-}C_5Me_4SiMe_2N^tBu)Y(CH_2SiMe_3)(THF)$ catalyzes the polymerization of the polar monomers *tert*-butylacrylate and acrylonitrile (Table 4). *tert*-Butylacrylate is polymerized in the presence of either $(\eta^5\text{-}\eta^1\text{-}C_5Me_4SiMe_2N^tBu)Y(CH_2SiMe_3)(THF)$ or $[(\eta^5\text{-}\eta^1\text{-}C_5Me_4SiMe_2N^tBu)YH(THF)]_2$ at temperatures as low as -30 °C (i. e., well below the decomposition temperature) to give poly(*tert*-butylacrylate) in high yields and with molecular weights $M_n > 20000$. Initiation seems to be somewhat slower when the hydride complex $[(\eta^5\text{-}\eta^1\text{-}C_5Me_4SiMe_2N^tBu)YH(THF)]_2$ is used. The molecular weight distributions of the resulting polymers are in the range of 1.5–2.0 and the polymer microstructure as judged by ^{13}C NMR spectroscopy is predominantly atactic. An intense red solution forms as soon as acrylonitrile is added to a toluene solution of $(\eta^5\text{-}\eta^1\text{-}C_5Me_4SiMe_2N^tBu)Y(CH_2SiMe_3)(THF)$, followed by the precipitation of yellow, atactic polyacrylonitrile. Rapid chain propagation appears to be preceded by a slow initiation step where the coordinated THF at the yttrium center is substituted by the monomer to generate the active species, a keteneiminato complex $(\eta^5\text{-}\eta^1\text{-}C_5Me_4SiMe_2N^tBu)Y(N=CCHCH_2R)$, by 1,4-insertion.

Conclusion

The introduction of the linked amido-cyclopentadienyl ligand as a replacement for the bridged bis(cyclopentadienyl) ligand in *ansa*-metallocenes has led to a new

class of homogeneous olefin polymerization catalysts. By now it is obvious that the complexes of the type $M(\eta^5:\eta^1-C_5R_4ZNR')L'_mX'_n$ exhibit properties intermediate to those of *ansa*-metallocenes and half-sandwich complexes. Many coordination chemical aspects, however, have not been fully explored yet and it remains to be seen whether this ligand framework provides a metal template as versatile as the ubiquitous metallocene unit $M(\eta^5-C_5R_5)_2$. On the other hand, the linked amido-cyclopentadienyl complexes may be also regarded as a hybrid between *ansa*-metallocenes and complexes containing chelating bis(amido) ligands derived from the diamines $R'HN(Z)NHR'$. The latter type of complexes has only just begun to emerge as yet another type of replacement for the bis(cyclopentadienyl) ligand and as single-site olefin catalyst system with novel features complementary to both metallocenes and linked amido-cyclopentadienyl complexes [25].

Acknowledgment

Financial support by the Bundesministerium für Bildung, Wissenschaft, Forschung und Technologie (project no. 03N1028), the BASF AG (Kunststofflaboratorium), the European Community, and the Fonds der Chemischen Industrie is acknowledged. I thank all my co-workers, past and present, for contributing to this research and Professor Rolf Mülhaupt and his group in Freiburg for collaborative efforts.

References

1. P. J. Shapiro, E. E. Bunel, W. P. Schaefer, J. E. Bercaw, *Organometallics* **1990**, *9*, 867.
P. J. Shapiro, W. D. Cotter, W. P. Schaefer, J. A. Labinger, J. E. Bercaw, *J. Am. Chem. Soc.* **1994**, *116*, 4623.
2. (a) H.-H. Brintzinger, D. Fischer, R. Mülhaupt, B. Rieger, R. Waymouth, *Angew. Chem.* **1995**, *107*, 1255, *Angew. Chem. Int. Ed. Engl.* **1995**, *34*, 1652. (b) P. C. Möhring, N. J. Coville, *J. Organomet. Chem.* **1994**, *479*, 1.
3. (a) J. Okuda, *Chem. Ber.* **1990**, *123*, 1649. (b) J. Okuda, *Comments Inorg. Chem.* **1994**, *16*, 185. (c) J. Okuda, T. Eberle, Half-Sandwich Complexes as Metallocene Analogs. In: *Metallocenes* (Eds. Halterman, R. L.; Togni, A.), Wiley-VCH, 1998, p. 418-57.
4. (a) J. C. Stevens, F. J. Timmers, G. W. Rosen, G. W. Knight, S. Y. Lai (Dow Chemical Co.), *European Patent Application, EP 0 416 815 A2*, **1991** (filed August 30, 1990). (b) J. A. Canich (Exxon Chemical Co.), *European Patent Application, EP 0 420 436 A1*, **1991** (filed September 10, 1990).
5. (a) J. C. Stevens, *Metcon 93*, Houston, 26-28 May, **1993**, p. 157. (b) J. C. Stevens, *Stud. Surface Sci. Cat.* **1994**, *89*, 277.
6. (a) K. Soga, T. Uozumi, S. Nakamura, T. Toneri, T. Teranishi, T. Sano, T. Arai, *Macromol. Chem. Phys.* **1996**, *197*, 4237. (b) F. G. Sernetz, R. Mülhaupt, F. Amor, T. Eberle, J. Okuda, *J. Polym. Sci., Part A* **1997**, *35*, 1571. (c) A. L. McKnight, M. A. Masood, R. M. Waymouth, *Organometallics* **1997**, *16*, 2879. (d) T. D. Shaffer, J. A. Canich, K. R. Squire, *Macromolecules* **1998**, *31*, 5145. (e) B. A. Harrington, D. J. Crowther, *J. Mol. Cat.* **1998**, *128*, 79.

7. D. W. Carpenetti, L. Kloppenburg, J. T. Kupec, J. L. Petersen, *Organometallics* **1996**, *15*, 1572.
8. (a) A. K. Hughes, A. Meetsma, J. H. Teuben, *Organometallics* **1993**, *12*, 1936. (b) P.-J. Sinnema, L. van der Veen, A. L. Spek, N. Veldman, J. H. Teuben, *Organometallics* **1997**, *16*, 4245.
9. S. Ciruelos, T. Cuenca, P. Gomez-Sal, A. Manzanero, P. Royo, *Organometallics* **1995**, *14*, 177.
10. J. Okuda, S. Verch, T. P. Spaniol, *Chem. Ber.* **1996**, *129*, 1429.
11. J. Okuda, T. Eberle, T. P. Spaniol, *Chem. Ber.* **1997**, *130*, 209.
12. R. M. Pulpi, J. N. Coalter, J. L. Petersen, *J. Organomet. Chem.* **1995**, *497*, 17.
13. (a) K. E. du Plooy, U. Moll, S. Wocadlo, W. Massa, J. Okuda, *Organometallics* **1995**, *14*, 3129. (b) F. Amor, T. P. Spaniol, J. Okuda, *Organometallics* **1997**, *16*, 4765. (c) F. Amor, K. E. du Plooy, T. P. Spaniol, J. Okuda, *J. Organomet. Chem.* **1998**, *558*, 139.
14. J. Okuda, K. E. du Plooy, W. Massa, H.-C. Kang, U. Rose, *Chem. Ber.* **1996**, *129*, 275.
15. F. Amor, A. Butt, K. E. du Plooy, T. P. Spaniol, J. Okuda, *Organometallics* in press.
16. (a) Y.-X. Chen, C. L. Stern, S. Yang, T. J. Marks, *J. Am. Chem. Soc.* **1996**, *118*, 12451. (b) L. Jia, X. Yang, C. L. Stern, T. J. Marks, *Organometallics* **1997**, *16*, 842.
17. P.-J. Sinnema, K. Liekelema, O. K. B. Stall, B. Hessen, J. H. Teuben, *J. Mol. Cat.* **1998**, *128*, 143.
18. J. Okuda, T. Eberle, T. P. Spaniol, *Eur. J. Inorg. Chem.* **1998**, 237.
19. A. D. Horton, J. de With, A. J. van der Linden, H. van de Weg, *Organometallics* **1996**, *15*, 2672.
20. (a) Pellicchia, C.; Immirzi, A.; Grassi, A.; Zambelli, A. *Organometallics* **1993**, *12*, 4473. (b) Bochmann, M.; Lancaster, S. J.; Hursthouse, M. B.; Malik, K. M. A. *Organometallics* **1994**, *13*, 2235.
21. A similar scenario was reported during the syndiospecific polymerization using the titanium catalyst $[\text{Ti}(\eta^5\text{-}\eta^x\text{-C}_5\text{Me}_4\text{CH}_2\text{CH}_2\text{Ph})\text{R}]^+$: J. C. Flores, J. S. Wood, J. C. W. Chien, M. D. Rausch, *Organometallics* **1996**, *15*, 4944.
22. J. Okuda, F. Amor, K. E. du Plooy, T. Eberle, K. C. Hultzsich, T. P. Spaniol, *Polyhedron* **1998**, *17*, 1073.
23. (a) K. C. Hultzsich, T. P. Spaniol, J. Okuda, *Organometallics* **1997**, *16*, 4845. (b) K. C. Hultzsich, T. P. Spaniol, J. Okuda, *Organometallics* **1998**, *17*, 485.
24. K. C. Hultzsich, T. P. Spaniol, J. Okuda, *Angew. Chem.* in press.
25. (a) J. D. Scollard, D. H. McConville, *J. Am. Chem. Soc.* **1996**, *118*, 10008. (b) R. Baumann, W. D. Davis, R. R. Schrock, *J. Am. Chem. Soc.* **1997**, *119*, 3830.

Late Transition Metal Catalysts for Olefin Polymerization

Oliver Pyrlík, Mattis Gosmann, Michael Arndt-Rosenau*

Institute for Technical and Macromolecular Chemistry
University of Hamburg
Bundesstr. 45, 20146 Hamburg
e-mail: arndt@chemie.uni-hamburg.de

Abstract. The polymerization behavior of $[(2\text{-}^{\text{tert}}\text{BuPh})_2\text{AND}]\text{NiBr}_2$ and $[(2,6\text{-}^{\text{iso}}\text{Pr}_2\text{Ph})_2\text{AND}]\text{NiBr}_2$ activated by methylaluminoxane (MAO) and diethylaluminium chloride (DEAC) are investigated using central composite experimental designs to model response surfaces for catalytic activity and polymer properties. Beside the catalyst and experimental conditions the catalytic performance is influenced by the choice of the cocatalyst. DEAC activation yields lower catalytic activity and polymers featuring a lower molecular weight but increased branching than MAO activation.

1. Introduction

Diimine-complexes of Ni and Pd in combination with methylaluminoxane have recently been reported to catalyze the polymerization of ethene, α -olefins and cycloolefins [1-3]. We have used experimental design techniques to study and quantify the influence of polymerization conditions on the polymerization behavior of $[(2\text{-}^{\text{tert}}\text{BuPh})_2\text{AND}]\text{NiBr}_2$ and $[(2,6\text{-}^{\text{iso}}\text{Pr}_2\text{Ph})_2\text{AND}]\text{NiBr}_2$ activated by methylaluminoxane (MAO) and diethylaluminium chloride (DEAC).

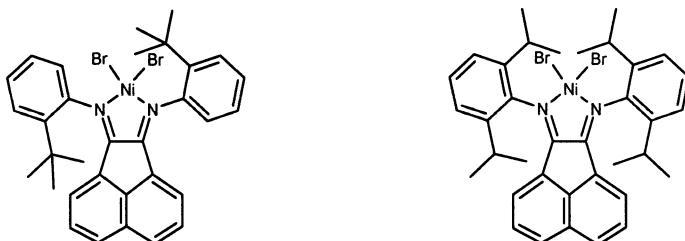


Fig. 1. Structure of the catalyst-precursors used in this study: $[(2\text{-}^{\text{tert}}\text{BuPh})_2\text{AND}]\text{NiBr}_2$ (left) and $[(2,6\text{-}^{\text{iso}}\text{Pr}_2\text{Ph})_2\text{AND}]\text{NiBr}_2$ (right).

A *central composite design* provides the experimental data needed to evaluate the *response surface* showing the effects the experimental conditions (“factors”) have on the target properties (e.g. catalyst activity, melting point, microstructure, etc..) using a small number of planned experiments [4].

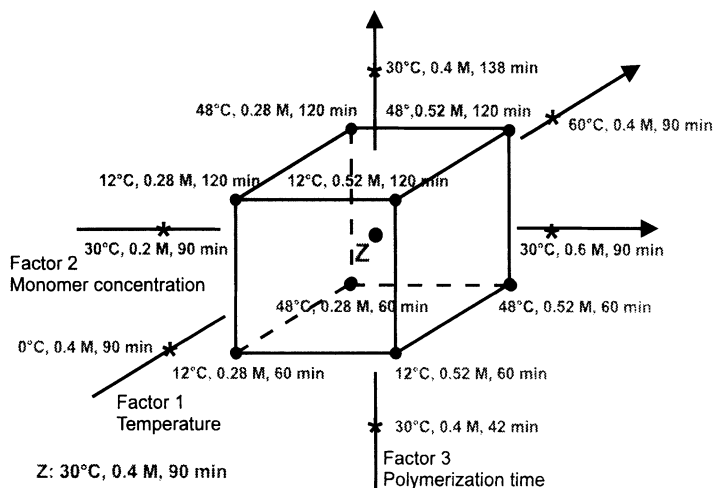


Fig. 2. Schematic drawing of the experimental conditions used for the central composite design. Temperature is varied from 0 to 60°C, ethene concentration from 0.2 to 0.6 mol/l and polymerization time from 42 to 138 min.

An empirical model is used to describe the target property Ψ as a function of the factors. In our study the factors were temperature (T), ethene concentration (c), and polymerization time (t). Therefore Ψ is approximated by:

$$\Psi = [k_1 \cdot T + k_2 \cdot c + k_3 \cdot t] + [k_4 \cdot T \cdot c + k_5 \cdot T \cdot t + k_6 \cdot c \cdot t] + [k_7 \cdot T^2 + k_8 \cdot c^2 + k_9 \cdot t^2] + k_{10} \quad (1)$$

2. Catalytic Activity

One of the important characteristics of a catalyst is the catalytic activity expressed in turnovers or, more commonly used in polymerization catalysis, kg polymer produced per mol of catalyst and hour. If the rate of polymerization is constant and the concentration of active sites equals that of the catalyst the catalytic activity, which is calculated from the yield, is equivalent to the rate of polymerization. The rate of polymerization r_p depends on the reaction rate constant k_p , the monomer concentration and the concentration of active sites Ni^* :

$$r_p = k_p \cdot [Ni^*]^n \cdot [ethene]^m \quad (2)$$

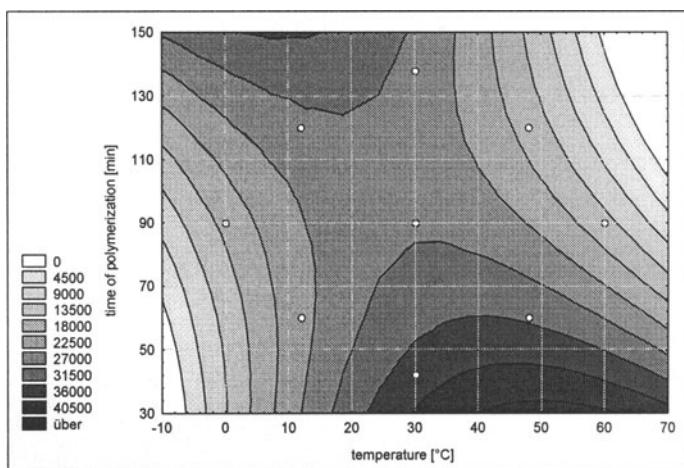


Fig. 3. Response surface showing the influence of the temperature and polymerization time on the catalytic activity of $[(2,6\text{-isoPr}_2\text{Ph})_2\text{AND}]\text{NiBr}_2$ using MAO as cocatalyst at an ethene concentration of 0.5 mol/l.

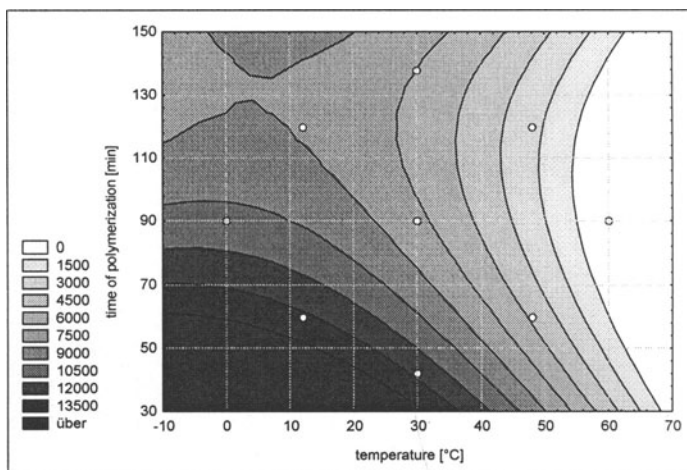


Fig. 4. Response surface showing the influence of the temperature and polymerization time on the catalytic activity of $[(2\text{-tertBuPh})_2\text{AND}]\text{NiBr}_2$ using MAO as cocatalyst at an ethene concentration of 0.5 mol/l.

$[(2,6\text{-isoPr}_2\text{Ph})_2\text{AND}]\text{NiBr}_2$, independent of the type of activator, has a much higher activity than $[(2\text{-tertBuPh})_2\text{AND}]\text{NiBr}_2$ under the same experimental conditions. Activation by DEAC yields strongly decreased activities independent on the Ni-compound. The experimental factors found to influence the catalytic

activity significantly are the monomer concentration and a temperature-polymerization time interaction. The observed temperature time interaction indicates a change of the number of active sites during polymerization time. This is clearly seen in the kinetic profiles of the polymerization.

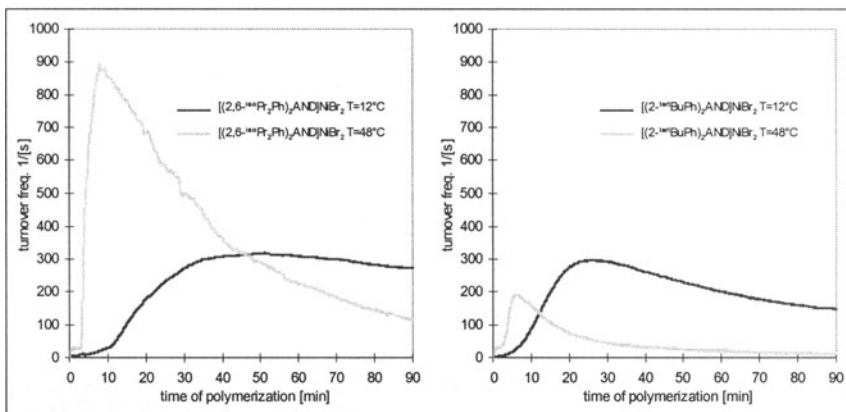


Fig. 5. Kinetics of ethene polymerization by $[(2,6\text{-}^{iso}\text{Pr}_2\text{Ph})_2\text{AND}]\text{NiBr}_2$ and $[(2\text{-}^{tert}\text{BuPh})_2\text{AND}]\text{NiBr}_2$ activated with MAO (0.26 mol/l ethene).

At 48°C the polymerization rate of $[(2,6\text{-}^{iso}\text{Pr}_2\text{Ph})_2\text{AND}]\text{NiBr}_2/\text{MAO}$ reaches its maximum within a few minutes followed by a rapid decrease. At 12°C an induction period is observed and the maximum rate of polymerization is reached after about 35–40 min followed by almost no deactivation. Catalyst deactivation is even more dramatic for $[(2\text{-}^{tert}\text{BuPh})_2\text{AND}]\text{NiBr}_2/\text{MAO}$: at 12°C an induction period is observed before the rate of polymerization reaches its maximum which is followed by significant decay; at 48°C the maximum activity is even lower than that at 12°C indicating a strong decrease of the maximum number of active centers.

3. Microstructure of the Polymers

One of the most interesting features of the diimine-Ni(II) catalyzed polymerization of ethene is chain branching that occurs due to isomerization of the growing chains. The central composite designs showed that the total number of branches depends on the temperature and the monomer concentration. Polymerizations carried out at elevated temperature and low monomer concentration result in highly branched polyethylenes. The melting point of these products decreases from about 140°C (linear) to 30°C (branched). The use of DEAC as cocatalyst instead of MAO results in extended branching. Notable is that the fraction of long branches (hexyl- and longer) is increased significantly. The polymers produced at elevated temperatures and low monomer concentration are amorphous and show glass transition temperatures between –60°C and –40°C.

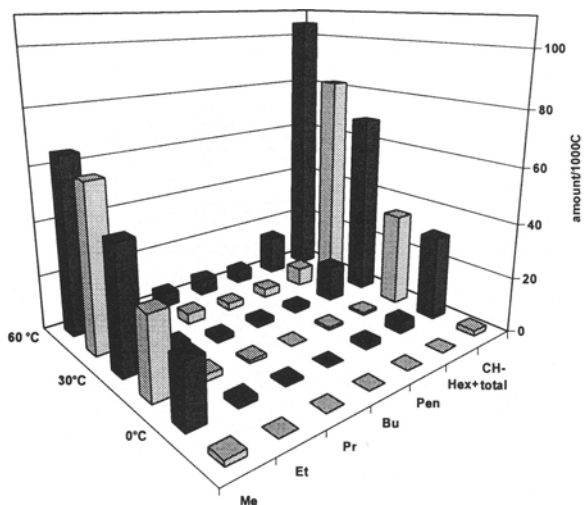


Fig. 6. Influence of the temperature of polymerization on the microstructure of polyethene produced by $[(2,6\text{-}^{i\text{iso}}\text{Pr}_2\text{Ph})_2\text{AND}]\text{NiBr}_2$ using MAO (■) and DEAC (■) as cocatalyst (0.4 mol/l ethene).

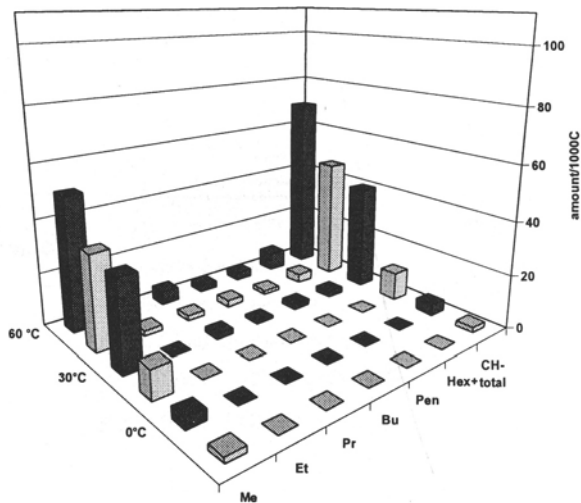


Fig. 7. Influence of the temperature of polymerization on the microstructure of polyethene produced by $[(2\text{-}^{t\text{ert}}\text{BuPh})_2\text{AND}]\text{NiBr}_2$ using MAO (■) and DEAC (■) as cocatalyst (0.4 mol/l ethene).

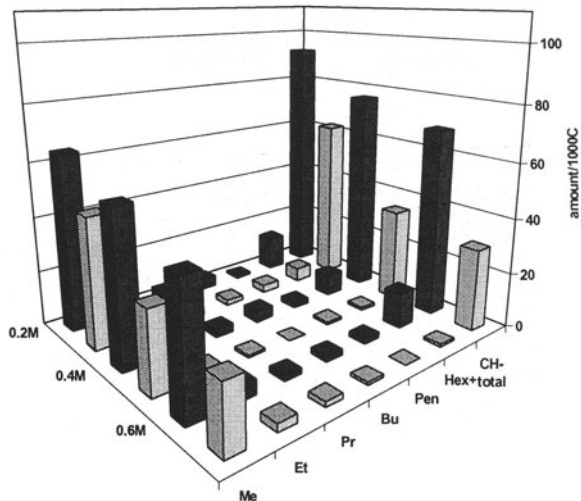


Fig. 8. Influence of the monomer concentration on the microstructure of polyethene produced by $[(2,6\text{-}i\text{Pr}_2\text{Ph})_2\text{AND}]\text{NiBr}_2$ using MAO (■) and DEAC (■) as cocatalyst (temperature of polymerization 30°C).

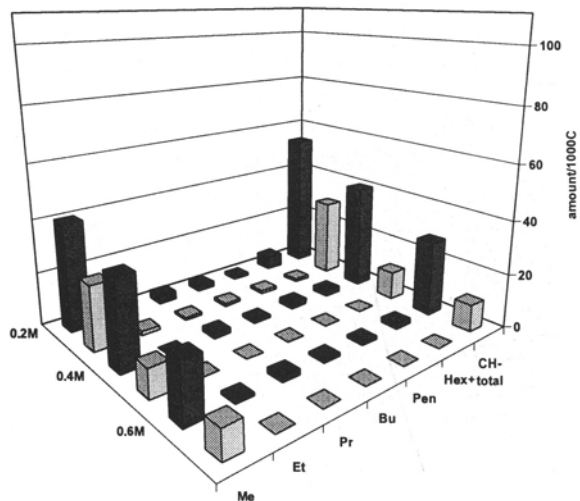


Fig. 9. Influence of the monomer concentration on the microstructure of polyethene produced by $[(2\text{-}t\text{er}t\text{BuPh})_2\text{AND}]\text{NiBr}_2$ using MAO (■) and DEAC (■) as cocatalyst (temperature of polymerization 30°C).

4. Molecular weight of the Polymers

The molecular weights of the polyethenes produced by all four catalyst systems only depend on the temperature of polymerization. They show a rapid decrease with increasing temperature ranging from about 1.5-2 mio g/mol at temperatures of 0°C to about 1-200000 at 60°C.

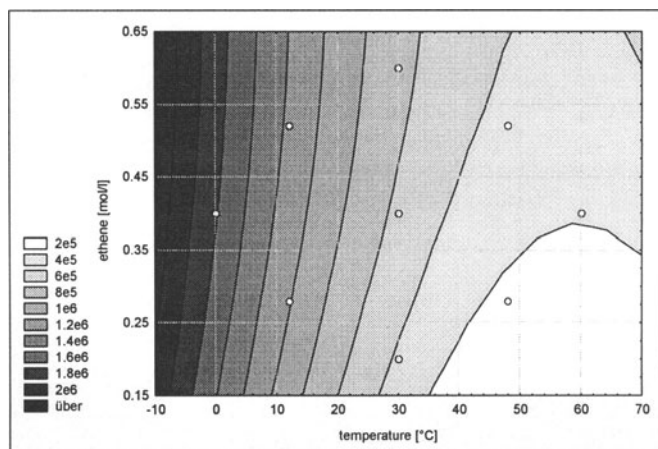


Fig. 10. Response surface showing the influence of the temperature and ethene concentration on the molecular weight of polyethene produced by [(2,6-*iso*Pr₂Ph)₂AND]NiBr₂/MAO.

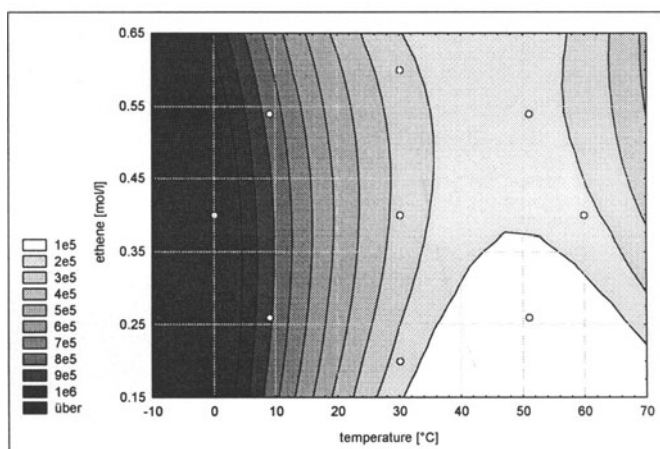


Fig. 11. Response surface showing the influence of the temperature and ethene concentration on the molecular weight of polyethene produced by [(2,6-*iso*Pr₂Ph)₂AND]NiBr₂/DEAC.

Polymerization using $[(2,6\text{-}^{180}\text{Pr}_2\text{Ph})_2\text{AND}]\text{NiBr}_2$ yields higher molecular weights than polymerization by $[(2\text{-}^{\text{tert}}\text{BuPh})_2\text{AND}]\text{NiBr}_2$. The extended amount of branching obtained by using DEAC as cocatalyst has to be paid not only by the price of decreased catalytic activity but also by lowered molecular weights.

5. Conclusion

Design of experiments has been shown to be a valuable method to study the polymerization behavior of Ni-based catalysts. The use of response surface methods enables a quantitative correlation of the experimental setup with the catalysts and polymer properties [5]. Further investigations in order to classify diimine based catalysts using these correlations are in progress.

For the specific cases under investigation we observed that the degree of branching depends on the temperature, concentration of ethene and the diimine ligand as well as on the cocatalyst used. The influence of the cocatalyst indicates that the kinetic schemes proposed until now are not complete.

Both catalyst precursors enable the production of highly linear UHMWPE at low temperatures ($<0^\circ\text{C}$), especially if activated by MAO. At elevated temperatures highly branched amorphous polymers of significantly lower molecular weights are produced.

References

- [1] a) L.K. Johnson, C.M. Killian, M. Brookhart, *J. Am. Chem. Soc.* 117 (1995), 6414; b) L.K. Johnson, S. Mecking, M. Brookhart, *J. Am. Chem. Soc.* 118 (1996), 267; c) C.M. Killian, D.J. Tempel, L.K. Johnson, M. Brookhart, *J. Am. Chem. Soc.* 118 (1996), 11664; C.M. Killian, L.K. Johnson, M. Brookhart, *Organometallics* 16 (1997), 2005; M.S. Brookhart, L.K. Johnson, C.M. Killian, S.D. Arthur, J. Feldman, E.F. McCord, K.A. Kreutzer, A.M. Bennett, B.E. Coughlin, S.D. Ittel, A. Parthasarathy, D.J. Tempel; Pat Appl. WO 96/23010 (1996) to DuPont.
- [2] a) C. Pellecchia, A. Zambelli; *Macromol. Rapid. Commun.* 17 (1996), 333; b) C. Pellecchia, A. Zambelli, L. Oliva, D. Pappalardo; *Macromolecules* 29 (1996), 6990.
- [3] D. Pappalardo, M. Mazzeo, C. Pellecchia; *Macromol. Rapid. Commun.* 18 (1997), 1017.
- [4] G.E.P. Box, N.R. Draper: "Empirical Model Building and Response Surface", J. Wiley Sons, New York (1987).
- [5] Details of the quantitative correlations, significance evaluation, and experimental results will be given in subsequent publications. M. Arndt-Rosenau, O. Pyrlík in preparation.

3. Homogeneous Catalysis, Mechanism of Polymerization

Chain growth in zirconocene-catalyzed olefin polymerization - DFT studies on possible reaction paths and the influence of a second olefin ligand

Marc-Heinrich Prosenč*, Frank Schaper and Hans-Herbert Brintzinger

Fakultät für Chemie, Universität Konstanz, D-78457 Konstanz

e-mail: marc.prosenč@uni-konstanz.de; present address: Department of Chemistry, University of North Carolina, Chapel Hill, North Carolina 27599, USA.

Abstract. To clarify the nature of the reaction barriers which limit the rate of propene insertion into the Zr-C bond of an alkyl zirconocene cation, the energy surface available to a species $[(C_2H_5)_2Zr\text{-ethyl(propene)}]^+$ has been explored as a function of the orientation of the ethyl C(α)-C(β) bond and of the distance between the ethyl-C(α) and the propene-C(2) atoms. The two-dimensional energy surface thus obtained shows three local minima each containing a distinct intermediate: (i) The "starting" geometry **I1** arises by coordination of propene to the β -agostic resting state **I0** and has the ethyl group still bound to the Zr center by a β -agostic bond, (ii) a "freed" species **I2** has a widely rotatable ethyl group and an energy close to that of geometry **I1**, but is separated from it by a transition state **T1** with an activation barrier of 20-25 kJ/mol and (iii) the γ -agostic insertion product **I3**, with an energy of ca. -30 kJ/mol, which is reached *via* an α -agostic transition state **T2**, with an activation energy of 25-30 kJ/mol. Especially for catalyst systems with sterically burdened zirconocene and alkyl moieties, the olefin insertion step **I2**→[**T2**]→**I3** will be rate-limiting for polymer-chain growth. We have further explored the effects of a second propene in the vicinity of the cation $[(C_2H_5)_2Zr\text{-ethyl(propene)}]^+$ on the course of polymer-chain growth. Whereas little interaction is found for the corresponding states **I1^P** and **I2^P**, a weak but significant binding of the external olefin arises in the transition state **T2^P**. Approach to the insertion product **I3^P**, finally, is associated with a steep descent in energy, which signifies attraction of the external olefin toward the metal. As the final state **I3^P** has the olefin already in place for the next insertion, chain growth can now proceed with increased efficiency through an alternative catalytic cycle involving only intermediates **I2^P** and **I3^P**. A kinetic analysis of polymer formation rates based on the operation of both catalytic cycles leads to an estimate of kinetic and equilibrium constants compatible with the observed olefin concentration exponents of 1.4-1.8 in the polymer formation rate law. Other experimental observations are discussed in relation to these alternative reaction paths in zirconocene-catalyzed α -olefin polymerization.

Introduction

Kinetic studies on zirconocene-based olefin polymerization catalysts have repeatedly revealed that the rates of monomer consumption in these systems depend on the monomer concentration to an order higher than one [1-4]. These *prima-facie* inexplicable observations have given rise to the proposal, made by Ystenes [5], that the insertion of an olefin into the metal-alkyl bond of an active polymerization catalyst is aided - or "triggered" - when a second olefin coordinates to the metal center. This proposal has met with considerable scepticism, however, since molecular model considerations suggest that it is impossible for steric reasons to have two olefin ligands simultaneously coordinated to an alkyl-zirconocene cation. Recent reports that activities of high-performance, industrially utilized zirconocene catalysts also depend on monomer concentrations to an order between 1 and 2 [6-8], have generated renewed incentive, however, to search for an explanation of these phenomena.

In order to explore the nature of the reaction barriers encountered along the reaction paths followed by typical zirconocene-based catalysts, as well as possible ways in which these might be influenced by a second olefin, we have undertaken a theoretical study of the energy surface accessible to a cationic alkyl-zirconocene olefin reaction complex, by means of density-functional methods. In the following we report the results of these studies which appear to furnish plausible explanations for a number of experimental data reported for these catalytic reaction systems.

Computational Methods

For all calculations on the density functional theory level, the Program RIDFT was used [9]. Energies and geometries were developed on the nonlocal level of theory. For geometry optimization the energies were corrected for nonlocal exchange according to Becke [10,11] and for nonlocal correlation according to Perdew (BP-86) [12] in the selfconsistent procedure. Final energies were corrected for nonlocal exchange according to Becke [10,11] and for nonlocal correlation according to the procedure of Lee, Yang and Parr (B-LYP) [13]. The SVP-split valence base set was used for C and H atoms [14,15]. For zirconium we used an effective core potential base set (ECP-28-mwb) with triple-zeta functions for the valence region and an additional d-polarization function [14]. For the J_{ij} -term approximation an additional auxiliary base set was used [9,16].

A two-dimensional energy surface for an ethyl zirconocene cation containing a propene ligand, $[(C_5H_5)_2Zr-CH_2CH_3(H_2C=CHCH_3)]^+$, was generated by varying the distance between the inner olefin terminus and the Zr-bound ethyl C atom, $d(C2-C3)$, and the rotation of the ethyl group about its Zr-C bond, $\theta(C1-Zr-C3-C4)$, in steps of ca 20 pm for d and of ca 10° for θ (Fig. 1). Each set was

optimized until the maximum internal energy gradient was lower than $2 \cdot 10^{-4}$. For the reaction path leading from the π -complex **I2** to the final product **I3**, additional energies were calculated separately, using only $d(\text{C2-C3})$ as an independent variable whilst all other geometry parameters being allowed to relax.

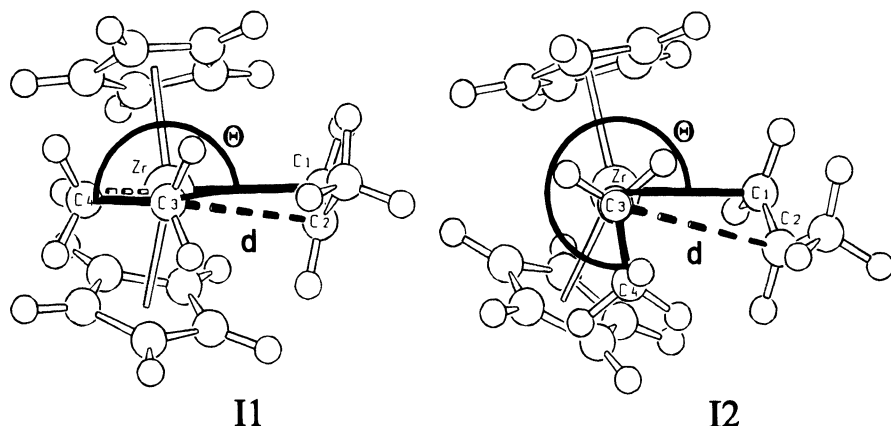


Fig. 1. Definition of the geometry parameters $d(\text{C2-C3})$ and $\theta(\text{C1-Zr-C3-C4})$,

Stationary points were checked by frequency calculations which resulted in no negative force constant for the minima and only one for the transition state. Calculations of the force constant matrix were carried out numerically with double finite differences with a step width of 5 pm to diminish numerical errors in the lower vibrational region (0 - 500 cm^{-1}).

Results and Discussion

1. Reaction path with a single propene ligand.

To characterize the nature of the reaction barriers which limit the rate of the Zr-mediated growth of a polypropene chain, we have first analyzed the geometries and trajectories accessible for a cationic alkyl zirconocene species containing a single propene ligand. Although a growing polypropene chain would probably be more closely approximated by an isobutyl group, we have chosen for this study, as a reasonably complete yet computationally still tractable system, a reaction complex containing a Zr-bound ethyl group, $[(\text{C}_5\text{H}_5)_2\text{Zr-ethyl (propene)}]^+$. Due to the presence of CH_3 substituents at its olefin and its alkyl ligands, this complex contains the elements necessary to define the essential interligand interactions.

To assess the possible fates of such a species, we have chosen as relevant reaction coordinates the distance from the inner olefin terminus C(2) to the Zr-bound alkyl atom C(3), $d(\text{C}(2)\text{-C}(3))$, and the dihedral angle between the $\text{C}(\alpha)\text{-C}(\beta)$ chain segment and the bond from Zr to the outer olefin terminus C(1), $\theta(\text{C}(1)\text{-Zr-C}(3)\text{-C}(4))$ (see Fig. 1). By variation of d between 150 and 350 pm and of θ between 180° and 300° , we obtain the two-dimensional energy surface mapped in Fig. 2.

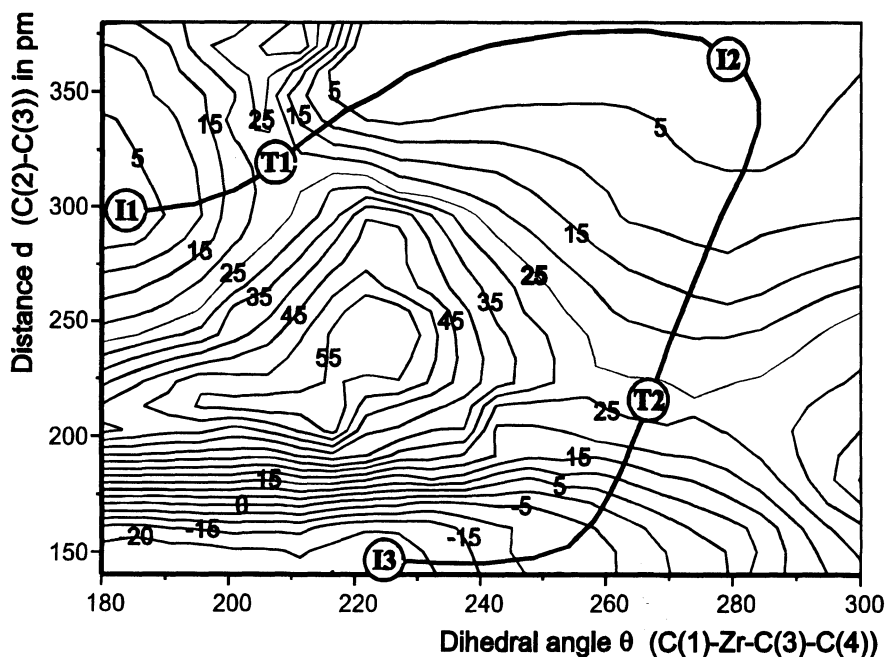


Fig. 2. Two-dimensional energy surface of a cation $[(\text{C}_5\text{H}_5)_2\text{Zr-ethyl (propene)}]^+$ as a function of the geometry parameters $d(\text{C}(2)\text{-C}(3))$ and $\theta(\text{C}(1)\text{-Zr-C}(3)\text{-C}(4))$.

This energy surface contains three distinct minima, each corresponding to a discrete reaction intermediate with geometries which are listed in Table 1 and graphically represented in Fig. 3:

- a "starting" geometry **I1**, in which a short Zr-H contact of 204 pm, an elongated $\text{C}(\beta)\text{-H}$ distance of 116 pm and a decreased $\text{Zr-C}(3)\text{-C}(4)$ angle of 84° are indicative of a β -agostic interaction.
- a "freed" geometry **I2**, which has a freely rotatable ethyl group and an energy close to that of the starting geometry **I1**,
- the insertion product **I3**, with an energy of ca. -30 kJ/mol, for which a short $\text{Zr-H}(\gamma)$ contact of 222 pm and a long $\text{C-H}(\gamma)$ bond distance of 116 pm indicate a strong γ -agostic bond of the newly formed alkyl chain to the Zr center.

Table 1. Distances (in pm), bond and dihedral angles (in degree) and relative energies (in kJ/mol) calculated for propene insertion intermediates and transition states in a cation [(C₅H₅)₂Zr-ethyl(propene)]⁺ with one propene ligand (**I1-I3**, c. f. Fig. 2 and 3) and in a cation [(C₅H₅)₂Zr-ethyl(propene)₂]⁺ with two propene ligands (**I2^P-I3^P**, c. f. Fig. 5).

| | I1 | I2 | T2 | I3 | I2^P | T2^P | I3^P ≈ | I2^d |
|-------------------|-----------|------------------|-----------|------------------|-----------------------|-----------------------|-------------------------|-----------------------|
| C(2)-C(3) | 292 | 356 | 210 | 156 | 362 | 210 | 155 | 380 ^d |
| Zr-C(1) | 274 | 264 | 232 | 225 | 263 | 232 | 229 | 264 ^d |
| Zr-C(2) | 301 | 311 | 266 | 291 ^a | 314 | 266 | 348 ^a | 321 ^d |
| Zr-C(3) | 231 | 228 | 239 | 285 ^a | 228 | 239 | 401 ^a | 229 ^d |
| Zr-H(agost) | 213 | _b | 207 | 217 | _b | 208 | _b | - |
| C-H(agost) | 117 | 111 ^b | 116 | 115 | 111 ^b | 116 | 111 ^b | - |
| Zr-Z(1,2) | 224 | 223 | 223 | 223 | 223 | 222 | 223 | 223 ^d |
| Zr-C(5) | - | - | - | - | 526 | 482 | 264 | - |
| Zr-C(6) | - | - | - | - | 559 | 561 | 321 | - |
| Z(1)-Zr-Z(2) | 132 | 131 | 133 | 134 | 131 | 133 | 132 | 132 ^d |
| Zr-C(3)-C(4) | 84 | 140 | 137 | - | 124 | 137 | - | 129 ^d |
| C(1)-Zr-C(3)-C(4) | 178 | 219 | 266 | 224 ^c | 284 | 267 | 243 ^c | 297 ^d |
| C(2)-C(1)-Zr-C(3) | 20 | 4 | 6 | 21 ^c | 42 | 5 | 34 ^c | 61 ^d |
| Energy | 0 | +21 | +26 | -23 | -5 | +17 | -58 | -58 |

^a Non-bonding Zr-C distance; ^b no agostic Zr-H interaction present; ^c C(3) no longer connected to Zr; ^d C atoms renumbered for comparison with **I2**.

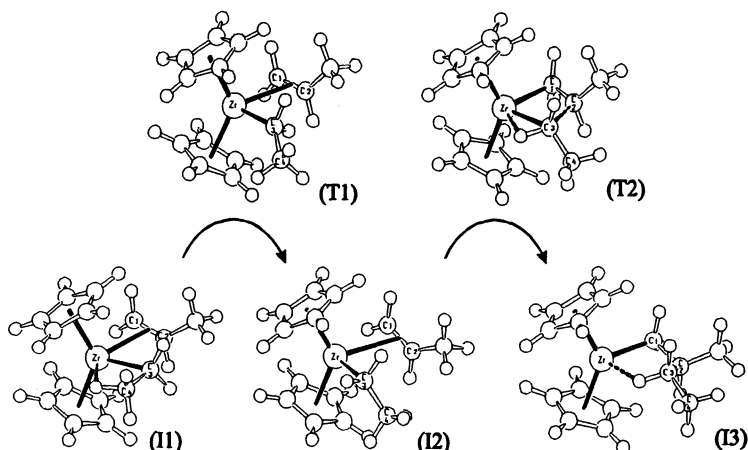


Fig. 3. Reaction sequence leading from an initial olefin complex with β -agostic ethyl group (I1) to the γ -agostic insertion product (I3)

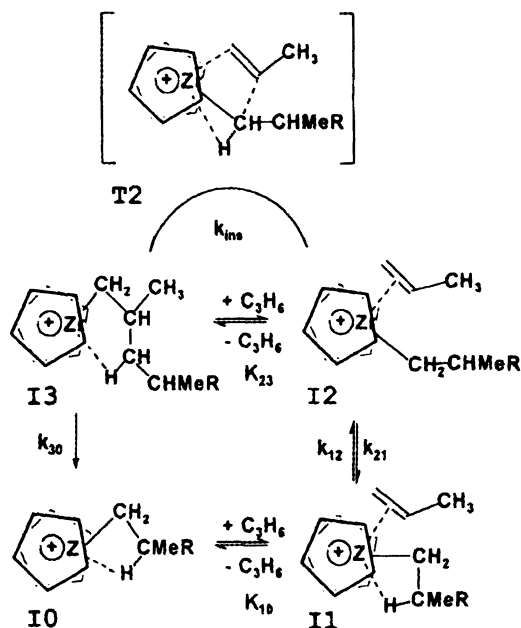
In a working catalyst system, π -complex I1 will arise through uptake of a propene ligand by the presumed resting state, i.e. by the cation $[(C_3H_5)_2Zr\text{-ethyl}]^+$, in which a β -agostic bond connects the alkyl ligand to the Zr atom. An increase of the dihedral angle θ from 180° in species I1 converts the latter to another π -complex I2, in which the β -H atom of the ethyl group is detached from the Zr center. For this species I2, in which the alkyl group can freely assume a wide range of θ values between ca. 220° and more than 320° , we find practically the same energy as for species I1. Apparently, an agostic interaction has lost most of its stabilizing effect in the presence of a π -bound olefin ligand and represents more of a steric burden now: To place five ligand atoms in the mid-plane of the zirconocene cation I1, the olefin CH_2 terminus and the ethyl CH_3 group have to be wedged into the narrow lateral parts of the metallocene framework. This mutual repulsion is apparent also from the short distance of only 300 pm, substantially below the sum of the Van-der-Waals radii, between the inner olefin and alkyl C atoms.

The rearrangement from I1 to I2 leads, as previously noted [21-24], over an activation barrier of ca. 20-25 kJ/mol. The transition state T1 for this process appears to be destabilized mainly by the necessity to move the ethyl group past one of the ring ligands with an unfavorably wide Zr-C(3)-C(4) angle of ca. 140° .

The relative energies of species I1 and I2 as well as that of the intervening transition state T1 will undoubtedly vary with the steric burdening of the alkyl group and the zirconocene ligand framework. Increased repulsive interactions will destabilize the β -agostic species I1 certainly more than the "freed" π -complex I2 and probably also more than the transition state T1 which lies between I1 and I2. For this reason, the β -agostic π -complex T1 will become less stable with respect to its conversion to I2, both in thermodynamic and in kinetic terms, the more a zirconocene catalyst is sterically encumbered.

From intermediate **I2**, the insertion of the propene ligand proceeds by way of transition state **T2**. A C(1)-H(α) bond elongated to 116 pm and a short Zr-H(α) distance of 211 pm document an α -agostic interaction for this state, in accord with experimental and theoretical data reported for this reaction sequence [17-23].

The insertion product **I3**, finally, contains the newly formed 2-methylbutyl chain in γ -agostic contact to the Zr center. While we have not investigated the further fate of this olefin-free species, previous studies leave is no doubts that it will rather rapidly decay to a species **I0** with a β -agostic bond [17-22]. Uptake of a new olefin ligand will then regenerate a homolog of species **I1** and thus complete the catalytic cycle represented in Scheme 1.



Scheme 1. Catalytic cycle for the polymerization of propene comprised of intermediates **I0-I3**

The energy of the insertion transition state **T2** is found to be only slightly higher (ca. 25 vs. 20 kJ/mol) than that of transition state **T1** for the rearrangement **I1**→**I2**. As discussed above, increased steric burdening of the alkyl chain and the zirconocene ligands is likely to accelerate the rearrangement **I1**→**I2** while it would rather inhibit the insertion step. We can thus assume that the olefin-insertion itself represents the rate-limiting process in the overall kinetics of polypropene formation, at least for the sterically demanding zirconocene catalysts of recent practical interest [6,24]. In Fig. 4, **T2** would thus represent the crucial transition state for the catalytic cycle.

2. Reaction path involving a second propene molecule.

To determine the influence of a second propene molecule on the reaction path for the insertion of the propene ligand into the Zr-C bond of the cation $[(C_5H_5)_2Zr\text{-ethyl (propene)}]^+$, we have added a second propene molecule to the structures obtained for intermediates **I2** and **I3** and for transition state **T2** and reoptimized the respective geometries. In these calculations, all geometry parameters were allowed to relax, except for the coordinate *d*, which was kept fixed at the value determined for **I2**, **I3** and **T2**.

Geometry optimization of complex **I2^P**, i.e. of the "freed" intermediate **I2** in the presence of a second olefin, leaves the geometry parameters for the $[(C_5H_5)_2Zr\text{-ethyl (propene)}]^+$ fragment practically unchanged (see Tab. 1). The ligand sphere around the Zr center appears to be sterically so congested already by two cyclopentadienyl ligands, the alkyl ligand and the coordination of one propene molecule that the second propene molecule is only weakly bound to the cation $[(C_5H_5)_2Zr\text{-ethyl (propene)}]^+$, as indicated by a long Zr-olefin distance *d*(Zr-C5) of 526 pm and by an energy difference of only ca. -5 kJ/mol (relative to species **I2** plus an infinitely remote olefin), hardly beyond the error margin.

As the reaction proceeds toward transition state **T2^P**, the energy difference due to the approach of the second olefin (i.e. relative to **T2** plus an infinitely remote olefin), is approximately doubled to ca -10 kJ/mol, while the olefin is now found at a distance *d*(Zr-C(5)) of ca. 480 pm from the Zr center. Apparently, the increased electron deficiency of this transition state begins to attract the π -electron density of the olefin. In accord with this view, the more negatively polarized CH₂ propene end is found closer to the Zr center than the CHMe terminus.

During the last section of the reaction sequence, the energy difference due to the presence of the second olefin grows dramatically, to reach finally ca. -35 kJ/mol in the insertion product **I3^P** (see Fig. 4). Quite obviously, the electron deficiency of the 14-electron insertion product **I3** reaches such a degree that direct coordination of the second olefin becomes highly exothermic. Part of this increased exothermicity is apparently felt already in the energy decrease of the insertion transition state **T2^P**.

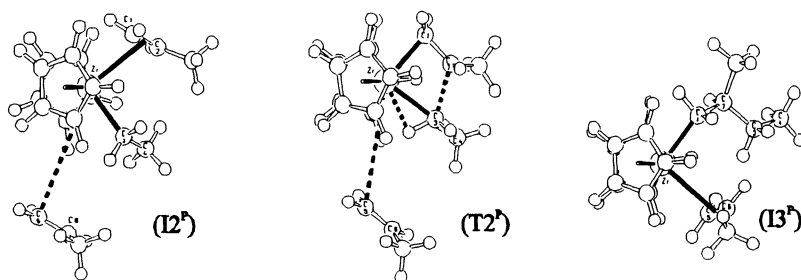
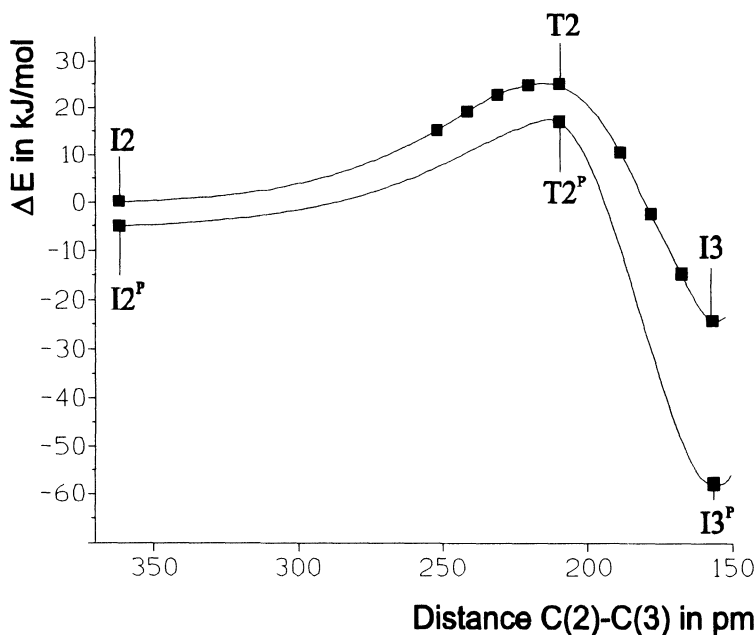
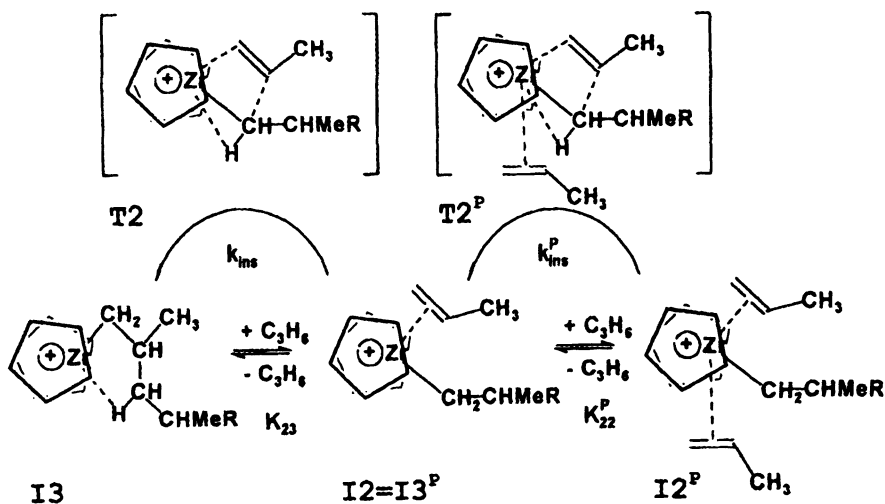


Fig. 4. Energy changes (top) and geometries (bottom) resulting from the presence of a second olefin ligand in the vicinity of the reaction complex $[(C_5H_5)_2Zr\text{-ethyl (propene)}]^+$.

An essential aspect of this modified reaction sequence is the circumstance that the final insertion product has its next olefin substrate already in place for another insertion and might thus escape some otherwise imminent deactivation reactions. Intermediate $I3^P$ has a geometry which is very similar indeed to that of the previously discussed intermediate $I2$. This is apparent from the data in Tab. 1 when alkyl and propene C atoms of $I3^P$ are renumbered in the appropriate sequence. We can thus represent chain growth under the influence of a second olefin by the catalytic cycle represented at the right of Scheme 2.



Scheme 2. Alternative catalytic cycles involving transition states with one propene ligand (left) and with two propene ligands (right).

The presence of two possible insertion transition states, **T2** and **T2^P**, in conjunction with the decreased activation energy of the latter, would *prima facie* suggest that two reaction branches, one with first-order dependence and one with second-order dependence on olefin concentration, might contribute to the overall rate of polymer formation. This conclusion turns out to be contingent, however, on a number of assumptions concerning rates and equilibria of individual reaction steps in each of the catalytic cycles, which will be discussed in detail in a subsequent section below.

Here, we want to address some still incompletely explored ramifications of the concept of the two-olefin cycle discussed above. One of these concerns the fact that our model calculations are based on the assumption of a cationic species *in vacuo*, rather than in a solution medium. It is likely that inclusion of the latter would show that solvent molecules, especially aromatics like toluene or dipolar solvents like dichloromethane, can cause similar stabilizing effects as a propene molecule on an insertion transition state corresponding to **T2**. This raises the question whether the presence of an extraneous propene molecule could still open up, even in such a solvent medium, a sufficiently favored reaction path to make its presence felt.

In this regard, we can state with certainty: Only to that measure to which a propene rather than a solvent molecule stabilizes the insertion transition state - and is subsequently „pulled“ into coordination to the Zr center - will the cycle to the right of Figure 6 remain operative, which avoids the formation of a „deactivated“ β -agostic species. The kinetic consequences of this assertion remain to be clarified, however.

Another intriguing aspect of the two-olefin reaction path discussed above is the possibility that part of the reaction enthalpy of each insertion step might get channelled into the activation of the reaction complex for the next olefin insertion: By the downhill slide along the final section of the energy profile in Figure 4, an entering olefin molecule will be accelerated almost exactly toward the Zr-bound alkyl chain, i.e. in the direction of the reaction coordinate of the next insertion step. There will thus be a finite probability that part of this reaction enthalpy escapes immediate thermalization, being temporarily stored e.g. in a relatively „soft“ scissoring vibration of the propene and alkyl ligands toward each other, which overlaps with the reaction coordinate leading from $\mathbf{I2}^P$ to $\mathbf{T2}^P$.

Which proportion of the reaction enthalpy might thus escape immediate dissipation into the reaction medium will be difficult to assess. Qualitatively, one can estimate that interactions with solvent molecules and conformational motions of the polymer chain will be the main leaks toward thermalization. It would thus appear possible that zirconocenes with especially extended π -ligands owe part of their unusually high activities to the fact that the „greasy“ inner surface of these π -ligands shields the entering propene ligand from losing all of its kinetic energy to the reaction medium at once. Even if only a minor fraction of this kinetic energy is transferred into the reaction coordinate of the next insertion, the two-olefin path would gain significant advantage over the one-olefin alternative. Since this advantage can accrue only to that measure to which a propene rather than a solvent molecule acts as a stabilizing outer-sphere ligand, the rate of polymer formation would gain its additional order in monomer concentration even if solvent molecules compete with the olefin for interaction with the electrophilic zirconocene cation.

3. Kinetic analysis.

The following kinetic analysis is based on reaction Scheme 2. Not included in this initial analysis are thus e.g. contact ion pairs with direct coordination of the counter-anion to the Zr center or species leading to side reactions such as regioirregularities, chain-end isomerizations or chain-transfer reactions. To analyse how the competition between transition states $\mathbf{T2}$ and $\mathbf{T2}^P$ affects the rate of polymer formation, v_{pol} , we neglect also the presence of intermediates $\mathbf{I0}$ and $\mathbf{I1}$. We set the rate of polymer formation $v_{\text{pol}} = [\mathbf{I2}] \cdot k_{\text{ins}} + [\mathbf{I2}^P] \cdot k_{\text{ins}}^P$ and solve for $[\mathbf{I2}]$ and $[\mathbf{I2}^P]$ by standard steady-state algorithms. Under the assumption that olefin uptake and release equilibria are fast compared to all other reaction steps and completely described by the dissociation constants $K_{23} = [\mathbf{I3}] \cdot [\mathbf{M}] / [\mathbf{I2}]$ and $K_{22}^P = [\mathbf{I2}] \cdot [\mathbf{M}] / [\mathbf{I2}^P]$, we obtain equation 1 for the rate of polymer formation as a function of the monomer concentration $[\mathbf{M}]$.

$$v_{\text{pol}} = [\text{Zr}]_{\text{tot}} \cdot ([\text{M}]^2 \cdot k_{\text{ins}}^{\text{P}} + [\text{M}] \cdot K_{22}^{\text{P}} \cdot k_{\text{ins}}) / ([\text{M}]^2 + [\text{M}] \cdot K_{22}^{\text{P}} + K_{23} \cdot K_{22}^{\text{P}}) \quad (1)$$

The rate of polymer formation will thus grow according to first- and second-order terms of $[\text{M}]$, whenever the first two terms in the denominator vanish relative to the third. To arrive at some semiquantitative estimates as to possible values of the rate and equilibrium constants in equation 1, we have converted rate data for the catalyst system $\text{Me}_2\text{Si}(\text{2-Me-benzind})_2\text{ZrCl}_2/\text{MAO}$ reported in ref. [9] to turnover frequencies (insertions/s) and used them for a calibration of these parameters (Figure 5).

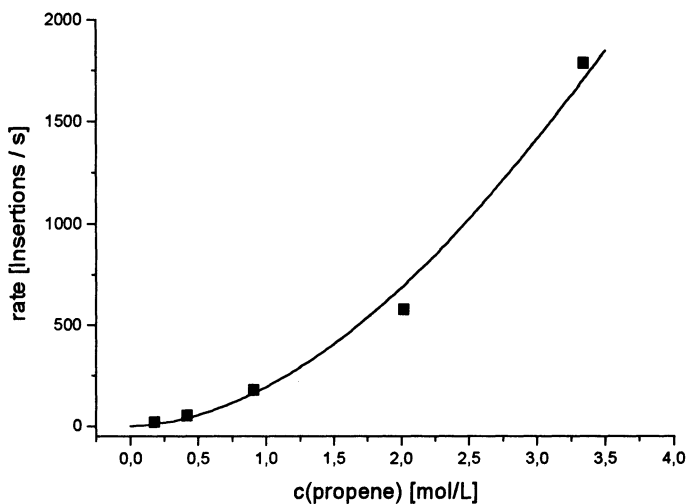


Fig. 4. Reproduction of the experimental rate data from ref. [9] by equation 1 with values of $k_{\text{ins}} = 3000 \text{ s}^{-1}$, $k_{\text{ins}}^{\text{P}} = 5 \cdot k_{\text{ins}} = 15000 \text{ s}^{-1}$, $K_{23} = 100 \text{ mol/L}$ and $K_{22}^{\text{P}} = 1 \text{ mol/L}$.

The experimental rate data are adequately reproduced only under the following conditions:

- The maximally attainable rate, $k_{\text{ins}}^{\text{P}}$, must be greater than the highest rate observed (ca. 2000 s^{-1}) by a factor of about 5; otherwise saturation would be observed.
- The ratio $k_{\text{ins}}^{\text{P}}/k_{\text{ins}}$ must be distinctly greater than 1, i.e. the second olefin must induce a noticeable rate increase, to give reasonable values for the other constants.
- The value of K_{22}^{P} must be comparable to the monomer concentrations considered, i.e. $K_{22}^{\text{P}} \cong 1 \text{ mol/L}$. This corresponds to a 50% probability of finding another olefin molecule within ca. 5 \AA from the Zr center of a cation $[(\text{C}_5\text{H}_5)_2\text{Zr-ethyl (propene)}]^+$, in reasonable agreement with the estimates represented in Table 1 and Figure 5.
- The dissociation constant of the first olefin, K_{23} , however, must be much greater than 1 mol/L , such that the fraction $[(\text{C}_5\text{H}_5)_2\text{Zr-ethyl (propene)}]^+ / [\text{Zr}]_{\text{tot}}$ always remains small and proportional to $[\text{M}]$.

That the first olefin should be less firmly bound than the second appears incompatible with Scheme 2 at first sight. It is evident that only the intervention of an additional intermediate of still lower free energy can explain that the concentration of the crucial intermediate **I2** remains low and proportional to $[M]$ even at olefin concentrations where substantial proportions of **I2** are converted to **I2^P**. The most likely candidate for such an additional low-energy intermediate is a contact ion pair with direct coordination of the anion to the Zr center. For a reasonably complete analysis of such a more realistic situation, equilibrium and rate constants for the mutual displacement of anion and olefin ligands have to be known, however. We are presently trying to gain access to data of this kind, in particular with a view to their dependence on the structure of individual zirconocene catalysts of practical interest.

References

- 1 Pino, P.; Rotzinger, B.; von Achenbach, E., *Makromol. Chem., Suppl.* **1985**, *13*, 105.
- 2 Fischer, D., *Dissertation*: Universität Freiburg, **1992**, p 100f.
- 3 Herfert, N.; Fink, G., *Makromol. Chem.* **1992**, *193*, 1359; *Makromol. Chem., Macromol. Symp.* **1993**, *66*, 157.
- 4 Siedle, A.R.; Lamanna, W.M.; Olofson, J.M.; Nerad, B.A.; Newmark, R.A., in *Selectivity in Catalysis, ACS Symp. Series* **1993**, *517*, 156.
- 5 Ystenes, M., *J. Catal.* **1991**, *129*, 383; *Makromol. Chem. Macromol. Symp.* **1993**, *66*, 71.
- 6 Stehling, U.; Diebold, J.; Kirsten, R.; Röhl, W.; Brintzinger, H.H.; Jüngling, S.; Mühlhaupt R.; Langhauser, F., *Organometallics* **1994**, *13*, 964.
- 7 Jüngling, S.; Mühlhaupt, R.; Stehling, U.; Brintzinger, H.H.; Fischer, D.; Langhauser, F., *J. Polym. Science Part A: Polymer Chemistry* **1995**, *33*, 1305.
- 8 Chien, J.C.W.; Yu, Z.; Marques, M.M.; Flores, J.C.; Rausch, M.D., *J. Polym. Sci.* **1998**, *A-36*, 319.
- 9 Eichhorn, K.; Treutler, O.; Öhm, H.; Häser, M.; Ahlrichs, R., *Chem. Phys. Lett.* **1995**, *242*, 652.
- 10 Becke, A. D., *J. Chem. Phys.* **1986**, *84*, 4524; *ibid* **1988**, *88*, 1053.
- 11 Becke, A. D., *Phys. Rev. A* **1988**, *38*, 3098.
- 12 Perdew, J. P., *Phys. Rev* **1986**, *B33*, 8822; *ibid. Phys. Rev.* **1986**, *B34*, 7406.
- 13 Lee, C.; Yang, W.; Parr, R., *G. Phys. Rev.* **1988**, *B37*, 785.
- 14 Ahlrichs, R.; Bär, M.; Häser, M.; Horn, H.; Kölmel, C., *Chem. Phys. Lett.* **1989**, *162*, 165.
- 15 Häser, M.; Ahlrichs, R., *J. Comp. Chem.* **1989**, *10*, 104.
- 16 Dunlap, B. I.; Connolly, J. W. D.; Sabin, J. R., *J. Chem. Phys.* **1979**, *71*, 339.
- 17 Lohrenz, J. C. W.; Woo, T. K.; Ziegler, T., *J. Am. Chem. Soc.* **1995**, *117*, 12893.
- 18 Woo, T. K.; Fan, L.; Ziegler, T., *Organometallics* **1994**, *13*, 2252.
- 19 Woo, T.K.; Margl, P.M.; Lohrenz, J.C.W.; Blöchl, P.E. Ziegler, T. *J. Am. Chem. Soc.* **1996**, *118*, 13021.
- 20 Lohrenz, J. C. W.; Woo, T. K.; Fan, L. and Ziegler, T. *J. Organomet. Chem.* **1995**, *497*, 91.
- 21 Weiss, H.; Ehrig, M. and Ahlrichs, R. *J. Am. Chem. Soc.* **1994**, *116*, 4919.
- 22 Yoshida, T.; Koga, N.; Morokuma, K., *Organometallics* **1995**, *14*, 746; *ibid.* **1996**, *15*, 766.
- 23 Leclerc, M.K.; Brintzinger, H.H., *J. Am. Chem. Soc.* **1995**, *117*, 1651; *ibid.* **1996**, *118*, 9024.
- 24 Spaleck, W.; Küber, F.; Winter, A.; Rohrmann, J.; Bachmann, B.; Antberg, M.; Dolle, V. and Paulus, E. F. *Organometallics* **1994**, *13*, 954.

Syndiotactic and Isotactic Specific Metallocene Catalysts with Hapto-flexible Cyclopentadienyl-Fluorenyl Ligand

Abbas Razavi, Vincenzo Bellia, Yves De Brauwer, Kai Hortmann, Marine Lambrecht, Olivier Miserque, Liliane Peters, Stéphane Van Belle

Fina Research, Centre de Recherche du Groupe PetroFina, Zone Industrielle C, B-7181 Feluy (Belgium)

Abstract.

The unbridged metallocenes can generally be classified as stereo-chemically non-rigid molecules. The fast rotation of the aromatic rings about their bond axis to the transition metal attributes a very high fluxionality to these molecules. Non-rigid character can be considered for bridged metallocenes if one extends the notion of fluxionality of the ring(s) to their capability of rapidly and reversibly changing their bonding order (hapticity) to the transition metal. The hapto-tropic behavior of metallocenes with substituted and unsubstituted cyclopentadienyl ring(s) is known as common occurrence in transition metal organometallic chemistry and homogeneous catalysis [1]. The hapto-flexible aromatic ligands bound to the transition metal can facilitate the ligand exchange reaction by lowering “temporarily” the hapticity in the transition state and permitting the increase of the formal co-ordination number without breaking the canonic electronic rules [2]. In this article we have reviewed the basic ideas of stereoselectivity in the light of recent metallocene structure discoveries revealing the presence of haptotropy. The quasi five fold increase of the molecular weight of the syndiotactic polypropylene produced with diphenylmethylened- μ -(cyclopentadienyl-fluorenyl)ZrCl₂/MAO catalyst system with respect to the molecular weight of the syndiotactic polymer produced with the parent isopropylidene- μ -(cyclopentadienyl-fluorenyl)ZrCl₂ is brought in direct relation to the difference in hapticity of these molecules in solution and in their cationic forms as active species. The experimental proof for this assumption is given unequivocally through facile hydrogenation of the fluorenyl’s six-member rings in the former and complete inertness of the benzenic rings of the latter to the hydrogenation. In an extension of the same idea haptotropy is also proposed to be responsible for the formation of short blocks of syndiotactic sequences in predominantly isotactic chains formed with the zirconocene isopropylidene- μ -(3-trimethylsilylcyclopentadienyl-fluorenyl)zirconium dichloride. It is further demonstrated that a change in the size and nature of the catalyst’s substituents could increase the probability of occurrence of the haptotropic behavior. The possibility of haptotropy being involved in occasional isospecific/syndiospecific site transformation via a reversible $\eta^5 \leftrightarrow \eta^3 \leftrightarrow \eta^1$ mechanism is discussed. The argument is reinforced by introduction of a new syndiotactic specific monocyclic η^5 , η^1 metallocene structure exhibiting similar symmetry properties.

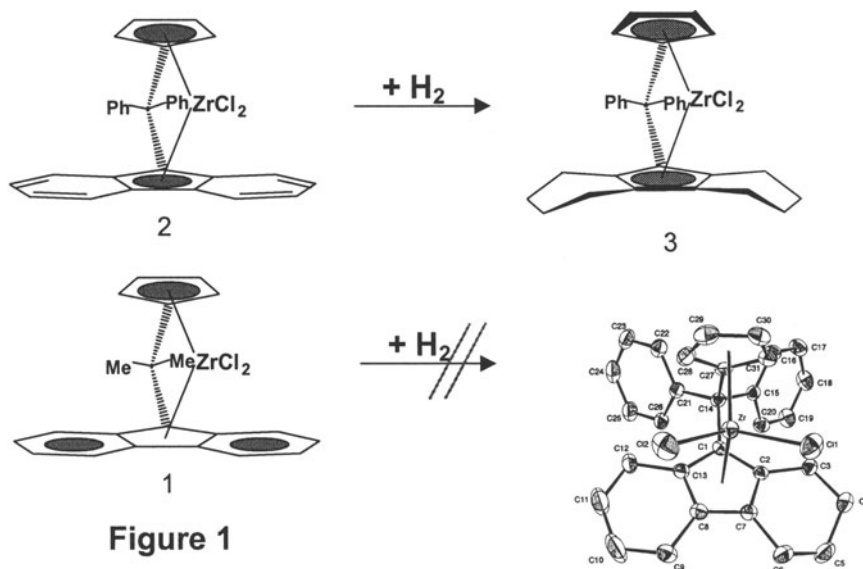
Results and discussion

The model and mechanism that have been developed and proposed in the last ten years for the syndiospecific polymerization of propylene with Cs symmetric metallocene catalysts [3] are perfectly apt to account and rationalize the polymerization behavior of isopropylidene- μ -(cyclopentadienyl-fluorenyl) zirconium dichloride **1** and diphenylmethylidene- μ -(cyclopentadienyl-fluorenyl) zirconium dichloride **2** as well as the properties of their polymers separately. However, the comparison of the molecular weights of the polymers produced with these two metallocenes based catalyst systems reveals a major discrepancy. In fact the catalyst derived from **2** produces syndiotactic polymers having molecular weights five times higher than the molecular weight of syndiotactic polymers produced with corresponding catalyst formed with **1** [4].

A brief review of the inter-atomic parameters published [4] for **1** and **2** reveal that upon introduction of the phenyl groups in the bridge, the important Zr-C bond distances do not undergo palpable changes and the observed variations are well within the expected experimental uncertainties. However, the Cent-Zr-Cent and Cl-Zr-Cl angles have been decreased from values of 118.60° and 98.20° for **1** to values of 117.60° and 96.60° for **2** by 1.00° and 1.60° respectively. These angular changes imply that in **2** as a result of the repulsive interaction between the two phenyl groups in the bridge the external tetrahedral angle is increased. As a consequence the internal tetrahedral angle around the bridging carbon of the ligand will be decreased and forces the transition metal to move slightly outward to fit better inside the ligand. Except for these minor differences, in the solid state under the compacting crystal effect the two metallocenes do not differ much structurally from each other. A comparison of the ¹H NMR spectrum [4] of **1** and **2** reveals, however, that the differences can be substantial in solution. The comparison shows that for both molecules, the proton signals related to the cyclopentadienyl groups have the same coupling pattern (virtual triplets) and very similar chemical shift values, however, the examination of the fluorenyl proton signals indicates that the protons belonging to the fluorenyl part of **2** have been subjected to different shielding and deshielding forces giving rise to completely different chemical shifts and signal pattern. The dramatic differences in chemical shifts and signal pattern of the fluorenyl protons for compounds **1** and **2** strongly suggest that their fluorenyl moieties are engaged in a different bonding relations or hapticities with the transition metal.

To verify this hypothesis a hydrogenation experiment proved to be very revealing. Since different hapticities for **1** and **2** has been assumed (only η^5 or η^3 since η^1 can be positively excluded based on X-ray data) the task would be to attribute the correct hapticity to each metallocene. Theoretically, if in one of the metallocenes the fluorenyl-Zr bond is η^3 in nature one would expect the corresponding six membered rings to be aromatic and not subject to hydrogenation. On the contrary if in one of the metallocenes the fluorenyl-Zr bond is η^5 the six membered rings are supposed to be diene like and prone to hydrogenation. Figure 1 shows the hydrogenation scheme for the two metallocenes and the crystal structure of the only resulting product diphenylmethylidene- μ -(cyclopentadienyl-

octahydrofluorenyl)ZrCl₂ **3**. Metallocene **3** was obtained from **2** under mild hydrogenation conditions [5]. All attempts to hydrogenate metallocene **1** under similar and even more vigorous conditions have failed. We therefore concluded that the structures given in Figure 1 (left) represent the correct hapticity (η^3) for **1** and (η^5) for **2**. We also suggest that the difference in hapticity in **1** and **2** is at the origin of the different catalytic behavior and different molecular weights of their polymers. Metallocene **3** is aspecific.



Hapticity change, though in a less significant extend, can also be suspected for the cyclopentadienyl part of the bridged cyclopentadienyl-fluorenyl based metallocene catalysts. The difference in the length of the Zr-cyclopentadienyl distal and proximal carbon bonds, measured for the solid state structures of the metallocene precursors, could be regarded as a hint of what can eventually happen in solution and during the polymerization to the active site. For **1** and **2** the Zr-C distal bonds are longer by about 0.1Å than the corresponding Zr-C proximal bonds Table 3 (vide infra, first and second row). Additionally the data given in Table 3 (third, fourth and fifth row) prove that the RCp-Zr distal carbon bond distances will become substantially longer after placing a sizable and bulky substituent at one of the cyclopentadienyl distal positions. In these cases the repulsive interactions of the substituent with the underlying non-aromatic ligands provoke further lengthening and weakening of the two Zr-C distal bonds. During the polymerization the interaction of the growing polymer chain and the substituent will become even stronger and could lead to further destabilization of the Zr carbon bonds in the RCp-Zr moiety of the complex and eventually to a change of hapticity $\eta^5 \leftrightarrow \eta^3 \leftrightarrow \eta^1$ in a more or less systematic way. The effect would be more pronounced for cases where the fluorenyl part has already a reinforced η^5 bonding to Zr (for example by introduction of phenyl groups in the bridge).

The formation of isotactic polypropylene with the C_1 symmetric metallocene isopropylidene- μ -(3-tert-butyl-cyclopentadienyl-fluorenyl) zirconium dichloride, **4** was rationalized by us on the basis of a hindered chain migratory insertion (chain "stationary" insertion) mechanism [6] at two diastereotopic coordination positions. Noteworthy for our present discussion regarding catalyst haptotropy is the presence of a minor syndiotactic fraction in the isotactic polymer that was produced with **4** (rrrr = 0.5%). The Hf analogue of **4**, the metallocene isopropylidene- μ -(3-tert-butylcyclopentadienyl-fluorenyl) hafnium dichloride **5** provides a very unstable catalyst. During its short life time, however, **5** produces an isotactic polymer which contains more than 3% of syndiotactic fraction (rrrr = 3.5%). The micro-structural characterization of the polymers with ^{13}C NMR spectroscopy and the identification of the signals related to juncture sequences, nevertheless, failed for these polymers to be conclusive. In the polymers of **4** the syndiotactic sequences were too short to permit their unequivocal identification as such within the rest of the isotactic polymeric chains. And in the case of the polymer produced with the Hf analogue **5** (rrrr = 3.5 %) because of short catalytic life time, relative purity, and small quantity of the polymer an exact assessment of its microstructure and composition was not possible. Nevertheless, what ever the origin and the mechanism, for the formation of syndiotactic blocks or fractions in these predominantly isotactic polymers the presence of a second type of active site with C_s symmetry characteristics had to be suspected either by a irreversible transformation of C_1 site to C_s or via a reversible RCp-Zr hapticity change (vide infra).

In an attempt to produce more stereoregular isotactic chains with longer syndiotactic sequences with stable catalysts for an unequivocal ^{13}C NMR characterization, we synthesized other similarly structured metallocenes. Figure 2 gives the single crystal X-ray structure of the metallocene isopropylidene- μ -(3-trimethylsilyl-cyclopentadienyl-fluorenyl)MCl₂, M = Zr **6**, and its Hf analogue M = Hf **7**. Metallocene **6**, after its activation with MAO, polymerizes propylene to isotactic polypropylene at a broad range of polymerization temperatures. The polymerization conditions, results and general polymer properties are given in Table 1. At 40°C the catalyst produces an isotactic polymer which contains 1.14% syndiotactic fractions (rrrr = 1.14%) by increasing the polymerization temperature to 60°C the catalyst activity increases to more than three fold and the percentage of the syndiotactic fraction in the polymer increases to the level of rrrr = 1.65%. At 80°C the catalyst starts to decompose (activity drop!) and the percentage of rrrr in the resulting polymer drops below 1%. The Hf analog **7** was too unstable in solution as a cation and decomposed rapidly before producing any reasonable quantities of polymer. The polymerization results with **6** confirms the formation of longer syndiotactic sequences with a stable catalyst, yet the increase of the syndiotactic fraction to 1.65 % [7] was still not sufficient for proper ^{13}C NMR analysis. The sequences were still too short to provide reliable sources for statistical investigation and determination of polymer stereosequences. In order to further increase the length of the syndiotactic sequences we decided to modify the bridge substituents in **6** from methyl to phenyl and synthesized the complex diphenylmethyldiene- μ -(3-trimethylsilylcyclopentadienyl-fluorenyl) zirconium

dichloride, **8**. The phenyl substituents should, as in the case of **2**, enhance an η^5 bonding between the fluorenyl part of the ligand and the Zr and facilitate the $\eta^5 \leftrightarrow \eta^3 \leftrightarrow \eta^1$ transformation of the RCp-Zr part during the polymerization. Table 2 gives the polymerization conditions, results, and polymer analysis for **8**/MAO catalyst system at different polymerization temperatures. The data presented in this table indicate that at 40-60°C the catalyst produces isotactic polypropylene polymers with about 4% of syndiotactic fraction (with or without H₂). With increasing polymerization temperature from 60 to 80°C by maintaining the activity (stability !) an isotactic polymer with a syndiotactic fraction of rrrr = 6% is produced.

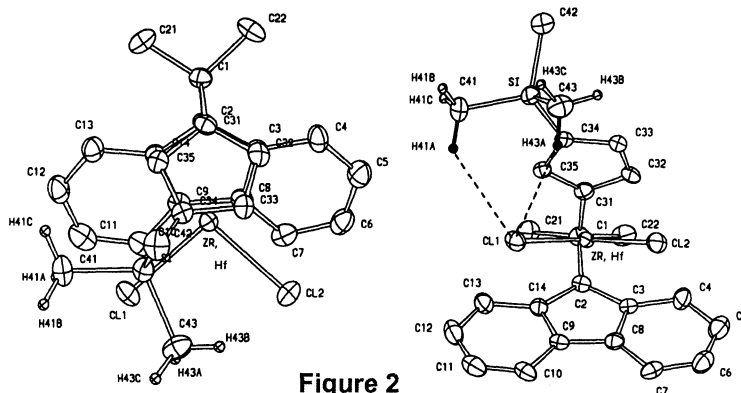


Figure 2

| Cat (mg) | Temp. (°C) | Activ. (kg/g) | Mw (kDa) | MWD | Mp (°C) | mmmm (%) | Rrrr (%) |
|----------|------------|---------------|----------|-----|---------|----------|----------|
| 2 | 40 | 4.2 | 134 | 3.0 | 105.4 | 66.57 | 1.14 |
| 2 | 60 | 14.5 | 64 | 2.5 | 109.0 | 66.98 | 1.65 |
| 2 | 80 | 4.7 | 42 | 2.4 | 114.6 | 69.06 | 0.94 |

| Temp. (°C) | Activ. (kg/g) | Mw (kDa) | MWD | Mp (°C) | mmmm (%) | Rrrr (%) |
|------------|---------------|------------------|-----|---------|----------|----------|
| 40 | 30 | 23 ^{a)} | 2.5 | 89 | 51.63 | 4.10 |
| 60 | 56 | 97 | 3.3 | 91 | 56.47 | 3.96 |
| 60 | 85 | 59 ^{b)} | 2.4 | 102 | 59.81 | 3.42 |
| 80 | 71 | 52 | 3.8 | 116 | 63.13 | 6.00 |

a) With 5 NI hydrogen

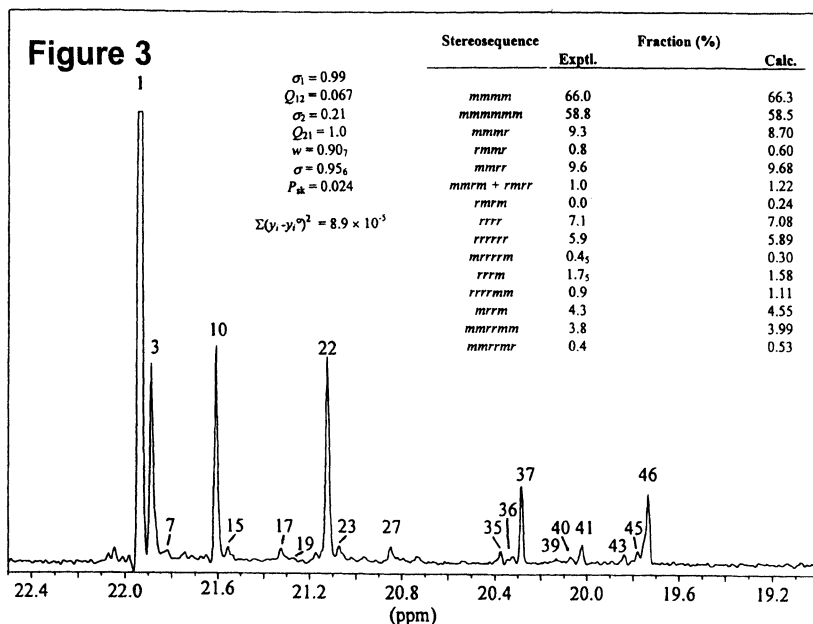
b) With 1 NI hydrogen

Figure 3 shows the methyl region of the 150 MHz ¹³C NMR spectrum of a hexane-soluble polymer fraction [8] produced with **8** at 60°C (peak numbering refers to the assignment reported in ref. [9a]). It is readily apparent that the sample contains both predominantly isotactic and syndiotactic sequences, and that the former are produced at C1-symmetric sites, according to the model discussed above for **4** [6]. Indeed, peak no. 17, arising from the mrrmmrrm nonad (which

contains two non-consecutive stereodefects), is well detectable, whereas no intensity is observed in the region of the rrrm pentad (which would have been diagnostic of two consecutive stereodefects).

In the same figure, the experimental stereosequence distribution is compared with the best-fit one in the framework of a simple two-site model (C1-symmetric isotactic + Cs-symmetric syndiotactic). The fit is rather good, and indicates that the enantioselectivity of the active species producing the syndiotactic sequences is very similar to that of the active species which are formed with 1,2 or 9 (vide infra). As a matter of fact, most errors in such sequences are due to "skipped insertions" (note the low intensity of peak no. 39, due to the rrrmr heptad, compared to peak no. 40, mostly due to the rrrrrmmr nonad).

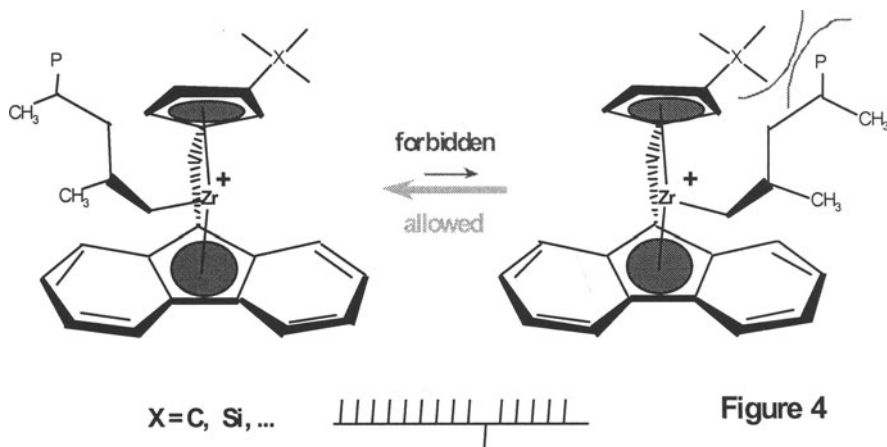
Finally, the fact that peak no. 41, associated with the mrrrrmmm+rrrrrmmm nonads, is rather intense, might indicate that it receives a significant contribution from the latter nonad, arising mainly from junctions between isotactic and syndiotactic stereoblocks. [9b]



The presence of short syndiotactic sequences in the predominantly isotactic chains can not be explained by mechanisms considering the active site as a simple geometrically invariant entity with identical catalytic behavior during the entire course of polymerization and different stages of each insertion step. Considering all potential dynamic changes such as ring slippage, molecular symmetry and hapticity changes [1,2] that a metallocenium active site can potentially undergo it is not far fetched to co-relate the above mentioned chain microstructure "anomalies"

to a reversible site transformation mechanism triggered by occasional hapticity change caused in turn by a substituent/chain repulsive interaction mechanism. Since the chain microstructure consists of isotactic and syndiotactic parts a combinatory mechanism with an originally C_1 symmetric site is required. Therefore the proposed mechanism must be a mixed chain stationary / chain migratory insertion mechanism [10a]. The active site must undergo occasional $C_1 \leftrightarrow C_s$ site geometry transformation. And the transformation could only occur if a reversible hapticity change for the RCp-Zr bond is possible.

The formation of isotactic polypropylene with a metallocene having bulky group (tert-butyl, or trimethylsilyl) is visualized in Figure 4. Because of the steric interaction between the large substituent and the growing polymer chain its migration to the crowded position is hindered or completely blocked. The chain becomes either "stationary" and remains "permanently" at the less crowded positions or even if it migrates it returns to its initial position immediately after each insertion by a site epimerization mechanism [10b]. This results in the formation of isotactic part of the polymer chain. Additionally, the possibility exists that occasionally, the chain manages to move to the energetically less favorable position (the probability is low but not zero) and comes into a very strong non-bonded steric interaction with the cyclopentadienyl substituent. To avoid this interaction the chain can change its conformation by rotating towards fluorenyl where it comes in contact with the six membered ring (Figure 5). Sandwiched between two substituents the site must change its hapticity or it will decompose (Hf sites 5 and 7). Figure 6 visualizes pictorially this situation. By changing the hapticity from penta to tri and eventually to mono in a reversible way, however, it permits the chain to become progressively mobile intermittently and shuttle freely between the two lateral pseudo enantiotopic coordination positions back and forth after each insertion and to produce syndiotactic sequences. In extreme situations the Cp could be even detached and reattached explaining in some cases partial and in some cases total decomposition of the catalyst at higher temperatures.



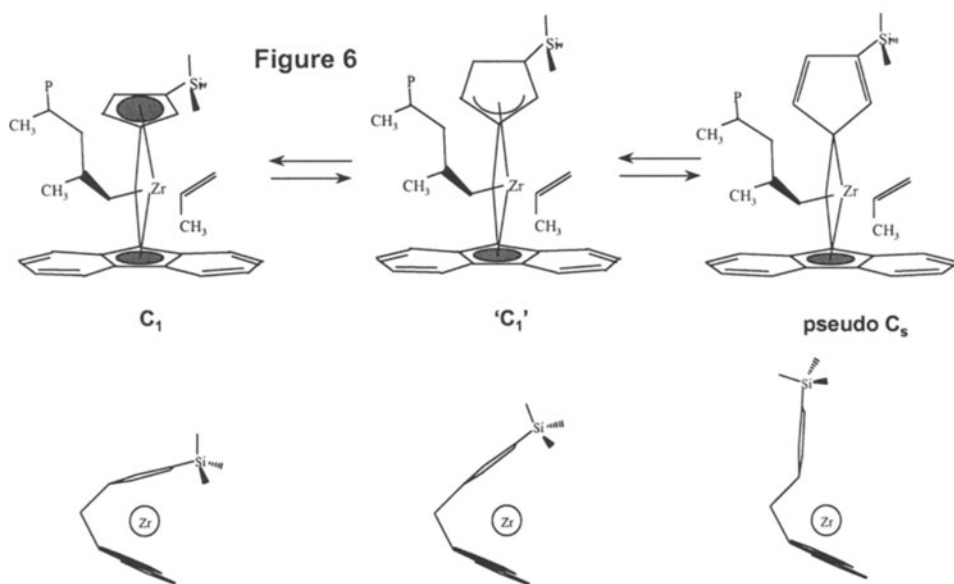
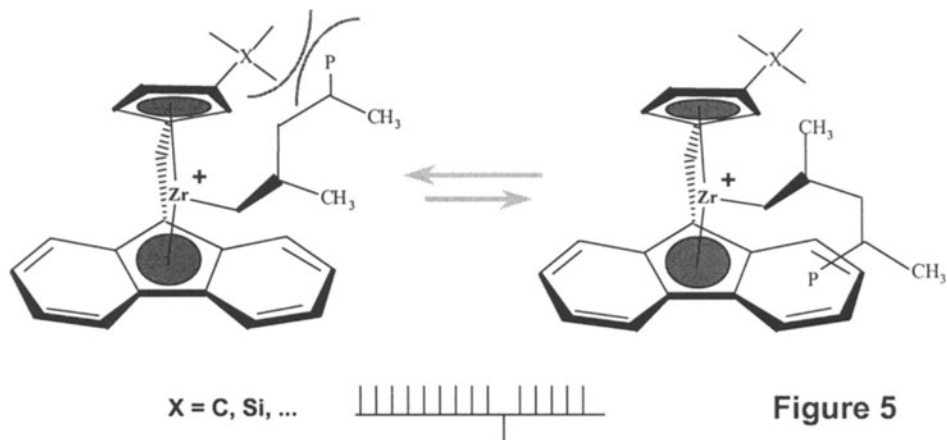


Table 3 compares the most important bond distances for the metallocenes **1**, **2**, **4**, **6**, and **7**. The substituted distal carbon atoms show increasingly longer bond distances to the Zr going from **1** (and **2**) to **4**, however, no substantial difference between the Cp-Zr bonds for the tert-butyl and trimethylsilyl (TMS) substituted systems can be observed. In the case of TMS substituted metallocene additional stereo - electronic factors must be taken into consideration. Longer Si distal carbon distance and different electron configuration (potentially available d-orbitals) can cause an increased repulsive interaction of the trimethylsilyl group with the growing chain and enhances the distal carbon bond loosening. The ^{13}C NMR data [11a] and DFT calculations indicate that the carbons attached to Si are charged more negatively (higher field chemical shifts). It seems that the Si atom acts as a

sort of insulator blocking the flow of the electrons from the methyl groups towards the cyclopentadienyl and the carbon atoms connected to it remains largely negatively charged and more repulsive towards the chain [11b]. Additionally in **8** since the phenyl substituents have strengthened the fluorenyl-Zr bond to a “perfect” pentahapto system the only way for molecule to relax is through a hapticity change in the RCp-Zr moiety.

Table 3

| Zr-Cp | Ci | Cps | Cp | Cds | Cd |
|--------|-------|-------|-------|-------|-------|
| 1 | 2.436 | 2.444 | 2.452 | 2.519 | 2.528 |
| 2 | 2.452 | 2.450 | 2.450 | 2.523 | 2.523 |
| 4 | 2.428 | 2.472 | 2.427 | 2.618 | 2.548 |
| 6 | 2.427 | 2.439 | 2.464 | 2.554 | 2.547 |
| 7 | 2.425 | 2.422 | 2.460 | 2.524 | 2.529 |
| Zr-Flu | iC | AC | a'C | dC | d'C |
| 1 | 2.401 | 2.528 | 2.501 | 2.651 | 2.667 |
| 2 | 2.417 | 2.513 | 2.513 | 2.680 | 2.680 |
| 4 | 2.411 | 2.514 | 2.554 | 2.650 | 2.677 |
| 6 | 2.422 | 2.523 | 2.667 | 2.671 | 2.677 |
| 7 | 2.424 | 2.541 | 2.512 | 2.675 | 2.653 |

Ci = bridge head C, Cp= prox. C, Cps = Prox. subst., Cd= distal subst, Cd=distal

There is no direct way to prove that the proposed reversible hapticity change is actually operative for the cases discussed above. What can be verified, however, is to see whether – if such phenomena are involved – the resulting mono-hapto-pentahapto bonded ligand can provide the syndiospecific environment to the site. Thus instead of looking for spectroscopic evidences for the hapticity change we took the indirect approach to verify the syndiotactic selective nature of Cs symmetric catalysts with a η^1, η^5 bonded ligand system in which the cyclopentadienyl moiety is replaced by a single atom and the second aromatic ring is a fluorenyl group. The eventual syndiospecificity of such metallocene would imply that the presence of the cyclopentadienyl ring as a whole is not really a necessity for its syndiospecificity. The bridge head carbon atom of the cyclopentadienyl like any other single atom (linked to the fluorenyl part by a bridge) coordinated to the transition metal could maintain the required stereo-rigidity and guarantee the symmetry prerequisites (prochiral and bilateral). Figure 7 shows the front view of such a hypothetical molecule compared with the parent syndiospecific metallocene **1** and the putative monohapto bonded trimethylsilyl substituted system **8** emphasizing thus the Cs or pseudo Cs symmetric character of the molecules. The polymerization results published in the literature [12] with monocyclic metallocenes with the desired structure were rather discouraging and potential molecules falling in this category have not been providing high polymers with acceptable syndiotacticity. However, by some substitutional modifications of the basic structure we finally managed to synthesize a new syndiotactic specific metallocene with the searched structural properties [13].

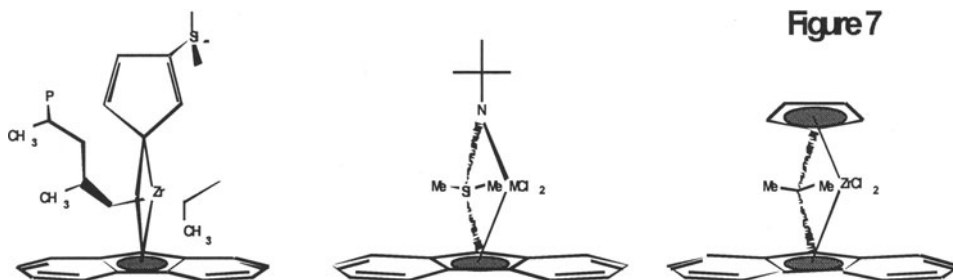


Figure 7

Figure 8 shows the molecular structure and symmetry of the amido-fluorenyl compound (η^1, η^5 -tert-butyl(bis-2,7-tert-butylfluorenyl-dimethylsilyl)amido-dichlorotitanium **9** as well as ^{13}C NMR characteristics of its polymers. It is prepared in rather good yields. Once activated, **9** produces high molecular weight syndiotactic polypropylene with very high activities. The polymerization conditions and polymer analyses are given in Table 4. The microstructure of the polymer is very similar to the microstructure of the polymers produced with the parent syndiospecific metallocenes **1** and **2** and syndiotactic stretches of **8**. From these results it can be concluded that a fluorenyl based η^1, η^5 bound ligand is perfectly capable of imparting the stereo-rigidity and symmetry environment prerequisite for syndiospecificity of the site and at least in this respect the proposed mechanism for **8** is justifiable. Additionally, the ^{13}C NMR data and microstructural similarity between the syndiotactic polymer produced with **1**, (**2**), **8** (sequences) and **9** indicate clearly that the formation of the polymer with **9** proceeds according to the chain migratory insertion mechanism operating on an enantiomorphic C_s -symmetric site (Figure 9). The lower stereoregularity (higher heterotactic pentads fractions) of the new syndiotactic chains is probably the result of lower stereo-rigidity of **9** due to the dynamic environment of nitrogen atom and/or possible ring slippage bond rearrangement mechanism leading occasionally to the dissymmetry of the site and short heterotactic sequences (Figure 10). The zirconium analogue of **9** produces only oligomeric materials.

Table 4

| Temp. (°C) | Activ. (kg/g) | Mw (kDa) | Mw (kDa) | MWD | Mp (°C) | rrrr (%) |
|------------|---------------|----------|----------|-----|---------|----------|
| 40 | 27 * | 157 | 405 * | 2.6 | 101.1 | 75.74 |
| 60 | 160 | 116 | 506 | 4.3 | n.d. | 63.92 |
| 80 | 75 | 119 | 367 | 3.1 | n.d. | 55.98 |

* diffusion problem, n.d.= not determined

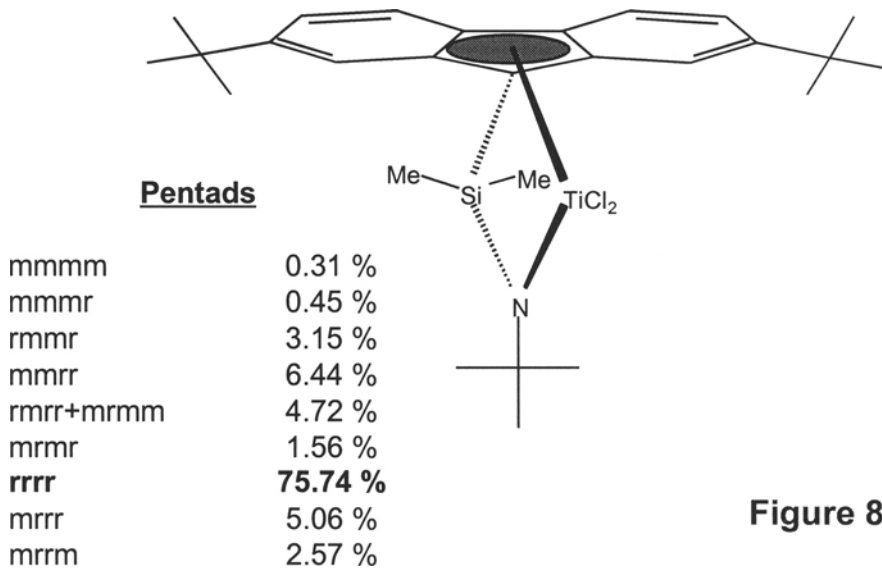


Figure 8

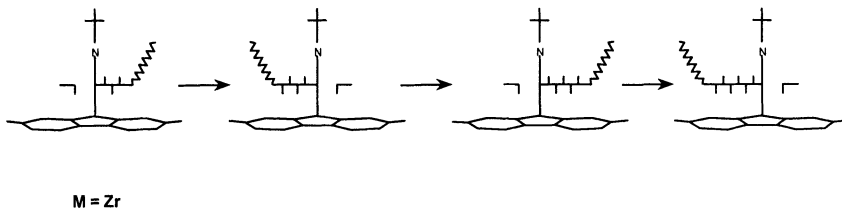


Figure 9

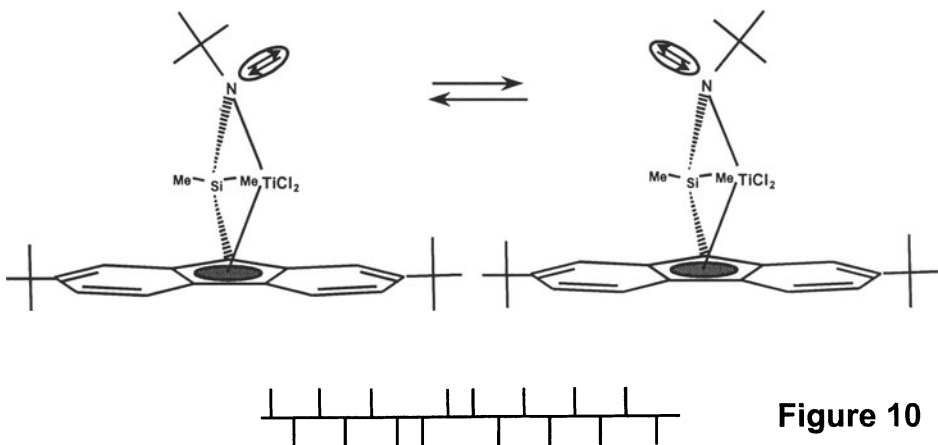


Figure 10

REFERENCES

- [1] Basolo, F., *Israel Journal of Chemistry* 27 (1986)233, Nesmeyanov, A.N., Ustynyuk, N.A., Makraova, L.G., Andrinov,V.G., Struchkov,Y.T., Andrae ,S., *J. Organomet. Chem.*, 159 (1978) 199, Huttner, G., Brintzinger, H. H., Bell, L.G., *J. Organomet. Chem.*, 145 (1978) 329
- [2] Faller, J.W., Crabtree, R.H., Habib, A., *Organometallics*,4 (1985) 929
- [3] a) Cavallo, L., Guerra, G., Vacatello, M. M., Corradini, P., *Macromolecules* 24 (1991) 1784. (b) Herzog, T. A, Zubris, W. L, Bercaw, J.E., *J. Am. Chem. Soc.* 118 (1996) 11988
- [4] Razavi, A., Ferrara, J., *J. Organomet. Chem.* 435 (1992) 299, Razavi, A. Thewalt, U., *J. Organomet. Chem.* 445 (1993) 111
- [5] Wild, F., Zsolnai, L., Huttner, G., Brintzinger, H. H., *J. Organomet. Chem.* 232 (1982) 233
- [6] Razavi, A., Vereecke, D., Peters, L., Den Daw, K. Nafpliotis, L, Atwood, J.L. " Mechanisms and Models in Ziegler-Natta Catalysis" , *Int. Symp. 40 years Ziegler Catalysts, 1993, Freiburg I.Br, Germany, R. Muelhaupt, G. Fink and H.H. Brintzinger (Eds)*
- [7] Razavi, A., Peters, L., Nafpliotis, L., Vereecke, D., Den Daw, K. *Makromol. Symp.* 89 (1995) 345
- [8] The hexane insoluble fractions could not be measured with this instrument since it is not soluble at 70°C upper working temperature for the 600 MHz instrument in question and the 400MHz spectra provided only pentad information insufficient for this kind of analysis.
- [9] a) Busico,V., Cippullo, R., Monaco, G, Vacatello,M, Segre, A. L. *Macromolecules*, 30 (1997) 6251; b) Busico, V., private communication
- [10] a) From the perspective of the incoming monomers the chain is "seen" to be always at the same position. This is why we prefer the call this mechanism chain stationary mechanism for the catalysts with large distal substituents and two energetically non-equivalent diastereotopic positions to differentiate from site epimerization mechanism occurring in unsubstituted Cs symmetric systems with energetically equivalents enantiotopic positions. b) From the intermediate position it had taken during the metalacyclobutane formation transition state.
- [11] a) Bajgur, C.S., Tikkanen, W. R., Petersen, J. *Inorg. Chem.* 24 (1985) 2539. b) Smith, J.A., Seyere, J.V., Huttner, G., Brintzinger, H.H. *J.Organomet. Chem.* 173 (1979) 175. c) Razavi, A. unpublished results
- [12] Okuda, J., Schattenmann, F.J., Swacadlo, S., Massa, W., *Organometallics* 14 (1995) 789, Okuda, J., Amer, F. *J.Organomet. Chem.* 520 (1996)245, Shiomura,T., Asanuma ,T., Inoue, N. *Macromol. Rapid Commun.* 17 (1996) 9, Hagihara,H., Shiono, T, Ikeda, T. *Macromolecules* 30 (1997) 4783.
- [13] Razavi, A., European Patent application No 96111127,5 and international patent application PCT/EP97/03649 (WO 98/02469)

Current Vitality of Ziegler's Monumental Discovery of Zirconium Catalysis in Olefin Polymerization: Metallocene and Nonmetallocene Catalysts via Reductive Dimerization

John J. Eisch, Xian Shi and Fredrick A. Owuor

Department of Chemistry, State University of New York at Binghamton, Binghamton, New York 13902-6016 U.S.A.

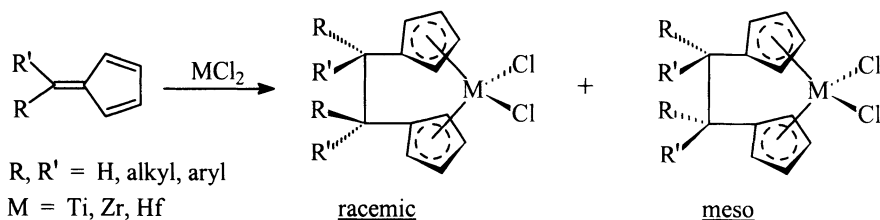
Abstract.

Although the avalanche of technical advances unleashed by Ziegler's discovery of the low-pressure polymerization of ethylene is most often associated with the use of titanium procatalysts, it is well to recall that the key initial experiment leading to the formation of polyethylene was achieved in 1953 with zirconium(IV) acetylacetonate.¹ Titanium salts maintained their superiority in the heterogeneous Ziegler-Natta catalysts used for olefin polymerization during the next two decades. With the reawakening of interest in homogeneous, single-site metallocene polymerization catalysts in the late 1970s, the zirconocene(IV) derivatives have regained a marked ascendancy, because they undergo deactivating reduction much less readily than titanocene(IV) derivatives.

The synthesis of such metallocenes of titanium, zirconium and hafnium generally requires the interaction of the Group 4 MCl_4 with the appropriately substituted cyclopentadienyl salt. In the present work we show how a great variety of bridge-substituted *ansa*-metallocenes can be prepared by the reductive dimerization of a suitable fulvene by the preformed Group 4 MCl_2 .²

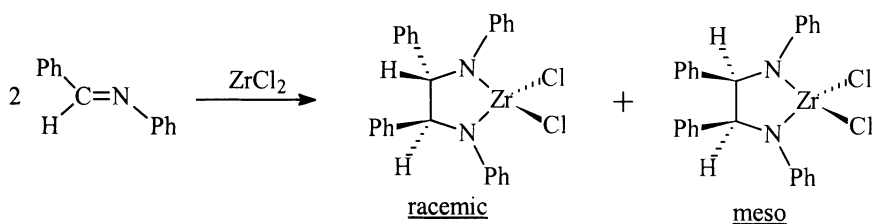
¹ K. Ziegler, E. Holzkamp, H. Breil and H. Martin, *Angew. Chem.*, **67**, 541 (1955).

² J.J. Eisch, X. Shi, J.R. Alila and S. Thiele, *Chem. Ber./Recl.*, **130**, 1175 (1997).



If R and R' are methyl, the tetramethylethylene-bridged ansa-metallocene can readily be obtained. If R = H and R' = alkyl or aryl, varying proportions of racemic and meso isomers can be obtained and separated into individual isomers.

This reductive coupling can also be applied to imines and even carbonyl derivatives and thus can lead to nonmetallocene catalyst systems as exemplified by the reductive coupling of benzalaniline:



All the foregoing metallocene and nonmetallocene procatalysts, when combined with MAO, are efficient polymerization catalysts for ethylene. The possible stereoselectivity of the racemic isomers for the polymerization of propylene is under investigation.

Introduction

The International Symposium on Metalorganic Catalysts for Synthesis and Polymerization has fittingly scheduled at its midpoint a Karl Ziegler Symposium, in order to commemorate the 100th anniversary of that brilliant scientist's birth and at the same time to acknowledge with gratitude his outstanding discoveries to which we owe the birth of the field of organometallic catalysis of hydrocarbon reactions just 45 years ago.

Ziegler's particular discovery of the low-pressure polymerization of ethylene by combinations of zirconium or titanium salts and aluminum alkyls certainly contains strong elements of accident, luck and serendipity, because Ziegler and his coworker, Hans Breil, came upon this revolutionary discovery while hoping to find something entirely different, an explanation for and the promotion of the so-called

Nickel Effect. But whether a great deal of their discovery be ascribed to fortuity or not, it is instructive to note that the sequence of experiments that led them to expose a Group 4 metal salt and triethylaluminum to ethylene was not the random mixings of ingredients but consequential experiments whose results suggested the succeeding trial. The focus was thus on careful experimental observation and not on any preconceived theory of what to expect. Ziegler did recognize what kind of result would be uninteresting and what would be startling. Thus Ziegler was alert and prepared in the sense expressed by Pasteur: Chance favors the prepared mind. The details of the background of the researches that led up to the experiment of Ziegler and Breil, whereby zirconium(IV) acetylacetonate and triethylaluminum were allowed to interact with ethylene to produce polyethylene, is a most inspiring and exciting story of a pioneering discovery, whose details can be found in accounts by Ziegler himself[1] and by his associates[2,3]. Such accounts are especially uplifting for younger chemists who may occasionally be depressed by the completely unsubstantiated impression that “all the important scientific discoveries have already been made”.

Background

Although Ziegler and Breil's historic discovery of transition-metal ethylene polymerization in 1953 was realized with zirconium(IV) acetylacetonate, they immediately investigated the possible suitability of other transition and actinide metal salts, such as those of iron, chromium, titanium, thorium and uranium, and finally determined that titanium derivatives, such as TiCl_4 , produced the most active heterogeneous polymerization catalysts for ethylene[4]. The momentous findings of Giulio Natta's group in 1954, namely that Ziegler catalysts prepared from TiCl_3 could effect the stereoselective polymerization of alpha-olefins, were also achieved with heterogeneous catalyst systems[5]. For the next two decades such Ziegler-Natta catalysts, which revolutionized the polymer industry worldwide, were titanium(III)-based heterogeneous systems on solid supports, whose catalytic activity was usually modified by the addition of various Lewis acids[5].

Not until the mid 1970s did homogeneous polymerization catalysts begin to attract attention. Kaminsky and Sinn demonstrated between 1975 and 1980 that titanocene and zirconocene derivatives, when combined with poly(methylaluminoxane) (MAO), were excellent ethylene polymerization catalysts[6]. That such metallocenes cocatalyzed by aluminum alkyls can effect the polymerization of ethylene in homogeneous media, albeit slowly, had already been observed in 1957 with titanocene dichloride by Natta's group[7] and independently by Breslow at the Hercules Corporation[8]. But the important insight concerned the significant stereoselective properties exhibited by ansa-metallocene catalysts in homogeneous media. The initial breakthrough was achieved with the ethylene(bisindenyl) derivatives of titanium(IV) and zirconium(IV) dichloride, which were first synthesized and separated into their

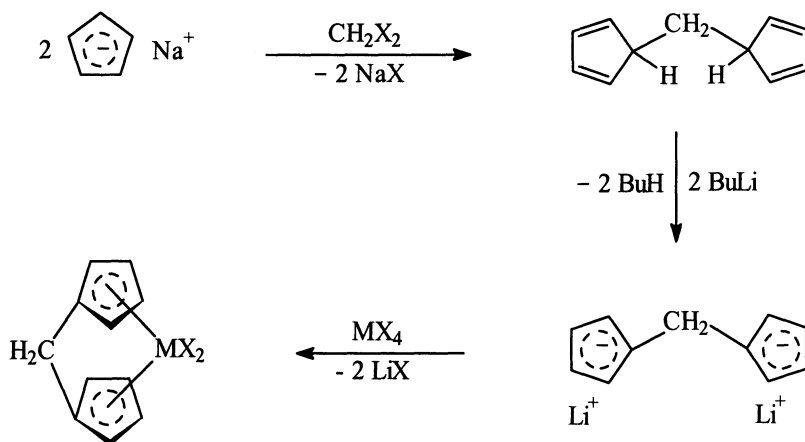
meso- and racemic-isomers by Brintzinger's group[9]. In 1984 Ewen reported that the specific metallocene employed with MAO could influence the stereoselectivity with which propylene is polymerized in this homogeneous system. Particularly noteworthy was his finding that rac-ethylene(bis-indenyl)titanium dichloride and MAO produced polypropylene of significant isotactic content.[10] In the very next year Kaminsky and Brintzinger reported that the analogous racemic zirconium derivative with MAO polymerized propylene to polypropylene of 86-91% isotactic content[11].

The second breakthrough with ansa-metallocenes was the discovery in 1988 by Ewen of the syndiospecific polymerization of propylene by agency of isopropylidene(cyclopentadienyl)(9-fluorenyl)zirconium dichloride and MAO, once again in a homogeneous phase and at rates of industrial feasibility[12].

Continuing developments in such single-site metallocene procatalysts are focusing on the introduction of substituents into such ansa-metallocenes, so as to modulate the stereoselectivity of the resulting catalyst and thereby to permit the synthesis of polymers with tailored properties.[13]. Because such metallocene catalysts owe their activity to their high oxidation states, interest has shifted back to zirconium derivatives and away from titanium derivatives because titanium(IV) is so readily reduced to titanium(III) with consequent loss of polymerization activity.

Results

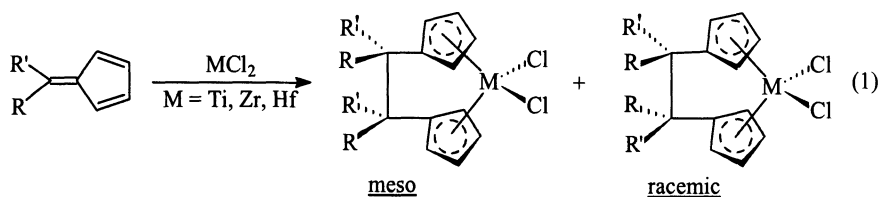
The importance of ansa-metallocenes in current industrial research and development requires that methods for their synthesis be available that are at once efficient, convenient and economical. Up to the present, some variant of the basic approach of Brintzinger has been employed (Scheme 1): 1) synthesis of the bicyclopentadiene derivative with its bridging group (here, $-\text{CH}_2-$); 2) metallation to form the dimetallo salt (usually achieved with BuLi); and 3) reaction of the dimetallo salt with MCl_4 , $\text{M} = \text{Ti, Zr and Hf}$ [14].



Scheme 1.

In connection with our recent investigations of the reducing action of subvalent transition metal salts on organic substrates[15], we noted with interest the ability of TiCl_2 [16] and ZrCl_2 [15] to effect the reductive dimerization of various organic derivatives with the formation of a carbon-carbon bond (Figure 1).

Such observations prompted us to ask whether such reductive dimerization induced by Group 4 metal dichlorides could be achieved between fulvenes. Were such reduction possible, two important outcomes might be realized: 1) the MCl_2 unit might remain as a π -complex with the two cyclopentadienyl rings to form an ansa-metallocene; and 2) with a 6,6'-unsymmetrically substituted fulvene, a mixture of meso and racemic ansa-metallocenes should thereby be formed (eq. 1).



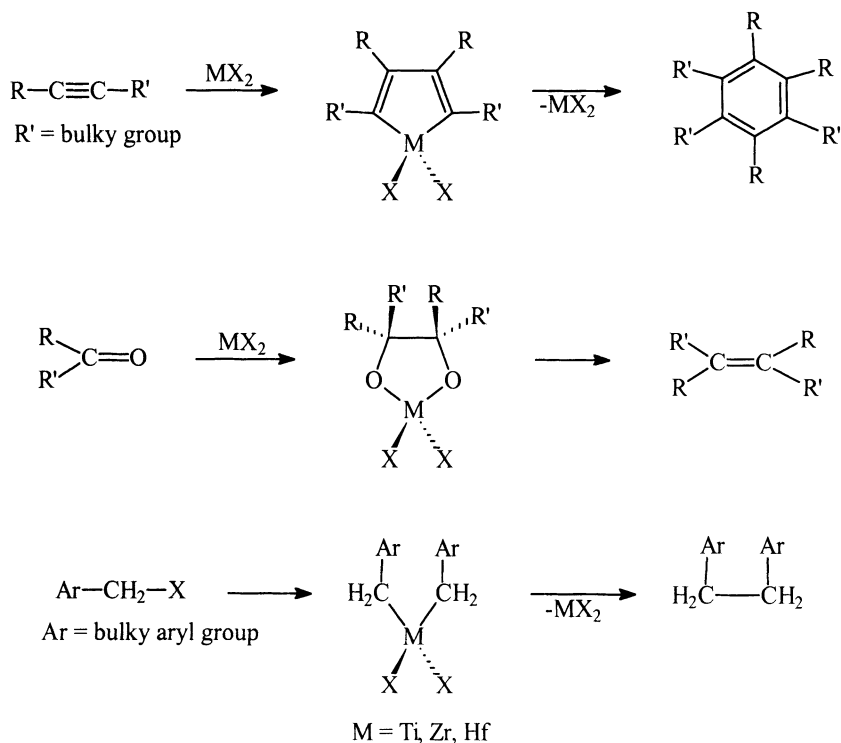
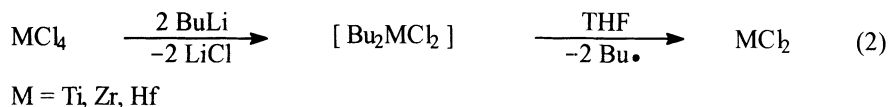


Fig. 1. Reductive Dimerizations of Group 4 Metal Dihalides

The proposed synthesis of ansa-metallocenes seemed both convenient and efficient, because a wide variety of fulvenes can be readily prepared from cyclopentadiene and the appropriate carbonyl derivatives[17] and the requisite Group 4 dichloride can be generated by the alkylative reduction of the Group 4 tetrachloride by treatment with 2 equiv. of butyllithium in THF (Eq. 2)[15, 16, 18].



Our initial test of this proposal with 6,6-dimethylfulvene was gratifyingly successful: heating the fulvene with MCl_2 (containing the LiCl from its preparation) in refluxing toluene gave good to excellent yields of the Group 4 ansa-metallocene dichloride, which could be freed from the LiCl by Soxhlet extraction with alkanes or arenes[19] (Figure 2).

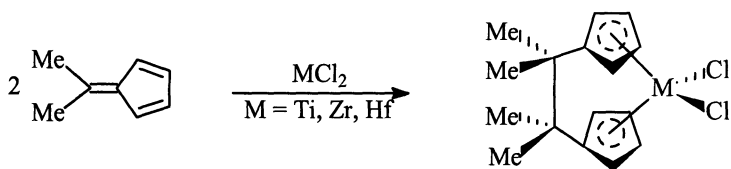


Fig. 2. ansa-Tetramethylene-Bridged Metallocenes

To determine the possibility of synthesizing both meso and racemic ansa-metallocenes, 6-phenylfulvene was treated individually with TiCl_2 and with ZrCl_2 . In both experiments the ansa-metallocene isomers were formed in at least 90% overall yield and by integration of the methine H signals in their ^1H NMR spectra in both cases a 50:50 mixture of the meso and racemic isomers was obtained. With the hope of steering the dimerization toward the racemic isomer by steric bulk, corresponding couplings by ZrCl_2 were undertaken with 6-(1-naphthyl)fulvene and 6-(9-anthryl)fulvene. In these experiments similar ^1H NMR analyses of the methine H signals showed in the case of the 1-naphthyl derivative the presence of 83% of the racemic derivative and in the case of the 9-anthryl fulvene the presence of only one isomer, which for steric reasons must necessarily be the racemic isomer[19] (Figure 3).

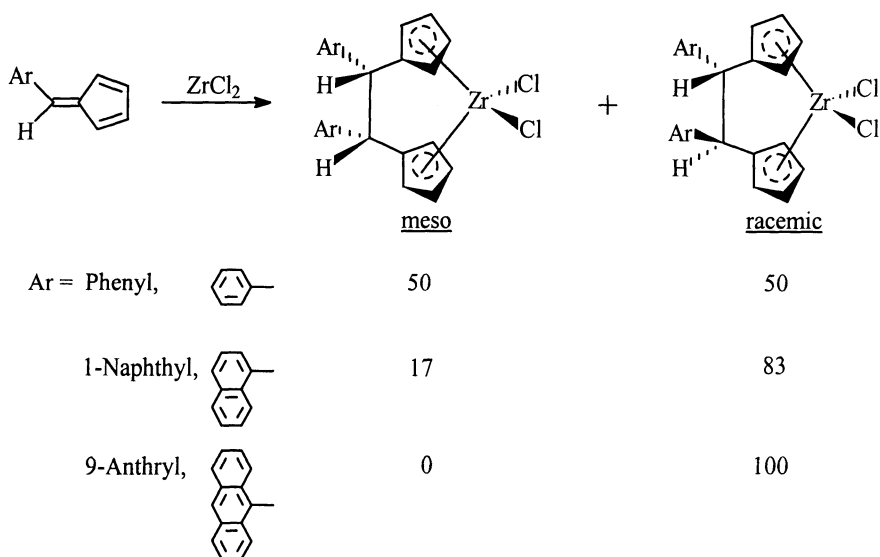


Fig. 3. ansa-1,2-Diarylethylene-Bridged Zirconocenes

To probe the suitability of our approach for the generation of ansa-indenyl metallocenes, 1', 1'-dimethylbenzofulvene was allowed to react with $ZrCl_2$ in refluxing toluene. The dimerization proceeded in high yield to the ansa-tetramethylethylene-bridged benzozirconocene dichlorides having the meso- and racemic-isomers in an equimolar ratio[19] (Figure 4).

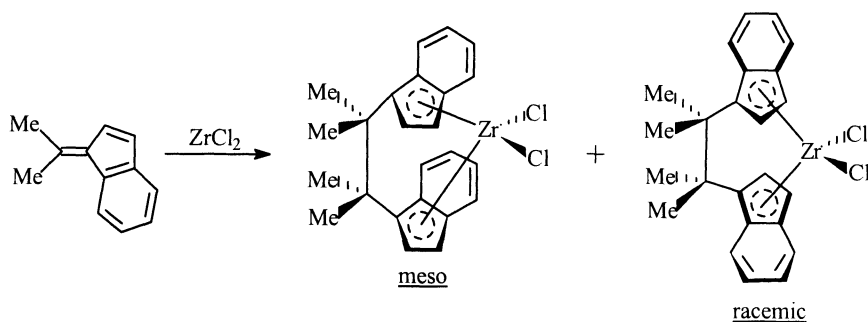


Fig. 4. ansa-Tetramethylethylene-Bridged Benzozirconocenes

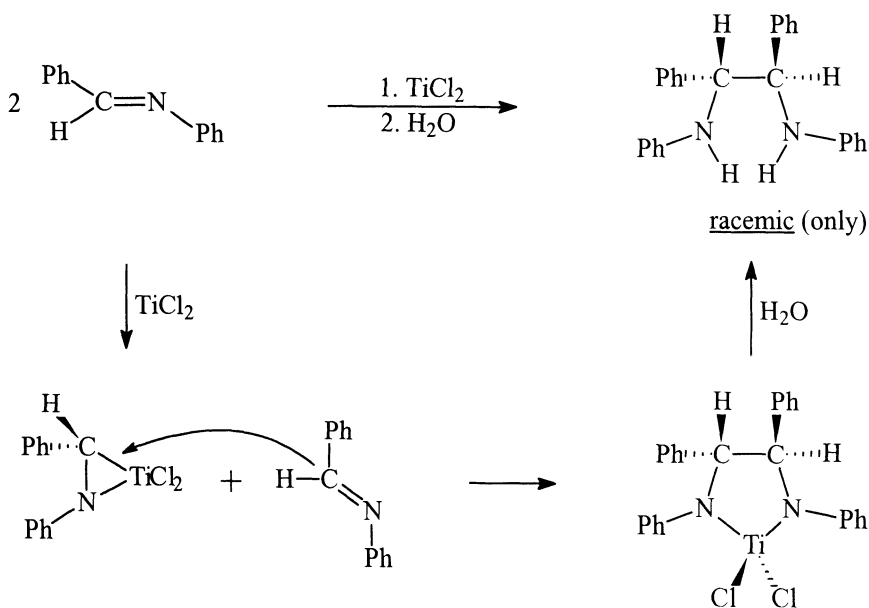


Fig. 5. Possible Mechanism of Oxidative Addition to Imines

The success of this novel synthesis of ansa-metallocenes has encouraged us to examine the suitability of such Group 4 metal dichlorides for the reductive dimerization of carbonyl and imine derivatives and thus for the synthesis of ansa-nonmetallocene Group 4 olefin polymerization catalysts. Indeed, the interaction of benzalaniline with TiCl_2 led to the dimerization of the imine into the TiCl_2 salt of exclusively the racemic isomer of 1,2-dianilino-1,2-diphenylethane (Figure 5). To explain such high selectivity in carbon-carbon bond formation, we suggest that a titanaazacyclopropane intermediate is formed by the oxidative addition of TiCl_2 to the $\text{C}=\text{N}$ bond and that then a second benzalaniline inserts, with steric control, into the $\text{C}-\text{Ti}$ bond of the titanaazacyclopropane intermediate[15] (Figure 5). The reductive dimerization of benzalaniline and related imines by ZrCl_2 is not nearly as selected and the ratio of the racemic : meso nonmetallocenes is about 75:25 (Figure 6). Possibly the larger atomic radius of zirconium (1.60Å) compared with

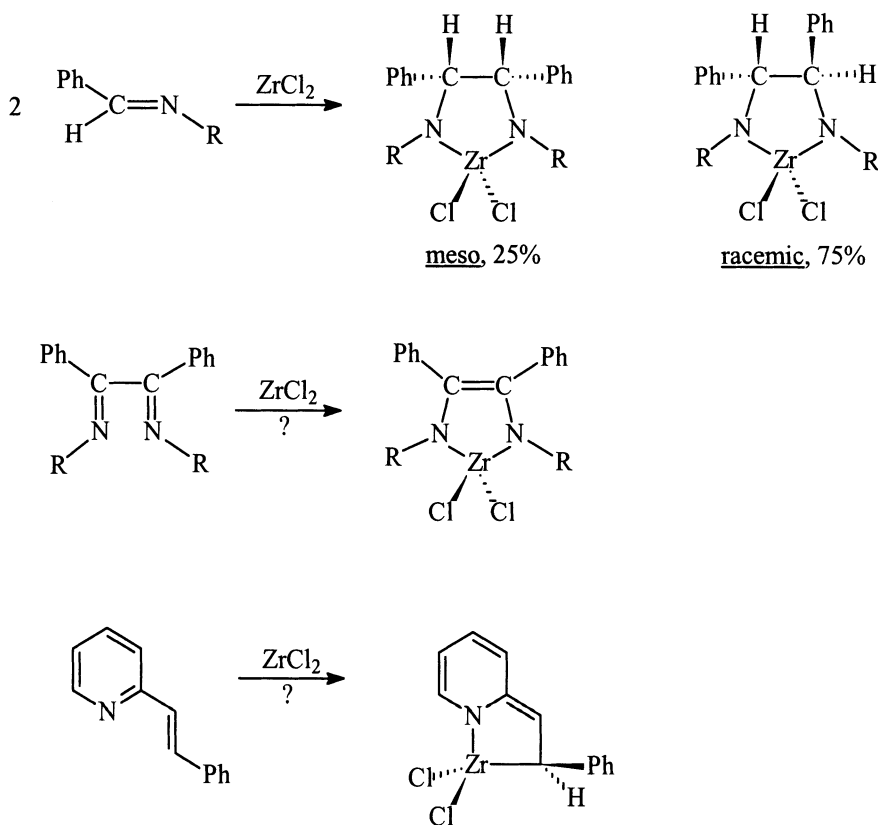


Fig. 6. Oxidative Additions of ZrCl_2 to Imines

titanium (1.46Å), diminishes steric influence in the carbon-carbon bond formation step. Two other potential intramolecular oxidative additions of $ZrCl_2$ to imines, which are also depicted in Figure 6, are currently under investigation[20].

In an analogous manner, ansa-nonmetallocene derivatives involving oxygen have been synthesized from carbonyl derivatives and $ZrCl_2$. In such reductive dimerizations of aldehydes and ketones, it is important to choose bulky organic substituents, lest the intermediate glycolate salt undergo rapid deoxygenation to the olefin (McMurry reaction). Our studies have shown that pivalaldehyde can undergo reductive dimerization with $ZrCl_2$ to produce solely the racemic isomer of the $ZrCl_2$ salt of the pinacol (Figure 7). Two other potential intramolecular oxidative additions of $ZrCl_2$ to ketonic derivatives are also suggested in Figure 7[20].

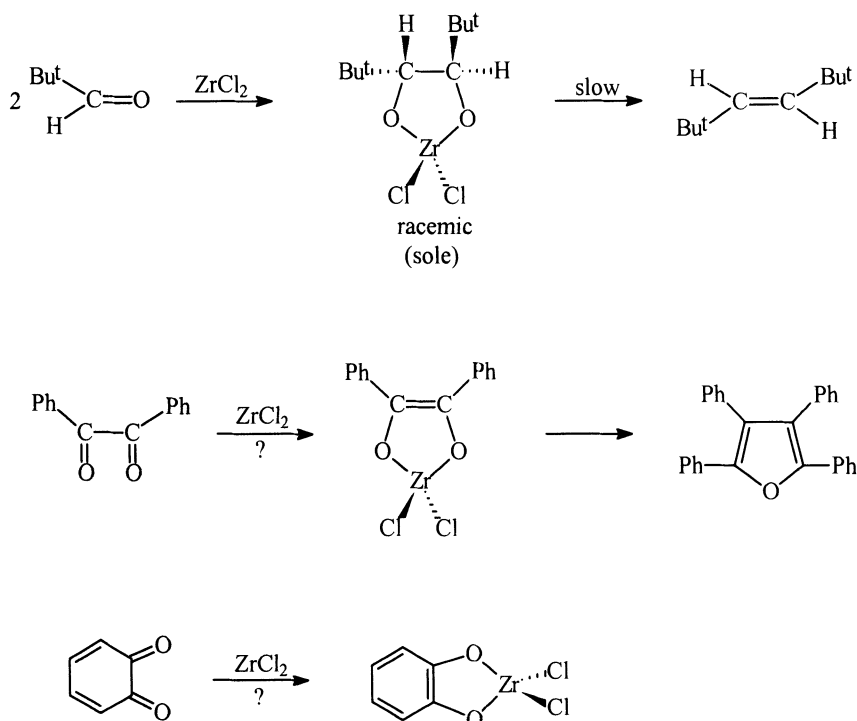


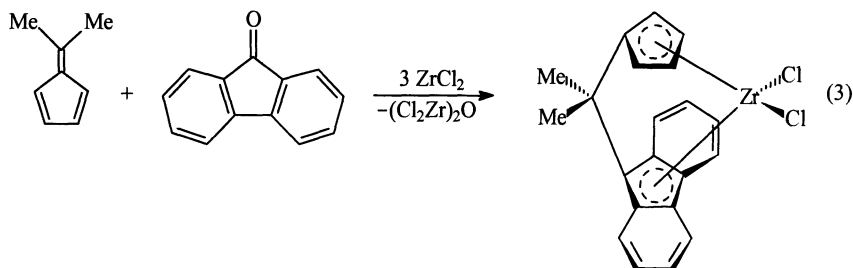
Fig. 7. Oxidative Additions of $ZrCl_2$ to Carbonyl Derivatives

All the foregoing ansa-metallocene procatalysts generated from imines or from carbonyl derivatives, once combined with MAO, have proved to form efficient

catalysts for the polymerization of ethylene to linear high-density polyethylene. The possible suitability of the racemic ansa-metallocenes or racemic ansa-nonmetallocene complexes for the stereoselective polymerization of propylene is under evaluation.

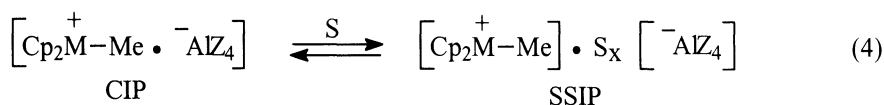
Discussion

The interaction of Group 4 metal dihalides with fulvenes in the present investigation has been shown capable of producing preponderantly racemic ansa-metallocenes having C_2 symmetry and potentially capable of fostering the isospecific polymerization of propylene (racemic isomers in Figures 3 and 4). In order to generate one-carbon bridged ansa-metallocenes like isopropylidene(cyclopentadienyl)(9-fluorenyl)zirconocene dichloride (Eq. 3), one would have to effect a cross-coupling, such as the following proposed deoxygenative coupling between a fulvene and a cyclopentadienone (Eq. 3). Having C_s symmetry, such a mixed ansa-metallocene can greatly favor the syndiospecific polymerization of alpha-olefins. Achieving such cross-couplings as that depicted in Eq. 3 is a prime goal of our current investigations[21].



But over and above attaining a certain stereoselectivity in polymerizing alpha-olefins with ansa-metallocenes having C_2 or C_s symmetry, there are significant advantages in employing ansa-metallocenes with MAO for the polymerization of ethylene or alpha-olefins, compared with unbridged metallocenes. Bridged metallocenes exhibit a higher rate of propagation and hence lead to higher molecular weights of the resulting polymer than unbridged metallocenes. Such higher polymer molecular weights could result from higher rates of olefin monomer insertion into the transition metal-carbon bond combining with lower rates of chain transfer occurring by metal-hydride elimination[22]. Also, in copolymerization of ethylene and alpha-olefins unbridged metallocenes tend to produce copolymers of lower molecular weight than those obtained with bridged metallocenes[23]. Again, the molecular explanation appears to be that the metal-carbon bond of the unbridged metallocenium cation appears to insert olefin monomer more slowly and to undergo chain transfer by metal-hydride elimination more rapidly.

The foregoing superiority of bridged metallocenes over unbridged metallocenes can be related to the current view of the active site of such metallocene catalysts as generated by alkylaluminum derivatives, namely that the active site is an ion-pairing of a metallocenium cation with an anionic aluminum anion. Furthermore, the ion-pairing can be an equilibration of a contact ion-pair (CIP) with a solvent-separated ion-pair (SSIP) (Eq. 4). Studies involving solvent polarity and concentration in such catalyst systems have concluded that solvent-separated ion-pairs are the more active sites in ethylene polymerization[18, 24-29].



With this ion-pairing model in mind, it becomes clear why bridged metallocenes should generate more active polymerization catalysts: the two-carbon ansa-bridge and its substituents will block the close approach of the AlZ_4 anion to one side of the metallocene, thereby reducing the formation of contact ion-pairs (Figure 8).

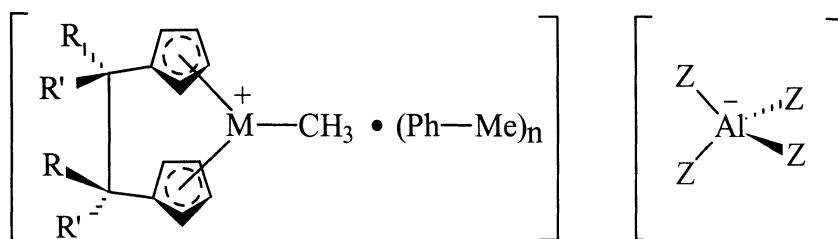


Fig. 8. ansa-Bridged metallocenes likely raise the steric barrier to tight ion-pairing and thereby promote the more reactive solvent-separated ion-pairing in toluene solution.

If the promotion of solvent-separated ion-pairs would lead to more reactive catalyst systems, we decided to design and synthesize organoalanes having two aluminum centers situated in the resulting Lewis acid, so that a chelating Lewis acidic action could be exerted on the neutral methylmetallocene derivative, $\text{Cp}_2\text{M}(\text{Me})\text{A}$, and the compound converted into solvent-separated ion-pairs (Figure 9). Thus by using the chelating o-bis(methylchloroalumino)benzene in toluene, the anion A would be bound in a chelate and thus be prevented from forming a CIP complex with the metallocenium cation.

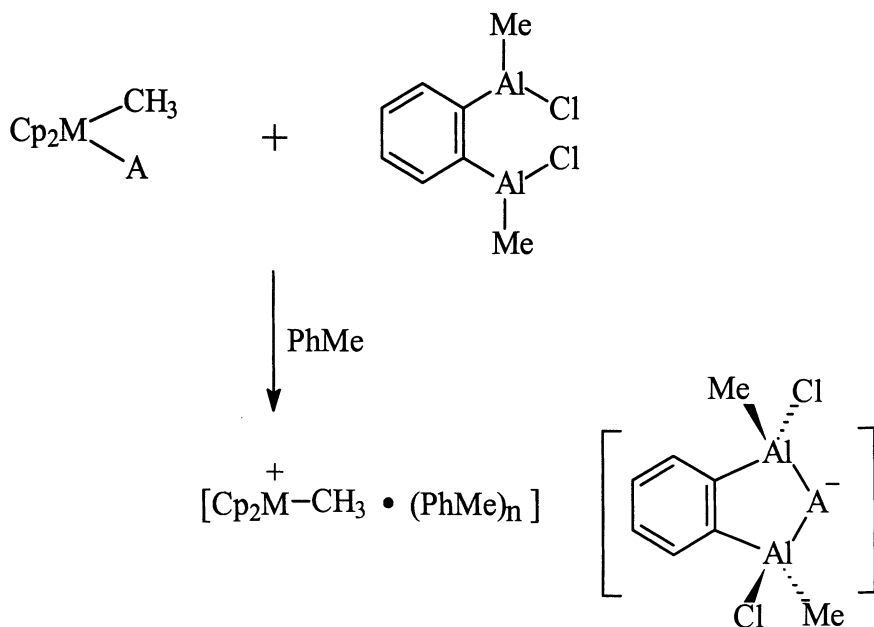


Fig. 9. Chelating Organodialanes Promote Solvent-Separated Ion Pairs in Metallocene Catalysis

In order to test this concept, the two chelating arylalanes depicted in Figure 10, namely structures **1** and **2**, were individually synthesized from the corresponding organotin derivatives in an efficient manner, according to novel procedures recently patented or published[30, 31]. The cocatalytic action of these chelating organoalanes was compared with that of MAO, MeAlCl_2 , and the *meta*- and *para*-isomers of bis(methylchloroaluminum)benzene by combining the individual aluminum cocatalyst with titanocene methyl chloride in an atomic Ti:Al ratio of 1:8 and measuring the productivity numbers of the individual catalyst systems for polymerizing ethylene (Figure 11). From the results it is evident that chelating aluminum cocatalysts, **1** and **2**, under the stated conditions, are markedly superior to MAO and display productivities about 2.5-3.0 times greater. Noteworthy is that the *meta*- or *para*-isomers of **1**, namely **3** and **4**, which cannot function as a chelating Lewis acid, show a low productivity as a cocatalyst, comparable to the rather ineffectual MeAlCl_2 itself. These composite findings confirm the value of the concept that has motivated this aspect of our work on Ziegler-Natta catalysis, namely that chelating Lewis acids make superior cocatalysts for olefin polymerization by promoting the generation of solvent-separated ion-pairs, the most active sites in such catalyst systems. Finally, we can combine the findings with *ansa*-metallocenes with those on chelating Lewis acids and conclude that the

most active olefin polymerization systems will be composed of ansa-metallocenes and chelating Lewis acids.

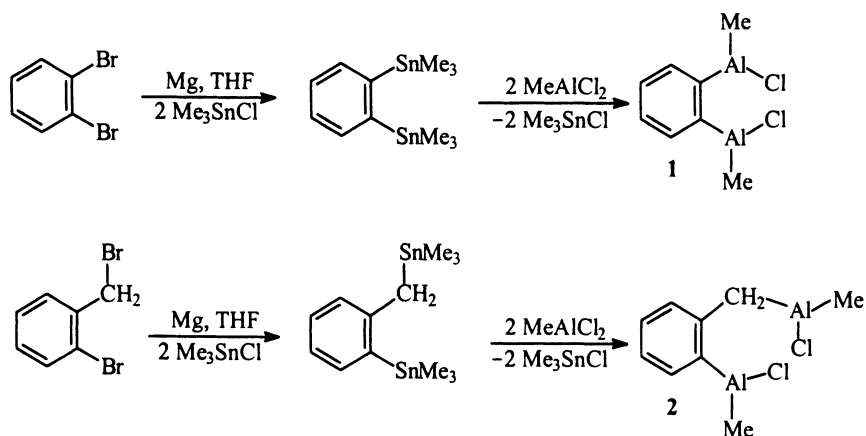
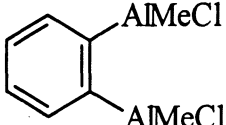
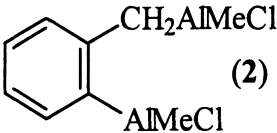
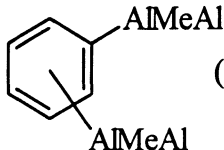


Fig. 10. Chelating Organoalanes

Acknowledgment

The research with subvalent Group 4 metal halides originated in a materials science project sponsored by Akzo Corporate Research USA. The research results obtained on chelating organoaluminum compounds were obtained under a grant from Witco GmbH, Bergkamen, Germany, and those involving the synthesis of metallocenes from fulvenes by research support from Solvay S.A., Brussels,

| <u>Cocatalyst</u> | <u>PN</u> |
|---|-----------|
|  <div style="display: inline-block; vertical-align: middle; margin-left: 10px;">(1)</div> | 2,340 |
|  <div style="display: inline-block; vertical-align: middle; margin-left: 10px;">(2)</div> | 1,925 |
| MAO | 810 |
| MeAlCl ₂ | 200 |
|  <div style="display: inline-block; vertical-align: middle; margin-left: 10px;">(3) (4)</div> | ~ 200 |

Conditions: start at ambient temperature in toluene with Ti:Al ratio of 1:8

Productivity numbers: grams PE/gram Ti · h · bar

Fig. 11. Polymerization Activity of Organoaluminum Cocatalysts with Titanocene methyl chloride, Cp₂Ti(Me)Cl

Belgium. Further support was provided by grants from the National Science Foundation and a Senior Scientist Award from the Alexander von Humboldt Foundation, Bad Godesberg, Germany, to the senior author. We are indebted to all these organizations for their indispensable financial aid.

References

- [1] K. Ziegler, Brennst.-Chem. **1954**, 35, 321.
- [2] G. Wilke, Angew. Chem. **1975**, 87, 805.
- [3] J.J. Eisch, J. Chem. Ed. **1983**, 60, 1009.
- [4] K. Ziegler, E. Holzkamp, H. Breil, H. Martin, Angew. Chem. **1955**, 67, 541.
- [5] J. Boor, Jr., Ziegler-Natta Catalysts and Polymerizations, Academic Press, New York, 1979, pp. 670.
- [6] A. Andresen, H. Cordes, J. Herwig, W. Kaminsky, A. Merck, R. Mottweiler, J. Pein, H. Sinn, H. Vollmer, Angew. Chem. Int. Ed. Engl. **1976**, 15, 629.
- [7] G. Natta, P. Pino, G. Mazzanti, R. Lanzo, Chim. Ind. (Milan) **1957**, 39, 1032.
- [8] D.S. Breslow, N.R. Newburg, J. Am. Chem. Soc. **1957**, 79, 5073.
- [9] F.R.W.P. Wild, L. Zsolnai, G. Huttner, H.H. Brintzinger, J. Organomet. Chem. **1982**, 232, 233.
- [10] J.A. Ewen, J. Am. Chem. Soc. **1984**, 106, 6355.
- [11] W. Kaminsky, K. K ulper, H.H. Brintzinger, F.R.W.P. Wild, Angew. Chem. Int. Ed. Engl. **1985**, 24, 507.
- [12] J.A. Ewen, L. Jones, A. Razavi, J. Am. Chem. Soc. **1988**, 110, 6255.
- [13] W. Spaleck, M. Antberg, M. Aulbach, B. Bachmann, V. Dolle, S. Haftka, F. K uber, J. Rohrmann, A. Winter, Ziegler Catalysts, G. Finke and R. M ulhaupt, Eds., Springer-Verlag, Berlin, 1995.
- [14] F. Wochner, L. Zsolnai, G. Huttner, H.H. Brintzinger, J. Organomet. Chem. **1985**, 288, 69.
- [15] J.J. Eisch, X. Shi, J.R. Alila, S. Thiele, Chem. Ber./Recl. **1997**, 130, 1175.
- [16] J.J. Eisch, X. Shi, J. Lasota, Z. Naturforsch. **1995**, 50b, 342.
- [17] K.J. Stone, R.D. Little, J. Org. Chem. **1984**, 49, 1849.
- [18] J.J. Eisch, S.I. Pombrik, X. Shi, S.C. Wu, Macromol. Symp. **1995**, 89, 221.
- [19] J.J. Eisch, X. Shi, F.A. Owuor, Organometallics, in press.
- [20] J.J. Eisch, F.A. Owuor, investigation in progress.
- [21] J.J. Eisch, P.O. Fregene, investigation in progress.
- [22] W. Spaleck, F. K uber, A. Winter, J. Rohrmann, B. Bachmann, M. Antberg, Volker Dolle, E.F. Paulus, Organometallics, **1994**, 13, 954.
- [23] F.J. Carol, S.C. Kao, E.P. Wasserman, R.C. Brady, New J. Chem. **1997**, 21, 797.
- [24] J.J. Eisch, J.E. Galle, A. Piotrowski, Transition Metal Catalyzed Polymerizations. Alkenes and Dienes, Harwood Academic Publishers, 1983, pp. 799-823.
- [25] J.J. Eisch, A.M. Piotrowski, S.K. Brownstein, E.J. Gabe, F.L. Lee, J. Am. Chem. Soc., **1985**, 107, 7219.
- [26] J.J. Eisch, M.P. Boleslawski, A.M. Piotrowski, Transition Metals and Organometallics as Catalysts for Olefin Polymerization, W. Kaminsky and H. Sinn, Eds., Springer-Verlag, Berlin, 1988, pp. 371-378.
- [27] J.J. Eisch, K.R. Caldwell, S. Werner, C. Kr uger, Organometallics, **1991**, 10, 3417.
- [28] J.J. Eisch, S.I. Pombrik, G.X. Zheng, Organometallics, **1993**, 12, 3856.
- [29] J.J. Eisch, S.I. Pombrik, S. G urtzgen, R. Rieger, W. Uzick, Catalyst Design for Tailor-Made Polyolefins, K. Soga and M. Terano, Eds., Kodansha, Tokyo, 1994, pp. 221-235.
- [30] J.J. Eisch, W. Uzick, K. Mackenzie, S. G urtzgen, R. Rieger, U.S. Patent 5,726,332, Mar. 10, 1998.
- [31] J.J. Eisch, K. Mackenzie, H. Windisch, C. Kr uger, Eur. J. Inorg. Chem., in press.

Kinetic Features of Living Polymerization of Propene with the $[t\text{-BuNSiMe}_2\text{Flu}]\text{TiMe}_2/\text{B}(\text{C}_6\text{F}_5)_3$ Catalyst

Takeshi Shiono, Hideaki Hagihara, Satoru Yoshida, Tomiki Ikeda

Research Laboratory of Resources Utilization, Tokyo Institute of Technology, Nagatsuta 4259, Midori-ku, Yokohama 226-8503, Japan
tshiono@res.titech.ac.jp

Abstract. Propene polymerization was conducted by $[\eta^1\text{-}t\text{-butyl}(\text{dimethylfluorenylsilyl})\text{amido}]\text{dimethyltitanium}$ combined with $\text{B}(\text{C}_6\text{F}_5)_3$ as a cocatalyst. Living polymerization proceeded at $-50\text{ }^\circ\text{C}$ in the presence of suitable amounts of $\text{B}(\text{C}_6\text{F}_5)_3$ and AlOct_3 . Addition of AlOct_3 and excess $\text{B}(\text{C}_6\text{F}_5)_3$ drastically increased the polymer yield and molecular weight with a small increase in the number of polymer chains. The results indicated that these Lewis bases enhanced the propagation rate although chain transfer reaction was slightly induced. The time-conversion curve showed that the polymerization rate depended on almost second order of propene concentration

Introduction

Living polymerization system, in which neither chain transfer nor deactivation occurs, affords polymers with predictable molecular weights and narrow molecular weight distributions. The living polymerization techniques can be also utilized for synthesis of terminally-functionalized polymers and block copolymers. Development of homogeneous single-site catalysts for α -olefin polymerization has enabled us to control the stereoregularity and the regioregularity of polyolefins. However, only the $\text{V}(\text{acac})_3/\text{AlEt}_2\text{Cl}$ (acac = acetylacetonate or its analog) system had been known as a homogeneous catalyst for living polymerization of propene at $-78\text{ }^\circ\text{C}$.¹⁾

Recently, several living systems for α -olefin polymerizations have been found by using transition metal catalysts including N-based ligands. Brookhart *et al.*²⁾ found that the living polymerization of α -olefins (propene, 1-hexene, and 1-octadecene) proceeded at $-10\text{ }^\circ\text{C}$ with Ni-diimine catalysts. McConville *et al.*³⁾ reported that the regiospecific living polymerization of higher α -olefins (1-hexene, 1-octene, and 1-decene) was achieved by chelating diamido complexes of titanium at $23\text{ }^\circ\text{C}$. Schrock *et al.*⁴⁾ also reported the living polymerization of 1-hexene by zirconium complex which contains the tridentate diamido ligand. More recently, Jeon *et al.*⁵⁾ found that the zirconium complexes with 2,2'-ethylenebis(N,N'-(trisisopropylsilyl)anilino) ligand conducted the living polymerization of 1-hexene

at -10 °C. These results indicate that the N-based ligands play an important role in the living polymerization of α -olefin by the transition metal catalyst.

The monocyclopentadienyl-amido complexes, which were found by Bercaw⁶⁾ and Okuda⁷⁾, have also attracted much attention because the complexes are excellent catalysts for copolymerization of ethene with higher α -olefin or styrene⁸⁻¹⁰⁾. We have recently found that $[\eta^1:\eta^3\text{-}t\text{-butyl}(\text{dimethylfluorenylsilyl})\text{ amido}]\text{-dimethyl-titanium } ([t\text{-BuNSiMe}_2\text{Flu}]\text{TiMe}_2)^{11)}$ conducted living polymerization of propene and 1-hexene combined with tris(pentafluorophenyl)borane ($\text{B}(\text{C}_6\text{F}_5)_3$) at -50 °C in a highly regiospecific manner¹²⁾. This paper described some kinetic features of propene polymerization with this catalyst.

Experimental Part

Materials Trioctylaluminum (AlOct_3) and $\text{B}(\text{C}_6\text{F}_5)_3$ were provided by Tosoh-Akzo Co. Propene from Mitsubishi Petrochemical was purified by bubbling it through a $\text{NaAlH}_2(i\text{-Bu})_2/1,2,3,4\text{-tetrahydronaphthalene}$ solution. Research grade TiCl_3 and PbCl_2 were used without further purification. Research grade toluene commercially obtained was purified according to the usual procedures. $[t\text{-BuNSiMe}_2\text{Flu}]\text{TiMe}_2$ was synthesized according to the procedures described in the previous report¹²⁾.

Polymerization Procedure Polymerization of propene was conducted in a 100 mL glass reactor by batchwise operation at -50 °C. To a reactor toluene was added (total vol. = 30 mL) and stirred in a ethanol bath equipped with a cryostat. Gaseous propene was introduced and liquefied at -50 °C. After addition of AlOct_3 as a scavenger, polymerization was started by successive introduction of $[t\text{-BuNSiMe}_2\text{Flu}]\text{TiMe}_2$ and cocatalyst. The polymerization was quenched by addition of HCl /methanol solution. The polymer obtained was washed several times with methanol and dried under vacuum at 60 °C.

Analytical Procedure Molecular weights and molecular weight distributions of PPs were determined by Waters 150C at 140 °C using *o*-dichlorobenzene as solvent. The following parameters were employed for universal calibration: $K = 1.38 \times 10^{-4}$ and $\alpha = 0.70$ for polystyrene standard; $K = 1.00 \times 10^{-4}$ and $\alpha = 0.74$ for polypropene. ^{13}C NMR spectra were recorded at 120 °C on a JEOL GX-500 spectrometer operated at 125.65 MHz in pulse Fourier-Transform mode. The pulse angle was 45°, and about 1000 scans were accumulated in pulse repetitions of 3.3 s. Sample solutions were made in tetrachloroethane- d_2 up to 10 % by weight. The central peak of tetrachloroethane- d_2 (74.47 ppm) was used as internal reference.

Results and Discussion

Influence of AlOct₃ Concentration

We used AlOct₃ in order to scavenge impurities like oxygen and water in the polymerization system. It is plausible, however, that AlOct₃ takes part in the polymerization such as initiation and chain transfer reactions. To investigate the effect of AlOct₃, we carried out propene polymerization in the absence or presence of AlOct₃.

Table 1 summarizes the results of the polymerization. Polymerization proceeded even in the absence of AlOct₃ although the activity was very low (run nos. 1 and 2). Addition of AlOct₃ drastically enhanced the activity as shown in run nos. 3 - 5. The plots of the polymer yield and the *M_n* value against polymerization time gave straight lines as displayed in Fig. 1A, which indicates that living polymerization proceeded under these conditions. The number of polymer chains calculated from the yields and the *M_n* values are independent of the presence of AlOct₃, whereas the *M_n* value with AlOct₃ was much larger than that without AlOct₃, even though the polymerization time with AlOct₃ was much shorter than that without AlOct₃. The results indicate that the addition of AlOct₃ enhanced the propagation rate but did not affect the initiation efficiency.

Table 1. Effects of AlOct₃ on propene polymerization with the [t-BuNSiMe₂Flu]TiMe₂/B(C₆F₅)₃ catalyst

| Run | Al/Ti (mol/mol) | [Al] (mM) | Time (h) | Yield (g) | <i>M_n</i> ^b (×10 ⁻⁴) | <i>M_w/M_n</i> ^b | N (μmol) ^c |
|----------------|--------------------|--------------|-------------|--------------|---|---|--------------------------|
| 1 ^a | 0 | 0 | 0.5 | trace | - | - | - |
| 2 ^a | 0 | 0 | 12 | 0.04 | 0.51 | 1.4 | 0.39 |
| 3 ^a | 10 | 12 | 0.1 | 0.12 | 1.4 | 1.7 | 0.44 |
| 4 ^a | 10 | 12 | 0.3 | 0.52 | 6.3 | 1.2 | 0.41 |
| 5 ^a | 10 | 12 | 0.5 | 1.04 | 10.2 | 1.3 | 0.51 |
| 6 ^b | 20 | 54 | 2 | 0.06 | 0.27 | 1.2 | 0.39 |
| 7 ^b | 20 | 54 | 4 | 0.13 | 0.38 | 1.2 | 0.66 |
| 8 ^b | 20 | 54 | 6 | 0.21 | 0.42 | 1.2 | 0.82 |

^a Polymerization conditions: Ti = 20 μmol, B = 40 μmol, toluene = 10 mL, C₃H₆ = 3.5 g, temp = -50 °C. ^b Polymerization conditions: Ti = 60 μmol, B = 60 μmol, toluene = 8.4 mL, C₃H₆ = 7 g, temp = -50 °C. ^c Determined by GPC using PS standard by universal calibration. ^d Number of polymer chains calculated from yield and *M_n*.

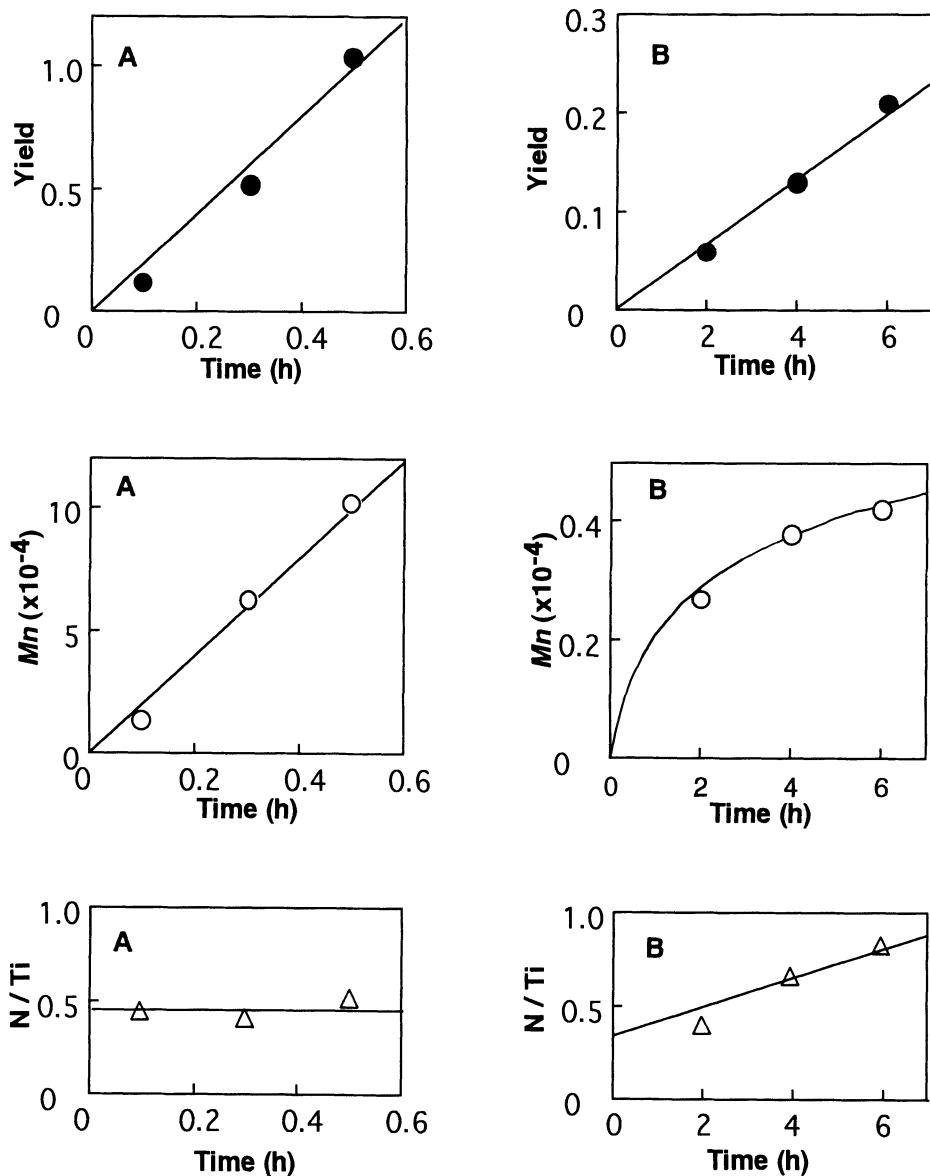


Fig. 1. Plots of Yield, Mn and N/Ti against polymerization time: **A**, $[Al]/[Ti] = 10$; **B**, $[Al]/[Ti] = 20$: The other polymerization conditions are shown in Table 1.

We conducted propene polymerization under higher concentration of AlOct_3 as shown in run nos. 6 - 8 although the other conditions were also slightly different. The polymer yield linearly increased against polymerization time, whereas the M_n value was gradually saturated. The number of polymer chains consequently increased with increase in polymerization time. The results indicate that higher concentration of AlOct_3 induced a chain transfer reaction.

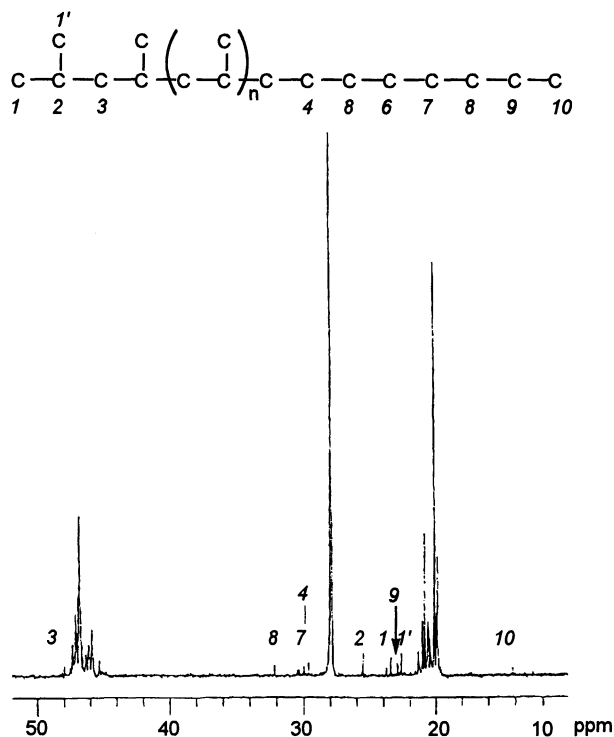


Fig. 2. 100 MHz ^{13}C -NMR spectrum of polypropene obtained with $[\textit{t}\text{-BuNSiMe}_2\text{Flu}]\text{TiMe}_2 / \text{B}(\text{C}_6\text{F}_5)_3$ in the presence of AlOct_3

In order to investigate what kind of chain transfer was induced by AlOct_3 , we measured the ^{13}C NMR spectrum of the polymer obtained in run no. 8. Beside the strong resonances of main-chain carbons around 20, 28 and 46 ppm, weak resonances of chain-end carbons were observed in the spectrum shown in Fig. 2. All these weak resonances can be assigned to 2-methyl-propyl and octyl end groups. The former could be formed by both the initiation at a Ti-Me bond and the termination with AlOct_3 followed by hydrolysis, and the latter by the initiation at a Ti-Octyl bond which is produced by chain transfer with AlOct_3 . Any other resonances cannot be detected in the olefinic regions of both the ^{13}C and ^1H NMR spectra, which indicated that AlOct_3 did not induce β -hydrogen transfer.

Influence of $B(C_6F_5)_3$ Concentration

Propene polymerization was conducted by $[t\text{-BuNSiMe}_2\text{Flu}]TiMe_2$ in various concentration of $B(C_6F_5)_3$, and the results are shown in Table 2. Theoretically, one equivalent of $B(C_6F_5)_3$ is enough for the activation of $[t\text{-BuNSiMe}_2\text{Flu}]TiMe_2$. A small excess of $B(C_6F_5)_3$, however, drastically improved the polymer yield. For example, the increase of the $[B(C_6F_5)_3]/[Ti]$ ratio from 1.0 to 1.25 increased both the yield and the Mn value by a factor of ca. 4.5, whereas the number of polymer chains increased only by a factor of ca. 1.3. The relations between the yield and Mn against the $[B(C_6F_5)_3]/[Ti]$ ratio in the same polymerization time are illustrated in Fig. 3. The yield and the Mn value were steeply increased and saturated around the $B(C_6F_5)_3]/[Ti]$ ratio of 2 to 3. The saturation is probably due to high conversion of propene. These results indicate that the improvement of activity was mainly attributed to the increase in propagation rate.

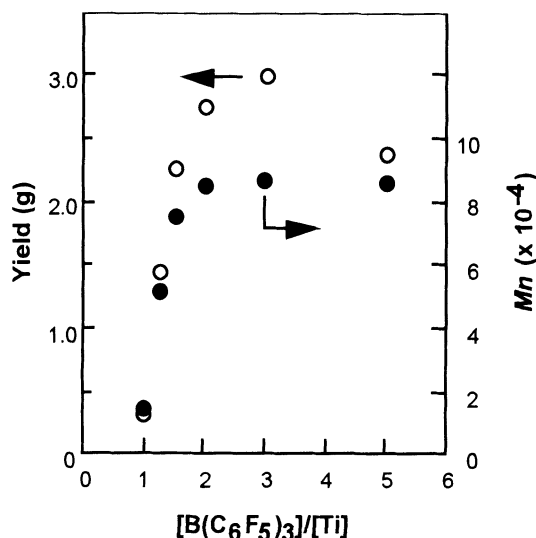


Fig. 3 Plots of polymer yield(O) and $Mn(\bullet)$ vs. $[B(C_6F_5)_3]/[Ti]$

The kinetic profiles in the presence of 3 equivalent of $B(C_6F_5)_3$ to the Ti complex were investigated (run nos. 20 - 23). The relation between the polymer yield and Mn is illustrated in Fig. 4. The Mn value linearly increased during most course of polymerization but slightly saturated in the later stage followed by an increase of the number of polymer chains. The result indicates that some chain transfer reaction occurred under higher concentration of $B(C_6F_5)_3$, although efficiency of the chain transfer is extremely low. We tried to identify the chain transfer reaction by NMR but failed due to high molecular weight of the polymers produced.

Table 2. Effects of $B(C_6F_5)_3$ concentration on propene polymerization with [*t*-BuNSiMe₂F]u[TiMe₂/B(C₆F₅)₃] catalyst^a

| Run | Ti (μmol) | $B(C_6F_5)_3$ (μmol) | Time (h) | Yield (g) | Mn^b ($\times 10^{-4}$) | M_w/Mn^b | N^c (μmol) | mm | mr | Triad (%) ^d π |
|-----|---------------------------|--------------------------------------|-------------|--------------|--------------------------------|------------|------------------------------|----|----|---------------------------------|
| 16 | 40 | 40 | 12 | 0.32 | 1.5 | 1.2 | 22 | 13 | 40 | 47 |
| 17 | 40 | 50 | 12 | 1.44 | 5.2 | 1.1 | 28 | - | - | - |
| 18 | 40 | 60 | 12 | 2.27 | 7.6 | 1.1 | 30 | - | - | - |
| 19 | 40 | 80 | 12 | 2.75 | 8.6 | 1.2 | 32 | - | - | - |
| 20 | 40 | 120 | 2 | 1.60 | 5.7 | 1.2 | 28 | - | - | - |
| 21 | 40 | 120 | 4 | 2.35 | 8.0 | 1.2 | 29 | - | - | - |
| 22 | 40 | 120 | 6 | 2.57 | 8.2 | 1.2 | 31 | - | - | - |
| 23 | 40 | 120 | 12 | 3.01 | 8.7 | 1.2 | 34 | 13 | 42 | 45 |
| 24 | 40 | 200 | 12 | 2.37 | 8.6 | 1.2 | 28 | 14 | 42 | 44 |

^a Polymerization conditions: toluene = 30 mL, C_3H_6 = 3.5 g, -50 °C. ^b Determined by GPC using universal calibration. ^c Number of polymer chains determined from yield and Mn . ^d Determined by ¹³C NMR.

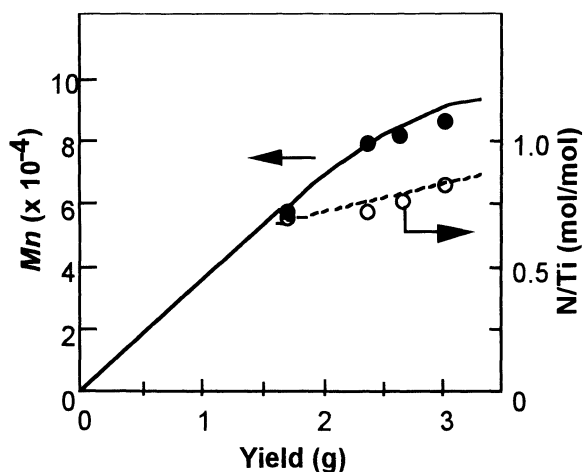


Fig. 4 Plots of Mn (●) and N/Ti (○) against polymer yield

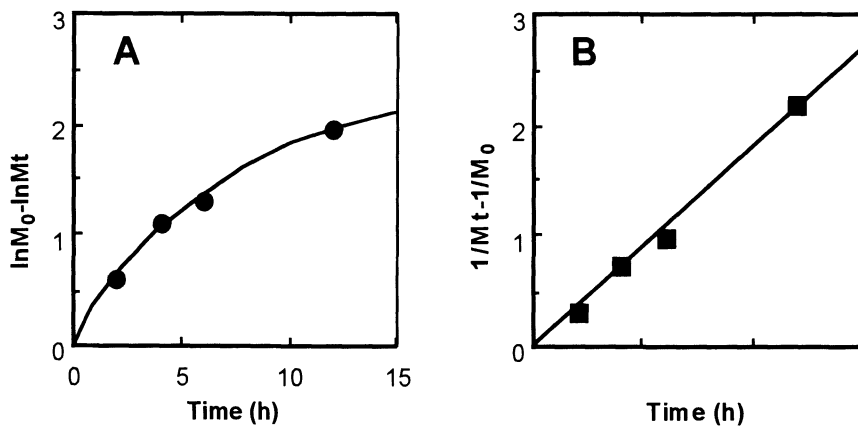


Fig. 5. First (A) and second (B) order plots for propene concentration

Fig. 5 shows the first order (A) and second (B) order plots for monomer consumption, which indicated that the polymerization rate was on second order to monomer concentration. The second order dependence of propagation rate on propene concentration was also confirmed from the dependence of M_n on propene concentration by means of the living nature¹³.

Similar results concerning the relationship between polymerization rate and monomer concentration have been observed in several metallocene catalyst systems. Jüngling *et al.* reported that the reaction order of the polymerization rate with respect to propene concentration was 1.7 for $\text{Me}_2\text{Si}(2\text{-Me-Benz[e]indenyl})\text{ZrCl}_2/\text{MAO}$ catalyst¹⁴. Chien *et al.* reported that the dependence of activity on olefin concentration was about 2.0 in homopolymerization of ethene and propene with the $[2\text{-(dimethylamino)ethyl}]\text{cyclopentadienyltitanium trichloride}/\text{MAO}$ catalyst¹⁵.

These values are much higher than that expected for the model of monomer-metal π complex formation followed by the insertion. If the number of active centers depends on concentration of monomer, the propagation rate could show more than first-order dependence on monomer concentration. Jüngling *et al.* actually proposed that propene might be involved in an equilibrium between dormant and active centers to improve the number of active centers. Such a possibility can be excluded in the time-conversion profile in this experiment, because the number of polymer chains, hence the number of active centers was almost constant during the polymerization.

Ystenes proposed the "trigger mechanism" which involves a two-monomer transition state as a model for the higher order system¹⁶. In the model, the incoming monomer triggers the insertion of the monomer coordinated previously. Chien *et al.* explained the higher-order dependence of polymerization rate by the model in which active site can complex either one or two monomers and insertion occurs with both complexes. Similar model might be applied to the propene polymerization with the [*t*-BuNSiMe₂Flu]TiMe₂/B(C₆F₅)₃ catalyst, since [*t*-BuNSiMe₂Flu]TiMe₂ is highly constrained and less sterically hindered.

The microtacticities of the polymers obtained were also investigated and listed in Table 2. The stereospecificity of the catalyst was almost independent of B(C₆F₅)₃ concentration.

A plausible mechanism of rate enhancement by Lewis acids

The above results clearly indicates that the addition of Lewis acid like B(C₆F₅)₃ and AlOct₃ enhanced propagation rate of propene polymerization. These results may be interpreted as follows.

When B(C₆F₅)₃ is used as a cocatalyst in olefin polymerization with metallocene catalyst, the ion pair, [Cp₂MR⁺ + MeB(C₆F₅)₃⁻], should be formed as active species¹⁷. The ion pair is in equilibrium with [Cp₂MRMe + B(C₆F₅)₃] and the excess B(C₆F₅)₃ can shift the equilibrium to the ion pair side. Such an effect consequently improves the coordinative unsaturation of the cationic metal center. The other possibility is that Lewis acid like B(C₆F₅)₃ and AlOct₃ coordinates to the counter anion to enhance the separation of the ion pairs, which also increases the degree of coordinative unsaturation of the cationic metal center. The increase in the degree of coordinative unsaturation promotes coordination of propene to enhance the propagation rate. The coordinative unsaturation might also induce chain transfer reaction such as β -H elimination and transmetalation with alkylaluminum.

Summary

The effects of B(C₆F₅)₃ and AlOct₃ on propene polymerization was investigated in the living system by [*t*-BuNSiMe₂Flu]TiMe₂/B(C₆F₅)₃. Both the addition of AlOct₃ and excess B(C₆F₅)₃ enhanced the propagation rate, although the chain

transfer reaction was slightly induced. The results suggest that the control of the interaction between the cationic metal center and the counter anion is very important to achieve living polymerization as well as to improve propagation rate.

References and notes

- [1] Doi, Y., Suzuki, S., Soga, K., *Macromolecules*, **1986**, *19*, 2896 and references therein.
- [2] Killian, C. M., Tempel, D. J., Johnson, L. K., Brookhart, M., *J. Am. Chem. Soc.*, **1996**, *118*, 11664.
- [3] Scollard, J. D., McConville, D. H., *J. Am. Chem. Soc.*, **1996**, *118*, 10008; Scollard, J. D., McConville, D. H., Rettig, S. J., *Organometallics*, **1997**, *16*, 1810.
- [4] Baumann, R., Davis, W. M., Schrock, R. R., *J. Am. Chem. Soc.*, **1997**, *119*, 3830.
- [5] Jeon, Y.-M., Park, S. J., Heo, J., Kim, K., *Organometallics*, **1998**, *17*, 3161.
- [6] (a) Shapiro, P. J., Bunel, E., Schaefer, W. P., Bercaw, J. E. *Organometallics* **1990**, *9*, 867. (b) Shapiro, P. J., Cotter, W. D., Schaefer, W. P., Labinger, J. A., Bercaw, J. E. *J. Am. Chem. Soc.* **1994**, *116*, 4623.
- [7] Okuda, *J. Chem. Ber.* **1990**, *123*, 1649.
- [8] (a) Stevens, J. C., Timmers, F. J., Wilson, D. R., Schmidt, G. F., Nickias, P. N., Rosen, R. K., Knight, G. W., Lai, S. Y. (Dow Chemical Company), Eur. Pat. Appl. 0416 815 A2; U. S. Pat. Appl. 401,345 (1990), *Chem. Abstr.*, **1991**, *115*, 93163m. (b) Stevens, J. C. In *Catalytic Olefin Polymerization*; Keii, T., Soga, K., Eds.; Kodansha-Elsevier, Tokyo 1994, p 277.
- [9] (a) Turner, H. W., Halatky, G. G., Canish, J. A. M. (Exxon Chemical Patents, Inc.), PCT Int. Appl. WO 93 19,103 (1993), *Chem. Abstr.* **1994**, *120*, 271442q. (b) Canish, J. A. M. (Exxon Chemical Patents, Inc.), U. S. US 5,026,798 (1991), *Chem. Abstr.* **1993**, *118*, 60284k.
- [10] (a) Sernetz, F. G., Mülhaupt, R., Waymouth, R. M. *Macromol. Chem. Phys.* **1996**, *197*, 1071. (b) Sernetz, F. G., Mülhaupt, R., Amor, F., Eberle, T., Okuda, J. *J. Polym. Sci., Part A: Polym. Chem.* **1997**, *35*, 1571. (c) Sernetz, F. G., Mülhaupt, R. *J. Polym. Sci., Part A: Polym. Chem.* **1997**, *35*, 2549.
- [11] We have recently succeeded in determining X-ray crystal structure of [t-BuNSiMe₂Flu]TiMe₂, which reveals that the fluorenyl ligand coordinates to Ti in a η^3 -manner. The detailed structure of the complex will be reported elsewhere.
- [12] Hagihara, H., Shiono, T., Ikeda, T., *Macromolecules*, **1998**, *31*, 3184.
- [13] Hagihara, H., Shiono, T., Ikeda, T., submitted to *Macromol. Rapid Commun.*
- [14] Jüngling, S., Mülhaupt, R., Stehling, U., Brintzinger, H. H., Ficher, D., Langhauser, F., *J. Polym. Sci. A. Polym. Chem.*, **1995**, *33*, 1305.
- [15] Chien, J. C. W., Yu, Z., Marques, M. M., Flores, J. C., Rausch, M. D., *J. Polym. Sci. A. Polym. Chem.* **36**, 319 (1998) and references therein.
- [16] Ystenes, M., *J. Catal.*, **1991**, *129*, 383.
- [17] Deck, P. A., Marks, T. J., *J. Am. Chem. Soc.*, **1995**, *117*, 6128.

Quantitative Structure-Activity Relationships for Unbridged Zirconocene Catalysts During Ethene Polymerization

J. A. Støvneng^(1,2), A. Stokvold⁽¹⁾, K. Thorshaug⁽¹⁾, and E. Rytter^(1,2)

⁽¹⁾Department of Industrial Chemistry, Norwegian University of Science and Technology (NTNU), N-7034 Trondheim, Norway, and

⁽²⁾Statoil Research Centre, N-7005 Trondheim, Norway

Jon.Andreas.Stovneng@Statoil.com

ASTO@Nycomed.com

Knut.Thorshaug@Chembio.ntnu.no

Erling.Rytter@Statoil.com

Abstract. Polymerization of ethene catalyzed by alkyl-substituted dicyclopentadienyl zirconium dichlorides [(R-Cp)₂ZrCl₂] was performed with methylaluminumoxane as cocatalyst in toluene at $T=50^{\circ}\text{C}$ and $P_{\text{Ethene}}=2$ bar. A kinetic model which includes activation of the dichloride, propagation of the polymer chain, and (non-permanent) deactivation of the active site was used to extract rate constants from the time-dependent polymerization activity curves. A calibration set of nine catalysts (R=H; Me; 1,2Me₂; 1,3Me₂; 1Me2Et; *n*-Pr; *n*-Bu; Me₄; Me₅) was used to establish quantitative structure-property relationships, both for the average polymerization activity over one hour and the propagation rate constant derived with the kinetic model. Structural parameters were obtained from low-energy conformations of γ -agostic (R-Cp)₂ZrC₄H₉⁺ cations, assumed to be reasonable representations of the active site. Geometries were optimized within the PM3(tm) semiempirical model, and electronic descriptors were computed via density-functional energy calculations on the PM3(tm) geometries. A principal-component analysis (PCA) followed by partial least-squares (PLS) regression indicates that the catalyst with R=1Me2Et is an “outlier”. Better linear models were found for the propagation rate constant than for the average polymerization activity. Several steric and electronic parameters have significant regression coefficients, indicating that the propagation rate is a complex function of molecular structure. Quantitative predictions were made for the propagation rate constant of catalysts that were not members of the calibration set: R=Et, *n*-Pen, *t*-Bu, and *i*-Pr, and Ind₂ZrCl₂.

1. Introduction

The idea of quantitative structure-activity/property relationship modeling

(QSAR/QSPR) is to derive empirical models that relate a measured *property* to the electronic and geometric *structure* of a set of samples (calibration set), with the aim of predicting this property for untested samples, and obtain better insight into the structure-property relationships [1].

We have applied these ideas to the catalytic activity of various unbridged alkyl-substituted zirconocenes during polymerization of ethene. In the experiments, we have kept constant as many parameters as possible, in an attempt to extract the influence of the alkyl substituents on the catalytic activity and determine which structural parameters of the active species that are responsible for the variation in activity. A similar study has been reported by Möhring and Coville [2] and Bravaya *et al.* [3].

The activity in our experiments is not a constant in time, but typically goes through periods of activation and deactivation. With a simple kinetic model, we have tried to separate the intrinsic propagation rate from activation and deactivation mechanisms. The multivariate analysis is applied to the propagation rate constant that results from the kinetic modeling.

2. Ethene Polymerization Experiments

Ethene was polymerized with $(R-Cp)_2ZrCl_2$ ($R=H; Me; 1,2Me_2; 1,3Me_2; 1Me2Et; n-Pr; n-Bu; Me_4; Me_5$) in toluene, with methylaluminoxane (MAO) as cocatalyst ($[Al]/[Zr]=2000$) at a temperature $T \approx 50^\circ C$ and a total pressure of 2.1 bar. The dichlorides were delivered by Boulder Scientific Co. and the MAO by Albemarle S.A. Further experimental details can be found in Ref. [4]. Results of the polymerization experiments are presented in Table 1. In order to avoid excessive polymer production and problems with controlling the reactor temperature, a three times lower Zr concentration was used for the $R=n-Pr$ and $n-Bu$ catalysts. Still, the temperature increased by a few degrees in these experiments.

Table 1. Results of ethene polymerization experiments in $(R-Cp)_2ZrCl_2 / MAO /$ toluene. P_{total} and T_{pol} are average values over one hour of the total pressure and the polymerization temperature, respectively.

| R | [Zr] ($\mu mol/L$) | P_{total} (bar) | T_{pol} ($^\circ C$) | $\langle Activity \rangle$ (tonPE/molZr h $[C_2H_4]$) | k_2 (tonPE/molZr h $[C_2H_4]$) |
|--------------------|-------------------------|----------------------|-----------------------------|--|---|
| <i>n</i> -Bu | 1.1 | 2.10 | 56.7 | 474 | 1420 |
| <i>n</i> -Pr | 1.1 | 2.12 | 54.9 | 608 | 1170 |
| Me ₄ | 3.6 | 2.10 | 53.0 | 99 | 600 |
| Me ₅ | 3.6 | 2.10 | 52.4 | 140 | 490 |
| 1,3Me ₂ | 3.6 | 2.11 | 52.1 | 87 | 460 |
| 1,2Me ₂ | 3.6 | 2.12 | 52.0 | 83 | 435 |
| 1Me2Et | 3.6 | 2.12 | 52.6 | 73 | 175 |
| Me | 3.6 | 2.11 | 51.7 | 80 | 161 |
| H | 3.6 | 2.11 | 51.8 | 73 | 121 |

Examples of activity-time profiles are given in Fig. 1. A general feature appears to be that the monoalkyl substituted zirconocenes have a considerably "smoother" profile than the others, with slow activation and deactivation.

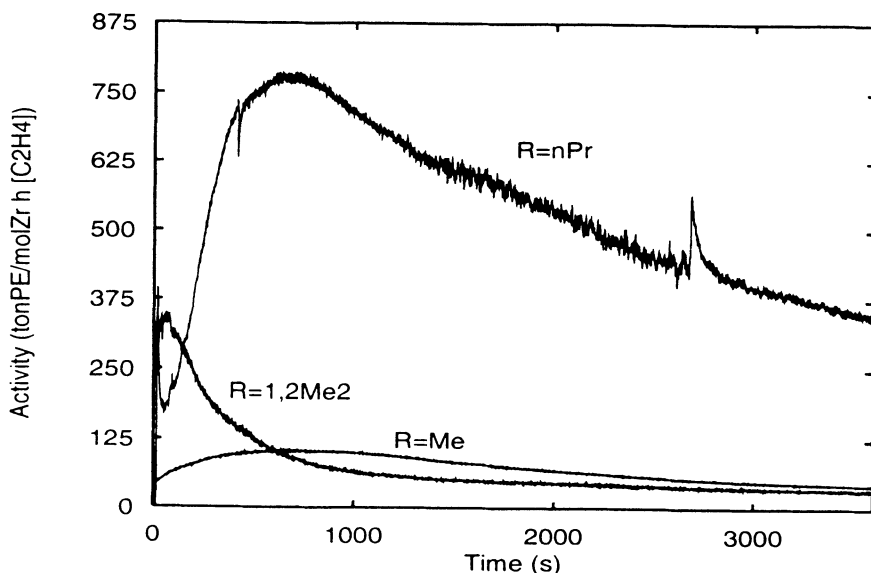
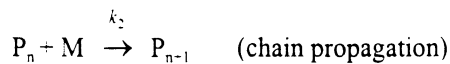
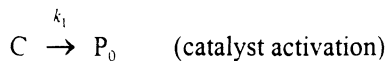
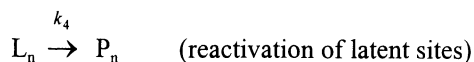


Fig. 1. Experimental activity-time profiles for the $(R-Cp)_2ZrCl_2$ catalysts with $R=n$ -Pr, 1,2Me₂, and Me.

3. Kinetic Modeling

The activity curves in Fig. 1 indicate that the kinetics can be described with a set of reactions that involves activation, propagation, and deactivation. A possible formulation of a simple kinetic model of this kind is given in Scheme 1 [5].





Scheme 1. Kinetic model, including activation, propagation, and nonpermanent deactivation.

Here, C represents the initial dichloride, P_0 is the $(R-Cp)_2ZrCH_3^+$ cation, assumed to be the active species after reaction with MAO, P_n is the active site after insertion of n monomers M, and L_n is an inactive (“latent”) site. The corresponding kinetic equations result in the following expression for the time dependent activity:

$$r_4(t) = c_0 k_2 m_0 \left(\frac{k_4}{k_3 + k_4} - \frac{k_1 - k_4}{k_1 - k_3 - k_4} e^{-k_1 t} + \frac{k_1 k_3}{(k_1 - k_3 - k_4)(k_3 + k_4)} e^{-(k_3 + k_4)t} \right)$$

Here, m_0 is the (constant) monomer concentration, c_0 is the Zr concentration, and k_1, k_4 are the rate constants of the kinetic model. By fitting $r_4(t)$ to the experimental activity curves, we obtain the propagation rate constants k_2 given in Table 1. The values of k_2 are very little affected by the exact choice of kinetic model. For example, inclusion of a permanent deactivation term changes the k_2 values by less than 2 percent.

Note that the chosen model results in a reaction order of 1.0 relative to ethene. However, only a slight modification, e.g., $L_n + M \rightarrow P_n$ for the reactivation reaction, gives an $r_4(t)$ that is nonlinear in m_0 , and for typical values of the rate constants, a reaction order between 1.0 and 2.0 may easily be obtained. In other words, a reaction order higher than 1 can be explained with a simple kinetic model, without resorting to a “trigger” mechanism [6] or a multisite model.

4. Derivation of Structure Data

In order to correlate catalytic activity with molecular structure, it appeared more natural to use the structure of active metallocene alkyl cations rather than that of the inactive dichlorides. Since experimental structure data were not available for the active species, geometry and electronic structure were based on quantum-chemical calculations.

Reaction-pathway modeling of Cossee-like mechanisms has shown that chain propagation may start from β - or γ -agostic cations in these systems [7-10]. Since β -agostic structures are the typical starting point for chain termination, we have chosen γ -agostic conformations as models for the active site.

With 1 to 4 alkyl substituents on the Cp ring, there are up to 25 different conformations depending on the relative orientation of the substituents. A conformational average was performed based on geometries optimized with the

semiempirical PM3(tm) method [11] and energies calculated with gradient-corrected density functional theory [12] (Becke88 [13] and Perdew-Wang 91 [14] gradient corrections). This approach represents a reasonable compromise between computational accuracy and efficiency¹ [15]. In Fig. 2, the conformations with lowest energy are shown for the two catalysts with R=1,3Me₂ and *n*-Pr. The agostic interaction is well reproduced with the PM3(tm) method.

As a basis for the QSAR analysis, we have included the following geometric descriptors: Cp-Cp opening angle, Zr-H_γ distance, exposed area on Zr, principal moment of inertia, radius of gyration, ovality, number of rotatable bonds, number of carbons in substituent R, number of substituents on Cp ligand. The following electronic descriptors were used: Mulliken charge on Zr, Hirshfeld charge on Zr, Voronoi charge on Zr, HOMO energy, LUMO energy, LUMO-HOMO energy gap, electronegativity, hardness.

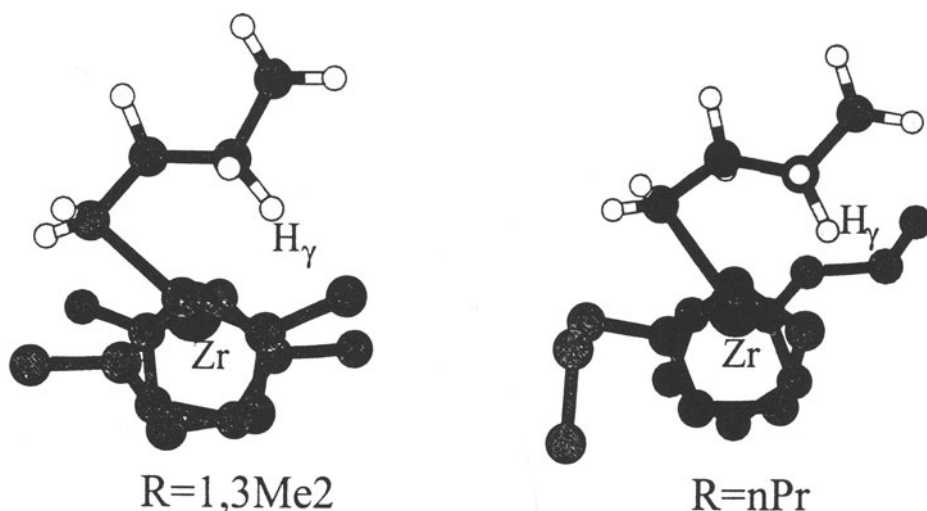


Fig. 2. Low energy γ -agostic conformations of $(1,3\text{Me}_2\text{Cp})_2\text{ZrC}_4\text{H}_9^+$ and $(n\text{-PrCp})_2\text{ZrC}_4\text{H}_9^+$ optimized with PM3(tm). Hydrogens on the ligands have been omitted for clarity. The agostic hydrogen on the γ -carbon has been labeled H _{γ} .

¹ For one of the catalysts, R=Me, we have verified the soundness of the present approach by comparing geometries optimized with PM3(tm) and DFT. The variation in structure parameters between the different conformations is very similar in the two cases.

5. Multivariate Analysis of the Data

We used principal component analysis (PCA) and partial least squares (PLS) regression to construct QSAR models [16]. In a PCA, the original descriptors are transformed into new, orthogonal variables, "principal components", in such a way that the 1. PC lies along the direction of maximum variance in the data set. In the PLS regression analysis, orthogonal PLS components are based on the variation in both descriptors and measured property. In our case, the latter will be the propagation rate constant k_2 resulting from the kinetic modeling described above or the average catalytic activity during one hour.

A standard measure of the quality of a regression model is the squared correlation coefficient r^2 which equals 1.0 for a perfect model. When all 9 catalysts were included in the calibration set, it was not possible to construct good regression models. After "leave-one-out" cross validation, the highest values of r^2 were only about 0.5. The analysis showed that the catalyst with R=1Me2Et is a so-called "outlier".² When this sample was removed from the calibration set, much better regression models were obtained. With all 17 descriptors in the model (see Sec. 4), only a single PLS component was used in the regression analysis (to avoid overfitting). After "leave-one-out" cross validation, we obtain $r^2=0.75$. In Fig. 3, this result is illustrated in a plot of modeled versus predicted propagation rate constant k_2 . The regression coefficients reveal a positive correlation between k_2 and the partial charge on Zr. Increasing Cp-Cp angle also seems to have a positive effect on the propagation rate. Negative correlation is found for the LUMO-HOMO energy gap and the distance between Zr and H₁. However, the largest regression coefficients are found for descriptors related to the size of the catalyst, e.g., principal moment of inertia, radius of gyration, and the number of rotatable bonds. This is mainly caused by the presence of the two catalysts with R=*n*-Pr and *n*-Bu in the calibration set, both having high propagation rates together with large values of these steric descriptors. The catalyst with R=Me₃ is in the cross validation predicted to have a propagation rate considerably lower than what is "measured" due to low values of the Cp-Cp angle and exposed area on Zr, and a large LUMO-HOMO energy gap.

² There are several possible reasons why R=1Me2Et is an outlier: One or more important molecular descriptors may be missing, the method of deriving structure data may have resulted in certain non-representative values for this catalyst, or the mechanism and kinetics may be different, resulting in a low propagation rate constant. Further, the amount of *meso*-complexes is not known. The calculated structure is based on a 50/50 mixture of *meso*- and *rac*-complexes.

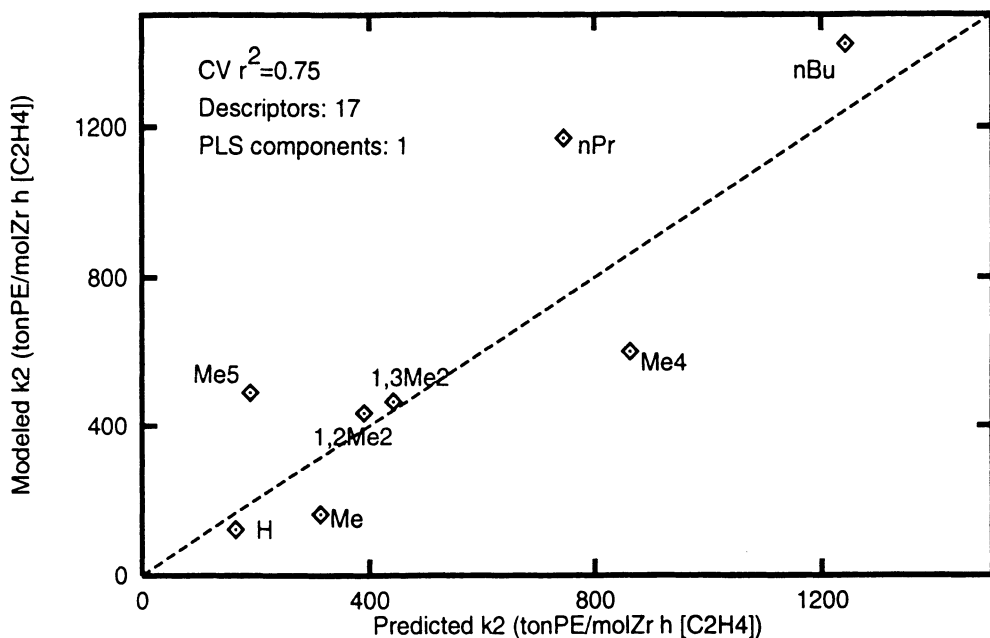


Fig. 3. Modeled (see Scheme 1) versus predicted propagation rate constant k_2 after “leave-one-out” cross validation. The calibration set consists of 8 catalysts; R=1Me₂Et is an “outlier” and has been removed. With all 17 descriptors in the model, a single PLS component gives the best compromise between under- and overfitting.

The value of r^2 can be significantly increased by removing certain molecular descriptors from the model. Actually, taking the Cp-Cp angle and the exposed area on Zr out of the analysis yields $r^2=0.94$ for a model based on 2 PLS components. The main change is a much better prediction of the propagation rate for the R=Me₅ catalyst. However, since the correlation between k_2 and these descriptors is “reasonable”, we have used the model in Fig. 3 for the prediction of k_2 for untested samples (see below).

We also tried to construct models based on the average catalytic activity over one hour. However, the quality of these models was significantly worse than that of the models based on the propagation rate constant, in particular when all the descriptors were used. Models with high values of r^2 could only be obtained with a careful selection of 5-6 descriptors and using up to 4 or 5 PLS components. A small data set like ours can typically support no more than two components.

The model presented in Fig. 3 was subsequently used to predict values of k_2 for catalysts which were not in the calibration set. The results are given in Table 2.

The accuracy of these predictions is not very high. In particular, the prediction for the catalyst with R=*t*-Bu changes considerably when certain molecular descriptors are removed from the model. Still, under the present experimental conditions, we expect a high propagation rate with R=*n*-Pen, intermediate values for R=Et, *i*-Pr, and for Ind₂ZrCl₂, and low propagation rate with R= *t*-Bu.

Table 2. Predicted values of k_2 for the catalysts in the prediction set, based on the model presented in Fig. 3.

| R | k_2 |
|---------------|-------|
| Et | 611 |
| <i>i</i> -Pr | 867 |
| <i>t</i> -Bu | 242 |
| <i>n</i> -Pen | 1821 |
| Ind | 638 |

6. Discussion and Conclusions

In the present work, we have used multivariate analysis in an attempt to resolve relationships between molecular structure of zirconocenes and their catalytic activity during ethene polymerization. The calibration set used in this study consists of only 9 samples - further reduced to 8 after detection of R=1Me2Et as an outlier - which were selected without paying much attention to experimental design.

An obvious extension of this work would be to increase the calibration set. This would enable so-called test set validation, where a model is constructed for one part of the measured samples and subsequently used to predict the desired property for the other part, the test set. This method is always superior to cross validation.

Inclusion of samples, e.g., R=*n*-Dodecyl, with very large values of the influential steric descriptors discussed above is expected to reduce their importance since we do not expect a corresponding dramatic increase in the propagation rate.

Finally, we would like to emphasize application of the methodology rather than the particular numerical results obtained. Other properties that should be suitable for a similar analysis include e.g. molecular weight and composition of polymer unsaturation. We expect both properties to correlate with structures derived from β -agostic conformations, which are known to be relevant for chain termination and isomerization [4].

Acknowledgments

Financial support from the Norwegian Research Council (NFR) under the Polymer Science Program and Borealis is gratefully acknowledged. Discussions with Endre Anderssen, Dept. of physical chemistry, NTNU are acknowledged.

References

1. For an introduction to multivariate analysis, see, e.g., T. W. Anderson, *An introduction to multivariate statistical analysis* (Wiley, New York, 1958).
2. P. C. Möhring and N. J. Coville, *J. Mol. Catal.* **1992**, *77*, 41.
3. N. M. Bravaya, V. V. Strelets, Z. M. Dzhabieva, O. N. Babkina, and V. P. Maryin, *Russ. Chem. Bull.*, **1998**, *47*, 1491.
4. K. Thorshaug, J. A. Støvneng, E. Rytter, and M. Ystenes, *Macromolecules* **1998**, *31*, 7149.
5. A more elaborate discussion of various similar kinetic models is given in T. S. Wester, H. Johnsen, P. Kittilsen, and E. Rytter, *Macromol. Chem. Phys.*, **1998**, *199*, 1989.
6. M. Ystenes, *J. Catal.* **1991**, *129*, 383.
7. T. K. Woo, L. Fan, T. Ziegler, *Organometallics* **1994**, *13*, 2252.
8. T. Yoshida, N. Koga, and K. Morokuma, *Organometallics* **1994**, *14*, 746.
9. L. Cavallo and G. Guerra, *Macromolecules* **1996**, *29*, 2729.
10. J. A. Støvneng and E. Rytter, *J. Organomet. Chem.* **1996**, *519*, 277.
11. *SPARTAN 4.0*, Wavefunction, Inc., 18401 Von Karman, Suite 370, Irvine, CA 92612, USA.
12. *ADF 2.3*, Scientific Computing and Modeling, Chemistry Department, Vrije Universiteit, De Boelelaan 1083, 1081 HV Amsterdam, The Netherlands.
13. A. D. Becke, *Phys. Rev. A* **1988**, *38*, 3090.
14. J. P. Perdew and Y. Wang, *Phys. Rev. B* **1992**, *45*, 13244.
15. K. J. Børve, V. R. Jensen, T. Karlsen, J. A. Støvneng, and O. Swang, *J. Mol. Model.* **1997**, *3*, 193.
16. *The Unscrambler 6.11*, CAMO AS, Olav Tryggvasons gt. 24, N-7011 Trondheim, Norway, and *Cerius² QSAR+*, April 1997. San Diego: Molecular Simulations Inc., 1997.

Coexistence of two active species in the polymerization of 1-hexene catalyzed with zirconocene / MAO catalysts

Holger Frauenrath, Helmut Keul, Hartwig Höcker*

Lehrstuhl für Textilchemie und Makromolekulare Chemie der Rheinisch-Westfälischen Technischen Hochschule Aachen, Worringerweg 1, 52056 Aachen, Germany
E-mail: Hoecker@dw1.rwth-aachen.de

Abstract. The polymerization behaviour of 1-hexene with catalyst systems consisting of different zirconocene dichlorides and MAO as the cocatalyst has been studied as a function of the polymerization temperature. The shape of the GPC curves obtained and the „Arrhenius plot“ of the temperature dependence of the number average molecular weight suggest the coexistence of two different active species. A model mechanism for the treatment of the polymerization kinetics was developed, and some thermodynamical parameters of the polymerization reaction were calculated.

1. Introduction

For many years the mechanism of metallocene/ MAO catalyzed polymerizations has been studied intensively. Good arguments have been put forward that the active species in these polymerizations are metallocenium cations generated by the MAO cocatalyst by methylation of the respective metallocene dichlorides and abstraction of one methyl group from the products (Fig. 1) [1]. The synthesis of cationic complexes with borate counterions and their use as polymerization catalysts has confirmed this hypothesis [2].

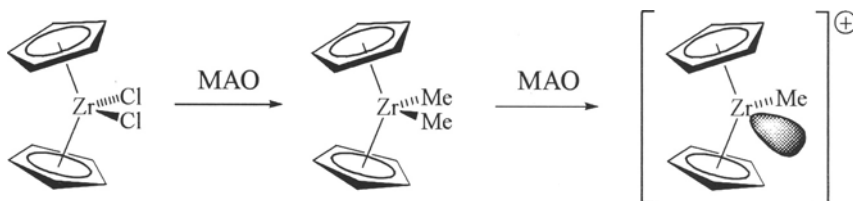


Fig. 1. Generation of the active species in zirconocenium catalyzed polymerizations from zirconocenium dichloride and MAO.

Still, many questions remain unanswered. Why is a large excess of the cocatalyst necessary? In order to achieve acceptable activities, generally Al/Zr ratios > 1000 are needed. Recent studies show that this cannot be attributed to the extent of methyl abstraction alone [3], which is almost complete for Al/Zr = 20 at

temperatures as low as -20°C . Can a cationic metallocenium species exist as a "solvated ion" in a solvent as apolar as toluene? Due to the low dielectric constant of organic solvents, one should expect the solvation of ions to be highly endothermic, and calculations [4] support this thesis, although solvation of MAO counterions is not to that extent disfavoured as solvation of AlR_4^- or BR_4^- counterions. This is well reflected by the low solubility of cationic complexes with borate counterions in toluene. With MAO much higher catalyst concentrations can be achieved, and at the same time the catalysts are much more stable against degradation than are the cationic catalysts, especially those which are referred to as „base-free“. It has also been reported [5] that polymerizations with zirconocene / MAO catalysts, usually regarded as true single-site catalysts, can show non-single-site behaviour of the catalyst.

In our study, the number average molecular weight \overline{M}_n was chosen as a probe for the nature of the active site in the polymerization of 1-hexene with zirconocene / MAO catalyst systems, because in contrast to the activity of polymerization it should be independent of catalyst and cocatalyst concentrations and consequently also of the actual degree of generation of the active species by the MAO cocatalyst, which is an unknown parameter. A similar idea was raised by Karol et al. [6] who chose the ethylene/1-hexene copolymerization behaviour of zirconocenes as a probe for the nature of the active site.

2. Experimental

Materials

Starting materials and reagents used for polymerization were of high purity. 1-Hexene (from Aldrich) was dried over CaH_2 and distilled before use (b.p. = $65-66^{\circ}\text{C}$). Cp_2ZrCl_2 , $\text{Et}(\text{Ind})_2\text{ZrCl}_2$ and $^i\text{Pr}(\text{Cp})(\text{Flu})\text{ZrCl}_2$ were used without further purification. A stock solution of $2 \cdot 10^{-3}$ mol/L in toluene was prepared and served as initiator. A 10% solution of MAO in toluene (from Witco GmbH) was used as a cocatalyst without further purification. Toluene was distilled over sodium/benzophenone and stored over molecular sieves 4\AA .

Measurements

^1H NMR and ^{13}C NMR spectra were recorded on a Bruker DPX-300 FT-NMR spectrometer at 300 MHz and 75 MHz, respectively. Deuterated chloroform (CDCl_3) was used as a solvent, and tetramethylsilane (TMS) served as internal standard.

Gel-permeation chromatography (GPC) was carried out using a high pressure liquid chromatography pump and a refractive index detector. The column combination applied consisted of 3 columns (length 300 mm, diameter 7.5 mm, particle size 5μ , pore size 10^4\AA ; 300 mm, 7.5 mm, 5μ , 10^3\AA ; 300 mm, 8 mm, 5μ , 10^2\AA). The eluting solvent was THF stabilized with 250 mg/L 2,6-di-tert.-butyl-4-

methylphenol with a flow rate of 1 mL/min. Polystyrene standards were used for calibration.

Polymerizations

A mixture of 9.5 mL MAO-solution and 0.5 mL Cp_2ZrCl_2 -solution was stirred at room temperature for 1h and at the desired temperature T_p for 1h. Then the polymerization was started by addition of 2 mL 1-hexene. After the polymerization time given in Table 1 the polymerization was terminated by pouring the polymerization mixture into 5% aqueous HCl. The organic layer was separated, dried over Na_2SO_4 and the polymer was isolated by filtration of the solution and evaporation of the solvent. The yield was determined gravimetrically, the molecular weight and the polydispersity index by means of GPC.

3. Results

The number average molecular weights \overline{M}_n of poly(1-hexene)s obtained with Cp_2ZrCl_2 **1**, $\text{Et}(\text{Ind})_2\text{ZrCl}_2$ **2**, and ${}^i\text{Pr}(\text{Cp})(\text{Flu})\text{ZrCl}_2$ **3** (Fig. 2) at different polymerization temperatures T_p are shown in Table 1 and the corresponding GPC curves in Fig. 3. An „Arrhenius-plot“ of $\ln(\overline{M}_n)$ versus $1/T_p$ is presented in Fig. 4.

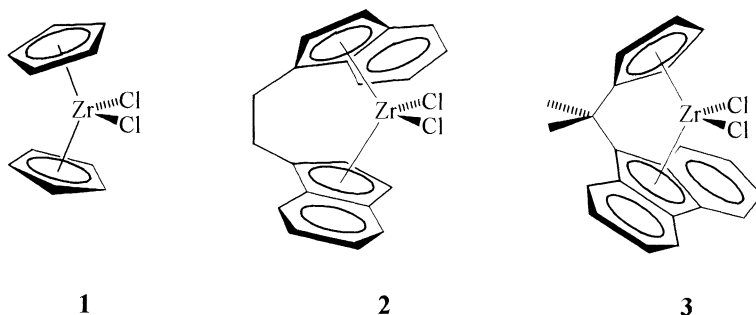


Fig. 2. Zirconocene catalysts with different symmetries employed in this study: Cp_2ZrCl_2 **1**, $\text{Et}(\text{Ind})_2\text{ZrCl}_2$ **2**, and ${}^i\text{Pr}(\text{Cp})(\text{Flu})\text{ZrCl}_2$ **3**.

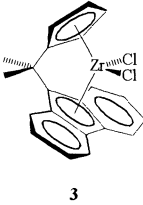
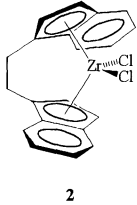

It can be observed that

- the number average molecular weight increases with decreasing polymerization temperature and that for all three catalysts there is no linear dependence of $\ln(\overline{M}_n)$ from $1/T_p$,
- the molecular weight distributions of poly(1-hexene)s obtained with Cp_2ZrCl_2 **1** at temperatures between 0°C and -60°C are bimodal, whereas they are not at higher and lower temperatures. This can also be seen in the polydispersity

indices $Q = \overline{M}_w / \overline{M}_n$ (Table 1). Proceeding from high to low temperatures, a high molecular weight shoulder develops at $T_p = 0^\circ\text{C}$, which increases with decreasing temperatures. At -20°C two peaks of the same height can be observed, and at lower temperatures the high molecular weight fraction is predominant. The same is observed for polymerizations with $\text{Et}(\text{Ind})_2\text{ZrCl}_2$ **2** and $^i\text{Pr}(\text{Cp})(\text{Flu})\text{ZrCl}_2$ **3** in a temperature range from 25°C to 65°C ,

- Cp_2ZrCl_2 **1** produces lower molecular weight poly(1-hexene)s than the other catalysts, whereas the molecular weights of poly(1-hexene)s produced with $\text{Et}(\text{Ind})_2\text{ZrCl}_2$ **2** and $^i\text{Pr}(\text{Cp})(\text{Flu})\text{ZrCl}_2$ **3** at temperatures between 5°C and 65°C are nearly identical.

Table 1. Examples for experimental results of 1-hexene polymerizations with Cp_2ZrCl_2 **1**, $\text{Et}(\text{Ind})_2\text{ZrCl}_2$ **2**, and $^i\text{Pr}(\text{Cp})(\text{Flu})\text{ZrCl}_2$ **3**.

| Catalyst | T_p $^\circ\text{C}$ | t_p h | Yield in % ¹⁾ | \overline{M}_n ²⁾ | $\overline{M}_w/\overline{M}_n$ |
|---|---------------------------|------------|-----------------------------|--------------------------------|---------------------------------|
|  3 | 65 | 24 | 72 | 1600 | 5,40 |
| | 55 | 24 | 82 | 2700 | 4,01 |
| | 45 | 24 | 63 | 6700 | 2,38 |
| | 25 | 24 | 66 | 18600 | 1,86 |
| | 10 | 48 | 93 | 27400 | 1,72 |
| | -5 | 48 | 66 | 37900 | 1,79 |
| | -35 | 120 | 11 | 64600 | 1,74 |
| | < -35 | > 120 | | < 10% yield | |
|  2 | 65 | 24 | 100 | 2000 | 4,70 |
| | 55 | 24 | 90 | 3400 | 4,27 |
| | 45 | 24 | 89 | 7900 | 2,72 |
| | 25 | 24 | 70 | 19500 | 1,96 |
| | 5 | 48 | 31 | 32400 | 1,94 |
| | -10 | 48 | 17 | 25600 | 1,93 |
| | -35 | 120 | 12 | 36100 | 2,09 |
| | < -35 | > 120 | | < 10% yield | |
|  1 | 65 | 24 | 89 | 460 | 1,57 |
| | 45 | 24 | 86 | 590 | 1,49 |
| | 30 | 24 | 85 | 850 | 1,82 |
| | 10 | 24 | 88 | 1200 | 2,15 |
| | -5 | 36 | 90 | 2900 | 2,75 |
| | -20 | 48 | 96 | 3700 | 3,10 |
| | -35 | 48 | 63 | 6500 | 2,07 |
| | -60 | 120 | 47 | 13000 | 1,92 |
| -80 | 120 | 28 | 17900 | 2,15 | |

¹⁾ Initial conditions: 2 mL 1-hexene, $[\text{Zr}] = 1 \cdot 10^{-4}$ mol/L, Al/Zr = 5000.

²⁾ Number average molecular weight and polydispersity index determined by GPC.

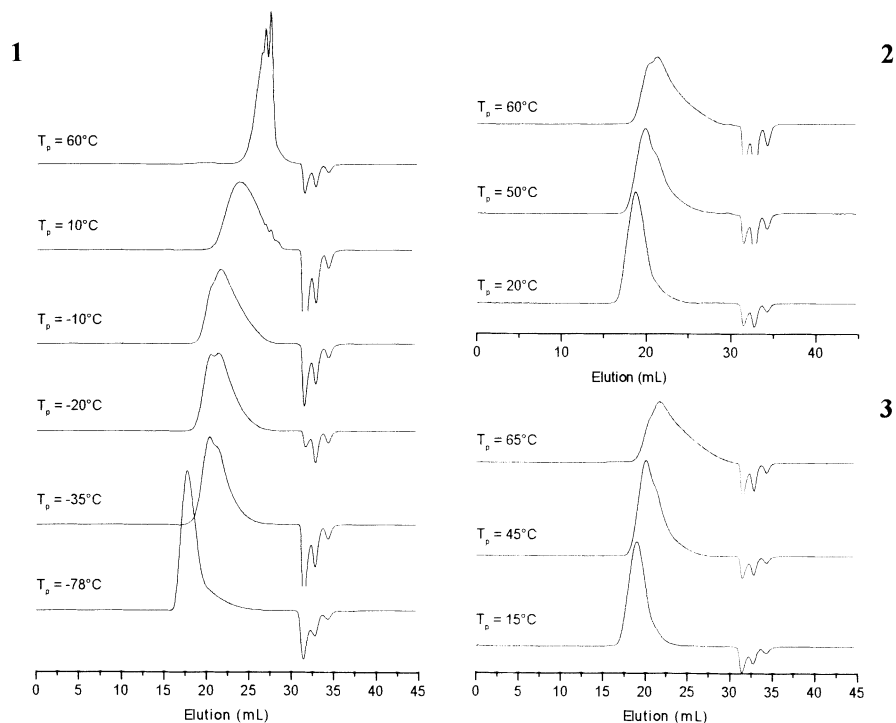


Fig. 3. GPC curves of poly(1-hexene)s obtained at different polymerization temperatures T_p with Cp_2ZrCl_2 **1**, $\text{Et}(\text{Ind})_2\text{ZrCl}_2$ **2**, and ${}^i\text{Pr}(\text{Cp})(\text{Flu})\text{ZrCl}_2$ **3**.

4. Discussion

The temperature dependence of the molecular weights does not have the characteristics one should expect for a mechanism with only one active species and one rate-determining step. In this case one should observe a linear dependence of $\ln(\overline{M}_n)$ on $1/T_p$. The sigmoidal shape of the curve in the case of Cp_2ZrCl_2 rather suggests the existence of two different types of active species at the high and the low temperature limit, respectively, with a transition temperature interval between them, where the molecular weights increase dramatically with decreasing temperature. This phenomenon resembles the situation in anionic polymerizations, where contact ion pairs (CIP) and solvent separated ion pairs (SIP) of the anionic chain end and the counterion are in a temperature-dependent equilibrium and chain growth proceeds via two distinct transition states with two respective Arrhenius straight lines [7].

The bimodal molecular weight distributions of poly(1-hexene)s obtained at polymerization temperatures within this transition interval are a clear proof for the coexistence of two active species at these temperatures. In the case of $\text{Et}(\text{Ind})_2\text{ZrCl}_2$ and ${}^1\text{Pr}(\text{Cp})(\text{Flu})\text{ZrCl}_2$ the high temperature limit cannot be reached because of the boiling point of 1-hexene at atmospheric pressure.

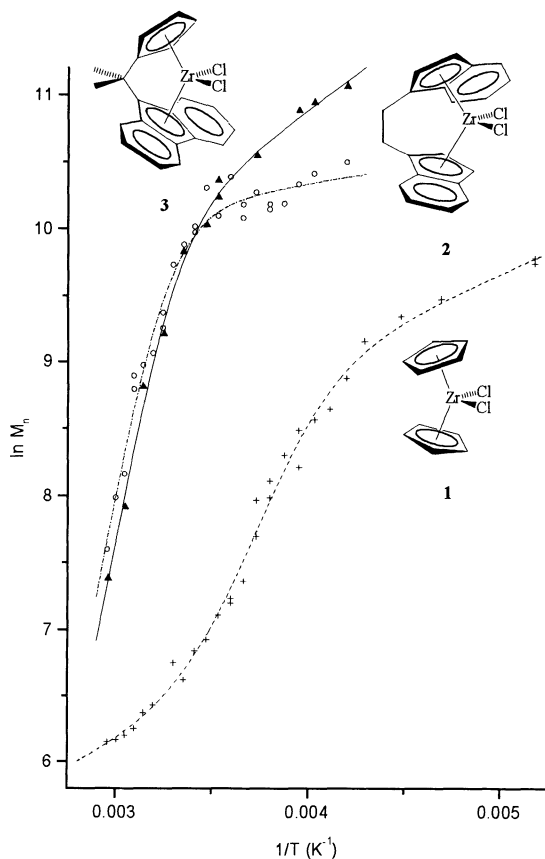


Fig. 4. Arrhenius plot of the experimentally determined molecular weights \bar{M}_n as a function of the polymerization temperature T_p for the catalyst systems $\text{Cp}_2\text{ZrCl}_2 / \text{MAO}$ (+), $\text{Et}(\text{Ind})_2\text{ZrCl}_2 / \text{MAO}$ (o), and ${}^1\text{Pr}(\text{Cp})(\text{Flu})\text{ZrCl}_2 / \text{MAO}$ (▲). The lines represent the fitting functions derived from Equation (14).

The much higher molecular weights of poly(1-hexene)s obtained with $\text{Et}(\text{Ind})_2\text{ZrCl}_2/\text{MAO}$ and ${}^1\text{Pr}(\text{Cp})(\text{Flu})\text{ZrCl}_2/\text{MAO}$ are i) due to the fact that the geometric constraints of the bridged and substituted Cp ligands affect the activation barriers of both the propagation and the termination reaction, and ii) also a consequence of the later „drop“ of the molecular weights as one proceeds to higher temperatures, where the equilibrium of the active species is shifted to the

one with the slower rate of polymerization. Obviously, the degree of substitution at the Cp ligands plays an important role for the equilibrium of the two active species, while the symmetry of the complex does not (at least for the active species at the high temperature limit).

To explain our experimental results, we propose the coexistence of two active species in a slow equilibrium in terms of the chain growth time scale. If they were in a fast equilibrium, every chain would grow with an averaged propagation rate and no bimodal molecular weight distribution would be observed. Both active species show different rates of propagation r_{p1} and r_{p2} and rates of termination r_{t1} and r_{t2} . This model mechanism is shown in Fig. 5. As we do not have any experimental evidence for what kind of species might be involved, the two identically drawn species Zr^*_1 and Zr^*_2 shown in Fig. 5 are to be understood as structurally different species, the equilibrium of which can of course be affected by other reagents.

The equilibrium constant K_{act} can be defined as

$$K_{act} = \frac{[Zr^*_2]}{[Zr^*_1]} \cdot \prod_i [Y_i]^{v_i} \quad (1)$$

where $[Zr^*_1]$ and $[Zr^*_2]$ are the concentrations of the two active zirconium species, Y_i are other reactants involved in this equilibrium and v_i are their stoichiometric coefficients. With the molecular weight of the repeating unit M_0 an expression for the molecular weight on the basis of the postulated mechanism is derived.

$$\bar{M}_n = M_0 \cdot P = M_0 \cdot \frac{r_p}{r_t} \quad (2)$$

$$\bar{M}_n = \frac{k_{p1}[\text{Mon}][Zr^*_1] + k_{p2}[\text{Mon}][Zr^*_2]}{k_{t1}[Zr^*_1] + k_{t2}[Zr^*_2]} \quad (3)$$

$$\bar{M}_n = M_0 \cdot [\text{Mon}] \cdot \frac{k_{p1}[Zr^*_1] + k_{p2}K_{act}[Zr^*_1] \cdot \prod_i [Y_i]^{-v_i}}{k_{t1}[Zr^*_1] + k_{t2}K_{act}[Zr^*_1] \cdot \prod_i [Y_i]^{-v_i}} \quad (4)$$

$$\bar{M}_n = M_0 \cdot [\text{Mon}] \cdot \frac{k_{p1} + k_{p2}K_{act} \cdot \prod_i [Y_i]^{-v_i}}{k_{t1} + k_{t2}K_{act} \cdot \prod_i [Y_i]^{-v_i}} \quad (5)$$

$$\bar{M}_n = M_0 \cdot [\text{Mon}] \cdot \frac{k_{p1}}{k_{t1}} \cdot \frac{1 + \frac{k_{p2}}{k_{p1}} \cdot K_{act} \cdot \prod_i [Y_i]^{-v_i}}{1 + \frac{k_{t2}}{k_{t1}} \cdot K_{act} \cdot \prod_i [Y_i]^{-v_i}} \quad (6)$$

$$\bar{M}_n = M_0 \cdot [\text{Mon}] \cdot \frac{A_{p1}^\infty}{A_{t1}^\infty} \cdot e^{\frac{-(E_{Ap1} - E_{At1})}{RT_p}} \cdot \frac{1 + \frac{A_{p2}^\infty}{A_{p1}^\infty} \cdot e^{\frac{-(\Delta G_{act} + E_{Ap2} - E_{Ap1})}{RT_p}} \cdot \prod_i [Y_i]^{-\nu_i}}{1 + \frac{A_{t2}^\infty}{A_{t1}^\infty} \cdot e^{\frac{-(\Delta G_{act} + E_{At2} - E_{At1})}{RT_p}} \cdot \prod_i [Y_i]^{-\nu_i}} \quad (7)$$

With $x = 1/T_p$ and with

$$C_0 = M_0 \cdot [\text{Mon}] \cdot \frac{A_{p1}^\infty}{A_{t1}^\infty} \quad (8)$$

$$B = -\frac{E_{Ap1} - E_{At1}}{R} \quad (9)$$

$$D_p = -\frac{\Delta G_{act} + E_{Ap2} - E_{Ap1}}{R} \quad (10)$$

$$D_t = -\frac{\Delta G_{act} + E_{At2} - E_{At1}}{R} \quad (11)$$

$$C_p = \ln \left(\frac{A_{p2}^\infty}{A_{p1}^\infty} \cdot \prod_i [Y_i]^{-\nu_i} \right) \quad (12)$$

$$C_t = \ln \left(\frac{A_{t2}^\infty}{A_{t1}^\infty} \cdot \prod_i [Y_i]^{-\nu_i} \right) \quad (13)$$

the following fitting function for the experimental data is derived:

$$\ln(\bar{M}_n) = \ln C_0 + B \cdot x + \ln \left(\frac{1 + e^{D_p \cdot x + C_p}}{1 + e^{D_t \cdot x + C_t}} \right) \quad (14)$$

The fitting curves are shown as dashed lines in Fig. 4. The parameters obtained and some thermodynamical parameters of the chain growth reactions calculated according to Equations (10)-(11) are given in Table 2. Of course the standard deviations of the parameters are relatively high because of the high number of parameters, and interpretation of the calculated thermodynamical parameters should be taken with precaution. But they do at least give an idea of the size of the thermodynamical and kinetical parameters. It is worth to notice that equations with less parameters derived from simplified models turned out to be unsuitable for a fitting of the experimental data.

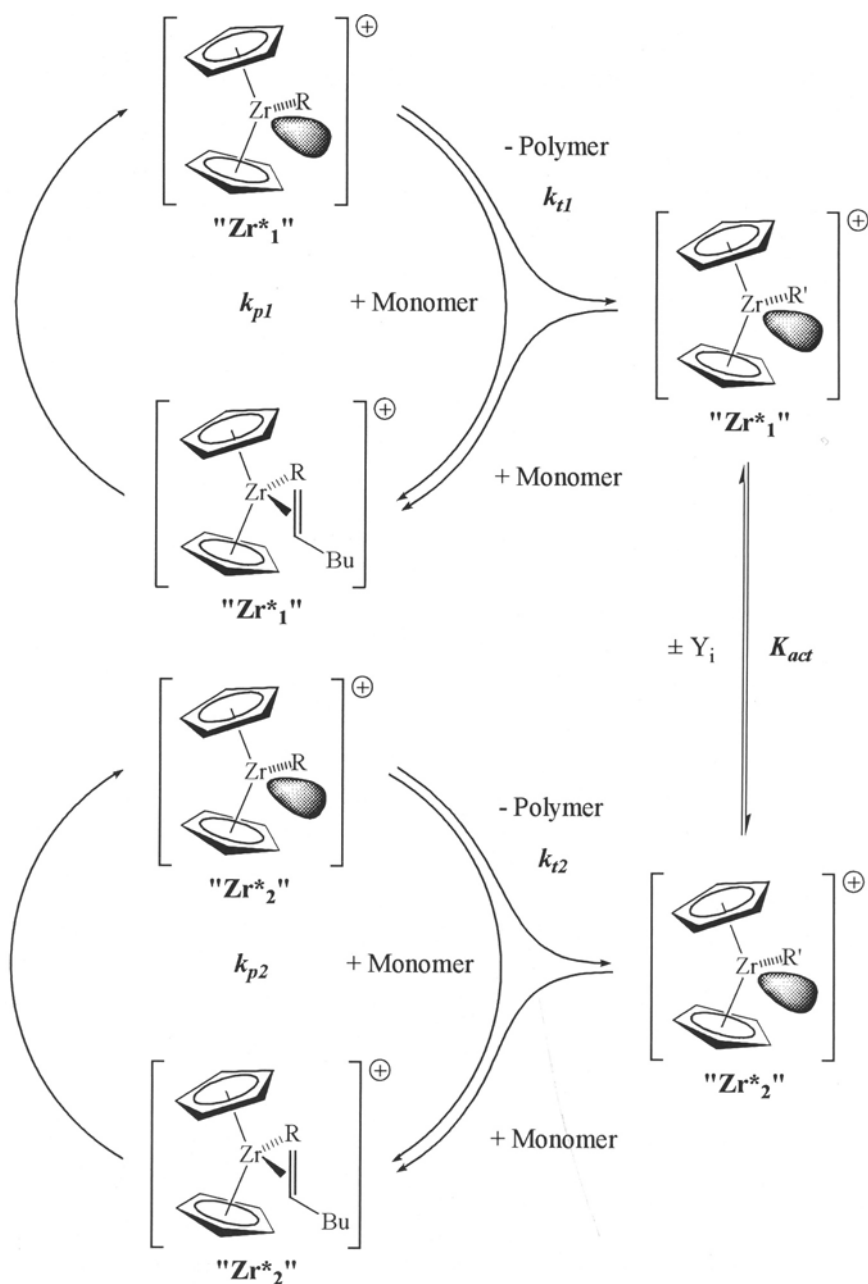


Fig. 5. Model mechanism assuming a slow equilibrium of two structurally different active species " Zr^*_1 " and " Zr^*_2 " with different rate constants of propagation k_{p1} and k_{p2} and of termination k_{t1} and k_{t2} , with the equilibrium constant K_{act} ($\text{R} = \text{Me}$, growing chain; $\text{R}' = \text{H}$, Me).

Table 2. Fitting parameters, and thermodynamical parameters¹⁾ of the polymerization reactions obtained by fitting the experimental data of poly(1-hexene) polymerizations with Cp₂ZrCl₂ **1** / MAO, Et(Ind)₂ZrCl₂ **2** / MAO, and ¹Pr(Cp)(Flu)ZrCl₂ **3** / MAO.

| Catalyst | 1 / MAO | 2 / MAO | 3 / MAO |
|--|----------------|----------------|----------------|
| D _p | 5104 (±836) | 8273 (±902) | 8839 (±2432) |
| D _t | 5172 (±1312) | 8031 (±758) | 7774 (±2211) |
| $\frac{\Delta G_{act}^0}{\text{kJ} \cdot \text{mol}^{-1}}$ ²⁾ | 42 (±6,9) | 69 (±7,5) | 73 (±20,2) |

¹⁾ Standard deviations for a 95% confidence interval.

²⁾ Calculated from D_p according to Equation (10), assuming that the difference of the activation energies is small.

5. Conclusions

From the experimental data presented here it is not possible to determine, which species are the two active species in the polymerization reaction. Different possibilities have been discussed in previous studies:

- Bimetallic zirconium complexes that were proposed as a part of the catalyst degradation reactions by Fischer and Mühlhaupt [8], as well as Huang and Rempel [9]. Brintzinger et al. [10] as well as Herfert and Fink [11] pointed out that these complexes are not necessarily inactive for ethylene polymerizations. The zirconocene concentrations used in our experiments was relatively high (1·10⁻⁴ mol/L) and could be the reason for the strong deviation from the expected behaviour we observed.
- Mixed bimetallic zirconium/aluminium complexes or contact ion pairs of the zirconocenium catalyst with the (Me-MAO)⁻ counterion like it was formulated by Fink et al. [12], Tritto et al. [3], Eisch et al. [13]. If the MAO cocatalyst generates the active species, solubilizes, and stabilizes it, like it was outlined in the introduction, why should it not be involved in the polymerization mechanism itself? Experiments and theoretical calculations of other groups [4,5] support this hypothesis.

There is one remarkable feature of the interconversion of the active species that has not been discussed before. The equilibrium of the two active species must be **slow** on the chain growth time scale. In other words, once a single chain has started to grow with one sort of active species at its end, the latter stays as it is until the termination of this chain. This is the reason why we do not only observe broadened, but clearly bimodal molecular weight distributions, and it is a clear

distinction from previously discussed model mechanisms like the intermittent chain growth proposed by Fink et al. [11]. To our opinion, the slow equilibrium could be explained by the assumption that diffusion of one of the reactants to and also away from the metallocenium cation is hindered, once the chain has started to grow.

Further experiments with other cocatalysts (e.g. $B(C_6F_5)_3$), more polar solvents (e.g. C_6H_5Cl) and different catalyst/cocatalyst concentrations are in progress to obtain a deeper insight into the polymerization process.

6. References

- [1] H.-H. Brintzinger, D. Fischer, R. Mühlhaupt, B. Rieger, R. Waymouth, *Angew. Chem.* **1995**, *107*, 1255 and references therein.
- [2] X. Yang, C. L. Stern, T. J. Marks, *Organometallics* **1991**, *10*, 840.
- [3] I. Tritto, R. Donetti, M. C. Sacchi, P. Locatelli, G. Zannoni, *Macromolecules* **1997**, *30*, 1247.
- [4] a) R. Fusco, L. Longo, A. Proto, F. Masi, F. Garbassi, *Macromol. Rapid Commun.* **1998**, *19*, 257-262; b) R. Fusco, L. Longo, F. Masi, F. Garbassi, *Macromol. Rapid Commun.* **1997**, *18*, 433-441; c) R. Fusco, L. Longo, F. Masi, F. Garbassi, *Macromolecules* **1997**, *30*, 7673-7685.
- [5] a) N. Naga, K. Mizunuma, *Macromol. Chem. Phys.* **1998**, *199*, 113; b) H. Frauenrath, H. Keul, H. Höcker, *Macromol. Rapid Commun.* **1998**, *19*, 391-395.
- [6] F. J. Karol, S.-C. Kao, E. P. Wasserman, R. C. Brady, *New J. Chem.* **1997**, *21*, 797-805.
- [7] M. Szwarc, M. Van Beylen, "Ionic polymerization and living polymers", Chapman & Hall, London, **1993**.
- [8] D. Fischer, R. Mühlhaupt, *J. Organomet. Chem.* **1991**, *417*, C7-C11.
- [9] J. Huang, G. L. Rempel, *Ind. Eng. Chem. Res.* **1997**, *36*, 1151-1157.
- [10] T. Haselwander, S. Beck, H.-H. Brintzinger in "Ziegler Catalysts: Recent Innovations and Technological Improvements", G. Fink, R. Mühlhaupt, H.-H. Brintzinger (eds.), Springer Verlag, Berlin, **1995**.
- [11] N. Herfert, G. Fink, *Makromol. Chem., Rapid Commun.* **1993**, *14*, 91-96.
- [12] G. Fink, D. Schnell, *Angew. Makromol. Chem.* **1982**, *105*, 15-30.
- [13] J. J. Eisch, S. I. Pombrik, G.-X. Zheng, *Angew. Chem.* **1995**, *107*, 1255-1283.

In-depth Investigation of Unsaturated Chain-end Groups: a Tool for Understanding Hydrogen Activation Mechanism in Zirconocene Catalysed Propene Polymerization

Maria Carmela Sacchi, Fabrizio Forlini, Incoronata Tritto, Paolo Locatelli

Istituto di Chimica delle Macromolecole del C.N.R. Via E. Bassini 15 - 20133 Milano, Italy

Andrew Carvill

National Microelectronics Research Centre, University College Cork, Cork, Ireland

Abstract.

Detailed NMR analysis of the microstructure of polypropenes prepared using a range of methylaluminoxane-activated zirconocene catalysts, with and without hydrogen present, have shown that chain transfer to hydrogen by the hindered metal polymeryls which result from secondary monomer insertion cannot be the only mechanism for the well known hydrogen activation effect. It is proposed that another mechanism which may give rise to the activation is that hydrogen should renew catalytic sites which have reacted with unsaturated chain terminal groups in the polymerization mixture to form inert species (such as metal allylics or other sterically hindered sites). Propene was polymerized in solution at partial pressures from 0.4 to 1.1 bar and temperatures ranging from 30°C to 100°C, using a range of three methylaluminoxane-activated zirconocene catalysts. It was found that of the several types of unsaturated terminal group observed using NMR spectroscopy, only vinylidene, 2-butenyl and 4-butenyl are actually formed during polymerization reactions conducted at less than 60°C. Preliminary investigations have shown that the activity of the zirconocene based catalysts is lessened on addition of low molecular weight olefins as models for unsaturated chain-end groups.

Introduction

Although many studies on the effects of hydrogen on heterogeneous Mg/Ti based catalysts [1-8] and homogeneous metallocene based catalysts [9-11] have been conducted, the reasons for the increase in catalyst activity which is observed in

many cases to accompany the molecular weight reduction have not been clarified yet. Several theories on how hydrogen may increase polymer yields have been suggested, among which the most significant are:

1. That hydrogen reacts with the surfaces of heterogeneous catalysts to increase the number of potentially active sites [2].
2. That hydrogen adds to inactive Ti(II) to give higher valence active Ti species [1c].
3. That the hydrogen chain transfer reactions increase the overall activity of the catalyst by shortcutting the slow propagation steps which occur a) after isolated secondary insertions [5,6] and b) possibly also after isolated stereoerrors in isotactic sequences [6c,7], renewing fast propagation starting from metal-hydride species.
4. That hydrogen prevents the formation of unsaturated chain-end groups which may act as poisons for the active sites [4].
5. That hydrogen renews sites which have been deactivated to inert species (such as metal allylics [3a,b,c] or sites sterically hindered due to insertion of unsaturated terminals [3d])

Of these proposed explanations, the first has been ruled out by studies in which it was shown that hydrogen does not increase the number of active sites present at the initial propagation stage [4,3d]. The second explanation has also been abandoned since the addition of hydrogen to supported and unsupported systems based on well defined divalent Ti compounds of type η^6 -areneTiAl₂Cl₆ did not show the expected activation with hydrogen [6b].

Work to verify or dismiss the remaining explanations has usually been done either on a single catalytic system or on a number of catalytic systems but under different conditions. The results are consequently not easily comparable and are insufficient to give a clear general picture of the problem of hydrogen activation. The idea of our work was to attempt to rationalize the complexity of the results presented so far. The method adopted was to test the validity of the different theories on a selected group of catalytic systems. In spite of the fact that the hydrogen effect has been studied and utilized principally with industrial heterogeneous catalysts, we used the new metallocene based catalysts for our investigation because they permitted comparison of widely different polymerization behaviours, which was not possible with heterogeneous catalysts. Moreover the relatively low molecular weights obtained with most of these catalysts permitted us to make a comprehensive NMR analysis of chain-end groups.

Propene polymerizations were conducted under uniform conditions both with and without hydrogen by using a range of isospecific *ansa*-zirconocene catalysts: Et(Ind)₂ZrCl₂ (I), Et(IndH₄)₂ZrCl₂ (II), Me₂Si(Ind)₂ZrCl₂ (III), Me₂Si(2-Me-Ind)₂ZrCl₂ (IV), Me₂Si(Benz[e]Ind)₂ZrCl₂ (V) and Me₂Si(2-Me-Benz[e]Ind)₂ZrCl₂ (VI) which show different polymerization behaviours as well as different hydrogen activation effects. On the basis of detailed NMR analyses of the regio- and stereoirregularities and of the chain-end groups of the samples

obtained, it was possible to evaluate the validity of some of the principal hypotheses on the mechanism of hydrogen activation [12]. The most relevant results regard the hypothesis related to regioerrors (point 3a) which has been considered almost definitive by many authors, especially with regard to heterogeneous catalysts. From a close examination of the ways in which the hydrogen-induced variations of regioirregularities/end groups with the different catalysts could be correlated to the degree of hydrogen activation, it was apparent that the reactivation of dormant sites following a 2,1 insertion could be only one of the causes of hydrogen activation effect. The analysis of these samples also allowed us to re-examine the hypothesis regarding isolated stereoerrors (point 3b) according to which not only regioirregular but also stereoirregular insertions may slow down the rate of chain propagation, leading to an increased chance of chain transfer to hydrogen. This had been suggested by the observation that in propene polymerization with some MgCl_2 -supported catalysts the stereoregularity of isotactic polymer chains increased upon increasing hydrogen concentration. In contrast with these results we have observed that the stereoregularity of the polymers produced with the above mentioned zirconocene catalysts did not change substantially in the presence of hydrogen, with only minimal increases being apparent in some cases [12a,b]. The analysis of chain-end groups was used to re-examine the hypothesis that hydrogen prevents the formation of unsaturated terminals which could act as polymerization inhibitors (point 4). In our trials, unsaturated terminals were never completely suppressed by hydrogen and also their decrease was not well correlated to the corresponding hydrogen activation [12a,b]. In fact in one case (catalyst II) a slight *increase* in the amount of vinylidene terminals was observed with hydrogen, while the activation was more than 200%.

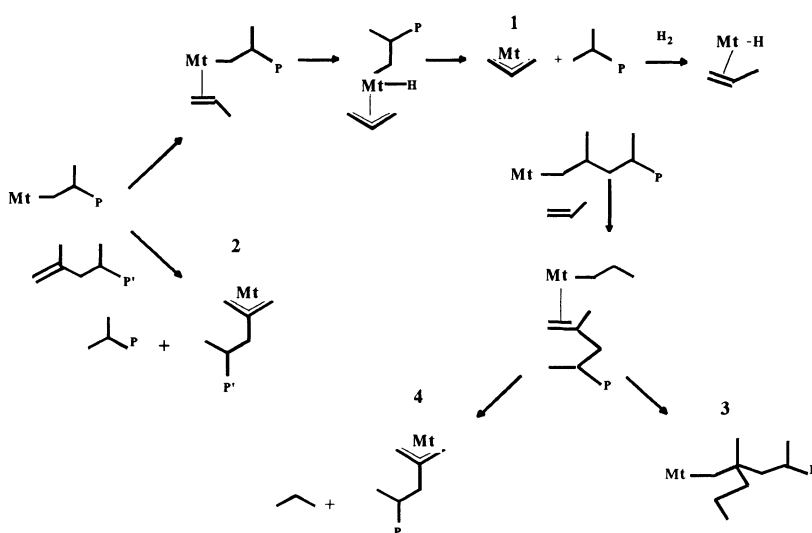
The final explanation (point 5) is still to be explored. A few years ago Guyot and Spitz [3a,b,c] suggested that, after a given propene monomer coordination, there is competition between further monomer insertion into the growing polymer chain and an allylic C-H activation process giving a π -allyl dormant species and a polymer chain with isobutyl chain-end group (Scheme 1.1). Site reactivation would then occur on reaction of these π -allyl species with hydrogen. A similar hypothesis was put forward by Teuben [13] to account for the deactivation of the catalyst system $[\text{Cp}^*_2\text{MMe}(\text{THT})]^+ [\text{BPh}_4]^-$ catalyst ($\text{Cp}^* = \eta^5\text{-C}_5\text{Me}_5$, $\text{M} = \text{Zr}/\text{Hf}$, $\text{THT} = \text{tetrahydrothiophene}$) observed during propene oligomerization. Some experimental evidence was produced for the formation of an allyl complex; moreover the addition of hydrogen was observed to restore oligomerization activity.

We propose a mechanism in some respects similar to the above: an allylic dormant species could derive from the unsaturated chain-end groups which have already formed during polymerization, rather than from the monomer. Allylic C-H activation should be easier for a vinylidene group than for a vinylic one. In Scheme 1.2 the vinylidene end group is shown as an example, among the terminals possibly involved. Alternatively it is possible that unsaturated chain-end groups formed by chain transfer to monomer do not eliminate but remain

coordinated to the active center and eventually reinsert (as proposed by Bukatov et al. [3d]) thereby creating sterically hindered active centers, to which next addition of propene should be very slow (Scheme 1.3). This process could also ultimately lead to the formation of an allylic species (Scheme 1.4).

In all these cases it is proposed that unsaturated chain-end groups react with catalyst to form dormant sites which could be reactivated by hydrogen. We are currently exploring this last hypothesis. To do this an in-depth knowledge of all the unsaturated species present in the polymerization system has become important.

Scheme 1. Possible mechanisms involving unsaturated chain-end groups

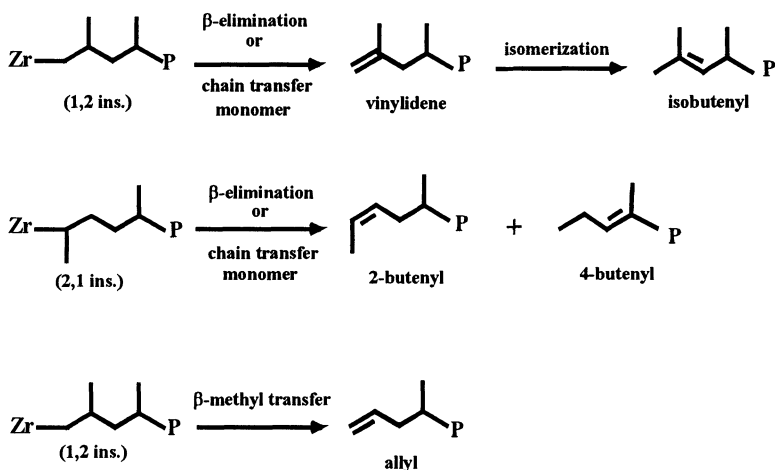


Results and discussion

Five unsaturated chain-end groups have been so far identified in propene homopolymers [1b,5a,9,10,12,14]. Vinylidene terminals derive from transfer of a β -hydrogen of the growing chain to monomer or to metal after regular (1,2) monomer insertion. Isobutenyl terminals derive from vinylidene isomerization. 2-butenyl terminals derive from chain transfer to monomer or to metal after secondary (2,1) monomer insertion. The origin of 4-butenyl has not been clarified yet. Allyl terminals derive from β -methyl transfer to metal after primary (1,2) monomer insertion (Scheme 2). A further chain termination leading to an internal vinylidene group has been recently proposed [14]. The steps in the present investigation have been: i) distinction between unsaturated species formed during the polymerization reactions (and therefore of possible relevance to the activation mechanism) and those formed afterwards due to thermal treatment (i.e. during the

NMR experiments); ii) determination of the dependence of the quantities of different types of terminals on the polymerization conditions (monomer partial pressure and temperature); iii) polymerization of propene in the presence of olefins which are models for the various unsaturated chain-end groups, to check their inhibition power on polymerization activity.

Scheme 2. Unsaturated chain terminal groups in polypropylene



Distinction between the unsaturated species formed during polymerization and those due to subsequent treatment of the polymer

Isobutenyl and 4-butenyl end groups could be formed during polymerization (in which case they could be involved in the hydrogen activation mechanism) or after polymerization, when the polymer samples are heated e.g. during the NMR experiments. To solve this problem we have analyzed the proton NMR spectra of two polymers before and after treatment at the temperature of the solution NMR experiments. One of them (prepared using the catalyst *rac*-Et(IndH₄)₂ZrCl₂ / MAO) is a low molecular weight polymer with vinylidene as the principal unsaturated terminal group (Fig.1). It is apparent that, after 48 h of heating at 103°C, the doublet assigned to isobutenyl end group is greatly enhanced at the expense of vinylidene signal and that its amount increases with time of heating. However, when the polymer had been completely freed from catalyst traces, the doublet due to isobutenyl did not appear even after a prolonged thermal treatment. So we can conclude that variable amounts of isobutenyls are not formed during polymerization, at least with this catalyst system under our conditions. An acid catalyzed vinylidene isomerization could be promoted by residual catalyst during the heating of the polymer. Fig.2 shows the proton NMR spectrum of a sample (prepared using *rac*-Me₂Si(Benz-[e]-Ind)₂ZrCl₂ / MAO) in which the triplet T assigned to 4-butenyl is present with about the same intensity as the multiplet due

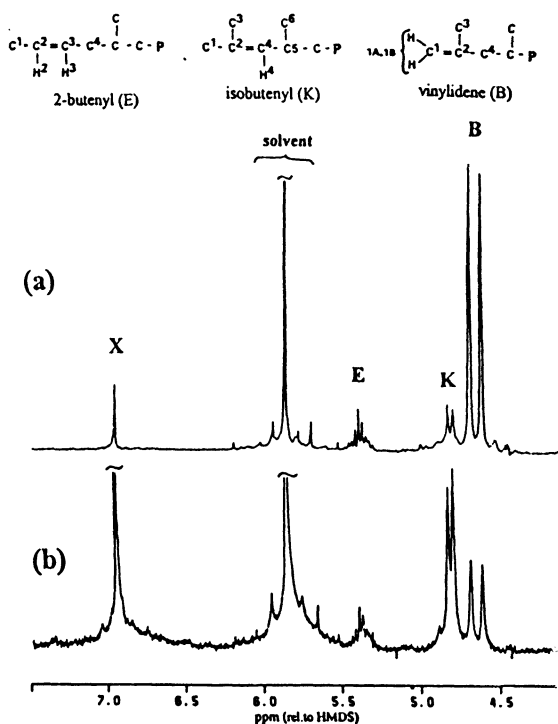


Fig. 1. ¹H NMR spectra (recorded in 1,1,2,2-tetrachloroethane-*d*₂ at 103°C) of the olefinic region of polypropene prepared using rac-Et(IndH₄)₂ZrCl₂/MAO: (a) fresh sample, recorded over 12 h; (b) same sample, recorded after heating at 103°C for a further 48 h.

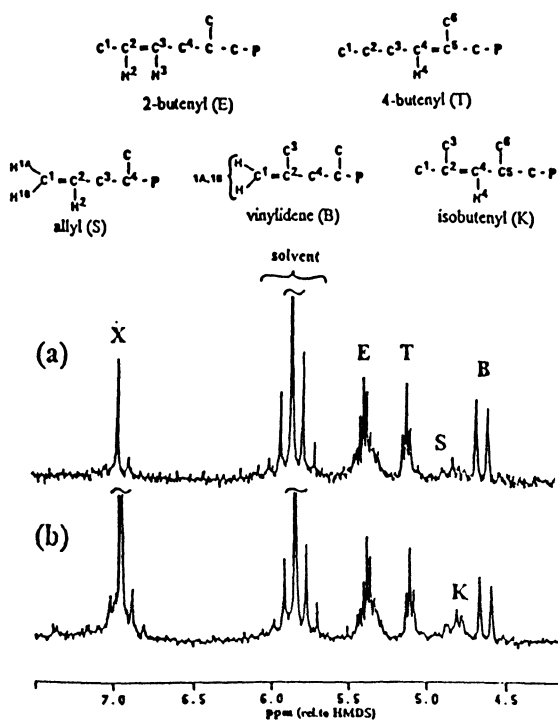


Fig. 2. ¹H NMR spectra (recorded in 1,1,2,2-tetrachloroethane-*d*₂ at 103°C) of the olefinic region of polypropene prepared using rac-Me₂Si(benz[e]Ind)₂ZrCl₂/MAO: (a) fresh sample, recorded over 12 h; (b) same sample, recorded after heating at 103°C for a further 48 h.

Table 1. Dependence of chain-end group trends on polymerization conditions:¹³C and ¹H NMR analysis of unsaturated chain terminals per 10,000 monomer insertions

| Run | Catalyst ^a | P(C ₃ H ₆) | solvent ^b | T | unsaturated terminals | | | |
|-----|-----------------------|-----------------------------------|----------------------|-----|-----------------------------|-----------|-----------|-------|
| | | | | | / 10,000 monomer insertions | | | |
| | | bar | | °C | vinylidene | 2-butenyl | 4-butenyl | allyl |
| 1 | (I) | 0.4 | Tol | 30 | 22 | 11 | 6 | n.d. |
| 2 | (I) | 1.1 | Tol | 30 | 15 | 7 | 4 | n.d. |
| 3 | (III) | 0.4 | Tol | 30 | 9 | 7 | 3 | n.d. |
| 4 | (III) | 1.1 | Tol | 30 | 9 | 4 | trace | n.d. |
| 5 | (V) | 0.4 | Tol | 30 | 8 | 14 | 6 | n.d. |
| 6 | (V) | 1.1 | Tol | 30 | 6 | 10 | 2 | n.d. |
| 7 | (V) | 1.1 | DCB | 60 | 9 | 17 | 19 | trace |
| 8 | (V) | 1.1 | DCB | 100 | 94 | 13 | 19 | 15 |
| 7a | (V) ^c | 1.1 | DCB | 60 | 38 | 61 | 30 | 6 |

^a(I): Et(Ind)₂ZrCl₂; (III): Me₂Si(Ind)₂ZrCl₂; (V): Me₂Si(Benz[e]Ind)₂ZrCl₂. ^bTol: toluene; DCB: o-dichlorobenzene. ^c minor oligomeric fraction of run 7, recovered by evaporation of precipitation mixture.

to the 2-butenyl end group E. This sample was also heated at 103°C for 48 h. We see that after this treatment (besides a partial isomerization of vinylidene B to isobutenyl K, and a large increase in the amount of the decomposition product X) no evolution of the system is observed, the ratio of E to T being the same as prior to the treatment. On the other hand the triplet T assigned to 4-butenyl was always present in the same amount from the outset of the thermal treatment for a given sample, independently of whether the sample had been previously freed from traces of catalyst.

Dependence of chain-end group trends on polymerization conditions

Polymerizations were conducted using three different zirconocenes, *rac*-Et(Ind)₂ZrCl₂ (I), *rac*-Me₂Si(Ind)₂ZrCl₂ (III) and *rac*-Me₂Si(Benz-[e]-Ind)₂ZrCl₂ (V) at the same temperature (30°C) varying propene pressure from 0.4 to 1.1 bar. A second series of polymerizations were conducted using Me₂Si(Benz-[e]-Ind)₂ZrCl₂ at propene partial pressure 1.1 bar and at a range of temperatures from 30 to 100°C. Table 1 shows that the numbers of unsaturated chain-end groups increased in general, with decreasing monomer pressure and increasing temperature. An exception is represented by 2-butenyls at 100 °C, which decrease giving place to 1,3 enchainned misinsertions [12c]. The only new terminals appearing at higher temperatures were allyl groups. In run 7, we recovered the small oligomeric fraction (7a) which remained in solution in the DCB / ethanol

Table 2. Propene polymerization^a with increasing amounts of different chain-end models

| Model ^b | model/propene molar ratio | Yield g | Yield decrease ^c % | Molecular weight and polydispersity | | | Tacticity ^e mmmm % |
|--------------------|---------------------------|---------|-------------------------------|-------------------------------------|----------------------|--------------------------------------|-------------------------------|
| | | | | M _n (NMR) ^d | M _n (GPC) | M _w /M _n (GPC) | |
| none | 0.00 | 1.70 | | 12,400 | 12,800 | 2.20 | 87 |
| 2-H | 0.17 | 1.24 | 27 | | 13,650 | 2.16 | |
| 2-H | 0.34 | 0.93 | 45 | | 11,140 | 2.17 | |
| 2-H | 0.70 | 0.61 | 64 | 9,700 | 9,170 | 2.15 | 89 |
| 2M1P | 0.17 | 1.26 | 26 | | 10,910 | 2.06 | |
| 2M1P | 0.34 | 0.83 | 51 | | 9,240 | 2.27 | |
| 2M1P | 0.70 | 0.73 | 57 | 7,200 | 6,640 | 2.29 | 88 |
| 2M1P | 1.03 | 0.29 | 83 | | 7,710 | 2.12 | |

^a Catalyst: Et (Ind)₂Zr₂(I) ; polymerizations conducted for 1 h, at 0.40 bar partial pressure propene, using 1.5 μmol Zirconocene / methylaluminoxane (MAO) (Zr : Al = 1 : 3,000) in 100 cm³ toluene at 30°C ± 1°C. ^b2-H: cis/trans 2-hexene; 2M1P: 2-methyl-1-pentene. ^cdecrease in yield by comparison with run without model olefin ^dcalculated as (10,000 × mol. wt. of monomer) ÷ (0.5 × total terminals per 10,000 monomer insertions) based on NMR. ^ecalculated according to best fit of integrals of ¹³C methyl signals for the four principal pentads to an enantiomorphic site control model (ref. 15).

Table 3. ¹³C and ¹H NMR analysis of regioirregularities and chain terminals, per 10,000 monomer insertions.

| Chain-end model ^a | Enchained secondary insertions: | | | Terminals following secondary insertion: | | Terminals following primary insertions: | |
|------------------------------|---------------------------------|------------------------|------------------|--|------------------------|---|----------------------|
| | 2,1 erythro ^b | 2,1 threo ^b | 1,3 ^b | 2-butenyl ^c | 4-butenyl ^c | vinylidene ^c | i-butyl ^b |
| none | 31 | 16 | 14 | 11 | 3 | 21 | 5 |
| 2-H | 26 | 14 | 15 | 10 | 3 | 33 | 6 |
| 2M1P | 31 | 19 | 19 | 11 | 3 | 35 | 15 |

^aPolymerization conditions as shown in Table 2, chain-end model/propene molar ratio= 0.7 ^bfrom ¹³C NMR spectra (assignments as given in ref. 12c). ^c from ¹H NMR spectra (assignments as given in ref. 12c)

mixture, that is the fraction which is usually lost on precipitation of these polymers. The ¹H and ¹³C NMR analysis shows that the unsaturated chain-end groups of this fraction were qualitatively the same as in the main fraction, but in

greater numbers, due to the low molecular weight. Therefore, with all three catalysts and under all the conditions described, only the five unsaturated terminals shown in Scheme 2 are detected, in variable proportions. Among these, allyls are formed only at higher temperatures and isobutenyls are formed during the polymer thermal treatment subsequent to the reaction. Therefore, if unsaturated groups formed during the polymerization act as inhibitors, the unsaturated groups involved should be found among the vinylidene, 2-butenyl and 4-butenyl terminals.

Molecular models of chain-end groups as polymerization inhibitors

The third step of our investigation consisted in checking whether molecular models of these three chain-end groups can work as polymerization inhibitors. A similar experiment has been performed by Imaoka [4] and Ystenes [16] with a heterogeneous catalyst. So far we have used 2-methyl-1-pentene (2M1P) and cis/trans 2-hexene (2H) with $\text{Et}(\text{Ind})_2\text{ZrCl}_2$, which has the highest hydrogen activation among the catalysts we have studied. Table 2 shows the results of propene polymerizations conducted in the presence of increasing concentrations of these model olefins. Both olefins act as polymerization inhibitors, but without completely poisoning the catalyst even when the concentration of olefin is almost as great as that of propene. From ^{13}C NMR analysis (Table 3) we have found that the model olefins i) do not affect stereoregularity or numbers of regiomisinsertions; ii) do not insert into the metal-polymeryl bond (i.e. no appreciable signs of inserted monomer and/or of new kinds of terminals are observed) and iii) lessen molecular weights with increases in the numbers of vinylidene and isobutyl terminations. Of the two model olefins, these effects are more evident when 2M1P is used.

Conclusion

On the basis of the results presented here and previously, it is possible to have a preliminary general overview of the mechanism of hydrogen activation effect. It has become apparent that there are several rather than one main cause of hydrogen activation, and that one or more of these may contribute to the effect, depending on the catalyst and conditions. In particular we now understand that with metallocene type catalysts: i) the reactivation of dormant sites following a 2,1 insertion is certainly one of the causes of the hydrogen activation, but not the only cause as had been supposed by some authors; ii) chain transfer to hydrogen after isolated stereoirregular insertions seems to contribute only marginally to the activation, at least with metallocenes; iii) there is a first positive indication that unsaturated chain-end groups could be involved in activation effect. We are continuing our examination of this last hypothesis, in which the preliminary results presented in this paper will be examined in greater detail. In particular it is of fundamental importance firstly to check whether the introduction of

hydrogen reverses the deactivation effects caused by the models and secondly to compare catalysts which have already shown different capacities for hydrogen activation, in order to find a relationship between the degree of the activation and the poisoning effect of the model olefins.

Acknowledgment. The authors would like to thank Professor Umberto Giannini for his constant interest in this work and his precious advice and Dr. Lucia Zetta and Mr. Giulio Zannoni for their valuable cooperation in NMR analysis.

References

1. (a) Guastalla, G.; Giannini, U. 1983. *Makromol. Chem., Rapid Commun*, 4, 519. (b) Hayashi, T.; Inoue, Y.; Chûjô, R.; Asakura, T. 1988, *Macromolecules*, 21, 2675. (c) Chien, J.C.W.; Nosaki, T. 1991. *J. Polym. Sci. Part A, Polym. Chem.*, 29, 505.
2. (a) Parsons, I. W.; Al-Turki, T. M. 1989. *Polymer Commun*. 30, 72. (b) Kioka, M.; Kashiwa, N. J. 1991. *Macromol. Sci.- Part A (Chem) A28*, 865.
3. (a) Spitz, R.; Masson, P.; Bobichon, C.; Guyot, A. 1988. *Makromol. Chem.* 189, 1043. (b) Spitz, R.; Masson, P.; Bobichon, C.; Guyot, A. 1989. *Makromol. Chem.* 190, 717. (c) Guyot, A.; Spitz, R.; Dassaud, J. P.; Gomez, C. 1993. *J. Mol. Catal.* 82, 29. (d) Bukatov, G.D.; Goncharov, V.S.; Zakharov, V.A. 1995. *Macromol. Chem. Phys.*, 196, 1751.
4. Imaoka, K.; Ikai, S.; Tamura, M.; Yoshikiyo, M.; Yano, T. 1993. *J. Mol. Catal.* 82, 37.
5. (a) Kojoh, S.; Kioka, M.; Kashiwa, N.; Itoh, M.; Mizuno, A. 1995. *Polymer* 36, 5015. (b) Mori, H.; Tashino, K.; Terano, M.; 1995. *Macromol. Chem. Phys.* 196, 651.
6. (a) Chadwick, J. C.; Miedema, A.; Sudmeijer, O. 1994. *Macromol. Chem. Phys.* 195, 167. (b) Albizzati, E.; Giannini, U.; Balbontin, G.; Camurati, I.; Chadwick, J. C.; Dall'Occo, T.; Dubitsky, Y.; Galimberti, M.; Morini, G.; Maldotti, A. 1997. *J. Polym. Sci.* 35, 2645. (c) Chadwick, J. C.; van Kessel, G. M. M.; Sudmeijer, O. 1995. *Macromol. Chem. Phys.* 196, 1431.
7. Chadwick, J. C.; Morini, G.; Albizzati, E.; Balbontin, G.; Mingozi, I.; Cristofori, A.; Sudmeijer, O.; van Kessel, G. M. M. 1996. *Macromol. Chem. Phys.* 197, 2501.
8. Busico, V.; Cipullo, R.; Chadwick, J. C.; Modder, J. F.; Sudmeijer, O. 1994. *Macromolecules* 27, 7538.
9. Tsutsui, T.; Kashiwa, N.; Mizuno, A. 1990. *Makromol. Chem., Rapid Commun.* 11, 565.
10. Jüngling, S.; Mülhaupt, R.; Stehling, U.; Brintzinger, H. H.; Fischer, D.; Langhauser, F. 1995. *J. Polymer Sci. Part A* 33, 1305.
11. Schupfner, G.; Kaminsky, W. 1995. *J. Mol. Catal. A* C102, 59.
12. a) Carvill, A.; Tritto, I.; Locatelli, P.; Sacchi, M.C. 1997. *Macromolecules* 30, 7056. (b) Sacchi, M.C.; Carvill, A. 1997. *MetCon '97, "Polymers in Transition"*. June 4-5, Houston, TX USA. c) Carvill, A.; Zetta, L.; Zannoni, G.; Sacchi, M.C. 1998. *Macromolecules* 31, 3783.
13. Eshuis, J.J.W.; Tan, Y.Y.; Meetsma, A.; Teuben, J.H. 1992. *Organometallics* 11, 362.
14. Resconi, L.; Piemontesi, F.; Camurati, I.; Sudmeijer, O.; Nifant'ev, I.E.; Ivchenko, P.V.; Kuz'mina, L.G. 1998. *J. Am. Chem. Soc.*, 120, 2308.
15. Resconi, L.; Fait, A.; Piemontesi, F.; Colonesi, M.; Rychlicki, H.; Ziegler, R. 1995. *Macromolecules*, 28, 6667.
16. Wester, T.S.; Ystenes, M. 1997. *Macromol. Chem. Phys.*, 198, 1623.

4. Supported Metallocene Catalysts

Supported Metallocene Catalysts for Propene Polymerization

Peter J.T. Tait and Ratna Ediati,

Department of Chemistry, UMIST, Manchester, England, UK.

Abstract.

A series of silica supported ethylenebisindenylzirconium dichloride catalysts have been prepared using a number of different experimental procedures and using different types of silica also pretreated under differing conditions. The kinetic and activity behaviour of these catalysts when used with methylaluminoxane (MAO) cocatalyst have been investigated for the polymerization of propene at various MAO concentrations. The activities of these supported catalysts were shown to be affected significantly by their methods of preparation and by the thermal treatment of the silica supports. Higher catalyst activities were obtained by first pretreating dehydrated silica with MAO and then reacting the product either with the metallocene or with a precontacted mixture of the metallocene and MAO. The use of a lower dehydration temperature, 260 °C rather than 460 °C, increased the activity of the supported catalyst systems. The catalyst activities also initially increased with increase in the concentration of external MAO. The order of treatment used for the supported catalyst preparation affected the shapes of the rate-time profiles which were obtained. MAO pretreated silica catalysts were shown by SEM studies to yield polymer of good morphology and evidence for silica fragmentation was also obtained. Leaching experiments were performed using selected MAO pretreated catalysts and showed the significance of leaching processes in these polymerization systems. These results are discussed in terms of a pore restricted model for the polymerization process.

1. INTRODUCTION

A considerable number of publications describing the preparation of supported metallocene catalysts have appeared in the scientific and patent literature [1-6]. The majority of these preparations have involved the use of silica supports. In these publications it is possible to identify three types of supported metallocene systems, as described in terms of the chemical bonding which is involved.

- (a) Systems in which the metallocene molecule is simply adsorbed onto or into the support structure.
- (b) Systems in which the metallocene is firmly and directly attached to the support by means of covalent linkages, e.g., Soga, Kim and Shiona [7]. A variant on this method is the linking of the cyclopentadienyl ring via a bridge to the support surface, e.g., Antberg, Lüker and Böhm [8]. An earlier and related example has been discussed by Booth et al [9].
- (c) Systems in which the metallocene molecule is embedded in a “sandwich” type layer structure of the form, support/MAO/metallocene/MAO, e.g., Janiak and Rieger [10]. In this structure the bonding is very likely that of ionic interactions arising from the formation of an ionic pair, e.g., Jordan [11].

In previous publications [3-4] we have discussed the kinetic behaviours of homogeneous and supported metallocene catalyst systems when used for the polymerization of ethylene. Also some preliminary results have been published on the polymerization of propene [5]. This paper now presents a fuller account of the comparative behaviour of selected catalysts, prepared using different procedures, for the polymerization of propene and using ethylenebisindenylzirconium dichloride supported on silica and activated by methylaluminoxane.

2. EXPERIMENTAL

2.1 Materials

EP10 silica was kindly donated by Crosfields, Warrington, UK. The sample had a surface area of $291 \text{ m}^2\text{g}^{-1}$, a pore diameter of 269 Å, a pore volume of $1.8 \text{ cm}^3\text{g}^{-1}$, and a median particle size of 100 μm .

MS3040 silica was kindly donated by the PQ Corporation, Conshohocken, USA. The sample had a surface area of $460 \text{ m}^2\text{g}^{-1}$, a pore diameter of 260 Å, a pore volume of $3.0 \text{ cm}^3\text{g}^{-1}$, and a median particle size of 45 μm .

2.2 Preparation of Catalysts

The following silica supported catalysts were prepared using procedures similar to those described previously [5]. Fuller details will be published elsewhere [12].

$\text{SiO}_2/\text{Et}(\text{Ind})_2\text{ZrCl}_2$ (EP46A): Zr = 1.53% (w/w).

$\text{SiO}_2/\text{Et}(\text{Ind})_2\text{ZrCl}_2/\text{MAO}$ (EP46B): Zr = 0.96% (w/w); Al = 7.7% (w/w).

$\text{SiO}_2/\text{MAO}/\text{Et}(\text{Ind})_2\text{ZrCl}_2$ (EP46C): Zr = 0.44% (w/w); Al = 7.4% (w/w).

SiO₂/MAO/Et(Ind)₂ZrCl₂ (EP26C): Zr = 0.18% (w/w); Al = 8.8% (w/w).

SiO₂/MAO/Et(Ind)₂ZrCl₂ (EP46CB): Zr = 0.40% (w/w); Al = 4.1% (w/w).

SiO₂/MAO/Et(Ind)₂ZrCl₂ (MS26C and MS46C) :

MS26C: Zr = 0.40% (w/w); Al = 4.0% (w/w);

MS46C: Zr = 0.39% (w/w); Al = 8.3% (w/w).

SiO₂/MAO/Et(Ind)₂ZrCl₂/MAO (EP46D) : Zr = 0.40% (w/w); Al = 9.0% (w/w).

SiO₂/[Et(Ind)₂ZrCl₂ + MAO] (EP46E) : Zr = 0.30% (w/w); Al = 12.2% (w/w).

SiO₂/MAO/[Et(Ind)₂ZrCl₂ + MAO] (EP46F) :

Zr = 0.32% (w/w); Al = 14.3% (w/w).

SiO₂/MAO/[Et(Ind)₂ZrCl₂ + MAO] (EP26F, EP26FB and MS26F) :

EP26F: Zr = 0.08% (w/w); Al = 10.4% (w/w);

EP26FB: Zr = 0.40% (w/w); Al = 4.2% (w/w);

MS26F: Zr = 0.32% (w/w); Al = 14.1% (w/w).

2.3 Polymerization Procedure

Details of the polymerization procedure are similar to those described previously [5]. Fuller details will be published elsewhere [12].

3. RESULTS

3.1 The Effect of Order of Reaction of Catalyst Components in Catalyst Formation.

The effect of the order of reaction of the catalyst components, viz., SiO₂, MAO and Et(Ind)₂ZrCl₂, during catalyst preparation was investigated by carrying out a series of polymerizations using SiO/Et(Ind)₂ZrCl₂, SiO₂/Et(Ind)₂ZrCl₂/MAO, SiO₂/MAO/Et(Ind)₂ZrCl₂ and SiO₂/MAO/Et(Ind)₂ZrCl₂/MAO supported catalyst systems containing similar zirconium contents. The results obtained are listed in Table 1. It is apparent that the activities of silica supported metallocene catalysts are strongly influenced by their method of preparation. Pretreatment of silica with MAO prior to reaction with a metallocene can be seen to yield a catalyst system of higher activity for propene polymerization than a catalyst prepared by direct reaction of silica with a metallocene, or by direct reaction of a silica with a metallocene followed by treatment with MAO.

Table 1. Comparative activities of supported $\text{SiO}_2 / \text{Et}(\text{Ind})_2\text{ZrCl}_2$, $\text{SiO}_2 / \text{Et}(\text{Ind})_2\text{ZrCl}_2 / \text{MAO}$, $\text{SiO}_2 / \text{MAO} / \text{Et}(\text{Ind})_2\text{ZrCl}_2$ and $\text{SiO}_2 / \text{MAO} / \text{Et}(\text{Ind})_2\text{ZrCl}_2 / \text{MAO}$ - MAO catalyst systems for the polymerization of propene.

| Catalyst | Type of catalyst | $[\text{Al}]_{\text{external}} / \text{mol dm}^{-3}$ | Al / Zr | Yield / g | $\text{Rp}_{\text{av}} \times 10^{-3} / \text{kg PP (mol Zr} \cdot \text{h)}^{-1}$ | $\text{Rp}_{\text{max}} \times 10^{-3} / \text{kg PP (mol Zr} \cdot \text{h)}^{-1}$ |
|----------|---|--|-------------|-----------|--|---|
| EP46A | $\text{SiO}_2 / \text{Et}(\text{Ind})_2\text{ZrCl}_2$ | 0.030 | 110 | 1.2 | 0.017 | 0.21 |
| EP46B | $\text{SiO}_2 / \text{Et}(\text{Ind})_2\text{ZrCl}_2 / \text{MAO}$ | 0.030 | 120 | 1.0 | 0.016 | 0.20 |
| EP46C | $\text{SiO}_2 / \text{MAO} / \text{Et}(\text{Ind})_2\text{ZrCl}_2$ | 0.009 0.030 | 230 4000 | 9.2 25 | 0.39 5.7 | 1.2 8.0 |
| EP46D | $\text{SiO}_2 / \text{MAO} / \text{Et}(\text{Ind})_2\text{ZrCl}_2 / \text{MAO}$ | 0.040 | 4000 | 1.1 | 0.39 | 3.9 |

EP46A: Zr = 1.53 % w/w; EP46B: Al = 7.7 % w/w, Zr = 0.96 % w/w;

EP46C: Al = 7.4 % w/w, Zr = 0.44 % w/w; EP46D: Al = 9.0 % w/w, Zr = 0.40 % w/w.

Polymerization conditions: Toluene; 6 bar; 60 °C.

The reason for this behaviour is evident from a comparison of the rate-time profiles for these catalyst systems. Figure 1 shows that the catalyst system $\text{SiO}_2 / \text{Et}(\text{Ind})_2\text{ZrCl}_2 - \text{MAO}$ rapidly loses its activity with increase in polymerization time. A maximum rate is shown at the beginning of the polymerization after which the rate decreases sharply with polymerization time. The same situation is true for the polymerization system, $\text{SiO}_2 / \text{Et}(\text{Ind})_2\text{ZrCl}_2 / \text{MAO} - \text{MAO}$ as is also shown in Figure 1. The catalyst system $\text{SiO}_2 / \text{MAO} / \text{Et}(\text{Ind})_2\text{ZrCl}_2 / \text{MAO} - \text{MAO}$ also behaves in the same way.

On the other hand the rate-time profile for the polymerization system, $\text{SiO}_2 / \text{MAO} / \text{Et}(\text{Ind})_2\text{ZrCl}_2 - \text{MAO}$, shows a different type of behaviour (Figure 2). These polymerization systems show an initial settling period during which the instantaneous rate decreases. This decrease is followed by a significant increase in rate reaches a limiting value which then remains constant for 2 h polymerizations.

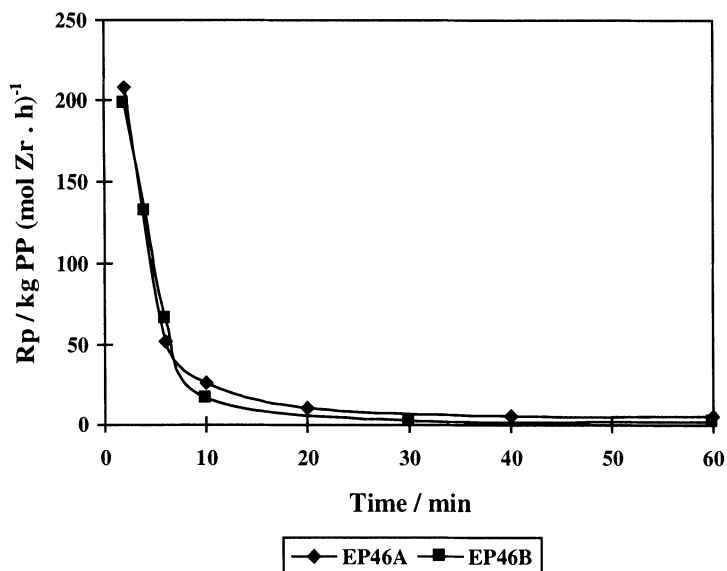
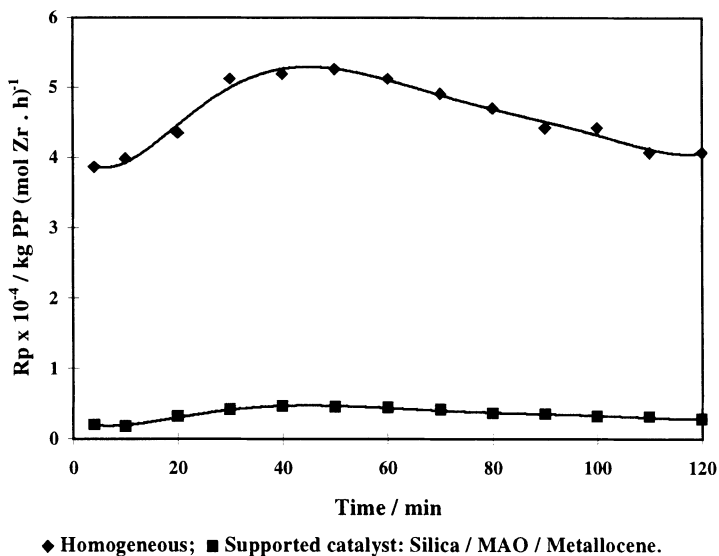


Figure 1. Rate-time profiles for polymerizations of propene using catalyst systems $\text{SiO}_2 / \text{Et}(\text{Ind})_2\text{ZrCl}_2$ (EP46A) – MAO and $\text{SiO}_2 / \text{Et}(\text{Ind})_2\text{ZrCl}_2 / \text{MAO}$ (EP46B) – MAO.

Polymerization conditions: Toluene = 250 cm³, 6 bar, 60 °C, 1 hour.

EP46A: [Zr] = 2.7 × 10⁻⁴ mol dm⁻³, Al/Zr = 110;

EP46B: [Zr] = 2.5 × 10⁻⁴ mol dm⁻³, Al/Zr = 120.



◆ Homogeneous; ■ Supported catalyst: Silica / MAO / Metallocene.

Figure 2. Comparative rate-time profiles for polymerizations of propene using homogeneous $\text{Et}(\text{Ind})_2\text{ZrCl}_2$ and silica supported $\text{SiO}_2 / \text{MAO} / \text{Et}(\text{Ind})_2\text{ZrCl}_2$ (EP46C) – MAO catalyst systems.

Polymerization conditions: Toluene = 300 cm³, 6 bar, 60 °C, 2 hour.

Homogeneous: [Al] = 0.030 mol dm⁻³; Al/Zr = 15000;

Heterogeneous: [Al] = 0.030 mol dm⁻³; Al/Zr = 1500;

Figure 2 also shows a rate-time plot for the homogeneous catalyst system $\text{Et}(\text{Ind})_2\text{ZrCl}_2\text{-MAO}$ when used under similar conditions for the polymerization of propene. This plot which shows a relatively stable polymerization rate throughout the polymerization time (2 h) is included to facilitate comparison of polymerization behaviour and to establish benchmark behaviour. The homogeneous catalyst system is much more active than the supported catalyst .

3.2 The Effect of Precontacting during Catalyst Formation

The effect of precontacting $\text{Et}(\text{Ind})_2\text{ZrCl}_2$ and MAO prior to reaction with MAO treated silica was investigated using two different types of silica dehydrated at two different temperatures. The results are shown in Table 2 and show a somewhat complex pattern.

For EP10 type silica dehydrated at 460 °C precontacting $\text{Et}(\text{Ind})_2\text{ZrCl}_2$ and MAO before reaction with MAO-treated silica gave rise to catalysts of the highest activity both in terms of $R_p(\text{av})$ and $R_p(\text{max})$, i.e., $\text{SiO}_2/\text{MAO}/\{\text{Et}(\text{Ind})_2\text{ZrCl}_2+\text{MAO}\}\text{-MAO}$ catalyst systems. For EP10 type silica dehydrated at 260 °C $\text{SiO}_2/\text{MAO}/\text{Et}(\text{Ind})_2\text{ZrCl}_2\text{-MAO}$ catalyst systems still showed the highest values of $R_p(\text{av})$ and $R_p(\text{max})$. For MS 3040 silica, dehydrated at 260 °C, the two catalyst systems, $\text{SiO}_2/\text{MAO}/\text{Et}(\text{Ind})_2\text{ZrCl}_2$ and $\text{SiO}_2/\text{MAO}/\{\text{Et}(\text{Ind})_2\text{ZrCl}_2+\text{MAO}\}$ showed similar high activities. The comparative rate-time plots of these polymerization systems are shown in Figure 3.

Apart from reducing the length of the settling period the use of precontacting had little effect on the overall shapes of the relevant rate-time profiles, as is evident in Figure 3.

3.3 The Effect of Silica Dehydration Temperature

The effect of the silica dehydration temperature was investigated by studying the behaviour of supported catalysts prepared using two types of silica, EP10 and MS 3040, dehydrated at two different temperatures. Results obtained for the catalyst system $\text{SiO}_2/\text{MAO}/\text{Et}(\text{Ind})_2\text{ZrCl}_2$ are listed in Table 3.

For both types of silica higher values for $R_p(\text{av})$ and $R_p(\text{max})$ were obtained when the lower dehydration temperature of 260 °C was used.

The reason for the higher activities of catalysts prepared using silica dehydrated at lower temperatures is evident from an examination of the relevant rate-time profiles. Inspection of Figure 4 shows that catalysts obtained using silica dehydrated at 260 °C reach a higher value of $R_p(\text{max})$ more quickly, i.e., the length of the setting period is reduced and in addition $R_p(\text{max})$ has a higher value both for the EP10 and MS 3040 silica.

Table 2. Effects of precontacting : Comparative activities of supported $\text{SiO}_2 / \text{MAO} / \text{Et}(\text{Ind})_2\text{ZrCl}_2$, $\text{SiO}_2 / \{\text{MAO} + \text{Et}(\text{Ind})_2\text{ZrCl}_2\}$ and $\text{SiO}_2 / \text{MAO} / \{\text{MAO} + \text{Et}(\text{Ind})_2\text{ZrCl}_2\}$ - MAO catalyst systems for the polymerization of propene.

| Catalyst | Type of catalyst | $[\text{Al}]_{\text{external}} / \text{mol dm}^{-3}$ | Yield / g | $\text{Rp}_{\text{av}} \times 10^{-3} / \text{kg PP (mol Zr} \cdot \text{h)}^{-1}$ | $\text{Rp}_{\text{max}} \times 10^{-3} / \text{kg PP (mol Zr} \cdot \text{h)}^{-1}$ |
|----------|---|--|-----------|--|---|
| EP46C | $\text{SiO}_2 / \text{MAO} / \text{Et}(\text{Ind})_2\text{ZrCl}_2$ | 0.030 | 25 | 5.7 | 8.0 |
| EP46E | $\text{SiO}_2 / \{\text{MAO} + \text{Et}(\text{Ind})_2\text{ZrCl}_2\}$ | 0.040 | 16 | 2.6 | 4.0 |
| EP46F | $\text{SiO}_2 / \text{MAO} / \{\text{Et}(\text{Ind})_2\text{ZrCl}_2 + \text{MAO}\}$ | 0.030 | 29 | 7.5 | 9.4 |
| EP26C | $\text{SiO}_2 / \text{MAO} / \text{Et}(\text{Ind})_2\text{ZrCl}_2$ | 0.030 | 37 | 8.4 | 10 |
| EP26E | $\text{SiO}_2 / \{\text{MAO} + \text{Et}(\text{Ind})_2\text{ZrCl}_2\}$ | 0.030 | 4.9 | 1.2 | 3.0 |
| EP26F | $\text{SiO}_2 / \text{MAO} / \{\text{Et}(\text{Ind})_2\text{ZrCl}_2 + \text{MAO}\}$ | 0.030 | 4.3 | 1.1 | 2.4 |
| MS26C | $\text{SiO}_2 / \text{MAO} / \text{Et}(\text{Ind})_2\text{ZrCl}_2$ | 0.030 | 34 | 8.6 | 12 |
| MS26F | $\text{SiO}_2 / \text{MAO} / \{\text{Et}(\text{Ind})_2\text{ZrCl}_2 + \text{MAO}\}$ | 0.030 | 35 | 8.7 | 13 |

EP46C: Al = 7.4 % w/w; Zr = 0.44 % w/w; EP46E: Al = 12.2 % w/w, Zr = 0.30 % w/w;

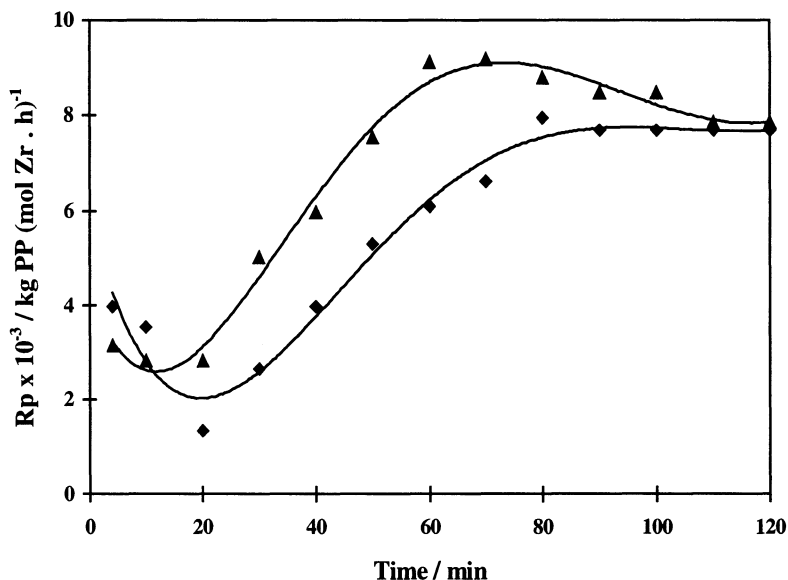
EP46F: Al = 14.3 % w/w, Zr = 0.32 % w/w.

EP26C: Al = 8.8 % w/w; Zr = 0.18 % w/w; EP26E: Al = 10.1 % w/w, Zr = 0.16 % w/w;

EP26F: Al = 10.4 % w/w, Zr = 0.08 % w/w.

MS26C: Al = 4.0 % w/w; Zr = 0.40 % w/w; MS26F: Al = 14.1 % w/w, Zr = 0.32 % w/w;

Polymerization conditions: Toluene = 300 cm³, Al/Zr = 4000, 6 bar, 2 hour, 60 °C.



◆ EP46C (Silica/MAO/Met); ▲ EP46F {Silica/MAO/(Met+MAO)}.

Figure 3. Effect of precontacting: comparative rate-time profiles for polymerizations of propene using catalyst systems $\text{SiO}_2 / \text{MAO} / \text{Et}(\text{Ind})_2\text{ZrCl}_2 - \text{MAO}$ and $\text{SiO}_2 / \text{MAO} / \{\text{Et}(\text{Ind})_2\text{ZrCl}_2 + \text{MAO}\} - \text{MAO}$.

Polymerization conditions: Toluene = 300 cm^3 , Al/Zr = 4000, 6 bar, 60°C , 2 hour.

Table 3. Effect of dehydration temperature of the silica on the activities of supported $\text{SiO}_2 / \text{MAO} / \text{Et}(\text{Ind})_2\text{ZrCl}_2 - \text{MAO}$ catalyst systems for the polymerization of propene.

| Catalyst | Type of silica | Dehydration temperature of silica / $^\circ\text{C}$ | $[\text{Al}]_{\text{external}} / \text{mol dm}^{-3}$ | Yield / g | $\text{Rp}_{\text{av}} \times 10^{-3} / \text{Kg PP (mol Zr . h)}^{-1}$ | $\text{Rp}_{\text{max}} \times 10^{-3} / \text{kg PP (mol Zr . h)}^{-1}$ |
|----------|----------------|--|--|-----------|---|--|
| EP26C | EP10 | 260 | 0.030 | 37 | 8.4 | 10 |
| EP46C | EP10 | 460 | 0.030 | 25 | 5.7 | 8.0 |
| MS26C | MS3040 | 260 | 0.030 | 35 | 8.6 | 12 |
| MS46C | MS3040 | 460 | 0.030 | 1.3 | 0.03 | 1.8 |

EP26C: Al = 8.8 % w/w; Zr = 0.18 % w/w; EP46C: Al = 7.4 % w/w, Zr = 0.44 % w/w; MS26C: Al = 4.0 % w/w, Zr = 0.40 % w/w; MS46C: Al = 8.3 % w/w Zr = 0.39 % w/w. Polymerization conditions: Toluene = 300 cm^3 , Al/Zr = 4000, 6 bar, 2 hour, 60°C .

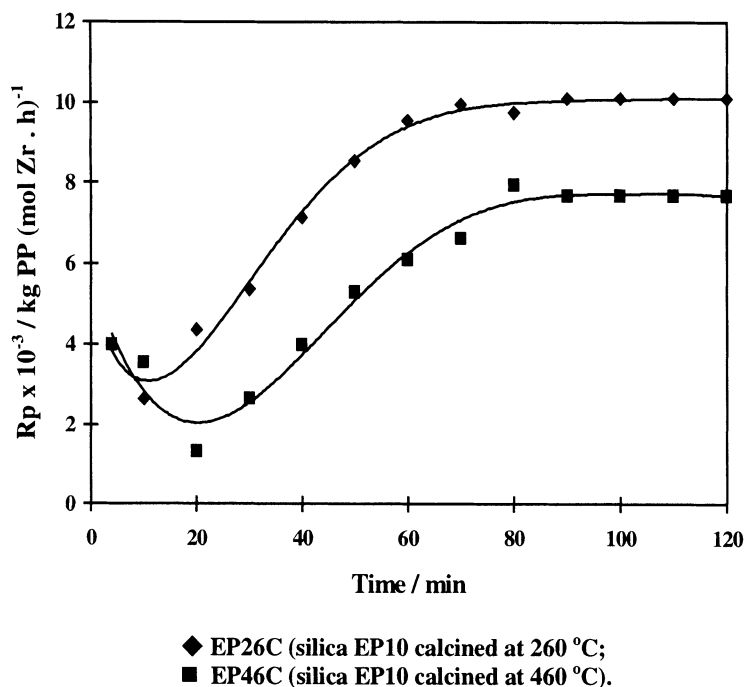


Figure 4. Rate-time profiles for polymerizations of propene using supported $\text{SiO}_2 / \text{MAO} / \text{Et}(\text{Ind})_2\text{ZrCl}_2 - \text{MAO}$ catalyst systems; Effect of dehydration temperature of the silica EP10.

Polymerization conditions: Toluene = 300 cm^3 , 6 bar, $60 \text{ }^\circ\text{C}$, 2 hour,
 $[\text{Al}]_{\text{external}} = 0.030 \text{ mol dm}^{-3}$; Al/Zr = 4000.

3.4 The Effect of External Methylaluminoxane Concentration

The effects of variation of external MAO concentration at constant $\text{Et}(\text{Ind})_2\text{ZrCl}_2$ concentration are shown in Figure 5 for the catalyst system $\text{SiO}_2/\text{MAO}/\text{Et}(\text{Ind})_2\text{ZrCl}_2$ (EP46C)-MAO. Both $R_p(\text{av})$ and $R_p(\text{max})$ increase rapidly with increase in MAO concentration to reach maximum values (at Al/Zr ratios of approximately 6000:1), after which both decrease gently with further increase in MAO concentration.

The effects of external MAO concentration on the kinetic behaviour of the $\text{SiO}_2/\text{MAO}/\{\text{Et}(\text{Ind})_2\text{ZrCl}_2 + \text{MAO}\}$ MS26F-MAO catalyst system is more or less similar apart from the higher values of $R_p(\text{av})$ and $R_p(\text{max})$ but show a somewhat greater sensitivity to deactivation at higher MAO concentrations - as is often observed for higher activity catalyst systems. This effect is also shown in Figure 5. The highest values of $R_p(\text{av})$ and $R_p(\text{max})$ at about Al:Zr ratios of approximately 5000:1.

It is considered that these effects are more properly regarded as MAO concentration rather than Al:Zr ratio dependent.

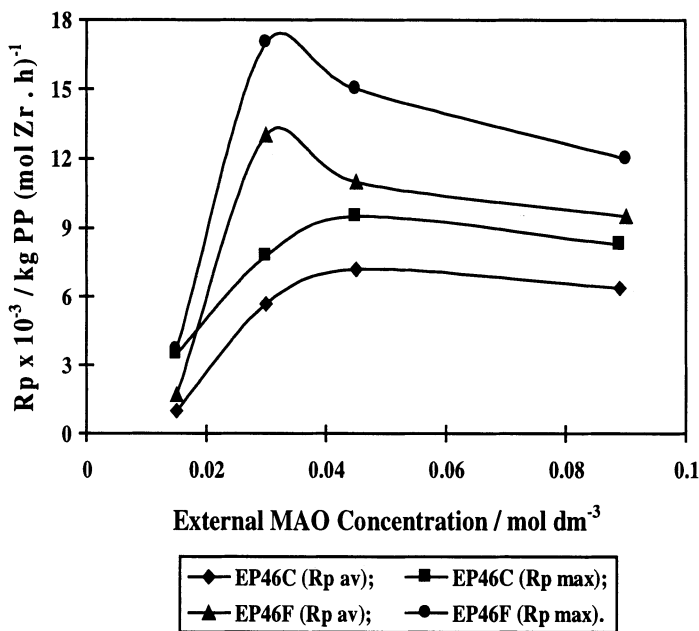


Figure 5. Effect of concentration of external MAO on activities of propene polymerizations using catalyst systems $\text{SiO}_2 / \text{MAO} / \text{Et}(\text{Ind})_2\text{ZrCl}_2$ (EP46C) – MAO and $\text{SiO}_2 / \text{MAO} / \{\text{Et}(\text{Ind})_2\text{ZrCl}_2 + \text{MAO}\}$ (EP46F) – MAO.
 Polymerization conditions: Toluene = 300 cm³, 6 bar, 60 °C, 2 hour,
 $[\text{Zr}] = 7.4 \times 10^{-6}$ mol dm⁻³.

3.5 Effect of Leaching

We have previously reported that a significant amount of leaching takes place when a supported $\text{SiO}_2/\text{Cp}_2\text{ZrCl}_2$ catalyst is treated with MAO under slurry conditions, and that the liquid fraction of the precontacted supported catalyst together with MAO was able to polymerize ethene [4]. In the present study leaching experiments were investigated using the supported catalyst systems $\text{SiO}_2/\text{MAO}/\text{Et}(\text{Ind})_2\text{ZrCl}_2$ and $\text{SiO}_2/\text{MAO}/\{\text{Et}(\text{Ind})_2\text{ZrCl}_2 + \text{MAO}\}$ for the polymerization of propene. The supported catalyst was precontacted with MAO in 50 cm³ toluene using a catalyst preparation reactor and the catalyst then subsequently filtered. The resultant liquid fraction was then used for the polymerization of propene. As a comparison, the mixture of precontacted supported catalyst and MAO was also used in the polymerization of propene under corresponding conditions. These leaching experiments were carried out for various Al/Zr molar ratios, precontacting temperatures and times.

Table 4 shows that the liquid fractions are active in the polymerization of propene, indicating that under the conditions employed significant leaching can take place. The yields of polymers resulting from the liquid fractions depend on the Al/Zr molar ratio and on precontacting temperature.

Table 4. Leaching of the metallocene from the silica support.

| Precontact Effect | Type of catalyst | Al/Zr | Precontact Temperat./ °C | Precontact Time / min | Yield / g | | $\frac{Y_L}{Y_{Total}}$ / % |
|----------------------------------|---|-------|--------------------------|-----------------------|-------------|-------------------|-----------------------------|
| | | | | | $Y_L^{(a)}$ | $Y_{Total}^{(b)}$ | |
| Effect of Al / Zr molar ratio | SiO ₂ / MAO / Et(Ind) ₂ ZrCl ₂ | 2000 | 60 | 30 | 24 | 77 | 31 |
| | SiO ₂ / MAO / Et(Ind) ₂ ZrCl ₂ | 4000 | 60 | 30 | 36 | 76 | 46 |
| | SiO ₂ / MAO / Et(Ind) ₂ ZrCl ₂ | 6000 | 60 | 30 | 23 | 36 | 64 |
| Effect of Precontact Temperature | SiO ₂ / MAO / Et(Ind) ₂ ZrCl ₂ | 4000 | No precontact | No precontact | - | 42 | - |
| | SiO ₂ / MAO / Et(Ind) ₂ ZrCl ₂ | 4000 | 25 | 30 | 9.7 | 51 | 19 |
| | SiO ₂ / MAO / Et(Ind) ₂ ZrCl ₂ | 4000 | 40 | 30 | 26 | 51 | 51 |
| | SiO ₂ / MAO / Et(Ind) ₂ ZrCl ₂ | 4000 | 60 | 30 | 36 | 76 | 46 |
| Effect of Precontact Time | SiO ₂ / MAO / {Et(Ind) ₂ ZrCl ₂ + MAO} | 2500 | No precontact | No precontact | - | 44 | - |
| | SiO ₂ / MAO / {Et(Ind) ₂ ZrCl ₂ + MAO} | 2500 | 60 | 30 | 23 | 56 | 41 |
| | SiO ₂ / MAO / {Et(Ind) ₂ ZrCl ₂ + MAO} | 2500 | 60 | 60 | 27 | 38 | 71 |
| | SiO ₂ / MAO / {Et(Ind) ₂ ZrCl ₂ + MAO} | 2500 | 60 | 90 | 23 | 31 | 74 |
| | SiO ₂ / MAO / {Et(Ind) ₂ ZrCl ₂ + MAO} | 2500 | 60 | 120 | 20 | 30 | 66 |

(a) : Yield of polymer obtained using the liquid fraction of the catalyst slurry,

(b) : Yield of polymer obtained using the catalyst slurry.

Polymerization conditions: Toluene = 300 cm³, [Al]_{external} = 0.028 mol dm⁻³, 6 bar, 60 °C, 2 hour.

Increase in the Al/Zr molar ratio in the range of 2000 - 4000 increased the yield of polypropene obtained using the liquid fraction; increasing the precontacting temperature also increases significantly the yield of polymer. Table 4 also shows that there is no significant effect of precontacting time on the yields of polymers resulting from the liquid fractions. However the ratio of the yield obtained using the liquid fraction (Y_L) to the yield obtained using the catalyst slurry (Y_{Total}) increases with increase in precontacting time to reach a more or less constant value after some 60 min precontacting at 60 °C.

3.6 Catalyst and Polymer Morphology

The morphology of the supporting silica is the same before and after the catalyst preparation as can be seen from an examination of Figure 6 which shows a SEM picture of MS3040 silica after preparation of the $\text{SiO}_2/\text{MAO}/\text{Et}(\text{Ind})_2\text{ZrCl}_2$ -type catalyst.

Figure 7 shows a SEM picture of the polymer produced using the catalyst system $\text{SiO}_2/\text{MAO}/\text{Et}(\text{Ind})_2\text{ZrCl}_2$ - MAO. This micrograph is particularly instructive in that it highlights that the greater activities of $\text{SiO}_2/\text{MAO}/\text{Et}(\text{Ind})_2\text{ZrCl}_2$ catalysts are associated with greater fragmentation of the catalyst support.

It is suggested that prior treatment of dehydrated silica with MAO before reaction with $\text{Et}(\text{Ind})_2\text{ZrCl}_2$ leads to a more homogeneous distribution of catalyst centres within the silica structure.

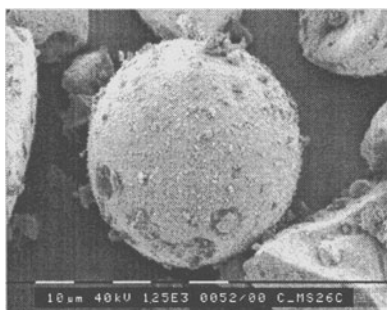


Figure 6. Morphology of SiO_2 after catalyst preparation (1250x).

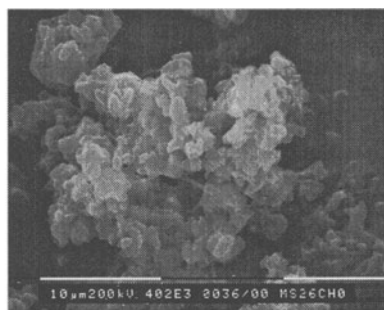


Figure 7. Morphology of the polymer produced using catalyst system $\text{SiO}_2/\text{MAO}/\text{Et}(\text{Ind})_2\text{ZrCl}_2$ -MAO.

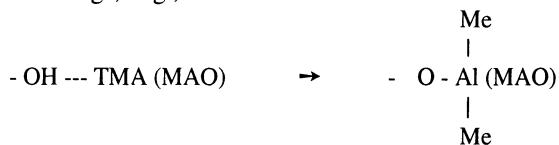
4. DISCUSSION

The MAO used in the present investigation contains 25-30% trimethylaluminium (TMA), and as a consequence the interaction of this MAO(TMA) with silica can be considered as occurring as follows:

Firstly, adsorption of MAO (TMA) onto the surface hydroxyl groups and siloxane rings, e.g.,



Secondly, the reaction between the adsorbed TMA (MAO) and the hydroxyl groups and siloxane rings, e.g.,



When such MAO-treated silica is then interacted with $\text{Et}(\text{Ind})_2\text{ZrCl}_2$ adsorption onto the TMA (MAO) coated surface can take place, followed by the formation of a Zr^+ - C zirconium cation and an anchored MAO anion. This zirconium species may then be regarded as 'free' to float in the vicinity of the charged surface in what may be described as a pore restricted ion pair metallocene-MAO- catalyst system [13].

The mechanism of leaching is illustrated in Figure 8 which depicts the situation in an idealized pore within the silica support. Leaching is visualized as taking place via two equilibrium reactions, one within the pores (Internal Equilibrium) and a second between charged entities within and without the pore structure (External Equilibrium). By means of this mechanism charged entities can be leached from the pore structure of the catalyst system.

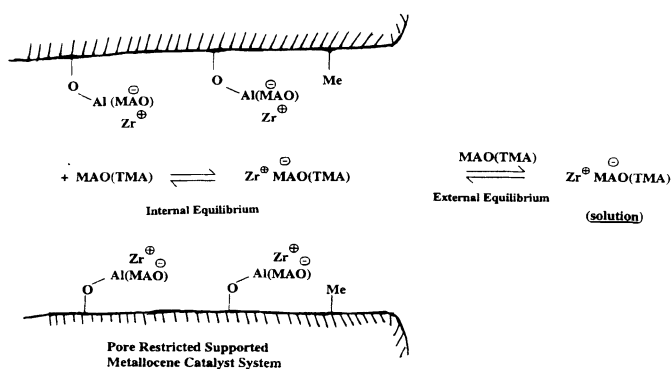
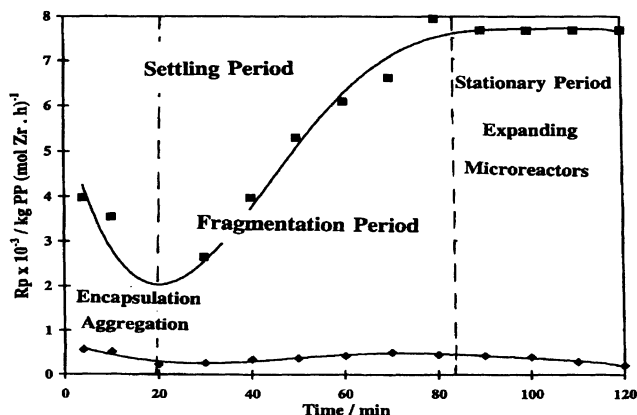


Figure 8. Mechanism of Leaching

The kinetic features of the polymerization of propene with supported $\text{SiO}_2/\text{MAO}/\text{Et}(\text{Ind})_2\text{ZrCl}_2\text{-MAO}$ catalyst systems are quite distinctive: an initial period during which the rate falls with increasing polymerization time, typically for 30 min under the experimental conditions used for the present investigation; then a period of increasing rate for about 60 min; followed by a period of limiting more or less constant rate. It is considered that these features arise from initial encapsulation and/or aggregation of sticky catalyst/polymer particles, followed by a period of catalyst fragmentation leading to a stationary period during which the polymerization behaviour is controlled by a discrete number of expanding microreactors [14,15]. The situation is illustrated in Figure 9. Evidence for fragmentation comes from SEM studies (See Figure 7).

Supported $\text{SiO}_2/\text{Et}(\text{Ind})_2\text{ZrCl}_2\text{-MAO}$ and $\text{SiO}_2/\text{Et}(\text{Ind})_2\text{ZrCl}_2/\text{MAO-MAO}$ catalyst systems behave very differently (Figure 1). The dramatic decrease in rate with increase in polymerization time which is observed can be attributed to either catalyst encapsulation before catalyst fragmentation can take place and/or catalyst deactivation.



◆ $[Al] = 0.009 \text{ mol dm}^{-3}$, $Al/Zr = 230$; ■ $[Al] = 0.030 \text{ mol dm}^{-3}$, $Al/Zr = 4000$.

Figure 9. Periods during R_p vs Time plot

Catalyst system: $SiO_2 / MAO / Et(Ind)_2ZrCl_2 - MAO$

Polymerization conditions: Toluene = 300 cm^3 , 6 bar, 60°C , 2 hour.

REFERENCES

1. W. Kaminsky and F. Renner, *Makromol. Chem., Rapid Commun.*, **14**, 239 (1993).
2. W. Kaminsky, *Macromol. Sym.*, **97**, 79 (1995).
3. P.J.T. Tait, A.1. Abozeid and A.S. Paghaleh, *Metallocenes '95*, Internat. Congress on Metallocene Polymers, 26-27 April, 1995, Brussels, p.89.
4. P.J.T. Tait, M.G.K. Monteiro, M. Yang and J.L. Richardson, *MetCon'97*, June 12-13, 1996, Houston.
5. P.J.T. Tait and R. Ediati, *MetCon'97*, June 4-5, 1997.
6. P.J.T. Tait in "Developments in Catalyst Support Technology", The Catalyst Group, Spring House, PA, p.99 (1996).
7. K. Soga, H.J. Kim and T. Shiona, *Macromol. Chem. Phys.*, **195**, 3347 (1994).
8. M. Antberg, H. Lüker and L. Böhm, US 5 202 398 (1993), assigned to Hoechst.
9. B.L. Booth, G.C. Ofunne, C. Stacey and P.J.T. Tait, *Organomet. Chem.*, **315**, 143 (1986).
10. C. Janiak and B. Rieger, *Angew. Makromol. Chem.*, **215**, 47 (1994).
11. R.F. Jordan, *Adv. Organomet. Chem.*, **32**, 325 (1991).
12. P.J.T. Tait and R. Ediati (To be published).
13. G.G. Hlatky and D.J. Upton, *Polymer Preprints*, **37**, No 1, 249 (1996).
14. P.J.T. Tait, G.H. Zohuri, A.M. Kells and I.D. McKenzie in "Ziegler Catalysts", Eds. G. Fink, R. Mulhaupt and H.H. Brintzinger, Springer-Verlag, Berlin, 1995, p.343.
15. F. Bonini, V. Fraaije and G. Fink, *J. Polymer Sci: Part A: Polymer Chemistry*, **33**, 2393 (1995).

Influence of the particle size of silica support on the kinetics and the resulting polymer properties at the polypropylene polymerization with heterogeneous metallocene catalysts; Part I: experimental studies and kinetic analysis

Christian Przybyla, Joachim Zechlin, Bernd Steinmetz, Bernd Tesche, Gerhard Fink*,

Max-Planck-Institut für Kohlenforschung, Kaiser-Wilhelm-Platz 1, D-45470 Mülheim/Ruhr

Abstract. The main focus of this study is the polypropylene polymerization with silica supported metallocene catalysts and especially the investigation of the influence of particle diameter on polymerization activity as well as the changing product properties in dependence on pellet size. The metallocene used was $\text{rac-Me}_2\text{Si}[\text{IndR}_2]_2\text{ZrCl}_2$ which was supported on a Grace silica/MAO system of four different particle sizes (10 μm , 35 μm , 50 μm , 80 μm). The propene-polymerizations were carried out in a toluene slurry at 40°C. It was observed that the highest activity is obtained with the smallest catalyst particles and the least activity results from the largest pellets. Also the molecular weights (M_w) strongly depend on the diameter of the support. The M_w of polypropylene produced by an 80 μm catalyst system is smaller by about 50 % compared to polypropylene obtained with a 10 μm catalyst system. Furthermore, the polymer growth and the polymer properties were investigated in dependence on time by SEM-images, microtome sections, ^{13}C -NMRs and DSC measurements.

1. Introduction

Homogeneous metallocene/methylaluminumoxan (MAO) catalysts, compared to conventional Ziegler catalyst, offer the unique possibility of tailoring the stereoregularity of polypropylene through ligand design at the transition metal center. They also offer the chance to alter the molecular weight by ligand

substitution. One additional as well as essential advantage of using metallocenes is the narrow molecular weight distribution of the produced polymer¹.

For practical applications homogeneous metallocenes present some drastic disadvantages. First of all the existing gas-phase as well as bulk production plants (Montell Spheripol technology, BASF-Novolen-technology, Amoco-Chisso-technology and Unipol-Shell-technology) require the support of the active species. Furtheron the production of well-shaped and uniform pellets with a narrow particle size distribution (including a high bulk density) cannot be reached by using homogeneous metallocenes. For these reasons the fixing of the metallocenes on a supporting material is inalienable for industrial interests. Another advantage of immobilization of the catalytic system is the dramatic reduction of cocatalyst needed^{2,3}.

Many different supporting materials were examined in the past as for example copolymers of styrene⁴, polystyrene⁵, pumice⁶, many oxides and halides of magnesium, calcium and aluminium⁷, but the supporting materials most applied are the manifold modifications of SiO₂^{8,9}. Beside the investigated zeolithes¹⁰ and molecular sieves¹¹, the amorphous silica obtained by the sol-gel process stand the test in the best way.

The differences of particle growth in early polymerization stages and the reaction kinetics as well as the product qualities in dependence on the dimension of the supporting material are unknown and this relation should be investigated in this paper.

2. Experimental section

2.1 Materials

All solvents and air-sensitive compounds were handled under an argon atmosphere using the Schlenk technique. The propylene gas was purified by passing through a series of columns of NaAl(Et)₄ to remove residual traces of moisture and oxygen. Toluene was purified by distillation under argon over NaAl(Et)₄.

2.2 Catalyst

Grace silica was calcinated at high temperatures (no more information can be given because of patent laws and claims). 7,5 g of this silica were added to a solution of $9 \cdot 10^{-5}$ mol rac-Me₂Si[IndR₂]₂ZrCl₂ and $2,8 \cdot 10^{-2}$ mol MAO in a solvent. The suspension was stirred, the solvent was removed, the catalyst was washed and dried in high vacuum (no details can be given because of patent claims also).

2.3. Propylene polymerization

The polymerizations were carried out in a 250 mL glass-autoclave equipped with a variable speed stirrer (1200 rpm) under constant propylene pressure of 2 bar. The temperature was always 40°C.

100 mL of anhydrous toluene were added to the reactor followed by 5 mL of an Al(*i*-Bu)₃ or Al(Et)₃ solution in toluene (10 vol.-%). The solution was thermostated and saturated with monomer gas reaching up to 2 bar. The heterogeneous catalyst ($[Zr]=5 \cdot 10^{-5}$ mol) was injected into the reactor as a powder with an argon pressure of 4 bar by an injection system. The consumption of monomer gas was registered by way of mass flow-meters. The polymerization time was varied from 1 to 90 minutes. The polymerizations were terminated by the slow addition of methanol. Precipitated polymers were adequately washed twice with 600 mL of methanol and twice with 20 mL of HCl and then dried in vacuum at 50°C for 12 h.

2.4 Electron microscopy

Scanning electron micrographs were obtained by using an Instrumental Scientific Instruments Model 60 electron microscope at 2 kV and varying levels of magnification. For the bulk analysis of the catalyst and the polymers the samples were embedded in an epoxy resin (Low Viskosity Kit, Spurr) and cured at 60°C for 24 h. Afterwards the samples were cut with a diamond knife in a Reichert Model Ultracut microtome at room temperature using standard methods. Both the cross-sectioned and unsectioned specimen were coated with a 100 Å tungsten layer by using an electron impact evaporator to increase the conductivity.

2.5 Polymer analytics

Weight-average molecular weights (M_w) and molecular weight distributions (M_w/M_n) of the polypropylene copolymers were determined by gel-permeation chromatography. The molecular weights were calculated from a universal calibration curve of polystyrene.

The ¹³C-NMR spectra of the polypropylenes were recorded on a Bruker AMX 300 spectrometer operating at 75 MHz and at 120°C. 2 mL of 1,2,4-trichlorobenzene served as solvent for 300 mg of the polymer and as reference. The lock was 1 mL of C₂D₂Cl₄.

Melting points of the polypropylenes were determined by differential scanning calorimetry.

BET measurements were carried out on a Sorptomatic 1900 with nitrogen as adsorbent at room temperature because of possible of destruction of catalyst at high temperature.

3. Results

Scanning electron microscopy was applied to characterize and to analyze the bulk structure as well as the composition of the supporting material. Fig. 1 represents the microtome sections and the aluminium linescans of heterogeneous catalyst particles consisting of the same silica support, equal cocatalyst concentration and identical metallocene species but with different particle diameters. It is obvious that a gradient of the aluminium (aluminumoxan (MAO)) concentration exists in case of the 50 μm catalyst. The MAO content on the surface is higher than inside the pellet. The smaller 10 μm particles show a homogeneous and uniform distribution of the cocatalyst MAO over the pellet diameter. It seems that the sterically crowded methylaluminumoxan has reached the center of the catalyst in the same concentration as the surface in spite of its hindrance.

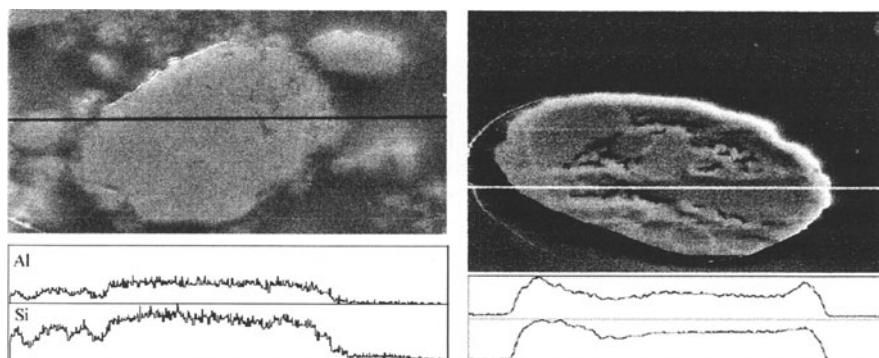


Fig. 1. Microtome sections and Al-linescans of the industrial catalyst with 10 μm (on the left) and 50 μm (on the right) particle diameter.

Among other factors, this fact could be the reason for the huge kinetic differences in the propylene polymerizations of the heterogeneous catalyst system $\text{SiO}_2/\text{MAO}/\text{rac-Me}_2\text{Si}[\text{IndR}_2]_2\text{ZrCl}_2$ with various particle diameters (Fig. 2). Four characteristic features of polymerization rate in dependence on particle size, are remarkable:

The period of low activity ('induction period'), before the polymerization reaction truly takes place, increases with increasing catalyst particle diameter.

The steepness of the increasing polymerization activity depends also on the pellet radius. The small particles enhance the turnover frequency more quickly than the larger ones.

The maximum activity also depends on catalyst partial diameter. The larger pellets show less maximum polymerization rate. At the beginning of all polymerization curves of the catalyst systems $\text{SiO}_2/\text{MAO}/\text{rac-Me}_2\text{Si}[\text{IndR}_2]_2\text{ZrCl}_2$, a prepolymerization peak appears that is independent of the particle radius.

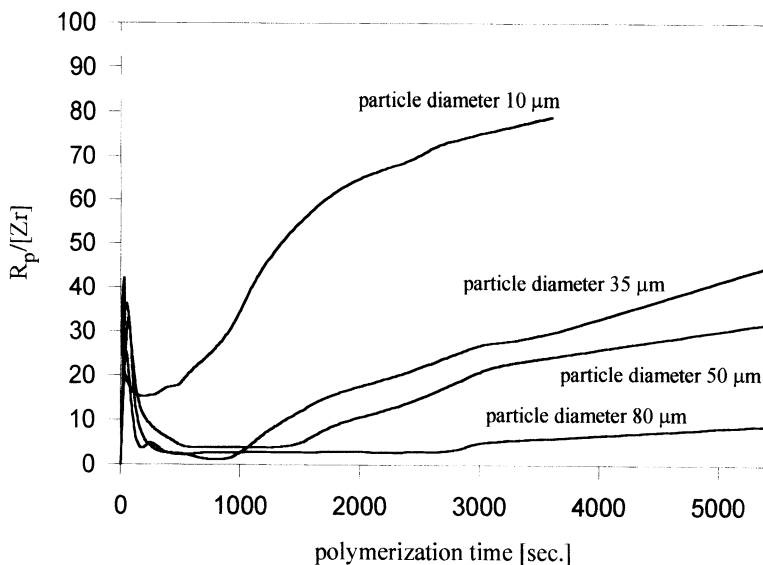
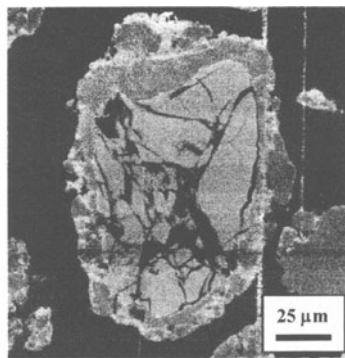
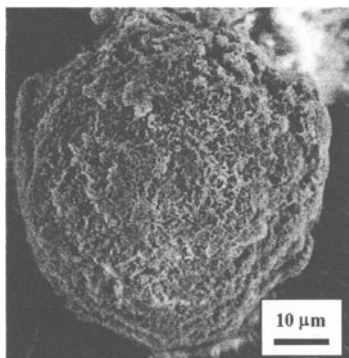


Fig. 2. Propene polymerization rate in dependence on catalyst particle size and polymerization time.

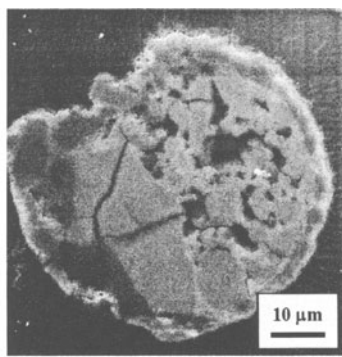
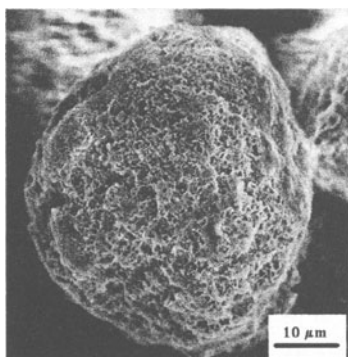
To obtain information about the different polymerization stages ('prepolymerization', 'induction period' etc.) it was necessary to stop the polymerization experiments at different stages. Fig. 3 presents SEM images and microtome sections of the 50 μm catalyst particle that was polymerized in various space of time (1 minute, 20 minutes, 90 minutes). It is conspicuous that the morphology of the polymer particle remains the same during the whole polymerization time and that the polymer represents a replica of the source catalyst in each case. The polymer structure on the pellet surface does not alter significantly relative to the polymerization time.

The microtome sections offers the possibility to observe the polypropylene growth inside the particle. After one minute of polymerization time a thin polypropylene layer around the pellets becomes visible. The microtome sections of the particles which were polymerized for 20 minutes also shows an identical thin polymer layer. The silica structure of the support is no longer visible in the sectioned pellet after 90 minutes of polymerization time. The supporting material is totally been filled with polymer.

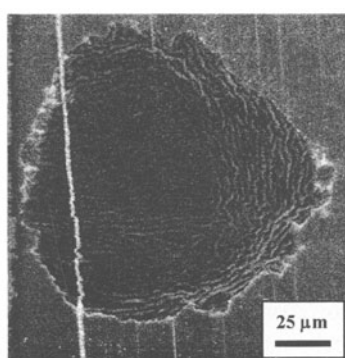
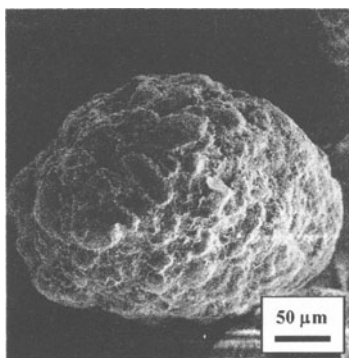
It seems that the 'prepolymerization' spike in the kinetic curve is due to the development of a polypropylene 'envelope'. The unchanged thickness of the polymer layer after 20 minutes of polymerization time compared to the layer after 1 minute of polymerization time points to a monomer diffusion problem. The propene molecule has to diffuse through the polymer layer to the active centers



50 μm catalyst, 1 min. polymerization time (SEM-image of the surface and bulk-structure)



50 μm catalyst, 20 min. polymerization time (SEM-image of the surface and bulk-structure)



50 μm catalyst, 90 min. polymerization time (SEM-image of the surface and bulk-structure)

Fig. 3. SEM-micrographs of the surface and bulk-structures of polypropylene produced by a heterogeneous catalyst system with particle diameter of 50 μm with different polymerization times.

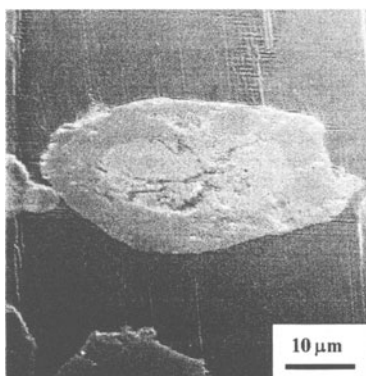
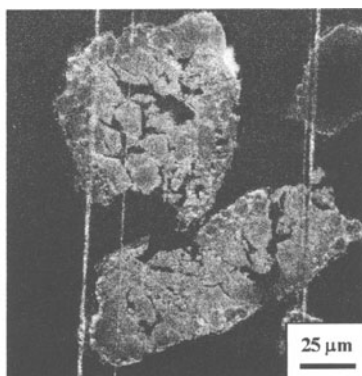
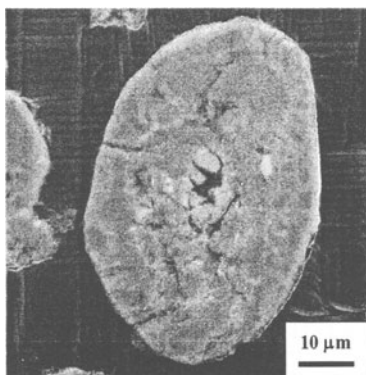
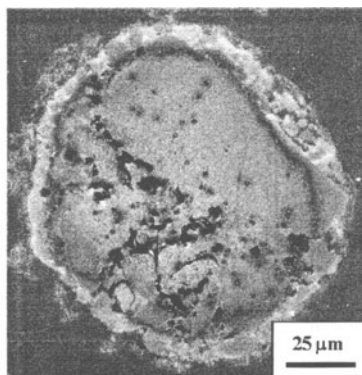
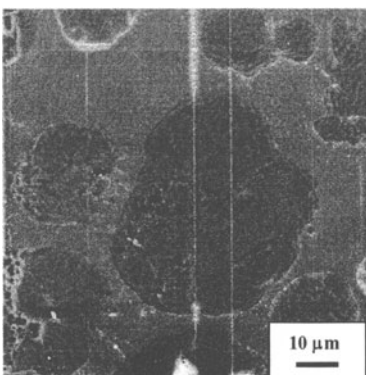
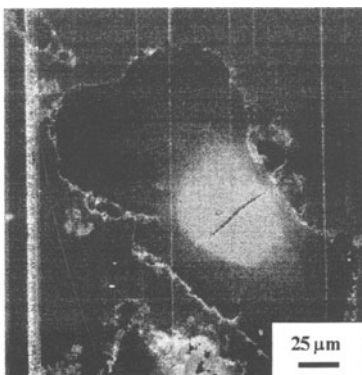
35 μm catalyst, 1 min. polymerization time80 μm catalyst, 1 min. polymerization time35 μm catalyst, 20 min. polymerization time80 μm catalyst, 20 min. polymerization time35 μm catalyst, 60 min. polymerization time80 μm catalyst, 90 min. polymerization time

Fig. 4. SEM-microtome sections of catalyst particles with varying diameters (35 μm and 80 μm) and different polymerization time 1, 20 and 60 minutes.

which leads to an induction period in kinetic curves. After the monomer has gone through the external polypropylene and has reached the first inner active species, the polymerization rate increases and the pellet starts fragmentation slowly from the outside to the center. The polymerization activity comes up to the maximum when the particle is completely fragmented.

Fig. 4 represents the microtome sections of the polymer particles that were produced by the 35 μm and the 80 μm catalyst. As has been the case for the 50 μm catalyst, the development of a polymer envelope around the pellet after a one minute reaction time can also be seen when applying the 35 μm and 80 μm catalyst systems. But the layer of the 35 μm particle is thicker than the layer of the larger material. A nearly full fragmentation even at 20 minutes of polymerization time can be found in the case of the 35 μm catalyst whereas the 80 μm catalyst system, at this moment, still has the initial thin polymer layer around the particle. After a reaction time of 60 minutes the supporting material of the 35 μm pellet has been completely penetrated by the polymer (similar to that of the 50 μm catalyst) but on the other hand the 80 μm catalyst particle contains an unfragmented silica center when given a polymerization time of 90 minutes.

The SEM-study of the propene-polymerization process elucidates the different reaction kinetics of the various dimensioned catalyst pellets as well as the dependence of catalyst particle size on the length of induction period and maximum activity.

Results of BET-measurements of the pure catalyst material and the 1 minute polymerized pellet as well as the 13 minutes polymerized particles are shown in Fig. 5. First of all it is generally noticed that the specific surface of the catalyst decreases with an increasing average particle size. This fact could be one of the

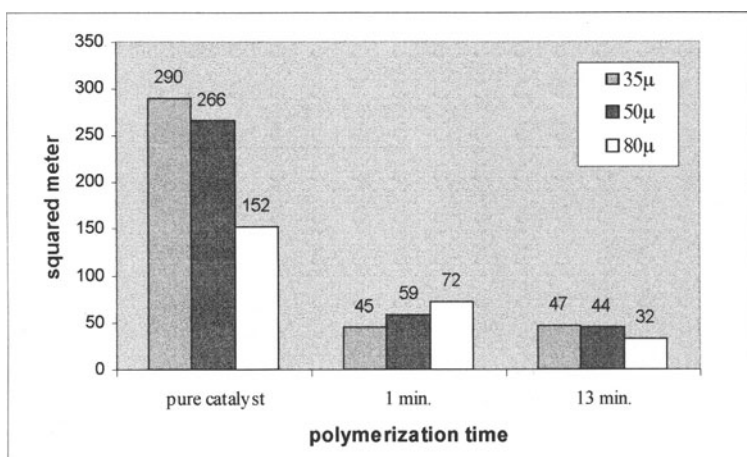


Fig. 5. Particle surface in dependence on propene-polymerization time and pellet diameter.

reasons for the higher activity of the smaller pellets compared to that of the larger ones. Moreover a very important fact signifies the enormous reduction of the specific surface of the pellets after a very short reaction time. The surface of the largest particles decreases in the slowest progression (reduction of 50 %) whereas the surface of the smallest pellets decreases in the fastest progression (reduction of 85 %). The lowering of the specific surface has to be equated with the reduction of such active centers that are accessible for the monomer in a direct way. This is another factor which is responsible for the induction period after the prepolymerization with its polymer layer formation. The specific surface remains stable with progressive polymerization time in consideration of the inaccuracy of BET-measurements.

The melting points of the produced polypropylenes are shown in Tab. 1. These melting points only depend on the polymerization time and not on the catalyst particle size. Polypropylenes obtained in the early polymerization stages have high melting points reaching to about 153°C, but the melting points decrease after termination of the 'induction period'. After the monomer has reached the inner active metallocenes and the polymerization rate increases, the melting point of the produced polymers decreases. According to this study the active species on the surface polymerize in a different way than the inner active species.

The ^{13}C -NMR data and the resulting microstructures of the products (Tab. 2) confirm this assertion. The isotacticity and the defect pentades of the polypropylenes neither change in dependence on particle size nor alter in dependence on reaction time. But the frequency of meso-2,1-misinsertion increases with a longer residence time in the reactor. In the beginning of propene polymerization the catalyst produces macromolecules with a misinsertion rate of 0.1 to 0.7 %, but after 60 minutes of polymerization time the misinsertion rate increases to about 0.9 up to 1.3 %. Again, it must be assumed that the metallocenes on the surface of the catalyst particle, which produce the first polymer layer around

Table 1. Melting points in dependence on polymerization time and catalyst particle diameter.

| Polymerization time | 10 μ melting point [°C] | 35 μ melting point [°C] | 50 μ melting point [°C] | 80 μ melting point [°C] |
|---------------------|-----------------------------|-----------------------------|-----------------------------|-----------------------------|
| 1 min. | 158,58 | n.d. | n.d. | n.d. |
| 6 min. | 157,70 | 153,69 | 153,10 | 153,33 |
| 13 min. | n.d. | 153,52 | 153,06 | 153,84 |
| 20 min. | 147,85 / 158,81(S) | 153,24 | 152,87 | 153,91 |
| 30 min. | 148,06 / 158,54 (S) | 150,58 | 149,65 | 152,49 |
| 60 min. | 148,47 / 158,81(S) | 148,77 | 148,17 | 152,32 |
| 90 min. | n.d. | 148,64 | 147,95 | 148,30 |

Table 2. Microstructure (isotacticity, defect pentades and meso-2,1-misinsertion) in dependence on polymerization time and catalyst particle diameter.

| Pellet Ø | Polym. time | Isotacticity [%] | mmmr- pentade [%] | mmrr- pentade [%] | mrrm- pentade [%] | meso-2,1- misinsert. [%] |
|-------------|----------------|---------------------|-------------------------|-------------------------|-------------------------|--------------------------------|
| 35µm | 6 min | 97,77 | 0,85 | 0,80 | 0,58 | 0,68 |
| | 30 min | 97,62 | 0,99 | 0,95 | 0,44 | 0,91 |
| | 60 min. | 96,22 | 1,55 | 1,53 | 0,70 | 1,08 |
| 50 µm | 6 min | 96,28 | 1,46 | 1,47 | 0,79 | 0,72 |
| | 30 min | 96,88 | 1,27 | 1,19 | 0,66 | 0,80 |
| | 60 min. | 95,74 | 1,93 | 1,56 | 0,77 | 1,29 |
| 80 µm | 6 min | 95,97 | 1,53 | 1,74 | 0,76 | 0,11 |
| | 30 min | 97,93 | 0,78 | 0,88 | 0,41 | 0,52 |
| | 60 min. | 97,35 | 0,94 | 1,19 | 0,52 | 0,87 |

the pellet, work more regioselectively than the inner active species which are reached by the monomer after a while.

The molecular weights and the molecular weight distributions of the polypropylenes are not influenced by the reaction time, but a strong relation between molecular weight and catalyst particle size can be observed. The molecular weight of the polymers that were obtained with the 80 µm catalyst amounts to 250 000 g/mol whereas the M_w of the macromolecules using the 35 µm catalyst amounts to about 450 000 g/mol. According to this we can perceive that the [MAO]/[Metallocene]-ratio on the surface and inside the pellet plays an important role. A homogeneous MAO-concentration along the whole particle diameter was found for the 10 µm catalyst particle which enables us to assume an optimized ratio of MAO and metallocene at each location of the material. A high MAO concentration on the surface and a small MAO concentration inside the particle was observed for the larger particles which indicates no optimized [MAO]/[metallocene]-ratio. Too much aluminiumalkyl furthers the chain transfer and reduces the molecular weight whereas less amounts of MAO reduces the activity and therefore the molecular weights, too. Accordingly it can be summarized that the homogeneous distribution of MAO and the resulting optimal [MAO]/[metallocene]-ratio on every place of the pellet are responsible for the high molecular weights of the small catalyst particles.

The very slow increase in the MWDs with progressive polymerization time is due to the fragmentation of the catalyst and the access to new active species for the monomer in the course of reaction.

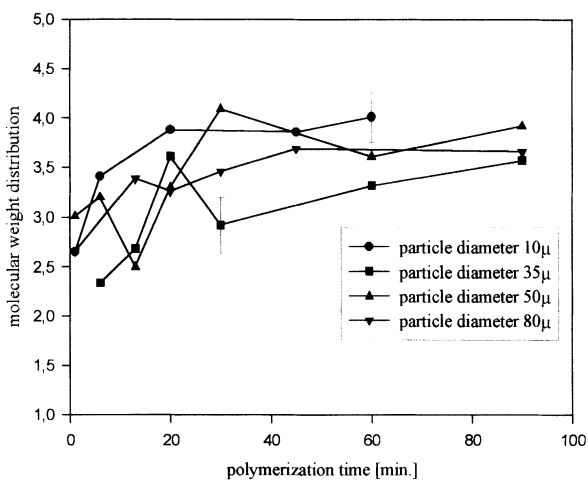
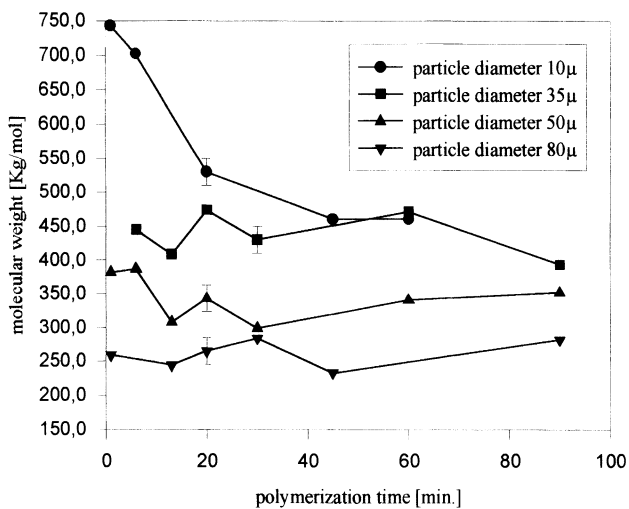


Fig. 6. Molecular weights and molecular weight distributions in dependence on polymerization time and catalyst particle diameter.

4. Conclusion

It was shown that the kinetic of the propene polymerization of the supported catalyst system $\text{SiO}_2/\text{MAO}/\text{rac-Me}_2\text{Si}[\text{IndR}_2]_2\text{ZrCl}_2$ as well as the molecular weights of the reaction products strongly depend on the catalyst particle size. In early polymerization stages a polymer layer is formed around the catalyst pellets which represents a diffusion hindrance for the following monomer. After an 'induction period' during which the monomer diffuses through the polymer envelope to new active species and which also depends on the pellet radius, the catalyst particle is fragmented by hydraulic forces due to the production of polypropylene inside the particle. The polymerization rate increases because of new active centers which are available after fragmentation. The maximum activity of the reaction for the smallest catalyst particle is eight times higher than for the largest system. This fact is due to the inhomogeneous cocatalyst distribution over the particle radius in case of the bigger pellets. The $[\text{MAO}]/[\text{metallocene}]$ -ratio is too high on the surface and too small inside the pellet. This leads to a reduced catalyst activity. The $10\ \mu\text{m}$ catalytic system has a homogeneous MAO distribution as well as an optimum $[\text{MAO}]/[\text{metallocene}]$ -ratio all over the particle. The maximum activity is quite high. Just like the polymerization rate, the molecular weight also depends on the pellet size of the catalyst which is also due to the MAO distribution over the particle.

One final observation made in our studies was the decrease of the melting points as well as the increase of the regioselectivity in relation to an increasing polymerization time. The different chemical environment of the active species on the catalyst surface and the metallocenes inside the pellet are responsible for that.

References :

- [1] M. Aulbach, F. Küber, *CHIUZ* **1994**, 28, 197.
- [2] G.G. Arzoumanidis, N.M. Karayannis, *Chemtech* **1993**, July, 43.
- [3] D.F. Oxley, *Chemistry&Industry* **1998**, 20 April, 305.
- [4] T. Kitagawa, T. Uozumi, K. Soga, T. Takata, *Polymer* **1997**, 38, 615.
- [5] H. Nishida, T. Uozumi, T. Arai, K. Soga, *Macromol. Rapid Commun.* **1995**, 16, 821.
- [6] G. Deganello, D. Duca, L.F. Liotta, A. Martorana, A.M. Venezia, *Gazzetta Chimica Italiana* **1994**, 124, 229.
- [7] K. Soga, M. Kaminaka, *Makromol. Chem.* **1993**, 194, 1745.
- [8] M.C. Sacchi, D. Zucchi, I. Tritto, P. Locatelli, *Macromol. Rapid Commun.* **1995**, 16, 581.
- [9] R. Quijada, R. Rojas, L. Alzamora, J. Retuert, F.M. Rabagliati, *Catalysis Letters* **1997**, 46, 107.
- [10] W. Kaminsky, F. Renner, *Makromol. Chem., Rapid Commun.* **1993**, 14, 239.
- [11] S.I. Woo, Y.S. Ko, T.K. Han, *Macromol. Rapid Commun.* **1995**, 16, 489.

Influence of the particle size of silica support on the kinetics and the resulting polymer properties at the polypropylene polymerization with heterogeneous metallocene catalysts; Part II: development of a model as well as a mathematical simulation

Christian Przybyla, Bruno Weimann, Gerhard Fink*,

Max-Planck-Institut für Kohlenforschung, Kaiser-Wilhelm-Platz 1, D-45470 Mülheim/Ruhr

Abstract. In heterogeneous olefin polymerization, the influence of monomer mass transport in the growing particle and the fragmentation of the support have been comprehensively modeled for conventional Ziegler catalyst but the simulation of the polymerization process of silica supported metallocene catalyst was calculated only by few authors. The expansion and modification of the existing 'particle growth model' for the catalytic system $\text{SiO}_2/\text{MAO}/\text{rac-Me}_2\text{Si}[\text{IndR}_2]_2\text{ZrCl}_2$ of Bonini et al. is presented. Especially the influence of the catalyst particle size on the kinetics and the fragmentation behaviour was modeled. It was observed experimentally that the maximum polymerization rate as well as the polymer properties depend on the average particle size of the catalyst pellet. In our calculations we were able to demonstrate that the propagation rate and the chain transfer rate alter relative to the varying pellet radius due to the different gradients of $[\text{MAO}]/[\text{metallocene}]$ -ratios from the particle surface to the granule center.

1. Introduction

For the mathematical modeling of the polymerization process as well as for the calculation of the molecular weights and the molecular weight distributions there are a few well-known estimations in literature with various basic conceptions:

The most common and simplest type of model is based on a spherical catalyst particle with a spherical shell of polymer growing around it. The monomer diffusion through the polymer shell to the active centers is the main focus of these models. Simulations which are based on such a catalyst geometry are generally called 'solid core models'. Bergley¹ assumed such a model and asserted that

diffusion is not a factor but a gradient across the polymer shell which is calculated analytically.

Schmeal and Street² derived the 'polymeric core model'. In this model the homogeneous dispersion of the catalyst pellet is predicted but the diameter of the catalyst-polymer core remains stable and only the thickness of the polymer shell growth with higher turnover frequencies.

The 'polymeric flow model' takes into consideration the increase of the polymer particle size relative to the polymerization time as well as the drifting apart of the active species. A small increasing of the polymerization rate results from this model³. Copolymerizations were also simulated by the 'polymeric flow model'⁹.

A more complex but more realistic model of the polymerizing particle is the 'multigrain model'. Yermakov et al.⁴ suggested this model conception, but they only simulated the mass transfer resistance and did not carry out the complete model calculations which were done by Ray et al.^{5,6} later on. The experimental observations that the catalyst particle is broken up into many small fragments in early polymerization stages formed the basic idea of the model. An idealization of this physical picture is a macroparticle which consists of many small microparticles. Each microparticle can be regarded as 'solid core' pellet.

All models described were made for conventional Ziegler catalyst and the completely different kinetics of slurry polymerizations of silica supported metallocene catalysts need a modified mathematical calculation. Fink et al.⁷ developed a 'particle growth model' for metallocenes which is based on the 'multigrain model'. Main differences of the 'particle growth'- and the 'multigrain'-model are the moments when the catalyst is completely fragmented. The total fragmentation of the catalyst pellet in the first few seconds of the reaction is predicted for the multigrain model whereas this stage is reached after a long polymerization time in Fink's model. Now, in this paper we try to calculate the influence of catalyst particle size on the kinetics for the 'particle growth model'.

2. Summary of the experimental results

Propene polymerizations were carried out in a toluene slurry by the use of the catalyst system $\text{SiO}_2/\text{MAO}/\text{rac-Me}_2\text{Si}[\text{IndR}_2]_2\text{ZrCl}_2$. As support an amorphous silica of different pellet radius was applied and so it was possible to investigate the influence of the particle diameter of the support on the kinetics as well as on the product qualities.

Detailed results of the studies are given in the preceding paper ('Influence of the particle size of silica support on the kinetics and the resulting polymer properties at the polypropylene polymerization with heterogeneous metallocene catalysts; Part I: experimental studies') but the most important findings were:

The kinetics of the propene polymerization of the supported catalyst system $\text{SiO}_2/\text{MAO}/\text{rac-Me}_2\text{Si}[\text{IndR}_2]_2\text{ZrCl}_2$ as well as the molecular weights of the reaction products strongly depend on the catalyst particle size. SEM-images and microtome sections proved that in early polymerization stages a polymer layer is

formed around the catalyst pellets. After an 'induction period' which symbolizes the space of time for the monomer diffusion through the polymer envelope to new active species and which also depends on the pellet radius, the catalyst particle is fragmented by hydraulic forces due to the production of polypropylene inside the particle. Then the polymerization rate increases because of new active centers which are available after fragmentation.

The maximum activity of the reaction for the smallest catalyst particle is eight times higher than for the largest system. This fact is due to the more inhomogeneous cocatalyst distribution over the particle radius in case of the bigger pellets.

One final observation in our studies was the decreasing of the melting temperature as well as the increasing of the regioselectivity in relation to increasing polymerization time. The different chemical environment of the active species on the catalyst surface and the metallocenes inside the pellet is responsible for that.

A schematic conception of the catalyst fragmentation is shown in Fig. 1. The main points are the development of a polymer envelope around the particle as well as the slow fragmentation of the granule from the surface to the center due to growing polymer.

3. The model for the catalyst system $\text{SiO}_2/\text{MAO}/\text{rac-Me}_2\text{Si}[\text{IndR}_2]_2\text{ZrCl}_2$

For the development of a model of the kinetics and of the polymer properties it is necessary to formulate a kinetic scheme which represents a sufficient description of the reaction (Tab. 1). This scheme is very similar to the suggestions made by Fink et al.⁷ but it is much more simplified relative to the conceptions of Hutchinson⁸.

We consider that each metallocene on the support is active when it enters the reactor. The first modification of Fink's particle growth model is made by the role of triisobutylaluminium (TIBA). In Fink's model the alkyle neither has the scavenger function only nor the cocatalyst function only but more than that it works as transformation agent for the active species. For that reason each reaction step (propagation, transfer, reactivation and deactivation) receives two rate constants. We assume only one rate constant for the methylalumoxane (MAO) cocatalyzed as well as for the TIBA transformed reaction.

The kinetic scheme of the modified 'particle growth model' additionally includes one more transfer reaction. In contrast to Fink's proposal, our scheme takes into consideration the chain-transfer to the alkyle.

The following reaction steps and resulting products are involved in the renewed model: The activation and transformation of the metallocenes on the support by aluminiumalkyles lead to active species. The propagation reaction is the main aspect of polymerization reactions. Two transfer reactions (transfer to the aluminiumalkyle and β -H-transfer) result in dead polymer chains and vacant active sites. The reactivation of these vacant sites leads again to a growing polymer chain. And finally we have taken into account the possibility of a second order deactivation reaction as reported by Fink et al. as well as by other authors¹⁰.

Table 1. Kinetic Scheme for Catalyzed Propene Polymerization with Supported Metallocenes.

| | | |
|-----------------------|---|--|
| Activation : | $Zr + MAO \rightarrow P_0^1$ | k_i |
| Transformation : | $P_i^1 + TIBA \rightarrow P_i^2$ | $k_a \quad i = 0, \dots, \infty$ |
| Propagation : | $P_i^1 + M \rightarrow P_{i+1}^1$ | $k_p \quad i = 0, \dots, \infty$ |
| | $P_i^2 + M \rightarrow P_{i+1}^2$ | |
| Chain Transfer to Al: | $P_i^1 + Al \rightarrow PH^1 + D_i^1$ | $k_{tr}^{Alk.} \quad i = 0, \dots, \infty$ |
| | $P_i^2 + Al \rightarrow PH^2 + D_i^2$ | |
| β -H-Transfer : | $P_i^1 \rightarrow PH^1 + D_i^1$ | $k_t^{\beta-H} \quad i = 0, \dots, \infty$ |
| | $P_i^2 \rightarrow PH^2 + D_i^2$ | |
| Reactivation : | $PH^1 + M \rightarrow P_1^1$ | k_r |
| | $PH^2 + M \rightarrow P_1^2$ | |
| Deactivation : | $P_i^1 + P_j^1 \rightarrow 2 C_d + D_i^1 + D_j^1$ | $k_d \quad i = 0, \dots, \infty$ $j = 0, \dots, \infty$ |
| | $P_i^2 + P_j^2 \rightarrow 2 C_d + D_i^2 + D_j^2$ | |

| | | |
|-----------------|---|--|
| Zr | = | metallocene that is not yet activated |
| MAO/TIBA | = | Methylalumoxane or Tri- <i>i</i> -Butylaluminium |
| P_i | = | living polymer chain containing <i>i</i> monomer units |
| M | = | monomer |
| PH | = | vacant active species resulting from chain transfer |
| D_i | = | dead polymer chain containing <i>i</i> monomer units |
| C_d | = | deactivated metallocene |
| k_i | = | activation rate constant |
| k_a | = | transformation rate constant |
| k_p | = | propagation rate constant |
| $k_t^{\beta-H}$ | = | rate constant for β -H-transfer |
| $k_{tr}^{Alk.}$ | = | rate constant for transfer to aluminium alkyl |
| k_r | = | reactivation rate constant |
| k_d | = | deactivation rate constant |

Beside the kinetic measurements and the kinetic scheme, the SEM-images, the microtome sections as well as the BET-measurements are the basis of the modified model. The experimental results exemplifies that the polymerization behaviour of the system $SiO_2/MAO/rac-Me_2Si[IndR_2]_2ZrCl_2$ is not in agreement with the 'multigrain model' and its complete fragmentation of the catalyst granule in the first polymerization steps. We assume the development of a polymer envelope around the particle in the early reaction moments and after that a slow fragmentation of the supporting material step by step from the surface up to the center due to the hydraulic forces of the polymer which penetrates into the support (Fig. 1).

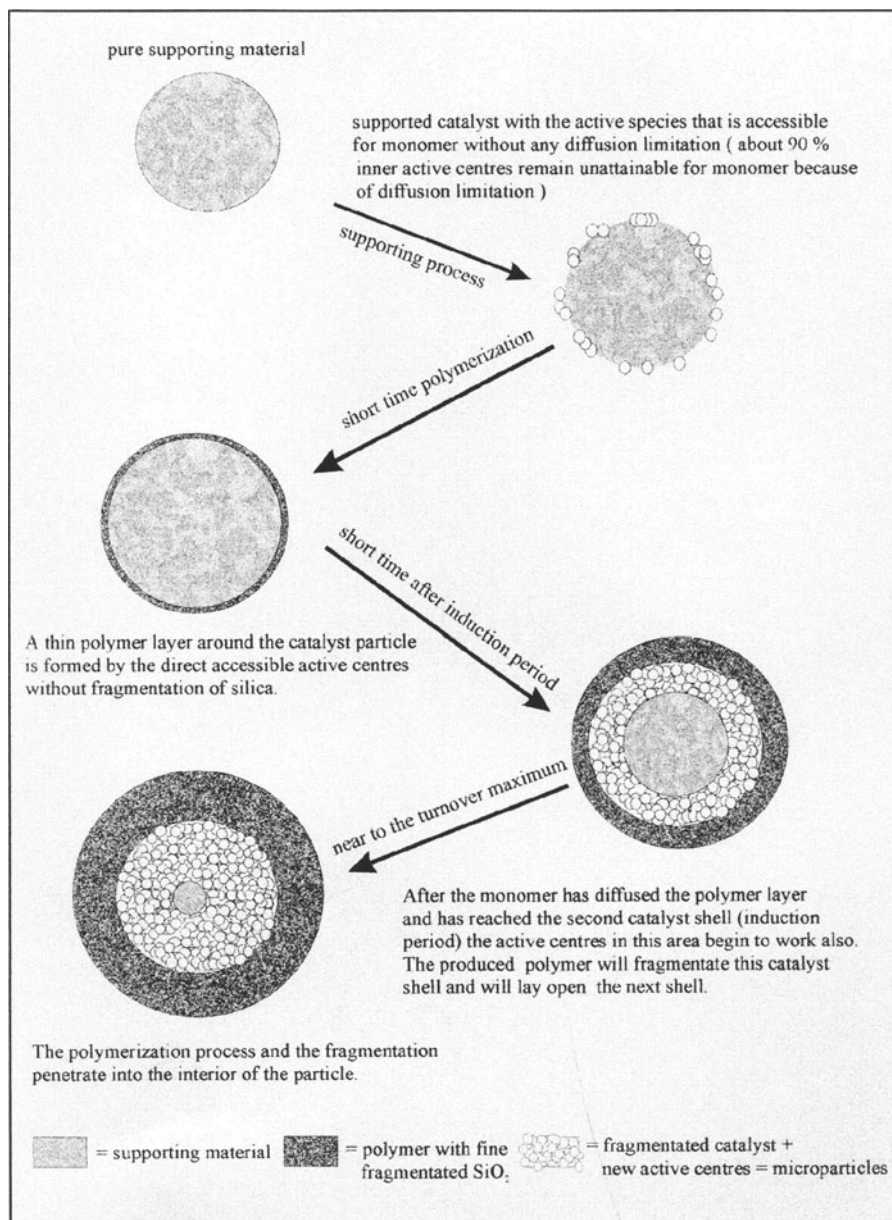


Fig. 1. Schematic lapse of the propene polymerization with the catalyst system $\text{SiO}_2/\text{MAO}/\text{rac-Me}_2\text{Si}[\text{IndR}_2]_2\text{ZrCl}_2$.

4. Mathematical modeling

From SEM images and BET-measurements we know the shape and the characteristics of the supporting material very well. It is a porous and spherical granule that is divided into a lot of shells for mathematical modeling. Exclusively the external layer is accessible to the monomer in the beginning of the reaction. The inner shells are not available for polymerization because of diffusion limitation of the monomer. The monomer concentration in all other shells out of the surface amounts to zero. When the monomer has diffused through the polymer layer on the surface and has reached the second shell, the arising polymer will break off this second shell. Now the first and the second shell have to be considered mathematically. Now, the monomer penetrates successively into the following shells up to the center and in like manner the catalyst shells fragments because of the growing polymer. When the whole silica particle is completely fragmented by polymer and all active centers are accessible for monomer, the equations describing our model are the same as for the 'multigrain model'. The full mass and the energy balances are shown in Tab. 2.

The system formed by these equations cannot be solved analytically; a numerical solution is carried out considering the macroparticle divided in N concentric shells where macroparticle full mass and energy balances can be rewritten using a centered finite difference method. The discretization leads to a set of ordinary differential equations for macroparticle monomer concentrations, one for each grid point in space. The complete set of discretized macroparticle mass balances and corresponding sets of microparticle mass balances and moment equations are sent to a differential-algebraic system equation solver.

The solution of microparticle full mass balances can be carried out analytically taking the possibility of quasi steady state assumption into account, since at this level the reaction is not diffusion-limited. Then we can compute temperature and monomer concentration values in the macroparticle at any time for everything among the N grid points determined, integrating the obtained equation over a very small interval of time. In this interval we consider as constant the geometric characteristics of particle and the rate of monomer consumption is evaluated as follows:

$$R_v = \frac{1 - \varepsilon}{\varphi^3(i)} \cdot R_p$$

$$R_p = -[C^*] \left(\frac{d[M]_c}{dt} \right) = [C^*] [M]_c \sum_{j=1}^2 k_p^j [P^j] + k_r^j [PH^j]$$

R_v = polymerization rate per macroparticle shell unity

R_p = total polymerization rate

ε = macroparticle void fraction

$\varphi(i)$ = microparticle growth factor

$[C^*]$ = concentration of active species in the support

$[M]_c$ = monomer concentration on the particle surface

$[P^j]$ = living polymer chain concentration produced by the j^{th} active site

$[PH^j]$ = concentr. of vacant metallocene species produced by the j^{th} active site

Table 2. Full mass and energy balances of the „Particle growth model“.

Macroparticle ($0 \leq r_1 \leq R_1$)

$$\varepsilon \cdot \frac{\partial [M]_l}{\partial t} = \frac{1}{r_1^2} \cdot \frac{\partial}{\partial r_1} (D_l \cdot r_1^2 \cdot \frac{\partial [M]_l}{\partial r_1}) - R_v \quad \text{Mass Balance}$$

$$\frac{\partial T_1}{\partial t} = \frac{1}{r_1^2} \cdot \frac{\partial}{\partial r_1} \left(\left(\frac{k_e}{\rho_{pol} C_p} \right) \cdot r_1^2 \cdot \frac{\partial T_1}{\partial r_1} \right) + \frac{(-\Delta H_p)}{\rho_{pol} C_p} \cdot R_v \quad \text{Energy Balance}$$

Boundary Conditions

$$r_1 = 0 \Rightarrow \frac{\partial [M]_l}{\partial r_1} = 0 \quad r_1 = R_1 \Rightarrow D_l \cdot \frac{\partial [M]_l}{\partial r_1} = k_s \cdot ([M]_b - [M]_l)$$

$$\frac{\partial T_1}{\partial r_1} = 0 \quad k_e \cdot \frac{\partial T_1}{\partial r_1} = h \cdot (T_b - T_1)$$

Initial Conditions

$$t = 0 \Rightarrow [M]_l = [M]_l^0, \quad T_1 = T_1^0, \quad R_1 = R_{cat}$$

Microparticle ($R_c \leq r_s \leq R_s$)

$$\alpha_v \cdot \frac{\partial [M]_s}{\partial t} = \frac{1}{r_s^2} \cdot \frac{\partial}{\partial r_s} (D_s \cdot r_s^2 \cdot \frac{\partial [M]_s}{\partial r_s}) \quad \text{Mass Balance}$$

$$\frac{\partial T_s}{\partial t} = \frac{1}{r_s^2} \cdot \frac{\partial}{\partial r_s} \left(\left(\frac{k_e}{\rho_{pol} C_p} \right) \cdot r_s^2 \cdot \frac{\partial T_s}{\partial r_s} \right) \quad \text{Energy Balance}$$

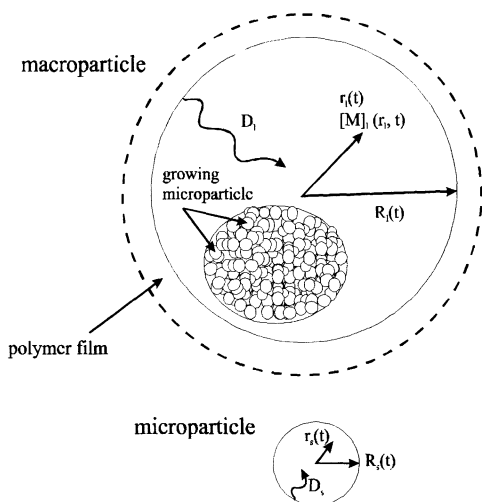
Boundary Conditions

$$r_s = R_s \Rightarrow [M]_s = \eta \cdot [M]_l \quad r_s = R_c \Rightarrow 4\pi R_c^2 D_s \cdot \frac{\partial [M]_s}{\partial r_s} = \left(\frac{4\pi}{3} \cdot R_c^3 \right) \cdot R_p$$

$$T_s = T_1 \quad -4\pi R_c^2 k_e \cdot \frac{\partial T_s}{\partial r_s} = \left(\frac{4\pi}{3} \cdot R_c^3 \right) \cdot (-\Delta H_p) \cdot R_p$$

Initial Conditions

$$t = 0 \Rightarrow [M]_s = [M]_s^0, \quad T_s = T_s^0, \quad R_s = R_c$$



| | |
|-----------------|---|
| C_p | specific heat (cal/g K) |
| $D_l; D_s$ | monomer diffusion coefficient into the macro- and microparticle (cm^2/s) |
| h | heat transfer coeff. in the external film surrounding the particle ($\text{cal}/\text{cm}^2\text{s K}$) |
| ΔH_p | heat of polymerization reaction (cal/mol) |
| k_e | heat transfer coefficient (cal/cm s K) |
| k_s | mass transfer coefficient in the external film (cm/s) |
| $[M]_b$ | monomer concentration in solution (mol/cm^3) |
| $[M]_l; [M]_s$ | monomer concentration in macro- and microparticle (mol/cm^3) |
| $[M]_s$ | monomer concentration on the microparticle surface (mol/cm^3) |
| $r_l; r_s$ | variable along the macro- and microparticle radius (cm) |
| R_c | initial microparticle radius (cm) |
| R_{cat} | radius of the virgin catalyst particle (cm) |
| $R_l; R_s$ | macroparticle radius ; microparticle radius (cm) |
| R_v | polymerization rate per macroparticle shell unity ($\text{mol}/\text{cm}^3\text{s}$) |
| t | polymerization time (s) |
| T_b | reaction temperature (K) |
| T_l bzw T_s | temperature in macroparticle (K) and temperature in microparticle (K) |
| α_v | amorphous phase fraction in polymer |
| ρ | polymer density (g/cm^3) |
| ω_{Zr} | weight percent zirconium on the support |
| $r_{ext.}$ | thickness of the external catalyst shell |
| η | sorption factor |

The microparticle growth factor $\phi(i)$, which means the ratio of the actual microparticle radius and the radius of the catalyst fragment, is the most important factor for the breaking off of the shell and for the monomer access to the inner active species. It was fixed that the external shell fragments if the microparticle

growth factor $\varphi(i)^{\text{ext}}$ becomes higher than the critical value $\varphi(i)^{\text{ext}}_{\text{crit}}$. The inner shells will fragment, if their microparticle growth factor $\varphi(i)$ reaches the critical value $\varphi(i)_{\text{crit}}$. In this way the slow fragmentation process which was observed experimentally can be simulated mathematically, whereas only differential equations for shells filled with monomer are calculated.

5. Calculation of polymer properties

The calculation of polymer properties was carried out similar to the method applied by Fink⁷ and Hutchinson⁸. First of all it was necessary to determine the balance on living (growing) polymer chains as well as the balance on dead polymer chains. The l^{th} moment of live polymer in the i^{th} shell is given by a weighted sum of polymer concentrations of :

$$\lambda_l^k(i) \equiv \sum_{n=1}^{\infty} n_l P_n^k(i)$$

Also the l^{th} moment of dead polymer is defined as :

$$\Lambda_l^k(i) \equiv \sum_{n=1}^{\infty} n_l D_n^k(i)$$

λ_l^k = growing polymer chains in the l^{th} moment at active site of type k .

Λ_l^k = dead polymer chains in the l^{th} moment produced by active site of type k .

P_n^k = growing polymer chain of length n produced at active site type k .

D_n^k = dead polymer chain of length n produced at active site type k .

The evaluation of the molecular weights and the molecular weight distribution is performed by calculating its leading moments, both for living and dead polymer. In this case we solve for any grid point the equations of moments of zero, first and second order for living and dead chain produced by any active center. The value of the molecular weight (number average as well as weight average) results in the ratio of the sums of living and dead polymer distributions of different order moments:

$$M_n = \frac{\lambda_1^k + \Lambda_1^k}{\lambda_0^k + \Lambda_0^k} M_{\text{mon}}$$

$$M_w = \frac{\lambda_2^k + \Lambda_2^k}{\lambda_1^k + \Lambda_1^k} M_{\text{mon}}$$

The polydispersity index amounts to :

$$P_d = \frac{M_w}{M_n}$$

6. Comparison of experimental and calculated data

For the simulation of the propene polymerization process by the aid of 'particle growth' model it is necessary to fix some physical and chemical parameters. Tab. 3 represents several parameters used. Most values were taken from literature or they were adjusted to literature parameters as for example the heat of polymerization reaction as well as the polymer density or the diffusion coefficients. Other parameters were determined by SEM images and microtome sections as for example the catalyst fragment radius. The resulting kinetic constants are obtained by a fitting process of the experimental and calculated data.

Table 3. Simulation parameters for propylene polymerization with SiO₂/MAO/rac-Me₂Si-[IndR₂]₂ZrCl₂ system in toluene.

| <u>Polym.</u> <u>Conditions</u> | ∅ | ∅ | ∅ | <u>Catalyst</u> <u>parameters</u> | ∅ | ∅ | ∅ |
|--|----------------------|----------------------|----------------------|---------------------------------------|--------------------|--------------------|--------------------|
| | pellet 10 μm | pellet 50 μm | pellet 80 μm | | pellet 10 μm | pellet 50 μm | pellet 80 μm |
| p [atm] | 2 | 2 | 2 | ε ₀ ^{lit.8} | 0.25 | 0.25 | 0.25 |
| T [K] | 313 | 313 | 313 | ρ _{cat} | 2.25 | 2.25 | 2.25 |
| | | | | R _c [cm] | 1•10 ⁻⁶ | 1•10 ⁻⁶ | 1•10 ⁻⁶ |
| | | | | ω _{Zr} [w.-%] | 0.0011 | 0.0011 | 0.0011 |
| | | | | MW [g/mol] | 628.83 | 628.83 | 628.83 |
| <u>Physical</u> <u>Param.</u> | | | | <u>Polymer parameters</u> | | | |
| φ _{crit} ^{lit.7} | 1.5 | 1.5 | 1.5 | ρ _{pol} [g/cm ³] | 0.950 | 0.950 | 0.950 |
| φ _{crit} ^{ext lit.7} | 2.15 | 2.15 | 2.15 | α _v ^{lit.8} | 0.4 | 0.4 | 0.4 |
| r _{ext} [cm] | 2.0•10 ⁻⁴ | 2.0•10 ⁻⁴ | 2.0•10 ⁻⁴ | C _p | 0.48 | 0.48 | 0.48 |
| N _{Shell} | 15 | 25 | 40 | [cal/g K] ^{lit.11} | | | |
| D _{macro} | 9•10 ⁻⁷ | 9•10 ⁻⁷ | 9•10 ⁻⁷ | -ΔH _p | 25.50 | 25.50 | 25.50 |
| [cm ² /s] ^{lit.5,12} | | | | [kcal/mol] ^{lit.11} | | | |
| D _{micro} | 10 ⁻⁸ | 10 ⁻⁸ | 10 ⁻⁸ | | | | |
| [cm ² /s] ^{lit.5,12} | | | | | | | |

Resulting kinetic constants

| | | | |
|--|----------------------|----------------------|----------------------|
| k _a [cm ³ /mol s] | 1 | 1 | 1 |
| k _p [cm ³ /mol s] | 3.5•10 ⁵ | 2.4•10 ⁵ | 1.9•10 ⁵ |
| k _t ^{β-H} [s ⁻¹] | 1.9•10 ⁻² | 2.2•10 ⁻² | 2.2•10 ⁻² |
| k _{tr} ^{Alk} [cm ³ /mols] | 9.0•10 ³ | 9.0•10 ³ | 9.0•10 ³ |
| k _r [cm ³ /mol s] | 4•10 ¹ | 4•10 ¹ | 4•10 ¹ |
| k _d [cm ³ /mol s] | 0.5 | 0.5 | 0.5 |

The changing values of the propagation rate constant and β -H-transfer rate constant relative to the particle size are due to the different $[\text{MAO}]/[\text{Metallocene}]$ -gradients in the pellets with different diameters. The homogeneous distribution of MAO and active species ($10\ \mu\text{m}$ catalyst) leads to high propagation constants whereas enrichments of cocatalyst on the surface as well as absence of MAO in the

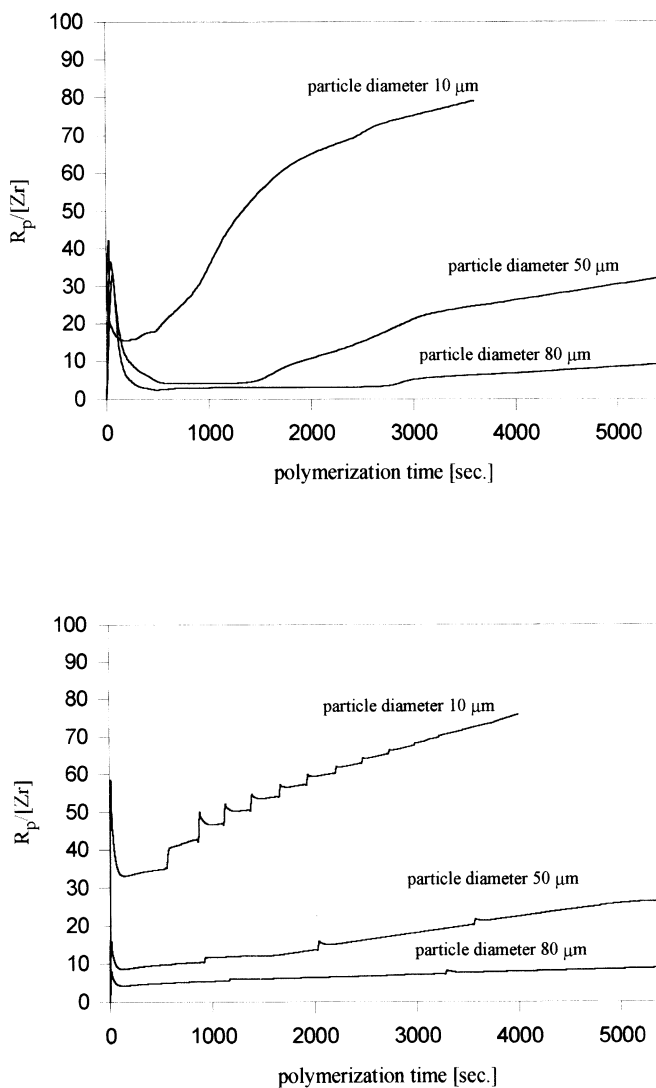


Fig. 2. Experimental (above) and simulated (below) polymerization rate in dependence on polymerization time and catalyst particle diameter.

center of the granule (80 μm catalyst) leads to a decreasing of the propagation constant. Fig. 2 shows the propene polymerization rate of the catalyst system $\text{SiO}_2/\text{MAO}/\text{rac-Me}_2\text{Si}[\text{IndR}_2]_2\text{ZrCl}_2$ received experimentally (above) and by calculation (below). It is obvious that the curves resulted by experiments correspond with the simulated curves in every detail. The prepolymerization peak appears in the calculation as well as the induction period which depends on the pellet radius in the evaluation also. The different final activities of the various dimensioned catalyst exist, both in the experimental and the calculated polymerization diagram. Finally we can sum up that the shape of polymerization rate is well-described by the model and furthermore the trends in the change of particle radius are in good agreement with the experiment. Also the computed molecular weights and the estimated molecular weight distributions correspond very well with the experimental dispersities and chain lengths (Tab. 4). Only the calculated dispersities are smaller than the determined ones. This could be based on the weak consideration of temperature gradient inside the pellet. The decreasing molecular weight relative to the growing catalyst particle radius that was observed in experiment can be found also in simulation.

Table 4. Calculated and experimentally determined molecular weights as well as MWD's in dependence on catalyst particle diameter.

| Particle diameter | $M_w^{\text{exp.}}$ [g/mol] | $M_w^{\text{calc.}}$ [g/mol] | Pd^{exp} | Pd^{calc} |
|-------------------|-----------------------------|------------------------------|--------------------------|---------------------------|
| 10 μm | 580 000 | 633 100 | 3.55 | 2.22 |
| 50 μm | 344 000 | 384 000 | 3.37 | 2.30 |
| 80 μm | 262 000 | 310 900 | 3.30 | 2.32 |

Fig. 3 represents the results of calculation of the monomer diffusion into the catalyst granule in dependence on polymerization time for the pellet size of 10 μm , 50 μm and 80 μm . One important fact which explains the different kinetic behaviours of the various dimensioned pellets can be seen there. The monomer has penetrated into the smallest particle (10 μm diameter) up to the center after 3000 seconds. In the case of the largest particle (80 μm diameter) the diffusion process needs much longer time. After 4000 seconds only 50% of the catalyst are penetrated by monomer. That means all active species are reached by monomer after 4000 seconds in case of the smallest pellet but only 50% of the active species are available for monomer in the same space of time by use of the larger pellets. The microparticle growth factor ϕ (ratio of the actual microparticle radius and the initial microparticle radius) for all three catalyst sizes show different time dependences (Fig. 3). The condition for catalyst shell fragmentation was $\phi > 1.5$ (the external shell $\phi > 2.15$).

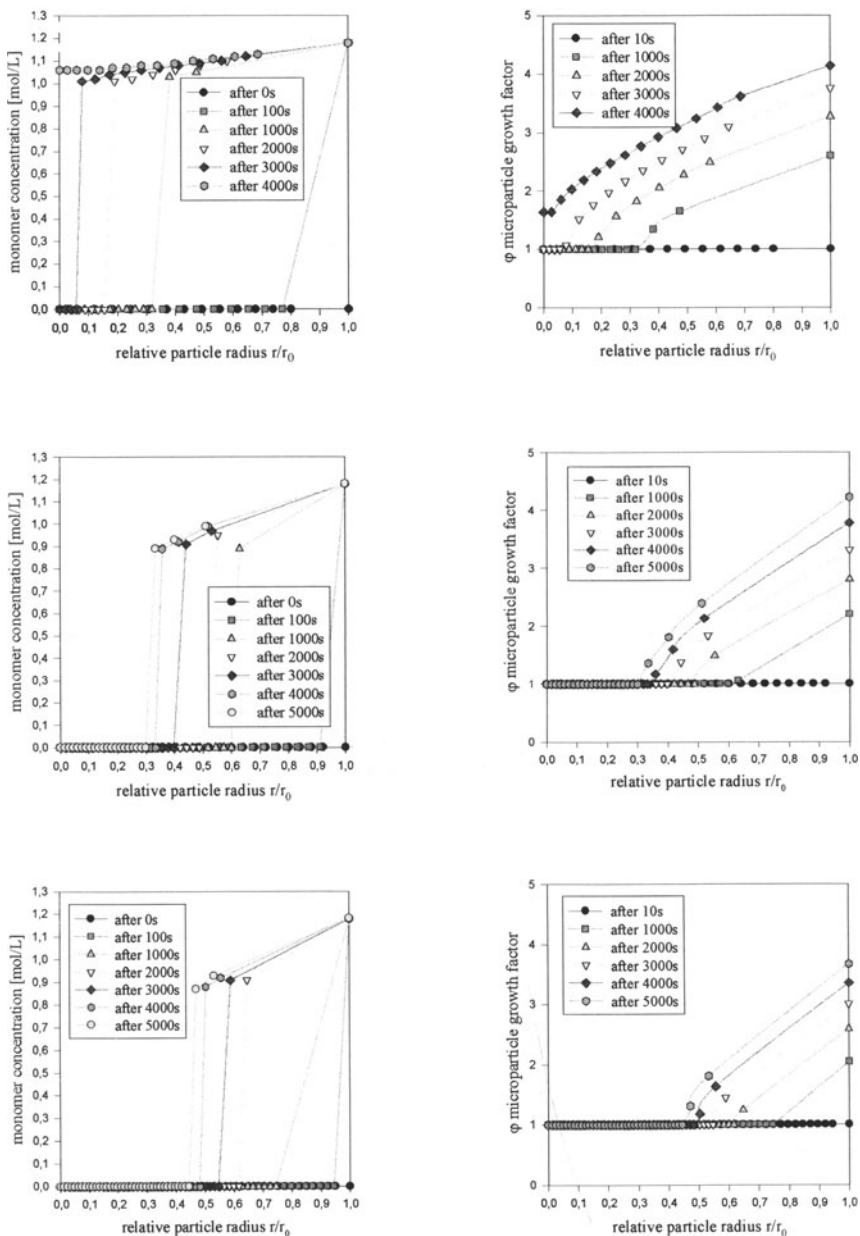


Fig. 3. Monomer concentration und microparticle growth factor in dependence on relative particle radius for the catalyst particles with different diameters (top 10 μm , center 50 μm , bottom 80 μm)

For the 10 μm catalyst granule the growth factor ϕ is larger than 1.5 in each place of the pellet after 4000 seconds which means that a complete fragmentation of the particle took place. In contrast to that after 4000 seconds the huge 80 μm pellet has a ϕ -value larger than 1.5 only for relative particle radius larger than 0.55. Less than half of the catalyst particle is fragmented at that moment.

From all the above we can conclude that the particle growth process is represented very close to reality by our model. The diffusion problems by use of heterogeneous metallocene catalysts in comparison to homogeneous catalysts play the most important role for the kinetics as well as for the polymer properties. Further catalyst systems (as for example systems based on other metallocene structures and other types of silica) are going to be calculated with this model estimation.

References :

- [1] J. Begley, *J. Polym. Sci., Polym. Chem. Ed.* 1966, 4, 319.
- [2] W.R. Schmeal, J.R. Street, *AIChE J.* 1971, 17, 1188.
- [3] L.L. Böhm, *Chem. Ing. Techn.* 1984, 56, 674.
- [4] Yu.I. Yermakov, V.G. Mikhalchenko, V.S. Breskov, Yu.P. Grabowskii, I.V. Emirova, *Plast. Massy* 1970, 9, 7.
- [5] S. Floyd, K.Y. Choi, T.W. Taylor, W.H. Ray, *J. Appl. Poly. Sci.* 1986, 32, 2935.
- [6] S. Floyd, T. Heiskanen, T.W. Taylor, G.E. Mann, W.H. Ray, *J. Appl. Poly. Sci.* 1987, 33, 1021.
- [7] F. Bonini, V. Fraaije, G. Fink, *J. Polym. Sci. A, Polym. Chem.* 1995, 33, 2393.
- [8] R.A. Hutchinson, C.M. Chen, W.H. Ray, *J. Appl. Poly. Sci.* 1992, 44, 1389.
- [9] E.L. Hoel, C. Cozewith, G.D. Byrne, *AIChE Journal* 1994, 40 (10), 1669.
- [10] J.C.W. Chien, B.P. Wang, *J. Polym. Sci. Part A: Polym. Chem.* 1988, 26, 3089.
- [11] F. Bonini, G. Storti, M. Morbidelli, S. Carra, *Gazetta Chimica Italiana* 1996, 126, 75.
- [12] S. Floyd, K.Y. Choi, T.W. Taylor, W.H. Ray, *J. Appl. Poly. Sci.* 1986, 31, 2231.

Supported metallocene catalysts in olefin polymerization: toward high performances

R. Spitz, N. Verdel, V. Pasquet, J. Dupuy, J.P. Broyer and T. Saudemont^{a)}

e-mail: spitz@lcpp.cpe.fr

LCPP CNRS/CPE BP 2077 69616 Villeurbanne Cedex France

a) GRL-Elf-Atochem BP34 64170 Lacq France

Abstract

In order to get a supported metallocene type catalyst, different methods have been used to link the group IV metal to the surface. The simplest procedure starts with a metal chloride (titanium or zirconium tetrachloride) supported on magnesium chloride or silica. This solid precursors are modified by a chemical treatment in order to replace in one step one of the chlorines by a cyclopentadienyl or a modified cyclopentadienyl ligand. The results are very different when titanium or zirconium are considered: the titanium catalyst is not different from a conventional Ziegler-Natta catalyst. On the contrary, the zirconium catalyst is similar to a metallocene system, producing polyethylene homo and copolymers with narrow molecular weight distribution which can not be fractionated by solvents. Another approach consists of the metal to the surface using a silicium bridging 2 indenyl ligands. In both cases the zirconium catalysts seem to be very close to the definition of a single site system. High activities have been observed in ethylene polymerization but in it was never possible to produce any isotactic polypropylene.

Introduction

Most of the industrial processes for olefin polymerization have been adapted for the use of solid catalysts, thus avoiding to add any solvent. The homogeneous metallocene systems are in principle not suited for heterogeneous polymerization and have been used first in solution processes. Solid systems are prepared by different methods [1] which can be summarized as follows: methylaluminumoxane (MAO) deposited or built on a support [2-6], preformed metallocenes complexes [7-11] interacted with a support, complete preparation of a complex on a support [12-14]. We will present results corresponding to the third method. If the

catalysts are derived from precursors which are similar to conventional systems they may in principle fulfill most of the requirement of heterogeneous processes. Similar approaches have already been described in the literature and we intend to present results obtained in pressure/temperature/activity/process conditions corresponding to industrial processes. The choice of catalysts will be restricted to systems where the active center is directly linked by a permanent link to the surface. We try to get catalysts with high activities, at least not less active than conventional supported systems and showing single site properties.

Modified conventional Ziegler-Natta catalyst

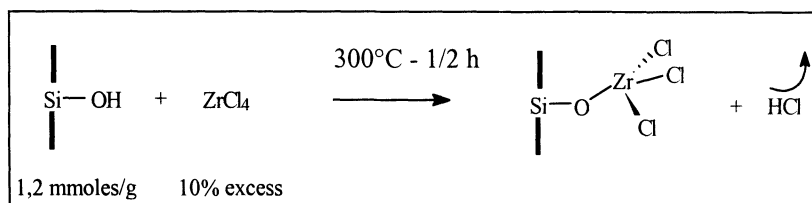
A very simple method to produce metallocene catalysts makes use of modifications of conventional Ziegler-Natta systems. The Ziegler-Natta catalysts are based on titanium chlorides and bear labile chlorine on their surface. It is in principle very simple to use any of the well known pathways which allow to substitute such a chlorine by a Cp or a modified Cp group. Sodium, lithium magnesium or any other Cp salt are often used in that way, performing substitution and producing a metal chloride as a by product. We have adapted this method in order to avoid to destroy the properties of the solid. We start with a catalyst supported on magnesium chloride. Such catalysts are very sensitive to solvents having Lewis base properties. These solvents may complex on the surface but also swell or dissolve the support as for example in the case of tetrahydrofuran which was used in our recipe. The Cp salts are generally used in solution in basic solvents. In order to keep the properties of the solid, we have preferred to perform the Cp substitution using a poor solvent, toluene. Of course the instantaneous concentration of the reagent is low in toluene but it does not forbid the substitution, as the continuous dissolution compensates the consumption of the soluble reagent. Details have been already published [15]. In this special case it appears that the activity of the modified catalyst, if any, is far below the conventional activity of the system. The catalyst, activated by common aluminum trialkyls is much more active than the starting catalyst and has none of the properties which are assumed to be characteristic of metallocenes type compound, even when activated by methylaluminoxane. It excludes in that case that an titanium metallocene catalyst has been leached from the surface when MAO is used as cocatalyst.

Supported zirconium based catalyst

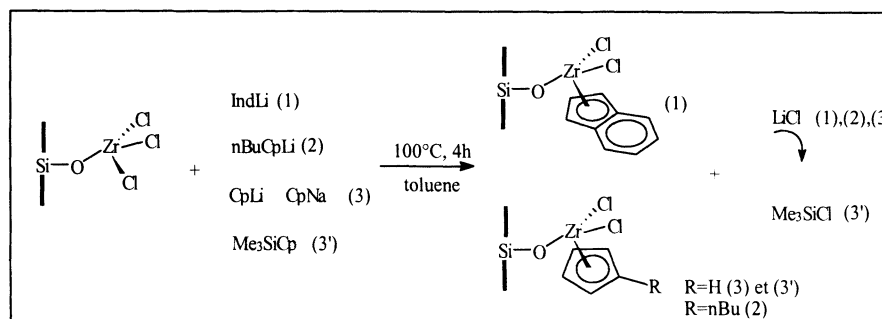
In a second step we tried to examine the opposite situation: start with a low activity conventional catalyst and convert it to a high activity system. Zirconium is much better suited for that purpose as it is difficult to get very high activities with conventional zirconium systems. Zr metallocene are known to be sometimes very

active. As there is no general recipe for a zirconium supported system, we have used a very simple preparation method. Zirconium tetrachloride is sublimated and reacted with the silanol groups on a silica surface. Details are given in the experimental part. The elemental analysis confirms that a part of the chlorines are eliminated, so that the reaction occurs as expected. Engaged in polymerization with trialkylaluminium compounds or MAO, a similar level of activity is observed, which remains below 2 Kg/g/h at pressures up to 16 bars and remains in the range of a few 100 g/g/h at 4 bars pressure. An interesting point is that the catalyst produces a very high molecular weight polymer. The solution viscosities (145 °C in trichlorobenzene) correspond to a molecular weight always above 500 000 g/mol in all polymerization conditions. This means that the possible contribution of these active centers will be easily identified by the presence of a very high molecular weight fraction in size exclusion chromatography.

The next step is the functionalization by a Cp compound. The step is also followed by elemental analysis, showing that the Cl- Cp' (Cp' holds for all the different substituted Cp used) exchange occurs. All the steps are summarized in the scheme 1 and 2.



Scheme 1. Zirconium chloride functionalisation of a silica surface



Scheme 2. Conversion to a half-metallocene system

The catalysts are named according to the following code: S holds for silica supported, Z for zirconium Cp for cyclopentadienyl, BuCp for n-butyl cyclopentadienyl, Ind for indenyl.

| Catalyst | %Zr ^{a)} | %Cl | %C | Cl/Zr* | C/Zr |
|----------|-------------------|------|------|--------|------|
| SZInd | 8,2 | 6,4 | 8,65 | 2 | 8 |
| SZCp | 8,6 | 6,7 | 5,65 | 2 | 5 |
| SZnBuCp | 8,15 | 6,35 | 9,70 | 2 | 9 |

a) with 1.2 mmol OH per g

* assuming no Cl remains from the Li or Na

Table 1. Expected elemental analysis of the solid component

| Catalyst | ligand | %Zr | %Cl | %C | Cl/Zr | C/Zr |
|----------|----------------------|------|------|-------|-------|-------|
| SZCpLi | CpLi | 8,40 | 8,06 | 5,19 | 2,47 | 4,70 |
| SZCpNa | CpNa | 8,95 | 7,32 | 5,07 | 2,10 | 4,30 |
| SZCp | Me ₃ SiCp | 8,80 | 8,15 | 7,18 | 2,38 | 6,20 |
| SZInd | IndLi | 8,50 | 9,20 | 6,30 | 2,78 | 5,63 |
| SZnBuCp | nBuCpLi | 7,50 | 8,56 | 10,65 | 2,93 | 10,79 |

Table 2. Observed composition of the catalyst

It is clear from the table 1 and 2 that we find more chlorine and less carbon than expected. It seems nevertheless that the active zirconium sites have been modified as it was no more possible to detect their activity. It appeared that even using a ratio Cp'/Zr above 1, it was not possible to exchange more than 1 Cl per Zr. In most cases, the exchanged chlorines remain on the surface of silica as a salt, but the use of a Cp'SiMe₃ compound produces ClSiMe₃ which is easily washed from the surface. Nevertheless, we did not observe clear differences in polymerization activity when the chlorine salt residue is present or absent. In all case, the Cp' modified catalyst, which can be considered as half metallocenes and bear 2 electron rich ligands, has lost its activity in the presence of a trialkylaluminium compound but polymerizes ethylene in the presence of MAO. In some cases, especially in copolymerization, very high activities are observed. The activity and the productivity of the catalysts are increased in the presence of an α -olefin. Examples of kinetics are presented on fig. 1. Activation effects are summarized on fig. 2.

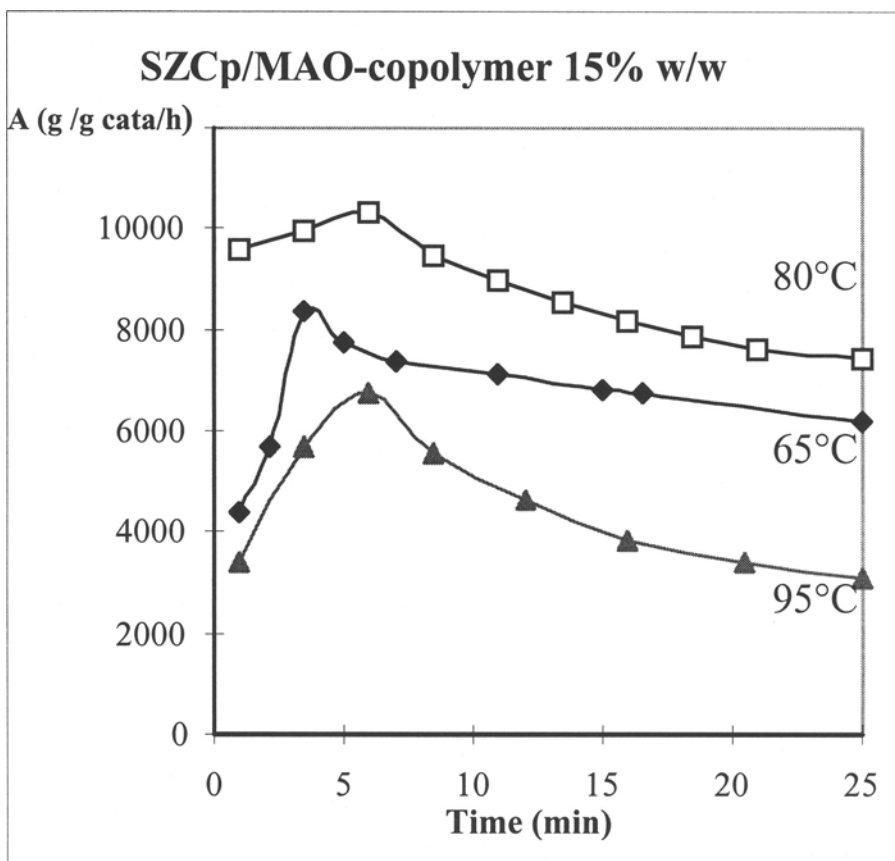


Fig. 1. Kinetic curves observed in ethylene hexene-1 copolymerization using a silica supported zirconium chloride catalyst modified by CpSiMe₃. Heptane suspension (65, 80 °C) or solution (95 °C), catalyst: 5 mg, cocatalyst: MAO 10 mMol.

The kinetic curves reported on fig. 1 correspond to a silica-zirconium chloride catalyst modified by a Cp ligand (using CpSiMe₃ as a reagent). All the polymerization are performed in the same conditions at constant pressure with a monomer ratio corresponding to 15 % hexene by weight in the copolymer. The activities show generally a maximum with temperature, corresponding to a change of monomer concentration and/or the deactivation of the catalyst at 95 °C and present also a maximum with the polymerization time.

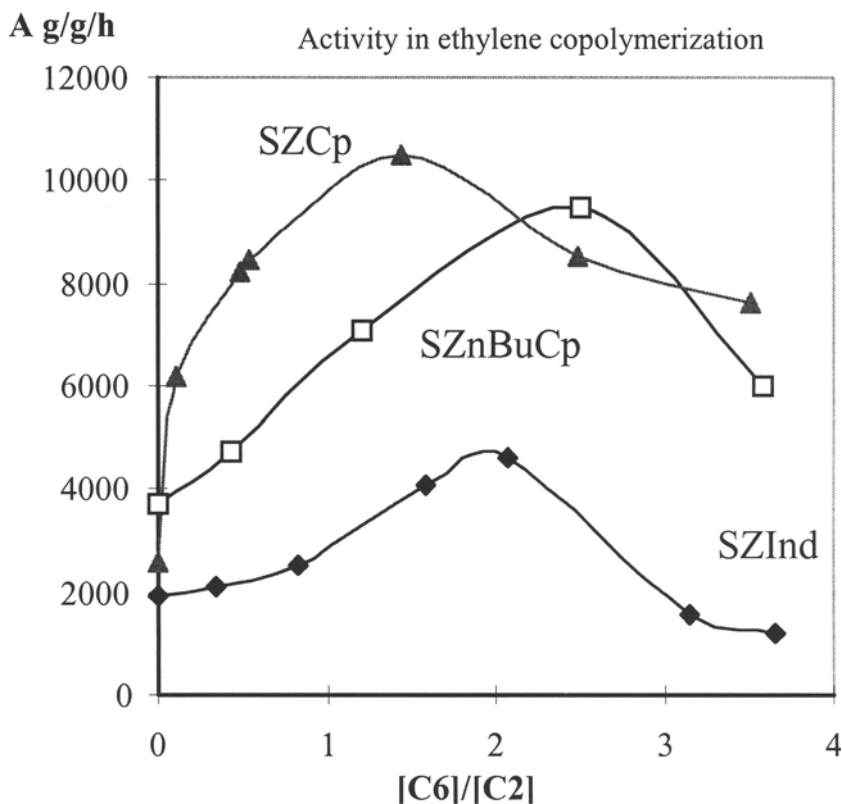


Fig. 2. Ethylene consumption rate measured in ethylene-1-hexene-1 copolymerization as a function of the monomer mole ratio in the reactor, using 3 different catalysts at 80 °C. Other conditions similar to fig. 1.

The fig. 2 shows the similar behavior of different systems when the monomer ratio is varied in each experiment, highlighting not only the well known activation effect of the comonomer (ethylene consumption increases with comonomer content) but also the fact that this activation effect remains limited (activity decreases at higher comonomer concentration).

The 1-hexene is copolymerized and a random copolymer is produced. The sensitivity of the polymer composition to monomer ratio is presented on fig. 3 for the catalyst used in fig. 1. It is interesting to observe that the competition between the 2 monomers is not very sensitive to temperature and also that the reactivity of hexene increases at higher hexene contents as it can be deduced from the shape of the curves. Fig. 4 compares not only the copolymerization behavior of all these solid catalysts but also the behavior of 2 homogeneous systems in the same conditions. All the solid catalysts are closer to the unbridged system and do not incorporate hexene as well as the ethenyl bridged system (bis ethenyl dicyclopentadienyl zirconium dichloride copolymerize hexene) does.

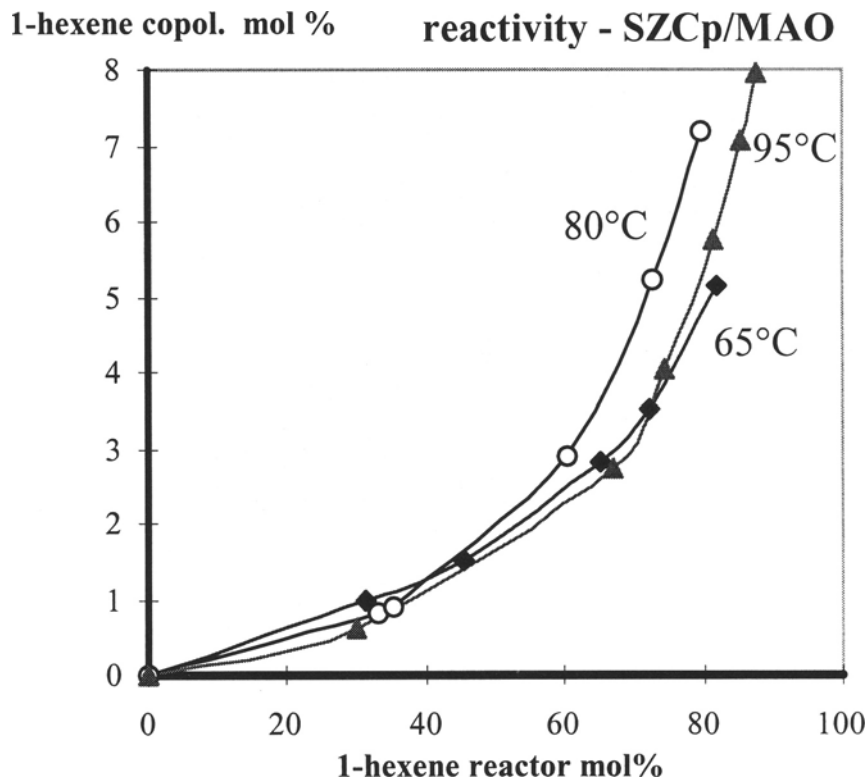


Fig. 3. Polymer composition as a function of reactor content in ethylene-hexene copolymerization using the silica zirconium cyclopentadienyl modified catalyst. Other conditions similar to fig. 1.

As a complement to fig. 4, copolymerization reactivity ratios have been determined by conventional kinetic experiments or by NMR analysis but will not be detailed in this paper. The reactivity ratios are in the same range than those observed with soluble metallocenes used in the same temperature and monomer conditions. The polydispersity index M_w/M_n (PDI) of all polymers and copolymers obtained is slightly above 2.5. There is no evidence of a diffusion control of the experiments, even at the highest activities.

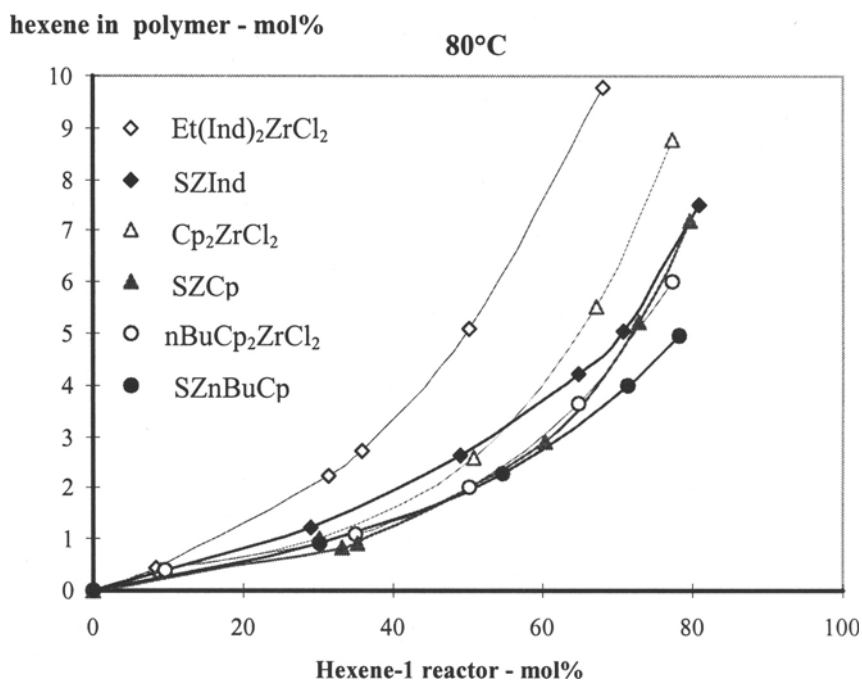


Fig. 4. Polymer composition as a function of reactor content in ethylene-hexene copolymerization using different homogeneous and heterogeneous catalysts. Other conditions similar to fig. 1.

The copolymers are not easily fractionated by solvents in fractions of different compositions. The DSC traces are very similar to those obtained using in the same conditions a soluble metallocene catalyst like dicyclopentadienyldichlorozirconium instead of the solid catalyst. The melting points, which may characterize the presence of a fraction of copolymer with low monomer content show the same trend than those observed using a soluble metallocene: fig. 5 shows that all the melting point range on a single line when polymer composition is varied. All these observations suggest a single site tendency.

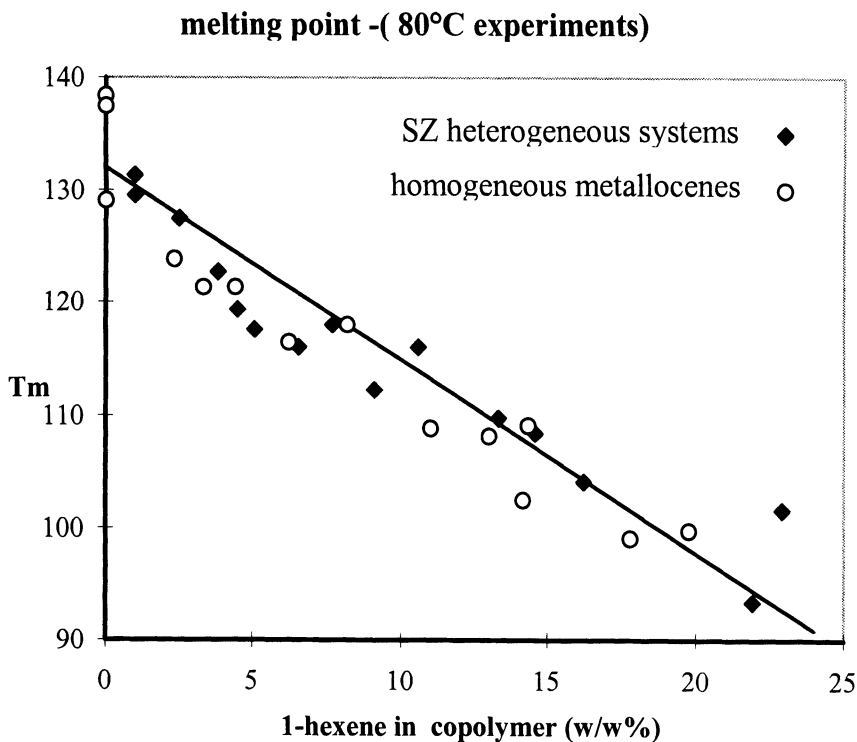
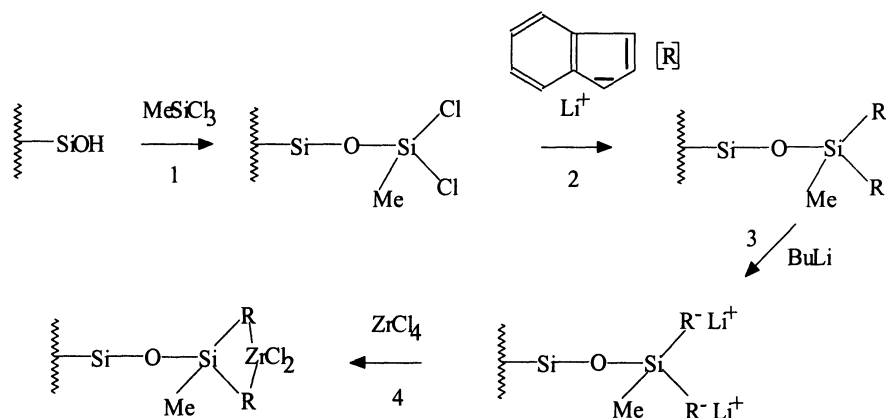


Fig. 5. Melting points T_m for ethylene- hexene copolymers with different compositions obtained with silica zirconium Cp' modified systems or homogeneous metallocenes. MAO is always used as activator.

Another approach: linking by a Si bridge to the surface

Soga et al [12-13] have presented a simple method to link a metallocene to a surface: the catalyst is built starting from a silicium dichloride linked by 2 siloxane bridges to the surface, the 2 chlorines being replaced by 2 indenyl groups to start a bridged complex preparation. We have slightly modified this principle. In order to have more flexibility, the silicium is substituted by a methyl group and only one siloxane bridge is formed. Details are given on the scheme 3.



Scheme 3. Catalyst preparation starting from a silicium bridge

This catalyst is active in ethylene polymerization. Depending on the treatment used to define the silanol group density on the surface (thermal treatment which may be followed by a chemical treatment using ClSiMe_3), more or less active catalysts are obtained. At intermediate activities, up to a few kg polymer produced by 1 g catalyst in one hour, polydispersity indexes near 2.5 or 3 are observed. Keeping in mind that the neighboring of active centers linked to the surface may be slightly different, this value is not too different from what is expected for a single site system. On the opposite, if the activities becomes very high (up to 20Kg/g catalyst/h) due to the particle size of the silica used (larger than 40 μ) diffusion control of the reaction is observed leading to very broad molecular weight distribution with a PDI above 20.

In propene polymerization an activity not exceeding of a few hundred g/g is observed with the best catalysts at a propene pressure of 4 bars. These values are far above the activities reported by Soga [12-13] but even at low temperature (30-40 $^{\circ}\text{C}$) no tacticity at all is observed. The product is recovered as a liquid oligomer with a polymerization degree below 20 and no indication of any stereospecificity on the NMR spectra.

Conclusion

The different catalysts reported have properties in common and also some differences. We were not able to convert a conventional titanium system to a single site system by the introduction of Cp' ligands. On the contrary, silica supported zirconium chloride catalysts, which are very similar to Ziegler conventional catalysts are easily converted to systems selectively activated by MAO and showing most of the properties of a single site catalyst and high activities in ethylene polymerization. Catalyst linked to the surface by the ligands have been also prepared with high activities and narrow molecular weight distributions. In no case we could get any isotactic high molecular weight polypropylene fraction from

zirconium systems and the activity remains low in most cases. It seems to be related to the fact that the active centers are attached by a rigid link to a solid surface.

Experimental

All the catalyst preparation are made under dry oxygen free argon using Schlenck tube techniques. All solvents are dried under argon. Silica (Grace 332: 320 m².g⁻¹) is generally dried under argon flow for 2 hours at 450 °C or 550 °C. The principles of the catalyst preparations are detailed in the text.

Heptane slurry polymerization are performed in a 500 ml stirred glass reactor at 4 bars constant total pressure using 300 ml of heptane. The ethylene consumption is registered. The activator generally used is methylaluminoxane (MAO) at 10 mMol. In the case of copolymerization, the quantity of catalyst is adjusted in order to maintain negligible the comonomer composition drift. The quantity of catalyst is typically 3 to 20 mg.

Acknowledgment

The authors thank the Elf-Atochem Company for support and especially Jean Malinge for discussions.

References

- [1] M. R. Ribeiro, A. Deffieux and M.F. Portela *Ind. Eng. Chem. Res.* 1997, 1224-1237 (1997)
- [2] C.Janiak, B.Rieger, *Angew. Makromol. Chem.*, 215, 47-57 (1994)
- [3] D.Lee, S.Shin, *Macromol. Symp.*, 97, 195-203 (1995)
- [4] K.Soga, M.Kaminaka, *Makromol. Chem. Rapid Commun.*, 13, 221-224 (1992)
- [5] K.Soga, M.Kaminaka, *Macromol. Chem. Phys.*, 195, 1369-1379 (1994)
- [6] S.Jüngling, S.Koltzenburg, R.Mülhaupt, *J. Polym. Sci. Part A, Polym. Chem.*, 35, 1-8 (1997)
- [7] S.Collins, W.M.Kelly, D.A.Holden, *Macromolecules*, 25, 1780-1785 (1992)
- [8] M.C.Sacchi, D.Zucchi, I.Tritto, P.Locatelli, *Macromol. Rapid Commun.*, 16, 581-590 (1995)
- [9] G.Satyanarayana, S.Sivaram, *Macromolecules*, 26, 4712-4714 (1993)
- [10] EP 293,815 (1987), Hoechst A.-G, invs : M.Antgerg, H.Lueker, L.Boehm; C.A 111:195585k
- [11] W.Kaminsky, M.Arndt, *Adv. Polym. Sci.*, 127, 143-157 (1997)
- [12] K.Soga, H.J.Kim, T.Shiono, *Macromol. Rapid Comm.*, 15, 139-143 (1994)
- [13] K.Soga, H.J.Kim, T.Shiono, *Macromol. Chem. Phys.*, 195, 3347-3360 (1994)
- [14] JP 0485306 to Mistubishi Yuka KK, invs: K. Soga , T. Sugano , CA 117:112258 (1990)
- [15] J. Dupuy and R. Spitz, *J. Appl. Polym. Sci.* 65, 2281 1997

Zeolite Supported Metallocene Catalysts: Effect of Support Structure and Surface Groups on the Polymerization Process

F. Ciardelli^{a)}, A. Altomare^{a)}, M. Michelotti^{a)}, G. Arribas^{b)}, S. Bronco^{a)}

a) Department of Chemistry and Industrial Chemistry, University of Pisa, Italy

b) UCV Caracas, Venezuela

E-mail: a) fciard@dcci.unipi.it - b) garribas@strix.ciens.ucv.ve

Abstract. The preparation and catalytic properties in monoalkene polymerization with various metallocene complexes of group IV transition metals (Ti, Zr, Hf) supported on HY zeolites and mesoporous silica MCM-41 are reported. These systems, as indicated by results obtained in a few laboratories and in the authors' laboratory, polymerize monoalkenes with significant productivity, which is lower than in homogeneous phase, but in general give polymer with higher molecular weight. Selectivity effects, catalyst leaching, role of support surface and pore size are discussed in case of ethylene and propylene polymerization, as well as of ethylene copolymerization with different α -olefins.

1. Introduction

The problem of converting soluble metallocene polymerization catalysts into physically heterogeneous but chemically homogeneous catalysts has been approached by many research groups by the pretreatment of a support with MAO followed by the addition of the metallocene [1]. In this way the transition metal part of the catalyst remains attached to the support through the same forces existing between the metallocene cation and the alumoxane counteranion in solution. Then the support acts as a solid matrix and its possible chemical and structural roles should be negligible thus allowing to maintain the same catalytic behavior as in solution. On the other side the support surface can be modified by reaction with several reagents providing different functional groups allowing to attach the metallocene complex directly to the support while maintaining its structure.

In order to contribute to understand in more detail the role of the support, as a way to develop innovative heterogeneous metallocene polymerization catalysts, the use of zeolites was investigated through the two above approaches.

The interest in zeolite based catalysts arises from the unique properties of these inorganic materials. These are: a) the activity related to both the composition and the geometry of the structure; b) the large number of available structures, ranging from the very narrow pore systems to large pores; c) the possibility to control, in a

variety of ways, the composition in a relatively wide range; d) the capability to act as hosts for transition metal ions, small metal clusters or transition metal complexes.

In this paper we report on the use of different zeolites as supports for metallocene complexes. While zeolites must contain in their framework structure both silicon and aluminium atoms, we have considered it very convenient to use also silica with a mesoporous crystalline structure (MCM-41) [2].

Results from our and other laboratories are discussed with reference to chemical composition, pore dimensions, surface chemical treatment and structure of the metallocene complex. Due to difficult molecular characterization of the final catalyst and the limited information available at present, the discussion is mainly based on productivity and polymer properties.

2. Preparation of supported catalyst

Previous papers devoted to the supportation of metallocene complexes onto inorganic matrices have shown the necessity to remove free hydroxyl groups from the support surface in order to maintain the complex integrity [3-5].

This holds true also for zeolites and in this paper we shall discuss only systems based on zeolites preventively treated with chemicals that remove hydroxyl groups. Indeed when free hydroxyl groups are present on the surface of the inorganic support the structure of the metallocene complex is not maintained [6]. The modification of the metallocene complex structure has been clearly demonstrated when reacting Cp_2TiCl_2 with MCM-41 in chloroform. In this case in the presence of traces of amine, the reaction between surface silanol groups and the metallocene led to fixation of titanium species inside the pores of this microporous crystalline support. EXAFS and FTIR analysis, as well as chemical considerations allowed to propose that the Ti(IV) ion is anchored to three oxygens (each linked to silicon) and one Cp ring [7].

The pretreatment of HY zeolite ($\text{Si}/\text{Al} = 7.25$) with AlMe_3 or ClSiMe_3 allows to support Cp_2ZrMe_2 without methane evolution. This catalyst showed lower initial activity, but better time stability as compared to the same system in solution [8].

NaY zeolite pretreated with either MAO or AlMe_3 , gave with Cp_2ZrCl_2 a supported catalyst having lower activity than in solution, particularly in the first minutes of the polymerization. According to extraction experiments it was concluded that the metallocene (Cp_2ZrCl_2) was confined inside the supercage of NaY zeolite pretreated with MAO without any leaching under polymerization conditions [9].

NaY zeolites after pretreatment with MAO were also used in another laboratory. Again lower activity and higher molecular weights were observed. The authors, by accurate chemical analysis, suggest that the concentration of framework aluminium atoms is the dominant factor but also the external surface affects the catalytic behavior [10].

Similarly ansa-metallocenes supported on MAO pretreated MCM-41 ($\text{SiO}_2 \sim 100\%$) gave a catalyst with good activity and slightly improved isotacticity and molecular weight [11] of the produced polymer.

On the basis of these results from the few different laboratories where zeolites or crystalline silica were used, as well as of many others in the case of silica gels [1,3,6,7], elimination of silanol groups appears necessary to heterogenize metallocenes without alteration.

Then the metallocene complex is linked to the support surface through weak cooperative bonds (macromolecular effect) [5] involving oxygen atoms attached to Si and/or Al. When the support is pretreated with MAO, it is likely that the metallocene cation is solvated and linked by the MAO-macromolecules. As in general, additional MAO is added to improve activity the possibility of metal leaching must be taken into account. Desorption in case of $\text{Cp}_2\text{Zr}(\text{CH}_3)_2$ supported on $(\text{CH}_3)_3\text{SiCl}$ treated silica was observed on addition of MAO as cocatalyst [6]. In that sense entrapping in the zeolite pores should limit or eliminate leaching effects and the occurrence of polymerization in solution.

In order to get information about this last possibility the supported catalyst HY-MAO- Cp_2ZrCl_2 was treated with a MAO toluene solution at 20°C and then filtered. Ethylene was submitted to polymerization with the filtrate as such and with the added residue of the proper amount of MAO in toluene, respectively. The latter system was 14 times more active, thus demonstrating that the zeolite supported catalyst was responsible for more than 93% of the polymer produced [12]. The main role of the supported catalyst is also in keeping with the polymer morphology rather different from that of the polymer obtained in the presence of the same metallocenes in homogeneous phase [12,13].

3. Homopolymerization of ethylene and propylene

As observed in previous reports, the polymerization of ethylene in the presence of Y zeolite supported metallocenes is characterized by a lower productivity in respect to the homogeneous case. Higher activity can be obtained by using crystalline silica MCM-41. In the case of the ethylene polymerization with Cp_2ZrCl_2 supported on HY-zeolite the increased amount of framework aluminum seems to produce a negative effect on productivity and molecular weight. The latter indeed is generally up to two times higher, with supported catalysts, HY zeolites with low Al content and MCM-41 pretreated with Me_3SiCl giving the best results in terms of molecular weight. MAO pretreatment of the support surface seems to be more efficient than AlMe_3 (Table 1).

The results obtained during ethylene polymerization in the presence of a catalyst prepared by supporting Cp_2TiCl_2 on the same MAO or AlMe_3 pretreated supports confirm the above data also for the molecular weight, even if these are already high with the homogeneous systems. Interestingly, higher activity is obtained by treating the support with MAO (Table 2) at 50°C ; (Runs PE60, PE61, PE68), even if these results may be simply related to a better elimination of free silanol groups [13].

Table 1. Homopolymerization of ethylene in the presence of supported Cp₂ZrCl₂/MAO catalysts^a

| Run | Support | | Al/Zr | Productivity ^b | \overline{M}_v^c x 10 ⁻³ | |
|------|---------|--|----------------------|---------------------------|--|--------------|
| | Type | SiO ₂ /Al ₂ O ₃ | | | | Pretreatment |
| EZ01 | | none | | 1,000 | 1,270 | 136 |
| EZ05 | HY | 27 | MAO | 1,000 | 190 | 232 |
| EZ07 | HY | 27 | MAO | 2,000 | 316 | 252 |
| EZ13 | HY | 5.7 | MAO | 1,000 | 58 | 170 |
| EZ41 | MCM41 | ∞ | MAO | 300 | 920 | 188 |
| EZ08 | HY | 27 | AlMe ₃ | 1,000 | 60 | 214 |
| EZ15 | HY | 5.7 | AlMe ₃ | 1,000 | 36 | 193 |
| EZ42 | MCM41 | ∞ | AlMe ₃ | 100 ^d | 50 | 149 |
| EZ36 | MCM41 | ∞ | AlMe ₃ | 1,000 | 467 | 246 |
| EZ38 | MCM41 | ∞ | Me ₃ SiCl | 1,000 | 528 | 293 |

a) In 80 ml toluene with 10 μmol of Zr for 60 min and MAO cocatalyst, P_{C₂H₄} = 1 bar and T = 20°C.

b) kg PE/g·atom Zr·bar·h

c) From viscosity measurements in decalin at 135°C.

d) Al(iBu)₃ cocatalyst.

Table 2. Homopolymerization of ethylene in the presence of supported Cp₂TiCl₂ catalysts^a

| Run | Support | | Pretreatment | Duration (min) | Productivity ^b | \overline{M}_v^c x 10 ⁻³ |
|------|---------|--|-------------------|-------------------|---------------------------|--|
| | Type | SiO ₂ /Al ₂ O ₃ | | | | |
| PE1 | | none | | 30 | 720 | 170 |
| PE26 | HY | 63 | MAO | 20 | 60 | 258 |
| PE60 | HY | 63 | MAO | 50 | 15 | 1,200 |
| PE20 | HY | 5.7 | MAO | 20 | 60 | 108 |
| PE59 | HY | 5.7 | MAO | 50 | 30 | 300 |
| PE50 | MCM41 | ∞ | MAO | 20 | 30 | 560 |
| PE61 | MCM41 | ∞ | MAO | 50 | 15 | 2,560 |
| PE31 | HY | 63 | AlMe ₃ | 20 | 60 | 125 |
| PE68 | HY | 63 | AlMe ₃ | 50 | 15 | 920 |
| PE13 | HY | 5.7 | AlMe ₃ | 20 | 60 | 113 |
| PE49 | MCM41 | ∞ | AlMe ₃ | 20 | 30 | 402 |

a) In 80 ml toluene with 5 μmol of Ti at 20°C; P_{ethylene} = 1 bar with MAO as cocatalyst (MAO/Ti = 1,000).

b) kg PE/g·atom Ti·bar·h

c) From viscosity measurements at 135°C in decalin.

The use of ansa-metallocenes reduces substantially the support effect even if same variation is still observable. In particular with MCM-41 and $\text{Et}(\text{Ind})_2\text{ZrCl}_2$ comparable activity and molecular weight are obtained as in solution. On the contrary the analogous Hf complex, both on HY zeolite with high aluminum content or on MCM-41 gives lower activity and higher polymer molecular weight than in solution. Analogous considerations appear to be valid for the corresponding propylene polymerization (Table 3). Indeed as observed for ethylene polymerization, $\text{Et}(\text{Ind})_2\text{ZrCl}_2$ gives lower activity than in solution and comparable molecular weight, whereas with MCM-41 both processes are very comparable for activity and chain length. $\text{Et}(\text{Ind})_2\text{HfCl}_2$ for propylene shows lower productivity and appreciably increased molecular weight.

Even if the general trends observed in our experiments are similar to those reported by other authors with zeolite or even silica supported metallocenes, there are also differences. These last can be connected to the different samples of support used which make difficult to clearly separate significant support effects on chemical effects. Also in many cases a partial release of catalytic species into the solution may occur, so the observed results are a combination of processes occurring in solution and in solid phase. The main evidence of the support role is generally provided by the higher molecular weight and a certain stability of catalytic species observable during kinetic experiments [12,14].

Table 3. Homopolymerization of ethylene and propylene in the presence of supported ansa-metallocenes/MAO catalysts ^a

| Metallocene | Support Type | Ethylene | | | Propylene | | |
|--|-----------------|----------|--------------------|---|-----------|--------------------|---|
| | | Run | Prod. ^b | \overline{M}_v ^c $\times 10^{-3}$ | Run | Prod. ^b | \overline{M}_v ^c $\times 10^{-3}$ |
| $\text{Et}(\text{Ind})_2\text{ZrCl}_2$ | none | EZ01 | 1,270 | 136 | AZ14 | 2,270 | 31 |
| $\text{Et}(\text{Ind})_2\text{ZrCl}_2$ | HY (5.7) | AZ2 | 390 | 155 | AZ15 | 885 | 38 |
| $\text{Et}(\text{Ind})_2\text{ZrCl}_2$ ^d | HY (5.7) | AZ5 | 45 | 178 | — | — | — |
| $\text{Et}(\text{Ind})_2\text{ZrCl}_2$ ^e | MCM41 | AZ13 | 1,780 | 127 | AZ18 | 2,010 | 35 |
| $\text{Me}_2\text{Si}(\text{Ind})_2\text{ZrCl}_2$ ^e | None | SZ2 | 1,140 | 197 | SZ3 | 2,520 | 61 |
| $\text{Me}_2\text{Si}(\text{Ind})_2\text{ZrCl}_2$ ^e | MCM41 | SZ1 | 1,680 | 169 | SZ4 | 1,730 | 64 |
| $\text{Et}(\text{Ind})_2\text{HfCl}_2$ | None | AH1 | 110 | 310 | AH5 | 620 | 390 |
| $\text{Et}(\text{Ind})_2\text{HfCl}_2$ | HY (5.7) | AH2 | 40 | 423 | AH6 | 160 | 480 |
| $\text{Et}(\text{Ind})_2\text{HfCl}_2$ | MCM41 | AH4 | 60 | 361 | AH8 | 390 | 495 |

a) In 80 ml of toluene with 10 μmol of Mt (Zr or Hf) for 60 min and MAO cocatalyst, $P_{\text{monomer}} = 1$ bar and $T = 20^\circ\text{C}$; $\text{Al}/\text{Mt} = 1,000$ in ethylene polymerization; $\text{Al}/\text{Mt} = 1,500$ in propylene polymerization; reaction time = 1 h.

b) kg Pol/g-atom Mt, bar-h.

c) From viscosity measurements in decalin at 135°C .

d) $\text{Al}(\text{iBu})_3$ cocatalyst; $\text{Al}/\text{Mt} = 50$.

e) Reaction time = 20 min.

4. Copolymerization of α -olefins with ethylene

As reported in the previous paragraph the use of ansa-metallocene reduces to a large extent the effect of the support. Indeed ansa-metallocenes when supported, particularly on MCM-41, show a behavior similar to that in solution. Thus the homopolymerization of α -olefins is not very informative.

In the copolymerization of ethylene with 1-hexene, both zirconium- and hafnium-ethylene-bis(indenyl)dichloride give products with similar composition both in homogeneous phase and supported on HY zeolites respectively. Again the activity is about two times lower and the molecular weight 1.5 to 2.0 times higher in the presence of supported catalysts [15]. On the other side Cp_2ZrCl_2 in homogeneous phase polymerizes α -olefins to polymers with very low molecular weight [16]. Copolymerization of α -olefins with ethylene using zeolite supported Cp_2ZrCl_2 appeared therefore the best way to evidence the role of the support on the polymerization process. Indeed the ethylene/1-hexene copolymer obtained in the presence of HY-zeolite supported Cp_2ZrCl_2 had a molecular weight 9 times higher and C_6 units content almost 2.5 times lower than the same copolymer prepared with the homogeneous Cp_2ZrCl_2 catalyst. Also the former showed one melting point only at 112.0°C, whereas the latter had two melting peaks at 89.4 and 116.8°C (Table 4). In this case, as in the case of the homopolymers, the copolymers obtained with supported catalysts exhibit a higher molecular weight regardless of the type of metallocene, thus indicating a minor incidence of the chain transfer to comonomer or β -hydride elimination, compared to that observed operating in solution.

Table 4. Copolymerization of ethylene with 1-hexene in the presence of supported Cp_2ZrCl_2 ^a

| Run | Support ^b | Durati on (min) | Productivity ^c | % C_6 (mol) ^d | \overline{M}_v $\times 10^{-3}$ ^e | Tm (°C) ^f |
|-----|---|-----------------------|---------------------------|--------------------------------------|---|----------------------|
| CZ1 | none | 60 | 652 | 20 | 7 | 89.4/116.8 |
| CZ2 | HY(SiO ₂ /Al ₂ O ₃ =5.7) | 60 | 228 | 8 | 63 | 112.0 |
| MC1 | none | 30 | 1,490 | 20 | 8 | 88.6/117.1 |
| MC2 | MCM-41 | 30 | 1,070 | 17 | 10 | 96.3/114.3 |

a) In 80 ml of 1.0 M 1-hexene solution at 20°C with 5 μmol Cp_2ZrCl_2 ; MAO/Zr = 2,000, $P_{\text{ethylene}} = 5$ bar.

b) Pretreated with MAO.

c) kg Pol/g-atom Zr-bar-h.

d) Determined by ¹H-NMR.

e) Determined by viscosity in decalin at 135°C.

f) Determined by DSC.

According to what has previously been published, bridged hafnium derivatives in solution afforded higher molecular weights and a quite similar trend was observed operating in the presence of the supported systems, thus indicating a substantial maintenance of the original metallocene nature following zeolite supportation [17].

Both DSC and ^1H NMR spectroscopy analysis gave evidence of a peculiar difference in the composition of the reaction products, which was dependent on the type of metallocene. While a minor concentration of 1-hexene units was observed in the copolymers obtained with supported biscyclopentadienyl derivatives compared to those observed in homogeneous phase, no composition difference was noticed in the case of the stereorigid complexes.

In the former case the disappearance of one of the two melting points observed with the solution product could be the consequence of a different compositional homogeneity, connected to a lower content of 1-hexene. Solvent fractionation of the homogeneous phase copolymer gave up to 65% of product soluble in low temperature boiling solvents with low molecular weight and high degree of branching. In contrast 90% of the product obtained with the supported catalytic system was extractable only with cyclohexane and toluene, according to the major length and linearity of the polymer chains (Table 5). This data also confirms the strict correlation between decrease of molecular weight and increased incorporation of α -olefin.

Table 5. Comonomer distribution in poly(ethylene-*co*-1-hexene) samples ^a

| Fraction extracted with: | Cp_2ZrCl_2 (homogeneous) | | | | Cp_2ZrCl_2 (supported) ^b | | | |
|--------------------------|--|-----------------------------|-------------------------------|--------------------|---|-----------------------------|-------------------------------|--------------------|
| | % | % C_6 ^c | \overline{M}_v ^d | T_m ^e | % | % C_6 ^c | \overline{M}_v ^d | T_m ^e |
| Acetone | 39 | 34 | 800 | - | 8 | 32 | 600 | - |
| Ethyl acetate | 20 | 26 | 2,500 | 83 | 2 | 20 | 3,100 | - |
| Diethyl ether | 5 | 15 | 6,000 | 97 | 0 | - | - | - |
| Cyclohexane | 30 | 6 | 13,000 | 116 | 81 | 6 | 65,000 | 110 |
| Toluene | 6 | <1 | 38,000 | 122 | 9 | 4 | 93,000 | 112 |

a) Copolymerization carried out in 80 ml of 1.0 M 1-hexene solution in toluene, with 5 (homogeneous) or 10 (supported) μmol of Zr; MAO/Zr = 2,000, P_{ethylene} = 5 bar and polymerization time = 60 min.

b) HY zeolite ($\text{SiO}_2/\text{Al}_2\text{O}_3 = 5.7$) pretreated with MAO.

c) Molar fraction determined by ^1H NMR analysis.

d) Determined by viscosity measurements in decalin at 135°C.

e) Melting point of the polymer fraction in °C.

The effect exerted by the impregnation on the HY zeolite in the case of Cp_2ZrCl_2 seems to be related to the particular size of the pores and cavities of this support. This was furthermore confirmed by copolymerization experiments with the same catalyst supported on the MCM-41 mesoporous silica. In this last case the differences between supported and unsupported catalyst were very modest.

Indeed the productivity with the supported catalyst was only 30% lower than with the homogeneous catalyst, while 1-hexene incorporation, molecular weight

and melting points were very similar (Table 4). The most reasonable explanation is therefore that the large pores of MCM-41 allow supportation of the nonbridged metallocene without affecting it sterically in a more or less direct way. The shape selectivity exerted by the HY zeolite supported Cp_2ZrCl_2 catalyst is furthermore confirmed by copolymerization of ethylene with either linear or branched α -olefins having variable steric demand.

In all cases the supported catalyst gave lower activity, lower incorporation of α -olefins, higher molecular weight and a single melting temperature. The differences particularly in activity and α -olefin content were the largest for branched α -olefins such as 4-methyl-1-pentene in respect to linear α -olefins (1-hexene to 1-dodecene). It is also of interest to note that all the above features showed the same qualitative dependence on the comonomer structure in the case of both the supported and homogeneous catalysts [15].

The comparison in the catalytic behavior for ethylene/ α -olefin copolymerization with Cp_2ZrCl_2 in solution and supported on zeolite was investigated by using α -olefins as reaction solvents (Table 6). The zirconocene in homogeneous phase led to the exclusive formation of oligomers, in the range (estimated by NMR) of 390-1,240 and characterized by terminal vinylidenic bonds as proven by FT-IR and NMR analysis [18]. In contrast, the zeolite supported catalyst gave, under the same experimental conditions, polymeric products with much higher molecular weights (up to two orders of magnitude), though with the usual decline in catalytic activity.

Table 6. Ethylene/ α -olefin copolymerization in α -olefin solution with unsupported or supported Cp_2ZrCl_2 ^a

| Run | α -Olefin | Support | Productivity ^b | $\overline{\text{MW}}$ | α -Olefin in copolymer (mol.-%) ^d |
|-----|------------------|-------------------------|---------------------------|------------------------|---|
| CM1 | 4MP | none | 1,736 | 390 | 50.0 ca |
| CM2 | 4MP | HY-zeolite ^e | 224 | 62,000 | 7.9 |
| CM3 | HEX | none | 1,876 | 1,240 | 50.0 ca |
| CM4 | HEX | HY-zeolite ^e | 348 | 19,000 | 22.1 |
| CM5 | OCT | none | 2,300 | 560 | 50.0 ca |
| CM6 | OCT | HY-zeolite ^e | 164 | 22,000 | 18.5 |

a) Reaction carried out at 20°C in 80 ml of α -olefin (4MP = 4-methyl-1-pentene, HEX = 1-hexene, OCT = 1-octene), with 5 μmol of Zr in solution or 10 μmol of supported Zr, cocatalyst MAO, $[\text{Al}]/[\text{Zr}] = 2,000$, ethylene pressure 5 bars, polymerization time 60 min.

b) kg Pol/g-atom Zr-bar-h.

c) Determined by ¹H NMR analysis for runs CM1, CM3 and CM5 and by viscosity measurements in decalin at 135°C for runs CM2, CM4 and CM6.

d) Determined by ¹H NMR analysis.

e) Pretreated with MAO.

These elastomeric copolymers revealed a totally amorphous nature because of the high incorporation of α -olefin (in the molar range 8-22 %), which was dependent on the type of comonomer and always below the value observed in solution. In this last case the oligomers always contain about 50% moles of α -olefin but this evaluation is clearly of little significance in connection with the very low molecular weight with a large contribution due to the end groups, which derive in all cases from the α -olefin with the formation of vinylidenic double bond at the end of the chain.

4. Final Remarks

The data reported in the present paper confirms that both zeolite and mesoporous crystalline silica can be used as well defined supports for metallocene complexes to yield heterogenized catalysts with good productivity. Like amorphous silica, these monoalkene polymerization in supports need that the surface hydroxyl groups are fully removed by chemical treatment in order to save the metallocene structure. Even after this treatment the heterogenized systems, show lower activity than the corresponding complexes in homogeneous phase but give polymers with higher molecular weight.

The increase in molecular weight is probably connected to the fact that the microporous structure of the support and pore sizes exert a significant role on transfer reactions, thus increasing chain length, particularly when α -olefins are present. During the copolymerization of ethylene with α -olefins a partial shape selectivity is observed with HY zeolite which is probably connected to inclusion of the active species in the support pores and seems to be related to molecular weight variation.

The various steric effects connected to the support may be reduced by increasing the pore sizes from the HY to the MCM-41 support. Also a certain increase in activity can be reached in the same way as well as by selecting proper conditions for catalyst pretreatment. Moreover the inclusion of the metallocene in the support pores limits to less than 10% catalyst leaching during polymerization.

Finally even if productivity is lower than in homogeneous phase it cannot be explained with the polymerization occurring only inside the support cavities. Indeed preliminary studies by SEM suggest that the support suprastructure is disseggregated during the polymerization thus allowing better site accessibility and lower diffusion limitation. Further studies in due course on the formed polymer morphology at different conversions should shed more light on this point.

References

1. O. Olabisi, M. Atiqullah, W. Kaminsky, *J.M.S. – Rev. Macromol. Chem. Phys.*, **C37** (3), 519-554 (1997).
2. F. Ramoa Ribeiro, F. Alvarez, C. Henriques, F. Lemos, J.M. Lopes, M.F. Ribeiro, *J. Mol. Catal. A. Chem.*, **96**, 245-270 (1995).
3. S. Collins, W.M. Kelly, D.A. Holden, *Macromolecules*, **25**, 1780 (1992).
4. K. Soga, M. Kaminaka, *Makromol. Chem. Rapid Commun.*, **13**, 221 (1992).
5. F. Ciardelli, A. Altomare, G. Conti, G. Arribas, B. Mendez, A. Ismayel, *Makromol. Chem. Macromol. Symp.*, **80**, 29 (1994).
6. N.V. Semikolenova, V.A. Zakharov, *Macromol. Chem. Phys.*, **198**, 2889-2897 (1997).
7. T. Maschmeyer, F. Rey, G. Sankar, J.M. Thomas, *Nature*, **378**, 159-162 (1995).
8. F. Ciardelli, A. Altomare, G. Arribas, G. Conti, F. Masi, F. Menconi, in "Catalyst Design for Tailor-Made Polyolefins", K. Soga, M. Terano (Eds.), Kodansha, Tokyo, 1994, p. 257.
9. S.I. Woo, Y.S. Ko, T.K. Han, *Macromol. Rapid Commun.*, **16**, 489 (1995).
10. Y.S. Ko, T.K. Han, J.W. Park, S.I. Woo, *Macromol. Rapid Commun.*, **17**, 749-758 (1996).
11. M. de Fátima V. Marques, C.A. Henriques, J.L.F. Monteiro, S.M.C. Menezes, F.M.B. Coutinho, *Macromol. Chem. Phys.*, **198**, 3709-3717 (1997).
12. M. Michelotti, G. Arribas, A. Altomare, S. Bronco, submitted.
13. R. Balducci, M. Michelotti, A. Altomare, F. Ciardelli, *MMC-7 Book of Abstracts*, P006 (1997).
14. M.R. Ribeiro, A. Deffleux, M.F. Portela, *Ind. Eng. Chem. Rev.*, **36**, 1224-1237 (1997).
15. M. Michelotti, A. Altomare, F. Ciardelli, E. Roland, *J. Mol. Catal. A. Chem.*, **129**, 241-248 (1998).
16. M. Michelotti, A. Altomare, F. Ciardelli, P. Ferrarini, *Polymer*, **37**, 5011 (1996).
17. W. Kaminsky, R. Engehausen, K. Zoumis, W. Spaleck, J. Rohrmann, *Makromol. Chem.*, **193**, 1643 (1992).
18. M. Michelotti, A. Altomare, F. Ciardelli, P. Ferrarini, *Polymer*, **37**, 5011 (1996).

Acknowledgment.

Support by MURST – Roma is gratefully acknowledged. Data with MCM-41 were kindly provided by Mr. Lotfi Oulderrahmania (PhD Thesis, University of Pisa).

Thanks are also due to DEGUSSA Corporation for providing HY zeolite and MCM-41 samples.

Preparation of novel supported metallocene and their olefin polymerization capabilities

Young Soo Ko, Tae Seok Seo, Dae Sik Hong and Seong Ihl Woo*

Department of Chemical Engineering, Korea Advanced Institute of Science and Technology, 373-1 Kusong-dong, Yusong-gu, Taejeon, Korea

*To whom correspondence should be addressed, wsil@convex.kaist.ac.kr.

Abstract.

Cp_2ZrCl_2 confined inside the supercage of NaY zeolite ($\text{NaY}/\text{MAO}/\text{Cp}_2\text{ZrCl}_2$) provides shape-selective copolymerization in which comonomer reactivity ratio depends on the shape and size of comonomer. In ethylene/propylene copolymerization over $\text{NaY}/\text{MAO}/\text{Cp}_2\text{ZrCl}_2$, a comonomer enhancement effect on the polymerization rate was observed, whereas in ethylene/1-hexene copolymerization comonomer enhancement effect was not observed. Comonomer depression effect was observed in ethylene/1-octene copolymerization. In ethylene/isobutylene copolymerization, isobutylene did not influence the polymerization rate. Copolymerization rate was also the same as the ethylene homopolymerization rate, indicating that isobutylene could not diffuse into the pores of the NaY zeolite during copolymerization because the kinetic diameter of isobutylene is larger than the pore diameter of NaY preadsorbed with methylaluminumoxane (MAO). The comonomer content in the copolymer chain prepared with $\text{NaY}/\text{MAO}/\text{Cp}_2\text{ZrCl}_2$ was less by about one-half than that in the copolymer chain prepared with Cp_2ZrCl_2 . Melting endotherm measured with DSC after successive annealing of copolymer shows that copolymers prepared with $\text{NaY}/\text{MAO}/\text{Cp}_2\text{ZrCl}_2$ show a narrower comonomer distribution than that prepared with Cp_2ZrCl_2 .

$\text{Me}_2\text{SiCp}_2\text{ZrCl}_2$ and $(\text{MeCp})_2\text{ZrCl}_2$ catalysts were synthesized in NaY supercage by ship-in-bottle synthesis method, and used for ethylene homopolymerization.

The activity of $(\text{MeCp})_2\text{ZrCl}_2/\text{NaY}/\text{MAO}$ system was larger than that of $\text{Me}_2\text{SiCp}_2\text{ZrCl}_2/\text{NaY}/\text{MAO}$ system. However, the absolute magnitude of the catalytic activity was small because LiCl salt formed during metallation was not removed completely and might act as a poison. Because of the difficulty in separating unreacted compounds and inactive or less active by-products from the supercage of NaY, the polymerization activity per Zr atom must be quite low.

Introduction

Recently, we have found that NaY zeolite-entrapped metallocene catalyst can polymerize ethylene with a small amount of additional MAO [1] and that $\text{Et}(\text{ind})_2\text{ZrCl}_2$ confined into the pores of MCM-41 polymerizes propylene with a high activity [2]. Zeolites are well-known for their characteristic crystalline structures having large surface area and well-defined pores of extremely narrow pore size distribution [3]. The shape selectivity of a zeolite originates from its regular pore size and the supercage. Molecules of kinetic diameter larger than the pore diameter of the zeolite simply cannot diffuse into or out of the pores, which will change product selectivity in many chemical reactions [4].

For the first time, we report shape selectivity in olefin polymerization. The copolymerization rate and the content of comonomer in ethylene copolymerization were affected by the shape and the diffusion of monomer through the pores of the zeolite. This provides a means of controlling the insertion rate and the amount of comonomer in copolymer chain by the shape selectivity of the zeolite during copolymerization. Silica and the other inorganic oxide supports generally possess a relatively broad pore size distribution due to their irregular pore structures. This results in their pore structure not showing shape selectivity in ethylene and propylene homopolymerization, and ethylene/ α -olefin copolymerization [5,6].

Metallocene catalysts can be synthesized in the supercage of zeolite by ship-in-bottle synthesis. A reactant is small enough to diffuse through the zeolite pores but the product is too large to diffuse out once formed. Hence, metallocene cannot diffuse out to solvent during polymerization, which will suppress the polymerization in the solvent phase. This might improve the morphology of polymer particles.

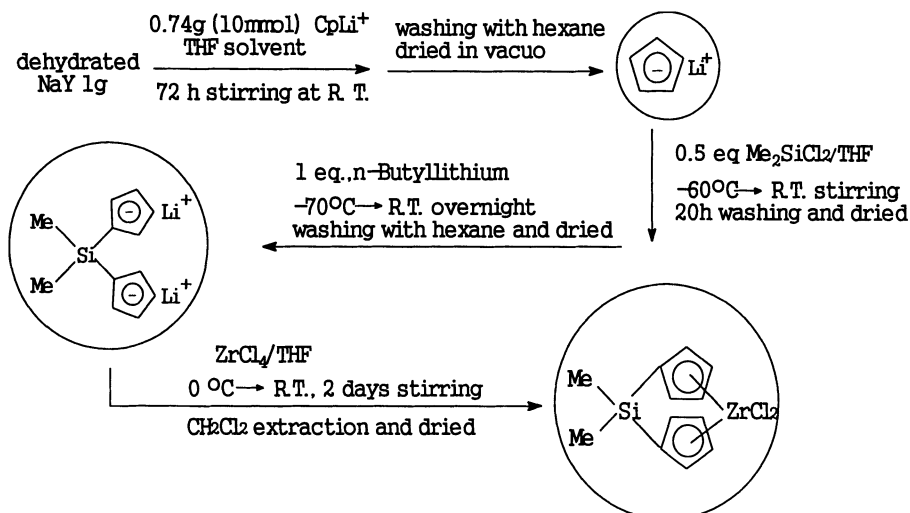
Experiments

Zeolite-Entrapped Metallocene Catalyst

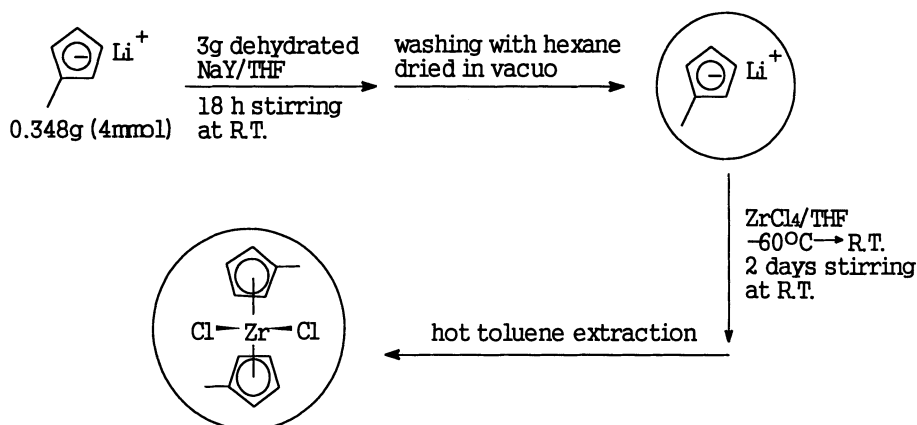
Cp_2ZrCl_2 confined the supercage of zeolite was synthesized as follows. 7.3g of dehydrated NaY zeolite and 20 mmol-Al of MAO solution (1.98 M-Al solution in toluene) were suspended in 100 cm³ of toluene and stirred for 24 h at 50°C. The resulting solid was washed more than 5 times with 150 cm³ of toluene and dried at 25 °C *in vacuo*. 1.0 mmol of Cp_2ZrCl_2 dissolved in 100cm³ of toluene was impregnated into MAO-pretreated NaY zeolite followed by vigorous stirring at 50°C for 48 h. Then solid part was washed more than 5 times with 150 cm³ of toluene to remove Cp_2ZrCl_2 physisorbed on the exterior surface of zeolite and dried *in vacuo*. The content of metal in the supported catalysts were measured by inductively coupled plasma (ICP) mass spectroscopy for zirconium (3.12 μmol Zr/g-catalyst). Polymerizations were carried out at 50 °C and at 1.2 atm or 8 atm.

Ship-in-Bottle Method to Encapsulate Metallocene in Zeolite

The detailed steps of ship-in-bottle synthesis are described as follows:



Scheme for the synthesis of $\text{Me}_2\text{SiCp}_2\text{ZrCl}_2$ in NaY zeolite



Scheme for the synthesis of $(\text{MeCp})_2\text{ZrCl}_2$ in NaY zeolite

Results and Discussion

Zeolite-Entrapped Metallocene Catalyst

Copolymerization of ethylene and propylene catalyzed over NaY/MAO/ Cp_2ZrCl_2 and unsupported Cp_2ZrCl_2 was conducted at 1.2 atm and 50 °C (Table 1). In the copolymerization of ethylene and propylene with

NaY/MAO/Cp₂ZrCl₂, the polymerization rate started to increase after 2-3 minutes of polymerization and increased as the molar ratio of propylene to ethylene in feed increased (Fig. 1). In the copolymerization of ethylene and propylene with Cp₂ZrCl₂, polymerization rates decreased as C₃/C₂ molar ratio in the feed increased. This depression effect of propylene on the polymerization rate does not indicate that there is an enhancement in the diffusion rate of ethylene through bulky polymer to the active site, which originates from the lower crystallinity after propylene is incorporated into the polymer chain [7, 8]. In contrast, comonomer enhancement effect was observed in the case of ethylene/propylene copolymerization with NaY/MAO/Cp₂ZrCl₂. The active site confined inside supercages of the NaY zeolite is very stable and maintains its polymerization activity for a long time. Hence, the molecular weight of the resulting polymer becomes much higher than that of the polymer prepared with Cp₂ZrCl₂. The resulting polymer becomes insoluble in toluene during polymerization. The incorporation of propylene into the ethylene polymer chain decreases the crystallinity of the polymer, which enhances the diffusion of ethylene, and hence, the polymerization rate increases. As shown in Table 1, the ethylene homopolymerization rate with NaY/MAO/Cp₂ZrCl₂ is much smaller than that with

Table 1. Results of Copolymerizations of ethylene (C₂) with propylene (C₃) or isobutylene (C₄) with NaY/MAO/Cp₂ZrCl₂ and unsupported Cp₂ZrCl₂.

| Catalyst | Mono- mer | mole ratio | yield (g) | Activity ^{d)} | Comono- mer Content (mol%) | M _n | MWD | T _m (°C) |
|---|--------------------------------|---------------|--------------------|------------------------|-------------------------------------|----------------|------|------------------------|
| NaY/ | | 0.0 | 0.29 | 258 | 0.0 | 101000 | 3.1 | 135.0 |
| MAO/ | C ₃ /C ₂ | 0.5 | 0.66 | 587 | 0.7 | 73000 | 2.8 | 132.2 |
| Cp ₂ ZrCl ₂ ^{a)} | | 1.0 | 0.79 | 702 | 1.7 | 36000 | 2.9 | 125.7 |
| | | 0.0 | 6.14 | 2558 | 0.0 | 46100 | 2.29 | 129.8 |
| Cp ₂ ZrCl ₂ ^{b)} | C ₃ /C ₂ | 0.5 | 3.85 | 1604 | 3.0 | 5900 | 2.38 | 120.7 |
| | | 1.0 | 3.24 | 1350 | 3.9 | 4300 | 2.17 | 118.2 |
| NaY/MAO | C ₄ /C ₂ | 0.5 | 1.19 ^{c)} | 215 | 0.0 | n.d. | n.d. | 137.5 |
| Cp ₂ ZrCl ₂ ^{a)} | | 1.0 | 1.19 ^{c)} | 212 | 0.0 | n.d. | n.d. | 135.8 |
| Cp ₂ ZrCl ₂ ^{b)} | C ₄ /C ₂ | 1.0 | 1.22 ^{c)} | 253 | 0.0 | n.d. | n.d. | 131.5 |

a) Polymerization condition : T = 50 °C, P = 1.2 atm, Al/Zr = 1000, t = 1 hr.

b) Polymerization condition : T = 50 °C, P = 1.2 atm, Al/Zr = 3000, t = 1 hr.

c) Polymerization time = 2 hr.

d) unit : kg-PE/molZr atm·hr

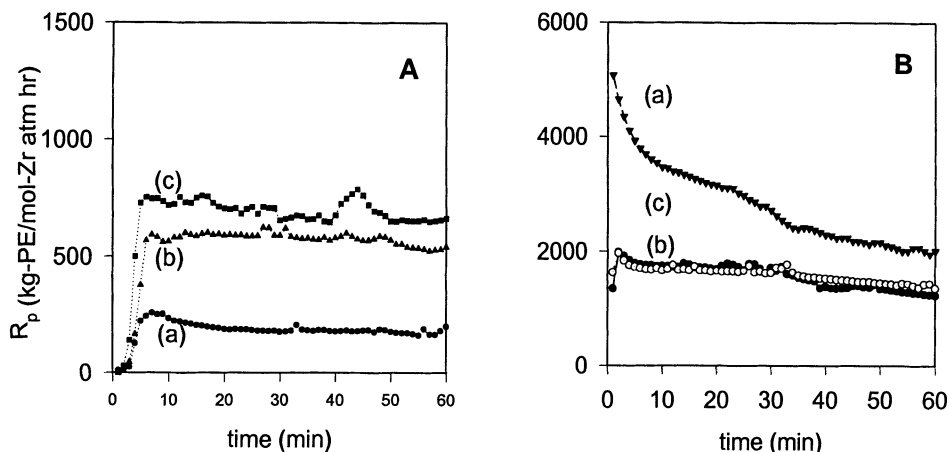


Fig. 1. The profile of ethylene consumption rate in ethylene/propylene copolymerization catalyzed over NaY/MAO/Cp₂ZrCl₂ (A) and unsupported Cp₂ZrCl₂ (B). Polymerization condition : T = 50 °C, P = 1.2 atm, Al/Zr = (A) 1000 and (B) 3000, C₃/C₂ molar ratio in feed = (a) 0.0, (b) 0.5 and (c) 1.0.

Cp₂ZrCl₂, indicating that the diffusion rate of ethylene through the NaY pores determines the polymerization rate. The propylene content in the resulting ethylene/propylene copolymer (0.7 and 1.7 mol %) with NaY/MAO/Cp₂ZrCl₂ is smaller than that (3.0 and 3.9 mol %) with Cp₂ZrCl₂. This indicates that the diffusion rate of propylene through the pores of NaY is smaller than that through toluene in which low molecular weight ethylene/propylene copolymer was dissolved. The effect of molecular size of comonomer (propylene, 1-hexene and 1-octene) on the average polymerization rate with Cp₂ZrCl₂ and NaY/MAO/Cp₂ZrCl₂ is shown in Fig. 2. Little effect of comonomer on the polymerization rate (ethylene consumption rate) was observed in the copolymerization of ethylene/1-hexene with NaY/MAO/Cp₂ZrCl₂. Comonomer depression effect was observed in the ethylene/1-octene copolymerization with NaY/MAO/Cp₂ZrCl₂. The increase in concentration of 1-octene decreased the polymerization rate. This copolymerization behavior is quite different from that of Cp₂ZrCl₂. Under the polymerization conditions in this study, there was only comonomer depression effect rather than enhancement effect with Cp₂ZrCl₂. There was little difference in the ethylene consumption rate between the copolymerization of ethylene with 1-hexene and with 1-octene catalyzed over Cp₂ZrCl₂. With NaY/MAO/Cp₂ZrCl₂, it can be stated that as the branch length and molecule size of α -olefin increased, comonomer enhancement effect was diminished and comonomer depression effect was observed. To confirm the effect of shape and diffusion of comonomer on the copolymerization rate with NaY/MAO/Cp₂ZrCl₂, we conducted ethylene/isobutylene copolymerization.

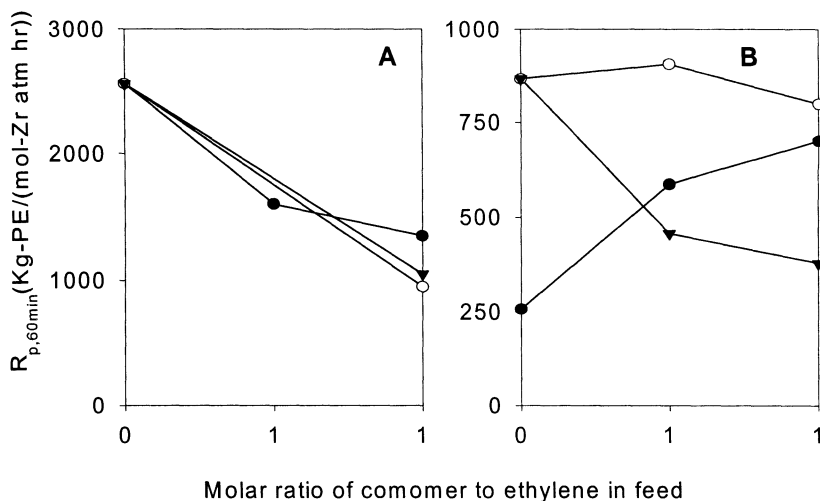


Fig. 2. Change in average activity of Cp_2ZrCl_2 (A) and $NaY/MAO/Cp_2ZrCl_2$ (B) with respect to the molar ratios of propylene (●), 1-hexene (○), and 1-octene (▼) to ethylene in the feed. Polymerization condition : $T = 50\text{ }^\circ\text{C}$, $P = 1.2\text{ atm}$ (in the case of 1-hexene and 1-octene copolymerization with $NaY/MAO/Cp_2ZrCl_2$, $P = 8\text{ atm}$), $Al/Zr =$ (A) 1000 and (B) 3000.

The ethylene consumption rate with Cp_2ZrCl_2 in the presence of isobutylene as a comonomer drastically decreased (Fig. 3). This might come from the formation of less active species between isobutylene and Cp_2ZrCl_2 . An isobutylene-unit was not found in the polymer chain when the copolymer was analyzed by $^{13}\text{C-NMR}$, indicating that isobutylene coordinated to an active Zr center prevented ethylene from accessing the active site. However, ethylene consumption rates were little changed in the copolymerization of ethylene and isobutylene with $NaY/MAO/Cp_2ZrCl_2$ from those in ethylene homopolymerization, indicating that Cp_2ZrCl_2 confined inside supercages did not complex with isobutylene. This can be explained by the difficulty in diffusion of isobutylene into the supercages of NaY zeolites because its kinetic diameter is larger than the pore diameter of NaY preadsorbed with MAO. It can be concluded that the copolymerization rate should be strongly influenced by the diffusion of comonomer through the pores of NaY zeolite, and that the insertion of α -olefins into the polymer chain is less preferred in comparison with ethylene. This can be called as shape-selective copolymerization.

NMR, DSC and GPC studies offered further insights into the effect of confinement of active sites into supercages of NaY on the microstructure of the copolymer. Molecular weights of polymers prepared with $NaY/MAO/Cp_2ZrCl_2$ catalyst were larger than those of unsupported Cp_2ZrCl_2 . This could result from the suppression of β -hydride elimination through β -H agostic interaction between the H of the β carbon of the polymer chain and the metal due to the

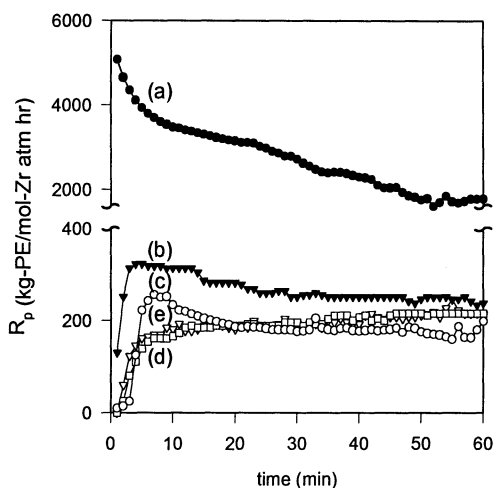


Fig. 3. The profile of ethylene consumption rate in ethylene/isobutylene copolymerization. Polymerization condition : $T = 50\text{ }^{\circ}\text{C}$, $P = 1.2\text{ atm}$, catalyst = Cp_2ZrCl_2 ((a) and (b)) and $\text{NaY/MAO/Cp}_2\text{ZrCl}_2$ ((c), (d) and (e)), $\text{Al/Zr} = 3000$ ((a) and (b)) and 1000 ((c), (d) and (e)), C_{i4}/C_2 molar ratio in feed = (a) 0.0 , (b) 1.0 , (c) 0.0 , (d) 0.5 , (e) 1.0 .

ellipsoidal contour of the supercage of the NaY zeolite [1]. It was also found that with $\text{NaY/MAO/Cp}_2\text{ZrCl}_2$ all the sequence distributions containing a propylene unit decreased, while only the [EEE] sequence distribution increased in comparison with those of unsupported Cp_2ZrCl_2 [9] (Table 2). This implies that a small pore diameter of NaY depresses the approach of more bulky propylene to the active sites, resulting in a decrease in the effective concentration of propylene during copolymerization. The product of r_E and r_P ($r_E r_P$) of $\text{NaY/MAO/Cp}_2\text{ZrCl}_2$ is larger than that of unsupported Cp_2ZrCl_2 . The $r_E r_P$ is unity for random sequences, higher than unity for blocky sequences, and lower than unity for alternating sequences of monomeric units in copolymers [10]. The $r_E r_P$ values indicate that the copolymer prepared with $\text{NaY/MAO/Cp}_2\text{ZrCl}_2$ was more blocky than that with homogeneous Cp_2ZrCl_2 catalyst. The number average sequence lengths of ethylene (n_E) of copolymers prepared with $\text{NaY/MAO/Cp}_2\text{ZrCl}_2$ were larger than that with Cp_2ZrCl_2 , providing another evidence of shape selectivity in ethylene/ α -olefin copolymerization.

Ethylene-propylene copolymers are characterized by a complicated melting behavior involving asymmetric broadening of the melting peak in the low temperature range (Fig. 4). This arises from the presence of families of macromolecules or a block of monomer units of various short chain branches [11]. The mechanical and thermal properties of copolymers are closely related to homogeneity in the comonomer distribution of the samples. To investigate the heterogeneity in the inter- and intramolecular distribution of comonomer, successive annealing of polymer was conducted (Fig. 5). Polymer samples were

Table 2. Chain sequence distribution, average sequence length, and reactivity ratio of ethylene-propylene copolymers obtained with NaY/MAO/Cp₂ZrCl₂ and unsupported Cp₂ZrCl₂.^{a)}

| Catalyst | mol. ^{b)} | [P]/[E] in feed | EEE | EEP+ PEE | PEP | EPE | PPE+ EPP | PPP |
|---|--------------------|--------------------|-------|-------------|-------|-------|-------------|-------|
| NaY/MAO/ Cp ₂ ZrCl ₂ | Exp. | 0.5 | 0.981 | 0.013 | 0.000 | 0.006 | 0.001 | 0.000 |
| | Cal. | | 0.981 | 0.013 | 0.000 | 0.006 | 0.001 | 0.002 |
| Cp ₂ ZrCl ₂ | Exp. | 1.0 | 0.953 | 0.030 | 0.000 | 0.014 | 0.003 | 0.000 |
| | Cal. | | 0.953 | 0.030 | 0.000 | 0.014 | 0.003 | 0.007 |
| Cp ₂ ZrCl ₂ | Exp. | 0.5 | 0.913 | 0.057 | 0.000 | 0.026 | 0.004 | 0.000 |
| | Cal. | | 0.914 | 0.055 | 0.001 | 0.026 | 0.004 | 0.004 |
| | Exp. | 1.0 | 0.888 | 0.073 | 0.000 | 0.034 | 0.005 | 0.000 |
| | Cal. | | 0.890 | 0.070 | 0.001 | 0.034 | 0.004 | 0.004 |

| Catalyst | mol. ^{b)} | [P]/[E] in feed | EE | EP+ PE | PP | E | P | n _E ^{c)} | n _P | r _E ×r _P |
|---|--------------------|--------------------|-------|-----------|-------|-------|-------|------------------------------|----------------|--------------------------------|
| NaY/MAO/ Cp ₂ ZrCl ₂ | Exp. | 0.5 | 0.987 | 0.013 | 0.000 | 0.993 | 0.007 | 155 | 1.046 | 7.13 |
| | Cal. | | | | | | | | | |
| Cp ₂ ZrCl ₂ | Exp. | 1.0 | 0.968 | 0.030 | 0.001 | 0.983 | 0.017 | 64.8 | 1.093 | 5.95 |
| | Cal. | | | | | | | | | |
| Cp ₂ ZrCl ₂ | Exp. | 0.5 | 0.941 | 0.057 | 0.002 | 0.970 | 0.030 | 34.2 | 1.07 | 2.32 |
| | Cal. | | | | | | | | | |
| | Exp. | 1.0 | 0.925 | 0.073 | 0.002 | 0.961 | 0.039 | 26.3 | 1.065 | 1.64 |
| | Cal. | | | | | | | | | |

a) Polymerization conditions are indicated in Fig. 1 and 2.

b) Exp.; measured triad distribution, Cal.; Markovian statistics of first order.

c) The number average sequence length of continuing ethylene sequence.

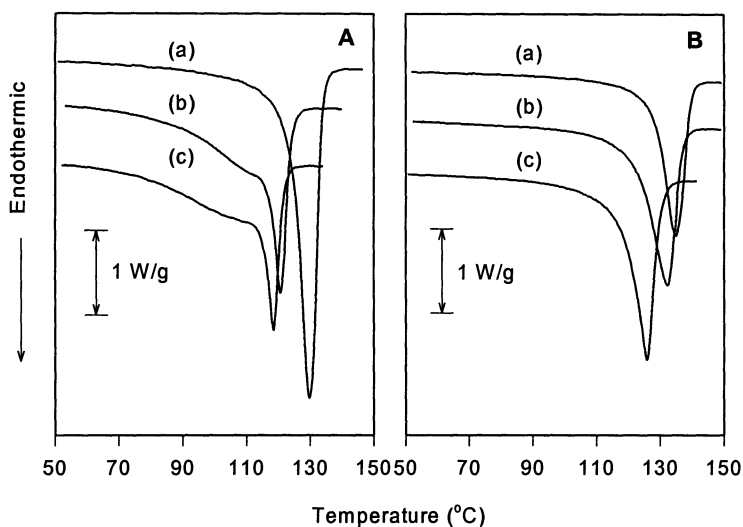


Fig. 4. DSC thermogram of ethylene/propylene copolymer prepared with Cp_2ZrCl_2 (A) and $NaY/MAO/Cp_2ZrCl_2$ (B). Polymerization condition : See Fig. 1. C_3/C_2 molar ratio in feed = (a) 0.0, (b) 0.5 and (c) 1.0.

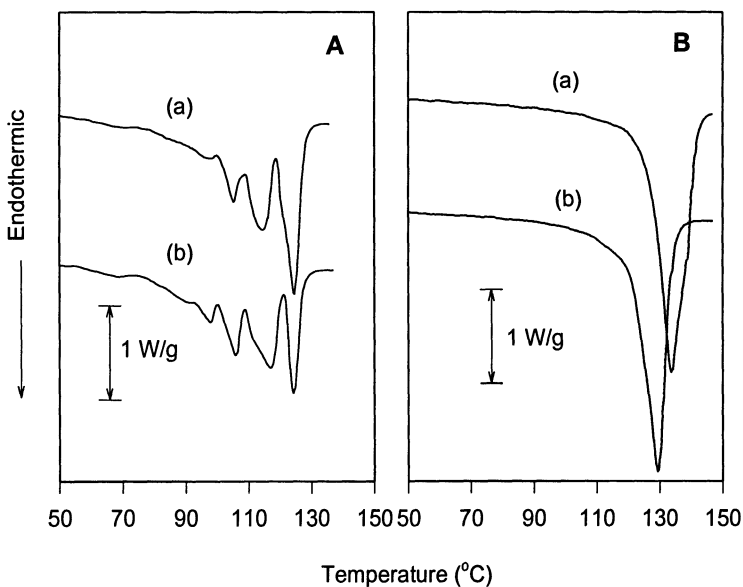


Fig. 5. DSC thermogram of ethylene/propylene copolymer prepared with Cp_2ZrCl_2 (A) and $NaY/MAO/Cp_2ZrCl_2$ (B). (C_3/C_2 molar ratio in the feed = 0.5 (a) and 1.0 (b))

melted at 160 °C in inert atmosphere for 20 min. and then were successively annealed at 125, 110, 100, 90, 80, 70, 60 and 30 °C for 12 hrs at each step. With a staged cooling procedure, ethylene-propylene copolymers prepared with unsupported Cp_2ZrCl_2 exhibit several well-resolved melting endotherms. These endotherms can be interpreted as the formation of crystallites of different thickness due to heterogeneity in comonomer distribution along polymer chains, and may be considered as representative of a homogeneous set of macromolecules or blocks with different short chain branches [12]. Those of $\text{NaY/MAO/Cp}_2\text{ZrCl}_2$ have only one melting endotherm, indicating a homogeneous inter- and intramolecular distribution of comonomer units.

This work suggests that the shape and diffusion of α -olefins should play a critical role in copolymerization due to the small pores of the NaY zeolite, which results in a change in apparent reactivity ratio. In the case of SiO_2 as a support, pore diameter distribution is wide and pore size is too large to affect the diffusion of various α -olefins into the active sites. Therefore, immobilization of metallocene catalyst onto the surface of silica did not show shape selectivity in ethylene/ α -olefin copolymerization [6]. The diffusivities of relatively large organic molecules in NaY zeolite are related to the molecular diameter and to the interaction of adsorbate molecules with the zeolite [3]. The difference in diffusivity arises from the steric hindrance through the pores of the NaY zeolite composed of a 12-membered oxygen ring [13]. The kinetic diameters of ethylene and α -olefin are 3.9 and larger than 4.5 Å, respectively [3]. Even though the NaY zeolite is fractured as polymerization progresses, the active sites are still surrounded by a part of the supercage and the pore structure. Therefore, shape selective copolymerization with $\text{NaY/MAO/Cp}_2\text{ZrCl}_2$ can be maintained. Furthermore, Cp_2ZrCl_2 confined inside a supercage imposes more steric hindrance between the polymer chain and the Zr active centers to make β -H elimination more difficult, resulting in higher molecular weight. Therefore, Cp_2ZrCl_2 confined inside supercage of NaY can copolymerize ethylene and comonomer into copolymer having narrow inter- and intramolecular comonomer distribution, higher molecular weight and less comonomer content as shown in Fig. 6.

Ship-in-Bottle Method to Encapsulate Metallocene in Zeolite

As shown in Fig. 7, a maximum activity was obtained about 2min with $\text{Me}_2\text{SiCp}_2\text{ZrCl}_2/\text{NaY/MAO}$ system, but the catalytic activity was drastically decreased later on. In case of $(\text{MeCp})_2\text{ZrCl}_2/\text{NaY/MAO}$ system, the activity increased slowly with polymerization time. The activity of $(\text{MeCp})_2\text{ZrCl}_2/\text{NaY}$ is larger than that of $\text{Me}_2\text{SiCp}_2\text{ZrCl}_2/\text{NaY}$, but the absolute magnitude of the catalytic activity was much smaller than that of unsupported $(\text{MeCp})_2\text{ZrCl}_2$. There are several reasons why the catalytic activity was low. First, when n-butyllithium reacted with metal complexes, LiCl salt was formed which can act as a poison to the catalytic center. Second, for each step, unreacted compound could occupy the supercage of NaY zeolite as inactive species. And the last, it was difficult to separate inactive or less active by-products formed in the supercage from the

desired product. However, these results indicate the possibility of preparing metallocene catalysts by ship-in-bottle synthesis method.

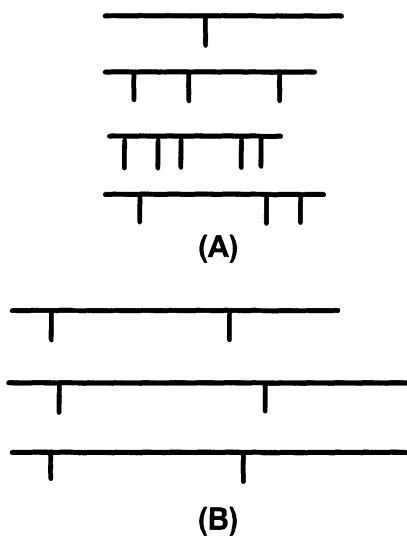
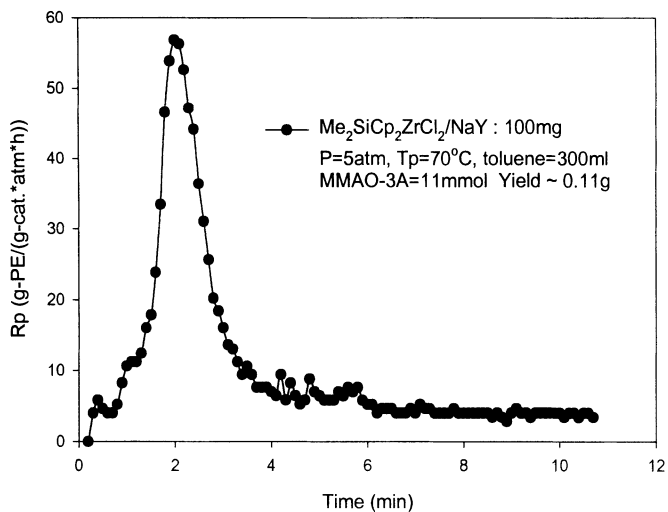
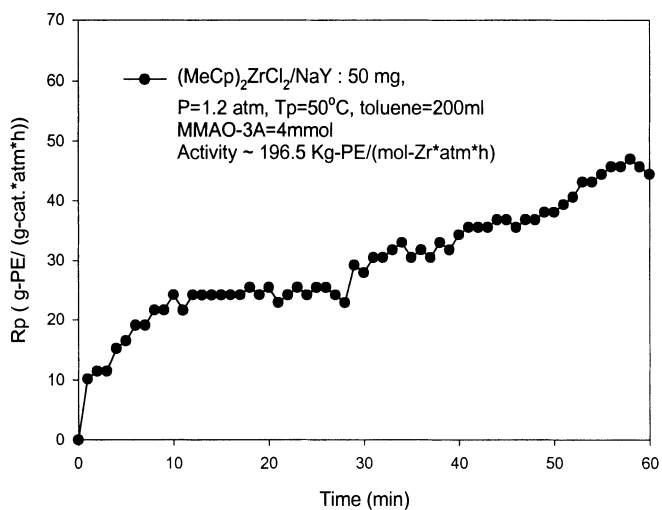


Fig. 6. Plausible molecular structure of copolymer prepared with Cp_2ZrCl_2 (A) and $\text{NaY/MAO/Cp}_2\text{ZrCl}_2$ (B).



(A)



(B)

Fig. 7. The profile of ethylene consumption rate in ethylene homopolymerization catalyzed over $\text{Me}_2\text{SiCp}_2\text{ZrCl}_2/\text{NaY}/\text{MAO}$ (A) and $(\text{MeCp})_2\text{ZrCl}_2/\text{NaY}/\text{MAO}$ (B).

Reference

- [1]. S.I. Woo, Y.S. Ko, T.K. Han, *Macromol. Rapid Commun.* **16**, 489(1995).
- [2]. Y.S. Ko, T.K. Han, J.W. Park, S.I. Woo, *Macromol. Rapid Commun.* **17**, 749 (1996).
- [3]. D.W. Breck, *Zeolite Molecular Sieves* (J. Wiley & Sons, New York, 1974).
- [4]. Sigmund M. Csicsery, *Zeolites* **4**, 202 (1984).
- [5]. S. Collins, W.M. Kelly, D. A. Holden, *Macromolecules* **25**, 1780 (1992).
- [6]. J.C.W. Chien, D. He, *J. Polym. Sci. Part A: Polym. Chem.* **29**, 1585 (1991).
- [7]. J.C.W. Chien, T. Nozaki, *J. Polym. Sci., Part A: Polym. Chem.* **31**, 227(1993).
- [8]. J. Koivumäki, J. Seppälä, *Macromolecules* **26**, 5535 (1993).
- [9]. J.C. Randall's paper, *JMS-REV. Makromol. Chem. Phys.* **C29(2&3)**, 201(1989).
- [10]. M. Kakugo, Y. Naito, K. Mizunuma, T. Miyatake, *Makromol. Chem.* **190**, 849 (1989).
- [11]. F. Defoor, G. Groeninckx, P. Schouterdeu, B.V. Heijden, *Polymer*, **33**, 3878(1992).
- [12]. E. Adisson, M. Ribeiro, A. Deffieux, M. Fontanille, *Polymer*, **33**, 20, 4337(1992).
- [13]. D.M. Ruthven, *Principles of Adsorption and Adsorption Processes* (J. Wiley & Sons, New York, 1984).

DEVELOPMENT OF SUPPORTED SINGLE-SITE CATALYSTS AND PRODUCED POLYETHYLENE

A. Muñoz-Escalona, L. Méndez, J. Sancho, P. Lafuente, B. Peña, W. Michiels, G. Hidalgo and M. F. Martínez-Nuñez

REPSOL, R & D, c/ Embajadores, 183. 28045 Madrid. Spain
e-mail: aescalonam@repsol.es

ABSTRACT

Following the development of conventional multi-site Ziegler-Natta catalysts during the 60-80s, large academic and industrial efforts are being devoted to the design and synthesis of a well defined new family of single-site olefin polymerization catalysts, with the group 4 metallocene class of compounds receiving the most attention. Recently, there is also a growing interest in the late transition metal catalysts based on nickel, palladium, iron and cobalt compounds.

The new generation of single-site catalysts can really impact the polyolefin industry if they can be used as dropped into large capacity production plants and produce resins that can be processed in the existing equipment without major modifications. Both requirements should be achieved at a favorable cost / performance balance respect to conventional polyolefin technologies. The main objectives of the present contribution is to address two of the most important issues the single-site catalysts technology is currently facing, namely, development of methods for supporting the new single-site catalysts suitable for dropping into slurry and gas-phase processes and the development of polyethylene with better properties and good processability. Firstly, after describing existing procedures for the preparation of supported metallocene catalysts, the method developed by Repsol is then followed. Repsol proprietary technology is based on functionalized metallocene that can react with appropriate carriers producing supported catalysts exhibiting: high activities (while retaining the essential characteristics of their homogeneous analogs), high stability, no reactor fouling or sheeting, good morphology (polymers replicate the catalyst morphology) and bulk densities of the resulting polymers. This method is also very suitable for the design of well defined multi-site catalysts that produce tailor-made bimodal or multimodal resins (either polymer molecular weight and/or chemical composition distributions) with controlled polymer architectures and showing good processability.

Finally, the advantages and disadvantages of supporting nickel α -diimine and iron pyridine bis-imine catalysts will be discussed together with the produced polyethylene.

INTRODUCTION.

Since the discovery of metallocene catalysts by Sinn and Kaminsky in 1980¹, they have caught the interest of the polymer industries due to their potential in producing tailor-made polymers. Metallocene catalysts have many advantage over conventional Ziegler-Natta or chromium catalysts. They are well defined organometallic transition metals compounds with only one active site for the polymerization reaction (single-site catalysts), while conventional catalysts are formed by complex chemical reactions leading to the formation of chemically ill defined multiple active centers, each of them with its own ability for (co)polymerization, transfer and termination rates, producing polymers with heterogeneous molecular and chemical composition. In contrast, single-site catalysts produce very homogeneous polymers with narrow molar weight distribution (MWD) (polydispersity of about 2) as well as chemical composition distribution (CCD). The development of single-site catalysts for olefins polymerization started in 1980 with metallocene catalysts (Fig.1), followed by the new single-site catalysts based on Ni, Pd, Fe and Co²⁻⁵, which have made their appearance recently in the polyolefin arena. The Ni diimine derivatives activated by MAO are capable of producing hyper-branched polyethylene², while the Pd based catalysts are capable of introduce polar monomers in the polymer chain³ producing functionalized polyolefin. More recently, during this year, high active catalysts based on substituted tridentate pyridine bis-imine ligands coordinated to Fe and Co have been reported^{4,5}.

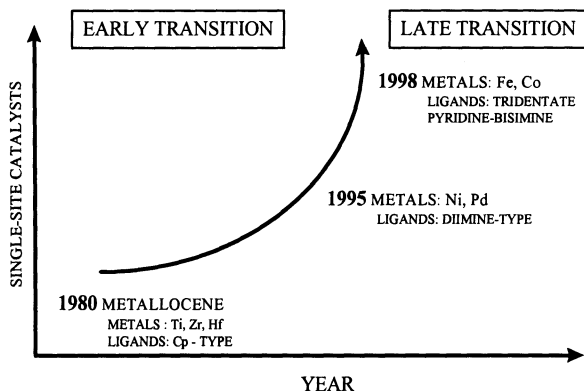


Fig. 1. Evolution of single-site catalysts for olefins polymerization

Conventional catalysts are solid substances (e.g. $\text{TiCl}_3\text{xAlCl}_3$, $\alpha\text{-TiCl}_3$, TiCl_4 , MgCl_2 and Cr/SiO_2)⁶, which are suited for the used in the slurry or gas-phase polymerization processes. To be dropped in slurry or gas phase processes, single-site catalysts need to be supported on appropriate carriers

To prepare supported metallocene catalysts different approaches have employed. First, we will describe briefly the state-of-the art of the methods for supporting metallocene catalysts, discussing the advantages and disadvantages of

each methods. Next, we will describe the method developed by Repsol based on the reaction of functionalized metallocene compounds with chemical groups attached to the carriers. Then, we will address the issue of producing polyethylene resins with controlled properties. We present, also, comparative results produced with soluble and heterogeneous single-site supported catalysts based on substituted nickel α -diimine compounds in the ethylene polymerization and their potential to produce low density polyethylene resins without the need of α -olefins as comonomer. Finally, preliminary results obtained with supported and unsupported iron pyridine bis-imine single-site catalysts are presented.

SUPPORTED SINGLE-SITE METALLOCENE CATALYSTS.

Supported metallocene catalysts can be prepared by a number of methods⁷, summarized as followed:

- I. Direct absorption on existing inorganic support materials: SiO₂, Al₂O₃, zeolite, MgCl₂, etc.
- II. Absorption on silica modified by reaction with: MAO, R₃Al, or others compounds
- III. Precontacting metallocene and MAO followed by subsequent absorption on silica or other carriers
- IV. Absorption on polymeric MAO produced by reacting with different compounds: bisphenol A, diol, p-hydroquinone, etc.
- V. Direct synthesis of metallocenes on carriers e.g.: SiO₂, Polymers (polysiloxane, polystyrene), etc.

Among them, the most investigated methods are based on the direct absorption of the metallocene on inorganic support materials (Method I)⁸⁻¹⁴ or on carriers previously modified or "passivated" by treatment with MAO (Method II)¹⁵⁻²¹. The other methods (III, IV and V) have been less employed²²⁻²⁶.

Method I, consisting in the direct reaction or absorption of metallocene compounds on silica, is the first and mostly used preparatory routes for supporting metallocene. Most of the fundamental understanding of the reactions that take place between the metallocene and the silica is due to the contribution of Marks and coworkers²⁷. Depending on the calcination temperature of the silica before supporting the metallocene, different complexes can be formed on the surface, some of them are schematically illustrated in fig.2.

μ -Oxo complexes (type A species) covalently bonded to the silica are believed to be inactive in polymerization, while ionic complexes weakly attached ("cation-like" type D species) in a concentration of about 1% are active. Interaction of metallocene compounds with silica surface generates other complexes (Type B). Depending on the Brönsted acidity of the silica, the absorption of the metallocene can be accompanied by significant decomposition, when reacting with surface vicinal hydroxyl groups giving double covalent bonded inactive type B species and free ligands. We have proved this reaction by following the decomposition of absorbed metallocene using thermogravimetric analysis coupled to mass spectrometry. It was observed that during catalysts preparation and by increasing

the temperature, the metallocene start to decompose gradually releasing the ligands. For example, when Cp_2ZrCl_2 is supported on silica, cyclopentadienyl ligands were observed to evolve at about 100°C reaching a maximum at 150°C . For this reason mild preparation conditions should be employed to obtain supported metallocene catalysts by direct absorption on silica or Al_2O_3 type carriers. Similar observations have been reported by Collin et al.²⁸. Additionally, type C species could also be formed when large amounts of metallocene are loaded on silica.

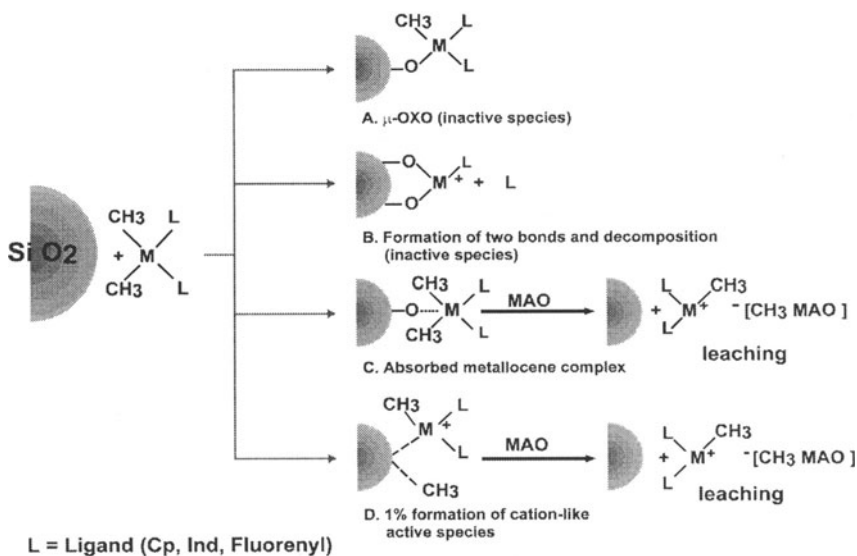


Fig. 2. Proposed reactions describing direct absorption of metallocene on silica

Taking into account all the reactions described before, it can be seen that only a small fraction of the total absorbed metallocene is actually active in olefin polymerization. Therefore, it is not surprising that activities found for this catalysts is roughly one or two orders of magnitude lower compared to their homogeneous analogs. Finally, if MAO is added to the reaction medium as cocatalyst for polymerizations, desorption of the metallocene due to the leaching of the weakly anchored active complexes C and D has been observed, producing certain amount of soluble species. The polymerization then takes place part in solution and part over the support.

However, some benefits can be obtained by direct support of metallocene catalysts over silica. Thus, polymers with higher molecular weight are obtained, compared to those produced by soluble analogs and lower amount of MAO is needed for the polymerization.

Method II is based in the "passivation" of the silica by chemical treatment (e.g. with MAO or trimethyl aluminum) before supporting the metallocene. Thus, by using silica covered with MAO the deleterious interaction of the metallocene with the Brönsted and Lewis groups of the silica can be avoided.

First at all, the most important factors to be considered are the morphology of the resulting MAO modified support and the distribution of the aluminum across the particle. In fig. 3 the morphology of a commercially high loaded silica (23% of Al content) is shown.

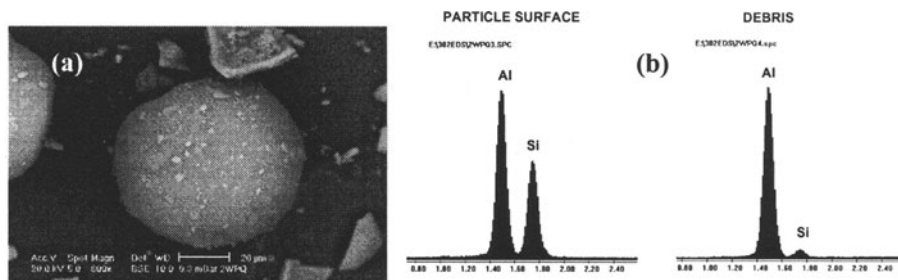


Fig. 3. (a) Morphology of commercial MAO SiO_2 and (b) EDX analysis

It can be observed that the morphology is not uniform. There are irregular fine particles present together with well formed spherical particles. By EDX analysis, it could be shown that unlike the spherical particles, the irregular fine particles are formed by practically pure Al (fig.3b). The debris come from layers of practically pure MAO covering the silica particles that detach from the rest of the particle²⁹. These can be removed by washing them with toluene. In order to examine the distribution of the aluminum across the silica particle, the commercial modified silica were embedded in epoxy resin and sectioned using a microtome provided with a diamond knife³⁰ (fig. 4a). The cross sectioned particles were analyzed under scanning electron microscope equipped with an energy dispersive X-ray analysis detector³¹. Semi-quantitative Al distributions were obtained by EDX point by point analysis across the particles (fig. 4b). The following observations can be made:

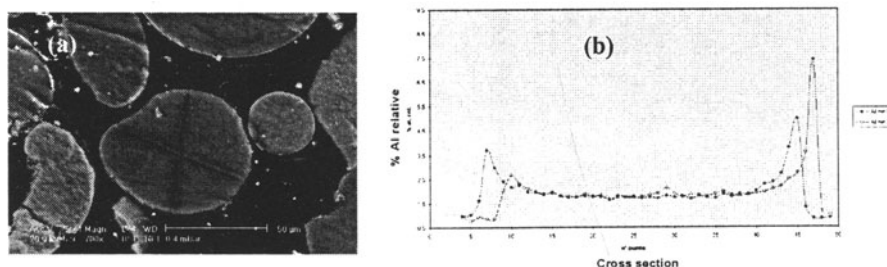


Fig. 4. Cross section of MAO/ SiO_2 (a) morphology (b) EDX analysis

1°. In the big particles the Al is not uniformly distributed across the section. The highest concentrations of Al were found on the surface and decreases inside of particles³²⁻³³. 2°. Small particles detached from the bigger spherical silica particles

are formed mostly of Al. It means, that the MAO is not strongly anchored to the SiO_2 .

After the absorption of MAO on the silica, catalysts are usually prepared by addition of the metallocene compound to the support. It is assumed that the immobilization of the metallocene on the MAO modified silicas proceeds through extraction of methide (or Cl) by the anchored MAO forming a “cation-like” metallocenium active species, so that no additional MAO is needed for activation (single-phase catalyst). In fig. 5(a), the scheme describing this procedure is presented.

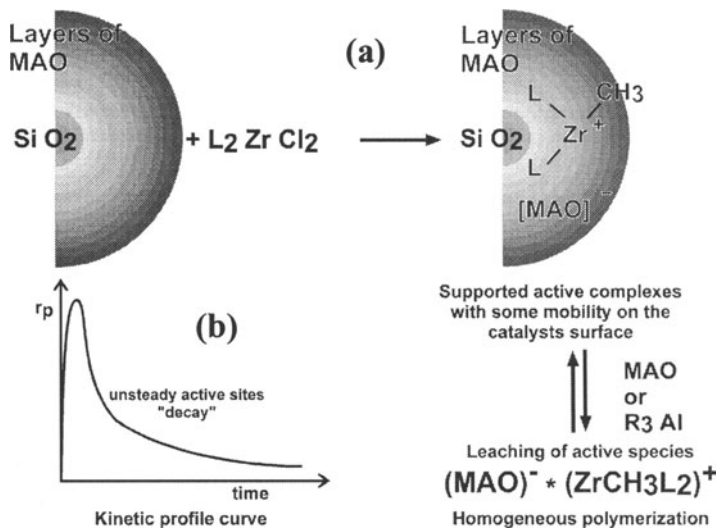


Fig. 5. (a) Proposed reactions describing formation of single-site metallocene catalysts of MAO/SiO₂; (b) Polymerization kinetic

As the metallocene complexes are bonded to the support by loosely ionic interaction, they can “float” over the MAO¹⁵ resembling, therefore, to homogeneous systems. The result is a more active catalytic system, but still lower than for the soluble or homogeneous catalysts. Due to the mobility of the active species, bimolecular deactivation can occur, producing polymers with lower molecular weights (MW) than polymers obtained with catalysts prepared with Method I, but similar to those obtained in solution polymerization. Also, they tend to give decay type kinetic curves similar to those found with soluble catalysts (see fig.5b).

The question is whether the polymerization takes place on the supported catalyst or in solution. To answer this question comparative leaching of catalysts prepared by Method I and II were performed by extraction using a solution of MAO in toluene. The extracted liquid fractions and the solid catalysts were used for polymerization after adding more MAO for activation³⁴. From the amount of polyethylene produced with the solid catalysts and filtered solutions the following conclusions can be drawn:

1°. Leaching was found to occur in both Methods (I and II). Catalysts prepared by Method I give lower leaching than Method II. Catalysts prepared by Method II are more active than those prepared by Method I.

Finally, due to the uneven distribution of MAO in modified MAO/SiO₂ there is higher concentration of the catalytic active complexes in the outer layers of the particles compared to the inner part. As a consequence, polymerization takes place in the outer layers of the catalyst and gradually decreases toward the center of the particles, giving rise to hollow and irregular polymer particles as a consequence of non-uniform catalyst fragmentation³³. Polymer particles grow layer by layer as represented in fig. 6.

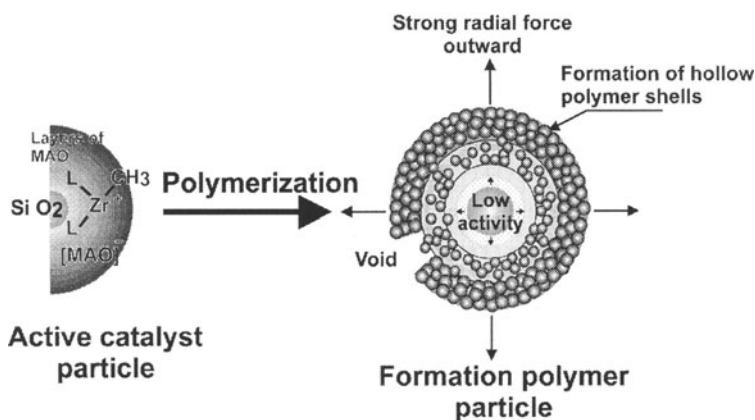


Fig. 6. (a) Proposed reactions describing formation of single-site metallocene catalysts of MAO/SiO₂; (b) Polymerization kinetic

The rapidly expanding outer layers are not followed by the less active growing inner part, resulting in a poorly filled polymer particles with not very high bulk density. The results are in accordance with the model proposed by Bonini et al.³⁵ to describe ethylene polymerization using this type of catalysts. Very fast catalyst fragmentation destroys the catalyst particles during the early stages of growth, producing fine polymer particles. Due to the mobility of the metallocene, migration from inside to the surface of the catalyst particles and to the reactor walls can take place leading to reactor fouling or sheeting.

SUPPORTING SINGLE-SITE FUNCTIONALIZED METALLOCENE CATALYSTS.

After evaluating the previously described preparatory methods and in order to overcome the mentioned disadvantages, we chose at Repsol a different approach to prepare supported metallocene catalysts. The method is based on the synthesis of metallocenes with functional chemical groups and supporting them by reaction

with organic and inorganic carriers (as such or previously modified with compounds having additional functional chemical groups)³³. The reactivity between the functional groups of the carriers and the metallocenes have been carefully controlled so that the reaction is very selective. By choosing the suitable impregnation conditions and type of carriers (specially with big porous diameters) an even distribution of anchored metallocene catalysts across the particle carriers can be obtained. Polymers with good morphology, replicating the catalyst morphology were obtained. Replication factors of 100 times were obtained while for conventional catalysts usually replication factor of 10-20 have been reported³⁶. The metallocenes are covalently anchored to the carrier by different reactions as represented in fig. 7, avoiding possible leaching of the active complexes^{37, 38}.

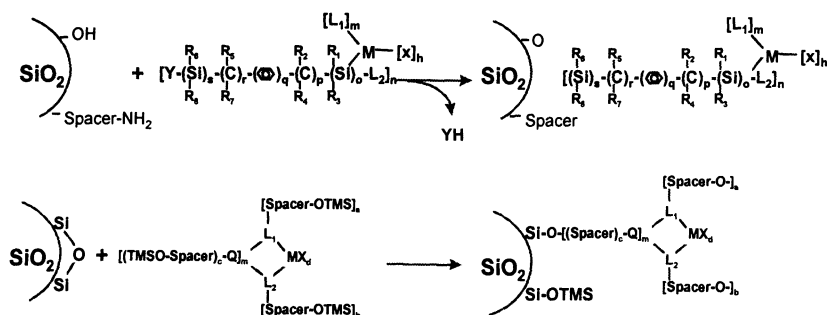


Fig. 7. Model reactions between SiO₂ and functionalized metallocenes

Due to the presence of spacers between the metallocene and the support a certain degree of mobility of the active species can be controlled but without bimolecular deactivation taking place. The numbers of functional groups attached to the metallocene and the length of the spacers between functional groups have a profound effect on the catalyst activities (see fig. 8).

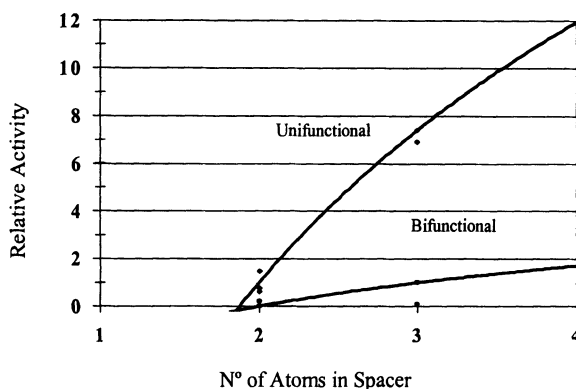


Fig. 8. Effect spacers length on catalytic activities

Thus, unfunctional metallocene are more active than bi-functional and metallocene with spacers with length of 2 atoms are less active than those with 3 and so on. Lee et al³⁹. have found similar results by introducing spacers between the silica surface and the metallocene. Activities nearly comparable to the homogeneous catalysts can be achieved. The catalysts display an initial build-up type kinetic curve, with a gradually accelerating part during fragmentation of the catalyst particles, followed by a long stationary period of particles growth, indicating very stable active species³³.

POLYETHYLENES PRODUCED WITH SUPPORTED SINGLE-SITE FUNTIONALIZED METALLOCENE.

Due to the fact that metallocene catalysts are single site catalysts, they produce polyethylenes with very narrow MWD (polydispersities about 2) compared to conventional Ziegler-Natta or chromium based polyethylenes. The result are resins with considerable processability problems. The difficulties in processing metallocene based polyethylenes are even more critical than LLDPE produced with conventional catalysts. Metallocene-catalyzed polyethylenes show melt flow instabilities (sharkskin and slip-stick or even volume melt fracture) when extruded through a capillary rheometer⁴⁰. This problem can be avoid by broadening the MWD of the PE by anchoring two or more different metallocene (dual or multi-sites supported metallocene catalysts) each of them giving their own molecular weight distribution, so that the resulting resin present bimodal or multimodal MWD⁴¹.

Mechanical properties can be also be controlled with high accuracy. This can be seen when comparing the tensile moduli of metallocene-catalyzed PEs (fig.9a) with the conventional ones as reported by Christ et al⁴², for narrow MW fractions of conventional PEs (fig. 9b).

It can be seen that the elastic modulus is mainly controlled by the density. Initial moduli for metallocene-catalyzed PEs are slightly higher than for conventional PEs with the same density. With only one metallocene catalysts, PEs with densities between 0.910 and 0.970 g/ml can be produced. The elastic moduli are depending from the density between 80 MPa and 1.000 MPa. Furthermore, the apparent moduli for amorphous and crystalline phase can be obtained by extrapolating the data in fig. 10a, to densities: $\rho_a = 0.85$ g/ml and $\rho_c = 1.003$, obtaining $E_a = 10$ MPa and $E_c = 7$ GPa, respectively. These value are of the same order of magnitude as the moduli for the amorphous and crystalline phase $E_a = 6$ MPa and $E_c = 7$ GPa, as calculated by different authors using conventional PEs (see reference 42). This give and indication of the potential of the metallocene catalysts for tailoring PE resins.

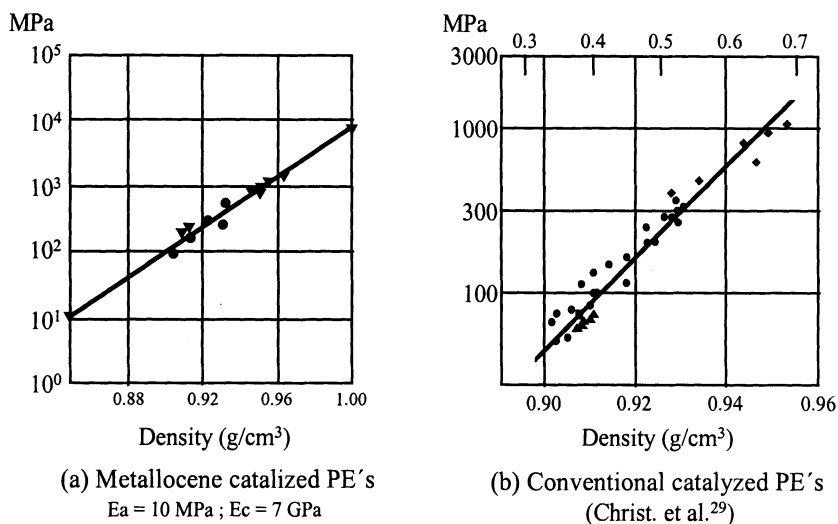
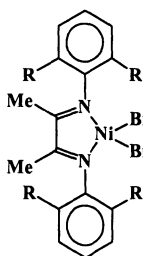


Fig. 9. Polyethylene design with supported single-site functionalized metallocene catalysts vs. Conventional products

SUPPORTED SINGLE-SITE Ni CATALYST.

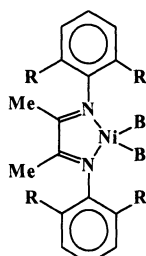
Ethylene polymerization was also carried out in *n*-heptane at 4,0 bar pressure using the following supported and unsupported Brookhart's type catalytic systems²:

Homogeneous catalyst



R = Me, ⁱPr MAO: Al/Ni = 700

Heterogeneous catalyst



R = Me, ⁱPr TIBA: Al/Ni = 600 (Total Al/Ni = 700)

For the preparation of heterogeneous catalysts the above mentioned **Method II** for supporting metallocene catalysts was used. Commercially available high loaded MAO/SiO₂ with a 23% of Al content was also used. Co-catalyst MAO was used for the soluble catalysts, and TIBA for the supported one. The polymerizations of ethylene were carried out in *n*-heptane at 4.0 bar using a Ni concentration of 0,0017 mmol. In case of the soluble homogeneous system, the active catalysts

were generated by addition of MAO at 700 Al/Ni ratio. As described before for supported catalysts, the active catalysts were directly formed after absorption on MAO/SiO₂, so that TIBA was added only as "scavenger". The total Al/Ni ratio was kept constant an equal to 700.

Ethylene polymerization activities obtained with both catalytic systems are comparable to those achieved with metallocene catalysts. Furthermore, activities decrease with polymerization temperature, as shown in fig. 10.

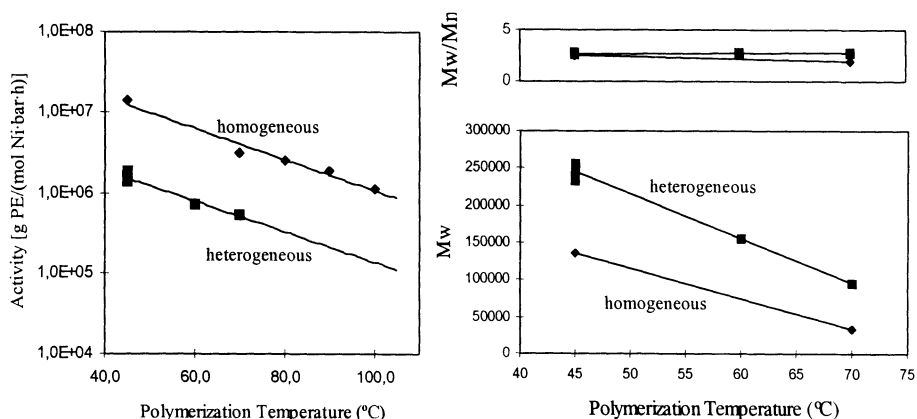


Fig. 10. Activity, Molecular Weight (Mw) & Polydispersity (Mw/Mn) vs. Polymerization temperature

Like metallocene catalysts for heterogeneous supported catalysts the polymerization activities are one order of magnitude lower compared to the homogeneous one. Also the polymer molecular weights follow the same tendency, e.g. supported or heterogeneous catalysts give higher molecular weight compared to homogeneous soluble catalysts (see fig. 10). With both catalytic systems molecular weights decrease with polymerization temperature due to favorable β -elimination reactions. Polydispersities (given as Mw/Mn) are around 2 confirming the single-site nature of the catalysts.

Due to the migratory insertion mechanism described by Brookhart et al.² for these type of catalysts highly branched polyethylene can be obtained. Among the type of branches, mostly short chain branched (SCB, Methyl, Ethyl, Butyl, Hexyl) are produced. Low concentration (0.9/1000C) of long chain branching (LCB) can be also formed. For both type of catalytic systems, branching contain increase with temperature as shown in fig. 11. Supported catalysts produce less branched compared to homogeneous catalysts, been methyl type branches the most frequently SCB found.

Regarding the polymer morphology, polymers produced with supported catalysts have granular forms while the polymers produced with the homogeneous, non-supported catalysts are not.

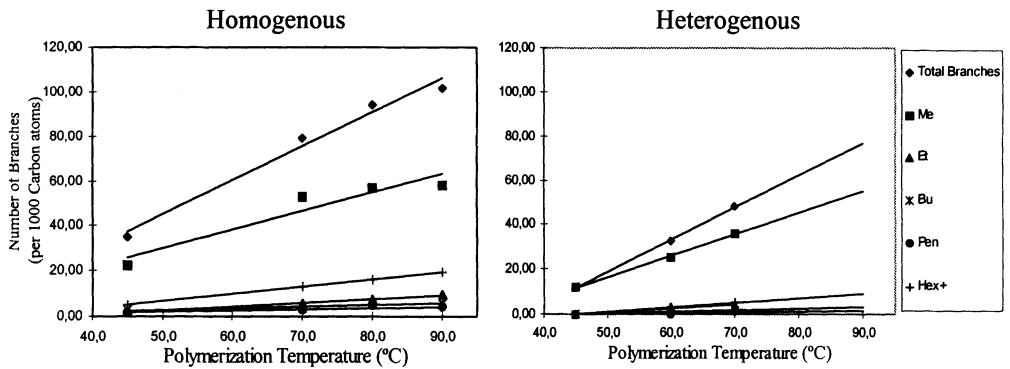


Fig. 11. Branching vs. Polymerization temperature for PEs obtained with Ni catalysts

POLYETHYLENES PRODUCED WITH Ni SINGLE-SITE CATALYSTS

Due to the fact that Ni catalysts produce highly branched polyethylene they present properties similar to products obtained by copolymerization of ethylene with α -olefins using metallocene catalysts.

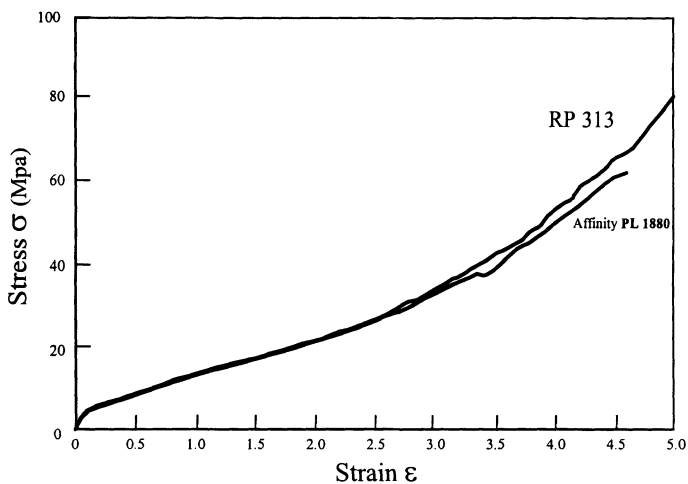


Fig. 12. Mechanical property of Ni catalyzed PEs and ethylene-octene-copolymer

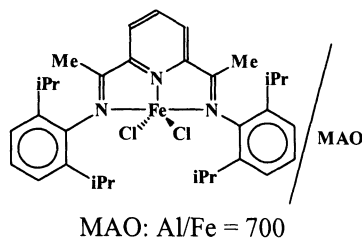
As example, in fig 12 the stress-strain curves of Affinity PL 1880 from Dow together with a product obtained by only ethylene polymerization with Ni single-site catalysts are presented. The Dow plastomers are produced by copolymerization of ethylene with 1-octene so that hexyl-type SCB are introduced. Both products have similar molecular weights (about $M_w = 118.000$), polydispersities (2.1) and densities of 0.901 g/cm^3 . The similarity in the stress-strain behavior is surprising good.

SUPPORTED Fe CATALYSTS.

Finally, the following iron catalysts, synthesized after Brookhart et al.⁵, were used unsupported and supported on MAO/SiO₂ for polymerization of ethylene

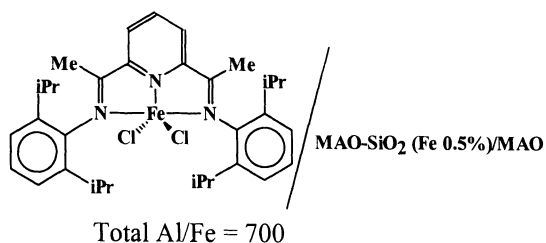
The type of method used for supporting the catalyst and the polymerization conditions are the same that those used for Ni based catalysts. However, the main difference of Fe supported catalysts, when using 23% Al high loaded MAO/SiO₂ as support is that they are not active using TIBA as scavenger. Therefore, in order to generate the active the catalysts additional MAO is needed in the reaction medium. Fig. 13, shows the dependence of the polymerization activities with temperature.

Homogenous catalytic system



Polymerization Conditions:
 [Fe] = 0.0033 mmol
 PC₂H₄ = 4.0 bar
 Solvent = Heptane

Heterogeneous catalytic system



Polymerization Conditions:
 [Fe] = .0132 mmol
 PC₂H₄ = 4.0 bar
 Solvent = Heptane

The polymerization activities are lower compared to Ni based catalysts. It can be also seen that for both catalytic systems the activities decrease as the temperature increases. In case of the homogeneous catalyst no activity was found at temperature over 70°C, probably due to catalyst decomposition. However, supported catalysts are more stable, so that activities were found at temperatures higher than 70°C.

Like Ni based catalysts, molecular weights of polymers produced with heterogeneous catalysts are considerable higher compared to soluble catalysts. However, with both catalytic systems (homo-and heterogeneous) the MWD of the polymers are very broad and even bimodals. Polydispersities were observed to

range between 4-27. These results are in agreement with Brookhart's finding (see reference 5). Therefore, more research is needed to improve the formation of the catalytic active species to produce single-site type catalysts, e.g. the use of different types of co-catalyst or anion for activation.

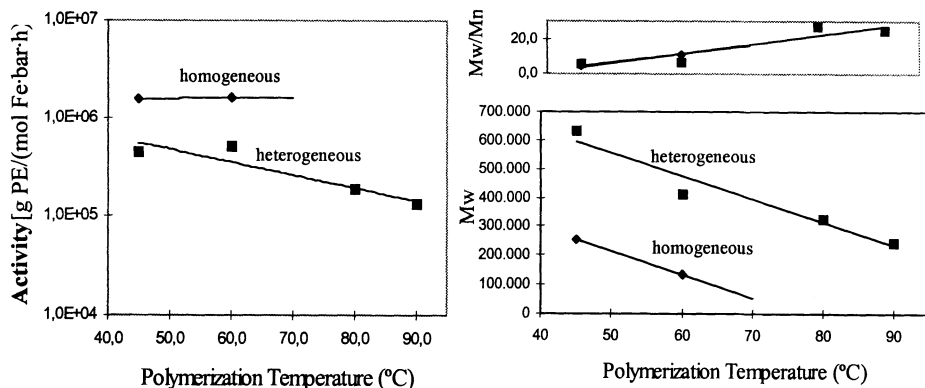


Fig. 13. Activity, Molecular weight (Mw) & Polydispersity (Mw/Mn) vs. Polymerization temperature

CONCLUSION

The following conclusions can be made:

- ❖ Single-site catalysts is a powerful molecular engineering tool for the development of a new generation of polyolefins
- ❖ Early transition metals metallocene catalysts have started this development, followed by late transition metals catalysts
- ❖ Single-site catalysts need however to be heterogeneized
- ❖ Among the heterogeneization methods, supporting functionalized metallocene catalysts open-up many opportunities compared to others methods (activity, stability, morphology, bimodals, etc.)
- ❖ Ni supported catalysts can be regarded as single-site catalyst but Fe based catalysts need further improvements
- ❖ Ni catalysts are very promising to produce branched PE's without comonomers, but developmental works is needed to control branching, sequencing, MW, etc.

REFERENCES.

- [1] Sinn, H. and Kaminsky, W., *Adv. Organomet. Chem.*, **18**, 99 (1980).
- [2] Johnson, L. K., Killian, Ch. M. and Brookhart, M. J. *Am. Chem. Soc.* **117**, 6414 (1995).
- [3] Johnson, L. K., Mecking, S. and Brookhart, M. J. *Am. Chem. Soc.* **118**, 267 (1996).
- [4] Britovsek, G. J. P., Gibson, V. C., Kimberley, B. S., Maddox, P. J. McTavish, S. J., Solan, G. A., White, J. P. and Williams, D. J. *Chem. Commun.* 849 (1998).
- [5] Boor, J., *Ziegler-Natta Catalysts and Polymerizations*. Academic Press, Inc. New York, 1979.
- [6] Small, B., L., Brookhart, M. and Bennett, A., M., *A. J. Am. Chem. Soc.* **120**, 4049 (1998)
- [7] Ribeiro, M. R., Deffieux, A. and Portela, M. F., *Ind. Eng. Chem. Res.*, **36**, 1224 (1997).
- [8] Pullukat, T. J., Shinomoto, R. and Gillings, C., *Proceeding POLYETHYLENE New Technology*, New Market. Institute of Materials, London (UK), 1997.
- [9] Chien, J. C. W. And He, D. J., *J. Polym. Sci. Part A: Polym. Chem.*, **29**, 1603 (1991).
- [10] Soga, K., Park, J. R. and Shiono, T., *Polym. Commun.* **32**, 310 (1991).
- [11] Tait, P. J. T., Abdulziz, I. A. and Paghaleh, A. S., *Metallocenes'95*, Brussels (Belgien), 1995.
- [12] Tait, P. J. T. and Monteiro, M. G. K. *Metcon,95*, Houston, TX (USA), 1995
- [13] Ciardelli, F., Altamore, A., Arribas, G., Conti, G., Massi, F. and Menconi, F. in "Catalyst Design for Taylor-Made Polyolefins, p. 257. Edited by K. Soga and M. Terano. Elsevier-Kodansha, Amsterdam, Tokyo, 1994.
- [14] Marques, M. F. V., Henriquez, C. A., Monteiro, J. L. F., Menezes, S. M. C. and Continho, F. B. *Polym. Bulletin*, **39**, 567 (1997).
- [15] Kamisky, W. And Renner, F., *Macromol. Chem. Rapid. Commun.* **14**, 239 (1993).
- [16] Chang, M., US Patent 5,006,6500 (1991) and Patent 5,086,025 (1992).
- [17] Soga, K. And Kaminaka, M., *Macromol. Chem. Rapid Commun.*, **13**, 221 (1992).
- [18] Janiak, Ch and Rieger, B. *Angew. Makrom. Chem.* **215**, 45 (1994).
- [19] Tait, P.T. and Monteiro, M., G. K. *Metcon,95*, Houston, TX (USA), 1995.
- [20] Ross, P., Meir, G. B., Samson, J., J., C. *macromol. Chem. Rapid. Commun.* **18**, 319 (1997).
- [21] Tait, P. J. T. and Ediaty, R., *Metcon'97*, Houston, TX (USA), 1997.
- [22] Ernst, E., Reussner, J. And Neissl, W. *Metcon'96*, Houston, TX (USA).
- [23] Jin, J., Uozumi, T. and Soga, K. *Macromol. Chem. Phys.*, **197**, 849 (1996).
- [24] Jin, J., Uozumi, T. and Soga, K., *Macromol. Rapid Commun.* **16**, 317 (1995).
- [25] Soga, K., Uozumi, T., Arai, T., Ban, H. T. and Kaji, E. *Metcon'97*, Houston, TX (USA).
- [26] Nishida, H., Uozumi, T., Arai, T. and Soga, K. *Macromol. Rapid Commun.* **16**, 821 (1995).
- [27] Marks, T. J., *Acc. Chem. Res.*, **25**, 57 (1992).
- [28] Collins, S., Kekky, W. M. and Holden, D. A., *Macromolecules*, **25**, 1780 (1992).
- [29] Muñoz-Escalona, A., Sancho, J., Peña, P., Michiels, W., Méndez, L., Marínez-Núñez, M., F., Lafuente, P. and Hidalgo, G. in *Proceeding of FLEXPO,98*. Chemical Market Resources, Inc. Houston, TX (USA) 1998.
- [30] Muñoz-Escalona, A., Hernández, J. G., Gallardo, J. A. and Sustic, A., in *Advances in Polyolefins*. Edited by R. B. Seymour and T. Cheng. Plenum Publishing, Co., New York (USA), p. 179 (1987).

- [31] Muñoz-Escalona, A., Villamizar, C. and Frias, P. in *Structure-Property Relationships in Polymeric Solid*. Edited by A. Hiltner. Plenum Press, New York (USA), p. 95 (1983).
- [32] Steinmetz, B., Tesche, B., Przybyla, C., Zechlin, J. And Fink G. *Acta Polymer.* **48**, 392 (1997).
- [33] Muñoz-Escalona, A., Hidalgo, G., Lafuente, P., Martínez-Nuñez, M. F., Méndez, L., Michiels, W., Peña, B. and Sancho, J., p.73, *Metallocenes Europe'98, Dusseldorf (Germany)*. 1998.
- [34] Semikolenova, N. V. and Zakharov, V. A., *Macromol. Chem. Phys.*, **198**, 2889 (1997).
- [35] Bonini, F., Fraaij, V. and Fink, G., *J. Polym. Sci. Part A: Polym. Chem.*, **33**, 2393 (1995).
- [36] Arzoumanides, G. G. and Karayannis, N. M. *Chemtech*, p. 43, July, 1993.
- [37] Michiels, W., Lafuente, P., Muñoz-Escalona, A., Hidalgo, G., Sancho, J. And Méndez, L. European Patent EP 757992 to Repsol. Sancho, J., Martín, C.,
- [38]. Hidalgo, G., Muñoz-Escalona, A. and Martínez-Nuñez, M. F. European Patent EP 839836 to Repsol.
- [39] Lee, D., Yoon, K. And Noh, S. *Macromol. Rapid Commun.* **18**, 427 (1997).
- [40] Vega, J. F., Muñoz-Escalona, A., Santamaría, A., Muñoz, M., E. and Lafuente, P. *Macromolecules*, **29**,960 (1996).
- [41] Muñoz-Escalona, A., Lafuente, P., Vega, J. F. and Santamaría, A. (to be published).
- [42] Christ, B., Fisher, C. J. and Howard, P. R., *Macromolecules*, **22**, 1709 (1989).

Ethylene Polymerization with the Heterogeneous Single Site CpIndZrCl₂ Catalyst

DONG-HO LEE

Department of Polymer Science, Engineering College, Kyungpook National University, Taegu 702-701, Korea . leedh@bh.kyungpook.ac.kr

SEOK KYUN NOH

School of Chemical Engineering and Technology, Yeungnam University, Kyoungsan, Korea

Abstract. For ethylene polymerization, the supported metallocene catalyst was prepared by anchoring CpIndZrCl₂ on silica with a hexamethyl-trisiloxane or pentamethylene spacer. The anchoring procedures exert a strong influence on the catalyst activity since the different anchoring methods lead to the formation of different structures of active sites. By the new anchoring route, it is possible to prepare a „heterogeneous single site“ catalyst which has only one catalyst structure on silica surface. The „heterogeneous single site“ catalyst exhibits a higher catalyst activity than other supported catalysts. In addition, the activity of the „heterogeneous single site“ catalyst was comparable to that of the unsupported homogeneous zirconocene at polymerization temperature of 70°C.

INTRODUCTION

Although the metallocene/methylaluminoxane (MAO) catalyst system exhibits some merits in comparison with the conventional heterogeneous Ziegler-Natta catalyst, the metallocene catalyst has to be immobilized on a support not only to be applicable for the existing fluidized bed process but also to control the morphology of the resulting polyolefin. In general, the immobilization of metallocenes on various supports has been accomplished by three different methods[1]: 1) direct impregnation of the metallocene on the support[2,3], 2) treatment of silica with MAO or alkylaluminum followed by reaction with the metallocene[4,5], 3) immobilization of an aryl ligand on the support followed by addition of the metal salt[6,7].

The beneficial points of the supported metallocene catalysts compared to the homogeneous ones are the enhancement of the molecular weight of the polymer and the applicability of smaller amounts of MAO as well as alkylaluminum. On the other hand, the heterogenized metallocenes lead to a reduction of catalytic activity compared to that of the corresponding soluble catalyst. In addition, the metal content of the immobilized metallocene is found to be very low (< 1.0 wt %).

We previously reported the examination of various polysiloxane-bridged dinuclear zirconocenes[8] which can be regarded as model compounds for a metallocene supported on silica. We have now proceeded to examine supported metallocenes possessing a spacer between the silica surface and the metallocene moiety. CpIndZrCl₂ anchored on silica with a spacer was prepared by reacting tosylated silica with the monoanion species holding the metallocene fragment through a spacer[9]. The catalyst activity of the spacer anchored metallocene was found to be much higher than that of the ordinarily supported one, but the synthesis of monoanion species was not simple.

Recently it has also been reported that the metallocene was supported on silica with a surface modified with silane compounds[10].

In this article, three different preparation methods were applied to anchor CpIndZrCl₂ on silica with hexamethyltrisiloxane or pentamethylene units as spacers. In order to detect any differences in catalyst properties resulting from the various anchoring methods, the zirconium content of the prepared catalyst was examined and the polymerization of ethylene was carried out. The experimental results can be explained by the plausible anchoring pathway of the zirconocene on the silica and the active site structure of the anchored zirconocene.

EXPERIMENTAL

Materials

Ethylene (Polymerization grade, 99.5 % purity, Korea Petrochemical Ind. Co., Korea) was dried by passing through two columns of P₂O₅, 1,5-dibromopentane (Aldrich Chem. Co., U.S.A.) and 1,5-dichlorohexamethyltrisiloxane (United Chem. Tech. Inc., U.S.A.) were distilled from calcium hydride just prior to use. CpNa (2.5 M solution in THF), TIOEt and n-BuLi were used as purchased from Aldrich Chem. Company. Methylaluminoxane (MAO) was commercial grade of modified MAO (MMAO-4, 6.4 wt %, Akzo, U.S.A.) and used as cocatalyst without further purification. Silica (SiO₂, Davidson, grade #952) was adopted after calcination at 600°C for 10 h. Toluene and tetrahydrofuran (Duksan Chem., Korea) were distilled from sodium-benzophenone complex.

Preparations of the Anchored Catalysts

As shown in Fig. 1, the supported catalysts on the basis of cyclopentadienylindenyl-zirconium dichloride (CpIndZrCl₂) anchored on silica with a hexamethyltrisiloxane spacer (ZATS) and a pentamethylene spacer (ZAPM) were prepared by three different procedures, Route 1, 2 and 3. The obtained catalysts were designated as ZATS-1, ZAPM-2, etc.

The silica-supported CpIndZrCl₂ (SiO₂/CpIndZrCl₂) was prepared by reacting zirconocene directly with a calcinated silica in toluene at 50°C for 15 h [2,3].

Polymerization

100 ml of toluene and the necessary amount of cocatalyst were added into a 400 ml glass reactor followed by saturation of ethylene under atmospheric pressure. With continuous flow of ethylene, the polymerization was initiated by injection of the catalyst. The produced polyethylene (PE) was precipitated in acidified methanol. The catalyst activity was calculated from the weight of polymer produced per mole of zirconium, hour and pressure of the monomer.

Measurements

The zirconium content of the catalysts prepared was measured by inductively coupled plasma emission spectrophotometry (ICP, JY38 Plus).

Thermal properties of PE were measured by differential scanning calorimetry (DSC, DuPont TA 2000) at 20°C/min. Molecular weight and molecular weight distribution were determined by gel-permeation chromatography (GPC, Waters 150C, Waters Associates) in 1,2,4-trichlorobenzene at 135°C, and data were analyzed using a polystyrene calibration curve.

RESULTS AND DISCUSSION

Zirconium Content of Anchored CpIndZrCl₂

The zirconium content of the various prepared catalysts was measured as shown in Table 1.

Table 1. Zirconium Content of Various Supported Catalysts

| Catalyst ¹ | Zr | |
|--|-----|-------------|
| | wt% | mmole/g-cat |
| SiO ₂ /CpIndZrCl ₂ | 0.8 | 0.09 |
| ZATS-1 | 0.6 | 0.07 |
| ZAPM-1 | 0.7 | 0.08 |
| ZATS-2 | 1.9 | 0.20 |
| ZAPM-2 | 2.0 | 0.21 |
| ZATS-3 | 3.4 | 0.39 |
| ZAPM-3 | 3.5 | 0.40 |

¹ ZATS-1 is the CpIndZrCl₂ catalyst anchored on silica with TS (hexamethyltrisiloxane spacer) by Route 1, and ZAPM-3 is the anchored catalyst with PM (pentamethylene spacer) by Route 3, etc.

It should be noted that the zirconium content of the anchored catalyst is strongly dependent on the anchoring method employed (Route 1 ; 0.6 - 0.7 wt % < Route 2 ; 1.9 - 2.0 wt % < Route 3 ; 3.4 - 3.5 wt %) and increases remarkably (5 - 6 times) with the new anchoring method (Route 3). It is also noteworthy that the anchoring method with more heterogeneous reaction steps leads to the formation of the catalyst with the lowest zirconium content. Another feature to be noted is that to our knowledge 3.5 wt % of zirconium attached to the silica surface is the largest amount ever reported. This result suggests positively that the characteristics of the heterogenized metallocene can be controlled by the newly employed method adopting a variety of types of ligands, metals, spacers, and silica.

In addition, it was observed that the anchored metallocenes made by the same procedure exhibited almost identical zirconium content regardless of the spacer structure. For example, ZATS-3 and ZAPM-3 obtained from the new Route 3 had a zirconium content of 3.4 wt % and 3.5 wt %, respectively.

The preparation procedures of the spacer anchoring and the proposed structure of the obtained catalysts are shown in Figure 1.

Route 1: Similar to reported procedures[11,12], the treatment of silica with *n*-BuLi resulted in the formation of -OLi sites and the lithiated silica was mixed with the dihalide (1) such as 1,5-dichlorohexamethyltrisiloxane or 1,5-dibromopentane to put in the TS or PM spacer group. After reaction with CpLi to incorporate the Cp ligand, the obtained silica was metallated with IndZrCl₃ to form the sites **A** as well as **B** by double anchoring. Site **B** was found to be less efficient in polymerization than site **A**. In addition, low active sites such as **C**, **D** and **E** can be formed by the reaction of IndZrCl₃ with the unconverted -OLi sites. These results clearly illustrate that many reaction steps under heterogeneous conditions lead to a drastic drop in the anchoring immobilization efficiency.

Route 2: The reaction between the tosylated silica and the dianion (2) of the spacer compound was performed followed by anchoring the zirconocene to form the active sites **A'** and **B'**. It can be assumed that site **B'** caused the decrease of the catalyst activity due to its low activity in spite of increased Zr content.

Route 3: The tosyl groups were reacted with the monoanion species to form the active site **A'**. The obtained catalyst had only one structure of active site so that it can be considered to be a real „heterogeneous single site“ catalyst.

The important feature to be noted for Route 3 is that there is no inefficient metallation step under heterogeneous conditions. The only heterogeneous reaction is the last step which is an anchoring step between the tosylated silica and the monoanion species connected with the metallocene fragment through a spacer.

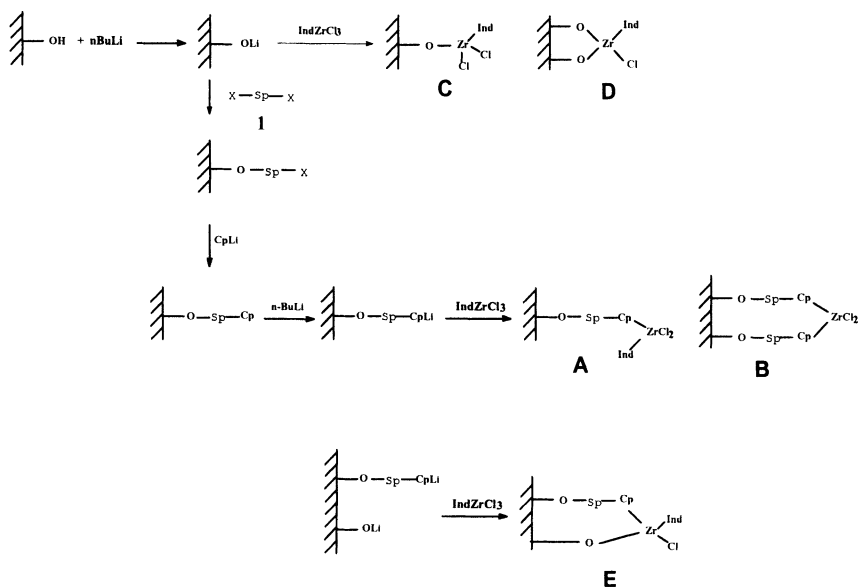
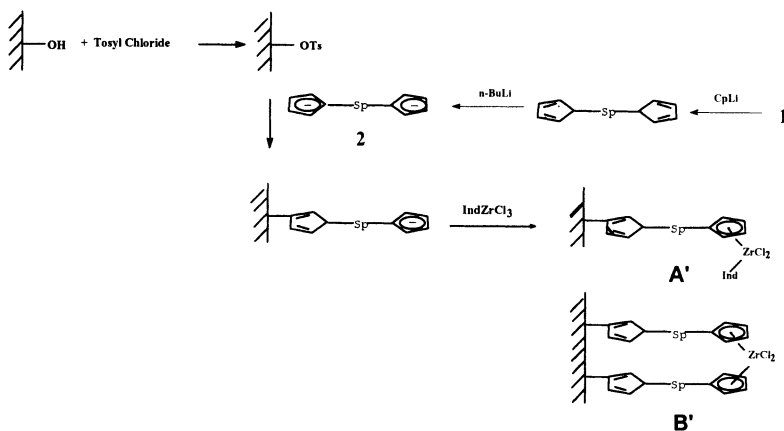
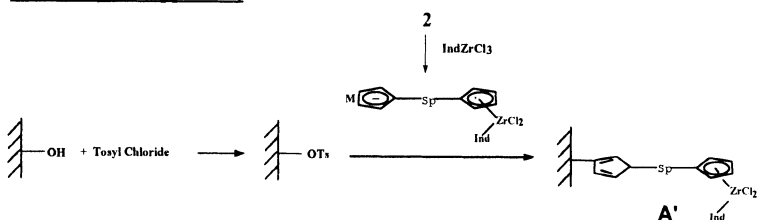
Route 1 (Known Procedure)**Route 2 (Modified Method)****Route 3 (New Approach)**

Figure 1. Plausible pathways and structures for the different preparation routes of anchoring CpIndZrCl₂ on silica

Polymerization Behaviors of the Anchored CpIndZrCl₂

To investigate the effect of the anchoring method on the catalytic properties the ethylene polymerization was carried out with the following catalysts and MMAO. These results were compared to the corresponding homogeneous CpIndZrCl₂ as well as the supported catalyst SiO₂/CpIndZrCl₂ which was obtained by a direct impregnation of CpIndZrCl₂ on SiO₂. The experiment was carried out with a constant [Al]/[Zr] ratio and the results are given in Table 2.

Table 2. Polymerization of Ethylene Initiated by Various Catalysts and MMAO

| Catalyst | Activity ^{a)} | M _w (x 10 ⁻³) | M _w /M _n | T _m (°C) |
|--|------------------------|--------------------------------------|--------------------------------|---------------------|
| CpIndZrCl ₂ | 1452 | 56 | 2.6 | 135 |
| SiO ₂ /CpIndZrCl ₂ | 162 | 102 | 3.4 | 135 |
| ZATS-1 | 289 | 96 | 3.0 | 135 |
| ZAPM-1 | 351 | 97 | 3.0 | 134 |
| ZATS-2 | 621 | 99 | 3.5 | 135 |
| ZAPM-2 | 864 | 101 | 3.4 | 134 |
| ZATS-3 | 1026 | 104 | 3.4 | 134 |
| ZAPM-3 | 1324 | 98 | 3.6 | 134 |

Polymerization conditions: [Zr] = 3.0 ~ 5.8 x 10⁻⁶ mol/L, [Al]/[Zr]=5000, 70 °C, 2h

a) Activity: kg-PE/mol-Zr · h · atm

The CpIndZrCl₂ anchored on silica with a hexamethyltrisiloxane or pentamethylene spacer (ZATS or ZAPM) shows a lower activity than the unsupported free CpIndZrCl₂. But the catalyst activity of ZATS and ZAPM is much higher than that of SiO₂/CpIndZrCl₂. In other words, the activity of the silica supported catalyst can be enhanced by introducing an appropriate spacer between the zirconocene fragment and the silica surface.

ZAPM exhibits a higher activity than ZATS. This result was interpreted in a way that the pentamethylene spacer acts as an electron donating alkyl group. The catalyst activity is increased by the electron enrichment of the metal center[13].

Among the anchored catalysts, ZATS-3 and ZAPM-3 generated by the new method of Route 3 exhibit two to three times higher activities than ZATS-1, 2 and ZAPM-1, 2 made by the other methods. This results can be understood taking into account that only one structure of site A' is obtained by Route 3 while less active sites such as B' can be formed following Route 2 as well as B, C, D and E following Route 1.

In summary, the catalyst activity of the ZATS and ZAPM series decreases in the following order: ZAPM-3 > ZATS-3 >> ZAPM-2 > ZATS-2 ~ ZAPM-1 > ZATS-1. The observed superiority of the new supporting method to the other ones could be a supporting evidence of the presence of a considerable amount of low active metal sites on the conventionally supported catalyst as mentioned previously.

At 70°C ZAPM-3 display almost identical activity as the unsupported homogeneous CpIndZrCl₂. This fact illustrates an increased tolerance of the supported catalyst towards higher temperatures and strongly suggest that the anchored catalyst maintains its thermal stability under the polymerization conditions.

The molecular weight (M_w) of PE obtained with the used catalysts decreases in the following order: SiO₂/CpIndZrCl₂ > ZATS ≥ ZAPM ≥ unsupported CpIndZrCl₂. The polydispersity index (M_w/M_n) of PE produced by ZATS and ZAPM is higher than that of the PE produced by CpIndZrCl₂. This can be explained by the different structures of the active sites as shown in Figure 1. Additionally the distances[13] between the active sites are randomly distributed. The melting point (T_m) of PE is almost independent of the types of catalyst. At a T_m of 135 °C indicates that the produced polymer is a linear PE.

The effects of the MMAO amount on the catalyst activity and M_w of PE were examined at 70°C and the results are given in Figure 2 and Figure 3, respectively.

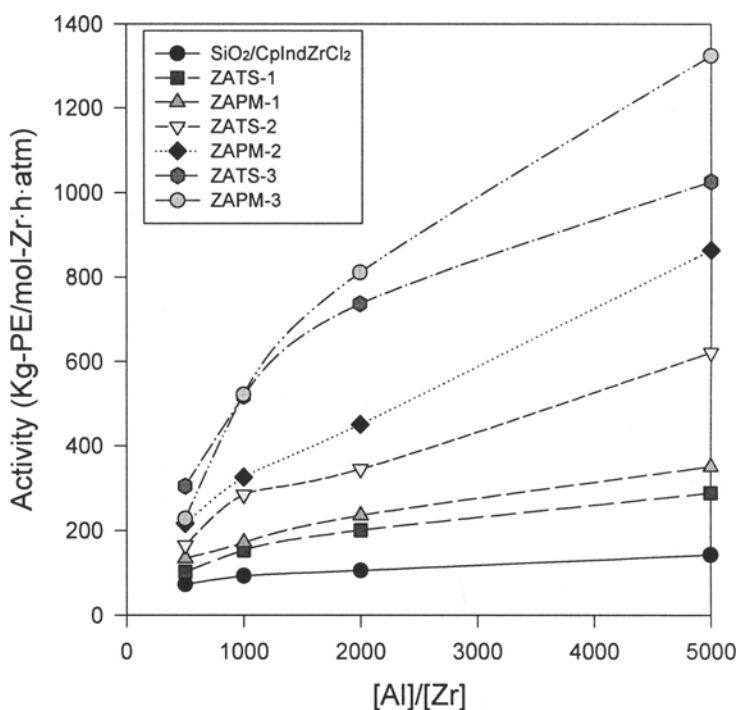


Figure 2. Effect of MMAO amount on the catalyst activity for ethylene polymerization with various supported catalysts.

Polymerization conditions : $[Zr] = 3.0 \sim 5.8 \times 10^{-6}$ mol/L, 70 °C, 2h.

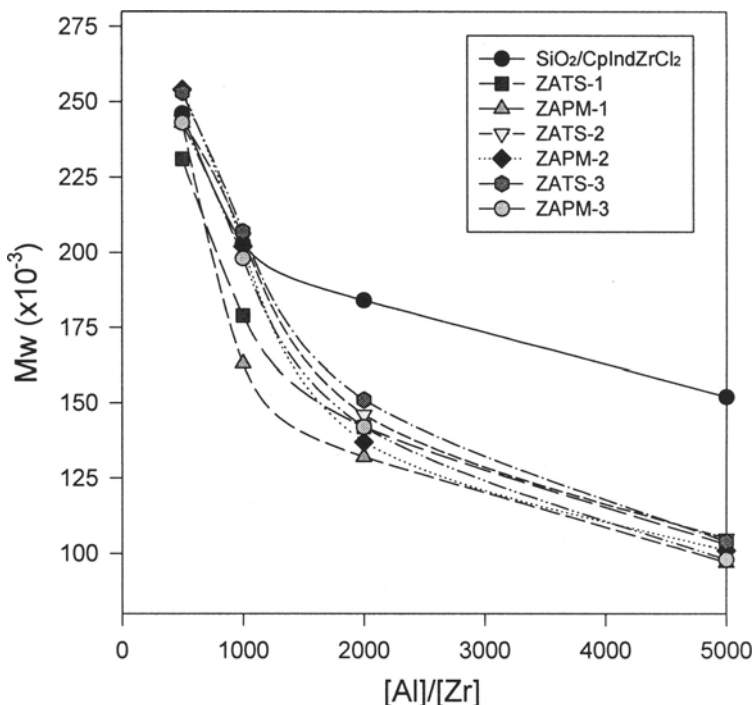


Figure 3. Effect of MMAO amount on the molecular weight of PE obtained with various supported catalysts.

Polymerization conditions : $[Zr] = 3.0 \sim 5.8 \times 10^{-6}$ mol/L, 70 °C, 2h.

As well-known, the catalyst activity increased with increasing MMAO amount as given in Figure 2. The increase in the catalyst activities of ZATS and ZAPM was stronger than that of $SiO_2/CpIndZrCl_2$. At $[Al]/[Zr]=5000$, the catalyst activity of ZAPM-3 was eight times higher than that of $SiO_2/CpIndZrCl_2$.

As shown in Figure 3, M_w of PE decreases with increasing MMAO amount due to the chain transfer reactions by MMAO[14]. The decrease in M_w of PE produced by ZATS and ZAPM was more significant than that of PE by $SiO_2/CpIndZrCl_2$.

Observation of the particle morphology by SEM confirmed that also for the anchored zirconocene the catalysts particle morphology is maintained by the polymer particle.

Judging from our experimental results the new method employed in this work can be one considered as a good alternative that allows the rapid practical application of heterogeneous metallocene catalysts.

REFERENCES

1. M.R. Ribeiro, A. Deffieux, and M.F. Portela, *Ind. Eng. Chem. Res.*, **36**, 1224 (1997)
2. W. Kaminsky and F. Renner, *Makromol. Rapid Commun.*, **14**, 239 (1994)
3. M. Kaminaka and K. Soga, *Makromol. Rapid Commun.*, **15**, 593 (1994)
4. J.C.W. Chien and D. He, *J. Polym. Sci.: Part A: Polym. Chem.*, **29**, 2603 (1991)
5. D.H. Lee, K.B. Yoon, and W.S. Huh, *Macromol. Symp.*, **97**, 185 (1995)
6. K. Soga, H.J. Kim, and T. Shiono, *Macromol. Chem. Phys.*, **195**, 3347 (1994)
7. K. Soga, T. Arai, B.T. Hoang and T. Uozumi, *Macromol. Rapid Commun.*, **16**, 905 (1995)
8. S.K. Noh, S.C. Kim, J.H. Kim, D.H. Lee, K.B. Yoon, H.B. Lee, S.W. Lee and W.S. Huh, *J. Polym. Sci.: Part A: Polym. Chem.*, **35**, 3717 (1997)
9. D.H. Lee, K.B. Yoon, and S.K. Noh, *Macromol. Rapid Commun.*, **18**, 427 (1997)
10. E.I. Iiskola, S. Timonen, T.T. Pakkanen, O. Haerki, P. Lehmus and J.V. Seppaelae, *Macromolecules*, **30**, 2853 (1997)
11. T.R. van den Ancker and C.L. Raston, *Organometallics*, **14**, 584 (1995)
12. H. Gao and R.J. Angelici, *J. Am. Chem. Soc.*, **119**, 6937 (1997)
13. P.C. Moehring and N.J. Coville, *J. Mol. Catal.*, **77**, 41 (1992)
14. J.C.W. Chien and H. De, *J. Polym. Sci., Polym. Chem. Ed.*, **29**, 1595 (1991)

The Impact of the Cocatalyst on the Polymerisation Behaviour of Supported Metallocenes

E. Ernst*, J. Reußner, P. Denifl

Borealis AG, St.-Peter-Str. 25, A-4021 Linz, Austria
Eberhard.Ernst@borealisgroup.com

Abstract

Recently a new supported metallocene catalyst system for the propylene polymerisation has been developed. For the activation of the catalyst common aluminium alkyls are necessary. The use of the cocatalysts has a great impact on the whole polymerisation behaviour. The aluminium alkyls effect the activation, the deactivation and the kinetic profile as well as the polymer properties of the resulting polypropylene.

The formation of a new kind of soluble MAO free metallocene catalyst as a result of the complex extraction from the catalyst particles by the cocatalyst has been assumed.

Introduction

The metallocene technology for polypropylene extends the range of technical materials by new property combinations. Homogeneous catalysts with MAO as activator generate fine polymer powders in liquid monomer processes, resulting in reactor fouling and separation problems in existing production plants. Therefore, the development of supported metallocene catalysts is a general requirement. For economic reasons the new catalyst systems should allow a simple replacement of the conventional Ziegler/Natta catalysts in existing plants without significant additional investment costs.

A new type of support has been developed by reaction of pre-dried silica with MAO and simultaneous cross-linking with aromatic diols [1-4]. The carrier material is a supported MAO network, which can be used as activator for the bridged metallocene dichlorides (figure 1).

The fixation is achieved by a simple addition of the dissolved complex and the formation of the cationic site. As metallocenes bisindenyl zirconium complexes with different substituents in 2 and 4 position and different bridges have been used (see table 1). The new catalysts enable an excellent control of the growing polypropylene particle morphology during polymerisation, but the pure supported metallocene catalysts show an unexpected low activity level in liquid propylene.

It has been found out that, the catalysts can be activated by common aluminium

alkyls. For technical processes it is necessary to use aluminium alkyls as cocatalysts and scavengers to ensure a constant catalyst performance and product quality.

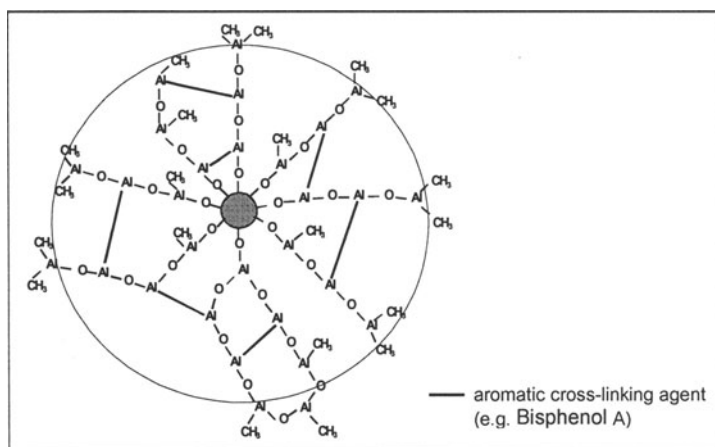


Fig. 1. Model of the silica supported organic cross-linked MAO network

The use of common aluminium alkyls, in combination with the new type of the discussed supported metallocene catalysts, has a great impact on the whole polymerisation behaviour.

The impact of the aluminium alkyl cocatalyst on the catalyst performance

The product of the catalyst formation reaction¹ is a free flowing powder. However, the pure solid catalyst shows a low activity in liquid propylene polymerisation as already pointed out. An addition of trialkyl aluminium compounds results in an enhancement of the catalyst activity by one or two orders of magnitude depending on the structure of the metallocene involved. The results

¹ Catalyst preparation procedure:

- pre-drying of Silica at 200 °C for 4 hours (material: Grace Davison Sylopol S5N)
- slurrying of Silica in toluene
- simultaneous feeding of MAO and Bisphenol A as divalent cross-linking agent
[Al(MAO)]:[OH] = 5 - 10 : 1; [Al(MAO)]:[Bisphenol A] = 15 - 25 : 1
- removal of unreacted, soluble aluminium compounds by extraction with toluene
- reaction of the cross-linked support with a solution of the metallocene in toluene gives a red-brown free flowing catalyst powder (containing 1 wt % of the metallocene)

of the polymerisation experiments using different supported complexes and aluminium alkyls are summarised in table 1.

Table 1. Activation of the supported metallocene catalyst by common aluminium alkyls

| supported metallocene | aluminium alkyl | Al(alkyl)/Zr mole ratio | kg PP/g cat.2h |
|--|-----------------|-------------------------|----------------|
| $\text{Me}_2\text{Si}(\text{Ind})_2\text{ZrCl}_2$ | none | 0 | 0,05 |
| $\text{Me}_2\text{Si}(\text{Ind})_2\text{ZrCl}_2$ | TIBAL | 400 | 2,7 |
| $\text{Me}_2\text{Si}(2\text{-Me-Ind})_2\text{ZrCl}_2$ | none | 0 | 0,01 |
| $\text{Me}_2\text{Si}(2\text{-Me-Ind})_2\text{ZrCl}_2$ | TIBAL | 400 | 5,8 |
| $(\text{Me}_3\text{Si})\text{MeSi}(2\text{-Me-4-Ph-Ind})_2\text{ZrCl}_2$ | none | 0 | 0,25 |
| $(\text{Me}_3\text{Si})\text{MeSi}(2\text{-me-4-ph-ind})_2\text{ZrCl}_2$ | TEAL | 600 | 1,0 |

Polymerisation conditions: liquid propylene; 70 °C; support Al(MAO) / Zr = 50-400

It is assumed that the low activity of the initial catalyst system derives from the well known methane formation during the fixation reaction. In this way inactive Zr-CH₂-Al bonds are formed [5]. Therefore, the function of the aluminium alkyl is the realkylation of the bonded zirconium complexes. In this sense the aluminium alkyl acts as real cocatalyst.

Table 2. The impact of the aluminium alkyl structure on the polymerisation behaviour of the supported $\text{rac}(\text{Me}_3\text{Si})\text{MeSi}(2\text{-Me-4-Ph-Ind})_2\text{ZrCl}_2$ system

| aluminium alkyl | Kg PP/ g cat * 2h | M _w [kg/mol] | M _w / M _n | T _m [°C] | XCS [%] |
|-----------------|-------------------|-------------------------|---------------------------------|---------------------|---------|
| TMAL | 1,0 | 271 | 4,8 | 152 | 3,0 |
| TEAL | 4,0 | 369 | 2,8 | 152 | 0,7 |
| TIBAL | 1,6 | 362 | 4,5 | 153 | 3,6 |
| TNHAL | 2,1 | 551 | 5,8 | 152 | 3,2 |
| DEAC | 0,1 | 72 | 5,6 | 147 | 3,3 |
| DEA(OEt) | 0,7 | 323 | 6,9 | 152 | 2,8 |

Polymerisation conditions: liquid propylene; 70 °C; mole ratio Al(alkyl):Zr = 400; 0,37 mole % hydrogen

If the aluminium alkyl acts as cocatalyst, as in the case of conventional supported titanium catalysts, there must be a strong influence of the structure of the aluminium alkyl on catalyst activity and polymer properties. Different types of commercial compounds have been tested under the same conditions. In table 2 the results are reported.

TEAL is the most effective cocatalyst for the supported $\text{Me}(\text{Me}_3\text{Si})\text{Si}$ -bis(2-methyl-4-phenylindenyl)zirconium dichloride system. At first, the structure of the cocatalyst determines the molecular weights by chain termination reactions. The generated fraction of xylene cold solubles (oligomers and atactic material) varies with the kind of cocatalyst and effects in this way the polydispersity M_w/M_n . As a consequence, the residual meso isomer of the supported metallocene is also influenced by the cocatalyst and causes side reactions in the presence of hydrogen.

In general, the activation of the catalyst also accelerates the deactivation. For many supported Z/N catalysts the cocatalyst titanium mole ratio has a significant impact on the catalyst performance [6,7]. The same effect can be noticed for the new types of supported metallocene catalysts. The results of comparative measurements for three different catalyst systems are depicted in figure 2.

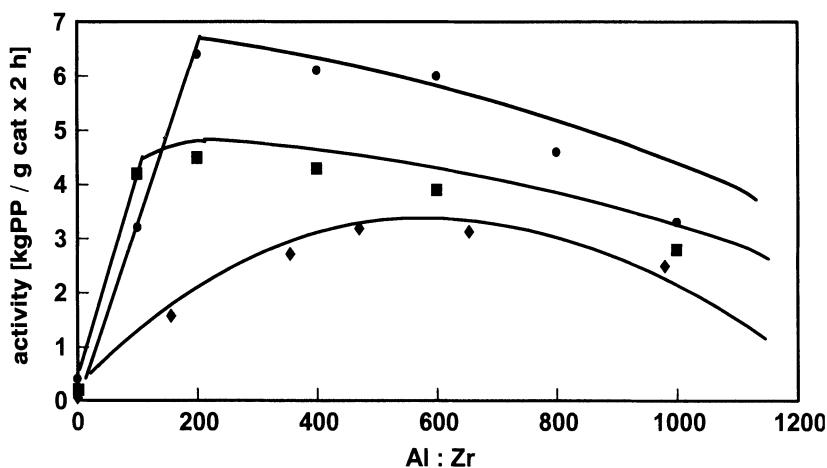


Fig. 2. Influence of the cocatalyst/zirconium mole ratio on the catalyst activity
 ● $\text{Me}_2\text{Si}(\text{2-Me-4-Ph-Ind})_2\text{ZrCl}_2$ ■ $\text{Me}(\text{Me}_3\text{Si})\text{Si}(\text{2-Me-4-Ph-Ind})_2\text{ZrCl}_2$ ◆ $\text{Me}_2\text{Si}(\text{2-Me-Ind})_2\text{ZrCl}_2$

For different bridged 2-methyl-4-phenylindenyl compounds the same profile has been observed. That of the 2-methylindenyl compound is somewhat broader. The activity maximum indicates the existence of a deactivation reaction caused by an excess of the cocatalyst compound. More information can be obtained from kinetic measurements. They have been performed under reduced pressure in hexane as solvent. Depending on the reaction conditions different kinetic profiles have been observed for the supported $\text{Me}_2\text{Si}(\text{2-Me-4-Ph-Ind})_2\text{ZrCl}_2$ system. The

results are reported in figure 3.

Preactivation means that the supported metallocene catalysts are treated with an aluminium alkyl solution before feeding the system into the reactor. If the activation reaction takes place, the kinetic profile changes dramatically. An additional activation in the first minutes of the polymerisation followed by a rapid deactivation of the active sites can be observed. These results correspond very well with the already mentioned realkylation reaction of the aluminium bonded zirconium complexes. The mechanism of the fast deactivation of the supported catalyst system is still unclear. It is believed that this effect is connected with further reactions of the metallocene with the cocatalyst. Hydrogen has also a detectable influence on the kinetic profile.

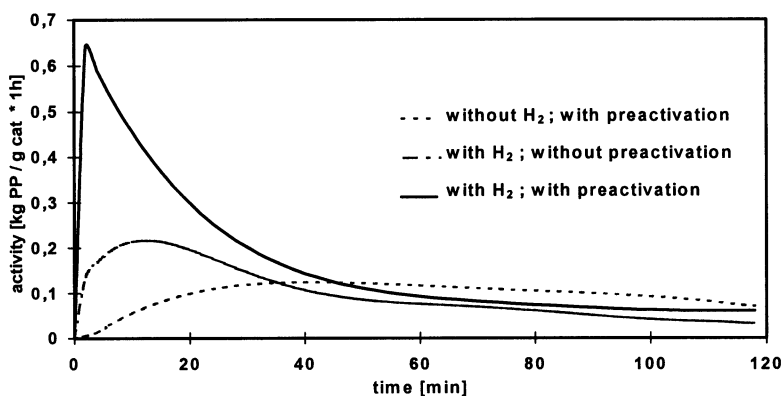


Fig. 3. The influence of catalyst preactivation on the kinetic profile (polymerisation conditions: 70°C; hexane; 5 bar propylene)

From the practical point of view metallocene leaching is the most critical influence of the aluminium alkyl. If the pure catalyst powder from the synthesis is treated with an aluminium alkyl solution, the aluminium partly extracts the metallocene from the catalyst surface. The extent of the leaching effect and the amount of generated soluble zirconium depends on the structure of the metallocene as well as on the kind of cocatalyst. It is lower for $\text{Me}_2\text{Si}(2\text{-Me-Ind})_2\text{ZrCl}_2$ than for the $\text{Me}_2\text{Si}(2\text{-Me-4-Ph-Ind})_2\text{ZrCl}_2$ system. And for the 4-phenyl substituted complex the effect is higher for TEAL than for TIBAL. The activity of the extracted metallocene/ AlR_3 mixture is very high. In table 3 the results are summarised.

To clear up if there is any influence of residual soluble MAO traces from the support synthesis the following correlations have been considered. The content of soluble aluminium deriving from the cross-linked MAO network is in the range of the detection limit of atomic absorption spectrometry measurements. On the one hand, if a small amount of MAO (mole ratio $\text{MAO}(\text{Al}) / \text{Zr} = 25$) is added, there is no visible influence on the catalyst activity. On the other hand, if the same

MAO(Al) / Zr mole ratio of around 1000 is used, the activity is much lower than for the metallocene / aluminium alkyl extract. Therefore, a qualitative new kind of MAO free metallocene catalyst has been generated by the extraction process.

The new soluble metallocene catalyst produces a fine polypropylene powder and can be regarded as source for reactor fouling in technical reactors.

Table 3. The interaction of the cocatalyst with the supported metallocene complex

| kind of soluble catalyst | Al / Zr mole ratio | soluble Zr [mole %] | kg PP/mmol Zr.2h |
|--|-----------------------|------------------------|---------------------|
| metallocene extracted from support by Al(alkyl) ₃ | | | |
| Me ₂ Si(2-Me-Ind) ₂ ZrCl ₂ / TIBAL | 1117 | 15 | 2 |
| Me ₂ Si(2-Me-4-Ph-Ind) ₂ ZrCl ₂ / TIBAL | 1097 | 24 | 100 |
| Me ₂ Si(2-Me-4-Ph-Ind) ₂ ZrCl ₂ / TIBAL Addition of MAO to the extract | 1097 + 25 | 24 | 100 |
| Me ₂ Si(2-Me-4-Ph-Ind) ₂ ZrCl ₂ / TEAL | 504 | 38 | 25 |
| soluble metallocene/MAO catalyst | | | |
| Me ₂ Si(2-Me-4-Ph-Ind) ₂ ZrCl ₂ / MAO | 1000 | 100 | 13 |
| Me ₂ Si(2-Me-4-Ph-Ind) ₂ ZrCl ₂ / MAO | 15000 | 100 | 1300 |
| supported metallocene catalyst activated with Al(alkyl) ₃ | | | |
| Me ₂ Si(2-Me-4-Ph-Ind) ₂ ZrCl ₂ / TEAL | 600 | n.d. | 220 |

n.d.: not determinable under polymerisation conditions

Conclusions

The aluminium alkyl acts not only as scavenger but also as a real cocatalyst. It has a strong impact on the catalyst performance. The following facts could be detected:

1. General activation of the supported metallocene

2. Additional increase of the activity for precontacting of catalyst and cocatalyst
3. Deactivation is caused by the interaction of the supported metallocene with the cocatalyst
4. The type of the cocatalyst influences the polymerisation behaviour and the polymer properties
5. Metallocene leaching is an undesirable side reaction for supported catalysts

References

- [1] E. Ernst, J. Reußner, W. Neißl
A new concept for supporting metallocenes
Metcon '96, June 1996, Houston, TX, USA
- [2] E. Ernst, J. Reußner, P. Denifl, W. Neißl
Metallocene polypropylene - alternative concepts for supported catalyst systems
SPO '97, September 1997, Houston, TX, USA
- [3] EP 685 494 A1 (1995) to PCD Polymere
- [4] EP 787 746 A1 (1996) to PCD Polymere
- [5] W. Kaminsky, A. Bark, R. Steiger
J. Molecular Catalysis 1992, 74, 109-119
- [6] L. Noristi, P.C. Barbè, G. Baruzzi
Macromol. Chem. 1991, 192, 1115-1127
- [7] P. Galli, P.C. Barbè, L. Norist
Die Angew. Makromol. Chem. 1994, 120, 73-90

Heterogenised MAO-free Metallocene Catalysts

Simon J. Lancaster, Sean M. O'Hara and Manfred Bochmann*

School of Chemistry, University of Leeds, Leeds LS2 9JT, UK

Abstract.

The treatment of dehydroxylated silica with $B(C_6F_5)_3$ in the presence of dimethylaniline results in borato-modified silica of the approximate composition $[HNMe_2Ph][(SiO_2)_{50}B(C_6F_5)_3]$ which on addition of metallocene dimethyls in the presence or absence of $AlMe_3$ give catalysts for the polymerisation of ethylene. Nanoparticulate silica gives materials of composition $[HNMe_2Ph][(SiO_2)_{35}B(C_6F_5)_3]$ and allows higher catalyst loading. Ion exchange of the ammonium salts with $[CPh_3][B(C_6F_5)_4]$ affords stable $[CPh_3][(SiO_2)_{50}B(C_6F_5)_3]$; the resulting catalyst give polymers of increased molecular weight. Trityl salts of siloxyborates as homogeneous models for silica-supported catalysts show that the stability of the anion towards one-electron processes, and hence its ability to generate stable catalysts, is crucially dependent on steric factors; e.g. the salts $[CPh_3][(C_6F_5)_3BOSiR_3]$ are stable and give active catalysts if $R_3 = Ph_3$ or Bu^tPh_2 but not if $R = Me$ or Pr^i .

Introduction

The advent of "single site" olefin polymerisation catalysts based on metallocene complexes has proved to be a major innovation step in Ziegler-Natta catalysis and has led, through ligand design and tuning of reaction conditions, to a widely extended range of polyolefin materials now being available.^{1,2} Typically, metallocene catalysts are generated by activating metallocene halides with an excess of methylaluminumoxane (MAO).³ Alternatively, catalysts may be generated in the absence of MAO by treating metallocene alkyls with a cation generating

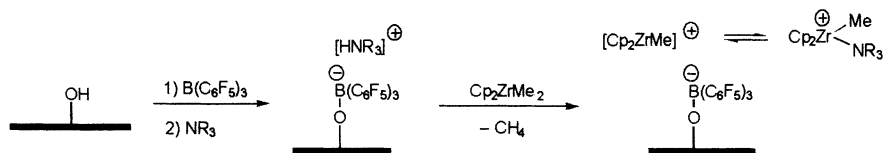
agent such as $[\text{HNR}_3][\text{B}(\text{C}_6\text{F}_5)_4]$, $[\text{CPh}_3][\text{B}(\text{C}_6\text{F}_5)_4]$ or $\text{B}(\text{C}_6\text{F}_5)_3$,⁴ to generate equilibrium concentrations of the catalytically active species $[\text{Cp}_2\text{MR}]^+$.^{5,6} The activity and stability of such MAO-free cationic catalysts are strongly dependent on the weakly coordinating nature of the counteranion,^{7,8} with $[\text{B}(\text{C}_6\text{F}_5)_4]^-$ and $[\text{RB}(\text{C}_6\text{F}_5)_3]^-$ being particularly successful.

The successful substitution of existing heterogeneous polymerisation catalysts in slurry and gas phase processes by metallocene catalysts requires heterogenisation, i.e. the attachment of the catalyst on a suitable support.⁹ Homogeneous metallocene catalysts do not allow control of polymer particle morphology which, in the case of less soluble polymers, can lead to serious reactor fouling. In heterogenised catalysts the growing polymer tends to form replicas of the original catalyst particles to give free-flowing powders which are easy to separate and process. Heterogenised catalysts prepared by reacting metallocenes with Lewis acidic supports such as Al_2O_3 or MgCl_2 followed by activation with aluminium alkyls,¹⁰ by covalent attachment of metallocenes,¹¹ and by ion exchange with crystalline silicates¹² have been reported. In most cases, however, heterogenisation is carried out by impregnating dehydroxylated high surface area silica with MAO and the metallocene, a method that has the added advantage of allowing a reduction of the excess of MAO necessary to achieve acceptable productivities. There is no firm attachment of the metallocene to the support with such catalysts; rather the polymerisation chemistry takes place in the MAO/alkene surface film along the lines known for homogeneous systems. Little is known, however, about the heterogenisation of MAO-free catalysts, a very recent example being the attachment of metallocenes to spherical polystyrene beads bearing amino functionalities.¹³ We report here the preparation of metallocene catalysts supported on silica modified with surface $-\text{OB}(\text{C}_6\text{F}_5)_3^-$ groups. Such supports act as polyanions to which the cationic active species are bound by electrostatic rather than covalent interactions.

Results and Discussion

Initial attempts to generate supported catalysts by treating dehydroxylated silica with $\text{B}(\text{C}_6\text{F}_5)_3$ followed by Cp_2ZrMe_2 and AlMe_3 failed to show appreciable activity after washing with toluene. Apparently the attachment of $\text{B}(\text{C}_6\text{F}_5)_3$ to surface hydroxyl groups is reversible under these conditions, resulting in the preferential formation of soluble $\text{Cp}_2\text{ZrMe}(\mu\text{-Me})\text{B}(\text{C}_6\text{F}_5)_3$. On the other hand, treatment of SiO_2 with $\text{B}(\text{C}_6\text{F}_5)_3$ followed by NMe_2Ph affords the anilinium salt of borato-modified silica. Elemental analysis indicates an approximate composition $[\text{HNMe}_2\text{Ph}]^+[(\text{SiO}_2)_{50}\text{B}(\text{C}_6\text{F}_5)_3]^-$ (Scheme 1). A similar approach has recently been reported by Exxon researchers.¹⁴

Scheme 1.



Monitoring this reaction by FT-IR indicates that not all OH groups of silica are accessible. Dehydroxylation of silica at 450°C gives a material with $\nu(\text{OH}) \approx 3695 \text{ cm}^{-1}$. After treatment with $\text{B}(\text{C}_6\text{F}_5)_3/\text{NMe}_2\text{Ph}$, according to Scheme 1, a band at 3678 cm^{-1} with reduced intensity is still apparent.

Catalysts were prepared by treating a slurry of $[\text{HNMe}_2\text{Ph}][(\text{SiO}_2)_{50}\text{B}(\text{C}_6\text{F}_5)_3]$ in toluene with an excess of Cp_2ZrMe_2 , initially with the addition of some AlMe_3 as scavenger and to stabilise the catalyst ($\text{Al}:\text{Zr} = 5:1$). There was rapid polymerisation at 1 bar ethene pressure at 60°C. The activities were about an order of magnitude lower than the homogeneous system activated with $[\text{HNMe}_2\text{Ph}][\text{B}(\text{C}_6\text{F}_5)_4]$ under comparable conditions. The gel permeation chromatography traces showed a tendency towards bimodal molecular weight distribution, with a significant low-molecular weight component, and correspondingly broad polydispersities (cf. Table 1, entries 1 - 4). This indicated the presence of several active species including the formation of some $\text{Cp}_2\text{ZrMe}(\mu\text{-Me})\text{B}(\text{C}_6\text{F}_5)_3$ in the solution phase. This was confirmed by comparing the activities of the toluene supernatant with that of the precipitated material: The precipitate gives high molecular weight polymer with good activity, whereas the supernatant shows reduced activity and affords very low molecular weight polyethylene (Table 1, entry 3). The homogeneous component could be eliminated by subjecting the as-prepared catalyst to a further toluene washing step. We have shown earlier that in the presence of AlMe_3 soluble cationic metallocene species form comparatively stable heterobinuclear complexes of the type $[\text{Cp}_2\text{Zr}(\mu\text{-Me})_2\text{AlMe}_2]^+$ which are capable of dissociation to generate active $[\text{Cp}_2\text{ZrMe}]^+$.¹⁵ It is likely therefore that in the presence of AlMe_3 the heterogenised catalyst contains the same cations, $[\text{Cp}_2\text{Zr}(\mu\text{-Me})_2\text{AlMe}_2][(\text{SiO}_2)_{50}\text{B}(\text{C}_6\text{F}_5)_3]$.

Table 1.

Ethene Polymerisations with metallocene dialkyls activated by $[(\text{SiO}_2)_{50}\text{B}(\text{C}_6\text{F}_5)_3][\text{HNMe}_2\text{Ph}]$ in the presence and absence of AlMe_3 .^a

| Run | Metallocene | Supported activator [μmol] | M [μmol] | T. [°C] | Polymer Yield [g] | Prod. b | M_w | M_w/M_n |
|----------------|---|----------------------------|----------|---------|-------------------|---------|-------------|-------------|
| 1 ^c | Cp_2ZrMe_2 | 8.4 | 100 | 50 | 0.495 | 0.36 | 94,000 | 45 |
| 2 ^d | Cp_2ZrMe_2 | 42 | 500 | 50 | 1.243 | 0.18 | 78,000 | 50 |
| 3 ^d | Cp_2ZrMe_2 | supernat. | 500 | 60 | 0.515 | 0.07 | 1,900 | 1.8 |
| 4 | Cp_2ZrMe_2 | precipit. of run 3 | | 60 | 1.518 | 0.21 | 105,000 | 14 |
| 5 | Cp_2ZrMe_2 | 8.4 | 100 | 30 | 0.646 | 0.15 | 477,000 | 9.5 |
| 6 | Cp_2ZrMe_2 | 8.4 | 100 | 60 | 1.040 | 0.24 | 192,500 | 8.2 |
| 7 | Cp_2ZrMe_2 | 8.4 | 100 | 60 | 1.244 | 0.28 | <i>n.d.</i> | <i>n.d.</i> |
| 8 | Cp_2ZrMe_2 | 8.4 | 100 | 80 | 0.44 | 0.10 | 133,000 | 12 |
| 9 ^e | Cp_2ZrMe_2 | 56 | 500 | 60 | 16.4 | 0.29 | 260,000 | 6.6 |
| 10 | $\text{Me}_2\text{Si}(\text{Ind})_2\text{ZrMe}_2$ | 8.4 | 100 | 60 | 2.64 | 0.63 | 75,000 | 12 |
| 11 | $\text{Me}_2\text{Si}(\text{Ind})_2\text{ZrMe}_2$ | 8.4 | 50 | 60 | 2.68 | 0.44 | 110,000 | 11 |
| 12 | $\text{Me}_2\text{Si}(\text{Ind})_2\text{ZrMe}_2$ | 8.4 | 100 | 80 | 0.818 | 0.19 | 122,000 | 9.3 |
| 13 | $\text{CGCTi}(\text{CH}_2\text{Ph})_2$ | 8.6 | 100 | 60 | 0.194 | 0.05 | 925,000 | 13 |
| 14 | DADNiMe_2 | 10 | 100 | 60 | 0.412 | 0.082 | <i>n.d.</i> | <i>n.d.</i> |
| 15 | DADNiMe_2 | 20 | 200 | 25 | 0.38 | 0.038 | <i>n.d.</i> | <i>n.d.</i> |

^a Conditions: 40 mL toluene, 1 bar ethene, 30 min reaction time. ^b In 10^6 g PE $(\text{mol Zr})^{-1} \text{h}^{-1} \text{bar}^{-1}$. ^c 500 μmol AlMe_3 added. ^d 2500 μmol AlMe_3 added. ^e 6 bar ethene.

Catalysts prepared without the addition of AlMe_3 have similar activity. In these cases, the homodinuclear cation $[(\text{Cp}_2\text{ZrMe}_2)(\mu\text{-Me})]^+$ is likely to be formed. The productivities of these aluminium-free catalysts do not vary significantly over the temperature range of 30 - 80 °C. Increasing the ethene pressure from 1 to 6 bars does not lead to a noticeable productivity increase but gives polymers of higher molecular weight. As expected the polymer molecular weight decreases with increasing temperature, from $M_w \approx 480,000$ at 30°C to 130,000 at 80°C. This contrasts with recent propene polymerisation data by Mülhaupt et al. who found that catalysts supported on MAO-impregnated silica showed less temperature dependence of polymer molecular weights than homogeneous analogues and better performance at higher operating temperatures.¹⁶

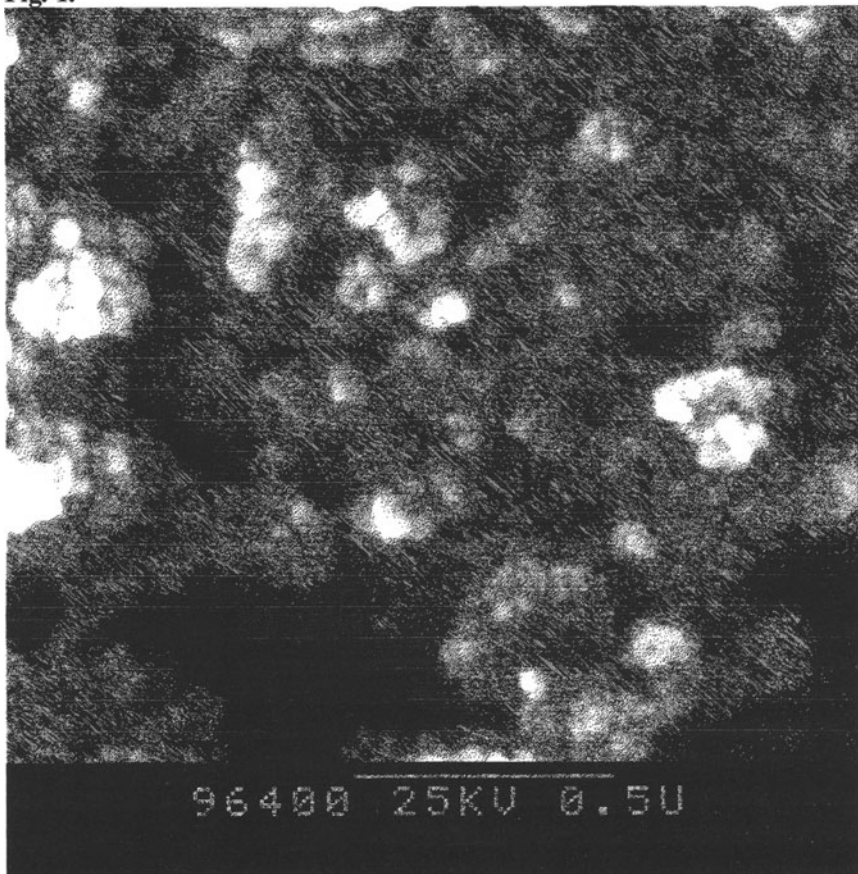
The productivities of supported *rac*- $\text{Me}_2\text{Si}(\text{Ind})_2\text{ZrMe}_2$ are comparable to those of Cp_2ZrMe_2 , while the M_w values are slightly lower. By contrast, the "constrained geometry" catalyst $(\text{CGC})\text{Ti}(\text{CH}_2\text{Ph})_2$ / $[\text{HNMe}_2\text{Ph}][(\text{SiO}_2)_{50}\text{B}(\text{C}_6\text{F}_5)_3]$ (CGC = $\eta^1\text{-}\eta^5\text{-C}_5\text{Me}_4\text{SiMe}_2\text{NBu}^t$) is an order of magnitude less active than zirconocenes but gives polyethylene of substantially higher molecular weight, $M_w = 925,000$ (Table 1, entry 13). Similar differences have been seen in homogeneous systems.¹⁷ The nickel diazadiene (DAD) NiMe_2

derived catalyst¹⁸ produces a low melting polymer with a productivity of ca. 8×10^4 g PE mol⁻¹ h⁻¹ (Table 1, entries 14 and 15) under comparable conditions (DAD = 2,6-C₆H₃Prⁱ₂N=C(Me)-C(Me)=N-2,6-C₆H₃Prⁱ₂).

The polydispersities of all polymers prepared with supported catalysts are broader than those obtained under homogeneous conditions. It seems likely that coordination of cationic active species to either surface oxygen atoms of the silica support, the oxygen atom of the -OB(C₆F₅)₃⁻ groups, and possibly also ortho-F atoms are resting states that will interrupt the propagation process at various stages of chain growth and will lead to the "intermittent growth" behaviour of the catalyst.¹⁹ Since re-activation of a dormant species by dissociation of these resting states is slow compared to the rate of propagation, broad polydispersities will result.

Nanoparticulate silica is accessible by the combustion of hexamethyldisiloxane in a methane/air stream at 700°C, to give globular silica particles of ca. 20 nm diameter.^{20,21} Although there is some agglomeration of the nanoparticles, these supports should possess higher accessible surface areas. An SEM image of nano-silica powder is shown in Fig. 1.

Fig. 1.



Nanoparticulate silica prepared in this way contains significantly less adsorbed water than conventional silica. Because the nanostructure is prone to sintering above 100°C, the material was dried in vacuo at 90°C. Treatment with $B(C_6F_5)_3$ / NMe_2Ph following Scheme 1 gives a support with a somewhat higher borate loading, $[HNMe_2Ph][(SiO_2)_{35}B(C_6F_5)_3]$. Polymerisation results with nanoparticulate supports are collected in Table 2. The catalyst performance is similar to the data given in Table 1. The morphology and the flow behaviour of the resulting polymer particles closely resembles that made with conventional silica.

Table 2.

Ethene polymerisations with nanoparticulate supports.^{a,b}

| Run | supported activator [μmol] | metallocene (μmol) | polymer yield [g] | productivity 10^6 g PE $(mol\ Zr)^{-1} h^{-1} bar^{-1}$ | M_w | M_w/M_n |
|-----|----------------------------|----------------------------|-------------------|---|-------------|-------------|
| 1 | 11.4 | Cp_2ZrMe_2 (100) | 2.111 | 0.37 | 187,000 | 11 |
| 2 | 11.4 | Cp_2ZrMe_2 (100) | 1.493 | 0.26 | <i>n.d.</i> | <i>n.d.</i> |
| 3 | 11.8 | $(CGC)TiCH_2Ph_2$ (100) | 0.194 | 0.033 | <i>n.d.</i> | <i>n.d.</i> |

^a Catalyst system $[(SiO_2)_{35}B(C_6F_5)_3][HNMe_2Ph]$ / metallocene. ^b Conditions: 40 mL toluene, 1 bar ethene pressure, 60°C, 30 min reaction time.

Ion exchange of a slurry of $[HNMe_2Ph][(SiO_2)_{50}B(C_6F_5)_3]$ in dichloromethane with $[CPh_3][B(C_6F_5)_4]$ leads to $[CPh_3][(SiO_2)_{50}B(C_6F_5)_3]$ as a thermally stable yellow solid (Scheme 2). Toluene suspensions of $[CPh_3][(SiO_2)_{50}B(C_6F_5)_3]$ discolour immediately on treatment with Cp_2ZrMe_2 . As is the case in the homogeneous system, Ph_3CMe is formed, together with a colourless catalytically active solid. The productivities of these catalysts are somewhat lower than those of the anilinium analogues, though the polymer molecular weights are significantly higher, $2.5 - 3 \times 10^5$ at 1 bar, with a further increase when the ethene pressure is raised to 6 bar (Table 3).²²

Scheme 2.

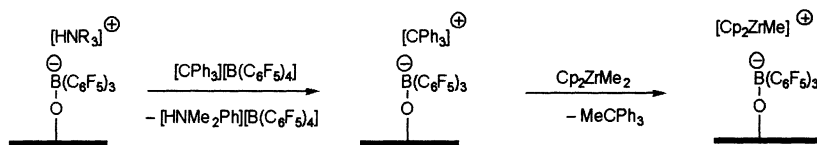
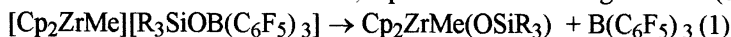


Table 3.Ethene polymerisations with $[\text{CPh}_3][(\text{SiO}_2)_{50}\text{B}(\text{C}_6\text{F}_5)_3] / \text{Cp}_2\text{ZrMe}_2^{\text{a}}$

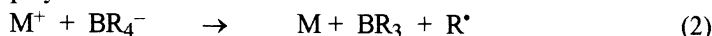
| Run | supported activator [μmol] | Zr [μmol] | T. [$^{\circ}\text{C}$] | polymer yield [g] | Prod. b | M_w | M_w/M_n |
|----------------|--|---------------------------|------------------------------|----------------------|------------|---------|-----------|
| 1 | 8.4 | 50 | 60 | 0.555 | 0.13 | 296,000 | 16 |
| 2 | 8.4 | 100 | 60 | 0.605 | 0.14 | 261,000 | 14 |
| 3 ^c | 50 | 500 | 60 | 6.44 | 0.13 | 360,000 | 3.4 |

^a Conditions: 40 mL toluene, 1 bar ethene, 30 min reaction time. ^b In 10^6 g PE $(\text{mol Zr})^{-1} \text{h}^{-1} \text{bar}^{-1}$. ^c 2500 $\mu\text{mol AlMe}_3$, 6 bar ethene pressure.

The reactivity of these heterogeneous trityl activators was compared to that of homogeneous analogues, both in order to allow closer comparison between heterogeneous and homogeneous systems and to probe the extent of siloxy transfer from borate to the transition metal centre, a possible deactivating reaction (eq. 1).



A number of trityl salts of siloxyborates $[\text{CPh}_3][(\text{C}_6\text{F}_5)_3\text{BOSiR}_3]$ were therefore prepared. A counteranion capable of stabilising highly electrophilic catalytically active species such as $[\text{Cp}_2\text{ZrMe}]^+$ must not only be essentially non-nucleophilic and chemically inert,²³ but must also be redox inactive and resist one-electron transfer reactions (eq. 2). The stability of triphenylmethyl salts towards formation of CPh_3^{\bullet} is therefore a useful indicator for the suitability of an anion in polymerisation reactions.



The stability of siloxyborates is a function of steric bulk. $[\text{CPh}_3][(\text{C}_6\text{F}_5)_3\text{BOSiMe}_3]$ readily decomposes at room temperature, as indicated by the formation of deeply coloured products. $[\text{CPh}_3][(\text{C}_6\text{F}_5)_3\text{BOSiPr}^t_3]$ is more stable but slowly decomposes, while $[\text{CPh}_3][(\text{C}_6\text{F}_5)_3\text{BOSiPh}_3]$ and $[\text{CPh}_3][(\text{C}_6\text{F}_5)_3\text{BOSiBu}^t\text{Ph}_2]$ showed no sign of decomposition at room temperature. Polymerisation results for the latter two anions are collected in Table 4. The productivities of $\text{Cp}_2\text{ZrMe}_2 / [\text{CPh}_3][(\text{C}_6\text{F}_5)_3\text{BOSiPh}_3]$ catalysts at 25°C are higher than those of heterogenised catalysts at 60°C . At 25°C the polymer molecular weights are comparable to those obtained with the heterogenised system at 60°C . On warming, however, the homogeneous system shows a significant decrease both in polymer molecular weight and in activity, and at 60°C the $\text{Cp}_2\text{ZrMe}_2 / [\text{CPh}_3][(\text{C}_6\text{F}_5)_3\text{BOSiPh}_3]$ system has become essentially inactive after 4 minutes. The anion $[(\text{C}_6\text{F}_5)_3\text{BOSiBu}^t\text{Ph}_2]$ behaves similarly but gives generally lower molecular weights. By contrast, silica attached to $-\text{B}(\text{C}_6\text{F}_5)_3$ behaves in essence like a sterically highly encumbered non-nucleophilic siloxy substituent; neither of the homogeneous anion systems shows the stability of the heterogenised catalyst.

Table 4.Ethene polymerisations with $[\text{CPh}_3][(\text{C}_6\text{F}_5)_3\text{BOSiR}_3] / \text{Cp}_2\text{ZrMe}_2^{\text{a}}$

| Run | CPh_3^+ [μmol] | SiR_3 | Zr [μmol] | polymer yield [g] | Prod. ^c | M_w | M_w/M_n |
|----------------|---|-----------------------------------|---------------------------|-------------------------|--------------------|---------|-----------|
| 1 | 5 | SiPh ₃ | 25 | 0.562 | 1.35 | 120,000 | 4.0 |
| 2 | 5 | SiPh ₃ | 10 | 0.455 | 1.1 | 281,000 | 7.0 |
| 3 | 10 | SiPh ₃ | 100 | 1.385 | 0.83 | 78,800 | 6.3 |
| 4 ^b | 10 | SiPh ₃ | 100 | 0.294 | 0.18 ^d | 9,400 | 2.8 |
| 5 | 5 | SiBu ^t Ph ₂ | 25 | 0.587 | 1.41 | 98,000 | 4.3 |
| 6 | 10 | SiBu ^t Ph ₂ | 100 | 1.021 | 0.61 | 53,000 | 4.6 |
| 7 ^b | 10 | SiBu ^t Ph ₂ | 100 | 0.231 | 0.14 ^d | 7,700 | 2.4 |

^a Conditions: 40 mL toluene, 1 bar ethene pressure, 10 min reaction time, 25°C. ^b 60°C. ^c In 10^6 g PE (mol Zr)⁻¹ h⁻¹ bar⁻¹. ^d Loss of catalytic activity within 4 min.

Conclusion

Treatment of dehydroxylated silica with $\text{B}(\text{C}_6\text{F}_5)_3$ in the presence of base leads to polyanionic borato-modified silica. The addition of metallocene dialkyls generates aluminium-free heterogenised polymerisation catalysts which give polyethylenes of higher molecular weights and broader polydispersities than analogous homogeneous catalysts. The supported catalysts show increased temperature stability. Activity and polymer molecular weight are a function of the mode of activation, e.g. $[\text{HNMe}_2\text{Ph}][(\text{SiO}_2)_{50}\text{B}(\text{C}_6\text{F}_5)_3]$ vs. $[\text{CPh}_3][(\text{SiO}_2)_{50}\text{B}(\text{C}_6\text{F}_5)_3]$.

Experimental Section

All manipulations were carried out using standard Schlenk, vacuum-line and glove box techniques. Light petroleum (bp 40 - 60 °C), toluene and diethyl ether were distilled under nitrogen from sodium-potassium alloy. CH_2Cl_2 was distilled under nitrogen from calcium hydride. Deuterated solvents were dried over 4-Å molecular sieves and deoxygenated *via* several freeze-thaw cycles. AlMe_3 (97%, Aldrich) was used as purchased. The compounds $\text{B}(\text{C}_6\text{F}_5)_3$ ²⁴ and $[\text{CPh}_3][\text{B}(\text{C}_6\text{F}_5)_4]$ ⁴ were prepared by literature methods. Ph_3SiOH , $\text{Bu}^t\text{Ph}_2\text{SiCl}$, Pr^i_3SiCl were purchased from Aldrich. $\text{Bu}^t\text{Ph}_2\text{SiOH}$ and Pr^i_3SiOH were prepared

by refluxing the corresponding chlorides with ethanol / KOH for 72 h. NMR spectra were recorded on Bruker DPX300, ARX250 and Jeol 270 instruments. Polymer molecular weights were determined by gel permeation chromatography (PL gel column, 1,2-dichlorobenzene, 140 °C). Powder samples for scanning electron microscopy (SEM) were mounted on conducting stubs and lightly gold coated prior to examination in a Hitachi S700 Field emission electron microscope with resolution of ca. 3 nm.

Synthesis of [HNMe₂Ph][(SiO₂)₅₀B(C₆F₅)₃]. To a suspension of 3.46 g (57 mmol) SiO₂ and 0.74 g (1.44 mmol) B(C₆F₅)₃ in 200 mL hexanes 0.19 mL (1.44 mmol) dimethylaniline was added. The suspension was stirred at room temperature for 4 h and allowed to settle overnight before filtering off the supernatant and washing with a further 200 mL hexane. The solid was dried at 0.1 torr / 20 °C for 4 h. Anal. C, 11.45%.

Synthesis of [CPh₃][(SiO₂)₅₀B(C₆F₅)₃]. A suspension of 7 g [(SiO₂)₅₀B(C₆F₅)₃] [HNMe₂Ph] was stirred at room temperature for 6 h, in the dark, with a solution of 2.3 g (2.5 mmol) [CPh₃][B(C₆F₅)₄] in 200 mL dichloromethane. The solid was allowed to settle and the supernatant filtered off. The process was then repeated with a second 200 mL aliquot of dichloromethane and 2.3 g [CPh₃][B(C₆F₅)₄]. After filtration the yellow residue was washed with 3 x 400 mL dichloromethane before drying at 0.1 torr / 20 °C for 4 h.

Synthesis of LiOSiPh₃. 7 g Ph₃SiOH (25 mmol) was dissolved in 80 mL diethyl ether and cooled to -78 °C. 25 mmol (10 mL of a 2.5 M soln.) BuⁿLi was added via a syringe. There was an instant precipitation of white solid which failed to dissolve on warming to room temperature. Filtration and drying under vacuum gave 6.5 g (23 mmol), 92%. Elemental Analysis: Calcd.: C, 76.54; H, 5.36. Found: C, 76.27; H, 5.42%. ¹H NMR (270MHz, d₅-pyridine, 23 °C): δ 7.88 (d, 6H, *J* = 7.26Hz, o-H, Ph), 7.31 (tr, 3H, *J* = 7.26Hz p-H, Ph), 7.23 (tr, 6H, *J* = 6.93Hz, m-H, Ph). ¹³C NMR (67.8MHz, d₅-pyridine, 23 °C): δ 144.81 (ipso-c, Ph), 136.09 (o-C, Ph), 128.1 (p-C, Ph), 127.3 (m-C, Ph). ²⁹Si NMR (53.54MHz, d₅-pyridine, 23 °C): δ -29.90.

Synthesis of Li[Ph₃SiOB(C₆F₅)₃]. LiOSiPh₃ 2.1 g (7.4 mmol) was suspended in 30 mL dichloromethane and 3.8 g (7.4 mmol) B(C₆F₅)₃ was added whilst stirring. The suspended solids dissolved rapidly. A small amount of fine solid was separated from the reaction mixture by centrifuge. Concentration to 10 mL led to crystallisation. The product was separated by filtration and washed with 50 mL light petroleum before drying in-vacuo. Yield 4 g (5 mmol), 68%. Elemental Analysis: Calcd.: C, 54.42; H, 1.91. Found: C, 54.20; H, 1.82%.

¹H NMR (270MHz, CD₂Cl₂, 22 °C): δ 7.56 (d, 6H, *J* = 8.25Hz, o-H, Ph), 7.48 (tr, 3H, *J* = 7.26Hz, p-H, Ph), 7.38 (tr, 6H, *J* = 7.26Hz, m-H, Ph). ¹³C NMR (67.9 MHz, CD₂Cl₂, 22 °C): δ 135.54 (o-C, Ph), 132.97 (ipso-C, Ph), 131.77 (p-C, Ph), 129.0 (m-C, Ph). ²⁹Si (53.54MHz, CD₂Cl₂, 22 °C): δ -17.13. ¹⁹F (84.10MHz, CD₂Cl₂, 23 °C): δ -140.6 (o-F, C₆F₅), -161.5 (p-F, C₆F₅), -165.93 (m-F, C₆F₅).

Synthesis of [CPh₃][(C₆F₅)₃BOSiPh₃]. Li[Ph₃SiOB(C₆F₅)₃], 2.0 g (2.5 mmol) was combined with 0.70 g Ph₃CCl and 10 mL of CH₂Cl₂ was added. The reaction was stirred for 1 h in the dark. A dark orange solution formed with a white suspended solid. The solid was separated by centrifuge. The solvent was removed to give an orange oil which crystallised on cooling to -20 °C. Yield 2.4 g (2.4 mmol), 93%. Elemental Analysis: Calcd.: C, 64.09; H, 2.93. Found: C, 64.05; H, 2.6%. ¹H NMR (270.05MHz, CDCl₃, 24°C): δ 8.02 (tr, 3H, p-H, CPh₃), 7.62 (tr, 6H, m-H, CPh₃), 7.39 (d, 6H, o-H, CPh₃), 7.07-6.93 (m, 15H, SiPh₃).

Synthesis of Li[(C₆F₅)₃BOSiMe₃]. B(C₆F₅)₃, 5.7 g (11.1 mmol) was dissolved in 30 mL of dichloromethane and 11.1 mmol (11.1 mL of a 1.0 M solution) NaOSiMe₃ was added. A white solid precipitated which was isolated by filtration and dried under vacuum. Yield 6 g (9.6 mmol), 86%. Elemental Analysis: Calcd.: C, 40.40; H, 1.46. Found: C, 40.27; H, 1.38%.

¹H NMR (270.05MHz, d₅-pyridine, 24°C): δ 0.24 (s, 9H, SiMe₃). ¹³C NMR (67.8MHz, d₅-pyridine, 24°C): δ 148.78 (d, J_{C-F} = 234Hz, o-C, C₆F₅), 138.52 (d, J_{C-F} = 244Hz, p-C, C₆F₅), 137.0 (d, J_{C-F} = 236Hz, m-C, C₆F₅). ²⁹Si NMR (53.54MHz, d₅-pyridine, 24°C): δ -3.70 ¹⁹F NMR (d₅-pyridine, 24°C): δ -136.31 (o-F, C₆F₅) -166.56 (p-F, C₆F₅), -169.95 (m-F, C₆F₅).

Attempted synthesis of [CPh₃][(C₆F₅)₃BOSiMe₃]. Combining the lithium salt and Ph₃CCl in dichloromethane led immediately to a dark green-blue solution. ¹H NMR analysis of the crude product showed no evidence for [CPh₃]⁺ cations.

Synthesis of [Li(Et₂O)_{1.25}][(C₆F₅)₃BOSiPrⁱ₃]. SiPrⁱ₃SiOH, 5.95 g (30 mmol) was dissolved in 300 mL diethyl ether and cooled to -78°C. 34 mmol, (21.4 mL of a 1.6 M soln.) BuⁿLi was added via a syringe. The reaction was warmed to room temperature and stirred for 3 h. 19.9 g (34 mmol) B(C₆F₅)₃.Et₂O was added in small portions via a bent finger. The solids fully dissolved after stirring overnight. Removal of the solvents under reduced pressure gave a sticky crystalline solid which after washing with light petroleum became a fine white powder. Yield 20 g, 25.5 mmol, 85%. Elemental analysis: Calcd.: C, 48.97; H, 4.3. Found: C, 48.55; H, 3.9%. ¹H NMR (300.13MHz, CDCl₃, 22°C): δ 3.75 (q, 5H, CH₃CH₂O), 1.26 (tr, 7.5H, CH₃CH₂O) 0.96 (d, 18H, J = 7.4Hz, CH(CH₃)₂), 0.72 (sep, 3H, J = 7.4Hz, CH(CH₃)₂). ¹³C NMR (75.47MHz, CDCl₃, 22°C): δ 147.99 (d, J_{C-F} = 234Hz, o-F, C₆F₅), 138.33 (d, J_{C-F} = 240Hz, p-F, C₆F₅), 137.19 (d, J_{C-F} = 226Hz, m-F, C₆F₅), 65.44 (CH₃CH₂O), 18.13 (CH(CH₃)₂), 14.68 (CH(CH₃)₂), 12.98 (CH₃CH₂O). ¹¹B NMR (96.29MHz, CDCl₃, 22°C): δ -3.43.

Attempted synthesis of [CPh₃][(C₆F₅)₃BOSiPrⁱ₃]. The reaction of the lithium salt [Li(Et₂O)_{1.25}][(C₆F₅)₃BOSiPrⁱ₃] 7.52 g (9.6 mmol) with an equimolar amount of Ph₃CCl (2.67g) in 80 mL dichloromethane at -78°C to room temperature led to a dark solution from which a pure material could not be isolated. ¹H NMR indicated the presence of [CPh₃]⁺ and CPh₃ radical in the crude sample.

Synthesis of [Li(Et₂O)_{2.25}][(C₆F₅)₃BOSiBu^tPh₂]. Bu^tPh₂SiOH, 7.68 g (29.9 mmol) was dissolved in 250 mL diethyl ether and cooled to -78°C. 29.9 mmol (18.7 mL of a 1.6M soln.) Bu^tLi was added dropwise. The reaction was warmed to room temperature and stirred for 3h. 29.9 mmol (17.5 g) B(C₆F₅)₃.Et₂O was added via a bent finger. The reaction was stirred overnight before removing the solvents under vacuum gave a white solid. Yield 20 g (21.3mmol), 71%. Elemental Analysis: Calcd. C, 54.88; H, 4.44. Found: C, 54.25; H, 4.65%.

¹H NMR (300.13MHz, CDCl₃, 20°C): δ 7.49-7.36 (m, 10H, Ph), 3.45 (q, 9H, J = 7.0Hz, CH₃CH₂O), 1.22 (s, 9H, Bu^t), 1.21 (tr, 13.5H, J = 7.0Hz, CH₃CH₂O). ¹³C NMR (75.47MHz, CDCl₃, 22°C): δ 147.78 (d, J_{C-F} = 228Hz, o-F, C₆F₅), 139.01 (d, J_{C-F} = 248Hz, p-F, C₆F₅), 136.80 (d, J_{C-F} = 240Hz, m-C, C₆F₅), 135.38 (o-C, Ph), 134.31 (ipso-C, Ph), 129.83 (p-C, Ph), 127.81(m-C, Ph), 65.3 (CH₃CH₂O), 28.29 (CH₃)₃C), 19.90 (CH₃)₃C), 14.66 (CH₃CH₂O). ¹¹B NMR (96.29MHz, CDCl₃, 20°C): δ -3.03.

Synthesis of [CPh₃][(C₆F₅)₃BOSiBu^tPh₂].

[Li(Et₂O)_{2.25}][(C₆F₅)₃BOSiBu^tPh₂] 8.11 g (8.62 mmol) was combined with 2.4 g Ph₃CCl and stirred for 6 h at room temperature in 200 mL light petroleum. The solvent was filtered off and the solid extracted with 100 mL dichloromethane to give a bright orange solution. Concentration to ca. 20 mL led to crystallisation. The crystals were separated by filtration and washed with light petroleum before drying under vacuum. Yield 5 g (4.95 mmol), 57.4%. Elemental Analysis: Calcd. C, 62.98; H, 3.39. Found: C, 62.6; H, 3.35%. ¹H NMR (250.13MHz, CDCl₃, 27°C): δ 8.14 (tr, 3H, J = 6.4Hz, p-H, CPh₃), 7.71 (tr, 6H, J = 7.6Hz, m-H, CPh₃), 7.54 (d, 6H, J = 8.3Hz, o-H, CPh₃), 7.12-7.00 (m, 6H, m&p-H, SiPh₂), 7.43 (d, 4H, J = 7.9Hz, o-H, SiPh₂), 0.89 (s, 9H, Bu^t). ¹³C NMR (62.90MHz, CDCl₃, 27°C): δ 210.66 (CPh₃), 143.60 (m-C, CPh₃), 142.35 (o-C, CPh₃), 139.76 (ipso-C, CPh₃), 138.75 (ipso-C, SiPh₂), 135.77 (p-C, CPh₃), 130.62 (o-C, SiPh₂), 127.40 (p-C, SiPh₂), 125.95 (m-C, SiPh₂), 27.78 (C(CH₃)₃), 19.88 (C(CH₃)₃). ¹¹B NMR (80.25MHz, CDCl₃, 27°C): δ -5.17.

General procedure for ethene polymerisations. Stock solutions of 0.1 M Cp₂ZrMe₂, 0.1 M Cp₂ZrMe₂ / 0.5 M AlMe₃ and 0.05 M *rac*-Me₂Si(Ind)₂ZrMe₂ in toluene were prepared. The heterogeneous activators were suspended in toluene and stirred rapidly. An all glass reactor vessel was flame dried and charged with 40 mL dry low-sulfur toluene. The toluene was saturated with ethylene at the desired temperature. An aliquot of the metallocene stock solution was introduced using a gas-tight syringe. The polymerisation was initiated by injection of an aliquot of the heterogeneous activator suspension. Polymerisations were terminated by injection of 2 mL methanol. Polymer samples were washed with acidified methanol and dried at 80 °C overnight.

Acknowledgements.

This work was supported by the Engineering and Physical Sciences Research Council and BP Chemicals, Sunbury. We are grateful to Dr. P. Brès, BP Chemicals, for supplying amorphous silica, to Dr. M.A. Keane, Department of Chemical Engineering, University of Leeds, for a sample of nanoparticulate silica, to Dr. R. Brydson, Department of Materials, University of Leeds, for SEM and EDX studies and to Dr Steve Holding, RAPRA Technology for GPC measurements.

References

- 1 W. Kaminsky and M. Arndt, *Adv. Polym. Sci.* **1997**, *127*, 144. W. Kaminsky, *J. Chem. Soc., Dalton Trans.* **1998**, 1413. M. Lee, *Chem. Brit.*, September **1998**, 22.
- 2 H.H. Brintzinger, D. Fischer, R. Mülhaupt, B. Rieger and R. Waymouth, *Angew. Chem.* **1995**, *107*, 1255; *Angew. Chem. Int. Ed. Engl.* **1995**, *34*, 1143. M. Aulbach and F. Küber, *Chemie Unserer Zeit* **1994**, *28*, 197.
- 3 H. Sinn and W. Kaminsky, *Adv. Organomet. Chem.* **1980**, *18*, 99.
- 4 H.W. Turner, *Eur. Pat. Applic.* 277,004 (**1988**, to Exxon Chemicals). J.A. Ewen and M.J. Elder, *Eur. Pat. Applic.* 426,637 (**1990**, to Fina technology). J.C.W. Chien, W.M. Tsai and M.D. Rausch, *J. Am. Chem. Soc.* **1991**, *113*, 8570. M. Bochman and S.J. Lancaster, *J. Organomet. Chem.* **1992**, *434*, C1. J.C.W. Chien, W. Song, and M.D. Rausch, *J. Polym. Sci., Part A: Polym. Chem.* **1994**, *32*, 2387. X. Yang, C.L. Stern and T.J. Marks, *J. Am. Chem. Soc.* **1991**, *113*, 3623.
- 5 M. Bochmann and L.M. Wilson, *J. Chem. Soc., Chem. Commun.* **1986**, 1610. R.F. Jordan, C.S. Bajgur, R. Wilett and B. Scott, *J. Am. Chem. Soc.* **1986**, *108*, 7410. J.J. Eisch, A.M. Piotrowski, S.K. Brownstein, E.J. Gabe and F.L. Lee, *J. Am. Chem. Soc.* **1985**, *107*, 7219. M. Bochmann, A.J. Jaggar and J.C. Nicholls, *Angew. Chem. Int. Ed. Engl.* **1990**, *29*, 780. T.J. Marks, *Acc. Chem. Res.* **1992**, *25*, 57.
- 6 M. Bochmann, *J. Chem. Soc., Dalton Trans.* **1996**, 255. A.S. Guram and R.F. Jordan in: *Comprehensive Organometallic Chemistry II*, eds. E.W. Abel, F.G.A. Stone and G. Wilkinson, Pergamon, Oxford **1995**, vol. 4, chapter 12.
- 7 X. Yang, C.L. Stern and T.J. Marks, *Organometallics* **1991**, *10*, 840. P.A. Deck, C.L. Beswick and T.J. Marks, *J. Am. Chem. Soc.* **1998**, *120*, 1772.
- 8 S.H. Strauss, *Chem. Rev.* **1993**, *93*, 927. A.J. Lupinetti and S.H. Strauss, *Chemtracts - Inorganic Chemistry*, **1998**, *11*, 565. A.R. Siedle, W.M. Lamanna, R.A. Newmark, J. Stevens, D.E. Richardson and M. Ryan, *Makromol. Chem., Macromol. Symp.* **1993**, *66*, 215.
- 9 F. Ciardelli, A. Altomare and M. Michelotti, *Catalysis Today* **1998**, *41*, 149. N.G. Dufrenne, J. P. Blitzand and C.C. Meverden, *Microchem. J.* **1997**, *55*, 192.
- 10 K. Soga and M. Kaminaka, *Makromol. Chem.* **1993**, *194*, 1745.
- 11 E.I. Iiskola, S. Timonen, T.T. Pakkanen, O. Härkki, P. Lehmus and J. V. Seppälä, *Macromolecules*, **1997**, *30*, 2853. E.I. Iiskola, S. Timonen, T.T. Pakkanen, O. Härkki and J. V. Seppälä, *Applied Surface Science*, **1997**, *121*, 372, and references cited therein.

- 12 J. Tudor, L. Willington, D. O'Hare and B. Royan, *Chem. Commun.* **1996**, 2031. S. O'Brien, J. Tudor, T. Maschmeyer and D. O'Hare, *Chem. Commun.* **1997**, 1905.
- 13 S.B. Roscoe, J.M.J. Frechet, J.F. Walzer and A.J. Dias, *Science* **1998**, *280*, 270.
- 14 J.E. Walzer and J.L. White, *Abstr. 215th Natl. ACS Meeting, Dallas 1998*, abstr. INOR051.
- 15 M. Bochmann and S.J. Lancaster, *Angew. Chem.* **1994**, *106*, 1715; *Angew. Chem. Int. Ed. Engl.* **1994**, *33*, 1634. M. Bochmann and S.J. Lancaster, *J. Organomet. Chem.* **1995**, *497*, 55.
- 16 S. Jüngling, S. Kotzenburg and R. Mülhaupt, *J. Polym. Sci., Part A: Polym. Chem.* **1997**, *35*, 1, and refereces therein.
- 17 Y.X. Chen, M.V. Metz, L. Li, C.L. Stern and T.J. Marks, *J. Am. Chem. Soc.* **1998**, *120*, 6287.
- 18 L.K. Johnson, C.M. Killian and M.C. Brookhart, *J. Am. Chem. Soc.* **1995**, *117*, 6414. C.M. Killian, D.J. Tempel, L.K. Johnson and M.C. Brookhart, *J. Am. Chem. Soc.*, **1996**, *118*, 11664. C. Pellechia and A. Zambelli, *Macromol. Rapid Commun.*, **1996**, *17*, 333. C. Pellechia, A. Zambelli, L. Olivia and D. Pappalardo, *Macromolecules*, **1996**, *29*, 6990. C. M. Killian, L. K. Johnson and M. Brookhart, *Organometallics*, **1997**, *16*, 2005.
- 19 G.Fink, W.Fenzl and R. Mynott, *Z. Naturforsch., Teil B*, **1985**, *40*, 158.
- 20 M.S. Wooldridge, *Prog. Energy & Combust. Sci.*, **1998**, *24*, 63.
- 21 M.A. Keane, personal communication.
- 22 For activities with homogeneous CPh_3^+ activated ethene polymerisation catalysts see for example M. Bochmann and S.J. Lancaster, *Organometallics* **1993**, *12*, 633.
- 23 G. Jiménez Pindado, M. Thornton-Pett, M. Bouwkamp, A. Meetsma, B. Hessen and M. Bochmann, *Angew. Chem. Int. Ed. Engl.* **1997**, *36*, 2358. G. Jiménez Pindado, M. Thornton-Pett and M. Bochmann, *J. Chem. Soc., Dalton Trans.* **1997**, 3115.
- 24 J.L. Pohlmann and F.E. Brinckmann, *Z. Naturforsch. B*, **1965**, *21b*, 5.

A NEW SUPPORTED ZIRCONOCENE CATALYST FOR ETHYLENE POLYMERIZATION

Wioletta Ochedzan-Siodlak, Maria Nowakowska,
Marek Wasielewski

University of Opole, Institute of Chemistry, 45-052 Opole, Oleska 48, Poland

INTRODUCTION

Metallocene catalysts enable the structure of polymers to be tailored in a way which has not been reached before. However, they are more active than the conventional Ziegler – Natta catalysts only as homogeneous metallocene systems, a fact that has essentially restricted their use to industrial processes producing polymers in solution. Modern polymerization processes are solvent free slurry (with liquid monomer) or gas phase processes. To use metallocene catalysts in these modern processes, it is necessary to convert them to heterogeneous catalysts [1, 2]. However, problems have appeared chiefly concerning the activity of the supported catalysts, because heterogeneous metallocene catalysts are much less active than supported Ziegler–Natta catalysts [3,4]. Most solid systems that have been reported cause a dramatic decrease in the activity when compared with the corresponding metallocenes in the solution. Generally, developing of heterogeneous catalyst, with the metallocene as active component supported on the surface of a solid carrier, is the point of extreme interest of recent years.

Recent reports are concerned heterogeneous metallocene catalyst supported on NaCl, SiO₂ and MgCl₂ [5, 6]. The catalyst activities of such a catalytic systems was about 5 kgPE/g-Ti·h.

We have decided to extend our research to include a complex MgCl₂(THF)₂ support, because it proved to be very good as a supporter of Ziegler - Natta catalysts. These results are presented in Tab. 1.

Table 1. The influence of the $\text{MgCl}_2(\text{THF})_2$ support on the activity of different metalorganic catalysts for ethylene polymerization.

| Catalyst | Cocatalyst | Mole ratio Al/M | Activity kgPE/gTi·h | Lit. |
|--|--------------------------|-----------------|---------------------|------|
| $\text{MgCl}_2(\text{THF})_2\text{TiCl}_4$ | AlEt_2Cl | 1300 | 50,00 | 7 |
| TiCl_4 | AlEt_2Cl | 360 | 358 | 8 |
| $\text{Cl}_4\text{Ti}(\mu\text{-Cl})_2\text{Mg}(\text{C}_4\text{H}_7\text{O}_2\text{CEt})_2$ | AlEt_3 | 100 | 4,98 | 9 |
| $\text{MgCl}_2(\text{THF})_2/$ $\text{Cl}_4\text{Ti}(\mu\text{-Cl})_2\text{Mg}(\text{C}_4\text{H}_7\text{O}_2\text{CEt})_2$ | AlEt_3 | 100 | 56,37 | 9 |
| VCl_3 | AlEt_2Cl | 100 | 9,74 | 9 |
| $\text{MgCl}_2(\text{THF})_2/\text{VCl}_3(\text{THF})_3$ | AlEt_2Cl | 100 | 254,41 | 9 |
| VOCl_3 | AlEt_2Cl | 30 | 7,6 | 10 |
| $\text{MgCl}_2(\text{THF})_2/\text{VOCl}_3$ | AlEt_2Cl | 1670 | 189,8 | 10 |
| $\text{MgCl}_2(\text{THF})_2/\text{VCl}_4$ | AlEt_2Cl | 5000 | 271,5 | 11 |

RESULTS

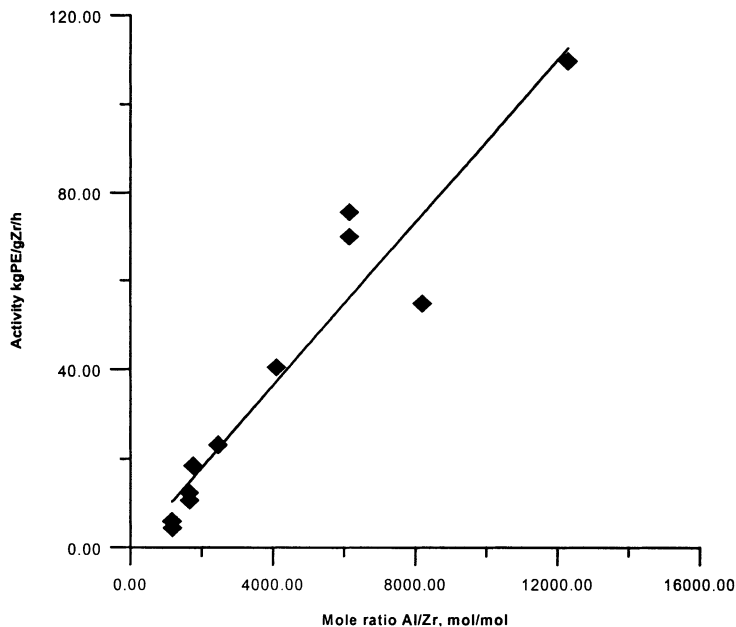
Our preliminary studies were carried out to determine the activity of zirconocene catalyst Cp_2ZrCl_2 supported on a complex of MgCl_2 with tetrahydrofuran $\{\text{MgCl}_2(\text{THF})_2\}$ by using methylaluminoxane (MAO) as a cocatalyst. These activities are presented in Tab. 2

The molar ratio Al / Zr was found to have a most important effect on the activity of this new catalytic system. The activity (A) as a function of mole ratio Al/Zr is a straight line as show in Fig.1.

Table 2. Conditions and results of ethylene polymerization. catalyst: $\text{MgCl}_2(\text{THF})_2/\text{Cp}_2\text{ZrCl}_2$, cocatalyst: MAO, polymerization conditions: $p=0.5\text{MPa}$, $T=323\text{K}$

| $\text{C}_{\text{Zr}} \times 10^5$ mol/dm ³ | Al:Zr mol/mol | Activity kg PE/gZr·h |
|---|------------------|-------------------------|
| 3.5 | 1180 | 15.23 |
| 2.5 | 1172 | 5.89 |
| 2.5 | 1652 | 12.34 |
| 2.5 | 1660 | 10.62 |
| 3.5 | 1180 | 4.37 |
| 3.5 | 1757 | 18.42 |
| 2.5 | 2460 | 23.06 |
| 1.5 | 4100 | 40.42 |
| 1.0 | 6150 | 69.95 |
| 1.0 | 6150 | 75.55 |
| 0.5 | 8200 | 54.82 |

Fig. 1. Activity of $\text{MgCl}_2(\text{THF})_2/\text{Cp}_2\text{ZrCl}_2/\text{MAO}$ catalytic system in ethylene polymerization as a function of mole ratio Al/Zr. Polymerization conditions: $C_{\text{Zr}} = (3.5 - 0.5) \times 10^{-5} \text{ mol/dm}^3$



Therefore, we can decrease considerably the concentration of the zirconium compound of catalyst system by using relatively high concentration of alkylaluminium compound, what is more environmental friendly. What should be stressed is that the obtained activity 110 kgPE/gZr-h, was a several time better than that obtained with other supported metallocene catalyst [3-6]. The studied catalytic system proved to be very stable in the polymerization process (Fig. 2.).

Molecular weights of resulting PE were determined by gel chromatography (Fig. 3, Tab. 3).

Fig. 2. Activity of $\text{MgCl}_2(\text{THF})_2/\text{Cp}_2\text{ZrCl}_2/\text{MAO}$ catalytic system in ethylene polymerization as a function of polymerization time; polymerization conditions: $C_{\text{Zr}} = 0.5 \times 10^{-5} \text{ mol/dm}^3$, $C_{\text{Al}} = 6.15 \times 10^{-2} \text{ mol/dm}^3$, $p = 0.5 \text{ MPa}$, $T = 323 \text{ K}$

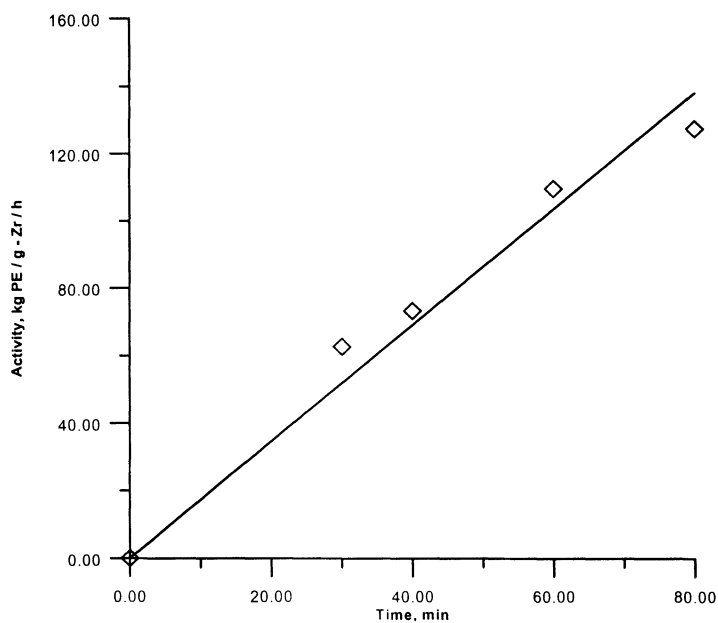


Fig. 3. Molecular weight distributions of PE obtained on the metallocene catalytic system: $\text{MgCl}_2(\text{THF})_2/\text{Cp}_2\text{ZrCl}_2/\text{MAO}$

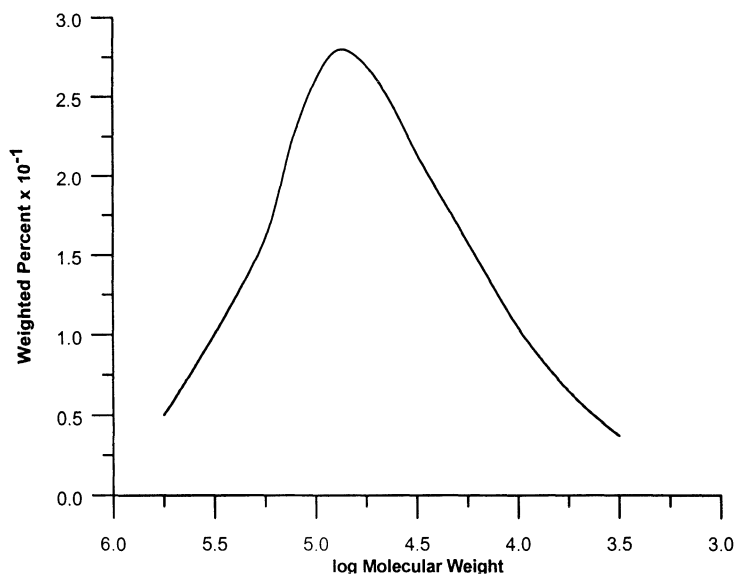


Table 3. Catalyst: $\text{MgCl}_2(\text{THF})_2/\text{Cp}_2\text{ZrCl}_2 + \text{MAO}$, polymerization conditions: $p=0.5\text{MPa}$, $T=323\text{K}$

| $C_{\text{Zr}} \times 10^5$ mol/dm ³ | Al:Zr mol/mol | t_{pol} min | Yield kg PE/g-Zr | M_w | M_w/M_n |
|--|------------------|-------------------------|---------------------|--------|-----------|
| 0.5 | 12300 | 60 | 109.81 | 113504 | 3.05 |
| 0.5 | 12300 | 30 | 62.66 | 135960 | 2.50 |
| 0.5 | 12300 | 40 | 73.31 | 136030 | 2.53 |
| 0.5 | 12300 | 80 | 127.66 | 134278 | 2.20 |

Table 4. Kinetic parameters of ethylene polymerization over the $\text{MgCl}_2(\text{THF})_2/\text{Cp}_2\text{ZrCl}_2/\text{MAO}$ catalytic system

| $C_{\text{Zr}} \times 10^5$ mol/dm ³ | R_p molEt /molZr·min | n_o^*/n_k mol/mol | k_p dm ³ /mol·min | k_r dm ³ /mol·min |
|--|------------------------------|------------------------|-----------------------------------|-----------------------------------|
| 0.5 | 4436 | 0.122 | 75751 | 15.64 |

$n_o^*=n^*$ - concentration of active sites, mol/dm³

n_k - catalyst concentration ($n_k=C_{\text{Zr}}$), mol Zr/dm³

n_o^*/n_k -share of active sites in the catalyst

k_p - the propagation rate constant

k_r - the regeneration rate constant of active sites

DP - polymerization degree of polyethylene

The obtained data (Tab.3) were used to perform a kinetic analysis of the polymerization process over the studied catalytic system. The kinetic model presented elsewhere [12] was used to calculate the concentration of active sites and rate constants for elementary reactions (Tab.4). In the supported catalyst, about 12% of zirconium atoms were found to be involved in the creation of active sites. In our system, the degree of polymerization DP, determined by the rate constants k_p/k_r was the similar to the DP measured by GPC, thus showing the kinetic analysis to be correct.

$$DP_{\text{exp.}} = 4641 \quad DP = k_p/k_r = 4843$$

CONCLUSIONS

The presented studies proved to obtain a new supported metallocene catalyst.

The catalytic activity of Cp_2ZrCl_2 supported on $\{\text{MgCl}_2(\text{THF})_2\}$ by using methylaluminoxane (MAO) as a cocatalyst was investigated in the low-pressure polymerization of ethylene.

This supported catalyst system found out to be active (110 kgPE/gZr·h) and stable during polymerization process.

The PE obtained has molecular weight (MW) about 135 000 and narrow MWD 2. The kinetic investigation of the polymerization process revealed 12% of the zirconium atoms to be involved in the forming catalytic active sites.

Acknowledgement

The authors would like to thanks, Prof. W. Kaminsky from University of Hamburg, for sample of MAO, which allowed us to do this work.

References

1. Soares J. B. P., Hamielec A. E.: Polym. React. Eng.1995, 3 (2), 131.
2. Kaminsky W., Renner F.: Macromol. Chem. Rapid Commun.1993, 14, 239.
3. Soga K., Kaminaka M.: Macromol. Chem. 1993, 194, 1745.
4. Sachii M. C., Zucchi D., Tritto I., Locatelli P.: Macromol. Rapid Commun. 1995, 16, 581-590.
5. Ross P., Meier G. B., Samson J. J. C., Weickert G., Westerterp K. R.: Macromol. Rapid Commun. 1997, 18, 319-324.
6. Sarma S. S., Sivaram S.: Macromol. Chem. Phys.1997, 198, 495-503.
7. Nowakowska M., Bosowska K., Macromol. Chem.1992, 193, 889.
8. Nowakowska M., Bosowska K., J. of Appl. Polymer Science 1998, 69, 1005-1011.
9. . Szczegot K., Prekursory katalizatorów polimeryzacji etylenu, Studia i monografie, Opole, 1995.
10. Czaja K., Bia ek M., Macromol. Rapid Commun. 1996, 17, 253 .
11. Czaja K., Bia ek M., Och dzan W., Polimery 1997, 42 (11 –12), 715.
12. Czaja K., Bia ek M, Polimery 1996, 41, 412.

5. Polystyrene and Copolymers

Syndiospecific Polymerization of Styrene

K. Yokota, T. Inoue, S. Naganuma, H. Shozaki, N. Tomotsu, M. Kuramoto, N. Ishihara*

1-1, ANESAKI-KAIGAN, ICHIHARA, CHIBA, 299-0193, JAPAN

● 16007675@ipc.idemitsu.co.jp

Abstract. Syndiotactic polystyrene, namely XAREC[®] is being developed by Idemitsu Petrochemical Co., Ltd. as a major new polymer family. XAREC[®] is a new crystalline engineering thermoplastic with a crystalline melting point of 270 °C. Because of its crystalline nature, XAREC[®] has a high heat resistance, an excellent chemical resistance and a water/steam resistance. XAREC[®] also has the dip soldering resistance. Potential applications for XAREC[®] include surface-mount electronic devices and electrical connectors. In this paper, some mechanistic models for polymerization and stereo-regulation as well as the factors which affect the activity and stereospecificity of the catalysts are discussed. The effects of substitutions on Cp ligand of half titanocene complexes were examined. The bulky substitution groups reduce the activity. Also, borate compounds as activator and effects of hydrogen are discussed.

1. Introduction

Polystyrene has been used as a commodity plastic for a long time. Especially it is an indispensable material in the field of electric appliances which require a certain stiffness. But its amorphous nature limits the application areas because of its poor resistance to heat and solvents.

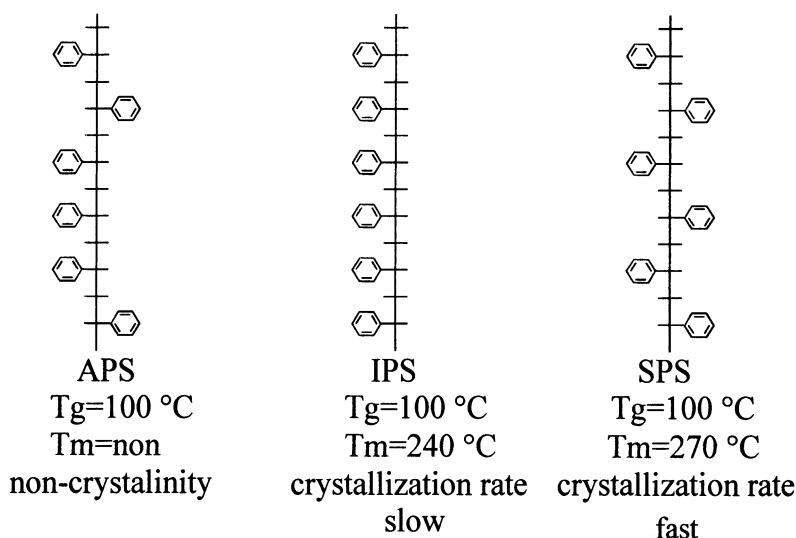
Since the discovery of Ziegler-Natta catalyst in the early 1950's, extensive studies concerning the stereospecific polymerization of olefins have been carried out [1,2]. In the field of polystyrene, isotactic polystyrene (IPS) was discovered by Natta in 1955 [3,4]. IPS is a crystalline polymer and has a high melting point ($T_m = 240^\circ\text{C}$), but the crystallization rate of IPS is too slow to be practical in injection moulding.

Ishihara et. al. succeeded in the synthesis of syndiotactic polystyrene (SPS) in 1985 [5]. This is the first known case of syndiospecific polymerization for styrene. The melting point of SPS is 270°C and its crystallization rate is extremely faster than that of

IPS. SPS is a crystalline polymer with high stereoregularity and this polymer is entirely different from conventional amorphous polystyrene in chemical and physical properties. Furthermore, the low specific gravity, low dielectric constant, high modulus of elasticity and excellent resistance to water and other chemical agents make SPS a promising material for a large number of applications in many markets.

The world first commercial plant, which has the ability to provide 5,000 ton of SPS in a year, was completed at Chiba factory of Idemitsu Petrochemical Co., Ltd. in Japan in 1996. And from this year SPS named XAREC® has been commercially provided.

Fig. 1. Structure and property derived from stereoregularity of polystyrene



2. Review of SPS catalyst systems

The catalyst for syndiospecific polymerization of styrene typically consists of transition metal compound and methylaluminumoxane (MAO). The evaluation of various transition metal compounds with MAO for styrene polymerization has been done [6]. To date, it was reported that many titanium and some zirconium complexes with MAO gave syndiospecific polystyrene

and polymerization activities of titanium complexes with one cyclopentadienyl ligand were relatively high for SPS.

It is explained the mechanisms of polymerization as following [7]. At first, titanium compound is reduced to trivalent species and alkylated by MAO. Secondly, styrene coordinates to metal center by η^4 mode and inserts to Ti-alkyl bond at secondary direction. Following phenyl group on chain end coordinates to metal center, inserted styrene is controlled to syndiospecific by steric repulsion with the coordinated chain end phenyl group. Then secondary insertion and coordination are continued to produce SPS.

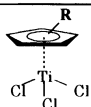
3. Results and discussion

3.1 Transition Metal Compounds

Among the SPS producing catalysts, titanocene complexes with one cyclopentadienyl ligand yield the highest for SPS. The polymerization activities of some titanium compounds with different substituents on the cyclopentadienyl ligand was reported [8].

Table 1. Polymerization activities of substituted cyclopentadienyltitaniumtrichloride

| R | Relative Activity ^{a)} | Mw | Mw/Mn | MIP(% ^{b)}) |
|---------------------------|---------------------------------|--------|-------|-----------------------|
| H (1) | 100 | 62000 | 2.2 | 80.1 |
| Me(2) | 110 | 63000 | 2.2 | 80.1 |
| 1,2,4-Me ₃ (3) | 110 | 63000 | 2.2 | 80.1 |
| Me ₅ (4) | 156 | 750000 | 2.2 | 93.2 |



a)Catalytic activity of CpTiCl₃ sets to100

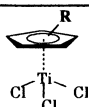
b)Methylethylketone insoluble portion

The catalyst activities increase with the number of methyl group on Cp ligand. Although an introduction of the substituents should disturb the polymerization reaction sterically, the polymerization activities increased by substitutions. It seems that the factor of the activity control is the electronic effect. Okuda et. al. [9] and Gassman et. al. [10] reported about the relationship between the electron donating ability of ligand and ⁴⁹Ti-NMR chemical shift. In the

titanium compounds ^{49}Ti -NMR peaks are shifted to the lower magnetic field by introducing the electron donating substituent on the cyclopentadienyl ligand. The values of ^{49}Ti NMR chemical shift of (1)~(4) are listed in Table 2. In the case of SPS polymerization by indenyl titanium complexes with MAO, the similar results were reported by Ready et al. [11] and Kim et al. [12]

Table 2. ^{49}Ti -NMR chemical shifts of titanium complexes

| R | Relative Activity ^{a)} | ^{49}Ti Chemical Shift ^{b)} |
|---------------------------|---------------------------------|---|
| H(1) | 100 | -394 |
| Me(2) | 110 | -332 |
| 1,2,4-Me ₃ (3) | 110 | — |
| Me ₅ (4) | 156 | -95.3 |



a)Catalytic activity of CpTiCl_3 sets to 100

b)use $^{49}\text{TiCl}_4$ as standard

In this work, the influences of electron donating ligands were investigated in more detail. In this experiments, polymerization was done on the same conditions [Cat. (mole ratio) : Ti / MAO / TIBA = 1 / 200 / 200 ; Polymn. temp.:70°C; Polymn. time:60min.].

Table 3. Polymerization of styrene using substituted cyclopentadienyltitaniumtrichloride and ^{49}Ti -NMR chemical shifts

| R | Activity(kg/gTi) | Mw | ^{49}Ti Chemical Shift ^{a)} |
|-------------------------|------------------|--------|---|
| Me(4) | 170 | 900000 | -95.29 |
| Et(5) | 180 | 870000 | -103.28 |
| nPr(6) | 47 | 945000 | -102.30 |
| nBu(7) | 107 | 906000 | -101.00 |
| iPr(8) | 62 | 406000 | - |
| cycHex(9) | 47 | 559000 | - |
| AdaCH ₂ (10) | 54 | 678000 | - |

Polym. Temp. 70 ° C, Polym. Time 1hr

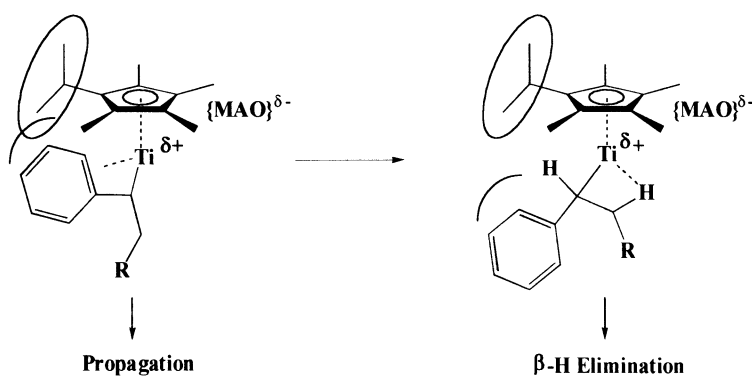
Ti:MAO:TIBA=1:200:200 a)use $^{49}\text{TiCl}_4$ as standard

At first, the influences of various linear alkyl substitutions were studied by displacing one of five methyl groups on pentamethylcyclopentadienyl ligand. Polymerization results using the compounds (4) to (7) are shown in Table 3.

The complex (5) substituted by ethyl group shows the same catalytic activity and the same molecular weight as (4). Otherwise, the substitutions by n-propyl (6) and n-butyl (7) groups extremely reduce the catalytic activities, but not change the molecular weight of polymers.

The catalytic activities and the ^{49}Ti chemical shifts of (4) to (7) are shown in Table 3. The difference of the ^{49}Ti chemical shifts is small. This means that the electron donating abilities of these alkyl groups are approximately equivalent. It is considered that the dominant factor of the propagation rate is the bulkiness of the substituents.

To evaluate the steric effect of the substituents, some complexes with branched alkyls were synthesized. It is considered that isopropyl group has the same bulkiness as ethyl group because $^1\text{H-NMR}$ spectrum of (8) shows that the isopropyl group rotates freely. But the isopropyl substitution extremely decreases the activity (Table 3). It can be explained that the ethyl group can open the coordination space by rotation but isopropyl always cover the coordination space. In this table, it is noteworthy that the molecular weights of the polymers are changed..



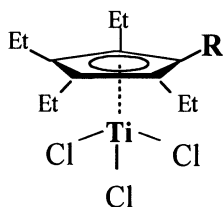
Scheme 1. Speculation for facilitation of β -H elimination

Different from the case of olefin polymerization, styrene is polymerized via coordination of the chain end phenyl group to the metal center. In the case of catalysts which contain alkyl substitutions, it is concluded that the low activities were due to the decrease of propagation rate. If the rate of chain transfer dose not change, the molecular weight of obtained polymer would decrease. But the linear alkyl groups do not decline their molecular weights. From the fact, it can be thought that the rate of chain transfer also decrease. Otherwise, in the case of branched alkyl substitutions, the molecular weights of obtained polymers decreased. It can be explained that the branched alkyl groups avoid the coordination of the phenyl group of the polymer end and facilitate β -H elimination (Scheme 4).

As shown in table 3, in the case of tetra methyl monoethyl substituent, the activity is the same as that of pentamethyl substituent. Therefore, ethylsubstituents were investigated. As can be seen in table 4, the polymerization actiivities were extremely decreased by pentaethyl groups in Cp ligands.

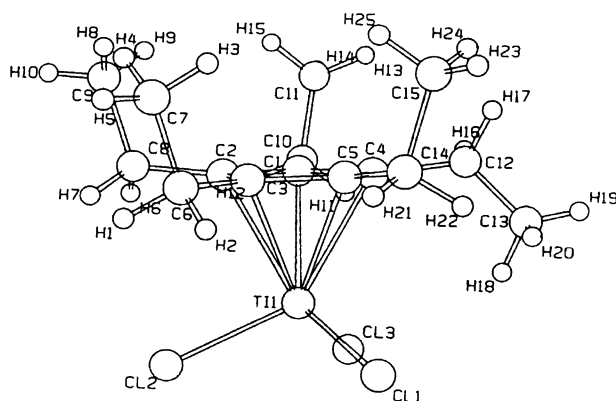
Table 4. Effects of alkyl substituents in Cp ligands for catalytic activities and molecular weight

| R | Activity(kg/gTi) | Mw |
|-----------|------------------|----------|
| Me | 120 | 1110,000 |
| Et | 54 | 1030,000 |



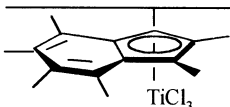
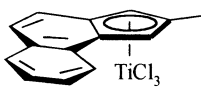
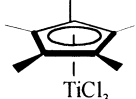
Polym. Temp. 70 ° C, Polym. Time 1hr
Ti:MAO:TIBA=1:200:200

The X-ray crystal structure of pentaethylcyclopentadienyl titanium trichloride is shown fig. 2. As to the bulkiness of ethyl group in Cp, only one ethyl group turns down. The ethyl group turned down Cp plane may approach of monomer to metal. Therefore the catalyst showed a low activity.

Fig. 2. The X-ray crystal structure of $(C_3Et_3)TiCl_3$ 

Cyclic substituents such as indenyl ligand were investigated. The bulkiness of indenyl ligand would be small than of alkyl ligand. The activity of heptamethyl indenyl titanium compound is an order of magnitude lower than that of pentamethyl Cp titanium compound. However the activity of 2-methylbenzindenyl

Table 5. Effects of substituents in indenyl ligands for catalytic activities

| Compounds | Activity(kg/gTi) |
|---|------------------|
|  | 10 |
|  | 340 |
|  | 270 |

Polym. Temp. 50 ° C, Polym. Time 1hr
Ti:MAO:TIBA=1:200:200

titanium compound is the same as that of pentamethyl Cp titanium compound. When the Ti compound have a large as a polymer chain,

the position of Ti on Cp ligand would shift from the center to the edge of Cp. At the moment, $\eta^5 \longleftrightarrow \eta^3$ ring slippage shown here would occur. Methyl-benzindenyl ligand would break the conjugation in the indenyl ring (fig. 3).

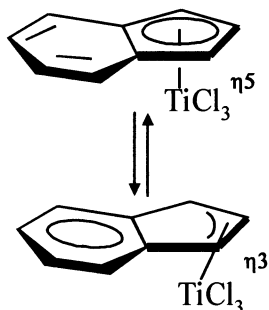


Fig. 3. The $\eta^5 \longleftrightarrow \eta^3$ ring slippage

3. 2 Borate Compounds

The syndiospecific polymerization of styrene results from the homogeneous coordinative polymerization. Borate and borane derivatives have been used as cocatalyst. We examined the catalytic activity of a titanium with several borate derivatives.

Table 6. Effects of fluorine of borate

| Borate compounds | Catalytic Activity (kg/gTi) |
|--|-----------------------------|
| $[\text{NMe}_2\text{PhH}][\text{B}(\text{C}_6\text{H}_5)_4]$ | 0 |
| $[\text{NMe}_2\text{PhH}][\text{B}(\text{C}_6\text{H}_4\text{F})_4]$ | 0 |
| $[\text{NMe}_2\text{PhH}][\text{B}(2,4\text{-F}_2\text{C}_6\text{H}_3)_4]$ | 5 |
| $[\text{NMe}_2\text{PhH}][\text{B}(3,4,5\text{-F}_3\text{C}_6\text{H}_2)_4]$ | 10 |
| $[\text{NMe}_2\text{PhH}][\text{B}(\text{C}_6\text{F}_5)_4]$ | 250 |
| $[\text{NMe}_2\text{PhH}][\text{B}(3\text{-(CF}_3\text{)C}_6\text{F}_4)_4]$ | 20 |

* Polym. Cond. ; Styrene 10ml, Cp*TiMe₃ 5x10⁻⁷ mol, [N][B] 5x10⁻⁷ mol, TIBA 3x10⁻⁶ mol
Polym. Temp. 70 ° C , time 4Hr

The active borate compounds have a tetraphenylborate anion. The effect of anions on the catalyst activity is summarized in Table 6. Fluorine substituents on the position of 3, 4, 5 increase the catalyst activity. It is thought that the delocalization of negative charge in borate may increase the catalyst activity. The effects of a cation part in a borate complex on a catalyst activity are listed in Table 7. The activity increases with decreasing the number of pKa of these complex. This suggests that pyridines which are formed in the reaction of titanium compound with a borate complex, may coordinate to active species.

Table 7. Effects of pyridinium anions of borate

$$\text{Cp}^*\text{TiMe}_3 + [\text{NR}^1\text{R}^2\text{R}^3\text{R}^4][\text{B}(\text{C}_6\text{F}_5)_4] \rightarrow [\text{Cp}^*\text{TiMe}_2][\text{B}(\text{C}_6\text{F}_5)_4] + \text{NR}^1\text{R}^2\text{R}^3 + \text{MeR}^4$$

| Borate compounds | | Catalytic Activity (kg/gTi) |
|---|--|-----------------------------|
| $[\text{NR}^1\text{R}^2\text{R}^3\text{R}^4]$ | pKa of $\text{NR}^1\text{R}^2\text{R}^3$ | |
| NMe ₂ PhMe | 5.1 | 2.0 |
| PyMe | 5.2 | 2.0 |
| 4-CN-PyMe | 1.9 | 2.8 |
| 3-CN-PyMe | 1.0 | 31.8 |
| 2-CN-PyMe | -0.3 | 40.5 |

* Polym. Cond. ; Styrene 10ml, Cp*TiMe₃, 5x10⁻⁷ mol, [N][B] 5x10⁻⁷ mol, TIBA 3x10⁻⁶ mol
Polym. Temp. 70 ° C , time 4Hr

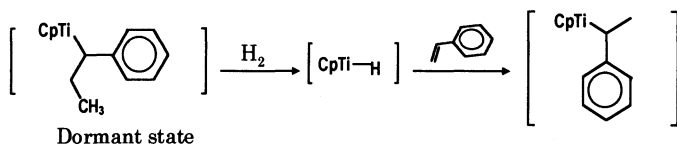
3.4 Effects of Hydrogen

The effects of addition of hydrogen on the catalyst activity are listed in Table 8. Addition of hydrogen increases catalytic activity. It is thought that in the presence of hydrogen, an active center would escape from its dormant state by a chain transfer. Then SPS polymerization proceeds via a Ti-H complex. Accordingly, hydrogen is a strong activator of syndiotactic polymerization of styrene.

Table 8. Effects of hydrogen on polymerization

| P_{H_2} (kg/cm ³) | Relative Activity ¹⁾ | Mw/Mn |
|---------------------------------|---------------------------------|-------|
| none | 100 | 2.1 |
| 0.1 | 160 | 2.5 |
| 0.5 | 210 | 4.5 |
| 1.0 | 220 | 12.0 |

¹⁾Catalytic activity without hydrogen sets to 100



4. Concluding remarks

The discovery of homogeneous metallocene catalysts in the 1980s has opened up new possibilities to fine-tune the stereochemical structure of polymer products. Using these novel catalysts, a large number of novel polymer products with specific properties have been obtained. The development of these catalysts for commercial processes and commercial polymers will be a dominant force in the polymer industry through the next century.

5. References

- [1] J. Boor Jr., Ziegler-Natta Catalyst and Polymerization, Academic Press, New York, 1979.
- [2] J. C. W. Chien, Coordination Polymerization, Academic Press, New York, 1975.
- [3] G. Natta, P. Pino, E. Mantica, F. Danusso, G. Mazzanti, M. Peraldo, *Chim. Ind.*, 38(1956)124.
- [4] G. Natta, F. Danusso, D. Sianesi, *Makromol. Chem.*, 28(1958)253.
- [5] N. Ishihara, T. Seimiya, M. Kuramoto, M. Uoi, *Macromolecules* 19(1986)2465.
- [6] N. Ishihara, M. Kuramoto, "Catalyst Design for Tailor-made Polyolefins" (Soga, Terano(eds)), Kodansha-Elsevier(Tokyo), 339(1994).
- [7] N. Mitani, N. Ishihara, T. Seimiya, T. Ijitsu, T. Takyuu, *Polymer Preprint Japan*, 37(1988)1152. C. Pellecchia, P. Longo, A. Grassi, P. Ammendola A. Zambelli, *Makromol. Chem., Rapid Commun.*, 8(1987)277. C. Pellecchia, D. Pappalardo, L. Oliva,

- A. Zambelli, *J. Am. Chem. Soc.*, 117(1995)6593. N. Ishihara, *Macromol. Symp.*, 89(1995)553. J. C. W. Chein, Z. Salajka, S. Dong, *Macromolecules*, 25(1992)3199.
- [8]N. Tomotsu, M. Kuramoto, M. Takeuti, H. Maezawa, *Metallocenes '96*, 179(1996)
- [9]A. Hafner, J. Okuda, *Organometallics*, 12(1993)949.
- [10]P. G. Gassman, W. H. Campbell, D. W. Macomber, *Organometallics*, 3(1984)385.
- [11]T. E. Ready, J. C. W. Chein, M. D. Rausch, *J. Organomet. Chem.*, 519(1996)21.
- [12]Y. Kim, B. H. Koo, Y. Do, *J. Organomet. Chem.*, 527(1997)155.

Monocyclopentadienyl Titanium Catalyst

James C. W. Chien* and Marvin D. Rausch*

Amherst Polymer Technology, Inc.
Department of Polymer Science and Engineering
Department of Chemistry, University of Massachusetts
Amherst, Massachusetts 01003, USA

Abstract. Monocyclopentadienyl titanium complexes are active catalysts for syndiotactic polymerization of styrene. The activity is severely suppressed when the Cp ligand has a substituent with a Lewis basic heteroatom. The active species is a titanium cation generated by the usual cocatalyst. Electron paramagnetic resonance and polymerization studies of a series of monocyclopentadienyl titanium precursors with different propensity for reduction showed that both the tetravalent and trivalent Ti^+ species are active, with the former having the greater activity than the latter. Very stable catalysts have been found as a result. In contrast, monocyclopentadienyl titanium complexes are poor for ethylene or propylene polymerization; but the activity is greatly improved with a coordinative substituent on the Cp ligand.

Introduction

Since the invention of organometallic mixed catalyst by Ziegler, whose 100th birthday we celebrate during this International Symposium, there were several major improvements variously regarded as new generations of Ziegler catalyst. Homogeneous systems allowed the preparation of many polyolefins having modified and improved molecular architecture in controlled manner. The most significant achievement is the polymerization of styrene to the new syndiotactic polystyrene (s-PS) by Ishihara et al. [1] Two types of catalysts have been found [1-4] homoleptic hydrocarbyl complexes and mono- η^5 -cyclopentadienyl (Cp) compounds of titanium activated by MAO. Other cocatalysts $(C_6H_5)_3C^+ B^-(C_6F_5)_4$ [5] and $B(C_6F_5)_4$ [6] were also found to be effective. On the other hand, titanocene precursors are poorly active. Organic compounds of most other transition metals are either inactive or non-stereoselective.

Kinetics

$CpTi(OBu)_3$ / MAO is a typical mono-Cp catalyst for styrene polymerization which is highly active and syndioselective.[8] The rate of polymerization is

constant (Figure 1); the yield of s-PS is directly proportional to the monomer concentration [S] (Figure 2). The activity under optimum conditions of [Ti], [Al], and solvent at 45°C is $A_S = 3 \times 10^7$ g PS / (mol Ti · mol S · h) which corresponds to a turn-over-rate of 88 styrene insertion/s.

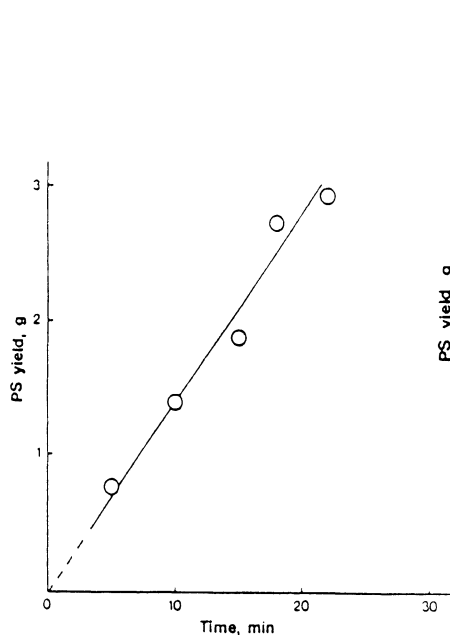


Fig. 1. Styrene polymerization profile catalyzed by $\text{CpTi}(\text{OBU})_3$ (83 μM) / MAO Al / Ti = 1000, in toluene/chlorobenzene solvent mixture (1:1).

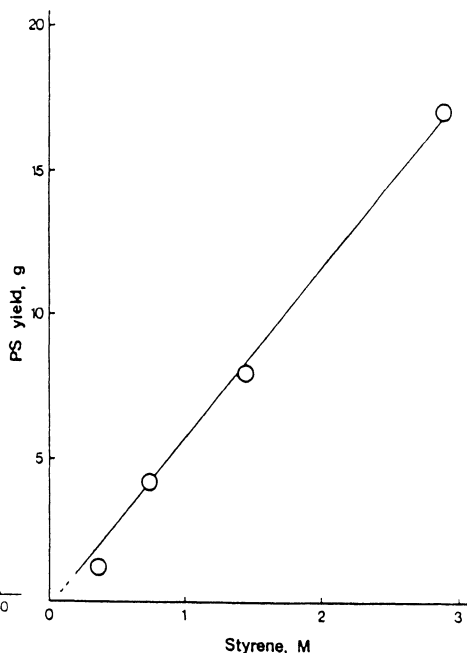


Fig. 2. Variation of PS yield with [S], $[\text{CpTi}(\text{OBU})_3] = 0.83 \mu\text{M}$, $[\text{MAO}] = 83 \text{ mM}$ in Al, $T_p = 60^\circ\text{C}$

The yield of 2-butanone insoluble highly stereoregular s-PS (SY) is 99%; it has $M_n = 1.5 \times 10^4$ ($\text{DP}_n = 144$), and polydispersity (PD) = $M_w / M_n = 2.8$. Both PD and SY increase with the increase of styrene concentration. The SY is quite dependent on the temperature of polymerization (T_p) as shown in Figure 3, it declines to a low s-PS content of only 49% at 90°C. Over the experimental conditions investigated, s-PS with PD ranging from 2.0 to 5.7 have been obtained. The melting transition temperature (T_m) also decreases with the increase of T_p , very similar behaviors have been reported for $\text{CpTiCl}_3 / \text{MAO}$ and $\text{Cp}^*\text{TiCl}_3 / \text{MAO}$.⁹ The polymerization activity increases with decreasing [Ti] (Figure 4) which is a characteristics commonly exhibited by metallocene catalysts.

The concentrations of the stereochemical tetrads have been determined from the areas of the methylene resonances [9], which can be fitted with the Bernoullian symmetric model of stereospecific propagation by a single P_r parameter. The effect of T_p on P_r afforded estimates for the stereocontrol energy which was found be 2 kcal/mol for CpTiCl_3 . This driving energy includes both opposite facial complexation of styrene, occasional configuration inversion of the Ti of the active

species lacking coordinated monomer, or occurrence of *cis* π -ligand insertion instead of the usual *cis* alkyl ligand migration.

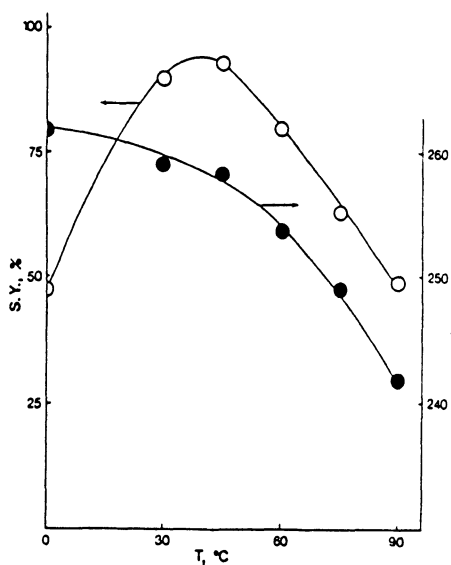


Fig. 3. Variation of SY and T_m of PS vs. temperature of polymerization for $[\text{CpTi}(\text{OBu})_3] = 83 \text{ gM}$, $\text{MAO/Ti} = 1000$ in Al.

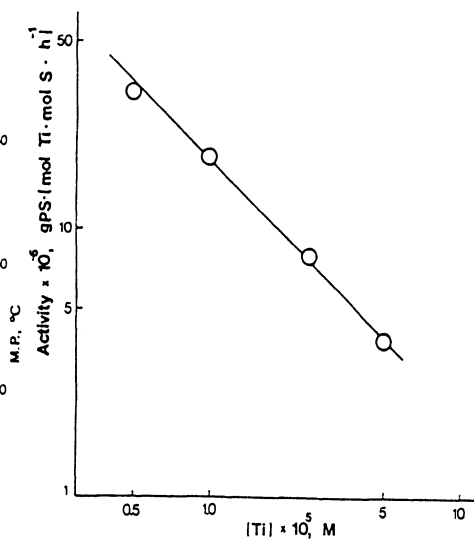
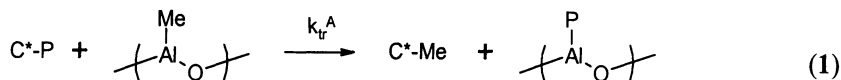


Fig. 4. Log-log plot of activity versus $[\text{Ti}]$ for $[\text{Al}]$ in $\text{MAO} = 83 \text{ mM}$.

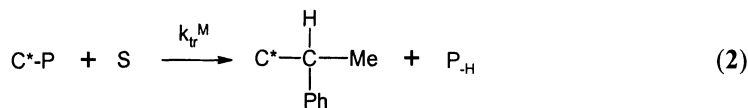
While the ketone insoluble fraction is high stereoregular, even the acetone soluble fraction is also prevailing syndiotactic and crystalline. However, the soluble material is less stereoregular and has lower M_w as well as lower T_m . It is denoted as a-PS even though the polymer is not entirely atactic.

The number of active site in a polymerization can be counted using CH_3OH .

Figure 5 is a plot of $[\text{metal polymer bond}]$ vis PS yield. The intercept gives the active site concentration, while the slope affords the increase of number of metal polymer bond due to chain transfer from Ti to MAO,



From the slope of a plot of DP_n vs $[\text{S}]^{-1}$ (Figure 6), one can obtain the chain transfer to monomer rate constant.



The spontaneous chain transfer is β -hydride elimination.

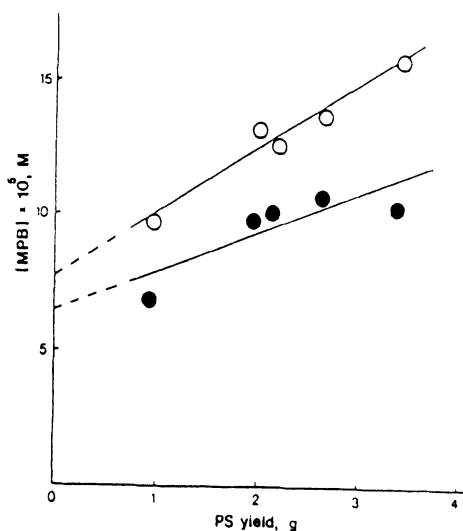


Fig. 5. Variation of [metal polymer bond] vs PS yield with $[CpTi(OBu)_3] = 83 \mu M$, $AL(MAO) / Ti = 1000$, $T_p = 45^\circ C$ in toluene.

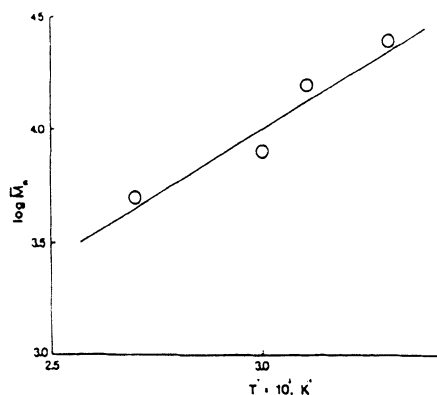


Fig. 6. Variation of $(DPn)^{-1}$ vs $[S]^{-1}$ for s-PS obtained in polymerizations of Figure 3.

The kinetic results are summarized in Table 1. The $CpTi(OBu)_3 / MAO$ system has very active stereospecific sites (Cs^*) with average $k_p = 10.8 (Ms)^{-1}$; the less stereospecific sites (Ca^*) have much smaller $k_p = 2 (Ms)^{-1}$. About 80% of the Ti forms the first type of active site; most of the remainder belongs to the second type.

The $TiBz_4 / MAO$ catalyst produce lower SY of PS, it has fewer number of C^* lower k_p value than $CpTi(OBu)_3 / MAO$.

Table 1. Kinetic parameters for styrene polymerization.

| Catalyst Fraction | Bz_4Ti/MAO | | $CpTi(OBu)_3/MAO$ | |
|--|--------------|-------|-------------------|------|
| | s | a | s | a |
| $A * 10^{-6}, g PS / (mol Ti mol S h)$ | 0.14 | 0.02 | 50.6 | 2.1 |
| $R_p * 10^5, Ms^{-1}$ | 5.5 | 2.2 | 51 | 1.6 |
| SY, % | 71 | | 96 | |
| C^* fraction of Ti | 1.7 | 17 | 79 | 13 |
| $[C^*] * 10^{-4}, M$ | 0.14 | 1.4 | 0.66 | 0.11 |
| $k_{p_s}, (Ms)^{-1}$ | 1.38 | 0.056 | 10.8 | 2.0 |
| $k_{tr}^A * 10^4, S^{-1}$ | 5.2 | 6.5 | 6.2 | 43 |
| $k_{tr}^M * 10^2, (MS)^{-1}$ | | | 6.7 | |
| $k_{tr}^{\beta} * 10^2, S^{-1}$ | | | 4.7 | |

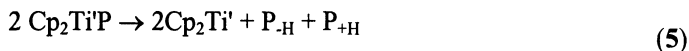
Its interesting to compare this s-PS catalyst with the ethylene bis(4,5,6,7-tetrahydro-1-indenyl)zirconium dichloride/MAO catalyst [10] for isospecific polymerization of propylene. The latter at 3500 : 1 [Al]/[Zr] has C* amounted to 66% of the zirconocene, 33% each of the isospecific and the less stereospecific sites. Their rate constants of propagations are 1,500 (Ms)⁻¹ and 100 (Ms)⁻¹, respectively with 0.02 s⁻¹ and 0.005 s⁻¹ for the k_{tr}^A values. Thus the rate of styrene insertion is about hundred times slower and the rate of transfer to Al about hundred times faster than this catalyst. Thus the s-PS molecular weight is much lower than the i-PP.

Reductive Decomposition

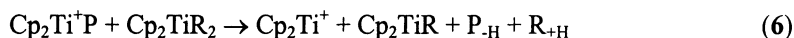
In the pioneering work of the first homogeneous Z-N catalyst system Cp₂TiCl₂ / AlR₂Cl [11], the active species is a tetravalent titanium complex which decomposes by bimolecular reductive disproportionation [12].



where P-H and P+H are the polyethylene molecules having vinyl and saturated end-groups, respectively. When cation generating cocatalyst is used, the reaction can be represented by



or

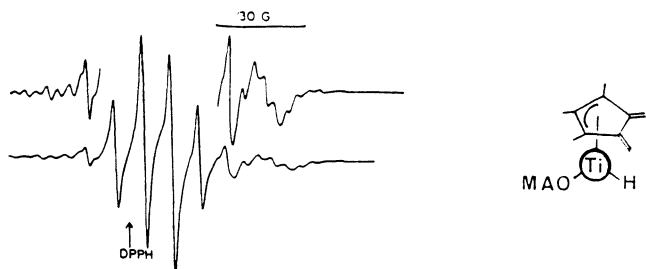


Reaction 6 does not need to overcome a coulombic repulsive barrier as it does in reaction 5. The trivalent Ti complexes can be partially reoxidized by air and reactivated for further polymerization of ethylene. The crystal structure Of Cp₂TiCl₂AlEt₂ was determined [13] and electron paramagnetic resonance (EPR) had been employed to follow the reductive decomposition of Cp₂TiCl₂ / EtAlCl₂ in toluene[14]. The reduction Of Cp₂ZrCl₂ by Et₃Al was studied by Sinn and coworkers [15-17].

CpTiCl₃ is readily reduced by MAO to a single Ti(III) species at g = 1.989 with proton splitting aH = 7.4 G [18]. The doublet coalesces to a singlet upon exposure to D₂. The reduction of Cp*TiCl₃ by MAO is slower, involving several different Ti(III) complex intermediates and took many hours to complete [18].The final product is a Ti(III) complex with an assigned structure comprising one η³-allyl and one η⁴-butadiene ligand (Figure 7).

Cp*TiMe₃ activated by either MAO, Ph₃C[⊕] or B(C₆F₅)₃, polymerizes styrene with very high stereospecificity (S.Y. = 99%) and high activity of 10⁷ g sPS / (mol Ti mol S h) using [Ti] = 0.1 mM, T_p = 50°C, t_p = 1 h. Under these condition, an equal stoichiometric mixture of Cp*TiMe₃ / Ph₃C[⊕] B⁻(C₆F₅)₄ or Cp*TiMe₃ / B(C₆F₅)₃ shows no detectable amount of unpaired spins [20]. In the case of the Cp*TiMe₃ / MAO (Al/Ti = 500) mixture, about 11% of the precursor was reduced

to Ti(III) [20]. Ewart et al. [21] also examined the EPR spectrum of a reaction mixture containing equal-stoichiometric amounts of Cp^*TiMe_3 and $\text{B}(\text{C}_6\text{F}_5)_3$ in chlorobenzene solution. A very weak doublet signal at $g = 1.994$ ($a\text{H} = 8.4$ G) was observed, which corresponds to 0.01% of the total titanium in solution.



The equivalency and facile H—D exchange of the five protons involved suggests the equilibria

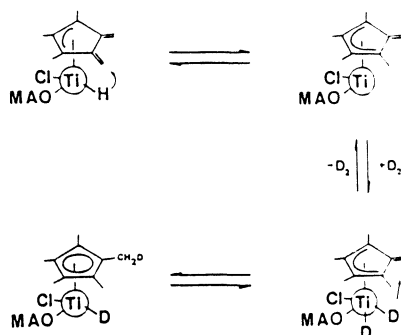


Fig. 7. EPR spectra of a reaction mixture of Cp^*TiCl_3 / MAO ($\text{Al}/\text{Ti} = 239$) after 10 h or longer reaction time. Species assignment for the spectra.

Grassi et al. [22,23] followed the reduction of $\text{Cp}^*\text{Ti}(\text{CH}_2\text{Ph})_3$ in the presence of $\text{B}(\text{C}_6\text{F}_5)_3$ at a very high conc. of 35 mM. About 60% of Ti was reduced in 3 h and no significant increase of Ti(III) afterwards. Since this reductive decomposition is a bimolecular process, the amount of Ti(III) formed in their polymerization at an initial Ti(IV) conc. of 1.7 mM would be orders of magnitude smaller than that observed by EPR [22,23]. In fact, quantitative determination of $[\text{Ti(III)}]$ at high concentration is unreliable because of excessive dipolar broadening or Heisenberg super-exchange.

There are pronounced effects of titanium precursor and cocatalyst concentrations on the reduction of $\text{CpTi}(\text{O}i\text{Bu})_3$ by MAO as well as the formed Ti(III) species as seen by EPR [19]. At low $[\text{CpTi}(\text{O}i\text{Bu})_3] = 0.08$ mM and high ratio of $\text{Al}/\text{Ti} = 1000$, which is the conditions for styrene polymerizations, the main EPR signal is a doublet at $g = 1.989$ and $a^{\text{H}} = 7.0$ G (Figure 8a) which is the same as observed previously [8] and subsequently [20-23]. It collapses to a broad singlet (Figure 8b) upon exposure to D_2 . One can discern a weak peak in both spectra on the low-field side (higher g -value). The major resonance may be assigned to the syndiospecific species $\text{CpTi}^{\oplus}\text{X}^-$ capable of maximal multi-hapto-coordinations

(*vide infra*). The species giving rise to the minor peak at $g = 1.995$, it is either lower in stereoselectivity, for instance allowing reduced haptic interactions between the monomer and the propagating chain with the metal center, or is catalytically inactive. The total spectrum integrated to 98% of the $[\text{CpTi}(\text{OBU})_3]$. This observation prompted Chien et al. [19] to propose that the stereoselective site *in this catalyst system* is a trivalent titanium (paramagnetic) complex. As the precursor concentration increases and Al/Ti ratio is lowered, the styrene polymerization activity decreases. This is accompanied by decrement of EPR signal intensity and the appearance of up to four more resonances (Figure 8c, d). At $[\text{CpTi}(\text{OBU})_3] = 29 \text{ mM}$, Al/Ti = 20 (with or without styrene), the Ti(III) signal integrated to only 40% of total titanium, and the EPR spectrum (Figure 8d, e) comprising $g = 1.992, 1.987, 1.980$ ($a^{\text{H}} = 9 \text{ G}$, $a^{\text{Al}} = 2.5 \text{ G}$), 1.965, 1.960, and 1.945.

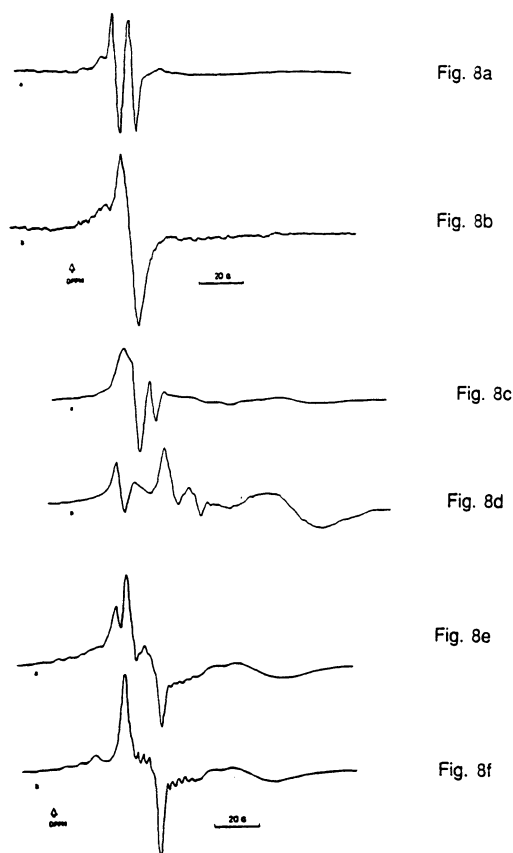
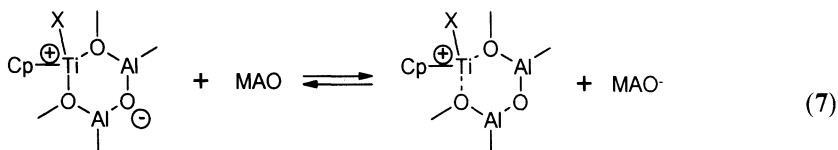


Fig. 8. EPR spectra of $\text{CpTi}(\text{OBU})_3 / \text{MAO}$ mixture from top to bottom: (a) $[\text{Ti}] = 83 \mu\text{M}$, $[\text{Al}]/[\text{Ti}]$ 1000. (b) Styrene (0.73 M) was added to (a). (c) $[\text{Ti}]$ 84 mM, $[\text{Al}] / [\text{Ti}] = 100$. (d) Styrene (0.73 M) was added to (c). (e) $[\text{Ti}] = 29 \text{ mM}$, $[\text{Al}] / [\text{Ti}] = 20$. (f) Styrene (0.73 M) was added to (e).

There are clearly eleven ^{27}Al shfs lines indicating that the metal center is coordinated to two Al atoms, the structure of which may be presented by that at the left of eq. 7.



In the presence of a larger quantity of MAO, the MAO⁻ may be displaced by neutral MAO, the coordination of which with CpTi[⊕]X is weak and dynamic. As a result there is no observable ^{27}Al shfs. It is essential for quantitative conclusion concerning the roles played by the various titanium oxidation states, that both the Ti(III) concentrations and polymerizations must be measured under identical conditions.

Active site model

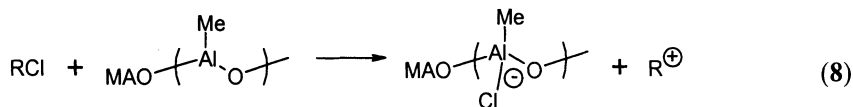
Our observation that the active species in the CpTi(OBu)₃ / MAO system are paramagnetic Ti(III) complexes fitted perfectly with Zambelli's vision of η^{n} interaction between the metal center with both the π -complexed monomer and the last inserted styrene unit. Otherwise it would be difficult to account for the exceeding regioselectiveness and stereoselectiveness of the monomer enchainment. The mechanism had been elegantly discussed several times [9,24-28].

Carbocationic (non-ZN) polymerization of styrene

a-PS can be formed by various pathways in the homogeneous catalyst promoted polymerization. The cation type cocatalyst, Ph₃C[⊕] is itself a very efficient cationic initiator of styrene polymerization. When it is employed to activate a stoichiometric amount of CpTiR₃ type precursor, a fraction of the latter is unavoidably consumed in scavenging impurities. This results in an imbalance of the two components of the catalyst systems, the excess Ph₃C[⊕] would initiate atactic carbocationic styrene polymerization.

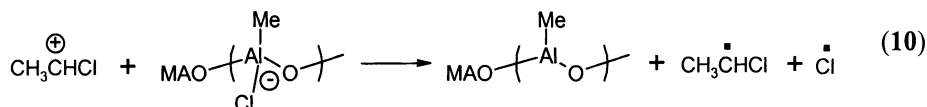
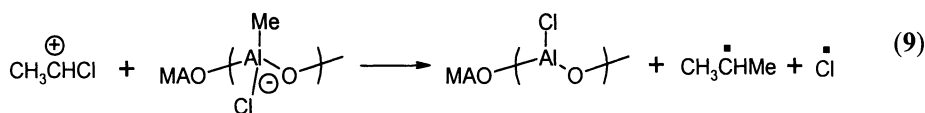
MAO is the ubiquitous cocatalyst, one of its several functions is to extract a X⁻ anion from the titanium precursor. CpTi(OPh)₃/MAO is a very active and syndiospecific catalyst producing 98% s-PS in a toluene medium. However, if the medium is changed to a 1 : 1 toluene/dichloroethane mixture or to dichloroethane entirely, the rate of polymerization was raised two and three-fold, respectively. The product is an entirely amorphous polystyrene (a-PS) devoid of a crystalline phase. This can be explained by production of the titanium cation by MAO, which reacted with dichloroethane to form carbocation which initiates atactic styrene polymerization [29].

We then found that $\text{CpTi}(\text{OPh})_3$ was not needed and in fact may not even be involved in this carbocationic formation process. A mixture of MAO / dichloroethane alone catalyzed even faster polymerization producing a-PS than with the Ti compound present. This could be caused by the direct extraction of a Cl^- anion from CH_3CHCl_2 by MAO,



Addition of NaN_3 in amount from 0.1 to 1.0 equivalent of Al suppresses this process completely because these quantities are all in excess compared to MAO which has an approximate M_n of 1200.

If the atactic styrene polymerization by MAO/RX is allowed to progress for a few minutes and then N_3^- was added, the polymerization rate decreased to certain degree but did not inhibit it completely. It seems that there is a different non-cationic initiators formed as a consequence of eq. 9. A possible initiator is a free radical which may be formed by,

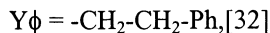
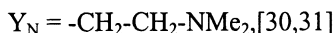


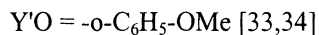
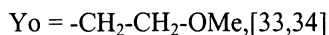
These polymerizations can be inhibited by the addition of 2,5-dimethyl-1-pyrrolinoxyl. Furthermore, a typical nitroxide electron spin resonance spectra appeared when *t*-butylphenylnitron was added to this polymerization mixture indicating the presence of a carbon (alkyl) radical.

In conclusion halogen containing solvent should not be used indiscriminately for metallocenium type system.

Effect of pendant-coordinative-group

If multi-hapto-coordination is requisite for syndiotactic styrene polymerization, then the attachment of a coordinative group on the Cp ring could profoundly interfere with this process. We have tested this hypothesis experimently with study of derivatives of CpTiCl_3 and Cp^*TiCl_3 with the following pendant-coordinative groups:





The compounds we synthesized, characterized and tested for polymerization are:

CpTiCl₃ (**1**), Cp*TiCl₃ (**2**), Y_NCpTiCl₃ (**3**), Y_NCp*TiCl₃ (**4**), (Y_NCp)₂TiCl₂ (**5**), [Y_N HClCpTiCl₂]₂O (**6**), Cp₂TiCl₂ (**7**), Y_{Ph}CpTiCl₃ (**8**), Y_{Ph}Cp*TiMe₃ (**9**), [Y_{Ph}Cp*TiMe₂]₂O (**10**), Y_oCpTiCl₃ (**11**), Y'_oIndTiCl₃ (**12**), Y'_oIndTiCl₃ (**13**).

Table 2. Comparison of polymerization^a

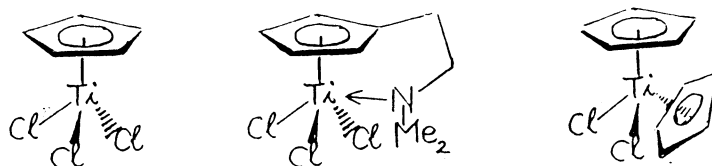
| Cat. | Styrene | | Ethylene | | | | Propylene | | | |
|----------|------------------|-----|------------------|-----------------------------|--------------------------------|-----------------------------|------------------|-----------------------------|--------------------------------|-----------------------------|
| | Act ^b | SY% | MAO | | Ph ₃ C [⊕] | | MAO | | Ph ₃ C [⊕] | |
| | | | Act ^b | M _w ^d | Act ^c | M _w ^d | Act ^b | M _w ^d | Act ^c | M _w ^d |
| 1 | 10 | 70 | 0,06 | 0,49 | 0,4 | 2,96 | 0 | | 0 | |
| 2 | 10 | 95 | 0,58 | 0,43 | 5,72 | 4,25 | 0 | | 0,04 | 4,78 |
| 3 | 0,27 | 88 | 4,96 | 2,14 | 12,3 | – | 1,9 | 4,52 | 4,82 | 4,52 |
| 4 | 0,19 | 73 | 0,2 | 1,0 | 0,98 | – | 0,15 | 0,49 | 0 | |
| 5 | | | 14,3 | 2,19 | 6,3 | 2,02 | 0,13 | 1,75 | 0 | |
| 6 | | | 12,8 | 2,65 | 1,9 | 1,99 | 0,07 | 0,66 | 0 | |
| 7 | | | 17,4 | 1,4 | 15,0 | 1,07 | 0,03 | 1,01 | 0,16 | 0,01 |

^a Tp = 25°C, [Ti] = 50-100 μM, ^b [Al]/[Ti] = 2000-4000, ^c [Ph₃C[⊕]] = [Ti], TIBA/Ti = 20, d g/mol*10⁻⁵, Activity unit is 10⁶ g polymer / (mol Ti [monomer] h).

Dimethylaminoethyl substituent

The dimethylamino group, when complexed to a metal center, has the electronic and steric features like a Cp ligand. Scheme 1 illustrates the difference between Cp₂, Y_NCp and Cp ligands.

Scheme 1.



The Y_N substituent affects polymerizations for the mono-Cp family of catalyst as can be seen in Table 2. The styrene polymerization activity of Y_NCpTiCl₃ and Y_NCp*TiCl₃ is 30 to 50 times smaller compared to unsubstituted CpTiCl₃ and Cp*TiCl₃. Unsubstituted Cp₂TiCl₂ has only 1% of the activity of CpTiCl₃ for styrene polymerization [1]. Multi-hapto-coordination of styrene would be hindered by the additional Cp ligand and supports the hypothesis that Y_N may be considered to be a pseudo-Cp ligand. The slightly higher activity for **4** compared with **3** can be attributed to the weaker Ti-N interaction.

In contrast to the negative effect of Y_N on A_S of CpTiCl₃ and Cp*TiCl₃ systems, there is a strong positive effect on A_E of the CpTiCl₃ systems. CpTiCl₃ has very low ethylene polymerization activity but Y_NCpTiCl₃ has 30 to 100 time

higher A_E values and produces polyethylene having several times greater molecular weight. Furthermore Cp_2TiCl_2 is three times more active than $\text{Y}_N\text{CpTiCl}_3$. This may be attributed to increase hindrance against bimolecular reductive decomposition (eqs. 5 and 6). Its interesting to note that Y_N does not have a similar effect on either the A_E or PE M_w of the Cp^*TiCl_3 complex. Probably the five methyl groups on the Cp ring already provide sufficient shielding to the metal center in this regard. A_E decreases in the order $3 > 4 > 2 > 1$, which is consistent with this idea.

There is different trend between mono-Cp and bis-Cp precursors, the latter complexes being more stable and active than the former. However, the difference in reactivity is considerably reduced in these bis-Cp compounds: $7 > 5 > 6$. Counterion association might be important for the mono-Cp systems 1 to 4 have A_E in the presence of $\text{Ph}_3\text{C}^\oplus$ and noncoordinating anion cocatalyst which are about 3 to 10-fold greater than using the MAO cocatalyst. On the other hand the bis-Cp systems 5-7 have A_E values which are all larger in the presence of MAO than with $\text{Ph}_3\text{C}^\oplus$ cocatalyst indicating that ion-pair coupling is not important for the bis-Cp complexes because of steric reasons. That 7 is more active than 5 and 6 may be due to Ti-N interaction in the latter during the catalytic process which could hinder the coordination of the monomer. The low activity of 6 with $\text{Ph}_3\text{C}^\oplus$ cocatalyst may be due to the requirement of reaction of TIBA with the HCl at the low Al/Ti ratio.

Only $\text{Y}_N\text{Cp}^*\text{TiCl}_3$ exhibits high activity for propylene polymerization of 2.5×10^6 g PP / (mol Ti $[\text{C}_3\text{H}_6]$ h) producing high M_w (4.6×10^5) atactic polypropylene. Compound 4, 5, and 6 exhibit less than one-tenth of this activity in the presence of MAO; $\text{Ph}_3\text{C}^\oplus \text{B}^-(\text{C}_6\text{F}_5)_4$ does not activate this system.

Kinetics and mechanism of olefin polymerization had been investigated [34]. Fig. 9a showed the $\log A_E$ vs $\log[\text{C}_2\text{H}_4]$ plot for $\text{Y}_N\text{CpTiCl}_3$; the slope is 2.0 ± 0.5 . A similar plot for propylene polymerization has a slope of 1.8 ± 0.2 (Figure 9b).

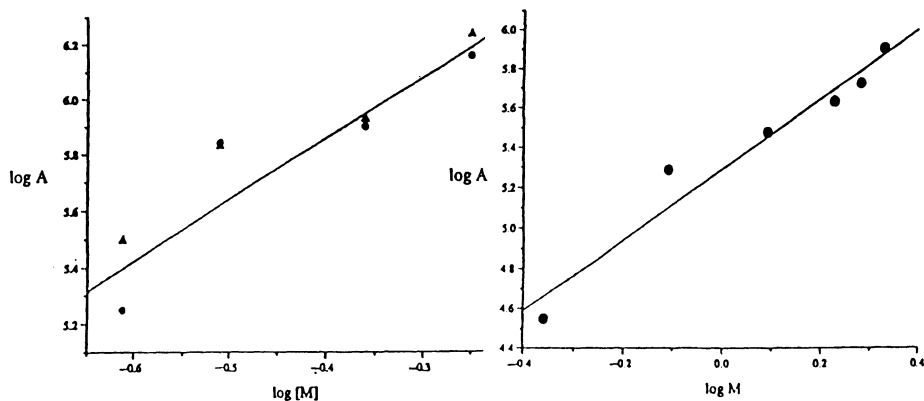
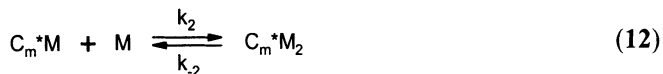


Fig. 9. Plot of $\log A$ vs. $\log[\text{monomer}]$ for $\text{Y}_N\text{CpTiCl}_3$ / MAO catalyzed polymerization (a) of ethylene; (b) of propylene.

This rate law of $1 < n < 2$ dependence on monomer concentration can be explained if the active site having m number of monomer molecules (M) inserted

(C_m^*) can complex either one monomer (C_m^*M) or two monomer ($C_m^*M_2$) molecules,



Migratory insertion may occur with either complex,



Assuming a constant Co and using steady-state approximation for C^*M and C^*M_2 , Marques et al. [35,36] derived

$$R_p = \frac{k_1 k_{p,1} [C_m^*][M]/(k_{-1} + k_{p,1})}{1 + k_1[M]/(k_{-1} + k_{p,1})} + \frac{k_1 k_2 k_{p,2} [C_m^*M_2][M]^{2/k-1}/(k_{-2} + k_{p,2})}{1 + k_1[M]/k_{-1} + k_1 k_2 [M]^{2/k-1}/(k_{-2} + k_{p,2})} \quad (15)$$

If $k_{p,2} \gg k_{p,1}$, then $n \sim 2$ [23]. In this analysis both $C_m^*M_1$ and $C_m^*M_2$ undergo migratory insertion (eqs. 3 and 4); it implies that 1^+ is not a "single-site" catalyst.

2-phenylethyl substituent

The effect of Y_{Ph} pendant group was investigated [32] with $Y_{Ph}Cp^*TiCl_3$ (**8**) and $Y_{Ph}Cp^*TiMe_3$ (**9**). 1H NMR of the ortho protons of the phenyl group are not appreciably shifted. η^6 -arene complexed to an electronically unsaturated group 4 metal should be shifted to low field compared to the ortho protons on the free arene (toluene) [37,38]. For benzyl complexes the electronic unsaturation is relieved via η^n -benzyl interaction ($n=1-3$) resulting in a shift of the ortho protons to higher field [39]. Since there is no significant shift of either kind there is no coordination of the phenyl group to Ti.

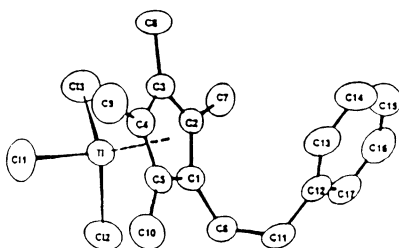


Fig. 10 Structure of $Y\phi Cp^*TiCl_3$ (**8**) showing the atomic number scheme.

X-ray structure of **8** is shown in Fig. 11, the bonding parameters are summarized in Table 3. The phenyl group and the Ti center are located at opposite side of the Cp ring. Thus there is also no coordination in the solid state.

Table 3. Selected Bond Lengths (Å) and Angles (deg) for **3a**

| Bond Lengths | | | |
|----------------|----------|-------------|----------|
| Ti-Cl(1) | 2.221(2) | Ti-Cl (3) | 2.245(2) |
| Ti-Cl(2) | 2.241(2) | Ti-Cp | 2.011(3) |
| Bond Angles | | | |
| Cl(1)-Ti-Cl(2) | 102.7(1) | Cl(1)-Ti-Cp | 115.8(1) |
| Cl(1)-Ti-Cl(3) | 103.9(1) | Cl(2)-Ti-Cp | 115.4(1) |
| Cl(2)-Ti-Cl(3) | 102.1(1) | Cl(3)-Ti-Cp | 115.1(1) |

a: Cp is the center of the cyclopentadienyl ring

The styrene polymerization by **8**/MAO has about one-third of the A_S by **2**/MAO for $T_p = 25-90^\circ\text{C}$ and $\text{Al/Ti} = 2000-4000$, they have the same syndiospecificity (% SY). **8**/MAO has A_E values of $3.75 \times 10^6 \text{ g} / (\text{mol Ti} [\text{C}_2\text{H}_4] \text{ h})$ which is about six-times greater than **2**/MAO. This suggests that during a polymerization the active species derived from **8** is in equilibrium between two states, one with (c) and one without (a) intramolecular phenyl coordination to Ti. As a result styrene polymerization can proceed with full η^n interaction in the c state but not in the a-state. Ethylene polymerization is catalyzed by the catalyst in either state but the reductive decomposition is suppressed for the a-state.

Methoxy substituent

The following compounds with methoxy substituents have been studied: $\text{Y}_0\text{CpTiCl}_3$ (**11**), $\text{Y}_0\text{IndTiCl}_3$ (**12**) and $\text{Y}'_0\text{IndTiCl}_3$ (**13**).

When **11** / MAO and **12** / MAO were used to polymerize styrene, both catalysts exhibited low activities of $ca\ 1 \times 10^4 \text{ g PS} / (\text{mol Ti mol S h})$ with SY > 92%. Both catalysts also had similar low ethylene polymerization activities of $ca\ 3 \times 10^4 \text{ g PE} / (\text{mol Ti} [\text{C}_2\text{H}_4] \text{ h})$. Neither catalyst has any activity for propylene polymerization. Catalyst **13**/MAO does not polymerize styrene, ethylene or propylene.

Possible factors for low polymerization activity are: oxygen-aluminium coordination between the precursor and cocatalyst which suppresses the resonance effect and enhances the inductive effects of the methoxy group; or the simple steric effect of the coordinated MAO, or that the coordination diminished the ability of MAO to abstract an anionic ligand to form the cationic organotitanium active species.

Electronic states of the catalytic species

One remarkable characteristics of the mono-Cp catalyst in styrene polymerization is that the tetravalent and trivalent titanium complex have very similar catalytic activities. This was reported by Ishihara et al. [1] for CpTiCl₃ and CpTiCl₂ and by Newman and Malanga [40] for Cp*Ti(OMe)₃ and Cp*Ti(OMe)₂. Ti⁺(III) complex was first proposed to be catalytically active species by Zambelli et al. [24,25] for a model of multi-hapto-coordinations. This proposal was supported by our finding that the CpTi(OBu)₃ / MAO catalyst have most of its catalytic species in paramagnetic states [8,19]. Grassie et al-[22,23] followed the reduction of Cp*Ti(CH₂Ph)₃ in the presence of B(C₆F₅)₃ at very high [Ti]. They concluded that Ti(III) complex is also the active species in this catalyst system for syndiospecific polymerization. A similar conclusion was reached for the Cp*Ti(OMe)₃ / MAO system [40]. However, other investigators [20,21] found very little reduction of Cp*TiMe₃ in the presence Of B(C₆F₅)₃, Ph₃C⁺ or MAO at low Ti concentration.

In this study, the styrene polymerization activities and EPR intensities for Ti(III) species are all measured under the *same conditions*. The [Ti] chosen is 50 μM, at which concentration even if all the Ti(IV) precursors were reduced, there is no appreciable dipolar broadening to interfere with quantitative EPR determination. Other studies [24,25] used 200 times higher concentration of the precursors. The catalyst concentration affect both the reduction of Ti and the polymerization process. At different [Ti] and [Al]/[Ti] ratio even the number of Ti(III) signals and their g-values can be different.

Change of CpTi(OBu)₃ concentration was also observed to markedly affect the polymerization activity [8,9]. For instance, the styrene polymerization activity at 60°C increase from 3.84 x 10⁶ to 32 x 10⁶ g PS [(mol Ti) (mol styrene) (h)]⁻¹ at [CpTi(OBu)₃] of 1.0 mM and 100 μM, respectively. Therefore, a relationship of catalytic activity and distribution of oxidation states of Ti is meaningful only when they are determined under exactly the same conditions of [Ti], [Al], T_p, time, medium, etc.

In general the rate of polymerization is comprised of:

$$\frac{R_p}{[\text{styrene}]} = \sum_{i=1}^n k_{p,i(\text{IV})}[\text{Ti}_i(\text{IV})] + \sum_{j=1}^m k_{p,j(\text{III})}[\text{Ti}_j(\text{III})] + \sum_{k=1}^r k_{p,k(\text{II})}[\text{Ti}_k(\text{II})] \quad (16)$$

where *n*, *m*, and *r* are the number of Ti(IV), Ti(III), and Ti(II) species either in the neutral or ionic state with the corresponding rate constant of propagation *k_p*. To a first approximation, the last term involving Ti(II) species may be neglected. The activity of η⁶-(arene)Ti(AlCl₄)₂ has A_S value of only 1.8x10³ g PS / (mol Ti [S] h) [3].

In this work we synthesized a number of η⁵-LTiCl₃ precursors which are known to exhibit different polymerization activities when compared under identical conditions. It is important to keep the nonhapto ancillary ligand the same. For instance CpTiF₃ and Cp*TiF₃ exhibit much higher activities than the corresponding chlorides [4] and differ in their dependence on T_p, Al(MAO)/Ti ratio, and time of polymerization.

Table 4 summarizes the % of Ti(III) for five η^5 -L-TiCl₃ compounds determined, which are the average of three runs. The reaction conditions are [Ti] = 50 μ M, Al/Ti = 4000, temp. = 25°C. Column 2 lists the results of 10 min. of activation while column 3 gives the amount of Ti(III) after 30 min. of reaction. There is only 25% to 40% more reduction of the precursor between 30 min. and 10 min. of reaction with MAO. Since polymerizations were run between 10 and 30 min., the results indicate that further reduction of the Ti precursor after aging, which may occur during the course of a polymerization, would be less than 40%.

Table 5 summarizes the activity of the various precursors in styrene polymerization catalysis. Column 2 gives the activity with preactivated catalyst for 10 min. of polymerization. Column 3 gives the activity with catalyst not preactivated for 30 min. of polymerization.

Table 4. Amount of Ti(III) as Measured by EPR

| | % Ti = Ti(III) at reaction time | | Fractional Increase of Ti(III) |
|--|---------------------------------|--------|-----------------------------------|
| | 10 min | 30 min | |
| η^5 -LTiCl ₃ | | | |
| 2-(Me)IndTiCl ₃ | 0.62 | 0.82 | 0.32 |
| 1-(Me)IndTiCl ₃ | 1.65 | 2.23 | 0.35 |
| IndTiCl ₃ | 5.05 | 6.31 | 0.25 |
| H ₄ IndTiCl ₃ ^a | 15.6 | 20.4 | 0.31 |
| CpTiCl ₃ | 22.0 | 29.1 | 0.32 |

a: H₄IndTiCl₃ is η^5 -(4,5,6,7-tetrahydroindenyl)trichlorotitanium.

Table 5. Styrene Polymerization Activity^a

| η^5 -L-TiCl ₃ | Activity x10 ⁻⁷ = g PS/[(mol Ti)(mol styrene)(h)] | |
|--|--|-----------------------|
| | With Preactivation | Without Preactivation |
| 2-(Me)IndTiCl ₃ | 24.9 | 16.6 |
| 1-(Me)IndTiCl ₃ | 17.2 | 5.1 |
| IndTiCl ₃ | 15.1 | 3.7 |
| H ₄ IndTiCl ₃ ^b | 8.8 | 2.7 |
| CpTiCl ₃ | 5.46 | 1.4 |

a: polymerization procedures have been previously reported [43]

b: H₄IndTiCl₃ is η^5 -(4,5,6,7-tetrahydroindenyl)trichlorotitanium.

Figure 11 (left) is a plot of log (polymerization activity) using preactivated catalyst vs. log[(% Ti(III))] after 10 min. of reaction. Figure 11 (right) plots log (polymerization activity) of catalyst without preactivation against log [(% Ti(III))] after 10 min. of stirring. The results suggest that both the Ti(IV) and Ti(III) η^5 -L-Ti⁺ complexes are catalytically active, and that the former is about 10 to 20 times more active than the latter. This is consistent with electrophilicity of the active species [9,24,41,42] as shown by I⁺ substituents on styrene that enhance the monomer reactivity [9,57]. Other factors such as steric and electronic effects also need to be taken into consideration. Certainly, the X-ray crystal structures of

$\text{Cp}^*\text{Zr}^+(\eta^7\text{-Bz})(\eta^3\text{-Bz})$ [30], of $\text{Cp}^*\text{Zr}^+(\eta^1 : \eta^6\text{-CH}_2\text{CHMeCH}_2\text{Ph})(\text{Bz})$ [31], and of $(\text{CpZr}^+\text{Bz}_2)(\eta^5\text{-PhCH}_2)\text{B}^-(\text{C}_6\text{F}_5)_3$ [34], indicate the steric viability of $\eta^5\text{-L-Ti}^+(\text{IV})\text{L}'\text{P}$ active species.

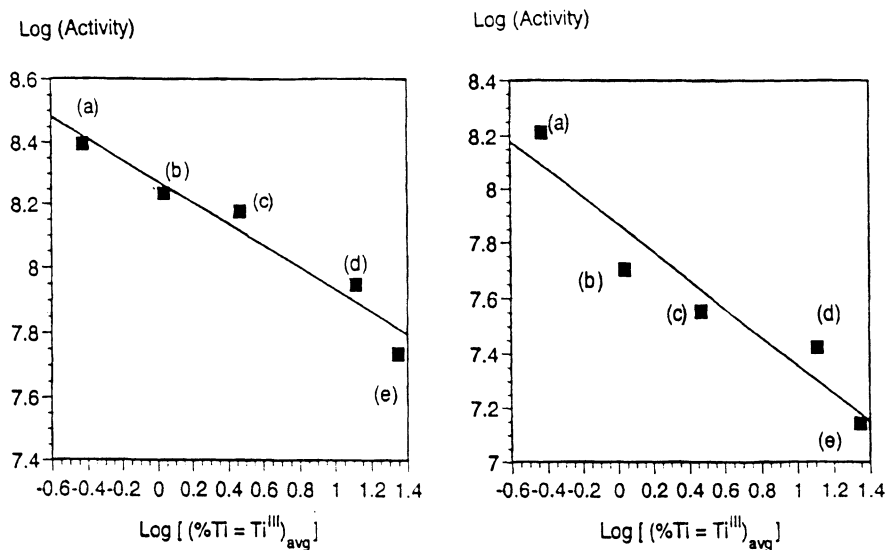


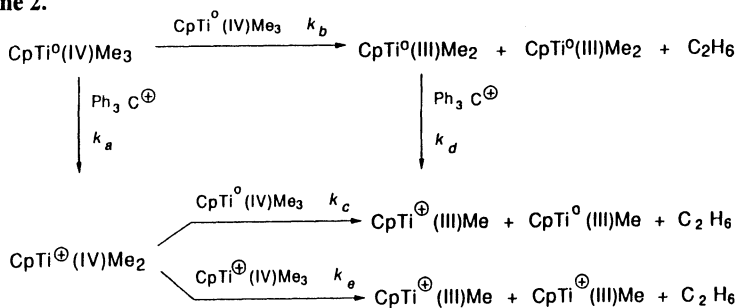
Fig. 11. Plot of $\log(\text{activity})$ vs. $\log(\text{Ti(III)}_{\text{avg}})$ for $\eta^5\text{-L-TiCl}_3$ catalysts. ESR sample aged for 10 min. (a) 2-(Me)IndTiCl₃, (b) 1-(Me)IndTiCl₃, (c) IndTiCl₃, (d) H₄IndTiCl₃, (e) CpTiCl₃. Top: catalyst preactivated for 10 min. prior to injection into polymerization vessel $f(x) = 0.343x + 8.274$; $R = 0.949$. Bottom: catalyst used without preactivation $f(x) = -0.513x + 7.871$; $R = 0.905$.

There is no strong evidence against a neutral trivalent $\eta^5\text{-L-Ti}^0(\text{III})\text{L}'\text{P}$ active species which is isolobal to the cationic $\eta^5\text{-L-Ti}^+(\text{IV})\text{L}'\text{P}$. However, even if the former is present, it is expected to be less active than the cationic species on the basis of its lower electrophilicity compared to $\eta^5\text{-L-Ti}^+(\text{III})\text{L}'\text{P}$.

Even though the syndiotactic polystyrene obtained with CpTiCl₃ / MAO by Ishihara et al. [1] has a narrow molecular weight distribution ($\text{MWD} = \text{M}_w/\text{M}_n = 1.74\text{-}2.57$), its not always observed. For example, the various Ti precursors employed by Zambelli et al. [2] produced PS with MWD ranging from 2.8 to 13.3, variation of experimental conditions in Ti(OBu)₄ / MAO catalysis afforded PS with MWD values ranging from 4.8 to 26 [44], MWD of 2.8 to 5.7 were obtained for PS polymerized by CpTi(OBu)₃ / MAO [19], Cp*TiF₃ gave PS with MWD up to 3.6 [4], and arene Ti(II) complexes afforded PS with 2.9 to 4.9 for MWD [3]. In other words, most of the syndiospecific styrene polymerization catalyst systems reported to date are multi-site catalysts. The fact is that styrene is a monomer susceptible to polymerization by free radical, anionic, as well as cationic initiators adds further complication to these catalysis and polymerization (*vide supra*).

There are two reaction pathways connecting Ti(IV) and Ti(III) species is delineated in Scheme 2 excluding the involvement of Ti(II) species.

Scheme 2.



Considerations of bond energies, ionization potentials, and redox potentials suggest the following order of decreasing exothermicity and rate constants,

$$k_a \sim k_d \sim k_b \sim k_c \sim k_e$$

Known chemistry of organotitanium compounds supports the formation of $\text{CpTi}^+(\text{IV})\text{Me}_2$ to be the most rapid reaction in Scheme 2. The formation of $\text{Cp}^+(\text{III})\text{Me}$ is slower by comparison and can proceed via either one of two probable pathways with relative rates of k_b , k_d and k_a , k_c . The third course is the slowest k_e , because it requires two half-titanocenium species to overcome the coulombic force in order to react.

Reduction of CpTiMe_3 in the presence of the other cocatalysts $\text{B}(\text{C}_6\text{F}_5)_3$, MAO and $\text{Me}_2\text{N}^+\text{H}_2\text{B}^-(\text{C}_6\text{F}_5)_4$ probably proceed by analogous reaction but are complicated by ion-pair coupling, μ -methyl dimerization, and acid-base complexation involving the reaction products.

Highly stable catalysts

If $\text{Ti}^+(\text{IV})$ is more active than $\text{Ti}^+(\text{III})$ species, then, it would desirable to design tetravalent titanium precursor which is resistant against reductive decomposition. The results of Table VII and VIII indicate that steric bulky η^5 -ligand can hinder close approach of two titanium centers for reactions 5 and 6. Alkyl or aryl substitution is a well-known way to increase the size of the η^5 -ligand. The substituent also increase the electron density at the metal center which enhances its catalytic activity. Eight new catalyst precursors were synthesized to explore this approach. They are two series of alkyl and aryl substituted IndTiCl_3 and $\text{benz}[e]\text{IndTiCl}_3$:

IndTiCl_3 (**14**), 1-Ph IndTiCl_3 (**15**), 1,3-Ph₂ IndTiCl_3 (**16**), 1-Bz IndTiCl_3 (**17**), 1-Ph(CH₂)₂- IndTiCl_3 (**18**) and Benz[e] IndTiCl_3 (**19**), 2-MeBenz[e] IndTiCl_3 (**20**), 1,2,3-Me₃benz[e] IndTiCl_3 (**21**).

Table 6 presents the polymerization data at 50°C. In order to indicate the dependencies on T_p , the change of value between 50°C to 100°C is given as Δ of the parameter. For example in the case of activity A_S , ΔA_S is

$$\Delta A_s(\%) = \frac{A_s(100^\circ\text{C}) - A_s(50^\circ\text{C})}{A_s(50^\circ\text{C})} \cdot 100 \quad (17)$$

Table 6. Styrene polymerization with substituted indenyl- and benz[e] indenyl-TiCl₃ / MAO catalyst

| Cat. | A _s ^a x 10 ⁻⁷ | Δ(A _s) ^b | S.Y. ^a [%] | Δ(S.Y.) ^b | T _m ^a [°C] | Δ(T _m) ^b | M _w ^a x 10 ⁻⁵ | Δ(M _w) ^b |
|------|---|---------------------------------|--------------------------|----------------------|-------------------------------------|---------------------------------|---|---------------------------------|
| 14 | 5,2 | -60% | 91,3 | -4% | 262,5 | -1,2% | 3,23 | -50% |
| 15 | 7,7 | -69% | 90,0 | -1,2% | 260,7 | +3% | 4,24 | -75% |
| 16 | 3,6 | -39% | 94,8 | -3,5% | 262,0 | -0,6% | 4,96 | -59% |
| 17 | 0,2 | -65% | 87,2 | -23% | 268,3 | -2,5% | 3,23 | -68% |
| 18 | 1,1 | -45% | 88,2 | -51% | 267,8 | -2,6% | 4,01 | -76% |
| 19 | 17 | -41% | 92,5 | -3,8% | 270,4 | -0,5% | 5,45 | -76% |
| 20 | 18 | -61% | 92,8 | -2,9% | 275,2 | -0,61% | 4,24 | -75% |
| 21 | 2 | 0% | 96,0 | -1% | 276 | -0,2% | 3,23 | -48% |

a: parameter for 50°C polymerization; unit is the same as in Table II.

b: change in the value of the parameter from 50°C to 100°C polymerizations.

The system 1,2,3-trimethylbenz[e]indenyl TiCl₃/MAO is clearly the most superior system. There was no loss of A_s up to 100°C, the highest syndioselectivity and smallest decrease for a 50°C increase of temp. as well as the smallest loss of T_m and decrement of M_w. The three methyl groups in this precursor provide both more electron donation and steric hinderance to help stabilize it against reduction [12], dimerization [18], or reaction with oxygen and moisture to form μ-oxo products, as well as β-hydride elimination. A solution of the catalyst precursor **20** retains most of its activity even after exposure to ambient atmosphere for 3 days.

Acknowledgement: This work is a joint research program of Professor James C. W. Chien and Professor Marvin D. Rausch. The works were performed by Z. Salajka, D.-H. Dong, U. Bueschges, A. Kucht, H. Kucht, T. E. Ready, P. Foster, M. Blaise, J. C. Flores, M. M. Marques, and Z.-T. Yu.

References

- [1] Ishihara, N.; Kuramoto, M.; Uoi, M. *Macromolecules* 1988, *21*, 3356.
- [2] Zambelli, A., Oliva, L.; Peilecchia, C. *Macromolecules* 1989, *22*, 2129.
- [3] Kaminsky, W.; Park, Y.-W. *Macromol. Rapid Commun.* 1995, *16*, 343.
- [4] Kaminsky, W.; Lenk, S., Scholz, V., Roesky, H. W.; Herzog, A. *Macromolecules* 1997, *30*, 7647.
- [5] Kucht, H.; Kucht, A.; Chien, J.C.W.; Rausch, M.D. *Appl. Organomet. Chem.* 1994, *8*, 393.
- [6] Pellecchia, C.; Longo, P.; Proto, A.; Zambelli, A. *Makromol. Chem., Rapid Commun.* 1992, *13*, 265.

- [7]Quyoum, R.; Wang, Q., Tudoret, M.-J.; Baird, M.C.; Gillis, D.J. *J. Am. Chem. Soc.* 1994, *116*, 6435.
- [8]Chien, J. C. W.; Salajka, Z. *J. Polym. Sci. Part A: Polym. Chem.* 1991, *29*, 1253.
- [9]Longo, P.; Proto, A.; Zambelli, A. *Macromol. Chem. Phys.* 1995, *196*, 3015.
- [10]Chien, J. C. W.; Sugimoto, R. *J. Polym. Sci. Part A: Polym. Chem.* 1991, *29*, 459.
- [11]Breslow, D. S.; Newburg, N. R. *J. Am. Chem. Soc.* 1957, *79*, 5072.
- [12]Chien, J. C. W. *J. Am. Chem. Soc.* 1959, *85*, 86.
- [13]Natta, G.; Corradini, P.; Bassi, I. W. *J. Am. Chem. Soc.* 1958, *80*, 75
- [14]Henrici-Olivö, G.; Olivö, S. *Angew. Chem. Int. Ed. Engl.* 1967, *6*, 790
- [15]Sinn, H.; Kolk, E. *J. Organomet. Chem.* 1966, *6*, 373.
- [16]Sinn, H.; Patat, F. *Angew. Chem. Int. Ed. Engl.* 1964, *3*, 93.
- [17]Sinn, H.; Kaminsky, W. *Adv. Organomet. Chem.* 1980, *18*, 99.
- [18]Bueschges, U.; Chien, J. C. W. *J. Polym. Sci. Part A: Polym. Chem.* 1989, *27*, 1525.
- [19]Chien, J. C. W.; Salajka, Z.; Dong, S.-H. *Macromolecules* 1992, *25*, 3199.
- [20]Kucht, H., Kucht, A.; Chien, J. C. W.; Rausch, M. D. *Appl. Organomet. Chem.* 1994, *8*, 393.
- [21]Ewart, S. W.; Sarstfield, M. J.; Seremic, D.; Tremblay, T. L.; Williams, E. F.; Baird, M. C. *Organometallics* 1998, *17*, 1502.
- [22]Grassi, A.; Pellicchia, C.; Oliva, L.; Laschi, F. *Makromol. Chem. Phys.* 1995, *196*, 1093.
- [23]Grassi, A.; Zambelli, A.; Laschi, F. *Organometallics* 1996, *15*, 480.
- [24]Zambelli, A.; Pellicchia, C.; Oliva L.; Longo, P.; Grassi, *Makromol. Chem.* 1991, *192*, 223.
- [25]Zambelli, A., Pellicchia, C.; Oliva, L. *Makromol. Chem. Macromol. Symp.* 1991, *48/49*, 297.
- [26]Zambelli, A.; Pellicchia, C.; Proto, A. *Macromol. Symp.* 1995, *89*, 373.
- [27]Pellicchia, C.; Pappalardo, D.; van Beek, J. A. M. *Macromol. Symp.* 1995, *89*, 335.
- [28]Pellicchia, C.; Grassi, A.; Immirzi, A. *J. Am. Chem. Soc.* 1993, *115*, 1160.
- [29]Chien, J. C. W.; Dong, S.-H. *Polym. Bull.* 1992, *29*, 515.
- [30]Flores, J. C.; Chien, J. C. W.; Rausch, M. D. *Organometallics* 1994, *13*, 4140.
- [31]Flores, J. C.; Chien, J. C. W.; Rausch, M. D. *Macromolecules* 1996, *29*, 8030.
- [32]Flores, J.C.; Wood, J.S.; Chien, J.C.W.; Rausch, M. D. *Organometallics* 1996, *15*, 4944.
- [33]Foster, P.; Rausch, M. D.; Chien, J. C. W. *J. Organomet. Chem.* 1997, *527*, 71.
- [34]Chien, J. C. W.; Yu, Z.-T.; Marques, M. M.; Flores, J. C.; Rausch, M. D. *J. Polym. Sci. Part A: Polym. Chem.* 1998, *36*, 319.
- [35]Marques, M.M.; Dias, H.R.; Costa, C.; Lemos, F.; Ribeiro, F.R. *Polym. Int.* 1997, *43*, 77.
- [36]Marques, M.; Dias, A.R.; Justino, J.; Dosta, C.; Lemos, F.; Ribeiro, F.R. *Polym. Int.* 1997, *43*, 86.
- [37]Gillis, D. J.; Tudoret, M.-J.; Baird, M. C. *J. Am. Chem. Soc.* 1993, *115*, 2543.
- [38]Horton, A. D.; Frijns, J. H. G. *Angew. Chem., Int. Ed. Engl.* 1991, *30*, 1152.
- [39]Hughes, A. K.; Meetsma, A.; Teuben, J. H. *Organometallics* 1993, *12*, 1936.
- [40]Newman, T. H.; Malanga, M. T. *J. M. S. Pure Appl. Chem.* 1997, *A34*, 1921.
- [41]Zambelli, A.; Proto, A.; Longo, P.; Oliva, L. *Macromol. Chem. Phys.* 1994, *195*, 2623.
- [42]Grassi, A.; Longo, P.; Proto, A.; Zambelli, A. *Macromolecules* 1989, *22*, 104.
- [43]Ready, T. E.; Chien, J. C. W.; Rausch, M. D. *J. Organomet. Chem.* 1996, *519*, 21.
- [44]Oliva, L.; Pellicchia, C.; Cinqira, P.; Zambelli, A. *Macromolecules* 1989, *22*, 1642.
- [45]Foster, P.; Chien, J. C. W.; Rausch, M. D. *Organometallics* 1996, *15*, 2404.

The effects of the bridge structure and the ligand system of zirconocene catalysts on the copolymerization of styrene and ethylene

Toru Arai, Toshiaki Ohtsu, and Shigeru Suzuki

Research Center of DENKI-KAGAKU KOGYO, 3-5-1 Asahimachi Machida-city Tokyo, Japan
fvbb0795@mb.infoweb.ne.jp

Abstract. The catalytic properties of zirconocene / MAO systems in the copolymerization of styrene and ethylene strongly depend on the structure of the zirconocene. An isopropylidene bridge leads to a relatively small bite angle and copolymers with a high styrene content. Fused ring substituents of cyclopentadienyl group such as indenyl or benzindenyl show remarkable effects on the styrene content, the catalytic yield and the molecular weights of the copolymers produced. Among the zirconocene complexes tested, *rac*-isopropylidenebis(4,5-benzindenyl) zirconiumdichloride exhibits the best catalytic performance in the copolymerization. The zirconocene formed a novel styrene-ethylene random copolymer with isotactic stereoregularity and head to tail styrene-styrene structures. The C_2 symmetry of the zirconocene is considered to be responsible for both the isotacticity and the formation of head to tail sequences.

Introduction

Recently, the single site catalyzed copolymerization of ethylene and styrene (Et-St) has been reported using various zirconium or titanium complexes. CGCT (constrained geometry catalysts technology) type complexes [(*t*-butylamido)dimethyl(tetramethylcyclopentadienyl)silane]titaniumdichloride [1], metallocene type complexes [isopropylidene(fluorenyl)(cyclopentadienyl)]zirconium dichloride[2] and half metallocene type $CpTiCl_3$ [3] activated by methylalumoxane (MAO) produce “pseudo-random” Et-St copolymers[1]. These copolymers were characterized by lack of head to tail St-St sequences, which limits the St content to 50 mol%. No stereoregularity of the phenyl group in the alternating Et-St sequence was observed. More recently, Oliva et al. reported a nearly alternating stereoregular copolymer produced at low temperatures (-25°C) using a Brintzinger-type zirconocene complex [5]. These results are similar to the alternating copolymer reported by Miyatake [4]. The copolymer also shows no head to tail styrene chain structure in a ^{13}C -NMR spectrum.

Our previous studies show that isopropylidene bridged zirconocene complexes with indenyl [6] or benzindenyl [7] ligands combined with MAO promote the Et-St copolymerization at 50°C with high activity. The formed copolymer has a random structure with head to tail St-St sequences and isotactic stereo-regularity in St-St and alternating Et-St sequences.

However, the effect of the complex structure on the Et-St copolymerization is still not clear. Here we report the relations between bridge structures (bite angle), ligand system and symmetry of the complexes and the catalytic properties for Et-St copolymerization.

Experimental

Complexes

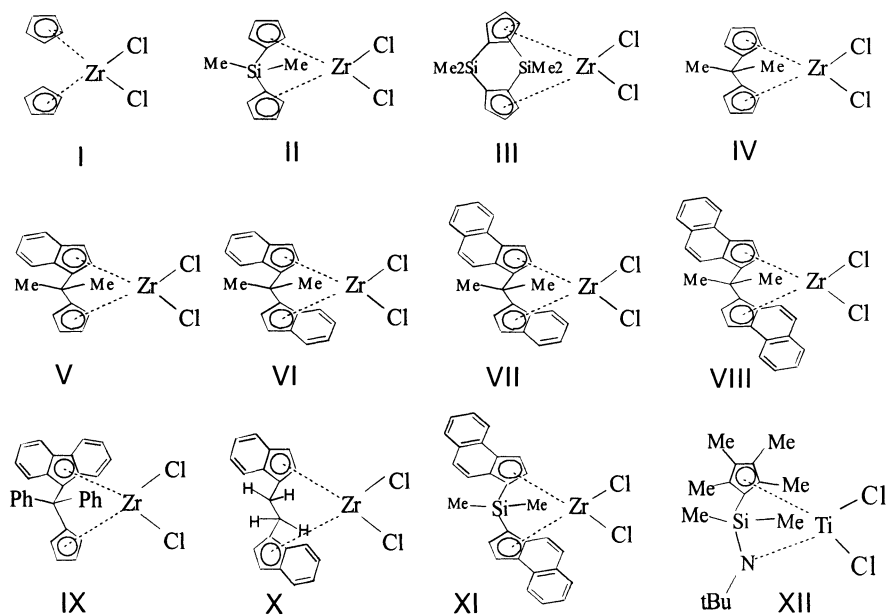


Fig. 1. Complexes.

The tested complexes are shown in Fig.1.

Biscyclopentadienyl zirconium dichloride (I) was purchased from Wako chemicals and following complexes were synthesized according to the literatures. (II)[dimethylsilylenebis(cyclopentadienyl)]zirconium dichloride [6], (III)[(1,1'-dimethylsilylene)(2,2'-dimethylsilylene)bis(cyclopentadienyl)]zirconium dichloride [8],

(IV)[isopropylidenebis(cyclopentadienyl)]zirconium dichloride [6],
 (V)[isopropylidene (cyclopentadienyl)(1-indenyl)]zirconium dichloride [9],
 (VI)rac-[isopropylidenebis(1-indenyl)]zirconium dichloride [9],
 (VII)rac-[isopropylidene(1-indenyl)(4,5-benz-1-indenyl)]zirconium dichloride [7],
 (VIII)rac-[isopropylidenebis(4,5-benz-1-indenyl)]zirconium dichloride [7],
 (IX)[Diphenylmethylene(fluorenyl)(cyclopentadienyl)]zirconium dichloride [10],
 (X)rac-[ethylenebis(indenyl)] zirconium dichloride [11],
 (XI)rac-[dimethylsilylenebis(4,5-benz-1-indenyl)]zirconium dichloride [12],
 (XII)[(t-Butylamido)dimethyl(tetramethylcyclopentadienyl)silane]titanium dichloride [1].

Polymerization

Screening polymerization runs were conducted in a 120 ml autoclave equipped with a magnetic stirrer and in a 10L autoclave with a mechanical stirrer and a heating and cooling jacket.

At the 120 ml scale, styrene and MAO were added to the autoclaves under a flow of ethylen at atmospheric pressure. A toluene solution of the complex was injected. The autoclave was then heated and pressurized to the reaction conditions within a few minutes.

In the case of the larger scale polymerizations, toluene and styrene were added and dehydrated by bubbling dry N₂ for 2 h at 50 °C, TIBA (tri-isobutyl aluminium; 8.4 mmol) as an inhibitor killer and MAO were injected, ethylene was introduced at the polymerization pressure, and then the complex solution was injected from a shot tank mounted on the autoclave. MAO(MMAO-3a) and TIBA were purchased from Tosoh-Akzo.

Characterization

The bite angle of the complexes was calculated by PM3(tm).

The ¹H and ¹³C-NMR spectra of the polymers were measured on an Alfa-500 NMR spectrometer (JEOL) using CDCl₃ or 1,1,2,2-tetrachloroethane with TMS as standard. The content of styrene was determined by ¹H-NMR comparing the peak intensities from phenyl, methylene and methine protons. Molecular weights and molecular weight distributions were determined by gel permeation chromatography (GPC) versus polystyrene standard.

Results and discussion

Screening runs

Some metallocene complexes were employed for the screening test. Typical conditions and results are summarized in Table 1. Except of the non-bridged zirconocene (I), Et-St copolymers were obtained. Narrow molecular weight distributions close to 2.0 indicate a single site catalysis. Under similar screening polymerization conditions, (VI) and (VII) yield a copolymer with a higher St content and molecular weight.

Table 1. Polymerization conditions and results.

| Run No. | Complexes (μmol) | St / Tol (ml / ml) | Yield (g) | Mw ($/10^4$) | Mw /Mn | St Cont. (mol%) | Bite angle (degree) |
|---------|-------------------------------|--------------------|-----------|----------------|--------|-----------------|---------------------|
| 1 | I; 23 | 10 / 16 | 1.3 | - | - | 0 | 132 |
| 2 | II; 23 | 10 / 16 | 8.8 | - | - | 12.5 | 124 |
| 3 | III; 23 | 10 / 16 | 6.2 | 1.2 | 2.0 | 18.7 | 119 |
| 4 | IV; 23 | 10 / 16 | 10.8 | 0.9 | 2.2 | 23.0 | 114 |
| 5 | V; 8.4 | 10 / 16 | 9.1 | 5.7 | 2.1 | 27.2 | 114 |
| 6 | VI; 8.4 | 10 / 26 | 7.5 | 14.0 | 2.2 | 39.1 | 114 |
| 7 | VII; 8.4 | 10 / 26 | 5.0 | 22.1 | 1.7 | 41.0 | 114 |

Conditions: MMAO, 14 mmol (run1-4) or 8.4 mmol (run 5-7),
Et pressure 0.6 MPa, 50 °C, 1h.

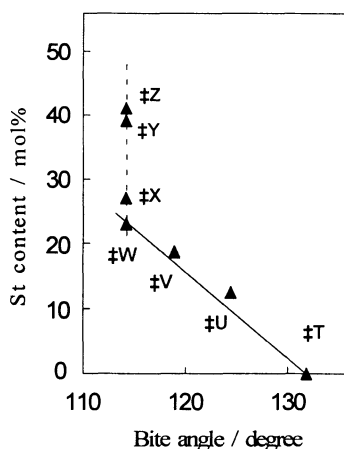


Fig. 2. Relations between St content and bite angle of the complex.

Fig.2 shows the relations between St content of the obtained copolymer and the bite angle of the zirconocenes. Among the zirconocenes with the same biscyclopentadienyl ligand system a smaller bite angle leads to the formation of copolymers with a higher St content (IV) > (III) > (II) > (I).

Comparison of the zirconocenes with the same isopropylidene bridge system, fused ring substituent of ligand such as indenyl or benzindenyl show remarkable effects on the St incorporation to form high St content copolymer of more than 40 mol% St. (VII) > (VI) > (V) > (IV). The molecular weight of the copolymers is also influenced by fused ring substituents of the ligand. The β -elimination reaction, which reduces the molecular weight, may be suppressed by the steric interaction between polymer chain end and the substituent of the cyclopentadienyl ligand.

However, this screening test is not suitable to determine the copolymerization properties of highly active complexes such as (VIII), due to the rapid exothermic polymerization.

Large scale runs

Large scale polymerization using 10L scale autoclave with cooling system is employed to compare catalytic properties of the highly active complexes under constant temperature conditions. Polymerization rate was estimated from Et feed rate monitored and each run was conducted until the polymerization was substantially completed. Table 2 shows the conditions and results.

Table 2. Polymerization conditions and results.

| Run No. | Complexes (μmol) | MAO (mmol) | Time (h) | Yield ^{d)} | Mw ($/10^4$) | Mw /Mn | St cont. (mol%) |
|------------------|-------------------------------|------------|----------|---------------------|----------------|--------|-----------------|
| 8 ^{a)} | VIII; 21 | 84 | 6.0 | 48 | 24.6 | 2.0 | 53.8 |
| 9 ^{a)} | VI; 84 | 84 | 7.0 | 15 | 15.5 | 1.8 | 49.8 |
| 10 ^{b)} | VI; 84 | 84 | 5.0 | 20 | 14.8 | 2.0 | 43.5 |
| 11 ^{a)} | XI; 21 | 84 | 5.0 | 3.4 | 11.9 | 3.4 | 4.5 |
| 12 ^{a)} | X; 84 | 84 | 6.0 | 4.6 | 5.0 | 2.0 | 9.0 |
| 13 ^{c)} | IX; 164 | 164 | 4.0 | 1.7 | 50.2 | 2.7 | 21.1 |
| 14 ^{a)} | XII; 84 | 84 | 3.0 | 6.8 | 35.3 | 2.1 | 49.8 |

a) Conditions: St 4000ml, Tol. 800ml, TIBA 8.4mmol, Et 0.2Mpa, 50° C.

b) Et 0.6MPa.

c) Et 0.4MPa.

d) Yield ($10^6\text{g-polym./mol-Zr}$).

Complex (VIII) shows the highest yield for St-Et copolymerization and gives high St content copolymers of more than 50 mol% under the conditions of large excess St monomer concentration (St; 7.3 mol/L, Et; 0.2 mol/L). The effect of the fused ring substituent of the ligand on St incorporation, yield and molecular weight of the copolymer is confirmed by comparison with results using complex (VI).

Dimethylsilylene and ethylene bridged complexes with fused ring substituent ligand (XI) and (X) produce low St content and molecular weight copolymer with

low yield compared to the corresponding isopropylidene bridged complexes (VIII) and (VI), respectively. These results indicate that the bite angle of the complexes affects not only St incorporation but also the catalytic yield and molecular weight of the copolymer produced.

The Ewen-type C_s symmetric zirconocene (IX) is less active and gives lower St content copolymer than the C_2 symmetric zirconocene (VI) under similar conditions (run 9,10 and 13). The CGCT-type C_s symmetric complex (XII) produces high St content copolymer close to 50 mol% with moderate yield.

The effects of the zirconocene symmetry on the formation of head to tail St-St sequences in St-Et copolymer have been reported [6,7]. The copolymers produced by (VI) and (VIII) show peaks attributable to head to tail St-St (isotactic polystyrene) sequences in ^{13}C -NMR spectra, whereas there is no peaks in the vicinity of 41-44 ppm produced by (IX) and (XII), as shown in Fig.3 and reported already [2]. In case of the C_s symmetric complex, there might be repulsive interactions between the close phenyl groups of polymer chain end and coordinated monomer, due to the steric interaction with the C_s symmetric ligand framework. This interaction will forbid the formation of the head to tail St-St sequences and reduce the catalytic yield and St content.

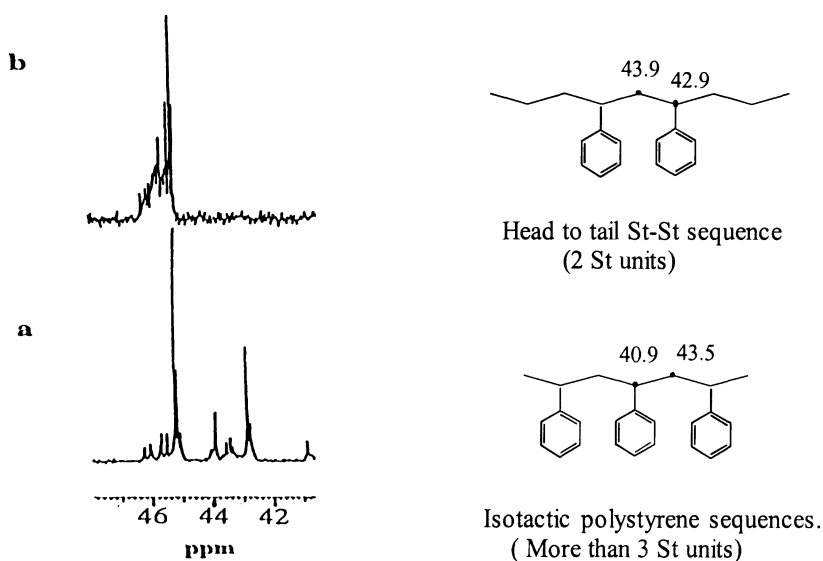


Fig. 3. ^{13}C -NMR spectra of the copolymers (TMS scale, 41-46ppm).

(a) Run 8 (complex VIII), (b) run 14 (complex XII).

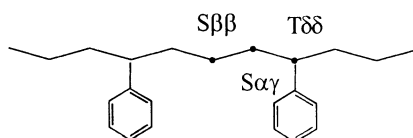
The copolymer produced by the complexes with C_s symmetry has meso- and rac-diad structure, while the copolymer produced by C_2 symmetric complexes has

only meso-diad (isotactic) structure in Et-St alternating sequence (Table 3), as reported already [6].

It could be considered that the steric interaction of the C_2 symmetric ligand framework to the polymer chain end and monomer phenyl groups controls the isotactic propagation of the head to tail St-St sequences, similar to the isotactic polymerization of propene reported with zirconocene with C_2 symmetry [11]. The isotactic stereo-regulation of Et-St alternating sequences is accounted for by the same consideration. C_2 symmetry of the complex seems to favor the isotactic propagation of the alternating sequence, even at higher temperatures, since the isotacticity is not influenced by migration error such as site isomerization (epimerization). To the contrast, C_s symmetric complex such as Ewen-type zirconocene and CGCT-type complex give the atactic alternating sequence, since the tacticity is sensitive to the migration error. The revelation of isotacticity using these C_s symmetric complexes may be limited under the lower temperature conditions [13].

Table 3. ^{13}C NMR assignment of the Et-St alternating sequence in Et-St copolymers [6].

| Carbon type | Tacticity | Chemical shifts in ppm from TMS. | | | |
|------------------|-----------|----------------------------------|----------------|-------|-------|
| | | (CDCl ₃) | | | |
| | | Ref. [4] | complexes (VI) | (IX) | (XII) |
| T $\delta\delta$ | rr | - | - | 45.78 | 45.68 |
| | mr | - | - | 45.56 | 45.55 |
| | mm | 45.4 | 45.44 | 45.45 | 45.43 |
| S $\alpha\gamma$ | rr | - | - | 37.02 | 37.04 |
| | rm | - | - | 36.95 | 36.94 |
| | mr | - | - | 36.74 | 36.73 |
| | mm | 36.6 | 36.62 | 36.63 | 36.64 |
| S $\beta\beta$ | r | - | - | 25.47 | 25.46 |
| | m | 25.2 | 25.26 | 25.30 | 25.25 |



Conclusion

Bridged zirconocene complexes activated with MAO promote the St-Et copolymerization. Smaller bite angle and fused ring substituents such as indenyl or benzindenyl ligand with C_2 symmetry of zirconocene lead to a high activity in the copolymerization and give high St content copolymers of more than 50 mol%. C_2 symmetry of the ligand framework is considered to be a key structure for the formation of head to tail St-St sequences and isotactic stereo-regularity.

References

- [1] Eur. Pat. Appl. 0416815A2 (1990), The Dow Chemical Company, J. C. Stevens, F. J. Timmers, D. R. Wilson, G. F. Schmidt, P. N. Nickias, R. K. Rosen, G. W. Knight, and S. -y. Lai; Chem. Abstr. 115, 93163.
F. G. Sernetz, R. Mulhaupt, F. Amor, T. Eberle, and J. Okuda, *J. Polym. Sci., Part A: Polym. Chem.*, **35**, 1571(1997).
- [2] N. Inoue, and T. Shiomura, *Polymer Preprints, Japan*, **42**, 2292 (1993).
- [3] P. Longo, A. Grassi, and L. Oliva, *Makromol. Chem.*, **191**, 2387 (1990).
- [4] M. Kakugo, T. Miyatake, and K. Mizunuma, *Stud. Surf. Sci. Catal.*, **517** (1990).
- [5] L. Oliva, L. Izzo, and P. Longo, *Macromol. Rapid Commun.*, **17**, 745 (1996).
- [6] T. Arai, T. Ohtsu, and S. Suzuki, *Macromol. Rapid Commun.*, **19**, 327 (1998).
Denki-kagaku kogyo Co. Ltd., JP97-309925, DE19711339A1.
- [7] T. Arai, T. Ohtsu, and S. Suzuki, *Polymer Preprints*, **39** (1), 220 (1998).
To be submitted.
- [8] A. Cano, T. Cuenca, P. Gomez-Sal, B. Royo, and P. Royo, *Organometallics*, **13**, 1688 (1994).
- [9] W. Spaleck, M. Antberg, V. Dolle, R. Klein, and J. Rohrmann, *New J. Chem.*, **14**, 499 (1990).
- [10] A. Razavi and J. L. Atwood, *J. Organomet. Chem.*, **459**, 117 (1993).
- [11] W. Kaminsky, K. Kulper, H. H. Brintzinger, F. W. W. P. Wild, *Angew. Chem., Int. Ed. Engl.* **24**, 507 (1985).
- [12] U. Stehling, J. Diebold, R. Kirsten, W. Röhl, H. H. Brintzinger, S. Jüngling, R. Mülhaupt, and F. Langhauser, *Organometallics*, **13**, 964 (1994).
- [13] L. Oliva, P. Longo, and L. Izzo, *Macromolecules*, **30**, 5616 (1997).

Branched Polyethenes Prepared via Olefin Copolymerization and Migratory Insertion

Johannes Heinemann, Philipp Walter, Dietmar Mäder, Rupert Schnell, Jürgen Suhm, Rolf Mülhaupt

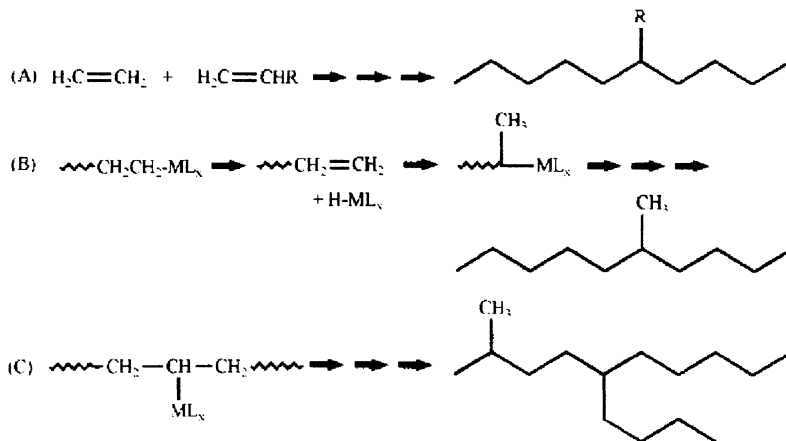
Freiburger Materialforschungszentrum und Institut für Makromolekulare Chemie der Albert-Ludwigs Universität Freiburg, Stefan-Meier-Str. 31, D-79104 Freiburg i.Br., Germany
mulhaupt@mfz.uni-freiburg.de

Abstract. Branched polyethenes with variable alkyl side chains were prepared via three routes: (1) metallocene-catalyzed copolymerization of ethene with propene, 1-octene, 1-eicosene, (2) simultaneous ethene polymerization and copolymerization of in-situ formed 1-alkenes resulting from ethene oligomerization, using a blend of Ni- and Ti-based catalysts ("hybrid catalysts"), and (3) Ni- and Pd-catalyzed ethene homopolymerization with branching occurring due to migratory insertion. The resulting families of materials included high density, low and ultralow density semicrystalline polyethenes as well as highly flexible and elastomeric polyethenes. The degree of branching (DB), as measured by the number of branched C/1000 C, was correlated with comonomer incorporation, catalyst structure, polymerization conditions, polyethene melting temperature and melting enthalpy. Polyethenes prepared by ethene/1-olefin copolymerization were compared with branched ethene homopolymers. Linear low density polyethenes with DB<50, produced with Ni-catalysts, resembled poly(ethene-co-propene). Highly branched polyethene elastomers were applied as toughening agents and blend components of isotactic polypropene in order to improve polypropene's impact resistance.

1. Introduction

During the 1930's, Fawcett, Gibson and coworkers at ICI discovered that high pressure free radical polymerization afforded branched low density semicrystalline polyethenes. Since then it is well recognized that short- and long-chain branching represents the key to achieving control of polyethene properties such as melting temperature, density, processability, optical clarity, stiffness, strength, toughness, stress crack resistance, and blend compatibility [1]. Pioneering advances by Ziegler during the 1950's led to group IV transition metal catalysts which can be used to copolymerize ethene with 1-alkenes and to

produce linear low density polyethenes at low pressure. Especially single-site metallocenes were found to yield ethene/1-alkene copolymers with narrow molecular weight distribution and very uniform comonomer incorporation. Metallocene catalysts can copolymerize less reactive long-chain 1-alkenes, cycloolefins, styrenes as well as macromonomers. Recent progress has been reviewed [2,3]. In contrast to metallocenes, many conventional catalysts gave rather complex copolymer mixtures with 1-alkene comonomer being incorporated predominantly in low molecular weight polyethylene fractions.



Scheme 1. Formation of branched polyethenes via 1-alkene copolymerization (A) and via migratory insertion ethene homopolymerization (B, C)

Branching of polyethenes can also be achieved in the absence of 1-alkene comonomer using exclusively ethene feedstock. During the 1980's Fink reported the formation of methyl-branched polyethenes via $2,\omega$ -polymerization, which later became known as migratory insertion polymerization [4-7]. For example, homopolymerization of 1-pentene on $\text{Ni}(\text{COD})_2$ / phosphorane catalysts produced methyl-branched poly(ethene-alt-propene) due to migration of the catalytically active transition metal alkyl resulting from β -hydride elimination followed by reinsertion. The distance between methyl branches was varied as a function of the 1-alkene molar mass. At the same time, branched ethene homopolymers were obtained by Ostoja-Starzewski by means of Ni-ylide-based catalysts as well as Ni/Cr hybrid catalysts [8-12]. At the Hamburg polyolefin symposium in 1987 he stated "it is thus possible to synthesize branched polyethylene from ethylene alone, i.e. without using comonomer" [12]. During the 1990's Brookhart's research led to the discovery of Ni- and Pd-catalysts containing diazadiene ligand frameworks [13-18]. As a function of ligand substitution pattern, transition metal type and especially process conditions such as polymerization temperature and pressure it was possible to control molar mass and degree of branching in ethene homopolymerization [14,18]. Brookhart's first patent application [13], jointly filed with Du Pont, claimed polyethenes with specific microstructures comprising 80 to 150 branches per 1000 methylene groups, which contain for every 100 branches that are methyl, about 30-90 ethyl branches, about 4-20 propyl

branches, 15-50 butyl branches, 3-25 amyl branches, 30-140 hexyl or longer n-alkyl branches. With diazadiene-Pd catalysts highly branched polyethenes with molar mass exceeding 100000 g/mol were obtained as viscous liquids. Moreover, polar comonomers such as methyl acrylate, were incorporated to form polyethene with n-alkyl and ester-alkyl side chains [16,17].

The routes to branched polyethenes via ethene/1-alkene copolymerization (route A) and ethene migratory insertion homopolymerization (route B and C) are displayed in Scheme 1. When insertion occurs only after migration of the transition metal alkyl to the chain end, methyl-branched polyethenes are formed exclusively. In contrast, highly branched polyethenes are obtained when insertion takes place during migration along backbone and side chains. Objective of this research was to compare branched polyethenes prepared by these different routes, including branched polyethene prepared by hybrid catalysts which give simultaneous ethene polymerization and oligomerization. Special emphasis was placed upon the correlations between degree of branching and catalysts structures as well as polyethene melting temperatures and melting enthalpies for semicrystalline polyethene. Blend formation of highly branched polyethene rubbers with isotactic polypropylene was evaluated in order to improve polypropylene's impact resistance.

2. Metallocene-Catalyzed Ethene/1-Alkene Copolymerization

The transition metal complexes displayed in Figure 1 were activated with methylalumoxane (MAO) to afford homogeneous catalysts which homo- and copolymerize ethene in toluene at temperatures varying between 20 and 60 °C and ethene pressures varying between 1 and 6 bar. According to branching route (A) in Scheme 1, single site metallocenes were applied to copolymerize ethene with 1-alkenes such as propene, 1-octene, and 1-eicosene. In accord with earlier observations by several other groups [19-24], copolymerization parameters can be varied as a function of metallocene structures. As apparent from Table 1, Cp*₂ZrCl₂/MAO gave very poor propene incorporation, as reflected by $r_E = 256$ ($r_p = 0.2$), while substitution of the dimethylsilylene-bridged bisindenyl ligand framework promoted propene incorporation with $r_E = 5.0$ ($r_p = 0.4$) for benzannulation and $r_E = 3.3$ ($r_p = 0.6$) for 4-phenyl substitution. This pronounced effect of the ligand substitution patterns is also clearly visible in Table 2, listing the results of ethene/1-octene copolymerization and including data reported previously by Schneider and Suhm [25-28]. Similar to observations by Spaleck and coworkers [29], the 2-methyl-substitution promoted formation of higher molecular weight copolymers and did not affect copolymerization. However, substitution in 4-position played the key role in ethene/1-octene copolymerization. Octene incorporation improved within the catalyst family containing the dimethylsilylene-bridged bisindenyl ligand framework with 4-

naphthyl > 4-phenyl > benzannelation. Comonomer incorporation of 4-naphthyl-substituted metallocenes (MNI, Table 2) was very similar to that of the half-sandwich complexes such as CBT (Fig. 1 and Table 2), which are referred to as “constrained geometry catalysts“. However, MNI/MAO gave around 100-fold activity with respect to CBT/MAO. It should be noted that CBT/MAO, which suffers rapid deactivation, was tailored to perform in solution processes with rather short hold-up times of a few minutes. Metallocene-catalyzed ethene/1-octene copolymerization yielded branched polyethylenes with degree of branching, measured as branched C/1000 C, ranging from 0 to 125. Also the entire feasible composition range of ethene/1-eicosene copolymers were prepared.

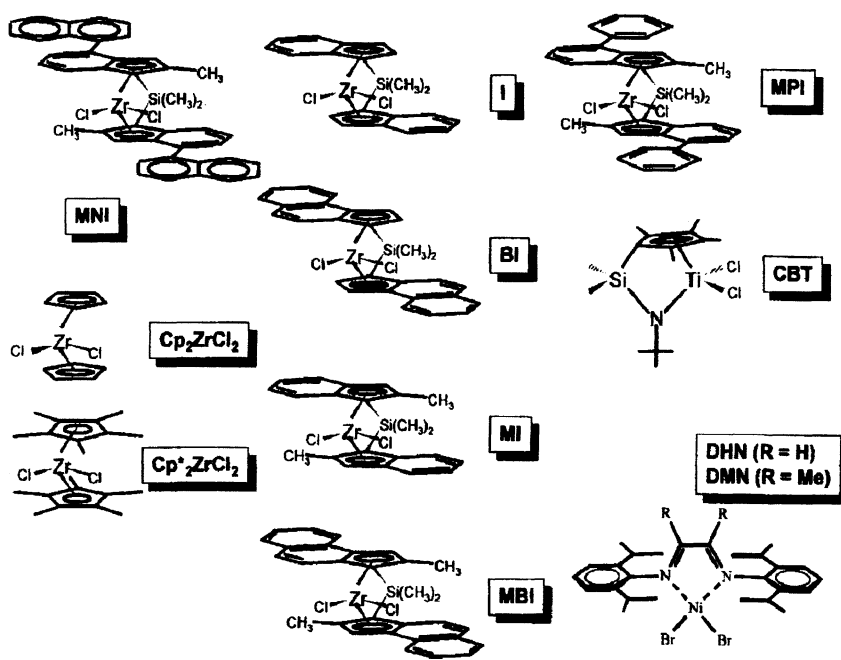


Fig. 1. Catalyst components

Table 1. Ethene/propene copolymerization catalyzed with MAO-activated metallocenes^{a)}

| metallocene type | MBI | MPI | Cp* ₂ ZrCl ₂ |
|--|-------|--------|------------------------------------|
| run no. 1 | 1 | 2 | 3 |
| [P] _{feed} (mol-%) | 76 | 76 | 76 |
| [P] _{polymer} ^{b)} (mol-%) | 51 | 59 | 2 |
| [P] _{polymer} ^{b)} (wt.-%) | 61 | 69 | 3 |
| r _E ^{c)} | 5.0 | 3.3 | 256 |
| r _P ^{c)} | 0.4 | 0.6 | 0.2 |
| r _E *r _P | 1.95 | 1.93 | 55.4 |
| activity ^{d)} | 22200 | 113500 | 40000 |
| M _n ^{e)} | 91900 | 32000 | 17000 |
| M _w /M _n ^{e)} | 1.5 | 2.0 | 1.9 |

a) p_E=2 bar, [E]=0.12 mol/l =24 mol-%, [P]=0.39 mol/l, run 1: [Zr]=2 μmol/l, Al/Zr=10000, run 2: [Zr]=0.375 μmol/l, Al/Zr=30000, run 3: [Zr]=3 μmol/l, Al/Zr=20000, 40 °C, toluene solvent, b) determined by means of ¹³C NMR, c) as determined according to Uozumi-Soga [30], d) kg(polymer) * mol_{Zr}⁻¹ * h⁻¹, d) determined by SEC with PE standard, run 4 with PP standard,

Table 2. Ethene/1-octene copolymerization catalyzed with MAO-activated metallocenes^{a)}

| metallocene | I | MI | BI | MBI | MPI | MNI | CBT | Cp ₂ Zr |
|--|------|------|------|------|------|------|------|--------------------|
| run-no. | 1 | 2 | 3 | 4 | 5 | 6 | 7 | 8 |
| [O] _{feed} (mol-%) | 75 | 75 | 75 | 75 | 75 | 75 | 75 | 75 |
| [O] _{pol.} (mol-%) ^{b)} | 12 | 11 | 19 | 22 | 32 | 42 | 43 | 14 |
| [O] _{pol.} (wt.-%) ^{b)} | 35 | 34 | 49 | 53 | 66 | 74 | 75 | 39 |
| r _E | 19 | 19 | 10 | 10 | 5 | 4 | 4 | 33 |
| r _O | 0.01 | 0.01 | 0.08 | 0.12 | 0.15 | 0.22 | 0.29 | 0.05 |
| r _E *r _O | 0.27 | 0.25 | 0.81 | 1.20 | 0.76 | 0.87 | 1.20 | 0.17 |
| activity ^{c)} * 10 ³ | 1600 | 890 | 1700 | 600 | 2500 | 2200 | 34 | 700 |
| M _n (g/mol) ^{d)} | | | | | | | | |
| * 10 ³ | 91 | 140 | 78 | 172 | 135 | 106 | 126 | 25 |
| P _n ^{e)} | 2390 | 3720 | 1750 | 3690 | 2450 | 1760 | 1970 | 630 |
| M _w /M _n ^{d)} | 1.6 | 1.8 | 1.6 | 1.8 | 2.5 | 2.5 | 2.3 | 2.5 |
| T _g ^{f)} [°C] | -49 | -46 | -57 | -59 | -65 | -66 | -63 | -50 |

a) p_E=2 bar, run 1-7 [E]=0.2 mol/l=25 mol-%, [O]=0.6 mol/l, run 8: [E]=0.2 mol/l, [O]=1.2 mol/l, run 1-5: [Zr]=2 μmol/l, run 6: 20 μmol/l, run 8: 5 μmol/l, run 1-8: [Al]=40 mmol/l, Al/Zr=10000, 40 °C, toluene, for more details concerning experimental conditions see [26-28]; b) determined by ¹³C NMR;

c) mol_{inserted monomeric units} * (mol/l_{total monomer conc})⁻¹ * (mol_{metallocene})⁻¹ * (h_{polym. time})⁻¹

d) determined by SEC and polystyrene standard, for run 5 PE standards were used;

e) degree of polymerization, f) determined by DSC, run 1-4,7,8: heating rate 20 Kmin⁻¹, run 5,6: heating rate 10 Kmin⁻¹

The potential of metallocene catalysts with respect to efficient 1-alkene incorporation was exploited to produce branched polyethene without feeding 1-alkene comonomer. A MAO-activated hybrid catalyst was composed of a blend of CBT (cf. Fig. 1) and Ni(acac)₂. It is well known that Ni(acac)₂/MAO forms 1-butene which is copolymerized with ethene on CBT/MAO. Simultaneous ethene dimerization and ethene copolymerization with in-situ formed 1-butene was performed in toluene at 40 °C and ethene pressure of 6 bar. The results are summarized in Table 3. As a function of the Ti/Ni molar ratio it was possible to control degree of ethyl branching and to vary melting temperature without drastic broadening of polydispersity of the resulting poly(ethene-co-1-butene). Similar to 1-butene copolymerization catalyst activity and molar mass decreased slightly at high content of the less reactive 1-butene.

3. Migratory Insertion Polymerization

Branched ethene homopolymers were prepared according to route B and C in Scheme 1 using diazadiene and methyl-substituted diazadiene (DAD) complexes of Ni and Pd. As reported by Brookhart [14,18], MAO-activated DAD(H,H)NiBr₂, abbreviated as DHN in Fig. 1, and DAD(Me,Me)NiBr₂, abbreviated as DMN in Fig. 1, produced polyethenes with predominant methyl branching at ethene pressures above 1.5 bar and low temperatures. Polymerization runs are listed in Table 4. More detailed description of Ni-catalyzed ethene polymerization was published in a previous communication [28].

Table 3. Ethene homopolymerization using the MAO-activated CBT/Ni(acac)₂ hybrid catalyst^{a)}

| run-no | Ti/Ni (mol/mol) | activity ^{b)} | M _n ^{c)} (g/mol) | M _w /M _n ^{c)} | T _m ^{d)} (°C) | C/1000C ^{e)} |
|--------|--------------------|------------------------|---|--|--------------------------------------|-----------------------|
| JH79 | 100/0 | 1400 | 280000 | 3.1 | 142 | 0 |
| JH138 | 1/5 | 3100 | 189000 | 2.8 | 130 | 9 |
| JH78 | 1/10 | 1100 | 200000 | 2.7 | 108 | 24 |
| JH124 | 1/30 | 540 | 70000 | 2.8 | 71 | 41 |

a) [Ti]=10 μmol/l, Al/Ti=4000, toluene, ethene pressure 6 bar, [E]=0.66 mol/l, 40 °C, polymerization time 1.5 h; b) kg_{polymer} * (mol_{Ti})⁻¹ * h⁻¹ * (mol/l_{ethene})⁻¹; c) SEC, polystyrene standard, d) DSC, 10 K min⁻¹; e) degree of branching determined by ¹H and ¹³C NMR.

Degree of branching was increased with increasing temperature, decreasing ethene pressure and with methyl substitution of the diazadiene ligand framework. With MAO-free cationic Pd complexes such as DAD(Me,Me)PdMe(NC-Me)⁺B[(CF₃)₂C₆H₃]₄⁻ highly branched liquid polyethenes were obtained. In contrast to Ni catalysts, the degree of branching was independent of ethene pressure in the case of Pd-catalyzed ethene polymerization.

Table 4. Ethene homopolymerization by means of Ni- and Pd-based catalysts^{a)}

| run no | catalyst | ethene (bar) | temp. (°C) | C/1000C ^{b)} | T _m ^{c)} (°C) | ΔH _m ^{c)} (J/g) |
|--------------------|----------|-----------------|---------------|-----------------------|--------------------------------------|--|
| JH05e | DHN | 4.6 | 20 | 6 | 137 | 278 |
| JH09e | DHN | 10.6 | 60 | 15 | 120 | 160 |
| JH06e | DHN | 5.2 | 60 | 23 | 112 | 100 |
| JH13e | DMN | 4.6 | 20 | 31 | 92 | 107 |
| JH64e | DMN | 1.5 | 20 | 64 | 52 | 70 |
| JH56e | DMN | 1.5 | 40 | 98 | -8 | 20 |
| JH41 ^{d)} | DMPN | 6.0 | 35 | 97 | -66 (T _g) | amorphous |
| JH53 ^{e)} | DMPN | 9.0 | 35 | 99 | -62 (T _g) | amorphous |

a) [Ni]=20 μmol/l, Al/Ni=1000 in toluene; [Pd]=0.25 mmol/l in CH₂Cl₂, for more detailed description of experimental conditions see [28]; b) degree of branching determined by ¹H and ¹³C NMR, c) determined by DSC, heating rate of 10 K min⁻¹, d) M_n=184000 g/mol, branched C/1000 C = 38 Me, 23 Et, 2 Pr, 9 Bu, 3 Pe, 35 Hex+; e) M_n=171000 g/mol, branched C/1000 C = 33 Me, 23 Et, 2 Pr, 8 Bu, 3 Pe, 33 Hex+.

4. Comparison of branched polyethenes

Semicrystalline and amorphous branched polyethenes with degree of branching (DB), expressed as number of branched C/1000 C of main and side chains, varying between 0 and 100 were prepared by means of copolymerization and migratory insertion. In the DB range of 0 to 60, both melting temperature and crystallinity, as determined by calorimetry (DSC), decreased with increasing DB. From Fig. 2 it is apparent that branched polyethene, prepared with Ni catalysts, exhibits very similar behavior with respect to that of poly(ethene-co-propene), prepared using MBI/MAO and Cp₂ZrCl₂/MAO metallocene catalysts. This is in accord with the NMR spectroscopic observation that Ni-catalysts such as DMN/MAO and especially DHN/MAO formed predominantly methyl-branched polyethene. At the same DB poly(ethene-co-1-octene) exhibited somewhat lower melting temperature because of higher 1-octene content with respect to propene. Moreover, in contrast to hexyl side chains, methyl branches can also be accommodated in crystal lamellae. It should be noted that for poly(ethene-co-propene) the maximum DB for 100 % comonomer incorporation is 330 for polypropene, whereas for poly(ethene-co-1-octene) the maximum DB is 125. The slight deviation observed for poly(ethene-co-1-eicosene) may be due to side chain crystallization, which occurs at 1-eicosene content when exceeding DB of 10.

These results are in good agreement with data reported by Arnold who investigated the influence of the degree of branching of model systems for short chain branched polyethene, prepared by hydrogenation of butadiene/ethene/1-olefin terpolymers [31,32]. Crystallinity, as reflected by the melting enthalpy displayed in Fig.3, appears to depend primarily on the branching probability.

However, since crystallization depends also upon thermal history, molecular weight and nucleation, more research is in progress to examine crystallization behavior of branched polyethene prepared by means of copolymerization and migratory insertion.

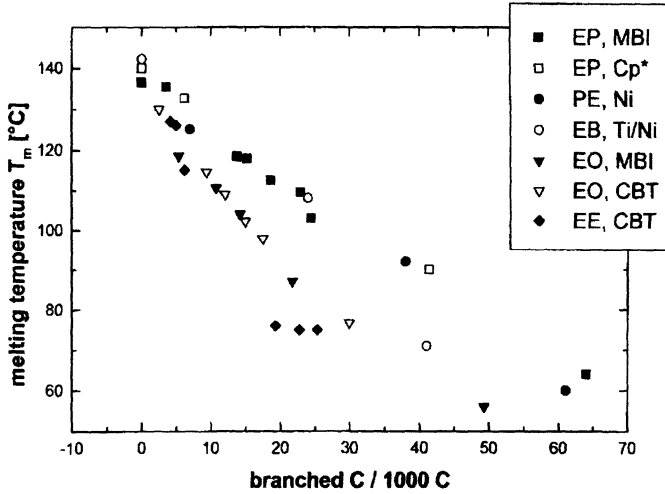


Fig. 2. Polyethene melting temperature as a function of degree of branching

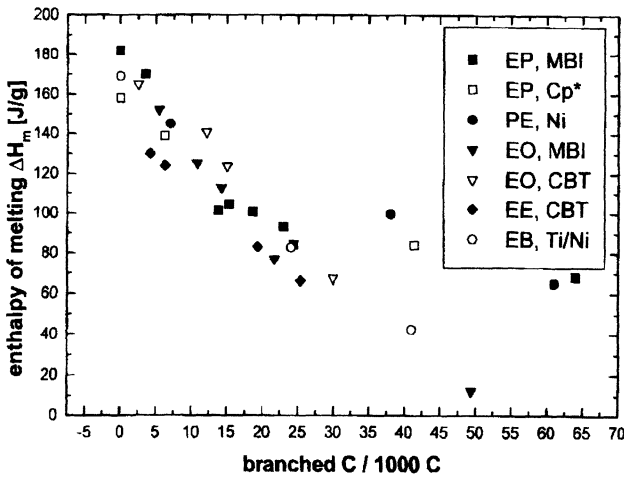


Fig. 3. Polyethene crystallinity as a function of degree of branching

In order to compare amorphous highly branched polyethenes prepared by routes (A) and (B) in Scheme 1, blends were prepared with isotactic polypropene. It is well established that polymer compatibility is a very sensitive probe for polymer microstructures [33-36]. Adequate polymer compatibility in two-phase blends is reflected by effective dispersion, i.e., small particle sizes, and good interfacial adhesion of the polyethylene microphases dispersed in the continuous polypropene matrix. Inadequate compatibility accounts for very large microphases which are readily pulled out of the surrounding matrix due to poor adhesion. Isotactic polypropene (Novolen M from Targor) was melt blended together with highly branched ethene homopolymer JH53 (Table 4) with DB = 99 and alternatively with poly(ethene-co-1octene), abbreviated as EO25, containing 7.6 mol-% 1-octene (equivalent to 25 wt-% 1-octene content and DB = 31), commercially available as Engage 8150 from Du Pont Dow Elastomers. Blending was performed in a Haake twin-screw blender at 200 °C at 60 rpm for the duration of 5 minutes in the presence of 4000 ppm stabilizer (80 wt.-% Irganox 1010/20 wt.-% Irgafos 168). The branched polyethylene content was varied from 0 to 20 wt.-%. Blend compositions and mechanical properties are listed in Table 5.

Table 5. Mechanical properties of blends containing isotactic polypropene (Novolen M, Targor) and branched polyethylene such as JH53 (cf. Table 4) and poly(ethene-co-1-octene), EO25, with 25 wt.-% (7.6 mol-%) 1-octene content (Engage 8150, Du Pont Dow Elastomers), prepared by melt blending at 200 °C^{a)}

| component | PE content (wt.-%) | T _g ^{c)} (°C) | Young's modulus (MPa) | yield stress (MPa) | elongation at break (%) | notched Izod impact str. (kJ/m ²) |
|-----------|--------------------|-----------------------------------|-----------------------|--------------------|-------------------------|---|
| Novolen M | 0 | + 6 | 1060 | 31 | 570 | 5.1 |
| EO25 | 5 | -57 | 980 | 29 | 680 | 7.7 |
| EO25 | 10 | -55 | 930 | 26 | 680 | 12.4 |
| EO25 | 20 | -51 | 720 | 21 | 670 | 47.7 ^{d)} |
| EO25 | 30 | -49 | 560 | 16 | 570 | 70.9 ^{d)} |
| JH53 | 10 | -71 | 870 | 25 | 580 | 13.6 |
| JH53 | 15 | -70 | 770 | 22 | 640 | 24.4 |
| JH53 | 20 ^{b)} | -68 | 640 | 17 | 250 | 12.9 |

a) processing was performed in a Haake twin-screw Rheomix blender with 60 ml chamber, b) processing problems due to handling of liquid JH53 accounted for poor mixing, c) glass temperature determined by means of DMA at 10 Kmin⁻¹, d) no fracture.

According to scanning electron microscopic analyses of fracture surfaces, both polyethenes formed microphases with average diameters of 1 μm for EO25 and 0.7 μm for JH53. As is apparent from Table 5, mechanical properties of both blend types were very similar. Poor performance of JH53 at 20 wt.-% content was a result of mixing problems related to difficult handling of the liquid JH53. Both highly branched polyethenes represent effective toughening agents which improve impact strength of isotactic polypropene. As shown by the trace of the dynamic mechanical analysis, displayed in Fig. 4 for iPP/PE (85 wt.-%/15 wt.-%

%), the first maximum of the $\tan(\delta)$ loss factor, which corresponds to the glass transition of the dispersed polyethene phase, occurs at $-70\text{ }^{\circ}\text{C}$ for JH53 and at $-51\text{ }^{\circ}\text{C}$ for EO25. Both glass temperatures of the dispersed polyethenes are much lower with respect to those of the corresponding bulk polyethenes ($-55\text{ }^{\circ}\text{C}$ for JH53 and $-43\text{ }^{\circ}\text{C}$ for EO25). The second maximum corresponds to the glass transition of the polypropylene matrix. Low rubber glass transition is of particular interest for improving low temperature toughness of isotactic polypropylene. Blend performance of highly branched polyethenes, prepared with Pd-catalysts, is similar to that of ethene/1-octene co- and terpolymers with much higher high 1-octene content, preferably around 50 wt.-%.

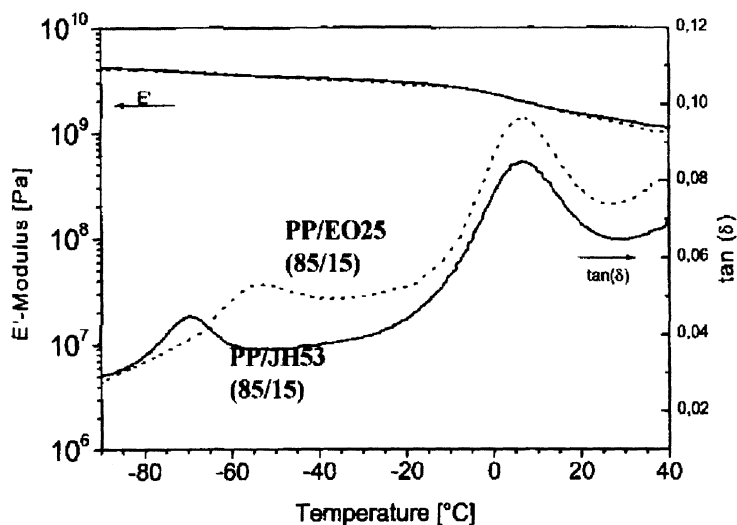


Fig. 4. Dynamic mechanical analysis (DMA) of polypropylene blends with 15 wt.-% branched polyethenes such as poly(ethene-co-octene) containing 25 wt.-% (7.6 mol-%) 1-octene (EO25) or polyethene JH53, prepared by means of Pd-catalyzed ethene homopolymerization.

5. Conclusions

Novel generations of single site catalysts based upon metallocenes with substituted dimethylsilylene-bridged bisindenyl ligand framework, half-sandwich complexes, and late transition metal complexes containing diazadiene-based ligands give excellent control of branching in polyethene synthesis. In contrast to many early catalyst generations of the 1970's, which were modified by trial-and-error-type research, the substitution pattern of such transition metal compounds can be tailored to produce very uniform polyethenes with well-defined microstructures, precisely controlled degree of branching, narrow molecular

weight distributions, and low organoleptics. Since the 1980's research is directed towards the development of catalyst systems which form branched polyethenes without requiring 1-alkene comonomer feedstocks. This is of special interest as alternative route to ethene copolymers with high comonomer content without requiring feed of expensive higher 1-alkenes, which are rather difficult to handle in gas phase polymerization. Two approaches have been identified to be very promising for controlling branching during ethene homopolymerization: (1) Ni- and Pd-based catalysts which give branching as a result of migratory insertion polymerization, and (2) multiple "single site" catalysts comprising blends of different single site catalysts in order to afford simultaneous oligomerization and in-situ copolymerization of in-situ formed vinyl-terminated macromonomers. Moreover, heterogeneous microreactors containing such single site metallocenes are attractive to achieve morphology control during polymerization. In many cases metallocene-catalyzed copolymerization and ethene homo- and copolymerization on multiple single site catalysts ("hybrid catalysts") yield polyethenes which match the performance of those produced by means of migratory insertion polymerization. More research is required to evaluate the formation of long-chain branches during metallocene copolymerization and migratory insertion polymerization. In addition to microstructure control via systematic ligand variations, the design of supported catalysts containing built-in multi-role microreactors represents a key challenge in catalyst development and polyolefin synthesis.

Acknowledgment

The authors gratefully acknowledge support by BASF AG and by the Bundesminister für Bildung und Forschung as part of the projects no. 03M40719 and no. 03N1028 0.

References

1. Ballard DGH (1986) in Seymour RB, Cheng T (eds.) *History of Polyolefins* Reidel D, Publishing Company Dordrecht p9
2. Brintzinger HH, Fischer D, Mülhaupt R, Rieger B, Waymouth RM (1995) *Angew Chem Int Ed Engl* 34:1143
3. Suhm J, Heinemann J, Wörner C, Müller P, Stricker F, Kressler J, Okuda J, Mülhaupt R (1998), *Macromol Symp* 129:1
4. Möhring V, Fink G (1985) *Angew Chem* 97:982
5. Schubbe R, Angermund K, Fink G, Goddard R (1995) *Macromol Chem Phys* 196:467
6. Fink G, Möhring VM, Heinrichs A, Denger C, Schubbe RH, Mühlenbrock PH (1996) in Salamone JC (ed.) *Polymeric Materials Encyclopedia* CRC Press Boca Raton vol 6:4720
7. Fink G, Möhring V, Heinrichs A, Denger C (1992) *ACS Symp Ser* 496:88

8. Ostoja Starzewski KHA, Witte J, Bartl H, Reichert KH, Vasillou G (1987) Eur Pat Appl 250999 assigned to Bayer AG
9. Ostoja Starzewski KA, Witte J (1985) *Angew Chem Int Ed Engl* 24:599
10. Ostoja Starzewski KA (1987) *Angew Chem Int Ed Engl* 26:23
11. Ostoja Starzewski, Witte J (1988) in Quirk RP (ed) *Transition Metal Catalyzed Polymerizations - Ziegler Natta and Metathesis Polymerization*, Cambridge University Press, New York
12. Ostoja Starzewski KA, Witte J, Reichert KH, Vasillou G (1988) in Kaminsky W, Sinn H (ed) *Transition Metals and Organometallics as Catalysts for Olefin Polymerization*, Springer Publishing Co., Berlin p.349
13. Johnson L, Killian C M, Arthur S M, Feldman J, McCord E F, McLain SJ, Kreutzer K A, Bennett M A, Coughlin E B, Ittel S D, Parthasarathy A, Tempel D J, Brookhart M, WO 96/23010, Aug.1, 1996, assigned to E.I. Du Pont de Nemours and Company and University of North Carolina
14. Killian CM, Johnson LK, Brookhart M (1997) *Organometallics* 16:2005
15. Killian CM, Tempel DJ, Johnson LK, Brookhart M (1996) *J Am Chem Soc* 118:11664
16. Mecking S, Johnson LK, Wang L, Brookhart M (1998) *J Am Chem Soc* 120:888
17. Johnson LK, Mecking S, Brookhart M (1996) *J Am Chem Soc* 118:267
18. Johnson LK, Killian CM, Brookhart M (1995) *J Am Chem Soc* 117:6414
19. Kaminsky W, Miri M (1985) *J Polym Sci Part A Polym Chem* 23:2151
20. Uozumi T, Soga K (1992) *Macromol Chem Phys* 193:8223
21. Chien JCW, He D (1991) *J Polym. Sci Part A Polym Chem* 29:1609
22. Herfert N, Fink G (1993) *Macromol Chem Phys* 194:3167
23. Uozumi T, Nakamura S, Toneri Teranshi T, Sano T, Arai T, Shiono T (1996) *Macromol Chem Phys* 197:4237
24. Fink G, Seppälä (1994) *Macromolecules* 27:6254
25. Schneider MJ, Mülhaupt R (1997) *Macromol Chem Phys* 198:1121
26. Schneider MJ, Suhm J, Mülhaupt R, Prosenc MH, Brintzinger HH (1997) *Macromolecules* 30:3164
27. Suhm J, Schneider MJ, Mülhaupt R (1998) *J Mol Catal A Chemical* 128:215
28. Suhm J, Heinemann J, Thomann Y, Thomann R, Maier RD, Schleis T, Okuda J, Kressler J. Mülhaupt R (1998), *J Mater Chem* 8:553
29. Spaleck W, Küber F, Winter A, Rohrmann J, Bachmann B, Aulberg M, Dolle V, Paulus EF (1994) *Organometallics* 13:954
30. Uozumi T, Soga K (1992) *Macromol Chem Phys* 193:823
31. Gerum W, Höhne GWH, Wilke W, Arnold M, Wegner T (1996), *Macromol Chem Phys* 197:1691
32. Reußner J, Höhne GWH, Utschik H, Arnold M, Wegner T, Wohlfarth L (1996), *J Thermal Analysis* 47:975
33. Yamaguchi M, Miyata H, Nitta K (1996) *J Appl Polym Sci* 62:87
34. Nitta K, Okamoto K, Yamaguchi M (1998) *Polymer* 39:53
35. Thomann Y, Suhm J, Thomann R, Bar G, Maier RD, Mülhaupt R (1998) *Macromolecules* 31:5441
36. Mäder D, Thomann Y, Suhm J, Mülhaupt R (1999), *J Appl Polym Sci* submitted

Metallocene Catalyzed Alternating Copolymerization of Olefins

Inken Beulich, Franck Freidanck, Anne-Meike Schauwienold, Ulrich Weingarten
Michael Arndt-Rosenau*, Walter Kaminsky

Institute for Technical and Macromolecular Chemistry
University of Hamburg
Bundesstr. 45, 20146 Hamburg
e-mail: arndt@chemie.uni-hamburg.de

Abstract. C_1 -symmetric metallocenes enable the production of alternating copolymers as well as that of blocky ones. A new model of copolymerization has been developed and applied to ethene/norbornene, ethene/propene and ethene/octene copolymerization. It is shown that the mechanism of polymerization depends on the catalysts structure, the monomer structure, and the temperature of polymerization.

Introduction

Olefin polymerization by metallocene catalysts has been proposed [1] to proceed by an *alternating mechanism* which involves a „migration“ of the growing polymer chain during insertion and, therefore, in the case of metallocenes with stereogenic transition metal centers inversion of the configuration takes place (the position formerly occupied by the polymer chain is available for the next olefin to approach, the configuration of the metallocene *alternates*).

In this context metallocenes with heterotopic active sites are interesting for copolymerization due to the fact that they offer a possibility to tailor the distribution of comonomers in copolymers at least to some extent [2-5].

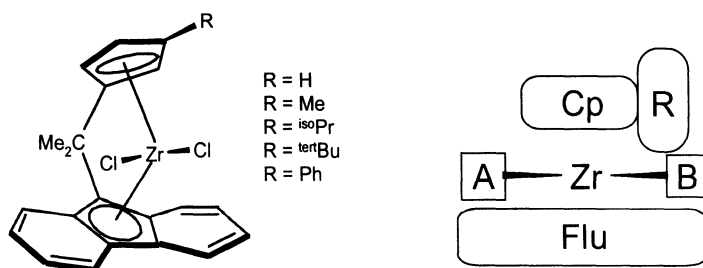


Fig. 1. Structure and schematic drawing of the metallocenes used in this study.

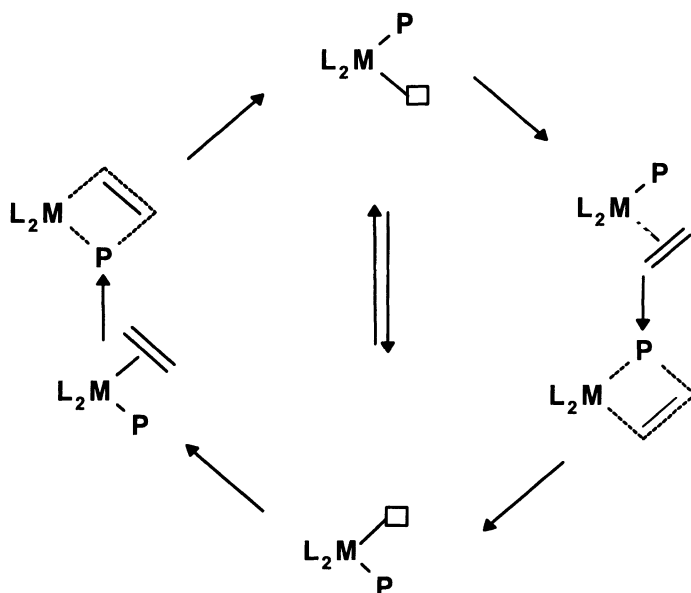


Fig. 2. Mechanism of olefin polymerization by metallocene catalysts. After two migratory insertions the polymer chain and the vacant site for olefin coordination are back in their original position (alternating mechanism). Isomerization of the active species after a migratory insertion results in the original arrangement without a second insertion (retention mechanism).

The simplest model one can think of is a metallocene having one site (A) available for coordination of both monomers and the other site (B) blocked for the bulkier comonomer; an alternating copolymer will be formed if a huge excess of the bulkier monomer is used.

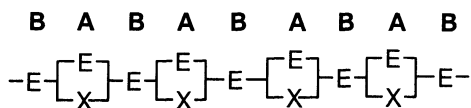


Fig. 3. Formation of an “alternating” copolymer by using a C_1 -symmetric catalysts.

If both sites are available for both monomers the copolymerization behavior of the catalyst is still beyond description by simple first (M1) or second order (M2) Markovian statistics (each site will have its own set of copolymerization parameters). We have developed a new copolymerization model for this case (TSAM – model) [2,3].

Ethene/Norbornene Copolymerization

Copolymerization of ethene with norbornene by $[\text{Me}_2\text{C}(3\text{-}^{1\text{er}}\text{tBuCp})(\text{Flu})]\text{ZrCl}_2/\text{MAO}$ at 30°C proceeds according to the "two sites alternating mechanism" as can be shown by comparison of the tetrad distribution observed to that calculated for the TSAM-model and a simple Markovian statistic [2]. The copolymerization parameter r_{ethene} for the site available for both monomers is 3.1 which is comparable to the parameter observed for $[\text{Me}_2\text{C}(\text{Cp})(\text{Flu})]\text{ZrCl}_2/\text{MAO}$ at 30°C , indicating that indeed the unsubstituted site (A) can be approached by both monomers.

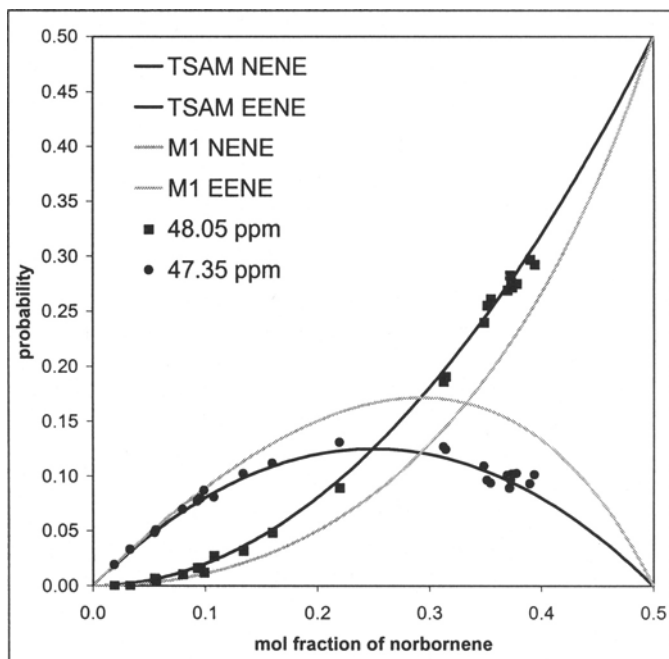


Fig. 4. Ethene/norbornene copolymerization by $[\text{Me}_2\text{C}(3\text{-}^{1\text{er}}\text{tBuCp})(\text{Flu})]\text{ZrCl}_2/\text{MAO}$ at 30°C . Comparison of the concentration of EN-centered tetrad estimated from ^{13}C -NMR spectra with the ones calculated based on the TSAM- (■) and the M1-model (◻).

Copolymerization by $[\text{Me}_2\text{C}(3\text{-MeCp})(\text{Flu})]\text{ZrCl}_2/\text{MAO}$ at 30°C is totally different. Copolymers containing up to 40 mol% of norbornene feature no blocks of norbornene as expected, but this time the alternating structure is most probably not due to the TSAM mechanism. The microstructure of copolymers obtained by using $[\text{Me}_2\text{C}(3\text{-MeCp})(\text{Flu})]\text{ZrCl}_2/\text{MAO}$ is described the M1-model and therefore insertion seems to proceed by a retention mechanism. At incorporation rates above 40 mol% blocks of norbornene are observed and the simple Markovian process is not able to describe the polymerization. The mechanism of polymerization seems

to change to an alternating one, which may be due to changes in the hapticity of the ligand induced by the bulky monomer.

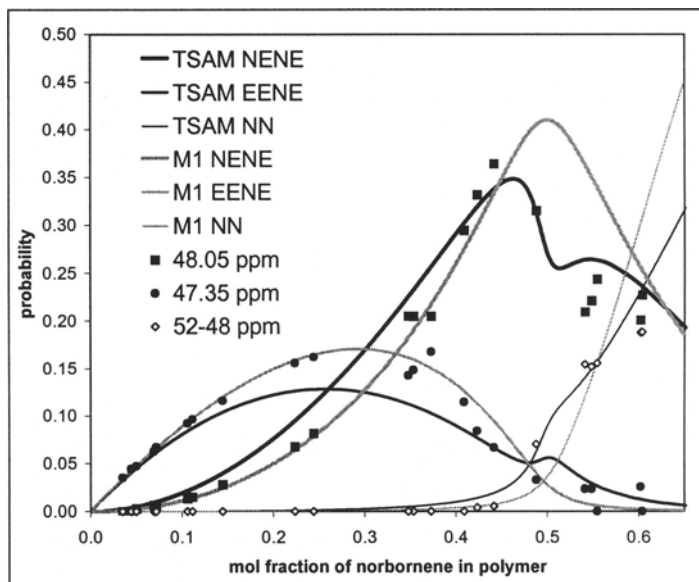


Fig. 5. Ethene/norbornene copolymerization by $[\text{Me}_2\text{C}(3\text{-MeCp})(\text{Flu})]\text{ZrCl}_2 / \text{MAO}$ at 30°C . Comparison of the concentration of EN-centered tetrads and NN-diads estimated from ^{13}C -NMR spectra with the ones calculated based on the TSAM-(■) and the M1-model (●).

The polymers obtained by using $[\text{Me}_2\text{C}(3\text{-MeCp})(\text{Flu})]\text{ZrCl}_2/\text{MAO}$ are semicrystalline if they contain 41–47 mol% of norbornene. At higher incorporation rates the formation of norbornene blocks leads to amorphous structures. In contrast semicrystalline polymers are obtained by using $[\text{Me}_2\text{C}(3\text{-}^{\text{tert}}\text{BuCp})(\text{Flu})]\text{ZrCl}_2$ if the norbornene content is 37–50 mol%. Crystallinity increases with increasing norbornene content as do the melting points which reach 320°C for a copolymer containing 49 mol% of norbornene. The semicrystalline, alternating copolymers obtained with both catalysts are transparent due to the small size of the crystallites.

Ethene/Propene Copolymerization

Ethene/propene copolymerization catalyzed by $[\text{Me}_2\text{C}(3\text{-RCp})(\text{Flu})]\text{ZrCl}_2/\text{MAO}$ ($\text{R} = \text{H}, \text{Me}, ^{\text{iso}}\text{Pr}, ^{\text{tert}}\text{Bu}$) has been investigated over the whole range of monomer compositions at 30°C and 60°C [3]. In contrast to the ethene/norbornene copolymerization the monomer sequence distributions of ethene/propene copolymers obtained with $[\text{Me}_2\text{C}(3\text{-MeCp})(\text{Flu})]\text{ZrCl}_2/\text{MAO}$ follow the TSAM-model, while those observed for $[\text{Me}_2\text{C}(3\text{-}^{\text{tert}}\text{BuCp})(\text{Flu})]\text{ZrCl}_2 / \text{MAO}$ catalysis can

be fitted to the M1-model. This explains the similarity of the monomer sequence distribution of copolymers obtained by using $[\text{Me}_2\text{C}(3\text{-}^{\text{tert}}\text{BuCp})(\text{Flu})]\text{ZrCl}_2 / \text{MAO}$ or $[\text{Me}_2\text{C}(\text{Cp})(\text{Flu})]\text{ZrCl}_2 / \text{MAO}$. A comparison of the copolymerization parameters for these two catalysts indicates that insertion for $[\text{Me}_2\text{C}(3\text{-}^{\text{tert}}\text{BuCp})(\text{Flu})]\text{ZrCl}_2$ most probably occurs from the substituted site.

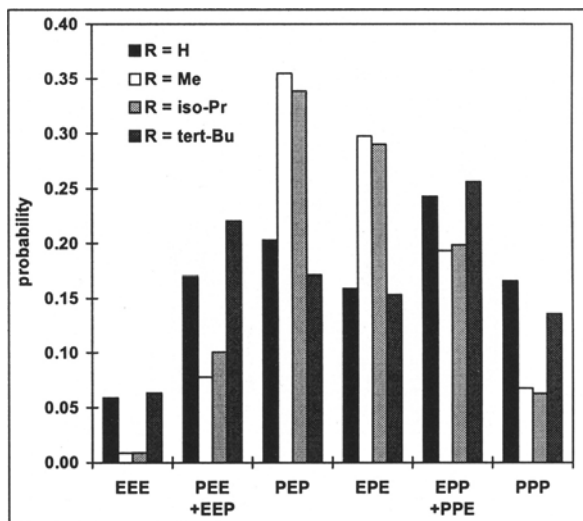


Fig. 6. Triad distributions of ethene/propene copolymers containing 55 mol% propene obtained by using $[\text{Me}_2\text{C}(3\text{-RCp})(\text{Flu})]\text{ZrCl}_2 / \text{MAO}$ at 30°C.

$[\text{Me}_2\text{C}(3\text{-}^{\text{iso}}\text{PrCp})(\text{Flu})]\text{ZrCl}_2/\text{MAO}$ is very similar to $[\text{Me}_2\text{C}(3\text{-MeCp})(\text{Flu})]\text{ZrCl}_2$ at 30°C, while the copolymerization behavior at 60°C is not described by one of the limiting cases. Molecular modeling yields an explanation for this. Rotation of the ^{iso}propyl-group yields two conformers: the more stable of them features the CH-proton directed towards the coordination sphere, while the second one has a Me-group in this position [6]. Thus at low temperature the catalyst will behave like $[\text{Me}_2\text{C}(3\text{-MeCp})(\text{Flu})]\text{ZrCl}_2$ and follow the TSAM-model, while at elevated temperature the second conformer, which is similar to $[\text{Me}_2\text{C}(3\text{-}^{\text{tert}}\text{BuCp})(\text{Flu})]\text{ZrCl}_2$ and works according to the M1-model, will contribute to the polymerization behavior.

Ethene/Octene Copolymerization

The results of ethene/norbornene and ethene/propene copolymerizations have already shown that the mechanism of polymerization by C₁-symmetric metallocene catalysts depends on the monomer used. While ethene/norbornene copolymers produced by $[\text{Me}_2\text{C}(3\text{-}^{\text{tert}}\text{BuCp})(\text{Flu})]\text{ZrCl}_2 / \text{MAO}$ are "alternating" and

ethene/propene copolymers are almost random, ethene/octene copolymerization features a tendency to form blocky structures.

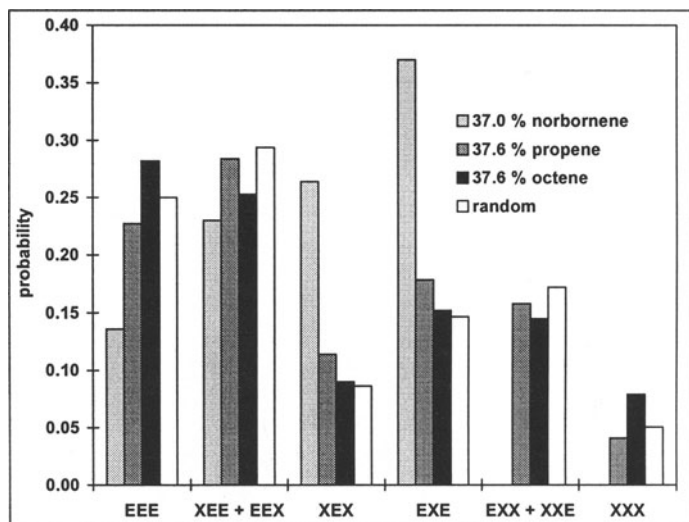


Fig. 7. Comparison of the microstructure of copolymers produced by [Me₂C(3-*tert*BuCp)(Flu)]ZrCl₂ / MAO at 30°C with a random copolymer.

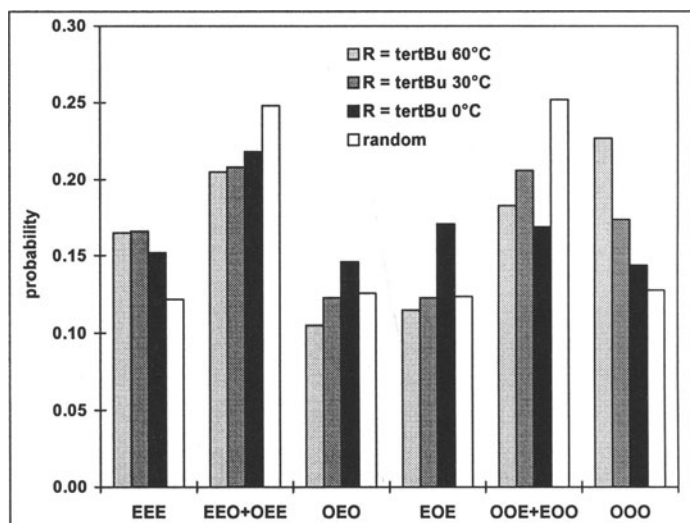


Fig. 8. Comparison of the microstructure of ethene/octene copolymers containing 51 mol% of octene produced by [Me₂C(3-*tert*BuCp)(Flu)]ZrCl₂ / MAO at 0, 30 and 60°C with a random copolymer.

The tendency to form blocks of octene is enhanced at elevated temperatures. The copolymerization behavior can be described neither by the M1- nor by the TSAM model [7]. In conjunction with the results of ethene/norbornene copolymerization it has to be assumed that the catalyst changes its structure depending on the size of the last monomer unit incorporated into the chain.

Nevertheless by using $[\text{Me}_2\text{C}(3\text{-PhCp})(\text{Flu})]\text{ZrCl}_2/\text{MAO}$ it is possible to generate copolymers of ethene and octene featuring a high amount of alternating sequences. At 30°C this catalyst works according to the TSAM model [7].

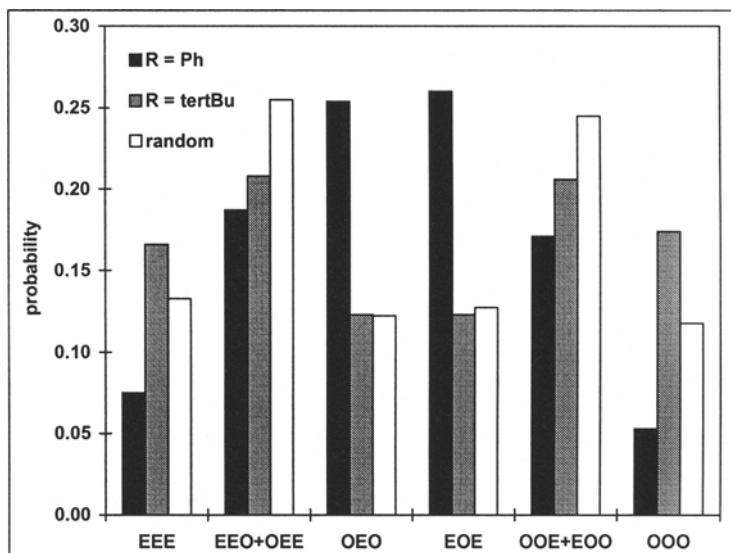


Fig. 9. Comparison of the microstructure of ethene/octene copolymers containing 49 mol% of octene produced by $[\text{Me}_2\text{C}(3\text{-tertBuCp})(\text{Flu})]\text{ZrCl}_2/\text{MAO}$ and $[\text{Me}_2\text{C}(3\text{-PhCp})(\text{Flu})]\text{ZrCl}_2/\text{MAO}$ at 30°C with a random copolymer.

Conclusions

Selected C_1 -symmetric metallocenes can catalyze the alternating copolymerization of ethene with cycloolefins or α -olefins due to the TSAM-mechanism. New semicrystalline polyolefins wait to be discovered.

Analysis of the microstructure of copolymers yields information about the mechanism of polymerization, it depends on: the monomer used, the catalysts used, and the temperature of polymerization.

The results of ethene/norbornene and ethene/propene copolymerization by $[\text{Me}_2\text{C}(3\text{-tertBuCp})(\text{Flu})]\text{ZrCl}_2/\text{MAO}$ indicate that the real mechanism may involve

an alternating mechanism for ethene insertion while in the case of propene a retention mechanism is in effect. Thus the subject of further studies will be the development and application of mixed models to investigate the microstructure of those copolymers.

Additionally the investigations have shown that metallocenes are able to produce blocky copolymers most probably due to change in their structure (hapticity of the ligand) [8].

A second type of changes in the structure of the metallocene may occur for $[\text{Me}_2\text{C}(3\text{-}^{150}\text{PrCp})(\text{Flu})]\text{ZrCl}_2$ and other metallocenes bearing unsymmetrical substituents which may rotate during chain growth. The third type is due to torsional isomers involving the cp-ligands of unbridged metallocenes like $(2\text{-PhInd})_2\text{ZrCl}_2$. New copolymerization models have to be developed to account for these effects.

References

- [1] H.H. Brintzinger, D. Fischer, R. Mühlhaupt, R.M. Waymouth, *Angew. Chem. Int. Ed. Engl.* 34 (1995), 1143 and references therein.
- [2] a) M. Arndt, I. Beulich, W. Kaminsky, *Proceedings of Met'Con 96* held in Houston, Texas, Catalyst Consultant Inc. (1996); b) M. Arndt, I. Beulich; *Macromol. Chem. Phys.* 199 (1998), 1221.
- [3] M. Arndt, W. Kaminsky, A.-M. Schaubwienold, U. Weingarten; *Macromol. Chem. Phys.* 199 (1998), 1135.
- [4] a) T. Uozumi, K. Miyazawa, T. Sano, K. Soga; *Macromol. Rapid Commun.* 18 (1997), 883; b) J. Jin, T. Uozumi, T. Sano, T. Teranishi, K. Soga, T. Shin; *Macromol. Rapid Commun.* 19 (1998), 337.
- [5] M.K. Leclerc, R.M. Waymouth; *Angew. Chem.* 110 (1998), 965.
- [6] M. Arndt-Rosenau; poster presented at the GDCH-symposium "Neue Horizonte der Polymerforschung" in Mainz (23-24.3.1998). Manuscript in preparation.
- [7] Details will be given in a subsequent publication by M. Arndt-Rosenau, F. Freidanck.
- [8] Similar effects may explain the blocky structure of ethene/propene copolymers formed by using $[\text{Me}_2\text{C}(3\text{-}^{\text{tert}}\text{BuCp})_2]\text{ZrCl}_2$ according to Galimberti et al. (*Macromolecules* 31 (1998), 3409).

Copolymer Microstructures of Ethylene Norbornene Copolymers Prepared with Homogeneous Metallocene Based Catalysts

Incoronata Tritto*, Laura Boggioni, Maria Carmela Sacchi, Paolo Locatelli, Dino R. Ferro, and Augusto Provasoli

Istituto di Chimica delle Macromolecole – CNR, Via E. Bassini, 15 – 20133 Milano (Italy)

Abstract. Series of ethylene-norbornene copolymers were synthesized in the presence of zirconocenes with different symmetries and ligand patterns and at different norbornene/ethylene ratios. Copolymers were characterized by ^{13}C NMR spectroscopy; Inadequate NMR sequences were used also. The comparison of ^{13}C NMR spectra of copolymers prepared with different norbornene content and the correlation between ^{13}C NMR chemical shifts and conformational structures of the chain on the basis of molecular mechanics calculations were performed. Preliminary assignments were revised and new comonomer sequences such as ENNE which contain *meso* and *racemo* NN dyads were assigned.

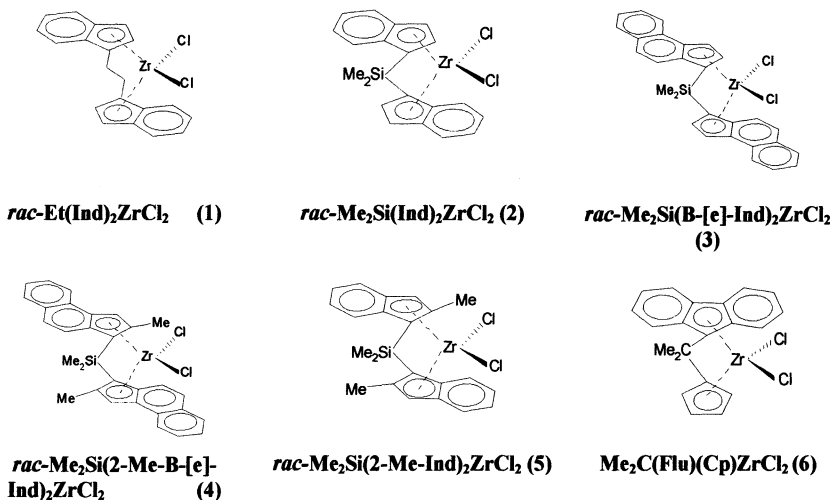
Introduction

Ethylene-norbornene (E-N) copolymers, first reported by Kaminsky, are of great practical interest [1, 2]. They are amorphous and resistant materials with good optical properties. The presence of flexible ethylene units among the rigid cyclic units of the polymer chain gives them the advantage of improved solubility and processability with respect to norbornene homopolymers prepared with the same catalysts. The properties of these materials depend upon comonomer compositions as well as upon the distribution of comonomers within the chain. However, a fundamental understanding of the processes and mechanisms involved in these copolymerizations has not been achieved so far.

Series of ethylene-norbornene copolymers were synthesized in the presence of zirconocenes with different symmetries and ligand patterns and at different norbornene/ethylene ratios. We will report the description of microstructures of ethylene - norbornene copolymers obtained by ^{13}C NMR spectroscopy. The comparison of the ^{13}C NMR spectra of these copolymers along with Inadequate ^{13}C - ^{13}C correlated NMR spectra and with the correlation between ^{13}C NMR chemical shifts and conformational structures of the chain on the basis of molecular mechanics calculations allowed us to: i) revise previous preliminary assignments, and ii) to assign new comonomer sequences.

Copolymer synthesis

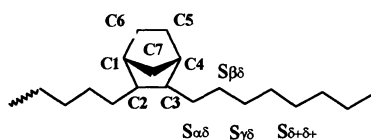
In order to probe the influence of the catalyst symmetry and structure on ethylene-norbornene copolymerization activity and copolymer microstructures, series of ethylene-norbornene copolymers were synthesized in the presence of the following zirconocenes:



Copolymerizations were carried out with metallocenes 1-6 activated by methylaluminoxane (MAO) ($[Zr] = 8 \cdot 10^{-5}$ mol/l, $[MAO]/[Zr] = 1000$, in toluene, at 30 °C, atmospheric pressure). The copolymerization reaction was stopped before 10% of the starting norbornene was consumed. Copolymers were characterized by ¹³C NMR spectroscopy. The activity and the norbornene content of copolymers obtained from a solution containing $[N]/[E] = 24$ and $[N] = 3$ mol/l are reported in Fig. 1.

NMR assignments and E-N copolymer microstructures

¹³C NMR spectra of E-N copolymers are quite complex. There is evidence that norbornene units are inserted through *exo*-addition in E-N copolymers prepared with metallocene based catalysts [1]. Only some NMR assignments of the regions of the methine and methylene carbons of the polymer chain of E-N copolymers with relatively low norbornene content are available. A number of groups are involved in NMR investigations of E-N copolymers in order to give more detailed Scheme 1.



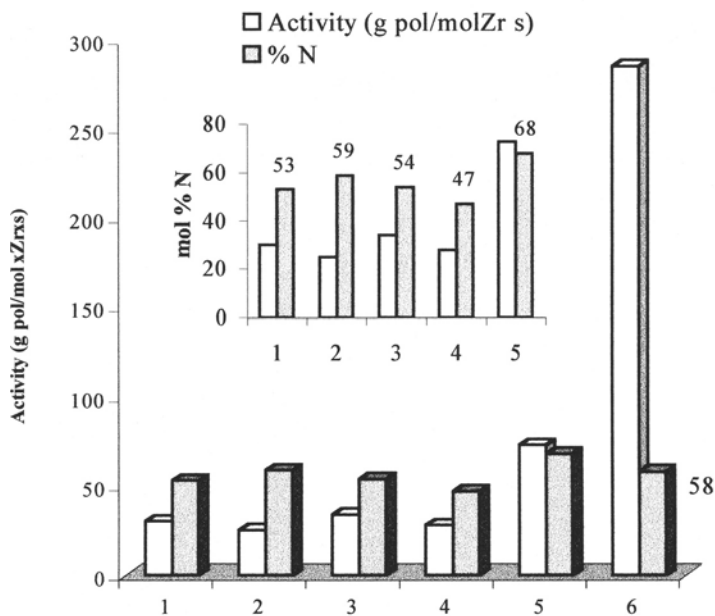


Fig. 1. Copolymerization of Norbornene and Ethylene by different metalocene / MAO catalysts: **1** = *rac*-Et(Ind)₂ZrCl₂, **2** = *rac*-Me₂Si(Ind)₂ZrCl₂, **3** = *rac*-Me₂Si(B-[e]-Ind)₂ZrCl₂, **4** = *rac*-Me₂Si(2Me-B-[e]-Ind)₂ZrCl₂, **5** = *rac*-Me₂Si(2Me-Ind)₂ZrCl₂, **6** = Me₂C(Flu)(Cp)ZrCl₂. Conditions: [N]/[E] = 24, [N] = 3 mol/l, [Zr] = 8•10⁻⁵ mol/l, Al/Zr = 1000 in toluene at 30°C, ethylene atmospheric pressure.

signal assignments in copolymers also with higher norbornene content [3, 4].

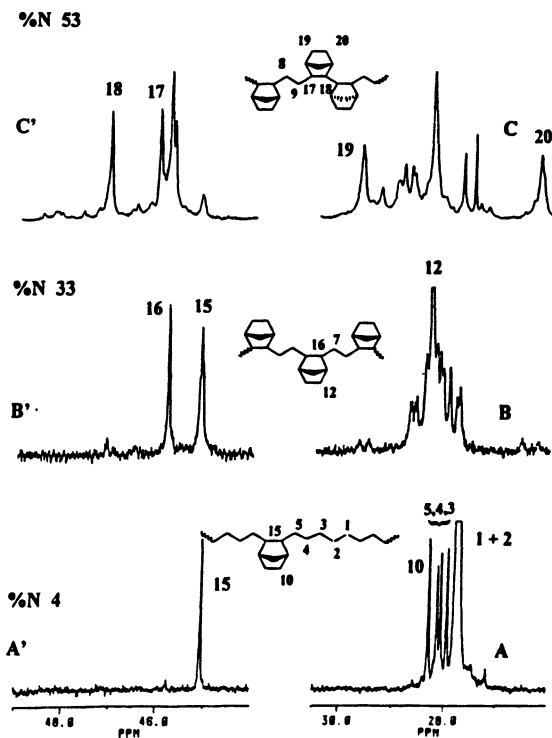
Fig. 2 shows the expansions from 26.5 to 30.5 ppm and from 45 to 49 ppm of the ¹³C NMR spectra of E-N copolymers with different compositions. In these regions methylene carbons of ethylene units and the secondary C5, C6 carbons of norbornene units (26.5-30.5 ppm) and tertiary norbornene C2, C3 carbons (45-49 ppm) of copolymers in the reported range of compositions appear. Copolymers of Fig. 2 were prepared in the presence of catalyst 1. Fig. 3 shows the same regions of the spectra of copolymer samples prepared with zirconocene 6. Fig. 4 shows the complete spectra of E-N copolymers prepared with catalysts 3, 4, and 5. The microstructural environments of carbons of norbornene units and of ethylene units in the copolymer sequences that are most characteristic of each spectrum are represented.

The spectrum of the copolymer with the highest ethylene content in Fig. 2A contains only isolated norbornene units. The methylene carbons of ethylene units, signals 3, 4 and 5 (at 27.93, 28.07, and 28.13 ppm) have been assigned to S_{γδ+}, S_{βδ+}, S_{αδ+} carbons of the EEEEN sequence on the basis of their changes in

Fig 2. ^{13}C NMR spectra of Ethylene-Norbornene copolymers prepared with the catalyst $\text{rac-Et(Ind)}_2\text{ZrCl}_2$ (in $\text{C}_2\text{D}_2\text{Cl}_4$, at 103 °C, HMDS as internal reference).

A, B, C: Expanded plot of methylene of Ethylene unit and of secondary C5, C6 carbons (Scheme 1) of Norbornene unit.

A', B', C': Expanded plot of tertiary C2, C3 carbons (Scheme 1) of Norbornene unit.



intensity depending on norbornene content. In this sequence the vicinity of a norbornene unit causes a downfield shift for the methylene carbons.

The sample of the spectrum in Fig. 2B contains 13 % of alternating NENEN and EENEN sequences also. Signals 7 and 12 at 28.74 and 28.39 ppm, respectively have been assigned to the $S_{\alpha\beta}$ methylene of ethylene and to C5, C6 carbons of norbornene, respectively with the help of an Inadequate ^{13}C - ^{13}C correlated NMR spectrum of a mainly alternating ethylene-norbornene copolymer (Fig. 4A).¹ Indeed signal 7 at 28.74 ppm correlates to the signal 16 at 45.82 ppm while #12 at 28.39 ppm correlates to the signal at 40.04 ppm due to C1, C4 carbons of norbornene units (see Scheme 1).

In the spectrum of a sample of a copolymer with the highest norbornene content (53 mol %) in Fig. 2C two groups of signals 19 and 20, at 29.68 and at 26.24 ppm, and signals 17 and 18, at 46.04 and 47.12 ppm, appear very intense. It is reasonable that, on increasing the norbornene content in the copolymer, sequences containing NN microblocks are formed and that for each NN dyad pairs of correlated signals appear. Moreover, Inadequate spectra reveal that # 20 at 26.24 ppm correlates to # 19 at 29.68 ppm which makes it possible to assign these signals to C5, C6 of

¹ The signal assignment checked by this method corresponds to assignments already reported apart from the fact that the ethylene signal at 28.74 ppm was mistaken for the C5 and C6 of norbornene units.

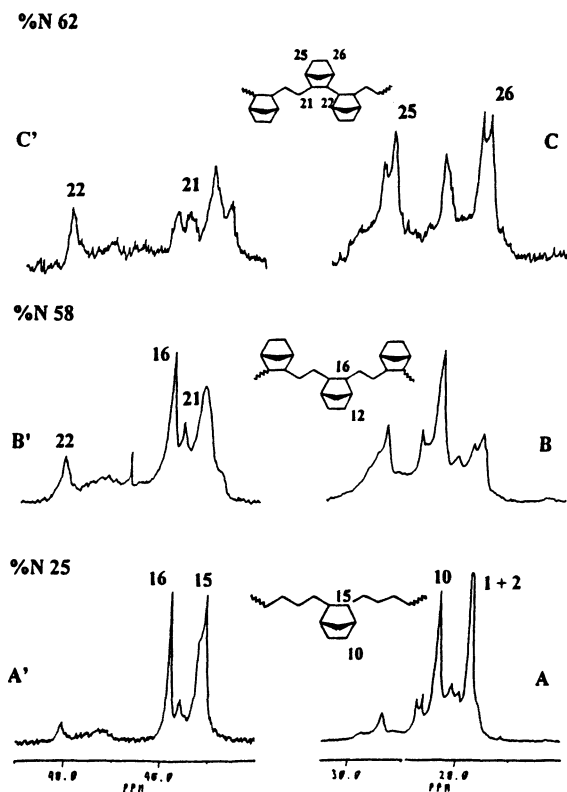


Fig. 3. ^{13}C NMR spectra (in $\text{C}_2\text{D}_2\text{Cl}_4$, at 103°C , HMDS as internal reference) of Ethylene-Norbornene copolymers prepared with the catalyst $\text{Me}_2\text{C}(\text{Flu})(\text{Cp})\text{ZrCl}_2$ A, B, C: Expanded plot of methylene of Ethylene unit and of secondary C5, C6 Norbornene unit. A', B', C': Expanded plot of tertiary C2, C3 carbons of Norbornene unit.

norbornene NN dyads. This is in agreement with recent assignments of Bergstrom et al. [4c]. They have also assigned the # 20 at 26.24 ppm and the signal 19 at 29.68 ppm to the internal and to the external (C5, C6) carbons of the same NN dyad contained in ENNE sequences.

The expansions of the region between 44 and 50 ppm (Fig. 2A', B', and C') show the signals due to C2, C3 norbornene tertiary carbons, which are the norbornene signals most sensitive to the comonomer environment. Signals 17 and 18 at 46.04 and at 47.12 ppm are assigned to NN dyads.

It is worth considering that NN dyads can be *meso* or *racemo*. In the spectrum of a copolymer with similar norbornene content prepared with $\text{Me}_2\text{C}(\text{Flu})(\text{Cp})\text{ZrCl}_2$ (Fig. 3C, C') we observe in the same regions two pairs of signals 21 and 22 at 48.07 and at 46.02 ppm, and 25 and 26 at 29.37 and 27.58 ppm. Differences between chemical shifts of pairs of signals in Fig. 2 and those in Fig. 3 should be due to the presence of dyads with different tacticity since the two catalysts used are known to yield prevalingly isotactic (1) or syndiotactic (6) polypropene. Moreover, it is worth noting that the isotacticity of ENNE sequences in copolymers prepared with catalyst 1-5 is very high, while syndiotacticity of ENNE sequences

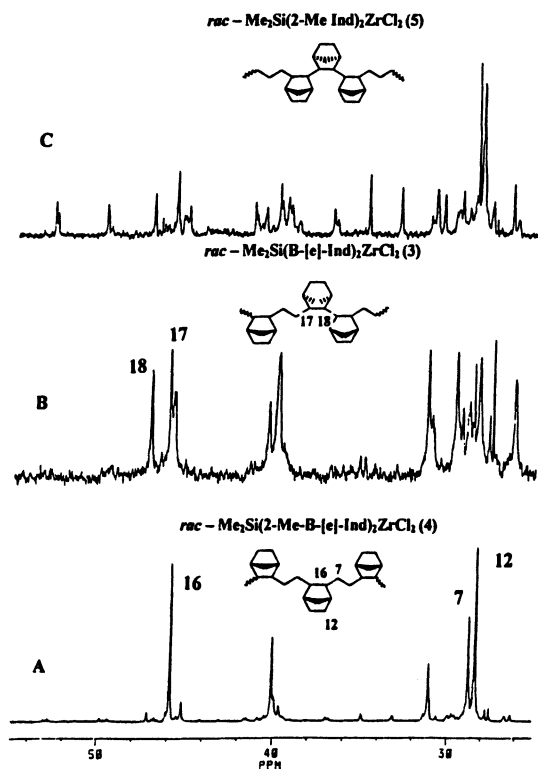


Fig. 4. ^{13}C NMR spectra of Ethylene – Norbornene copolymers prepared, under the experimental conditions of Fig. 1, with different catalysts: 4 (A) 3 (B) 5 (C).

in copolymers prepared with catalyst 6 is lower. Tacticity of ENNE sequences is higher than that observed in hydro-dimers and hydro-trimers with the same catalysts [5].

Fig. 4 shows the complete ^{13}C NMR spectra of E-N copolymers prepared with the C_2 symmetric catalysts 3, 4, and 5 under the same comonomer feed compositions and experimental conditions of copolymers in Fig. 1. Catalyst 4 gives an almost perfectly alternating copolymer. 3 yields a copolymer containing mainly *meso* NN dyads in ENNE sequences. The spectrum of the copolymer prepared with catalyst 5 shows a more complex picture with signals that are not present in the spectra of copolymers prepared with catalysts 3 and 4 and which are due to sequences containing longer norbornene blocks.

Correlation between chemical shifts and conformation

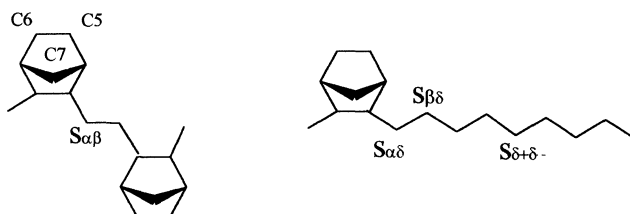
In order to provide an independent support to the chemical shift assignments presented above, we resorted to a traditional approach used in our laboratory for the interpretation of NMR spectra of polymers in terms of chain conformation. The approach is based on determining the stable conformers by means of molecular mechanics and on considering such conformation-dependent effects as the well-known γ -gauche effect [6, 7].

The results of molecular mechanics show that dimers and trimers are poor models of poly-norbornene and of its higher oligomers, due to strong steric interactions between non-adjacent units, which induce large deformations of the torsional angles (and of the ring geometry). Yet the differences between dimers and trimers can be used to understand the shifts.

Norbornene tertiary carbons C2-C3. The dihedral distortion from standard *gauche* conformation found in the racemic isomers is in the opposite direction in the hydro-dimer with respect to the alkyl dimers (Table 1). The significant weakening of the γ -*gauche* effect for carbon C3 in the 3,3'-di-ethyl *racemo* derivative appears to confirm the difference of 1 ppm between the *r* and *m* signals (#22 at 48.07 ppm, and #18 at 47.12) assigned to sequence ENNE. The significance of such torsional deformations is confirmed by a comparison with the assignment of the C3 chemical shifts of hydro-dimers and -trimers by Arndt *et al.* [1] (Table 2). It is noteworthy that the rather large *m* - *r* chemical shift differences (of opposite sign in dimers vs. trimers) are well correlated with torsional angle deformations. The same considerations hold for the complementary behaviour of carbon C1.



Ethylenic secondary carbons. It is at first surprising that in such sequences as **EENEE** and **ENENE** the signals of carbons $S_{\alpha\beta}$ (28.39 ppm) and $S_{\beta\delta+}$ (28.07 ppm) are shifted downfield relative to $S_{\alpha\delta}$ (28.13 ppm) and $S_{\delta+\delta+}$ (27.34 ppm), respectively. Usually a γ branching causes a shift of ca. -2 ppm with respect to a single γ substitution, owing to an increase of *gauche* conformations. Here the lack of such a shift must be due to the δ substituents C7 and C3'. Indeed for 5-decyl-norbornene, where only C7 is present, a small shift of -0.8 ppm is observed [8]. Calculations on various ethylene-norbornene oligomers suggest that the absence of such a shift may be due to molecular distortions.



Norbornene secondary carbons C5-C6. Non-equivalence of the two $\text{CH}_2\text{-CH}_2$ ($S_{\alpha\beta}$) norbornene carbons is observed for *meso* and *racemo* NN dyads (cf. signals 19/20 and 25/26 with signals #10 and #12). Such a splitting may arise from the ring distortion found in molecular models of **NENNEN** (larger for *meso* dyads).

Table 1. Conformational differences between *meso* and *racemo* stereoisomers concerning carbons C1 and C3 in hydro-dimer, 3,3' dimethyl-dimer and 3,3' diethyl-dimer.

| | | C1 | | C3 | |
|-----------------------|--------------------------|-----------|--------------------------|-----------|--|
| | | φ | | φ | |
| hydro - dimer | <i>meso</i> (C1...C3') | 64 | <i>meso</i> (C3...C1') | 64 | |
| | <i>racemo</i> (C1...C1') | 72 | <i>racemo</i> (C3...C3') | 57 | |
| 3,3' dimethyl - dimer | <i>meso</i> (C1...C3') | 61 | <i>meso</i> (C3...C1') | 61 | |
| | <i>racemo</i> (C1...C1') | 52 | <i>racemo</i> (C3...C3') | 70 | |
| 3,3' diethyl - dimer | <i>meso</i> (C1...C3') | 60 | <i>meso</i> (C3...C1') | 60 | |
| | <i>racemo</i> (C1...C1') | 49 | <i>racemo</i> (C3...C3') | 73 | |

Table 2. Correlation between observed chemical shifts for carbons C₃ and γ -gauche conformations in hydro-dimers and -trimers [1]

| Atom | | Config | Ch. Shift | γ -gauche Conformations | | | |
|--------|-----------|-----------|-----------|--------------------------------|-----------------------|-----------------------|-----------------------|
| | | | | φ (Popul.) | φ (Popul.) | φ (Popul.) | φ (Popul.) |
| Dimer | C3 | <i>m</i> | 38.23 | 64 (1.) | | | |
| | | <i>r</i> | 36.14 | 57 (1.) | | | |
| Trimer | C3a = C3b | <i>mm</i> | 37.84 | 51 (0.264) | 37 (0.264) | 81, -51 (0.236) | 46 (0.236) |
| | C3a = C3b | <i>rr</i> | 41.64 | 59 (0.255) | 99 (0.255) | 65 (0.245) | 64 (0.245) |
| | C3a | <i>mr</i> | 38.37 | 49 (0.444) | 49 (0.328) | 56, -70 (0.228) | |
| | C3b | <i>mr</i> | 42.10 | 69 (0.444) | 88 (0.328) | 70 (0.228) | |

Conclusions

As shown in Fig. 1, the C₃ symmetric metallocene Me₂C(Flu)(Cp)ZrCl₂ (**6**) is the most productive catalyst, as is already known. Among the C₂ symmetric catalysts, under the experimental conditions used, *rac*-Me₂Si(2-Me-Ind)₂ZrCl₂ (**5**) is noticeably more active than the others. The kind of the bridge does not have a great

influence on the activity. The ethane bridged *rac*-Et(Ind)₂ZrCl₂ (**1**) catalyst is only slightly more active than the Me₂Si< bridged *rac*-Me₂Si(Ind)₂ZrCl₂ (**2**). The norbornene content is not strongly affected under these polymerization conditions (Fig. 1).

On the other hand the microstructure of the E-N copolymers greatly depends on the catalyst symmetry and Cp substituents, as shown by the ¹³C NMR spectra (Figs 2-4). The most interesting features observed are:

1. the greatest tendency to alternating copolymerization of the *rac*-Me₂Si(2-Me-B-[e]-Ind)₂ZrCl₂ (**4**) catalyst, which, under the copolymerization conditions used, allows for the formation of ENNE sequences only to limited extent. This is especially evident in the region of ¹³C NMR spectra between 45 ppm and 54 ppm, which show small amounts of NN dyads (# 17, 18);
2. the highest activity and the greatest norbornene incorporation given by *rac*-Me₂Si(2-Me-Ind)₂ZrCl₂ (**5**) catalyst with respect to the other C₂ catalysts and especially with respect to **4**. Moreover, **5** seems to have a tendency to yield blockiness as revealed from the formation of long norbornene microblocks,

Finally, the signals of *meso* and *racemo* NN dyads in ENNE sequences have been identified. Worthy of note is that the tacticity of ENNE sequences in copolymers, especially isotacticity in copolymers prepared with C₂ catalysts **1-5**, is very high, higher than that observed in hydro-dimers and hydro-trimers with the same catalysts.

Acknowledgements. We gratefully thank Prof. H. H. Brintzinger for providing some of the metallocenes used and Dr. L. Zetta and Mr. G. Zannoni for their valuable cooperation in NMR analysis. Financial help from EC TMR Project Network N°ERB FMRX CT97-0116 GLASSCYCLICS is gratefully acknowledged.

References

1. (a) Kaminsky W., Bark A., Arndt M. Makromol. Chem. Macromol. Symp. (1991) 47: 83
(b) Kaminsky W., Noll A., Polymer Bulletin (1993) 31: 175
2. Cherdron H., Brekner M. J., Osan F., Angew. Makromol. Chem. (1994) 223: 121
3. (a) Tritto I., Boggioni L., Sacchi M.C., Locatelli J. Mol. Catalysis A: Chem. (1998) 133: 139. (b) Tritto I., Boggioni L., Sacchi M.C., Locatelli P., Ferro D. R., Provasoli A., presented at the Europolymer Conference (EUPOC'98) 31 May - 5 June 1998 Gargnano (Bs) Italy and Tritto I., Boggioni L., Locatelli P. Metcon'97, Session VII.
4. a) Ruchatz D., Fink G., Macromolecules (1998) 31: 4674. b) Rische T., Waddon A. J., Dickinson L., MacKnight W.J. Macromolecules (1998) 31: 1871. (c) Bergström C.H., Sperlich B.R., Ruotoistenmäki J., Seppälä J. V. J. Polymer Sci. Part A, Polym. Chem. (1998) 36: 1633
5. (a) Arndt M., Kaminsky W. Macromol. Symp. (1995) 97: 225 (b) Arndt M., Kaminsky W., Engenhausen R., Zoumis K., Journal of Molecular Catalysis (1995) C 101: 171.
6. Provasoli A., Ferro D. R., Macromolecules (1977) 10: 874,
7. Sacchi M. C., Tritto I., Locatelli P., Zetta L., Ferro D. R., Foster H. Macromolecules (1986) 19: 1634
8. Sagane T., Mizuno A. Makromol. Chem. (1993) 194: 37

Studies on Properties of Metallocene Catalysed Copolymers of Ethylene and Linear, Non-conjugated Dienes

P. Pietikäinen, A. Malmberg, B. Löfgren and J. Seppälä*

Helsinki University of Technology, Department of Chemical Engineering, P.O.Box 6100, FIN-02015 HUT, FINLAND
e-mail seppala@polte.hut.fi

Abstract. The effect of diene addition on the structure of ethylene copolymer was studied. The dienes used were 1,5-hexadiene (HD), 1,7-octadiene (OD), and 7-methyl-1,6-octadiene (MOD). Polymerizations were conducted in n-heptane in the presence of the metallocene catalyst cyclopentadienyl zirconium dichloride (Cp_2ZrCl_2) with methylaluminoxane (MAO) as a cocatalyst. The structure of the copolymer was determined by NMR-techniques. The 1,5-hexadiene comonomer was predominantly incorporated as a 5 member ring structure into the polyethylene backbone. OD and MOD formed branches in the polyethylene chain. The ethylene/HD copolymers were analysed using dynamic rheometry to study the effect of ring structures on the rheological properties of the product. The ring structures stiffen the chain, which was manifested as increasing viscosity and shear sensitivity of the melt. At low hexadiene ring content, the effect of the ring structure was masked by the long chain branching already present in the ethylene homopolymer.

1 Introduction

Metallocene catalysts have proven to be effective in olefin/diene copolymerizations [1]. Besides saturations in polymer backbone or in the end of diene branches, copolymerization of dienes allows the appearance of cyclic structures and long chain branching in the polyethylene chain (Figure 1). On the other hand, these modification reactions of polyolefins are usually accompanied by undesirable side reactions, such as the formation of gel in the polymer through incorporation of a second double bond as a crosslink in the copolymerization.

A number of non-conjugated dienes, such as 1,5-hexadiene, 1,4-pentadiene and 1,7-octadiene, are capable of undergoing cyclopolymerization in the presence of a coordination catalyst. In ethylene/1,5-hexadiene copolymers, hexadiene is predominantly incorporated as five member rings but may also react through 1,2-insertion to butene branches or form long chain branching [2]. Homopolymer of

HD is an optically active polyolefin consisting of consecutive five member rings [3].

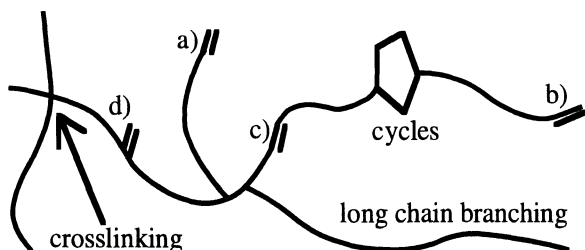


Fig. 1. Structures that can be formed into a ethylene/diene copolymer. Unsaturation in the polyethylene chain appear a) in the end of a branch due to the diene comonomer, b) in the end of the chain due to β -elimination, c) in the chain (*trans*-vinyl) and d) in the chain (vinylidene).

We used 1,5-hexadiene (HD), 1,7-octadiene (OD) and 7-methyl-1,6-octadiene (MOD) in copolymerizations of ethylene using $\text{Cp}_2\text{ZrCl}_2/\text{MAO}$ as the catalyst. The basic metallocene was chosen in order to minimize the electronic and ligand effects in the polymerization. The structure of the ethylene / diene copolymers was studied by NMR-techniques and dynamic rheometry.

2 Experimental

The polymerizations were conducted in heptane slurry at 80°C . Polymerization time was 1 h and ethylene pressure 2.5 bar. 1 mg of the catalyst was used and the Al/Zr molar ratio was either 2000 or 4000 depending on the amount of diene added.

The comonomer contents of the copolymers were calculated from NMR spectra recorded on a Varian Gemini 2000, 300 MHz spectrometer at 125°C from samples dissolved in 1,1,2,2-tetrachloroethane- d_2 . The melt temperature was measured using Perkin Elmer DSC 7 and the degree of crosslinking was determined by decaline extraction based on ASTM standard D-2765-84. A Waters 150-C ALC GPC instrument with a refractometer detector was used to determine the molecular weight and the molecular weight distribution of the samples. The samples were dissolved in trichlorobenzene, and the measurement was carried out at 140°C .

The dynamic rheological properties of the polymers were studied using a controlled stress dynamic rheometer SR-500 by Rheometric Scientific. The linear viscoelastic behaviour was measured as a function of the angular frequency between 0.02 rad/s and 100 rad/s using a 25 mm plate-plate geometry with 1 mm sample gap. The measurements were carried out in nitrogen at three different temperatures between 150°C and 210°C.

3 Results and discussion

3.1 Copolymerization

The results of the copolymerizations of ethylene with dienes are presented in Table 1. Satisfactorily high contents of functional groups in copolymers were achieved. The molecular weights of copolymers were quite low, especially with the MOD comonomer. The comonomer incorporation was most efficient in the HD copolymerizations.

Table 1. Polymerizations of ethylene and linear, non-conjugated dienes.

| Run | Diene | Diene feed, mol/dm ³ | T _m , °C | X-link, % | M _w , g/mol | MWD | Diene in the product | |
|-----|-------|---------------------------------|---------------------|-----------|------------------------|------|----------------------|-------------------|
| | | | | | | | mol-% | wt-% |
| P1 | - | - | 134 | * | 100 000 | 2.6 | - | - |
| P2 | HD | 0.40 | 115 | * | 71 000 | 3.5 | 3.5 ^b | 9.5 ^b |
| P3 | HD | 0.60 | 113 | * | 36 000 | 3.5 | 6.9 ^b | 17.7 ^b |
| P4 | HD | 1.00 | 111 | >80 | n.d. | n.d. | n.d. | n.d. |
| P5 | OD | 0.30 | 106 | * | n.d. | n.d. | 1.9 ^a | 7.1 ^a |
| P6 | OD | 0.48 | 102 | 65 | n.d. | n.d. | 2.4 ^a | 8.9 ^a |
| P7 | MOD | 0.30 | 116 | * | 33 000 | 2.3 | 1.9 ^a | 7.8 ^a |
| P8 | MOD | 0.40 | 111 | * | 19 000 | 2.1 | 2.4 ^a | 9.8 ^a |
| P9 | MOD | 0.70 | 94 | 36 | n.d. | n.d. | n.d. | n.d. |

Polymerization conditions: temperature 80°C, P_B 2.5 bar

* degree of crosslinking negligible

^a based on ¹H NMR, ^b based on ¹³C NMR

The melt temperature of the copolymers decreased significantly due to the diene incorporation. The effect of HD was not as strong as that of OD and MOD, which suggests that the five member ring with HD forms a relatively linear defect in the polyethylene chain. Crosslinking was also observed in the HD-copolymers with increasing diene content, even though in shorter polymerizations hardly any crosslinking occurred at 80°C [4].

3.2 Copolymer structure by NMR

According to the NMR analysis the HD-copolymer contained no butene branches, only ring structures [4-6]. The ratio of *cis* and *trans* conformer of the rings affects the properties of the product. Cyclopentane rings in *cis* conformer are reported to offer high heat stability [7]. In all our copolymers, about 25% of the rings were in *cis* conformation and about 75% in *trans* conformation, and the material obtained had significantly lower melt temperatures than homopolyethylene produced under the same conditions (Table 1). Polymerization temperature has no effect on this ratio with this catalyst [5].

The structure of the OD-containing copolymers was studied by DEPT-analysis. As shown in Figure 2, hexene branches in the ethylene/OD copolymers can also appear as branch pairs. No ring structures are observed [4-6]. The peak at 42.9 ppm may result either from the CH₂-group connecting the branch pair or from the CH₂-group belonging to the cyclopentane ring formed with octadiene. However, the absence of the methine peak at 34.6 ppm, which would be due to the carbons that connect the ring structure to the polyethylene chain, eliminated the possibility of this structure. The peaks at 35.6 ppm and in the area of 30-26.4 ppm come from carbons of hexene branches of the branch pairs and vinylidene bonds in the ethylene backbone. MOD formed only 1-methyl-hexene branches to the ethylene backbone in these experimental conditions, as expected.

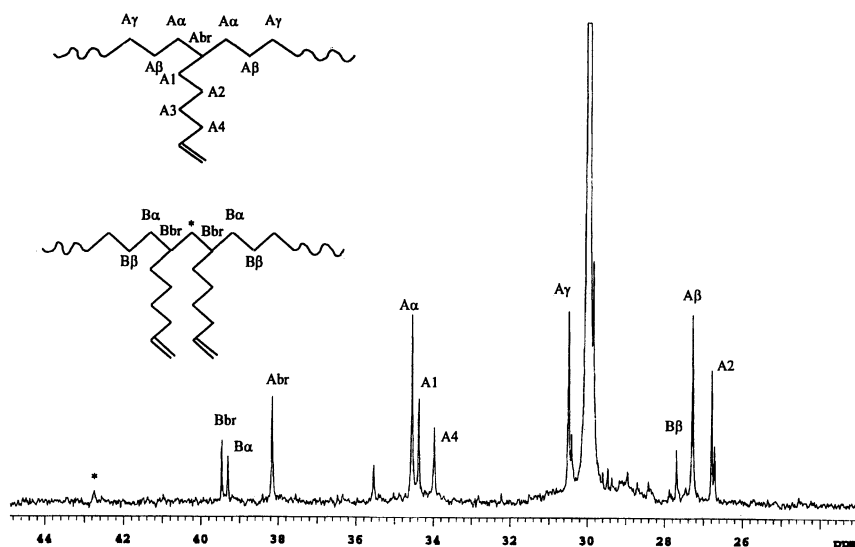


Fig. 2. ^{13}C NMR (300 MHz) spectra of ethylene/OD copolymer.

3.3 Dynamic rheological properties

With a fixed chemical structure, the polymer melt rheological properties are governed by the molecular weight, the MWD, and by long chain branching [8]. The chemical structure of the polymer chain sets the molecular mobility and thus the magnitude of the rheological properties of the polymer melt [9]. For example, the presence of bulky side groups in ethylene/styrene copolymers stiffens the polymer chain, which provides increased resistance to flow as compared to polyethylene [10].

To investigate the effect of the ring structures on the polymer melt flow behaviour, the dynamic rheological properties of the ethylene/HD copolymers were studied. Figure 3 shows the shear thinning behaviour of complex viscosity of the ethylene homopolymer and the HD-containing copolymers in comparison to a LDPE and a linear, narrow MWD HDPE sample. In ethylene polymers (with low amounts of linear comonomers), the flow activation energy is sensitive to the presence of long chain branches, increasing with an increasing content or increasing length of the long branches [9,11]. Thus, an Arrhenius type flow activation energy E_a of 59 kJ/mol was obtained for the long chain branched LDPE, whereas the linear HDPE sample yielded only 28 kJ/mol for E_a .

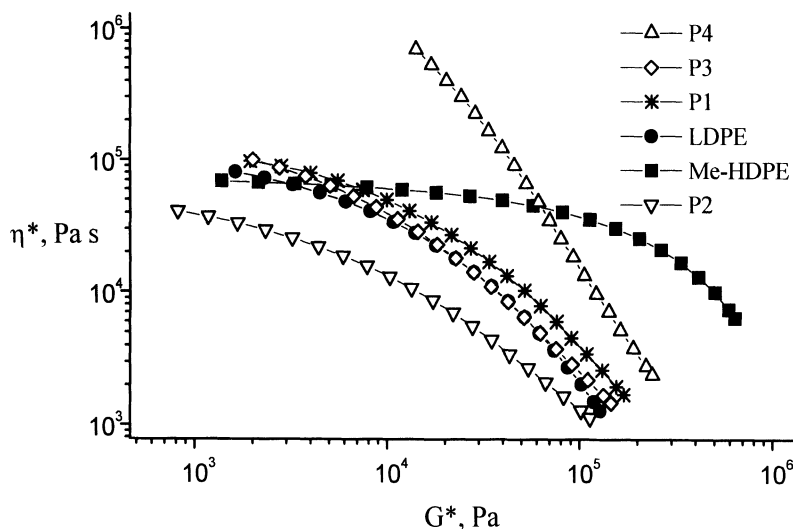


Fig. 3. Complex viscosity η^* of selected polymer samples as function of complex modulus G^* at 170°C. Reference materials: a broad MWD LDPE with long chain branching and a linear, narrow MWD metallocene catalysed HDPE sample.

Despite the narrow molecular weight distributions reported in Table 1, the polymers P1 and P2 showed pronounced shear thinning, comparable to that of the LDPE sample rather than to the narrow MWD Me-HDPE. This behaviour together with a high flow activation energy E_a of 55 kJ/mol obtained for the P1 suggest long chain branching already in the ethylene homopolymer P1. Long chain branching in metallocene catalysed ethylene homopolymers, suggested to arise from *in situ* copolymerization of ethylene and the vinyl terminated macromonomers at suitable conditions, has recently been reported by our group [12].

The ethylene homopolymer P1 and the sample P2 with 3.5 mol-% diene showed a high flow E_a and similar shear sensitivity, and seemed to differ only in their molecular weight. The possible effect of the hexadiene ring structure on the melt relaxation behaviour of P2 may be masked by the long chain branching. The sample P3 with 7 mol-% diene exhibited, in comparison to the measured molecular weight, a high complex viscosity at low frequencies. The copolymer P3 appeared also more shear sensitive than the ethylene homopolymer P1. An increasing content of ring structures in the main chain thus influenced the relaxation behaviour in the same manner as do higher molecular weights. Sample P4, with still higher 1,5-hexadiene feed in polymerization, showed the yield behaviour of a partly crosslinked material. Although a high degree of crosslinks was measured for this sample, it was still thermoplastic.

4 Conclusions

The studied dienes, 1,5-hexadiene (HD), 1,7-octadiene (OD), and 7-methyl-1,6-octadiene (MOD) were effectively incorporated into the polyethylene chain by the metallocene catalyst and they had a significant effect on the properties of the polymer. The HD comonomer was predominantly incorporated as a 5 member ring into the polyethylene backbone. At low hexadiene ring content, the effect of the ring structure on the melt flow behaviour was masked by the long chain branching present already in the ethylene homopolymer. With increasing content of ring structures, the chain flexibility was reduced, which manifested itself as increasing viscosity and shear sensitivity of the melt. At still higher HD concentration in polymerization, the copolymer was partly crosslinked, but still thermoplastic.

References

1. Brinzinger, H. H., Fischer, D., Mülhaupt, R., Rieger, B. and Waymouth, R. M., *Angew. Chem. Int. Ed. Engl.*, **34** (1995), 1143.
2. Bergemann, C., Croop, R. and Luft, G., *J. Mol. Cat. A: Chemistry*, **116** (1997), 317.
3. Coates, E. W. and Waymouth, R., *J. Am. Chem. Soc.*, **115** (1993), 91.
4. Pietikäinen, P., Seppälä, J.V., Ahjopalo, L. and Pietilä, L.-O., submitted to *Eur. Polym. J.*, (1998).
5. Pietikäinen, P., Väänänen, T. and Seppälä, J.V., *Eur. Polym. J.*, in press, (1998).
6. Pietikäinen, P., Starck, P. and Seppälä, J.V., *J. Pol. Sci. Part A*, in press, (1998).
7. Resconi, L., Mazzocchi, R. and Piemontesi, F. *Eur. Pat. 508450*.
8. Mavridis, H., Shroff, R., *J. Appl. Polym. Sci.* **57** (1995), 1605.
9. Dealy, J.M., and Wissbrun, K.F., *Melt rheology and its role in plastics processing*, Van Nostrand Rheinhold, New York 1990.
10. Lobbrecht, A., Friedrich, Chr., Sernetz, F.G., and Mühlhaupt, R., *J. Appl. Polym. Sci.* **65** (1997), 209.
11. Carella, J. M., Gotro, J. T., Graessley, W. W., *Macromolecules* **19** (1986), 659
12. Malmberg, A., Kokko, E., Lehmus, P., Löfgren, B., Seppälä, J.V., *Macromolecules*, in press, (1998).

Ethylene/ α -Olefin Copolymerization with Dimethylsilyl-bis(2-methyl-4-phenyl-indenyl) zirconium dichloride and Methylaluminumoxane: Influences on Polymerization Activity and Molecular Weight

Massoud Miri, David Hetzer, Adam Miles, Mark Pecak, and Brent Riscili

Department of Chemistry, Rochester Institute of Technology,
Rochester, New York 14623
Email: mjmsch@rit.edu

Abstract. The copolymerizations of ethylene with 1-hexene and of ethylene with 1-octene have been investigated using *rac*-Me₂Si [2-Me-4-Ph-Ind]₂ZrCl₂ and methylaluminumoxane as cocatalyst. This metallocene catalyst readily incorporates α -olefin, and at the same time the polymerization activities remain relatively high. Interestingly no comonomer effect can be observed with this catalyst in contrast to other metallocene catalysts, e.g. Cp₂ZrCl₂ or Me₂Si-[Ind]₂ZrCl₂. Also the mode of addition of catalyst components influences the polymerization rate. The separate addition of the metallocene from the MAO is accompanied by longer induction periods, whereas the combined addition induces copolymerization almost instantaneously. The activities obtained with 1-octene are slightly lower than those obtained with 1-hexene. The molecular weight drops with increasing α -olefin concentration, however it is relatively high compared to copolymers produced with other metallocene catalysts. With a highly racemic mixture of the title catalyst unprecedented activities were obtained of 1,170,000 kg polyethylene / (mol Zr x h x [mon]) at 40 °C, and 477,000 kg ethylene/1-hexene copolymer / (mol Zr x h x [mon]) at 45 °C and a monomer ratio of unity in the reaction.

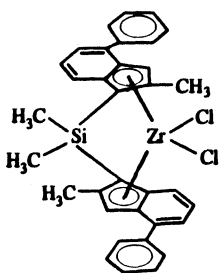
Introduction

Metallocenes have been intensely investigated as polymerization catalysts, and are continuously introduced as superb catalysts for the production of industrial polymers [1,2]. One major issue related to the synthesis of copolymers with high α -olefin content is that the polymerization activity is significantly lower than for the ethylene homopolymerization. Furthermore the incorporation of comonomer into the copolymer depends among other conditions also on the type of catalyst.

The main objective is to find a catalyst that inserts a high amount of comonomer at a comparably high polymerization activity.

Another issue with many metallocene catalysts is, that they produce relatively low molecular weight polymers. This is due to the high tendency of the metallocene catalysts to undergo several types of chain transfer reactions via β -H-elimination. The resulting reduction in molecular weight becomes particularly apparent in the presence of α -olefins, such as 1-hexene and 1-octene for the syntheses of linear low density polyethylene or elastomeric ethylene/ α -olefin copolymers.

In this work we investigate the polymerization activities and influence on molecular weight properties of racemic dimethylsilyl-bis(2-methyl-4-phenyl-indenyl) zirconium dichloride (structure shown below) using methylaluminoxane as cocatalyst for the copolymerization of ethylene with 1-hexene, as well as 1-octene. Previously it had been shown that substituents in the 2-position of the coordinated cyclopentadienyl ring effectively prevent chain transfer via β -H-elimination [3].



Results and Discussion

Initially two sets of polymerizations for each α -olefin, i.e. 1-hexene and 1-octene, were carried out at 60 °C introducing the catalysts components separately into the reaction (except Exp. No. 4). The metallocene, obtained in form of two racemic mixtures (with rac:meso -ratios of approximately 30:1 and 49:1) was purchased from Boulder Scientific, and the cocatalyst from Witco. The initial data, obtained only with the less racemic metallocene, are shown in Table 1.

Table 1. Influence of comonomer type and concentration on polymerization activity and related data, using $\text{Me}_2\text{Si}[\text{2-Me-4-Ph-Ind}]_2 \text{ZrCl}_2$, rac:meso $\geq 30:1$, without premixing of catalyst compounds, except for Run 4*

| Exp. No. | α -Olefin, Type | α -Olefin, M | Activity, $\frac{\text{kg polymer}}{\text{molZr h [mon]}}$ | Induction period, min | $R_{p, \max} 10^{-5} \frac{\text{g ethylene}}{\text{min molZr}}$ | α -Olefin in polymer, mol-% |
|----------|------------------------|---------------------|--|-----------------------|--|------------------------------------|
| 1 | -- | 0 | 96 800 | 2 | 6.00 | 0 |
| 2 | 1-hexene | 0.32 | 28 000 | 2 | 3.20 | 16 |
| 3 | 1-hexene | 0.64 | 13 300 | 24 | 2.72 | 21 |
| 4* | 1-hexene | 0.64 | 21 600 | 2 | 4.00 | 17 |
| 5 | 1-hexene | 1.92 | 4 500 | 39 | 1.20 | 50 |
| 6 | 1-hexene | 3.2 | 4 500 | 40 | 1.12 | 55 |
| 7 | 1-octene | 0.32 | 16 800 | 10 | 2.00 | 20 |
| 8 | 1-octene | 0.64 | 13 500 | 23 | 1.92 | 23 |
| 9 | 1-octene | 1.92 | 2 800 | 42 | 1.00 | 45 |
| 10 | 1-octene | 3.2 | 1 900 | 38 | 0.60 | 53 |

$p_{\text{ethylene}} = 4 \text{ bar (0.36 M)}$, $[\text{Al}] = 3.0 \times 10^{-2} \text{ M}$, $[\text{Zr}] = 1 \times 10^{-6} \text{ M}$, $T = 60 \text{ }^\circ\text{C}$, [mon]: total monomer concentration, α -olefin content in polymer estimated from mass balance of product minus ethylene polymerized

As indicated in Figure 1, it is apparent that the polymerization activity goes down as the α -olefin concentration increases. This is due to the bulkier structure and corresponding steric hindrance of the α -olefin as compared to ethylene. The drop in activity is steeper at low comonomer concentrations and levels off when the concentration of the α -olefin is about 50 mol %. This stays in contrast to many metallocene catalysts investigated so far, for which at ethylene/ α -olefin molar ratios close to unity an enhancement of activity has been observed.

This phenomenon, also called positive "comonomer effect", which has not been clearly explained yet, was mentioned earlier for ethylene/1-hexene copolymerizations with other metallocenes, e.g. zirconocene dichloride and dimethyl silyl zirconium dichloride [4,5,6]. With the present metallocene catalyst, no positive comonomer effect is observed, because of the high incorporation of α -olefin even at relatively low concentrations of the olefin, and the related decrease in the propagation rate constant. The factors that usually would cause an enhancement in activity could still be present, but they are here overshadowed by the more significant decrease in polymerization rate.

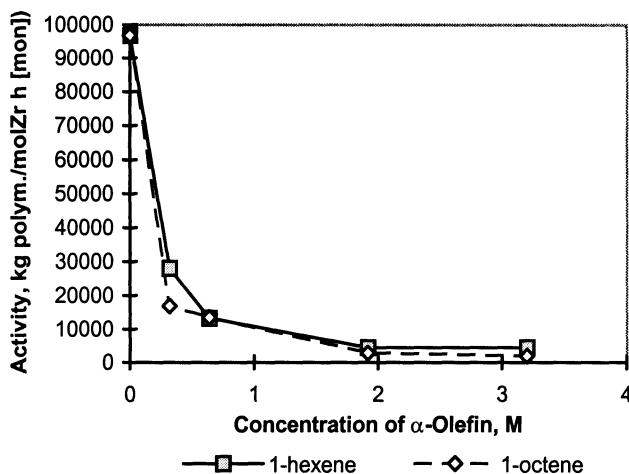


Fig. 1. Influence of α -olefin on polymerization activity

By monitoring the ethylene consumption during the polymerization with a mass flow measuring instrument, it is furthermore observed that as more α -olefin is provided in the reaction system, the polymerization requires more time to take up monomer, i.e. increased induction periods occur. These induction periods are not caused, as might be assumed, by an inertia in the measurement of the ethylene flow. Such a cause can be eliminated based on the homopolymerizations of ethylene, which start without any significant delay. Induction periods were observed previously in coordinative copolymerization for cases in which high amounts of α -olefin are incorporated [5,7]. The α -olefin slows down the formation of active complex, unless the catalyst compounds are combined prior to its addition, as shown below.

The monitored polymerization rate of ethylene is often more reliable for activity measurements than the one based on the polymer yield, which may become inaccurate due to loss of product in transfers. Furthermore this technique is advantageous in comparing the effects of different comonomers on activity without the need to consider the different properties of the comonomers (see also Figure 2). The ethylene polymerization rate indicates that 1-octene reduces the activity slightly more than 1-hexene.

The amount of α -olefin incorporated into the polymer was estimated here as the difference of purified product and the pure ethylene polymerized. It can be seen that 1-hexene and 1-octene are easily incorporated by the catalyst, yielding copolymers with 50 mol % comonomer when the molar feed ratio is about 5:1 ethylene/ α -olefin. The phenyl ring in the 4-position on each indenyl ligand seem to favor the incorporation of the bulky comonomer both due to steric and electronic effects compared to other related metallocenes.

The activity is significantly increased, when the metallocene is premixed prior to injection into the reaction system. This can be derived by comparing Exp. No. 3 and 4. With the premixing mode the activity is about one and a half times higher

than with the separate addition. This is caused by the combined effect of both an absence of a long induction period (2 instead of 24 min), and a higher ethylene polymerization rate (4.00 vs. 2.72 g ethylene/(min mol Zr)). For polyethylene formation no significant induction periods are observed even if the catalysts are added separately.

The copolymerizations with the premixed catalysts are better controllable at lower temperatures than 60 °C. Figure 2 shows the mass flow diagrams for the ethylene homopolymerization and ethylene/1-hexene copolymerization at 40 °C, again showing the absence of long induction periods and the establishment of relatively high, steady rates. The corresponding conditions for these runs are given in Table 2, Exp. No's 11 and 12. The 20 degree decrease in polymerization temperature results in a drop in the ethylene polymerization rate by more than one half (comparing Exp. No's 1 with 11, and 4 with 12).

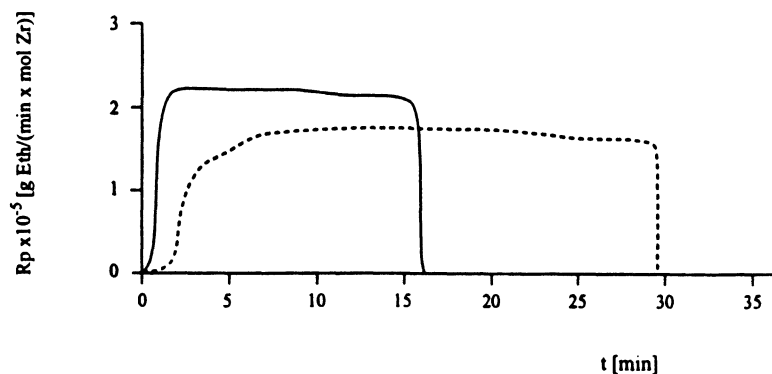


Fig. 2. Polymerization rate of ethylene versus polymerization time for $\text{Me}_2\text{Si}[\text{2-Me-4-Ph-Ind}]_2\text{ZrCl}_2$, 30/1 rac:meso using premixed catalyst components, at 40°C and 2.5 bar.

———— Ethylene Homopolymerization, Exp. No. 11

----- Ethylene/1-Hexene Copolymerization (molar feed ratio 1:1), Exp. No. 12

A remarkable increase in activities, surpassing those mentioned in the literature so far, occurs when a very highly racemic mixture (98 %) of the above mentioned catalyst is used. These results are given in Exp. No's 13 and 14. The polymerization activity for pure ethylene exceeds one million kg polymer/(mol Zr x h x [mon]). The polyethylene run had to be conducted at a lower zirconium concentration of 1×10^{-7} M, to be able to better control the temperature and ethylene mass flow. Prior two other polyethylene runs with the highly racemic mixture had been carried out that went out of control. Even for the

copolymerization with 1-hexene an unprecedented activity of close to one half a million kg copolymer/(molZr h [mon]) is obtained.

Table 2. Activities and related data obtained for the homopolymerization of ethylene and copolymerization with 1-hexene using premixed catalyst compounds

| Exp. No. | 1-Hexene M | rac:meso of metallocene \geq | Activity $\frac{\text{kg polymer}}{\text{molZr h [mon]}}$ | Induction period min | $R_{p, \max} 10^{-5} \frac{\text{g ethylene}}{\text{min molZr}}$ | 1-Hexene in polymer mol-% |
|----------|------------|--------------------------------|---|----------------------|--|---------------------------|
| 11 | 0 | 30 : 1 | 50 800 | 1 | 2.20 | 0 |
| 12 | 0.26 | 30 : 1 | 32 500 | 2 | 1.76 | 14 |
| 13 | 0 | 49 : 1 | 1 169 000 | 1 | 60.8 | 0 |
| 14 | 0.26 | 49 : 1 | 477 000 | 1 | 13 | - |

$P_{\text{ethylene}} = 2.5 \text{ bar (0.26 M)}$, $[Al] = 3.6 \times 10^{-2} \text{ M}$, $[Zr] = 1 \times 10^{-6} \text{ M}$, except for Exp. No. 13 with $1 \times 10^{-7} \text{ M}$ (for better control), $T = 40 \text{ }^\circ\text{C}$, except for Exp. No. 14 with $45 \text{ }^\circ\text{C}$

In Table 3 molecular weight data for the initial set of polymers are given (Exp. No's 1-10). The molecular weight of the polyethylene falls with $M_n = 181,000 \text{ g/mol}$ in the desired range of commercial polyolefins. However, with the presence of even small amounts of α -olefin, the molecular weight is reduced to below half the polyethylene molecular weight. This effect is mainly caused by chain transfer to the comonomer. At higher α -olefin concentrations the incremental decrease in molecular weight becomes less marked. This resembles the pattern of the decrease of polymerization rate or activity with increasing comonomer content. The difference between the two α -olefins lies in the range of experimental error. Since the polymers described in Table 1 were obtained at $60 \text{ }^\circ\text{C}$, it should be possible to obtain higher molecular weights for the copolymers by lowering the polymerization temperature, without the issue of operating below ambient conditions.

Table 3. Molecular weight properties of polyethylene and ethylene/ α -olefin copolymers produced with $\text{Me}_2\text{Si-[2-Me-4-Ph-Ind]}_2\text{ZrCl}_2$

| Exp. No. | α -Olefin, Type | \overline{M}_w g/mol | \overline{M}_n g/mol | M_w/M_n |
|----------|------------------------|------------------------|------------------------|-----------|
| 1 | -- | 477,000 | 181,000 | 2.63 |
| 2 | 1-hexene | 213,000 | 79,100 | 2.68 |
| 3 | 1-hexene | 182,000 | 65,500 | 2.78 |
| 5 | 1-hexene | 103,000 | 29,900 | 3.43 |
| 6 | 1-hexene | 96,400 | 29,500 | 3.27 |
| 7 | 1-octene | 200,000 | 72,600 | 2.90 |
| 8 | 1-octene | 173,000 | 59,500 | 2.90 |
| 9 | 1-octene | 148,000 | 38,100 | 3.87 |
| 10 | 1-octene | 140,000 | 41,600 | 3.37 |

Conditions of polymerization as in Table 1, molecular weight data determined by GPC at $135 \text{ }^\circ\text{C}$

Molecular weight distributions are on the average between 2.6 and 3.5, which is still relatively narrow and typical for metallocenes, i.e. single site catalysts. The tendency of broader distributions with higher α -olefin concentration is caused by the very high incorporation of the comonomer in the present case. Even though the copolymerizations were run at relatively low conversions (typically not exceeding half an hour of actual polymerization time to obtain a sufficient amount of polymer), the depletion of the comonomer causes the formation of higher molecular weight copolymer towards the end of the run.

The determination of the monomer reactivity ratios of the copolymerizations and the study of the monomer sequence distribution and microstructure determined by C 13 NMR spectroscopy of the ethylene/ α -olefin copolymers described here, will be discussed in a subsequent publication.

As a major conclusion, the discussed catalyst, racemic dimethylsilyl bis(2-methyl-4-phenyl-indenyl) zirconium dichloride, produces the highest activities among the metallocenes both in ethylene homopolymerization and copolymerization with α -olefins, even without the appearance of a comonomer effect. At the same time this catalyst incorporates relatively high amounts of α -olefin, and produces molecular weights and polydispersities that fall in the range of commercially desirable polymers. With these properties this metallocene can be utilized both for the production of LLDPE type copolymers and elastomeric copolymers with higher α -olefin content.

Acknowledgments

The authors would like to thank Dow Chemical, and especially Dr. P. Nickias, for providing us with GPC data of our copolymer samples.

We would also like to thank the Dean of the College of Science, Dr. R. Clark, and the Chair of the Department of Chemistry, Dr. G. Takacs, for their support.

References:

- [1] W.Kaminsky and M. Arndt, *Advances in Polymer Science*, **127**, 145-187 (1997)
- [2] H.H. Brintzinger, D. Fischer, R. Mulhaupt, B. Rieger and R. Waymouth, *Angew. Chem. Int. Ed. Engl.*, **34**, 1143-1170 (1995)
- [3] W. Spaleck, F.Kuber, A. Winter, J. Rohrmann, B. Bachmann, M. Antberg, V. Dolle, E.F. Paulus, *Organometallics*, **13**, 954-963 (1994)
- [4] W. Kaminsky and M. Miri, *Proc. Int. Symp. Relat. Heterog. Homog. Catal.*, **5**, 327-341 (1986)
- [5] N. Herfert, P. Montag, G. Fink, *Makromol. Chem.* **194**, 3167-3182 (1993)
- [6] J.C.W. Chien and T. Nozaki, *J. Polym. Sci., Part A: Polym. Chem.*, **31**, 227-237 (1993)
- [7] B.A. Krentsel, Y.V. Kissin, V.J. Kleiner, L.L. Stotskaya, "Polymers and Copolymers of Higher α -Olefins", Hanser Publishers, 1997, e.g. page 280.

6. Functional Polyolefins and Polydienes

The Role of the Cyclopentadienyl Ligand in Catalysts for 1,3-Diene Polymerization

Lido Porri, Giovanni Ricci ¹, Antonino Giarrusso

Department of Industrial Chemistry and Chemical Engineering, Politecnico di Milano, Piazza Leonardo da Vinci 32, 20133 Milan (Italy)

¹Istituto di Chimica delle Macromolecole - CNR, Via Bassini 15, 20133, Milan (Italy)

Abstract. CpTiCl₃-MAO is active for the polymerization of various types of 1,3-dienes. Polymers with a 1,2, a cis-1,4 or a mixed cis/1,2 structure are obtained depending on the type of monomer and the polymerization temperature. An interpretation of the factors that determine chemoselectivity and stereospecificity is presented. CpVCl₂-MAO gives predominantly cis polymers from various dienes. The systems Cp₂TiCl-MAO and Cp₂VCl-MAO are also active catalysts; hypotheses are presented on the nature of the active species in these systems.

Introduction

It is now well established that the role of the cyclopentadienyl ligand in catalysts for stereospecific propene polymerization is to block the conformation of the growing polymer chain in a chiral orientation [1]. Fig. 1a shows a schematic representation of the active sites for the polymerization of propene with catalysts derived from a C₂ symmetry complex. The ligand has little or no effect on monomer enantiofacial selection, which is essentially determined by the steric interaction between the new monomer and the growing chain.

In diene polymerization the situation is different because the bond between the growing polymer chain and the transition metal (Mt) is of the η³-allyl type (Fig. 1b). This type of bond is conformationally much more rigid than the Mt-C bond of σ-type, and the Mt-η³-butenyl group is chiral, independently of whether the butenyl group has an anti or a syn form [2]. Hence, in diene polymerization, a chiral situation is automatically formed after the first diene insertion.

This is the reason why isotactic diene polymers can be synthesized using soluble catalysts prepared from non-chiral precursors. Isotactic 1,2-polybutadiene was synthesized in 1955 [3] using catalysts derived from AlEt₃ and chromium compounds such as Cr(CO)₆, Cr(CO)₃(pyridine)₃, Cr(CNPh)₆, Cr(acac)₃. Isotactic cis-1,4 poly[(E)-1,3-pentadiene] was prepared a few years later using AlEt₃-Ti(OBu)₄ [4].

Another important difference between the polymerization of dienes and that of monoalkenes regards the mode of monomer coordination. While an alkene

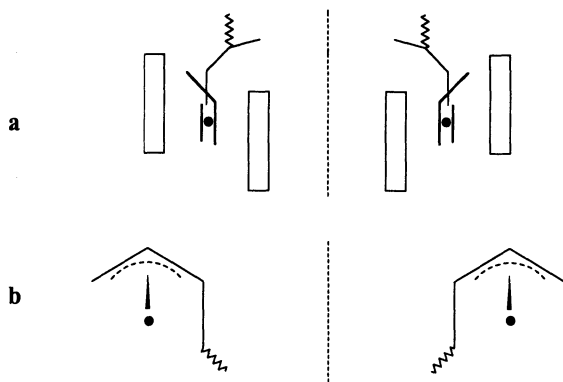


Fig. 1. Schematic representation of the active site for the polymerization of
 (a) propylene with a catalyst derived from a C₂ symmetry complex, and
 (b) butadiene (only the anti form is shown)
 ● transition metal

coordinates η^2 , a common diene usually coordinates η^4 , the *cis*- η^4 coordination being by far that energetically favored. As a consequence, the catalysts derived from bis-cyclopentadienyl derivatives of Zr, e.g., Cp₂ZrCl₂-MAO, are inactive for the polymerization of dienes, because an η^4 coordinated monomer along with an η^3 -bonded growing chain would give rise to a 20-electron zirconium cation. However, catalysts based on bis-cyclopentadienyl derivatives of Zr are active for the copolymerization of alkenes with 1,3-dienes. Ethylene can be incorporated after butadiene, and butadiene after ethylene [5].

Notwithstanding the fact that the cyclopentadienyl ligand has little or no effect on the stereochemistry of diene polymerization, metallocene catalysts have proved to be of great interest for the polymerization of this class of monomers. They have made possible the preparation of new polymers, some of which are very stereoregular, and have also allowed for a deeper insight into some mechanistic aspects of diene polymerization. Catalysts based on Ti, Zr [6], V and Mo [7] have been used, but Ti- and V-based systems have been particularly investigated. This paper reports on the most significant results obtained with the latter systems.

Polymerization with CpTiCl₃-MAO

The polymerization of dienes with CpTiCl₃-MAO has been extensively studied [6,8-15]. This system is active for the polymerization of various dienes (Table 1). The structure of the polymers is strongly dependent on the structure of the monomer.

Table 1. Polymerization of some 1,3-dienes with CpTiCl₃-MAO^a

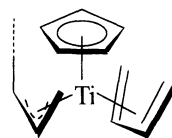
| Monomer ^b | Time (h) | Conv (%) | [η] ^c (dL·g ⁻¹) | m.p. ^d (°C) | Polymer Microstructure ^e |
|----------------------|----------|----------|--|------------------------|-------------------------------------|
| B | 0.15 | 82 | 4.1 | | 81.5 % cis-1,4; 18.5% 1,2 |
| DMB | 70 | 85 | | 120 | ≥98 cis-1,4 |
| 2MP | 18 | 15 | | 136 | ≥98 cis-1,4 |
| EP | 1 | 24 | 1.9 | | 56 % cis-1,4; 44 % 1,2 trans |
| ZP | 2 | 4 | waxy | | 85% cis-1,4; 15% 1,2 |
| 4MP | 1/60 | 100 | 0.4 | | 100 % 1,2 syndiotactic |

- a. Polymerization conditions: temperature, 20°C; monomer, 2 mL; toluene, 16 mL; CpTiCl₃, 1·10⁻⁵ mol; Al/Ti molar ratio, 1000 (in the case of (Z)-1,3-pentadiene, 5·10⁻⁵ mol of CpTiCl₃ and Al/Ti molar ratio of 500 were used)
- b. B, butadiene; DMB, 2,3-dimethyl-1,3-butadiene; 2MP, (E)-2-methyl-1,3-pentadiene; EP, (E)-1,3-pentadiene; ZP, (Z)-1,3-pentadiene; 4MP, 4-methyl-1,3-pentadiene.
- c. intrinsic viscosity, determined in toluene at 25°C.
- d. determined by DSC analysis.
- e. determined by IR and NMR analysis.

Some monomers (butadiene, B; (Z)-1,3-pentadiene, ZP; 2,3-dimethylbutadiene, DMB; (E)-2-methyl-1,3-pentadiene, 2MP) give cis or predominantly cis polymers. (E)-1,3-pentadiene, EP, gives polymers with a mixed cis/1,2 structure, while 4-methyl-1,3-pentadiene, 4MP, gives 1,2 syndiotactic polymer. The results obtained with CpTiCl₃-MAO give some indications on the factors that determine chemo- and stereoselectivity in 1,3-diene polymerization.

The polymers with a cis or a mixed cis/1,2 structure derive from a situation as that shown in Fig. 2, that is, with the new monomer coordinated cis-η⁴ and the last inserted unit anti-η³-bonded. We shall first examine the case of two symmetric monomers, B and DMB. The fact that DMB gives almost exclusively cis units, while B gives polymers ca. 80% cis and 20% 1,2, depends on the relative reactivity of C1 and C3 of the allyl groups derived from each monomer. In the butenyl group derived from DMB, C3 is much less reactive than C1, because of the methyl group (Fig. 3). As a consequence practically only cis DMB units are formed.

More difficult is to interpret the results obtained from non-symmetric monomers, because these can give, at least in principle, two types of η³-butenyl groups on insertion into the growing polymer chain. In addition, these monomers have two prochiral faces and can react with one or the other enantioface. A plausible interpretation of the results obtained from EP and 2MP is as follows. Although each of these monomers can give, in principle, two types of butenyl groups, only groups **a** (Fig. 4) are actually formed, as shown by the fact that vinyl groups are completely absent in poly(EP) and vinylidene groups are absent in

**Fig. 2**

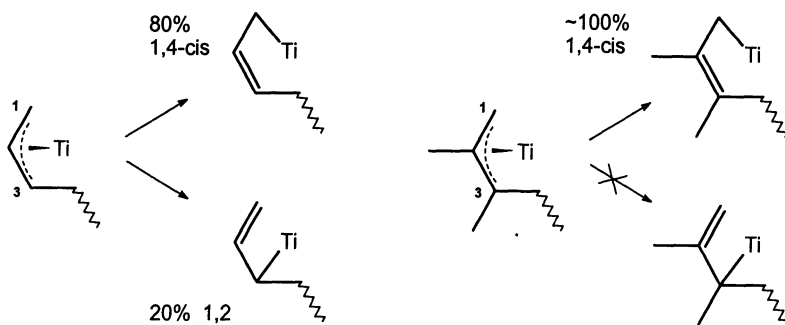


Fig. 3. Scheme for the formation of a polybutadiene with a cis-1,4 / 1,2 structure and of a poly(2,3-dimethylbutadiene) with about 100% cis-1,4 structure

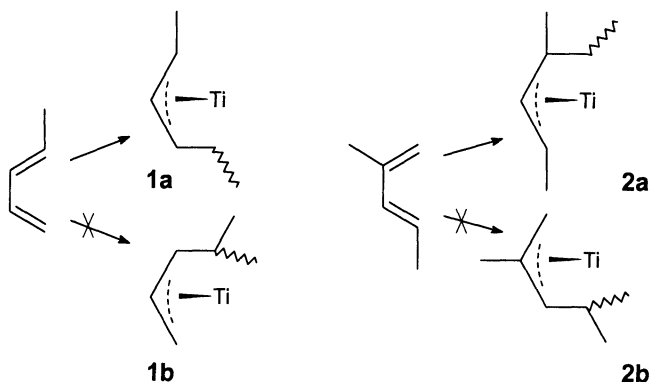
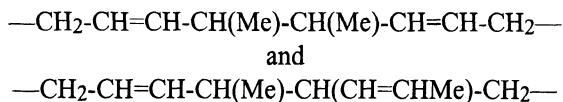


Fig. 4. η^3 -Butenyl groups that can be obtained from (E)-1,3-pentadiene (**1a**, **1b**) and (E)-2-methyl-1,3-pentadiene (**2a**, **2b**) on insertion into the growing polymer chain. Only the anti forms are shown

poly(2MP). These groups should be present, at least in a very small amount, if butenyl groups **b** are formed.

Some structural features of the polymer of EP give an indication of its mode of formation. Inversions such as



are not present in the polymer, according to NMR analysis. This suggests that the formation of a polymer with a mixed cis/1,2 structure likely occurs according to the scheme of Fig. 5 (**a**, **b**).

Presentation of pentadiene as in **a** gives rise to a cis-1,4 unit, while presentation with the other enantioface, as in **b**, gives rise to a 1,2 unit, if the butenyl group **1a** of Fig. 4 is to be formed. In other words, the catalyst is not capable of discriminating between the two monomer enantiofaces and the chemoselectivity

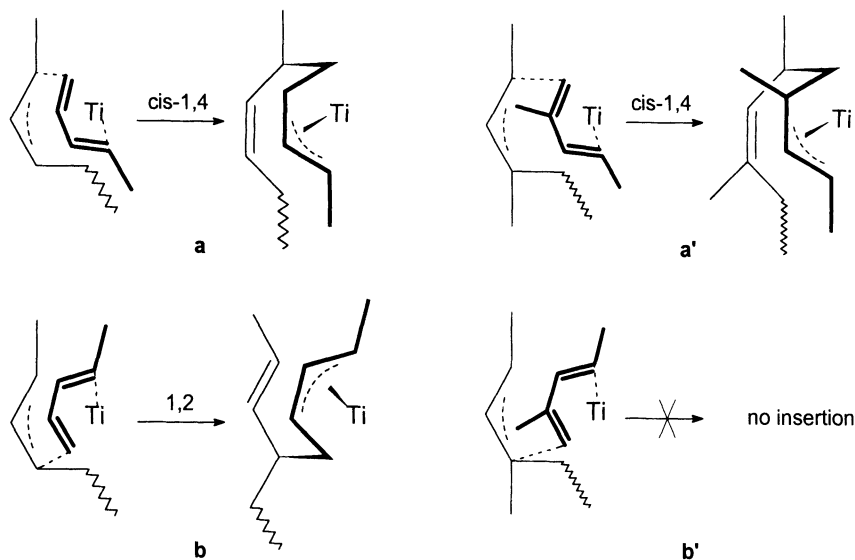


Fig. 5. Scheme for the formation of a polypentadiene with a mixed 1,2/*cis*-1,4 structure (**a**, **b**) and of a poly(2-methylpentadiene) with a *cis*-1,4 isotactic structure (**a'**, **b'**)

depends on which enantioface reacts. A mechanism of this type gives a polymer without the inversions indicated above and this supports its validity.

In our interpretation, this scheme is also valid for the polymerization of 2MP (Fig. 5, **a'** and **b'**). This monomer likely can coordinate with one or the other enantioface, and a rapid equilibrium between the coordinated and non-coordinated monomer is established. However, reaction with one face (**b'**) is not followed by insertion, because reaction of the new monomer at C3 of the butenyl group is too slow (Fig. 5, **b'**). The result is the formation of a poly(2MP) consisting practically of *cis* units only. It may be noted that the scheme of Fig. 5 **a'** accounts well for the formation of a polymer with an isotactic structure, as shown in previous papers by our group [2a,2c,8,16-20]. Presentation of the monomer as in **a'** gives in fact, after insertion, an η^3 -butenyl group having the same chirality as the previous one. If this interpretation is correct, the polymerization of 2MP to *cis* 1,4 isotactic polymer represents a case where isospecificity does not depend on the fact that the catalyst is capable of discriminating between the two monomer enantiofaces. Isospecificity seems to depend on the fact that presentation with one enantioface is not followed by insertion, for kinetic factors.

Another case on which the use of CpTiCl_3 -MAO has shed some light regards the polymerization of ZP and 4MP. These monomers had been polymerized with the heterogeneous systems AlEt_3 - $\alpha\text{-TiCl}_3$ and AlEt_3 - VCl_3 , and a *trans*-1,4 isotactic poly(ZP) and 1,2 isotactic poly(4MP) were obtained [21]. Conventional homogeneous systems (e.g., those based on Ni, Co, Cr) are in general poor catalysts for the polymerization of both ZP and 4MP.

Using CpTiCl_3 -MAO, ZP gives a polymer consisting predominantly of *cis* units, at room temperature (ca. 85% *cis*-1,4, the other units being 1,2) [9,13]. This

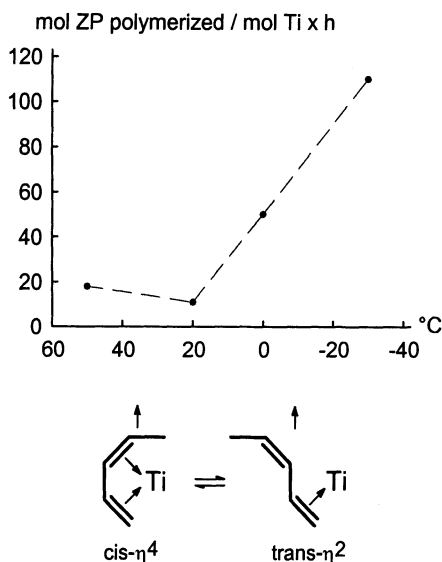


Fig. 6. Temperature effect on the polymerization rate of (Z)-1,3-pentadiene (ZP) with $\text{CpTiCl}_3\text{-MAO}$

polymer likely derives from a $\text{cis-}\eta^4$ coordination of the monomer. However, at -20°C , ZP gives a polymer with a 1,2 syndiotactic structure. In addition, the polymerization rate was found to be higher at -20°C than at $+20^\circ\text{C}$ (Fig. 6) [9]. This phenomenon seems indicative of different modes of monomer insertion at $+20^\circ\text{C}$ and at -20°C , respectively. All the other monomers used in this work (B, EP, DMB) give the same type of polymer either at $+20^\circ\text{C}$ or at -20°C . The particular behavior of ZP is likely related to its mode of coordination to the transition metal of the catalyst. The mode of coordination by far energetically more favored for the most common dienes (butadiene, isoprene, (E)-1,3-pentadiene, 2,3-dimethylbutadiene) is $\text{cis-}\eta^4$. For ZP this type of coordination is less favored, for steric reasons, and there is probably an equilibrium between the $\text{cis-}\eta^4$ and $\text{trans-}\eta^2$ coordination. The equilibrium is likely shifted toward the η^4 coordination at room temperature, but both forms presumably coexist either at $+20^\circ\text{C}$ or -20°C . The experimental results can be accounted for by assuming that i) at -20°C , the monomer coordinated η^2 is inserted much more rapidly than that coordinated η^4 , and ii) the activation energy of the insertion reaction is higher for the η^4 - than for the η^2 -coordinated monomer.

A scheme for the formation of a polymer of ZP with a 1,2 syndiotactic structure, based on an η^2 -coordination of the monomer, had already been proposed [22]. Some new data supporting this scheme will be examined in the following.

4MP gives a 1,2 syndiotactic polymer both at $+50^\circ\text{C}$ and at -50°C . It seems reasonable that also for this monomer there is an equilibrium between the $\text{cis-}\eta^4$ and the $\text{trans-}\eta^2$ coordination. The reason why 4MP, unlike ZP, gives polymers with a 1,2 syndiotactic structure both at $+50^\circ\text{C}$ and at -50°C , may be due to the fact that the $\text{cis-}\eta^4$ coordinated monomer is not incorporated, because its insertion

is by far much slower than that of the η^2 -coordinated monomer, at least in the range of temperature investigated (from +50°C to -50°C). An anomalous effect of the temperature on the polymerization rate has been observed also for 4MP, although much less pronounced than for ZP: the polymerization rate at -20°C is of the same order of magnitude as that at +20°C. Our interpretation is that only the η^2 -coordinated monomer is incorporated and that the concentration of the η^2 form, in the $\text{cis-}\eta^4 \rightleftharpoons \text{trans-}\eta^2$ equilibrium, increases with decreasing temperature. In conclusion, our interpretation of the mode of formation of 1,2 syndiotactic poly(4MP) is that an equilibrium is formed between the η^4 - and η^2 -coordinated monomer, but the insertion of the monomer coordinated η^4 practically does not occur for kinetic reasons.

In order to find a support to this interpretation, the following copolymerizations were examined: ZP/4MP, B/EP and 4MP/B. The expectation was that the mode of monomer coordination would in some way affect the copolymerization behavior. The results of the copolymerizations (Table 2) can be summarized as follows [22].

1. ZP and 4MP give copolymers in which both 4MP and ZP have a 1,2 structure. This fact proves by itself that a true copolymer is obtained, because ZP gives, at room temperature, homopolymers consisting predominantly of cis units. Even in copolymers containing ca. 20% 4MP, the ZP units have a 1,2 structure. In our opinion this result supports the hypothesis that 4MP units derive from an η^2 coordination. The coordination geometry around the transition metal is different if the monomer is coordinated η^2 rather than η^4 . If 4MP units derive from a $\text{trans-}\eta^2$ coordination, ZP too will coordinate η^2 , since the catalytic complex is slow in modifying its coordination geometry. It is also to be considered that for ZP likely there is a low energy difference between η^2 and η^4 coordination. In

Table 2. Copolymerization of (Z)-1,3-pentadiene (ZP) with 4-methyl-1,3-pentadiene (4MP), butadiene (B) with 4MP and (E)-1,3-pentadiene (EP) with B, using $\text{CpTiCl}_3/\text{MAO}$ as catalyst ^a

| M1 | Feed Composition | | M2 | Time (min) | Conv (%) | Copolymer Composition | | [η] (dl·g ⁻¹) |
|----|------------------|---------|----|------------|----------|-----------------------|------------|----------------------------------|
| | mol (%) | mol (%) | | | | M1 (mol %) | M2 (mol %) | |
| ZP | 16 | 4MP | 84 | 0.75 | 37 | 9.5 | 90.5 | 0.2 |
| ZP | 53 | 4MP | 47 | 15 | 16 | 38 | 62 | 0.2 |
| ZP | 71 | 4MP | 29 | 14 | 8 | 51 | 49 | 0.1 |
| ZP | 84 | 4MP | 16 | 14 | 10 | 58 | 42 | |
| ZP | 95 | 4MP | 5 | 240 | 13 | 74 | 26 | |
| B | 50 | 4MP | 50 | 27 | 22 | 99 | | |
| B | 20 | 4MP | 80 | 164 | 16 | 93 | 7 | |
| B | 20 | EP | 80 | 12 | 17 | 48 | 52 | 2.1 |
| B | 50 | EP | 50 | 9 | 18 | 68.5 | 31.5 | 2.8 |

- a. Polymerization conditions: temperature, 20°C; toluene, 32 mL; CpTiCl_3 , $1 \cdot 10^{-5}$ mol; MAO/Ti = 1000.

conclusion the results of the copolymerization are consistent with the hypothesis that both 4MP and ZP coordinate η^2 in the copolymerization.

2. B and EP also give random copolymers. This is likely due to the fact that both B and EP coordinate $\text{cis-}\eta^4$.
3. B and 4MP give block copolymers. When the comonomer molar ratio in the feed is 50:50, the product obtained at ca. 15% conversion is practically polybutadiene only. If 4MP in the feed is more than 50%, block copolymers are obtained. Our interpretation is that B coordinates η^4 , while the active coordination for 4MP is η^2 . It is to be noted that while the homopolymerization of 4MP is much more rapid than that of B [10], the B/4MP copolymerization, at a feed composition 50/50, gives practically only PB.

In our view, the results of the ZP/4MP, B/EP and B/4MP copolymerizations support the interpretation that 4MP units derive from a $\text{trans-}\eta^2$ monomer coordination.

Polymerization with Cp_2TiCl_2 -MAO and Cp_2TiCl -MAO

Although Cp_2ZrCl_2 -MAO is inactive for the polymerization of dienes at room temperature, it has been found that Cp_2TiCl_2 -MAO exhibits some activity, although modest. Some data on the polymerization of butadiene, 4-methylpentadiene and styrene are reported in Table 3 [23].

The low activity was attributed to the formation of a small amount of Ti(III) in the reaction of Cp_2TiCl_2 with MAO. Actually Cp_2TiCl -MAO was found significantly more active than Cp_2TiCl_2 -MAO for the polymerization of dienes and styrene [23]. The two systems, however, have comparable activity for ethylene and propylene polymerization.

The nature of the active species in Cp_2TiCl -MAO represents an intriguing problem. The first step of the catalyst forming reaction is likely the alkylation of Cp_2TiCl , with formation of Cp_2TiMe , which in turn gives an ionic species on further reaction with MAO:

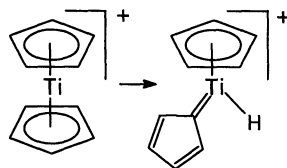


Fig. 7



Table 3. Polymerization of butadiene (B), 4-methyl-1,3-pentadiene (4MP) and styrene (STY) with Cp₂TiCl₂/MAO, Cp₂TiCl/MAO and CpTiCl₃-MAO^a

| Monomer | Temp (°C) | Cp ₂ TiCl ₂ -MAO | | Cp ₂ TiCl-MAO | | CpTiCl ₃ -MAO | |
|---------|--------------|--|--------------|--------------------------|--------------|--------------------------|--------------|
| | | Time (min) | Conv. (%) | Time (min) | Conv. (%) | Time (min) | Conv. (%) |
| B | +20 | 180 | 11 | 30 | 39 | 9 | 82 |
| B | -30 | 7000 | traces | 1350 | 7 | 300 | 7 |
| 4MP | +20 | 17 | 43 | 2 | 66 | 1 | 100 |
| 4MP | -30 | 14 | 10 | 2 | 19 | 1 | 100 |
| STY | +50 | 1440 | 5 | 17 | 24 | 10 | 56 |
| STY | +20 | 1440 | 2 | 11 | 8 | 10 | 15 |

a. Polymerization conditions: monomer, 2 mL; toluene, 16 mL; Ti, 1·10⁻⁵ mol; MAO/Ti=1000.

The cation [Cp₂Ti]⁺ does not possess the requisite Ti-C bond. In our view this cation rearranges to give a carbene-like structure containing a Ti-H bond (Fig. 7). The monomer, on reaction with the Ti-H bond, gives the Ti-C bond on which the polymer chain grows. There are various pieces of evidence that make plausible this working hypothesis. Cp₂Ti was reported to rearrange in solution to give the species Cp(C₅H₄)Ti-H [24]. Cp₂Zr(CH₂Ph)₂ is stable at +100°C and can be recrystallized from boiling heptane. Cp₂Ti(CH₂Ph)₂, instead, decomposes at +30°C to give [(C₅H₄)Ti]_n and toluene [25]. There are other examples in the literature of H-migration from Ti-bonded C₅H₅ ligand [26,27]. Although the hypothesis of the formation of a carbene-like structure seems plausible, a different interpretation was reported for the reaction of Cp₂TiCl with aluminum alkyls [28].

Cp₂TiCl-MAO gives from butadiene, 4-methyl-1,3-pentadiene and styrene polymers having practically the same structure as those obtained with CpTiCl₃-MAO, although the latter system is more active, as said before. The fact that Cp₂TiCl-MAO gives 1,2 syndiotactic poly(4MP) and syndiotactic polystyrene is of some interest for an interpretation of the mode of formation of these polymers.

Four years ago we proposed [10] an interpretation for the formation of 1,2 syndiotactic poly(4MP) based on the hypothesis that the growing polymer chain is η³-bonded to Ti and the new monomer is η²-coordinated. More recently it has been proposed that a back-biting coordination of the double bond of the penultimate monomer unit is an important factor in determining the formation of 1,2 units, using CpTiCl₃-MAO as catalyst [14,15].

The back-biting coordination appears improbable with Cp₂TiCl-MAO, because of the two Cp groups bonded to Ti, even if we accept the interpretation of the rearrangement of the [Cp₂Ti]⁺ cation to a carbene-like structure. The fact that 1,2 syndiotactic poly(4MP) can be obtained with Cp₂TiCl-MAO seems to indicate that the back-biting coordination of the penultimate monomer unit is not essential to chemoselectivity.

A scheme for the formation of syndiotactic polystyrene, based on the hypothesis that the growing polymer chain is η³-bonded to Ti and the monomer is

η^2 -coordinated, was proposed by us in 1994 [10]. Recently a different scheme has been proposed, in which the growing polymer chain is η^7 -bonded to Ti [29]. As reported above, $\text{Cp}_2\text{TiCl-MAO}$ polymerizes styrene to syndiotactic polymer. At least with this system, it seems highly improbable that the growing chain is η^7 -bonded to Ti. A bond of this type would create a too electron rich configuration around the Ti atom of the active species.

Polymerization with catalysts based on cyclopentadienyl vanadium compounds

Two systems have been used in our laboratory, $(\text{C}_5\text{H}_4\text{Me})\text{VCl}_2 \cdot 2 \text{PEt}_3\text{-MAO}$ and $\text{Cp}_2\text{VCl-MAO}$ [30]. Some data on the polymerization of dienes with these systems are reported in Table 4. For the first system, the complex of $(\text{C}_5\text{H}_4\text{Me})\text{VCl}_2$ with PEt_3 was used because $(\text{C}_5\text{H}_4\text{Me})\text{VCl}_2$ tends to disproportionate at room temperature [31]. $(\text{C}_5\text{H}_4\text{Me})\text{VCl}_2 \cdot 2 \text{PEt}_3\text{-MAO}$ is much more active than $\text{Cp}_2\text{VCl-MAO}$. It is also more active than $\text{CpTiCl}_3\text{-MAO}$, and this may be due to the fact that a higher percentage of the transition metal is active in the vanadium system.

The polymers obtained have a predominantly cis structure, ca. 80-85%, the other units being predominantly 1,2. $\text{Cp}_2\text{VCl-MAO}$ also gives predominantly cis polymers, but while it has a good activity for butadiene polymerization it is much less active for the polymerization of other dienes.

Soluble vanadium catalysts (e.g., $\text{AlEt}_2\text{Cl-V}(\text{acac})_3$; $\text{AlEt}_2\text{Cl-VCl}_3 \cdot 3 \text{THF}$) have long been used for the polymerization of butadiene and other dienes and generally give polymers with a trans-1,4 or a mixed trans-1,4/1,2 structure [2a]. $\text{MAO-V}(\text{acac})_3$ also gives trans polybutadiene at high Al/V molar ratio [32]. To our knowledge, vanadocene catalysts are the only vanadium catalysts that give high cis polymers. It is well known that trans-1,4 structures in diene polymers often derive from an anti \rightarrow syn isomerization of the last inserted unit [2a,2b,32]. The formation of a trans vs. a cis unit depends on the relative rate of two processes, i) monomer insertion, and ii) anti \rightarrow syn isomerization of the last inserted unit. If the isomerization process is more rapid than monomer insertion, a trans-1,4 unit is formed. The formation of predominantly cis polymers with vanadocene catalysts may be due to one or both of the following factors: i) anti \rightarrow syn isomerization of the last inserted unit is slower than with other vanadium catalysts, because of the Cp ligand; ii) monomer insertion is more rapid than with other soluble vanadium catalysts.

Conclusions

1. In catalysts for diene polymerization, the cyclopentadienyl ligand has little influence, if any, in determining the formation of iso- or syndiotactic polymers.

Table 4. Polymerization of some 1,3-dienes with $\text{Cp}^*\text{VCl}_2 \cdot (\text{PEt}_3)_2$ -MAO ($\text{Cp}^* = \text{C}_5\text{H}_4\text{Me}$) and Cp_2VCl -MAO^a

| Monomer ^b | V-comp. | Time (h) | Conv. (%) | Polymer Microstructure | | |
|----------------------|---------------------------|----------|-----------|------------------------|---------------|---------|
| | | | | cis-1,4 (%) | trans-1,4 (%) | 1,2 (%) |
| B | Cp^*VCl_2 | 1/6 | 82 | 80.5 | 2.5 | 17 |
| I | Cp^*VCl_2 | 5 | 76 | 78 | | 22 |
| EP | Cp^*VCl_2 | 1 | 57 | 71 | | 29 |
| ZP | Cp^*VCl_2 | 116 | 11 | 85 | 15 | |
| 2MP | Cp^*VCl_2 | 6 | 25 | 50 | 50 | |
| 4MP | Cp^*VCl_2 | 8 | 70 | | 18 | 82 |
| B | Cp_2VCl | 1 | 42 | 85 | 2 | 13 |
| I | Cp_2VCl | 24 | 7 | 82 | | 18 |

- a. Polymerization conditions: temperature, 20°C; monomer, 2 ml; toluene, 16 ml (10 ml of monomer and 80 ml of solvent for butadiene); V, 1×10^{-5} mol; Al/V = 1000 (in polymerization of isoprene with Cp_2VCl , 1×10^{-4} mol of V and Al/V molar ratio of 500 were used).
- b. B, butadiene; I, isoprene; EP, (E)-1,3-pentadiene; ZP, (Z)-1,3-pentadiene; 2MP, (E)-2-methyl-1,3-pentadiene; 4MP, 4-methyl-1,3-pentadiene.

In some cases, for instance in the case of vanadium systems, it has been found that the cyclopentadienyl ligand affects the cis/trans ratio in the polymers. The advantages of metallocene catalysts lie in the fact that they are soluble systems and have a high activity.

2. The polymerization with CpTiCl_3 -MAO has shown that the presence of substituents at C1 and C3 of the allyl group can affect both chemoselectivity and stereospecificity in diene polymerization. An interesting example is the formation of a polymer with a mixed cis/1,2 structure from pentadiene and of a polymer with a cis-1,4 isotactic structure from 2-methylpentadiene. In addition, the polymerization with the CpTiCl_3 system has given some indications on the factors that determine the different behavior of (Z)-pentadiene and 4-methylpentadiene with respect to other dienes.

References

- 1 a) Corradini, P.; Guerra, G. *Prog. Polym. Sci.* **16**, 239 (1991); b) Guerra, G.; Cavallo, L.; Moscardi, L.; Vacatello, M.; Corradini, P. *J. Am. Chem. Soc.* **116**, 2988 (1994); c) Bierwagen, E.P.; Bercaw, J.E.; Goddard, W. A. *J. Am. Chem. Soc.* **116**, 1481 (1994); d) Pino, P.; Cioni, P.; Wei, J. *J. Am. Chem. Soc.* **109**, 6189 (1994).
- 2 For reviews on 1,3 diene polymerization with transition metal catalysts: a) Porri, L.; Giarrusso, A. in *"Comprehensive Polymer Science"*, G.C. Eastmond, A. Ledwith, S. Russo, P. Sigwalt, Editors, Pergamon Press Ltd, Oxford 1989, Vol.4., Part II, p.53-108; b) Porri, L.; Giarrusso, A.; Ricci, G. *Prog. Polym. Sci.* **16**, 405 (1991).
- 3 Natta, G.; Porri, L.; Zanini, G.; Palvarini, A. *Chim. Ind. (Milan)* **41**, 1163 (1958)
- 4 Natta, G.; Porri, L.; Stoppa, G.; Allegra, G.; Ciampelli, F. *J. Polym. Sci., Part B* **1**, 67 (1963)
- 5 Kaminsky, W.; Schlobohm, M. *Makromol. Chem., Macromol. Symp.* **4**, 103 (1986)

- 6 Longo, P.; Oliva, P.; Proto, A.; Zambelli, A. *Gazz. Chim. It.* **126**, 377 (1996)
- 7 Unpublished results from our lab.
- 8 Ricci, G.; Italia, S.; Giarrusso, A.; Porri, L. *J. Organomet. Chem.* **451**, 67 (1993)
- 9 Ricci, G.; Italia, S.; Porri, L. *Macromolecules* **27**, 868 (1994)
- 10 Porri, L.; Giarrusso, A.; Ricci, G. *Macromol. Symp.* **89**, 383 (1995)
- 11 Meille, S. V.; Capelli, S.; Ricci, G. *Macromol. Rapid Commun.* **16**, 891 (1995)
- 12 Longo, P.; Grisi, F.; Proto, A.; Zambelli, A. *Macromol. Rapid Commun.* **16**, 891 (1995)
- 13 Oliva, L.; Longo, P.; Grassi, A.; Ammendola, P.; Pellecchia, C. *Makromol. Chem., Rapid Commun.* **11**, 519 (1990)
- 14 Longo, P.; Proto, A.; Oliva, P.; Zambelli, A. *Macromolecules* **29**, 5500 (1996)
- 15 Longo, P.; Grisi, F.; Proto, A. *Macromol. Rapid Commun.* **18**, 183 (1997)
- 16 Gallazzi, M.C.; Giarrusso, A.; Porri, L. *Makromol. Chem., Rapid Commun.* **2**, 59 (1981)
- 17 Bolognesi, A.; Destri, S.; Porri, L. *Makromol. Chem., Rapid Commun.* **3**, 187 (1982)
- 18 Porri, L.; Gallazzi, M.C.; Destri, S.; Bolognesi, A.; *Makromol. Chem., Rapid Commun. Makromol. Chem., Rapid Commun.* **4**, 485 (1983)
- 19 Porri, L.; Giarrusso, A.; Ricci, G. *Makromol. Chem. Macromol. Symp.* **48/49**, 239 (1991)
- 20 Porri, L.; Giarrusso, A.; Ricci, G. *Makromol. Chem. Macromol. Symp.* **66**, 231 (1993)
- 21 Porri, L.; Gallazzi, M. C. *Eur. Polym. J.* **2**, 189 (1966)
- 22 Ricci, G.; Porri, L. *Macromol. Chem. Phys.* **198**, 3647 (1997)
- 23 Ricci, G.; Bosisio, C.; Porri, L. *Macromol. Rapid Commun.* **17**, 781 (1996)
- 24 Brintzinger, H.H.; Bercaw, J. J. *J. Am. Chem. Soc.* **92**, 6182 (1970)
- 25 Fachinetti, C.; Floriani, G. *Chem. Commun.* 654 (1972)
- 26 Volpin, M. E. ; Belyi, A. A.; Shur, V. B.; Lyakhovetsky, Yu. I.; Kudryavtes, R. V.; Buhnov, N. N. *J. Organomet. Chem.* **27**, C5 (1970)
- 27 van Tamelen, E. E.; Seeley, D.; Schneller, S.; Rudler, H.; Cretney, W. *J. Am. Chem. Soc.* **92**, 5251 (1970)
- 28 Eisch, J. J.; Pombrik, S. I.; Xian Shi, Shu-Ching Wu *Macromol. Symp.* **89**, 221 (1995)
- 29 Zambelli, A.; Pellecchia, C.; Proto, A. *Macromol. Symp.* **89**, 373 (1995)
- 30 Ricci, G.; Panagia, A.; Porri, L. *Polymer* **37**, 363 (1996)
- 31 Nieman, J.; Teuben, J. H.; Huffman, J. C.; Caulton, K. G. *J. Organomet. Chem.* **255**, 193 (1983)
- 32 Ricci, G.; Italia, S.; Porri, L. *Macromol. Chem. Phys.* **195**, 1389 (1994)

Catalytic Reaction Mechanisms and Structure-Reactivity Relationships in the Stereospecific Butadiene Polymerization

R. Taube, Anorganisch-Chemisches Institut, Technische Universität München, Lichtenbergstraße 4, D-85747 Garching b. München, Germany

Abstract

Starting with the reaction model of the allylnickel complex catalyzed butadiene polymerization, some essential mechanistic aspects and details, which have been elucidated by DFT quantum chemical calculations are reported. In comparison the present state of the knowledge about the allyllanthanide complex catalyzed butadiene polymerization is outlined. Besides neutral tris(allyl) lanthanide complexes as first one-component lanthanide catalysts for the *trans*-1,4 polymerization, also bis(allyl) and mono(allyl)lanthanide halides as well as cationic bis(allyl)lanthanide complexes of the general type $[\text{Ln}(\eta^3\text{-C}_3\text{H}_5)_2\text{L}_4]\text{B}(\text{C}_6\text{F}_5)_4$ (Ln: La, Nd; L: THF, dioxane) have been synthesized. Allylneodymium halides combined with MAO result in highly active complex catalysts for the *cis*-1,4-polymerization of butadiene, while cationic bis(allyl)neodymium complexes catalyze the *cis*-1,4 polymerization without any cocatalyst. Polymerization degree and polydispersity of the polybutadienes allow important conclusions concerning the catalytic reaction mechanism which give further support to the suggested reaction model for the allyllanthanide complex catalyzed butadiene polymerization.

Introduction

Mechanistic investigations concerning the complex catalyzed stereospecific butadiene polymerization are relatively rare and over decades no experimentally well-founded, convincing reaction model to explain the mechanism of stereoregulation - for example in the case of the allylnickel(II) complex catalyzed butadiene polymerization which was known since the middle of the sixties [1, 2, 3] - could be found in the actual literature [4].

We came to this area of research from coordination chemistry in the early 70ties with the aim of developing a fruitful cooperation with industry. In our first publication, which appeared in 1977 [5], we introduced a series of cationic allylbis-(ligand)nickel(II) complexes $[\text{Ni}(\eta^3\text{-C}_3\text{H}_5)_2\text{L}_2]\text{X}$ (L: P(OPh)₃, P(O-*o*-Tol)₃, PPh₃, 0,5 COD; X: BF₄, PF₆) as new structurally defined, highly active and selective one-component catalysts for the stereospecific butadiene polymerization. To explain our own experimental results and those known from literature at that time, concerning the neutral dimeric allylnickel(II) complexes $[\text{Ni}(\eta^3\text{-C}_3\text{H}_5)_2\text{X}]_2$ (X: Cl, Br, I, CF₃CO₂) [6], we suggested a simple thermodynamically controlled two-channel reaction model. This was based on the assumption, that the butenyl-monoligand complex $[\text{Ni}(\text{RC}_3\text{H}_4)\text{L}]^+$ or $[\text{Ni}(\text{RC}_3\text{H}_4)\text{X}]$ generates the *trans* and

the ligand-free butenyl complex $[\text{Ni}(\text{RC}_3\text{H}_4)]^+$ the *cis* units in the growing polybutadienyl chain by η^2 or η^4 coordination of butadiene and insertion into the allylnickel bond.

In the following years the catalytic mechanism of stereoregulation has gradually been elucidated more thoroughly on the basis of further experimental investigations. For the first time a comprehensive, experimentally well-founded reaction model could be derived [7], which allows to explain the catalytic structure-reactivity relationships for the allylnickel(II) complex catalyzed butadiene polymerization in a convincing manner [8, 9], including also the industrially used Ziegler-Natta catalyst system $\text{Ni}(\text{O}_2\text{CR})_2/\text{BF}_3 \cdot \text{OEt}_2/\text{Al}_2\text{Et}_6$ [10]. Recently, the reaction model could be established in all essential aspects and further developed by DFT quantum calculations [11, 12].

The two-channel reaction model for the allylnickel(II) complex catalyzed *trans*- and *cis*-1,4 polymerization of butadiene

The course of the catalytic reaction is shown schematically in Fig. 1. The butenylbis(ligand)nickel(II) complex, which does exist in the *anti* and in the thermodynamically more stable *syn* form, acts as a precatalyst under polymerization conditions. In the reaction with butadiene two structurally different butadiene complexes are formed by successive ligand substitution, corresponding to the equilibria K_1 and K_2 for the *syn* and K_1' and K_2' for the *anti* form. These butadiene complexes are the active catalysts. Via butadiene insertion into the allylnickel bond the growing chain R is extended by another olefinic C_4 unit and a new butenyl group is formed. In accordance with the principle of least structure variation the *syn* or the *anti* structure of the reacting butenyl group leads to a *trans* or a *cis* double bond in the growing chain. From these *syn-trans* and *anti-cis* correlation it follows that the *cis-trans* selectivity can be determined by the different reactivity of the two catalyst complexes in the *syn* and in the *anti* form, respectively. Thus, the monoligand complex, which is more reactive in the *syn* form, catalyzes the *trans* polymerization via reaction channel k_{1t} , whereas the ligand-free complex by its higher reactivity in the *anti* form generates the *cis* units via the reaction channel k_{2c} .

The higher reactivity of the *syn* form has been confirmed by NMR spectroscopy for the typical *trans* catalysts $[\text{Ni}(\eta^3\text{-C}_4\text{H}_7)\text{I}]_2$ [13] and $[\text{Ni}(\eta^3\text{-C}_4\text{H}_7)(\text{P}(\text{OPh})_3)_2]\text{PF}_6$ [14], and the *cis* selectivity of the ligand-free complex is established by the synthesis of the cationic C_{12} -allylnickel(II) complexes $[\text{Ni}(\eta^3, \eta^2, \eta^2\text{-C}_{12}\text{H}_{19})]\text{X}$ (see below) as extremely active catalysts for the *cis*-1,4 polymerization of butadiene [15].

In the case of nickel the butadiene insertion proceeds always under formation of an *anti* butenyl group. Therefore the *anti-syn* isomerization is a necessary reaction step in the catalysis of the *trans* polymerization and can be rate-determining, as it

has been proved by NMR spectroscopy for the bis(triphenyl-phosphite) complex $[\text{Ni}(\eta^3\text{-C}_4\text{H}_7)(\text{P}(\text{OPh})_3)_2]\text{PF}_6$ [14].

The different reactivity of the *anti* and the *syn* form of the butenylnickel(II) complex in dependence of its different structure is the crucial idea to deduce the correct mechanism for the *cis-trans* regulation in the allylnickel complex catalyzed butadiene polymerization.

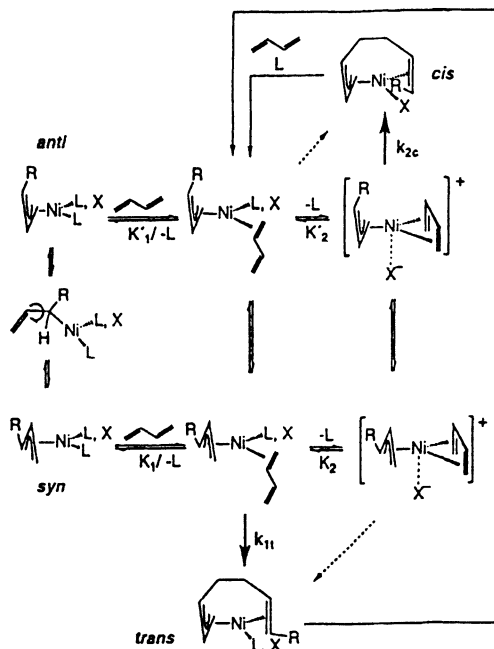


Fig. 1. General reaction model of the allylnickel(II) complex catalyzed *trans*- and *cis*-1,4 polymerization of butadiene to explain the thermodynamic and kinetic control of the catalytic reaction course.

The different reactivity of the *syn*- and *anti*- η^3 -butenylnickel(II) complex as consequence of the π -allyl insertion mechanism

To explain the different reactivity of the catalytically active butenyl(butadiene)-nickel(II) complexes in the *syn* and in the *anti* form, respectively, we introduced the π -allyl insertion mechanism. In contrast to the generally assumed Cossee-Arlman mechanism, where the allyl group should react like an alkyl group from the σ -bonded state, we suggested for the first time, that with nickel the C-C bond formation takes place through a nucleophilic attack of the π -coordinated butenyl group on the η^4 -*cis* coordinated butadiene. This is schematically shown in Fig. 2 by the corresponding interaction of the two shaded 2p orbitals of the terminal carbon atoms of both reactants in the plane of the nickel(II) complexes. Since in the monoligand *syn* complex the growing chain R is *trans* orientated to the ligand L or X in the *z*-position, a higher reactivity than for the *anti* form can be expected,

which leads to the formation of a *trans* double bond in the next C₄ unit. On the other hand, in the ligand-free complex the C-C bond formation must be supported energetically by the coordination of the next double bond in agreement with Tolmans 18-16 electron rule. Under these conditions, obviously, the *anti* form can become the more stable and reactive one giving rise to the formation of a *cis* double bond in the insertion step.

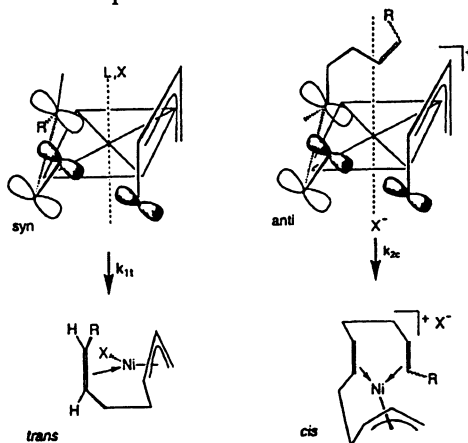


Fig. 2. Structure of the monoligand and the ligand-free butenyl(butadiene)-nickel(II) complex for the butadiene insertion reaction according to the π -allyl insertion mechanism generating a *trans* and a *cis* double bond, respectively, in the growing chain corresponding to the reaction channels k_{1t} and k_{2c} .

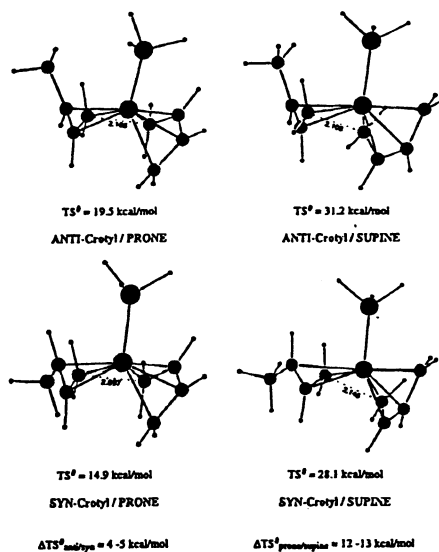


Fig. 3. Structures and relative stabilities of the transition states for the *anti*- and *syn*- η^3 -crotyl(monoligand)nickel(II) catalyst complexes with η^4 -*cis* coordinated butadiene in the prone and in the supine configuration ($L = \text{PH}_3$).

All these fundamental mechanistic aspects have been supported substantially by comprehensive and methodically well-established DFT quantum chemical calculations in cooperation with Dr. S. Tobisch from the Institute of Physical Chemistry of the University of Halle [11, 12].

Some essential results concerning the structure and stability of the transition states for the insertion step in the monoligand and the ligand-free complex catalyst are shown in Fig. 3 and Fig. 4. For the monoligand complex it was found, that independent of the nature of the ligand L (e.g. PH_3 , I^- or C_2H_4) the transition state of the insertion step in the *syn* form is about 4-5 kcal mol⁻¹ more stable than the transition state of the corresponding *anti* complex, which agrees with the observed *trans* selectivity of the *syn* complex.

Furthermore, a preferred reactivity of the butadiene from the η^4 -*cis* coordination state in the prone configuration was found, whereas the *syn* butenyl group shows nearly the same reactivity in the prone and in the supine configuration. This result nicely explains the missing stereoregularity in the methylene groups of the *trans* polybutadiene generated by allylnickel catalysts, as it is described in the literature [16, 17].

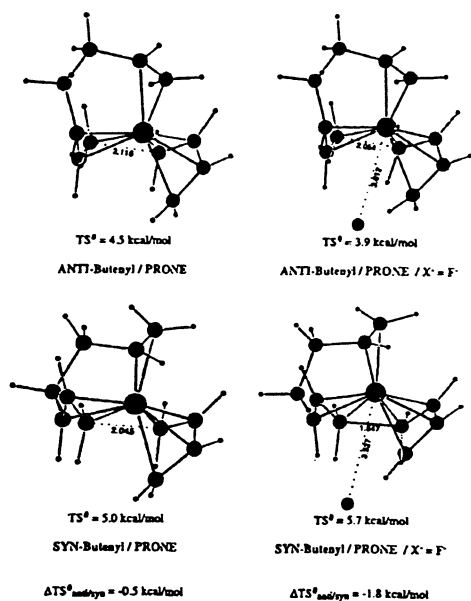


Fig. 4. Structures and relative stabilities of the transition states for the ligand-free *anti*- and *syn*- η^3 -butenylnickel(II) catalyst complexes with one η^2 coordinated double bond from the growing chain, with η^4 -*cis* coordinated butadiene in prone configuration, and a weak anion interaction (X⁻ = F⁻)

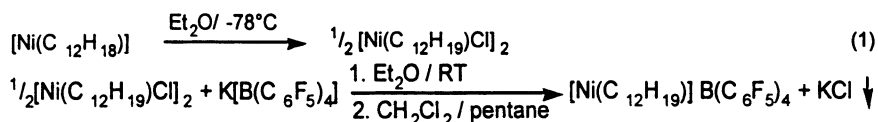
On the other hand, in the case of the ligand-free complex the transition state for the butadiene insertion in the *anti* form becomes the more stable one by coordination of the next double bond, giving rise to the formation of a *cis* double bond in agreement with the reaction model. As the calculation showed, the reactivity of the *anti* form compared to the *syn* form can be additionally increased by a weak anion coordination in the - z-position.

Since the *anti* butenyl group is fixed in its configuration in relation to the prone coordinated butadiene the experimentally proved stereoregularity in the methylene groups of the *cis* polybutadiene from nickel catalysts [16, 17] becomes quite understandable.

Cationic η^3, η^2, η^2 -dodeca-2(*E*),6(*E*),10(*Z*)-triene-1-yl-nickel(II) complexes as extremely active catalysts for the *cis*-1,4 polymerization of butadiene

As we have shown already some years ago, cationic C₁₂-allylnickel(II) complexes of the type [Ni(η^3, η^2, η^2 -C₁₂H₁₉)]X with weakly or non-coordinating anions, like X⁻: PF₆⁻, SbF₆⁻ [15, 18], B(C₆H₃(CF₃)₂)₄⁻ [19], and others [20], can be synthesized from the C₁₂-bis(allyl)nickel(II) complex [Ni(η^3, η^3, η^2 -C₁₂H₁₈)] [21] by partial protolysis with the respective Brønsted acid HX. Besides the η^3 -coordinated butenyl group these complexes contain two olefinic C₄ units π -coordinated to the nickel, and correspond directly to the ligand-free butenylnickel(II) complex under polymerization conditions. X-ray crystal structure analyses [22,23] and ¹³C-NMR measurements [24] indicate the possibility of a weak coordinative interaction between the anion and the nickel in this type of complex.

More recently we also succeeded in the synthesis of the tetrakis(pentafluoro) borate (X⁻:B(C₆F₅)₄⁻) by simple anion exchange in the already known C₁₂-allylnickel(II) chloride [21], c.f. the following reaction scheme (1):



With a turnover frequency (TOF) between 10 and 20 thousand mol butadiene per mol Ni and hour at room temperature under standard conditions - c.f. the results in Table 1 - these cationic C₁₂-allylnickel(II) complexes are the most active nickel catalysts for the stereospecific butadiene polymerization and their identity with the ligand-free complex catalyst giving rise to a high *cis*-selectivity. Concerning the *cis* content and also the polydispersity of the polybutadiene, there

seems to be a delicate influence of the anion, which needs further investigations to become fully elucidated.

Table 1. Catalytic properties of cationic C₁₂-allylnickel(II) complexes for the *cis*-1,4 polymerization of butadiene in toluene at 25 °C^{a)}

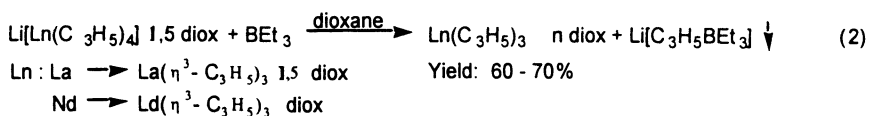
| [Ni(C ₁₂ H ₁₉)]X | C % | TOF | cis % | \bar{M}_w/\bar{M}_n |
|--|-----|-------|-------|-----------------------|
| X: B(C ₆ H ₃ (CF ₃) ₂) ₄ | 60 | 12000 | 93 | ≈ 2 |
| X: PF ₆ | 80 | 16000 | 89 | ≈ 2 |
| X: SbF ₆ | 70 | 14000 | 91 | n.d. |
| X: B(C ₆ F ₅) ₄ | 90 | 18000 | 86 | ≈ 6 |

a) [Ni] = 2·10⁻⁴M, [BD]₀ = 2M, t_p : 30 min; C = conversion, TOF : mol BD / (mol Ni h)

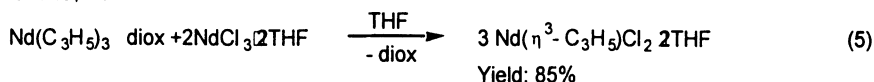
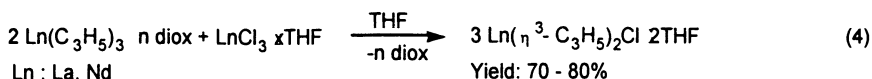
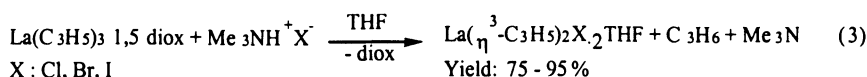
Additional studies during the last years were directed to derive also an experimentally well-founded reaction model for the allyllanthanide complex catalyzed butadiene polymerization [25, 26].

Synthesis and characterization of three different types of allyllanthanide(III) complexes as new catalysts for the stereospecific butadiene polymerization

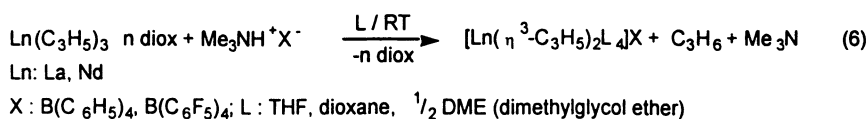
As already published [27], we synthesized the first tris(allyl)lanthanide complexes with lanthanum and neodymium from the known tetrakis(allyl) complexes [28] by allyl anion abstraction with boron triethyl as the Lewis acidic acceptor, according to equation (2):



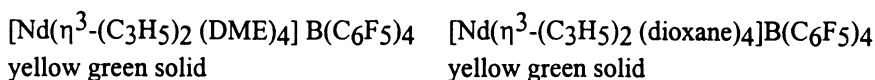
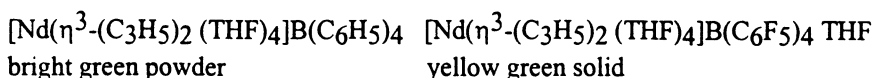
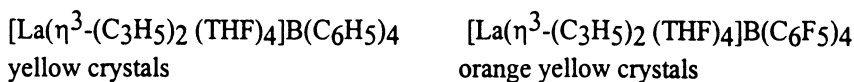
From the tris(allyl)lanthanide complexes we could also synthesize for the first time bis- and mono(allyl)lanthanide halides [26, 29], either by partial protolysis with trimethylammonium halides as the Brønsted acid or by comproportionation with the lanthanide trichloride in the corresponding molar ratio of 2:1 and 1:2, respectively, c.f. the following equations (3), (4) and (5):



Quite recently we succeeded in the synthesis of cationic bis(allyl)lanthanide complexes by partial protolysis of the tris(allyl) complexes with trimethylammonium salts of the tetrakis(phenyl)- or tetrakis(pentafluorophenyl)borate anion as non-coordinating counteranion in proper donor solvents (L), c.f. equation (6):



The following cationic bis(allyl)lanthanide complexes have been isolated and fully characterized:



The lanthanum(III) complexes could also be characterized by X-ray crystal structure analysis. In Fig. 5 the unit cell for the tetrakis(pentafluoro)borate complex is shown. As can be seen both allyl anions are η^3 coordinated and the four THF ligands are η^1 coordinated to the lanthanum resulting in the coordination number of 8, which has been found also in all other types of allyl complexes of La(III) and Nd(III) [26, 27, 29, 30]. The B(C₆F₅)₄-anion is well separated from the bis(η^3 -allyl) complex cation. Therefore, three different types of allyllanthanide complexes are available and can be used as structurally defined polymerization catalysts.

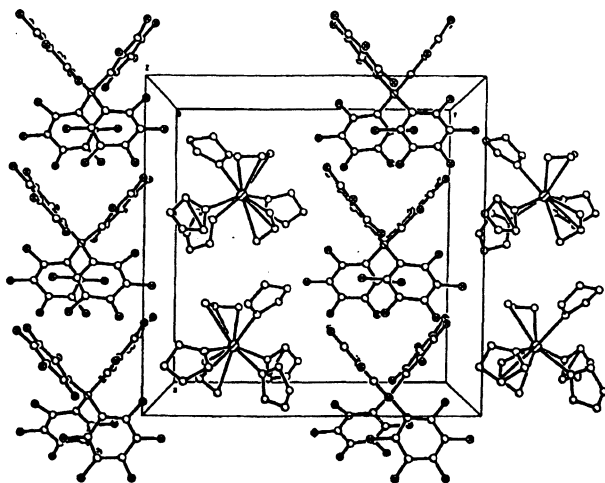


Fig. 5. Arrangement of the lattice constituents in the unit cell for $[\text{La}(\eta^3\text{-C}_3\text{H}_5)_2(\text{THF})_4]\text{B}(\text{C}_6\text{F}_5)_4$ [31]

Catalytic properties of the different allyllanthanide(III) complexes for the stereospecific butadiene polymerization

1. Tris(η^3 -allyl)lanthanides $\text{Ln}(\eta^3\text{-C}_3\text{H}_5)_3 \cdot n$ diox ($\text{Ln} : \text{La}, \text{Nd}$)

The catalytic properties of the tris(allyl)lanthanide complexes in toluene at 50 °C under standard conditions are shown in Table 2. The tris(allyl)lanthanides were the first one-component catalysts in the lanthanide complex catalyzed butadiene polymerization. They show a high *trans* selectivity, but their catalytic activity is only moderate. For the neodymium complex with one dioxane ligand the TOF amounts about 600 per hour and can be doubled by removing the donor ligand. At the same time, the *trans* selectivity decreases slightly from 94 to 89 % and correspondingly the *cis* selectivity increases from 3 to 7 %. Obviously, donor ligands act as inhibitors in the catalytic reaction and can also diminish the *cis* selectivity [32].

Table 2. . Catalytic properties of tris(η^3 -allyl)lanthanides as one component catalysts with high *trans* selectivity in toluene at 50 °C under standard conditions^{a)}

| Complex | C % | TOF | cis % | \bar{M}_w/\bar{M}_n |
|--|-----|------|-------|-----------------------|
| $\text{La}(\eta^3\text{-C}_3\text{H}_5)_3 \cdot 1,5$ diox | 60 | 500 | 83 | n.d. |
| $\text{Nd}(\eta^3\text{-C}_3\text{H}_5)_3 \cdot \text{diox}$ | 40 | 600 | 94 | n.d. |
| $\text{Nd}(\eta^3\text{-C}_3\text{H}_5)_3$ | 50 | 1300 | 89 | $\approx 1,2$ |

^{a)} $[\text{Ln}] = 1 \cdot 10^{-3}\text{M}$, $[\text{BD}]_0 = 2\text{M}$, t_p : 50-150 min; C=conversion, TOF: mol BD/(mol Ln h)

In case of the donor ligand-free $\text{Nd}(\eta^3\text{-C}_3\text{H}_5)_3$ a kinetic analysis gave the bimolecular rate law $r_p = k_p [\text{Nd}] [\text{BD}]$ with $k_p = 0,28 \text{ mol l}^{-1} \text{ s}^{-1}$ at 50°C , as it is expected if a butadiene complex of Nd(III) is involved in the rate determining step of the catalysis. The degree of polymerization \bar{n}_{exp} increases in an almost linear mode with the conversion, indicating a living polymerization in agreement with the low polydispersity in the range of 1. From the comparison of the theoretical chain length n_{calc} with \bar{n}_{exp} - the ratio $n_{\text{calc}}/\bar{n}_{\text{exp}} \approx 2 - 2,5$ was found - it can be concluded that about three chains per Nd are generated.

Thus it can be assumed that the tris(allyl)neodymium complex in the investigated experimental range works as a single-site catalyst, without chain transfer and with reaction of all three allyl groups in the catalysis of chain propagation.

If the tris(allyl)lanthanide complexes are combined with Lewis acids like EtAlCl_2 or methylaluminoxane the catalytic activity can be increased considerably and the selectivity is changed from *trans* to *cis*, c.f. in Table 3.

The polydispersity was determined again in a range below 2 ($\bar{M}_w/\bar{M}_n \approx 1,4 - 1,7$), the degree of polymerization \bar{n}_{exp} increases also nearly linearly with conversion, but the ratio $n_{\text{calc}}/\bar{n}_{\text{exp}}$ was found near 1 indicating that only one allyl group is catalytically active in the chain propagation reaction.

Table 3. . Catalytic properties of tris(η^3 -allyl)lanthanides in combination with the Lewis acids EtAlCl_2 and methylaluminoxane ($\text{MAO} \hat{=} \text{CH}_3\text{AlO}$) in toluene at 50°C under standard conditions ($[\text{BD}]_0 = 2\text{M}$)

| Catalytic system | $[\text{BD}]_0/[\text{Ln}]$ | TOF | cis | trans | 1,2 [%] |
|---|-----------------------------|-------|-----|-------|---------|
| $\text{La}(\eta^3\text{-C}_3\text{H}_5)_3 \cdot 1,5\text{diox}$ | | | | | |
| + 2EtAlCl_2 | 2000 | 140 | 88 | 11 | 1 |
| + 30 MAO | 2000 | 2900 | 55 | 43 | 2 |
| + 30 MAO | 5000 | 4700 | 65 | 32 | 3 |
| $\text{Nd}(\eta^3\text{-C}_3\text{H}_5)_3 \cdot \text{diox}$ | | | | | |
| + 2EtAlCl_2 | 2000 | 8300 | 94 | 5 | 1 |
| + 30 MAO | 5000 | 10000 | 59 | 37 | 4 |
| + 30 MAO | 5000 | 14000 | 79 | 18 | 3 |

TOF : mol BD / (mol Ln · h)

The simplest mechanistic interpretation of these results is to assume that two allyl anions can be abstracted by the Lewis acid from the tris(allyl)lanthanide complex. Thus, a monoallyllanthanide dicationic fragment is generated, which

might be stabilized by different coordinative interactions, especially with donor atoms of the Lewis acid, and can be regarded as the functional unit responsible for the *cis* selectivity in the allyllanthanide complex catalyzed butadiene polymerization. Further support to this mechanistic explanation comes from the catalytic properties of the bis- and mono(allyl)neodymium chlorides.

2. Bis- and mono(η^3 -allyl)neodymium chloride $\text{Nd}(\eta^3\text{-C}_3\text{H}_5)_2\text{Cl}\cdot 1,5 \text{ THF}$ and $\text{Nd}(\eta^3\text{-C}_3\text{H}_5)\text{Cl}_2\cdot 2\text{THF}$

In combination with hexaisobutylaluminumoxane (HIBAO) and especially with methylaluminumoxane (MAO) as cocatalysts both allylneodymium complexes form highly active and selective catalysts for the *cis*-1,4 polymerization, c.f. in Table 4.

The extremely high TOF of nearly 600 000 per hour and a *cis* selectivity of 98 % are reached for both allylneodymium chlorides in combination with 30 equivalents of MAO (CH_3AlO) in heptane as solvent.

For three combinations the course of the catalytic reaction in toluene has been investigated in some detail, the results are summarized in Table 5.

Table 4. Catalytic properties of bis- and mono(η^3 -allyl)neodymium chloride in combination with alkylaluminumoxanes in toluene and heptane at 35 - 50 °C under standard conditions^{a)}

| Catalytic system | solvent | [BD] ₀ /[Nd] | TOF | <i>cis</i> | <i>trans</i> | 1,2 [%] |
|---|---------|-------------------------|--------|------------|--------------|---------|
| $\text{Nd}(\text{C}_3\text{H}_5)_2\text{Cl}\cdot 1,5\text{THF}$ | | | | | | |
| + 30 HIBAO | toluene | 10000 | 25000 | 97 | 2 | 1 |
| + 30 MAO | toluene | 10000 | 12500 | 92 | 7 | 1 |
| + 30 MAO | heptane | 20000 | 575000 | 98 | 1 | 1 |
| $\text{Nd}(\text{C}_3\text{H}_5)\text{Cl}_2\cdot 2\text{THF}$ | | | | | | |
| + 30 HIBAO | toluene | 10000 | 19000 | 97 | 2 | 1 |
| + 30 MAO | toluene | 7500 | 12000 | 94 | 5 | 1 |
| + 30 MAO | heptane | 40000 | 570000 | 98 | 1 | 1 |

^{a)} [Nd] = $1\cdot 10^{-4}$ M, [BD]₀ = 1-3M; TOF : mol BD / (mol Ln · h)

(HIBAO $\hat{=}$ $i\text{-C}_4\text{H}_9\text{AlO}$; MAO $\hat{=}$ CH_3AlO)

Table 5. Results and conclusions from kinetic measurements and polymer analysis (in cooperation with Prof. Dr. G. Müller, Institute of Technical and Macromolecular Chemistry of the University Halle) for three catalytic systems generated from bis- and mono(allyl)neodymium chloride and 30 equivalents of alkylaluminumoxane in toluene

| | Nd(C ₃ H ₅) ₂ Cl·2THF + 30 HIBAO | Nd(C ₃ H ₅)Cl ₂ ·2THF + 30 HIBAO | Nd(C ₃ H ₅)Cl ₂ ·2THF + 30 MAO |
|--|---|---|---|
| Rate law | $r_p = k_p[\text{Nd}][\text{BD}]^{1,8}$ | - | $r_p = k_p[\text{Nd}][\text{BD}]^2$ |
| K_p (at 35°C) | - | - | 3,24 l ² mol ⁻² s ⁻¹ |
| \bar{M}_w/\bar{M}_n | ≈ 1,1 - 1,3 | ≈ 1,1 - 1,3 | ≈ 1,1 - 1,2 |
| \bar{n}_{exp} | ~ conversion | ~ [BD] ₀ / [Ln] | ~ conversion |
| $N_{\text{calc}}/\bar{n}_{\text{exp}}$ | ≈ 1 | ≈ 0,5 - 0,9 | ≈ 1 |

In the case of the combination Nd(η^3 -C₃H₅)₂Cl·1,5 THF / HIBAO a first order rate law for neodymium and 1,8 order for butadiene was found. From the polydispersity of around 1, the linear increase of the polymerization degree \bar{n}_{exp} with conversion and its ratio to the theoretical chain length n_{calc} of about 1 it can be deduced that all the neodymium is catalytically active with only one allyl group and without any chain transfer reaction.

If the mono(allyl)neodymium(III) dichloride is combined with HIBAO the polymerization degree \bar{n}_{exp} increases linearly with decreasing concentration of Nd thus indicating a living polymerization. But from the lower polymerization degree in comparison with the theoretical chain length it can be seen, that only 50 - 90 % of the neodymium complex is catalytically active. Probably the Lewis acidity of the HIBAO is not strong enough to transform the mono(allyl)neodymium chloride complex completely into the catalytically active dicationic mono(allyl)-neodymium(III) fragment.

When MAO as a stronger Lewis acid is used a complete activation of all the neodymium can be reached. The rate law, besides first order in Nd, becomes exactly second order in butadiene. The degree of polymerization \bar{n}_{exp} increases linearly with conversion and from its identity with the theoretical chain length n_{calc} one can conclude that now all the neodymium with one allyl group acts as the polymerization catalyst. Direct evidence for the formation of a cationic allyllanthanide complex fragment as the catalytically active structure for the *cis*-1,4 polymerization of butadiene is given by the catalytic properties of the cationic bis(allyl)lanthanide complexes.

3. Cationic bis(η^3 -allyl)lanthanide complexes $[\text{Ln}(\eta^3\text{-C}_3\text{H}_5)_2\text{L}_4]\text{X}$ (Ln : La, Nd; L : THF, dioxane; X : $\text{B}(\text{C}_6\text{F}_5)_4$)

The catalytic properties of three cationic bis(η^3 -allyl)lanthanide complexes are summarized in Table 6.

Table 6. Catalytic properties of cationic bis(η^3 -allyl)lanthanide(III) complexes in toluene at 50 °C ($[\text{BD}]_0 = 2\text{M}$): $[\text{La}(\text{C}_3\text{H}_5)_2(\text{THF})_4]\text{B}(\text{C}_6\text{F}_5)_4$ **1**, $[\text{Nd}(\text{C}_3\text{H}_5)_2(\text{THF})_4]\text{B}(\text{C}_6\text{F}_5)_4$ **2**, $[\text{Nd}(\text{C}_3\text{H}_5)_2(\text{diox})_4]\text{B}(\text{C}_6\text{F}_5)_4$ **3**

| # | $[\text{Ln}]$ M | $\frac{[\text{BD}]_0}{[\text{Ln}]}$ | t_p [min] | Yield [%] | TOF | Cis/ trans/1,2 | M_n [g/mol] | PD | $n_{\text{calc}}/n_{\text{exp}}$ |
|----------|--------------------|-------------------------------------|----------------|--------------|-------|-------------------|------------------|------|----------------------------------|
| 1 | $1 \cdot 10^{-3}$ | 2000 | 60 | 56 | 1100 | 27/68/5 | 31000 | 1,04 | 1,91 |
| 1 | $5 \cdot 10^{-4}$ | 4000 | 120 | 46 | 950 | 36/60/4 | 64000 | 1,28 | 160 |
| 2 | $1 \cdot 10^{-3}$ | 2000 | 20 | 23 | 1300 | 42/52/6 | 36000 | 1,16 | 0,66 |
| 2 | $5 \cdot 10^{-4}$ | 4000 | 40 | 41 | 2400 | 43/51/6 | 87000 | 1,88 | 0,98 |
| 2 | $2 \cdot 10^{-4}$ | 10000 | 90 | 35 | 2300 | 45/39/7 | 189000 | 1,81 | 0,96 |
| 3 | $1 \cdot 10^{-3}$ | 2000 | 7 | 57 | 10000 | 78/19/3 | 58000 | 1,70 | 1,05 |
| 3 | $5 \cdot 10^{-4}$ | 4000 | 10 | 48 | 11200 | 88/10/2 | 127000 | 1,44 | 0,81 |
| 3 | $2 \cdot 10^{-4}$ | 10000 | 35 | 40 | 6900 | 92/ 7/1 | 254000 | 1,58 | 0,84 |

TOF: mol BD / (mol Ln h); M_n = viscosimetric; PD = M_w/M_n

The cationic bis(allyl)lanthanide complexes are the first one-component lanthanide catalysts, which can perform a high *cis* selectivity. The lanthanum complex **1**, with the stronger coordinating THF as stabilizing donor ligand, shows only moderate catalytic activity with a TOF of about 1000 per hour and a *cis* selectivity of about 35 %. With the isostructural neodymium complex **2** the activity is doubled and the *cis* selectivity increases to 45 %. But if, as in the neodymium complex **3**, the dioxane, which is easier to substitute is introduced as a donor ligand, a high activity with a TOF of about 10 000 per hour and a *cis* selectivity of more than 90 % can be reached. The polydispersity is found in all cases in a range distinctly below 2, the polymerization degree increases linearly with the conversion and from the comparison with the theoretical chain length, $n_{\text{calc}}/\bar{n}_{\text{exp}}$, it can be concluded that all the lanthanide is active and that two chains are formed per lanthanum and only one chain is formed at the neodymium. These results give strong support for the assumption that the *cis* selectivity in the allyllanthanide complex catalyzed butadiene polymerization is structurally determined by the formation and reactivity of a dicationic mono-(allyl)lanthanide complex fragment.

Tentative reaction model of the allyllanthanide(III) complex catalyzed *trans*- and *cis*-1,4 polymerization of butadiene

As it is well known there are essential differences in the coordination chemistry of Ni(II) and the Ln(III) ions. These originate from the much lower electronegativities and the larger ionic radii, giving rise to the higher coordination number, and the missing ability of the Ln(III) ions to form $d_{\pi}-p_{\pi}$ back bonding interactions. Thus, the Ln(III) ions can be defined as much "harder". Therefore the allyl anion is bonded in a highly polar, almost purely ionic manner, while unsaturated hydrocarbons can be coordinated only by cation-quadrupole interactions, similar as it is described for the alkali metal ions [33].

Under these conditions the σ -allyl insertion mechanism seems to be more favoured from an energetic point of view. Furthermore it is to be expected that depending on the coordinative accessibility of the Ln(III) ion the butadiene can react with the σ -bonded butenyl group either vinylene-like from the η^2 -*trans* coordinated state to give a *syn* butenyl group or from the η^4 -*cis* coordinated state in supine configuration with formation of an *anti* butenyl group.

By the supine configuration of the η^4 -*cis* coordinated butadiene in relation to the σ -butenyl group the facial *cis* arrangement of the two terminal methylene groups from butadiene with the C(1) atom of the σ -butenyl group is realized as a necessary structural condition for the σ -allyl insertion mechanism in agreement with the results of the stereochemical investigations of Porri et al. [34].

One further consequence of the σ -allyl insertion mechanism is the preferred reactivity of the σ -butenyl group via the C(1) atom, where the negative charge is mostly stabilized in the strong electrostatic field of the Ln(III) ion. This explains quite simply the high 1,4 selectivity in the allyllanthanide(III) complex catalyzed butadiene polymerization. The lower stability of the C(3)- σ form of the butenyl group implies on the other hand a correspondingly slow *anti-syn* isomerization, for which an activation barrier ΔG^{\ddagger} of more than 16 kcal mol⁻¹ have been estimated from NMR-measurements at allyllanthanum complexes [27, 35].

Finally it can be assumed that in the case of the lanthanides in contrast to Ni(II) the *anti* and the *syn* butenyl group show virtually the same stability and an equal reactivity. Since in the coordination sphere of the Ln(III) ion only non-directed electrostatic forces are effective no difference in the steric conditions for the η^3 coordination of both forms and thus also in their stability is to be expected. Furthermore, in the σ -bonded state there should be practically no influence of the double bond configuration on the bond strength to the Ln(III) ion so that equal reactivity of the butenyl group in the *anti* and in the *syn* form results.

From these different constitutional conditions one has to conclude that in contrast to nickel the *cis-trans* selectivity must be determined by the mode of butadiene coordination in the catalytically active butenyl lanthanide complex as it is formulated schematically in Fig. 6 to describe the corresponding catalytic cycles.

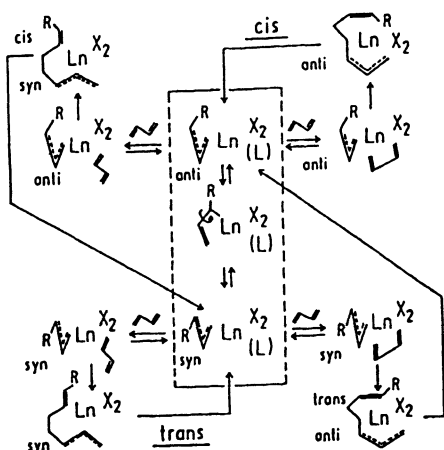


Fig. 6. General reaction model for the allyllanthanide(III) complex catalyzed *trans*- and *cis*-1,4 polymerization of butadiene (X: anion, including a further butenyl anion; L: donor ligand or solvent molecule including also one double bond from the growing chain).

Accordingly *trans* or *cis* selectivity arise if the butadiene is η^2 -*trans* or η^4 -*cis* coordinated, respectively, and becomes inserted with formation of the new butenyl group in the *syn* or *anti* configuration so rapidly, that no isomerization can take place. To explain the *trans* selectivity of the tris(allyl)lanthanides it seems plausible to assume an η^2 coordination of butadiene owing to steric constraints in the tris(polybutadienyl) complex, which must be supposed as the store complex under polymerization conditions. If a better accessibility of the Ln(III) ion is realized by allyl anion abstraction the η^4 -*cis* coordination becomes possible and *cis* selectivity is initiated correspondingly, as it is observed in the catalytic systems with Lewis acids and with the cationic bis(allyl)lanthanide complexes. The coherent increase in propagation rate might also reflect the stronger activation of the η^4 -*cis* coordinated butadiene in the cationic butenyllanthanide(III) complex. The highest activity and *cis* selectivity is to be expected if the coordinative competition of any donor influence from other ligands, the solvent or the anions is reduced as much as possible.

Finally it can be stated that the suggested reaction model seems to be appropriate to give some understanding of essential mechanistic aspects in the allyllanthanide complex catalyzed butadiene polymerization and to rationalize the further experimental investigations for the full elucidation of the catalytic structure-reactivity relationship.

Acknowledgement

I am deeply indebted to the very engaged experimental research activities of my co-workers, which are named in the references. Financial support was given from the Bundesministerium für Forschung und Technologie, Deutsche Forschungsgemeinschaft and Fonds der Chemischen Industrie.

References

- [1] G. Wilke, B. Bogdanović, P. Hardt, P. Heimbach, W. Keim, M. Kröner, W. Oberkirch, K. Tanaka, E. Steinrücke, D. Walter, H. Zimmermann, *Angew. Chem.* **1966**, *78*, 157; *Angew. Chem., Int. Ed. Engl.* **1966**, *5*, 151
- [2] L. Porri, G. N. Natta, M.C. Gallazzi, *Chim. Ind.* **1964**, *46*, 428; *J. Polym. Sci. C*, **1967**, *16*, 2525
- [3] B. D. Babitzkii, B. A. Dolgoplosk, V. A. Kormer, M. I. Lobach, E. I. Tinyakova, V. A. Yakovlev, *Isv. Akad. Nauk. SSSR Ser. Chem.* **1965**, 1507
- [4] W. Keim, *Angew. Chem.* **1990**, *102*, 251; *Angew. Chem. Int. Ed. Engl.* **1990**, *29*, 235
- [5] R. Taube, U. Schmidt, *Z. Chem.* **1977**, *17*, 349
- [6] P. W. Jolly, G. Wilke, *The Organic Chemistry of Nickel*, Vol. 2, Organic Synthesis, Academic Press, New York **1975**
- [7] R. Taube, J.-P. Gehrke, P. Böhme, *Wiss. Zeitschrift THLM*, **1987**, *29*, 310
- [8] R. Taube, U. Schmidt, J.-P. Gehrke, P. Böhme, J. Langlotz, S. Wache, *Makromol. Chem., Makromol. Symp.* **1993**, *66*, 245
- [9] R. Taube, G. Sylvester, *Stereospecific Polymerization of Butadiene or Isoprene*, in B. Cornils, W. A. Herrmann, (Eds.) *Applied Homogeneous Catalysis with Organometallic Compounds*, Vol. 1, VCH Weinheim **1996**, p. 296 ff.
- [10] R. Taube, J. Langlotz, G. Müller, J. Müller, *Makromol. Chem.* **1993**, *194*, 1273
- [11] S. Tobisch, H. Bögel, R. Taube, *Organometallics*, **1996**, *15*, 3563
- [12] S. Tobisch, H. Bögel, R. Taube, *Organometallics* **1998**, *17*, 1177
- [13] V. I. Klepikova, G. P. Kondratenkov, V. A. Kormer, M. I. Lobach, L. A. Churlyayeva, *J. Polym. Sci. Polym. Lett.* **1973**, *11*, 193
- [14] R. Taube, J.-P. Gehrke, R. Radeaglia, *J. Organomet. Chem.* **1985**, *291*, 101
- [15] R. Taube, P. Böhme, J.-P. Gehrke, *J. Organomet. Chem.* **1990**, *399*, 327
- [16] L. Porri, M. Aglietto, *Makromol. Chemie* **1976**, *177*, 1465
- [17] L. M. Stephenson, L. M. Kovac, *C. A. ACS Symp. Ser.* **1983**, *212*, 30
- [18] R. Taube, J. Langlotz, *Makromol. Chem.* **1993**, *194*, 705
- [19] R. Taube, S. Wache, *J. Organomet. Chem.* **1992**, *428*, 431
- [20] R. Taube, J.-P. Gehrke, P. Böhme, K. Scherzer, *J. Organomet. Chem.* **1991**, *410*, 403
- [21] B. Bogdanović, P. Heimbach, M. Kröner, G. Wilke, E. G. Hoffmann, J. Brandt, *Liebigs Ann. Chem.* **1969**, *727*, 143

- [22] R. Taube, S. Wache, J. Sieler, R. Kempe, *J. Organomet. Chem.* **1993**, *456*, 131
- [23] R. Taube, S. Wache, J. Sieler, *J. Organomet. Chem.* **1993**, *459*, 335
- [24] S. Wache, R. Taube, *J. Organomet. Chem.* **1993**, *456*, 137
- [25] R. Taube, H. Windisch, S. Maiwald, *Macromol. Symp.* **1995**, *89*, 393
- [26] R. Taube, H. Windisch, H. Hemling, H. Schumann, *J. Organomet. Chem.* **1998**, *555*, 210
- [27] R. Taube, H. Windisch, S. Maiwald, H. Hemling, H. Schumann, *J. Organomet. Chem.* **1996**, *513*, 49
- [28] A. Mazzei, *Makromol. Chem. Suppl.* **1981**, *4*, 61
- [29] S. Maiwald, R. Taube, H. Hemling, H. Schumann, *J. Organomet. Chem.* **1998**, *552*, 195
- [30] R. Taube, H. Windisch, H. Weißenborn, H. Hemling, H. Schumann, *J. Organomet. Chem.* **1997**, *548*, 229
- [31] J. Sieler, S. Maiwald, R. Taube, unpublished results
- [32] R. Taube, H. Windisch, H. Weißenborn, H. Hemling, H. Schumann, *J. Organomet. Chem.* **1997**, *548*, 229
- [33] S. Mecozzi, A.P. West jr., D. A. Dougherty, *J. Am. Chem. Soc.* **1996**, *118*, 2307
- [34] L. Porri, A. Giarrusso, G. Ricci, *Prog. Polym. Sci.* **1991**, *16*, 405
- [35] R. Taube, H. Windisch, *J. Organomet. Chem.* **1994**, *472*, 71

Styrene and Conjugated Dienes Polymerization with Half Sandwich Titanocene Catalysts

Adolfo Zambelli, Alfonso Grassi, Pasquale Longo

Università di Salerno - Dipartimento di Chimica - 84081 - Baronissi - Italy
zambelli @ chem.unisa.it

Abstract.

The Cp'TiX₃ - MAO catalytic system (Cp' = η⁵-C₅H₅, η⁵-C₅Me₅; X= halide, alkyl, alkoxy; MAO = methylalumoxane) promotes polymerization of ethylene, α-olefins, styrene and conjugated diolefins.

Polymerization of styrene and conjugated diolefins is stereospecific and the results, for this last class of monomers, dramatically depend on the structure of the monomer.

This presentation mainly reports some results of polymerizations performed with isotopically labelled reagents suggesting some hypothesis on the polymerization mechanism and the organometallic active species.

Introduction

Cp'TiX₃ complexes activated with MAO (Cp' = η⁵-C₅H₅, η⁵-C₅Me₅; X = halide, alkyl, alkoxy; MAO = methylalumoxane) provide versatile catalytic systems promoting polymerization of ethylene and linear α-olefins (1,2), styrene and substituted styrenes (3-5), conjugated diolefins (6-8).

Propene polymerization by these catalysts is not stereospecific whereas styrene and substituted styrenes are polymerized to highly syndiotactic polymers under the same conditions.

1,3-Butadiene and isoprene prevalingly afford *cis*-1,4 polymer.

4-methyl-1,3-pentadiene affords the 1,2 syndiotactic polymer with exceptional rate, while (*Z*)-1,3-pentadiene can be polymerized to a mixture of *cis*-1,4 and 1,2 polymers, at room temperature, and to 1,2 syndiotactic polymer, at low temperature (*see infra*).

Several lines of experimental evidence suggest that the Cp'TiX₃ - MAO systems include different organometallic species with different reactivity towards the mentioned monomers (9,10).

The hapticity of the growing chain end and that of the monomer coordinated to the Ti atom of the active species, most probably depend on the particular polymerization considered.

The oxidation state of the active species might be +3 or +4. Some evidence reported in the literature suggest the oxidation state +4 for ethylene polymerization and +3 for conjugated diolefins and styrene polymerization (*see infra*).

In this communication we will show some results on this intriguing catalytic system.

Oxidation state of the active species

The Cp*TiCl₃-MAO catalyst (Cp* = η⁵-C₅Me₅) promotes fast ethylene polymerization at low temperature (0°C). The same system is poorly active in styrene and conjugated diolefins polymerizations, under the same conditions. When the catalyst is pre-treated at higher temperature (e.g. 20 min at 70°C), it becomes very effective in styrene and butadiene polymerizations but less efficient in promoting ethylene polymerization (11). Considering that Ti(IV) compounds can be easily reduced to lower oxidation states by aluminum organometallics, one can suspect that the polymerization of ethylene is promoted by Ti(IV) species while that of styrene and 1,3-butadiene is promoted by Ti(III) species.

In order to confirm this hypothesis we carried out ESR investigations of the half titanocene catalysts (12-14). In the Figure 1 are compared the EPR spectra of chlorobenzene solutions of the Cp*TiMe₃ - MAO system in the presence of p-chlorostyrene (Figure 1A) and α-¹³C-p-chlorostyrene (Figure 1B). The former spectrum exhibits an anisotropic ESR signal (with the parallel component observed at $g_{\parallel} = 1.968$ and the perpendicular component at $g_{\perp} = 1.974$) which was assigned to a Ti(III) species with reduced mobility in the viscous solution containing the polymer product. When the ¹³C-enriched monomer was added in the ESR tube, this signal was quantitatively converted in the ESR signal pictured in the Figure 1B. Computer simulation suggests that it arises from the coupling of both the perpendicular and parallel components of the former signal with the ¹³C-enriched nuclei ($a_{\parallel} (^{13}\text{C}) = 4.7 \text{ G}$; $a_{\perp} (^{13}\text{C}) = 1.7 \text{ G}$; the corresponding isotropic value is $a_{\text{iso}} (^{13}\text{C}) = 2.7 \text{ G}$). This result clearly indicates 2,1 (or secondary) insertion of the styrene monomer on Ti-growing polymer chain bond.

It is worth noting that the coupling constant observed between the d¹ electron of Ti(III) species and the ¹³C-enriched methine carbon of the last monomer in the chain ($a_{\text{iso}} (^{13}\text{C}) = 2.7 \text{ G}$) is smaller than the coupling constant previously found for the σ alkyl bond Ti(III)-¹³CH₃ ($a_{\text{iso}} (^{13}\text{C}) = 6.0 \text{ G}$) (13). This smaller value suggests a partial delocalization of the d¹ electron on the aromatic ring of the last styrene unit in the polymer.

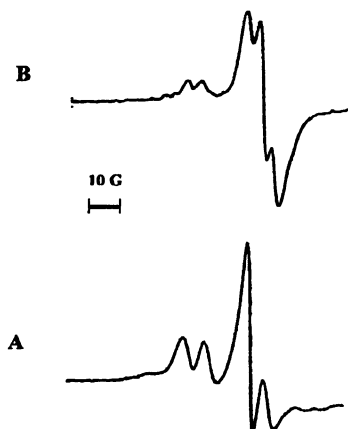


Fig. 1. ESR Spectra of the $\text{Cp}^*\text{Ti}(\text{CH}_3)_3$ - MAO catalytic system in the presence of p-chlorostyrene (1A) and after the addition of α - ^{13}C -enriched-p-chlorostyrene (1B) (chlorobenzene, 293K, $[\text{Ti}] = 0.01 \text{ M}$; Al/Ti molar ratio = 100)

The results confirm our previous suggestion of a “ η^n benzyl coordination” of the last styrene unit of the growing polymer chain to the metal of the active species (see Figure 2) (9).

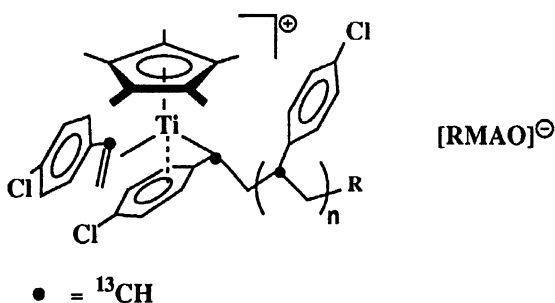


Fig. 2. Chemical structure of the active species in the syndiospecific styrene polymerization promoted by half titanocene catalysts.

4-methyl-1,3-pentadiene polymerization

Polymerization of this monomer is extremely fast and highly regio and stereospecific to 1,2 syndiotactic polymer (15,16).

When polymerization is performed in the presence of CpTiCl_3 - ^{13}C -enriched MAO (17) two different ^{13}C -enriched end groups, in comparable amounts, are

detected in the NMR spectrum of the resulting polymer (see Figure 3). These ^{13}C enriched end groups result from 2,1-insertion (end group t_1) and 4,1-insertion (end group t_2) of the monomer unit into $\text{Ti-}^{13}\text{CH}_3$ bond.

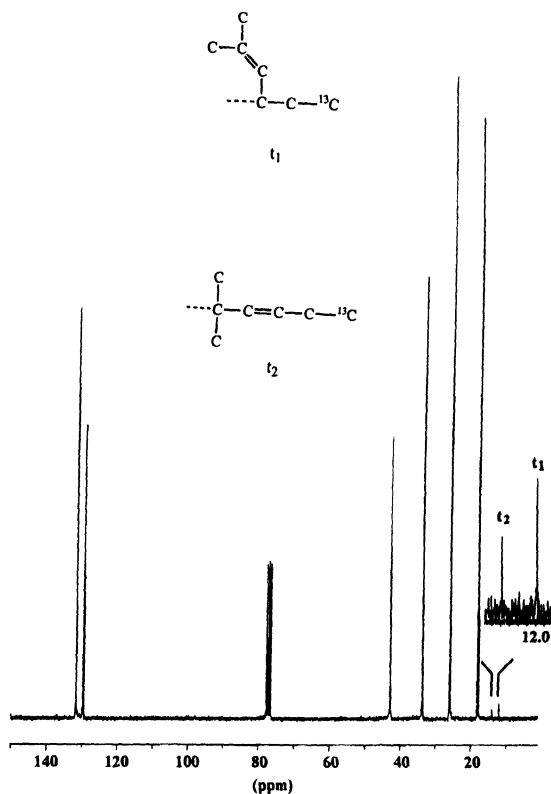
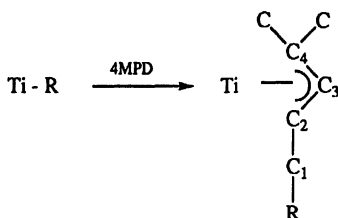


Fig. 3. ^{13}C NMR spectrum of poly-4-methyl-1,3-pentadiene obtained with the CpTiCl_3 - ^{13}C -enriched MAO catalytic system.

In both cases the monomer is attached by the ^{13}C -enriched methyl at the less hindered carbon. However it is surprising that the arrangement of the first unit is not as regular as that of the next ones. Actually no 1,4 units are detected along the polymer chain. Dealing with a conjugated diolefin, one has to consider that the arrangement of a given monomer unit can be considered irreversible only after insertion of the next one, since the growing chain end is likely η^3 -bonded to the metal of the active species, and either one or the other allyl carbon (C_2 or C_4 of Figure 4) can attack the incoming new monomer.

Apparently, when $\text{R} = \text{CH}_3$, the C_2 and C_4 carbons have comparable chances of attacking the incoming monomer, while when R is the polymer chain, the attack occurs almost exclusively by the C_2 carbon.



4MPD = 4-methyl-1,3-pentadiene

Fig. 4. η^3 -coordination of the last inserted monomer unit

A tentative explanation of the observed experimental fact could be that back biting coordination of the penultimate monomer unit of the growing chain end could shift the coordination equilibrium reported in the Figure 5 towards the σ -alkyl form, forcing the 1,2 insertion.

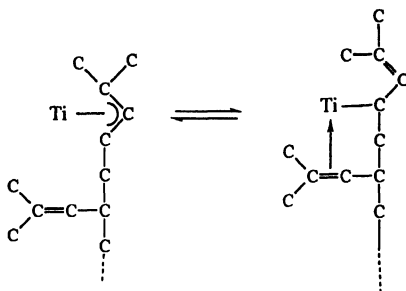


Fig. 5. η^3 - η^1 coordination equilibrium of the polymer chain end in the conjugated diene polymerization. The η^1 coordination is stabilized by the back-biting of the penultimate monomer unit of the growing polymer chain.

Possibly the σ -coordination of the chain, stabilized by the back biting coordination of the penultimate monomeric unit, could also account for the exceedingly high reactivity of this monomer.

This hypothesis was checked by copolymerizing 4-methyl-1,3-pentadiene with ethylene (18). The product present a random distribution of the two comonomers, and a considerable amount of 1,4-diene units chemically bound to ethylene units was detected in the corresponding ^{13}C NMR spectrum. Apparently as expected, the lack of a double bond in the penultimate unit of the growing chain decreases the chemoselectivity of the incorporation of 4-methyl-1,3 pentadiene as well as during the initiation step.

When attempting to copolymerize 1,3-butadiene with 4-methyl-1,3-pentadiene, Porri had previously obtained essentially *cis*-1,4-polybutadiene while the other monomer did not appreciably react (19). Since 4-methyl-1,3-pentadiene is by far more reactive than 1,3-butadiene in the homopolymerization, Porri suggested that

butadiene coordination (quite likely η^4) is much more favoured than that (possibly η^2 due to the steric demand of the two geminal methyl substituents) of 4-methyl-1,3-pentadiene (20).

Polymerization of selectively deuteriated (Z)-1,3-pentadiene

As reported by Porri and coworkers (15,20), polymerization of (Z)-1,3-pentadiene in the presence of the CpTiCl₃-MAO catalytic system affords prevalingly isotactic 1,4-*cis* polymer, at +20 °C, and 1,2 syndiotactic polymer at low temperature (-20°C). In addition, the polymerization is much faster at -20 °C than at +20 °C. These authors tentatively explain the intriguing behavior of this monomer suggesting *trans* η^2 coordination of (Z)-1,3-pentadiene to Ti at low temperature, followed by the attack of the growing chain end. At +20 °C the η^2 coordination of the monomer could evolve to η^4 before insertion ensues. This hypothesis is able to rationalize the higher polymerization rates for lower temperature and the 1,4-monomer units observed at higher temperature.

Other authors (21) suggest that although the *cisoid* conformation of the isolated monomer is less stable than the *trans* one, η^4 coordination could be stabilized by H-agostic interactions between the methyl of the coordinated monomer and the metal, overcoming the higher energy of the *cisoid* conformation. Then, *cis*-1,4 or 1,2 syndiotactic insertion would occur through the attack of the C₄ or the C₂ of the η^3 coordinated growing chain end to the C₁ of the η^4 coordinated monomer (see Figure 6). The temperature dependence of the chemoselectivity could be due to the formation of H-agostic bonds with the metal involving the methyl group of the anti- η^3 -coordinated terminal of the growing chain, which could make the C₂ atom more accessible for the insertion reaction.

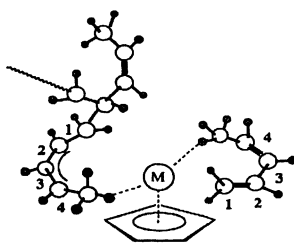


Fig. 6. H-agostic interactions of the methyl groups of the coordinated monomer unit and of last inserted monomer unit with the metal of the active species.

However, polymerization of 4,5,5,5-(Z)-1,3-pentadiene-*d*₄ and (Z)-1,3-pentadiene in the presence of CpTiCl₃-MAO at different temperatures (22) have shown that the chemoselectivity and its temperature dependence are not affected by the isotopic substitution on the monomer (see Table 1).

Copolymerization of the two monomers provided copolymers with identical composition as the feed, within the limits of the experimental accuracy. The lack of any appreciable isotopic effect suggests that agostic interactions might not play noticeable role in the mechanism of this polymerization probably due to the much stronger interactions of the unsaturations of both the monomer and the growing chain end with Ti, as suggested, in the previous section, for 4-methyl-1,3-pentadiene (see Figure 5).

Table 1. Polymerization conditions and structures of poly-(*Z*)-1,3-pentadiene (*Z*-PD).

| run ^a | Z-PD (g) | Z-PD-d ^b (g) | T (°C) | t (h) | yield (g) | polymer structure |
|------------------|----------|-------------------------|--------|-------|-----------|---|
| 1 | - | 0.30 | -20 | 18 | 0.155 | 1,2-syndiotactic |
| 2 | 0.30 | - | -20 | 18 | 0.152 | 1,2-syndiotactic |
| 3 | - | 0.30 | +10 | 20 | 0.102 | 1,4-cis (82%) 1,2-syndiotactic (18%) |
| 4 | 0.30 | - | +10 | 20 | 0.101 | 1,4-cis (82%) 1,2-syndiotactic (18%) |
| 5 | 0.33 | 0.34 | -20 | 18 | 0.118 | 1,2-syndiotactic ^c |
| 6 | 0.33 | 0.34 | +20 | 20 | 0.100 | 1,4 cis ^c |

^a) All the runs were performed in a 100 ml glass-flask using 700 mg of MAO, 5.5 ml of toluene, and 2×10^{-5} mol of CpTiCl₃.

^b) 4,5,5,5-tetradeutero-(*Z*)-1,3-pentadiene.

^c) The relative abundance of the two monomers in the polymer is the same as in the feed.

As a matter of fact, copolymerization of (*Z*)-1,3-pentadiene with ethylene at -20 °C produces random copolymers containing a relevant amount of *cis*-1,4-pentadiene adjacent to ethylene, suggesting once again a relevant role of the growing chain-end in determining the chemoselectivity of the insertion of the incoming monomer.

Possibly, the back biting coordination of the penultimate unsaturated monomeric unit to the titanium of the active species could be temperature dependent and determine chemoselectivity of the insertion reaction. (see Figure 7)

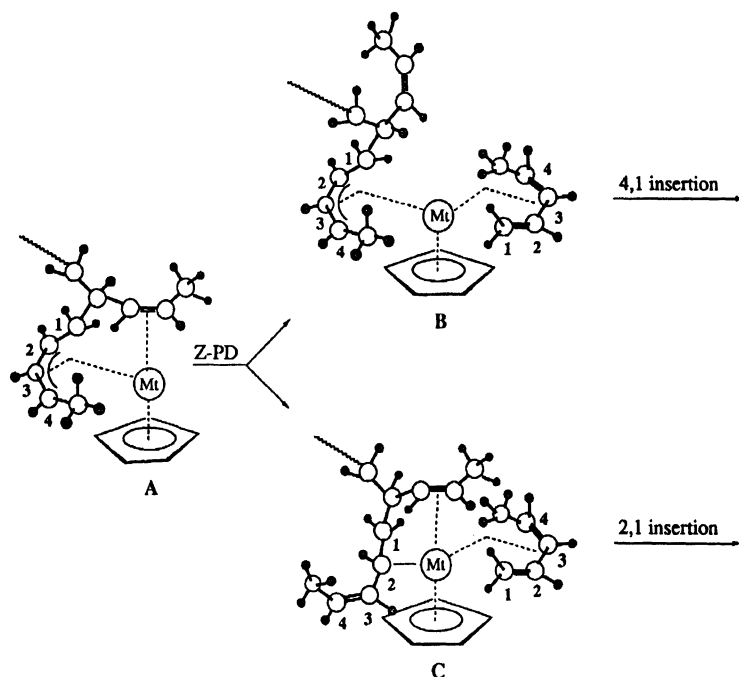


Fig. 7. Schematic presentation of a possible mechanism for chemoselective polymerization of (*Z*)-1,3-pentadiene in the presence of CpTiCl₃ - MAO: (A) post-insertion intermediate following a 2,1 insertion. It involves a simultaneous *anti*- η^3 coordination of the allyl terminal and an η^2 coordination of the last double bond of the growing chain (“back-biting” coordination), (B) pre insertion intermediate involving an *anti*- η^3 coordination of the allyl terminal of the growing chain, leading to *cis*-4,1 insertion, (C) pre insertion intermediate involving an η^1 coordination of the allyl terminal and an η^2 coordination of the last double bond of the growing-chain, leading to 2,1 syndiotactic insertion

Styrene - 1,3-Butadiene Copolymerization

In a previous paper we tried to copolymerize 1,3-butadiene with styrene in the presence of the CpTiCl₃-MAO catalytic system (23). While 1,3-butadiene can be homopolymerized with higher activity than styrene by this catalyst, mixture of 1,3-butadiene and styrene turned out to produce less polymer than either monomer alone, under the same conditions. Even very low amount of 1,3-butadiene greatly depresses the polymerization rate.

We attempted to evaluate the reactivity ratios by plotting the composition of the feeds and that of the resulting polymers according to the Fineman and Ross equation. Unfortunately, the values we found are not quite reliable, because what actually happens is that styrene polymerization by the CpTiCl₃ - MAO catalyst is inhibited by 1,3-butadiene, at least under the conditions we used, and some stereoirregular polystyrene is produced through a mechanism unrelated to syndiotactic polymerization. A similar inhibition of 4-methyl-1,3-pentadiene

polymerization by 1,3-butadiene was previously reported by Porri for the 1,3-butadiene - 4-methyl-1,3-pentadiene pair (24). Most probably 1,3-butadiene coordination (likely η^4) almost completely prevent coordination (possibly η^2) of styrene and 4-methyl-1,3-pentadiene.

While styrene and substituted styrenes copolymerize giving *co*-syndiotactic copolymers (4) and 1,3-butadiene copolymerizes with isoprene giving *cis*-1-4 copolymers (23) the behavior of other comonomer pairs need further investigation since the results are much less easily predictable.

Conclusion

The polymerization behavior of conjugated diolefins, in the presence of CpTiCl₃-MAO catalytic system, is much less predictable than that of α -olefins or styrene monomers. The presence of two conjugated unsaturations may lead to different coordination modes of both the monomer and the growing chain, depending on the particular diolefin investigated. While this greatly complicates investigation of the reaction mechanism, these monomers can likely disclose particularly valuable information on the matter.

REFERENCES

- 1 Soga K, Park JR, Shioni Y (1991) *Polym Commun* 32:310
- 2 Canich JM, Hlatky GG, Turner HW Int Pat Appl WO 92 00,333, Chem Abstr (1992) 116:174967z
- 3 Ishihara N, Seimiya T, Kuramoto M, Uoi M (1986) *Macromolecules* 19: 2464
- 4 Grassi A, Longo P, Proto A, Zambelli A (1989) *Macromolecules* 22:104
- 5 Ready TE, Day RO, Chien JCW, Rausch MD (1993) *Macromolecules* 26:5822
- 6 Oliva L, Longo P, Grassi A, Ammendola P, Pellicchia C (1990) *Makromol Chem, Rapid Commun* 11:519
- 7 Longo P, Oliva P, Proto A, Zambelli A (1996) *Gazz Chim Ital* 126:377
- 8 Ricci G, Italia S, Porri L (1994) *Macromolecules* 27:868
- 9 Zambelli A, Pellicchia C, Oliva L, Longo P, Grassi A (1991) *Makromol Chem* 192:223
- 10 Chien JCW, Salajka Z, Dong S (1992) *Macromolecules* 25:3199
- 11 Longo P, Proto A, Zambelli A (1995) *Makromol Chem Phys* 196:3015
- 12 Grassi A, Pellicchia C, Oliva L, Laschi F (1995) *Macromol Chem Phys* 196:1093
- 13 Grassi A, Zambelli A, Laschi F (1996) *Organometallics* 15:480
- 14 Grassi A, Saccheo S, Zambelli A, Laschi F (1998) *Macromolecules* 31:5588
- 15 Ricci G, Italia S, Porri L (1994) *Macromolecules* 22:2186
- 16 Zambelli A, Ammendola P, Proto A (1989) *Macromolecules* 22:2186
- 17 Longo P, Proto A, Oliva P, Zambelli A (1996) *Macromolecules* 29:5500
- 18 Longo P, Grisi F, Proto A, Zambelli A (1997) *Macromol Rapid Commun* 18:183
- 19 Ricci G, Porri L (1997) *Macromol Chem Phys* 198:3647
- 20 Ricci G, Porri L, Giarrusso A (1995) *Macromol Symp* 89:383
- 21 Guerra G, Cavallo L, Corradini P, Fusco R (1997) *Macromolecules* 30:677

- 22 Longo P, Guerra G, Grisi F, Pizzuti S, Zambelli A (1997) *Macromol Chem Phys* 199:149
- 23 Zambelli A, Proto A, Longo P, Oliva P (1994) *Macromol Chem Phys* 195:2623
- 24 Ricci G, Porri L (1997) *Macromol Chem Phys* 198:3655

Half-Vanadocene Catalyst for Butadiene Polymerization

S.Ikai, M.Suzuki, N.Tsujimoto, Y.Iwamoto, S.Yuasa, J.Yamashita,

M.Murakami, Y.Kai, and T.Yano

UBE INDUSTRIES LTD. Polymer Research Laboratory
8-1, Goiminamikaigan, Ichihara, Chiba 290-0045 Japan
Email:14573u@ube-ind.co.jp

Abstract.

CpVCl_3 in combination with either MAO or $(\text{C}_6\text{H}_5)_3\text{CB}(\text{C}_6\text{F}_5)_4/\text{TEA}$ was found a remarkably active catalyst system in butadiene polymerization relative to catalyst systems formed from a titanium analogue, Cp_2VCl_2 and Cp_2VCl . For the $\text{CpVCl}_3/(\text{C}_6\text{H}_5)_3\text{CB}(\text{C}_6\text{F}_5)_4/\text{TEA}$ system, the dependencies of conversion on time, B/V mole ratio, an amount of TEA, and the dependency of molecular weight of polybutadiene on time have been examined. The catalyst system gives polymers with very high molecular weights and narrow polydispersities. The molecular weight and the conversion decrease with an increase in a feed of hydrogen gas as a chain transfer agent. The polymers consist of high 1,4-cis units and nearly 10% of 1,2-vinyl units. The sequence distribution of 1,4 and 1,2 units was found random by ^{13}C -NMR analysis.

Introduction

Metallocene/MAO catalyst systems have been developed for olefin polymerization, in particular, because of the advantages in catalyst activity and the controls of polymer structure, comonomer incorporation and etc., by modifying the ligand structure. From this, it can be of great interest to study the catalyst performances of metallocenes on conjugated diene polymerization. Until now, various Ziegler Natta type catalysts are known to give polybutadienes with their respective structures such as 1,4-cis, 1,4-trans, and syndio-1,2-vinyl units[1]. However, the application of metallocene/MAO catalyst systems to conjugated diolefin polymerization has been limited to a few kinds of metallocenes. Some of the reported metallocenes as precatalysts having substantial activities are CpTiCl_3 , CpTiCl_2 [2], $(\text{RCp})\text{TiCl}_3$; ($\text{R}=\text{MeOCOCH}_2$, Me_3Si , tBu)[3], $(\text{MeCp})\text{VCl}_2(\text{PEt}_3)_2$, and Cp_2VCl [4]. Our study on butadiene polymerization has been directed to the half-vanadocene/MAO or $(\text{C}_6\text{H}_5)_3\text{CB}(\text{C}_6\text{F}_5)_4$ catalyst system in an attempt to probe the above mentioned advantages of homogeneous catalysts observed in olefin polymerizations.

Experimental

Metallocenes and half-metallocenes as precatalysts have been prepared by the methods reported; CpTiCl_3 [5], Cp_2VCl and $\text{CpVCl}_2(\text{PMe}_3)_2$ [6,7], and Cp_2VCl_2 and CpVCl_3 [8]. We obtained cocatalysts from TOSOH AKZO CORP., as toluene solutions of triethylaluminum (TEA), modified methylalumoxane (MMAO) which comprises hydrolyzed triisobutylaluminum in part and hydrolyzed trimethylaluminum, and a powder of $(\text{C}_6\text{H}_5)_3\text{CB}(\text{C}_6\text{F}_5)_4$.

Butadiene polymerizations were carried out in a mixture of toluene and butadiene in a 300ml flask with a stirrer under nitrogen atmospheric pressure. The polymerization was initiated by adding the toluene solutions of a cocatalyst and a precatalyst under the conditions as indicated in each table and figure. Hydrogen gas of 1 to 10ml was introduced by a syringe into the reactor before adding a precatalyst toluene solution. Polymerization was terminated by adding an antioxidant of Irganox 1076 dissolved in a HCl-EtOH solution.

Molecular weights (M_n and M_w) of polymers were obtained by TOSOH SC-8010 GPC equipped with TSK gel (HXL-H and GMHXL) columns at 40°C using THF as an eluent and polystyrene as a standard. Microstructures were measured by an IR spectrometer for CS_2 solutions of polymers measuring absorption peaks at 740cm^{-1} , 910cm^{-1} , and 980cm^{-1} for 1,4-cis, 1,2-vinyl, and 1,4-trans units, respectively. Sequence distributions were determined [9,10] by JEOL EX-400 ^{13}C -NMR (100MHz) at 130°C using *o*-DCB/ $\text{C}_6\text{D}_6(4/1)$ as a solvent and TMS as an internal standard.

Results and Discussion

The polymerizations of butadiene were performed with the new catalyst systems, CpVCl_3 in combination with either modified MAO (MMAO) or $(\text{C}_6\text{H}_5)_3\text{CB}(\text{C}_6\text{F}_5)_4/\text{TEA}$ as an activator. Table 1 summarizes the results of butadiene polymerization with various metallocenes and half-metallocenes for the comparison of the present CpVCl_3 catalyst with other known catalysts.

A half-metallocene and a metallocene of vanadium form much active catalyst systems relative to the titanium analogs (Run 1 vs. 7, 2 vs. 8 and 3 vs. 6). The vanadocenes, $\text{Cp}_2\text{VCl}_2(+4)$ and $\text{Cp}_2\text{VCl}(+3)$ is much less active than the half-vanadocene, $\text{CpVCl}_3(+4)$ (Run 4,6 vs. 7) as observed for the titanium analogs (Run 1 vs. 3) presumably because of the coordinatively saturated metallocenes for butadiene. For the half-vanadocenes, $\text{CpVCl}_3(+4)$ is much more active than $\text{CpVCl}_2\text{L}_2(+3)$ (Run 5 vs. 7) and the less activity for the latter would be ascribed to coordinative blocking to butadiene by two equivalents of PMe_3 as a strong Lewis base. In fact, we have found that the addition of triethylphosphine ($\text{P}/\text{V}=2$) to the $\text{CpVCl}_3/(\text{C}_6\text{H}_5)_3\text{CB}(\text{C}_6\text{F}_5)_4/\text{TEA}$ catalyst system decreased the catalyst activity intensively.

The Borate/TEA activator is superior to MMAO for CpVCl_3 (Run 7 vs. 8) and the former catalyst system was found to have a remarkably high activity as much as $30\text{kg}/\text{mmol V}(\text{Bd}:11[\text{M}])\text{hr}$.

Both the metallocenes(+4) and the half-metallocenes(+4) shown in Table 1 gave polybutadienes with very high molecular weights, narrow molecular weight distributions, and microstructures of predominant 1,4-cis units (83 to 91%). The difference of polymer structure observed among the titanium and the vanadium catalysts is not distinctive. It is assumed that the active species from the CpVCl_3 catalyst is a cationic complex with one Cp ligand, its structure being geometrically similar to $[\text{CpTiR}(\text{C}_4\text{H}_6)]^+$ proposed for CpTiCl_3 catalyst[11].

Table 1. Butadiene Polymerization with Various Metallocenes

| Run No. | catalyst | mole 10^{-6} | Al/V ratio | time min. | conversion % | Mw 10^{-4} | Mw/Mn | structure(%) ^{*3} | | |
|---------|----------------------------|----------------|------------|-----------|--------------|--------------|-------|----------------------------|-----|------|
| | | | | | | | | trans | 1,2 | cis |
| 1 | CpTiCl_3 | 5 | 1000 | 60 | 12.9 | 221 | 1.82 | 1.1 | 15 | 83.6 |
| 2 | CpTiCl_3 | 5 | *1 | 60 | 30.3 | 209 | 1.88 | 1.0 | 15 | 83.9 |
| 3 | Cp_2TiCl_2 | 5 | 1000 | 60 | 0 | --- | --- | --- | --- | --- |
| 4 | Cp_2VCl | 1 | 5000 | 60 | 1.46 | 15 | 3.09 | 1.5 | 8.6 | 89.9 |
| 5 | CpVCl_2L_2 | 1 | *2 | 5000 | 0.61 | 11 | 3.21 | 1.7 | 8.8 | 89.5 |
| 6 | Cp_2VCl_2 | 5 | 1000 | 60 | 4.55 | 189 | 2.94 | 1.3 | 7.6 | 91.1 |
| 7 | CpVCl_3 | 1 | 5000 | 30 | 14.4 | 272 | 2.69 | 1.4 | 8.2 | 90.4 |
| 8 | CpVCl_3 | 1 | *1 | 20 | 28.6 | 203 | 2.80 | 1.3 | 8.4 | 90.3 |

Polymerization conditions: temperature 30°C, toluene 169ml, butadiene 32ml, *1 Metal/Borate/TEA=1/1.5/200, *2 L= PMe_3 , *3 IR spectroscopy

The dependencies of conversion on B/V mole ratio are shown in Fig. 1 for the $\text{CpVCl}_3/(\text{C}_6\text{H}_5)_3\text{CB}(\text{C}_6\text{F}_5)_4/\text{TEA}$ catalyst system. The maximum conversions were achieved at a ratio of nearly 1.4-1.5 for two different CpVCl_3 concentrations.

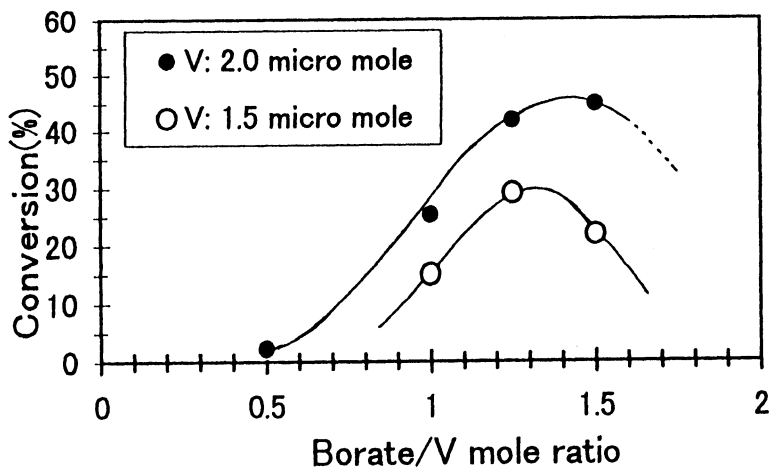


Fig. 1. The dependencies of conversion on B/V mole ratio(Bd:2M, TEA:200 micro moles)

Since butadiene polymerization was not observed without $(C_6H_5)_3CB(C_6F_5)_4$, the formation of cationic active species by the borate/TEA activator is highly assumed.

Fig. 2 gives conversion as a function of an amount of TEA used for three different $CpVCl_3$ concentrations ($B/V=1.5$). The polymerizations occurred only by the use of TEA of more than 100 micro moles and the maximum conversions were achieved by the use of TEA of 150-200 micro moles (Al/V mole ratio = 75-150).

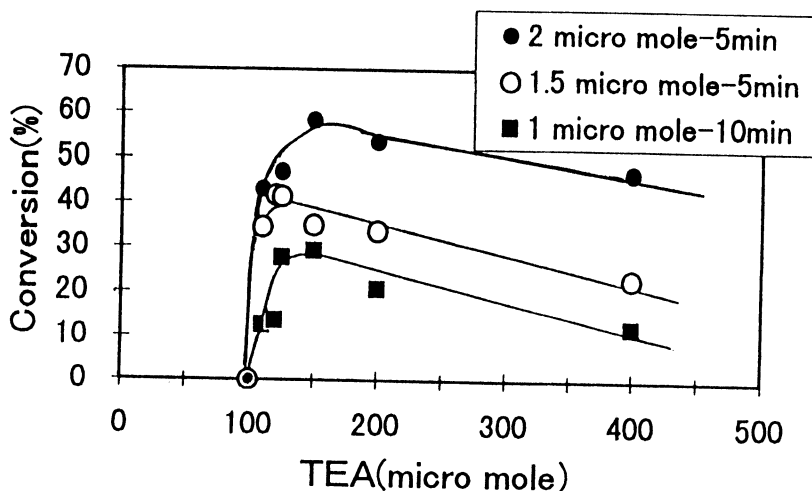


Fig. 2. The dependencies of conversion on an amount of TEA ($B/V:1.5$, $Bd:2M$)

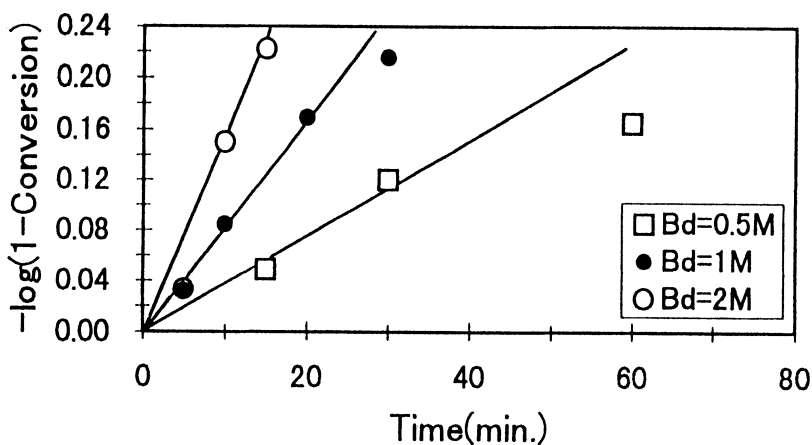


Fig. 3. Polymerization time vs. $-\log(1-\text{conversion})$ ($V:1\text{micro mole}$, $B/V:1.5$, $TEA:150\text{micro moles}$)

When a propagation rate(R_p) is expressed in the following equation, $R_p = k_p[Bd]F(V^*)$, wherein k_p is a propagation rate constant, $[Bd]$ is a concentration of butadiene, and $F(V^*)$ is a function of active species concentration, a plot of time vs. $-\log(1-\text{conversion})$ would exhibit a linear relationship with $k_pF(V^*)$ as a slope of the straight line, provided that $F(V^*)$ is constant in a course of polymerization. Fig. 3 shows plots of time vs. $-\log(1-\text{conversion})$ for three different $[Bd]$, having linearity at the early stage of polymerization.

Fig. 4 shows a relationship between $[Bd]$ and the slope of the lines obtained from Fig. 3. The slope increases with the concentration of $[Bd]$ and this result would indicate that $F(V^*)$ is dependent on $[Bd]$. Then, in that case, the deviations from the straight lines at a longer polymerization time observed in Fig. 3 can be ascribed to a decrease of $[Bd]$ and a consequent decrease of $F(V^*)$ with an increase of conversion.

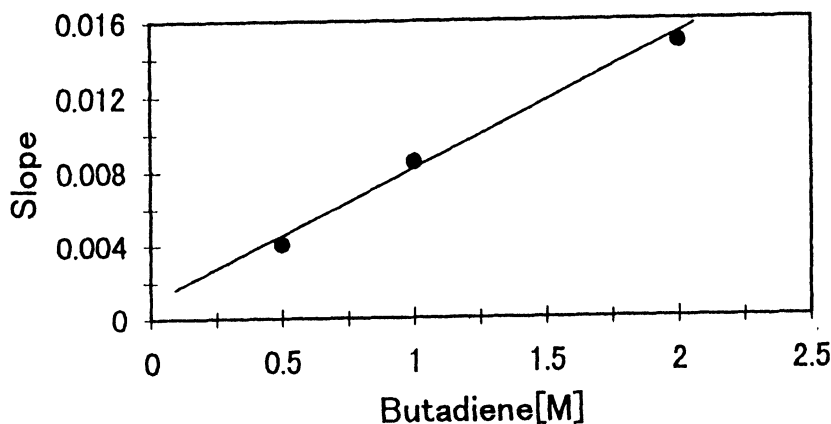


Fig. 4. Butadiene concentration vs. slope

As shown in Fig. 5, molecular weight(M_w) increases with time, but level off after 10min., indicating the presence of a chain transfer reaction. Since the molecular weight of the polymers are very high, a mechanistic study of the chain transfer reaction was not possible by the structural analysis of the polymer chain ends with a ^{13}C -NMR spectrometer.

The molecular weight of polybutadienes was decreased by the introduction of hydrogen gas to the polymerization system as have been well known in olefin polymerization with metallocene catalysts. As Fig. 6 shows, the molecular weight decreases sharply with an increase in a hydrogen feed while the conversion decreases gradually.

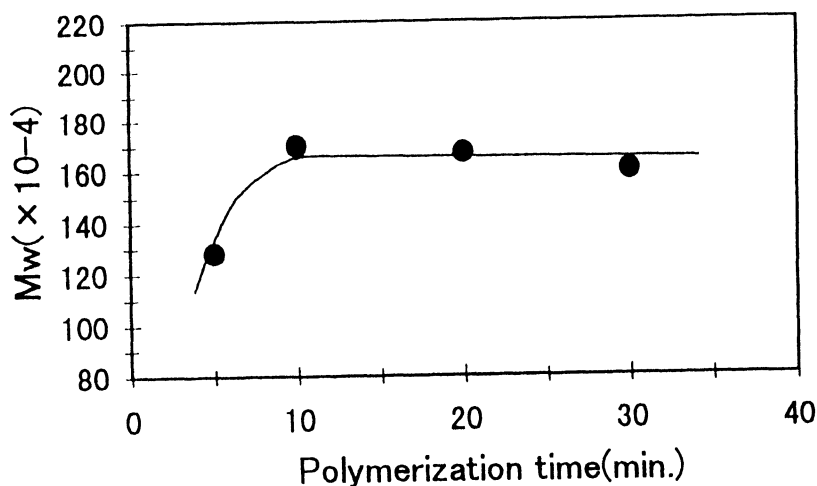


Fig. 5. The time dependency of Mw (V:1micro mole, Bd:1M, B/V:1.5, TEA:150micro moles)

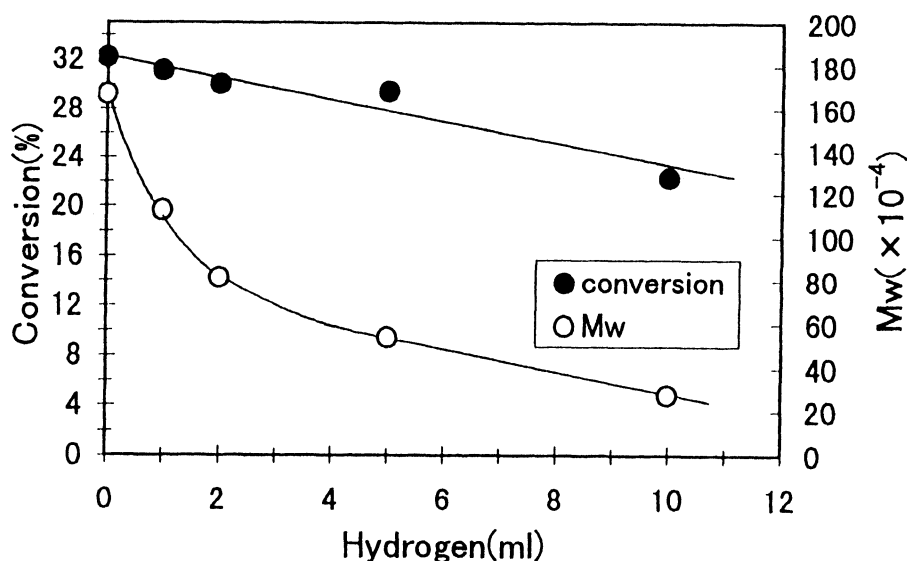


Fig. 6. The dependencies of Mw and conversion on hydrogen feed (V:1micro mole, Bd:1M, TEA:150micro moles)

The structural analysis of polybutadiene was performed by ^{13}C -NMR (Fig. 7) and the assignment of carbon chemical shifts based on sequences of trans, cis, and 1,2-vinyl units was listed in Table 2. Table 3 summarizes the fractions of cis, trans, and 1,2-vinyl units, and of the diad distribution of them, and the randomness of the distribution of 1,4 and 1,2 units. The observed value (1.05) of $P_{v-1,4}/2P_{vP_{1,4}}$ is close to the calculated value for a statistical random distribution. The random distribution of 1,4 and 1,2 units for polybutadiene is also reported for other polymers produced with

such as alkyl lithium and cobalt catalysts[9]. It can be said that even the present half-vanadocene catalyst system does not regulate the sequence distribution.

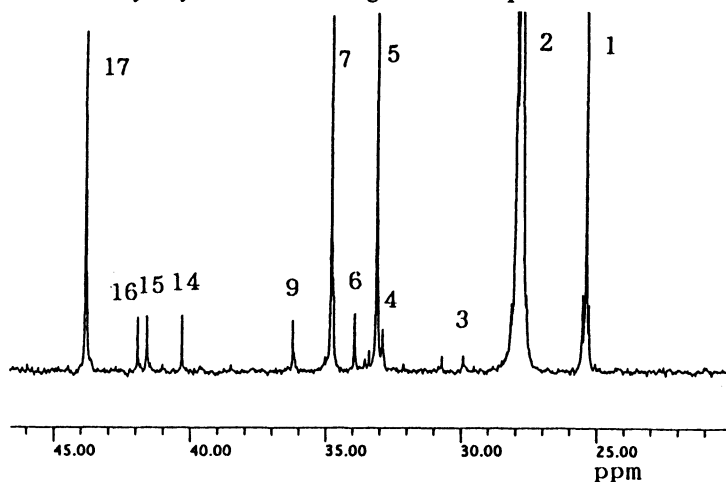


Fig. 7. ^{13}C -NMR spectrum of butadiene

Table 2. Structural analysis of polybutadiene by ^{13}C -NMR

| Sequence | Carbon*1 | Signal | Chemical shift | |
|-----------------------|-----------------------------------|--------|----------------|--------------|
| | | | Observed(ppm) | intensity(%) |
| Cis-1,2 | $\text{CH}_2(4)$ | 1 | 25.40 | 5.9 |
| Cis-1,4 / 1,4-Cis | $\text{CH}_2(4) / \text{CH}_2(1)$ | 2 | 27.84 | 74.5 |
| Trans-1,2 | $\text{CH}_2(4)$ | 3 | 29.93 | 0.2 |
| 1,2-1,2-cis(m) | $\text{CH}_2(1)$ | | ----- | 0 |
| Trans-1,4 / 1,4-trans | $\text{CH}_2(4) / \text{CH}_2(1)$ | 4 | 32.90 | 0.4 |
| 1,4-1,2-cis | $\text{CH}_2(1)$ | 5 | 33.13 | 5.7 |
| 1,2-1,2-cis(r) | $\text{CH}_2(1)$ | 6 | 33.94 | 0.7 |
| 1,4-1,2-1,4 | $\text{CH}_2(1)$ | 7 | 34.73 | 5.4 |
| 1,4-1,2-1,2(m) | $\text{CH}_2(1)$ | 8 | ----- | 0 |
| 1,4-1,2-1,2(r) | $\text{CH}_2(1)$ | 9 | 36.22 | 0.7 |
| 1,2-1,2-trans(m) | $\text{CH}_2(1)$ | 10 | ----- | 0 |
| 1,4-1,2-trans | $\text{CH}_2(1)$ | 11 | ----- | 0 |
| 1,2-1,2-1,2 | $\text{CH}_2(2)$ | 12 | ----- | 0 |
| 1,2-1,2-trans(r) | $\text{CH}_2(1)$ | 13 | ----- | 0 |
| 1,2-1,2 | $\text{CH}_2(1)$ | 14 | 40.32 | 0.6 |
| 1,4-1,2-1,2 | $\text{CH}_2(2)$ | 15 | 41.58 | 0.6 |
| 1,2-1,2-1,4 | $\text{CH}_2(2)$ | 16 | 41.92 | 0.6 |
| 1,4-1,2-1,4 | $\text{CH}_2(1)$ | 17 | 43.81 | 4.7 |

*1 Carbon: 1,4 unit $-\text{C}(1)\text{H}_2\text{C}(2)\text{H}=\text{C}(3)\text{HC}(4)\text{H}_2-$,
 1,2 unit $-\text{C}(1)\text{H}_2\text{C}(2)\text{H}(\text{C}(3)\text{H})=\text{C}(4)\text{H}_2-$

Table 3. Sequence distribution of polybutadiene

| Sequence | Observed(%) | Random calculated (%) | Alternative calculated(%) | IR method |
|-------------------------|-------------|--------------------------|------------------------------|-----------|
| Cis-1,2 | 11.5 | 11.2 | 12.8 | |
| 1,2-cis | 11.9 | 11.2 | 12.8 | |
| Trans-1,2 | 0.4 | 0.14 | 0.16 | |
| 1,2-trans | 0 | 0.14 | 0.16 | |
| Cis-Cis | 73.9 | 73.8 | 73.1 | |
| Trans-Cis | 0.9 | 0.94 | 0.9 | |
| Cis | 85.9 | 85.0 | 85.9 | 88.3 |
| Trans | 1.1 | 1.1 | 1.1 | 0.7 |
| 1,2 | 13.0 | 13.1 | 13.0 | 11.0 |
| $P_{v-1,4/2}$ | 0.119 | 0.113 | 0.130 | |
| $P_vP_{1,4}$ | 0.113 | 0.113 | 0.113 | |
| $P_{v-1,4}/2P_vP_{1,4}$ | 1.05 | 1.00 | 1.15 | |

References

- [1] G. Ricci, S. Italia, C. Comitani, and L. Porri, *Polymer Commun.*, 32(1991) 514.
- [2] P. Longo, P. Oliva, A. Proto, and A. Zambelli, *Gazzetta Chimica Italiana*, 126(1996)377.
- [3] T. Kase, A. Miyazawa, K. Soga, et al., *Polymer Prepr. Jpn.*, 47(1998)293.
- [4] G. Ricci, A. Panagia, and L. Porri, *Polymer* 37(1996)363.
- [5] A. M. Cardoso, R. J. H. Clark, and S. Moorhouse, *J. Chem. Soc., Dalton Trans.*, 7(1980) 1156.
- [6] J. Nieman, J. H. Teuben, J. C. Huffman, and K. G. Cauiton, *J. Organomet. Chem.*, 255(1983)193.
- [7] L. E. Manzer, *J. Organomet. Chem.*, 110(1976)291.
- [8] D. B. Morse, D. N. Hendrickson, T. B. Rauchfuss, and S. R. Wilson, *Organometallics*, 7(1988)496.
- [9] H. Sato, K. Takebayashi, and Y. Tanaka, *Macromolecules*, 20(1987)2418.
- [10] J. Furukawa, E. Kobayashi, *Die Makromolekulare Chemie*, 175(1974)237.
- [11] G. Ricci, S. Italia, A. Giarrusso and L. Porri, *J. Organomet. Chem.*, 451(1993) 67.

Chemical Functionalization of Polypropylene with a V-based Living Polymerization Catalyst

Masahide Murata, Yoshifumi Fukui,

Japan Chemical Innovation Institute
NIMC,1-1 Higashi, Tsukuba, Ibaraki 305,Japan

Kazuo Soga

Japan Advanced Institute of Science and Technology
1-1 Asahidai, Tatsunokuchi, Nomi-gun, Ishikawa 923-12, Japan

Abstract.

The $V(acac)_3$ ($acac = acetylacetonato$)/ $AlEt_2Cl$ catalyst was modified by reacting with α,ω -unconjugated diene compound, and the resulting catalyst was applied to the polymerization of propylene. The polymer produced showed a bimodal molar mass distribution, where the higher molecular weight ($M_n(h)$) was approximately twice of the lower molecular weight ($M_n(l)$). From a detailed analysis of the polymer quenched with CO , the $M_n(h)$ fraction was confirmed to have a telechelic structure. Such a telechelic polymer might be produced by the dinuclear vanadium species formed between $V(acac)_3$ and an α,ω -unconjugated diene compound.

INTRODUCTION

A soluble $V(acac)_3/AlEt_2Cl$ system as a catalyst for olefin polymerizations was studied from the initial stage of the coordination polymerization chemistry opened by Ziegler and Natta. Natta found as early as in 1962 that the vanadium catalyst system initiates the polymerization of propylene at a low temperature[1]. It was also demonstrated that the polymerization of propylene preferentially proceeds through 2,1-insertion mechanism [2-4]. On the other hand, Doi found in 1986 that the living polymerization of propylene takes place with the catalyst[5].

Afterwards, a big research effort has been put to develop the terminally functionalized polypropylenes, and a variety of many different types of functional groups have been successfully introduced into the propagation chain ends[6-9]. Novel A-B type block copolymers have been also synthesized by using this technique[10].

Thus, the development of such a new methodology has certainly expanded the potential appreciability of polypropylene. However, synthesis of a „telechelic“

polypropylene, i.e., introduction of two functional groups at both chain ends of polypropylene, is not easy with this technique. Shiono has demonstrated that such a telechelic polypropylene can be synthesized with a conventional Ti-based Ziegler-Natta catalyst[11] using a specially designed cocatalyst (alkylaluminiums or alkylzincs), which functions as a transfer reagent to incorporate a functional group at the initiation chain end. But the functional groups available are limited due to the deactivation by most of polar groups.

We have recently developed a new technology which potentially affords to yield a variety of telechelic polypropylenes[12]. This paper summarizes the results of propylene polymerization obtained so far with the technology.

EXPERIMENTAL

Living Polymerization of Propylene

In a 50 ml schlenk flask with a magnetic stirrer, 5 ml of an AlEt_2Cl (5 mmol) solution in toluene and, if necessary, the prescribed amount of cyclohexene was introduced. The solution was cooled down to $-78\text{ }^\circ\text{C}$ in a dry ice methanol bath, followed by the addition of 0.025 mmol of unconjugated diene and 2 ml of a $\text{V}(\text{acac})_3$ (0.5 mmol) solution in toluene. After the mixture was aged for 60 to 120 min at $-78\text{ }^\circ\text{C}$, the solution was put into the polymerization reactor (300 ml flask) containing 0.83 mol of liquid propylene to start the polymerization. Polymerization was quenched at $-78\text{ }^\circ\text{C}$ by adding of acidic methanol. The polymer produced was washed several times with methanol and dried under vacuum at room temperature.

CO Quenching Method

The fundamental experimental method of the quenching reaction of living polymerization system with CO was described in the literature[8]. Polymerization used for the CO quenching was carried out in a stainless steel autoclave (100 ml of volume) with 0.28 mol of liquid propylene at $-65\text{ }^\circ\text{C}$. The reactor was connected to another autoclave charged with 30 atm of CO through a stop valve. The CO gas was introduced into the polymerization reactor by opening the valve after 2 h of polymerization. The polymer terminated by CO was purified by washing with plenty of methanol.

Polymer Analyses

In the case of bimodal molar mass distribution, the curve deconvolution was conducted based on the Gaussian distribution to evaluate the weight fraction ratio of higher and lower molecular weight polymers.

The CO terminated polymer was fractionated by a circulated chromatographic method with Nippon Bunseki Kogyo LC-908 in chloroform at room temperature. The molecular weights of the fractionated samples were measured at 140 °C with a Senshu Science SSC7100 using ODCB as the solvent and calibrated by polystyrene standards. The IR analysis of the fractionated polymer was conducted with a Perkin Elmer PARAGON1000 spectrometer. The number of CO groups per one polypropylene chain was calculated by using the correlation established in a reference[8].

Analysis of the reaction products of $V(acac)_3/AlEt_2Cl$ with unconjugated dienes

The reaction of the $V(acac)_3/AlEt_2Cl$ catalyst with a unconjugated diene was conducted in deuterated toluene (toluene- d_8) under similar conditions to those of the propylene polymerization. The reaction was terminated by adding a concentrated hydrochloric acid solution in ice water. The toluene- d_8 solution was washed with aqueous HCl and dried over magnesium sulfate. The reaction products in the organic layer were analyzed by 270 MHz 1H -NMR spectrometer (JEOL GSX series) and GPC.

RESULTS AND DISCUSSION

Prior to polymerization, the catalyst system was aged either in the absence or presence of cyclohexene (CH) as described above. It was confirmed that CH is not polymerized under these conditions. Three kinds of unconjugated dienes, i.e., 1,7-octadiene (OD), 1,8-nonadiene (ND) and 1,9-decadiene (DD) were tested in this study. Since we have already found that the fraction of the active vanadium, which functions as the living polymerization initiator in the ordinary propylene polymerization with $V(acac)_3/AlEt_2Cl$ catalyst system, is approximately 10 % [13], we used here each of the unconjugated dienes in the amount of 5 mol % for the $V(acac)_3$ compound (active $V(acac)_3$ /unconjugated diene = 2/1 mol/mol). Table 1 summarizes the results of propylene polymerization together with some analytical data of resulting polymers. In the case of bimodal molar mass distribution (MMD), the GPC curve was deconvoluted. The area ratio of the two deconvoluted MMD curves is expressed as area% (h/l) in Table 1.

It is evident from the results obtained in Runs No. 1 and 2 that the number of the active species markedly increases when the catalyst system is aged in the presence of cyclohexene (CH). Similar results were also obtained even when the catalyst system was aged in the presence of OD (cf. Runs No.3 to 5). Taking the previous information [14] into consideration, it may be plausible to speculate that the active vanadium species are stabilized by the coordination of a CH molecule. More quantitative analyses on the number of active sites will be made later on.

The polymers produced with the catalysts aged in the presence of the unconjugated dienes display bimodal MMD's. The relative area of the $M_n(h)$ fraction increased up to 11.2 % when 25 ml of CH was used. It should be noted here that the ratio of $M_n(h)/M_n(l)$ is always kept at around 2. The use of 1,8-

nonadiene (ND) or 1,9-decadiene (DD) in place of OD (Run 6 and Run 7) also gave similar results. However, the relative area % (h/l) was dependent upon the unconjugated dienes. Among the three unconjugated dienes employed in the present study, ND gave the highest area % (h/l).

Table 1. Results of propylene polymerization with the $V(acac)_3/AlEt_2Cl$ catalyst^{a)}

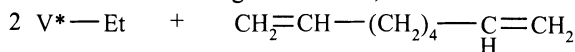
| Run No. | CH in ml | Diene | Polymer yield in g | M_n (h/l) | Area-% (h/l) ^{b)} | $M_n(h)/M_n(l)$ |
|---------|----------|-------|--------------------|-------------|----------------------------|-----------------|
| 1 | 0 | - | 0.15 | none/16200 | 0/100 | - |
| 2 | 25 | - | 0.68 | none/16200 | 0/100 | - |
| 3 | 0 | OD | 0.10 | 29000/14000 | <1/>99 | 2.1 |
| 4 | 2.5 | OD | 0.16 | 30000/15100 | 4.3/95.7 | 2.0 |
| 5 | 25 | OD | 0.46 | 23600/12000 | 11.2/88.8 | 2.0 |
| 6 | 25 | ND | 0.83 | 29200/15200 | 22.8/77.2 | 1.9 |
| 7 | 25 | DD | 0.72 | 27900/14200 | 17.2/82.8 | 2.0 |

a) Conditions; aging: toluene = 6.4 ml, temperature = -78 °C
aging time: 1 h for the systems without diene and with OD, 2 h for those with ND and DD; $V(acac)_3$ = 0.5 mmol, $AlEt_2Cl$ = 5 mmol, diene = 0.025 mmol.

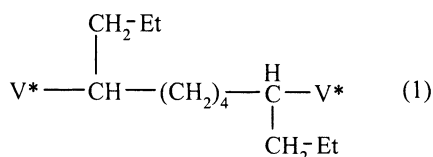
Polymerization: propylene (liq). = 0.83 mol, temperature = -78 °C, time = 2 h.

b) h/l: high/low molecular weight

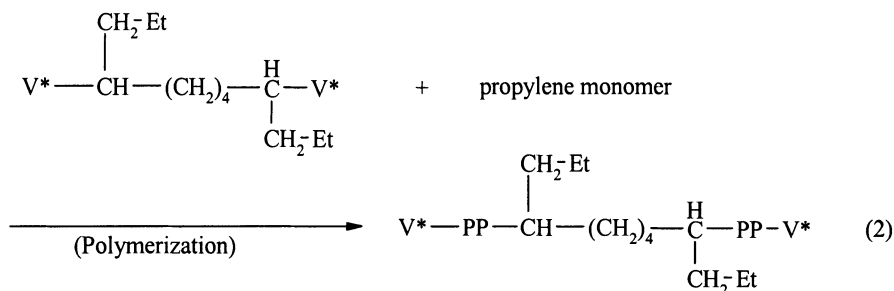
Fig.1. illustrates the MMD curve for the polymer obtained in Run. 6, which clearly displays a bimodal shape. It could be confirmed that each fractions of polymers had narrow M_w/M_n values at around 1.1. The $M_n(h)$ fraction might be formed in terms of the following mechanism;



(Formation of dinuclear active species) \longrightarrow



where V^*-Et denotes the active vanadium species formed in the original catalyst. The two C=C bonds in the unconjugated diene may react with the two V^*-Et bonds by 2,1-insertion mode[15], resulting in the formation of a bifunctional species (V^*-V^*). Accordingly, the polymer chain grows up to two directions simultaneously, maintaining the living polymerization characteristic.



Since the reaction (1) does not proceed quantitatively, the resulting catalyst might contain a part of the original mononuclear active species ($\text{V}^*\text{-Et}$). The number of each active species was estimated from the polymer yield and M_n in Tab. 1. The results are given in Tab. 2.

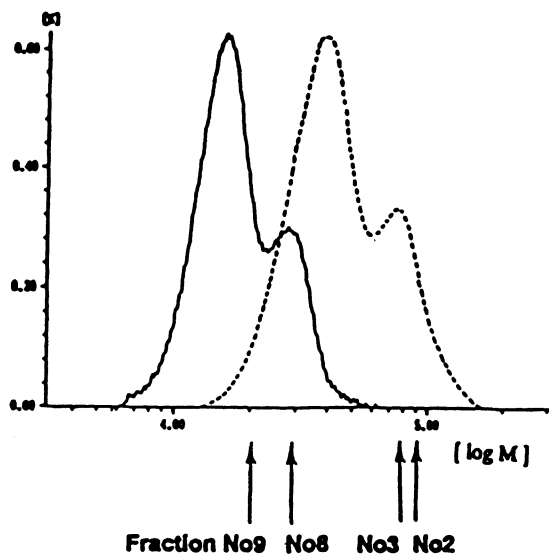


Fig. 1. MMD curves for polypropylenes: (—)MMD of the polymer obtained in Run No. 6; (---): MMD of the polymer quenched with CO. Fractions No. correspond to those in Tab. 6.

Table 2. The number of each active sites formed in the present catalysts

| Run No. ^{a)} | Cyclohexene in ml | Diene | Active Vanadium ^{b)} | |
|-----------------------|-------------------|-------|-------------------------------|-----------|
| | | | V*-Et | V*-V* |
| | | | in % of V | in % of V |
| 1 | - | - | 1.9 | |
| 2 | 25 | - | 8.4 | |
| 3 | 0 | OD | 0.007 | 1.4 |
| 4 | 2.5 | OD | 0.05 | 2.0 |
| 5 | 25 | OD | 0.44 | 6.8 |
| 6 | 25 | ND | 1.3 | 8.4 |
| 7 | 25 | DD | 0.89 | 8.4 |

a) Runs No. correspond to those in Tab.1.

b) Active vanadium was calculated by the following equations;

Total active vanadium = Polymer Yield/ $M_n(l)$ /0.5 mmol of Vanadium x 100

V*-Et = Total active vanadium x weight fraction of $M_n(l)$

V*-V* = Total active vanadium x weight fraction of $M_n(h)$

As seen in Tab. 2, when the enough amount of CH was present, the total number of active sites was recovered to approximately 10 %, which is the equivalent level of the case of the ordinary living polymerization of propylene with the catalyst system[13]. This strongly suggests that CH should stabilize the active species. However, the selectivity to form the dinuclear active species (V*-V*) is not so high at the moment. To get a better information on this point, some additional experiments were conducted as follows.

Figures 2 and 3 show the ¹H-NMR spectra of the reaction products of the OD and ND with the catalyst mixture, where those of the OD and ND monomers are also shown for reference. In the spectra of reaction products, the signals assignable to the protons of C=C (5 to 6 ppm region) disappeared completely, clearly indicating that all the C=C bonds in diene molecule have been consumed by the reaction with the V catalyst. It has been reported that the oligomerization is took place when some linear type non-conjugate dienes are contacted with the V-based catalyst[16]. Indeed, a measurable amount of oligomers were produced when 1,7-octadiene or 2,6-bis(3-butenyl)-naphthalene was reacted with the V(acac)₃/AlEt₂Cl catalyst (Tab. 3).

Table 3. Results of oligomerization obtained from the mixture of dienes and $V(acac)_3/AlEt_2Cl$

| Diene | Oligomer Yield | M_n |
|---------------------------------|----------------|-------|
| | in mg | |
| 1,7-octadiene | 6 | 1100 |
| 2,6-bis(3-butenyl)- naphthalene | 14 | 620 |

Oligomerization conditions; $V = 0.5$ mmol, $AlEt_2Cl = 5$ mmol, diene = 0.025 mmol
 temperature = -78 °C

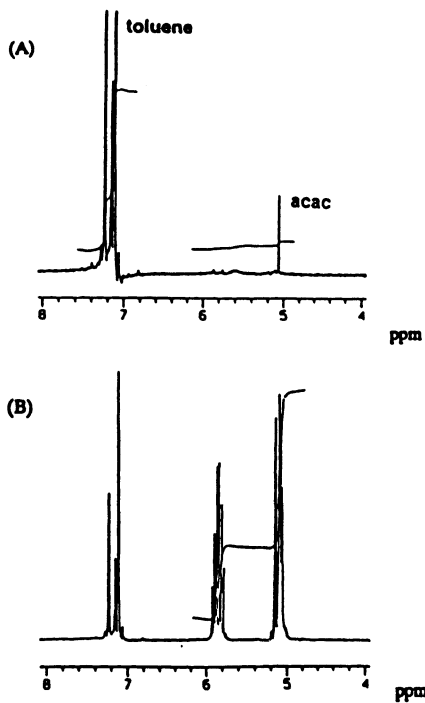


Fig. 2. 1H NMR spectra of (A) reaction product between $V(acac)_3/AlEt_2Cl$ and 1,7-octadiene and (B) 1,7-octadiene

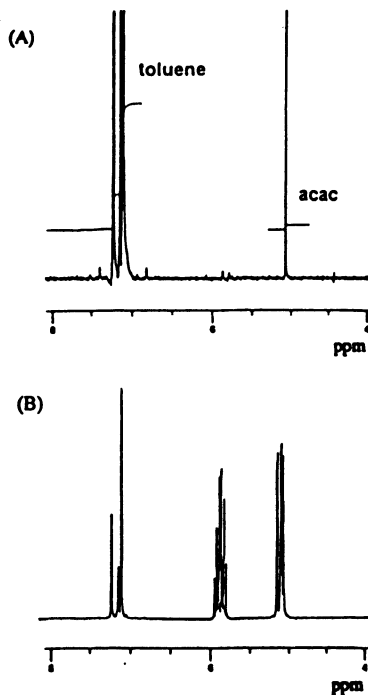


Fig. 3. 1H NMR spectra of (A) reaction product between $V(acac)_3/AlEt_2Cl$ and 1,8-nonadiene and (B) 1,8-nonadiene



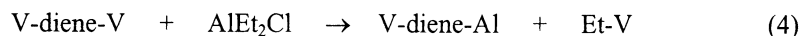
It is known that the cyclization also takes place simultaneously during the oligomerization of some linear non-conjugate dienes[16]. To suppress the cyclization reaction, 2,6-bis(3-butenyl)-naphthalene having a rigid structure was employed as a diene compound. However, the $M_n(\text{h})$ fraction did not increase so much as shown in Tab. 4.

Table 4. The results of propylene polymerization obtained with the catalyst abed in the presence of 2,6-bis(3-butenyl)-naphthalene ^{a)}

| Polymer | $M_n(\text{h/l})$ | Area-% | $M_n(\text{h})/M_n(\text{l})$ |
|------------|-------------------|--------------------|-------------------------------|
| Yield in g | | (h/l) ^b | |
| 0.90 | 30000/15100 | 13.0/87.0 | 2.0 |

- a) Conditions; aging: toluene = 6.4 ml, temperature = -78
 aging time = 1 h, $\text{V}(\text{acac})_3 = 0.5$ mmol, $\text{AlEt}_2\text{Cl} = 5$ mmol, diene = 0.025mmol.
 propylene (liq.) = 0.83mol, temperature = -78, time = 2 h.
 b) h/l: high/low molecular weight

We have carefully checked the previous data on the oligomerization/cyclization of dienes[16], and found that the oligomers have relatively broad MMD's ($M_w/M_n = 1.4$). Accordingly, slow chain transfer reactions might proceed during the oligomerization with the V-based catalyst. It is also known that some chain transfer reactions take place even in the ethylene polymerization with the V-based catalyst[5]. Taking these facts into account, we are currently considering the occurrence of such a chain transfer reaction as shown below.



These two side reactions as expressed in the eqs. (3) and (4) might be the main factors to suppress the selectivity to form the dinuclear active sites. However, a further study is necessary to fully understand the reaction mechanism between the V catalyst and a diene compound.

In order to confirm the structures of both $M_n(\text{h})$ and $M_n(\text{l})$ polymers, the propylene polymerization was terminated with CO. Since the polymerization was conducted at -65 °C, the MMD of resulting polymer shifted toward a higher molecular weight region as shown by a dotted line in Fig. 1. The polymer obtained was fractionated into 12 samples with circulated LC method. Four typical samples, which had been collected in the early and late stages of fractionation, were selected and subjected to the GPC and IR[8] analyses. The analytical results are shown in Tab. 5. The data

given in Tab. 5 clearly indicate that the lower and higher molecular weight polymers contain approximately one and two equivalents of CO, respectively.

Table 5. Analytical results of CO terminated polymers

| Fraction NO. | Weight in % | M_n | M_w/M_n | [CO] in mol/mol-PP |
|--------------|-------------|-------|-----------|--------------------|
| 2 | 4.2 | 92700 | 1.3 | 2.1 |
| 3 | 6.6 | 77300 | 1.3 | 2.3 |
| 8 | 7.6 | 30300 | 1.2 | 1.1 |
| 9 | 2.3 | 21500 | 1.2 | 1.3 |

Accordingly, the polymer fractions with higher molar mass is considered to have a telechelic structure (eq.(5)).



CONCLUSIONS

It was demonstrated that a telechelic polypropylene can be prepared by using the living vanadium catalyst combined with a suitable unconjugated diene compound. As the first telechelic sample, polypropylene possessing two aldehyde groups at both chain ends was synthesized. Due to the side reactions like diene oligomerization and the chain transfer by AlEt_2Cl , the selectivity to produce a telechelic polypropylene is not so high at the moment. A further study is thus in progress putting an emphasis on the improvement of the selectivity.

ACKNOWLEDGEMENT

This work was supported by NEDO for the project on Technology for Novel High-Functional Materials in Industrial Science and Technology Frontier Program, AIST.

REFERENCES

- [1] G. Natta, I. Pasquon, A. Zambelli, *J. Am. Chem. Soc.* **84** (1962) 1488
- [2] Y. Takegami, T. Suzuki, *Bull. Chem. Soc. Jpn.* **42** (1969) 848
- [3] T. Suzuki, Y. Takegami, *ibid.* **43** (1990) 1848

- [4] A. Zambelli, C. Tosi, M. C. Sacchi, *Macromolecules* **5** (1972) 649
- [5] Y. Doi, T. Keii, *Adv. Polym. Sci.* **73/74** (1986) 201
- [6] M. Murata, S. Ueki, *Kobunshi* **44** (1995) 436
- [7] Y. Doi, Y. Watanabe, S. Ueki, K. Soga, *Makromol. Chem. Rapid Commun.* **4** (1983) 533
- [8] Y. Doi, M. Murata, K. Soga, *ibid* **5** (1984) 811
- [9] Y. Doi, G. Hizal, K. Soga, *Makromol. Chem.* **188** (1987) 1273
- [10] H. Furuhashi, N. Murakami, S. Ueki, Y. Doi, *Polymer Preprint Jpn.* **40** (1991) 1755
- [11] T. Shiono, K. Yoshida, K. Soga, *Makromol. Chem. Rapid Commun.* **11** (1990) 169
- [12] M. Murata, Y. Fukui, K. Soga, *ibid.* **19** (1998) 267
- [13] Y. Doi, T. Koyama, K. Soga, *Makromol. Chem.* **186** (1985) 11
- [14] J. Boor, Jr., "Ziegler-Natta Catalysts and Polymerizations", Academic Press, New York (1979)
- [15] Y. Doi, F. Nozawa, M. Murata S. Suzuki, K. Soga, *Makromol. Chem.* **186** (1985) 1825
- [16] Y. Doi, N. Tokuhiko, K. Soga, *Kobunshi Ronbunshu* **46** (1989) 215

COPOLYMERIZATION OF ETHYLENE / ω -HYDROXY α -OLEFINS

Maria M. Marques¹; Sandra G. Correia¹; J. Ascenso¹; Alberto R. Dias¹; Mathew Blais²; Marvin D. Rausch² and James C.W. Chien^{2,3,4}

1. Centro de Química Estrutural, I. S.T., Av. Rovisco Pais 1049-001 Lisboa, Portugal.
2. Department of Chemistry, University of Massachusetts at Amherst, Amherst MA 01002, USA.
3. Department of Polymer Science and Engineering, University of Massachusetts, Amherst MA 01003, USA.
4. Amherst Polymer Technology, Inc. Amherst, MA 01002, USA.

Abstract. Two different homogenous catalyst systems, a C_2 symmetric *ansa*-zirconocene (1) and a α -Diimine Ni complexes (2) activated by methylaluminoxane were used in copolymerization of ethylene / α -olefins with OH functional groups. The α -olefins with OH functional group used as co-monomer in the polymerisation reactions were 5-Hexen-1-ol (3) and 10-Undecen-1-ol (4).

Catalyst (1) shows low activities when monomer (3) is used. Only with very small concentrations of monomer the activities are comparable to those obtained in the absence of the polar monomer (3). The activities obtained with catalyst (2) are higher, even when high concentrations of monomer (3) and (4) are used. ¹H and ¹³C NMR spectra, used to characterise the polymers, show the presence of carbons linked to OH groups. So, these catalysts systems allow us to obtain functionalised copolymers by direct polymerisation of ethylene / hydroxy- α -olefins.

Key words: Copolymerisation, Metallocenes, Hydroxy-Copolymers

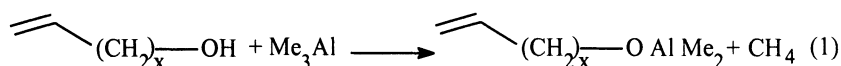
INTRODUCTION

This study has two objectives: The first is to develop methods to polymerize ethylene directly with α -olefins possessing active hydrogens such as OH. Secondly, we aimed to find catalyst structures, which are more tolerant to the polar monomers.

In this communication we report the results obtained with a C_2 - symmetric catalyst, *rac*-ethylene-bis(1- η^5 -indenyl)zirconium dichloride and a α -diimine nickel complex based catalyst.

RESULTS

Ziegler-Natta catalysts are usually poisoned by oxygen containing molecules. In this work the functional groups of polar monomers are protected by trimethylaluminium (TMA).



Et(Ind)₂ZrCl₂ (1)

The results of the copolymerizations of ethylene / 5-hexen-1-ol and ethylene / 10-undecen-1-ol obtained with the catalyst system (1) / MAO are given in the Tables 1 and 2.

In spite of the OH group being protected by TMA, the activities of the copolymerizations decrease with the increase of comonomer concentration in the feed.

Aaltonen et al. [1] have also studied the copolymerization of ethylene / 10-Undecen-1-ol using catalyst (1) but in their work MAO instead of TMA was employed to block the hydroxy groups. Our results, given in Table 2, show slightly higher activities than their's for the same concentration of alcohol in the feed thus proving that TMA is a better blocking agent for the hydroxy groups.

Table 1. Copolymerization of 5-Hexen-1-ol Catalysed by Et(Ind)₂ZrCl₂ / MAO System

| Run | [5-hexen-1-ol] | [Ethylene] | Polymer OH | Activity×10 ⁻⁶ |
|------------------|----------------|------------|---------------|---------------------------|
| No | mM | M | mol% | g /molZr.h |
| 246 ^b | 33 | 0.36 | 1.4 | 0.05 |
| 247 ^b | 82 | 0.36 | 5.0 | 0.03 |
| 248 ^b | 365 | 0.36 | | - |

Experimental conditions: 50 ml toluene; T=25°C; ^a[Zr]= 46 μM, [Al]/[Zr]=3500; ^b [Zr]= 57 μM, [Al]/[Zr]=2500; Method of treatment of the monomer - TMA 1/1 *in situ*.

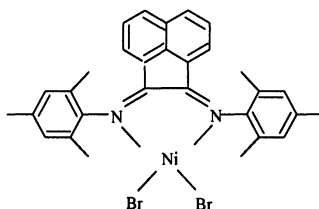
Table 2. Copolymerization of 10-Undecen-1-ol Catalysed by Et(Ind)₂ZrCl₂ / MAO System

| Run | [10-undecen-1-ol] | [Ethylene] | Polymer OH | Activity×10 ⁻⁶ |
|------------------|-------------------|------------|---------------|---------------------------|
| No | mM | M | mol% | g /molZr.h |
| 201 ^a | 49 | 0.36 | 4.5 | 1.40 |
| 202 ^a | 97 | 0.36 | 7 | 0.35 |
| 203 ^a | 196 | 0.36 | | 0.06 |
| 204 ^a | 293 | 0.36 | 10 | 0.04 |

Experimental conditions: 50 ml toluene; Method of treatment of the monomer -TMA 1/1 *in situ*. ^a[Zr]= 67 μM, [Al]/[Zr]=2140, T=25°C; ^b[Zr]= 66 μM, [Al]/[Zr]=2190, T=25°C; ^c[Zr]= 67 μM, [Al]/[Zr]=2140, T=25°C.

MesNDABNiBr₂ (2)

The catalyst precursor (2) has the structure shown below; the results obtained with the catalyst system, (2) / MAO are given in the Tables III and IV.



(2)

The amount of hydroxy group incorporated in the polymer was determined by ¹H. Typical ¹H and ¹³C spectra are shown in Figure 1.

Table 3. Copolymerization of 5-Hexen-1-ol Catalyzed by MesNDABNiBr₂ / MAO System

| Run <i>No</i> | [5-hexen-1-ol] <i>mM</i> | Treatment of monomer | [Ethylene] <i>M</i> | Polymer | Activity $\times 10^{-6}$ <i>g/molNi.h</i> |
|------------------|-----------------------------|----------------------------|------------------------|--------------------|---|
| | | | | OH <i>mol %</i> | |
| 159 ^b | - | | 0.30 | - | 2.57 |
| 51 ^a | 17 | MAO 1/1 | 0.30 | | 0.47 |
| 52 ^a | 35 | „ | 0.30 | | 0.42 |
| 53 ^a | 82 | not blocked | 0.30 | 1.0 | 0.17 |
| 155 ^b | 82 | TMA 1/1 <i>in situ</i> | 0.35 | 1.7 | 1.74 |
| 156 ^b | 165 | „ | 0.35 | 2.5 | 1.25 |
| 164 ^c | - | - | 0.20 | | 0.12 |
| 163 ^c | 50 | TMA 1/1 <i>in situ</i> | 0.20 | 1.1 | 0.38 |
| 162 ^c | 82 | „ | 0.20 | 2.4 | 0.22 |

Experimental conditions: V=50 ml toluene; ^a[Ni]= 37 μ M, [Al]/[Ni]=2200; T=25 °C ^b[Ni] = 58.6 μ M, [Al]/[Ni]=2100, T=25 C; ^c[Ni] = 59 μ M, [Al]/[Ni] = 2100, T=70 °C.

Table 4. Copolymerization of 10-Undecen-1-ol Catalyzed by MesNDABNiBr₂ / MAO System

| Run <i>No</i> | [10-undecen-1-ol] <i>mM</i> | [Ethylene] <i>M</i> | Polymer | Activity $\times 10^{-6}$ <i>g/mol.Ni.h</i> |
|------------------|--------------------------------|------------------------|--------------------|--|
| | | | OH <i>mol %</i> | |
| 159 ^a | - | 0.35 | | 2.57 |
| 157 ^a | 78 | 0.35 | 3.3 | 2.23 |
| 158 ^a | 156 | 0.35 | | 2.07 |
| 160 ^a | 196 | 0.35 | 8.0 | 1.73 |
| 161 ^a | 293 | 0.35 | 9.0 | 1.96 |

Experimental conditions: V=50 ml toluene; T=25 C; Method of treatment of the monomer - TMA 1/1 *in situ*; ^a[Ni]= 58.6 μ M, [Al]/[Ni]=2100; T=25 °C; ^b[Ni]= 51 μ M, [Al]/[Ni]=1900.

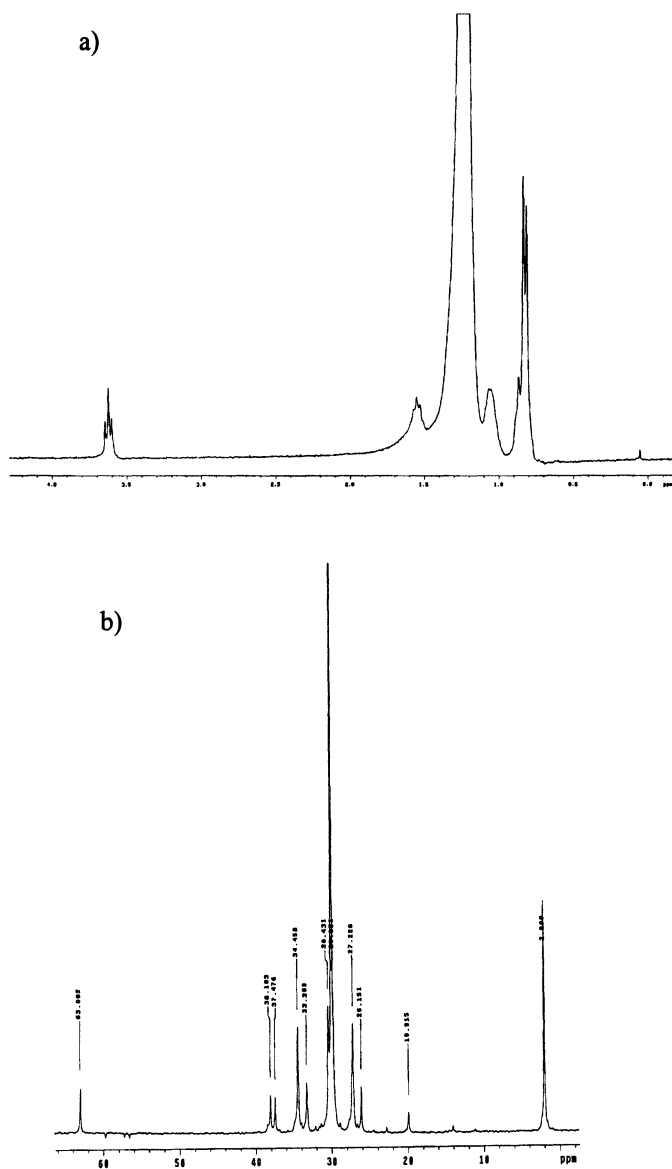


Fig. 1. Catalyst system (2) / MAO; (a) ^1H NMR spectra of copolymer of ethylene / 5-hexen-1-ol (run 162). (b) ^{13}C NMR spectra of copolymer of ethylene / 10-undecen-1-ol (run 162).

COMPARISON OF CATALYST SYSTEMS

The activities of the Ni catalyst with α -diimine ligands (**2**) in copolymerization of ethylene / hydroxy- α -olefins are in some cases considerably higher than the C₂-symmetric *rac*-ethylenebis(1- η^5 -indenyl)zirconium dichloride catalyst (**1**).

If we compare the results, we will see that for similar concentrations of alcohol in the feed the values obtained with catalyst (**1**) show lower activities than those obtained with the catalyst (**2**) (run 247 vs 155 and run 204 vs 161).

The activities of (**1**) / MAO decrease with the increase of monomer concentration in the feed (runs 201 to 204) but with the catalyst system (**2**) /MAO the activity remains approximately constant when the concentration of monomer in the feed increases (runs 157 to 161).

The amount of alcohol incorporated in copolymers depends on the monomer used. In the case 10-undecen-1-ol quite similar results are obtained either with the catalyst (**1**) or (**2**) (run 204 vs 161) but 5-hexen-1-ol seems to incorporate better when (**1**) is used as catalyst.

Regarding activities, it seems that the catalyst system (**2**) based on an α -diimine Ni complex is in fact much better for use with hydroxy monomers than the zirconium Cp based one (**1**) consistent with the relative oxophilicities of the two metals.

CONCLUSIONS

The studied α -diimine Ni complex based catalyst system, (**2**) / MAO, show very promising results since good rates of hydroxy incorporation were obtained. The activities were in a general way several times higher (up to 50 times higher) than those obtained with the zirconium Cp based catalyst system (**1**) / MAO and did not decrease with the increase of monomer concentration in the feed as it was the case with the zirconium Cp based system.

Recently two groups led by Gibson [2] and Brookhart [3] discovered new catalysts based on triimine complexes of Fe and Co. They could be even less

electrophilic and oxophilic than the α -diimine complexes of Ni. Studies on their co- and terpolymerization behaviors of protected polar vinyl monomers are under investigation.

BIBLIOGRAPHY

- (1) (a) P. Aaltonen, B. Löfgren, *Macromolecules* **28**, 5353 (1995); (b) P. Aaltonen, G. Fink, B. Löfgren, J. Seppala, *Macromolecules* **29**, 5255, (1996).
- (2) G.J.P. Britovsek, V. C. Gibson, B. S. Kimberley, P. J. Maddox, S. J. McTavish, G. A. Solan, A. J. P. White, D. J. Williams, *Chem. Commun.* **1998**, 849.
- (3) B.L.Small, M. Brookhart and A.M.A. Bennet, *J. Am. Chem. Soc.* **120**, 4049 (1998).

ACKNOWLEDGMENT

This work was supported in part by NATO (Collaborative Research Grant 960548) and by Fundação para a Ciência e Tecnologia (Projects PRAXIS/PCEX/C/QUI/77/96 and PRAXIS 2/2.1/QUI/143/94). We also thank Fundação para a Ciência e Tecnologia for grant PRAXIS XXI BTL/7586/96 (to SGC). We appreciate the support by Borealis in polymerization equipment and FTIR analysis of polymers. We thank Eng. Luzia Filipe for useful discussions on FTIR determination of acid content in polymers.

Stereospecific Polymerization of Methacrylates with Dimethylsilylene-bridged Zirconocene Catalysts

Nobuya Saegusa¹, Tetsuya Saito¹, Takeshi Shiono¹, Tomiki Ikeda¹, Hai Deng², Kazuo Soga²

¹Research Laboratory of Resources Utilization, Tokyo Institute of Technology, 4259 Nagatsuta, Midori-ku, Yokohama 226-8503, Japan

²Japan Advanced Institute of Science and Technology, 15 Asahidai, Tatsunokuti, Ishikawa 923-12, Japan
tshiono@res.titech.ac.jp

Abstract. Polymerization of methyl methacrylate (MMA) was conducted with a series of dimethylsilylene-bridged zirconocene complexes (*rac*-Me₂SiInd₂ZrMe₂, **1**; Me₂SiCpIndZrMe₂, **2**; Me₂SiCpFluZrMe₂, **3**: Cp, cyclopentadienyl; Ind, indenyl; Flu, fluorenyl) to investigate the effects of the cyclopentadienyl ligand. The zirconocene complexes were activated by [Ph₃C][B(C₆F₅)₄] or [PhMe₂NH][B(C₆F₅)₄] in the presence of diethylzinc. It was found that **1** and **2** gave polymers but **3** did not at 0°C. The dependence of polymer yield and molecular weight on polymerization time indicated that some chain transfer reaction occurred in both systems. ¹³C NMR analysis revealed that *C*₁-symmetric **2** as well as *C*₂-symmetric **1** gave isotactic rich polymer (mmmm = 84–87 %) by enantiomorphic-site controlled mechanism. Polymerization of allyl methacrylate (ALMA) was also conducted with Cp₂ZrMe₂ and **1**. These catalysts selectively polymerized the methacryl group to give syndiotactic-rich and isotactic polymers, respectively with pendant allyl group.

Introduction

Group 4 metallocene catalysts have been paid much attention for their high activity and high stereospecificity in polymerization of α -olefins since the discovery of Kaminsky and Sinn. Recently, some papers reported that metallocene catalysts are also active for polymerization of methacrylate and acrylate monomers^{1–3}. Yasuda *et al.* found that lanthanocene complexes proceed living polymerization of methyl methacrylate (MMA) and acrylate monomers. Collins *et al.* reported that a cationic zirconocenealkyl compound also promotes polymerization of MMA in the presence of neutral bis(cyclopentadienyl)dimethylzirconium (Cp₂ZrMe₂). These catalysts gave

syndiotactic-rich polymers. The NMR analysis of the polymer indicated that the syndiospecific polymerization proceeded via chain-end control mechanism. We found that cationic Cp_2ZrMe_2 species conducted polymerization of MMA in the presence of a suitable Lewis acid, and C_2 -symmetric zirconocenes produced isotactic poly(MMA) by enantiomorphic-site control⁴⁻⁶. We have previously investigated the effects of cyclopentadienyl ligand on MMA polymerization using non-bridged zirconocene compounds i. e., Cp_2ZrMe_2 , $\text{Ind}_2\text{ZrMe}_2$, CpFluZrMe_2 and $\text{CpCp}^*\text{ZrMe}_2$ ($\text{Cp}^* = \eta^5\text{-C}_5\text{Me}_5$), and found that the cyclopentadienyl ligands affected the kinetic features but did not change the stereoregularity of poly(MMA)⁷.

In this work, to investigate the effects of the cyclopentadienyl ligand on the polymerization of MMA with ansa-zirconocenes, a series of dimethylsilylene-bridged zirconocene complexes *rac*- $\text{Me}_2\text{SiInd}_2\text{ZrMe}_2$, (**1**); $\text{Me}_2\text{SiCpIndZrMe}_2$ (**2**); and $\text{Me}_2\text{SiCpFluZrMe}_2$ (**3**) was employed as a catalyst combined with $[\text{Ph}_3\text{C}][\text{B}(\text{C}_6\text{F}_5)_4]$ or $[\text{PhMe}_2\text{NH}][\text{B}(\text{C}_6\text{F}_5)_4]$ in the presence of diethylzinc.

Polymerization of other methacrylate monomers, namely allyl methacrylate (ALMA) and vinyl methacrylate (VIMA), was also conducted with Cp_2ZrMe_2 and the ansa-zirconocene complex **1**.

Experimental Part

Methacrylate monomers were dried over calcium hydride and distilled before use. Toluene was dried and distilled from sodium and benzophenone. Dimethylsilylene-bridged zirconocene complexes, **1**, **2**, and **3** were synthesized from the corresponding zirconocene chloride and methyl lithium according to the similar procedure reported previously⁸. ZnEt_2 , $[\text{Ph}_3\text{C}][\text{B}(\text{C}_6\text{F}_5)_4]$ and $[\text{PhMe}_2\text{NH}][\text{B}(\text{C}_6\text{F}_5)_4]$ were donated from Tosoh Akzo Co. Ltd.

Polymerization of MMA was carried out under a dry nitrogen atmosphere in a 50 ml round-bottomed flask equipped with a magnetic stirrer. A typical polymerization process is as follows: toluene 6.0 ml, methacrylate 1.0 ml, and the toluene solution of ZnEt_2 (2.0 M) 1.0 ml were injected into the flask and stirred 0.5 h at 0°C. After the addition of the zirconocene complex in toluene (10 mM) 1.0 ml, the toluene solution of $[\text{Ph}_3\text{C}][\text{B}(\text{C}_6\text{F}_5)_4]$ or $[\text{PhMe}_2\text{NH}][\text{B}(\text{C}_6\text{F}_5)_4]$ (10 mM) 1.0 ml was immediately injected to start polymerization. The polymerization was quenched with a methanol solution of hydrochloric acid. The produced polymer was precipitated in methanol, followed by drying in vacuo at 60°C for 6 h.

Results and Discussion

Polymerization of MMA

Polymerization of MMA was conducted by the dimethylsilylene-bridged zirconocenes with different symmetries, that is C_2 -symmetric complex **1**, C_1 -symmetric complex **2** and C_s -symmetric complex **3**. The results are summarized in Table 1. The activity depended on the structure of zirconocene complexes. The activity of **1** was almost twice as high as that of **2**. However, **3** did not produce any polymer in the same conditions. The molecular weight of the polymer obtained with **1** was also higher than that obtained with **2**. $\text{PhMe}_2\text{NHB}(\text{C}_6\text{F}_5)_4$ gave better results than $\text{Ph}_3\text{CB}(\text{C}_6\text{F}_5)_4$ both in polymer yields and molecular weights. However, the difference was not significant.

Then, the kinetic features of the **1** / $\text{Ph}_3\text{CB}(\text{C}_6\text{F}_5)_4$ and the **2** / $\text{Ph}_3\text{CB}(\text{C}_6\text{F}_5)_4$ systems were investigated. The plots of the polymer yields and the molecular weights against polymerization time are displayed in Fig. 1. In both systems, the polymer yields increased against polymerization time, while the molecular weight reached a certain value. As a consequence, the number of polymer chains was increased with increasing the polymerization time. This result indicates that some chain transfer reaction occurred in these systems.

Table 1. Polymerization of MMA with the zirconocene complexes

| Cat. | Co-Cat. | Time(h) | Yield (%) | $M_n^a)$ ($\times 10^{-4}$) | MWD | $N^b)$ |
|----------|---|---------|-----------|----------------------------------|-----|--------|
| 1 | $\text{Ph}_3\text{CB}(\text{C}_6\text{F}_5)_4$ | 1 | 15 | 5.9 | 1.3 | 0.27 |
| | | 3 | 31 | 13 | 1.4 | 0.23 |
| | | 6 | 40 | 14 | 1.5 | 0.28 |
| | | 9 | 54 | 12 | 1.8 | 0.43 |
| 2 | $\text{Ph}_3\text{CB}(\text{C}_6\text{F}_5)_4$ | 0.5 | 4.4 | 2.0 | 2.0 | 0.21 |
| | | 1 | 6.8 | 3.3 | 1.8 | 0.20 |
| | | 3 | 13 | 3.9 | 1.7 | 0.31 |
| | | 6 | 16 | 3.7 | 2.0 | 0.41 |
| | | 9 | 24 | 4.3 | 1.8 | 0.52 |
| 3 | | 24 | 0 | - | - | - |
| 1 | $\text{PhMe}_2\text{NHB}(\text{C}_6\text{F}_5)_4$ | 3 | 38 | 12 | 1.3 | 0.31 |
| 2 | | 1 | 11 | 4.9 | 1.7 | 0.21 |
| | | 3 | 24 | 5.3 | 2.1 | 0.42 |
| | | 6 | 33 | 5.6 | 2.3 | 0.56 |

Polymerization conditions: $[\text{Zr}] = 1.0 \text{ mM}$, $[\text{B}] = 1.0 \text{ mM}$, $[\text{Zn}] = 0.2 \text{ M}$, $[\text{MMA}]_0 = 1.89 \text{ M}$, at 0°C , in 9.0 ml of toluene. a) Determined by GPC using PMMA stds. b) Number of polymer chains.

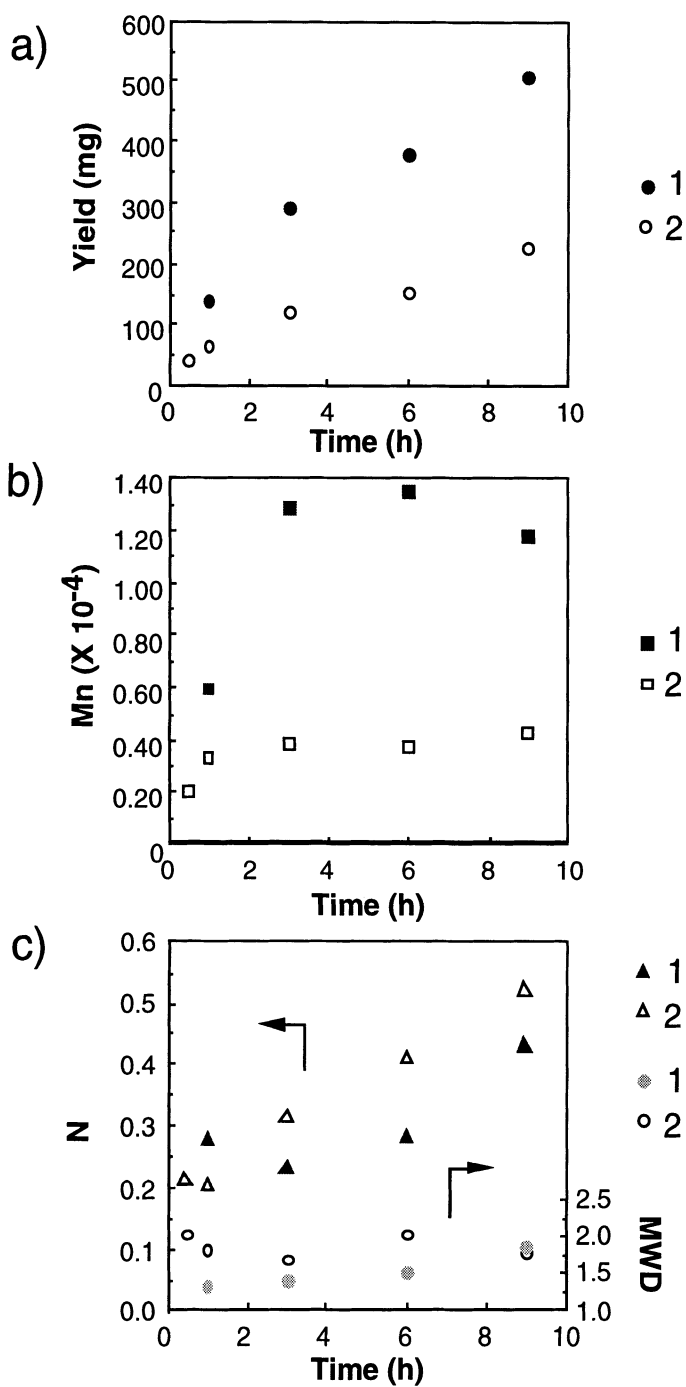


Fig. 1. Plots of a) polymer yield, b) number-average molecular weight (Mn), and c) number of polymer chains (N) and molecular weight distribution (MWD) against polymerization time

Table 2. Microtacticity of MMA obtained with the zirconocene complexes

| Cat. | Co-Cat. | Pentad Fraction ^{a)} | | | | | | | $\beta^b)$ | $\sigma^c)$ | $\omega^d)$ | |
|----------|--|-------------------------------|------|------|------|------|------|------|------------|-------------|-------------|------|
| | | mmmm | mmmr | rmmr | mmrr | mrmm | rrrr | mrrr | | | | mrrm |
| 1 | Ph ₃ CB(C ₆ F ₅) ₄ calc. ^{e)} | 0.83 | 0.05 | 0.00 | 0.07 | 0.01 | 0.02 | 0.01 | 0.02 | 0.97 | (0.80) | 0.96 |
| | | 0.83 | 0.05 | 0.00 | 0.06 | 0.00 | 0.02 | 0.01 | 0.03 | | | |
| 1 | PhMe ₂ NHB(C ₆ F ₅) ₄ calc. | 0.82 | 0.05 | 0.01 | 0.06 | 0.00 | 0.02 | 0.01 | 0.02 | 0.97 | (0.83) | 0.96 |
| | | 0.82 | 0.05 | 0.00 | 0.06 | 0.01 | 0.02 | 0.01 | 0.03 | | | |
| 2 | Ph ₃ CB(C ₆ F ₅) ₄ calc. | 0.83 | 0.05 | 0.00 | 0.06 | 0.00 | 0.02 | 0.02 | 0.02 | 0.97 | (0.81) | 0.95 |
| | | 0.83 | 0.05 | 0.00 | 0.06 | 0.00 | 0.02 | 0.01 | 0.02 | | | |
| 2 | PhMe ₂ NHB(C ₆ F ₅) ₄ calc. | 0.82 | 0.04 | 0.00 | 0.05 | 0.01 | 0.04 | 0.02 | 0.01 | 0.98 | (0.85) | 0.93 |
| | | 0.82 | 0.04 | 0.00 | 0.06 | 0.00 | 0.04 | 0.01 | 0.02 | | | |

Polymerization conditions are shown in Table 1; polymerization time was 3 h. a) Determined by ¹³C NMR. b) Selectivity of one prochiral face on the enantiomorphous site. c) Probability of syndiotactic propagation in the chain-end control site. d) Weight fraction of polymer derived from the enantiomorphous site. e) Calculated values by the two-site model.

The microtacticity of the polymers was investigated by ¹³C NMR (Table 2). It was found that the C₁-symmetric complex **2** gave isotactic polymers whose stereoregularity was almost the same with those obtained by the C₂-symmetric complex **1**. The microtacticity was, however, independent of the borate compounds employed. Besides the strong isotactic pentad resonance, weak resonances of syndiotactic structure were also observed in all the spectra. Therefore, we analyzed these polymer by the two site model, in which isotactic and syndiotactic polymers are produced by enantiomorphous-site and chain-end controlled mechanism, respectively. The observed values are in agreement with the calculated ones. The selectivity of one prochiral face on the enantiomorphous site (β) and probability of syndiotactic propagation in the chain-end control site (σ) were proper values compared with our previous work⁶⁾, although the σ values contain an unavoidable error because of the low intensities of syndiotactic structures. It is noteworthy that C₁-symmetric complex **2** conducted isospecific polymerization of MMA by enantiomorphous-site controlled mechanism.

Polymerization of allyl methacrylate

Polymerization of ALMA and VIMA, which have allyl and vinyl ester groups, respectively, was conducted by a non-bridged zirconocene (Cp₂ZrMe₂) combined with PhMe₂NHB(C₆F₅)₄ in the presence of ZnEt₂ (Table 3). Relation between polymer yield and polymerization time indicated the presence of induction period in this system. The gel-permeation chromatograms of these polymers show broader molecular-weight distribution than that of PMMA obtained under the same conditions⁵⁾. The comparison

of the results of 2 h and 3 h polymerization suggested that the polymerization proceeded steadily with a chain transfer reaction after the induction period. When $\text{Al}(i\text{-Bu})_3$ was used in place of ZnEt_2 , however, only a trace of polymer was obtained. On the other hand, no polymer was obtained in the case of VIMA.

Therefore, polymerization of ALMA was conducted with the C_2 -symmetric ansa-zirconocene **1** combined with $\text{PhMe}_2\text{NHB}(\text{C}_6\text{F}_5)_4$ and ZnEt_2 . Although the activity was lower than that by Cp_2ZrMe_2 , **1** gave a polymer with high molecular weight. Compared with the results shown in Table 1, ALMA was less active than MMA.

Table 3. Polymerization of methacrylates with zirconocene complexes

| Cat. | Monomer | Time | Yield (%) | Mn^{a} | | MWD | N^{b} |
|----------------------------|-------------------|------|-----------|------------------------|-----|--------------|-----------------------|
| | | | | $(\times 10^{-4})$ | | | |
| Cp_2ZrMe_2 | ALMA | 0.5 | 0.93 | 3.8 | 2.1 | 0.02 | |
| | | 1 | 9.0 | 5.0 | 3.8 | 0.17 | |
| | | 2 | 38 | 15 | 3.0 | 0.24 | |
| | | 3 | 74 | 14 | 2.8 | 0.50 | |
| | VIMA | 6 | 0 | - | - | - | |
| | ALMA ^c | 6 | trace | - | - | - | |
| 1 | ALMA | 6 | 38 | 12 | 1.8 | 0.31 | |

Polymerization conditions: $[\text{Zr}] = 1.0 \text{ mM}$, $[\text{PhMe}_2\text{NHB}(\text{C}_6\text{F}_5)_4] = 1.0 \text{ mM}$, $[\text{ZnEt}_2] = 0.2 \text{ M}$, $[\text{Monomer}]_0 = 1.0 \text{ M}$, at 0°C , in 9.0 ml of toluene. a) Determined by GPC using PMMA stds. b) Number of polymer chains. c) $\text{Al}(i\text{-Bu})_3$ was used in place of ZnEt_2 .

Table 4. Microtacticity of PALMA obtained with zirconocene complexes

| Cat. | Triad Fraction ^a | | | $4[\text{mm}][\text{rr}]^{\text{b}}$ | $2[\text{rr}]^{\text{b}}$ |
|----------------------------|-----------------------------|------|------|--------------------------------------|---------------------------|
| | mm | mr | rr | $[\text{mr}]^2$ | $[\text{mr}]$ |
| Cp_2ZrMe_2 | 0.02 | 0.24 | 0.74 | 1.0 | - |
| 1 | 0.91 | 0.06 | 0.03 | (30) | 1.0 |

Polymerization conditions are shown in Table 3: a) Determined by ^{13}C NMR. b) $4[\text{mm}][\text{rr}] / [\text{mr}]^2 = 1$ for a chain end-controlled mechanism; $2[\text{rr}] / [\text{mr}] = 1$ for an enantiomorphic site-controlled mechanism.

^1H and ^{13}C NMR spectra of the poly(ALMA)s obtained with these systems showed the resonances of allyl group. The relative peak intensities indicated that these catalyst systems selectively polymerized methacryl group of ALMA and gave a polymer with pendant allyl group. The steric triad fraction of the polymers were estimated from the ^1H NMR resonances of the methyl group by a similar procedure for PMMA (Table 4). The results indicate that the syndiotactic-rich polymer was derived from Cp_2ZrMe_2 via chain-end controlled mechanism, and the isotactic polymer was obtained with **1** via enantiomorphic-site controlled mechanism. These results indicated that the replacement of methyl to allyl group did not affect the stereospecificity of the catalysts.

Summary

Polymerization of MMA was conducted using three types of dimethylsilylene-bridged zirconocene complexes. The C_1 -symmetric complex **2** as well as the C_2 -symmetric complex **1** gave highly isotactic polymer by enantiomorphic-site controlled mechanism. The kinetic data suggested that some chain transfer reaction occurred in both systems. However, C_s -symmetric complex **3** gave no polymer in the same conditions.

Cp_2ZrMe_2 and **1** combined with $PhMe_2NHB(C_6F_5)_4$ and $ZnEt_2$ selectively polymerized the methacryl group of ALMA to give the polymers with pendant allyl groups. Microtacticity of the polymer depended on the structure of zirconocene complexes, as is observed in the polymerization of MMA, namely Cp_2ZrMe_2 and **1** gave syndiotactic-rich and isotactic polymers respectively, by chain-end controlled and enantiomorphic-site controlled mechanism.

References

- [1] Yasuda, H., Yamamoto, H., Yamashita, M.; *Macromolecules*, 1993, **26**, 7134.
- [2] Collins, S., Ward, D. G., *J. Am. Chem. Soc.*, 1992, **114**, 5460.
- [3] Collins, S., Ward, D. G., Suddaby, K. H.; *Macromolecules*, 1994, **27**, 7222.
- [4] Soga, K., Deng, H., Yano, T., Shiono, T., *Macromolecules*, 1994, **27**, 7938.
- [5] Deng, H., Shiono, T., Soga, K., *Macromol. Chem. Phys.*, 1995, **196**, 1971.
- [6] Deng, H., Shiono, T., Soga, K., *Macromolecules*, 1995, **28**, 3067.
- [7] Shiono, T., Saito, T., Saegusa, N., Hagihara, H., Ikeda, T., Deng, H., Soga, K., *Macromol. Chem. Phys.*, 1998, **199**, 1573.
- [8] Chien, J. C. W., Tsai, W. M., Rausch, M. D., *J. Am. Chem. Soc.*, 1991, **113**, 8570 and references therein.

DEVELOPMENT OF CATALYTIC SYSTEMS BASED ON LANTHANOÏD COMPLEXES FOR OLEFIN POLYMERIZATION

Karel BUJADOUX, Thomas CHENAL, Christine FOUGA, Xavier OLONDE,

Jean-François PELLETIER, and André MORTREUX

Laboratoire de Catalyse Hétérogène et Homogène, URA CNRS 402, Groupe de Chimie Organique Appliquée ENSCLille BP 108 59652 VILLENEUVE D'ASCQ Cedex France

andre.mortreux@ensc-lille.fr

The use of the alkylation technique of $\text{Cp}^*_2\text{LnCl}_2\text{Li}(\text{OEt})_2$ complexes for the synthesis of lanthanocene active species which are useful for olefin polymerization, is described. Both butyl lithium and butyl-ethyl magnesium (BEM) are shown to be suitable as alkylating reagents for ethylene polymerization. Using BEM in excess allows the synthesis of higher dialkylmagnesium compounds via a chain transfer reaction between magnesium and lanthanoid atoms following the insertion reaction of the monomer into the Ln-alkyl bond. For methyl methacrylate polymerization, using a butyl lithium/Ln ratio of 2 gives the best results, leading to the production of syndiotactic (>80%) PMMA with low molecular weight distributions (<2), in high yields and molecular weights (up to $2 \cdot 10^5$).

INTRODUCTION

The use of d^0 alkylzirconocene cationic catalysts for olefin polymerization is currently the subject of thorough studies in both academic and industrial groups, as proved by many papers in the present proceedings.

However, the neutral lanthanocene alkyl isoelectronic analogous complexes, although recognized as extremely active catalysts for ethylene polymerization since the early eighties⁽¹⁻³⁾, have only given rise to a few studies since then.

This may be due, at least in part, to the high sensitivity of lanthanoid – alkyl or hydride complexes towards oxygen and moisture, and to some extent to their lack of reactivity towards α -olefin polymerization.

A renewed interest in this field appeared in 1992 via the application of these catalysts as initiators for the syndiospecific polymerization of methylmethacrylate (MMA), as well as their use for the production of block copolymers^(4,5).

The aim of this paper is to present our results related to the use of preformed catalytic systems obtained via reaction of bis-(pentamethylcyclopentadienyl) lanthanoid chloro complexes with alkylating reagents, providing solutions

containing the expected metal alkyl species necessary for these polymerization reactions.

The use of such systems in ethylene homopolymerization, block (PE-PMMA) copolymerization and MMA homopolymerization is described in turn.

ETHYLENE HOMOPOLYMERIZATION

Preliminary experiments have been conducted in a stainless steel autoclave monitored with a stirring bar at room temperature after premixing 0.1 mmol of $\text{Cp}^*\text{NdCl}_2\text{Li}(\text{OEt}_2)_2$ for 30 min in 10 ml toluene with 0.2 mmol of alkylating reagents such as AlR_3 (R = Et, iBu), ZnEt_2 , BuLi, BuMgEt (BEM). Only the alkyllithium and dialkylmagnesium reagents gave satisfactory results after introduction into the autoclave initially charged with 40 ml toluene and further pressurized with ethylene (50 bars). Upon stirring starting from ambient temperature, a rapid increase of temperature (ca 100-120°C) was observed; 15 g of polymer were obtained within 4 min.

These first observations led us to carry out a series of experiments using these alkylating reagents, at different ratios, under atmospheric pressure at 80°, using a 1 liter, double envelope flask in 500 ml ISOPAR L as solvent^(6,7).

Whereas an excess of BuLi did not give a result any different from that obtained with 2 eq, a strong effect was observed using different BEM/Nd ratios. The results are summarized in Table 1.

Table 1 - Influence of the BEM/Sm ratio on the polymer yield and characteristics^a

| Run | Mg/Sm | Yield [g] | \bar{M}_n | \bar{M}_w / \bar{M}_n |
|-----|-------|-----------|-------------|-------------------------|
| 1 | 0.5 | 0.8 | 12020 | 2.2 |
| 2 | 1 | 7.1 | 6290 | 2.4 |
| 3 | 5 | 8.2 | 2820 | 1.6 |
| 4 | 10 | 4.4 | 1900 | 1.3 |
| 5 | 20 | 3.1 | 690 | 1.3 |
| 6 | 50 | 2.6 | 400 | 1.3 |

^a Conditions: catalyst $\text{Cp}^*\text{SmCl}_2\text{Li}(\text{OEt}_2)_2 = 0.1$ mmol; 500 ml ISOPAR L; alkylation: 2h, 20°C; reaction time = 5min; T = 80°C

It appears that an excess of BEM decreases the reaction rate as well as the polydispersity index, and lowers the molecular weight. Interestingly, a precipitation was observed in the first 5 minutes during runs 1 and 2, but the polymer remained soluble in runs 3-6. Moreover, the ethylene consumption vs time had a profile systematically similar to that given in figure 1.

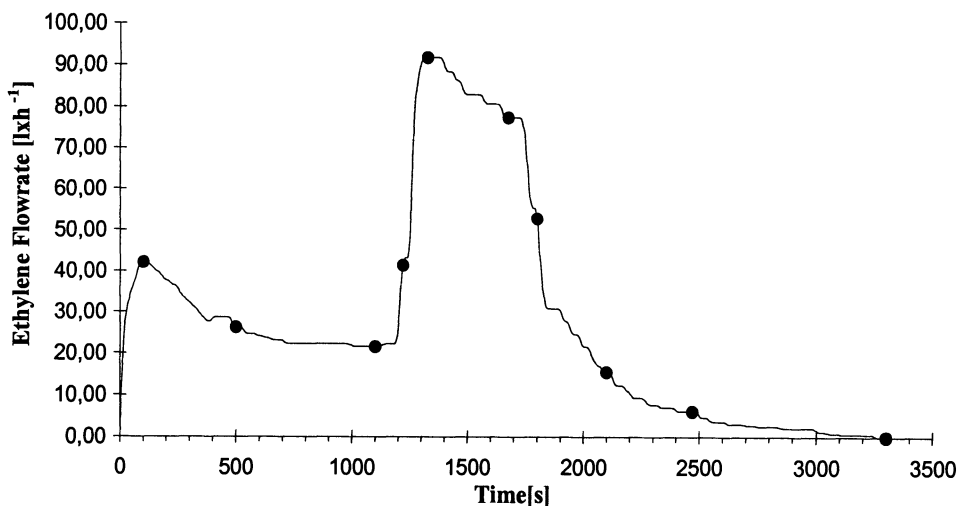


Fig.1: Ethylene flowrate vs time using conditions described in run 6.

One characteristic of the ethylene consumption rate is that it is initially steady stage (until ca 1200s for a BEM/Nd ratio of 50) and then increases rapidly just after the beginning of the polymer precipitation.

10 samples of polymers have been analyzed carefully at different reaction times (Table 2), to try to determine which phenomenon could explain this behavior

Table 2 -Polymer characteristics as a function of the reaction time ^a

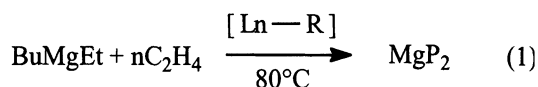
| Time[s] | \bar{M}_n | \bar{M}_w / \bar{M}_n | Ethylene consumption [g] | Average C=C content [%] ^b |
|---------|-------------|-------------------------|--------------------------|--------------------------------------|
| 100 | 485 | 1.2 | 1.1 | nd |
| 500 | 580 | 1.2 | 5.5 | 2.2 |
| 1100 | 900 | 1.2 | 10.2 | 3 |
| 1220 | 950 | 1.3 | 11 | 2.3 |
| 1325 | 1130 | 1.5 | 13.5 | 8 |
| 1675 | 1420 | 1.8 | 23.4 | 11 |
| 1800 | 1550 | 2 | 26.4 | 9 |
| 2100 | 1715 | 3.8 | 29 | 10 |
| 2470 | 1530 | 4 | 30.1 | 9 |
| 3300 | 1870 | 5.9 | 30.7 | 11 |

^a Conditions: same as in table 1; Mg/Sm = 50

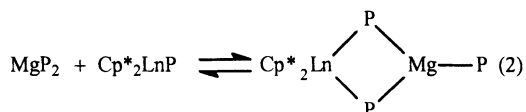
^b estimated by infrared spectroscopy

The results depicted in this table show that the polydispersity index is low before precipitation and increases as soon as the precipitate appears, as does the

C=C content in the polymer. Furthermore, from the molecular weight values and the ethylene consumption and assuming a quasi living polymerization, one could calculate the average chain number, which corresponds, before precipitation, to 2 chains per magnesium atom. This indicates that the polymer grows on magnesium as well as on the lanthanoid complex. Obviously, this can be explained by a chain transfer reaction between the two metals, which allows the synthesis of higher dialkyl magnesium compounds MgP_2 where P represents the linear, growing alkyl chain (eqn.1) [8].



A plausible interpretation of an increase in the polydispersity index together with that of the double bond content in the polymer could arise from the decrease of Mg-C bonds in the solution due to MgP_2 precipitation: this allows the equilibrium depicted in eqn2 to shift to the left, therefore leading to an increase in β hydrogen elimination on the free Cp^*_2LnP .



PILOT SCALE EXPERIMENTS, ETHYLENE POLYMERIZATION

The above reactions were run at 80°C. Nevertheless, increasing the temperature to 100°C leads to an ethylene consumption profile different from that described in fig 1. After 4 hours reaction, the ethylene consumption rate was almost the same as after 1 hour (ca 35 l/h) and no precipitate was observed, whereas 180 g polyethylene were produced after precipitation using ethanol. GPC ($\bar{M}_n = 2110$; PDI = 2) and IR analysis (high vinyl content) suggest that at 100°C, the β H transfer reaction occurs. This result, associated with other data already reported under 6 bar at 160°C (6), led us to use this catalyst under supercritical conditions in a pilot plant, typically those used on an industrial scale for ethylene polymerization over Ziegler Natta catalysts (9). At 200°C / 1200 bar, using a BEM/Ln ratio of 3, the productivity into highly linear polyethylene ($\bar{M}_n = 23\,700$; PDI = 1.8) could reach up to 20t per mole of lanthanoid. Kgs of polyethylene produced using this technology had a (Mg + Ln) content lower than 10 ppm. Interestingly, the "activity" of the system can be calculated, giving values as high as $2 \cdot 10^4$ insertions per second per lanthanoid atom, close to industrial conditions. Unfortunately, although transfer reactions were occurring due to an increase of the melt flow index of the polymer, the introduction of 1-butene as comonomer could not result in the production of any copolymer (6).

ETHYLENE – METHYLMETHACRYLATE COPOLYMERIZATION

Biblock (PE–PMMA) copolymers have been synthesized using a first reaction on Cp^*_2SmR with ethylene (living ethylene polymerization), followed by introduction of methylmethacrylate (MMA) ⁽⁵⁾. However, as stated by the authors, the length of the ethylene polymer chain had to be carefully adjusted (less than ca. 10 000 dalton) in order to avoid mass transfer problems related to the fact, that the alkyl chain may hinder the metal towards its accessibility for the polar comonomer, if the polymer particles are too bulky.

We now have the possibility to synthesize new MgP_2 compounds as described in the first part of this paper, with a narrow polydispersity index provided; a control correlates to the soluble nature of the growing dialkylmagnesium.

A first reaction using 5 mmol BuMgEt and 0.1 mmol $\text{Cp}^*_2\text{SmCl}_2\text{Li}(\text{OEt}_2)_2$ in 500 ml ISOPAR L conducted under 1.1 bar ethylene for 30 min at 80°C gave 12.4 g of polymer after hydrolysis ($\overline{M}_n = 445$ da; $\overline{M}_w / \overline{M}_n = 1.2$)

A second run using exactly the same conditions, followed by the addition at -78°C of 50 mmol (5 g) of MMA for 2 h, gave 16.7 g of polymer. After extraction using acetone during 4 days, 8.9 g of insoluble compound could be recovered ($\overline{M}_n = 890$, $\overline{M}_w / \overline{M}_n = 1.1$). A comparison between the GPC characteristics allows us to conclude that the average number of ethylene and MMA moities in the copolymer are 16 and 4.5 respectively, a ratio which could be undoubtedly adjusted by controlling both steps.

METHYLMETHACRYLATE HOMOPOLYMERIZATION

Using $(\text{Cp}^*_2\text{SmH})_2$ as initiator, Yasuda and coworkers ^(4,10) have attained the best results ever reported for MMA polymerization in terms of polydispersity index (living polymerization, PDI = 1.04), syndiotacticity (82.3%) as well as molecular weight ($\overline{M}_n = 563\ 000$) at 0°C. Our first idea was to try to use the former system $\text{Cp}^*_2\text{SmCl}_2\text{Li}(\text{OEt}_2)_2$ / BEM as initiator for this reaction, at different BEM/Sm ratio as for ethylene polymerization.

Table 3 - MMA polymerization on $\text{Cp}^*_2\text{SmCl}_2\text{Li}(\text{OEt}_2)_2$ / BEM ^a

| Mg/Sm | Conv % | $\overline{M}_n \times 10^{-3}$ | PDI | Tacticity | | |
|-------|--------|---------------------------------|------|-----------|----|----|
| | | | | rr | mr | mm |
| 0.5 | 17 | 33 | 6.67 | 84 | 8 | 8 |
| 1 | 23 | nd | nd | 63 | 12 | 25 |
| 3 | 5 | nd | nd | 50 | 23 | 27 |

^a Alkylation: 0.1 mmol $\text{Cp}^*_2\text{SmCl}_2\text{Li}(\text{OEt}_2)_2$ + BEM in 20 ml PhMe, 20°C, 1h
 Polymerization: MMA = 50 mmol, in 80 ml PhMe; T = 0°C; 3.5 h

Although a good syndiotacticity is obtained upon using a low Mg/Sm ratio, the molecular weight distribution (PDI) is much higher than what could be expected from a putative $\text{Cp}^*_2\text{Sm-R}$ species. An increase of the magnesium alkyl gave even

poorer results, especially for the tacticity. In any case, the conversions are low. This may be due to the presence of the binuclear, bridged compound $\text{Cp}^*_2\text{Sm}(\text{R})_2\text{MgR}$ already proposed during ethylene polymerization studies, giving rise to a slow initiation process.

Although alkyllithium compounds are well known as initiators for MMA polymerizations, we have tried to use butyl lithium (BuLi) as alkylating reagent for the synthesis of the Cp^*_2SmBu . Indeed, the use of BuLi as initiator for this polymerization needs low temperature conditions to avoid side reactions. This was confirmed by using BuLi alone (0.4 mmol) in toluene for 2 hours at 0°C to polymerize 50 mmol MMA: only a 7% conversion was obtained ($\overline{M}_n = 12\ 000$, PDI = 2.7, 25% rr, 26%mr and 49% mm).

In table 4 the results which are obtained by using different $\text{Cp}^*_2\text{SmCl}_2\text{Li}(\text{OEt}_2)_2/\text{BuLi}$ ratios for the synthesis of Cp^*_2SmBu initiators are given.

Table 4 - MMA polymerisation on $\text{Cp}^*_2\text{SmCl}_2\text{Li}(\text{OEt}_2)_2/\text{BuLi}$ ^a

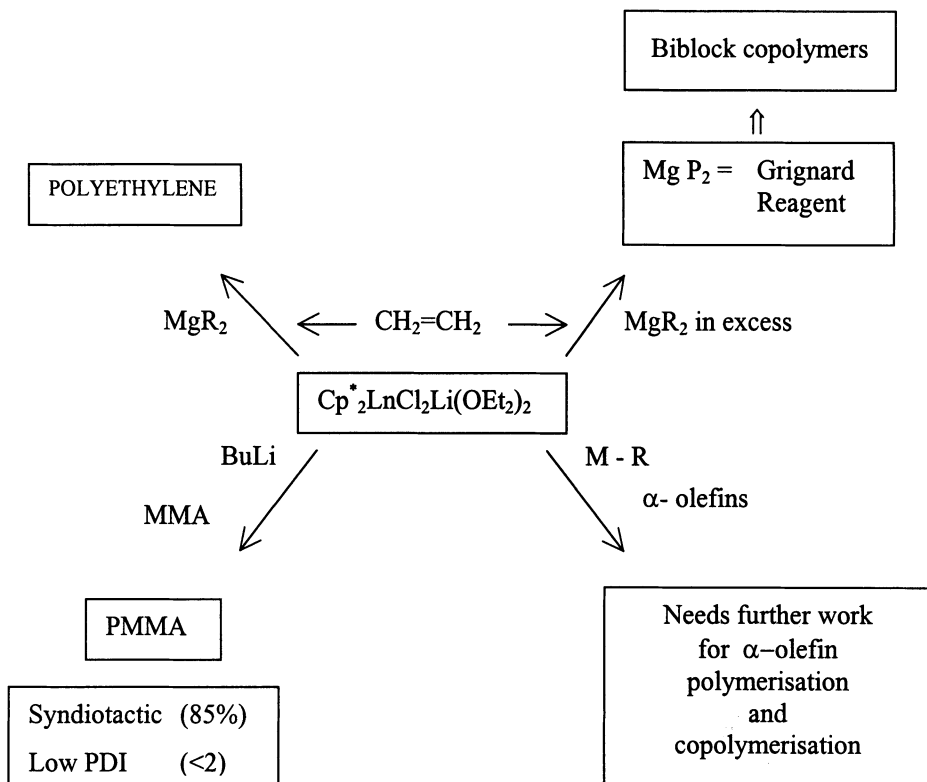
| BuLi/Sm | $\overline{M}_n \times 10^{-3}$ | PDI | Tacticity | | |
|---------|---------------------------------|-----|-----------|----|----|
| | | | rr | mr | mm |
| 1 | 50 | 4.3 | 77 | 17 | 6 |
| 1.25 | 122 | 2.5 | 84 | 13 | 3 |
| 1.5 | 93 | 2 | 86 | 12 | 2 |
| 1.75 | 80 | 2 | 80 | 15 | 5 |
| 2 | 67 | 2 | 80 | 14 | 6 |
| 5.6 | 23 | 10 | 51 | 29 | 20 |
| 10 | 14 | 20 | 41 | 21 | 38 |

^a Conditions: same as in table 3; polymerization reaction time = 1 h; apart from BuLi/Sm = 1 (23% yield), all reactions gave total conversions of MMA

Interestingly, the results obtained with BuLi/Sm ratios ranging from 1.5 to 2 indicate that the expected samarium alkyl species are produced (the syndiotacticity is equivalent to that obtained using the $(\text{Cp}^*_2\text{SmH})_2$ hydride complex); even if the molecular weight distribution is higher, this technique offers the great advantage of easy synthesis, without isolation of the samarium hydride or alkyl complex, both active and stereoselective species for the production of large amounts of highly syndiotactic PMMA. In line with this, experiments have been undertaken using increasing amounts of MMA (5, 10 and 20 g) in separate experiments on 0.1 mmol $\text{Cp}^*_2\text{SmCl}_2\text{Li}(\text{OEt}_2)_2$ alkylated with 0.2 mmol BuLi. As expected, syndiotactic PMMA was obtained in high yields (100, 93 and 95 %, respectively) in each case (ca 80% rr), with increasing molecular weights (60, 85 and 190×10^3) as well as narrow molecular weight distributions (1.82, 1.76 and 1.75).

CONCLUSION

This paper shows that the alkylation technique and a careful choice of the alkylating reagent could afford in situ alkyl lanthanide complexes which may be used as catalysts and/or initiators in a variety of polymerization reactions as depicted in the scheme below.



Compared to zirconocene cationic species, one can see some important aspects:

- i. The catalytic species for ethylene polymerization can be prepared easily without isolation of the active lanthanoid – alkyl complex using a low amount of alkylating reagent; as a result, this technique has been the subject of several patents^(11, 12).
- ii. A pseudo living transfer between the lanthanoid and magnesium occurs during polymerization of ethylene at high BEM/Ln ratios and low temperature (80°C). This new process can be applied in the synthesis of higher dialkylmagnesium compounds which can be either functionalized or used in the production of biblock copolymers⁽¹³⁾.

- iii. In contrast to classical zirconocene catalysts, the lanthanoid alkyl species can also act as initiators for MMA polymerization, leading to syndiotactic PMMA.

On the other hand, the polymerization of α -olefins has only been realized successfully, using lanthanocenes, by introducing more sophisticated, silicon bridged silylated cyclopentadienyl ligands, and even then with low activities⁽¹⁴⁾. In this respect, more work needs to be done by tuning the ligands to develop the same chemistry with lanthanoides as is presently occurring on group 4 metallocenes for either propylene homopolymerization or ethylene- α -olefin copolymerization.

Acknowledgments: The financial support of Enichem, Elf-Atochem Co, the Centre National de la Recherche Scientifique and the Ministry of Research and Technology is greatly acknowledged.

REFERENCES

- 1 Watson, P.L.; Parshall, G.W.; *Acc. Chem. Res.*, 1976, 98, 1729.
- 2 Jeske, G.; Lauke, H.; Mauermann, H; Swepson, P.N.; Schumann, H; Marks, T.J.; *J. Am. Chem. Soc.*, 1985, 107, 8091.
- 3 Mauermann, H; Swepston, P.N.; Marks, T.J.; *Organometallics*, 1985, 4, 200.
- 4 Yasuda, H.; Yamamoto, K.; Yakoya, K.; Miyaka, S.; Nakamura, A.; *J. Am. Chem. Soc.*, 1992, 114, 4908.
- 5 Yasuda, H.; Furo, M.; Yamamoto, H.; Nakamura, H.; Miyake, S.; Kibino, N.; *Macromolecules*, 1992, 25, 5115.
- 6 Olonde, X.; Mortreux, A.; Petit, F.; Bujadoux, K.; *J. Mol. Catal.*, 1993, 82, 75.
- 7 Pelletier, J.F.; Mortreux, A.; Petit, F.; Olonde, X.; Bujadoux, K.; in "*Catalyst design for tailor made polyolefins*". Studies in Surface Sciences and Catalysis vol 89; K. Soga and M. Terano Ed.; Kodansha : Tokyo. 1994 pp 249-258.
- 8 Pelletier, J.F.; Mortreux, A.; Olonde, X.; Bujadoux, K.; *Angew Chem Int Ed Eng*, 1996, 35, 1854.
- 9 Brusson, J.M.; Mortreux, A.; Petit, F.; Bujadoux, K.; Leprévost, B.; *Macromolecular Chemistry and Physics*, 1995, 196, 4083.
- 10 Yasuda, H.; Yamamoto, H.; Yamashita, M.; Yakota, K.; Nakamura, A.; Miyake, S.; Kai, Y.; Kanehisa, N.; *Macromolecules*, 1993, 26, 7134.
- 11 Pettijohn, T.M.; Hsieh, H.L.; US Pat 5, 109, 085 to Phillips Petroleum Co
- 12 Bujadoux, K.; Olonde, X.; Mortreux, A.; Petit, F.; WO 93.07180 A1
- 13 Pelletier, J. F.; Bujadoux K.; Olonde, X.; Adisson, E.; Mortreux, A.; Chenal, T.; Eur.Pat. 96 40 07 31.4-2110 to ECP Enichem Polymères France
- 14 Ihara, E.; Nodono, M.; Yasuda, H.; *Macromol Chem. Phys.*; 1996, 197, 1909.

7. Polymer Characterization and Processes

INITIAL 2,1-INSERTIONS IN METALLOCENE POLYMERIZATIONS OF POLYPROPYLENE

J. C. Randall, C. J. Ruff, J. C. Vizzini, A. N. Speca, T. J. Burkhardt

Baytown Polymers Center, Exxon Chemical Company, 5200 Bayway Drive, Baytown, Texas, USA 77522-5200

Abstract. 2,1-insertions during propylene polymerizations with a metallocene catalyst produce regio defects within the polypropylene chain and n-butyl end groups after chain transfer with hydrogen of a terminal 2,1-inserted propylene unit. In this study, initial 2,1-insertions, which produce 2,3-dimethylbutyl end groups, are reported for the first time. The structural proof was obtained with model compounds, a NMR DEPT experiment and gc-mass spectrometry of propylene oligomers. The mole percent of initial 2,1-insertions ranges from 25 to 40%. From ^{13}C NMR, a conservation of end group concentrations is established through the observation that the sum of n-propyl + 2,3-dimethylbutyl initial groups is equal to the sum of the n-butyl + iso-butyl final groups. Number average molecular weights calculated from the end group concentrations are in excellent agreement with number average molecular weights from GPC. A linear relationship is observed when the total 2,1-insertions per molecule are plotted versus the degree of polymerization.

INTRODUCTION

The identification and characterization of a propylene 2,1-insertion into a metallocene metal-hydride bond are reported for the first time in this study. Non stereoselective 1,2-insertions of the first propylene unit into the metal-methyl or metal hydride bond have been well established during metallocene catalyzed α -olefin polymerizations(1,2). For example, an enantioselectivity ranging from 0.5 to about 0.65 has been observed for initial 1,2-insertions in metallocene catalyzed 3-methyl-1-pentene polymerizations(1). The upper end of this enantioselective range is associated with the catalyst ligand structure(1), which can impart a small, but definite enantioselectivity. Much higher enantioselectivities in α -olefin polymerizations develop with chain growth(2). This effect has also been observed in classical magnesium chloride supported Ziegler-Natta catalysis(3). Evidence is given in this study that an initial insertion of a propylene monomer into a metal hydride bond also may not have a high level of regioselectivity.

The total 2,1-insertions per chain, including interior 2,1- regio defect structures and both types of 2,1-end groups, are examined as a function of degrees of polymerization. From the relationship between 2,1-insertions and the degrees of

polymerization, a steady state probability for 2,1-insertions is obtained. We have found that initial 2,1-insertions manifested as 2,3-dimethylbutyl end groups represent at least 30% of the initial end groups in the polypropylenes examined in this study.

EXPERIMENTAL

Carbon 13 NMR data were obtained at 100.556 MHz at 125°C on a Varian 400 NMR spectrometer. A 90° pulse, an acquisition time of 4.0 seconds and a pulse delay of 10 seconds were employed. The spectra were broad band decoupled and were acquired without gated decoupling. Typical numbers of transients collected ranged from 4,000 to 6,000. Spectral resonance area measurements were made by integration and measured manually with scale settings between 5000 and 1,000,000, depending upon the strength of the observed signal. At completion, all resonance intensities were converted to a common scale factor. The samples were dissolved in tetrachloroethane-d₂ at concentrations between 10 and 15% by weight. Spectral frequencies were recorded with respect to 21.80 ppm for the *mmmm* methyl resonance, which had been determined with respect to an internal tetramethylsilane standard and is close to the reported literature value of 21.855 ppm(5). The polypropylene methyl pentad/heptad assignments used in this study are well established(5,6,7). A ¹³C NMR DEPT experiment was performed to establish the carbon types and confirm the assignments for the 2,3-dimethylbutyl end group. Normal and DEPT ¹³C NMR spectra are shown in Figure 1.

The first step in determining end group mole fractions is to measure independently the ten methyl pentad ¹³C NMR resonance intensities by spectral integration and then to sum the intensities after conversion to a common scale factor. It is necessary to measure the integrated area of each methyl pentad resonance separately to avoid overlap with resonances from end groups and erythro 2,1-regio defects. The *rr*-centered methyl pentad resonance intensities were actually determined from the corresponding heptad resonances. Each end group produces an array of resonances from which an average resonance intensity corresponding to one carbon atom can be readily determined. It is necessary to use resonance intensities from single carbons for both the end groups and propylene repeat units to express the results in terms of mole fractions. Each end group resonance intensity is converted to a common basis by using the same scale factor as in the methyl pentad intensity measurements. A similar approach was used for the erythro regio defect measurement where an array of resonances was also utilized. No resonances were observed for the corresponding threo isomer. The specific resonances employed for the end group and regio defect area determinations are listed in Table 1, below, and were chosen because they were the least affected by overlap.

Table 1. ^{13}C NMR resonance intensities used to determine end group and regio defect fractions.

| 2,1-regio defect (erythro) ppm | n-propyl ppm | 2,3-dimethylbutyl ppm | n-butyl ppm | iso-butyl ppm |
|-----------------------------------|-----------------|--------------------------|----------------|------------------|
| 42.1 | 39.8 | 43.1 | 36.9 | 25.8 |
| 38.4 | 20.13 | 36.5 | 23.2 | 23.8 |
| 35.8 | 14.5 | 32.0 | 20.85 | 22.5 |
| 35.7 | | 20.53 | 14.1 | |
| 31.4 | | 17.8 | | |
| 40.4 | | 16.3 | | |
| 17.5 | | | | |
| 17.2 | | | | |

The end group mole fractions are calculated by dividing each end group intensity for a single carbon by the sum of the methyl pentad intensities and the single carbon intensities for the erythro 2,1-regio defect and the four types of end groups. These fractions can be converted to a frequency per 10,000 repeat units by simply multiplying each mole fraction by 10,000. The total fraction of 2,1-insertions is determined by adding the regio defect, n-butyl and 2,3-dimethylbutyl fractions. The total 2,1-insertions per molecule is calculated by dividing the total 2,1-insertion fraction by $0.5 \times (\text{sum of the four end group fractions})$.

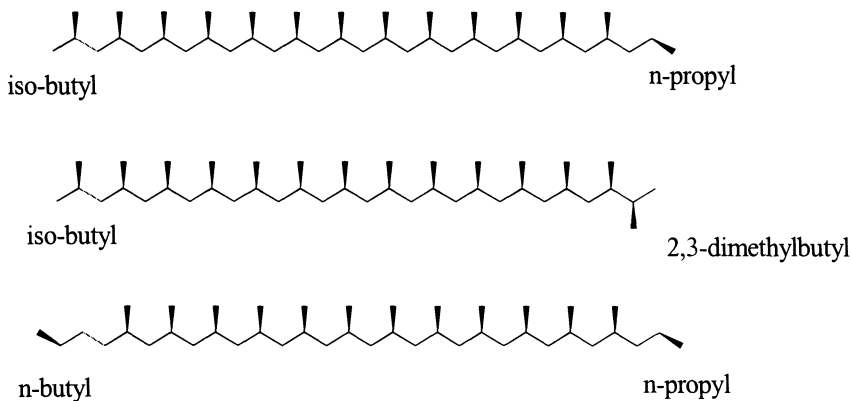
A hydrooligomerization experiment, closely following the conditions of Busico, et al.(8), was performed with a C_2 symmetric metallocene catalyst. The hydrooligomerization conditions are given in Table 2 below. The polymerization utilized high levels of hydrogen to create essentially propylene oligomers, which would lend themselves to GC-mass spectroscopy characterization. Any polymer that formed was removed as a thin film and an aliquot from the hexane solution was submitted for GC-mass spectroscopy analysis. The hexane solution containing the oligomers was separated with an HP 6890 gas chromatograph equipped with a poly(dimethylsiloxane) column. The eluents were analyzed with an HP 5973 mass selective detector. The distribution of observed isomers from the C_9 oligomers confirmed the existence of 2,3-dimethylbutyl end groups.

Table 2. Hydrooligomerization conditions.

| | |
|-----------------|---------------------|
| Catalyst | 1.0 μmol |
| TEAL | 0.25 mmol |
| Propylene | 2.68 moles |
| Hydrogen | 1.67 mol |
| Hexane(solvent) | 300 ml. |
| Temperature | 70° C |

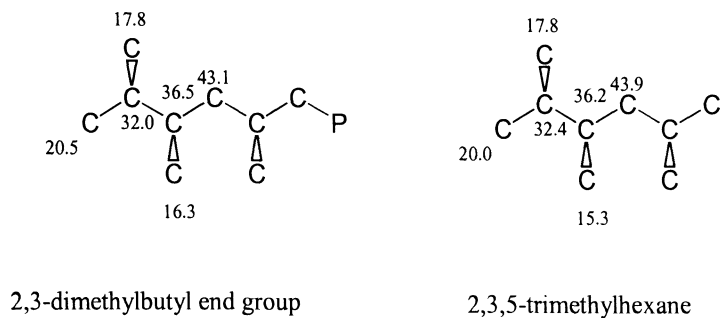
RESULTS AND DISCUSSION

The following types of end groups are expected for polypropylenes prepared with metallocene catalysts in the presence of hydrogen:



A 1,2 insertion of the first propylene unit into a metal-hydride bond produces an n-propyl initial end group. Chain termination by hydrogen of a 1,2-terminal unit produces an isobutyl structure for the final end group, while hydrogenolysis of any terminal 2,1-insertion will lead to a final n-butyl end group(4). What has not been addressed previously is the possibility of an initial 2,1-insertion into a metal-hydride bond followed by a normal 1,2-insertion. This insertion sequence will produce an initial 2,3-dimethylbutyl end group.

The following weak resonances were observed for the 2,3-dimethyl butyl end group, which were assigned by comparison with a model compound, 2,3,5-trimethylhexane(9).



Assignments for the three types of methyl groups, two types of methine carbons and a methylene carbon were also confirmed by a DEPT experiment shown in Figure 1 where the 32.0 and 36.5 methine resonances, the 16.3, 17.8 and 20.5 methyl resonances and the 43.1 methylene resonance are clearly identified. Resonances for 2,3-dimethylbutyl end groups can also be seen in polypropylene ^{13}C NMR spectra published by other investigators(4,10), although the presence of 2,3-dimethylbutyl end groups was not mentioned in either article. The DEPT experiment reported by Carvill, et al.(10), where the 2,3-dimethylbutyl resonances were overlooked, gave the same DEPT results for the 2,3-dimethylbutyl end group reported in this study. Examination of a low molecular weight polypropylene fraction obtained by collecting xylene soluble polymers at room temperature affords a better opportunity to observe 2,3-dimethylbutyl end groups as shown in Figure 2.

GC mass spectroscopy results were obtained for the low molecular weight oligomers from the hydrooligomerization experiment. It was possible to observe the C_9 trimer distribution by GC-mass spectroscopy as shown in Table 3. The C_9 trimers must uniquely arise from initial propylene insertions into a metal-hydride bond. Eight skeletal isomers are possible: four with 1,2- centers and four with 2,1-centers. No isomers were observed for consecutive 2,1-insertions. The remaining five isomers are given in Table 3. The GC mass-spectroscopy results have a valuable feature in that they not only show initial 2,1-insertions, but give identifications and estimates of 2,1-insertions for the second and third insertions as well. A 2,1-insertion for the second insertion is a regio defect while 2,1-insertions for the one and three positions of the oligomer give the structures expected for end groups. 2,3-Dimethyl-1-heptene arises uniquely from a 1,2-2,1-1,2 insertion sequence because the double bond establishes the direction of chain growth. It is interesting to note that the observed approximately 1 - 2 % of 2,1-insertions for the second insertion is close to the approximately 1% regio defects observed for polypropylenes prepared with the same catalyst system in the presence of hydrogen. The 1 to 2 % of regio defects observed for the middle repeat unit of the trimers suggest that regio selectivity develops rapidly after initial 2,1-insertions. A relatively high percentage of final 2,1-insertions among the trimers is expected because of the more favorable conditions for chain transfer with hydrogen over propagation for a terminal 2,1-unit(4).

Table 3. GC-mass spectrometry of propylene trimers after hydro-oligomerization.

| Retention Time (min.) | Relative Abundance | Trimer | Insertion Sequence |
|--------------------------|-----------------------|------------------------|-------------------------------|
| 18.002 | 4.9 | 2,3,5-trimethylhexane | 2,1-1,2-1,2 |
| 18.322 | 72.2 | 2,4-dimethylheptane | 1,2-1,2-1,2 |
| 18.738 | 1.2 | 5-methyl-2-octene | 1,2-1,2-2,1 |
| 18.823 | 1.2 | 2,3-dimethyl-1-heptene | 1,2-2,1-1,2 |
| 19.004 | 5.4 | 2,4-dimethyl-1-heptene | 1,2-1,2-1,2 |
| 19.511 | 1.0 | 2,3-dimethylheptane | 2,1-1,2-2,1 or 1,2-2,1-1,2 |
| 19.806 | 14.1 | 4-methyl-1-octane | 1,2-1,2-2,1 |

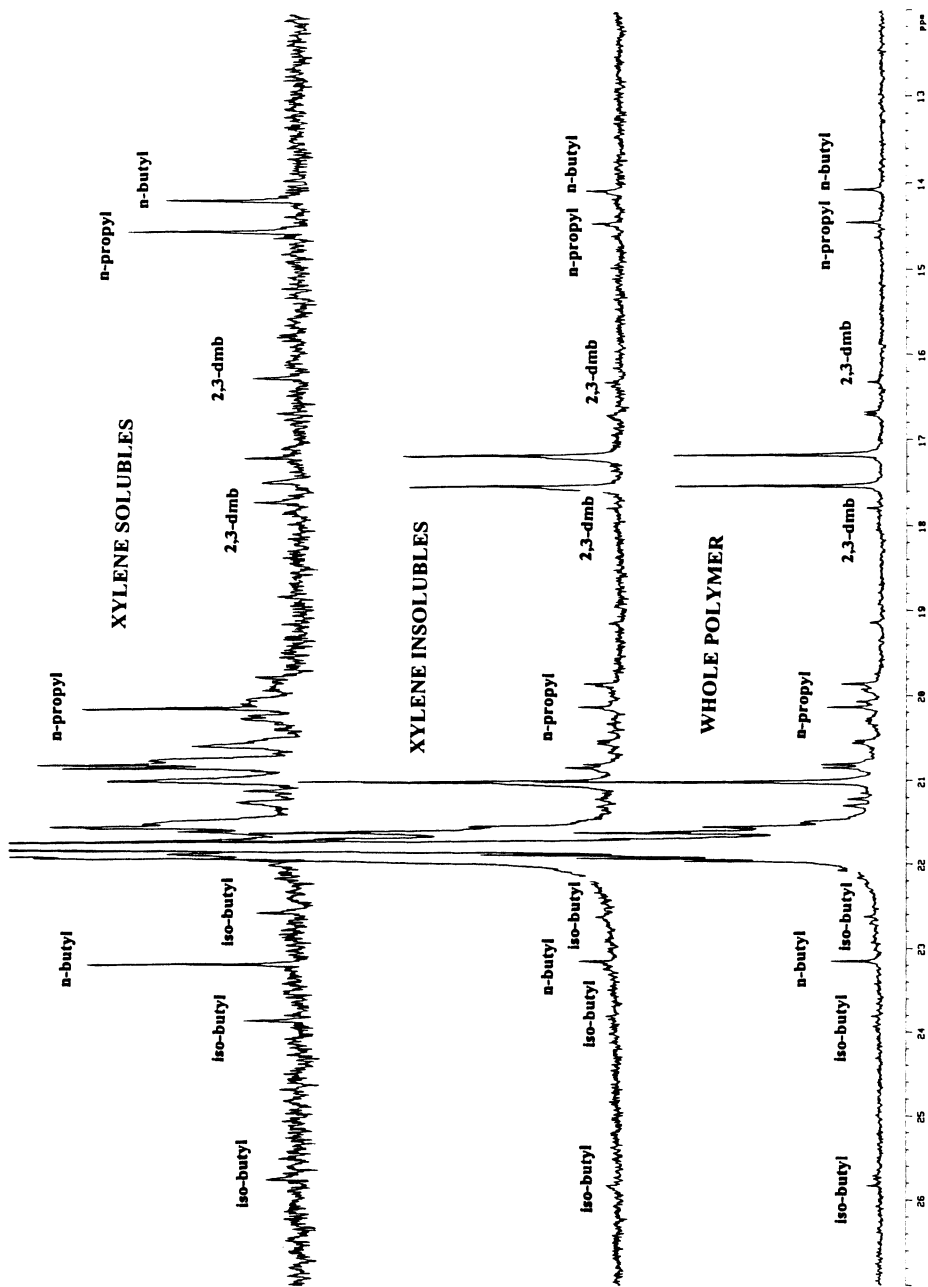


Fig. 2. ^{13}C NMR Spectra at 100 MHz of the Xylene Soluble and Xylene Insoluble Fractions from a Polypropylene Produced with a C2 Symmetric Metallocene Catalyst in the Presence of Hydrogen

If all of the major end groups have been properly identified, the sum of the initial (n-propyl plus 2,3-dimethylbutyl) end groups in the polypropylenes, made with the same catalyst system and in the presence of hydrogen, should equal the sum of the final (n-butyl plus isobutyl) end groups. This conservation of end groups is demonstrated in Table 4 over a broad range of end group concentrations.

Table 4. Conservation of end groups for polypropylenes prepared with a C₂ symmetric catalyst in the presence of hydrogen.

| Polypropylene | n-propyl + 2,3-dimethylbutyl end groups/10,000 repeat units | iso-butyl + n-butyl end groups/10,000 repeat units |
|---------------|---|---|
| 1 | 455 | 443 |
| 2 | 48 | 43 |
| 3 | 20 | 18 |
| 4 | 18 | 18 |
| 5 | 11 | 13 |
| 6 | 9 | 11 |
| 7 | 9.8 | 10.8 |
| 8 | 6.9 | 6.6 |
| 9 | 6.5 | 6.7 |
| 10 | 2.5 | 2.6 |
| 11 | 2.4 | 2.0 |
| 12 | 1.8 | 1.6 |
| 13 | 1.5 | 0.9 |
| 14 | 1.4 | 1.3 |
| 15 | 1.2 | 1.1 |
| 16 | 1.2 | 1.3 |
| 17 | 1.1 | 1.1 |
| 18 | 0.5 | 0.5 |
| 19 | 0.2 | 0.7 |

An important feature obtained from end group analyses of polypropylenes is the end group distribution. Table 5 contains the percent of initial 2,1-insertions (2,3-dimethylbutyl vs. n-propyl) as a function of polypropylene melt flow rate (MFR). It can be seen that the per cent of 2,3-dimethylbutyl initial units shows a slight downward trend over an MFR range of 86 to 788. Hydrogenolysis of initial 2,1-insertions creating propane could cause such a downward trend at the higher levels of hydrogen.

Table 5. Percent initial 2,1-mis-insertions as a function of melt flow rate (MFR).

| MFR | % Initial 2,1-Mis-insertions |
|-----|------------------------------|
| 86 | 33 |
| 224 | 27 |
| 507 | 29 |
| 788 | 25 |

With the 2,3-dimethylbutyl end group positively identified, it is instructive to examine end group distributions as a function of degrees of polymerization for a series of polypropylenes prepared with the same supported C_2 symmetric metallocene catalyst. A 1:1 ratio of n-propyl to n-butyl end groups is typically observed over a broad range of degrees of polymerization, which directly relates to the levels of hydrogen employed in the polymerizations. Correspondingly, the isobutyl to 2,3-dimethylbutyl end group ratio is also close to 1:1. A 1:1 ratio of n-propyl to n-butyl end groups has been observed by others for metallocene polymerizations conducted in the presence of hydrogen(4). Figure 3 contains a plot of the distribution of the four types of end groups as a function of degree of polymerization. After a degree of polymerization of 500, the distribution remains fairly consistent as the chains become longer. It is interesting that more scatter is observed in the low molecular weight regime where the end group measurements are the most accurate. As discussed previously, high levels of hydrogen could cause initial 2,1-insertions to be lost through a generation of propane. This would create changes in the end group distributions for very low molecular weight polymers. Just why there should be scatter in the data for the low molecular weight polypropylenes is not entirely clear. The data for each type of end group in Figure 3 was also used to give fractional averages for the various types of end groups. From 19 observations of the end group distribution, the iso-butyl end groups give an average of 13%, the 2,3-dimethylbutyl end groups give 16%, and the n-propyl and n-butyl end groups represent 35 and 36% of the total end groups, respectively. (The standard deviations were similar and ranged from 4 - 5%.)

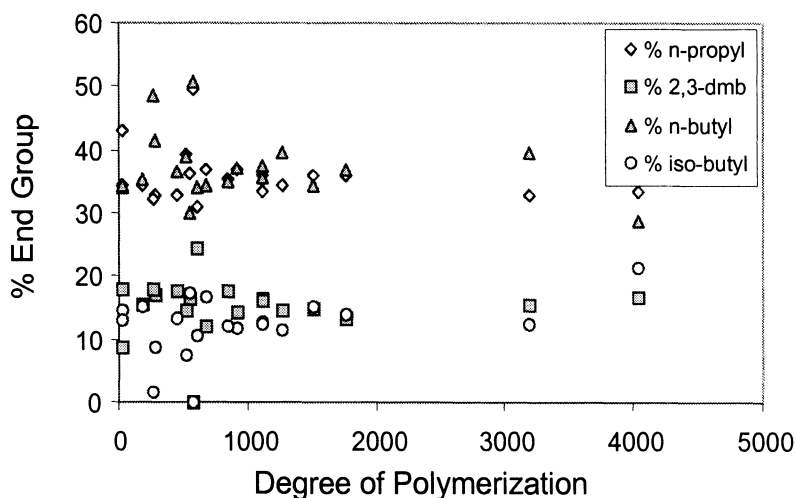


Fig. 3. The End Group Distribution for Polypropylenes Produced with a C_2 Symmetric Metallocene Catalyst in the Presence of Hydrogen

From the end group concentration data determined from ^{13}C NMR, it is also possible to calculate a number average molecular weight. This is done after assuming that the contributing concentrations from any other types of end groups types are insignificant. A comparison of number average molecular weights obtained by ^{13}C NMR and GPC is given in Table 6. Overall, satisfactory agreement is obtained and this result lends credence to the assumption that the four types of end groups identified and utilized in the analyses are the major types of end groups that are present.

Table 6. Number average molecular weights by GPC and ^{13}C NMR.

| Polypropylene | M_n by ^{13}C NMR | M_n by GPC |
|---------------|------------------------------|--------------|
| A | 7600 | 10400 |
| B | 9200* | 8200 |
| C | 10400 | 11500 |
| D | 11800 | 12400 |
| E | 15100 | 18300 |
| F | 21400 | 24100 |
| G | 21800* | 27900 |
| H | 22000 | 23800 |
| I | 22400 | 25100 |
| J | 46700 | 47500 |

*measured on xylene insolubles

From the ^{13}C NMR structural data, it is possible to combine the concentrations for n-butyl, 2,3-dimethylbutyl end groups with the concentrations observed for 2,1-regio defects to give either the total number of 2,1-insertions per average polymer molecule or per 10,000 repeat units. The total 2,1-insertions per molecule is plotted versus degree of polymerization (D.P.) in Figure 4. A linear relationship is observed. Data from whole polymers, xylene soluble fractions and xylene insoluble fractions are included in Figure 4. The fact that uniform results are obtained from fractions and whole polymers is an indicator of the completely random nature of the 2,1-regio defect distribution. Linear regression gave the following equation for the best fit:

$$\text{Total misinsertions/molecule} = 0.0095 (\text{D.P.}) + 0.3947$$

$$r^2 = 0.995$$

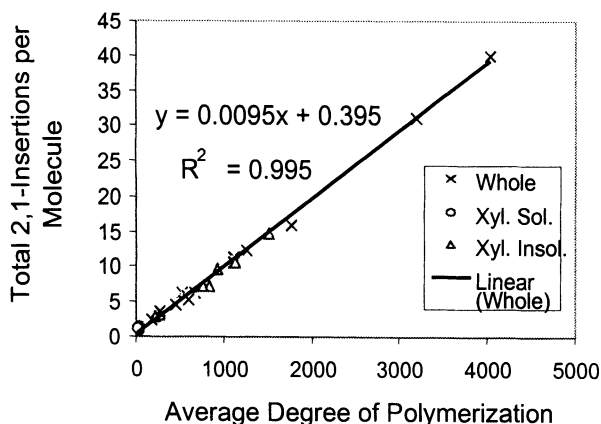


Fig. 4. 2,1-Insertions per Molecule versus Average Degree of Polymerization

The slope, 0.0095, is the probability for a 2,1-insertion with each monomer insertion. The fraction of total 2,1-insertions expressed per 10,000 repeat units versus degree of polymerization is plotted in Figure 5. The two calculated points are 95, as given by the 0.0095 slope from Figure 4. It can be seen that the number of total 2,1-insertions per 10,000 repeat units reaches a steady state value of 95 around a degree of polymerization of 500. The shape of the curve in Figure 5 is a result of the behavior of the end group concentrations, which become less significant with increasing molecular weight. Polymerizations conducted with the same unsupported C_2 symmetric catalyst give a different probability for 2,1-insertions with each monomer insertion, as can be seen in Figure 6. In this case, the slope is 0.0042 with an r^2 of 0.996.

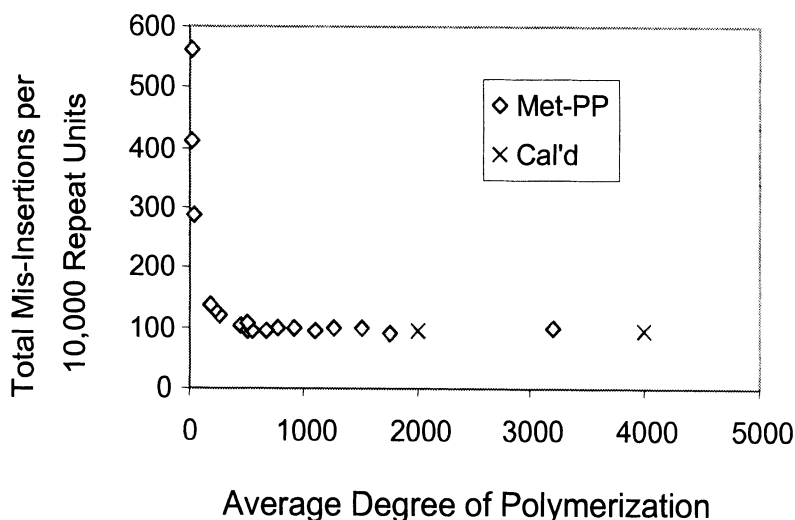


Fig. 5. 2,1-Insertions per 10,000 Repeat Units versus Average Degree of Polymerization

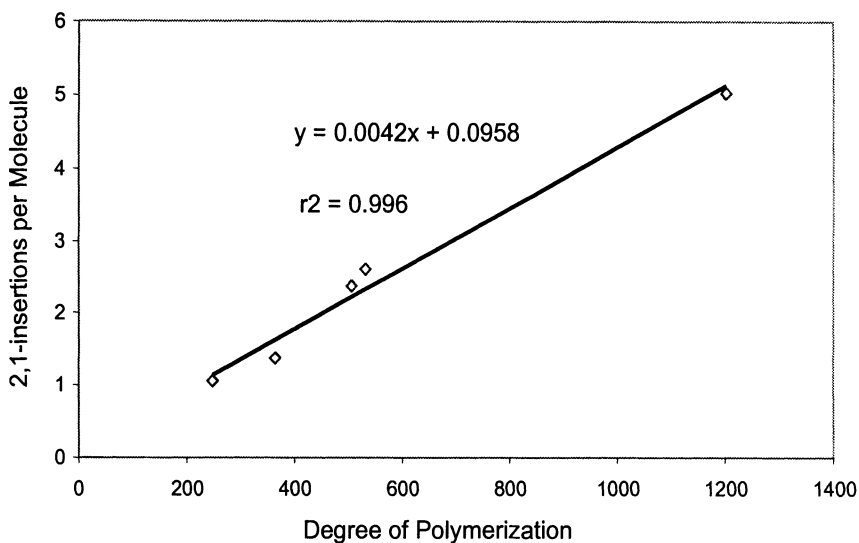


Fig. 6. 2,1-Insertions per Molecule versus Average Degree of Polymerization for Polypropylenes Prepared in Solution

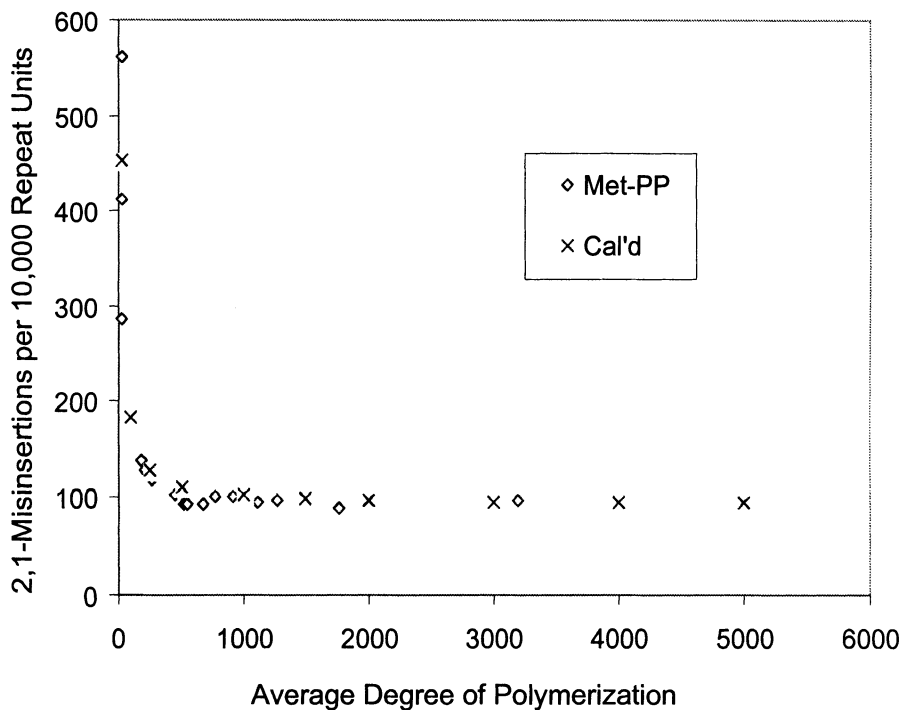


Fig. 7. Calculated 2,1-Insertions per 10,000 Repeat Units versus Average Degree of Polymerization Based on a Model Assuming Random Regio Defects

A calculated fit for total 2,1-insertions per 10,000 repeat units versus degree of polymerization is given in Figure 7. The calculated points that give a good fit utilized 30% initial misinsertions, 60% terminal misinsertions and a probability of a 2,1-insertion with each monomer insertion of 0.0095. The fact that a calculation of this type reproduces the observed behavior once again demonstrates the random nature of the 2,1-regio defect distribution.

Finally, it is instructive to examine the behavior of the 2,1 regio defects as a function of degrees of polymerization excluding 2,1-insertions from end groups. A plot of 2,1-regio defects per molecule versus average degree of polymerization is given in Figure 8.

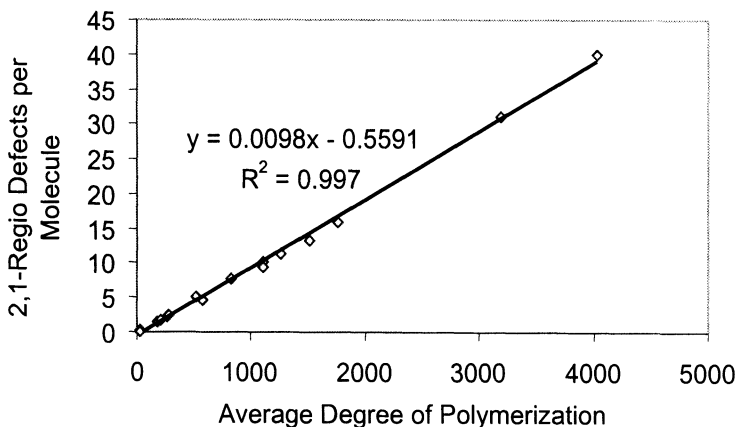


Fig. 8. 2,1-Regio Defects per Molecule Average Degree of Polymerization

The best fit, after linear regression is,

$$2,1 \text{ regio defects/molecule} = 0.0098*(D.P.) - 0.5591$$

$$r^2 = 0.997$$

It is not surprising that a negative intercept and a higher slope was obtained for the 2,1-regio defects versus total 2,1-insertions. The concentrations of 2,1-regio defects must diminish significantly at the lower molecular weights because of hydrogenolysis of terminal 2,1-inserted propylene units.

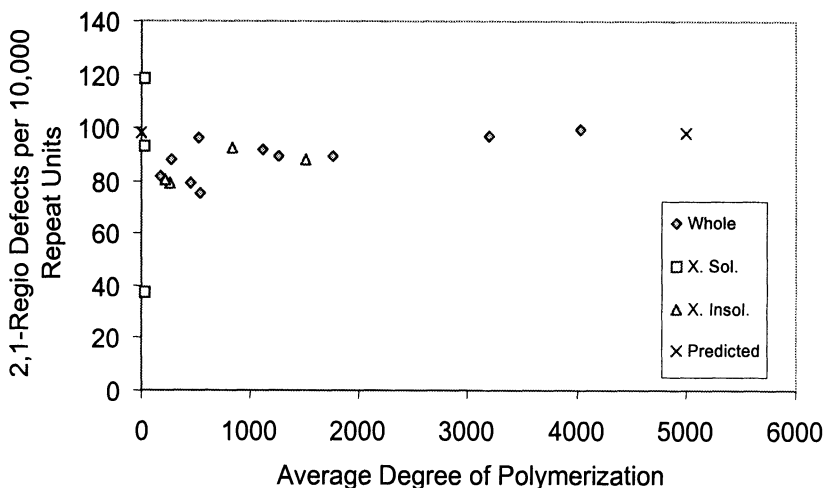


Fig. 9. 2,1-Regio Defects per 10,000 Repeat Units versus Average Degree of Polymerization

This behavior can be more clearly seen in Figure 9 where regio defects per 10,000 repeat units are plotted versus degree of polymerization. The calculated points are determined from the slope of the line (0.0098) in Figure 8. There is scatter among the data for the low molecular weights because of the weakness of the 2,1-regio resonances, but typically the number of 2,1-regio defects per 10,000 repeat units approaches 80 as the degrees of polymerization fall below 1000. Clearly, the sounder approach is to consider the total 2,1-insertions per molecule or per 10,000 repeat units when examining the behavior of 2,1-insertions as a function of molecular weight.

SUMMARY AND CONCLUSIONS

Initial 2,1-misinserted propylene units have been identified for the first time in this study. Although the observed initial 2,1-insertions occur nominally at around 30 percent, it is possible for the actual amount to be higher. Hydrogenolysis can convert initial 2,1-insertions to propane, which was detected among the off gases during polymerization although quantitative results could not be obtained. A value of 50% initial 2,1-insertions would be the point at which initial propylene insertions into a metal-hydride bond are non-regioselective and are simply random. Finally, it was observed that the probability for 2,1-insertions was affected neither by the presence of hydrogen nor for two different counter ions.

The presence of initial 2,1-inserted propylene units is not just related to the specific C_2 symmetric catalyst employed in this study. Although previously overlooked, resonances for initial 2,1-misinserted propylene units can be observed in published ^{13}C NMR spectra of polypropylenes prepared with other C_2 symmetric catalysts(4,10). In addition, we have observed 2,3-dimethylbutyl end groups for polypropylenes produced with classical magnesium chloride supported Ziegler-

Natta catalysts. This may not be surprising in view of the fact that n-butyl end groups are also observed(11).

Good agreement is obtained between number average molecular weights determined by GPC versus that calculated from ^{13}C NMR end group data. This result indicates that the most important end groups have been identified and there are no significant contributions from vinylidene, 2-butenyl and 4-butenyl end groups(10). Resonances characteristic of these end groups were not observed. It is also likely that any original, residual vinylidene end groups underwent double bond re-arrangements that left the isobutyl skeletal unit intact. The NMR experiments utilized tetrachloroethane- d_2 as the NMR solvent, which is known to lead to vinylidene rearrangements at the temperature of the NMR experiments(12).

ACKNOWLEDGMENTS

The authors gratefully acknowledge helpful discussions with Drs. Jeff Brinen and Main Chang. Appreciation is also expressed to Exxon Chemical Company who granted permission to publish this work.

REFERENCES

- 1.) M. C. Sacchi, E. Barsties, I. Tritto, P. Locatelli, H.H. Brintzinger and U. Stehling *Macromolecules*, **30**, 1267 (1997)
- 2.) P. Longo, A. Proto, A. Grassi and P. Ammendola, *Macromolecules*, **24**, 4624, (1991)
- 3.) M. C. Saachi, F. Forlini, I. Tritto, R. Mendichi, G. Zannoni and L. Noristi, *Macromolecules*, **25**, 5914 (1992); M. C. Saachi, P. Locatelli and I. Tritto, *Makromol. Chem.*, **190**, 139 (1989)
- 4.) S. Jüngling, R. Mülhaupt, U. Stehling, H. H. Brintzinger, D. Fischer and F. Langhauser, *J. Polym. Sci., Polym. Chem.*, **33**,1305 (1995)
- 5.) T. Hayashi, Y. Inoue, R. Chûjo, and T. Asakura, *Polymer*, **29**, 138 (1988)
- 6.) F. C. Schilling and A. E. Tonelli, *Macromolecules*, **13**, 270 (1980)
- 7.) V. Busico, P. Corradini, R. De Biasio, L. Landriani and A. L. Segre, *Macromolecules*, **27**, 4521 (1994)
- 8.) V. Busico, R. Cipullo, and P. Corradini, *Makromol. Chem.* **194**, 1079 (1993)
- 9.) N. Chamberlain, Private Communication
- 10.) A. Carvill, L. Zetta, G. Zannoni and M. C. Sacchi, *Macromolecules*, **31**, 3783 (1998)
- 11.) J. C. Chadwick, G. M. M. van Kessel and O. Sudmeijer, *Macromol. Chem. Phys.* **196**, 1431 (1995)
- 12.) B. Rieger, A. Reinmuth, W. Röhl and H. H. Brintzinger, *J. Mol. Cat.*, **82**, 67 (1993)

Olefin Polymerization with DuPont's Versipol™ Catalyst System

Steven D. Ittel

DuPont, Central Research and Development
Experimental Station
Wilmington, DE 19880-0328, USA
Steven.D.Ittel@usa.dupont.com

Abstract. In collaboration with the University of North Carolina, DuPont is developing a new catalyst technology for olefin polymerization. Versipol™ catalyst technology is based upon the late transition metals. The steps in DuPont's commercialization effort are outlined.

Introduction

DuPont has a major business in the copolymerization of ethylene with polar comonomers to produce high value-added products for the packaging and industrial polymer industries. This line of products is based upon copolymerization of ethylene with monomers like acrylic acid or methyl methacrylate. These polymerizations are carried out under the relatively forcing conditions of 1-3 kilobars pressure and temperatures of 150-250 °C. It was clear that milder conditions could provide a lower-cost or lower investment opportunity.

Over twenty years ago, George Parshall initiated a program on coordination polymerization of ethylene with polar comonomers. He correctly predicted that the successful catalyst would be nickel derived. In spite of that prediction and considerable effort, a viable catalyst system was not discovered and the program was abandoned.

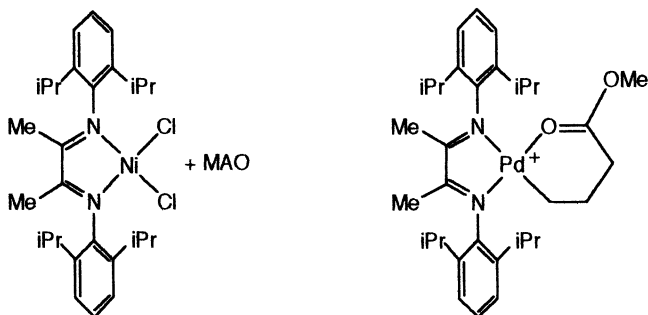
It was decided to reinitiate the program; the approach was predicated upon the following presumptions:

- The polymerization would be late metal catalyzed.
- The desired catalyst could be identified by searching under ambient conditions even though it was presumed that optimal conditions would not be ambient.
- Coordination polymerization will yield linear polymers.
- Post-polymerization modification is an acceptable method for lab synthesis of polymers, but would not be reasonable for a commercial process.

It was decided to enhance DuPont's effort by identifying a university partner. Professor Maurice Brookhart at the University of North Carolina had a very strong program on electrophilic, late transition metal catalysts. He had recently entered the area of polymerization catalysis through his studies on styrene/CO alternating

copolymerizations. DuPont had established a high level of comfort with Brookhart through consulting, collaboration, and sharing of students. Professor Brookhart found DuPont's description of the copolymerization challenge of interest. Lynda Johnson, then a postdoctoral student, accepted the challenge and initiated a program on ethylene polymerizations with late metals. The rest is history.¹

The initial catalysts presented to DuPont were based primarily, but not exclusively upon cationic complexes of nickel and palladium with bulky α -diimine ligands. Typical examples are shown [MAO (methyl aluminoxane) converting Ni^{II} dihalides into an active cationic form]:



The cationic nature of the catalysts promotes ethylene coordination and the bulky nature of the ligands reduces the associative displacement of growing polymer chains, leading to high molecular weight.

The Approach

With the initial invention in hand, it was clear that a major effort was going to be required to fully exploit the new polymerization technology. The scope of the catalysts would have to be expanded significantly. Very early in the program, it was clear that type of polymers being generated were unlike those seen previously and the new structures could provide valuable patent protection. To facilitate both of these efforts, a fundamental understanding of the underlying technology would be essential.

Laboratory investigation quickly demonstrated that the α -diimine ligands were not unique. A robust catalyst screening method would facilitate the discovery of new catalyst families. Screening many polymerizations with the identified catalysts was a secondary, but important objective. This became particularly important through its impact on the mechanistic studies.

These scouting and fundamental programs can be thought of as "looking out" – expanding the scope of knowledge and expanding the patent scope. It was also necessary to have clearly identified commercial targets – "focussing problems" – those objectives which are a reality check and a measure of ones progress. Does

¹ L. K. Johnson, C. M. Killian and M. Brookhart, *J. Am. Chem. Soc.*, **117**, 6414 (1995).

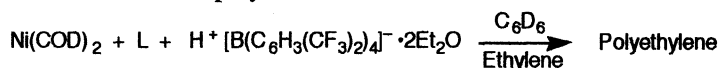
one have sufficient catalyst activity? Catalyst productivity? Is there a potential commercial process? Is there some commercially attractive attribute of the polymer?

As the program was initiated, the name "Versipol™" was coined to describe this late metal olefin polymerization technology. It is particularly apt because this technology is very versatile in its abilities to catalyze commercially-significant transformations. "The Approach" above constitutes an outline for the remainder of this paper.

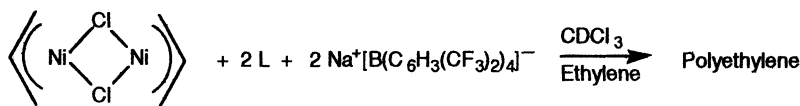
Catalyst and Ligand Screening

Due to the (apparent) simplicity of preparation of α -diimine ligands, it became possible to generate a wide range of ligands in a short period of time through what would be a "combinatorial," or more aptly, a "parallel synthesis" approach. To be able to test these catalysts, a simple, robust screening procedure needed to be implemented. What we settled upon was an array of tests.

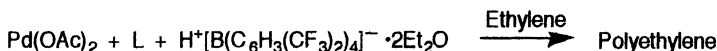
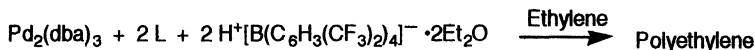
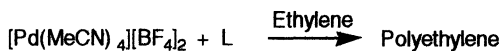
Starting from Ni^0 , protonation with a non-coordinating acid in the presence of ethylene leads to initiation of polymerization.



Initiation from a Ni^{II} allyl complex by abstraction of halide was an alternative approach.



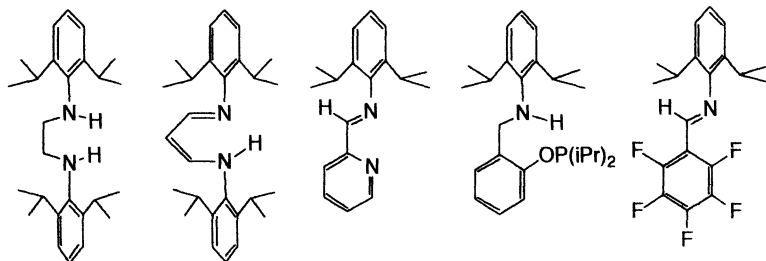
Similar screens utilizing Pd^{II} and Pd^0 were also established.



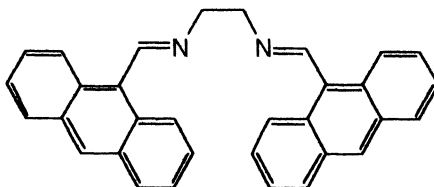
The ease of these screens was a strong positive. Isolation of the organometallic was not required. By carrying out the polymerizations directly in an NMR solvent, the polymers could go directly to initial characterization of branching density. Nonetheless, this type of screening has serious limitations. Many things have to go occur in the proper sequence to get a positive polymerization result. The ligand has to displace the existing ligands, conversion to an active cationic form has to occur, and the initiation of polymerization has to occur – all in the order indicated. Thus it is easy to see that any single approach could miss potential catalysts.

In addition, these catalysts are not necessarily "innocent" - there can be active communication between catalysts. One catalyst can be very active in butene or α -olefin formation. An adjacent catalyst could be very active in ethylene copolymerization with α -olefins and incorporate the product being produced by its neighbor. In this case, one would still get a positive, but the polymer would not be representative of what one would expect. In a worse case, a catalyst could be very active for ethylene homopolymerization but inhibited by α -olefins - it would show a "negative result" even though it was active for ethylene homopolymerization. By employing an array of screens, it was more likely that active species would not be overlooked. Clearly, there is no substitute for preparation, isolation, careful characterization and finally isolated testing of a catalyst.

The initial results of the screening effort resulted in the largest single case ever filed by DuPont.² It focuses largely on the α -diimine catalysts from both UNC and DuPont, together with the resulting polymers and their applications. In addition to this case, a subsequent filing became the first patent to issue on Versipol™ technology.³ These cases disclosed a wide variety of ligands, which formed effective catalysts for ethylene polymerization. They include α -diamines, β -diimines (shown in its enamine structure), pyridylmonoimines, and monoimines.



Another interesting class of compounds was the diimines represented by the structure:

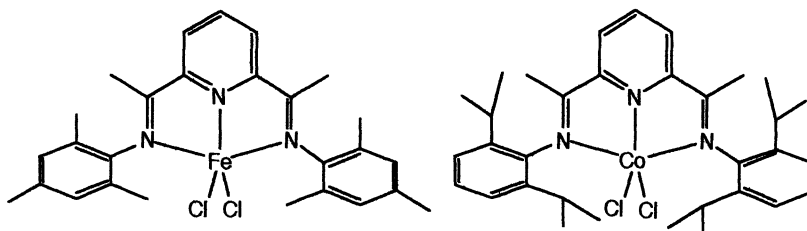


² WO 96/23010 - "The 500/500/500 Case" - L. K. Johnson, C. M. Killian, S. D. Arthur, J. Feldman, E. F. McCord, S. J. McLain, K. A. Kreutzer, A. M. A. Bennett, E. B. Coughlin, S. D. Ittel, A. Parthasarathy, D. J. Tempel, M. S. Brookhart

³ US 5,714,556 (Feb 3, 1998), L. K. Johnson, J. Feldman, K. A. Kreutzer, S. J. McLain, A. M. A. Bennett, E. B. Coughlin, D. S. Donald, L. T. J. Nelson, A. Parthasarathy, X. Shen, W. Tam, Y. Wang

where the chelate bite is the same as the α -diimines, but the unsaturation is exo-metallo-cyclic in the resulting metal complex. This library of ligands greatly expands the range of Versipol™ catalysts, each providing its own set of polymerization properties with unique attributes and liabilities. For any particular application, one must identify the preferred catalyst system.

As mentioned above, the α -diimine-based catalysts were not limited to nickel and palladium; they also worked with Co^{II} and Fe^{II} . Not satisfied with their low activity, a program to discover more active iron and cobalt catalysts was undertaken. Tridentate, pyridyldiimine ligands were found to yield much higher activity.⁴



Like the nickel catalysts, these catalysts are most active in their cationic form, especially when activated with MAO. Unlike the nickel catalysts, ethylene homopolymerization provide high density, high molecular weight polyethylene. Ethylene copolymerizations with α -olefins yield linear low density polyethylenes. When the sterics of these catalysts are tuned back, they can also produce α -olefins with very high rates and productivities.⁵

After broadening the scope of the neutral chelating ligands, it was decided that there could well be families of anionic ligands that would yield "neutral nickel" catalysts. This was confirmed with the discovery of a broad range of catalysts.⁶ The steric requirement to obtain high molecular weights, observed in the neutral ligands, was maintained in the anionic ligands. In general, these complexes perform best if activated with a non-coordinating Lewis acid activator.

The catalyst synthesis and screening program continues. The range of polymerizations being scouted has been increased as additional, robust screens have been developed.

⁴ a) WO 98/27124, A. M. A. Bennett. b) WO 98/30612, M. Brookhart, B. L. Small. c) G. J. P. Britovsek, V. C. Gibson, B. S. Kimberley, P. J. Maddox, S. J. McTavish, A. J. P. White, D. L. Williams *Chem. Commun.* 849 (1998). d) B. L. Small, M. Brookhart, A. M. A. Bennett, *J. Am. Chem. Soc.*, 120, 4049 (1998)

⁵ B. L. Small, M. Brookhart, *J. Am. Chem. Soc.*, 120, 7143 (1998).

⁶ a) WO 98/30609 L. K. Johnson, A. M. A. Bennett, E. B. Coughlin, J. Feldman, E. Hauptman, S. D. Ittel, A. Parthasarathy, R. D. Simpson, L. Wang. b) WO 98/30610 J. Bennett, M. Brookhart, L. K. Johnson, C. M. Killian. c) C. Wang, S. Friedrich, T. R. Younkin, R. T. Li, R. H. Grubbs, D. A. Bansleben, M. W. Day, *Organometallics*, 17, 3149 (1998)

The Polymers

From inception of this program, it was observed that the polymers resulting from most of the polymerizations did not behave as one might expect. For instance, ethylene homopolymerizations with the Ni^{II} or Pd^{II} catalysts did not produce the white crystalline powder. Rather, the products ranged from LLDPE to plastomers to elastomers to oils, all with appreciable molecular weights. Polymerization of lower α -olefins resulted in elastomers but as the molecular weight of the α -olefin was increased, the resulting polymer began to look like LLDPE. All of these observations had to be explained.

The first job was to begin to quantify the branching. With branching levels between 20 and 160 per 1000 methylene carbons, there was considerable variation between samples. Through a series of sophisticated multidimensional NMR experiments, it was possible to individually quantify each of the branches between methyl and pentyl (C₁-C₅) as well as some branches-upon-branches such as sec-butyl. Figure 1 indicates the branching distribution in several samples. It can be seen that for several Ni-derived polymers, there are more methyl than ethyl than propyl, etc. The same relationship holds for the even or the odd branches of a Pd-derived polymer, but there are a disproportionate number of even branches (dotted line).

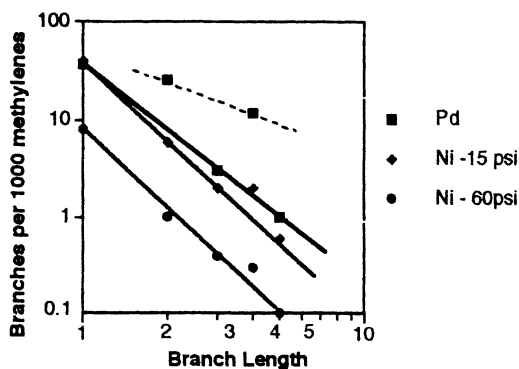


Fig. 1. Distribution of branches in typical Ni- and Pd-derived polyethylenes as a function of branch length.

This distribution can be explained by a "chain-walking" mechanism in which the growing polymer chain undergoes a series of β -hydride eliminations and reinsertions. In Figure 2, the growing polymer chain is indicated at the top. Beta-elimination and reinsertion would move the metal center down the polymer chain. Insertion of an ethylene at any point terminates the walking and propagates the polymer chain. Short side-branches are more likely than long ones because more steps are required to obtain the longer branches.

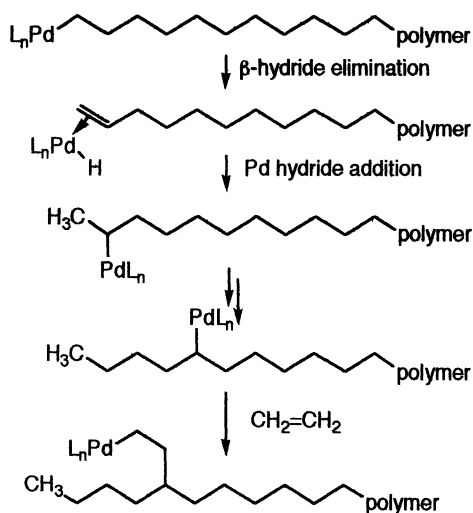


Fig. 2. Illustration of the chain walking mechanism.

If the metal center inserts one ethylene and then walks back to the main chain, an ethyl branch is produced (a butyl if there are two insertions before walking). This particular variation of the mechanism yields only even branches. Thus the total distribution of branches observed is the superposition of the two mechanisms, one making even and odd branches and the other making only even.

It is important to note two important features of this mechanism. First, chain walking is not a new mechanism. It has been observed in a number of polymerizations including α -olefin polymerization⁷ and cyclopentene polymerizations⁸ in which insertion is 1,3- or α,ω - rather than 1,2-. Propylene polymerizations in which propylene 1,3-insertions have occurred are also known so there is ample precedent for an elimination-reinsertion mechanism. Highly branched polyethylenes from ethylene homopolymerizations are also known.⁹ Mixed-catalyst systems that make α -olefins and copolymerize them in the same reactor are an example and can be traced back to Ziegler who combined Ni- and V-derived catalysts. The process described here can be differentiated from both of these approaches, because high molecular weight polymers with statistically mixed branching are obtained. The polymers are free of any unincorporated α -olefin, a feature that contributes greatly to the commercial prospects of the technology. A process that produced and incorporated only butene or hexene could be attractive,

⁷ V. Möhring, G. Fink, *Angew. Chem., Int. Ed., Engl.* 17, 466 (1978).

⁸ W. Kaminsky, A. Bark, R. Spiehl, M. Moller-Lindenhoff, S. Niedoba, pp 291 in W. Kaminsky and H. Sinn (Eds.) "Transition Metals and Organometallics as Catalysts for Olefin Polymerization," Springer Verlag, Berlin Heidelberg (1988). W. M. Kelly, N. J. Taylor, S. Collins, *Macromolecules*, 27, 4477 (1994).

⁹ K. A. Ostoja Starzewski, J. Witte, K. H. Reichert, G. Vasiliou, pp 349 in W. Kaminsky and H. Sinn (Eds.) "Transition Metals and Organometallics as Catalysts for Olefin Polymerization," Springer Verlag, Berlin Heidelberg (1988).

but production of higher olefins in a polymerization would require a prohibitive extraction process to reduce odor. Nonetheless, it should be noted that certain of the late-metal catalysts reported here are among the most active α -olefin synthesis catalysts known and they would fit admirably into such a concept.

Polymerizations of higher olefins than ethylene gave interesting results that are illustrated very briefly here. Propylene polymerization yields a low T_g (-30 to -50 °C) polymer unlike other polypropylenes. NMR investigation of the enchainment identified polyethylene segments, polypropylene segments and even 4-methyl-1-pentene segments. Figure 3 illustrates the similarity between this polymer and a polymer of 4-methyl-1-pentene. The various monomers are indicated by sets of common symbols (sets of three for propylene and six for 4-methyl-1-pentene). Insertion of propylene at the end of a branch yields the same structure as 1,2-insertion of 4-methyl-1-pentene. A 1,5-insertion of 4-methyl-1-pentene yields the same structure as combined 1,3 and 1,2-insertions of propylene.

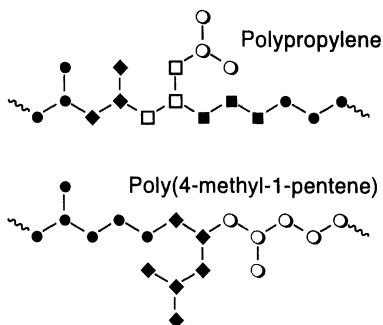


Fig. 3. Comparison of the structures of propylene and 4-methyl-1-pentene polymerizations with a palladium catalyst.

These observations indicate that the catalyst centers can walk through tertiary centers on a growing polymer chain. This is in accord with the observation of sec-butyl groups in ethylene polymerizations. It also indicates that α -olefins are incorporated only at the end of a growing chain, but that a methyl branch on a polyolefin chain represents enough of an "end" to allow insertion. In contrast, ethylene can insert anywhere on a polyolefin chain except at a tertiary center or at a carbon adjacent to a tertiary center.

The palladium catalysts are capable of copolymerizing ethylene with a variety of polar comonomers.¹⁰ Depending upon polymerization conditions, incorporation levels of methyl acrylate from 5-40% have been obtained. The copolymerization at first appears to be random, but detailed NMR analysis of the polymers combined with detailed NMR analysis of the copolymerization mechanism reveals that much of the methyl acrylate incorporation is not along the polymer chain as might be expected, but rather, at the ends of branches. In addition to these functional

¹⁰ S. Mecking, L. K. Johnson, L. Wang, M. Brookhart, *J. Am. Chem. Soc.*, **120**, 888 (1998).

branches, the catalyst also makes the branches expected for chain walking. The resulting polymer can be very low in crystallinity. This structure makes the acid groups of the acrylic groups more available for functionalization reactions such as ionomer formation or crosslinking.

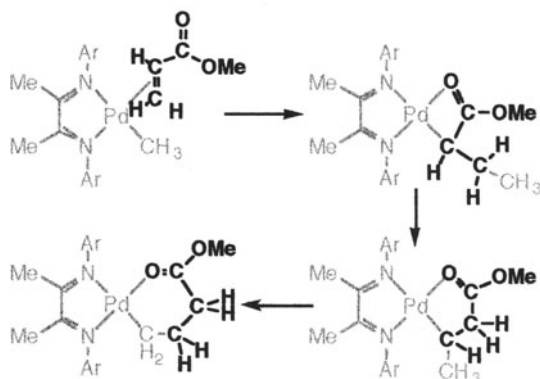


Fig. 4. Mechanism of methyl acrylate incorporation at the end of polymer branches. This is also the mechanism of formation of the palladium metallocycle complex illustrated at the beginning of the paper. Incoming monomer and its fate are in black.

The chain-walking mechanism indicated in Figure 4 is responsible for the acrylate incorporation at the end of branches. The six-membered metallocycle is a stable resting state for the catalyst. As a result, the polar monomer copolymerizations are very slow in comparison with normal ethylene homopolymerizations.

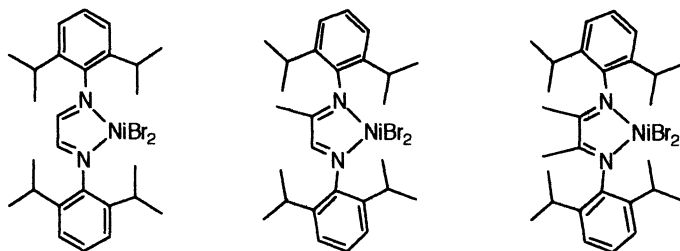
In addition to methyl and other alkyl acrylates, the α -diimine catalysts will copolymerize other acrylics including functional esters such as glycidyl acrylate and acrylic acid. Internal olefins, α -olefins, and cyclic olefin are also copolymerized, as are vinyl ketones and carbon monoxide. Traditional monomers which will not copolymerize but which do not stop ethylene homopolymerization include methacrylates, maleic anhydride, vinyl ethers and fluoroalkylethylenes; some of these inhibit homopolymerization slightly. Monomers which do not copolymerize and completely inhibit ethylene homopolymerization include styrene, vinyl acetate, polycyclic olefins like norbornenes, and diolefins which can be isomerized to conjugated species faster than monomer incorporation.

Processes

It is clear that to have a commercial success, one must have a viable commercial process. A process for LLDPE will be the focus of this section of the paper, because it illustrates all of the issues that must be addressed. Polymerizations have

been run from -90 (for NMR) to $+150$ °C and under pressures of 0.1 to 300 atm. The pressure of 0.1 atm may seem unusual, but as will be seen in a moment, the branching of the polymer is pressure-dependent, so to achieve the very highest levels of branching, low pressures are useful. To date, polymerizations have been demonstrated in solution, slurry, suspension, and gas phase. In the polymer industry, each of these processes has its own advantages and limitations. Slurry and gas phase are appropriate to HDPE and LLDPE production. Solution and gas phase polymerizations are appropriate for LLDPE, but as the density of the polymer is lowered, solution becomes more viable.

There are a variety of controls on the polymerizations. Firstly, the polymer is dependent upon the particular catalyst chosen. For instance, simply changing the number of methyls on the backbone of the α -diimine catalysts can have a pronounced effect on the molecular weight and density of the resulting polymers. Under one set of conditions, the following behavior was observed.



| | | | |
|-------------------|--------|---------|---------|
| $M_n =$ | 19,000 | 72,000 | 340,000 |
| $M_w =$ | 40,000 | 154,000 | 710,000 |
| $CH_3/1000CH_2 =$ | 34 | 75 | 100 |

Molecular weight goes up and density goes down with increasing substitution on the catalyst backbone. Beyond these variables based upon catalyst structure, there are a variety of parameters that can be varied during polymerizations. These include temperature, pressure (both of which influence the concentration of ethylene available to the catalysts), and the presence of chain transfer agents such as hydrogen.

Molecular weight drops with increasing temperature (Figure 5), branching increases with increasing temperature (Figure 6) and molecular weight decreases with increasing hydrogen content in the ethylene feed stream (Figure 7). Thus, with this combination of controls, it is possible to independently control density and molecular weight without having the normal additional control of added α -olefin for density control.

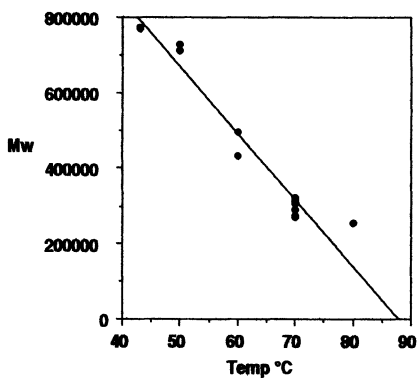


Fig. 5. Response of molecular weight to temperature for a nickel α -diimine catalyst.

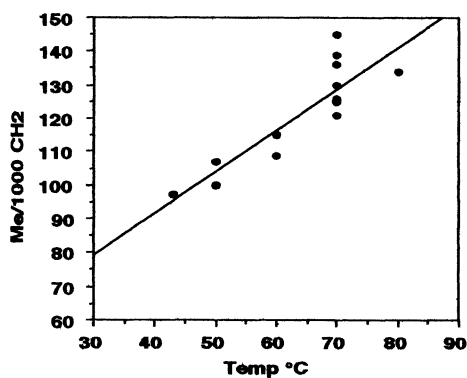


Fig. 6. Response of branching to temperature for a nickel α -diimine catalyst.

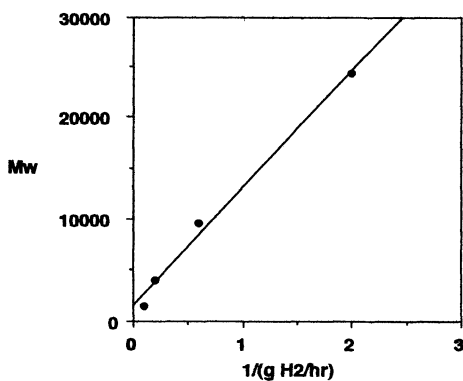


Fig. 7. Response of molecular weight to hydrogen for a nickel α -diimine catalyst.

For gas phase polymerization, morphology control of the particles in the fluidized polymer bed requires carefully supported catalysts. Versipol™ catalysts are amenable to supporting in a variety of means, many of which are in common with metallocenes. Upon being supported, the general behavior of the catalysts is similar to that observed in solvent-based polymerizations, but changes in several critical catalytic rates means that extrapolation between solution and gas-phase requires considerable experience. For instance, to change density, one does not change the ratio of two monomers; rather, it is dependent upon only the local concentration of ethylene. Differences in local concentrations of ethylene between gas phase and solution and the transport of ethylene through a polymer particle are different in their particulars. Nonetheless, gas-phase polymerizations can be controlled quite successfully.

Conclusions

Versipol™ polymerization technology is a remarkable advance whose full impact remains to be discovered. The intent of this paper was to indicate the breadth of possibilities and outline the remaining challenges.

It is possible to utilize ethylene homopolymerization to produce everything from HDPE to LLDPE to VLDPE to high molecular weight polyolefin fluids. Demonstrated molecular weights range from UHMW (>2,000,000) to high-purity α -olefins. The polymerization is not limited to ethylene – α -olefins can be copolymerized or homopolymerized, as can cyclic olefins.

Reminding us of our original objective, copolymerizations of ethylene with functional monomers like methyl acrylate yield polar polyolefins that should find high-value applications.

Acknowledgements

As I have tried to indicate throughout this paper, this work has been a team effort. I would like to acknowledge those individuals whose contributions have already be made known through published patent applications or other contributions to the scientific literature. From the University of North Carolina, I particularly thank the three original inventors, Professor Maurice Brookhart, Lynda Johnson and Chris Killian. I also recognize Jordan Bennett, Amy Collins, Eric Dias, Derek Gates, Leigh Huff, Stefan Mecking, Enrique Onate, Michael Rachita, Scott Schultz, Brooke Small, Steve Svedja, and Dan Tempel. DuPont contributors include Sam Arthur, Alison Bennett, Patricia Cotts, Bryan Coughlin, Geraldine DiRenzo, Dennis Donald, Jerry Feldman, Kenn Gardner, Zhibin Guan, Elisabeth Hauptman, Lynda Johnson (again), Kristina Kreutzer, Betsy McCord, Steve McLain, John McMinn, Lissa Nelson, Anju Parthasarathy, Jose Rodriguez-Parada, Bryan Sauer, Xing Shen, Hsiang Shih, Bob Simpson, Jeff Sweetman, Wilson Tam, Mark Teasley, Bill Tuminello, Bill Uy, Mark Wagman, Lin Wang, Ying Wang,

and Yueli Wang. In addition to all of these individuals who have appeared on patents or publications, there are many others whose work to this point has gone unrecognized outside DuPont. Finally, Joel Citron has managed to keep the monumental patent effort organized and flowing smoothly.

FEATURES OF CYCLOPENTADIENYL METAL CATALYSTS FOR ETHYLENE COPOLYMERIZATION IN GAS AND LIQUID PHASE

Frederick J. Karol, Sun-Chueh Kao, Eric P. Wasserman and Zhengtian Yu

UNIVATION Technologies, Polymers Research and Development,
PO Box 670, Bound Brook, NJ 08805, USA

INTRODUCTION

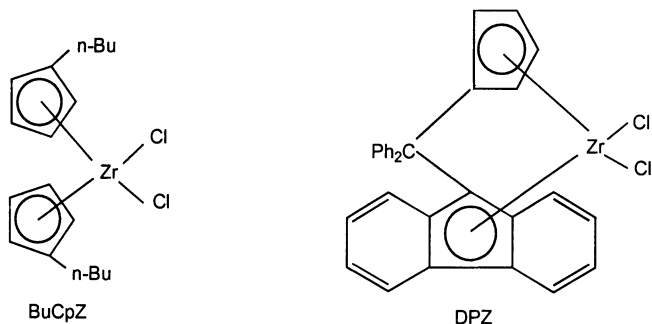
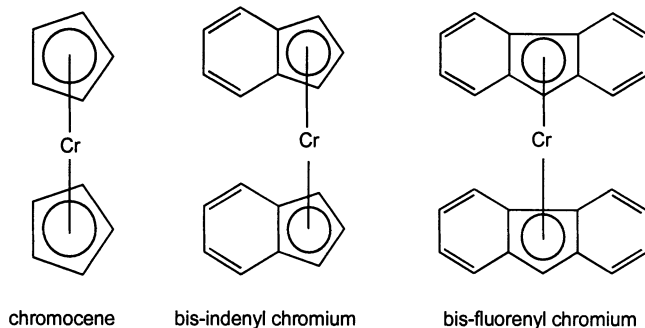
Catalysis in gas phase reactions for the production of olefin polymers is well known in the polyolefin industry [1]. Developments in the UNIPOL® process for polyethylene, EPR/EPDM, and polypropylene continue to demonstrate the broad versatility of the process. The emergence of metallocene catalysis in many laboratories around the world has added yet another significant catalytic tool for manipulating and controlling the molecular framework of polyolefins. Selection of the appropriate metallocene catalyst, with control of ligand environment at the active site, continues to provide the basis of improved process operations and unique product opportunities.

Early work in the late 1960s and 1970s demonstrated the effect of directly synthesized π -organic ligands attached to chromium on the polymerization parameters of several supported, chromium-based catalysts [2,3]. Silica-supported bis(cyclopentadienyl)-, bis(indenyl)-, and bis(fluorenyl)-chromium catalysts showed good activity in ethylene polymerization. The differences in process parameters among these supported catalysts were ascribed to different organic ligands complexed to the active chromium sites. These catalysts do not require any external activating agent for realizing high polymerization activities. The supported chromocene catalyst in gas phase ethylene polymerization displayed an outstanding chain transfer response to hydrogen. Comonomer incorporation of α -olefins such as propylene and 1-butene was poor unless the cyclopentadienyl ligand was removed by thermal means [4].

Many Group IV metallocene catalysts run in the gas phase have been identified as single-site catalysts capable of providing polyethylenes of narrow molecular weight distribution. These catalysts can produce ethylene, α -olefin copolymers of narrow comonomer compositional distribution. Such a capability of these catalysts has been used to differentiate metallocene catalysts from traditional titanium-based Ziegler-Natta catalysts.

Metalloenes Described in This Study

Certain metallocenes (with abbreviations) described in this study are shown below.



Catalysts Make It All Possible

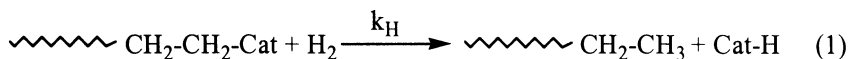
Activities and overall productivities with Group IV metallocene catalysts can be extremely high in the gas phase leading to a residual transition metal content of one ppm or less in the polymer. In many cases the catalyst sustains a high level of activity for many hours, with little evidence of catalyst decay. However, changes in catalyst composition and process conditions can alter such a kinetic profile. With methylalumoxane (MAO) as an activator, alumoxane/ zirconium ratios can be 300/1 or lower depending upon the specific metallocene used and reaction conditions under which polymerization takes place. Selection of the final catalyst composition reflects a consideration of both polymerization rates in the reactor and the costs associated with a specific catalyst.

Polymer molecular weights produced with metallocene catalysts depend upon the specific family of metallocene catalysts (e.g., bridged or unbridged) as well as the specific ligand composition. Many of the unbridged metallocenes have a

tendency to produce ethylene copolymers of lower molecular weight. Bridged metallocene catalysts typically provide a means to reach higher molecular weights. Precise control of ligand environment at the metal center in unbridged metallocenes can provide a route to higher molecular weight. In copolymerization with α -olefins, chain transfer to comonomer can be a significant kinetic process leading to lower molecular weights for the resultant copolymers [5].

Chain Transfer to Hydrogen

Chain transfer to hydrogen can be a highly efficient process with many metallocene catalysts. Such a high sensitivity was first noted with a chromocene catalyst for ethylene polymerization [2]. This high response to hydrogen led directly to highly saturated polyethylenes containing methyl groups as the major terminal functionality in the polymers (eq. 1). Metallocene catalysts based on



zirconium also display a high sensitivity to hydrogen as a chain transfer agent [6]. With some zirconium metallocene catalysts an unusually low $[\text{H}_2]/[\text{C}_2]$ ratio may be used to control polyethylene molecular weight within the commercial range (Table I). However, the sensitivity to changes in this ratio is generally higher with a chromocene catalyst.

Table 1. Effect of $[\text{H}_2]/[\text{C}_2\text{H}_4]$ Ratio on Polyethylene Melt Index¹

| Catalyst | $[\text{H}_2]/[\text{C}_2\text{H}_4] \times 10^3$ | MI, dg/min |
|--|---|------------|
| $(\text{C}_5\text{H}_5)_2\text{Cr}/\text{SiO}_2$ | 1.9 | 0.21 |
| | 3.8 | 1.0 |
| | 6.1 | 3.0 |
| | 7.5 | 5.5 |
| Unbridged Zr Metallocene | 0.04 | 3.0 |
| | 0.16 | 5.9 |
| | 0.32 | 14 |

¹For chromocene catalyst in the gas phase, the relationship was reported earlier [3]: $\text{MI} = A([\text{H}_2]/[\text{C}_2\text{H}_4])^{3.6}$

Results from kinetic studies and unsaturation measurements with certain metallocene catalysts suggested that a dehydrogenation process liberating hydrogen can occur [5,7-9]. Such a transformation was proposed to lead to a π -allyl intermediate that could subsequently participate in the polymerization process. Support for such a mechanism came from detection of hydrogen in the

gas phase during the polymerization process (Table II). The hydrogen liberated by such a dehydrogenation process can act as a highly efficient chain transfer agent to reduce the polymer molecular weight during copolymerizations. Hydrogen generation was not detected during the homopolymerization of ethylene.

Table 2. Hydrogen Generation with DPZ/MAO Catalyst

| | | | |
|-----------------------------|-------|-------|-------|
| 1-Hexene, mL | 0 | 50 | 200 |
| $[C_6]/[C_2]$, molar | 0 | 1.3 | 5.0 |
| Polymer Yield, g | 6.6 | 38.1 | 68 |
| SCB/1000C ¹ | -- | 51.6 | 129 |
| Mn X 10 ⁻³ (SEC) | 201.7 | 99.3 | 63.1 |
| Polymer, mmol | 0.03 | 0.38 | 1.08 |
| Mw/Mn (SEC) | 3.2 | 2.4 | 2.2 |
| Vinyl, wt. % | 0.005 | 0.007 | 0.015 |
| Internal, wt. % | 0.001 | 0.059 | 0.109 |
| Pendant, wt. % | 0.000 | 0.009 | 0.039 |
| Mn X 10 ⁻³ (IR) | 413.7 | 34.4 | 16.1 |
| Mol C = C/mol Polymer | 0.46 | 2.9 | 3.9 |
| H ₂ , ppm (GC) | 0 | 2100 | 5300 |
| H ₂ , mmol | 0 | 0.37 | 0.93 |

¹SCB = butyl branches

Comonomer Ratios in Gas Phase to Produce Copolymers

Many members of the metallocene family display an outstanding capacity to incorporate comonomer in ethylene, α -olefin copolymerization. These catalysts are among the best of all coordination catalysts for copolymerization. One way (Table III) to describe such a capacity for copolymerization in the gas phase is to determine the comonomer/ethylene (C_x/C_2) molar ratio necessary to be maintained in the reactor to achieve a copolymer of 0.92 g/cc density [10,11]. Such ratios for catalysts with outstanding copolymerization capabilities for 1-hexene would be in the range of $C_6/C_2 = 0.004$ - 0.005 . Comparable ratios in ethylene, 1-butene copolymerizations were $C_4/C_2 = 0.02$ - 0.03 . With a high activity Ziegler-Natta titanium catalyst such ratios would be $C_6/C_2 = 0.12$ and $C_4/C_2 = 0.35$. For a chromium oxide catalyst a typical value would be $C_4/C_2 = 0.08$. The poor copolymerization capability of the supported chromocene catalyst was reflected in the high $C_3/C_2 = 0.45$ value when propylene was used as a comonomer. Such a C_3/C_2 value was required to produce a copolymer density of 0.946 g/cc.

Table 3. Comonomer Ratios in Gas Phase to Produce Copolymers (0.92 g/cc)

| <u>Catalyst</u> | C_6/C_2 | C_4/C_2 |
|-----------------------|-------------|-----------|
| Bridged Metallocene | 0.004-0.005 | 0.02-0.03 |
| Unbridged Metallocene | 0.02 | -- |
| Mono-Cp Metallocene | 0.03 | -- |
| CrO ₃ | 0.03 | 0.08 |
| Vanadium | 0.06 | 0.13 |
| Mg/Titanium | 0.12 | 0.35 |

Several groups have carried out ethylene copolymerization studies in a hydrocarbon diluent with a variety of α -olefins (C₃-C₁₈) using Group IV metallocene catalysts with MAO [12-28]. Among the observations from this earlier work was that ansa-metallocenes with one or more atoms as bridging groups were more effective for incorporating comonomer than the unbridged metallocenes. The ethylene reactivity ratio (r_1) varied by factor of 200 within the family of zirconocene catalysts. In most cases the products of the reactivity ratios were below one, indicating an alternating tendency during the monomer/comonomer insertion process. For 1-hexene as a comonomer, the incorporation varied by as much as sixfold for six bridged and unbridged metallocenes studied [5]. The presence of an α -olefin generally results in an accelerating rate effect in ethylene copolymerization. Rate enhancements as high as twelve times the ethylene homopolymerization rate have been observed in the presence of the α -olefin [29]. Causes for such rate enhancements have not been clearly elucidated. Analytical measurements for the extent of chain branching and copolymer unsaturation provided the basis for probing changes in the nature of the active sites when using different catalyst compositions. Computational chemistry has proven useful in understanding changes in the cation-anion interaction when different ligands are complexed to the active zirconium cationic centers (see below).

Control of Molecular Weight and Compositional Distribution

Many metallocene catalysts have been identified as single-site catalysts capable of providing polyethylenes of narrow molecular weight distribution (polydispersity~2). In many cases such catalysts run in a gas phase process also produce polyethylenes of narrow molecular weight distribution. It is not necessary for these single-site catalysts to remain in solution in order to provide polyethylenes of narrow molecular weight distributions. However, there are other metallocene catalysts that behave differently as they produce polyethylenes with molecular weight distributions as high as 4-5 (Table IV). In-situ routes to more than one type of active site during the polymerization process may be one explanation for such a broadening of molecular weight distribution.

Table 4. Comparison of MWD and CCLD for Four Metallocene Catalysts in Gas Phase

| <u>Catalyst</u> | <u>Mw/Mn</u> | <u>Lw/Ln</u> |
|-----------------|--------------|--------------|
| A | 2.1-2.3 | 3.0-3.1 |
| B | 2.3-2.6 | 3.6-4.5 |
| C | 2.8-3.7 | 1.5-2.2 |
| D | 4.0-5.3 | 1.4-2.4 |

Metallocene catalysts can produce ethylene, α -olefin copolymers of narrow comonomer compositional distribution. Such a capability of these catalysts have been used to differentiate metallocene catalysts from traditional titanium-based Ziegler-Natta catalysts. In gas phase copolymerizations with metallocene catalysts, the degree of uniformity in compositional distribution may be controlled over a wide range depending upon the catalyst and process conditions under investigation. Such control of compositional and molecular weight distributions by selection of the appropriate metallocene catalyst provides the basis of expanding the range of product opportunities.

Temperature Rising Elution Fractionation (TREF) was used to provide information on comonomer compositional distribution. From the TREF temperature data, the branch frequency may be obtained for a given comonomer. Consequently, the main chain lengths between branches, expressed as Lw and Ln may be calculated. Lw is the weight average chain length between branches:

$$L_w = \sum_i W_i L_i$$

and Ln is the number average chain length between branches:

$$L_n = 1 / \sum_i (W_i / L_i)$$

wherein W_i is the weight fraction of the component i having an average backbone spacing L_i between two adjacent branch points. A Crystallizable Chain Length Distribution (CCLD), L_w/L_n , of less than about 3, preferably less than about 2, is indicative of narrow comonomer compositional distribution.

Comonomer compositional distribution among polymer chains relates to relative monomer/comonomer incorporation rates during chain propagation. It is possible by selection of the appropriate catalyst to manipulate independently the breadth of polymer molecular weight distribution and comonomer compositional distribution.

Certain bridged metallocene catalysts, namely those having facial chirality, when used for ethylene polymerization in the gas phase provided the unexpected combination of a broad molecular weight distribution and narrow comonomer distribution [30]. The presence of both the racemic and meso stereoisomers during the polymerization of ethylene was important to the formation of polyethylene having the combination of broad molecular weight distribution and narrow comonomer distribution.

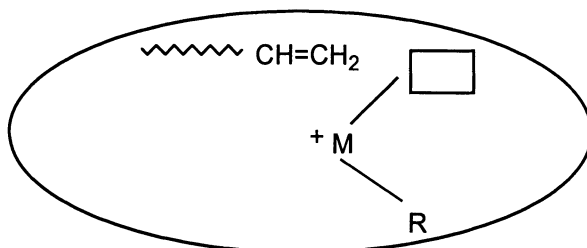
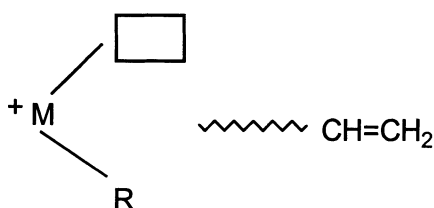
Long Chain Branching in Gas Phase

Polyethylenes containing long chain branches possess high strength and low viscosity under high shear conditions, permitting high processing rates. Early work to introduce and take advantage of long chain branching in polyethylene was carried out using low pressure, chromium oxide catalysis [31]. Introduction of long chain branches into polyethylene can occur when vinyl-terminated long chain polymer molecules copolymerize with ethylene monomer during polymerization. This reincorporation mechanism has been accepted for a long time as a route to long chain branching. Such unsaturated long chain polymer molecules are not expected to be in the vapor state under the reaction conditions typically employed in gas phase processes, but rather are expected to be solids or high boiling liquids having lower mobility. Accordingly, it was believed that serious difficulties might be encountered in attempting to introduce long chain branches into polyethylene in a gas phase polymerization, and that it might not be possible to accomplish this under industrially acceptable conditions. It has surprisingly now been found that long chain branches can be introduced into polyethylene in a gas phase process using certain bridged metallocene catalysts and appropriate reaction conditions (Table V) [32-33].

Table 5. Introduction of Long Chain Branching in C_2/C_6 Copolymers Using Bridged Metallocene Catalysts

| | | | | |
|-----------------------|-------|-------|-------|-------|
| Cat E/Cat F | 1:1 | 5:1 | 3:1 | 0:1 |
| Reaction Temp. °C | 85 | 85 | 65 | 85 |
| Density, g/cc | 0.933 | 0.940 | 0.908 | 0.920 |
| LCB/1000 Carbon Atoms | 0.3 | 2.0 | 0.0 | 0.8 |

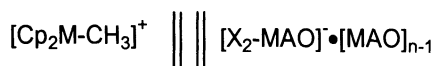
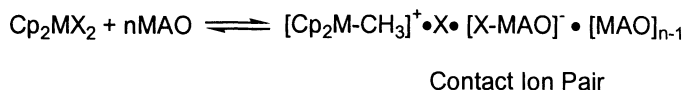
In gas phase polymerizations the polymer particle may be viewed as a microreactor within which polymer chains are created. In the process of polymer chain transfer, some polymer chains will be terminated and generate terminal vinyl groups. Polymer chains with these vinyl groups should remain in the vicinity of the active sites. Such a presence creates an opportunity for the vinyl-terminated polymer chain to incorporate as a comonomer into a growing polymer chain within the polymer particle (Figure 1). Such incorporation provides a means of introducing long chain branching. Proximity effects of this type are particularly significant in gas phase polymerizations where polymer chains and active sites are contained within the growing polymer particle.

Fig. 1. Proximity Effect for Long Chain Branching in Polymer Particle ReactorGas Phase PolymerizationSolution Phase Polymerization

The ability of the catalyst system to introduce long chain branching was significantly better in the gas phase than in hydrocarbon diluent. Long chain branching contents of 0.3-2.0 LCB/1000 carbon atoms were estimated for gas phase copolymerization studies under conditions where slurry polymerizations showed no long chain branching content.

Ion-Pair Effect in Metallocene-Catalyzed Ethylene Copolymerization

The response of zirconocenes to changes in Al/Zr ratio and MAO structure has been interpreted in terms of a mechanistic model involving ion-pairs [5]. Metal centers with higher mobility, lower steric hindrance and higher electrophilicity are believed to form stronger contact ion-pairs (Scheme A). As the MAO ratio increases, the MAO aggregates are postulated to become larger, and thereby the cationic species becomes more separated from the anion. This less sterically hindered species is proposed as largely responsible for the enhanced activity.

Scheme 1. Ion-Pair Model

Solvent Separated Ion Pair

A route to modify the structure of MAO aggregates is by supporting these molecules on solids such as silica. This modification would constrain MAO on the surface and thus minimize possible equilibria among various aggregates. The ion-pair model predicts that under these conditions the cationic zirconocene center would experience little or no influence by changing the Al/Zr ratio. These was no significant change in molecular weight, polydispersity, butyl branch frequency, and total unsaturation when using a BuCpZ catalyst in the presence of a silica-supported MAO (Table VI). Small decreases in polydispersity and butyl branch frequencies suggest the active sites in the supported systems are somewhat more homogeneous, tighter ion-pairs than the centers in the soluble catalysts.

Table 6. Effect of Heterogenization on Activity, Mw, PDI, BBF and TCE of BuCpZ Catalyzed Ethylene/1-Hexene Copolymerization¹

Solution MAO

| <u>Al/Zr</u> | <u>Activity</u> ² | <u>Mw</u> | <u>PDI</u> | <u>BBF</u> | <u>TCE</u> |
|--------------|------------------------------|-----------|------------|------------|------------|
| 150 | 52842 | 80182 | 3.0 | 8 | 0.0934 |
| 350 | 59469 | 39118 | 2.6 | 10 | 0.1654 |
| 750 | 71358 | 26956 | 2.7 | 13 | 0.2435 |
| 1500 | 81784 | 19687 | 2.4 | 14 | 0.3208 |

Supported MAO

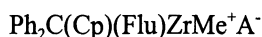
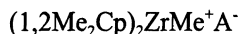
| | | | | | |
|------|-------|--------|-----|---|--------|
| 250 | 26737 | 110292 | 2.2 | 7 | 0.0261 |
| 500 | 60858 | 96262 | 2.1 | 8 | 0.0256 |
| 1000 | 78105 | 98770 | 2.1 | 8 | 0.0269 |

¹PDI= polydispersity, BBF= butyl branch frequency, TCE= wt% of total unsaturated chain ends

²gPE/(mmol Zr-hr-100psi C₂H₄)

Results From Computational Chemistry

In recent years molecular modeling techniques have been applied to metallocene catalysis, mostly on the cationic species, without accounting for the anion part derived from the cocatalyst [34-40]. In general, both ligand structure of the cation and the size of the anion should influence the contact ion-pair interaction. In order to illustrate this, we have done PM3 semi-empirical quantum calculations on four different single-site catalyst systems:

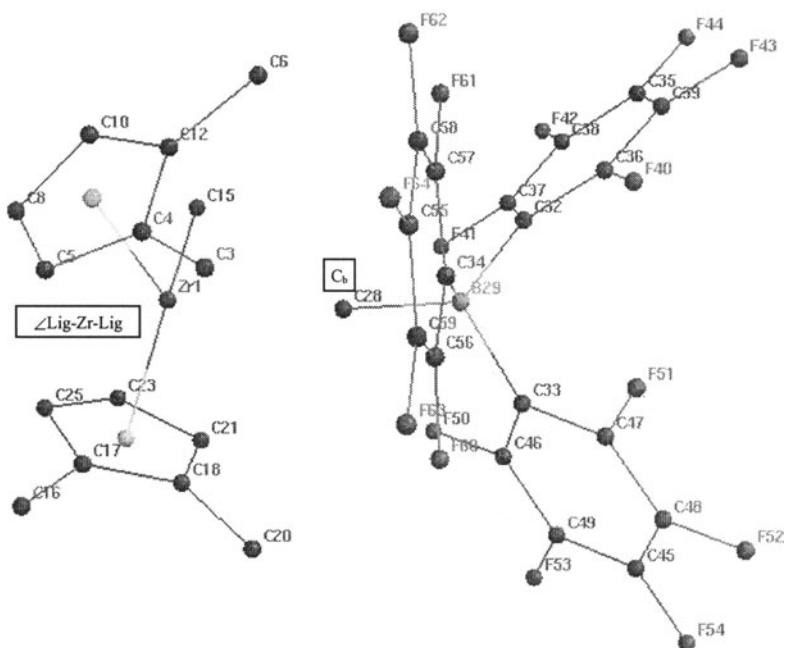


where A⁻ represents an anion of either [MeB(C₆F₅)₃]⁻ or [Me(MAO)₉]⁻.

PM3 in Spartan® (product of Wavefunction, Inc. version 4.1) was used as a primary tool to obtain the different structures. PM3 code was installed on Power Challenge (R8000) server and was performed remotely through an Indigo2 workstation. The structure of Group IV cation can be reproduced by PM3 as compared with a higher level calculation [41]. Our test calculations on Group IV metallocene precursors show that the error is generally less than 0.06 Å for the bond lengths and less than 8 degree for the angles. Table VII lists the selected geometries of (1,2Me₂Cp)₂ZrMe⁺[MeB(C₆F₅)₃]⁻ between X-ray [42] and PM3 calculated structure and PM3 (Figure 2). The calculated structure shows that PM3 can fairly reproduce the cation-anion separation parameters

Table 7. Selected Geometries of (1,2Me₂Cp)₂ZrMe⁺[MeB(C₆F₅)₃]⁻

| <u>Geometry</u> | <u>PM3 Calculated</u> | <u>X-Ray [42]</u> |
|-------------------------------------|-----------------------|-------------------|
| Zr-C _b (b = bridging, Å) | 2.520 | 2.549 |
| Zr-B (Å) | 4.19 | 4.16 |
| ∠Zr-C _b -B (deg.) | 170.4 | 161.8 |
| ∠Lig-Zr-Lig (deg.) | 133.2 | 131.1 |
| Zr-C (terminal, Å) | 2.304 | 2.252 |

Fig. 2. PM3 Calculated Structure of $(1,2\text{Me}_2\text{Cp})_2\text{ZrMe}^+[\text{MeB}(\text{C}_6\text{F}_5)_3]^-$ 

The structure of $[\text{cation}][\text{Me}(\text{MAO})_9]^-$ is similar to that of $(\text{Cp})_2\text{ZrMe}^+[\text{Me}(t\text{BuAlO})_6]^-$ proposed by Barron [43] except the cage of $(t\text{BuAlO})_6$ is replaced by $(\text{MeAlO})_9$.

The contact cation-anion interaction can be measured by the perturbation of certain geometric parameters of cation with/without the anion. Table VIII shows how the $\angle\text{Lig-Zr-Lig}$ angle changes with/without $[\text{MeB}(\text{C}_6\text{F}_5)_3]^-$ or $[\text{Me}(\text{MAO})_9]^-$ for the four different cations studied.

The anion impacting effect, which is defined by the difference in angle between the 'naked' cation and the cation-anion complex, is listed in the second column. The separation parameters are listed in the third column.

The data in Table VIII indicate that the resistance to the impacting effect of the anion decreases in the order $\text{Ph}_2\text{C}(\text{Cp})(\text{Flu})\text{ZrMe}^+ > \text{Me}_2\text{Si}(2\text{MeInd})_2\text{ZrMe}^+ > (1,2\text{Me}_2\text{Cp})_2\text{ZrMe}^+ > (\text{Ind})\text{ZrMe}^+$. The structures of both monoCp and unbridged bisCp type ligand-metal complexes are more sensitive to the anion than are those of bridged ligand-metal complexes. $[\text{Me}(\text{MAO})_9]^-$ has greater impact than $[\text{MeB}(\text{C}_6\text{F}_5)_3]^-$, although the former is twice as far away from the cation as the latter.

It is tempting to relate the effect of Al/Zr ratio on polymerization behavior with the calculations on cation-anion interaction. Because of the higher impacting effect

of the MAO anion with $(1,2\text{Me}_2\text{Cp})_2\text{ZrMe}^+$ than the bridged cations, we believe that at the higher Al/Zr ratios this interaction is reduced, leading to higher polymerization rates. Unbridged metallocenes such as $(\text{BuCp})_2\text{ZrMe}^+$ would fall into the category modeled by $(1,2\text{Me}_2\text{Cp})_2\text{ZrMe}^+$. Higher rates of comonomer incorporation with the bridged metallocene are no doubt related to the smaller angle of $\angle\text{Lig-Zr-Lig}$ and also to a weaker interaction of the anion with the cationic center.

Table 8. Anion Effect of $\angle\text{Lig-Zr-Lig}$ Angle

| Composition | (A) ¹ | $\angle\text{Lig-Zr-Lig}$, deg. | Anion Effect, ² deg. | Cation-anion Zr-C _b | Separation ³ (Å) Zr-B |
|---|------------------|----------------------------------|---------------------------------|-----------------------------------|-------------------------------------|
| (Ind)ZrMe ₂ ⁺ | | 130 | --- | --- | --- |
| (Ind)ZrMe ₂ ⁺ A ⁻ | 1 | 116.8 | 13.2 | 2.45 | 4.15 |
| | 2 | 98.5 | 31.5 | 5.30 | --- |
| $(1,2\text{Me}_2\text{Cp})_2\text{ZrMe}^+$ | | 141 | --- | --- | --- |
| $(1,2\text{Me}_2\text{Cp})_2\text{ZrMe}_2^+\text{A}^-$ | 1 | 133.2 | 7.8 | 2.52 | 4.19 |
| | 2 | 119 | 22 | 5.31 | --- |
| $\text{Me}_2\text{Si}(2\text{MeInd})_2\text{ZrMe}^+$ | | 131 | --- | --- | --- |
| $\text{Me}_2\text{Si}(2\text{MeInd})_2\text{ZrMe}_2^+\text{A}^-$ | 1 | 128.4 | ~3 | 2.52 | 4.2 |
| | 2 | 112 | 19 | 5.35 | --- |
| $\text{Ph}_2\text{C}(\text{Cp})(\text{Flu})\text{ZrMe}^+$ | | 118 | --- | --- | --- |
| $\text{Ph}_2\text{C}(\text{Cp})(\text{Flu})\text{ZrMe}_2^+\text{A}^-$ | 1 | 113.4 | ~5 | 2.60 | 4.09 |
| | 2 | 107 | 11 | 5.32 | --- |

¹A⁻ = anion type: 1=[MeB(C₆F₅)₃]⁻, 2=[Me(MAO)₉]⁻

²Anion effect is difference in angle between the 'naked' cation and cation-anion complex

³See reference [42]

⁴Average values of $\angle\text{Lig-Zr-Me}$

REFERENCES

- [1] Karol, F. J., *Macromol. Symp.*, **89**, 563 (1995).
- [2] Karol, F. J., Karapinka, G. L., Wu, C., Dow, A. W., Johnson, R. N., *J. Polym. Sci. A-1*, **10**, 2621 (1972).
- [3] Karol, F. J., Brown, G. L., Davison, J. M., *J. Polym. Sci. A-1*, **11**, 413 (1973).
- [4] Karol, F. J., Wu, C., *J. Polym. Sci., A-1*, **12**, 1549 (1974).
- [5] Karol, F. J., Kao, S. C., Wasserman, E. P., Brady, R. C., *New J. Chem.*, **21**, 797 (1997).
- [6] Kaminsky, W. Lüker, H., *Makromol. Chem., Rapid Commun.*, **5**, 225 (1984).
- [7] Brinen, J. L., Muhle, M. E., Paper presented at the Polymer Reaction Engineering Foundation Conference, Palm Coast, Florida, March 18, 1997.
- [8] Richardson, D. E., Alameddin, N. G., Ryan, M. F., Hayes, T., Eyler, J. R., and Siedle, A. R., *J. Am. Chem. Soc.*, **118**, 11244 (1996).
- [9] Christ, C. S., Eyler, J. R., Richardson, D. E., *J. Am. Chem. Soc.*, **110**, 4038 (1988).
- [10] Karol, F. J., Paper presented at International Conference on Polyolefins: RETEC, February 23-26, 1997; Houston, Texas, pp. 88-107.

- [11]Fraser, W. A., Williams, C. C., Sachs, W. H., Paper Presented at Metallocene Technology '97, Chicago, Illinois, June 16-17, 1997.
- [12]Ewen, J. A. In *Catalytic Polymerization of Olefins*, Keii T., Soga, K., Eds., Kodansha, Tokyo, 1986, p. 271.
- [13]Kaminsky, W., Miri M., *J. Polym. Sci., Polym. Chem. Ed.*, **23**, 2151 (1985).
- [14]Drögemüller, H., Heiland, K., Kaminsky, W., in *Transition Metals and Organometallics as Catalysts for Olefin Polymerization*, Kaminsky, W., Sinn, H., Eds., Springer-Verlag, Berlin, 1988, p. 303.
- [15]Herfert, N., Montag, P., Fink, G., *Makromol. Chem.*, **194**, 3167 (1993).
- [16]Koivumäki, J., Fink, G., Seppälä, J. V., *Macromolecules*, **27**, 6254 (1994).
- [17]Seppälä, J. V., Koivumäki, J., Liu, X., *J. Polym. Sci., Part A: Polym. Chem.*, **31**, 3447 (1993).
- [18]Koivumäki, J., Seppälä, J. V., *Polymer Sci., Part A: Polym. Chem.*, **26**, 5535 (1993).
- [19]Koivumäki, J., Seppälä, J. V., *Polymer*, **34**(9), 1958 (1993).
- [20]Pietikäinen, P., Seppälä, J. V., *Macromolecules*, **27**, 1325 (1994).
- [21]Koivumäki, J., Seppälä, J. V., *Macromolecules*, **27**, 2008 (1994).
- [22]Koivumäki, J., *Polym. Bull.*, **34**, 413 (1995).
- [23]Zambelli, A., Grassi, A., Galimberti, M., Mazzocchi, R., Piemontesi, F., *Makromol. Chem., Rapid Commun.*, **12**, 523 (1991).
- [24]Karol, F. J., Kao, S. C., *New J. Chem.*, **18**, 97 (1994).
- [25]Karol, F. J., Kao, S. C., In *Catalyst Design for Tailor-made Polyolefins*, Soga, K., Terano, J., Eds., Elsevier, Amsterdam, 1994, pp. 389.
- [26]Heiland, K., Kaminsky, W., *Makromol. Chem.*, **193**, 601 (1992).
- [27]Katayamo, H., Shiraiski, H., Hino, T., Ogane, T., Imai, A., *Macromol. Symp.*, **97**, 109 (1995).
- [28]Bergemann, C., Cropp, R., Luft, G., *J. Mol. Catal. A: Chemical*, **105**, 87 (1996).
- [29]Tsutsui, T., Kashiwa, J., *Polym. Commun.*, **29**(6), 180 (1988).
- [30]European Patent Application 0743324A2 (Union Carbide), Priority Date 5/16/95.
- [31]Hogan, J. P., Levett, C. T., and Werkman, R. T., *SPE Journal*, **23**, 87 (1967).
- [32]European Patent Application 0659773A1 (Union Carbide), Priority Date 12/21/93.
- [33]Ohgizawa, M., Takahashi, M., and Kashiwa, N., MetCon 95, Houston, Texas, May 17-19, 1995.
- [34]Hoffmann, R., Lauher, J. W., *J. Am. Chem. Soc.*, **98**, 1729 (1976).
- [35](a): Proscenc, M.-H., Janiak, C. J., Brintzinger, H. H., *Organometallics*, **11**, 4036 (1992). (b): Janiak, C. J., *Organomet. Chem.* **452**, 63 (1992).
- [36](a): Kawamura-Kuribayashi, H., Koga, N., Morokuma, K., *J. Am. Chem. Soc.* **114**, 2359 (1992). (b): Kawamura-Kuribayashi, H., Koga, N., Morokuma, K., *J. Am. Chem. Soc.* **114**, 8687 (1992). (c): Yoshida, T., Koga, N. *Organometallics* **14**, 746 (1995). (d): Koga, N., Yoshida, T., Morokuma, K., in *40-Year Ziegler-Catalyses*; Fink/Mulhaupt/Brintzinger (Eds); Freiburg/Breisgau, Germany, 274 (1993). (e): Yoshida, T., Koga, N., Morokuma, K., *Organometallics* **15**, 766 (1996).
- [37]Bierwagen, E. P., Bercaw, J. E., Goddard, W. A. III, *J. Am. Chem. Soc.* **116**, 1481 (1994).
- [38](a): Woo, T. K., Fan, L., Ziegler, T., *Organometallics* **13**, 432 (1994). (b): Woo, T. K., Fan, L., Ziegler, T., in *40-Year Ziegler-Catalyses*, Fink/Mulhaupt/Brintzinger (Eds), Freiburg/Breisgau, Germany, 291, (1993). (c): Fan, L., Harrison, D., Deng, L., Woo, T. K., Swerhone, D., Ziegler, T., *Can. J. Chem.* **73**, 989 (1995). (d): Fan, L., Harrison, D.,

- Deng, L., Woo, T. K., Swerhone, D., Ziegler, T., *Organometallics* **14**, 2918 (1995). (e): Lohrenz, J. C., Woo, T. K., Ziegler, T., *J. Am. Chem. Soc.* **117**, 12793 (1995).
- [39](a): Corradini, P., Guerra, G., Vacatello, M., Villani, V., *Gazz. Chim. Ital.*, **118**, 173 (1988). (b) Cavallo, L., Guerra, G., Oliva, L., Vacatello, M., Corradini, P., *Polym. Commun.*, **30**, 16 (1989). (c) Venditto, G., Guerra, P., Corradini, P., Fusco, R., *Polymer*, **31**, 530 (1990). (d) Cavallo, L., Corradini, P., Guerra, G., Vacatello, M., *Polymer*, **32**, 1329 (1991). (e) Corradini, P., Guerra, G., *Progr. Polym. Sci.*, **16**, 239 (1991). (f) Cavallo, L., Guerra, G., Vacatello, M., Corradini, P., *Macromolecules*, **24**, 1784 (1991).
- [40]Yu, Z., Chien, J. C. W., *J. Polym. Sci, Part A*, **33**, 125 (1995); *ibid*, **33**, 1085 (1995).
- [41]Hehre, W. J., Presentation in Inorganic Division, ACS Meeting (Chicago) (1995).
- [42]Yang, X., Stern, C. L., Marks, T. J., *J. Am. Chem. Soc.*, **116**, 10015 (1994).
- [43]Harlan, C. J., Bott, S. G., Barron, A. R., *J. Am. Chem Soc.*, **117**, 6465 (1995).

How to Avoid Gas-Liquid Mass Transfer Limitations during Polymerization of Olefins

Pål Kittilsen^a, Rune Tøgersen^b, Erling Rytter^{b,c}, Hallvard Svendsen^a

^aDepartment of Chemical Engineering, Norwegian University of Science and Technology, 7034 Trondheim, Norway

^bDepartment of Industrial Chemistry, Norwegian University of Science and Technology
^cStatoil Research Centre, 7005 Trondheim, Norway
e-mail: paal.kittilsen@chembio.ntnu.no

Abstract. Propene was polymerized using a modern Ziegler-Natta catalyst dispersed in decane. The stirring rate was changed during polymerization, and the observed monomer feed rates were analyzed using a steady state and a dynamic mass balance to obtain mass transfer coefficients. A theoretically founded mass transfer model for a semi batch stirred laboratory reactor was developed. It is shown how the model can be used to secure minimal transport limitations in kinetic experiments during polymerization of olefins. It is found that introducing baffles and sparging considerably decrease the transport resistance at high stirring rates.

1. Introduction

The present work is focused on slurry phase olefin polymerization. In order to avoid gas-liquid mass transfer limitations during polymerization of olefins, there is a need to understand and quantify the effect of gas-liquid mass transfer and to provide criteria for how reactors should be operated and designed.

We wanted to investigate mass transfer effects in an apparatus that is in use for kinetic studies. A relevant method was described by Keii et al. [5]. They showed how to obtain mass transfer factors¹ using mass balances in an analysis of the dynamic and steady state reaction rates resulting from variation in stirring speed in a first order polymer reaction. We have extended the method to also include other reaction orders and discussed the influence of deactivation.

A common model for describing gas-liquid mass transfer at a moving surface is the penetration model concept [2]. The contact time between gas and liquid is a key parameter. It can be related to the turbulence intensity and to the mean flow of the liquid. Theofanous et al. [11] found that two distinct mass-transfer regimes, associated with small scale and macro scale turbulent motion respectively, are

¹ The notation *mass transfer factor* for denoting $k_t A$ and *mass transfer coefficient* for denoting k_t , is used.

controlling the mass transfer. A criterion based on the turbulence Reynolds number was derived.

Bin [1] found a correlation, based on a theoretical relation between the turbulence intensity and the mass transfer coefficient, which fitted a large number of data. The turbulence intensity is related to the energy dissipation, which in turn can be calculated from the geometry of the agitator-reactor system and the agitation rate. However, Bin failed to correlate experiments in the low Reynolds number regime.

This low Reynolds number regime was investigated by Dong et al. [4], who measured corresponding surface flow rates and mass transfer rates in a stirred vessel. They found good agreement between predicted and measured mass transfer coefficients when using the mean flow as the basis for calculating the contact time and thus the mass transfer coefficient. We have derived a new theoretically based correlation based on this work.

2. Experimental

A 600 ml semi batch cylindrical vessel equipped with a two-bladed possibly self-sparging stirrer was used for the experimental investigation. The monomer was propene, the solvent 175 ml of decane and the catalyst was 40 mg of a modern Ziegler-Natta catalyst (Ti on a support, Borealis BC-1). The feed rate of propene was recorded at 1 Hz. The reactor was operated at 70°C and 4 bar total pressure² unless stated otherwise. For details of the method see Thorshaug et al. [12].

3. Methods to determine the mass transfer factor

The mass transfer factor can be determined through an analysis of the steady state and dynamic feed rates of monomer as the stirring rate is changed. Fig. 1 shows how the feed rate changes with time and stirring rate. The methods used in this section are based on the ideas of Keii et al. [5] who analyzed a non-deactivating, first order polymer reaction. Details of this section are given by Kittilsen et al. [6].

The basis is the general monomer mass balance for an ideal mixed semi batch reactor with constant volume and catalyst concentration:

$$V \frac{dM}{dt} = k_L A (M_0 - M) - k_p GM^n \quad (1)$$

Steady state method: At steady state in a non-deactivating system, the monomer concentration is constant and the dynamic term of the general mass balance can be disregarded. Using this together with the mass balance for no mass transfer resistance ($F_0 = k_p GM_0^n$), the mass transfer factor $\beta = k_L A$, is expressed as

² The vapor pressure of the solvent plus the partial pressure of the monomer gas.

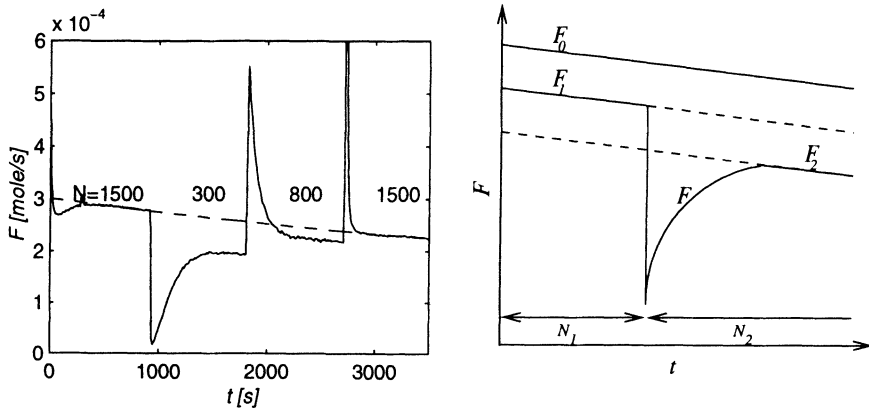


Fig. 1. The left figure shows a typical experiment where the stirring rate, N , has been changed during the run. The stirring rates are in rpm . The dashed line shows the approximate level of no mass transfer resistance. The figure to the right shows corresponding feed rates and stirrer rates schematically.

$$\beta_i = F_i / M_0 \left[1 - (F_i / F_0)^{1/n} \right] \tag{2}$$

The method for non-deactivating system may also be used for slow deactivating systems obtaining quasi steady states. F_i and F_0 must then be taken at the same level of deactivation. Also the deactivation must be independent of monomer concentration. These assumptions were proven valid in a kinetic study (see Section 5) and by a numerical analysis of the deactivation rate.

Dynamic method: Keii et al. [5] solved the general mass balance (Eq. 1) analytically for the first order non-deactivating case. A plot of $\ln |F - F_i|$ versus t should give a linear relation with slope $-\alpha_i$. The mass transfer factor is

$$\beta_i = \alpha_i V - F_0 / M_0. \tag{3}$$

For systems with a relatively small deactivation rate and a monomer reaction order close to one, the solution found for the non-deactivation system can be used. In this case the deactivation is neglected and the reaction is considered first order. A numerical investigation was done in which extrapolated values were used for F_2 (shown to be slightly better than a mean value) and mean values were used for F_0 . It was found that Eq. 3 gave β -values with deviations of $\pm 0-15\%$ from the "true" values when the system was a 1.2-order deactivating system with parameters typical for systems considered in this work. These errors are smaller than the observed uncertainty in β_i and we have used this analytical method when analyzing the transient responses.

4. Mass transfer across a gas-liquid interface

The gas-liquid contact area, the rate of renewal of the surface and the deviation from equilibrium monomer concentration are controlling the mass transfer at a free interface.

Contact area: In a non-spraying reactor the contact area equals the area of the free surface. This changes with stirring rate: At higher stirring rates a vortex forms and at even higher rates the surface becomes rippled. The changes in area, up to a factor two, are taken into account in the present investigation [7].

Mean flow dominated mass transfer: At low stirring the mean circulating flow will dominate the mass transfer process. Dong et al. [4] have shown that this approach is appropriate in a study of calculated mass transfer coefficients from measured surface velocities. Based on the penetration theory concept and assuming the surface velocity proportional to the impeller Reynolds number we derived a relation between the Sherwood, the Reynolds and the Schmidt. The details of the derivation are given by Kittilsen et al. [7]. The constants in the relation were estimated by fitting the data of Dong [3]:

$$Sh = 0.071 Re^{0.76} Sc^{1/2} \quad (4)$$

Small scale turbulence dominated mass transfer: At sufficiently high stirring rates small scale turbulence takes over as the dominating effect controlling the gas-liquid mass transfer. The rate of surface renewal is now related to the turbulent intensity, which is coupled to the viscous energy dissipation. Bin [1] examined several reported mass transfer experiments, and developed a correlation valid for organic liquids:

$$k_L = 0.372(d_i / d_r)^{0.865} (\bar{\epsilon}v)^{1/4} Sc^{-1/2} \quad (5)$$

The energy dissipation, $\bar{\epsilon}$, can be found through a power correlation for the stirrer used. In this study a correlation for a two-bladed stirrer given by Nagata et al. [9] was used.

Controlling mechanism for mass transfer: Theofanous et al. [11] defined a turbulent Reynolds number which provides a measure of the relative time scale of small- and macro turbulent scales, and can thus be used to determine which mechanism is controlling. Based on turbulent macro length scale and macro velocity scale [1,12] gave the turbulent Reynolds number as

$$Re_t = 0.07 d_i^{4/3} \bar{\epsilon}^{1/3} / \nu \quad (6)$$

A suggested shift between the two mass transfer models was taken at $Re_t = 200$. A model which approaches the right values at the limits $Re_t \gg 200$ and $Re_t \ll 200$ is

$$k_L = \frac{(200 / Re_t)^4 k_L^{mf} + (Re_t / 200)^4 k_L^{sst}}{(200 / Re_t)^4 + (Re_t / 200)^4} \quad (7)$$

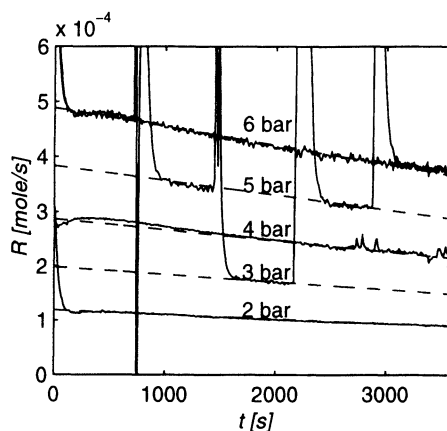


Fig. 2. Reaction rates at various pressures as function of time. Three experiments were performed with constant pressures at levels 2, 4 and 6 bar and one was performed with varying the pressure during the polymerization at the levels 6, 5, 3, 5, 6 bar. The dashed lines are the modeled rates using a linear deactivation model.

5. Results and discussion

Kinetics: A kinetic study of the system was performed through a variation of the monomer concentration (total pressure of 2, 3, 4, 5 and 6 bar), keeping all other parameters constant. A logarithmic plot of reaction rate as function of monomer concentration (from SRK-EOS) revealed monomer dependency of order 1.18 to 1.22, with an average of 1.20. The deactivation was independent of amount of polymer produced and the reaction rate could be well described by a linear deactivation model:

$$R = (c_0 - c_d t) M^n \quad (8)$$

The observed and modeled reaction rates at various pressures are shown in Fig. 2.

Effect of stirring rate: The reactor was operated unbaffled and non-spraying. Every experiment started and ended with a period of low mass transfer resistance (high stirring rate), thereby ensuring the assumption of equilibrium between the two phases to be reasonable. The response of a typical experiment is shown in Fig. 1.

The mass transfer factors were calculated using the methods described in Section 3 and are plotted together with the modeled factors in Fig. 3.

The results from the steady state and the dynamic experiments differed significantly. The most likely reason for this discrepancy is departure from an ideal mixed reactor.

Numerical calculations were done using a two-compartment model with both external and internal mass transfer and a possible catalyst concentration variation. The model could qualitatively explain the discrepancies between the observed

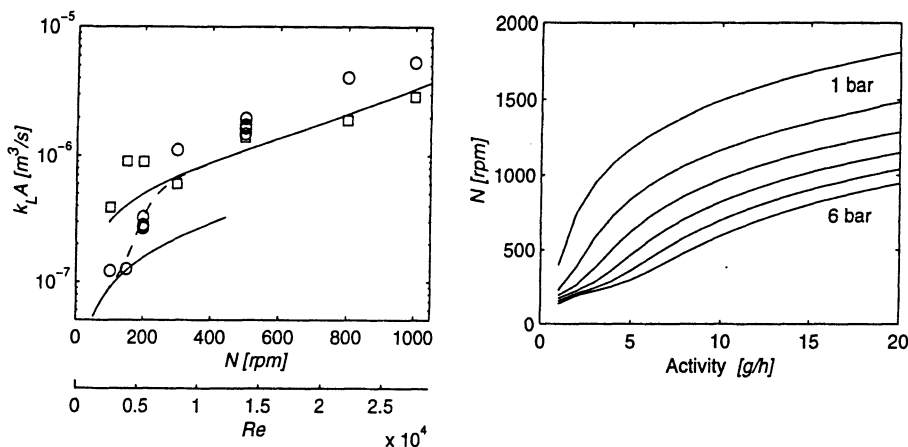


Fig. 3. Gas-liquid mass transfer of propene in decane in an unbaffled and non-sparging reactor. Left: Experimental and modeled mass transfer factors as functions of stirrer speed. The upper solid line represent the turbulence based model, the lower line the mean flow based model. \circ = steady state based coefficients, \square = dynamic based coefficients. Right: Calculated necessary stirring rates to assure negligible mass transfer resistance. The criterion was that $R \geq 0.95R_0$. The predicted uncertainty is ± 200 rpm.

dynamic- and steady state based mass transfer factors. The calculations showed that assuming all catalyst in the bulk compartment, then the steady state based coefficients were the correct ones. This case is not unlikely since centrifugal forces will pull the polymer/catalyst particles to the reactor wall, were the disturbance of the flow from the wall will cause turbulence and good mixing properties. The steady state values are thus most reliable.

Modeling: The unbaffled, non-sparging system was modeled using the equations derived in the last section. Data for viscosity and surface tension were taken as interpolations of pure decane literature values at several temperatures [8]. Density was estimated by the Hankinson-Brobst-Thomson technique [10]. Diffusivity coefficients were estimated using Wilke-Chang's method [10] for propene in decane. The limiting stirrer rate for significant mass transfer resistance was evaluated as a function of reaction rate (in g/h). The criterion for neglecting the effect of mass transfer was chosen as a conversion rate greater than 95% of the reaction rate without mass transfer limitation. The measured mass transfer factors together with the modeled factors and the mass transfer limit chart are shown in Fig. 3.

In a parameter sensitivity analysis it was found that the largest uncertainty was related to the estimate of the diffusion coefficient, which is believed to be correct only within $\pm 50\%$. The resulting error in the modeled mass transfer factors is about $\pm 20\%$. Bin's empirical relation has an uncertainty of $\pm 20\text{-}30\%$ [1] and the interfacial area is believed to be accurate to within $\pm 20\%$. A higher uncertainty is expected in the low Reynolds number region. This adds up to a total uncertainty in the predicted mass transfer factors of order two, and translates to an uncertainty in the estimated necessary stirring rates of ± 200 rpm. This uncertainty can be significantly reduced if better physical data were available.

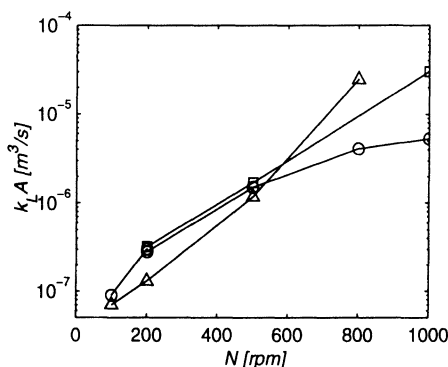


Fig. 4. The effects of baffles and sparging on the gas-liquid mass transfer of propene in decane. Mass transfer factors as function of stirring rate. \circ = normal reactor, Δ = with baffles, \square = with self-sparging.

Effect of baffles and sparging: Mass transfer factors were determined as function of stirring rate with/without baffles and with/without a hollow-tube self-sparging impeller. The results are presented in Fig. 4. Baffles increase the mass transfer factor for high stirring rates, but lower the factor at low stirring rates. The baffles may have a stabilizing effect on the liquid at lower stirring rates. Self-sparging increases the mass transfer factor above a certain stirring speed. The self-sparger starts to function when the induced suction overcomes the hydrostatic pressure.

7. Conclusions

The gas-liquid mass transfer in a stirred semi batch lab reactor was investigated experimentally and theoretically. The system was polymerization of propene using a Ziegler-Natta catalyst dispersed in decane.

The kinetic study of the system revealed the deactivation independent of amount of polymer produced, and a monomer reaction order of 1.2.

The transient- and steady state monomer feed rates were measured as function of stirring rate. The results from the two methods differed significantly. The discrepancy was qualitatively explained by the presence of dead zones in the reactor. The steady state based factors were found to be most reliable.

The model developed for an unbaffled, non-sparging reactor was based on the gas-liquid mass transfer being controlled by the renewal of liquid surface. The theoretically founded model described the observed trend accurately and fitted the experimental mass transfer factors within a factor of two, which is also the estimated uncertainty in the model. The model can be used to provide criteria for the necessary stirring rate to secure minimal gas-liquid transport limitations during polymerization of olefins.

Introducing baffles and sparging considerably decreased the gas-liquid mass transfer resistance at high stirring rates. Baffles caused an increased mass transfer resistance at low stirring rates.

References

- [1] Bin, A.K., Chem. Eng. Commun. 1984;31:155.
- [2] Cussler, E. L. *Diffusion. Mass transfer in fluid systems*. New York: Cambridge University Press; 1984.
- [3] Dong, L. *Flow Generated by an Impeller and Mass Transfer Across Gas-Liquid Interfaces in Stirred Vessels*. Trondheim, Norway: Ph.D. thesis, The Norwegian Institute of Technology; 1991.
- [4] Dong, L.; Johansen, S. T., and Engh, T. A., Can. Met. Quart. 1992; 31(4):299.
- [5] Keii, T.; Doi, Y., and Kobayashi, H., J. Polym. Sci., Part A: Polym. Chem. 1973; 11:1881.
- [6] Kittilsen, P.; Tøgersen, R.; Rytter, E., and Svendsen, H., *Experimental Study of Gas-Liquid Mass Transfer Limitations in Olefin Polymerization*. To be published.
- [7] Kittilsen, P.; Tøgersen, R.; Rytter, E., and Svendsen, H., *Modeling of Gas-Liquid Mass Transfer in Semi Batch Olefin Polymerization*. To be published.
- [8] Lide, D. R. *Handbook of Chemistry and Physics*. 78 ed. New York: CRC; 1996.
- [9] Nagata, S.; Yokotama, T., and Maeda, H., Mem. Fac. Eng., Kyoto Univ. 1956; 18:13.
- [10] Reid, R. C.; Praunsnitz, J. M., and Poling, B. E. *The Properties of Gases and Liquids*. New York: McGraw-Hill; 1987.
- [11] Theofanous, T. G.; Houze, R. N., and Brumfield, L. K., Int. J. Heat Mass Transfer. 1976; 19:613.
- [12] Thorshaug, K., Støvneng, J.A., Rytter, E., Ystnes, M., *Macromolecules*, In press.

Symbols

| | |
|--|---|
| <p>A : interfacial area</p> <p>α_i : slope of $\ln F - F_i$ vs. t</p> <p>β_i : mass transfer factor at stirrer rate N_i ($=k_L A$)</p> <p>c_o : reaction rate constant</p> <p>c_d : deactivation rate constant</p> <p>D : diffusion coefficient</p> <p>d_i : impeller diameter</p> <p>d_r : reactor diameter</p> <p>$\bar{\epsilon}$: mean energy dissipation</p> <p>F : monomer feed rate</p> <p>F_i : steady state monomer feed rate at stirrer speed N_i</p> <p>F_o : monomer feed rate at no mass transfer limitation</p> <p>G : amount of catalyst</p> <p>k_L : mass transfer coefficient</p> <p>k_L^{mf} : mean flow mass transfer coeff.</p> | <p>k_L^{st} : small scale turbulence mass transfer coeff.</p> <p>$k_L A$: mass transfer factor ($=\beta$)</p> <p>k_p : propagation constant</p> <p>M : monomer concentration</p> <p>M_o : monomer concentration at equilibrium</p> <p>N_i : stirrer rate i</p> <p>n : monomer reaction order</p> <p>ν : kinematic viscosity</p> <p>R : reaction rate</p> <p>Re : Reynolds number ($=Nd_i^2/\nu$)</p> <p>Re_t : turbulent Reynolds number ($=0.07d_i^{4/3}\bar{\epsilon}^{1/3}/\nu$)</p> <p>$Sc$: Schmidt number ($=\nu/D$)</p> <p>Sh : Sherwood number ($=k_L d/D$)</p> <p>T : Temperature</p> <p>V : reactor volume</p> |
|--|---|

Ternary Metallocene Based Catalysts in High Temperature, High Pressure Polymerization

G. Luft, A. Rau, A. Dyroff, C. Götz, S. Schmitz, T. Wieczorek,
R. Klimesch* and A. Gonioukh*

Technical University Darmstadt, Department of chemical engineering, Petersenstraße 20
D-64287 Darmstadt.

* BASF AG, Polymer Laboratory, Department Polyolefins, D-67056 Ludwigshafen
Email: alex@bodo.ct.chemie.tu-darmstadt.de

Abstract. High pressure copolymerizations of ethene and 1-hexene were performed by use of a ternary catalyst system based on $\text{Me}_2\text{Si}[\text{Ind}]_2\text{ZrCl}_2$, $\text{Al}(\text{iBu})_3$ and $[\text{PhNHMe}_2][\text{B}(\text{C}_6\text{F}_5)_4]$. The productivity depends strongly on the molar ratio of $[\text{Al}]/[\text{Zr}]$ used. With small amounts of 1-hexene in the feed a rate enhancement of the ethene polymerization rate was observed. Incorporation of 1-hexene in the polymer was studied as well as the influence of 1-hexene on polymer density.

Introduction

MAO-free catalyst systems based on Group 4 metallocene alkyls L_2MR_2^1 and a cation-forming agent are inefficient in polymerization because most of the metallocene species are consumed by the reaction with impurities. Ternary catalyst systems based on a zirconocene dichloride L_2ZrCl_2 , an aluminium alkyl and a cation forming-agent are less sensitive to impurities and easy to handle. Chien and Naga used the ternary catalyst systems $\text{L}_2\text{ZrCl}_2/\text{AlR}_3/[\text{Ph}_3\text{C}][\text{B}(\text{C}_6\text{F}_5)_4]$ in low temperature olefin polymerization[1]. In order to activate the metallocene species and to start the polymerization they injected the components of the catalyst system step by step into the reactor.

In this article we are reporting on the performance of the premixed ternary catalyst system $\text{Me}_2\text{Si}[\text{Ind}]_2\text{ZrCl}_2/\text{Al}(\text{iBu})_3/[\text{PhNHMe}_2][\text{B}(\text{C}_6\text{F}_5)_4]$ in continuous high-pressure polymerizations at 210°C.

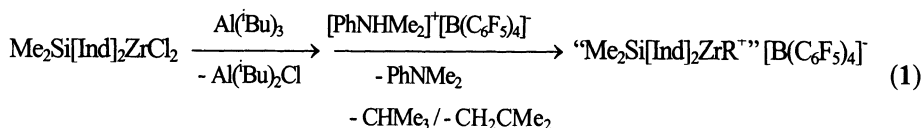
¹ L_2 = bridged or nonbridged η^5 -Ligands

Experimental

Formation of the active catalyst

To generate the active “metallocene cation” the components of the catalyst system were premixed in a two-step procedure. First a slurry of $\text{Me}_2\text{Si}[\text{Ind}]_2\text{ZrCl}_2$ in toluene was reacted with 5 to 200 mol equivalents of $\text{Al}(\text{}^i\text{Bu})_3$. The resulting solution was stirred for 30 min at room temperature and in a second step added to a solution of 1.3 mol equivalents of $[\text{PhNHMe}_2][\text{B}(\text{C}_6\text{F}_5)_4]$ in toluene. Within two hours the catalyst solution was metered into the reactor.

In the first step alkyl zirconocenes are formed by the reaction of the metallocene dichloride with $\text{Al}(\text{}^i\text{Bu})_3$. The second step is accompanied by the evolution of a gas that was identified as a mixture of isobutane and isobutene. The protonolysis of metallocene species like $\text{L}_2\text{Zr}(\text{CH}_2\text{CHMe}_2)\text{X}$ with $[\text{PhNHMe}_2][\text{B}(\text{C}_6\text{F}_5)_4]$ is expected to yield isobutane[2]. The isobutene most probably is formed by a β -H-elimination. This means that hydrido zirconocene complexes can be involved in the activation process. However, if a metallocene cation is formed the overall reaction of the activation may be represented by:



R = ${}^i\text{Bu}$ or H

Polymerization

The polymerization experiments were performed in a continuously operated, 100 -ml, high-pressure autoclave (figure 1). For the experiments described here the pressure was set to 150 MPa and the residence time to 240 s. Ethene was taken out of bombs, purified by molecular sieves and a copper catalyst and pressurized by means of a two-stage compressor. 1-hexene was distilled from CaH_2 and metered by a high pressure membrane pump. The mixture of the monomers was continuously fed into the reactor along the stirrer. The desired composition of the feed was adjusted by mass flow controllers. The pressure was maintained constant by means of a motor driven outlet valve controlled by a process computer. The catalyst solution was added into the reactor by a syringe-type pump. When the feeding of the catalyst solution was commenced the temperature inside increased and reached a constant level after 20 min. After the reactor the pressure was released to ambient and the polymer was collected in different separators.

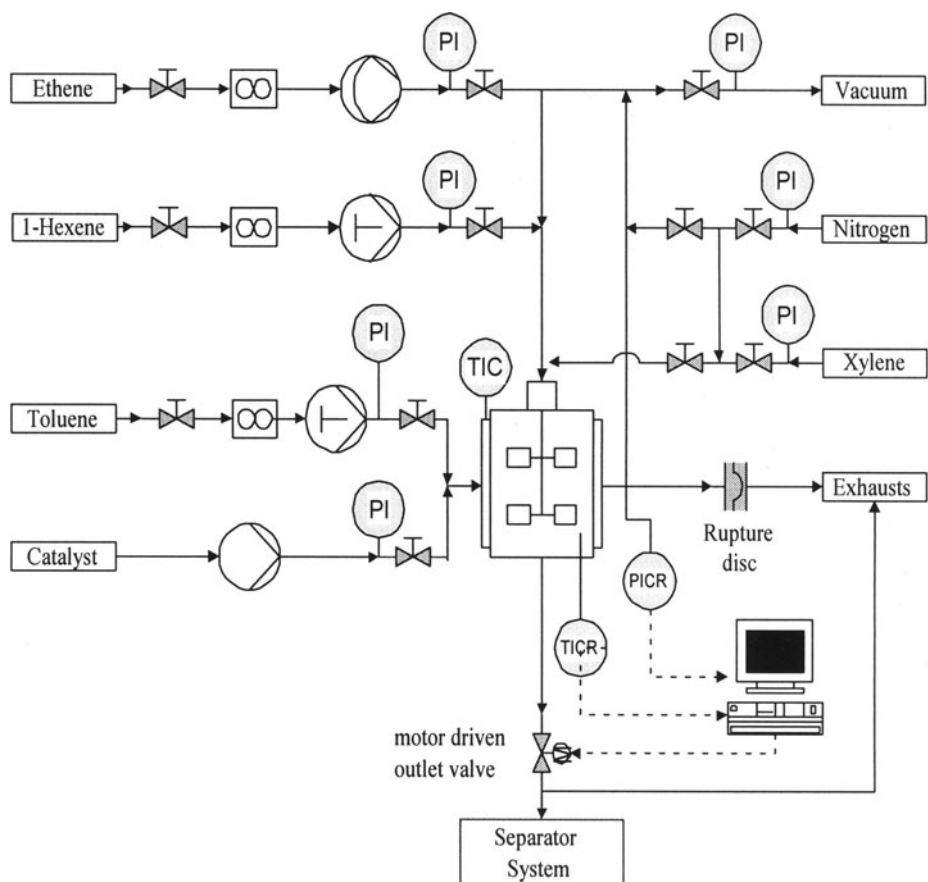


Fig. 1. High pressure polymerization unit

Results

Influence of the [Al]/[Zr] ratio on productivity

In two series of experiments we varied the molar ratio of [Al]/[Zr]. In the first series the content of [Zr] in the feed was maintained at 0.5 mol-ppm, whereas in the second series [Al] was adjusted to 40 mol-ppm. The plot of productivity as a function of the [Al]/[Zr] ratio shows nearly the same sigmoid shape for both series (figure 2). At small [Al]/[Zr] ratios the yield was very low; when this ratio was increased to 100 the productivity increased steeply to 300 kg polymer / g Zr. Further increase of the amount of aluminium alkyl leads only to a minimal increase in productivity. Figure 2 shows that for reaching optimal productivities it is not sufficient to adjust a minimum concentration of scavenger in the reactor. A definite Zr concentration must additionally be chosen and/or the activation requires a definite ratio of metallocene dichloride to tri-isobutyl aluminium. Except for the products obtained with very high catalyst concentrations the polymers showed narrow molecular weight distributions ($M_w/M_n \cong 2$).

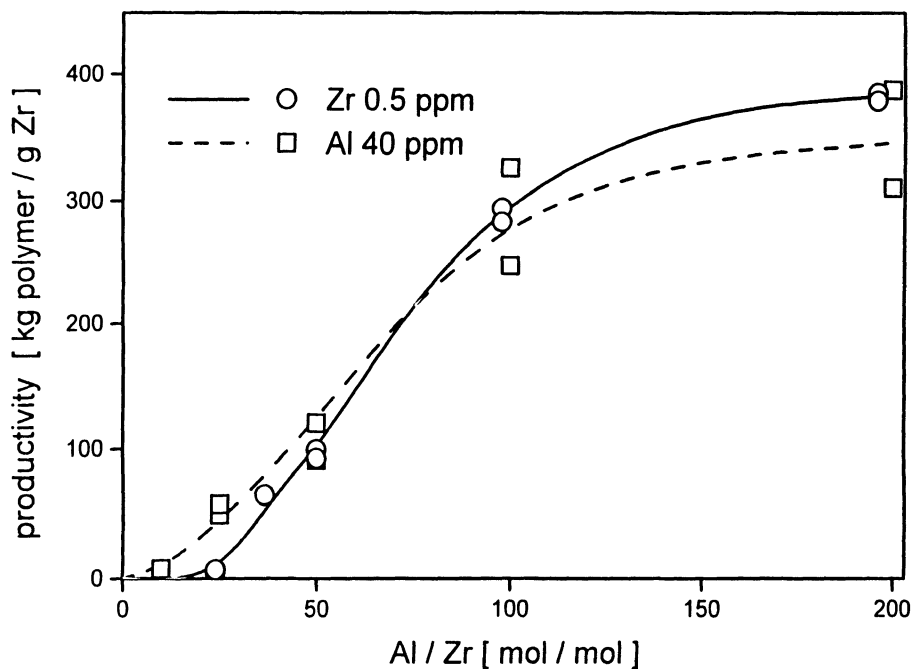


Fig. 2. Influence of the [Al]/[Zr] ratio on productivity

Rate enhancement effect

With small amounts of 1-hexene in the reactor an increase in the ethene polymerization rate is observed (figure 3). This phenomenon, called rate enhancement effect, is known from low pressure polymerizations with soluble and insoluble catalysts[3]. The conditions used in the high pressure polymerization result in a one-phase system in the reactor even in homopolymerization. Therefore the acceleration effect can not be attributed to a diffusion phenomenon.

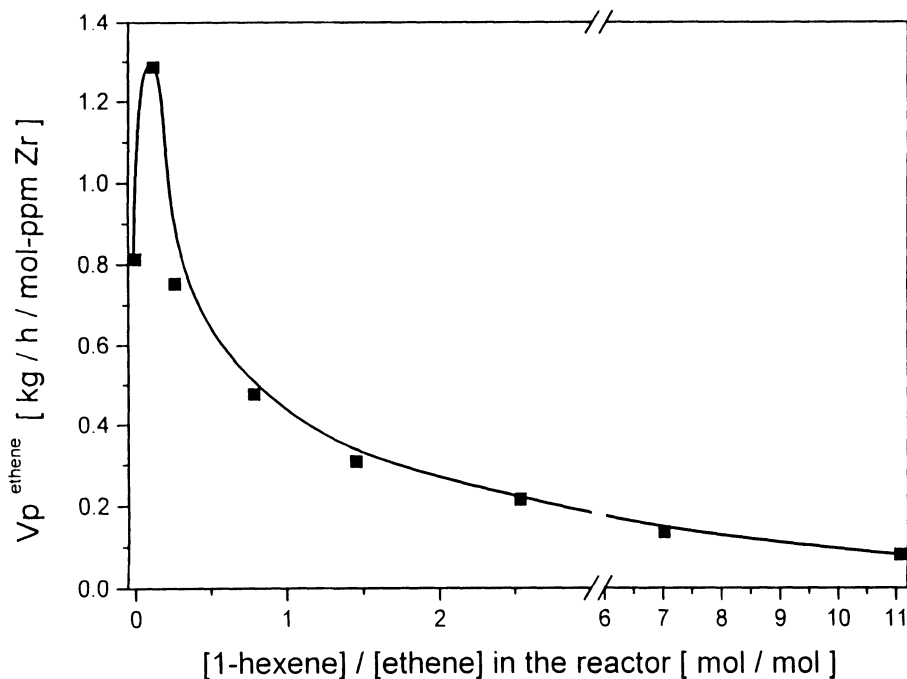


Fig. 3. Influence of [1-hexene]/[ethene] ratio on the polymerization rate of ethene

Incorporation of 1-hexene into the polymer

The incorporation of 1-hexene into the polymers was determined by means of ^{13}C -NMR and IR spectroscopy. The outlined copolymerization diagram clearly shows the preferential incorporation of ethene into the copolymer (figure 4). According to the method of Fineman-Ross, the copolymerization parameters were

determined as $r_e = 28$ and $r_h = 0.05$ with $r_e \cdot r_h \cong 1$. These values are quite similar to the values of $r_e = 63$ and $r_h = 0.02$ found in ethene/1-hexene high-pressure copolymerizations for the catalyst system $\text{Me}_2\text{Si}[\text{IndH}_4]_2\text{ZrCl}_2/\text{MAO}$ [4].

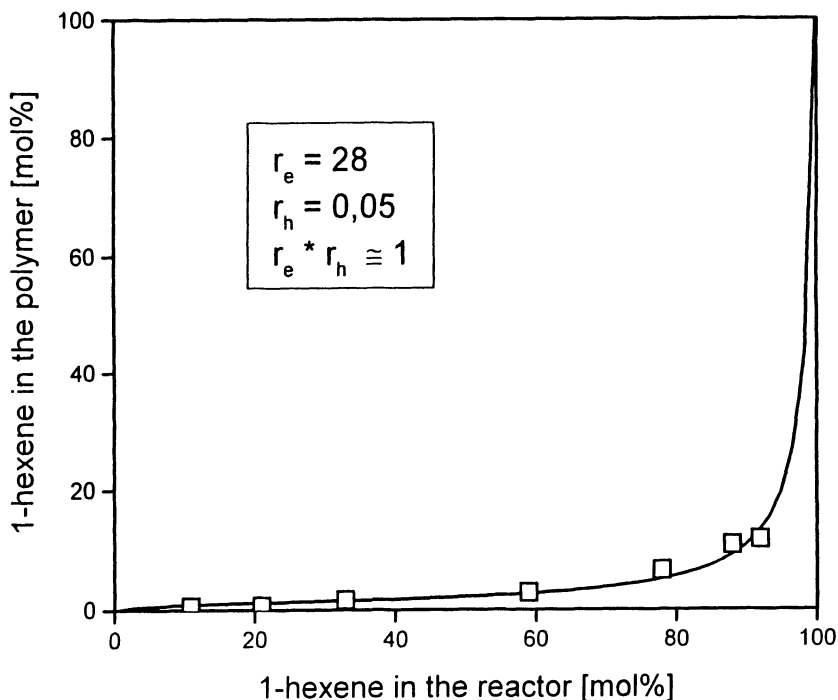


Fig. 4. Diagram of copolymerization

Influence of 1-hexene concentration on polymer density

The density of the copolymers decreased with an increasing 1-hexene concentration in the feed (figure 5). The density of the ethene homopolymer was 0.965 g/cm^3 , whereas the density of the copolymer obtained with 70 mol% 1-hexene in the feed was 0.876 g/cm^3 .

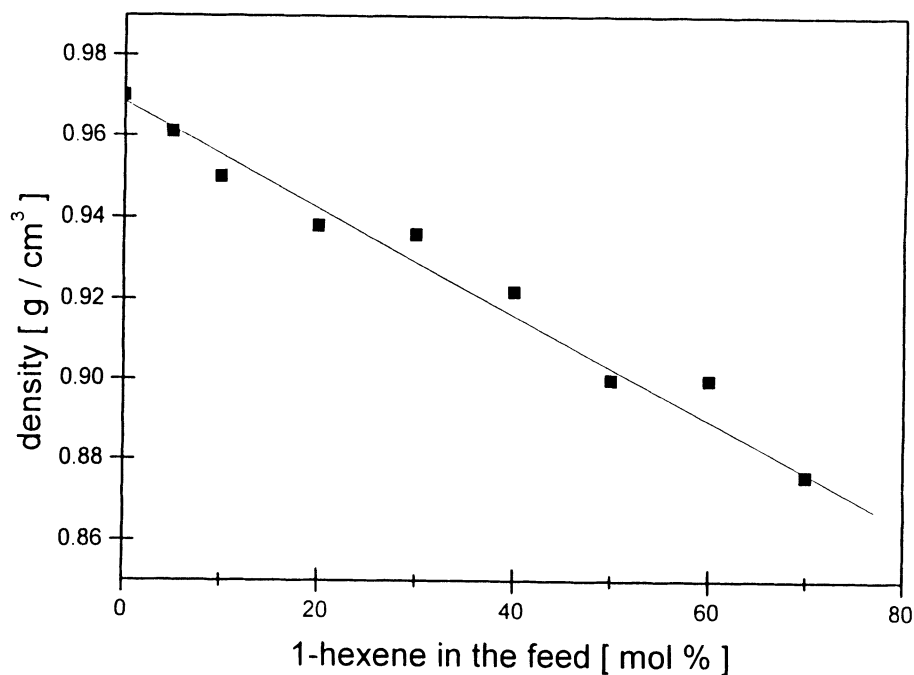


Fig. 5. Influence of 1-hexene concentration in the feed on polymer density

References

- (a) Tsai W, Rausch MD, Chien JCW (1993) *Appl Organomet Chem* 7: 71
(b) Tsai W, Chien JCW (1994) *J Polym Sci Part A, Polym Chem* 32: 149
(c) Chien JCW, Song W, Rausch MD (1994) *J Polym Sci Part A, Polym Chem* 32: 2387
(d) Naga N, Mizunuma K (1997) *Macromol Rapid Commun* 18: 581
- Guo Z, Swenson DC, Jordan RF (1994) *Organometallics* 13: 1424
- (a) Koivumäki K (1995) *Acta polytechnica Scandinavia, Chemical Technologies Series*: 227, Helsinki
(b) Herfert N, Fink G (1992) *Polym Mater Sci Eng* 67: 31
- Bergemann C, Cropp R, Luft G, *J Molecular Catalysis A Chemical* 105: 87

Acknowledgement. The authors thank the BMBF for support of this research.

Advances in the Use of Stopped-flow Techniques for Olefin Polymerization

Minoru Terano* , Mikio Yamahiro, Hideharu Mori

School of Materials Science, Japan Advanced Institute of Science and Technology, 1-1 Asahidai, Tatsunokuchi, Ishikawa 923-1292, Japan
e-mail: terano@jaist.ac.jp

Abstract. The stopped-flow method, by which a reaction can be conducted within an extremely short period (*ca.* 0.1 s), has been extensively applied to various kinds of investigations of olefin polymerization using Ziegler catalysts. The most important studies using this method are related to kinetic investigations of the polymerization. This method seems to be most suitable for the kinetic study of olefin polymerization with Ziegler catalysts, because the quasi-living polymerization stage can be attained, in which the states of the active sites are constant without a time-dependent change, and the chain-transfer reaction can be essentially negligible. For this reason, it is possible to clarify the effects of hydrogen and the co-catalyst, which are significant and indispensable factors that must be taken into account during the olefin polymerization, and for the polymerization behavior in the initial stage. Attention is also focused on the study of the active sites on the catalysts using the stopped-flow method. This can be done because the nature of the active sites just after their formation can be directly reflected in the polymer obtained during the initial polymerization stage. The method has been employed to produce a novel olefin block copolymer by taking advantage of the polymerization within an extremely short period, where the polymerization time is considered to be shorter than the lifetime of the growing polymer chain. In this article, we outline the various investigations related to the stopped-flow method for the polymerization of olefins with Ziegler catalysts.

1. Stopped-flow technique for olefin polymerization

In the field of polymer science, stopped-flow techniques with a spectroscopic detector have been widely employed to investigate the various kinds of polymerizations, such as cationic polymerization¹⁻⁶, anionic polymerization^{7,8}, and group-transfer polymerization⁹. A major objective of these studies was to obtain information concerning the active species and the polymerization kinetics. For UV-absorbing species, such as a vinyl aromatic cation, this method was most useful to observe, in real time, the active species that have a short lifetime.

Stopped-flow FTIR spectroscopy was recently developed in order to determine reaction kinetics during a polymerization with no UV-detectable moiety.

For Ziegler-catalyzed olefin polymerizations, the method was developed by Keii and Terano in 1987, now called the Keii method, to evaluate certain kinetic parameters during the polymerization of propylene with an MgCl_2 -supported Ziegler catalyst¹⁰. It must be noted that the polymerization system is heterogeneous and the active species can not be spectroscopically detected. These features are different from the other polymerization systems.

There is an elegant simplicity in the stopped-flow technique. In its basic form, two reagents are driven together through tubes to contact and flow into a flask containing a quenching agent. In order to fully display the ability of the stopped-flow technique, it is necessary to meet the following requirements.

- The active sites on the catalyst must be formed by interaction with the co-catalyst without any delay. Thus, complete mixing of the catalyst and co-catalyst is required.
- The time required for the formation of the active sites at the beginning of the polymerization must be negligible compared with the polymerization time.
- The stirring of the catalyst slurry in the vessel should be efficient in order to avoid temperature and concentration gradients.
- The monomer must be highly soluble in the solvent used in the polymerization in order to obtain an appropriate and relatively high monomer concentration.
- The flow velocity must be constant during the polymerization.
- The monomer conversion must be held below *ca.* 10% in order to ignore the changes of monomer concentration and polymerization temperature.
- The polymerization must be terminated immediately and completely in order to avoid any deviation in polymerization time, and to be able to neglect the evolution of unfavorable side-reactions induced by the slow and/or reversible termination reaction.
- Sufficient polymer must be obtained to perform all required analytical measurements.

In this decade, the stopped-flow method has been extensively applied to various kinds of investigations for olefin polymerization with Ziegler catalysts by taking advantage of the polymerization within an extremely short period. The objective of this paper is to summarize the most recent results of these studies and to demonstrate the advantages of the method for the basic studies of olefin polymerization, as well as of Ziegler catalysts.

2. Olefin polymerization kinetics

For olefin polymerization with a typical Ziegler catalyst, catalyst deactivation, as well as the various types of chain-transfer reactions, proceeds along with the

propagation reaction. On the other hand, using the stopped-flow method, the states of the active sites are constant without a time-dependent change, and chain-transfer reactions can be negligible within the extremely short period, indicating that a quasi-living polymerization can be performed. One of the most attractive features of the method is the ability to observe the polymer produced in the initial polymerization stage, which directly reflects the nature of the active sites just after their formation. Accordingly, the method was found to be useful for studying the polymerization behavior and the nature of active sites as well as for accurately estimating kinetic parameters.

It should be noted that the excellent characteristics mentioned above, such as constant catalyst activity and negligible chain-transfer reactions within the extremely short period, can not be found in any other polymerization system. However, the appropriate choice of suitable polymerization conditions and catalyst systems are required in order to get the desired results by taking advantage of the stopped-flow technique.

2-1. Effect of hydrogen

Hydrogen is used as a chain-transfer agent to control the molecular weight of the polymer during the commercial production of polyolefins, such as polypropene and polyethylene. Although a large number of reports have been published on the effect of hydrogen during the polymerization of olefins, the mechanism of the chain-transfer reaction with hydrogen has not yet been clarified, because the active sites on the heterogeneous catalysts are extremely complex and the variation in the nature of the active sites (e.g., the oxidation state of titanium species) may exert a significant influence on the effect of hydrogen. Furthermore, it is difficult to obtain exact information about the effect of hydrogen on the chain-transfer reaction using a conventional polymerization procedure because the state of the active sites on the catalyst varies with polymerization time, and the various types of chain-transfer reactions, including the elimination of β -hydrogen and transfer by co-catalyst or monomer, proceed with the propagation reaction.

With this in mind, the stopped-flow polymerization method was used for the study of the chain-transfer reaction by hydrogen during the initial stage of the propene polymerization¹¹. The addition of hydrogen had no apparent effect on either the yield or the molecular weight of the resulting polymer, as shown in Fig. 1(a). Accordingly, the method was successfully applied to find the region, in other words, the polymerization condition under which hydrogen does not act as a chain-transfer reagent. It is important that we have identified the region where hydrogen has no effect on either the molecular weight or the polymer yield of polypropene produced with an MgCl_2 -supported Ziegler catalyst. On the other hand, when the catalyst was treated with $\text{Al}(\text{C}_2\text{H}_5)_3$ before polymerization, the molecular weight of the produced polymer was decreased by using hydrogen, even though the yield was not affected (Fig. 1(b)). This indicates that the hydrogen acted as a chain-transfer agent for the catalyst modified by the pre-treatment. Furthermore, as can be seen by comparing Figs. 1(a) and 1(b), the activity of the catalyst is decreased

(compared to its original value) using the pretreated catalyst, as a result of catalysts deactivation and decreased monomer concentration. These results seem to indicate that the effect of hydrogen during the initial stage of propene polymerization is dependent upon the existence of a different state of the active sites, where the reduction of titanium species is believed to occur to yield lower oxidation states through the pre-treatment with $\text{Al}(\text{C}_2\text{H}_5)_3$.

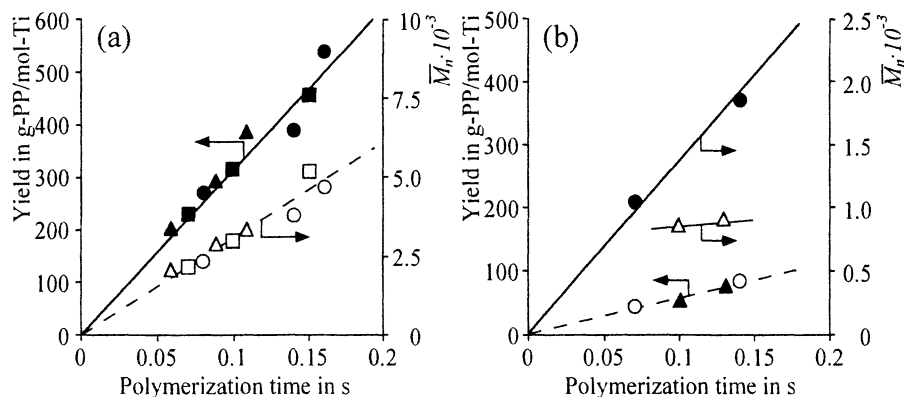


Fig. 1. Dependence of polymer yield ($\bullet, \blacktriangle, \blacksquare$) and \bar{M}_n ($\circ, \triangle, \square$) on polymerization time. (a) The polymerization was carried out with an MgCl_2 -supported Ziegler catalyst in the presence ($\blacktriangle, \triangle$, 1 atm; \blacksquare, \square , 4 atm) or absence (\bullet, \circ) of hydrogen. (b) The polymerization was performed with a pretreated MgCl_2 -supported Ziegler catalyst in the presence ($\blacktriangle, \triangle$, 1 atm) or absence (\bullet, \circ) of hydrogen.

As mentioned above, it was demonstrated that the state of the catalyst has a significant influence on the chain-transfer reaction with hydrogen. However, it was not clear whether it was hydrogen in the molecular or atomic state that affects the chain-transfer reaction. In order to make this point clear, the H_2 - D_2 exchange reaction, which is commonly used for the detection of the dissociation of a hydrogen molecule, was applied to study the olefin polymerization catalysts. The results of the H_2 - D_2 exchange reaction, combined with those from stopped-flow polymerization, appear to indicate that chain transfer by hydrogen occurred in the system in which HD was produced in an exchange reaction¹². In other words, only the pretreated catalyst showed activity for the H_2 - D_2 exchange reaction, as well as the chain transfer reaction with hydrogen. Thus, it is apparent that the zero effect of hydrogen during the initial stage of propene polymerization is due to the non-dissociation of the hydrogen molecule and that chain transfer with hydrogen takes place through atomic hydrogen.

PdCl_2 was successfully employed as the source of atomic hydrogen (by dissociation of the hydrogen molecule) in order to initiate the chain-transfer reaction during the initial stage of the propene polymerization¹³. PdCl_2 itself does not act as a chain-transfer agent nor does it start the propene polymerization. It was observed that chain transfer occurred even during the initial stage of the polymerization by the addition of PdCl_2 . Thus, it was clear that the introduction of

a material that can bring about the dissociation of a hydrogen molecule could induce the chain-transfer reaction with hydrogen. This result also suggested that the chain-transfer reaction with hydrogen occurred on the catalyst, even though atomic hydrogen was formed at another site, i.e., the solid PdCl_2 particle. The technique developed in the study might be further applied for the improvement of the hydrogen response of the catalyst system for olefin polymerization.

2-2. Effect of co-catalyst

The use of a co-catalyst, such as triethylaluminium as an activating agent is indispensable for olefin polymerization with Ziegler catalysts. The catalyst efficiency is known to be changed when using a different alkylaluminium compound as co-catalyst, as well as by using the same co-catalyst at different concentrations. However, no exact kinetic explanation concerning the active sites has been provided for this phenomenon. To obtain a clearer insight into this, the stopped-flow technique was applied to the investigation of the influence of triethylaluminium concentration on the kinetic parameters obtained in the initial stage of propene polymerization with an MgCl_2 -supported Ziegler catalyst¹⁴. From this study, it was clear that the change in the catalyst activity is solely due to the change of $[C^*]$ and is independent of the k_p value.

The effect of the nature of the alkylaluminium co-catalyst on the kinetic parameters for the initial stage of propene polymerization with an MgCl_2 -supported Ziegler catalyst was also studied by the stopped-flow polymerization method¹⁵. The value of $[C^*]$ significantly decreased with an increase in the bulkiness of the alkyl group of the aluminium compound. The change in the value of k_p was rather small. However, it was proportional to the meso pentad fraction of the resulting polypropene, suggesting that the order of the k_p corresponded to the ratio of isotactic polypropene to total polypropene. From this point of view, it might be presumed that k_p values on isospecific and aspecific active sites produced by trialkylaluminium were the same regardless of the alkyl group of the aluminum compound, and that the overall k_p was proportional to the ratio of the concentration of isospecific active sites to that of all the active sites.

In order to confirm this presumption, the kinetic parameters, $k_{p(\text{insol})}$ and $[C^*_{(\text{insol})}]$, were calculated from the yield and molecular weight of the fraction insoluble in boiling heptane. It was observed that the values of $k_{p(\text{insol})}$ were almost the same regardless of the co-catalyst, while the values of the overall k_p were dependent on the ratio of $[C^*_{(\text{insol})}]$ to overall $[C^*]$, as shown in Fig. 2. The results obtained in the study suggested that the nature of the isospecific active sites produced by various alkylaluminiums was essentially the same, but that the ratio of the different types of active sites formed with a variety of alkylaluminiums were different.

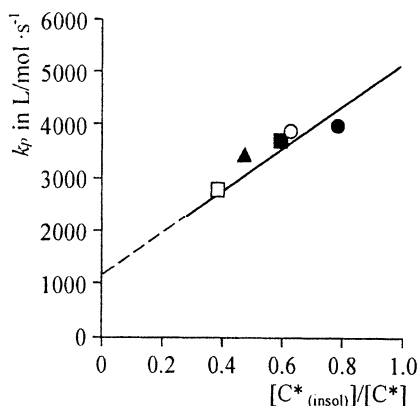


Fig. 2. The relationship between k_p values and $[C^*_{(insol)}]/[C^*]$. TEA (○), TNBA (●), TNHA (■), TNOA (▲), TIBA (□).

2-3. Insight into the broad molecular weight distribution

The molecular weight distributions of polyolefins produced with heterogeneous Ziegler catalysts are unusually broad, and this is one of the most important unanswered questions. Many attempts have been made to solve this problem. There have been three suggested explanations for the broad molecular weight distribution: a change in the rate constants for the propagation and transfer reactions at different polymer chain lengths; the existence of polymer layers leading to a monomer diffusion limitation; and the non-uniformity of the active sites, i.e., the existence of various active sites having different properties, such as different k_p values. From stopped-flow polymerization analysis with an $MgCl_2$ -supported Ziegler¹⁴, in which the transfer reaction is negligible and the existence of the polymer layer can be ignored, it was clear that polypropenes obtained during the initial polymerization stage up to *ca.* 0.2 s showed similar values in molecular weight distributions ($\overline{M}_w/\overline{M}_n=3.2-4.3$, determined by GPC). Furthermore, the value remained constant up to 10 s ($\overline{M}_w/\overline{M}_n=3.6$), at which point the chain-transfer reaction is considered to start in competition with the propagation reaction. Hence, the former two explanations could not be employed in this case. The only feasible reason for the broad molecular weight distribution is the last one, i.e., the existence of non-uniform active sites in the system.

3. Synthesis of a novel olefin block copolymer

An example of another application of the stopped-flow method is the synthesis of a novel olefin block copolymer, polypropene-*b*-poly(ethene-*co*-propene)¹⁶⁻¹⁸. An impact copolymer is one of the main grades of commercial polypropene, and it is produced by a sequential polymerization process; it is sometimes called a

"block-type copolymer", but it does not have such a true structure, as the lifetime of the growing polymer chain is extremely short (less than 1 s) due to the rapid chain transfer. Furthermore, the activity of the catalyst changes with the polymerization time. Thus, it has been impossible to synthesize the block copolymer by conventional sequential polymerization even on a laboratory scale.

3-1. Synthesis of polypropene-*b*-poly(ethene-*co*-propene)

To avoid an unfavorable chain transfer, the polymerization was performed using the stopped-flow method and terminated within *ca.* 0.2 s, which is shorter than the lifetime of the growing chain. The activity of the catalyst was constant without deactivation in the region up to *ca.* 0.2 s. Thus, the modified stopped-flow apparatus (Fig. 3) was successfully applied to synthesize this block copolymer, in which poly(ethene-*co*-propene) was chemically linked with polypropylene¹⁶.

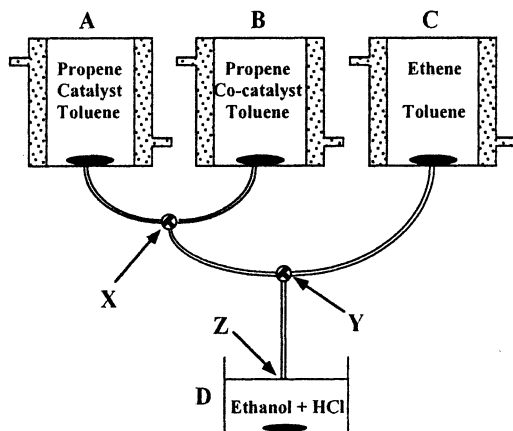


Fig. 3. Polymerization apparatus for the synthesis of the block copolymer. A, catalyst slurry in propene-saturated toluene; B, $\text{Al}(\text{C}_2\text{H}_5)_3$ solution in propene-saturated toluene; C, ethene-saturated toluene; D, ethanol with HCl; X and Y, three-way Teflon[®] tap. The polymerization of propene proceeds in the Teflon[®] tube from X to Y; then subsequent copolymerization of propene with ethene takes place from Y to Z.

The copolymers obtained showed unimodal GPC curves without any peak in the lower molecular weight region. In order to prove block formation, the copolymer obtained from the stopped-flow method, and a commercial, so-called "block-type" copolymer were extracted with heptane to check for the existence of free poly(ethene-*co*-propene) in these system using ¹³C NMR. After extraction, the fraction of poly(ethene-*co*-propene) remained unchanged for the copolymer obtained by the stopped-flow method (Fig.4) but disappeared from the commercial "block-type" copolymer (Fig.5). In all cases, the peaks due to the polypropene homopolymer remained the same after extraction. Therefore, these results suggest

the formation of the true block copolymer in the stopped-flow experiment, where almost all of the poly(ethene-*co*-propene) is chemically linked with polypropene.

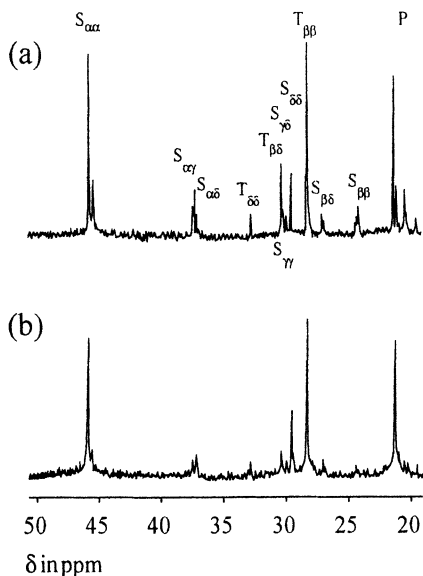


Fig. 4. ^{13}C NMR spectra of (a) polypropene-*b*-poly(ethene-*co*-propene) and (b) the unsolved part after extraction with heptane.

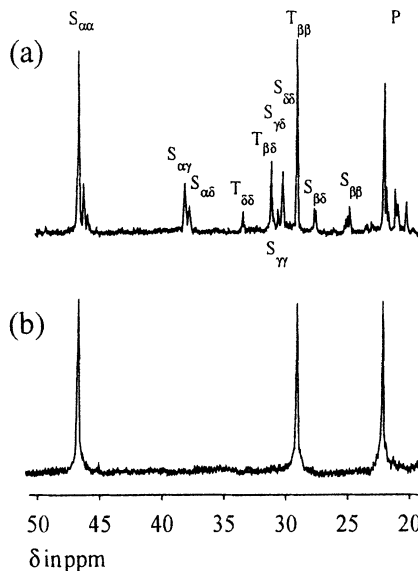


Fig. 5. ^{13}C NMR spectra of (a) commercial block-type copolymer and (b) the unsolved part after extraction with heptane.

3-2. Reactivates of ethene and propene

Polypropene-*b*-poly(ethene-*co*-propene) was employed to evaluate the reactivities of ethene and propene on each active site of the MgCl_2 -supported Ziegler catalyst using a temperature rising elution fractionation (TREF) technique. The MgCl_2 -supported Ziegler catalyst is considered to have non-uniform active sites^{19,20}. The heterogeneity of the active sites leads to a broad comonomer distribution as well as a broad molecular weight distribution. The block copolymer obtained in this study can be regarded as the mixture of polypropene-*b*-poly(ethene-*co*-propene) having different microstructures, which correspond to non-uniform active sites. The copolymer was fractionated on the basis of the crystallinity of the polypropene part in the block copolymer. Reactivities of ethene and propene on each active site were investigated based on the ^{13}C NMR analysis of the poly(ethene-*co*-propene) part of each fraction.

The results of the fractionation of polypropene obtained by the stopped-flow method are summarized in Tab. 1. The molecular weight and microtacticity of the fractionated polypropene increased with rising elution temperature. However, the molecular weight distributions ($\overline{M}_w/\overline{M}_n$) were equal to *ca.* 2, which indicated the nonuniformity of the active sites that produced each fraction under a quasi-living state.

Tab. 1. Characterization of fractionated polypropene^{a)}

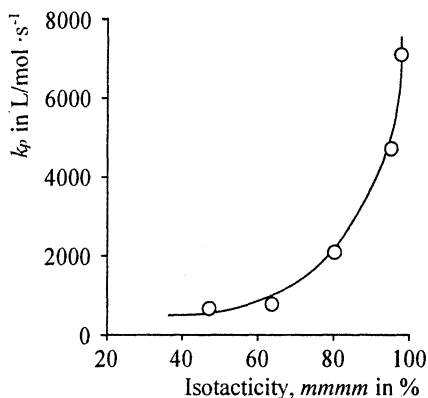
| Fraction No. | Extraction temp. in °C | \bar{M}_n ^{b)} | \bar{M}_w/\bar{M}_n ^{b)} | <i>mmmm</i> ^{c)} in % |
|--------------|------------------------|---------------------------|-------------------------------------|--------------------------------|
| P-1 | 32 | 3000 | 2.4 | 47.3 |
| P-2 | 50 | 3500 | 2.1 | 63.6 |
| P-3 | 100 | 6400 | 2.3 | 80.2 |
| P-4 | 105 | 16000 | 2.0 | 95.1 |
| P-5 | 140 | 27000 | 2.6 | 97.8 |

a) Fractionation was performed using TREF analysis system.

b) Determined by GPC.

c) Determined by ¹³C NMR.

Fig. 6 shows the relationship between the propagation rate constant (k_p) and the meso pentad fraction (*mmmm*) obtained from resulting fractionated polypropene. The value of k_p for the propene polymerization significantly increased with increasing stereospecificity of the active sites. These results seem to indicate that the distribution of the properties of active sites, such as k_p and stereospecificity, are continuous.

**Fig. 6.** Relationship between k_p values obtained from fractionated polypropene and *mmmm* pentad fraction.

On the basis of the polypropene homopolymer results, the fractionation of polypropene-*b*-poly(ethene-*co*-propene) obtained in this study was achieved based on the difference in the crystallinity of the polypropene part (Tab. 2).

Tab. 2. Characterization of fractionated polypropene-*b*-poly(ethene-*co*-propene)^{a)}

| Fraction No. | Extraction temp. in °C | \bar{M}_n ^{b)} | \bar{M}_w/\bar{M}_n ^{b)} | Ethene content ^{c)} in mol-% |
|--------------|------------------------|---------------------------|-------------------------------------|---------------------------------------|
| B-1 | 32 | 7400 | 2.7 | 36.0 |
| B-2 | 50 | 7800 | 2.7 | 26.0 |
| B-3 | 100 | 14000 | 2.3 | 11.2 |
| B-4 | 105 | 35000 | 1.9 | 6.3 |
| B-5 | 140 | 53000 | 2.2 | 2.7 |

a) Fractionation was performed using TREF analysis system.

b) Determined by GPC.

c) Determined by ¹³C NMR.

The ethene content in the block part significantly decreased with increasing elution temperature, in other words, with increasing crystallinity of the polymer and the stereospecificity of the active sites. The k_p values for ethene and propene were calculated using the ^{13}C NMR results of each fraction²¹. The k_p for propene in the copolymer significantly increased with the increase in the stereospecificity of the active sites (Fig. 7), the tendency of which was similar to that of the polypropene homopolymer. However, for ethene, k_p was constant for all active sites having the different stereospecificity for propene polymerization. This means that the stereospecificity of the active sites does not affect the reactivity of ethene.

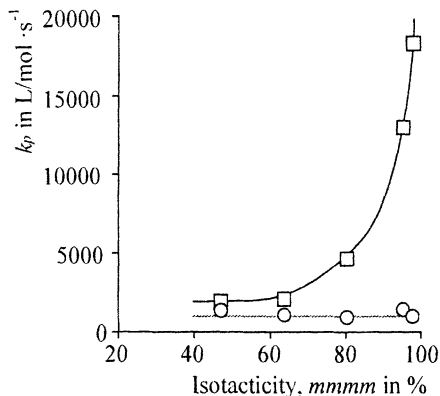


Fig. 7. Dependence of k_p values obtained from ethene unit (O) and propene unit (□) in poly(ethene-*co*-propene) part of the fractionated polypropene-*b*-poly(ethene-*co*-propene) on stereospecificity of active sites.

Various experiments including ethene homopolymerization and ethene-propene copolymerization with different conditions are now in progress to clarify the difference in k_p values for propene during the homo- and copolymerizations as well as the constant k_p value for ethene polymerization.

4. Future perspective

We have attempted to outline the variety of investigations that have used the stopped-flow method for olefin polymerization with Ziegler catalysts. We have also reported the various kinds of studies using the stopped-flow technique^{22,23}, such as the influence of the catalyst preparation method of the supported Ziegler catalyst on the kinetic parameters^{24,27}, the formation of active sites induced by catalyst fragmentation during polymerization²⁸, the interaction of a supported Ziegler catalyst with Lewis bases^{29,30}, and the cyclopolymerization of 1,5-hexadiene³¹. Here, it seems appropriate to close this article with some personal speculation about future work with the stopped-flow technique.

On the scientific side, we expect to see efforts directed towards the elucidation of the many unanswered questions that exist concerning olefin polymerization with Ziegler catalysts, such as the formation reaction and the structure of the active

sites, deactivation reactions related to the oxidative sites of titanium species, etc. The clear and detailed understanding of the basic aspects that should arise will lead to further development of the area. The kinetic study of olefin polymerization catalyzed by metallocene catalysts represents another important challenge for both academic and industrial interests. The work with a metallocene catalyst system has become an intensive research target of growing interest because the system has the capability of permitting the researcher to obtain a polymer having well-controlled properties and/or excellent performance. It is considered that the application of the stopped-flow technique would be one suitable approach to perform such detailed kinetic investigations, which are essential for finding an explicit relationship between the catalyst structure and polymerization mechanism, as well as for evaluating the critical parameters for stereoregularity during α -olefin polymerization³¹. Technologically, it is of interest to apply the stopped-flow method for the design and synthesis of novel olefin polymers having a well-defined structure and outstanding performance, which can open new areas of application for the polyolefins.

References

- 1 D. C. Pepper, *J. Polym. Sci., Polym. Symp.* **56**, 39 (1976)
- 2 M. Sawamoto, T. Higashimura, *Macromolecules* **12**, 581 (1979)
- 3 K. Takarabe, T. Kunitake, *Makromol. Chem.* **182**, 1587 (1981)
- 4 M. Villesange, A. Rives, C. Bunel, J.-P. Vairon, M. Froeyen, M. V. Beylen, A. Persoons, *Makromol. Chem., Macromol. Symp.* **47**, 271 (1991)
- 5 J.-P. Vairon, A. Rives, C. Bunel, *Makromol. Chem., Macromol. Symp.* **60**, 97 (1992)
- 6 B. Charleux, A. Rives, J.-P. Vairon, K. Matyjaszewski, *Macromolecules* **29**, 5777 (1996)
- 7 J.-P. Vairon, A. H. E. Müller, in *Comprehensive Polymer Science (Vol. 3)*, G. Allen, J. C. Bevington, Eds., Pergamon Press, UK 1988, pp. 571-577
- 8 V. Warzelhan, G. Löhr, H. Höcker, G. V. Schulz, *Makromol. Chem.* **179**, 2211 (1978)
- 9 W. J. Brittain, E. C. Aquino, I. B. Dicker, D. J. Brunelle, *Makromol. Chem.* **194**, 1249 (1993)
- 10 T. Keii, M. Terano, K. Kimura, K. Ishii, *Makromol. Chem., Rapid Commun.* **8**, 583 (1987)
- 11 H. Mori, K. Tashino, M. Terano, *Macromol. Rapid Commun.* **16**, 651 (1995)
- 12 H. Mori, K. Tashino, M. Terano, *Macromol. Chem. Phys.* **197**, 895 (1995)
- 13 H. Mori, T. Iizuka, K. Tashino, M. Terano, *Macromol. Chem. Phys.* **198**, 2499 (1997)
- 14 M. Terano, T. Kataoka, T. Keii, *J. Mol. Catal.* **56**, 203 (1989)
- 15 H. Mori, H. Iguchi, K. Hasebe, M. Terano, *Macromol. Chem. Phys.* **198**, 1249 (1997)
- 16 H. Mori, M. Yamahiro, K. Tashino, K. Ohnishi, K. Nitta, M. Terano, *Macromol. Rapid Commun.* **16**, 247 (1995)
- 17 M. Yamahiro, H. Mori, K. Nitta, M. Terano, *Macromol. Chem. Phys.* accepted.
- 18 M. Yamahiro, H. Mori, K. Nitta, M. Terano, *Polymer* accepted.
- 19 M. Kakugo, T. Miyatake, Y. Naito, K. Mizunuma, *Macromolecules* **21**, 314 (1988)
- 20 M. Kakugo, T. Miyatake, K. Mizunuma, Y. Kawai, *Macromolecules* **21**, 2309 (1988)
- 21 M. Yamahiro, H. Mori, M. Terano, to be published.

- 22 H. Mori, M. Terano, in *New trends in polyolefin science and technology*, S. Hosoda, Ed., Research Signpost, India 1996, pp. 37-49
- 23 H. Mori, M. Terano, *Trend in Polymer Science*, **5**, No.10, 314 (1997)
- 24 M. Terano, T. Kataoka, *Makromol. Chem., Rapid Commun.* **10**, 97 (1989)
- 25 M. Terano, T. Kataoka, T. Keii, *J. Polym. Sci., Part A: Polym. Chem.* **28**, 2035 (1990)
- 26 M. Terano, T. Kataoka, M. Hosaka, T. Keii, in *Olefin Polymerization Catalysts*, D. H. Lee, K. Soga, Eds, Hyung-Seul Publishing, Seoul 1990, pp. 31-46
- 27 M. Terano, T. Kataoka, and T. Keii, in *Catalytic Olefin Polymerization*, T. Keii, K. Soga, Eds, Kodansha-Elsevier, Tokyo 1990, pp. 55-61
- 28 H. Mori, M. Yoshitome, M. Terano, *Macromol. Chem. Phys.* **198**, 3207 (1997)
- 29 H. Mori, H. Saito, M. Terano, *Macromol. Chem. Phys.* **199**, 55 (1998)
- 30 H. Mori, H. Saito, M. Yamahiro, H. Kono, and M. Terano, *Macromol. Chem. Phys.* **199**, 613 (1998)
- 31 H. Mori, H. Yamada, H. Kono, M. Terano, *J. Mol. Cat. A: Chem.* **125**, L81 (1997)
- 32 M. Takahashi, N. Kawamoto, T. Matsukawa, M. Yamahiro, H. Mori, M. Terano, *Polymer Prepr. Jpn, English Ed.* **45**, E 56 (1996)

Contributors

A

Akimoto, A. 180
Altomare, A. 358
Arai, T. 465
Arndt-Rosenau, M. 212, 485
Arribas, G. 358
Ascenso, J. 576

B

van Belle, S. 236
Bellia, V. 236
Berthold, J. 3
Beulich, I. 485
Blais, M. 576
Bochmann, M. 413
Böhm, L.L. 3
Boggioni, L. 493
Botzenhardt, S. 97
Brandolini, A.J. 60
Brita, D. 142
de Brauwer, Y. 236
Brintzinger, H.-H. 223
Bronco, S. 358
Broyer, J.P. 347
Bujadoux, K. 590
Burkhardt, T.J. 601
Busico, V. 76

C

Camurati, I. 142
Carvill, A. 294
Cecchin, G. 14
Chadwick, J.C. 14, 76
Chenal, T. 590
Chien, J.C.W. 446, 576
Ciardelli, F. 358

Cipullo, R. 76
Correia, S.G. 576

D

Dall’Occo, T. 142
Del Duca, D. 14
Deng, H. 583
Denifl, P. 406
Destro, M. 142
Dias, A.R. 576
Dupuy, J. 347
Dyroff, A. 651

E

Ediati, R. 307
Eilertsen, J.L. 136
Eisch, J.J. 248
Elder, M.J. 150
Enderle, H.-F. 3
Ernst, E. 406
Ewen, J.A. 150

F

Ferro, D.R. 493
Fink, G. 321, 333
Fleissner, M. 3
Forlini, F. 294
Fouga, C. 590
Frauenrath, H. 283
Freidanck, F. 485
Fukui, Y. 566
Fusco, O. 142

G

Galimberti, M. 142
Galli, P. 14

Gavrilov, Y.A. 89
 Giarrusso, A. 519
 Gonioukh, A. 651
 Gosmann, M. 212
 Götz, C. 651
 Grassi, A. 548

H

Hagendorf, W. 105
 Hagihara, H. 264
 Harder, A. 105
 Haupt, E. 105
 Heinemann, J. 473
 Heitmann, B. 105
 Herzog, A. 123
 Hetzer, D. 509
 Hidalgo, G. 381
 Höcker, H. 283
 Hofmann, M. 97
 Hong, D.S. 368
 Hortmann, K. 236

I

Ikai, S. 558
 Ikeda, T. 264, 583
 Imaeda, K. 192
 Imuta, J.-I. 30
 Inoue, T. 435
 Ishihara, N. 435
 Ittel, S.D. 616
 Iwama, N. 192
 Iwamoto, Y. 558

J

Jones, R.L. 150

K

Kai, Y. 558
 Kaji, E. 50
 Kaminsky, W. 170, 485
 Kao, S.-C. 629
 Karol, F.J. 629
 Kashimoto, M. 192
 Kashiwa, N. 30
 Kato, T. 192

Keii, T. 38
 Keul, H. 283
 Kissin, Y.V. 60
 Kittilsen, P. 643
 Klimesch, R. 651
 Ko, Y.S. 368
 Kojoh, S.-J. 30
 Kovaleva, N.Y. 89
 Krashennikov, V.G. 89
 Kuramoto, M. 435
 Kuskov, M.L. 89

L

Ladygina, T.A. 89
 Lafuente, B. 381
 Lancaster, S.J. 413
 Lambrecht, M. 236
 Lee, D.-H. 397
 Leipunskii, I.O. 89
 Löfgren, B. 502
 Locatelli, P. 294, 493
 Longo, P. 548
 Luft, G. 651

M

Mäder, D. 473
 Malmberg, A. 502
 Marques, M.M. 576
 Martinez-Nuñez, M.F. 381
 Matsuzawa, T. 38
 Mendez, L. 381
 Michelotti, M. 358
 Michiels, W. 381
 Miles, A. 509
 Mink, R.I. 60
 Miri, M. 509
 Miserque, O. 236
 Monaco, G. 76
 Mori, H. 658
 Mortreux, A. 590
 Mülhaupt, R. 473
 Muñoz-Escalona, A. 381
 Murakami, M. 558
 Murata, M. 566

N

Naganuma, S. 435
Noh, S.K. 397
Novokshonova, L.A. 89
Nowakowska, M. 426
Nowlin, T.E. 60

O

Ochedzan-Siodlak, W. 426
O'Hara, S.M. 413
Ohtsu, T. 465
Okuda, J. 200
Olonde, X. 590
Osano, Y. 192
Ott, M. 105
Owuor, F.A. 248

P

Pasquet, V. 347
Pecak, M. 509
Pelletier, J.-F. 590
Peña, P. 381
Peters, L. 236
Pietikäinen, P. 502
Porri, L. 519
Prosenc, M.-H. 223
Provasoli, A. 493
Przybyla, C. 321, 333
Pyrlik, O. 212

R

Randall, J.C. 601
Rau, A. 651
Rausch, M.D. 446, 576
Razavi, A. 236
Reußner, J. 406
Ricci, G. 519
Riscili, B. 509
Roesky, H.W. 123
Ruff, C.J. 601
Rytter, E. 136, 274, 643

S

Sacchi, M.C. 294, 493
Saegusa, N. 583

Saito, T. 583
Sancho, J. 381
Saudemont, T. 347
Schaper, F. 223
Schauwienold, A.-M. 485
Schimmel, I. 105
Schmitz, S. 651
Schnell, R. 473
Segre, A.L. 76
Seo, T.S. 368
Seppälä, J. 502
Shi, X. 248
Shiono, T. 264, 583
Shozaki, H. 435
Sinn, H. 105
Soga, K. 50, 566, 583
Specca, A.N. 601
Spitz, R. 347
Steinmetz, B. 321
Støvneng, J.A. 274
Stokvold, A. 274
Sudmeijer, O. 76
Sugano, T. 192
Suhm, J. 473
Suzuki, M. 558
Suzuki, S. 465
Svendsen, H. 643

T

Tait, P.J.T. 307
Talarico, G. 76
Taube, R. 531
Terano, M. 658
Tesche, B. 321
von Thienen, N. 105
Thorshaug, K. 274
Tøgersen, R. 643
Tomotsu, N. 435
Tsujimoto, N. 558
Tsutsui, T. 30
Tritto, I. 294, 493

U

Uchino, H. 192
Uozumi, T. 50

V

Vacatello, M. 76
Vecellio, G. 14
Verdel, N. 347
Vizzini, J.C. 601

W

Walter, P. 473
Wasielewski, M. 426
Wasserman, E.P. 629
Wessel, H. 123
Weimann, B. 333
Weingarten, U. 485
Weiss, K. 97
Werner, R. 170
Wieczorek, T. 651
Woo, S.I. 368

Y

Yamahiro, M. 658
Yamashita, J. 558
Yano, A. 180
Yano, T. 558
Yokota, K. 435
Yoshida, S. 264
Ystenes, M. 136
Yu, P. 128
Yu, Z. 629
Yuasa, S. 558

Z

Zakharov, I.I. 128
Zakharov, V.A. 128
Zambelli, A. 548
Zechlin, J. 321
Zhidomirov, G.M. 128
Zhigach, A.M. 89